SEISMIC BEHAVIOUR OF REINFORCED CONCRETE WALLS WITH LOW SHEAR RATIO

A thesis submitted for the degree of Doctor of Philosophy in the Faculty of Engineering of the University of London and for the Diploma of Membership of Imperial College

by

Mário Manuel Paisana dos Santos Lopes

Engineering Seismology and Earthquake Engineering Section
Civil Engineering Department
Imperial College of Science Technology and Medicine
University of London

June 1991

BIBL. LONDN. UNIV.

À MANUELA

ABSTRACT

In this thesis the shear transfer mechanisms in plastic hinges of reinforced concrete walls and the mathematical modelling of their overall force-deformation relationship are studied.

Eight cyclic tests were performed on scaled models. In order to simulate the conditions more likely to lead to shear failure in the bottom storey of a R/C wall, a new test set-up was developed. The test rig, reinforcement patterns, manufacture of the models are described. The main variable studied in the experimental programme was the design of shear reinforcement.

A quantitative comparison of the provisions of the most relevant codes for the design of R/C walls was undertaken.

The overall force-deformation relationship of R/C walls was studied using an analytical model that separates the total deformation into flexural and shear components. The necessity to couple the shear component to the flexural component was demonstrated by comparing experimental and analytical results. A model based on previous work was implemented for the shear component. Several improvements were included and shown to provide a more accurate and realistic representation of the force-deformation response of walls with low shear ratios.

The analysis of the experimental results led to the identification of the shear resisting mechanisms and the parameters that control shear strength at the ultimate limit state in the plastic hinge zone. This yielded a safe design method, which is more economical than the most advanced code provisions for earthquake resistant design.

ACKNOWLEDGEMENTS

I would like to express my gratitude to my supervisor Dr. Elnashai for his patience and support, and for having made my experimental programme possible.

The support of Junta Nacional de Investigação Científica e Tecnológica (Lisbon), which funded my stay in London, is also acknowledged.

To all the researchers in the field of earthquake engineering at Imperial College who helped me during the tests and with their opinions I express my gratitude. In particular I want to thank Kypros Pilakoutas making available his computer program and for all the useful discussions we had.

I would like to thank all the technicians of the concrete laboratory for their technical advice and support, especially those closely involved with my work: the "A team" William Bobinski and Mike Hobbins, Andrew Hearnshaw, Roby Wilson and Stefan Algar.

I would like to thank Professor João Azevedo for his continuous interest in my work and for his logistic support. I am also grateful to Maria Helena for her help with formulas and tables.

Finally to my parents, wife and children I would like to thank for all their support, in particular during the moments of crisis. Especially, I would like to thank my wife Manuela for her dedication.

TABLE OF CONTENTS

	Page
ABSTRACT	3
ACKNOWLEDGMENTS	4
TABLE OF CONTENTS	5
LIST OF TABLES	11
LIST OF FIGURES	12
ABBREVIATIONS	28
NOTATION	29
ERRATA	34
1 INTRODUCTION	35
1.1 The Role of R/C Walls in Earthquake Resistant Design	35
1.2 Objectives of the Thesis	36
1.3 Layout of the Thesis	38
2 LITERATURE REVIEW AND IDENTIFICATION OF RESEARCH NEEDS	40
2.1 Literature Review	40
2.1.1 Reinforced Concrete Walls Testing	40
2.1.1.1 US Portland Cement Association	41
2.1.1.2 Earthquake Engineering Research Centre at the University of California, Berkeley	45
2.1.1.3 Other American and Japanese Programmes	48
2.1.1.4 New Zealand	50
2.1.1.5 Europe	52

2.1.2 Analytical Models for R/C Walls 55
2.2 Design Philosophies 63
2.2.1 Overall Structure 63
2.2.1.1 Preamble 63
2.2.1.2 Direct Design 65
2.2.1.3 Capacity Design 66
2.2.1.3.1 General 66
2.2.1.3.2 Application of Capacity Design Principles to Walls 67
2.2.2 Shear Design 68
2.2.2.1 Truss Model 68
2.2.2.2 Compressive Force Path Concept 69
2.3 Discussion 72
2.3.1 Reinforced Concrete Walls Testing 72
2.3.1.1 Shear Transfer Mechanisms 72
2.3.1.2 Reasons for the Development of Low Shear Ratios 80
2.3.2 Behaviour Factors 82
2.3.3 Analytical Models for R/C Walls 83
2.4 Summary 85

3 COMPARATIVE STUDY OF DESIGN CODES 112
3.1 Evaluation of Design Strengths 112
3.2 Strength Reduction Factors and Partial Safety Coefficients 114
3.3 Specified Properties of the Materials 115
3.4 Classification of Buildings Based on Ductility 115
3.5 Flexural Design 117
3.5.1 Design Assumptions for Flexure 117
3.5.2 Comparative Examples 119
3.6 Shear Design 121
3.6.1 Maximum Shear Stress 121
3.6.2 Contribution of Concrete to Shear Resistance 124
3.6.3 Design of Horizontal Shear Reinforcement 128
3.6.4 Comparison of Design Strengths 129
3.6.5 Provisions for Sliding Shear 130
3.6.6 Provisions for Vertical Web Reinforcement 132
3.7 Design for Ductility 133

3.7.1 Critical Zones 133
3.7.2 Design of Confinement Reinforcement 134
3.8 Provisions to Avoid Local Instability 139
3.9 Final Remarks 140

4. EXPERIMENTAL WORK 153
4.1 Experimental Methodology 153
4.1.1 Boundary Conditions 153
4.1.2 Experimental Set-Up 154
4.1.3 Details of the Specimens 156
4.1.3.1 Geometry 156
4.1.3.2 Concrete 157
4.1.3.3 Steel Reinforcement 157
4.1.3.3.1 Properties 157
4.1.3.3.2 Design of the Walls 158
4.1.3.4 Mould, Casting and Curing Procedure 161
4.1.4 Load History 162
4.1.5 Instrumentation and Data Acquisition 164
4.1.6 Evaluation of Shear and Flexural Deformations 166
4.2 Description of Tests and Results 167
4.2.1 Introduction 168
4.2.2 Wall SW11 170
4.2.2.1 Description of the Test 170
4.2.2.2 Results 171
4.2.3 Wall SW12 171
4.2.3.1 Description of the Test 171
4.2.3.2 Results 173
4.2.4 Wall SW13 173
4.2.4.1 Description of the Test 173
4.2.4.2 Results 175
4.2.5 Wall SW14 176
4.2.5.1 Description of the Test 176
4.2.5.2 Results 177
4.2.6 Wall SW15 177
4.2.6.1 Description of the Test 177
4.2.6.2 Results 178
4.2.7 Wall SW16 179
4.2.7.1 Description of the Test 179

4.2.7.2 Results 180
4.2.8 Wall SW17 181
4.2.8.1 Description of the Test 181
4.2.8.2 Results 181
4.2.9 Wall SW18 182
4.2.9.1 Description of the Test 182
4.2.9.2 Results 183
4.3 General Discussion of Results 184
4.3.1 Limit States 184
4.3.2 Deformational Characteristics 184
4.3.2.1 Stiffness 184
4.3.2.2 Ductility 186
4.3.2.3 Energy Dissipation 187
4.3.3 Force-Displacement Curves 187
4.3.3.1 Vertical Displacements 187
4.3.3.2 Horizontal Displacements 189
4.3.3.3 Flexural and Shear Deformations 191
4.3.3.4 Base Rotation 193
4.3.3.5 Out-of-Plane Displacements 194
4.3.4 Strain-Gauge Results 194
4.3.4.1 Bottom Edge Members 195
4.3.4.2 Bottom Web Vertical Strains 196
4.3.4.3 Second Level Vertical Strains 197
4.3.4.4 Vertical Strains at the Zero Moment Level 197
4.3.4.5 Vertical Strains on Top of the Wall 198
4.3.4.6 Stirrups 198
4.3.4.7 Confinement Reinforcement 200

5 ANALYTICAL STUDIES 221
5.1 Introduction 221
5.2 Description of Constitutive Relationships and Computer Programs 222
5.2.1 Constitutive Relationships for Steel 222
5.2.2 Constitutive Relationships for Concrete 223
5.2.3 Description of the Shear Model 225
5.2.4 Description of Computer Programs 229
5.3 Flexural Component 231
5.4 Shear Component 233

5.5 Balance Between Shear and Flexural Components 239
5.5.1 Coupling of Shear and Flexural Deformations 239
5.5.2 Post-Yield Segment of Shear Envelope 241
5.6 Discussion and Future Improvements 243
5.7 Summary 246

6 DISCUSSION OF RESULTS AND DESIGN IMPLICATIONS 258
6.1 Introduction 258
6.2 Shear Strength of R/C Walls 259
6.2.1 Shear Transfer Mechanisms 259
6.2.2 Shear Strength of the Compressive Zone 261
6.2.2.1 Design Concept of the Tests 261
6.2.2.2 Comparisons with Different Methods 262
6.2.2.3 Verification 263
6.2.3 The SRS Method 265
6.2.4 Comparisons With Experimental Data 267
6.2.5 Discussion 269
6.3 Effect of Confinement 272
6.4 Length of the Plastic Hinge Zone 274
6.5 Sliding Shear 276
6.6 Ductility 277
6.6.1 Effect of the Load History 277
6.6.2 Effect of the Failure Mode 278
6.6.3 Effect of the Shear Ratio 280
6.7 Effect of Shear Design and Failure Mode in Energy Dissipation 281
6.8 Behaviour Factors 286
6.9 Conclusions 287

7 CONCLUSIONS AND FUTURE DEVELOPMENTS 295
7.1 Conclusions 295
7.2 Future Developments 300

REFERENCES 302

APPENDIX A: PHOTOGRAPHS OF THE EXPERIMENTAL PROGRAMME 312
A(11) Wall SW11 313
A(12) Wall SW12 315
A(13) Wall SW13 317

A(14) Wall SW14 319
A(15) Wall SW15 321
A(16) Wall SW16 323
A(17) Wall SW17 325
A(18) Wall SW18 327

APPENDIX B: EXPERIMENTAL RESULTS **329**
B(11) Wall SW11 330
B(12) Wall SW12 345
B(13) Wall SW13 359
B(14) Wall SW14 375
B(15) Wall SW15 387
B(16) Wall SW16 397
B(17) Wall SW17 409
B(18) Wall SW18 417

APPENDIX C: RESULTS OF ANALYTICAL STUDIES **428**

LIST OF TABLES

		Page
2.1	Stress conditions causing failure of type I wall specimens (Lefas, 1988)	88
2.2	Basic behaviour factors q for $T>T_1$(EC8)	89
2.3	Failure modes of R/C walls critical regions (EC8)	91
3.1	Partial safety coefficients (EC2)	142
3.2	Strength reduction factors (ACI, UBC, NZ)	142
3.3	Limit characteristics of steel reinforcement (EC8)	142
4.1	Concrete mix proportions	202
4.2	Properties of steel reinforcement	202
4.3	Results of compressive tests in cubes	203
4.4	Width of largest diagonal crack of each wall	204
4.5	Force, displacement, stiffness and ductility at ultimate load and failure	205
4.6	Displacements due to the foundation	206
6.1	Shear capacity according to SRS method	291

LIST OF FIGURES

		Page
2.1	Test specimen (Barda et al, 1977)	92
2.2	Nominal dimensions of test specimens with rectangular cross-sections (Oesterle et al, 1980)	92
2.3	Nominal cross-section dimensions (Oesterle et al, 1980)	93
2.4	Nominal dimensions of test specimens (Cardenas et al, 1980)	93
2.5	Details of EERC/UBC tests (Wang et al, 1975 and Vallenas et al, 1979)	94
2.6	Test specimen geometry (Wagner and Bertero, 1982)	95
2.7	Experimental set-up (Wagner and Bertero, 1982)	95
2.8	Relationship of initial shear strength to normal stress (Wagner and Bertero, 1982)	96
2.9	Frictional shear resistance versus normal stress (Wagner and Bertero, 1982)	96
2.10	Direct load transfer in low-rise walls (Paulay et al, 1982)	96
2.11	Test assembly and loading arrangement (Goodsir, 1985)	97
2.12	Test rig arrangement (Lefas, 1988)	98
2.13	Details of test specimens (Lefas, 1988)	
	a) Walls with aspect-ratio 1	98
	b) Walls with aspect-ratio 2	99
2.14	Schematic representation of the failure mechanism of walls with aspect-ratio 1 (Lefas, 1988)	99
2.15	Test rig arrangement for models of scale 1:2.5 (Pilakoutas, 1990)	100
2.16	Reinforcement details for walls SW8 and SW9 (Pilakoutas, 1990)	100
2.17	Inelastic springs (Park et al, 1987)	101
2.18	Distribution of flexibility (Park et al, 1987)	101

2.19 Equivalent frame elements for walls (Smith and Girgis, 1984)
a) Braced wide column analogy 101
b) Braced frame analogy 101
2.20 Truss analogy model (Hirashi, 1984) 102
2.21 Inclined crack model of Huang and Sheu (1988) 102
2.22 Hysteresis relations of different models (Otani, 1984)
a) Large loop models 103
b) Narrow loop models 103
2.23 Origin Orientated Hysteresis Model 104
2.24 Wall model (Kabeyasawa et al, 1982) 104
2.25 Axial-Stiffness Hysteresis Model (Kabeyasawa et al, 1982) 104
2.26 Proposed R/C column model (Vulcano and Bertero, 1986) 105
2.27 Analytical and experimental curves of framed wall under cyclic loading - specimen 4 (Vulcano and Bertero, 1986)
a) Analytical 105
b) Experimental 105
2.28 Analytical and experimental curves of rectangular wall under cyclic loading - specimen 6 (Vulcano and Bertero, 1986)
a) Analytical 106
b) Experimental 106
2.29 New wall model (Vulcano et al, 1988) 106
2.30 New uniaxial element model (Vulcano et al, 1988) 107
2.31 Envelope of bending moments 107
2.32 Truss model for R/C linear Members 107
2.33 Beam under two point load (Kotsovos, 1983) 108
2.34 Types of behaviour exhibited by beams subjected to two point loading (Kotsovos, 1983) 108
2.35 Shear transfer across inclined cracks by concrete alone (Schlaich et al, 1987) 109
2.36 Vertical force at the point of load application due to friction (Pilakoutas and Elnashai, 1991) 109
2.37 Internal forces in wall with low aspect ratio 109
2.38 Interaction between walls and frames 110

2.39 Constitutive relationships of oscillators
a) Oscillator 1 111
b) Oscillator 2 111

3.1 Stress-strain diagram for steel 143
3.2 Parabola-rectangle diagram (EC2) 143
3.3 Rectangular stress diagram (EC2) 143
3.4 Cross-section of the walls
a) Wall 1 144
b) Wall 2 144
3.5 Moment - axial force interaction diagrams
a) Wall 1 144
b) Wall 2 144
3.6 Effect of amount and distribution of vertical reinforcement on ultimate curvature (Cardenas and Magura, 1973) 145
3.7 Flexural strength
a) Wall 1 N = 0 145
b) Wall 1 N = 2066 KN 145
c) Wall 1 N = 4131 KN 146
d) Wall 2 N = 0 146
e) Wall 2 N = 2066 KN 146
f) Wall 2 N = 4131 KN 146
3.8 ACI - contribution of concrete 147
3.9 NZ - contribution of concrete
a) In the PHZ 147
b) Outside the PHZ 147
3.10 EC8 - contribution of concrete outside the PHZ 148
3.11 Shear resistance of Wall 1 for N = 0
a) M/VL = 1 148
b) M/VL = 2 148
3.12 Shear resistance of Wall 1 for N = 2066 KN
a) M/VL = 1 149
b) M/VL = 2 149
c) M/VL = 5 149
3.13 Shear resistance of Wall 1 for N = 4131 KN
a) M/VL = 1 150
b) M/VL = 2 150
c) M/VL = 5 150

3.14 Sliding shear resistance of Wall 1 and Wall 2 151
3.15 Boundary elements according to ACI 1983 151
3.16 Length of the PHZ 152
3.17 Confinement reinforcement (EC8) 152
3.18 Stress-strain diagrams for concrete (EC8) 158

4.1 Wall specimen 207
4.2 Load transferring system 207
4.3 Bending moment diagram on the walls 208
4.4 Photo of the test-rig 208
4.5 Photos of the connection wall-steel frames
a) Wall with one frame - side view 209
b) Wall with the two frames and connecting plates
- side view 209
c) Front view 209
4.6 Schematic representation of the test-rig 210
4.7 Dimensions of test specimens 211
4.8 Trilinear representation of stress-strain diagram for steel 211
4.9 Reinforcement details of the specimens
a) SW11 and SW12 212
b) SW13 212
c) SW14 212
d) SW15 212
e) SW16 213
f) SW17 213
g) SW18 213
h) Detail of the cross section 213
4.10 Details of the stirrups
a) Walls SW11 and SW12 214
b) All other walls 214
4.11 Suggested path of the compressive force (Kotsovos, 1989) 214
4.12 Uneven closure of cracks 214
4.13 Location of the transducers (all walls) 215
4.14 Location of strain gauges in vertical bars (all walls) 215

4.15 Location of strain gauges in horizontal bars
a) Wall SW11 216
b) Wall SW12 216
c) Wall SW13 216
d) Wall SW14 216
e) Wall SW15 217
f) Wall SW16 217
g) Wall SW17 217
h) Wall SW18 217
4.16 Evaluation of flexural deformations
a) Real area α 218
b) Method of area α1 218
c) Method of area α2 218
d) Method of area α3 218
4.17 Evaluation of shear deformations using diagonal measurements. 218
4.18 Components of diagonal measurements 219
4.19 Measurement of flexural deformations using diagonals 219
4.20 External instrumentation 220
4.21 Sliping along diagonal cracks in the post-ultimate range 220
4.22 Balance between shear and flexure deformations for wall of shear ratio 2 (Pilakoutas, 1990) 220

5.1 Stress-strain diagram for steel used in the analysis (Pilakoutas, 1990) 248
5.2 Stress-strain model for monotonic loading of confined and unconfined concrete (Mander et al, 1988) 248
5.3 Factors α_n α_s for the evaluation of confining stresses (EC8) 249
5.4 Evaluation of the confined compressive strength (EC8) 249
5.5 Unloading segment of concrete model (Mander et al, 1988) 250
5.6 Constitutive relations for concrete
a) Element 1 250
b) Element 2 250

5.7 Slopes of the envelope used in defining unloading branches (Ozcebe and Saatcioglu, 1989) 251
5.8 Sample segments of shear model (Ozcebe and Saatcioglu, 1989) 251
5.9 Variation of unloading slope above cracking load with ductility in the shear model (Ozcebe and Saatcioglu, 1989) 252
5.10 Variation of unloading slope below cracking load with ductility in the shear model (Ozcebe and Saatcioglu, 1989) 252
5.11 Definition of reloading slopes of shear model (Ozcebe and Saatcioglu, 1989) 253
5.12 Iterative solution process in the generic step of the analysis 254
5.13 Stiffness matrix of wall element 255
5.14 Flow chart of program NONWALL 256
5.15 Discretization of the wall 257
5.16 Dimensions of walls SW3 and SW9 (Pilakoutas, 1990) 257

6.1 Possible minimum SRS (Pilakoutas, 1990) 292
6.2 Forces and stresses in the compressive edge member (Pilakoutas, 1990) 292
6.3 Mohr-Coulomb failure envelope for concrete (Pilakoutas, 1990) 293
6.4 Schematic representation of the failure surface of wall SW15 293
6.5 Dowel action of vertical web reinforcement along diagonal crack 294
6.6 Definition of relative energy dissipation 294

A(11)1 Description of test of wall SW11 313
A(11)2 Steel cage of wall SW11 314
A(11)3 Wall SW11 after the test 314
A(12)1 Description of test of wall SW12 315
A(12)2 Wall SW12 after the test 316
A(13)1 Description of test of wall SW13 317
A(13)2 Wall SW13 after the test 318
A(14)1 Description of test of wall SW14 319
A(14)2 Failure region of wall SW14 320

A(15)1 Description of test of wall SW15 321
A(15)2 Steel cage of wall SW15 322
A(15)3 Wall SW15 after the test 322
A(15)4 Detail of the top region of the failure surface of wall SW15 322
A(16)1 Description of test of wall SW16 323
A(16)2 Wall SW16 after the test 324
A(17)1 Description of test of wall SW17 325
A(17)2 Wall SW17 after the test 326
A(18)1 Description of test of wall SW18 327
A(18)2 Steel cage of wall SW18 328

B(11)1.a Wall SW11 - force versus displacement 1 (all readings) 330
B(11)1.b Wall SW11 - force versus displacement 1 330
B(11)2 Wall SW11 - force versus displacement 2 331
B(11)3 Wall SW11 - force versus displacement 3 331
B(11)4 Wall SW11 - force versus displacement 4 331
B(11)5 Wall SW11 - force versus displacement 5 332
B(11)6 Wall SW11 - force versus displacement 6 332
B(11)7 Wall SW11 - force versus displacement 7 332
B(11)8 Wall SW11 - force versus displacement 8 333
B(11)9 Wall SW11 - force versus displacement 9 333
B(11)10 Wall SW11 - force versus displacement 10 333
B(11)11 Wall SW11 - force versus displacement 11 334
B(11)12 Wall SW11 - force versus displacement 12 334
B(11)13 Wall SW11 - force versus displacement 13a 334
B(11)14 Wall SW11 - force versus displacement 14 335
B(11)15 Wall SW11 - force versus displacement 15a 335
B(11)16 Wall SW11 - force versus top horizontal displacement 335
B(11)17 Wall SW11 - force versus flexural component of top horizontal displacement 336
B(11)18 Wall SW11 - force versus shear component of top horizontal displacement 336
B(11)19 Wall SW11 - RSD,RFD versus top horizontal displacement 336
B(11)20 Wall SW11 - force versus opening on top 337

B(11)21 Wall SW11 - force versus extension at a quarter height 337
B(11)22 Wall SW11 - force versus extension on top 337
B(11)23.a Wall SW11 - force versus strain 1_I 338
B(11)23.b Wall SW11 - force versus strain 1_{II} 338
B(11)24.a Wall SW11 - force versus strain 2_I 338
B(11)24.b Wall SW11 - force versus strain 2_{II} 339
B(11)24.c Wall SW11 - force versus strain 2_{III} 339
B(11)25.a Wall SW11 - force versus strain 10_I 339
B(11)25.b Wall SW11 - force versus strain 10_{II} 340
B(11)25.c Wall SW11 - force versus strain 10_{III} 340
B(11)25.d Wall SW11 - force versus strain 10_{IV} 340
B(11)26 Wall SW11 - force versus strain 11 341
B(11)27 Wall SW11 - force versus strain 12 341
B(11)28 Wall SW11 - force versus strain 13 341
B(11)29 Wall SW11 - force versus strain 15 342
B(11)30.a Wall SW11 - force versus strain 17_I 342
B(11)30.b Wall SW11 - force versus strain 17_{II} 342
B(11)31 Wall SW11 - force versus strain 19 343
B(11)32 Wall SW11 - force versus strain 20 343
B(11)33 Wall SW11 - force versus strain 21 343
B(11)34 Wall SW11 - force versus strain 22 344
B(11)35 Wall SW11 - force versus strain 23 344
B(11)36.a Wall SW11 - force versus strain 24_I 344
B(11)36.b Wall SW11 - force versus strain 24_{II} 345
B(12)1 Wall SW12 - force versus displacement 1 345
B(12)2 Wall SW12 - force versus displacement 2 345
B(12)3 Wall SW12 - force versus displacement 3 346
B(12)4 Wall SW12 - force versus displacement 4 346
B(12)5 Wall SW12 - force versus displacement 5 346
B(12)6 Wall SW12 - force versus displacement 6 347
B(12)7 Wall SW12 - force versus displacement 7 347
B(12)8 Wall SW12 - force versus displacement 8 347
B(12)9 Wall SW12 - force versus displacement 9 348
B(12)10 Wall SW12 - force versus displacement 10 348
B(12)11 Wall SW12 - force versus displacement 11 348
B(12)12 Wall SW12 - force versus displacement 12 349
B(12)13 Wall SW12 - force versus displacement 13b 349
B(12)14 Wall SW12 - force versus displacement 14a 349

B(12)15	Wall SW12 - force versus displacement 15b	350
B(12)16	Wall SW12 - force versus top horizontal displacement	350
B(12)17	Wall SW12 - force versus flexural component of top horizontal displacement	350
B(12)18	Wall SW12 - force versus shear component of top horizontal displacement	351
B(12)19	Wall SW12 - RSD,RFD versus MD	351
B(12)20	Wall SW12 - force versus opening on top	351
B(12)21	Wall SW12 - force versus extension at a quarter height	352
B(12)22	Wall SW12 - force versus extension on top	352
B(12)23	Wall SW12 - force versus strain 1	352
B(12)24	Wall SW12 - force versus strain 3	353
B(12)25	Wall SW12 - force versus strain 5	353
B(12)26	Wall SW12 - force versus strain 9	353
B(12)27	Wall SW12 - force versus strain 10	354
B(12)28	Wall SW12 - force versus strain 11	354
B(12)29	Wall SW12 - force versus strain 12	354
B(12)30	Wall SW12 - force versus strain 13	355
B(12)31	Wall SW12 - force versus strain 14	355
B(12)32	Wall SW12 - force versus strain 15	355
B(12)33	Wall SW12 - force versus strain 16	356
B(12)34	Wall SW12 - force versus strain 17	356
B(12)35	Wall SW12 - force versus strain 18	356
B(12)36	Wall SW12 - force versus strain 19	357
B(12)37	Wall SW12 - force versus strain 20	357
B(12)38	Wall SW12 - force versus strain 21	357
B(12)39	Wall SW12 - force versus strain 22	358
B(12)40	Wall SW12 - force versus strain 23	358
B(12)41	Wall SW12 - force versus strain 24	358
B(13)1	Wall SW13 - force versus displacement 1	359
B(13)2	Wall SW13 - force versus displacement 2	359
B(13)3	Wall SW13 - force versus displacement 3	359
B(13)4	Wall SW13 - force versus displacement 4	360
B(13)5	Wall SW13 - force versus displacement 5	360
B(13)6	Wall SW13 - force versus displacement 6	360
B(13)7	Wall SW13 - force versus displacement 7	361
B(13)8	Wall SW13 - force versus displacement 8	361

B(13)9 Wall SW13 - force versus displacement 9 361
B(13)10 Wall SW13 - force versus displacement 10 362
B(13)11.a Wall SW13 - force versus displacement 11 362
B(13)11.b Wall SW13 - force versus displacement 11a 362
B(13)12 Wall SW13 - force versus displacement 12 363
B(13)13 Wall SW13 - force versus displacement 13 363
B(13)14 Wall SW13 - force versus displacement 15 363
B(13)15 Wall SW13 - force versus top horizontal displacement 364
B(13)16 Wall SW13 - force versus flexural component of top horizontal displacement 364
B(13)17 Wall SW13 - force versus shear component of top horizontal displacement 364
B(13)18 Wall SW13 - RSD,RFD versus MD 365
B(13)19 Wall SW13 - force versus opening on top 365
B(13)20 Wall SW13 - force versus extension at a quarter height 365
B(13)21 Wall SW13 - force versus extension on top 366
B(13)22.a Wall SW13 - force versus strain 1_I 366
B(13)22.b Wall SW13 - force versus strain 1_{II} 366
B(13)23.a Wall SW13 - force versus strain 2_I 367
B(13)23.b Wall SW13 - force versus strain 2_{II} 367
B(13)24 Wall SW13 - force versus strain 4 367
B(13)25 Wall SW13 - force versus strain 5 368
B(13)26 Wall SW13 - force versus strain 6 368
B(13)27 Wall SW13 - force versus strain 7 368
B(13)28 Wall SW13 - force versus strain 8 369
B(13)29 Wall SW13 - force versus strain 9 369
B(13)30 Wall SW13 - force versus strain 11 369
B(13)31 Wall SW13 - force versus strain 12 370
B(13)32 Wall SW13 - force versus strain 13 370
B(13)33 Wall SW13 - force versus strain 14 370
B(13)34 Wall SW13 - force versus strain 16 371
B(13)35 Wall SW13 - force versus strain 19 371
B(13)36 Wall SW13 - force versus strain 20 371
B(13)37 Wall SW13 - force versus strain 21 372
B(13)38 Wall SW13 - force versus strain 22 372
B(13)39 Wall SW13 - force versus strain 23 372
B(13)40 Wall SW13 - force versus strain 24 373

B(13)41 Wall SW13 - force versus strain 25 373
B(13)42 Wall SW13 - force versus strain 26 373
B(13)43 Wall SW13 - force versus strain 27 374
B(13)44 Wall SW13 - force versus strain 28 374
B(13)45 Wall SW13 - force versus strain 29 374
B(13)46 Wall SW13 - force versus strain 30 375
B(14)1 Wall SW14 - force versus displacement 1 375
B(14)2 Wall SW14 - force versus displacement 2 375
B(14)3 Wall SW14 - force versus displacement 3 376
B(14)4 Wall SW14 - force versus displacement 4 376
B(14)5 Wall SW14 - force versus displacement 5 376
B(14)6 Wall SW14 - force versus displacement 6 377
B(14)7 Wall SW14 - force versus displacement 7 377
B(14)8 Wall SW14 - force versus displacement 8 377
B(14)9 Wall SW14 - force versus displacement 9 378
B(14)10 Wall SW14 - force versus displacement 10 378
B(14)11 Wall SW14 - force versus displacement 11 378
B(14)12 Wall SW14 - force versus displacement 12 379
B(14)13 Wall SW14 - force versus displacement 13 379
B(14)14 Wall SW14 - force versus displacement 15 379
B(14)15 Wall SW14 - force versus top horizontal displacement 380
B(14)16 Wall SW14 - force versus flexural component of top horizontal displacement 380
B(14)17 Wall SW14 - force versus shear component of top horizontal displacement 380
B(14)18 Wall SW14 - RSD,RFD versus MD 381
B(14)19 Wall SW14 - force versus opening on top 381
B(14)20 Wall SW14 - force versus extension at a quarter height 381
B(14)21 Wall SW14 - force versus extension on top 382
B(14)22 Wall SW14 - force versus strain 3 382
B(14)23 Wall SW14 - force versus strain 4 382
B(14)24 Wall SW14 - force versus strain 5 383
B(14)25 Wall SW14 - force versus strain 6 383
B(14)26 Wall SW14 - force versus strain 7 383
B(14)27 Wall SW14 - force versus strain 9 384
B(14)28 Wall SW14 - force versus strain 10 384
B(14)29 Wall SW14 - force versus strain 11 384

B(14)30 Wall SW14 - force versus strain 12 385
B(14)31 Wall SW14 - force versus strain 13 385
B(14)32 Wall SW14 - force versus strain 14 385
B(14)33 Wall SW14 - force versus strain 19 386
B(14)34 Wall SW14 - force versus strain 20 386
B(14)35 Wall SW14 - force versus strain 21 386
B(14)36 Wall SW14 - force versus strain 22 387
B(14)37 Wall SW14 - force versus strain 23 387
B(15)1 Wall SW15 - force versus displacement 2 387
B(15)2 Wall SW15 - force versus displacement 3 388
B(15)3 Wall SW15 - force versus displacement 4 388
B(15)4 Wall SW15 - force versus displacement 9 388
B(15)5 Wall SW15 - force versus displacement 10 389
B(15)6 Wall SW15 - force versus displacement 11 389
B(15)7 Wall SW15 - force versus displacement 12 389
B(15)8 Wall SW15 - force versus displacement 13 390
B(15)9 Wall SW15 - force versus displacement 15 390
B(15)10 Wall SW15 - force versus extension on top 390
B(15)11 Wall SW15 - force versus strain 1 391
B(15)12 Wall SW15 - force versus strain 2 391
B(15)13 Wall SW15 - force versus strain 4 391
B(15)14 Wall SW15 - force versus strain 7 392
B(15)15 Wall SW15 - force versus strain 8 392
B(15)16 Wall SW15 - force versus strain 9 392
B(15)17 Wall SW15 - force versus strain 10 393
B(15)18 Wall SW15 - force versus strain 11 393
B(15)19 Wall SW15 - force versus strain 12 393
B(15)20 Wall SW15 - force versus strain 13 394
B(15)21 Wall SW15 - force versus strain 14 394
B(15)22 Wall SW15 - force versus strain 16 394
B(15)23 Wall SW15 - force versus strain 19 395
B(15)24 Wall SW15 - force versus strain 20 395
B(15)25 Wall SW15 - force versus strain 21 395
B(15)26 Wall SW15 - force versus strain 22 396
B(15)27 Wall SW15 - force versus strain 23 396
B(15)28 Wall SW15 - force versus strain 24 396
B(15)29 Wall SW15 - force versus strain 25 397
B(15)30 Wall SW15 - force versus strain 26 397
B(16)1 Wall SW16 - force versus displacement 1 397

B(16)2 Wall SW16 - force versus displacement 2 398
B(16)3 Wall SW16 - force versus displacement 3 398
B(16)4 Wall SW16 - force versus displacement 4 398
B(16)5 Wall SW16 - force versus displacement 5 399
B(16)6 Wall SW16 - force versus displacement 6 399
B(16)7 Wall SW16 - force versus displacement 7 399
B(16)8 Wall SW16 - force versus displacement 8 400
B(16)9 Wall SW16 - force versus displacement 9 400
B(16)10 Wall SW16 - force versus displacement 10 400
B(16)11 Wall SW16 - force versus displacement 11 401
B(16)12 Wall SW16 - force versus displacement 12 401
B(16)13 Wall SW16 - force versus displacement 13 401
B(16)14 Wall SW16 - force versus displacement 15 402
B(16)15 Wall SW16 - force versus top horizontal displacement 402
B(16)16 Wall SW16 - force versus flexural component of top horizontal displacement 402
B(16)17 Wall SW16 - force versus shear component of top horizontal displacement 403
B(16)18 Wall SW16 - RSD,RFD versus MD 403
B(16)19 Wall SW16 - force versus opening on top 403
B(16)20 Wall SW16 - force versus extension on top 404
B(16)21.a Wall SW16 - force versus strain 1_I 404
B(16)21.b Wall SW16 - force versus strain 1_{II} 404
B(16)22.a Wall SW16 - force versus strain 2_I 405
B(16)22.b Wall SW16 - force versus strain 2_{II} 405
B(16)23 Wall SW16 - force versus strain 5 405
B(16)24 Wall SW16 - force versus strain 9 406
B(16)25 Wall SW16 - force versus strain 10 406
B(16)26 Wall SW16 - force versus strain 12 406
B(16)27 Wall SW16 - force versus strain 19 407
B(16)28 Wall SW16 - force versus strain 20 407
B(16)29 Wall SW16 - force versus strain 21 407
B(16)30 Wall SW16 - force versus strain 22 408
B(16)31 Wall SW16 - force versus strain 23 408
B(16)32 Wall SW16 - force versus strain 24 408
B(17)1 Wall SW17 - force versus displacement 1 409
B(17)2 Wall SW17 - force versus displacement 2 409
B(17)3 Wall SW17 - force versus displacement 7 409

B(17)4 Wall SW17 - force versus displacement 8 410
B(17)5 Wall SW17 - force versus displacement 9 410
B(17)6 Wall SW17 - force versus displacement 10 410
B(17)7 Wall SW17 - force versus displacement 11 411
B(17)8 Wall SW17 - force versus displacement 12 411
B(17)9 Wall SW17 - force versus displacement 13 411
B(17)10.a Wall SW17 - force versus displacement 15a 412
B(17)10.b Wall SW17 - force versus displacement 15b 412
B(17)11 Wall SW17 - force versus top horizontal displacement 412
B(17)12 Wall SW17 - force versus opening at third level 413
B(17)13 Wall SW17 - force versus opening on top 413
B(17)14 Wall SW17 - force versus extension on top 413
B(17)15 Wall SW17 - force versus strain 1 414
B(17)16 Wall SW17 - force versus strain 2 414
B(17)17 Wall SW17 - force versus strain 10 414
B(17)18 Wall SW17 - force versus strain 12 415
B(17)19 Wall SW17 - force versus strain 13 415
B(17)20 Wall SW17 - force versus strain 19 415
B(17)21 Wall SW17 - force versus strain 20 416
B(17)22 Wall SW17 - force versus strain 21 416
B(17)23 Wall SW17 - force versus strain 22 416
B(17)24 Wall SW17 - force versus strain 23 417
B(17)25 Wall SW17 - force versus strain 24 417
B(18)1 Wall SW18 - force versus displacement 1 417
B(18)2 Wall SW18 - force versus displacement 2 418
B(18)3 Wall SW18 - force versus displacement 3 418
B(18)4 Wall SW18 - force versus displacement 4 418
B(18)5 Wall SW18 - force versus displacement 5 419
B(18)6 Wall SW18 - force versus displacement 6 419
B(18)7 Wall SW18 - force versus displacement 9 419
B(18)8 Wall SW18 - force versus displacement 10 420
B(18)9 Wall SW18 - force versus displacement 11 420
B(18)10 Wall SW18 - force versus displacement 12 420
B(18)11.a Wall SW18 - force versus displacement 15a 421
B(18)11.b Wall SW18 - force versus displacement 15b 421
B(18)12 Wall SW18 - force versus top horizontal displacement 421

B(18)13 Wall SW18 - force versus opening at third level 422
B(18)14 Wall SW18 - force versus opening on top 422
B(18)15 Wall SW18 - force versus extension on top 422
B(18)16.a Wall SW18 - force versus strain 1_I 423
B(18)16.b Wall SW18 - force versus strain 1_{II} 423
B(18)17.a Wall SW18 - force versus strain 2_I 423
B(18)17.b Wall SW18 - force versus strain 2_{II} 424
B(18)18 Wall SW18 - force versus strain 9 424
B(18)19 Wall SW18 - force versus strain 12 424
B(18)20 Wall SW18 - force versus strain 13 425
B(18)21 Wall SW18 - force versus strain 19 425
B(18)22 Wall SW18 - force versus strain 20 425
B(18)23 Wall SW18 - force versus strain 21 426
B(18)24 Wall SW18 - force versus strain 22 426
B(18)25 Wall SW18 - force versus strain 23 426
B(18)26 Wall SW18 - force versus strain 24 427

C.1 Comparison of results of programs CRELIC and NONWALL for different values of C 429
C.2 Comparison of results of programs CRELIC and NONWALL for different values of λ 429
C.3 Comparisons of predictions of programs CRELIC and NONWALL with data of wall SW13 430
C.4 Comparisons of predictions of programs CRELIC and NONWALL with data of wall SW9 430
C.5 Comparisons of predictions of programs CRELIC and NONWALL with data of wall SW3 430
C.6 Force versus shear displacement evaluated by the proposed shear model (wall SW13)
a) Full results 431
b) Results up to MD=2.0 431
C.7 Force versus shear displacement evaluated by the shear model after changing unloading branches (wall SW13)
a) Full results 432
b) Results up to MD=2.0 432
C.8 Force versus shear displacement evaluated by the shear model for β=0 (wall SW13) 432

C.9 Force versus shear displacement evaluated by the shear model after calibration of unloading stiffness (wall SW13) 433
C.10 Comparison of experimental data with predictions of the shear model (wall SW13) 433
C.11 Comparison of cumulative energy dissipation by the shear component (wall SW13) 433
C.12 Force versus shear displacement evaluated by the shear model (wall SW16) 434
C.13 Comparison of experimental data with predictions of the shear model (wall SW16) 434
C.14 Analytical results for V_y=120KN (wall SW13)
a) Force versus total displacement 435
b) Force versus flexural displacement 435
c) Force versus shear displacement 435
C.15 Analytical results with coupling (wall SW13)
a) Force versus total displacement 436
b) Force versus flexural displacement 436
c) Force versus shear displacement 436
C.16 Analytical results of coupled version for KH=6KN/mm
a) Force versus total displacement 437
b) Force versus flexural displacement 437
c) Force versus shear displacement 437
C.17 Analytical results of coupled version KH=15KN/mm
a) Force versus total displacement 438
b) Force versus flexural displacement 438
c) Force versus shear displacement 438
C.18 Total cumulative energy dissipation for different values of the post-yield stiffness of the shear model 439
C.19 Relative contribution of the shear component to the total deformation for different values of the post-yield stiffness of the shear model 439

ABBREVIATIONS

ACI	American Concrete Institute
ASHM	Axial Stiffness Hysteresis Model
CFP	Compressive Force Path
EC	EuroCode
IC	Imperial College
LHS	Left Hand Side
LVDT	Linear Voltage Differential Transducer
MD	Maximum Displacement amplitude in a given cycle
NZ	New Zealand Standards
OOHM	Origin Orientated Hysteresis Model
PHZ	Plastic Hinge Zone
R/C	Reinforced Concrete
RHS	Right Hand Side
SRS	Shear Resistance Surface
UBC	Uniform Building Code
USD	Unloading Stiffness Degradation index

NOTATION

A	pinching parameter
a	internal lever arm according to truss model
A_{ch}	cross sectional area along the confined length measured out-to-out of confinement reinforcement
A_g	gross area of section
A_{gb}	concrete gross area along confined length
A_l	total area of inclined reinforcement
A_{te}	area of one leg of tie
A_{st}	total area of longitudinal reinforcement
$(A_s/s)_{cr}$	amount of distributed confinement reinforcement
$(A_s/s)_h$	amount of distributed horizontal shear reinforcement
$(A_s/s)_v$	amount of distributed vertical web reinforcement
b	width of the web
b_o	width of confined area
C	parameter that defines the relative centre of rotation in a wall element (as proposed by Vulcano et al)
c	neutral axis depth
C_{cc}	compressive force in a wall edge member
cc	concrete cover
d	distance from the extreme compression fibre to centroid of tension reinforcement
d_s	distance from the extreme tension fibre to centroid of tension reinforcement
d_{se}	distance of centroid of total vertical reinforcement to extreme compression fibre
d_x	distance from centroid of total vertical reinforcement to extreme compression fibre
d'	distance from extreme compression fibre to centroid of compression reinforcement
E_c	elastic compressive Young's modulus of concrete
E_s	Young's modulus of steel
f_c	specified compressive strength of concrete (cylinder strength) if referring to ACI, UBC or

	NZ, or characteristic compressive strength of concrete if referring to the Euro-Codes
f_{cc}	compressive strength of confined concrete
f_{cx}	compressive stress of confined concrete in σ-ε diagram
f_y	specified yield strength of steel reinforcement if referring to ACI, UBC or NZ, or characteristic yield strength of steel reinforcement if referring to the Euro-Codes
f_{cd}	design compressive strength of concrete (EC2)
f_{un}	stress at a point in the σ-ε diagram for concrete where unloading starts
f_{yd}	design yield strength of steel reinforcement
g	depth of rectangular stress block in concrete
H	total height of wall
h_c	cross sectional dimension of concrete measured centre-to-centre of confinement reinforcement
h_o	height of the wall up to the level where M = 0
h_{phz}	length of the plastic hinge zone
h_s	distance between floors
K	tangent stiffness of shear model
KH	post-yield stiffness in the shear model
K_1	elastic shear stiffness
K_2	slope of the line connecting the yield point in one direction with the cracking point in the opposite direction in the shear envelope
K_f	secant stiffness at failure
K_u	secant stiffness at ultimate load
L	length of the wall cross section
l_c	length of confined region
M	bending moment in plane of the wall
n	counter that traces the successive number of cycles in one direction at the current maximum deflection in the shear model
N	axial force
N_o	nominal concentric axial compressive capacity based on ACI 318-83
N_r	relative axial stress
N_u	factored axial force

q	behaviour factor as defined in EC8
r	steel hardening ratio
S	structural type factor according to NZ
s	spacing of distributed reinforcement
V	shear force in plane of the wall
V_c	contribution of the concrete to shear resistance in terms of force
V_{cc}	shear resistance of a wall compressive edge member
v_c	contribution of the concrete to shear resistance in terms of stress
V_{dd}	dowel resistance of vertical bars
V_f	shear force correspondent to flexural capacity
V_{fc}	shear force correspondent to failure by crushing of the concrete after yielding of main flexural reinforcement
V_{id}	shear resistance of inclined bars
V_m, V_m'	variables used to define second reloading branches in the shear model
V_p, V_p'	variables used to define the first reloading branches in the shear model
V_r	design shear strength
V_s	contribution of the truss mechanism to shear resistance
V_{ss}	sliding shear resistance
V_{cr}	cracking load in the shear model
V_t	contribution of the zone of the wall under axial tension to shear strength
V_y	yield load in the shear model
V_u	ultimate shear force of a wall failing in shear by diagonal tension
V_θ	force resisted along shear failure surface in the compressive zone
W	percentage of vertical steel reinforcement
W_{wd}	design volumetric ratio of confinement reinforcement
W_w	volumetric ratio of confinement reinforcement used in design
ε	strain

ϵ_a	auxiliar value of strain used to define unloading branches of concrete
ϵ_c	compressive strain of confined concrete in σ-ϵ diagram
ϵ_{cc}	strain of compressive concrete at maximum stress
ϵ_{co}	strain of unconfined concrete at maximum stress (usually taken as 0.002)
ϵ_{pl}	strain at which an unloading branch from the σ-ϵ diagram intersects the strain axis
ϵ_{un}	strain at a point in the σ-ϵ diagram for concrete where unloading starts
ϵ_u	ultimate strain
δ_{hf}	horizontal displacement at the level where M=0 due to the rotation of the foundation
δ_h	top horizontal displacement
Δ	deflection where unloading starts in the shear model
Δ_{cr}	deflection at cracking in the shear model
Δ_m	maximum displacement in the shear model
Δ_p	previous peak displacement in the shear model
Δ_y	deflection at yield in the shear model
ϕ	strength reduction factor
ϕ_o	ratio of overstrength moment of resistance to moment resultant from specified code loading, where both moments refer to the base section of the wall
ϕ_s	angle of the shear failure surface with respect to the horizontal in the tension side of the wall
γ_c	partial safety coefficient for concrete
γ_s	partial safety coefficient for steel
θ	angle of friction
θ_o	angle of potential shear failure surface in the compressive zone with respect to the horizontal
φ	angle of the inclined bars with the horizontal
ρ_h	ratio of horizontal shear reinforcement area to concrete area
ρ_l	ratio of total vertical reinforcement area to gross area of the web only

ρ_n	ratio of vertical shear reinforcement area to area of concrete
ρ_v	ratio of total vertical reinforcement area to gross area of concrete
λ	variable that defines the length where bond is not effective in the uniaxial springs
λ_o	shear ratio (λ_o = M /V L)
$\mu_{1/r}$	curvature ductility demand
μ_{fr}	safe lower value of concrete-to-concrete friction coefficient under cyclic loading as defined in EC8
μ_f	displacement ductility factor at failure
μ_u	displacement ductility factor at ultimate load
ν	coefficient used in EC8 to distinguish between different modes of failure of critical regions of walls
ξ	normalised value of neutral axis depth with respect to the length of the wall cross section L
σ	axial stress
τ	tangential stress
τ_o	cohesion of the concrete
τ_{Rd}	design stress used to calculate the contribution of concrete to shear resistance in EC2 and EC8

The index "n" in subscript after a variable denotes reference to the nominal value of that variable.

ERRATA

CHAPTER 1

1 INTRODUCTION

1.1 The Role of R/C Walls in Earthquake Resistant Design

In the past it was considered that flexible buildings would perform well under earthquake actions due to the reduction in the inertia forces compared to stiffer, shorter period structures. However, observations from earthquake damage studies have shown that flexible buildings do not perform as well as it was expected. It was observed that due to high interstorey drifts extensive damage is inflicted on non-structural elements, rendering the buildings difficult to repair. High interstorey drifts may also impose excessive ductility demands and high forces due to secondary effects that could trigger failure. Buildings with a very flexible ground floor provided typical examples of failure due to high interstorey drifts.

Structural walls are very efficient in providing overall stiffness to reinforced concrete buildings due to their high stiffness. However, as they attract most of the total shear force at the lower levels, they were thought to be inherently brittle. This has led to conservative provisions in some codes that penalize buildings with R/C walls with higher seismic forces. Some codes assign all the inertia forces to the walls and use other structural resisting systems, such as frames, only as a reserve of strength. The idea that R/C walls are inherently brittle has been shown to be incorrect by research undertaken during the last two decades. Their ability to behave in a ductile flexural mode is now established.

The general design philosophy that forms the background to the codes states that structures should, in general, be able to:

- Resist minor earthquakes without damage.

- Resist earthquakes of moderate intensity without structural damage, but with some non-structural damage.

- Resist major earthquakes, of magnitude equal to the maximum that could be experienced in the area, without collapse but with some structural as well as non-structural damage.

In medium and high-rise R/C buildings the frames may not provide the necessary stiffness to ensure that the two first requirements are met. The use of structural walls provides an efficient solution for this problem. The contribution of the walls may also be indispensable to ensure that the third requirement is met. Properly designed walls should provide not only stiffness, but also strength, ductility and energy dissipation capacity. Therefore, in seismic zones, structural walls are essential elements in medium and high-rise reinforced concrete buildings.

1.2 Objectives of the Thesis

Despite all the efforts of the past decades to understand the behaviour of R/C walls under earthquake loading, some issues are still unclear or are the subject of disagreement. One of the most important issues is the effect of high shear forces, in particular in the plastic hinge zone (PHZ), where yielding of the main flexural reinforcement is expected. This work concentrates on this problem, with special emphasis on the following two aspects:

- Assessment of the shear transfer mechanisms in the PHZ and calculation of the contribution of each of these mechanisms to the shear capacity at the ultimate limit state, leading to design recommendations.

- Modelling of the overall force deformation of R/C walls in the presence of high shear forces by means of a simplified model able to be incorporated in a global model for the nonlinear analysis of an entire structure.

The current work was preceded by two other projects in the same Department; by Lefas (1988) and Pilakoutas (1990). Different and often contradictory conclusions were drawn by those two researchers regarding the shear transfer mechanisms and the evaluation of the shear capacity of R/C walls. It is the purpose of this thesis to assess their conclusions and compare them with proposals of other researchers. Also, comparison with the theory that forms the background to some of the most advanced code provisions, namely the draft of EC8, is sought.

An experimental programme comprising tests on eight walls was performed to achieve the above mentioned objectives. It was sought to simulate the conditions more likely to lead to a shear failure that may be found in R/C walls of multistorey buildings. In order to achieve this a new test set-up was developed. The boundary conditions imposed on the specimens are considered to simulate in a more realistic manner the load-transfer to critical regions of R/C walls of multistorey buildings.

Additional aspects of the behaviour of R/C walls with high shear forces are discussed in this work, with particular reference to the provisions of the draft of EC8. These aspects of behaviour are:

- Effect of confinement reinforcement. Although this is well established for flexural walls, it still remains unclear for walls with low shear ratios.

- Determination of the distance along the height of the wall where confinement reinforcement is necessary.

- The need for design against sliding shear.

- Influence of the load history, failure mode and shear ratio on the ductility and energy dissipation capacity of R/C walls with low shear ratios.

- Qualitative and quantitative effect of horizontal web reinforcement on the behaviour.

1.3 Layout of the Thesis

After the introductory chapter 1, a literature review of research pertinent to the thesis is presented in chapter 2. The philosophies that form the background to the codes and alternative concepts and methods are also presented. The conclusions given by the authors in the literature and the design philosophies and methods are discussed.

A quantitative comparison of the most relevant code provisions for the design of R/C walls is undertaken in chapter 3.

Chapter 4 contains a description of the new set-up developed for this test programme, a description of all the specimens and respective tests, the layout of the figures showing the results and a general discussion of those results.

In chapter 5 analytical studies concerning the development of a general model for the simulation of the overall force deformation relationship of R/C walls are presented. The chosen model simulates the overall deformation by separating it into shear and flexural components. The purpose of this study is to make a contribution towards the

development of the shear component and to improve the performance of the model in estimating the correct balance between both components of the deformation.

The main design-orientated discussion is presented in chapter 6. The contribution of different shear transfer mechanisms (horizontal and vertical web reinforcement, aggregate interlock, dowel action of flexural reinforcement, the compressive edge member and diagonal reinforcement) at different stages of loading and unloading, in particular at the ultimate limit state, are discussed. The main results of the different tests are compared, the ability of different theories to explain the observed behaviour is assessed and design recommendations regarding shear capacity are proposed.

The EC8 methodology for inclusion of R/C walls in the evaluation of the behaviour factors is assessed on a qualitative basis. Changes in that methodology are proposed. Other design issues already referred to in section 1.2 are also discussed.

In chapter 7 the main conclusions and developments presented in the previous chapters are summarised. Recommendations for future research and developments concerning both the experimental and analytical work are suggested.

CHAPTER 2

2 LITERATURE REVIEW AND IDENTIFICATION OF RESEARCH NEEDS

A review of the literature on aspects of R/C walls behaviour relevant to the current study is given herein. In section 2.1 previous research on testing and modelling the overall force-deformation relationship of reinforced concrete walls is reviewed. Where considered appropriate, reference is also made to tests of other R/C members. Section 2.2 presents the design philosophies that form the background to the codes and the compressive force path concept. Finally, in section 2.3 a discussion leading to identification of research needs is undertaken. Some of the subjects discussed in section 2.3 are further referred to in chapter 6.

2.1 Literature Review

2.1.1 Reinforced Concrete Walls Testing

Until the 1970's most research efforts had been directed towards understanding the behaviour of moment resisting frames. The capability of walls to sustain large inelastic deformations without substantial loss of load carrying capacity was questioned. Less work was performed to improve the understanding of how walls behave under earthquake loading. Before the 1960's, the most significant experimental investigation on the behaviour of R/C walls was carried out by Benjamin and Williams (1957, 1958 and 1960). These research trends have been changing in recent years due to more effort being applied to understand the behaviour of R/C walls. Most of the experimental work on the behaviour of R/C walls has been performed during the last two decades in the USA, New Zealand, Japan and Europe. The literature survey focusses on work which is considered of more significance for

earthquake resistant design, performed at selected research establishments.

2.1.1.1 US Portland Cement Association

The strength of shear walls for high-rise buildings was studied by Cardenas and Magura (1973). Three specimens had a shear-ratio M/VL of 2 at a distance L/2 of the base of the wall and were subjected to lateral and axial loading. Three more specimens had a shear-ratio of 1. The main variables were the amount and distribution of flexural reinforcement and the shear ratio. The main conclusions were as follows:

- Axial load increases moment capacity but reduces ultimate curvature.

- Minimum shear reinforcement (0.27% of the cross section area) was sufficient to allow the development of the flexural capacity in the walls with the higher shear ratio.

- Concentration of the flexural reinforcement near the edges resulted in higher ductility.

Results from tests of eight specimens representing low-rise shear walls with boundary elements were reported and analysed by Barda, Hanson and Corley (1977). The test programme aimed at determining the effect of load reversals intended to represent severe earthquake loading. One specimen was repaired and retested. The main parameters varied in this investigation were the amount of flexural reinforcement, the amounts of vertical and horizontal web reinforcement and the aspect ratio H/L. As shown in figure 2.1 the loads were applied to the wall through the top slab.

The major findings and conclusions of this test programme were:

- Specimens subjected to load reversals had a shear strength about 10% less than similar specimens which were subjected to loading in one direction. Notwithstanding, current design procedures underestimate the strength of the specimens subjected to load reversals.

- The amount of horizontal web reinforcement had little effect on the shear strength of walls whose aspect ratio was 1/2. However the shear strength increased significantly with added vertical web reinforcement.

- The presence of the top slab appeared to have a significant influence on the shear strength of specimens with an aspect ratio of 1/2 and 1/4.

- Shear force was observed to be transmitted from the top slab to the base through the formation of compressive "struts" in the wall between cracks.

- Frame action due to the boundary elements provided a mode of failure that was gradual rather than sudden.

Fiorato, Oesterle and Corley (1977), Oesterle, Fiorato, Aristizabal-Ochoa and Corley (1980) and Oesterle, Aristizabal-Ochoa, Shiu and Corley (1984) reported an extensive test programme on R/C walls. The test specimens were approximately one-third of full size. Their height was 4.57m, the length of the cross-section 1.91m and the width 0.1m, as shown in figure 2.2. Each specimen was loaded laterally as a vertical cantilever with forces applied through the top slab. The applied shear ratio M/VL was 2.4. Three cross-section shapes were considered as shown in figure 2.3; flanged, barbell and rectangular. Other parameters varied were axial load, concrete strength, loading history, level of shear stress at flexural yielding and the amount of horizontal shear reinforcement. The tests were performed under load control before yield and displacement control after yield.

The main conclusions were:

- Isolated structural walls possess significant inelastic deformation capacity under load reversals. Rotational ductility decreases with increased level of shear stress.

- Specimens subjected to high shear stresses developed inclined cracks giving rise to a truss mechanism which transferred shear after these cracks had formed. With repeated cycling in the inelastic range, loss of concrete by abrasion and surface spalling increased the shear deformation and reduced the compressive strength of the concrete struts between inclined cracks. Finally, the specimens failed by web crushing. Hence this failure mode depends on the magnitude of the shear stresses and the level of deformation.

- Walls subjected to low nominal shear stresses developed nearly horizontal cracks. Consequently little truss action developed to transmit shear. After yield, shear was transferred primarily by interface friction and dowel action until the walls failed in flexure.

- Axial compressive forces decreased ductility of specimens governed by flexure. However they had the opposite effect in walls subjected to high shear stresses, as axial compressive stresses stiffened the aggregate interlock mechanism and inhibited the degradation of shear stiffness and strength resulting from abrasion under load reversals.

- Shear failure can be avoided if horizontal web reinforcement is provided for the shear force developing at maximum flexural capacity of the section. Significant increases on the amount of horizontal web reinforcement beyond that level had little effect on the ductility of specimens failing by web crushing.

- The boundary elements may limit sliding shear by acting as large dowels.

- Rectangular walls are more susceptible to out-of-plane instability. Barbell and flanged walls have larger out-of-plane stiffness, but are more susceptible to web crushing by virtue of their generally higher moment-to-shear capacities.

- Concrete strength affects the crushing strength of the web and the boundary elements and the abrasion resistance at crack interfaces.

- Stiffness degradation was essentially a function of the maximum displacement previously achieved.

- The addition of confinement hoops resulted in an increase in capacity of walls limited by shear strength but no increase was apparent for walls limited by flexural strength.

- Confinement hoops doubled the top displacement ductility ratio for a wall limited by flexural strength but had no significant effect on the ductility of walls limited by shear strength.

Results from a series of seven tests on rectangular walls with aspect ratio H/L of 1, as shown in figure 2.4, were reported by Cardenas, Russel and Corley (1980). Variables in the test programme were the amount and distribution of vertical and horizontal reinforcement. Hoops were not provided and vertical load was not applied. Lateral load was applied at the top of the wall through an enlarged monolithic section.

Specimens containing the minimum amount of horizontal reinforcement and having the vertical reinforcement uniformly distributed failed by crushing of the compressive zone after yielding of the horizontal reinforcement. Specimens whose

vertical reinforcement was concentrated near the edges and whose horizontal reinforcement did not yield failed in a mode labelled shear-anchorage, explained as follows. When inclined cracks formed the force in the vertical reinforcement located near the right edge of the wall became constant along the height. The wall failed due to inadequate anchorage of that reinforcement on top. Walls with uniformly distributed vertical and horizontal reinforcement calculated according to ACI (1977) failed by crushing of the diagonal concrete struts after yielding of most of the vertical reinforcement. Both vertical and horizontal reinforcement were considered effective in contributing to shear strength. The strength of a wall subjected to monotonic loading resulted in a 7% increase as compared to a similar wall subjected to reversals of high shear forces.

2.1.1.2 Earthquake Engineering Research Centre at the University of California, Berkeley

Work on R/C structural walls has been performed since the 1970's at the Earthquake Engineering Research Centre, University of California, Berkeley (EERC/UCB). Despite earlier experimental research on the behaviour of reinforced concrete components, the results from the first tests on walls were reported in 1975 by Wang, Bertero and Popov (1975). The specimens intended to model, at scale 1/3, the three bottom storeys of two framed barbell walls of a multistorey building. The region of major interest, i.e. where plasticity was expected to spread, was unlikely to reach the third storey. However, it was decided to design the specimens with three stories in order to keep the local effect of the concentrated axial loads away from the critical region and to provide a realistic boundary condition for that region. Shear force, axial force and bending moment were applied to simulate the effects of gravity loads and earthquake excitations on the prototype. Details of the specimens and test arrangements are shown in figure 2.5. After testing, the units were repaired and retested.

Vallenas, Bertero and Popov (1979) tested two models similar to the above in addition to two of rectangular cross-section. Parameters studied included the wall cross-section type, the kind of transverse reinforcement used in the boundary elements (rectangular hoops vs spirals), load history (cyclic or monotonic) and repair techniques.

The main conclusions of the above investigation were as follows:

- Flexural strength could be adequately predicted by using the plane sections hypothesis and realistic material properties. However, it was considered that if strain hardening of the flexural steel and material strengths in excess of those assumed in design were neglected in the evaluation of the flexural capacity, shear forces in excess of those calculated according to code procedures would develop.

- The maximum nominal shear stresses recorded were $1.12\sqrt{f_c}$ MPa and $0.78\sqrt{f_c}$ MPa for barbell and rectangular sections respectively. Under high shear and moment, large diagonal cracks may develop and eventually lead to diagonal tension failure. Well confined boundary elements were effective in providing shear resistance when a sliding shear failure occurred in the wall web.

- Closely spaced confinement reinforcement can be used to control buckling of the main flexural reinforcement. Spirals are more effective than hoops. Instability of rectangular sections appears to be affected by the ratio of clear height to web thickness and the level of compressive strains in the flexural reinforcement.

The effect of the amount and arrangement of wall panel reinforcement on the overall seismic performance of walls was studied by Iliya and Bertero (1980) who subjected two specimens to three series of tests. Additional objectives were to study the effectiveness of epoxy injection techniques

for the repair of damaged walls, methods of strengthening walls after local failure and the effects of construction joints.

It was observed that the 45° arrangement of the wall reinforcing bars was more effective in resisting the effect of shear reversals; there was less deterioration, and energy dissipation capacity was improved. The relative contribution of shear deformations to the total deformation was higher at the first storey where the inelastic behaviour was concentrated, and increased with higher displacement ductility. This effect was less pronounced for the wall designed with diagonal reinforcement. However, it was considered that the most important detail seemed to be the use of barbell cross-section with well confined edge members rather than the amount of wall panel reinforcement. The amount of reinforcement has more effect on the ductility of cyclically loaded specimens than on the ductility of their monotonically loaded counterparts.

The shear resistance of vertical boundary members of walls was studied by Wagner and Bertero (1982). It was sought to duplicate prototype edge members with simple test specimens. Figure 2.6 shows the geometry of the test specimens and figure 2.7 shows the experimental set-up. Different levels of constant axial load were applied during the tests. Figure 2.8 shows an estimate of the maximum concrete shear resistance of the edge members under monotonic loading. The shear resistance of the cyclically loaded specimens decreases but stabilizes after a few shear displacement cycles. A lower bound of the edge member shear resistance at this stage was given by the frictional resistance, as shown in figure 2.9. It is observed that the frictional shear resistance increases linearly with the level of axial stress. This can be expressed in terms of the Mohr-Coulomb failure criterion as follows:

$$\tau = \sigma \tan\theta + \tau_o \qquad (2.1)$$

If a fully cracked surface had been formed the cohesion is zero. Hence, the frictional resistance is defined by:

$$\tau = \sigma \tan\theta \qquad \theta = 32^{\circ} \tag{2.2}$$

This data cannot be used to evaluate the ultimate shear resistance of the edge member since extra parameters have an effect, as discussed hereafter. A larger number of cycles and large openings of flexural cracks due to yielding of the flexural reinforcement would degrade shear resistance. It was also suggested that the higher the axial compression an edge member of a wall would be subjected to, the lower its shear strength would be (in terms of the angle of friction θ). However, the data was considered to provide insight into the participation of edge members in the shear resistance of laterally loaded R/C walls.

2.1.1.3 Other American and Japanese Programmes

At McMaster University, Alexander et al (1973) studied the effect of axial load in low rise walls. It was concluded that axial compression increased the horizontal load carrying capacity of the wall and reduced the rate of stiffness deterioration and attainable ductility.

Yamaguchi, Sugano, Higashibata and Nagashima (1980) reported results of tests on sixteen walls of scale 1:5 and barbell cross-section. The aspect ratio was varied from 0.6 to 2.4 and the axial stress from 0 to 4MPa. The amounts of reinforcement in the web and the boundary members were also varied. Different modes of failure were also observed. The ratio of shear to flexural capacities was considered to be a good indicator of which type of failure should be expected. For values of that ratio higher than 1.1 the mode of failure should be dominated by flexure and for values lower than 0.86 shear failure should be expected. For

intermediate values a mixed failure mode is likely to occur.

The effect of out-of-plane moments on the in-plane behaviour of walls was studied by Aoyama and Yoshimura (1982) who tested eight reinforced concrete walls under biaxial loading. It was concluded that the in-plane behaviour was not affected by out-of-plane moments as long as they were not larger than half the out-of-plane yield moment.

Twenty two scale 1:8 models and one full scale concrete wall were tested under alternating lateral load by Hernandez and Zermeno (1980) at the National Autonomous University of Mexico. The aim of this research programme was to study the effect on the strength and inelastic behaviour, when shear governs the failure, of several variables such as shear-ratio (M/VL), concrete strength, amount and distribution of reinforcement, axial loads, presence of intermediate slabs and boundary elements.

The most important conclusions were:

- Structural walls with shear failure have an inadequate hysteretic behaviour.

- The efficiency of boundary elements for improving behaviour is low even if the concrete at the end columns is confined with high amounts of confinement reinforcement.

- It is convenient to place similar amounts of reinforcement in both directions in the wall web in order to prevent accelerated shear failure due to yielding.

- Intermediate slabs behaved as stiffeners, increasing initial rigidity and improving deformation capacity

BIBL. LONDIN. UNIV.

at failure, but this did not increase the wall strength.

- The main variables that influence deformation capacity at failure were shear and reinforcement ratios and arrangements of web reinforcement.

- The amount and distribution of reinforcement at the boundary elements did not influence the deformation capacity at failure.

2.1.1.4 New Zealand

Four low-rise walls with an aspect ratio of 1/2 were tested at the University of Canterbury by Paulay, Priestley and Singe (1982). Two of the walls had rectangular cross-sections and the other two included small flanges. Two of the walls were designed with diagonal reinforcement. The horizontal load was applied on top by means of a beam. It was recognized that the diagonal tension strength of low-rise walls was significantly affected by the mode of load introduction on top. The aims of this study were as follows:

- Examine the ductility by flexural yielding and its consistent attainment under load reversals.

- Study the characteristics of the hysteretic behaviour of low-rise walls and compare their ability to dissipate energy with beams and columns.

- Establish maximum displacement ductility.

- Study the contribution of shear deformations to the energy dissipation and stiffness degradation.

- Observe the influence of the flanges on the hysteretic response.

- Study means of reducing sliding shear deformations.

It was concluded that it is possible to ensure a ductile behaviour with extensive yielding of the flexural reinforcement if shear failure was suppressed. This could be achieved if the supplied shear strength exceeded the demand when the wall developed its flexural overstrength. Diagonal reinforcement was found to produce a substantial increase in energy dissipation capacity and improvement on the control of sliding shear even when as little as 30% of the applied shear was resisted by such reinforcement. Nevertheless, the above amount of diagonal reinforcement was not enough to prevent slipping. A significant amount of energy was dissipated due to yielding of the diagonal reinforcement. Evaluation of stresses in the vertical and horizontal wall reinforcement suggested that a major part of the horizontal shear force was transferred directly from the top beam to the foundation by diagonal struts as shown in figure 2.10. It was found that flanged walls were more likely to be affected by sliding shear due to the lower depth of the neutral axis at the critical base section.

The validity of current code provisions for the prevention of premature inelastic instability and the effect of confinement reinforcement in regions subjected to large compressive strains were studied by Goodsir (1985). Four 1:3 scale walls were tested under eccentric axial and cyclic lateral loading simulating seismic actions. The test assembly and loading arrangement are shown in figure 2.11. Three walls had a rectangular (1500*100mm^2) cross-section and one a "T" section. All walls showed good energy dissipation capacity. In three of the walls failure was initiated by crushing of the unconfined concrete immediately adjacent to the well confined boundary element. The other wall failed due to buckling of the compression zone. It was concluded that if

the ratio of the clear height to the wall thickness was not larger than 10, as recommended by codes, rectangular walls were unlikely to fail by lateral instability. It was proposed that confinement reinforcement should cover 3/4 of the compressive zone and not only half of it as recommended in the New Zealand standards (3101:1982). This was considered necessary due to a neutral axis depth at failure larger than calculated. Strain distribution along the stirrups indicated that there was a general trend of increasing strain levels with maximum imposed displacement ductility which was attributed to the breakdown of shear resisting mechanisms.

2.1.1.5 Europe

The main features of two research projects at Imperial College are described herein. Lefas (1988) tested fifteen isolated walls of scale 1:3. The main variables in this experimental programme were the aspect ratio, axial force, amount of horizontal web reinforcement and concrete strength. Six specimens (SW1-SW6), of aspect ratio 1, were tested under monotonic loading. Six specimens (SW11-SW16), of aspect ratio 2, were tested under monotonic loading and three (SW31-SW33) were subjected to 4 to 5 cycles. The tests were performed under load control and the load was applied on the top beam. The test rig arrangement is shown in figure 2.12 and details of test specimens in figure 2.13.

All the specimens tested under monotonic loading were designed according to ACI-318 1983 with the exception of SW26 which had half the amount of horizontal shear reinforcement and a weaker concrete. The specimens tested cyclically had less horizontal and vertical web reinforcement than the other specimens of the same aspect ratio.

Significant flexural overstrength was reported. This was attributed to the high axial compressive stresses that were thought to have developed. Axial stresses of up to three times the uniaxial strength were claimed to exist in the compressive zone. That was considered to be due to the triaxial stress state. It was found that if all the shear was taken by the compressive zone, the triaxial state of stress that existed there would counteract the tensile stresses due to the shear force. Accordingly, the principal stresses are compressive. Table 2.1 shows the level of stresses that were calculated for walls with aspect-ratio 1. The average shear stress was obtained by dividing the measured shear force by the area of the compressive zone. The three principal stresses were then calculated and transformed to the octahedral stress space. The ultimate octahedral shear stress was calculated using a failure criterion (Kotsovos, 1980). The applied octahedral shear stress was always greater than the ultimate. A proposed failure mechanism for walls with aspect ratio 1 is shown in figure 2.14.

In all tests failure started with nearly vertical splitting of the compressive zone in the region of the tip of the inclined crack (aspect ratio 1) or the deepest flexural crack (aspect ratio 2). The ultimate load was higher than the contribution of the horizontal web reinforcement to the shear strength. It was therefore concluded that shear resistance of the walls was associated with triaxial stress conditions that developed in the compressive zone of the section at the base of the wall rather than the strength of the tensile zone of this section. Hence it was considered that the "Compressive Force Path" concept described in section 2.2.2.2 could suitably explain the behaviour of the walls.

From the comparison of the results of the monotonic and cyclic tests it was concluded that the response of the walls was not strongly influenced by the loading regime and the concrete strength. The load-carrying capacity of the

walls tested under cyclic loading was similar to that of walls subjected to monotonic loading. Modes of failure and failure mechanisms were also the same for both loading conditions. However slightly higher ductility ratios were registered for the cyclically loaded walls, which were partially attributed to differences in the amount of reinforcement. This point is further discussed in sections 4.3.3.2 and 6.6.1.

The data and conclusions given by Lefas are examined in section 2.3.1.1. The main conclusion of the work, that the concrete below the neutral axis gives an insignificant contribution to the shear strength, is appraised by testing wall SW15 as described in chapter 4 and discussed in section 6.2.1.

A total of nine (SW1-SW9) isolated R/C walls were tested at scales 1:5 and 1:2.5 by Pilakoutas (1990). One of the smaller models was tested on the Imperial College shaking table, whilst all the others were subjected to a severe cyclic loading regime under displacement control. Modelling was performed successfully with one significant difference; a larger deviation from the elastic stiffness was shown by the smaller scale models. This was attributed to higher shrinkage effects. The aspect ratio of the larger models was 2 and the horizontal load was transferred to the wall through a top beam. The test rig arrangement of the larger scale walls is shown in figure 2.15.

Most of the walls failed due to crushing of the compressive concrete or steel fracture, i.e., in a flexural mode. Wall SW5 failed in a diagonal tension mode and SW6 in a mixed mode influenced by shear. Despite having different amounts of horizontal web reinforcement and the same vertical reinforcement, walls SW8 and SW9 exhibited similar behaviour. Both failed in a flexural mode and exhibited similar strength and deformational characteristics. This shows that the provision of shear reinforcement beyond the level necessary to allow the

development of the flexural capacity had little effect on the behaviour. The reinforcement details of both walls are shown in figure 2.16.

Wall SW8 contained no horizontal web reinforcement on the top third of the wall. This did not affect the behaviour.

The contribution of pre-yield cycling and shear deformations to the overall energy dissipation capacity appeared to be rather low. Most of the energy dissipated was due to flexural deformations at high displacement ductilities even though the relative participation of shear tended to increase with ductility.

A method for the design against shear failure was proposed based on the evaluation of the minimum shear resistance surface (SRS). According to this method the resistance of the concrete in the compressive zone is proportional to the depth of the neutral axis and the concrete strength. With regard to the contribution of the part of the wall under tensile axial strain the method leads to results similar to the truss analogy. Comments on the validity of this method and on the evidence provided are offered in section 2.3.1.1. Further discussion is presented in chapter 6 considering the evidence of the experimental programme described in chapter 4.

2.1.2 Analytical Models for R/C Walls

The models which simulate the overall force-deformation relationship of R/C walls can be subdivided in two broad sub-groups. The first sub-group consists of detailed models, which in general make use of the finite element method, whilst the second sub-group consists of macroscopic models. The detailed models are based on the interpretation of material behaviour at stress-strain level. Their major drawbacks are:

- The lack of completely reliable constitutive relationships for the materials and the interaction between them for any load history.

- The large computational effort required. Hence this technique is mainly used for the study of individual elements and would not be realistic for entire structures.

The macroscopic model's purpose is to represent the overall behaviour by means of a simplified idealization. The main disadvantage of these models is their reduced versatility, as they are usually valid only for conditions similar to those used in their derivation. Their main advantage over the detailed models is that the former need much less computational effort. Therefore macroscopic models can be used to model the behaviour of elements of models which represent an entire structure. The present work is concerned only with macroscopic models.

The equivalent beam model represents the wall as a vertical line element at the centre of mass of the wall cross-section. The dimensions of the wall cross-section are considered by means of rigid links which connect the vertical element to the beams. In most programs, such as DRAIN-2D (Kanaan and Powell, 1973) and SAKE (Otani, 1974), the nonlinear behaviour is accounted for by means of nonlinear rotational springs. The latter elements are concentrated at the ends of the vertical member while the rest of the member remains linear elastic. The inelastic rotations at each end depend only on the moment at that end and any hysteretic model can be adopted for the springs. A new distributed model proposed by Park, Reinhorn and Kunnath (1987) simulates the nonlinear behaviour in a different way. The flexibility factor, 1/EI, is assumed to be linearly distributed along the member between the two critical sections and the point of contraflexure, if present, as shown in figures 2.17 and 2.18. The inelastic shear spring, which is connected to the flexural spring in

series, is modelled using the Origin Orientated Hysteresis Model (OOHM) which is described later in this section.

Smith and Girgis (1984) proposed two models to simulate the walls as equivalent frames. The first model is equivalent to the above-described beam model with two diagonal braces between each level, as shown in figure 2.19.a. It was considered that the diagonal braces prevent the interaction between bending and shear stiffness allowing the more accurate representation of shear walls with a high shear to moment ratio. The second analogous frame also includes horizontally rigid beams and braces, but the central column used in the previous frame is omitted. This is replaced by a column on one vertical edge and a hinged link on the other, as indicated in figure 2.19.b.

Another technique to analyse R/C walls is to utilize truss representation. Figure 2.20 shows a truss model of a wall as proposed by Hirashi (1984). The area of the non-prismatic member is evaluated considering the stresses along the height of the edge member of the wall under tension. The main object of the analysis is the assessment of deformations at the first storey, hence truss members above that level are assumed to be rigid.

Vecchio and Collins (1986, 1988) presented the Modified Compression Field Theory in order to predict the response of reinforced concrete elements to in-plane shear and axial stresses. The model relates average stresses to average strains in a cracked reinforced concrete element, satisfying conditions of compatibility and equilibrium. While the original Compression Field Theory ignored tension in the cracked concrete (Collins and Mitchel, 1980), this model takes into account tensile stresses in the uncracked concrete. The stress-strain relationship for the cracked concrete was determined by testing reinforced concrete panels under a variety of uniform biaxial stresses.

A new truss model was presented and applied to low-rise R/C walls by Hsu and Mo (1985) and Hsu, Mau and Chen (1987). The model is based on the assumption that the deformation is essentially due to shear deformations of the web. Axial stresses due to bending are assumed to be taken by flanges or boundary elements. Hence, it only applies to walls with low aspect ratios and boundary elements. It is also based on the assumption that the strength of the walls is conditioned by the strength of the concrete struts, which were modelled using a new stress-strain curve for softened concrete.

It was concluded that if the concrete had been modelled using stress-strain relationships for nonsoftened concrete the strength of the walls would have been overestimated. However results from tests of 24 low-rise walls compared well with analytical predictions when a softened concrete relationship was used. Nevertheless, the model could not be applied to dynamic analysis as it only predicts the force deformation relationship under monotonic loading. It was subsequently generalized for any variable amplitude cyclic loading by Mo (1988). However, due to the complexity of the problem it was necessary to rely on experimental observations to establish the rules that define the unloading and reloading branches.

Huang and Sheu (1988) analysed the cyclic behaviour of low-rise R/C walls without boundary elements, subjected to both lateral and axial loads. The model applies constitutive laws of concrete and reinforcing bars. An inclined crack model, shown in figure 2.21, and softening curvature approach were proposed to solve for bending, shear, total deflections and forces of steel bars across the inclined crack. The comparison with experimental results of low-rise walls showed good agreement.

Several models based on a prescribed envelope were proposed. Most of these were suitable or aimed at representing the hysteretic behaviour of R/C members whose

behaviour was mainly dominated by flexure; notably Ramberg-Osgood (Ramberg and Osgood, 1943), Clough (Degrading Stiffness) (Clough and Johnston, 1966), Degrading Trilinear (Fukada, 1969), Takeda (Takeda, Sozen and Nielsen, 1970), (Degrading) Bilinear (Nielsen and Imbeault, 1971) and others. The models comprise of a set of rules that define the unloading and reloading branches usually following experimental observations. The envelope, considered to represent the behaviour under monotonic load, may be given by a curve (Ramberg-Osgood model), a bilinear line (Clough and Bilinear models) or a trilinear line (Degrading Trilinear and Takeda models) with stiffness changes at cracking and yield points.

Figure 2.22 (Otani, 1984) shows hysteresis loops for the above mentioned models. The Clough model was modified to include the degradation in unloading stiffness kr from the initial yield stiffness ky with maximum displacement amplitude MD beyond the yield displacement Dy:

$$kr = ky \cdot ABS(Dy/MD)^{\alpha}$$

where α is the unloading stiffness degradation index (USD index). Its value may vary from 0 to 0.5 for reinforced concrete.

Comparatively few models have been proposed to simulate the behaviour of R/C members which are strongly influenced by shear. One of these models was drawn from a set of experiments (Vecchio, 1981). The latter reference showed that the unloading paths of a R/C specimen loaded in cyclic "pure shear" were straight lines merging at the vicinity of the origin. The reloading branches were aimed at the point of maximum previous displacement. This gave rise to the Origin Orientated Hysteresis Model (OOHM) already referred to and shown in figure 2.23 . Recently Ozcebe and Saatcioglu (1989) proposed a model to represent the shear component of the deformation of R/C members. This model demonstrated the capability of representing the

pinching effect which is in general associated with the presence of high shear forces. This model is described in detail in section 5.2.3.

Kabeyasawa et al (1982) concluded that the bending deformation of a wall was caused primarily by extension of the tension-side boundary column. The resistance of the wall was due to the resistances of the boundary columns and the central wall section. It was therefore proposed to model the wall as three vertical line elements with infinitely rigid beams at the top and bottom floor levels, as shown in figure 2.24. Two outside elements represented the axial stiffness of the boundary columns. The central vertical element was a one component model in which vertical, horizontal and rotational springs were concentrated at the base. This model was intended for the simulation of the wall deformation under constant curvature.

The shear deformation was expressed by the deformation of the horizontal spring. The OOHM was used to model the hysteretic behaviour of the rotational and horizontal springs. The definition of the yield point for the envelope of the horizontal spring was evaluated using empirically derived equations. The vertical springs were modeled using the Axial-Stiffness Hysteresis Model (ASHM) shown in figure 2.25. The axial rigidity was assumed to remain linear elastic in compression. When the axial load changed from compression to tension, the stiffness was reduced to 90% of the initial elastic stiffness. Tensile yielding was considered to occur when all the longitudinal reinforcement yielded under the tensile load. After this the stiffness was reduced to 0.1% of the initial stiffness. Two parameters α=0.9 and β=0.2, were introduced to describe the unloading stiffness degradation and the stiffness hardening point P, shown in figure 2.25.

Several improvements and studies using the model have been performed by Vulcano, Bertero and Colotti (1986, 1987,

1988). It was proposed to replace the existing ASHM by a new system shown in figure 2.26. Each axial element is divided into two elements in series, which represent the zones where the bond is still effective and where it is not. The length of each zone is defined by the parameter λ as shown. In the zone where the bond is ineffective the behaviour of steel (component 2) and concrete (component 3) are simulated by different springs which account for the different constitutive relationships of the two materials.

The model was considered able to simulate the main features of observed phenomena; degradation of bond between concrete and steel, opening and closure of cracks and the hysteretic behaviour of concrete and steel. The first studies using the new ASHM (Vulcano and Bertero, 1986, 1987) were performed using the following constitutive relationships:

- Component 1; linear elastic.

- Component 2; bilinear with the second slope depending on the value r assumed for the steel hardening ratio.

- Component 3; linear elastic in compression neglecting the tensile strength of concrete.

- The value of λ was considered constant.

Despite these simple assumptions the essential features of the above-mentioned observed phenomena were preserved and a first check of the accuracy of the model was performed. The performance of the model was assessed by comparing results with experimental data from tests by Vallenas et al (1979) as shown in figures 2.27 and 2.28. The results showed the difficulty of the analytical model in evaluating the relative contribution of each of the components of the deformation to the total deformation. This proved to be very sensitive to the choice of several parameters such as the bond degradation parameter λ, steel

hardening ratio r, yield shear value assumed for the horizontal spring. The results also showed the inadequacy of the OOHM to idealize the measured shear behaviour. However, satisfactory results were obtained in the idealization of the measured flexural behaviour using the proposed ASHM.

Further improvements on the flexural component of the model were later proposed (Vulcano et al, 1988) following two approaches:

- Use of more refined laws to describe the behaviour of steel, concrete and the interaction between them.

- Modification of the geometry of the wall model in order to account for the progressive yielding of the flexural reinforcement.

A new wall model, as indicated in figure 2.29, was proposed. The rotational and central vertical springs were replaced by a set of multi-uniaxial elements and a parameter C. This variable defines the ratio between the relative flexural displacement and the relative rotation between the two levels. Figure 2.30 shows the new uniaxial element model, which allows different constitutive relationships for steel and concrete in the zone where the bond is considered to be effective.

The performance of the model as far as the flexural component is concerned was improved by using more refined constitutive relationships for the materials. It was found that the accuracy in predicting the flexural response could be efficiently improved, rather than assuming a greater number of uniaxial elements, by calibrating adequately the parameter C. The shear component continued to be simulated by the OOHM, with poor results.

2.2 Design Philosophies

2.2.1 Overall Structure

2.2.1.1 Preamble

It is not practical to design structures to resist strong earthquakes with the materials behaving within their elastic limits. Hence, the idea that it is necessary to take advantage of the nonlinear behaviour of the materials to dissipate the energy the earthquakes impart to the structures (with the exception of special structures, such as nuclear power plants) is widely accepted. Hence, it is possible to design the structures to levels of forces below the elastically calculated actions.

In normal circumstances, undertaking nonlinear dynamic analysis of structures is not feasible. Therefore, the codes allow the evaluation of the forces induced in the structures by earthquakes, "correcting" the results obtained using models based on elastic properties of the materials. In the case of the draft EC8 (1988) the "correction" is performed by dividing the results of the elastic model by a behaviour coefficient "q". According to the New Zealand Standard 4203 (1984) the results of the elastic analysis must be multiplied by a structural type factor S to obtain the earthquake induced forces. These coefficients depend upon the ability of the structure to dissipate energy and also on the degree of redundancy of the structure. The more redundant a structure, the better its capacity as a whole to redistribute actions and to dissipate energy.

Owing to the significance of EC8 as a European standard, an in-depth discussion of some salient aspects of the code is given herein. The provisions dealing with the influence of wall behaviour on the "q" factors are one

of the most advanced features of this code. The basic behaviour factors q for structures with period $T \geq T_1$ are shown in table 2.2. These values should be modified to take into account the likely mode of failure of R/C walls. The prediction of the likely mode of failure (flexure or shear) is to be performed in terms of the ratio ν defined as follows:

$$\nu = V_{Rd} \; / \; (V_{MRd)} \cdot \gamma_{Rd}) \qquad (2.3)$$

V_{Rd} - design shear strength

$V_{(MRd)}$ - the shear force value at the state of the design flexural failure of the critical region under consideration, i.e. when the applied moment equals the design flexural strength M_{Rd}: this force depends on M_{Rd} and on the structural system (e.g. for a free cantilever wall with only one horizontal force acting on top, $V_{(MRd)}=M_{Rd}/H$). More generally, $V_{(MRd)}=M_{Rd}/\lambda_o L$, where the shear ratio λ_o ($\lambda_o=M/VL$) is calculated at the state of failure

γ_{Rd} - global factor expressing the uncertainties:

- Of the models predicting the shear and flexural strengths.

- Of the shear ratio value needed in order to translate M_{Rd} into $V_{(MRd)}$ values.

When more precise data is not available, γ_{Rd} may be taken equal to 1.4 for Ductility Class (DC) "H" and to 1.3 for DC "M" structures. The definition of Ductility Classes is given in section 3.4.

If $\nu > 1$,

then the q factors for wall systems may be taken equal to those for frame systems.

If $0.75 < \nu < 1$,

then the q values for wall systems apply.

If $0.50 < \nu < 0.75$,

then half the q values for wall systems should be taken but not less than unity.

If $\nu < 0.50$

then q-values for uncoupled walls should be taken equal to unity.

2.2.1.2 Direct Design

The Direct Design approach embodied in many codes such as ACI (1983), UBC (1988), etc., consists of the following:

- First the elastic analysis of the structure is performed.

- Then the nonlinear behaviour of the structure is taken into account by means of a factor by which the internal forces obtained from the elastic analysis are divided.

- The structure is then designed to withstand those forces.

2.2.1.3 Capacity Design

2.2.1.3.1 General

The a-priori definition of the ground motion characteristics to which a structure will be subjected is not possible. Consequently, the structural behaviour cannot be controlled using direct design methods. However, it is possible to "force" a structure to behave in the most desirable way by pre-defining the zones where the plastic hinges are to be formed and the sequence of their formation. In this way it is possible to achieve:

- Better damage control.
- Knowledge of the zones where damage will occur.
- Realistic evaluation of the ductility demand.
- The imposition of the most desirable failure mode through the formation of an appropriate mechanism.

In order to "force" a certain sequence on the formation of plastic hinges a deterministic allocation of strength and ductility is necessary. To achieve this it is necessary to know the probable strength of each link on the structure. This must be evaluated considering the real properties of the materials without any safety factors or strength reduction factors. The zones where the plastic hinges are expected to form must be suitably detailed to have the necessary strength and ductility. The rest of the structure must be provided with enough reserve strength in order to ensure that the chosen energy dissipation mechanism is maintained at near full strength throughout the deformations that may occur.

According to this philosophy (Park and Paulay, 1975), termed Capacity Design, within certain limits the

structural behaviour is controlled. Some codes, such as the New Zealand Standard 3101 (1982) and the draft EC8 (1988) already embody this philosophy.

2.2.1.3.2 Application of Capacity Design Principles to Walls

The most likely place for the formation of a plastic hinge in the structure of a building is the wall at the level of the ground floor or short coupling beams of coupled walls. Even if the wall interacts with frames that continues to be the case, due to the large difference of stiffness among the wall and the frames. So the plastification of the base of the wall is difficult to avoid and it is necessary to design for that. However, it is considered advantageous that above the base hinge the wall remains elastic. This helps to control overall displacements and interstorey drift, which must be limited due to considerations of overall stability and damage control. After the plastification at the base hinge, the wall rotates almost as a rigid body enabling the plastification of the frames. As above the plastic hinge the wall remains elastic it is likely to absorb most of the higher mode effects (Paulay, 1977). This can be beneficial, as it may lead to a more regular distribution of ductility demand in the beams of interacting frames.

The distribution of bending moments and shear forces along the height of a wall obtained for a code-prescribed equivalent lateral static load may lead to an underestimation of the moments and shear forces that develop during the nonlinear dynamic response (Paulay, 1977). Hence, for the wall to remain elastic above the plastic hinge zone, strength in excess of that evaluated by applying equivalent lateral static loads must be provided. For instance, according to the provisions of the draft EC8 (1988) a linear envelope of the calculated bending moment diagram vertically displaced a distance

equal to the length of the wall must be used, as shown in figure 2.31.

The overstrength in shear can be obtained by multiplying the shear forces derived for the specified lateral static loading by dynamic magnification factors and scaling up to correspond with the strain hardened flexural capacity at the wall base. The scaling up is necessary because the shear demand increases at every level with increased flexural capacity at the base (Paulay, 1977). The scaling up factor depends on the design moment and the expected flexural capacity. The latter must be evaluated considering the actual amount of flexural reinforcement used and not that required by the design, the strain hardening of the steel, the confinement of the concrete and no safety coefficients on the materials or the strength.

The dynamic magnification factors prescribed by EC8 (1988) are as follows:

$$\omega = 0.9 + 0.1\, n \qquad n \leq 5$$

$$\omega = 1.2 + 0.04\, n \qquad 5 \leq n \leq 15$$

$$\omega = 1.8 \qquad n \geq 15$$

where n is the number of storeys.

2.2.2 Shear Design

2.2.2.1 Truss Model

Despite the fact that there is still considerable debate and research concerning the design for shear, the truss model is widely used and forms the background for the shear design in most codes.

According to this model, after diagonal cracking due to shear occurs, R/C linear members behave as a truss as shown in figure 2.32. The compressive edge member of the wall on one side and the tensile flexural reinforcement on the other act as longitudinal cords. The concrete between the inclined cracks forms the compressive inclined struts and the horizontal web reinforcement forms the horizontal ties. The shear capacity of the member may be limited by the compressive strength of the concrete struts which is termed web crushing failure, or by the tensile strength of the horizontal web reinforcement which gives rise to diagonal tension failure.

However, numerous tests on walls and particularly on beams have shown that the truss analogy underestimates the shear strength of these members. The difference between the tests results and the theory is the so called "contribution of concrete". In most codes, this is empirically accounted for by assuming a nominal shear strength.

2.2.2.2 Compressive Force Path Concept

According to the Compressive Force Path concept proposed by Kotsovos (1983, 1987, 1988) and applied to R/C walls by Lefas (1988) and Lefas et al (1990), the strength of a R/C member is associated with the strength of concrete in the region of the path along which the compressive force is transferred to the support. Shear failure is considered to occur when tensile stresses develop within the path of the compressive force (Kotsovos, 1983). Such stresses may develop due to the following reasons (Kotsovos, 1988):

a) Changes in the path direction: a tensile force resultant develops for equilibrium purposes at the zones where the path changes direction. The location of such zones depend on the shear ratio and how the horizontal load is transferred to the wall.

b) Varying intensity of the compressive stress field along the path: the compressive stresses will reach a critical level in the sections where the compressive area is minimum. This will induce tensile stresses in the surrounding concrete. This type of failure is usually termed compressive failure.

c) Tip of inclined cracks: it is known from fracture mechanics that large tensile stresses develop perpendicular to the direction of the maximum principal compressive stress in the region of the crack tip.

d) Bond failure: after bond failure the stresses in the tension reinforcement will be the same along a certain length. The variation of the bending moment along this length causes a variation of the internal lever arm which means a reduction of the neutral axis depth for the sections where the moment is higher. This will increase the compressive stresses and will lead to failure in a manner similar to that described in b) above.

The analysis of the modes of failure (Kotsovos, 1983) by testing two point load beams without shear reinforcement is shown in figure 2.33. This indicates that the mode of failure depends on the ratio a_v/d as shown in figure 2.34. On the basis of this dependence, the beam behaviour may be divided into four types as follows:

Type I - Characterized by flexural failure with the beam developing its full flexural capacity.

Type II - Characterized by a mode of failure caused by a diagonal crack which initiates near the tip of the flexural crack closest to the support and propagates towards the load point. The flexural capacity reduces with a_v/d , decreasing to a

value dependent on the amount of longitudinal tension reinforcement.

Type III- Characterized by a mode of failure caused by a diagonal crack which forms independently from the flexural cracks. With increasing values of a_v/d the flexural capacity increases from the critical value in Type II to another value which is also dependent upon the amount of longitudinal reinforcement, at which it becomes equal to the full flexural capacity.

Type IV - Characterized by failure caused by a diagonal crack joining the support to the load point and allowing the beam to develop its full flexural capacity.

Types III and IV behaviour are only affected quantitatively by the presence of shear reinforcement, i.e. the load levels causing diagonal cracking and failure may be affected rather than the mode of diagonal cracking and failure.

In order to allow the development of the flexural capacity, transverse reinforcement must be provided for the cases of behaviour type II and type III. It is only necessary within the path of the compressive force to counteract tensile stresses (Kotsovos, 1988). It must be provided in the zones where the path changes direction and where the path is parallel to the axis of the member. Where the path changes direction, the required area of reinforcement may be calculated from the difference between the applied shear force and the shear force resisted by concrete alone.

An empirical formula for the calculation of the contribution of concrete in terms of bending was derived by Bobrowski for beams and applied by Lefas (1988) to walls. It is recommended to distribute the reinforcement

along a length equal to the width of the wall. Where the path of the compressive force is parallel to the longitudinal axis of the member confinement reinforcement should be provided to sustain the tensile stresses that may develop in the compressive zone.

2.3 Discussion

2.3.1 Reinforced Concrete Walls Testing

A degree of agreements exists on how to estimate the flexural capacity of R/C walls. This is reflected in the fact that flexural design is based on similar hypothesis for most codes. This is clearly shown in chapter 3 of this thesis. The standard approach is based on the plane sections hypothesis. Whereas this hypothesis is not strictly applicable to low-rise walls, the error margins resulting from the plane sections assumption are small. At flexural capacity most of the reinforcement has yielded, thus the stresses are independent of the strain if hardening is not considered.

2.3.1.1 Shear Transfer Mechanisms

The calculation of the shear resistance of R/C members has and continues to be a subject of research. The validity of the truss analogy has been questioned. One of the reasons for this is the fact that there is no coherent and accepted theory for the calculation of the "contribution of concrete". The nominal shear stress usually used to quantify it does not represent a real shear stress on the cross-section of the member. In general, it is only a value calibrated from data obtained from monotonic tests in beams and walls.

In the case of ACI (1983) the concrete contribution is considered to be equal to the shear causing significant inclined cracking. Hence, it is a function of the mechanism of resistance before cracking, i.e., of an elastic distribution of stresses. The writer considers that the interpretation of the behaviour (concerning shear resisting mechanisms) after the process of yielding and redistribution of stresses based on an elastic concept is highly questionable. These inconsistencies and the scatter of the experimental results are reflected by the large differences in the evaluation of the "contribution of concrete" by the different codes. The comparative code study presented in chapter 3 of this thesis highlights such problems.

The "contribution of concrete" is usually attributed to the fact that concrete struts are less inclined to the longitudinal axis of the member than the diagonal cracks (Schlaich, Schafer and Jennewein, 1987). This means that the shear force is transferred across diagonal cracks not only by the transverse reinforcement but also by aggregate interlock. The development of this mechanism relies on the concrete tensile strength, as shown in figure 2.35.

However, under earthquake loading, due to the yielding of the main flexural reinforcement and accumulation of plastic tensile strains, flexural cracks open much more than in the case of pre-yield monotonic loading. As diagonal cracks are usually extension of flexural cracks their opening will also be affected by the yielding of the main flexural reinforcement. Also, it has been shown that the effect of aggregate interlock decreases with increasing crack width (Fenwick and Paulay, 1968). This will diminish the aggregate interlock effect. Most researchers therefore advise that along the length of the potential plastic hinge the contribution of all mechanisms to the shear strength, except that of web reinforcement, are neglected in the absence of axial compression (Paulay, 1977). This view has received wide acceptance and is embodied in some of the

most advanced codes, such as the NZS 3101 (1982) and the draft EC8 (1988).

Nevertheless, it was observed that due to yielding of the main flexural reinforcement large horizontal flexural cracks open at the built-in section. In these situations the shear force is transferred across the compressive zone at this level (Park and Paulay, 1975, Paulay et al, 1982 and Oesterle et al, 1984). This seems to contradict the view expressed above that shear transfer mechanisms other than web reinforcement should be neglected in the plastic hinge zone. In fact, this type of reinforcement cannot contribute to the shear transfer across horizontal cracks because it is parallel to them. The truss analogy cannot explain shear transfer in these conditions because it is based on the assumption that in the presence of shear forces the cracks are inclined. Horizontal web reinforcement on its own only transfers shear from the compressive side of a section to the tension side. It does not provide shear strength if the concrete on the tension side of the wall cannot transfer the shear force to the foundations.

The above discussion would point to the possibility that the Compressive Force Path concept may provide the explanation. Nevertheless, careful analysis of the data given by Lefas (1988) raises serious doubts about the ability of the CFP concept, as applied by Lefas, to explain the observed behaviour. According to this concept failure occurs due to the development of tensile stresses within the compressive zone. Lefas attempted to show that the compressive zone was capable of resisting the shear force without developing any tensile stresses.

However, his calculations were based on a maximum compressive stress in the concrete evaluated considering that the ratio between maximum and average compressive stresses were 1.4 for walls with aspect ratio 1 (as depicted in table 2.1) and 2 for walls with aspect ratio

2. These values seem excessive. Some codes such as EC2 (1984), allow the use of a rectangular stress block which would lead to a ratio of 1.25. For confined concrete this ratio may be even less as the distribution of stresses may be more uniform due to the descendent branch of the stress strain-curve. Table 2.1 also shows in brackets the values of the maximum compressive stresses, confining stresses and principal stresses that would be obtained if the ratio between the maximum and average compressive stresses was 1.25. It is observed that tensile stresses develop showing that the compressive zone could only sustain part of the total shear.

Also the development of the confining stresses calculated by Lefas, and shown in table 2.1, would only be possible if the confinement reinforcement could sustain stresses higher than 3000MPa. The yield stress of the reinforcement used was reported to be 420MPa. The likely reason for the unrealistic overstrengths reported has already been pointed out by Pilakoutas (1990) and Pilakoutas and Elnashai (1991). The horizontal load was applied to the top beam of the specimens by means of a steel plate. Friction between the steel plate and the concrete beam generated a vertical force at the point of load application due to vertical movement of that point, as shown in figure 2.36. A friction coefficient of 0.1 would introduce an error of 7% in the evaluation of the moment at the base of a wall of aspect ratio 1. It has been shown (Pilakoutas, 1990) that back-calculations of concrete axial stresses from section strength are prone to very large errors. A 5% error in the evaluation of the bending moment may give raise to an error of more than 100% in the evaluation of concrete compressive axial stresses. Therefore, the extremely high values of the concrete axial stresses calculated by Lefas are probably a consequence of his boundary conditions error.

It should also be noted that no experimental evidence of the main conclusion of Lefas work, i.e., that no shear

was transferred by the part of the section of the walls below the neutral axis, was provided. All the walls were designed with a certain amount of horizontal web reinforcement which enabled them to transfer to the zone below the neutral axis a part of the total applied shear force. It was shown that the proposed wall resistance and failure mechanism would lead to the development of shear stresses in the octahedral stress space above the corresponding ultimate value. This also indicates that the failure mechanism proposed by Lefas could not have developed.

The literature survey showed that several researchers concluded that confined edge members of R/C walls acting as large dowels offered effective resistance to shear. Wagner and Bertero (1982) suggested that the shear resistance of the edge member was proportional to the axial compressive force on the same edge member. This can be expressed as follows:

$$V_{cc} = C_{cc} \tan\theta \qquad (2.4)$$

The above equation is equivalent to (2.2) but expressed in terms of forces in the compressive zone. In the absence of axial force, the compressive force in the edge member of a wall may be calculated as follows:

$$C_{cc} = M / d \qquad (2.5)$$

where d is the internal lever arm.

If the bending moment is expressed as a function of the shear force and the shear ratio, then replaced in (2.5) and (2.4), the following expression for V_{cc} is obtained:

$$M = \lambda_o V L$$

$$C_{cc} = \lambda_o V L / d$$

$$V_{cc} = \lambda_o V \tan\theta L / d \qquad (2.6)$$

Equation 2.6 shows that in this case the shear strength of the compressive zone would be a fraction of the total shear force which would depend essentially on the shear ratio.

The SRS method proposed by Pilakoutas (1990) established that the contribution of the compressive zone to the shear strength is dependent essentially on the depth of the neutral axis and the concrete strength. Although one of the walls was designed according to the SRS method, yielding good results, the experimental evidence was not conclusive. It is not shown that the neutral axis is the key parameter controlling the strength of the compressive zone and the test conditions are not the most severe as far as shear failure is concerned (since the shear ratio was 2 or more for all walls). Thus, no experimental evidence is given to support the validity of the method in more severe conditions, i.e. lower shear ratios.

As previously referred to, large differences exist between different codes for the evaluation of the shear strength. These differences are larger for walls with low shear ratios. This is due to the fact that the tests on low rise walls have apparently shown that the "contribution of concrete" is higher for such walls. The tests have also shown that vertical web reinforcement is effective in providing shear resistance for these walls while the effectiveness of horizontal web reinforcement decreases. This is reflected in the codes by empirically-based

provisions for the design of vertical web reinforcement if the shear ratio is low.

It is apparent from the above that there are still very important conceptual and practical disagreements about the shear transfer mechanisms and their evaluation. The quantitative comparison of code provisions presented in chapter 3 also leads to the same conclusion. These disagreements are stronger for the cases of plastic hinges and low shear ratios. As referred to in chapter 1, the main purpose of the current project was to understand and quantify the shear transfer mechanisms across plastic hinges of R/C walls of multistorey buildings under conditions favouring shear failure. These conditions are essentially (i) a low shear ratio and (ii) no axial compression, since the latter would enhance the shear strength. In order to induce a low shear ratio, of say 1, it is necessary that at a height similar to the length of the cross section the wall is acted upon by a transverse shear force and no bending moment.

In R/C walls testing, this is usually performed by building the specimens with an aspect ratio equal to the imposed shear ratio, i.e. the height of the wall is similar to the length of the cross section. The horizontal load is applied through a top loading beam, which is supposed to transfer the shear force uniformly along the section. However, Paulay, Priestley and Synge (1982) considered that the mode of load application at the top of the specimen affects the diagonal tension strength. They tested walls with aspect ratio 1/2 and found that part of the horizontal load was transferred directly to the foundation by means of diagonal concrete compressive struts. In fact, the wall can behave as a short cantilever in which the horizontal load applied on top is equilibrated by a compressive inclined force in the concrete and a vertical tension force in the reinforcement, as shown in figure 2.37. Such load transfer mechanism enhances the effectiveness of vertical

reinforcement in transferring shear and reduces the effectiveness of the horizontal reinforcement.

Barda, Hanson and Corley (1977) came to similar conclusions which were referred to in the literature review. Results from tests of walls of aspect ratio 1 by Cardenas, Russel and Corley (1980) indicated that in the walls whose horizontal web reinforcement did not yield, the force in the reinforcement located near the edge became constant along the wall height. This also points to the formation of an arch mechanism that transfers the load directly to the foundation. The design of walls SW8 and SW9 tested by Pilakoutas and shown in figure 2.16 also shows the influence of the top beam on the behaviour.

In multistorey buildings the horizontal forces are transferred to the wall by the floor slabs and beams along the entire height of the building. Hence, the shear force is transferred to the bottom region of a wall from its upper parts. It is questionable if the boundary conditions used in the tests can reproduce the ones existing in the bottom part of multistorey buildings if the shear ratio is close to 1 or less. The arch mechanism and the direct transfer of load to the foundation may not develop in the case of the bottom part of a wall in a multistorey building, since the whole member is more prone to beam behaviour.

It is concluded from the above that the boundary conditions usually used in tests of walls with low shear ratios are inadequate if the results are to be considered representative of the behaviour of the bottom part of walls in multistorey building. It was shown in the literature review that other researchers had already pointed out the importance of adequate boundary conditions. A solution for this problem is presented in chapter 4.

2.3.1.2 Reasons for the Development of Low Shear Ratios

Apparently in multistorey buildings the shear ratios should not be low because the total height of the walls will, in general, be much larger than the length of the cross-section. If the contribution of the frames is not considered, a triangular inverted distribution as usually prescribed by the codes for static analysis of earthquake effects will yield a resultant of the inertia forces in the walls at two thirds of their height. However, this resultant may be applied at a much lower level due to a number of reasons such as:

- Interaction with the frames. Due to their different deformed shapes along the height, a redistribution of forces occurs between frames and walls as shown in fig 2.39. The wall tends to deform as a flexural cantilever. If the axial deformation of the columns is disregarded, the deformation of the frame is due essentially to flexural deformations of the beams and columns. At each level their bending moments are proportional to the total shear force at that level. The interstory drift is therefore proportional to the shear force, and the frame behaves as a shear beam. Hence, similar distributions of load along the height induce different deformed shapes in the walls and the frames as shown in figure 2.39. As the floor slabs impose the compatibility of displacements between both systems, interaction forces are generated. The frame-wall compatibility forces tend to decrease the wall and increase the frame deformation at higher floor levels. At lower floor levels the compatibility forces decrease the frames and increase the wall deformations. The resultant of the inertia forces in the wall is likely to be applied lower than the 2/3 height implied by the inverted triangular distribution in codes.

- Influence of the higher modes of vibration. The deformed shape of the higher modes corresponds to a distribution of forces with a much lower level of application of the resultant than the triangular distribution derived from the first mode. Thus, the influence of the higher modes also tends to decrease the shear ratio. This has been verified by other researchers (Wang et al, 1975).

- The overall nonlinear behaviour of the wall tends to shift downwards the resultant of the inertia forces on the whole building. Therefore, the resultant of the inertia forces on the walls also shifts downwards. Nonlinear time-history analyses and experiments by Wang, Bertero and Popov (1975), Aktan and Bertero (1984) and Bertero (1984) have shown that the pattern of inertia forces along the height of mixed frame-wall system at the time of maximum wall shear demand is closer to a uniform pattern than to the triangular inverted distribution.

- The concentration of the nonlinear behaviour of the wall on its bottom region while the rest remains elastic also reduces the shear ratio at the base of the wall (Wang et al, 1975).

- Redistribution of shear from a wall in tension to a wall in compression. This effect may be important especially in coupled walls of high rise buildings due to the large number and stiffness of the coupling beams. It was reported that due to this effect a redistribution of shear may occur such that the wall under compression would take 90% of the shear (Aktan, Bertero and Piazza, 1982).

Wang et al (1975) found that the shear ratio of a wall of a ten storey R/C building may be as low as 1.5.

2.3.2 Behaviour Factors

The dependence of the behaviour factors on the likely mode of failure of the walls is due to the fact that a wall will exhibit different ductility and energy dissipation capacity for different failure modes. According to EC8 "the q factors can be derived as the average ratios between the seismic intensity inducing an ultimate limit state in the structure taking into account its actual nonlinear behaviour, and the design seismic intensity used in conjunction with a conventional linear model." Therefore, the q factors depend on a large number of parameters that influence the nonlinear behaviour of which the two most important are the ductility ratio and the sustainable energy dissipation capacity.

It should be noted that the concepts of ductility and energy dissipation capacity are not equivalent. Two oscillators can have the same ductility and different energy dissipation capabilities. This can be demonstrated considering two nonlinear single degree of freedom oscillators whose constitutive relationships are as shown in figure 2.39. Assume that the mass, the yield force F_y, the yield displacement δ_y, and the stiffness in the pre-yield and post-yield branches are the same for both oscillators. Also, assume that the maximum ductility factor $\mu_{max}=\delta_{max}/\delta_y$ is infinite for both. If both oscillators were subjected to a ground motion which would induce displacements larger than δ_y, in general oscillator 1 would undergo smaller displacements than oscillator 2 due to its larger energy dissipation capacity represented by the area within the loops. Hence, the ductility demand would be lower for the oscillator with the larger energy dissipation capacity. Several authors have recognized the importance of energy dissipation capacity in reducing the response of structures to earthquake ground motion (Popov, 1980, Otani 1984, Moss, Carr and Buchanan, 1986).

Table 2.3 shows qualitatively the influence of the failure modes on the energy dissipation capacity of critical regions (where yielding of the main flexural reinforcement should be expected) of R/C walls according to EC8. The table indicates that if a wall fails in shear or by lateral instability its energy dissipation capacity is less than if it fails in a ductile flexural manner. Its ductility also decreases as flexural failure would occur at a higher displacement. The flexural mode of failure 1a is associated with large ductility and energy dissipation capacity. This is achieved by yielding of the main flexural reinforcement while brittle failure of the compressive concrete is avoided by providing confinement reinforcement. It would appear from the above that shear failure and lateral instability should be avoided, instead of penalizing the whole structure by imposing low behaviour factors. If a wall fails in shear in a brittle manner, the large amount of energy it originally absorbed is suddenly released and acts as an impulse load of very short duration on the remainder of the building (Wang et al, 1975). This may lead to the collapse of the entire structure unless it possesses adequate reserve strength, ductility and energy dissipation. It should also be noted that the designer can act upon the value of V_{Rd} either by providing shear reinforcement or by changing the dimensions of the cross-section, thus controlling the value of ν. This means that even if the wall shear ratio is small the q factor may be increased to that of a frame system. These aspects of EC8 provisions for the calculation of the q factors are discussed in section 6.8 considering the experimental results.

2.3.3 Analytical Models for R/C Walls

The assessment of seismic performance of structures requires models that can predict their nonlinear dynamic response for any load history. In order to choose a model to simulate the overall nonlinear behaviour of R/C walls

it is important to understand and select the characteristics of the model that are relevant and influential. A study was performed by Otani (1984), who compared the performance of the hysteretic models shown in figure 2.22. It was reported that the earthquake response amplitude is strongly influenced by the yield level and the energy dissipation capacity, particularly for short period structures. The post-yield stiffness had some influence and the initial stiffness and cracking force level have little influence on the response amplitude if the ductility demand is high. However Carr et al (1986), pointed out that variations in the exciting accelerograms may be responsible for variations in ductility demand higher than variations caused by different flexural models. However, pinched models in general exhibited higher values of the response.

A shear wall model incorporated in the analysis of a multistorey building should not only be able to simulate the wall behaviour for arbitrary load histories but also for any combination of bending moment, shear and axial forces. The equivalent beam model with rotational springs at the ends has the disadvantage of not accounting for the spread of plasticity along a finite length of the wall. The distributed model overcomes this disadvantage. However, the main disadvantage of the beam model is the assumption that rotations occur around points lying on the mass centre of the wall cross-section. In this manner important features of experimentally observed behaviour, such as the shifting of the neutral axis to the compressive side, extension of the wall, effects due to the outriggering interaction with connecting beams, etc., are disregarded. These features are incorporated in the model proposed by Kabeyasawa et al (1982) and developed by Vulcano, Bertero and Colotti (1986,1987 and 1988).

The truss model accounts for redistribution of stresses due to diagonal cracking which the beam model does not account for. However, difficulties arise in defining the geometry and mechanical properties of the equivalent

truss system. Further problems arise from the changes of the structural topology depending on the crack propagation during the load history. Models such as those proposed by Huang and Sheu (1988) and Hsu et al (1985, 1987) are not suitable as they only apply to specific boundary conditions and types of walls. They do not possess adequate versatility as required for integration in a nonlinear model of a multistorey building.

It appears from the above that Kabeyasawa's model is the more suitable for this purpose as it simulates the most important features of observed behaviour. The progress in the past few years in improving the flexural component has lead to a model with an excellent performance for flexural-dominated wall behaviour. However, in the presence of high shear forces difficulties were reported in obtaining the correct balance between the two components of the deformation. The OOHM used to simulate the shear component was considered inadequate. Hoedejanto (1988) pointed out that the "Origin Orientated Hysteresis" behaviour observed in Vecchio's tests may not necessarily apply directly to conditions in a reinforced concrete element subjected to bending as well as shear.

As referred to in chapter 1, it is one of the purposes of the current work to propose improvements to the shear component, towards assembling a general model suitable for the nonlinear analysis of R/C walls for any level of applied shear.

2.4 Summary

The literature survey undertaken above highlighted the need for a concerted effort in shear design. Different and contradictory opinions are still expressed by different researchers.

Current code provisions for shear design are based on the truss analogy. The so called "contribution of concrete" is considered to vanish in the PHZ if the axial load is below a threshold value. This concept, embodied in the most advanced codes such as EC8 and NZ, was questioned. An alternative concept and design method, the compressive force path concept, was described. According to this concept the shear strength of a R/C member is associated with the strength of the path along which the compressive force is transferred to the supports. The contribution of the zone below the neutral axis is considered insignificant or non-existent. However, serious doubts were raised about the possibility of explaining observed behaviour using the compressive force path concept.

The boundary conditions usually used in tests of walls with low shear ratios were considered inadequate for simulating the behaviour of the bottom region of walls of multistorey buildings. This is due to the fact that these boundary conditions allowed transferring part of the load directly from the top beam to the foundations. This would not be possible if the element being tested obeyed beam behaviour, which is the case in a multistorey building. Thus, some features in the behaviour of walls with low shear ratios, which were observed to be different from walls with higher shear ratios, may be a consequence of these boundary conditions.

One of the most advanced features of EC8, the influence of the mode of failure of walls on the behaviour coefficients, was discussed. It was pointed out that EC8 provisions allow the designer to affect the behaviour coefficients by increasing the shear capacity, even for low shear ratios.

Finally, the literature review showed that macroscopic models were able to simulate satisfactorily the overall behaviour of flexural walls. One of the more advanced of these models, proposed by Kabeyasawa et al, was able to

simulate features of observed wall behaviour that other models did not consider. However, the model showed poor performance in simulating the shear component of the deformation, hence it is not adequately reliable in the presence of high shear forces.

The two most important research objectives identified in this chapter were:

- The understanding of shear transfer mechanisms in PHZ of R/C walls, and the ability of different theories to explain observed behaviour.

- To improve modelling of the shear component of the deformation of R/C walls in order to develop a model valid for any shear ratio and not only for flexural walls.

In conclusion, despite the large research efforts and advances in understanding the seismic behaviour of R/C walls, especially during the last two decades, some important issues are still object of discussion and disagreement. The widespread use of walls in earthquake resistant design of medium and high rise R/C buildings emphasises the need for continuing research efforts in this field.

SPECIMEN	DEPTH OF N.A	STRESSES DUE TO BENDING				STRESSES DUE TO SHEAR	COMBINED PRINCIPAL STRESS CONDITIONS			APPLIED STRESSES IN OCTAHEDRAL FORM		$\tau_{o,ult}$
	c (mm)	$\bar{\sigma}_x$	máx σ_x	máx $\frac{\sigma_x}{f_c'}$	$\sigma_y=\sigma_z$	$\tau_{xy}=\frac{F_H}{cb}$	σ_1	σ_2	σ_3	σ_o	τ_o	
SW 11	90	89.0	124.6 (111.3)	2.8 (2.5)	22.3 (15.1)	41.3	139.2 (126.6)	22.3 (15.1)	7.7 (-0.2)	56.4	58.9	51.3
SW 12	130	76.7	107.4 (95.9)	2.4 (2.1)	16.0 (11.9)	28.6	115.6 (104.7)	16.0 (11.9)	7.8 (3.1)	46.5	49.0	45.2
SW 13	190	56.9	79.7 (71.1)	2.3 (2.1)	12.1 (8.7)	24.8	87.8 (79.8)	12.1 (8.7)	4.0 (0.0)	34.6	37.7	33.8
SW 14	100	72.0	100.8 (90.0)	2.8 (2.5)	18.0 (12.3)	38.0	115.8 (105.5)	18.0 (12.3)	3.2 (-3.2)	46.0	50.0	42.0
SW 15	140	64.8	97.0 (81.0)	2.6 (2.2)	16.0 (10.3)	32.7	108.5 (93.8)	16.0 (10.3)	4.5 (-2.5)	43.0	46.6	40.2
SW 16	180	66.0	92.4 (82.5)	2.1 (1.9)	11.0 (9.5)	28.2	101.2 (92.1)	11.0 (9.5)	2.2 (-0.2)	38.1	44.7	39.0

All Stresses in MPa

Values in brackets were calculated by the author and not by Lefas

Table 2.1 Stress conditions causing failure of type I wall specimens (Lefas, 1988)

Structural System		Ductility Class	Regularity class	
			R_M	R_m
Frame		L	2.0 (1.5)	1.5 (1.0)
		M	3.0	2.5 (2.0)
		H	5.0	4.0
R.C. Walls	(b) Coupled	L	2.0 (1.5)	1.5 (1.0)
		M	3.0	2.5 (2.0)
		H	4.5	4.0
	(b) Uncoupled	L	1.5	1.0
		M	2.5 (c)	2.0 (c)
		H	3.5 (c)	3.0 (c)
Core Structures (d)		L	1.5	1.0
		M	2.0	1.5
		H	2.5	2.0
Dual	H_{frame} 65%	as per frame systems		
	H_{walls} 65%	as per wall systems		
Regular structures behaving essentially like inverted penduli (e)		L	1.0 (f)	
		M	1.3 (f)	
		H	1.7 (f)	

Footnotes (b) through (f) are given overleaf.

Table 2.2 Basic behaviour factors q for $T>T_1$ (EC8)

b - When both coupled and uncoupled walls are included in the structural system, the selection of the q-factor is made on the basis of the more resistant type of walls.

c - Higher values of the q-factors, equal to those valid for coupled wall systems may apply under the condition that:

$$\nu = V_{Rd} \; / \; (V_{MRd)} \; . \; \gamma_{Rd}) \; > \; 1.0$$

d - Core structures are defined as those in which more than 65% of the total seismic force is resisted by R/C core(s).

e - R/C structures are considered as behaving like inverted penduli when
  . 50% of their mass is located in the up 1/3 of the height of the building.
  . the dissipation of energy takes place mainly in one isolated region.

f - These values may be increased provided that the designer proves that a correspondingly higher energy dissipation is ensured in the critical region.

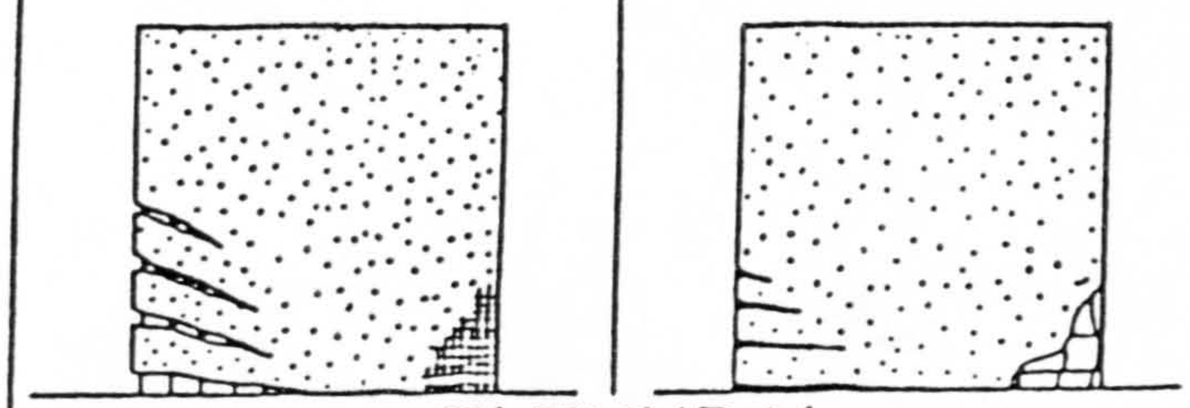
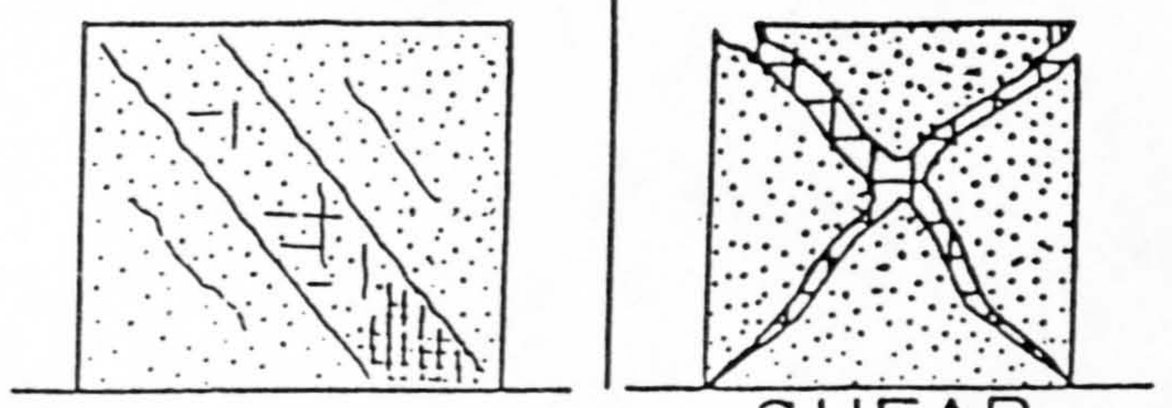
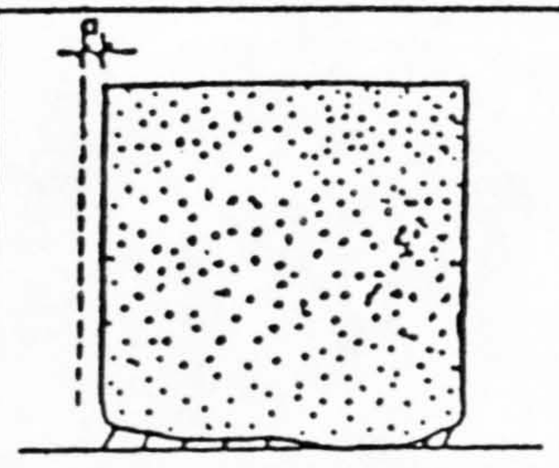
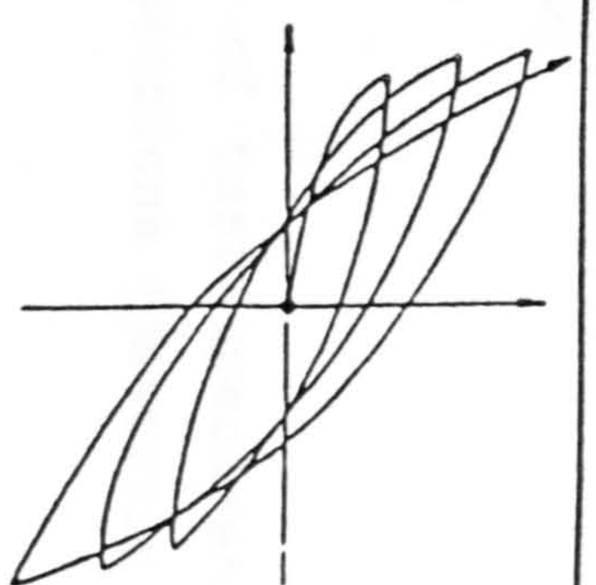
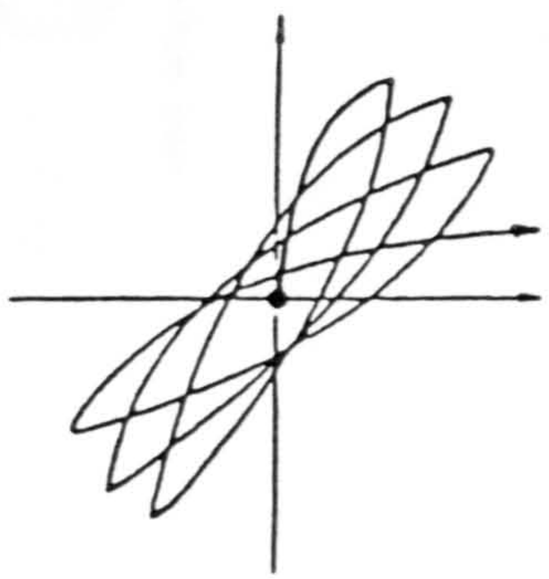
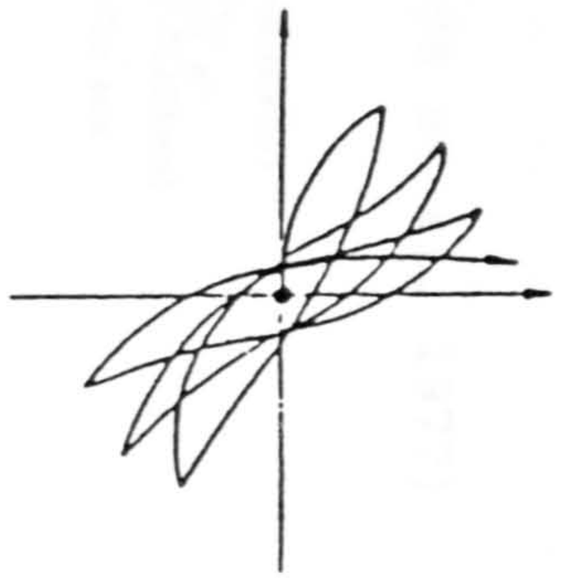
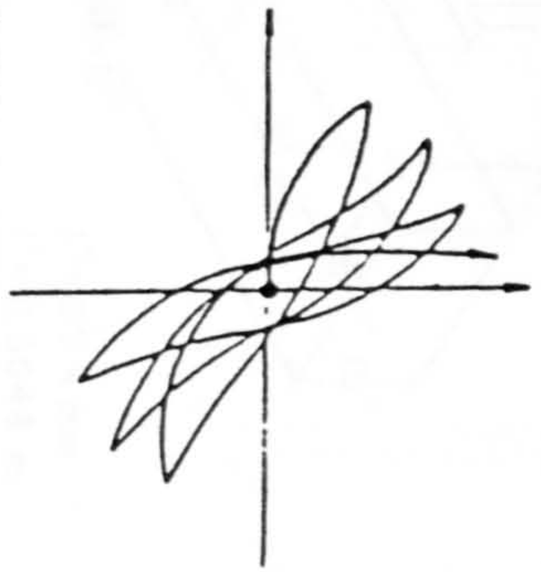
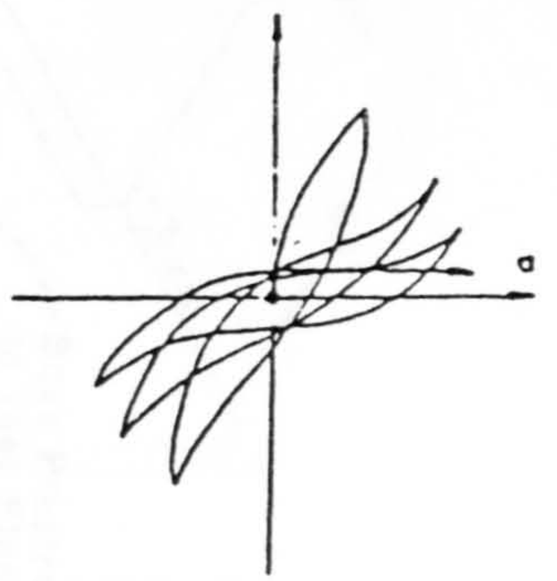
FAILURE MODE	1.a	1.b	2.a	2.b	3
	 FLEXURAL		 SHEAR		
	(ductile)	(brittle)	WEB DIAGONAL FAILURE (compression)	WEB DIAGONAL FAILURE (tension)	HORIZONTAL SLIDING
CAUSE	Almost simultaneous reaching of yield on both edges (mainly when h/l >>2)	• "Defective" boundary elements • Lateral instability of wall's edges	• Insufficient web thickness	• Insufficient web reinforcement • Low Ns-values	• Insufficient wall's base detailing (anchoring, splicing) • Low Ns-values
EXPECTED RESPONSE					

Table 2.3 Failure modes of R/C walls critical regions (EC8)

FIGURES

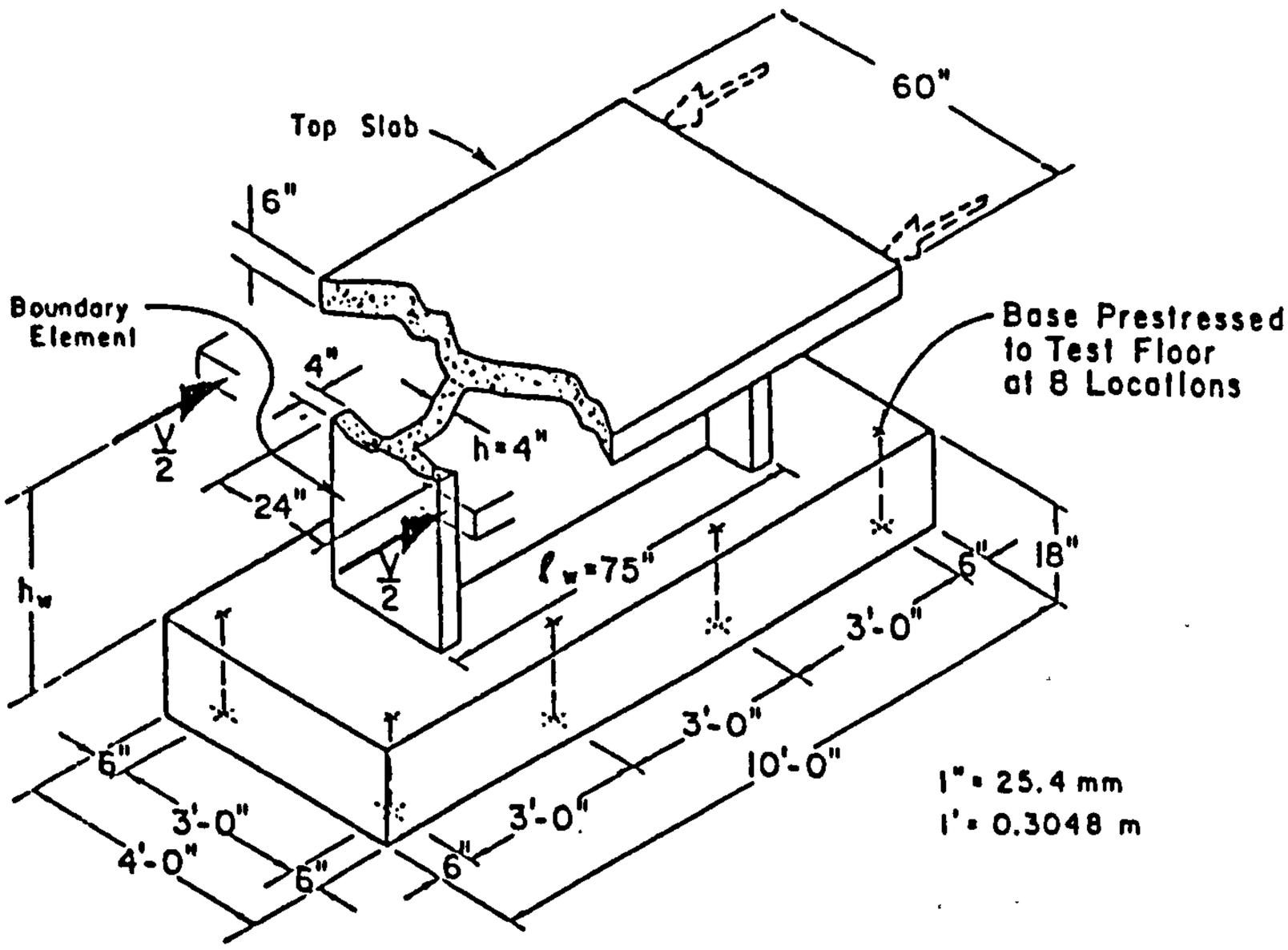


Figure 2.1 Test specimen (Barda et al, 1977)

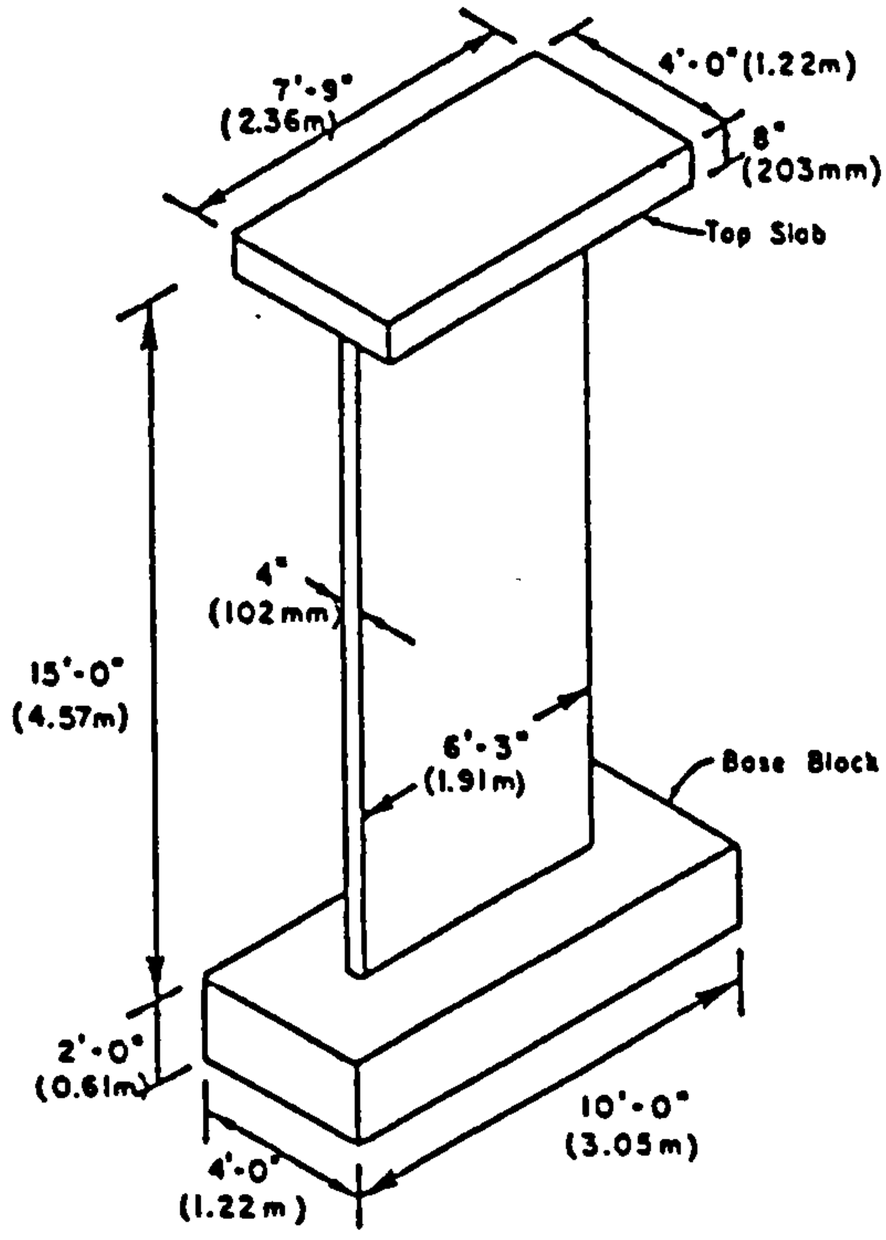


Figure 2.2 Nominal dimensions of test specimens with rectangular cross-sections (Oesterle et al, 1980)

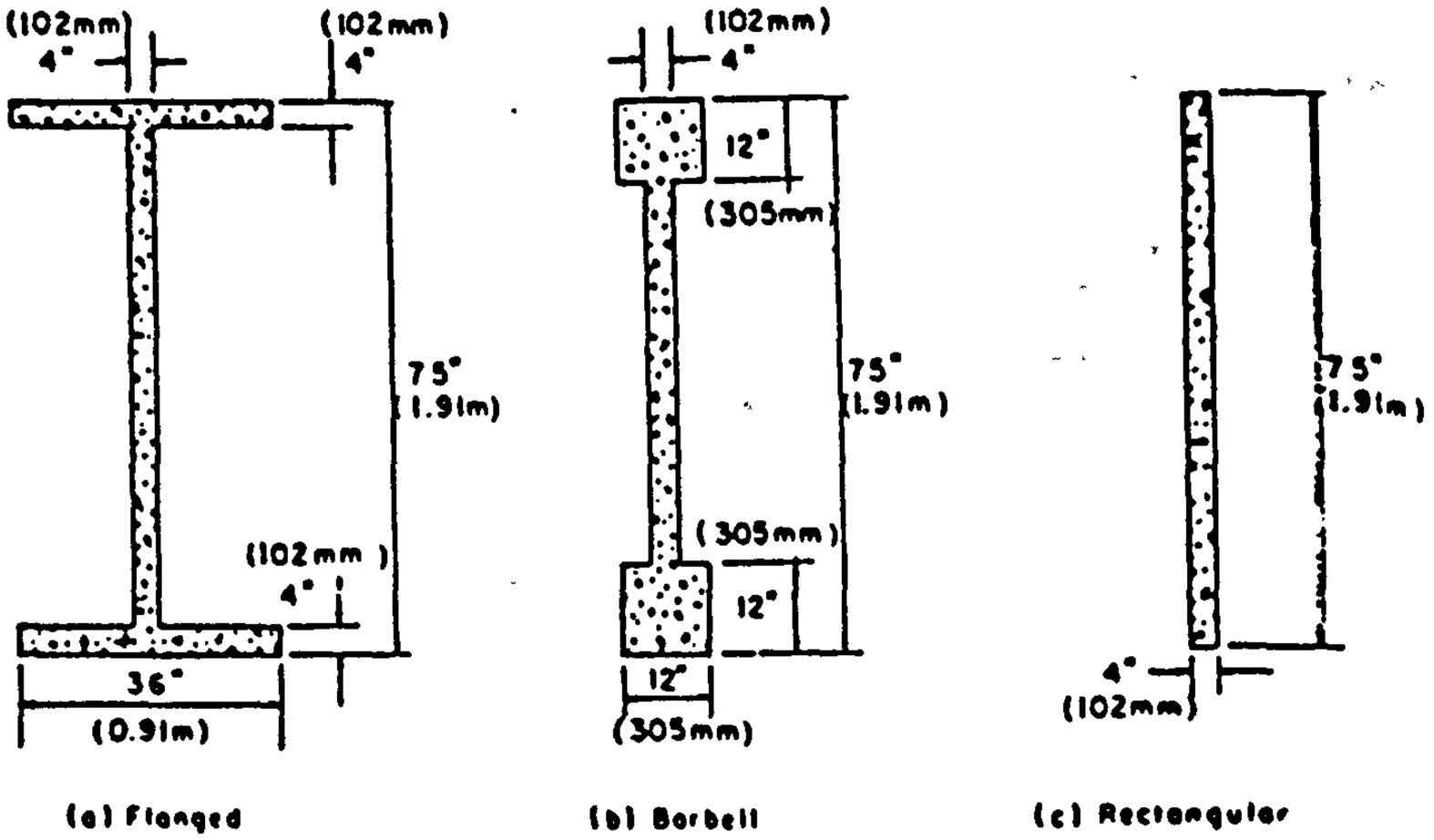


Figure 2.3 Nominal cross-section dimensions (Oesterle et al, 1980)

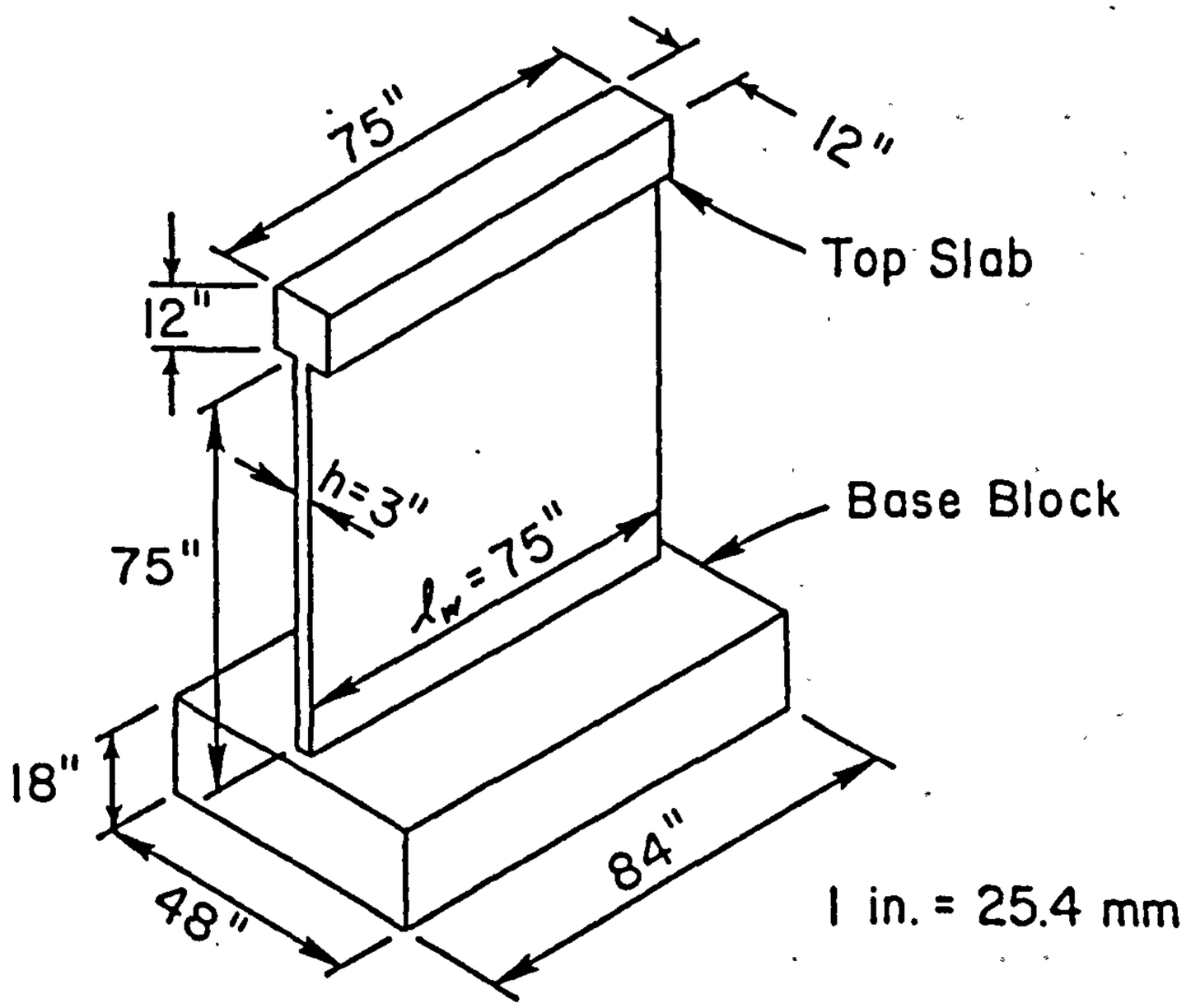
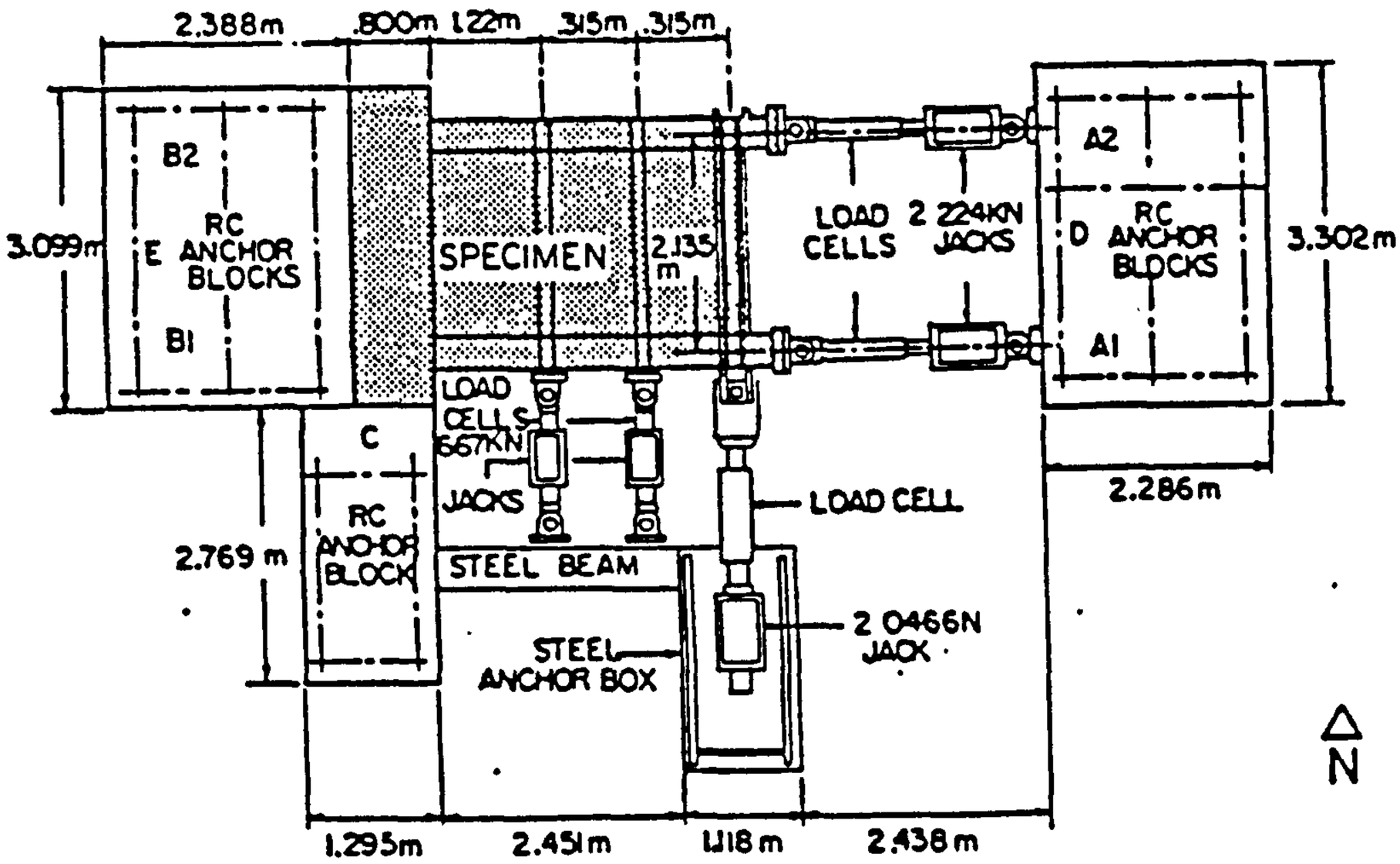


Figure 2.4 Nominal dimensions of test specimens (Cardenas et al, 1980)



(a) Plan

HORIZONTAL CROSS-SECTION

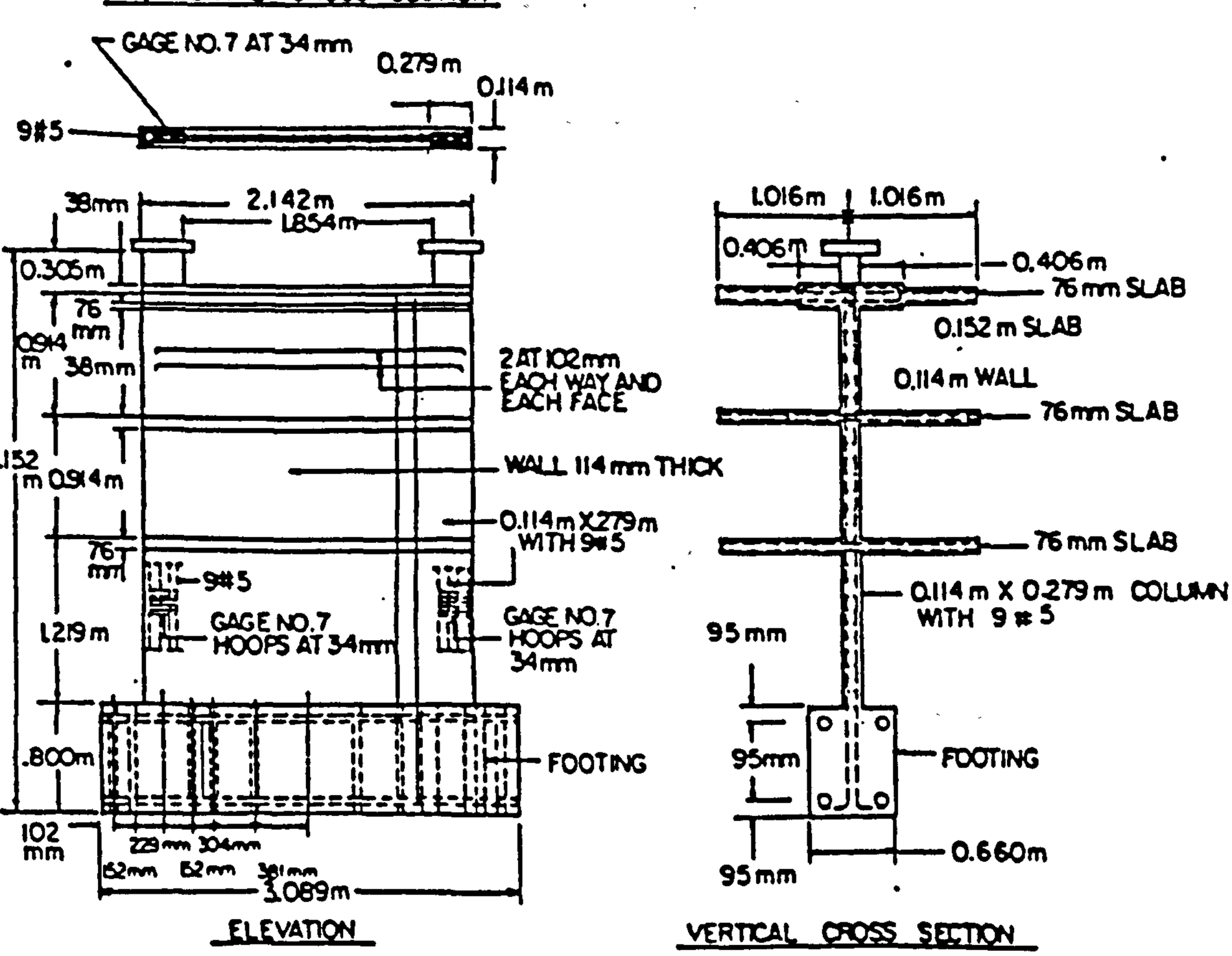


Figure 2.5 Details of EERC/UBC tests (Wang et al, 1975 and Vallenas et al, 1979)

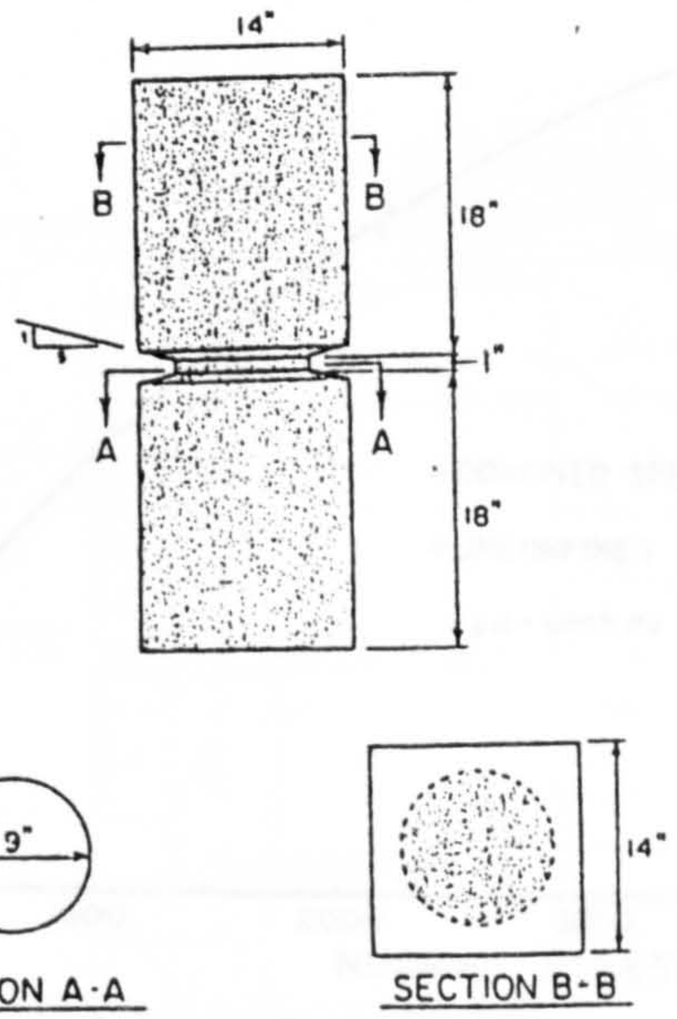


Figure 2.6 Test specimen geometry (Wagner and Bertero, 1982)

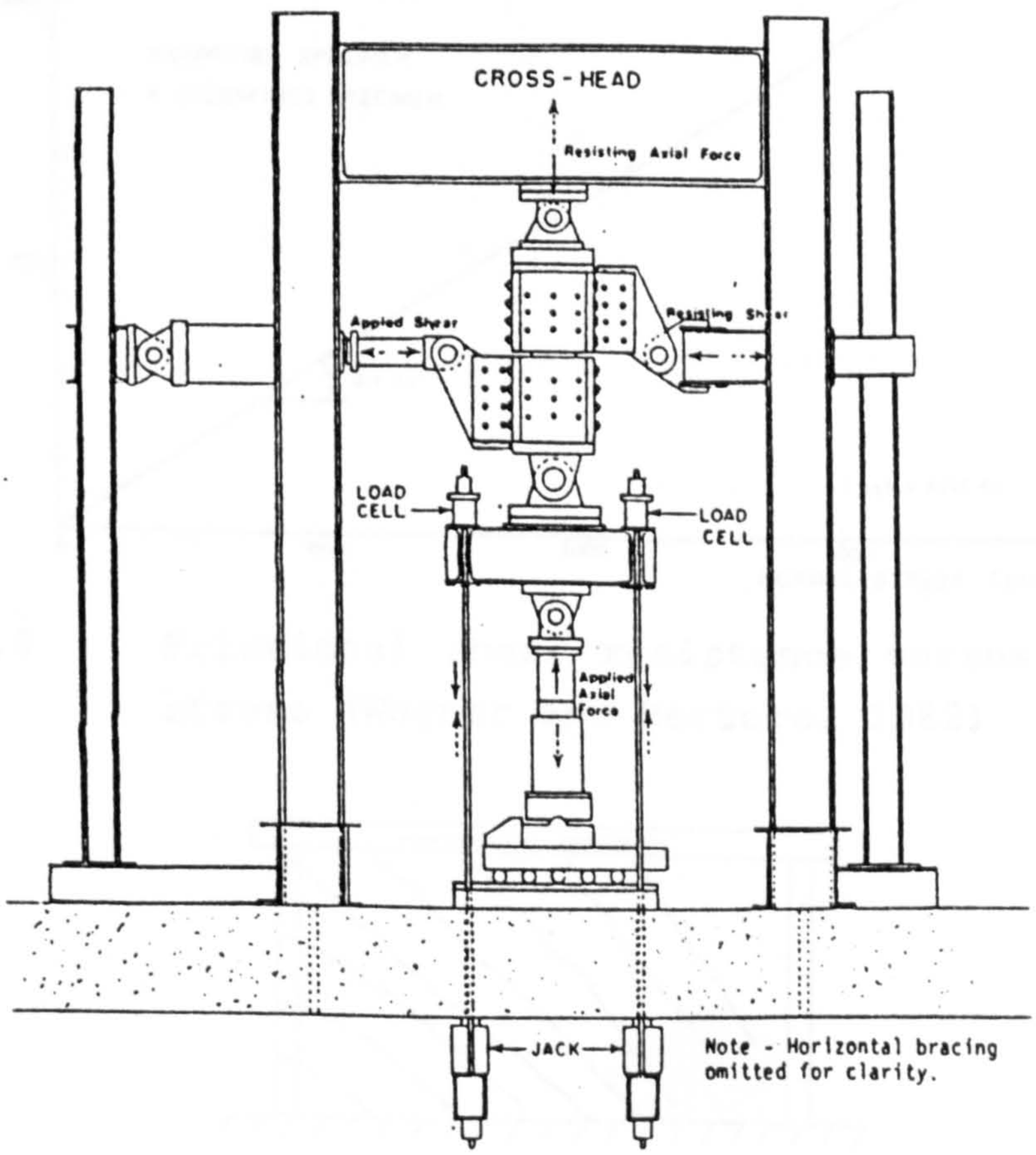


Figure 2.7 Experimental set-up (Wagner and Bertero, 1982)

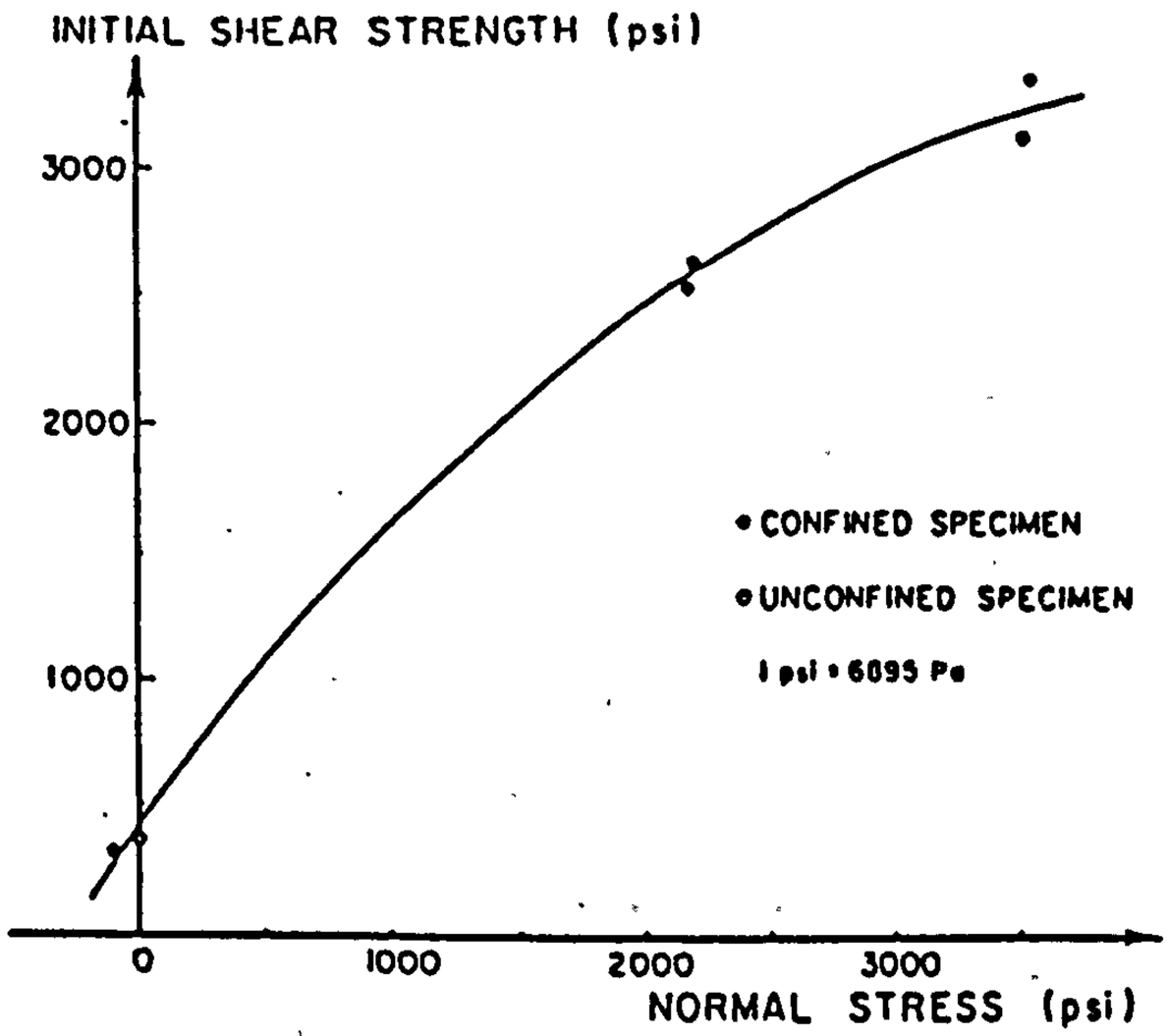


Figure 2.8 Relationship of initial shear strength to normal stress (Wagner and Bertero, 1982)

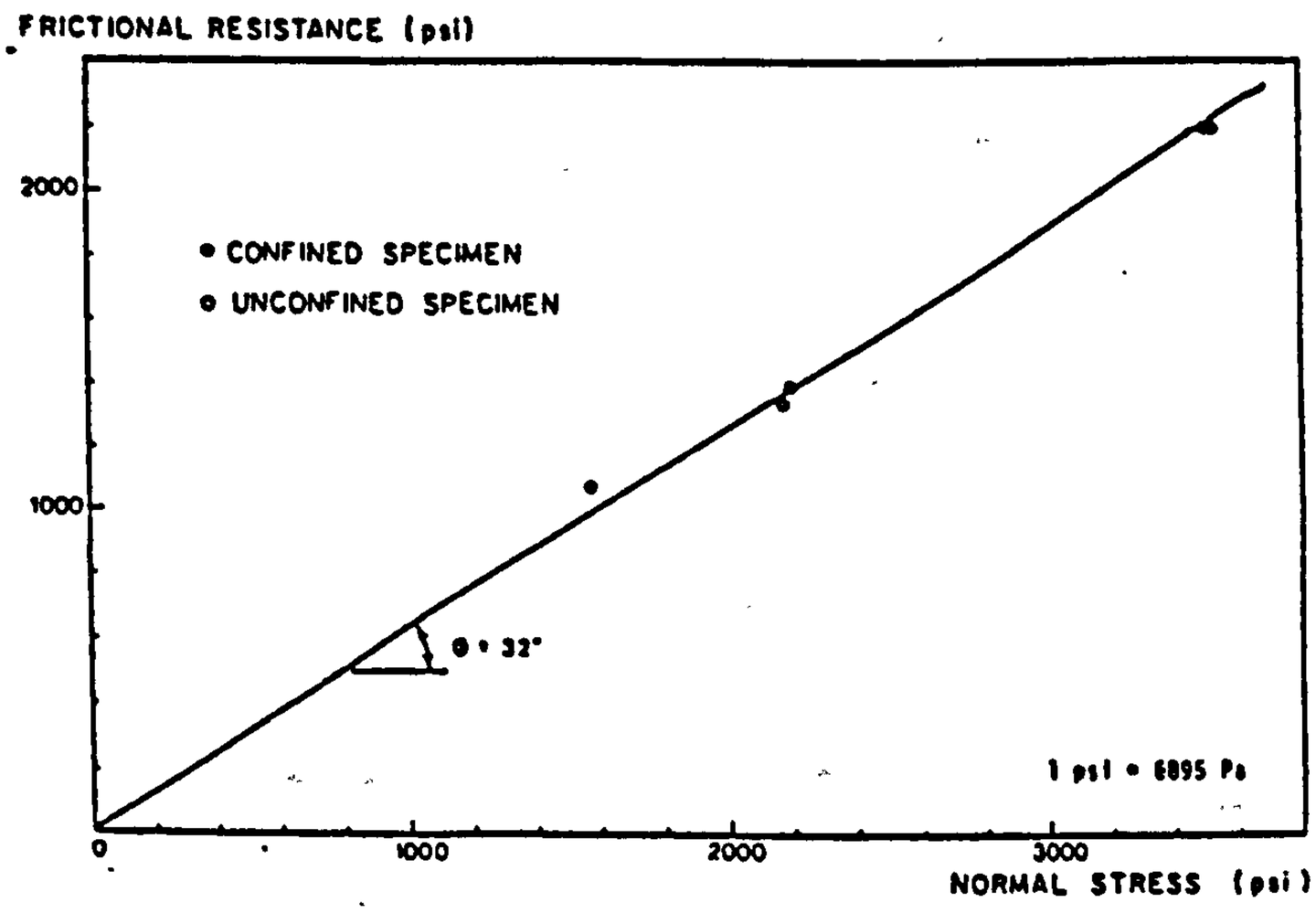


Figure 2.9 Frictional shear resistance versus normal stress (Wagner and Bertero, 1982)

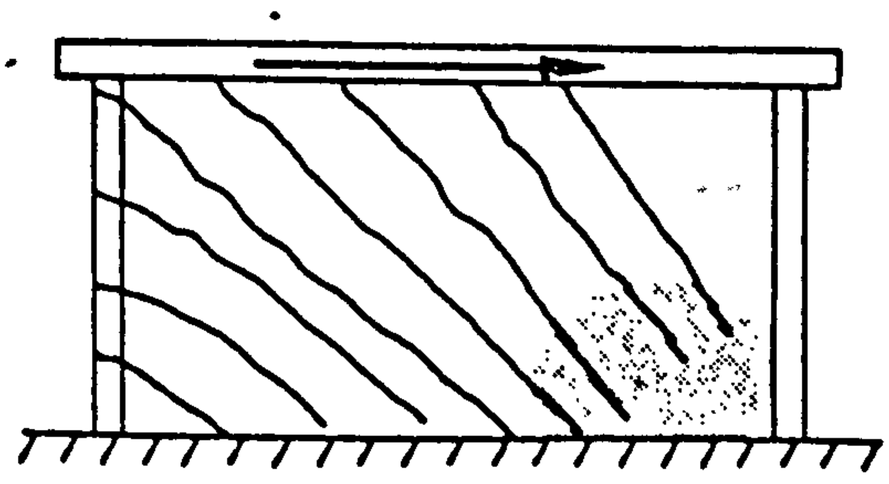
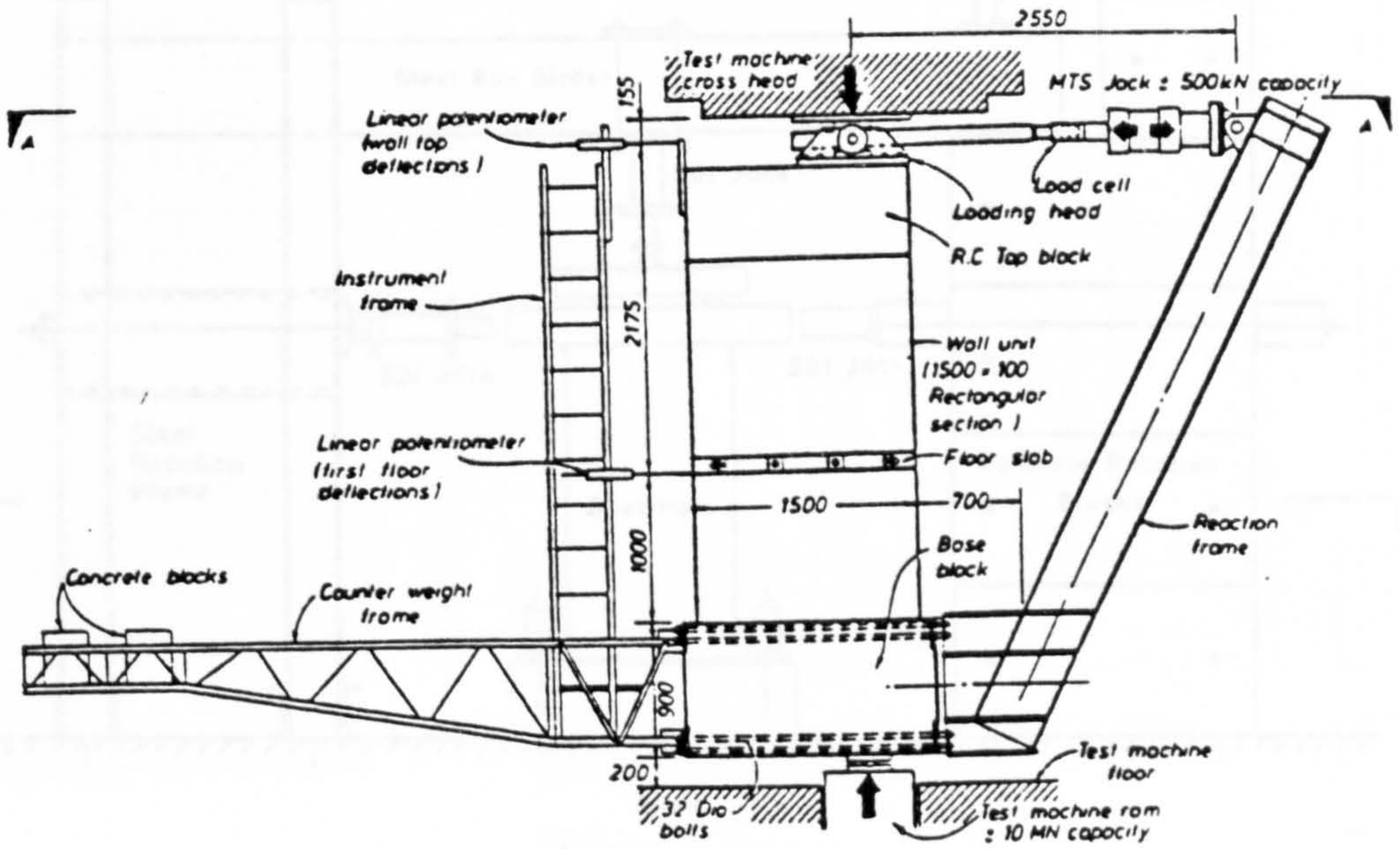
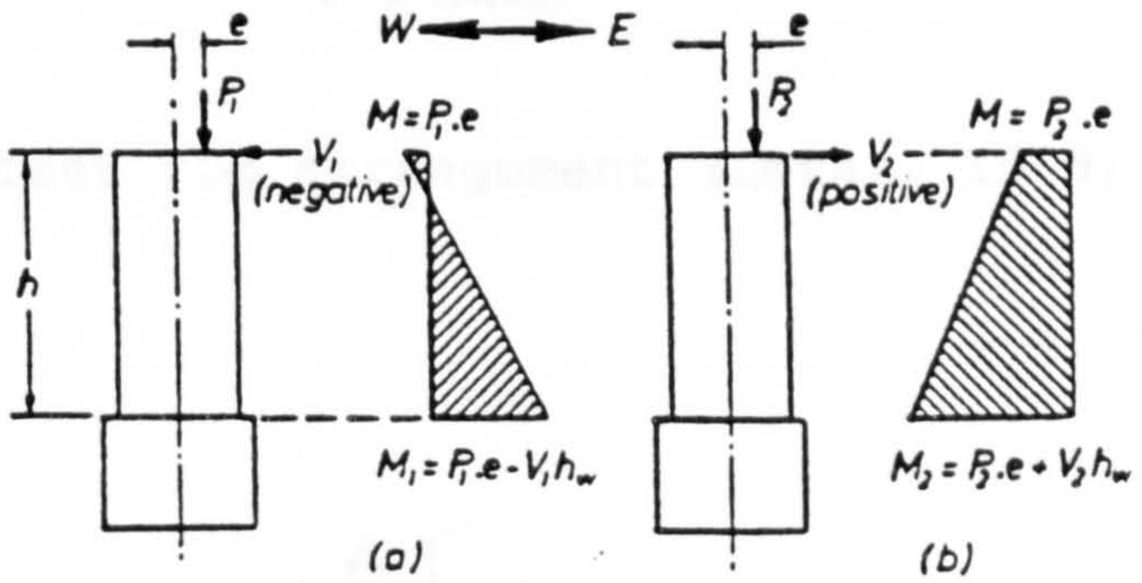


Figure 2.10 Direct load transfer in low-rise walls (Paulay et al, 1982)



ELEVATION



Bending Moment Patterns Applied to Test Specimens.

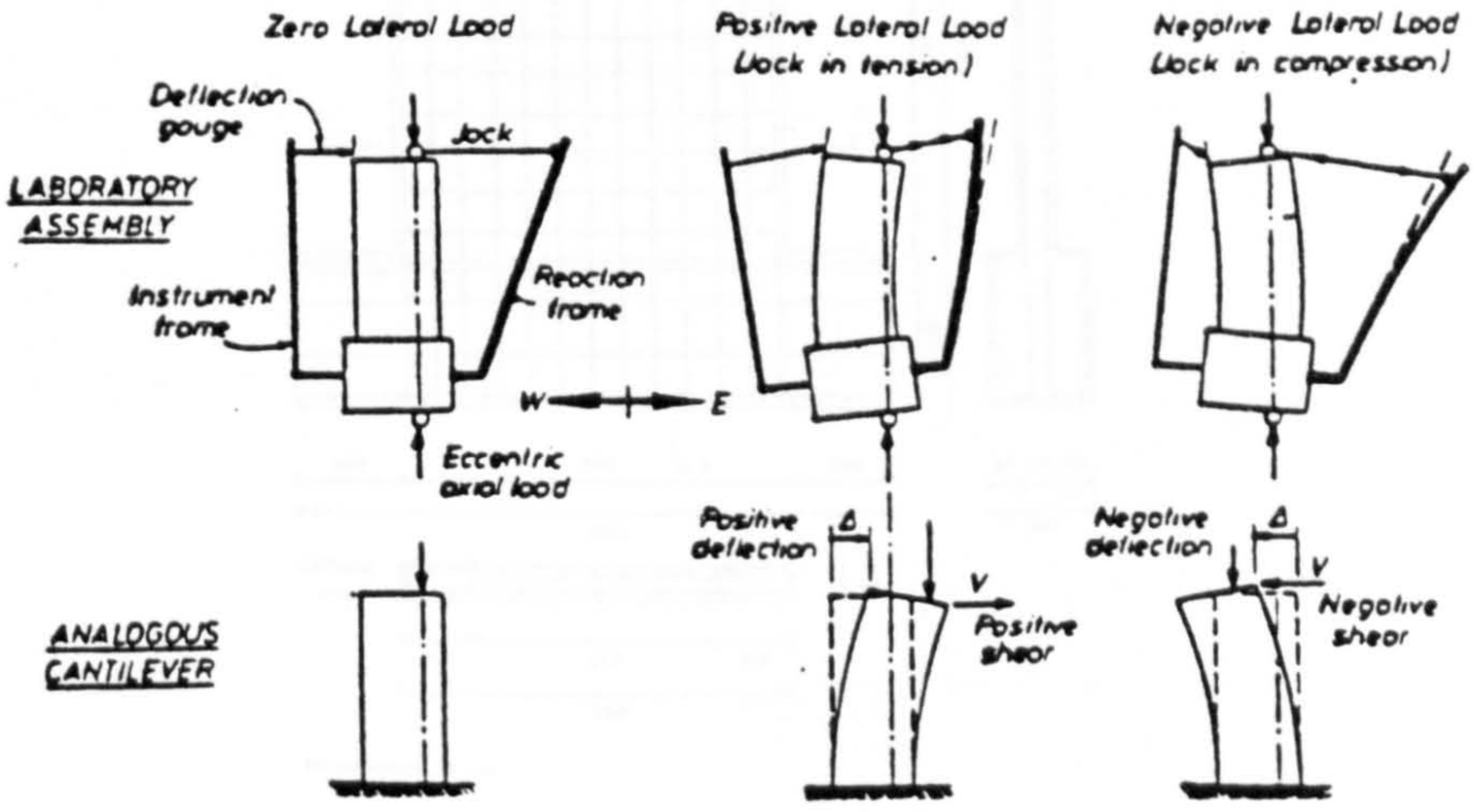


Figure 2.11 Test assembly and loading arrangement (Goodsir, 1985)

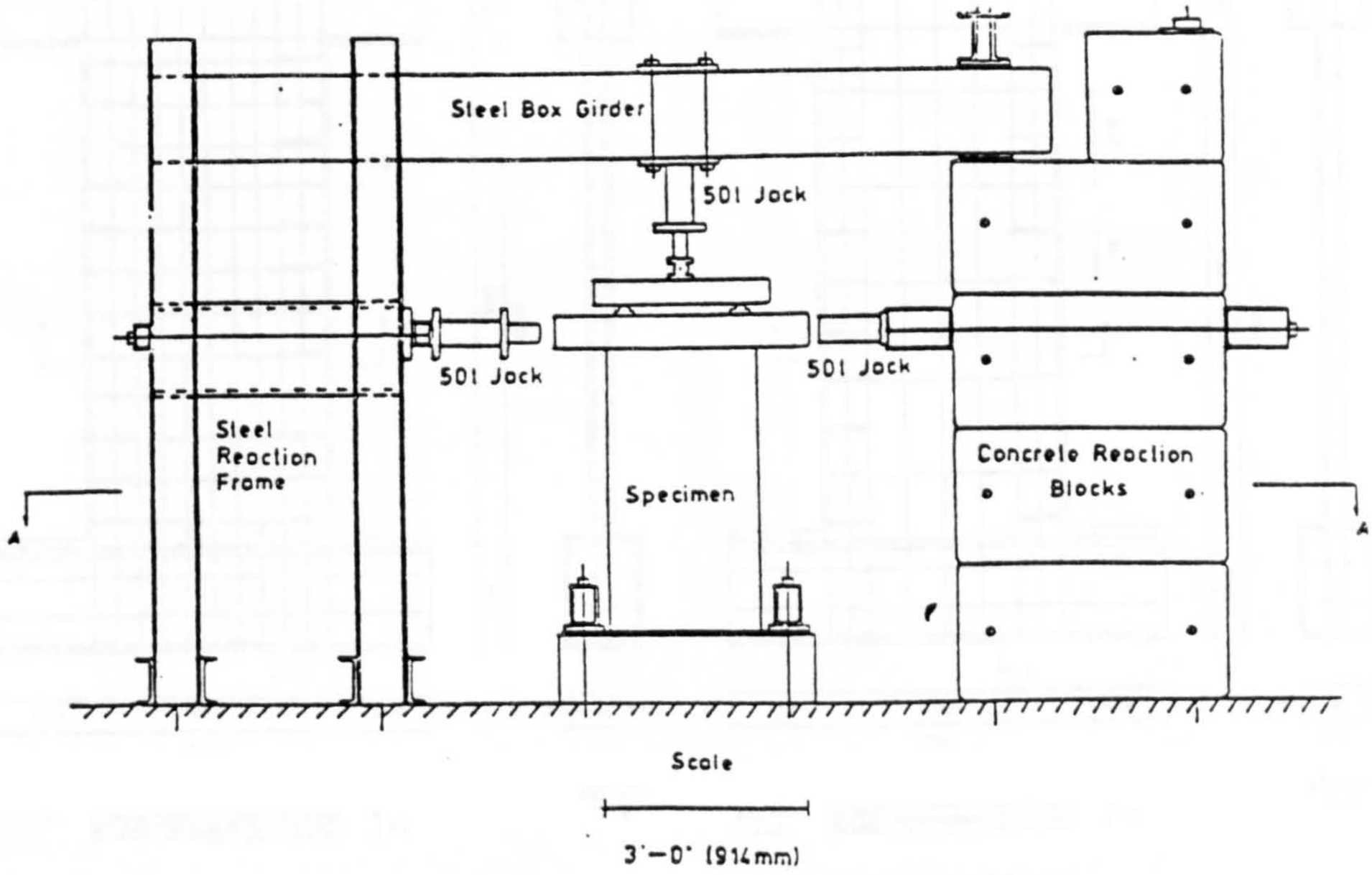
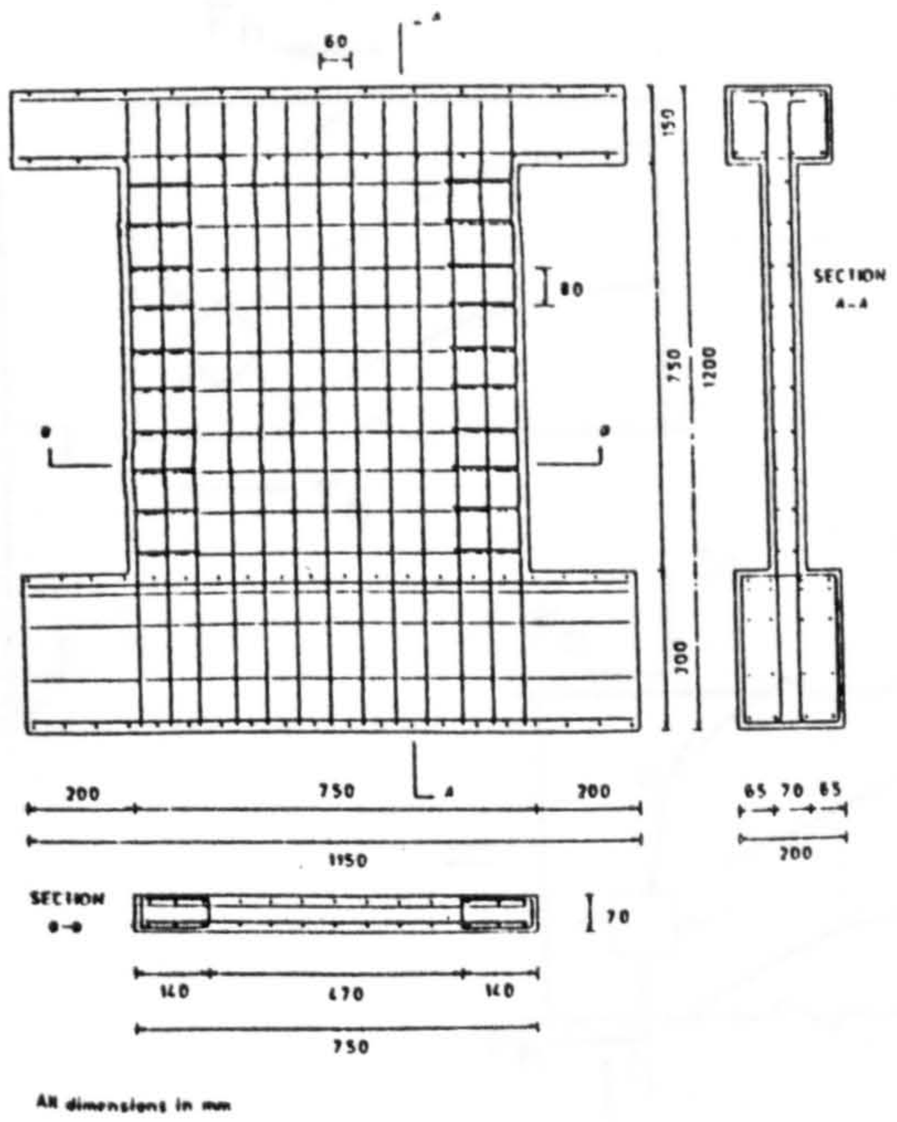
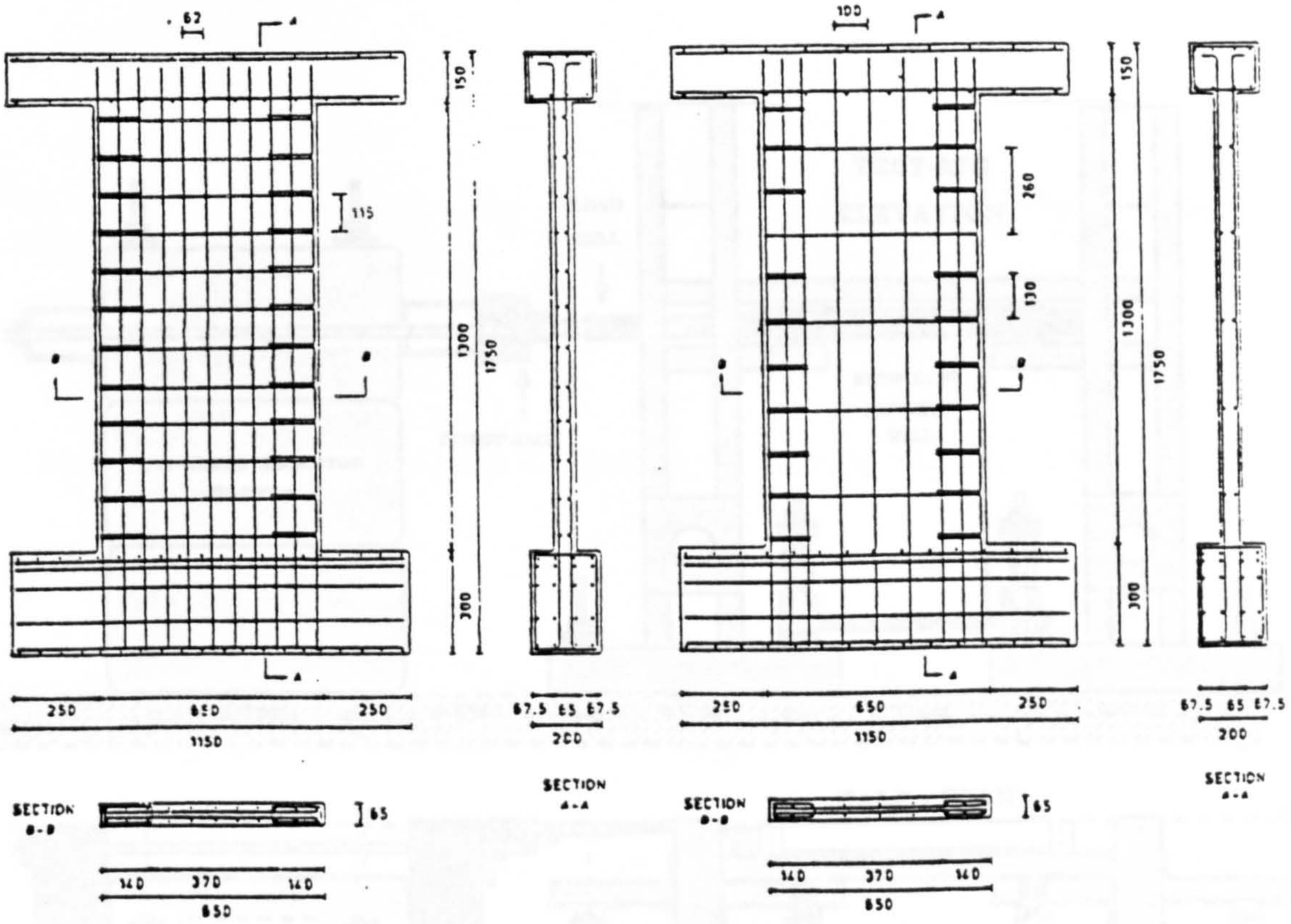


Figure 2.12 Test rig arrangement (Lefas, 1988)



a) Walls with aspect ratio 1

Figure 2.13 Details of test specimens (Lefas, 1988)



b) Walls with aspect ratio 2

Figure 2.13 Details of test specimens (Lefas, 1988)

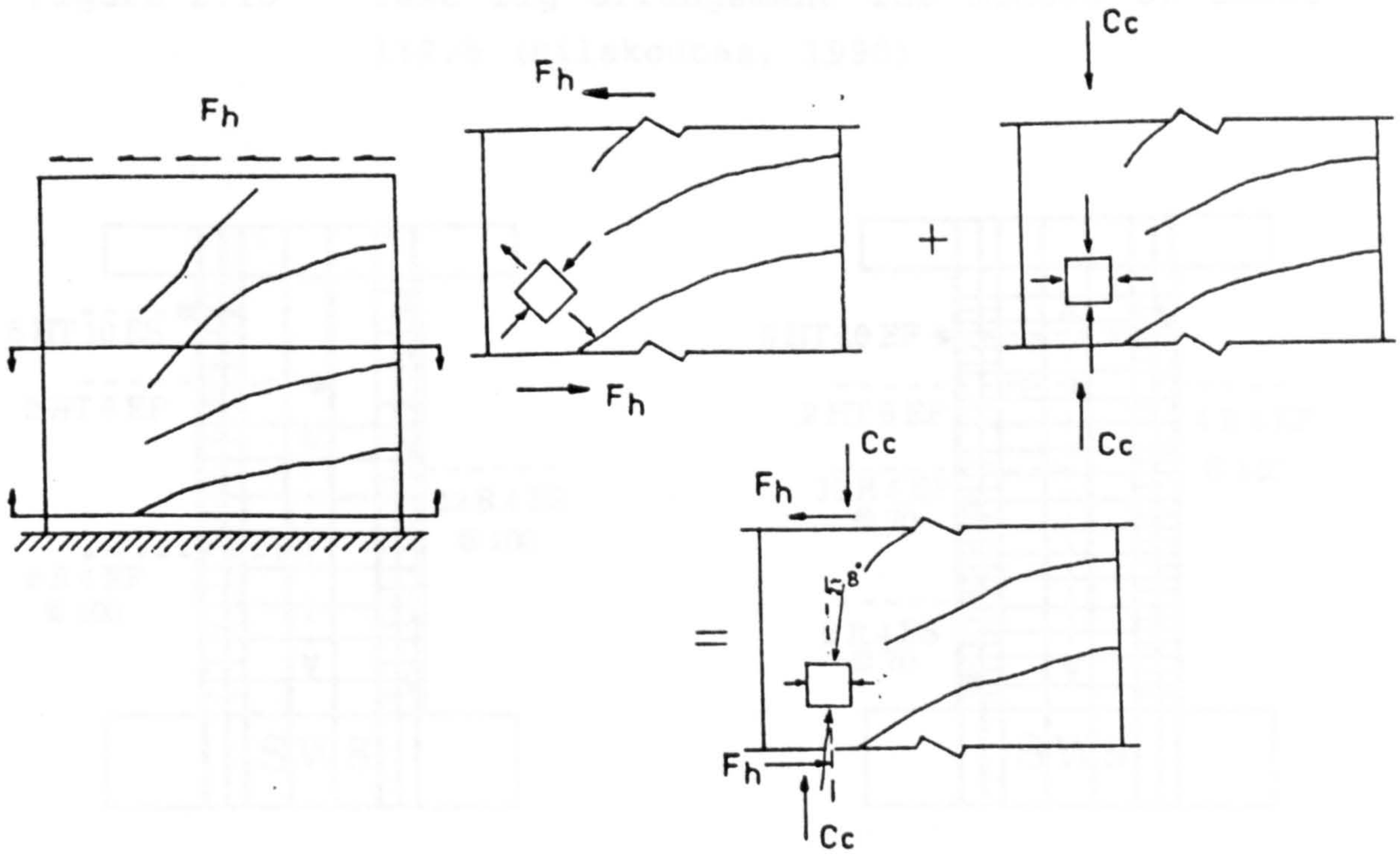


Figure 2.14 Schematic representation of the failure mechanism of walls with aspect ratio 1 (Lefas, 1988)

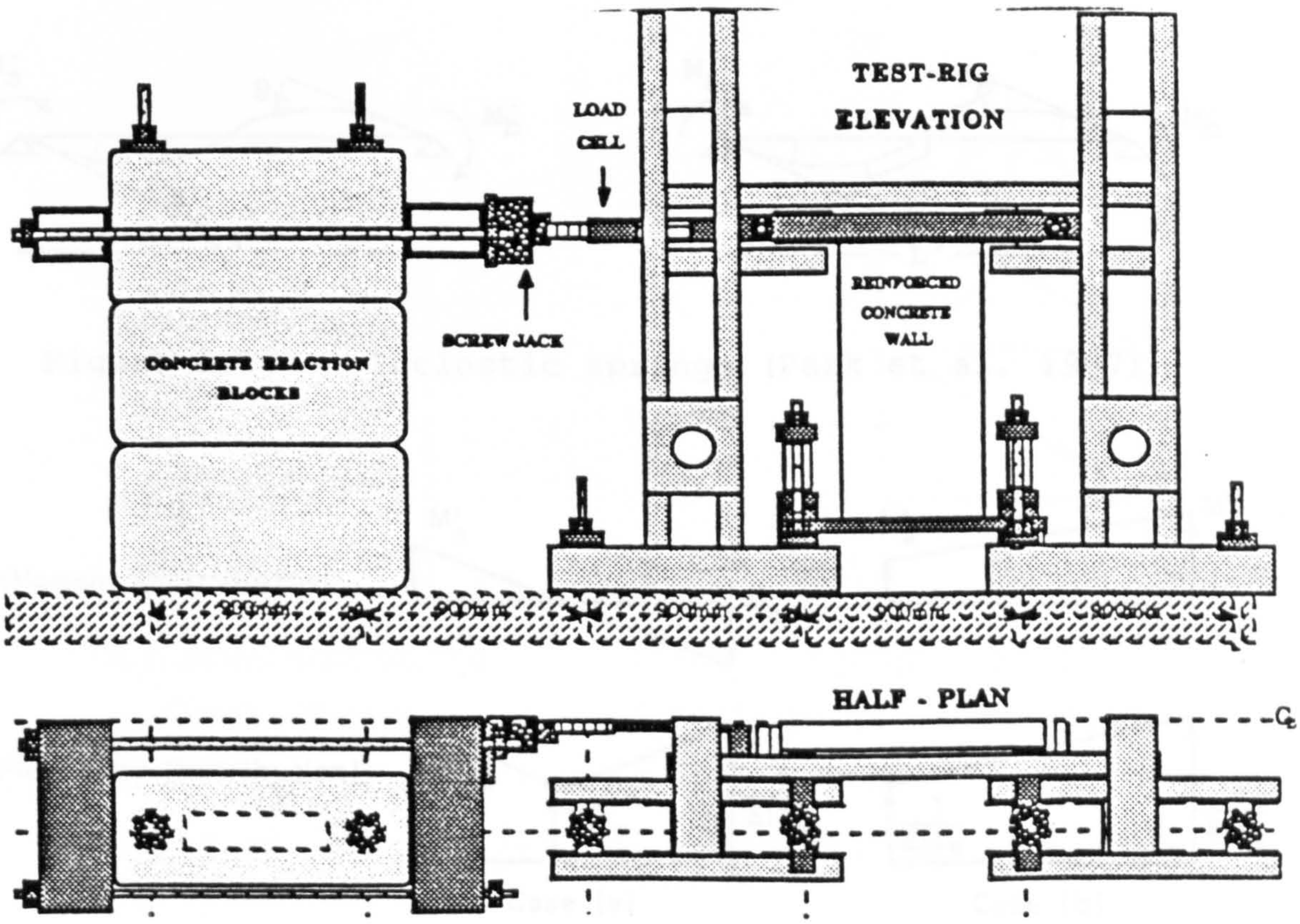


Figure 2.15 Test rig arrangement for models of scale 1:2.5 (Pilakoutas, 1990)

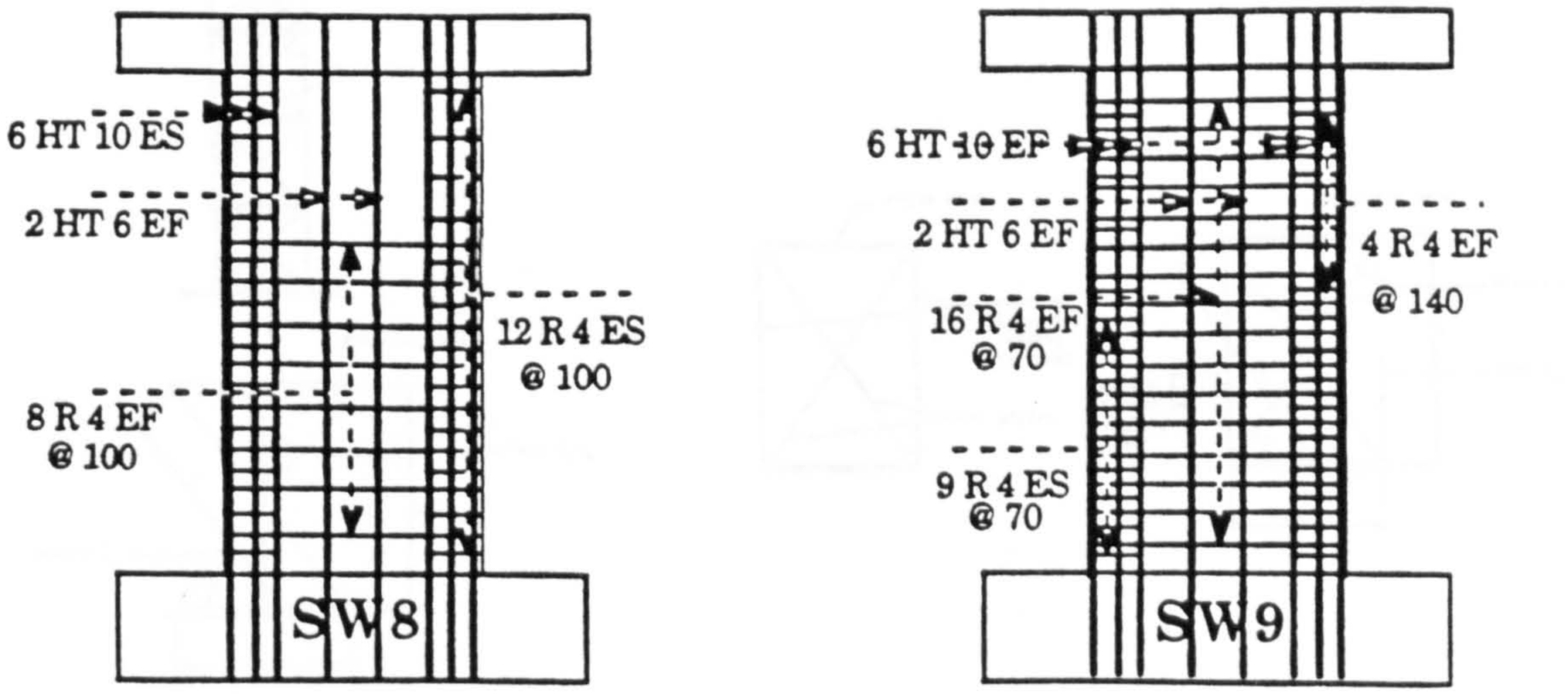


Figure 2.16 Reinforcement details for walls SW8 and SW9 (Pilakoutas, 1990)

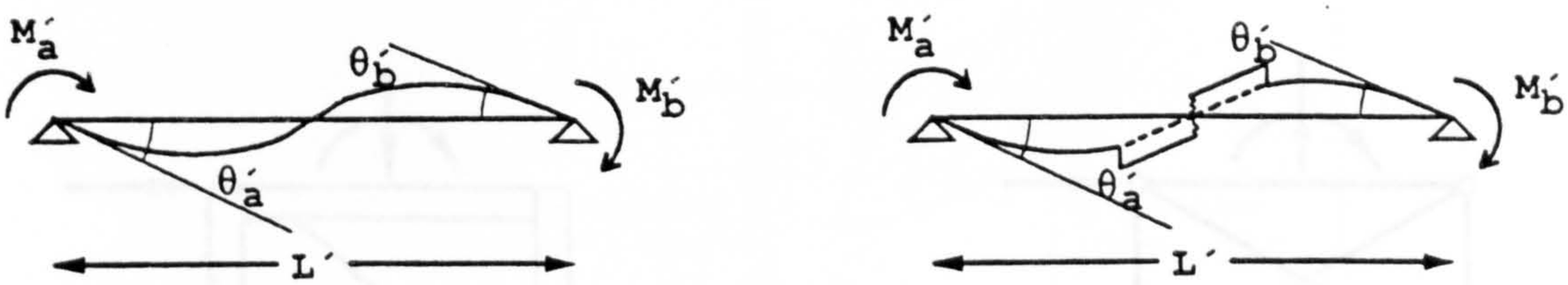


Figure 2.17 Inelastic springs (Park et al, 1987)

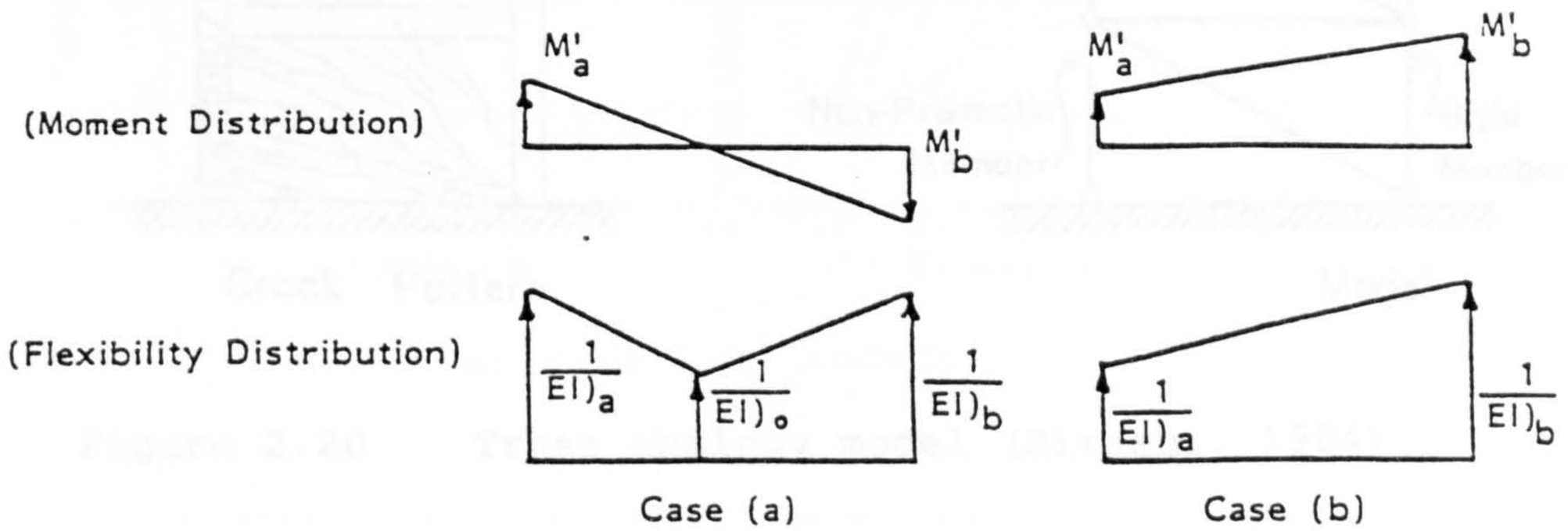
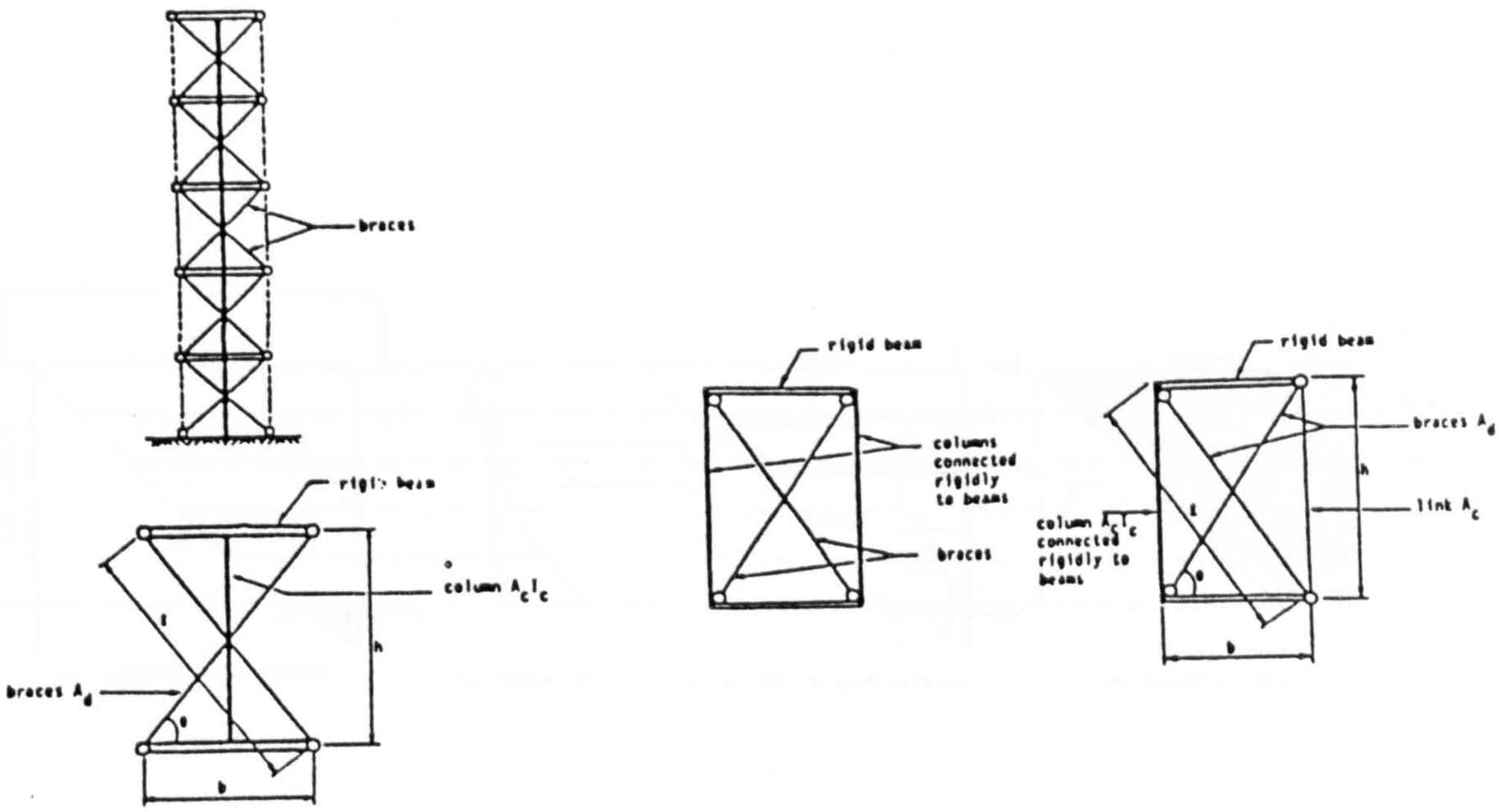


Figure 2.18 Distribution of flexibility (Park et al, 1987)



a)Braced wide column analogy b)Braced frame analogy

Figure 2.19 Equivalent frame elements for walls (Smith and Girgis, 1984)

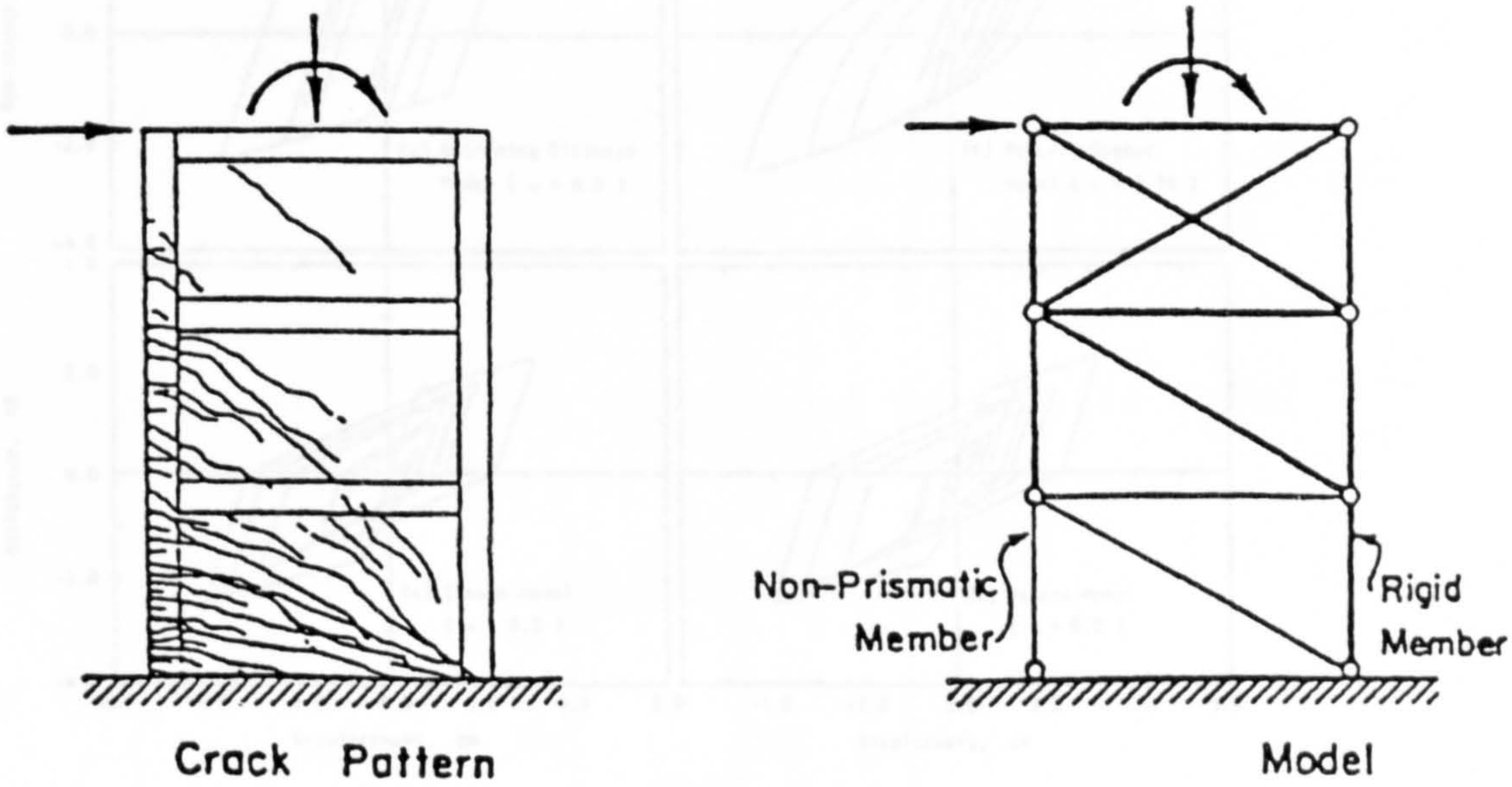


Figure 2.20 Truss analogy model (Hirashi, 1984)

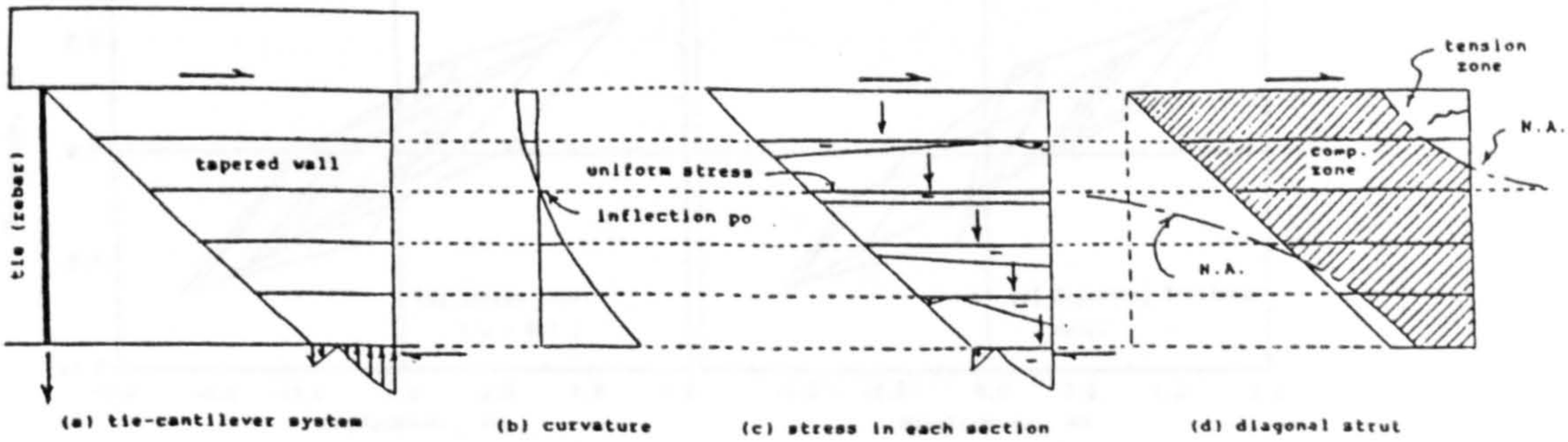
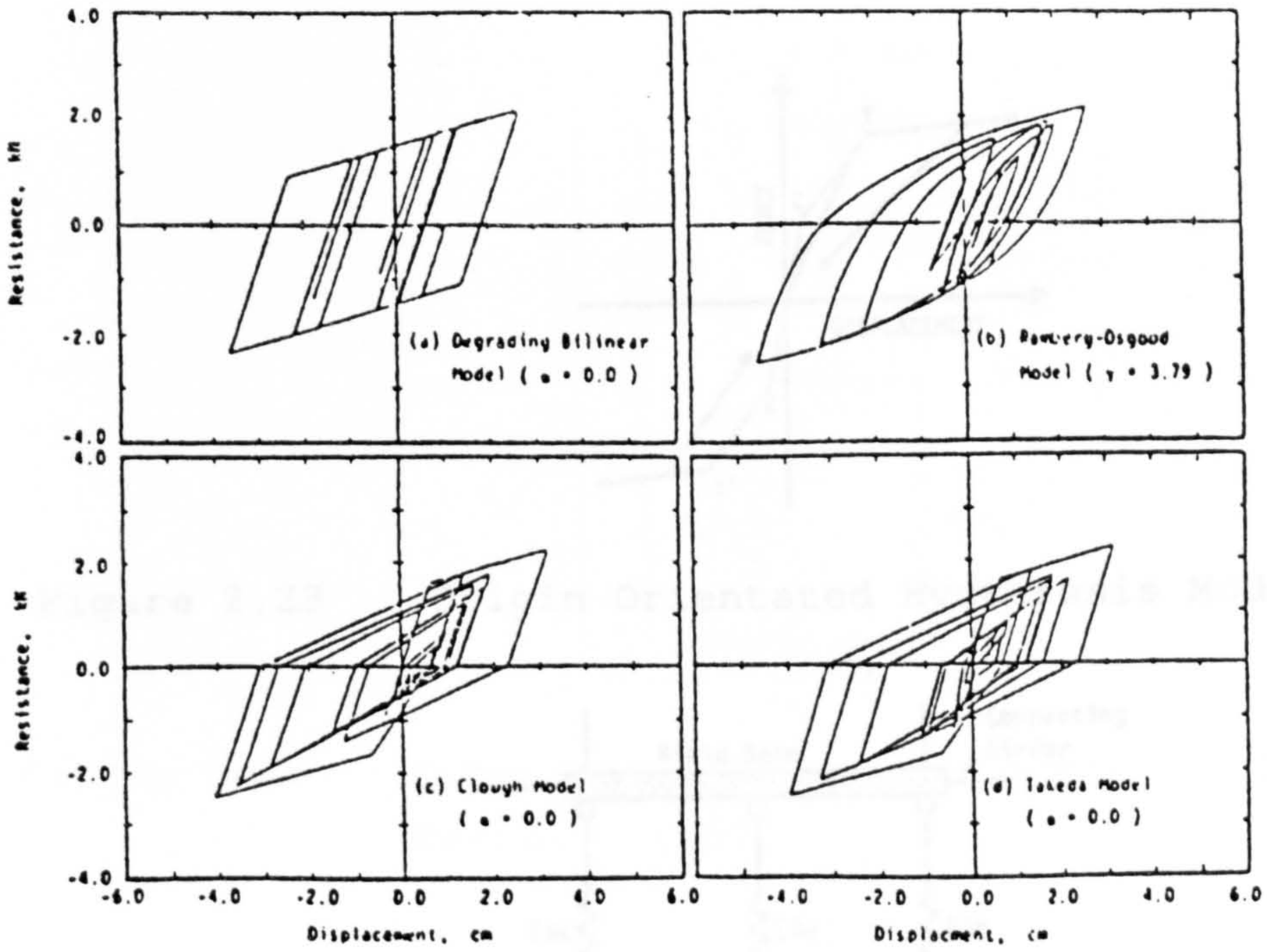
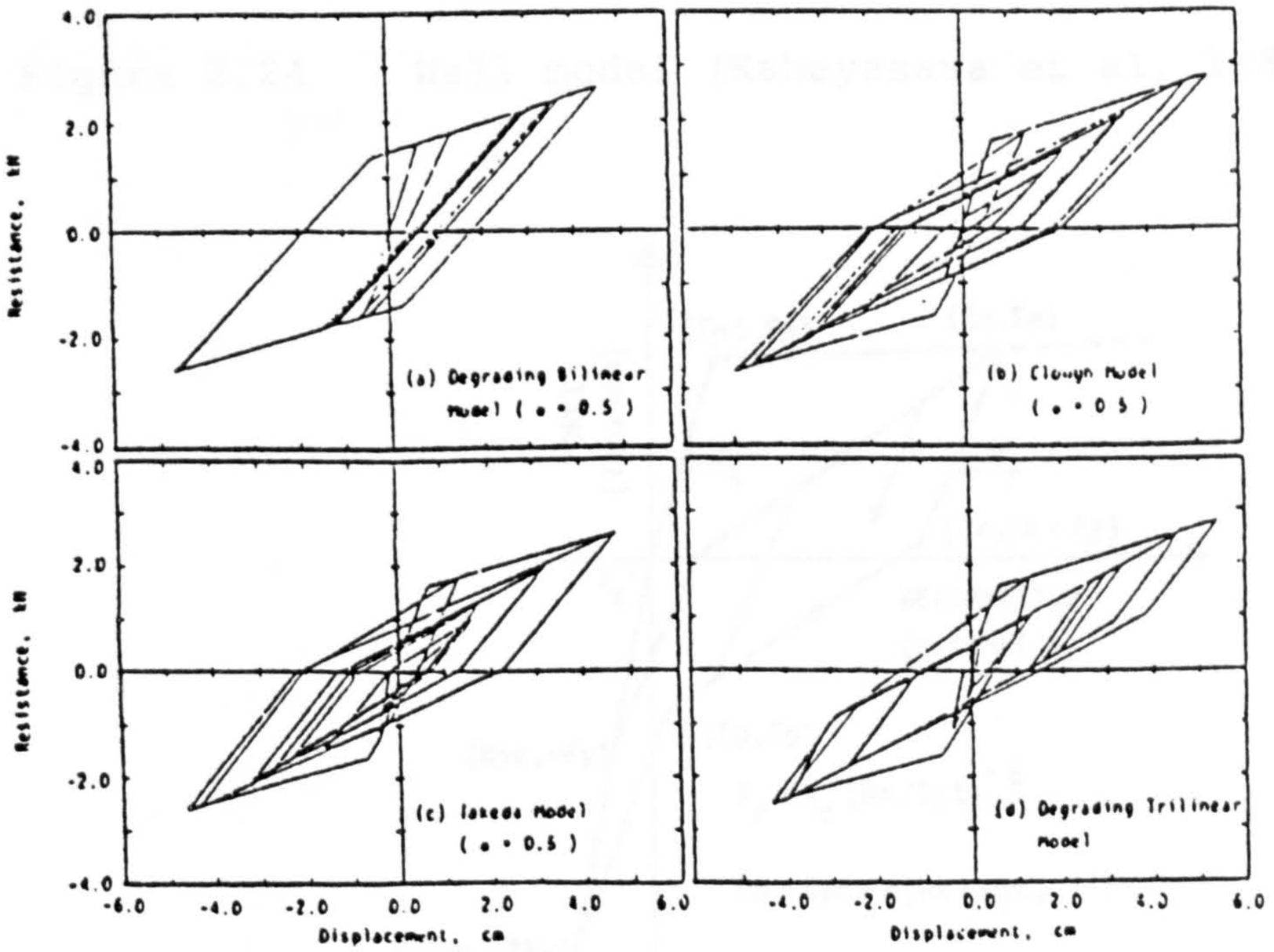


Figure 2.21 Inclined crack model of Huang and Sheu (1988)



a) Wide loop models



b) Narrow loop models

Figure 2.22 Hysteresis relations of different models (Otani, 1984)

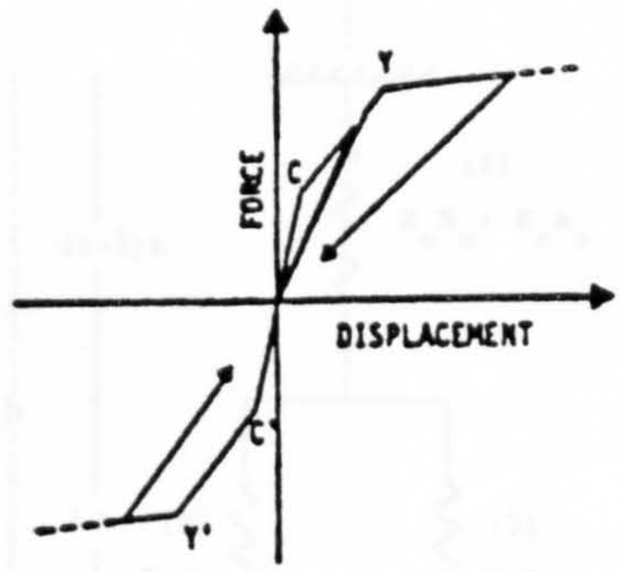


Figure 2.23 Origin Orientated Hysteresis Model

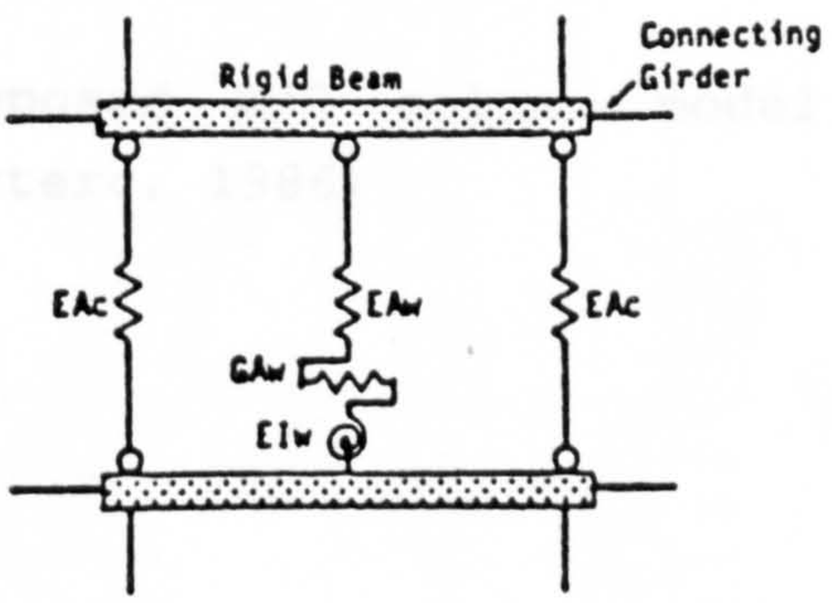


Figure 2.24 Wall model (Kabeyasawa et al, 1982)

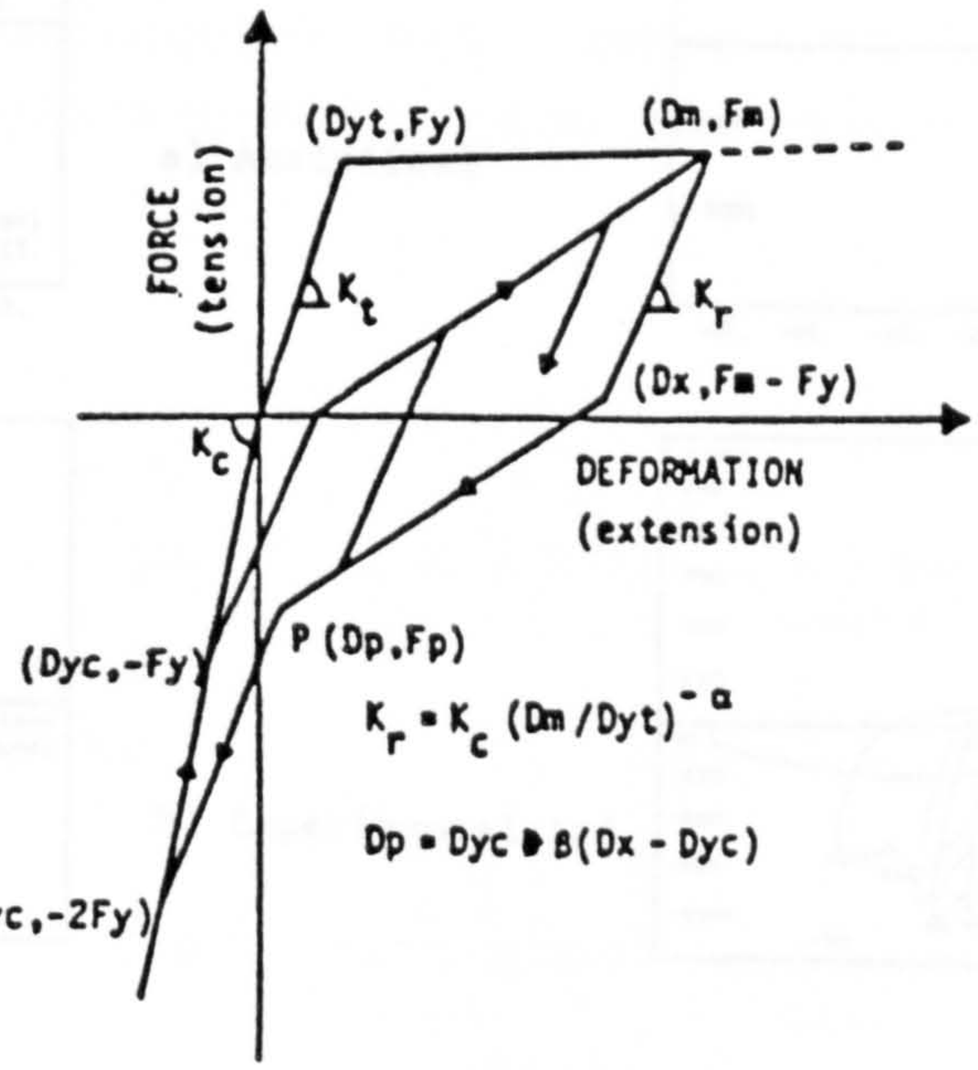


Figure 2.25 Axial-Stiffness Hysteresis Model (Kabeyasawa et al, 1982)

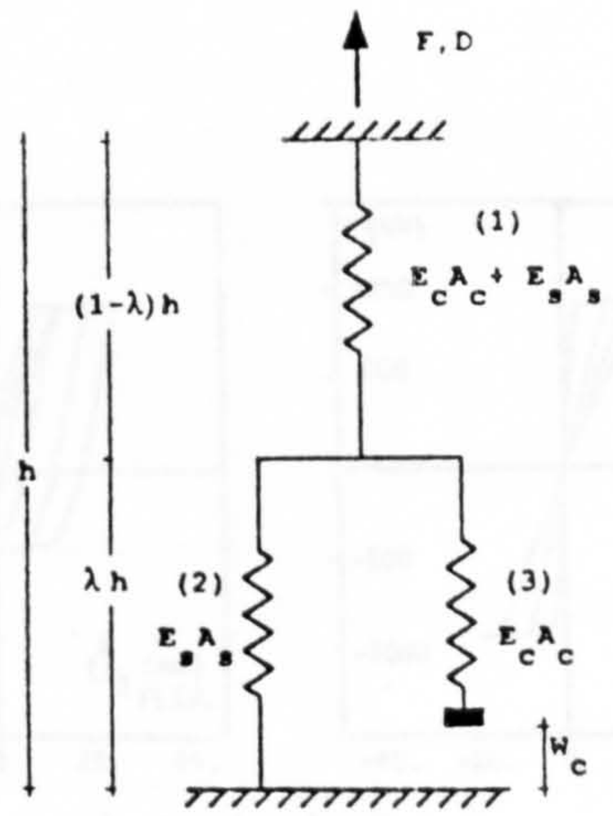
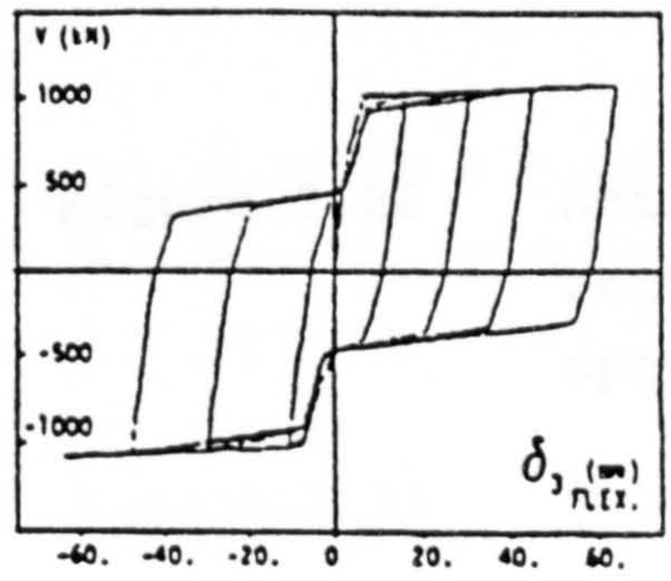
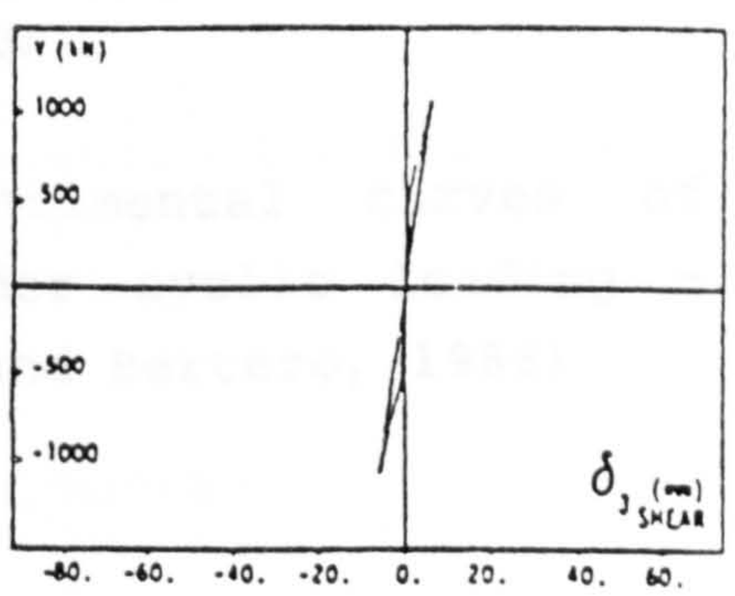
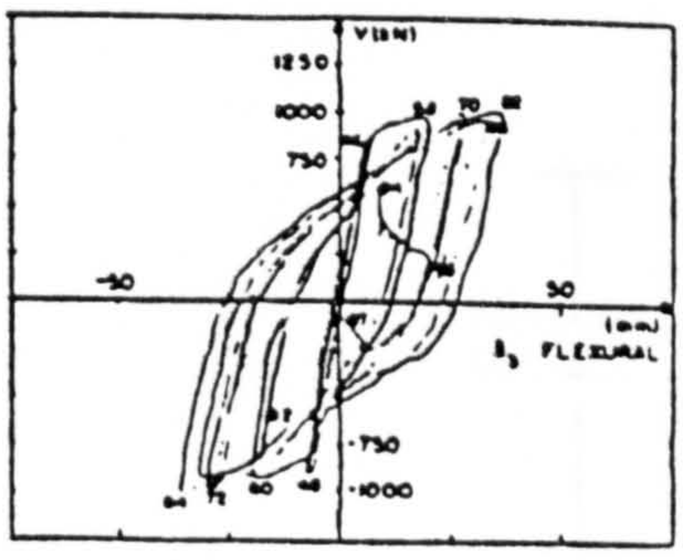


Figure 2.26 Proposed R/C column model (Vulcano and Bertero, 1986)



a) Analytical





b) Experimental(10)

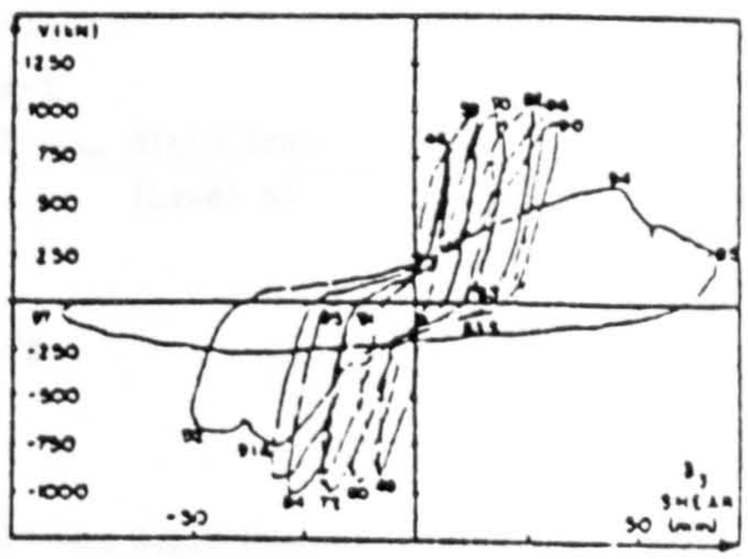
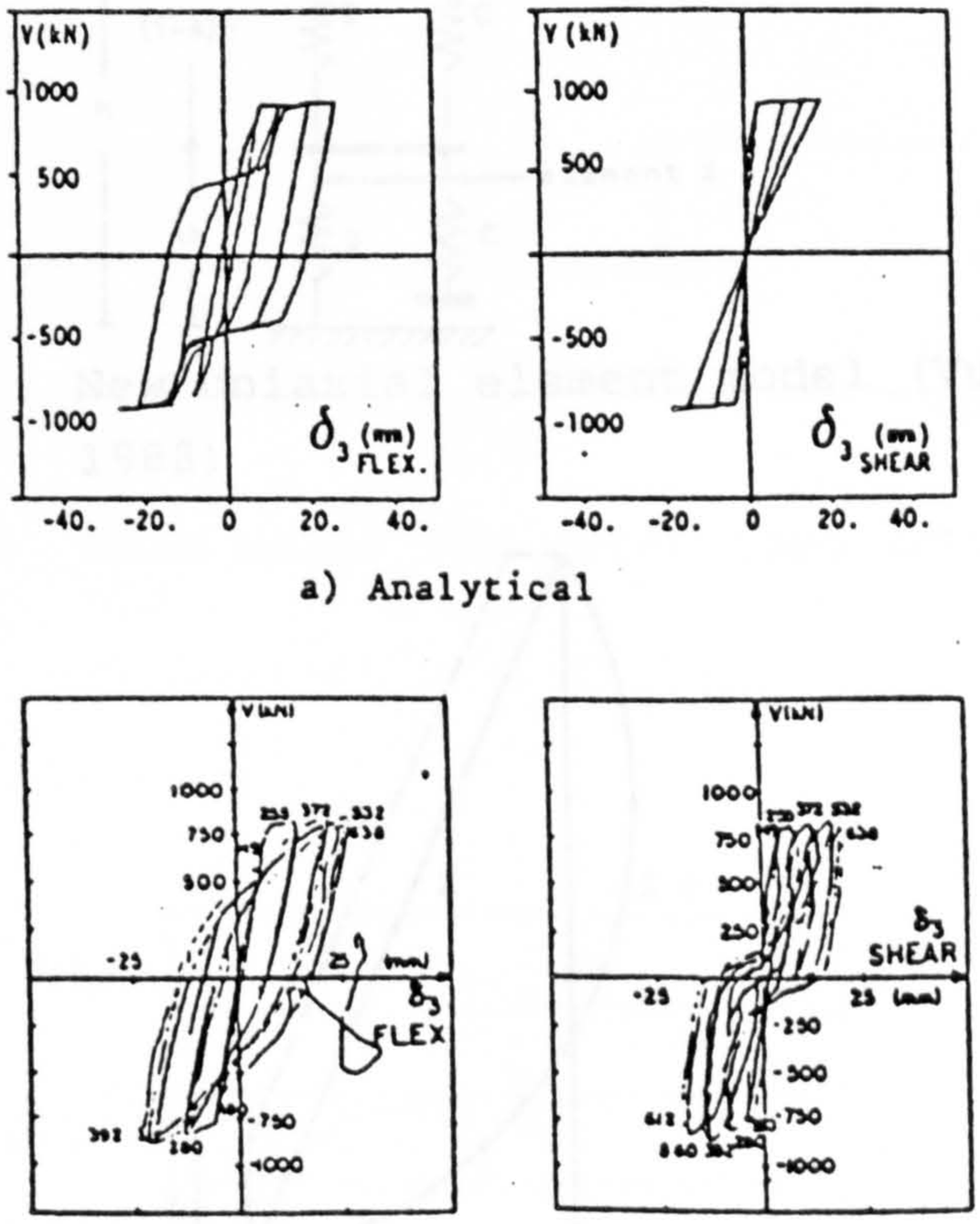


Figure 2.27 Analytical and experimental curves of framed wall under cyclic loading - specimen 4 (Vulcano and Bertero, 1986)



a) Analytical

b) Experimental (10)

Figure 2.28 Analytical and experimental curves of rectangular wall under cyclic loading - specimen 6 (Vulcano and Bertero, 1986)

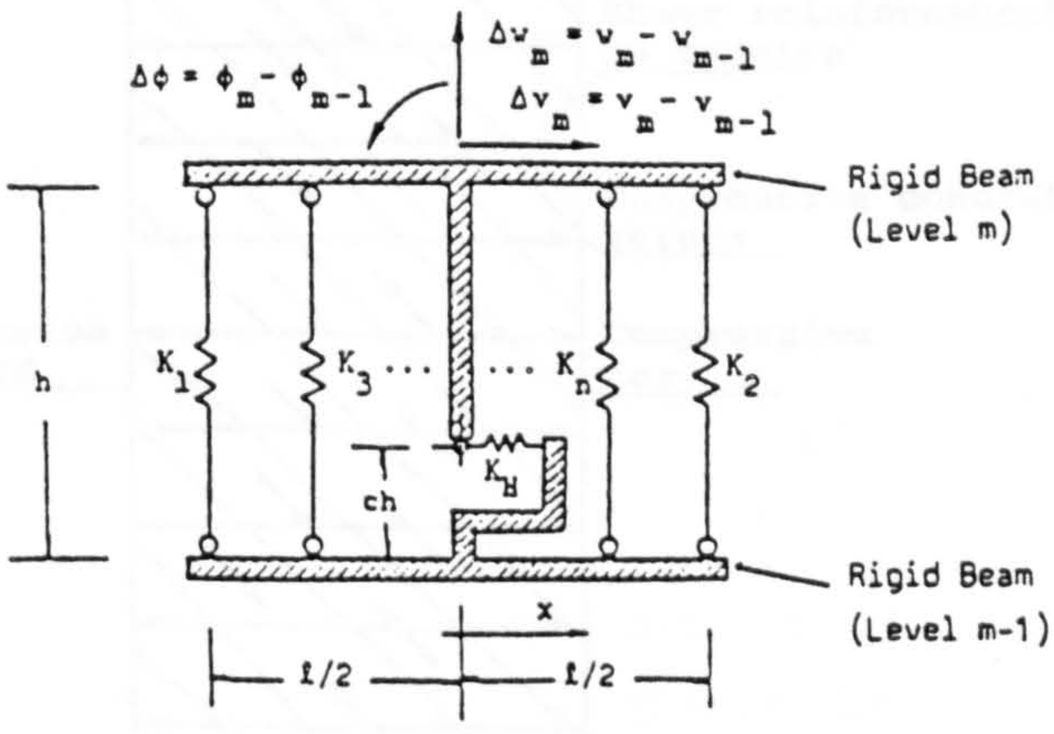


Figure 2.29 New wall model (Vulcano et al, 1988)

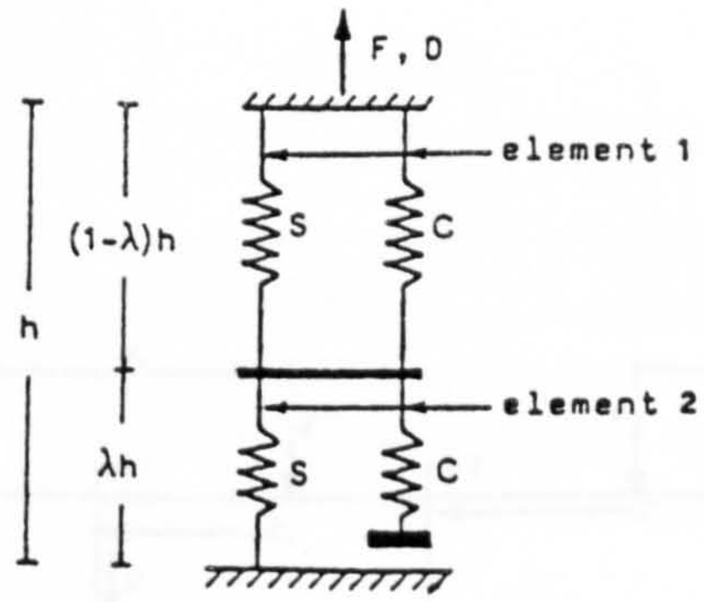
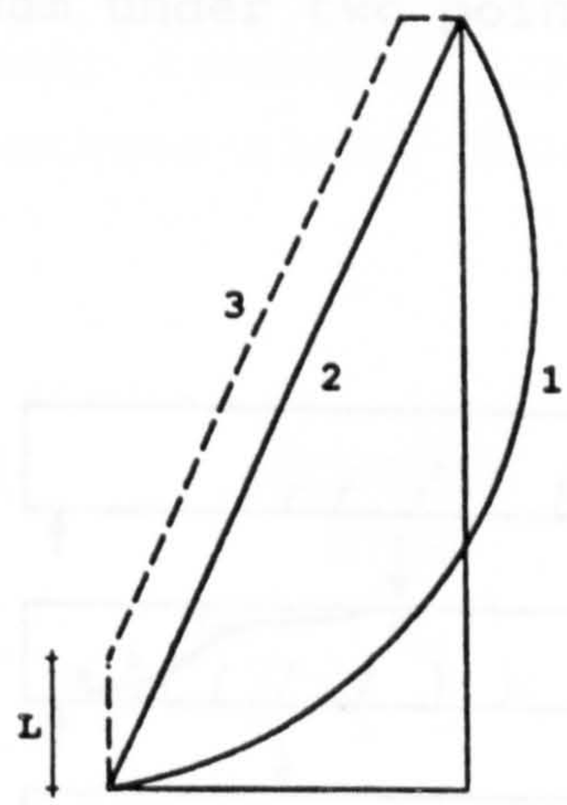


Figure 2.30 New uniaxial element model (Vulcano et al, 1988)



1 - diagram obtained from global analysis of the building
2 - linear envelope
3 - design envelope

Figure 2.31 Envelope of bending moments

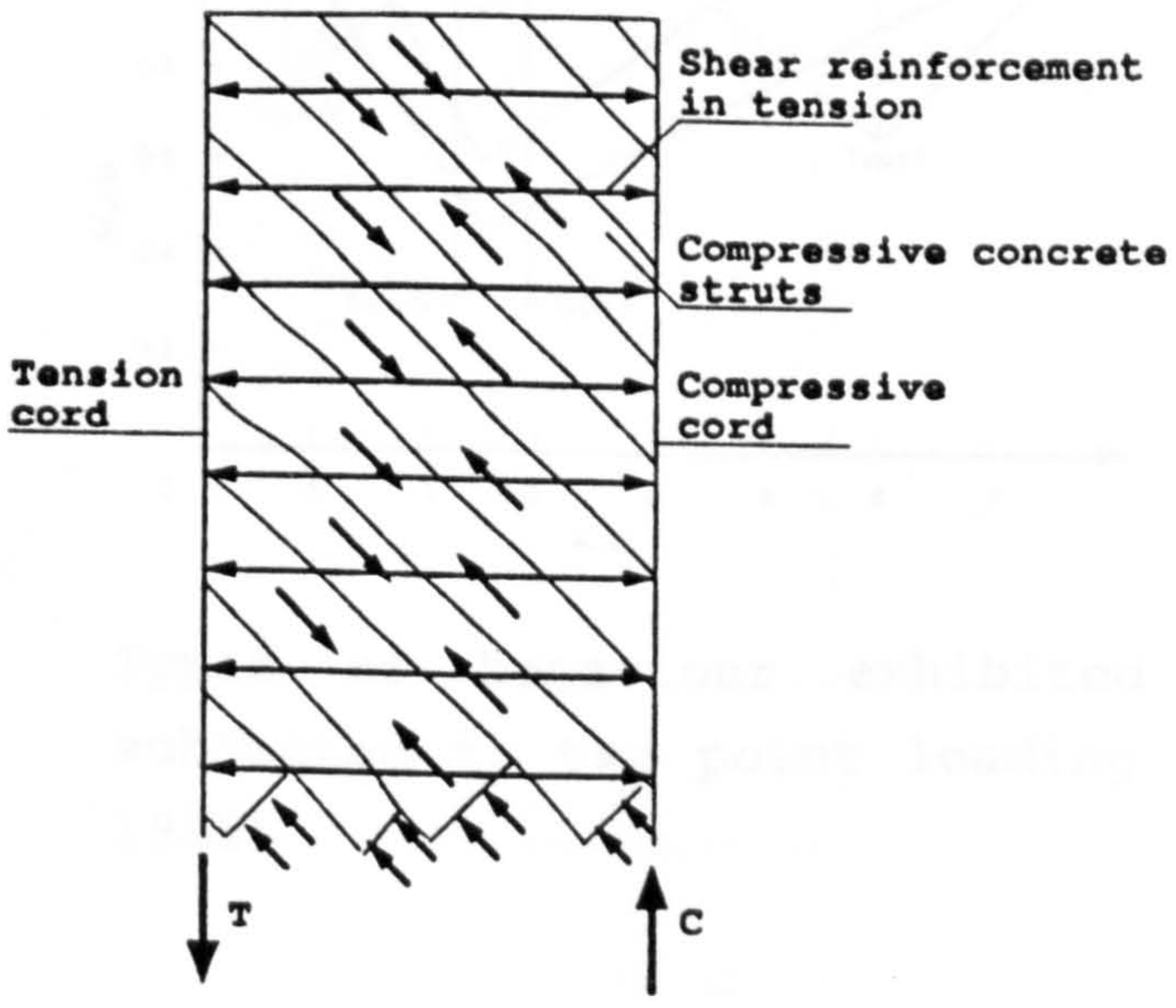


Figure 2.32 Truss Model for R/C Linear Members

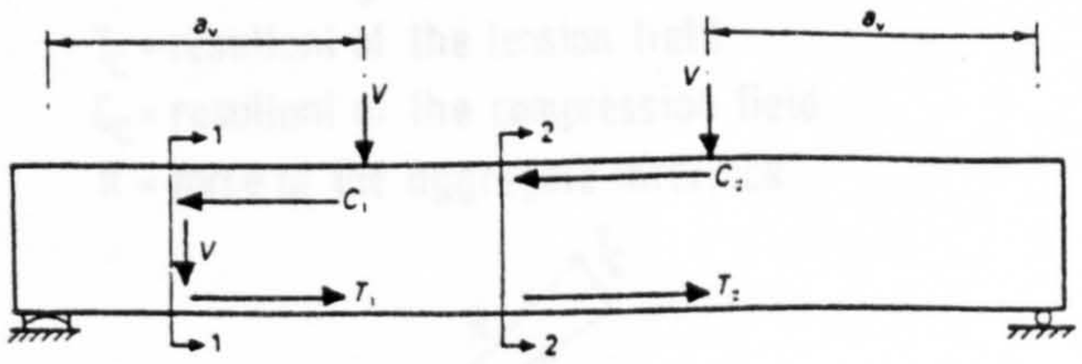


Figure 2.33 Beam under two point load (Kotsovos, 1983)

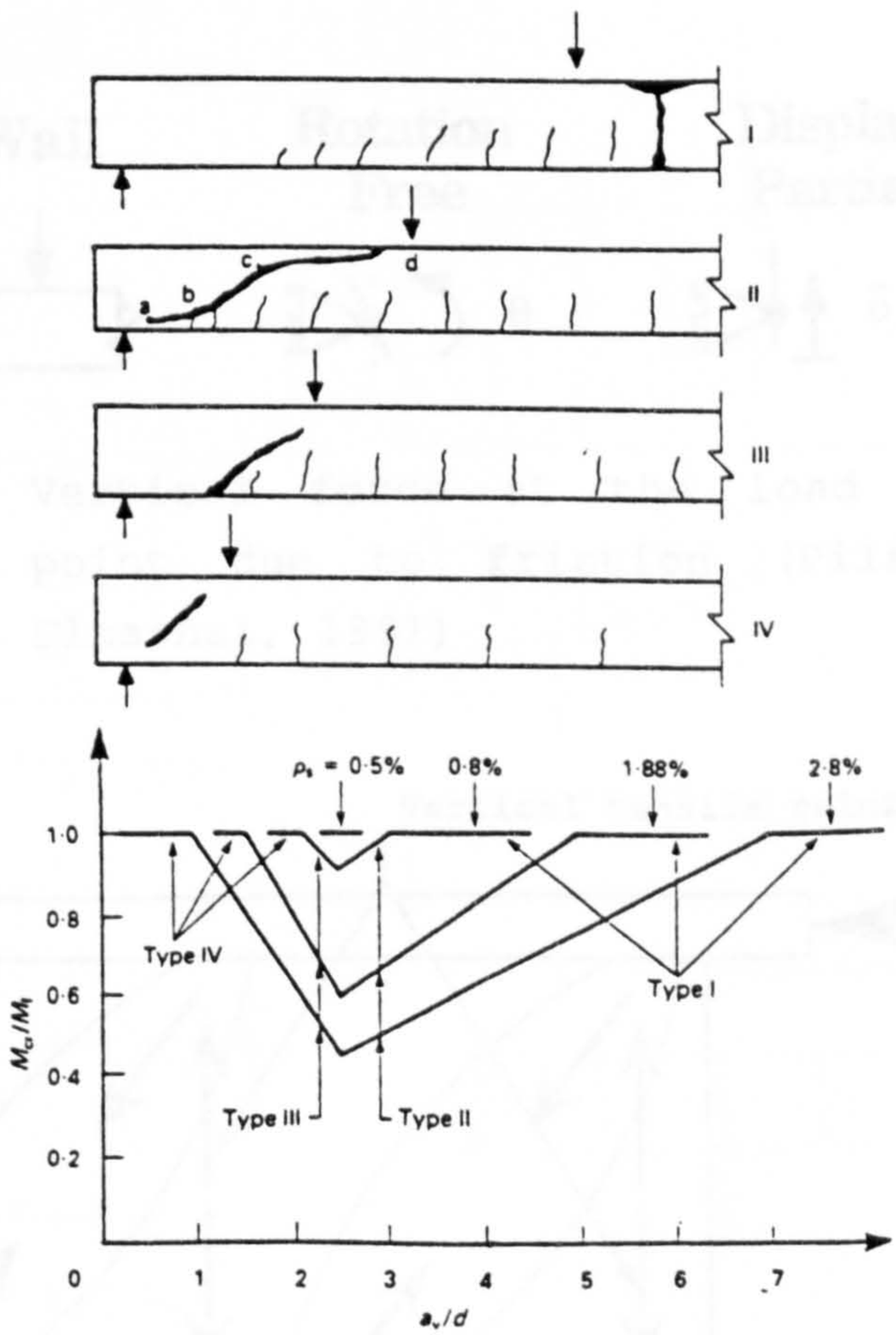
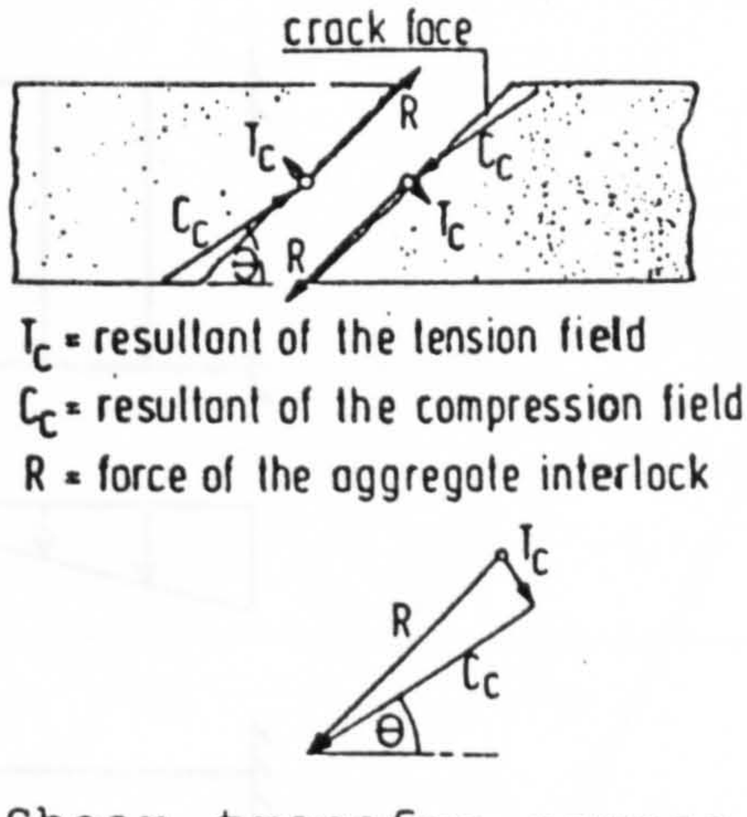


Figure 2.34 Types of behaviour exhibited by beams subjected to two point loading (Kotsovos, 1983)



T_c = resultant of the tension field

C_c = resultant of the compression field

R = force of the aggregate interlock

Figure 2.35 Shear transfer across inclined cracks by concrete alone (Schlaich et al, 1987)

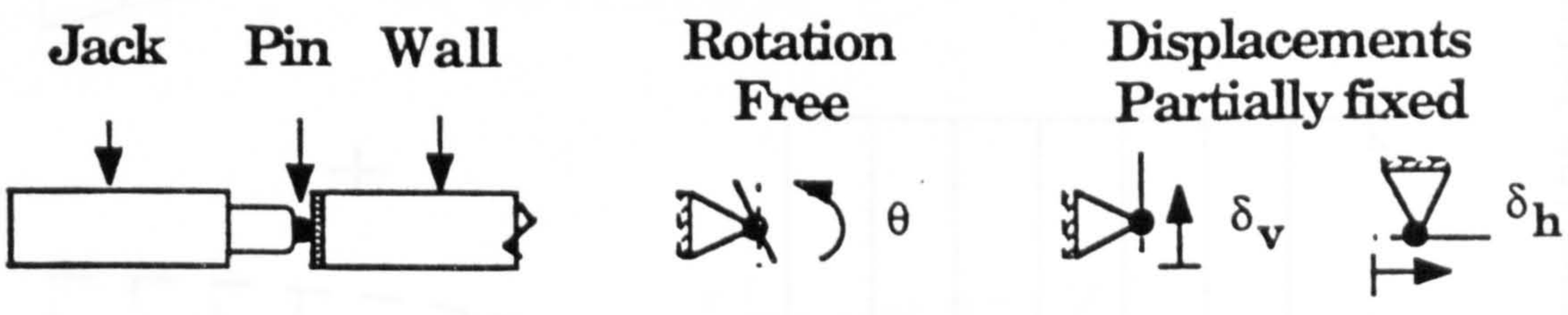


Figure 2.36 Vertical force at the load application point due to friction (Pilakoutas and Elnashai, 1991)

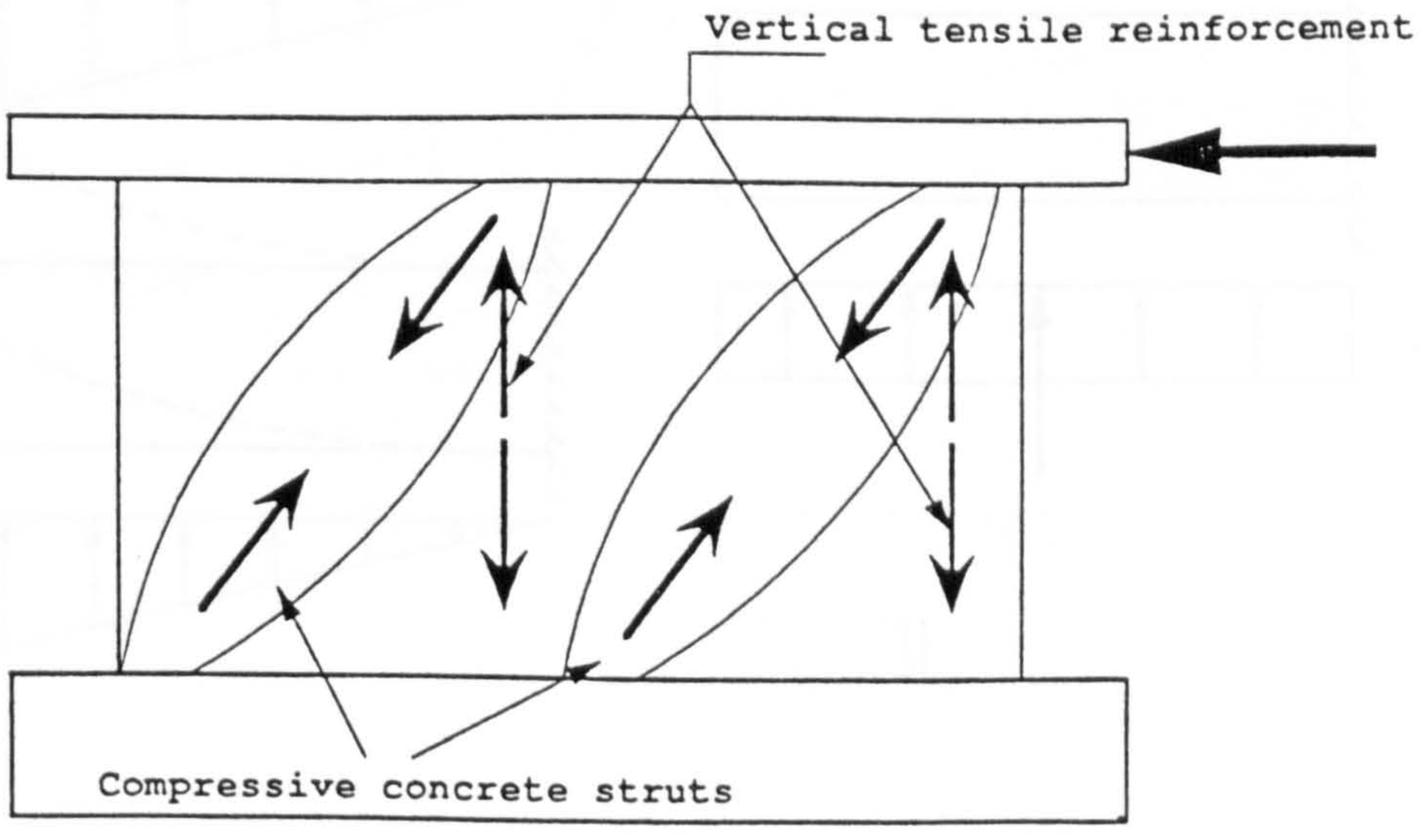


Figure 2.37 Internal forces in wall with low aspect ratio

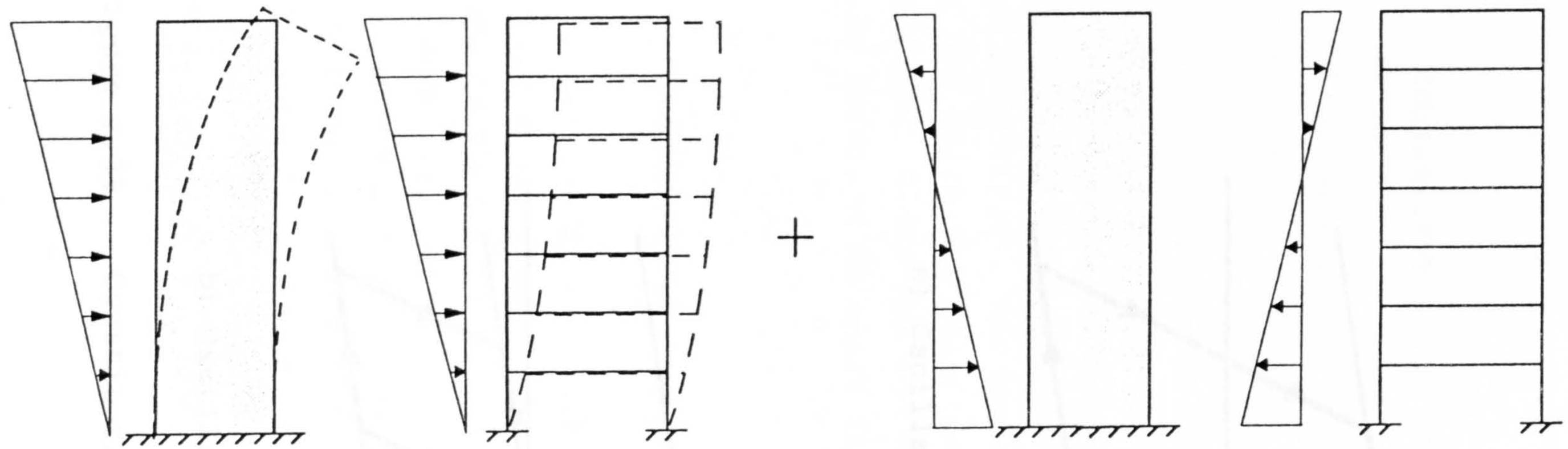
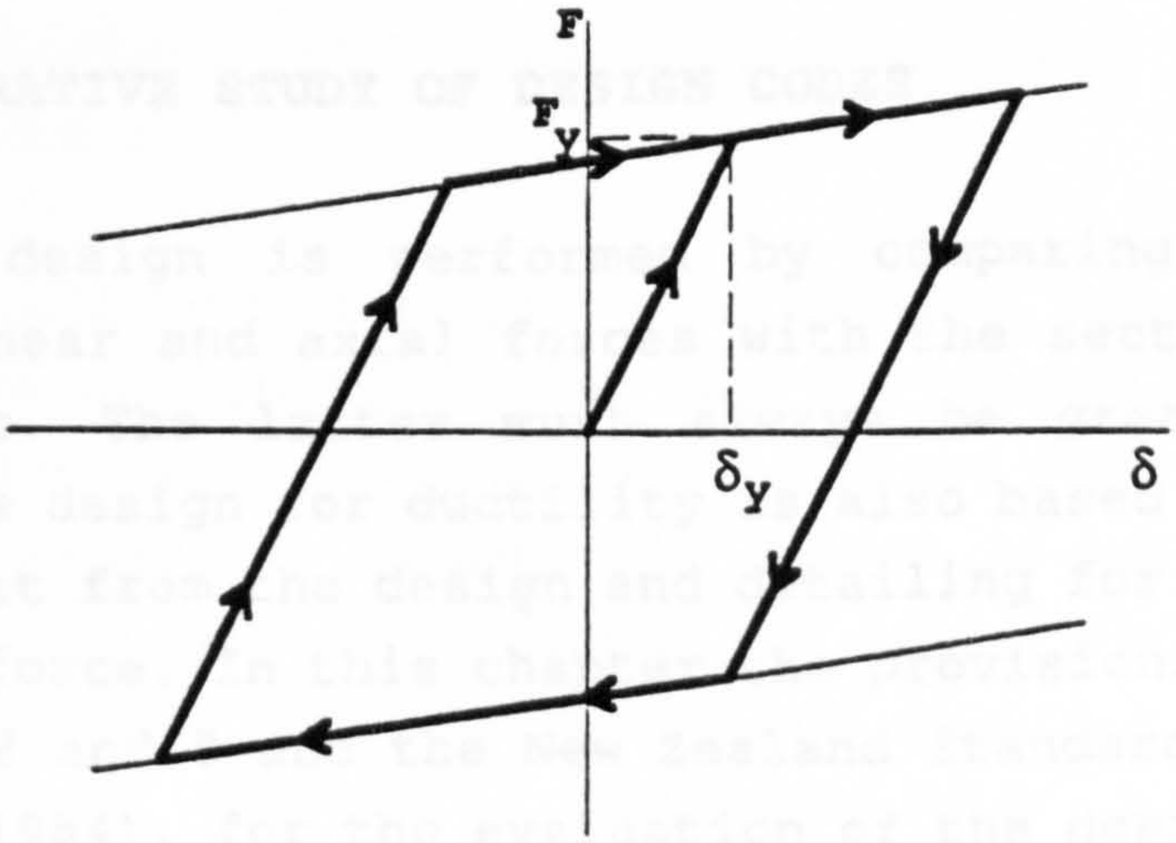


Figure 2.38 Interaction between walls and frames



a) Oscillator 1

b) Oscillator 2

Figure 2.39 Constitutive relationships of oscillators

CHAPTER 3

3 COMPARATIVE STUDY OF DESIGN CODES

Code design is performed by comparing the applied moments, shear and axial forces with the section or member resistances. The latter must always be greater than the former. The design for ductility is also based on parameters which result from the design and detailing for moment, shear and axial force. In this chapter the provisions of ACI, UBC, Eurocodes 2 and 8 and the New Zealand Standards 3101 (1982) and 4203 (1984), for the evaluation of the design resistance of R/C walls are described and in some cases quantitatively compared. Since ACI and UBC are very similar, the latter is only referred to where it differs from ACI.

3.1 Evaluation of Design Strengths

The design strength of reinforced concrete elements is obtained using two different approaches depending on which code is being used. According to ACI, UBC and NZ the design strength is obtained by multiplying the nominal strength by a strength reduction factor. The nominal strength is obtained using the corresponding design assumptions for each case and the specified value of the strength of the materials. According to the Commentary on ACI (1983), the objectives of using the strength reduction factors are:

- To allow for the probability of members having strength lower than the design values due to variations in material strengths and dimensions.

- To allow for inaccuracies in design equations.

- To reflect the level of ductility and the degree of reliability of member behaviour under the load effects being considered.

- To reflect the importance of the member in the structure.

The EC2 and EC8 use a different approach based on partial safety coefficients for the materials. Hence, the design strength of a reinforced concrete member or section is obtained using the respective design assumptions for each case and the design strength of steel and concrete. The design strength for both steel and concrete is obtained by dividing the respective characteristic strength by the corresponding partial safety coefficient. The characteristic strength is defined as that strength below which 5% of all possible strength test results may be expected to fall. According to EC2 the partial safety coefficients take account of :

- The possibility of unfavourable random deviations of the material properties from their specified or estimated characteristic values.

- The uncertainties in the relationship between the material properties in the structure and those measured by standardised tests.

- The conversion between the material properties in the structure and the properties of standardised specimens.

- The inaccuracy, compared with actual behaviour, of the mechanical model for the assessment of the resistance capacity in the limit state equation.

- The possibility of unfavourable random deviations of certain geometrical parameters from their nominal values. (e.g. the dimensions of the cross sections and the position of the reinforcement in these sections).

3.2 Strength Reduction Factors and Partial Safety Coefficients

The partial safety coefficients of the materials prescribed in EC2 for checking the ultimate limit states depend on the load combination and are as given in table 3.1. Those values may be increased if a certain level of quality control is not achieved. Structures subjected to seismic actions are considered to be subjected to accidental loading scenarios.

The strength reduction factors ϕ prescribed in ACI, UBC and NZ for seismic design of structural walls are as given in table 3.2. For members in which f_y does not exceed 415 MPa with symmetric reinforcement and with $(L-d'-d_s)/L \geq 0.7$, ϕ may be increased linearly to 0.9 as ϕN_u decreases from $0.1 f_c A_g$ to zero in the cases of ACI and UBC. This is due to the fact that for members with less axial load it is more likely that failure will be initiated by yielding of the flexural reinforcement, hence a more ductile behaviour will be expected. Also, less variability in strength is expected as the ultimate capacity is more dependent on steel properties.

The value of $\phi=0.6$ for shear in UBC may be increased to 0.85 if the nominal shear strength is greater or equal to the shear corresponding to the development of the nominal flexural strength. The value of ϕ for shear is the sole difference between ACI and UBC, hence only the former will be referred to hereafter. All the results presented in this chapter refer to design strengths, i.e., values obtained using the design strength of steel and concrete in the case of EC and the nominal strength multiplied by the strength reduction factor in the cases of ACI and NZ.

3.3 Specified Properties of the Materials

Concrete compressive strength is often evaluated by means of tests on cubes rather than cylinders. A cube strength of 30MPa, commonly used in practice, is specified. The cylinder strength is obtained by multiplying the cube strength by 0.85, i.e.:

$$f_c = 0.85 * 30 = 25.5 \text{ MPa}$$

The specified yield stress of all the steel reinforcement is 400MPa.

These are also the values of the characteristic stresses for concrete and steel as defined in EC2. The corresponding design stresses are:

$$f_{cd} = \frac{f_c}{\gamma_c} = \frac{25.5}{1.3} = 19.615 \text{ MPa}$$

$$f_{yd} = \frac{f_y}{\gamma_c} = \frac{400}{1.0} = 400 \text{ MPa}$$

3.4 Classification of Buildings Based on Ductility

As already discussed in section 2.2.1 it is usual to take advantage of the nonlinear behaviour of the materials in earthquake resistant design. For this design philosophy to be implemented, structures must possess adequate energy dissipation capacity without a substantial decrease of its overall resistance against horizontal and vertical loading. To this end, local ductility demands should be distributed over most of the structure and not concentrated in a few points. In this respect, EC8 distinguishes between three "Ductility Classes" (DC). No such distinction exist in ACI or NZ, whose provisions apply to all walls.

In EC8, different behaviour factors are assigned to each DC and different rules are given for the application of capacity design principles. It is recommended to adopt a unique DC for a given seismic region. The choice of the DC must be based on local seismicity, economical data and available workmanship considerations.

Three ductility classes (DC) are considered: high "H", medium "M" and low "L". The higher the DC, the better the seismic performance that can be expected. Higher values of the q factors are recommended for the DC "M" and "H" while for the DC "L", the values of the q factors are lower.

According to EC8, limits are imposed on the properties of steel reinforcement and concrete to be used. The higher the DC the more stringent the limits are. The use of concrete class lower than C16 (f_c=16MPa) for DC "L" or C20 for DC "M" and DC "H" is not allowed. Steel reinforcement should fulfil the additional rules of table 3.3. The purposes of these rules are:

(i) To ensure high local ductility in the case of beams with low steel ratio.

(ii) To secure the formation of a sufficiently long PHZ.

(iii) To render the application of capacity design principles more economical.

(iv) To reduce uncertainties in applying capacity design principles.

Since the q factors for walls of structures of DC "L" are close to unity the distinction between the different modes of failure is not needed. For walls in structures of DC "M" and "H", the q factors depend on the likely mode of failure. The distinction between the different modes of

failure can be made following the procedure described in section 2.2.1.1.

The design for shear and ductility also differ for different DC. Hereafter, the provisions for walls of DC "M" and "H" are discussed.

3.5 Flexural Design

3.5.1 Design Assumptions for Flexure

The flexural strength is calculated assuming that plane sections remain plane after deformation. Some codes as ACI and NZ state that for deep flexural members a nonlinear distribution of strains must be considered, but no guidance is given. As far as structural walls are concerned, it is generally accepted that walls with large height to width ratios may be designed as beams assuming a linear distribution of axial strains. This hypothesis is more seriously violated if a high shear force is present, which may be assessed by the shear ratio M/VL. However, as referred to in chapter 2, at ultimate flexural capacity when most of the flexural reinforcement has yielded and therefore stresses are independent of the strains, the departure from the assumption of plane sections has an insignificant effect.

Other design assumptions in flexural design are:

- Full strain compatibility between steel and concrete.
- The tensile strength of concrete is neglected.
- The stress-strain diagram for steel is elastic perfectly plastic, as shown in figure 3.1.

EC2 imposes a maximum steel strain (ε_u) of 0.01 while ACI and NZ impose no limit on the steel strain.

According to ACI and NZ the relation between concrete compressive stress distribution and concrete strain may be assumed to be rectangular, trapezoidal, parabolic or of any other shape that results in prediction of strength in good agreement with results of comprehensive tests. These requirements may be considered satisfied by an equivalent rectangular concrete stress distribution defined by assuming a concrete stress of $0.85f_c$ uniformly distributed over an equivalent compression zone bounded by edges of the cross section and a straight line located parallel to the neutral axis at a distance $g=\beta_1 c$ from the fibre of maximum compressive strains. The definition of β_1 is very similar for both codes as in some parts NZ is a copy or an adaptation of ACI.

In the following the values given refer to ACI and the bracketed values are the corresponding NZ code recommendations. Factor β_1 is taken as 0.85 for concrete strength f_c up to and including 27.6MPa (30MPa). For strengths above that level β_1 is reduced continuously at a rate of 0.05 (0.04) for each 6.7MPa (5MPa) of strength in excess of 27.6MPa (30MPa), but β_1 should not be taken less than 0.65. The maximum concrete compressive strain is $\epsilon_u=0.003$

According to EC2, the maximum concrete compressive strain is $\epsilon_u=0.0035$ in bending or bending with compression and if the section is not all under compression. The idealized stress-strain diagram for concrete is the parabola-rectangle as shown in figure 3.2.

If the section is not fully in compression, a simplified rectangular distribution can be assumed for the compressive stresses as shown in figure 3.3 and defined as follows:

- The stress is equal to zero along a height of 0.2c measured from the neutral axis.

- Along the remaining depth of 0.8c the stress is assumed to be constant and equal to $0.85f_{cd}$.

3.5.2 Comparative Examples

Two rectangular walls with the same cross-section (3000*300mm^2) are considered. Both have the same area of vertical steel reinforcement A_{st}=20100mm^2, what corresponds to a percentage of the gross concrete section of W=2.2%. Wall 1 has the flexural reinforcement concentrated near both edges while Wall 2 has the reinforcement uniformly distributed along the section as shown in figure 3.4. Therefore, the different results may be attributed only to the distribution of longitudinal reinforcement.

In figure 3.5 bending moment - axial force interaction diagrams of both walls are shown. The comparison of both figures shows that much higher resistances are obtained for the wall with the reinforcement concentrated near the edges as in this case the internal lever arm is much higher. The flexural strength of the wall with concentrated reinforcement is also more sensitive to the level of axial force. The concentration of vertical reinforcement near the edges or in the flanges also results in walls with increased curvature ductility when compared with the curvature ductility of walls with distributed reinforcement along the web, as shown in figure 3.6.

The differences between ACI and NZ are due only to the different strength reduction factors. With the exception of the very high levels of axial force, the highest flexural strengths are obtained for EC. This trend changes for high axial forces because the contribution of the concrete becomes more important and the design strength of the concrete is smaller for EC than the specified strength in NZ. Since this effect outweighs the influence of the strength reduction factor ϕ, the flexural strength obtained according to EC decreases in comparison with NZ. Due to the fact that the

walls are designed to resist primarily horizontal loads, they are over-designed for vertical loads. Hence, the level of axial force is generally low; below $0.20f_cA_g$, which corresponds to N=4590KN for Walls 1 and 2. Therefore only the bottom part of the diagrams is of interest as far as most of the practical applications are concerned.

In figure 3.7 the flexural strength of both walls is evaluated for different levels of axial force as a function of the total amount of longitudinal reinforcement. Three levels of axial force are considered, corresponding to the following axial stresses:

$N = 0$ KN

$N = 2066$ KN $= 0.09\ f_c\ A_g$

$N = 4131$ KN $= 0.18\ f_c\ A_g$

The longitudinal reinforcement was varied in proportion to the amounts shown in figure 3.4. keeping the same distribution in both cases. Note that particularly for Wall 1 the amount of vertical reinforcement that corresponds to the higher values of W would not be possible to place in practice because of lack of space. The problem could be resolved by increasing the size of the boundary elements or using flanges if the architectural design allow for it. Otherwise, it would be necessary to redesign the wall.

Figure 3.7 shows higher values of the flexural strength are always obtained for Wall 1. As most of the contribution to the compressive force is provided by the steel, the flexural strength varies almost linearly with the total amount of steel. In the case of Wall 2 as there is a more important contribution of the concrete, the increase in strength corresponding to a given increase in the amount of flexural reinforcement is smaller than for Wall 1. This is more clear for W>1.6%. For Wall 1 the highest resistances are always obtained for EC because there is no strength reduction

factor. For Wall 2 the differences are smaller because the contribution of the concrete is more important and the design stress prescribed by EC is lower than the specified concrete stress of NZ and ACI.

3.6 Shear Design

All codes are based on the same principles. To design against diagonal compression failure, they all impose a maximum nominal shear stress. This shear stress is equal to the shear force divided by the effective cross-sectional area. The values of d used in the examples were:

Wall 1 d = 2850 mm

Wall 2 d = 2400 mm

The design against diagonal tension failure is based on the following equation:

$$V_r \leq V_s + V_c \qquad (3.1)$$

in which the term V_s represents the contribution of the truss mechanism and V_c the contribution of concrete .

3.6.1 Maximum Shear Stress

The maximum nominal shear force according to ACI is:

$$V_{r,n} < 0.83 \sqrt{f_c}\, b\, d \qquad (3.2)$$

For Wall 1, this gives:

Wall 1 $V_{r,n} \leq 0.83 \sqrt{25.5} * 2850 * 300 = 3591000N$

$V_{r,n} \leq 3591$ KN

For Wall 2, it leads to:

Wall 2 $V_{r,n} \leq 0.83 \sqrt{25.5} * 2400 * 300 = 3024000N$

$V_{r,n} \leq 3024$ KN

The corresponding design values can be obtained as the product of the nominal values and the strength reduction factor for shear ϕ=0.85. This gives:

Wall 1, $V_r \leq 3591 * 0.85 = 3052$ KN

Wall 2, $V_r \leq 3024 * 0.85 = 2570$ KN

According to capacity design principles, EC and NZ have different provisions for the zone where a plastic hinge is expected to form and for the rest of the wall.

NZ provisions for the PHZ are as follows:

$$V_{r,n} \leq (0.3\ \phi_o\ S + 0.16)\ \sqrt{f_c}\ b\ d \qquad (3.3)$$

The flexural overstrength factor ϕ_o is equal to the ratio of the overstrength moment of resistance divided by the strength reduction factor, which in this case is ϕ=0.9. The overstrength moment of resistance is higher than the nominal moment of resistance mainly due to hardening of the flexural reinforcement. Hence it is dependent on the steel grade. NZ suggests the following values:

Steel Grade 275 overstrength = 1.25 nominal strength $\phi_o = \frac{1.25}{0.9} = 1.3$

Steel Grade 380 overstrength = 1.40 nominal strength $\phi_o = \frac{1.40}{0.9} = 1.56$

In general the higher the ductility demand, the smaller the value of S. The inclusion of S in equation (3.3) is intended for limiting the maximum shear force in walls of high ductility demand. It has been observed that web crushing may happen at the PHZ of cantilever walls after a few cycles

of displacement ductility of 4 or more. If the ductility demand is smaller, it is considered that higher shear forces can be repeatedly attained without web crushing.

In the examples shown in this chapter the value of ϕ_o used is 1.56. Values of S given in NZ are:

Coupled shear wall S = 0.8

Cantilever wall with limited ductility S = 1.6

The value used in the examples is 1.6. This leads to the following maximum values of $V_{r,n}$ and V_r:

Wall 1 $V_{r,n} \leq (0.3 * 1.56 * 1.6 + 0.16) \sqrt{25.5} * 2850 * 300 =$
$= 3249000N$

$V_{r,n} \leq 3249$ KN

$V_r \leq 0.85 * 3249 = 2762$ KN

Wall 2 $V_{r,n} \leq (0.3 * 1.56 * 1.6 + 0.16) \sqrt{25.5} * 2400 * 300 =$
$= 2736000N$

$V_{r,n} \leq 2736$ KN

$V_r \leq 0.85 * 2736 = 2326$ KN

Outside the PHZ the maximum shear stress is limited to 6MPa or $0.2f_c$ whichever is less.

$0.2\ f_c = 0.2 * 25.5 = 5.1$ MPa

Wall 1 $V_{r,n} \leq 5.1 * 2850 * 300 = 4360500$ N = 4361 KN

$V_r \leq 0.85 * 4361 = 3706$ KN

Wall 2 $V_{r,n} \leq 5.1 * 2400 * 300 = 3672000$ N = 3762 KN

$V_r \leq 0.85 * 3762 = 3121$ KN

EC8 provisions for the PHZ are as follows:

$$V_r \leq 0.2 f_{cd} b d \quad (3.4)$$

Wall 1 $V_r \leq 0.2 * 19.615 * 2850 * 300 = 3354165$ N

$V_r \leq 3354$ KN

Wall 2 $V_r \leq 0.2 * 19.615 * 2400 * 300 = 2824560$ N

$V_r \leq 2825$ KN

Outside the PHZ, EC8 provisions are as follows:

$$V_r \leq 0.3 f_{cd} b d \quad (3.5)$$

Wall 1 $V_r \leq 0.3 * 19.615 * 2850 * 300 = 5031248$ KN

$V_r \leq 5031$ KN

Wall 2 $V_r \leq 0.3 * 19.615 * 2400 * 300 = 4236840$ KN

$V_r \leq 4237$ KN

For walls in structures of DC "L" the provisions for walls in structures of other DC outside the PHZ apply throughout the wall.

3.6.2 Contribution of Concrete to Shear Resistance

According to ACI the contribution of concrete to shear resistance in walls designed for seismic loading is in general:

$$v_{c,n} = 0.166 \sqrt{f_c} \quad (3.6)$$

$v_{c,n}$ = 0.84 MPa

This upper limit may be increased if the shear ratio is low, as shown below:

$$M/VL \leq 2 \quad v_{c,n} = \alpha f_c \tag{3.7}$$

The coefficient α varies linearly from 0.166 for M/VL=2 to 0.249 for M/VL=1.5. For lower values of the shear ratio α=0.249.

The variation of α reflects the higher participation of concrete in shear resistance observed in tests of low rise walls. However, it should be noted that the discussion in section 2.3.1.1 raises doubts about the extension of this provision to the design of the bottom part of walls of multistorey buildings with lower shear ratios.

The provisions of ACI for walls not designed for seismic loading are also to be complied with. Unless a more detailed calculation is made, the maximum value of v_c is given by equation (3.6). A more detailed calculation involves choosing the lesser of the values of $v_{c,n}$ given by the following two formulae:

$$v_{c,n} = 0.27 \sqrt{f_c} + \frac{N_u}{4A_g} \tag{3.8}$$

$$v_{c,n} = 0.05 \sqrt{f_c} + \frac{L\ (0.1 \sqrt{f_c} + N_u\ ./A_g)}{M/V - L/2} \tag{3.9}$$

Equations (3.8) and (3.9) predict the occurrence of inclined cracking at any section through a wall. Equation (3.8) corresponds to the occurrence of a principal tensile stress of approximately $0.33\sqrt{f_c}$ at the centroid of the wall cross-section. Equation (3.9) corresponds approximately to the occurrence of a flexural tensile stress of $0.5\sqrt{f_c}$ at a section L/2 above the section being investigated. The values of v_c computed from equations (3.8) and (3.9) at a section

L/2 or h/2 (whichever is less) above the base also apply to all sections between this section and the base.

The contribution of concrete to shear resistance according to ACI is shown in figure 3.8. as a function of the shear ratio and axial force. All values refer to design strengths, i.e., they are already multiplied by the strength reduction factor for shear ϕ=0.85.

Equation (3.8) always gives higher results than the maximum allowed for walls designed for seismic loading and equation (3.9) is relevant for certain shear ratios if the axial load is small.

According to the principles of capacity design, NZ establishes more stringent provisions for the evaluation of the contribution of concrete in the PHZ than in the rest of the wall.

Equations (3.8) and (3.9) apply throughout the wall and a minimum value of v_c is established for the zones outside the PHZ, as follows:

$$v_{c,n} = 0.2 \sqrt{f_c} = 1.01 \text{ MPa} \qquad (3.10)$$

For the PHZ there is no minimum, yet a maximum is established by equation (3.11) below:

$$v_{c,n} = 0.6 \sqrt{\frac{N_u}{A_g}} \qquad (3.11)$$

The contribution of concrete to shear resistance according to NZ is shown in figure 3.9. Outside the PHZ the contribution of concrete is governed by equation (3.8) for the low values of M/VL and by the minimum value of equation (3.10) for the high values of M/VL. The transition between both levels is established by equation (3.9). In the PHZ equation (3.11) governs the design for low levels of axial force. For the higher levels of axial force equation (3.11)

applies to low levels of M/VL and equation (3.10) otherwise, the transition being made by equation (3.9).

EC8 follows the capacity design philosophy and establishes more stringent provisions for the PHZ. EC8 provisions for the PHZ are as follows:

$$N_u \leq 0.1\ L\ b\ f_{cd} \quad \Rightarrow \quad v_c = 0$$

$$N_u > 0.1\ L\ b\ f_{cd} \quad \Rightarrow \quad v_c = 2.5\ \tau_{rd} = 2.5 * 0.3 = 0.75\ MPa$$

The value of τ_{rd} is defined in EC2 and depends on the concrete compressive strength. Outside the PHZ, EC8 provisions are as follows:

$$N_u \leq 0.1\ L\ b\ f_{cd} \quad \Rightarrow \quad v_c = 2.5\ \tau_{rd} = 0.75\ MPa$$

$$N_u > 0.1\ L\ b\ f_{cd} \quad \Rightarrow \quad v_c = 2.5\ \tau_{rd}\ \beta_2 = 0.75\ \beta_2$$

$$\beta_2 = 1 + M_o\ /\ M$$

M_o is the moment that produces a maximum tensile stress equal to the longitudinal stress due to the axial force (both calculated using linear elastic constitutive relationships). For a rectangular section:

$$\sigma = \frac{N_u}{bL} = \frac{M_o}{bL^2/6} \qquad M_o = \frac{N_u\ L}{6}$$

$$\beta_2 = 1 + M_o\ /\ M = \frac{N_u\ L\ /\ 6}{VL\ \ (M\ /\ VL)}$$

$$\lambda_o = M\ /\ VL$$

$$v_c = 0.75 \left(1 + \frac{N_u\ /\ V}{6\ \lambda_o}\right) \qquad (3.12)$$

In figure 3.10 the value of v_c outside the PHZ according to EC8 is evaluated as a function of the shear ratio M/VL as

in the previous figures and for different values of N/V. The provisions for the walls of structures of DC "M" and DC "H" outside the PHZ and with high axial forces apply throughout in walls of structures of ductility class "L".

It is difficult to perform a direct comparison of EC with ACI and NZ because v_c does not depend on the same parameters, but some comments can be made. The most noticeable feature is the large difference between the different codes particularly for low shear ratios. This reflects the uncertainties that still exist regarding the evaluation of the contribution of concrete to shear resistance, as referred to in section 2.3.1.1. EC8 is in general the most conservative code. NZ is the code that relies more on the contribution of concrete if no yielding of the tensile reinforcement is expected. Another important feature is the much higher contribution of concrete outside the PHZ for EC and NZ, particularly NZ.

3.6.3 Design of Horizontal Shear Reinforcement

In all codes horizontal shear reinforcement is calculated according to the truss analogy, using equation (3.13) below:

$$\left(\frac{A_s}{s}\right)_h = \frac{V_s}{a\ f_y} \qquad (3.13)$$

Shear reinforcement is designed to withstand a shear force equal to the factored shear force for the specified code loading less the contribution of the concrete, as depicted in equation (3.1). EC uses f_{yd} instead of f_y. "a" represents the internal lever arm of the truss model and assumes the following values:

EC $\quad a = 0.9\ d$

ACI, NZ $\quad a = d$

According to ACI and NZ the nominal strength has to be multiplied by the strength reduction factor ϕ=0.85 to obtain the design strength. This is numerically equivalent to considering a lever arm a=0.85d. Therefore, for a certain variation in the amount of shear reinforcement, the variation in the design strength is slightly higher for EC than for ACI and NZ.

If the shear ratio λ_o=M/VL is smaller than 1.3, equation (3.13) does not apply in the case of EC8. In this situation the following empirical formula is proposed:

$$\left(\frac{A_s}{s}\right)_h (\lambda_o - 0.3) + \left(\frac{A_s}{s}\right)_v (1.3 - \lambda_o) = \frac{V_s}{a\ f_y} \qquad (3.14)$$

For walls of structures of DC "L" equation (3.13) applies for all shear ratios.

NZ establishes a minimum amount of horizontal shear reinforcement which may control the design for walls with low shear ratios, according to the following formula:

$$\rho_h = \frac{4}{3}\left(\frac{\rho_i}{\lambda_o}\ \frac{d_x}{d} - \frac{v_c}{f_y}\right) \qquad (3.15)$$

This is intended to avoid that diagonal tension failure developed before yielding of the flexural reinforcement if the shear ratio is low.

3.6.4 Comparison of Design Strengths

In figures 3.11, 3.12 and 3.13 the design shear strengths for the different codes and situations (in the PHZ or outside it) are expressed as a function of the amount of distributed horizontal web reinforcement. The contribution of concrete is calculated considering the section of Wall 1. The axial force levels are the same as referred to in 3.5.2 for the examples concerning the flexural strength. Three levels

of the shear ratio are considered as indicated in the figures, except for the case of N=0, because the results for λ_o=2 are equal to the results for λ_o=5.

The figures show that the largest discrepancies between the different codes occur for low values of the shear ratio and axial force. It is also for low shear ratios that the highest values of shear resistance are obtained as a consequence of higher values of the contribution of concrete. This question has already been discussed in section 2.3.1.1. It was then pointed out that these code provisions are the result of experimental observations from tests with boundary conditions that may not provide an adequate representation of the true situation in the bottom region of walls of multistorey buildings.

The figures also show considerable discrepancies on the values of the maximum allowable shear force. The lower slope of the EC curves for λ_o=1 is due to the factor (λ_o-0.3) in equation (3.14).

3.6.5 Provisions for Sliding Shear

NZ has no specific requirements concerning sliding shear in walls. There are provisions for beams, where it is necessary to provide diagonal reinforcement for shear stresses above certain levels. Nevertheless it is recommended that in walls with very high shear stresses or squat walls with flanges, diagonal reinforcement is used to resist part of the shear force. The only code that has provisions for sliding shear is EC8. To avoid the latter mode of failure, the shear force must be smaller than the value calculated as follows:

$$V_r \leq V_{dd} + V_{id} + \mu_{fr} \min N_u \qquad (3.16)$$

$$V_{dd} = 1.5\ \Sigma A_{st} \sqrt{f_{cd}\ f_{yd}}$$

$$V_{id} = 2\ \Sigma A_i\ f_{yd}\ \cos\varphi$$

$$\mu_{fr} = 1/3$$

To provide some guidance with regard to the situations in which sliding shear is likely to affect the design and the most important parameters involved, figure 3.14 is presented. The sliding shear resistance V_{ss} of Wall 1 and Wall 2 was calculated for the 3 values of the axial force indicated in figure 3.14. The shear force corresponding to the flexural capacity V_f was evaluated as a function of the shear ratio. Figure 3.14 presents the ratio V_{ss}/V_f as a function of the shear ratio for the different cases. If $V_{ss}/V_f \geq 1$ then sliding shear does not control the design of the wall. The wall would reach its flexural capacity before this type of failure could occur.

Figure 3.14 shows that Wall 2, which has the flexural reinforcement distributed along the web, is less prone to sliding shear failure than the wall with flexural reinforcement concentrated in the edge members. This is due to the fact that Wall 2 needs more flexural reinforcement than Wall 1 to achieve a certain flexural capacity. This increases the dowel action effect which increases the sliding shear resistance. The influence of the axial compressive force is positive, as it enhances the resistance to sliding shear more than the flexural capacity. However, figure 3.14 shows that the most important parameter is the shear ratio. For values of $M/VL \geq 1.4$ sliding shear failure is unlikely to occur. For lower values of M/VL the walls are more prone to sliding shear failure. This is the case of the walls described in chapter 4, which are expected to fail by sliding shear if diagonal tension failure is prevented. This corresponds to the situation represented by the left hand side of the bottom inclined line in figure 3.14. Therefore, the experimental results will help to assess EC8 provisions for sliding shear.

3.6.6 Provisions for Vertical Web Reinforcement

Besides specifying minimum amounts of vertical web reinforcement, some codes have more stringent provisions, especially for walls designed for seismic loading.

According to ACI, the amount of vertical web reinforcement must be evaluated using equation (3.17) given by:

$$\rho_n = 0.0025 + 0.5\ (2.5 - M / V L)\ (\rho_h - 0.0025) \qquad (3.17)$$

A minimum value of ρ_n, which does not need to be larger than ρ_h, is also established as given below:

$$\rho_n \geq 0.0025$$

The inclusion of the shear ratio in equation (3.17) reflects the observations from tests of low rise walls which indicate that vertical web reinforcement becomes effective in resisting shear, while the efficiency of the horizontal web reinforcement is expected to decrease. Again it is stressed that this may be a result of the boundary conditions in those tests which allowed a direct transfer of load to the foundations. ACI also specifies the following for walls designed for seismic loading:

$$\lambda_o \leq 2 \quad \Rightarrow \quad \rho_n \geq \rho_h$$

According to EC8 vertical web reinforcement is calculated using equation (3.14) if $\lambda_o<1.3$. If $\lambda_o \geq 1.3$ the vertical web reinforcement may be calculated as follows:

$$\left(\frac{A_s}{s}\right)_v = \frac{V - V_c - \min N_u}{d\ f_{yd}} \qquad (3.18)$$

The use of this formula will lead to amounts of vertical web reinforcement similar to the amount of horizontal shear reinforcement for the low values of N.

For walls of DC "L" only nominal vertical web reinforcement is needed.

3.7 Design for Ductility

3.7.1 Critical Zones

ACI does not follow capacity design principles and it may be necessary to design for ductility at any level along the height of a wall. The code specifies that boundary elements with special transverse reinforcement are necessary at any level in a wall where the maximum extreme compressive fibre stresses exceed $0.2f_c$. The stress must be calculated using a linear elastic model and gross section properties. The compressive stress of $0.2f_c$ is an index value and is not intended for the description of the actual state of stress that may develop at critical sections. The size of the boundary elements (figure 3.15) must be such that they carry all factored gravity loads on the wall, as well as the vertical force required to resist the overturning moment calculated from factored earthquake storey shear forces.

According to the capacity design philosophy it is necessary to design for ductility only in the zones where yielding of the main flexural reinforcement is expected; at the base of the walls. For codes that obey the capacity design philosophy, the length of the PHZ may be calculated as shown in figure 3.16

According to NZ it is necessary to confine the outer half of the compression zone if the neutral axis depth exceeds the value of c given below:

$$c = 0.10\ \phi_o\ S\ L \qquad (3.19)$$

or

$$c = \frac{8.6\ \phi_o\ S\ L}{(4 - 0.7\ S)\ (17 + H\ /\ L)} \qquad (3.20)$$

According to EC8 it is necessary to confine the part of the compression zone where $\varepsilon \geq 0.0015$. This must be evaluated for the maximum axial force and bending moment corresponding to the earthquake action. It is noteworthy that according to EC2 the maximum compressive strain in the concrete is $\varepsilon_u = 0.0035$. Therefore, for a rectangular section this provision enforces the confinement of 60% of the compression zone. Thus EC8 provisions are slightly more stringent than the NZ regulations.

3.7.2 Design of Confinement Reinforcement

Confinement reinforcement serves four main purposes:

- It increases the compressive strain capacity of concrete. Hence, the extreme compressive fibres which may undergo large strains due to large ductility demand must be properly confined.

- It provides lateral support to the main vertical reinforcement avoiding buckling of the bars.

- Together with the vertical bars forms a basket that contains the concrete core of the edge members.

- It is also thought that confinement reinforcement may have an effect on the strength of edge members but this is difficult to express reliably in terms of apparently critical material properties.

ACI specifies that the total cross-section area of rectangular hoop reinforcement should not be less than that given by equations (3.21) and (3.22) below.

$$\left(\frac{A_s}{s}\right)_{cr} = 0.3\ h_c\ \frac{f_c}{f_y}\left(\frac{A_{gb}}{A_{ch}} - 1\right) \qquad (3.21)$$

$$\left(\frac{A_s}{s}\right)_{cr} = 0.12\ h_c\ \frac{f_c}{f_y} \qquad (3.22)$$

The spacing of the confinement reinforcement should not be more than one quarter of the thickness of the wall or 100mm. According to NZ the area of rectangular hoops should be the larger of the two values calculated as follows:

$$\left(\frac{A_s}{s}\right)_{cr} = 0.3\ h_c\ \frac{f_c}{f_y}\ \left(\frac{A_{gb}}{A_{ch}} - 1\right)\left(0.5 + 0.9\ \frac{c}{L}\right) \qquad (3.23)$$

$$\left(\frac{A_s}{s}\right)_{cr} = 0.12\ h_c\ \frac{f_c}{f_y}\ \left(0.5 + 0.9\ \frac{c}{L}\right) \qquad (3.24)$$

The spacing of the hoops should not be less than 6 times the diameter of the longitudinal bars, one half the thickness of the confined region of the wall or 150mm.

NZ also enforces the use of transverse tie reinforcement to avoid buckling of the longitudinal bars, if the ratio of longitudinal reinforcement ρ_n exceeds $2/f_y$. The provisions for this are as follows:

- Ties suitably shaped should be arranged so that each longitudinal bar or bundle of bars, placed close to the wall surface, is restrained against buckling by a 90° bend or at least a 135° standard hook of a tie. When two or more bars not more than 200mm apart (centre to centre) are so restrained, any bars between them are exempted from this requirement.

- The area of one leg of a tie, A_{te}, in the direction of potential buckling of the longitudinal bar, shall be computed from equation (3.25) below, where ΣA_b is the sum of the areas of the longitudinal bars reliant on the tie, including the tributary area of any bars exempted

from being tied in accordance with the previous paragraph.

$$A_{te} = \frac{\Sigma A_b}{16} \frac{s}{100\ mm} \qquad (3.25)$$

where s is the spacing of the ties in mm. Longitudinal bars centred more than 75mm from the inner face of stirrup ties need not be considered in determining the value of ΣA_b.

- The spacing of ties along the longitudinal bars should not exceed six times the diameter of the longitudinal bar to be restrained.

The design of confinement reinforcement according to EC8 is aimed at providing a certain curvature ductility at the plastic hinge zone of the walls. The curvature ductility demand may be evaluated as follows:

$\mu_{1/r} = 1.2\ q^2$ for uncoupled walls

$\mu_{1/r} = 1.0\ q^2$ for coupled walls

The influence of the DC in the curvature ductility demand is considered within the value of the q factor.

The amount of confinement reinforcement (figure 3.17) necessary to provide the required curvature ductility may be calculated as follows:

$$W_{wd} = 0.9 \sqrt[3]{\mu_{1/r}}\ (0.01\ \mu_{1/r} + 0.15\ \frac{A_{gb}}{A_{ch}} + \max N_r - 0.4) \qquad (3.26)$$

$$N_r = \frac{N_u}{b\ L\ f_{cd}}$$

$$W_{wd} = \frac{\text{volume of stirrups and cross ties}}{\text{volume of confined concrete}} \frac{f_{yd}}{f_{cd}}$$

$$W_{wd} = \frac{4\ b_o\ A_{sw}}{b_o^2\ s}\ \frac{f_{yd}}{f_{cd}}$$

The following limits are also imposed:

DC "H" $W_{wd} \geq 0.2$ $s \leq b_o / 4$

DC "M" $W_{wd} \geq 0.15$ $s \leq b_o / 3$

For walls of structures of DC "L", W_{wd} may be evaluated as follows:

$$W_{wd} = \min \begin{cases} 1.45 \left(0.10 \frac{A_{gb}}{A_{ch}} + \max N_r - 0.37\right) \\ 0.10 \end{cases}$$

$s \leq b_o / 2$

EC8 also allows another method of evaluating the necessary amount of confinement reinforcement, applicable only to walls of rectangular cross section, as given below:

$$\mu_{1/r} = \min \begin{cases} \frac{\varepsilon_{cu}}{\varepsilon_{cy}}\ \frac{1 - \xi_{sy}}{\xi_{cu}} \\ \frac{\varepsilon_{su}}{\varepsilon_{sy}}\ \frac{1 - \xi_{sy}}{1 - \xi_{su}} \end{cases}$$

ε_{cu} - concrete strain at post-peak 0.85 f_{ck} level in the stress-strain diagram of confined concrete.

ε_{sy} - tensile steel strain at yield.

ε_{su} - uniform tensile steel strain at failure.

ξ_{cu} - normalized neutral axis depth at the post failure 85% strength level when concrete strain is critical.

ξ_{sy} - normalized neutral axis depth at yield of tensile steel.

ξ_{su} - normalized neutral axis depth when the tensile steel strain is critical.

EC8 provides constitutive relationships for confined concrete which can be used to evaluate some of the variables defined above.

The minimum amount of cross-ties to avoid local instability of the vertical bars is:

$4\ \phi\ 8\ /\ m^2$ for steel S400

$4\ \phi\ 10\ /\ m^2$ for steel S220

The quantitative comparison between the different code provisions for the design of confinement reinforcement is not straightforward, since they are not a function of the same parameters, but a very important qualitative comment can be made.

The need for confinement reinforcement in NZ and EC8 is restricted to the PHZ while in ACI it may be necessary at any level of a wall. ACI also has more stringent provisions concerning the spacing of the confinement reinforcement which makes steel fixing more difficult. The design according to NZ and EC8 demands more flexural reinforcement to provide the excess strength that is necessary for the wall to remain elastic above the PHZ. The cost associated with the provision of more flexural reinforcement is probably less than the cost associated with the provision of confinement reinforcement in large parts of the wall (Paulay, 1980), especially due to the high cost of workmanship to place the confinement

reinforcement. Hence, the codes based on the capacity design philosophy lead to a more rational and, in general, more economical design of reinforced concrete walls.

3.8 Provisions to Avoid Local Instability

In ACI the only provisions are the ones referred to in 3.7.1 regarding the dimensions of the boundary elements.

Both NZ and EC8 impose minimum values of thickness in some parts of the sections of the walls in the PHZ. The NZ code gives:

If $c \geq 4\,b$ and $c \geq 0.3\,L \Rightarrow$
$\Rightarrow b \geq h_s / 10$ in the outer half of the compressive zone.

This requirement may be waived in any part of a wall at a distance smaller than "3b" of a flange with a width of at least $h_s/5$. The EC8 provisions recommend the following:

$$l_c \geq \begin{cases} 2b \\ 0.2\,L \end{cases} \Rightarrow b \geq \begin{cases} 200\ mm \\ h_s\ /10 \end{cases}$$

$$l_c \leq \begin{cases} 2b \\ 0.2\,L \end{cases} \Rightarrow b \geq \begin{cases} 200\ mm \\ h_s\ /15 \end{cases}$$

This requirement only applies in the confined part of the section of the wall. If the most compressed edge of the wall is connected to a flange with adequate dimensions ($L \geq h_s/5$ and $b \geq h_s/15$), than if $l_c < 3b$:

$$b \geq \begin{cases} 150\ mm \\ h_s/\ 20 \end{cases}$$

This provisions do not apply to walls of DC "L".

3.9 Final Remarks

It was shown in section 3.5 that the differences in flexural design between the different codes are due essentially to the strength reduction factors and partial safety coefficients. Hence, they are not due to the hypothesis on which the calculations are based. This reflects the fact already referred to in section 2.3.1, that there are no significant disagreements concerning flexural design.

The results presented in section 3.6 show that extremely large differences still exist between different codes in the design for shear. These differences are not only numerical but also conceptual, as the parameters used to calculate the "concrete contribution" and the maximum allowable shear force are not the same for all codes. Most of the code provisions for shear, with the exception of the truss analogy formula, are empirically derived and are not backed by any theory describing the shear transfer mechanisms. This indicates that the present state of disagreement regarding the evaluation of the shear strength of R/C members is a consequence not only of the scatter of the experimental data, but also of a lack of understanding of the shear transfer mechanisms.

The calculation of the plastic hinge length in NZ and EC8 is similar. However, for walls with low shear ratios these provisions lead to a PHZ almost up to the point of contraflexure. This is compatible with observations from tests of low rise walls, in which the stresses in the vertical reinforcement were reported to be uniform along the height. However, in the author's opinion, the uniform steel stress is a consequence of the unrealistic boundary conditions leading to direct transfer of stresses from the loading beam to the foundations. This would lead to shorter lengths of the PHZ. This issue is further discussed in

section 6.4 considering the experimental results described in chapter 4, which were obtained in tests where more realistic boundary conditions were used.

TABLES

Combination	γ_c (concrete)	γ_s (steel)
Fundamental	1.5	1.15
Accidental	1.3	1.0

Table 3.1 - Partial safety coefficients (EC2)

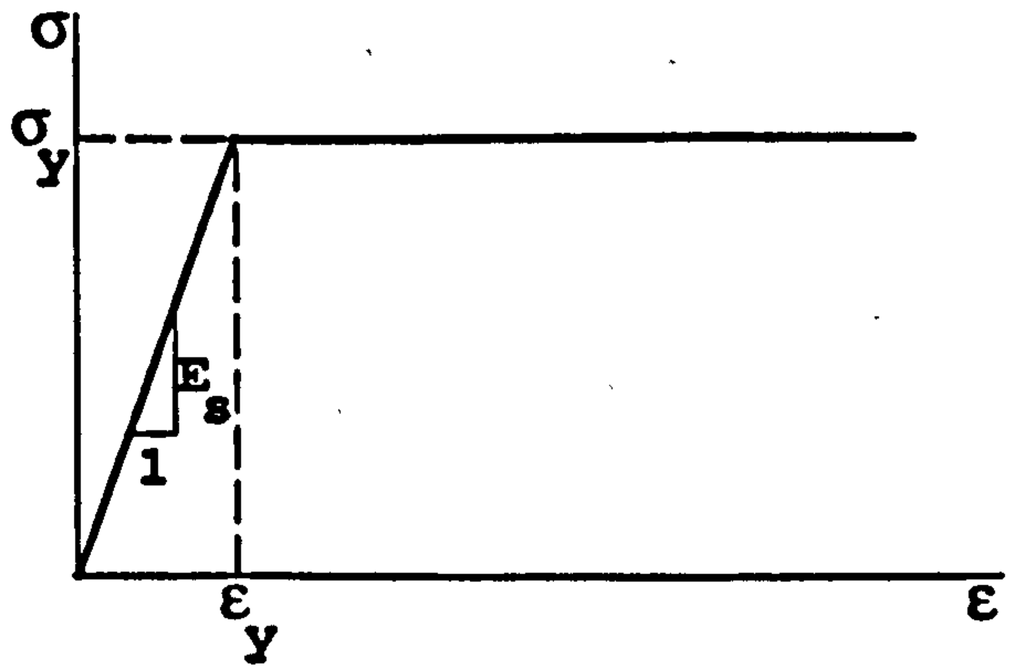
	ϕ - ACI	ϕ - UBC	ϕ - NZ
Shear	0.85	0.6	0.85
Flexure Nu = 0	0.9	0.9	0.9
Flexure Nu $\leq$ 0.1 f_c Ag	0.7	0.7	0.9

Table 3.2 - Strength reduction factors (ACI, UBC, EC8)

		DC L	DC M	DC H
(i)	Strain at failure	$\geq$ 6%	$\geq$ 9%	$\geq$ 12%
(ii) (iii)	Tensile failure strength to yield ratio	$\geq$ 1.2	$\geq$ 1.25 $\leq$ 1.45	$\geq$ 1.3 $\leq$ 1.45
(iv)	Actual to nominal yield strength ratio		$\leq$ 1.25	$\leq$ 1.15

Table 3.3 - Limit Characteristics of steel reinforcement (EC 8)

FIGURES



$\sigma_y = f_y$ in the cases of ACI and NZ

$\sigma_y = f_y / \gamma_s$ in the case of EC

Figure 3.1 Stress-strain diagram for steel

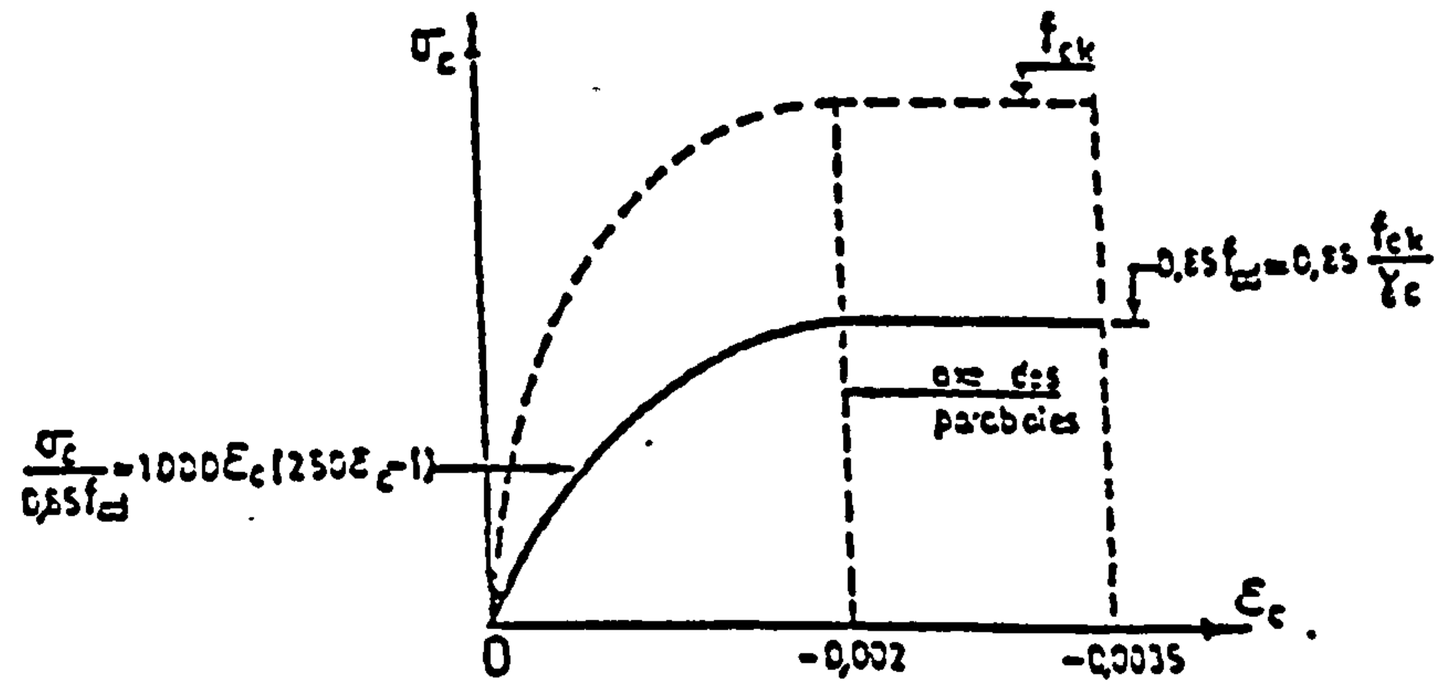


Figure 3.2 Parabolic/rectangular stress block for concrete (EC2)

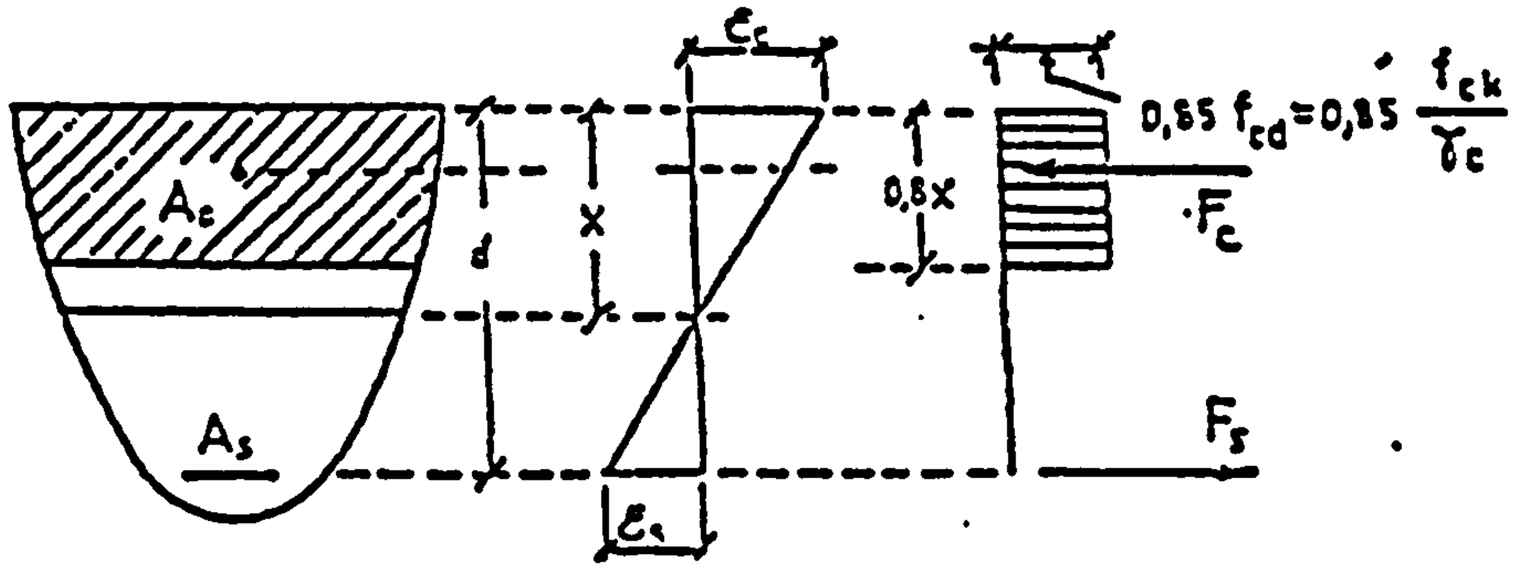
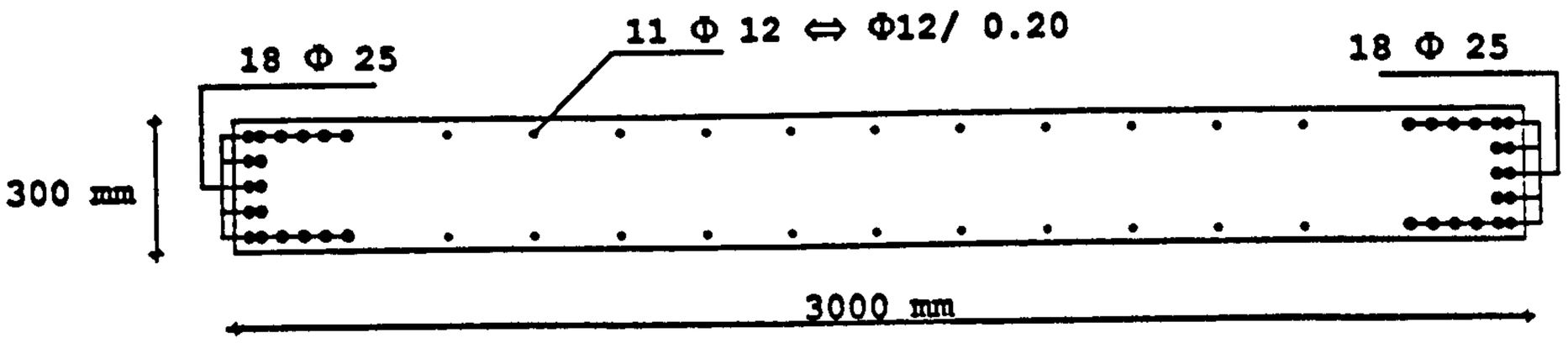
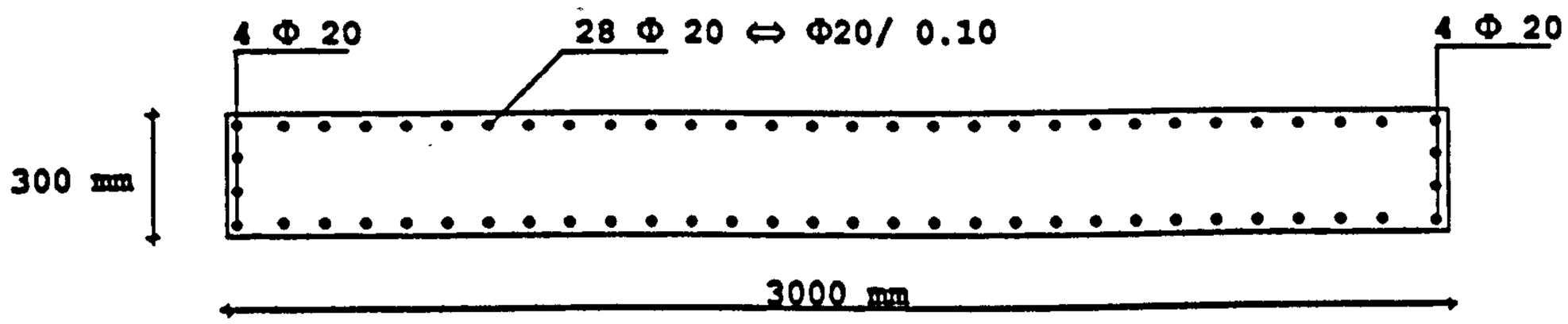


Figure 3.3 Rectangular stress block for concrete (EC2)

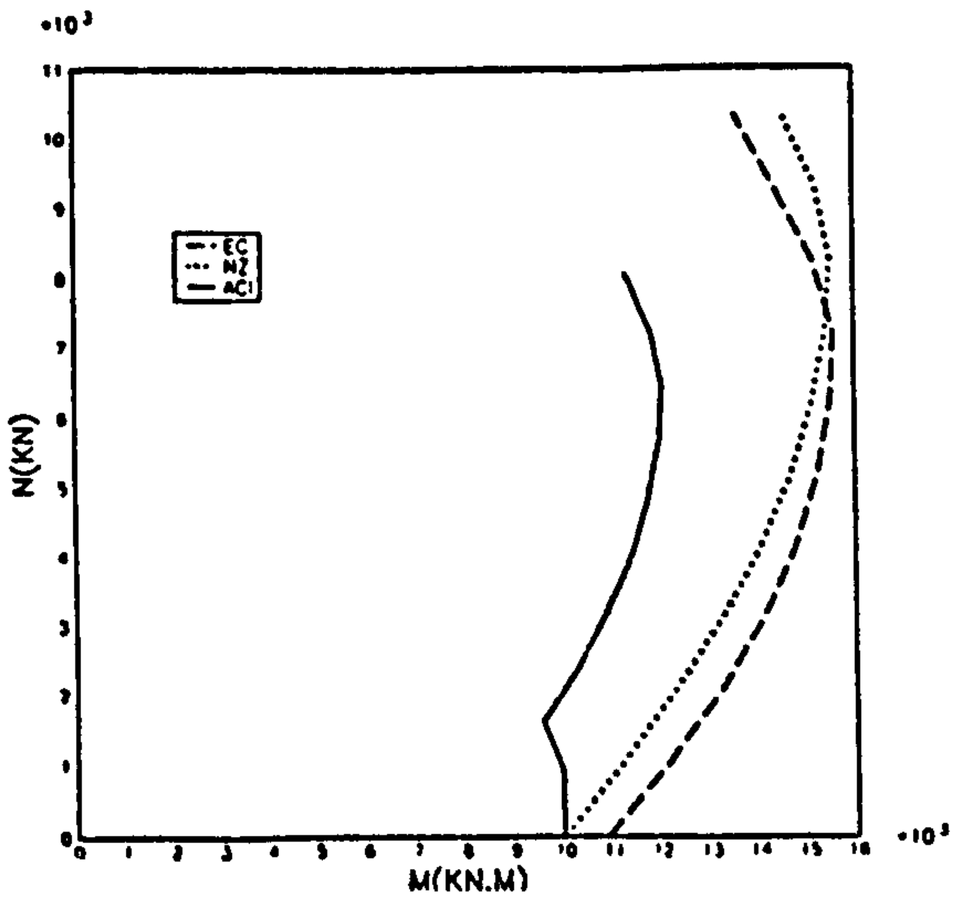


a) Wall 1

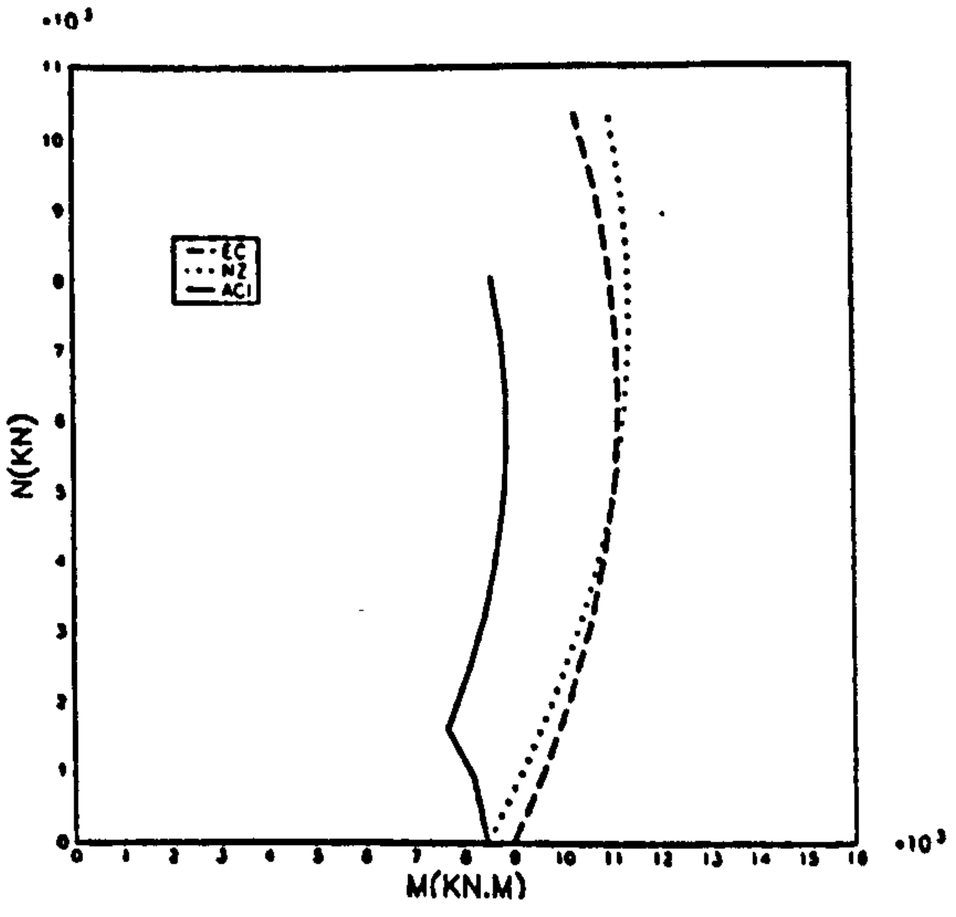


b) Wall 2

Figure 3.4 Cross-section of the walls



a) Wall 1



b) Wall 2

Figure 3.5 Bending moment axial-force interaction diagrams

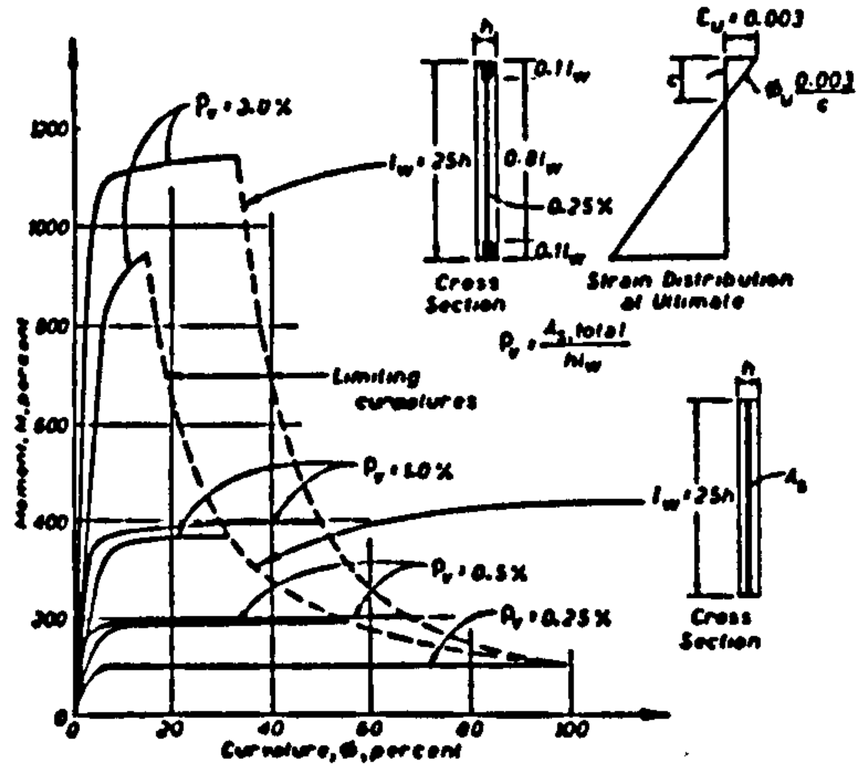
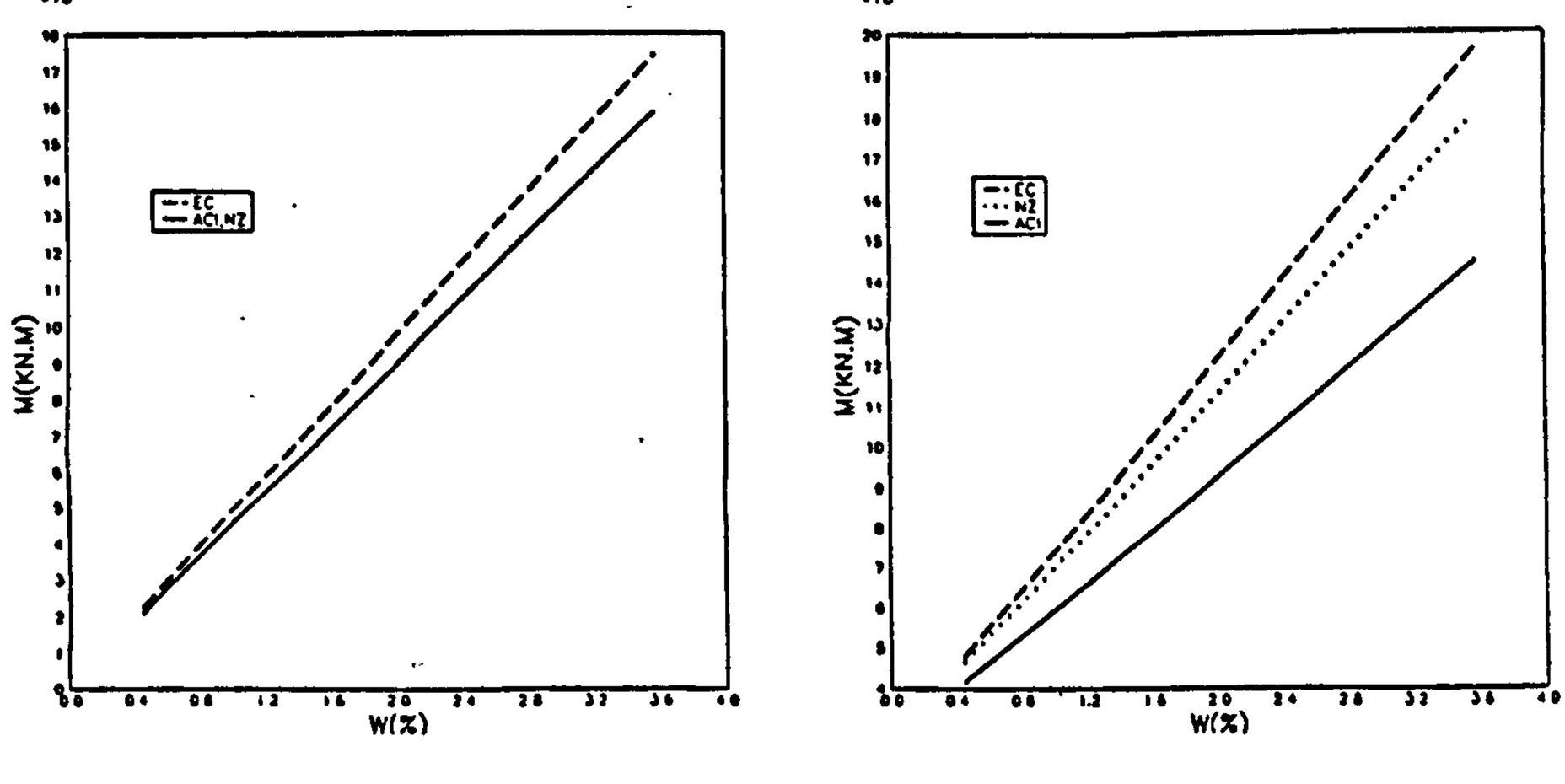
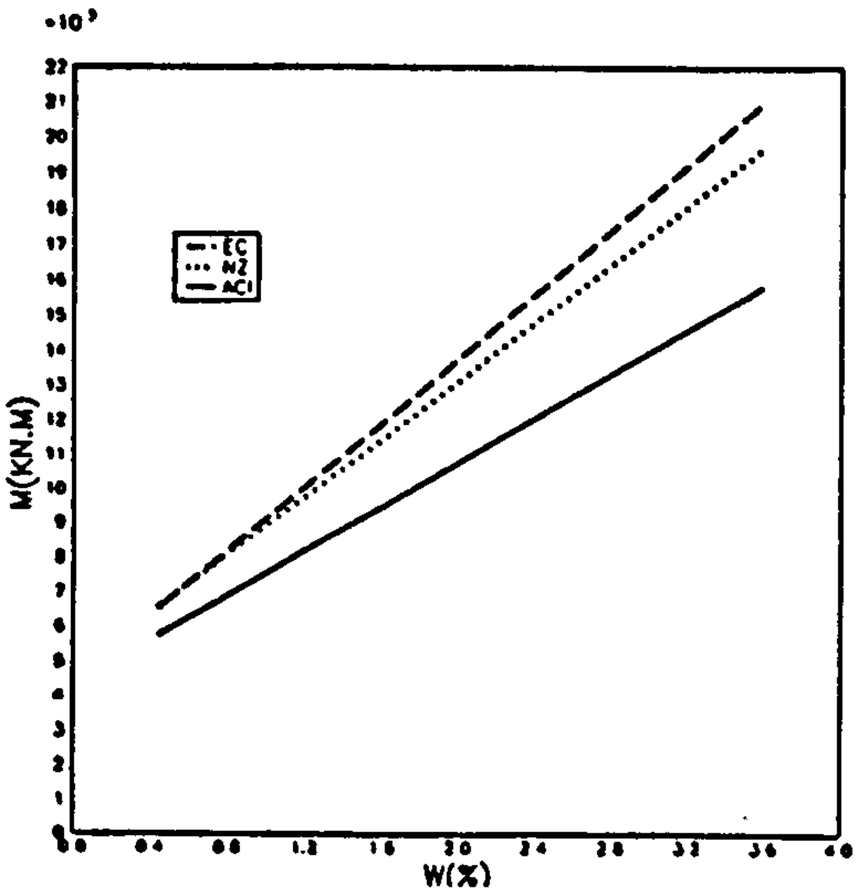


Figure 3.6 Effect of amount and distribution of vertical reinforcement on ultimate curvature (Cardenas and Magura, 1973)

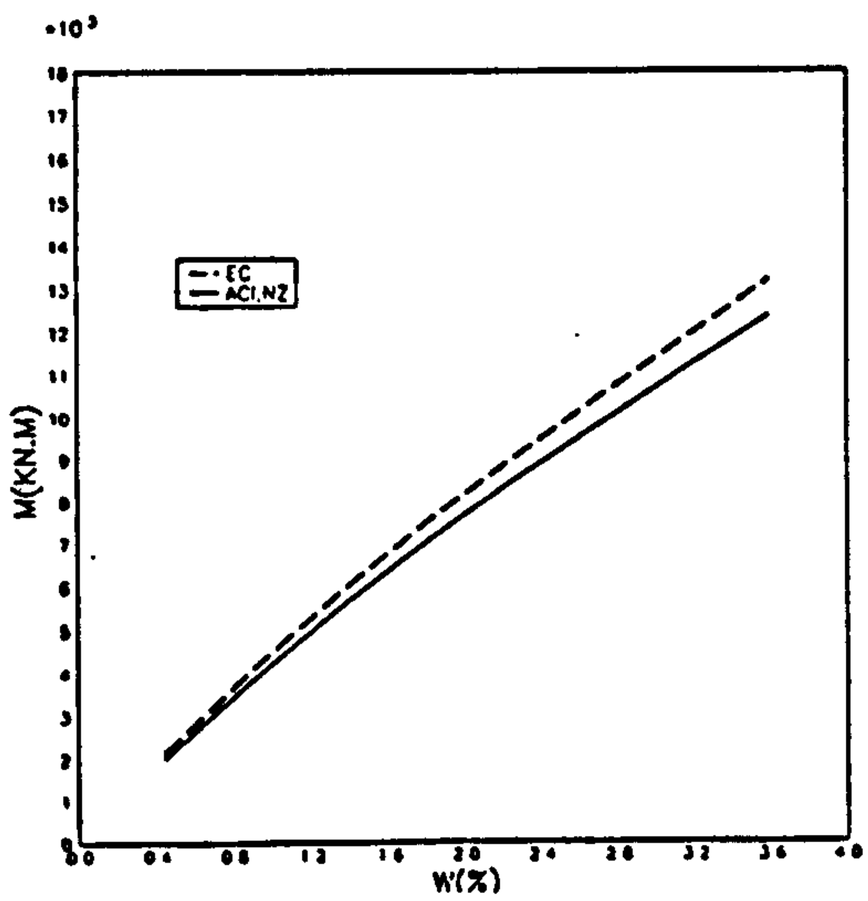


a) Wall 1 N = 0 b) Wall 1 N = 2066 KN

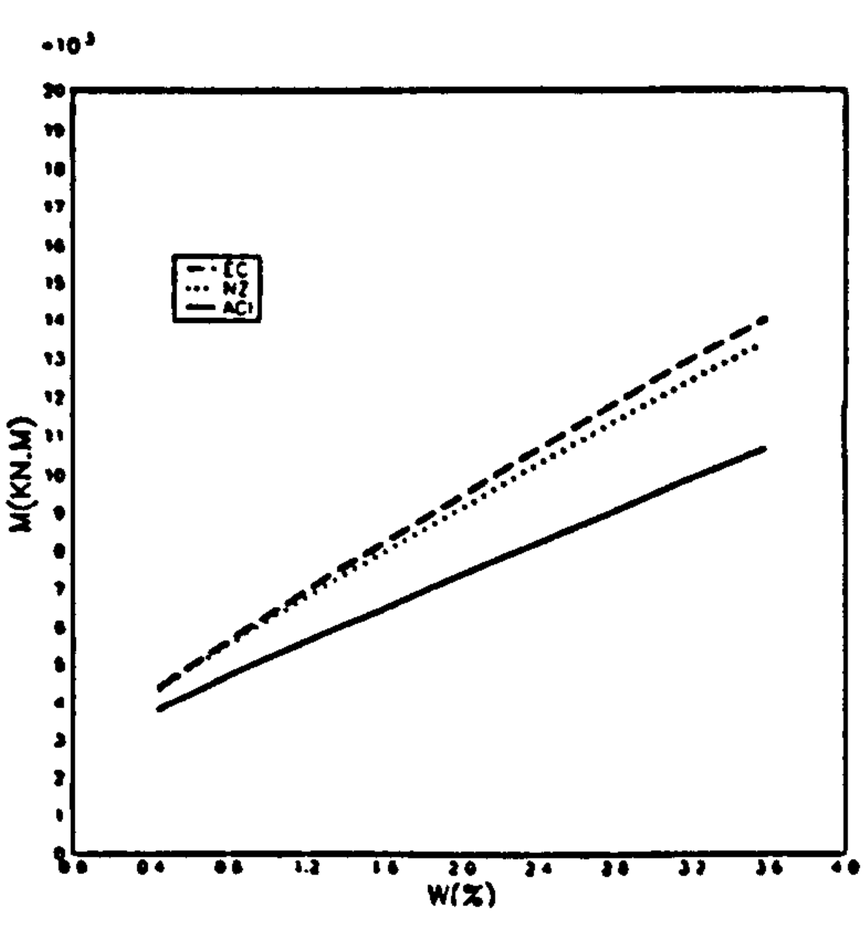
Figure 3.7 Flexural strength



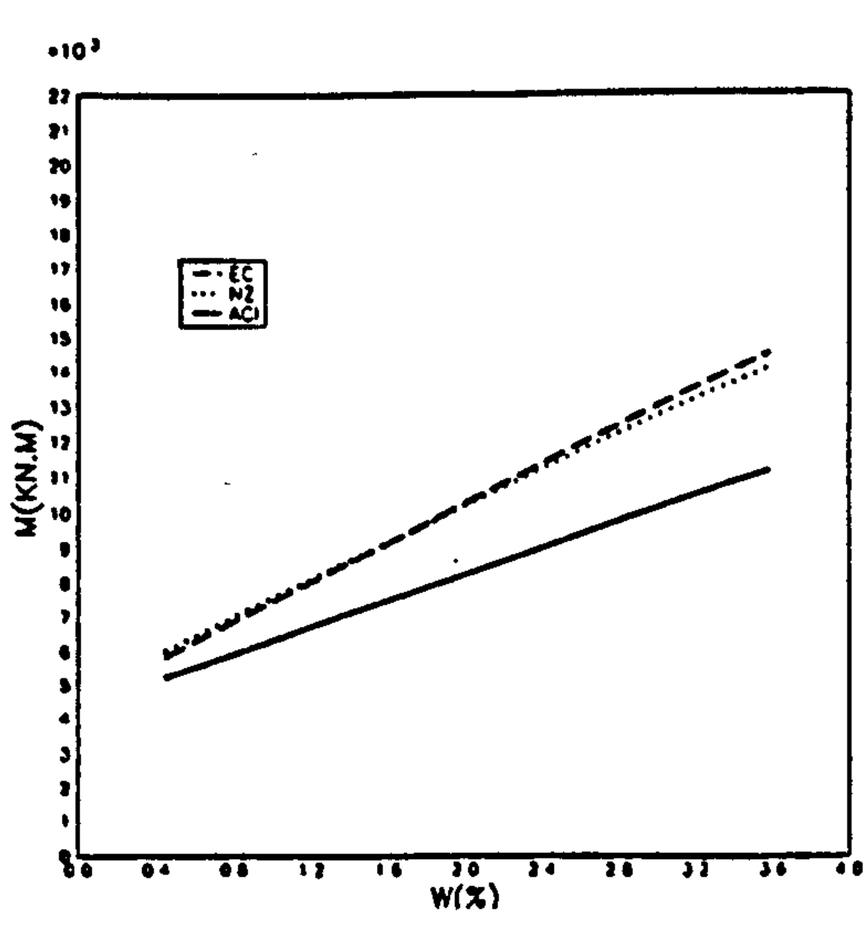
c) Wall 1 N = 4131 KN



d) Wall 2 N = 0



e) Wall 2 N = 2066 KN



f) Wall 2 N = 4131 KN

Figure 3.7 Flexural strength (cont.)

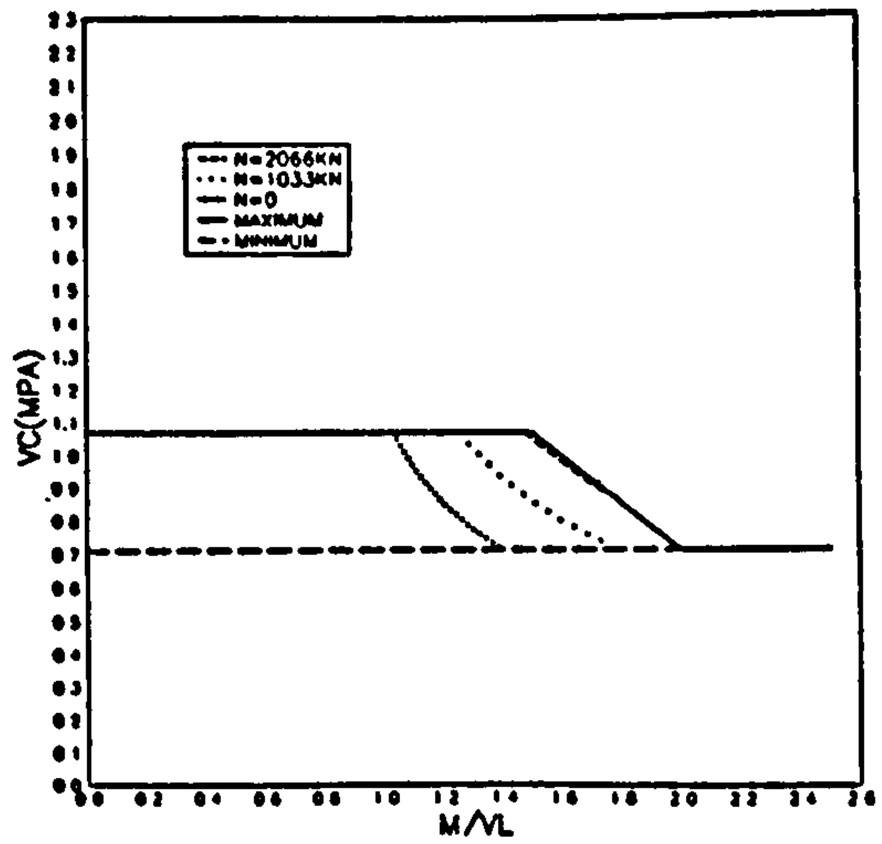
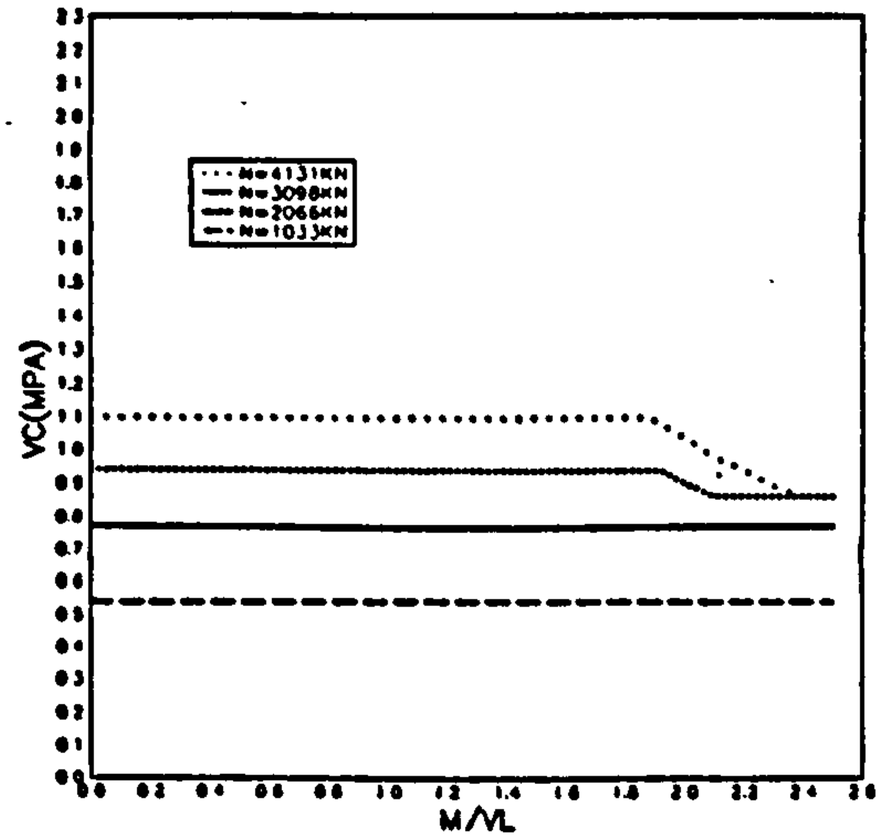
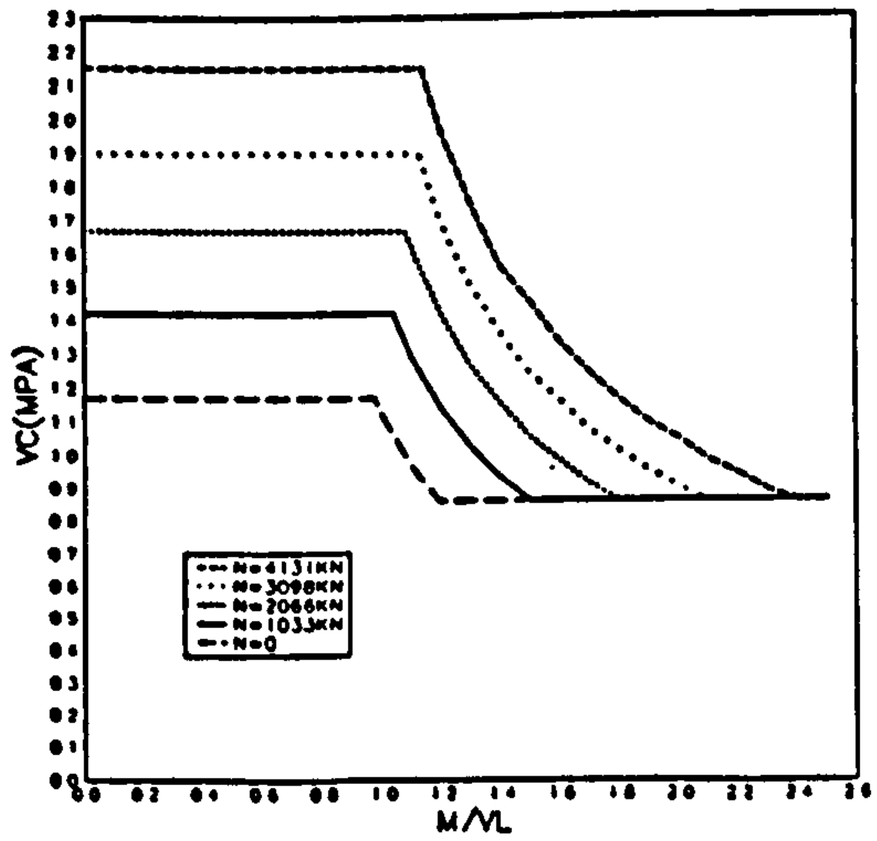


Figure 3.8 ACI - contribution of concrete



a) In the PHZ



b) Outside the PHZ

Figure 3.9 NZ - contribution of concrete

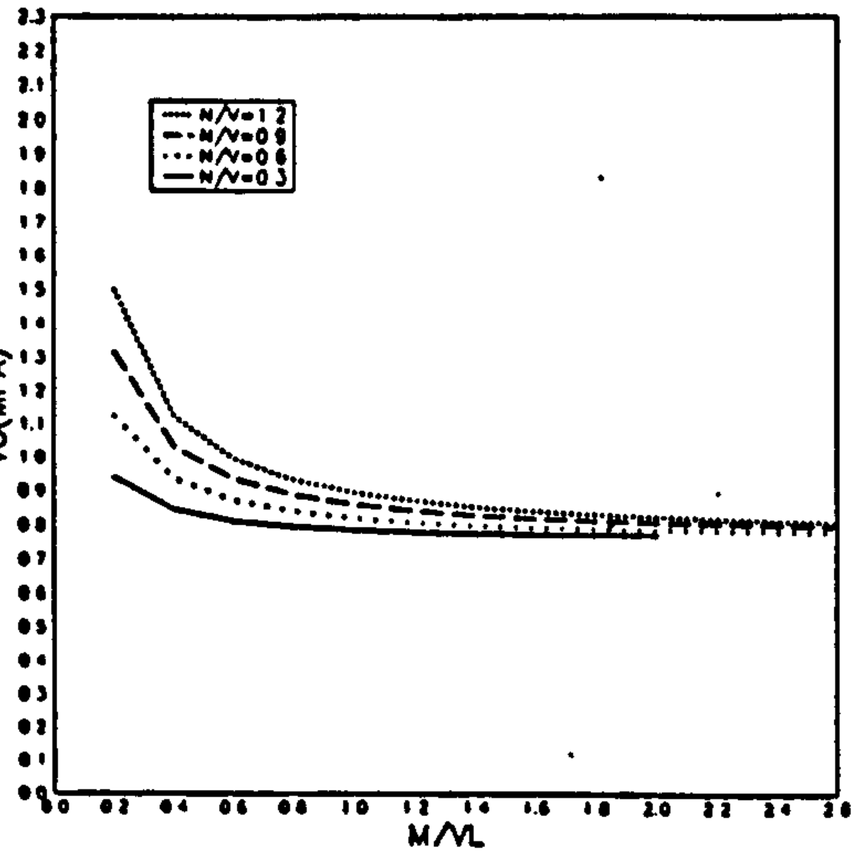
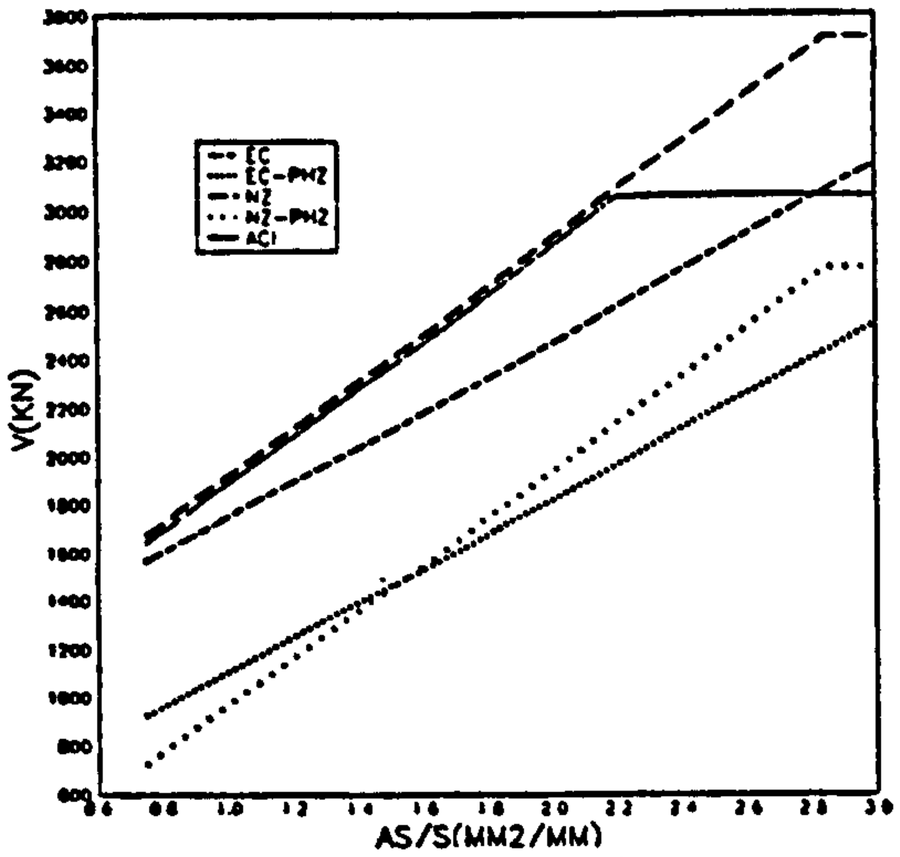
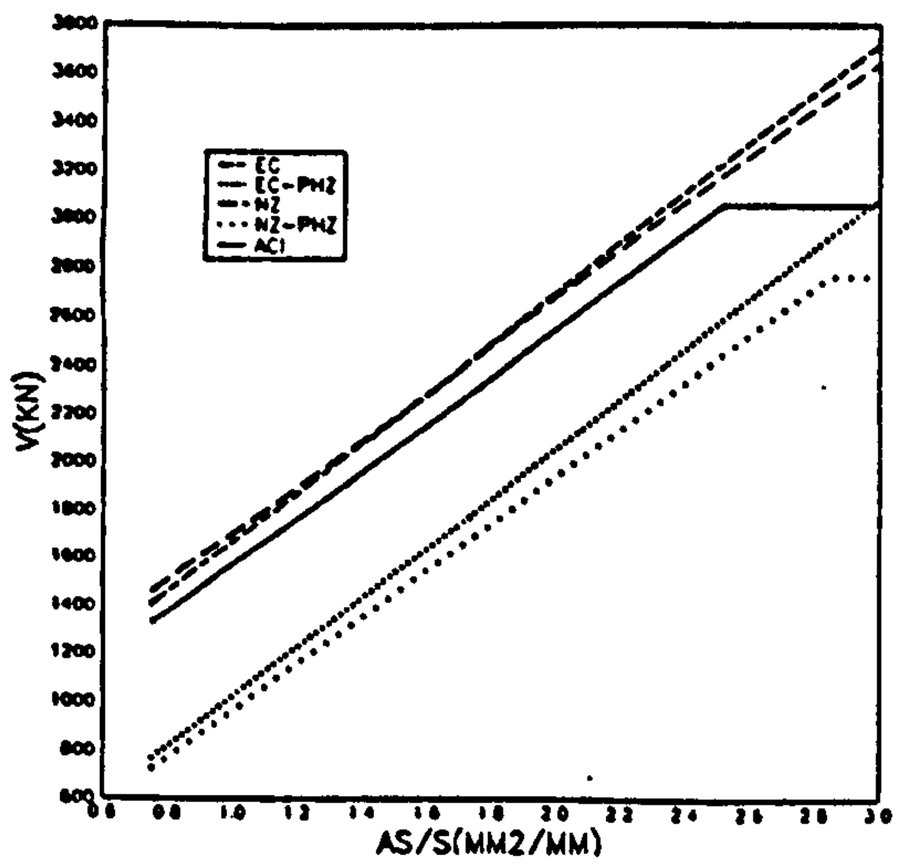


Figure 3.10 EC8 - contribution of concrete outside the PHZ

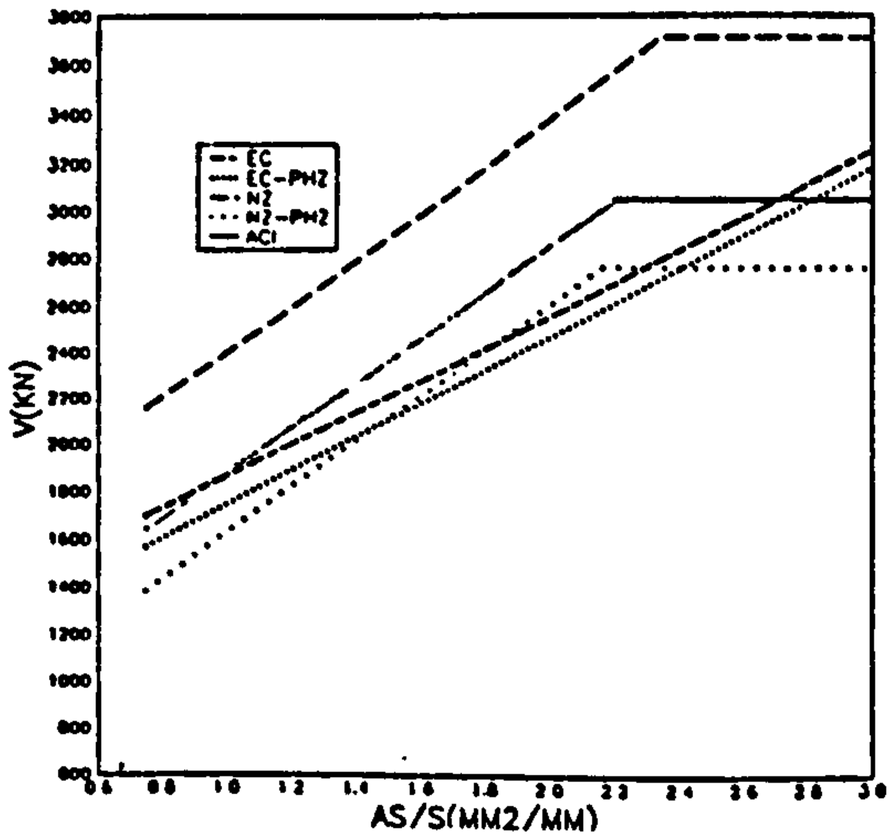


a) M / V L = 1

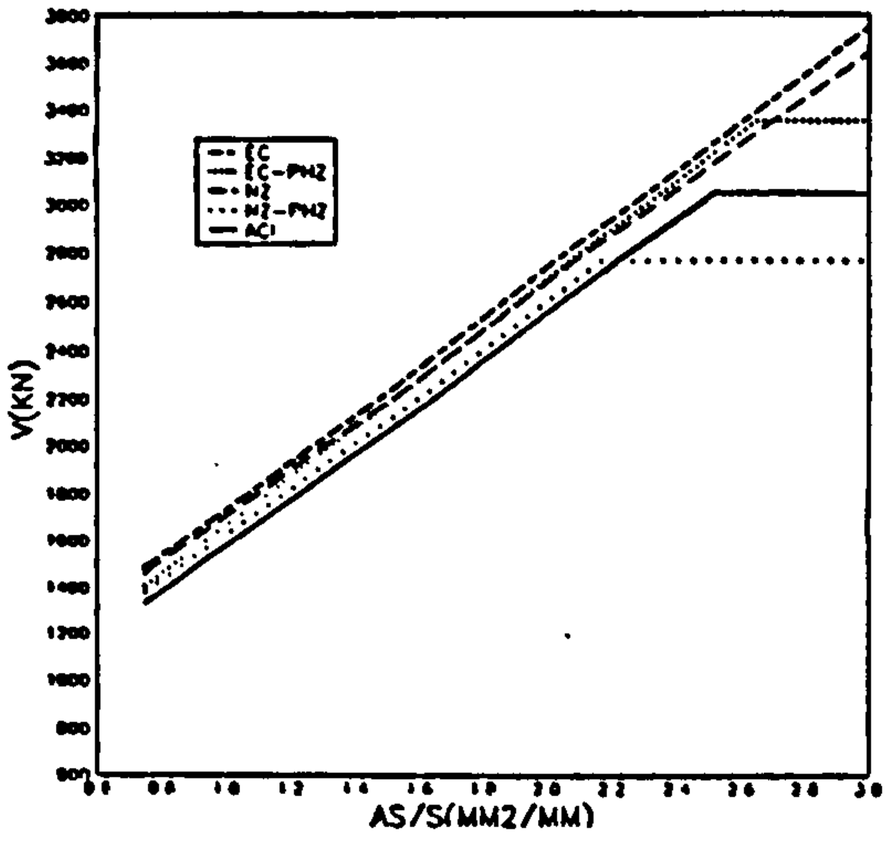


b) M / V L = 2

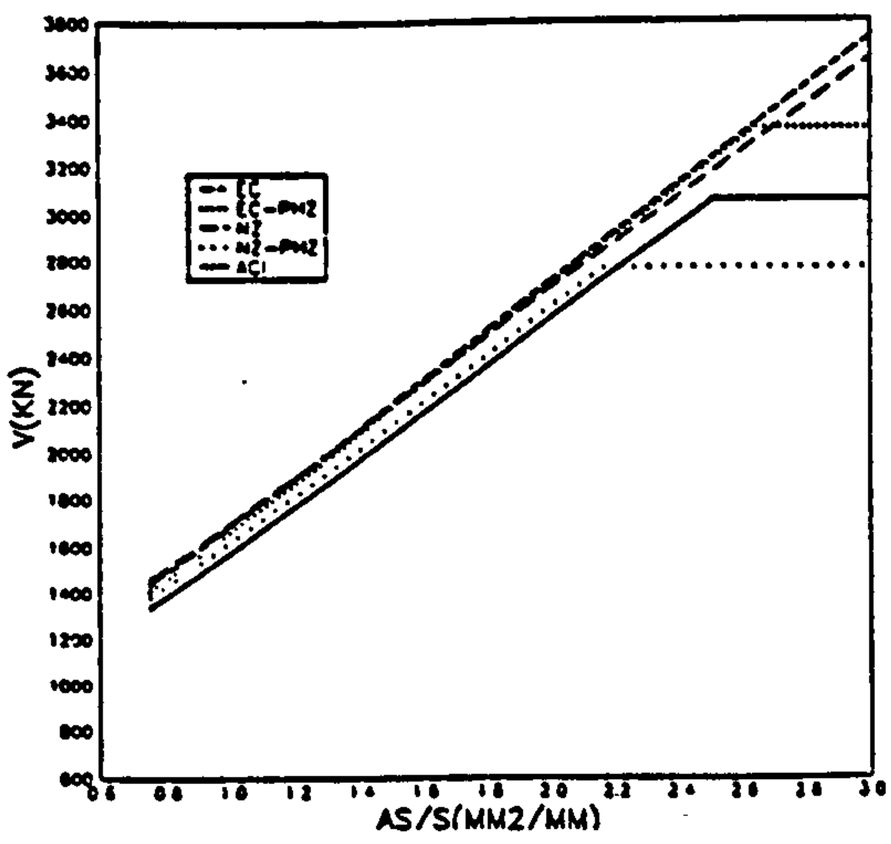
Figure 3.11 - Shear resistance of Wall 1 for N = 0



a) M / V L = 1

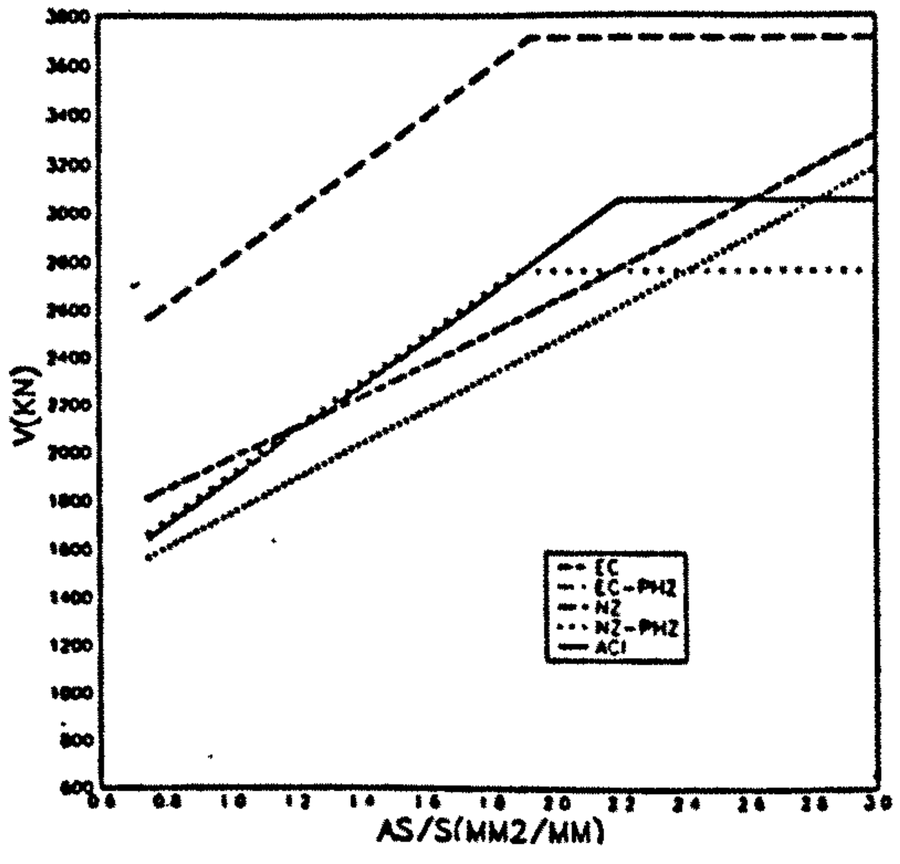


b) M / V L = 2

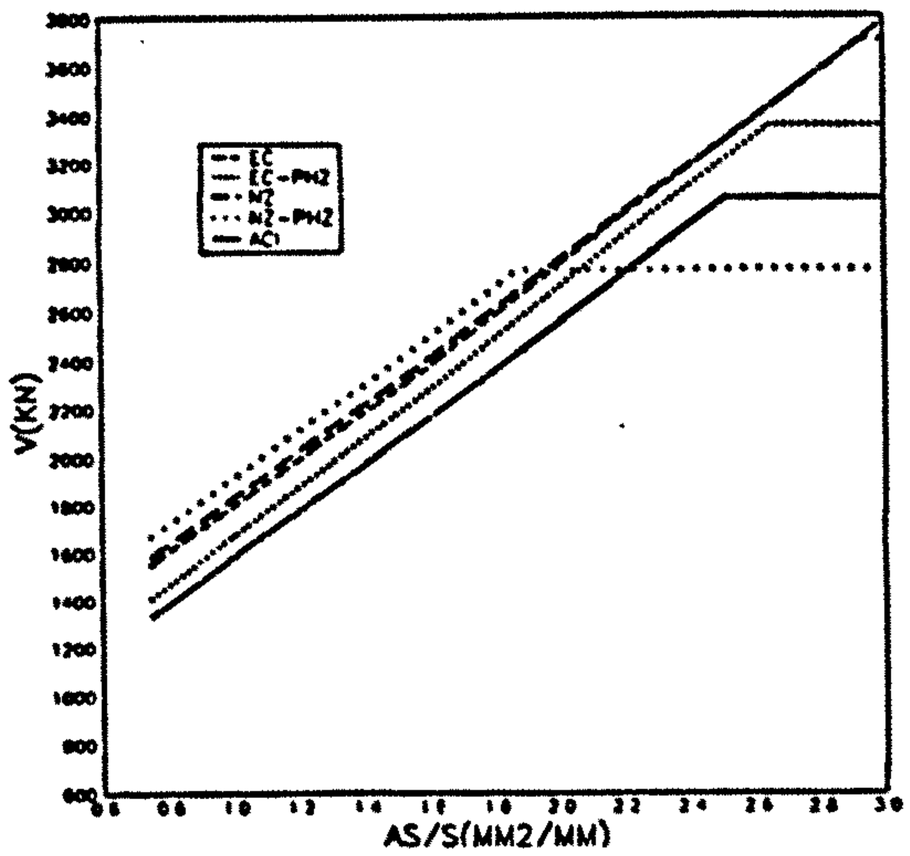


c) M / V L = 5

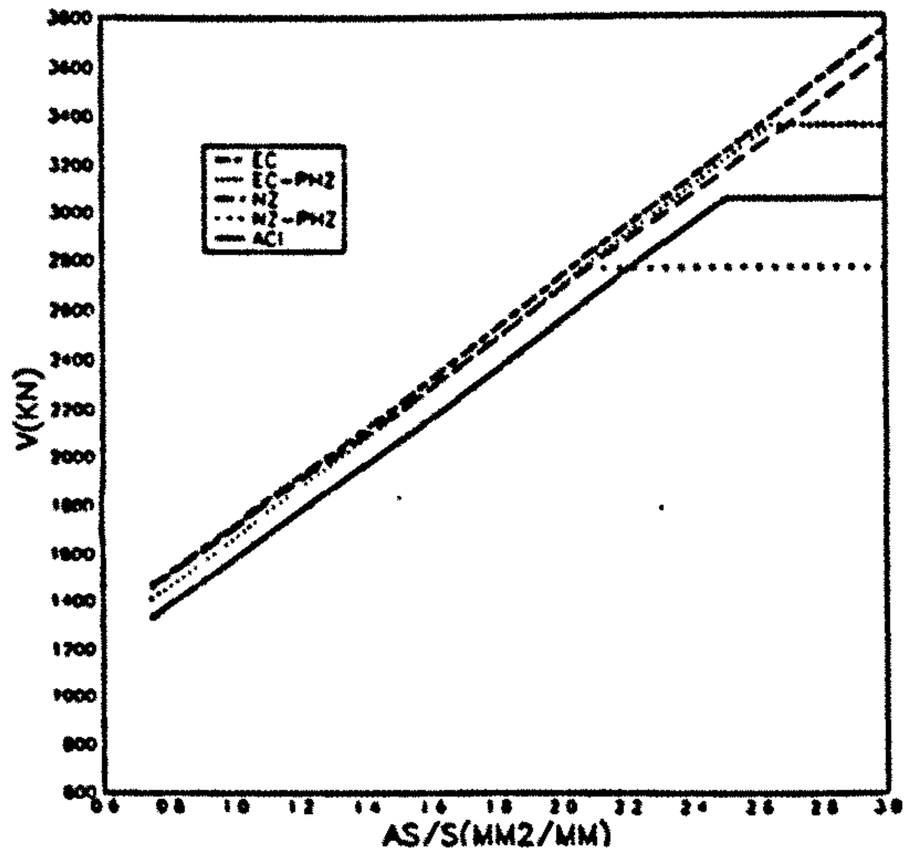
Figure 3.12 Shear resistance of Wall 1 for N = 2066 KN



a) M / V L = 1



b) M / V L = 2



c) M / V L = 5

3.13 Shear resistance of Wall 1 for N = 4131 KN

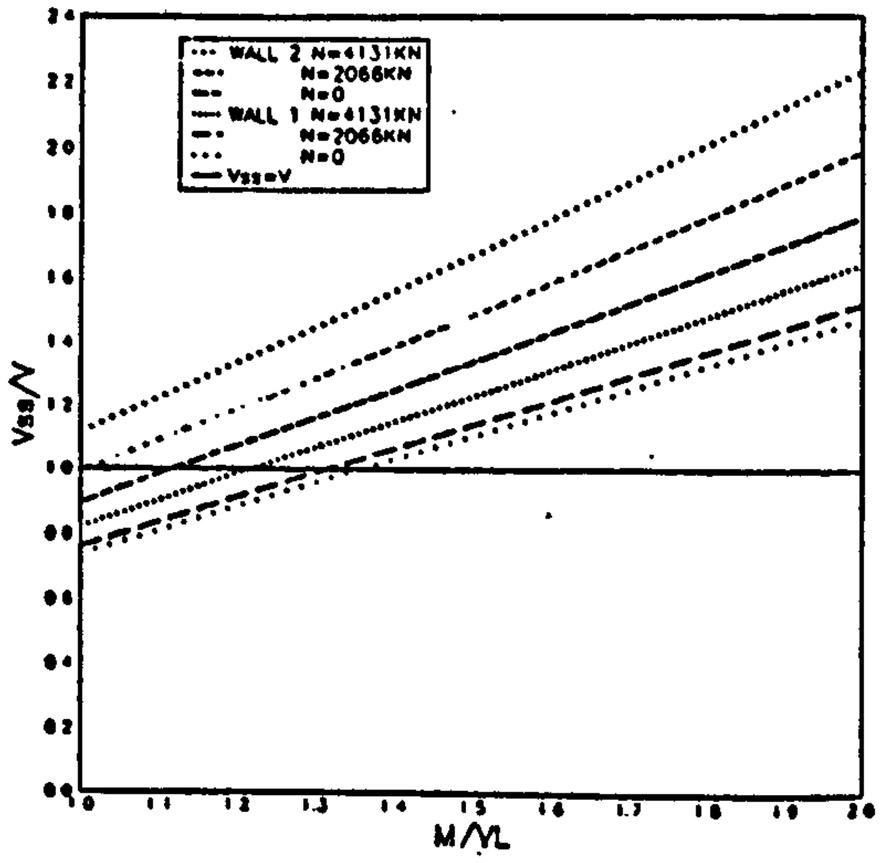


Figure 3.14 Sliding shear resistance of Wall 1 and Wall 2

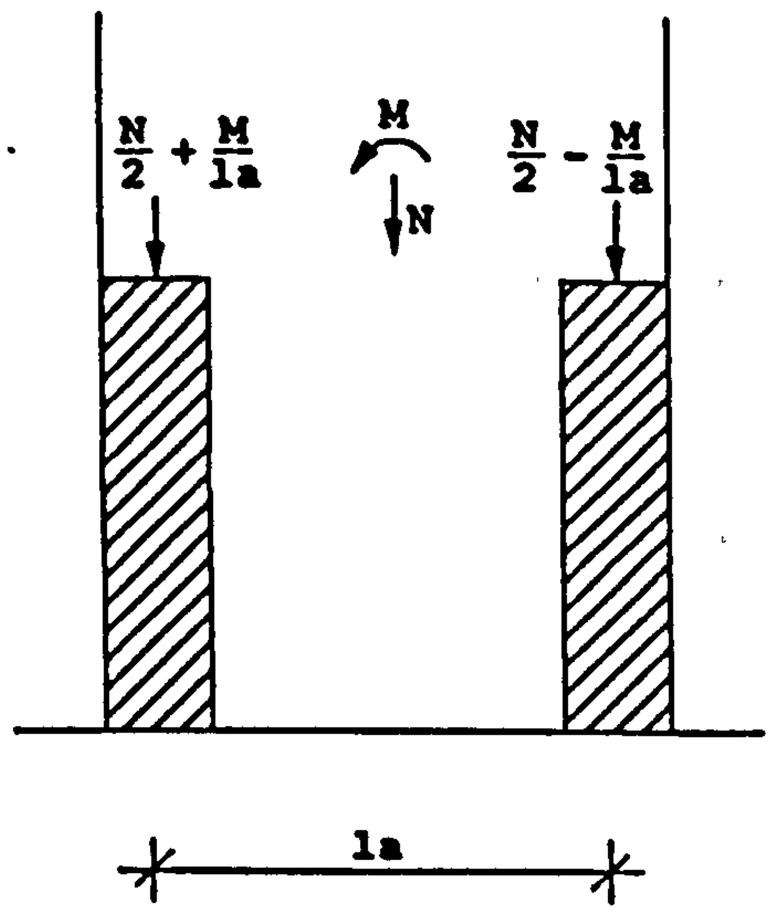


Figure 3.15 Boundary elements according to ACI 1983

EC 8 $h_{PHZ} \geq H / 6$

$h_{PHZ} \geq L$

$h_{PHZ} \geq h_s$

NZ $h_{PHZ} \geq H / 6$

$h_{PHZ} \geq L$

$h_{PHZ} \leq 2\ L$

If $H / 6 \geq 2\ L$ then $h_{PHZ} = 2\ L$

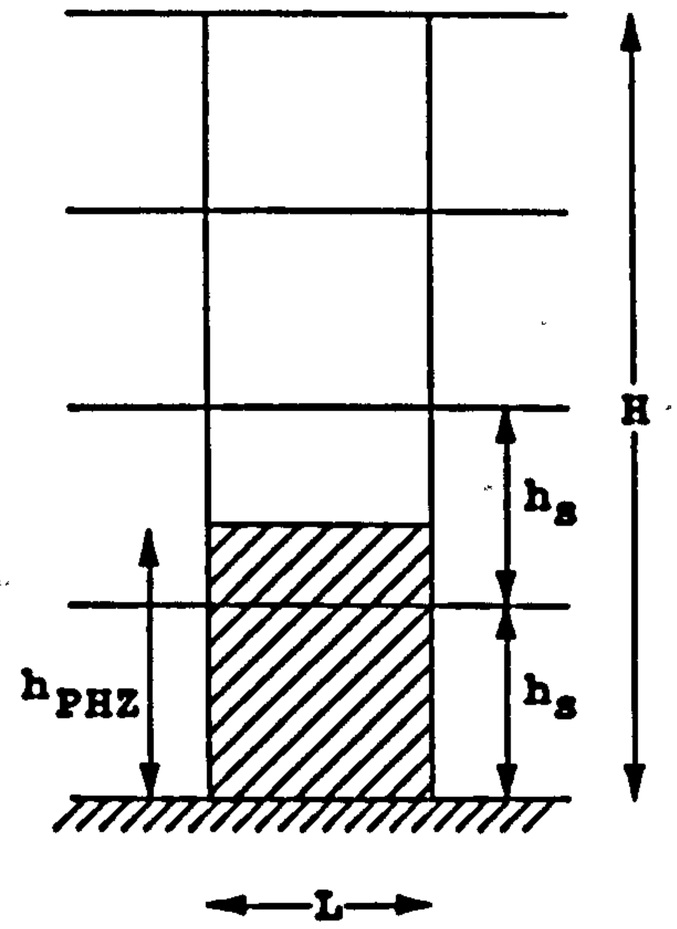


Figure 3.16 Length of the PHZ

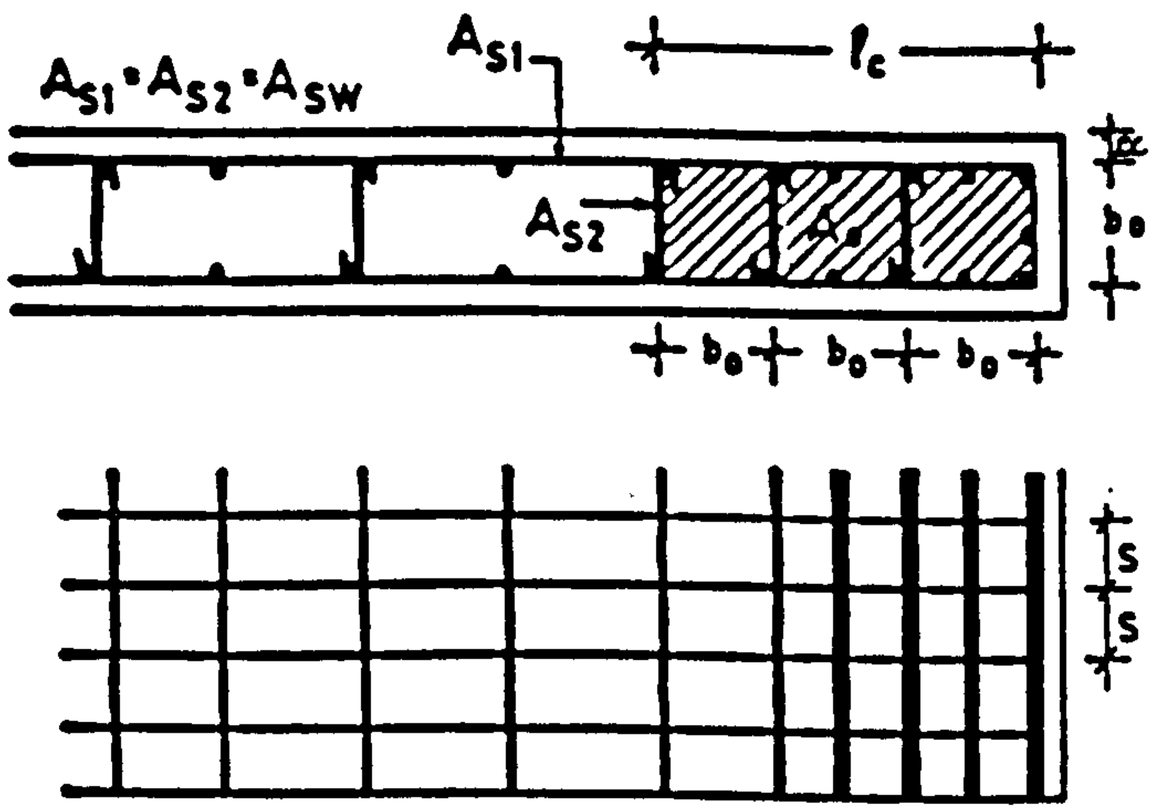


Figure 3.17 - Confinement reinforcement (EC8)

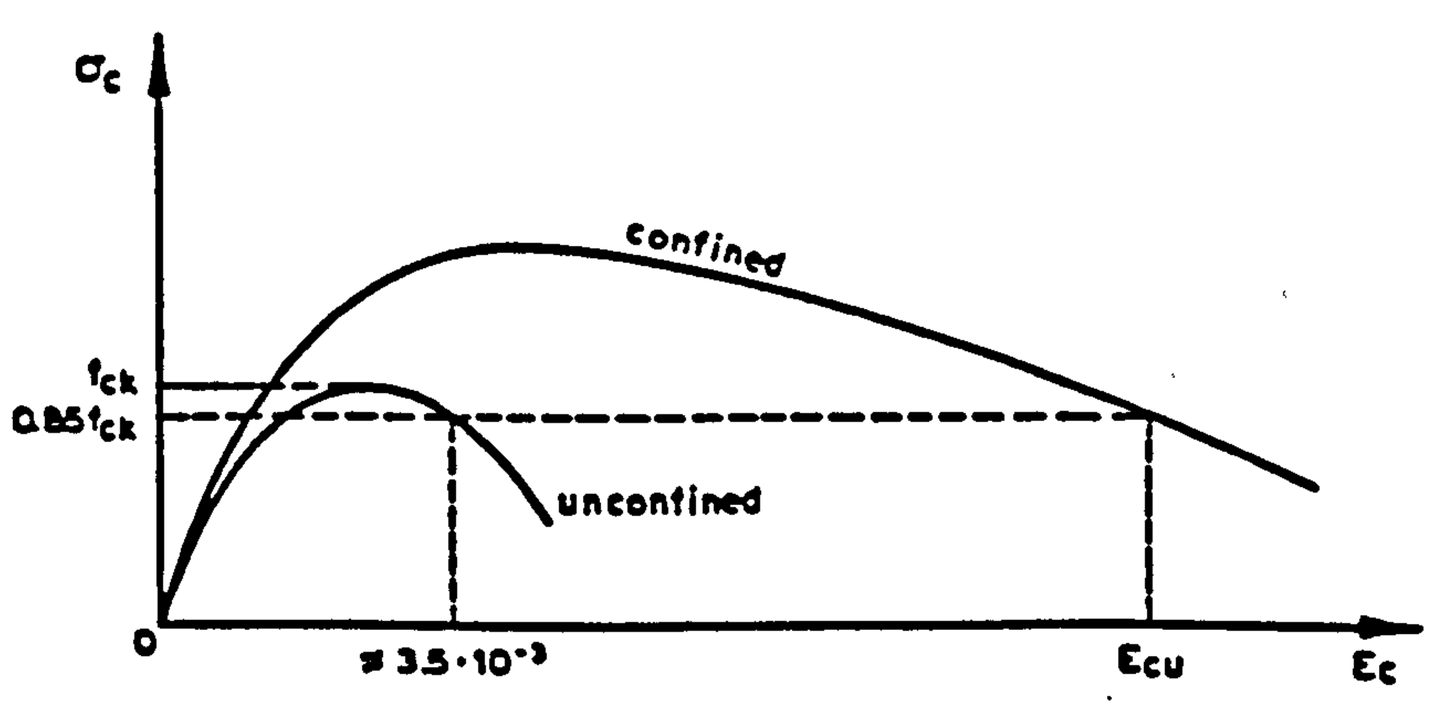


Figure 3.18 Stress-strain diagrams for concrete (EC8)

CHAPTER 4

4 EXPERIMENTAL WORK

In section 4.1 the test set-up and the wall specimens are described. The description of the tests and results is given in section 4.2. For the sake of compactness the photographs and the plots showing the results are presented in appendices A and B. A general discussion of the results is presented in section 4.3. Even though reference is made to design issues, the principal design-orientated discussion is presented in chapter 6.

4.1 Experimental Methodology

4.1.1 Boundary Conditions

As referred to in 2.3.1.1, the purpose of the tests was to reproduce the conditions more likely to lead to a shear failure in critical regions of R/C walls of multistorey buildings. These regions can be expected to extend up to a height similar to the length of the cross section of the walls. In order to avoid the direct transfer of load to the foundation by means of the formation of an arch mechanism, the horizontal load cannot be applied directly to the wall at this level. To solve this problem a new system of load application was developed and manufactured. The wall specimen was extended above the level of application of the horizontal force as shown in figure 4.1. The load is applied not directly to the wall but to steel frames that transfer it to the top beam, as shown in figure 4.2. Therefore, at the top of the wall a shear force and a bending moment are applied. At the level where the load is applied to the steel frames the system reduces to a single shear force. This is where the critical zone of the wall to be studied is considered to

start. The bending moment diagram in the wall is shown in figure 4.3. It is intended that the upper part of the wall remains elastic, as its sole purpose is to transfer the load to the bottom region. In order to ensure that, the top section was designed with extra flexural reinforcement to increase its flexural capacity and the point of load application is set closer to the top beam than to the foundation beam, as depicted in figure 4.1. The ratio between the moments on the top and bottom section is:

M_{TOP} / M_{BASE} = 0.8 F / 1.1 F = 0.73

The effectiveness of these measures was assessed by strain gauges placed at the top level on the vertical bars closer to the edge.

The wall model aspect ratio was 1.9 and the shear ratio was 1.1. These values were kept constant throughout the test program.

4.1.2 Experimental Set-Up

The test-rig used to apply the horizontal load to the steel frames was that used by Pilakoutas (1990) for the 1:2.5 scale walls and shown in figure 2.15. The only differences were the replacement of the wall by the wall-steel frame system discussed above, and the level of the jack that was lowered down in order to impose the required shear ratio on the wall specimens. A photograph of the set-up is shown in figure 4.4. Details of the connections between the steel frames and the wall are shown in figure 4.5. Each steel frame encased the top beam on either side of the wall. The width of the top beam was 300mm and the width of the steel frames was 100mm. This allowed each frame to be placed on the side of the wall leaving a small gap. This can be clearly seen in figure 4.5.a. The two frames were connected by means of a top plate and two side plates as shown in figure 4.5.b. The whole system was adjusted by means of a set of steel plates and

studs. The photograph of the front view of the system in figure 4.5.c shows the top beam encased by the frames. To avoid concentration of loads, a set of steel plates was placed between the top beam and the steel frames on all sides. The system was finally adjusted by a set of vertical and horizontal steel studs in such a way that the top beam was rigidly connected to the frames. This connecting system was preferred to alternative ones, such as grouting the gap between the frames and the top beam, due to its versatility. It could be assembled or dismantled in about 15 minutes, and misalignments could be easily corrected by releasing the studs and adjusting the position of the frames.

The concrete blocks shown in figure 2.15 formed a wall against which the jack reacted. The system comprised two sets of three superimposed blocks embedded in a thin layer of cement grout. The blocks were prestressed onto the concrete strong floor on the 900mmx900mm grid. A 400KN prestressing force was applied in each stud; two for each group of three blocks, as shown in figure 2.15. This provided the capacity to rigidly resist a moment of $720*10^3$KNmm. A yoke of two 300mmx200mm rectangular hollow sections was stressed at the right height on the reaction blocks so as to provide the push and pull capability for the jack. The load was applied by a 175mm stroke, 200KN capacity screw jack reacting against the concrete blocks. The jack was driven by an electrical motor at a constant speed of about 0.1mm per second. A hinge and a 10 volt (strain gauged cylinder type) load cell were connected between the jack and the rest of the structure that transferred the load to the steel frames, as shown in figure 4.6. The structure that transferred the load to the wall was essentially a stiff collar frame with a roller on either side. This loading frame could only move horizontally in the plane of the wall. Other possible movements were restrained by a system of flat rollers reacting against two standard laboratory assembly portal frames, as shown in figure 2.15.

With this arrangement the specimen, the encasing frames and the load transferring members were encased in a safe way.

The boundary conditions at the level of the jack were intended to apply a horizontal load at a constant height on the encasing frames. As figure 4.6 shows, according to the direction of loading one of the rollers pushes the encasing frames and the wall. Each cylindrical roller was connected to the loading frames by two circular bearings. This was intended to eliminate tangential frictional forces that could develop due to vertical movement of the point of load application in the encasing frames. The roller on the side of the jack was horizontally fixed to the stiff frame, while the roller on the open side of the frame could be adjusted in the horizontal direction by means of a system of steel studs. In order to avoid movement of the foundation beam two hollow section beams were prestressed against it. A total force of 500KN was applied on each side of the foundation beam.

4.1.3 Details of the Specimens

4.1.3.1 Geometry

All the specimens had the same geometry. The section of the walls was rectangular and their geometric aspect ratio was 1.9. The cross section dimensions were 45x450mm^2. The choice of the dimensions of the walls was dictated by the capacity of the jack and other components of the system which had been designed for a maximum horizontal force of 200KN. Although the specimens did not represent a scaled version of any particular prototype, they could be considered 1:5 scale models of walls used in current earthquake resistant design practice. The dimensions of the foundation beam were larger than the structural requirement would have given. This was due to the clamping system having the floor bolts 900mm apart and the need to leave room for the external instrumentation. This led to an increased length and therefore it was necessary to increase the other dimensions to provide full fixity to the wall. With regard to the top beam, due to the applied bending moment on top, the beam was subjected to

vertical forces on the sides, thus it behaved as two short cantilevers in the plane perpendicular to the wall. Usually its only function is to spread the horizontal load along the cross section of the wall on top. The dimensions of the specimens are shown in figure 4.7.

4.1.3.2 Concrete

Since the purpose of the tests was to simulate the conditions (in terms of moment, shear and axial force) more likely to lead to a shear failure, it was sought to impose a high shear force. However, most codes impose a limit on the maximum possible shear force at a certain section as a function of the concrete strength. As referred to in section 4.1.3.3.2, the first walls were designed according to ACI 1983. Hence, a concrete of high strength already used extensively in other research programmes at IC was chosen. However, the material supply source differed for the last three specimens. Details of the concrete mix are shown in table 4.1. The specified compressive cube strength at 28 days was 45MPa. At least three cubes were tested on the day of the structural test. The results of these tests are presented in table 4.3.

4.1.3.3 Steel Reinforcement

4.1.3.3.1 Properties

The properties of the steel reinforcement were measured in monotonic tensile tests. Six bars of each diameter were tested. Two were left unground and four were ground in two positions within the stressed area. Two kinds of 8mm steel were available and both were tested. It was found that in the 8mm square bars the reduction of area due to grinding was such that the ultimate resistance of these sections was below the yield resistance of the unground sections. Plasticity

could not spread and the overall behaviour of such bars was fragile, hence they were not used. All the 8mm bars used in the test programme were of circular cross section. The strains were measured both by strain gauges and by a device utilising a transducer to measure the extension within a sample length of 250mm. The extension device proved more successful in monitoring strains during the entire strain-controlled tests. In most cases the adhesive used for strain gauges broke at approximately 20000 microstrains whilst other gauges were unreliable after yield. The properties of steel reinforcement are shown in table 4.2. The 6mm bars results refer to unground bars as most of these bars were not gauged in all tests. The yield strength was well defined for the 8mm bars but for the other bars there was a progressive change in stiffness from the elastic value to the hardening stiffness.

In the analytical studies presented in the next chapters the stress-strain curves of steel are represented by a trilinear model as shown in figure 4.8. The parameters that define these curves for all kinds of steel are shown in table 4.2. For the 4mm and 6mm bars which exhibited a gradual change in stiffness around the yield point, the trilinear representation may differ slightly from the actual stress-strain characteristics of the steel around that point. The 8mm bars exhibited a yield plateau of almost no stiffness between the well defined yield point and the onset of strain hardening. The trilinear representation leads to a slight overestimation of the stresses in this area.

4.1.3.3.2 Design of the Walls

The experimental programme comprised testing of eight R/C walls. SW11 was tested under monotonic loading, walls SW12 to SW17 were tested under cyclic loading up to failure and wall SW18 was subjected to a large number of cycles before it was loaded monotonically to failure. With the exception of the vertical web reinforcement, the first two walls were designed according to ACI 1983 (without

considering the strength reduction factors) to resist the maximum shear force allowed by this code, which was 97KN for walls with this section and concrete strength. The flexural reinforcement was calculated for the bending moment corresponding to the shear force of 97KN. The confinement reinforcement was ϕ4/40mm which was more than necessary.

For walls designed for seismic loading the amount of vertical web reinforcement should be at least equal to the amount of horizontal web reinforcement (stirrups) according to ACI. However, due to reasons related with the design of wall SW15, it was decided to place less vertical web reinforcement. The reinforcement details of all walls are shown in figure 4.9. The tests of SW11 and SW12 showed that the detail used for the anchorage of the stirrups was not efficient enough to enable those bars to develop their full capacity. Therefore wall SW13 was designed similar to SW12 but with a different anchorage detail for the stirrups, as shown in figure 4.10. In the case of wall SW13 each stirrup comprised two steel bars, each one detailed as shown in figure 4.10.b. This detail was considered effective in providing confinement and therefore the stirrups were also considered to provide confinement at the edge members. This led to an increase to 60mm of the spacing of the reinforcement provided only for confinement purposes. In addition to differences in the load history, walls SW11 and SW12 exhibit another difference; in wall SW11 all the stirrups have the discontinuous side on the same side of the wall while in SW12 it is on alternate sides of the wall. This resulted in the model being symmetric.

It was sought to vary only one parameter from test to test to allow a clear interpretation of the results. Wall SW14 was similar to SW13 without confinement reinforcement. As the stirrups provided confinement, the three lower ones were shifted slightly upwards as compared with their counterparts in SW13 in order that the effect of confinement was not felt near the base section. The purpose of the test was to provide insight into the role of confinement

reinforcement on the behaviour of R/C walls with low shear ratios which is not well established.

Wall SW15 differs from SW13 in the amount and distribution of horizontal web reinforcement. It was the purpose of this test to investigate the behaviour of a wall designed according to the CFP concept. Although the path of the compressive force is well established for simply supported beams it is not for continuous systems or others with moments of different sign. However, it was suggested by Kotsovos (1989) that a continuous system may be studied as a set of simply supported beams between points of contraflexure. Due to the dimensions of the walls, both the part above and below the level where M=0 may be expected to exhibit type IV behaviour according to the CFP concept. The path of the compressive force would therefore be as shown in figure 4.11 (Kotsovos, 1989). Stirrups would only be needed at the level where M=0 to transfer the shear from one side to the other. Wall SW15 was designed in this way. As shown in figure 4.9.d the horizontal web reinforcement was distributed in a strip 240mm wide centred at the level where M=0. A photograph of the steel cage of wall SW15 is shown in figure A(15)2. The yield resistance of the horizontal reinforcement was 89KN. The remainding shear force was considered to be resisted by the concrete. Below and above the horizontally-reinforced strip 1.4mm diameter wire was placed to avoid lateral instability. The yield strength of each wire was 1KN. With regard to the vertical web reinforcement, there is a difference between code requirements and the CFP method. Whereas the former specifies a minimum required area, the latter makes no reference to the role of vertical reinforcing bars. To isolate parameters studied within the context of the CFP concept, vertical web reinforcement was reduced below code requirements in the first five tests. The resulting reinforcing detail is shown in figure 4.9.

In the tests of walls SW16, SW17 and SW18 it was sought to eliminate the possible contribution of vertical web reinforcement to the shear strength. Hence this kind of

reinforcement was not placed. The walls were designed to fail in shear by diagonal tension; to achieve such a mechanism, the amount of stirrups was reduced as compared to SW13. The stirrups were not uniformly distributed along the height of the wall for the reason discussed in section 6.2.2. With the exception of wall SW18 all walls throughout the experimental programme were designed with the same amount of vertical reinforcement in both edge members. In wall SW18 the 8mm bars were replaced by 12mm bars in the edge member which would be under tension at the base level at failure. The rest of the reinforcement of wall SW18 was exactly the same as in SW17.

In wall SW18 it was attempted to pre-form a crack in the same position of the diagonal crack that led to the failure of wall SW17 and eliminate any possible friction between its surfaces. The purpose of this procedure was the elimination of the aggregate interlock effect along the crack. To achieve this a 0.4mm thick steel plate coated with grease and wrapped in cling-film (to avoid the grease flowing away during casting) was fixed to the mould and the steel cage before casting. The position of this plate is shown in figure 4.9.g and can be seen in figure A(18)2. In figure A(17)2 that shows wall SW17 after the test, two arrows point to the extreme positions of the zone that corresponds to the location of the steel plate in SW18.

4.1.3.4 Mould, Casting and Curing Procedure

The moulds were made from 19mm plywood. Before each cast, the inside of the mould was coated with a releasing agent. The concrete was mixed in the laboratory using a suitable size concrete mixer. Each batch comprised the concrete of the wall and the corresponding control cubes. All specimens were cast in the horizontal position. The concrete for the beams was placed and vibrated in three layers. A 25mm diameter pocket vibrator was used to vibrate the beams and the wall web. An electrical hammer was applied on the sides of the mould to vibrate the edge members of the wall where

the pocket vibrator could not penetrate. The wall surface was carefully compacted and levelled to eliminate voids and geometric irregularities.

The specimens were trowel finished two hours after casting and covered with wet hessian and nylon approximately four hours after. The control cubes were demoulded on the day after casting and placed on top of the wall. After curing for one week, the walls were demoulded and stored in the upright position together with the cubes under standard laboratory conditions until tested.

4.1.4 Load History

Knowledge of the strength of the structures under monotonic load is sufficient to assess their performance for most actions. In the case of earthquake ground motion the structures are subjected to displacements at the foundations and no external forces are directly applied in the structure above the ground level. Seismic forces are generated due to the inertia of the mass of the structure. As already discussed in section 2.2.1.1, in most cases structures are designed to exceed their elastic limits when responding to this type of action. Consequently, knowledge of the strength, available ductility and energy dissipation capacity are needed to assess the performance of the structures.

It was pointed out in the literature survey that the strength and ductility of R/C members may not be the same under monotonic and cyclic loading conditions. Therefore, a large number of displacement reversals should be imposed on the walls if the results of the tests are to be used for earthquake resistant design. Results of monotonic tests should be used only as an indication, as these tests cannot simulate several phenomena observed under load reversals.

Under cyclic loading flexural cracks open on both sides of the sections and shear cracks open in two directions. When

the load is reversed after unloading, new cracks may open before the cracks previously opened (during loading in the opposite direction) have closed. This is more likely after yielding of the main flexural reinforcement occurs, due to accumulation of plastic strains. Therefore, a full depth crack may develop along an entire section along which shear may have to be transferred by aggregate interlock and dowel action. This phenomena already reported (Ma, Bertero and Popov, 1976) cannot be observed under monotonic loading. The shear transfer mechanisms are also more likely to degrade under cyclic loading. This has already been pointed out as one of the most important reasons for the shear failures which have caused severe damage and even collapse of many structures in past earthquakes (Bertero, Popov and Wang, 1974). Both aggregate interlock and dowel action tend to degrade under cyclic loading. If high shear forces are present, relative displacements occur between the crack surfaces. This leads to incomplete closure of the cracks now subjected to compression due to the mis-match between the two rough surfaces, as shown in figure 4.12. This in turn leads to the degradation of the aggregate interlock effect and increased displacements between the crack surfaces. This is one of the reasons for the observed stiffness degradation on reloading between successive loops at the same displacement ductility range observed in R/C members (Ma, Bertero and Popov, 1976).

It is also very important in cyclic testing for earthquake resistant design that the tests are displacement controlled after yielding of the main flexural reinforcement. At this stage the stiffness is reduced and large increases in displacement may correspond to small increases in applied load. Clearly, under force control it is possible to measure the ultimate load but not the corresponding displacement. As a load above the ultimate is applied, the displacement reading becomes meaningless. The last reliable displacement reading at a load just below the ultimate may be very different from the displacement corresponding to the ultimate due to the low stiffness of the system at this stage. In

force controlled tests it is also impossible to follow a descending branch. Thus, it may not possible to obtain any reliable measure of the ductility.

In the current test program all walls were tested under displacement control. The control displacement was the horizontal displacement of the wall at the level where M=0. Wall SW11 was loaded monotonically up to failure. All other walls were subjected to load reversals. In the first cyclic test (wall SW12) the reading of one of the top horizontal transducers was used as control displacement. From then onwards the tests were controlled using the average of the readings of the two top horizontal transducers, which is hereafter referred to as top horizontal displacement. The reason for this change was the considerable difference between the readings of the two top horizontal transducers.

Wall SW15 was an exception to the above mentioned procedure because the reading of one of the top horizontal transducers could not be registered, as explained in section 4.2.6.1. At each level of displacement, incremented by approximately 0.8mm, three cycles were applied. This criteria was established based on observations from an earlier study at Imperial College (Elnashai, Pilakoutas and Ambraseys, 1990). In the case of wall SW18 three cycles were applied at 0.4mm amplitude and six cycles were applied at a displacement level of 2.4mm before loading monotonically in one direction to failure. The extra number of cycles were applied in order that the wall was subjected to a number of cycles similar to wall SW17 before it would achieve the ultimate load .

4.1.5 Instrumentation and Data Acquisition

Data acquisition was performed through a Hewlett Packard data logging system. A maximum of 20 channels were available for the load cell, power supplies and linear voltage differential transducers (LVDT's). Hence, a maximum of 17

transducers could be used in each test. Forty quarter bridge circuits were available in the data logger for strain gauge readings. An X-Y plotter was used during testing to plot the load vs displacement curve. Cracks were marked on the specimens after every cycle and photographs were taken for each level of maximum imposed displacement.

The load applied to the wall through the stiff collar frame was measured by a tension/compression electrical load cell. The output was a single voltage as in the case of the transducers. Figure 4.13 shows the positions of the transducers and the number of the corresponding readings for all walls. The stroke length of the transducers used was 50mm. In order to measure absolute displacements, the transducers were fixed on a firm scaffold pole frame which was independent of the test rig. The out-of-plane transducers and the ones on the foundation beam were measuring displacements of plates glued to the concrete. Most of the others had plates at the end of the shaft. These plates measured the displacements of reference pins which were welded to plates glued to the concrete. The reference pins and respective plates can be seen in figure 4.5.a. The pins for the vertical readings at the bottom level were welded to the steel bars before casting because the concrete at that level could spall earlier in the test and those readings would be lost thereafter if the plates were used.

Strains in the steel reinforcement were measured using different types of electrical strain gauges depending on the diameter of the steel bars. The ribs in the high tensile 6, 8 and 12mm diameter bars were taken off with a file at the position where the gauges were to be placed. That zone was rubbed with emery paper and cleaned with a water-based degreasing surface cleaner. After fixing the gauges to the bars their bridge wires were connected to the water-proof wire and the gauges were then water-proofed and protected. The gauges were not placed on the outside of the steel cage in order to avoid damage during casting and levelling. The location of the gauges placed on vertical bars and the number

of the corresponding readings are shown in figure 4.14. The same notation applies to all walls, despite the fact that gauges were not placed in all those locations in all walls. In some cases more than one gauge was placed at a certain location. In this cases the readings have the same number with a subscript index. The position of the gauges on the horizontal bars are shown for each wall in figure 4.15. Only the position of gauges that worked during a significant part of the test are shown.

4.1.6 Evaluation of Shear and Flexural Deformations

The flexural component of the top horizontal displacement is due to deformations associated with rotations of the sections of the wall. Therefore it can be measured by integrating the diagram of rotations along the height of the wall from the base up to the level where M=0. The rotations were measured at selected levels as they could not be measured continuously. At each level two transducers measured the vertical displacement on both sides of the wall. The rotations were then calculated dividing the difference between both readings by the length of the cross section of the wall. The levels at which the transducers were placed were the same for all walls and are shown in figure 4.13. Their vertical spacing was smaller at the lower levels because that is where the highest curvatures are expected due to yielding of the main flexural reinforcement.

The integration of the rotations was performed considering a linear variation of the rotations between the levels of measurement. This is referred to as method of area $\alpha 2$ in figure 4.16.c, where it is demonstrated that the measured area is a good approximation of the real area α. Another approach was used by Lefas (1988) which calculated flexural deformations by multiplying the rotation on top of the wall by the total height of the wall. This corresponds to the method of area $\alpha 3$ shown in figure 4.16.d. As the figure shows, the method used by Lefas is likely to lead to a gross

overestimation of flexural deformations. Further discussion of this issue considering the experimental data obtained in the current test series is presented in section 4.3.3.3.

Shear deformations are the ones which are not associated with the rotation of the sections. These are often evaluated using the difference of two diagonal measurements as shown in figure 4.17. Many researchers use this procedure to evaluate shear deformations and the method of area $\alpha 2$ to evaluate flexural deformations. However, the two methods are based on incompatible hypothesis. Figure 4.18 shows that the evaluation of shear deformations by means of diagonal measurements is equivalent to evaluate them by subtracting the flexural deformations calculated using the method of area $\alpha 1$ (shown in figure 4.16.b) from the total. The use of method of area $\alpha 1$ may lead to an understimation of flexural deformations of approximately 25%, as shown in figures C.3 and C.4. Therefore, diagonal measurements would tend to lead to an overestimation of shear deformations. It should be noted that this measuring procedure, besides measuring shear deformations may also include part of the flexural deformations. An example of such a case is shown in figure 4.19.

In the current work, method of area $\alpha 2$ was used to evaluate flexural deformations. Shear deformations were calculated by subtracting flexural deformations from the total.

4.2 Description of Tests and Results

In this section the individual experiments are described and corresponding tables of results and graphical displays are identified.

4.2.1 Introduction

The plots showing the results of transducer and strain gauge readings are shown in appendix B. For easy identification each figure number has the number of the wall it refers to in brackets. The degree of success of strain gauge readings changed from wall to wall. Some gauges (or their water-proof protection) were damaged during steel fixing and casting; most gauges failed during the test. This could have been due to several reasons such as breaking of the bridge wires, loss of bond due to high strains, ageing of the adhesive or workmanship defects. When failure of the gauge was due to interruption of the electric current, the reading at which it occurred was easily identified and therefore only the results registered up to that stage are shown. However, for other types of failure it was not easy to identify the stage at which failure occurred. In such cases the readings are shown up to a stage in which it was clear the gauge readings were defective. In some cases they seemed to be working only in one direction of loading. Problems also arose with transducer readings. These problems were due to loss of bond between the concrete and the steel plates due to workmanship defects or loss of contact with the reference pin. The correct positioning of the transducers was a difficult task due to limited working space. This can be seen in figure 4.20 which shows the back of a wall with the instrumentation. Inaccuracies in some readings were present due to sliding of the transducer end plate along the reference pin. Both transducer and strain gauge data exhibited parasitic readings arising from noise or errors in the data acquisition system. Most of these readings were eliminated from the results.

The tests were stopped from time to time to take readings on all channels. This typically lasted for approximately 30 seconds. During this period some drop in load and a slight increase in displacement due to creep and relaxation were noticed. When the test continued the load was immediately recovered and the system would then follow along

the path it was following before the test was stopped. In the first test, readings were taken before continuing the test after each stop. These readings were then eliminated except for transducer 1. Figure B(11)1.a shows all the readings of transducer 1. On all other walls readings were not taken when restarting the tests. Readings were taken at the end and beginning of each half cycle, at zero load and when the stiffness was changing. However, the changes in stiffness were gradual and readings could only be taken at discrete points. Therefore, the results are presented as multilinear segments.

The results of the compressive tests on cubes are shown in table 4.3. In most cases the measured strength was very close to the specified value. The concrete specified strength was taken as 0.85 of the measured cube strength.

Table 4.4 shows the width of the largest diagonal crack in all tests. It was measured using a scaled magnifying lens whose resolution was 0.1mm. These values are later used in the main discussion of chapter 6 as an indication of the effectiveness of the aggregate interlock mechanism.

Sequences of photographs of all tests are given in appendix A, figures A(11) through A(18) inclusive. The numbers in brackets correspond to the numbers of the walls for easy identification. As only the part of the wall below the loading frame was visible, photographs of the whole wall could be taken only after testing. The values of MD shown in the photographs were not exact as the control system was not of sufficient accuracy to allow the tests to be stopped exactly at the desired point. Errors of a few tenths of millimetre may exist.

Several quantities were calculated using available data from transducer readings. The opening of the cross section, i.e., the increase in length of the wall cross section, was calculated using two horizontal readings at the same level on either side of the wall. Readings 1 and 2 were used to

calculate the opening on top and readings 15 and 15b to calculate the opening at the third height level. The extension of the walls on top was obtained as the average from readings 9 and 10. The extension at a quarter height was calculated as the average from readings 5 and 6. Shear and flexural deformations were evaluated using the method of area α2, described in 4.1.6. The relative contributions of the shear and flexural components to the top horizontal displacement, RSD and RFD respectively, are also shown.

4.2.2 Wall SW11

4.2.2.1 Description of the Test

The first visible diagonal crack formed at a displacement of approximately 0.6mm and at a load slightly above 30KN. The crack was inclined slightly more than 45° to the horizontal, as shown in figure A(11)1. Soon after, several flexural cracks were visible. They were almost horizontal and were of limited extent. With increased applied displacement the flexural cracks extended to the web of the wall and showed a downwards trend. No significant increase in the width of flexural cracks was noticed. At a displacement of 1.9mm several other diagonal cracks, which formed independently of flexural cracks, were visible. A continuous increase in the crack width of the first diagonal crack was clear even before first yield of the main flexural reinforcement.

The ultimate load was reached at a displacement of 4.7mm. At this stage the width of the main diagonal crack had increased to about 1.4mm and several cracks had already penetrated in the compressive zone. Thereafter the load dropped when the applied displacement was increased. However, the wall exhibited a considerable ability to sustain displacements in the post-ultimate range with moderate drop in load. The test was stopped when the load dropped to

approximately 72KN (78% of the ultimate). No sudden drop in load carrying capacity was observed.

The wall failed in shear by diagonal tension. Figure A(11)3 shows diagonal cracking also at the top of the wall. None of the cracks in this part of the wall opened as much as the diagonal crack along which failure occurred in the bottom part of the wall. Spalling in one side of the wall was noticeable shortly after the ultimate load was reached. This was due to the opening of the discontinuous side of the stirrups. Spalling of the concrete at the bottom level on the compressive side was not noticed during the test. However, after the test was stopped, concrete could be easily removed by hand, indicating that the cover ceased to contribute to the wall resistance probably before the end of the test.

4.2.2.2 Results

Results of transducer readings are presented in figures B(11)1 to B(11)15. Figures B(11)16 to B(11)22 show results calculated using data from the transducers. The top horizontal displacement is plotted in figure B(11)16 and is the displacement on the x-axis of figure B(11)19. Strain gauge readings are shown in figures B(11)23 to B(11)36.

4.2.3 Wall SW12

4.2.3.1 Description of the Test

The reading of one of the top horizontal transducers at the level where M=0 was used as the control displacement. However, it was observed during the test that the readings of this transducer were substantially different from the readings of the other transducer placed on the opposite side of the wall at the same level. As a consequence, the test showed bias in the left hand side direction.

The wall was loaded monotonically up to the first displacement step of 0.8mm. Independent shear and flexural cracks formed at a load of approximately 35KN. When the applied displacement was reversed, flexural cracks opened on the opposite side and shear cracks inclined in the opposite direction opened in the web. Subsequent cycles at the same displacement amplitude caused moderate extension of some of the cracks previously formed. After three cycles at 0.8mm some of the flexural cracks had penetrated the web showing some downwards inclination. With the continuation of the test more shear and flexural cracks formed, and the previous ones extended. Some flexural cracks became as inclined in the web as adjacent shear cracks which formed independently.

At MD 2.4 it was noticeable that one of the shear cracks in each direction was opening more than the others. It is thought that yielding of the extreme ϕ8mm bars occurred just before MD 2.4 was reached. Strain gauge readings on ϕ8mm bars of this wall are not conclusive in this respect as only one incomplete gauge reading is available. However, similar readings on other walls indicate that yielding must have occurred at this stage. Diagonal cracks seemed to be about to penetrate the compressive zone before MD 2.7. The width of the major diagonal cracks continued to increase with successive increases of MD. The ultimate load of 94.7KN was reached at a displacement of approximately 3.5mm. As in the case of wall SW11, the wall possessed a reasonable capacity to accommodate displacements in the post-ultimate range with moderate loss of load carrying capacity (the displacement at failure was 157% of the displacement at the ultimate load, as shown in table 4.5). The increase in the width of the main diagonal cracks progressed much faster after the ultimate load was achieved. The failure mode was the same as in the case of wall SW11. No horizontal crack along the entire cross section of the wall was visible.

Figure A(12)2 shows the wall after testing. It is clear that diagonal cracks also opened in the upper part of the wall, but the width was kept at much lower levels than the

width of the two main diagonal cracks in the bottom region. Spalling of the concrete cover at the bottom ends was not apparent before the ultimate load was achieved. However, this does not necessarily mean that the concrete cover was contributing to the wall resistance at this stage. After the tests, pieces of concrete which seemed to be still part of the wall were in fact detached from it and could be removed by hand. Figure A(12)2 shows localized spalling at upper levels. As in the case of wall SW11, this was due to the opening of the stirrups in the discontinuous side due to insufficient anchorage length, as already referred to in section 4.1.3.3.2. Another noticeable feature in figure A(12)2 is the increased length of the wall cross section along the height of the wall where the main diagonal cracks developed. This issue is further discussed in section 4.3.3.2.

4.2.3.2 Results

Results of transducer readings are presented in figures B(12)1 to B(12)15. Figures B(11)16 to B(11)22 show results calculated using the transducer data. In the figures showing the shear and flexural components of the top horizontal displacement some readings are missing due to the fact that the end plate of one of the vertical transducers lost contact with the reference pin. The values of RSD and RFD are plotted as a function of MD in figure B(12)19. Strain gauge readings are shown in figures B(12)23 to B(12)41.

4.2.4 Wall SW13

4.2.4.1 Description of the Test

In this test the average of the two top horizontal transducers was used as control displacement. The values of MD shown in the photographs are slightly higher than in

reality due to the rotation of the foundation beam. The only important difference in design between this wall and SW12 was the detail of the anchorage of the stirrups, as described in section 4.1.3.3.2.

First diagonal cracking was visible at a load of approximately 40KN. Flexural cracks only became visible thereafter. At the end of the cycles at MD 0.8 several diagonal cracks had formed but fewer flexural cracks on the sides were visible than in the case of wall SW12. At MD 1.8 more shear and flexural cracks had formed. Previously existing shear and flexural cracks increased in length. Some flexural cracks extended into the web with an increased angle of inclination similar to shear cracking. With increasing MD the same process of forming new cracks and extending the existing ones continued. Shear cracks that formed independently of flexural cracks were inclined a few degrees more than 45° to the horizontal. Diagonal cracks that formed as extension of flexural cracks lower down were less inclined. The width of the diagonal cracks increased steadily but none of them opened much more than the others.

Strain gauge readings point to the fact that yielding of the extreme vertical bars must have occurred just before MD 2.4 was reached at a load of approximately 72KN. At this stage the formation of several flexural cracks on the boundaries was visible. The propagation of diagonal cracks into the compressive zone seemed to have been halted up to a value of MD close to 6 mm while in the case of SW12 it was visible before MD 2.7. After diagonal cracks penetrated the compressive zone, spalling of the concrete at the extreme ends of the bottom section of the wall was noticeable. Small vertical cracks could also be seen in the compressive zone.

The test continued with steady increase in the width of the diagonal cracks. However, none of them opened as extensively as in the test of wall SW12. After MD was increased for the first time above 7mm the wall and the encasing frames were about to touch the external

instrumentation. It was then decided to remove all transducers before reloading in the opposite direction. Only the two main top horizontal transducers were placed again. The wall still sustained three full cycles at a MD of approximately 7.5mm with a decrease in resistance of 24KN. When MD was increased again the maximum load did not increase beyond the level achieved in the previous cycle. When reloading in the opposite direction, the wall failed by crushing of the concrete, a process that quickly spread along the whole cross section, as shown in figures A(13)1 A(13)2.

The exact location where crushing started was not very clear. It is thought it was in the concrete immediately adjacent to the confined edge member. The low levels of strain gauge readings recorded on confinement reinforcement and the fact that high compressive strains in the main flexural reinforcement were not recorded, indicate that failure did not occur due to compressive failure of the concrete of the edge members. A photograph of the wall, taken after the test, shows that the integrity of the concrete in the edge members was well protected by the confinement reinforcement. Signs of what could be considered as sliding shear failure were not observed. Therefore, it is considered that the wall failed by web crushing, also called diagonal compression failure.

4.2.4.2 Results

Results of transducer readings are shown in figures B(13)1 to B(13)14. No horizontal transducer was placed at the second level in this wall nor in any other wall tested after this. Figures B(13)15 to B(13)21 show the plots of variables calculated as a function of transducer readings. Strain gauge readings are shown in figures B(13)22 to B(13)46.

4.2.5 Wall SW14

4.2.5.1 Description of the Test

Wall SW14 was similar to SW13 but for the confinement reinforcement. The development and evolution of the cracking process in this wall was similar to wall SW13 in the initial phases of the test. There were no strain gauge readings on the bottom extreme bars. However, there was no indication that yielding may have occurred at a different stage than in wall SW13. From this stage onwards shear cracks seemed to have propagated faster than in wall SW13. However, the maximum width of the diagonal cracks was similar to the corresponding values of wall SW13.

At MD 3.2 there were external signs of deterioration of the compressive zone at the bottom level. This was clear at MD 4.0 when cracking and spalling could be observed in the compressive zone. At this stage the width of diagonal cracks still seemed to be kept at a moderate level. Table 4.4 shows that the maximum width of the diagonal cracks was only slightly higher than in wall SW13 at the same stage. When MD was increased beyond 4.0mm the maximum previous load was not achieved. Deterioration of the compressive zone and a sudden increase in the width of diagonal cracks was noticeable. During subsequent stages of the test the load dropped continuously. The degradation of the compressive zone continued and extended to the web. The width of diagonal cracks also increased at a fast rate, higher than before the ultimate load was achieved. When the deterioration of the concrete extended to the whole web the maximum load achieved on reloading was quite low and the test was stopped.

4.2.5.2 Results

Results of transducer readings are shown in figures B(14)1 to B(14)14. Figures B(14)15 to B(14)21 show the plots of variables calculated as a function of transducer readings. Figure B(14)9 shows that the end plate of transducer 9 was not free to move at the last stages of the test. The error due to this is also apparent in the results shown in figures B(14)16, B(14)17 and B(14)18. Strain gauge readings are shown in figures B(1)22 to B(14)37.

4.2.6 Wall SW15

4.2.6.1 Description of the Test

The horizontal web reinforcement of wall SW15 was concentrated within a strip centred at the level of contraflexure, as shown in figures 4.9.d and A(15)2.

A few cycles after the test had started, it was noticed that the plate of one of the reference pins for the horizontal transducers on top was not properly glued to the concrete. Thereafter the test was controlled only with the reading of the other transducer at this level. Due to this the test exhibited bias in one direction. However, the concentration of stirrups prevented a large opening of the wall at this level, therefore the assymmetry of the load history was not significant.

The cracking process seemed to have started with the formation of diagonal cracks at a load of approximately 30KN. There were several parallel cracks in both directions at an angle of approximately 45° to the horizontal. Flexural cracks started to became noticeable at higher loads of approximately 40KN. As in previous tests, both kinds of cracks were visible before the first displacement step at MD 0.8 was achieved. At MD 1.6 another large inclined crack was visible in both

directions above the ones already formed at MD 0.8. They were slightly more inclined than the others and their width increased faster than any other crack in the previous tests. Table 4.4 shows that before MD 2.4 was reached, the crack width was already larger than the width of the largest diagonal cracks of wall SW13 at failure. Nearly vertical cracking could be observed in the compressive zone in one of the sides before MD 2.4 and in both sides at MD 3.2.

Yield seemed to have occurred at a load of 70KN or slightly below. The width of the main diagonal cracks continued to increase rapidly. The other diagonal cracks opened more moderately. The maximum load of 85KN was registered at MD 3.2. Three cycles in each direction were effected at this displacement level with a moderate drop in load carrying capacity. The first increase in displacement beyond MD 3.2 was performed without achieving the previous maximum load in the same direction. Upon reloading in the opposite direction, a loud noise was heard and a sudden and considerable loss of load carrying capacity was registered. Failure in shear by diagonal tension had occurred in a very brittle manner. At this stage the part of the wall above the diagonal crack along which failure occurred was moving as a rigid body relative to the lower portion of the wall. Photographs taken after the test show the complete failure surface and a detail at the top end. In addition to the degraded state of the compressive zone at the bottom, it is noticeable that the crack that triggered failure was forced to change direction to avoid the ϕ6 mm stirrups.

4.2.6.2 Results

Two of the vertical transducers, at the second and third level, did not work properly or were damaged. Therefore, no vertical readings at these levels are shown and shear and flexural deformations were not evaluated. Figures B(15)1 to B(15)9 show the other transducer readings. Figure B(15)10

shows the average of vertical readings on top. Strain gauge readings are shown in figures B(15)11 to B(15)30.

4.2.7 Wall SW16

4.2.7.1 Description of the Test

The wall was monotonically loaded up to a displacement of 0.8mm at the start of the test. At this displacement shear and flexural cracks had already formed. After three cycles at MD 0.8 the web was crossed by two long diagonal cracks, one in each direction, and several flexural cracks were visible on the sides. At MD 1.6, more extensive flexural cracking could be observed. New cracks had formed and the existing ones extended. Shorter diagonal cracks appeared above and below the ones formed before. The width of the major diagonal crack increased rapidly and reached 0.5mm at MD 1.6, as shown in table 4.4. When MD was increased to 2.4 several flexural cracks almost uniformly distributed along the height of the edge members appeared.

Yielding of the extreme ϕ8mm bars seemed to have occurred shortly before this displacement was reached at a load of approximately 70KN. The main diagonal cracks continued to open fast. Small nearly vertical cracks were visible in the compressive zone on the right hand side. When MD was increased to 3.2mm more flexural cracks appeared, and existing ones extended and inclined downwards in the web. Cracking in the compressive zone could be observed clearly on both sides. The opening of diagonal cracks continued at a fast rate.

The maximum load was achieved at MD 4.1. The failure surface comprised one of the major diagonal cracks and a contiguous surface within the compressive zone. There was no sudden loss of load carrying capacity. In fact during the test there was no clear indication that the load achieved on

the first cycle at MD 4.1 was the ultimate. However, at the next displacement step the load registered at MD 4.1 was not achieved, although the drop in load was very small. From MD 4.1 onwards, the maximum load registered dropped continuously, but no sudden loss of load carrying capacity was registered. The width of the main diagonal cracks continued to increase at a rate noticeably higher than before the ultimate load was achieved. It is noteworthy that a similar feature was observed in the test of wall SW12, which exhibited the same mode of failure, where through-the-thickness cracks existed. Finally, the test was stopped when the maximum load achieved had dropped to slightly more than 60KN. As in the case of wall SW12 it seemed that after the test the length of the wall cross section was larger below the level where M = 0 than above that level.

4.2.7.2 Results

Most of the readings of the vertical transducers were unreliable after the ultimate load. Post ultimate readings are only shown for transducers 3, 4, 9 and 10 in order to illustrate errors that can occur after the resistance of the wall to diagonal tension is exhausted, as discussed in section 4.3.3.1. Shear and flexural deformations are only shown up to the ultimate load. Transducer readings are shown in figures B(16)1 to B(16)14. Figures B(16)15 to B(16)20 show the plots of variables calculated as a function of transducer readings. Strain gauge results are shown in figures B(16)21 to B(16)32.

4.2.8 Wall SW17

4.2.8.1 Description of the Test

The only difference in design between walls SW16 and SW17 was that the latter had one more stirrup in the region of the wall crossed by the main diagonal cracks along which failure occurred in wall SW16. The test of wall SW17 was very similar to the test of wall SW16. There were quantitative differences but the essential features were the same. The cracking process was similar and the mode of failure the same; shear by diagonal tension. The increase in the width of the main diagonal crack in each direction showed the same trends with slightly lower values of the crack opening for wall SW17, as shown in table 4.4. The maximum load was higher and was achieved 0.7mm later than in the case of wall SW16. Wall SW17 also showed ability to sustain large displacements with moderate loss of load carrying capacity after the ultimate load was achieved. The increase in the width of the wall cross section, also observed in other walls which failed in shear by diagonal tension, is apparent in figure A(17)2. This may be due to rigid body displacements above the main diagonal cracks after the ultimate load was achieved, as shown in figure 4.21. This problem is discussed in section 4.3.3.1.

4.2.8.2 Results

One vertical transducer at each of the two lower levels did not work properly. Therefore, no readings of transducers at these levels are presented. Figures B(17)1 to B(17)10 present the remaining transducer readings. Other force versus displacement curves, including the opening of the cross section of the wall at the third level and top, are shown in figures B(17)11 to B(17)14. Figures B(17)15 to B(17)25 show results of strain gauge readings.

4.2.9 Wall SW18

4.2.9.1 Description of the Test

Three cycles were performed at MD 0.4 in this test. When this displacement was first reached, a crack had already formed along the steel plate and extended downwards, as shown in figure A(18)1. This corresponds to the displacement of the wall to the right hand side in the photographs of figure A.(18). After three full cycles at MD 0.4 no other cracks were visible. Extension of the preformed diagonal crack was not observed during the second and third cycles. Loads of 35.5KN and 34.2KN were registered when loading to the right and left hand side, respectively. After three cycles at MD 0.8 some diagonal and flexural cracks formed when loading to the left hand side. Flexural cracks due to loading on the right hand side direction were also visible. The width of the preformed crack at this stage was larger than the width of any diagonal crack in the previous tests at similar stages. However, it was the only diagonal crack visible in this direction at MD 0.8.

After the cycles at MD 1.6, more shear and flexural cracks had formed in both directions. Some flexural cracks extended towards the web and inclined downwards as shear cracks. There was a larger number of cracks forming when loading to the right hand side. The width of all flexural cracks and most diagonal cracks was reduced. The preformed crack continued to increase its width at a rate similar to the main diagonal cracks in the previous tests. It also extended into the compressive zone. At MD 2.4 the crack pattern was more extensive with most cracks increasing in length and a few new ones appearing. The width of the preformed crack continued to increase and propagate into the compressive zone. The main flexural bars on the right hand side seemed at or very near to yield. At this stage a load of 74KN was achieved when displacements were imposed in the left hand side direction. As the shear strength in this

direction was not expected to be very different from the strength of wall SW17, it was decided not to increase displacements more in this direction. It was intended to impose failure in the opposite direction.

Six cycles were imposed at MD 2.4 before loading the wall monotonically to failure in the right hand side direction, for the reasons discussed in section 4.1.4. At MD 3.7 several nearly vertical cracks could be seen in the compressive zone. Spalling could also be observed there. The width of the preformed crack was already more than 1.5 mm. The maximum load of 99.9KN was registered at a displacement of 3.3mm. Thereafter the load started to drop at a moderate rate and the width of the preformed crack continued to increase, albeit at a faster rate. The mode of failure was the same as for walls SW12, SW16 and SW17. Sudden loss of load carrying capacity was not registered and a considerable ability to sustain large displacements in the post ultimate range was observed. The test was stopped when the load had dropped to about 75KN.

4.2.9.2 Results

Transducer readings are shown in figures B(18)1 to B(18)11. Two transducers, 10 and 13, did not work satisfactorily during most of the test. Their readings were eliminated. Figures B(18).12 to B(18)15 show other load displacement curves and figures B(18)16 B(18)26 shown strain gauge readings.

4.3 General Discussion of Results

4.3.1 Limit States

The yield load and the mode of failure were observed to be unrelated. Moreover, the loading regime has no noticeable effect on the yield load. Strain gauge readings indicate that yielding of the extreme bars started at loads of approximately 72KN.

Table 4.5 shows the values of the load, secant stiffness, top horizontal displacement and respective ductility level at two stages of the tests; ultimate load and failure. With the exception of SW13 and SW15, the envelope of the force vs top horizontal displacement curve of all the walls exhibited a post-ultimate load descending branch of considerable displacement amplitude. Therefore, failure was not considered to happen at the ultimate load but only when the load dropped to approximately 80% of the ultimate. The values on the four right hand side columns of table 4.5 refer to this stage, at which the tests were stopped.

4.3.2 Deformational Characteristics

4.3.2.1 Stiffness

For all modes of failure and walls, stiffness degradation was observed, especially after flexural yielding. However, the envelope of the force vs top horizontal displacement diagram of the walls which failed by diagonal tension showed higher displacements at similar loads, i.e., lower stiffness. The high stiffness registered for wall SW18 was due to the fact that it had a flexural design different to earlier models and the tensile reinforcement was still elastic at ultimate load and failure. However, a large decrease in stiffness was observed after the ultimate load,

not only in wall SW18 but also in SW16 and SW17. This was due essentially to the breakdown of shear resisting mechanisms. It is also noteworthy that wall SW13, which exhibited the best inelastic response, at the ultimate load possessed a secant stiffness that was approximately 11 times less than the elastic stiffness. The consequent shift in the period of vibration should be considered in earthquake resistant design, as it may change the design forces.

All walls exhibit two distinct segments with different stiffness on reloading. This can be observed in the curves that show the relationship top horizontal displacement vs force of all walls tested under cyclic loading (figures B(12)16, B(13)15, B(14)15, B(15)3, B(16)15, B(17)11 and B(18)12). However, it should be noted that the transition between both segments is not as sudden as the figures suggest, as the readings were not continuous. The transition was in fact progressive and a curve of considerable extension connects both segments. The existence of an initial reloading segment of reduced stiffness is termed pinching and is due to the cracks in both directions which were opened at the same time. When reloading started, the cracks opened when loading in the opposite direction did not close before the new ones opened. At this stage the contribution of the concrete to the load resisting mechanisms was much reduced and the strength and stiffness of the wall were due essentially to the steel cage. Therefore, the stiffness was low and large displacements occurred. When the cracks closed the load started to pick up again and the second segment of reloading started. The progressive variation in stiffness from one segment to another indicates that the closure of cracks is not sudden but a gradual phenomena.

The mode of failure has an influence on the intensity of the pinching effect. The walls that failed in shear by diagonal tension showed a more intense pinching effect. The first reloading stiffness was lower and the displacements before the load started to pick up again were larger. This was probably due to the fact that the horizontal web

reinforcement was insufficient to prevent the opening of large diagonal cracks. However, it is extremely important to note that a considerable pinching effect is present even if failure by diagonal tension is prevented.

The stiffness on reloading tended to decrease noticeably after yielding of the main flexural reinforcement. The reduction in stiffness seemed to depend essentially on the maximum displacement previously attained. Additional cycles at a given maximum displacement are also the source of some stiffness deterioration. This emphasises the importance of cyclic loading tests, where seismic design recomendations are sought.

The unloading stiffness tended to decrease when the maximum imposed displacement increased. At the lower levels of load, i.e., at the second segment of unloading, the stiffness was lower than at the initiation of unloading. The mode of failure does not seem to affect the rate of degradation of the unloading stiffness.

Comparisons with analytical predictions are discussed in chapter 5.

4.3.2.2 Ductility

Table 4.5 shows the displacements at ultimate load and at the state of failure for all walls. The influence of the mode of failure is evident. The results show the walls that failed by diagonal tension achieved their ultimate loads at much lower levels of displacement than wall SW13. However they possessed a considerable ability to deform in the post ultimate range with a moderate drop in strength. Wall SW15 was an exception to this pattern as it failed in an abrupt manner. The comparison of the results of walls SW13 and SW14 shows that confinement reinforcement affects both the strength and ductility of walls with low shear ratios. A more

detailed discussion and interpretation of these results is presented in section 6.3.

4.3.2.3 Energy Dissipation

The overall force deformation relationship of all walls shows a noticeable pinching effect, which leads to a considerable reduction in the energy dissipation capacity. The pinching effect varies quantitatively with the mode of failure. It is more intense for the walls failing in shear by diagonal tension. However, the fact that it is always present, shows that it is not possible to avoid a considerable reduction in energy dissipation capacity if the shear ratio is low and the walls are designed only with conventional reinforcement. This observation is important as it is not fully compatible with EC8 philosophy regarding the influence of shear forces in the evaluation of the q factors. This subject is further discussed in section 6.8.

4.3.3 Force-Displacement Curves

4.3.3.1 Vertical Displacements

The most important reason for placing vertical transducers on both sides of the walls at several levels was to evaluate the flexural deformations according to the methodology described in section 4.1.6. In this section comments are made on the readings themselves as well as on their average values at the level where M=0 and at a quarter of that level.

The most noticeable features of the vertical displacement curves are the tendency to accumulate upward displacements and the higher stiffness for downward displacements. The increase in the length of the wall is attributed to the accumulation of plastic strains in the

steel and dilatancy of the concrete. Plastic strains accumulate essentially in the lower region of the wall where plasticity spreads. Flexural cracks also open more in this region and therefore the dilatancy of the concrete should increase the length of the wall more in this region. Thus, if the failure mode of the wall is not diagonal tension, most of the increase in length should be concentrated along the lower region of the wall. The comparison of figures B(13)20, B(13)21, B(14)20 and B(14)21 which show the extension of walls SW13 and SW14 slightly below a quarter height and on top, indicate that most of the extension of the wall is concentrated in the lower region. However, the same comparison of the corresponding readings for wall SW12 (figures B(12)21 and B(12)22), which failed in shear by diagonal tension, shows a more even distribution of the extension of the wall along the height. Shear failure curtails the spread of plasticity along the height. Therefore, the increased extension in the upper parts of the wall is attributed to the large opening of diagonal cracks up to the level where M=0.

It is also noticeable that part of the extension of the walls is not recovered upon unloading. The extension at zero load tends to increase with maximum displacement amplitude. Both observations are consistent with the causes to which the extension of the wall was attributed. Steel tensile strains at zero load increased with increased displacement after yielding, and closure of cracks was uneven, particularly if there was slipping in the cracks interface. In the case of monotonic loading, plasticity only occurs in one side of the wall and there is no uneven closure of cracks. Therefore, extension of the wall should be less than in the case of cyclic loading. The lower values of the extension of wall SW11 as compared with the same values for the other walls, confirm this view.

An interesting feature in some readings is the accumulation of downward displacements. This can be seen in the readings at the lower levels of some of the walls which

failed in shear, such as SW15 and SW16 (figures B(15)3, B(16)3 and B(16)4). Even though a reverse of the general trend at the upper levels was not observed, the extension of these walls on top may increase at a lower rate or even decrease after the ultimate load. An example is shown in figure B(16)20. Pilakoutas (1989) has also pointed out similar observations, including the possibility of net shortening of the wall. This is not consistent with the reported observation that the width of diagonal cracks increased continuously throughout the tests. One possible explanation for this inconsistency is that after the ultimate shear force is achieved very large deformations occur between the faces of inclined cracks, as shown in figure 4.21. The figure shows that due to the slippage of the upper portion of the wall along the diagonal crack, the upper portion of the wall moves downwards. This casts doubts about the reliability of the separation of the total deformation into flexure and shear components, after the ultimate shear force is achieved. As figure 4.21 shows, vertical displacements that would be considered as a resultant of rotations of the wall cross sections may in fact be due to slippage along shear cracks.

4.3.3.2 Horizontal Displacements

The difference between the two horizontal readings on either side of the walls at the level where M=0 shows very large openings for the walls failing in shear by diagonal tension, specially the ones under cyclic loading. In the case of walls SW17 and SW18 the opening of the wall was also registered at the third level, slightly above half height. The registered values were somewhat larger or similar to the ones registered at the level where M = 0. This is consistent with observations previously reported in section 4.2, that the increase in the length of the wall cross section extended almost from the base up to the level where M=0. The figures also show that the walls started opening at loads similar to the ones at which the cracking process started. This observation may therefore be a consequence of the large

widths of the diagonal cracks that led to the failure of these walls. The figures show that the opening of the walls tends to increase with the maximum level of applied displacement and is not very sensitive to the level of applied load. Little recovery of opening is observed in unloading.

The same observation was registered for the walls that did not fail in shear by diagonal tension and in wall SW11 which was monotonically loaded. However, the values were distinctively lower. In the case of wall SW13 some stirrups did not yield, as discussed in section 4.3.4.6 below. This did not allow the development of the large crack widths observed in the walls failing by diagonal tension, thus restricting the opening of the wall.

The lower values of the opening registered for SW11 can only be attributed to the load history. Notice that SW11 failed in shear at a load lower than SW12. The uneven closure of cracks and the degradation along the cracks interface during cyclic loading may be responsible for the permanent opening registered at zero load and its increase with the maximum applied displacement. Therefore, it can be concluded that the shear resisting mechanisms degraded faster in wall SW12 (as compared to SW11) due to the cyclic nature of the loading regime. The faster degradation of the shear resisting mechanisms led to failure at a much lower level of applied displacement. This point is further discussed in section 6.6.1.

The comparison of the horizontal readings on the lower levels with the overall force-deformation curve does not show similar increase in displacement at any stage. Therefore, a translational deformation of the walls did not take place, which confirms that none of the walls suffered a sliding shear failure, as previously reported in section 4.2.

4.3.3.3 Flexural and Shear Deformations

The comparison of the flexural and shear component diagrams shows qualitative differences between both types of diagram. The pinching effect described in section 4.3.2.1 seemed to affect essentially shear deformations. The flexural displacement vs force diagrams only exhibited a small increase in stiffness during reloading. It should be noticed that when cracks due to loading in different directions are opened simultaneously, the shear force can only be transferred by aggregate interlock and dowel action. These mechanisms provide a very low shear stiffness to the wall at such stages. In contrast, for the case of the flexural component the decrease in stiffness due to the lack of contribution of the concrete is less significant. This can be attributed to the large amount of compressive reinforcement that continues to resist the axial force generated by bending moment. The increase in the pinching effect observed in the walls that failed by diagonal tension seemed to have been essentially due to the shear component, as it is more affected by the opening of large diagonal cracks.

The decrease in stiffness on reloading is more noticeable after yielding of the main flexural reinforcement and seemed to have affected both types of deformation. In both cases the reloading stiffness decreases with increased applied maximum displacement. This observation affects shear deformations even if diagonal tension failure is prevented.

The observed decrease in unloading stiffness with increased maximum displacement on the overall diagrams affected both components of the total deformation. The mode of failure did not appear to have any significant effect on the unloading segments of either of the components of the deformation.

Both envelopes of flexure and shear deformations showed a nonlinear pattern, such as the total deformation. The envelopes of both components of the deformation were affected

qualitatively by cracking and yielding of the main flexural reinforcement in the same way as the total deformation. This shows that what could be labelled as yielding of the envelope of the shear diagram is not associated with yielding of the horizontal web reinforcement. It is postulated herein that large shear deformations are triggered by yielding of the flexural reinforcement due to its effect on the opening of flexural and diagonal cracks. Both envelopes of shear and flexural deformations showed lower stiffness, even before yield, for the walls failing by diagonal tension. Whilst the above-mentioned effect has little quantitative consequences, it reflects the effect of diagonal cracks on the flexural component of the total displacement.

All walls under cyclic loading showed that after cracking and yielding of the main flexural reinforcement shear deformations increased faster than flexural deformations. Therefore elasticity provides an upper limit for the contribution of the flexural component to the total deformation. Wall SW11 showed increases in shear deformations at cracking and yielding, but no significant increase in between. This suggests that shear resisting mechanisms degrade faster under cyclic loading. Similar conclusions were drawn by other authors as referred to in chapter 2. However, an exception to this trend were the results presented by Lefas (1988), who came to the conclusion that at the ultimate load the contribution of flexural deformations would be higher than it would be given by elasticity. This can only be attributed to the errors associated with method of area $\alpha 3$ which Lefas used to calculate flexural deformations, as referred to in section 4.1.6.

The failure mode has a clear effect on the energy dissipation capacity of the walls. However, wall SW13 which did not fail in shear by diagonal tension, exhibited considerable pinching. The fact that this effect is associated essentially with shear deformations shows that for walls with a certain mode of failure, the balance between shear and flexure commands the energy dissipation capacity.

For each wall this balance is dependent essentially on the shear ratio. Figure 4.22 shows the balance between shear and flexural deformations for a wall of shear ratio 2 which failed in flexure (Pilakoutas, 1990). Figure 4.22 also shows the same trend of increasing shear deformations with maximum applied displacement. However the contribution of shear deformations is clearly lower than in the case of the walls of the current test programme, as the comparison of figure 4.22 with figure B(13)18 shows.

4.3.3.4 Base Rotation

The rotation of the foundation beam was assessed by the two vertical transducers placed on either side of the wall, as indicated in figure 4.13. The displacements are in general extremely small for all walls with the exception of SW13. In this case the condition of almost full fixity was not achieved. As the displacements of the foundation beam are known, the component of all the other displacements due to that movement could be calculated and subtracted from the corresponding readings. Therefore, all results of wall SW13 were processed to exclude the movement of the foundation beam. For all other walls the movement was sufficiently small to be disregarded. In these cases there are variations in stiffness but they are small, hence the rotational stiffness at the base of the wall was considered constant. Its value was calculated for all walls (with the exception of SW13) and is shown in table 4.6. The horizontal displacement at the level of the top horizontal displacement due to the foundation δ_{hf} was calculated at ultimate load and failure. The results are shown in table 4.6. The results show that the contribution of the rotation of the foundation to the top horizontal displacement at ultimate load and failure does not exceed 2.8% and 1.4% respectively. These values can be considered negligible and they were not considered in the evaluation of shear and flexural deformations.

4.3.3.5 Out-of-Plane Displacements

The out-of-plane displacements may be due to the fact that the walls were not perfectly symmetric or to any misalignment between the loading system and the specimens.

The ratio between length and width of the wall cross section was 10. Thus, in the weak axis direction its stiffness and yield moment were approximately 100 and 10 times less than in the testing direction. Therefore, the yield moment would be reached in the weak axis direction at a displacement approximately 10 times larger than in the strong axis direction. Hence, even if the full out-of-plane displacement was due to a moment, it would not exceed 15% of the out-of-plane yield moment before the ultimate load was reached in all cases. As already referred to in section 2.1.1.3, Aoyama and Yoshimura (1982) demonstrated experimentally that the in-plane behaviour is not affected by out-of-plane moments below 50% of the weak axis yield moment.

4.3.4 Strain-Gauge Results

In all walls there were locations, generally at the bottom of the ϕ8mm bars, where more than one gauge was placed, as already referred to in section 4.1.5. Usually one gauge was placed in each of the two bars in equivalent positions. In wall SW11 two gauges were placed in each bar at locations 2 and 10. The comparison of the readings taken at equivalent locations showed some variability. This can be due to bending of the bars, out-of-plane effects, differences of area at the ground sections, etc. Therefore, care must be taken in the interpretation of strain gauge readings.

4.3.4.1 Bottom Edge Members

Some of the gauges at these location failed before yield or shortly afterwards. Others performed satisfactorily up to strains several times the yield strain. The following observations are given on the readings:

- Before yielding, loading and unloading in tension and compression occur at constant stiffness. The stiffness is higher in compression.

- There is practically no energy dissipation before yielding.

- Pre-yield behaviour gave no indication of the failure mode. Yielding of the extreme bars appears to have occurred at similar loads in all walls, between 70KN and 74KN.

- After yielding the maximum plastic strain increases when a new MD is applied. The reloading stiffness in tension decreases with increased values of MD.

- Initial unloading stiffness is always higher than in the case of reloading.

- The area within the loops after yielding is large, especially in the ϕ8mm bars, indicating that yielding of the main flexural reinforcement is an important source of energy dissipation.

- With progressive increase in MD, plastic tensile strains are accumulated. Increased levels of irrecoverable strains are registered at zero load. The increase in plastic tensile strains is one of the major causes of the uplifting of the wall, already referred to in section 4.3.3.1.

- Walls that failed in shear by diagonal tension attained lower levels of plastic tensile strains. This should be expected, as failure by diagonal tension occurs at lower loads.

4.3.4.2 Bottom Web Vertical Strains

The readings of the gauges placed on the vertical web reinforcement at the bottom level are shown in figures B(13)27, B(13)28, B(14)26, B(15)14 and B(15)15. The most important feature in the readings is that they show the bars were in tension for both directions of loading. The maximum strains seemed to increase steadily after the yield load was attained. The largest strains were attained in walls SW13 and SW14. In general the bars did not yield. Accumulation of plastic tensile strains was moderate. This may have occurred due to the extension of the wall. The strains in the bars of wall SW15 showed lower levels of strains than the other walls.

It can be concluded that at early stages of the load history the neutral axis shifted away from the centre of the cross section. This can only be attributed to cracking. The increase in the maximum strains after the yield load was achieved suggests a continuous shift of the neutral axis towards the compressive side in the post- yield range. This effect may be attributed to the extension of existing cracks due to accumulation of plastic tensile strains in the main flexural reinforcement. It is also necessary to establish internal equilibrium of forces. The lower strains registered in wall SW15 were due to the fact that diagonal tension failure interrupted the process of decreasing the neutral axis depth. This process would probably continue until the ultimate flexural capacity was reached.

4.3.4.3 Second Level Vertical Strains

The purpose of registering strains on the main vertical reinforcement 190mm away from the base was to monitor the spreading of plastic tensile strains in that reinforcement.

The readings of walls SW13 and SW14 show that the flexural reinforcement at that level yielded. The readings of the walls that failed by diagonal tension showed lower levels of strain, which indicate that most bars did not yield above that level. It is obvious that diagonal tension failure curtails the spread of plasticity along the flexural reinforcement.

4.3.4.4 Vertical Strains at Zero Moment Level

The readings on the bars of the edge members showed the same pattern in all walls and readings. Very low levels of strain were registered before cracking. They became tensile for both directions of loading after the cracking process started. The yield strain was not exceeded but strains in excess of half the yield strain were recorded. On the diagrams of some bars, shift towards the tension side was visible, leading to moderate accumulation of tensile strains. This was due to the opening of cracks. The dissipation of energy is practically nil.

Much fewer readings are available for the inner $\phi 4$ bars. Very low compressive strains were registered before cracking started. After cracking some readings became tensile for both directions of loading. However, these strains tend to be more moderate than on the edge members. Other readings continued to register moderate levels of compressive strains.

The development of the truss mechanism to resist shear leads to a shifting of the tensile force in the flexural reinforcement. Therefore, at a point of contraflexure the reinforcement on both sides of the section should be in

tension. This could be the reason for the tensile strains registered at the edge members.

It was already shown that after cracking, the inner ϕ4 bars were in tension for both directions of loading at the base section. This can only be due to the bending moment and therefore the same situation should occur along most of the height of the wall. The spreading of tensile strains to the level where M=0 may be the reason why these strains were registered in some of the inner ϕ4mm bars at this level.

The resultant of the tensile stresses in the steel at the level where M=0 has to be equilibrated by compressive stresses in the concrete. This means that the tendency of the wall to uplift is resisted by the steel, which in turn induces compressive stresses the concrete in an effect similar to prestressing.

4.3.4.5 Vertical Strains on Top of the Wall

Gauges were placed on the extreme vertical bars below the top beam in walls SW11 and SW12. The purpose was to confirm that the vertical reinforcement on top of the walls worked only in the elastic range. The results show that no yielding of the main flexural reinforcement occurred. Hence, no changes in the design of the upper part of the wall were considered necessary and no more gauges were placed at this location in subsequent specimens.

4.3.4.6 Stirrups

Strain gauge readings of stirrups showed that very low levels of strain were recorded before cracking occurred in their vicinity. After cracking the stirrups developed tensile stresses for both directions of loading. Stiffness was in general not very different for the two directions with the exception of SW12. However, the stiffness showed a tendency

to decrease after yielding of the main flexural reinforcement.

In the case of wall SW12 there were larger differences of behaviour between the two directions. This was due to the inadequacy of the anchorage detail, as referred to in section 4.1.3.3.2. The stirrups could only develop their strength beyond the yield stress when the anchored side of the stirrups was on the compressive side of the wall. In the case of wall SW11 the same problem occurred with all stirrups, since they were all anchored in the tension side. It is therefore impossible to quantify the strength of the stirrups in these two walls. Hence, the results of walls SW11 and SW12 should in general be used only in a qualitative manner. However, it should be noted that the strength provided by the stirrups of wall SW12 should be higher than in the case of SW11, because at each stage half of the stirrups could be considered effective.

The results of walls SW13 and SW14 show that the stirrups slightly above the level where M=0 developed levels of strain similar to the other ones below. That illustrates the influence of the boundary conditions used, already referred to in section 2.3.1.1. If at that level a stiff loading beam had been used, the stirrups close to the loading beam would have registered much lower levels of strain, as reported by Pilakoutas (1990).

The readings showed that particularly after yielding of the main flexural reinforcement, there are large increases in strain with very little increase in load. The imperfect closure of diagonal cracks may tend to increase the length of the wall cross section, thus contributing to increased stirrup's strains. However, the increase in strain before the stirrups have yielded indicates that the increase in the force transferred by the stirrups is much larger than the increase in the shear force applied to the wall. This indicates that other shear resisting mechanisms are

degradating. A similar conclusion was drawn by Goodsir (1985), as referred to in section 2.1.1.4.

The readings of walls SW16, SW17 and SW18 in gauges that worked beyond the ultimate load (wall SW16 reads 19 and 20, wall SW17 reads 19 and 21 and wall SW18 reads 19, 20, 21 and 22) indicate that all stirrups underwent large tensile strains beyond the yield level. Most of the stirrup gauges of wall SW13 showed levels of strain slightly above the yield level, with the two lower ones showing strains below the yield level. This indicates that the total yield force the stirrups could mobilize was not far from its limit. The much lower strain exhibited by the bottom stirrup may be due to lack of effectiveness. These results seem to indicate that shear failure by diagonal tension is associated with the exhaustion of the yield strength of all the stirrups which cross the failure surface below the neutral axis. It also points to the fact that the diagonal tension strength of wall SW13 was not far in excess of its ultimate load.

The two stirrups ϕ6 in wall SW15 did not yield. However, shear failure happened despite the fact that stirrups still possessed a reserve of strength. This indicates that the concentration of the stirrups at the level where M=0 is not an efficient way of designing against shear.

4.3.4.7 Confinement Reinforcement

In general strain gauge readings of confinement reinforcement showed moderate values of extension of these bars. Of particular interest are the readings of wall SW13 which showed the highest strength, ductility and energy dissipation capacity. The low values of the strains registered indicate that the amount of confinement reinforcement was more than necessary. This points to the fact that designing walls with low shear ratios with rules applicable to more flexural walls is a safe procedure. In fact, it may lead to an excess supply of confinement

reinforcement. This should be expected as flexural walls undergo much larger compressive strains than walls with low shear ratios. It also points to the fact that failure of the concrete in wall SW13 must have started outside the well confined edge member.

TABLES

	Mix proportions by weight
Cement	1.00
10 mm aggregate	3.15
Course sand	2.00
Fine sand	0.89
Free water	0.68

Table 4.1 - Concrete mix proportions

Steel Type	E_s MPa	f_y MPa	E_{sh} MPa	f_{su} MPa	E_{ul} Strain x 10E6
ϕ 4 Round	200 000	414	2 600	471	60 000
ϕ 6 Deformed	200 000	608	2 200	667	40 000
ϕ 8 Deformed	200 000	436	2 500	623	140 000
ϕ12 Deformed	200 000	500	1 300	600	85 000

Table 4.2 - Properties of steel reinforcement

Wall	SW11	SW12	SW13	SW14	SW15	SW16	SW17	SW18
Testing Day	54	48	105	85	69	30	32	32
Cube Strength (MPa)	46.5	45.8	53.7x3*	45.2	48.6	46.2	44.0	46.8
	46.4	46.9	55.4	45.0	45.9	42.8	44.6	42.0
	44.7	48.8	56.6	47.2	48.8	43.5	45.8	42.0
	46.7	47.9	56.6	48.4	45.6	43.7	45.9	45.2
					48.8	46.2	45.0	47.0
Average (MPa)	46.1	47.4	55.0	46.5	47.5	44.5	45.1	44.6

* Tested between 28th day and day of testing

Table 4.3 - Results of compressive tests in cubes

Wall SW 11		Wall SW 12		Wall SW 13		Wall SW 14		Wall SW 15		Wall SW 16		Wall SW 17		Wall SW 18	
Disp. (mm)	Crack (mm)	Disp. (mm)	Crack (mm)	Disp. (mm)	Crack (mm)	Disp. (mm)	Crack (mm)	Disp. (mm)	Crack (mm)	Disp. (mm)	Crack (mm)	Disp. (mm)	Crack (mm)	Disp. (mm)	Crack (mm)
1.0	0.15	1.0	0.1	0.6	0.1	0.9	0.08	0.8	0.15	0.8	0.15	0.8	0.05	0.4	0.15
1.4	0.3	1.7	0.2	1.6	0.2	1.6	0.2	1.6	0.45	1.6	0.5	1.7	0.3	0.8	0.25
1.9	0.4	2.5	0.5	2.2	0.28	2.5	0.3	2.4	1.2	2.4	0.9	2.5	0.7	1.6	0.5
3.9	0.5	3.2	1.0	2.8	0.35	3.3	0.4	3.2	1.6	3.2	1.5	3.2	1.2	2.4	0.8
5.2	1.5	4.0	1.8	4.2	0.4	4.1	0.5	4.0	2.3	4.0	2.2	4.1	1.7	3.3	1.4
6.5	2.9	4.8	5.0	5.0	0.5	4.8	1.0			4.8	5.0	4.8	3.0		
				5.8	0.6	5.8	1.7			5.8	8.0	5.6	4.0		
				7.5	0.9	6.6	1.9								

Table 4.4 - Width of largest diagonal crack of each wall

Wall	Ultimate Load				Failure			
	Force (KN)	Displ. (mm)	Secant Stiffness K_u (KN/mm)	Displ. duct. ratio μ_u	Force (KN)	Displ. (mm)	Secant Stiffness K_f (KN/mm)	Displ. duct. ratio μ_f
SW 11	92.6	4.7	19.7	1.96	72.4	7.4	9.8	3.08
SW 12	94.7	3.5	27.1	1.46	88.8	5.5	16.1	2.29
SW 13	108.3	7.5	14.4	3.13	80.6	9.3	8.7	3.88
SW 14	98.8	4.1	24.1	1.71	79.0	6.6	11.1	2.75
SW 15	85.0	3.2	26.7	1.33	72.0	4.0	18.0	1.67
SW 16	80.3	4.1	19.6	2.93	65.0	8.1	8.0	3.38
SW 17	83.6	4.8	17.5	2.00	66.8	8.1	8.2	3.38
SW 18	99.9	3.3	30.3	1.38	80.0	8.2	9.8	3.42

Table 4.5 - Force, displacement, stiffness and ductility at ultimate load and failure

Wall	Rotational Stiffness (KN.mm/rad) x 10^6	δ_{HF} at ultimate load (mm)	δ_{HF}/δ_H control at yield (%)	δ_{HF}/δ_H control at failure (%)
SW 11	170	0.133	2.8	1.4
SW 12	336	0.069	2.0	1.2
SW 14	501	0.048	1.2	0.5
SW 15	646	0.032	1.0	
SW 16	556	0.035	0.9	0.4
SW 17	640	0.032	0.7	0.3
SW 18	954	0.026	0.8	0.3

Table 4.6 - Displacements due to the foundation

FIGURES

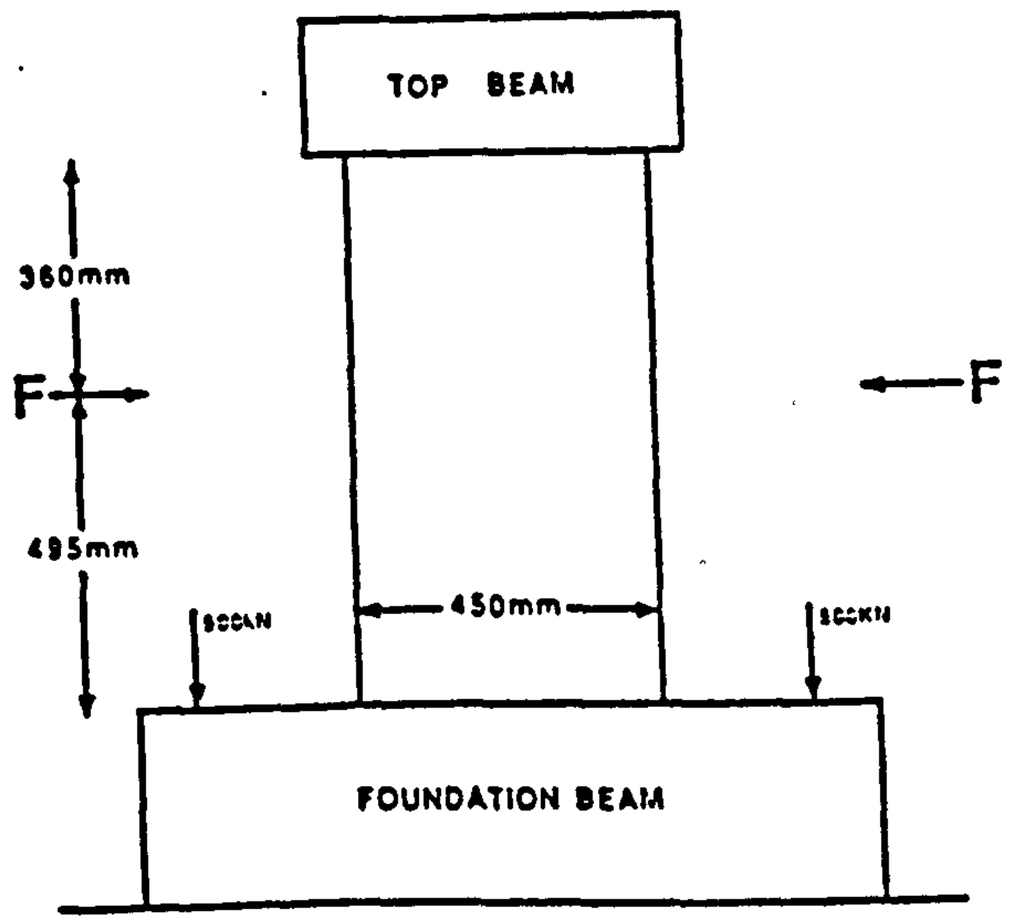


Figure 4.1 Wall specimen

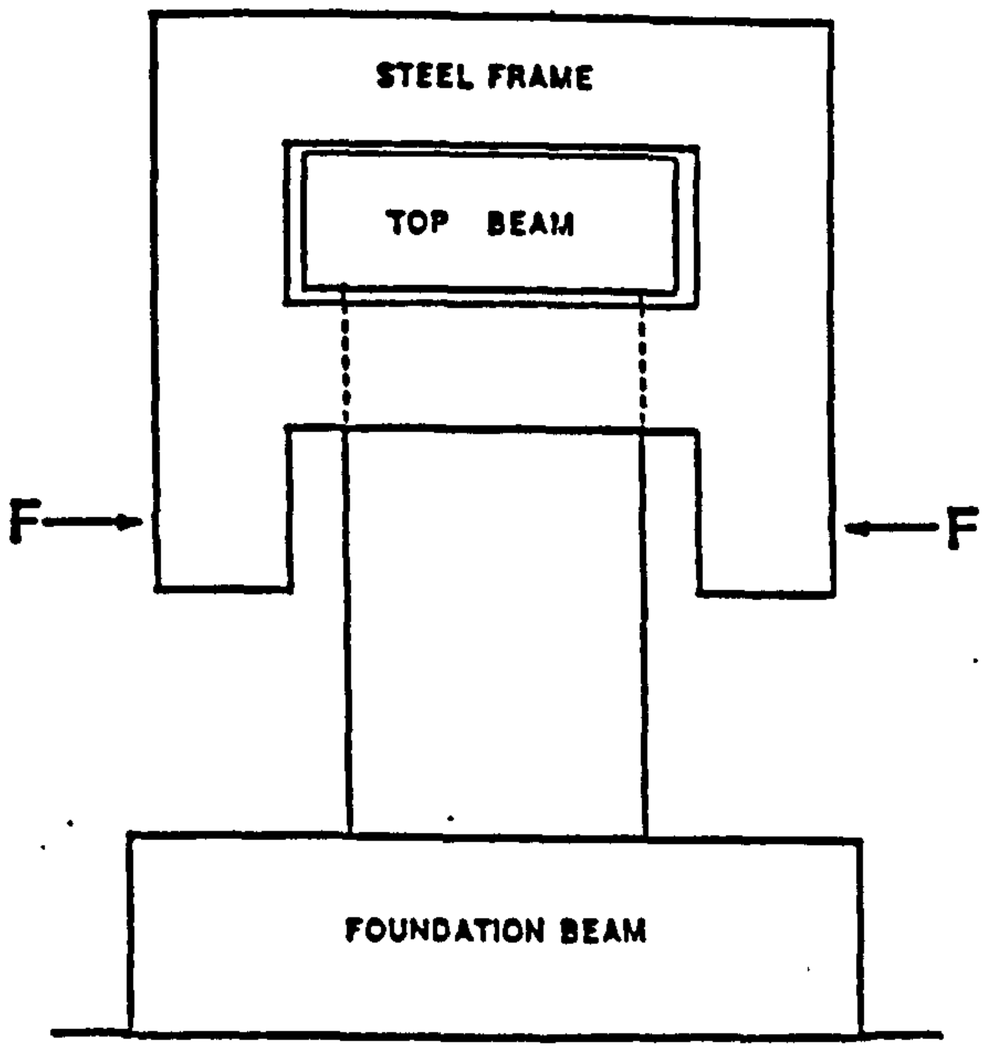


Figure 4.2 Load transferring system

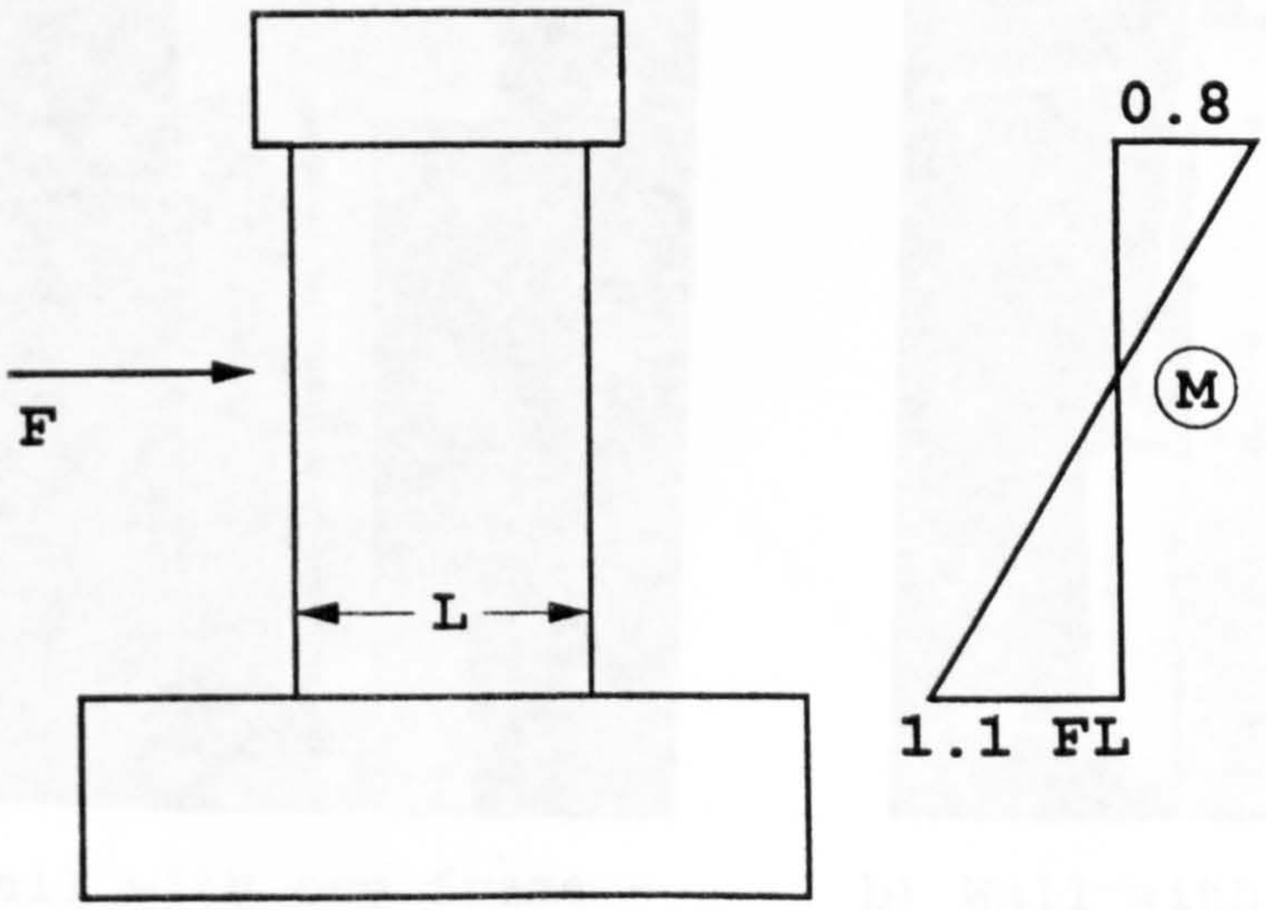


Figure 4.3 Bending moment diagram on the walls

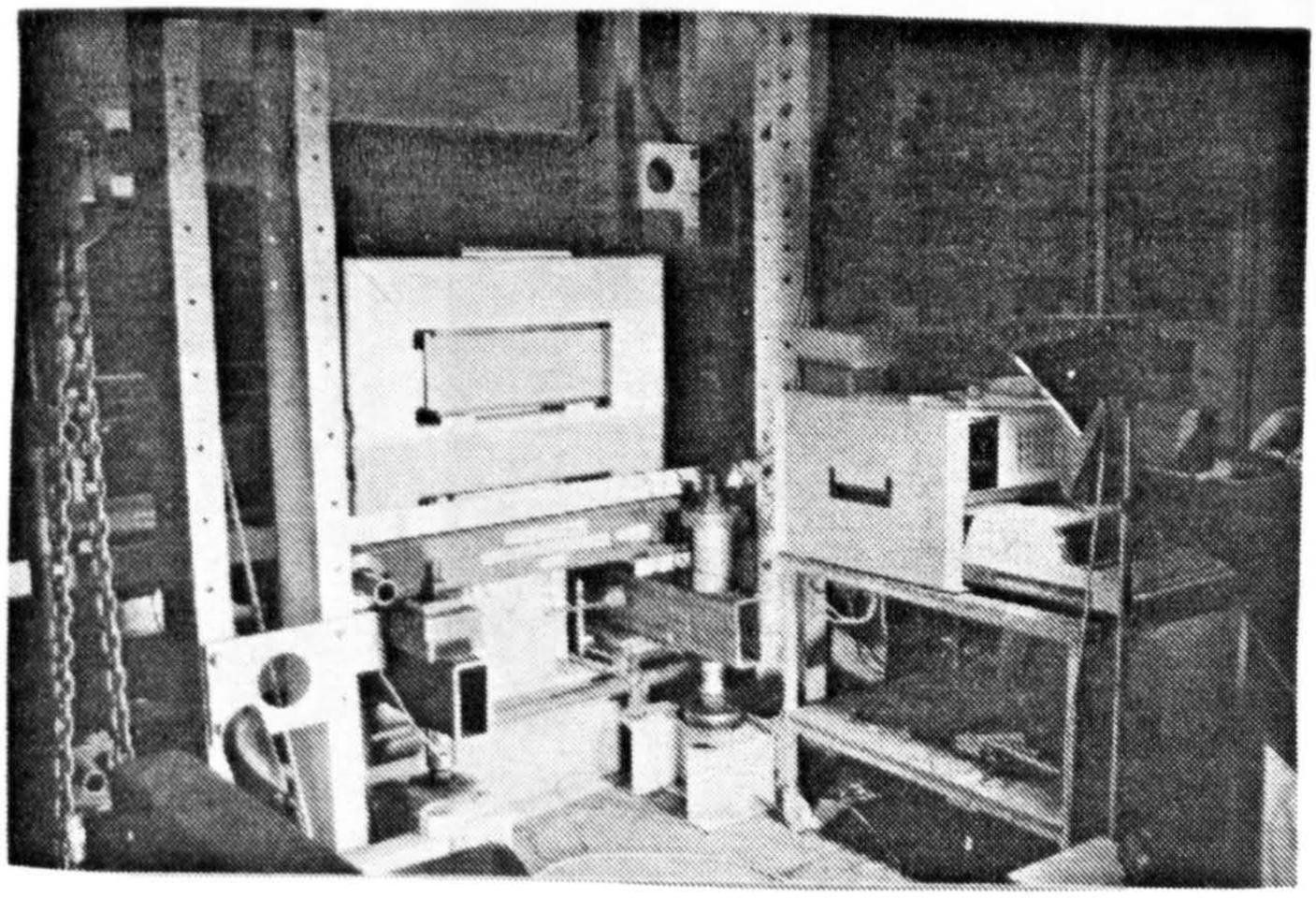
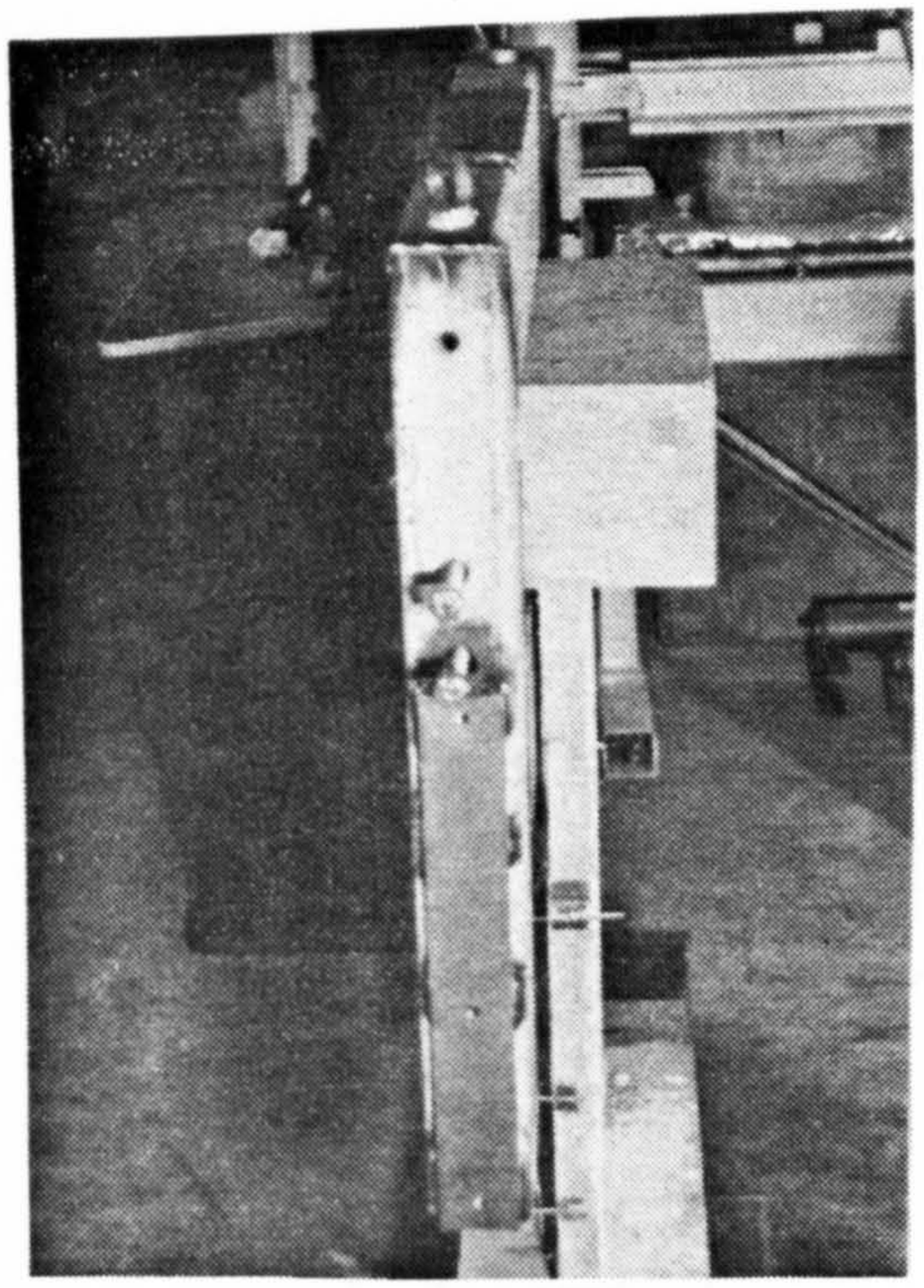
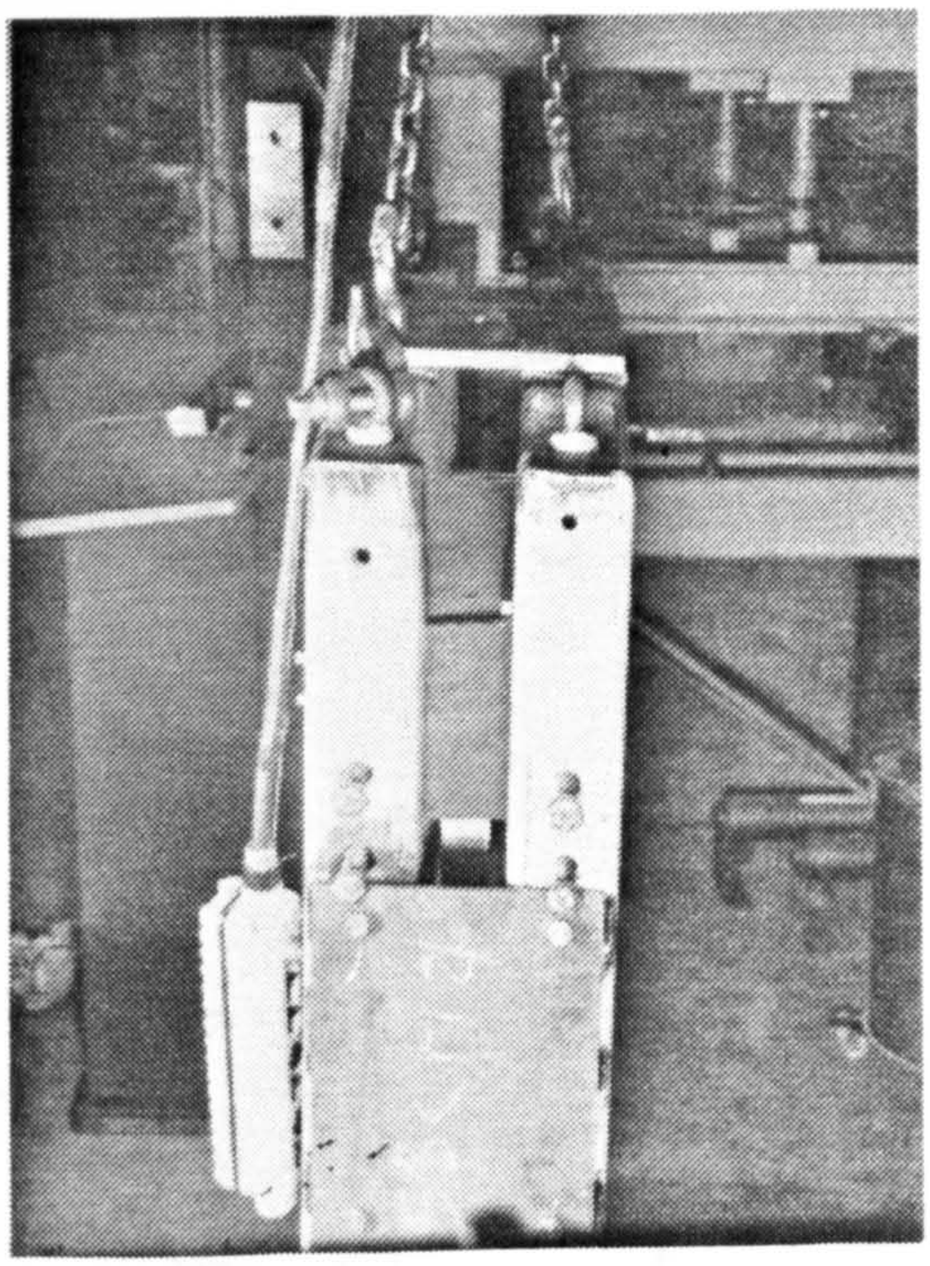


Figure 4.4 Photograph of the test-rig



a) Wall with one frame - side view



b) Wall with the two frames and connecting plates - side view

c) Front view

Figure 4.5 Photographs of the connection wall-steel frames

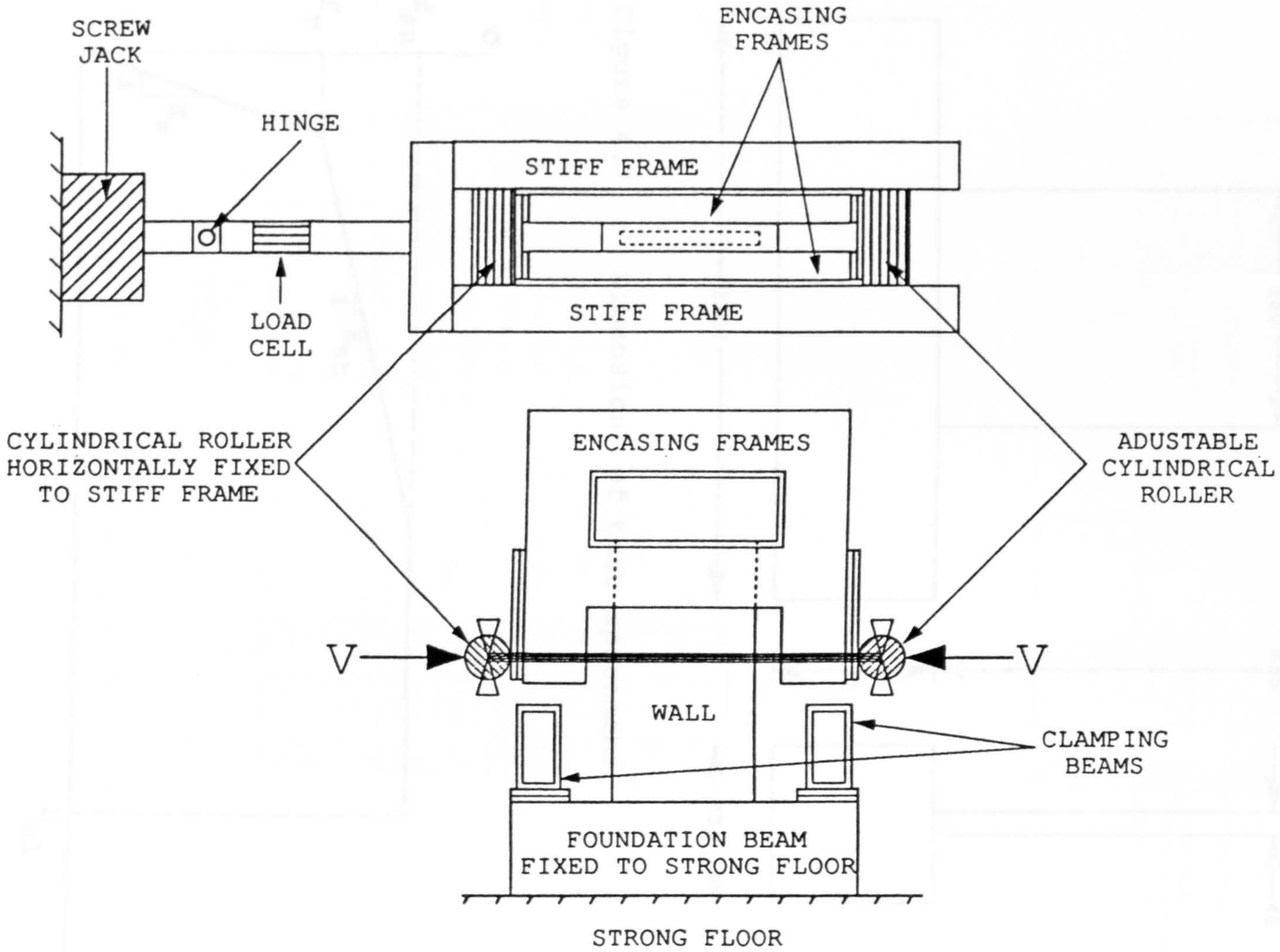


Figure 4.6 Schematic representation of the test-rig

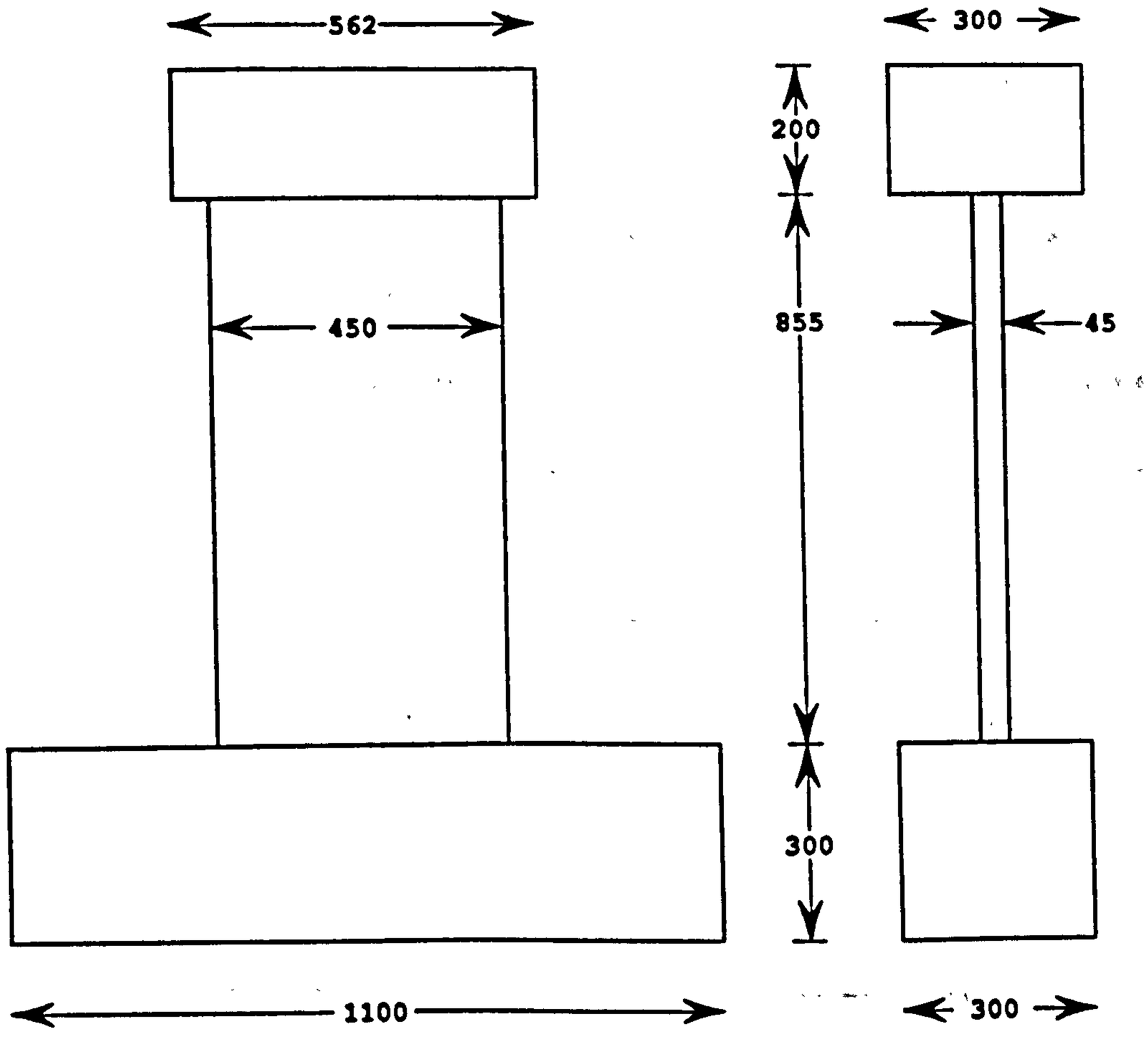


Figure 4.7 Dimensions of test specimens

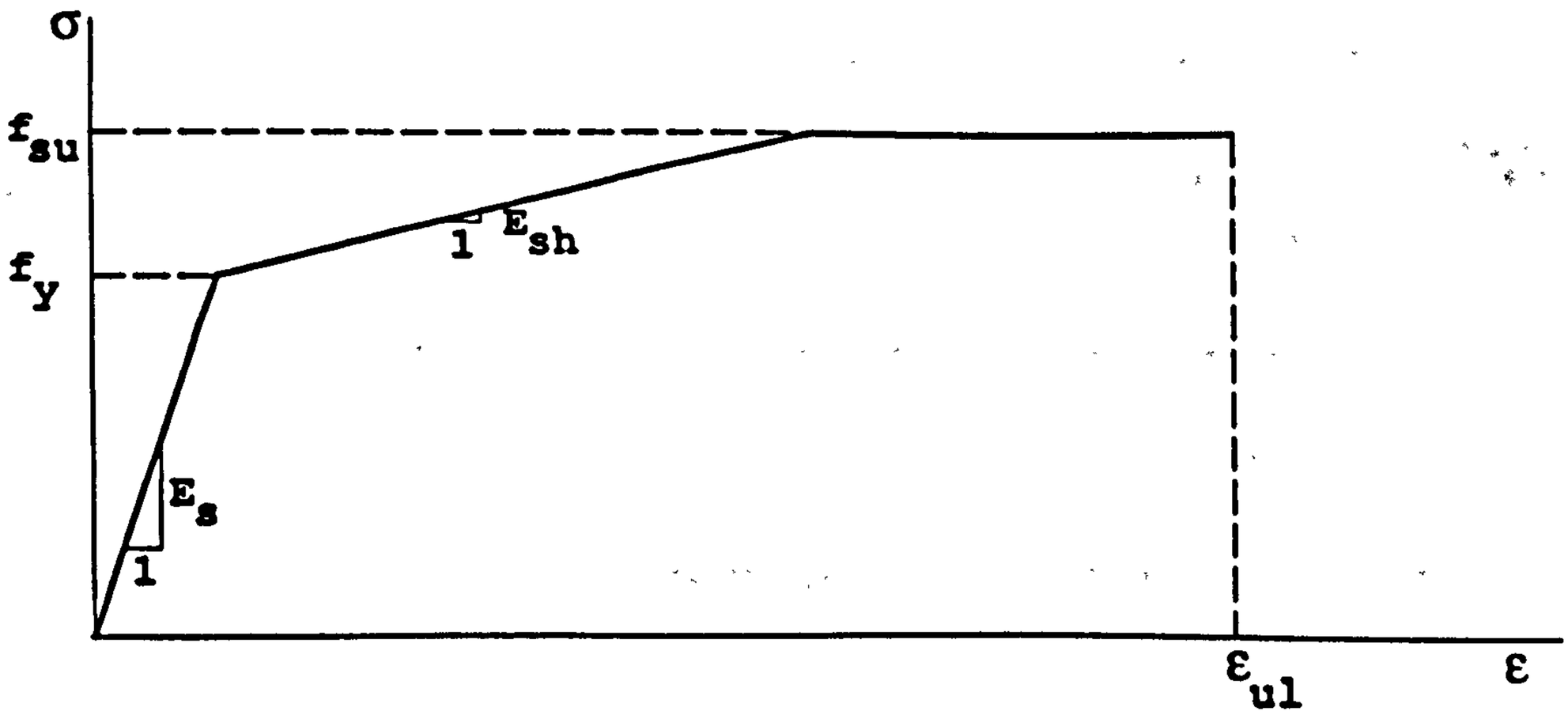
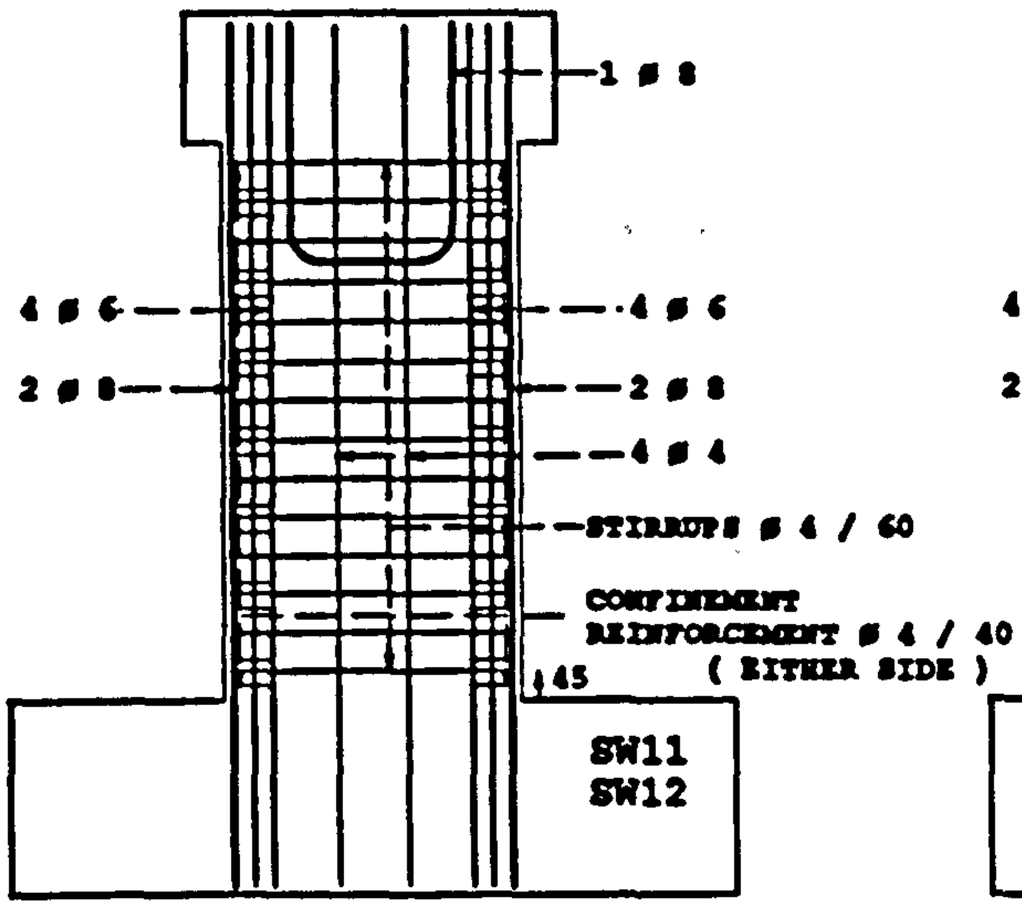
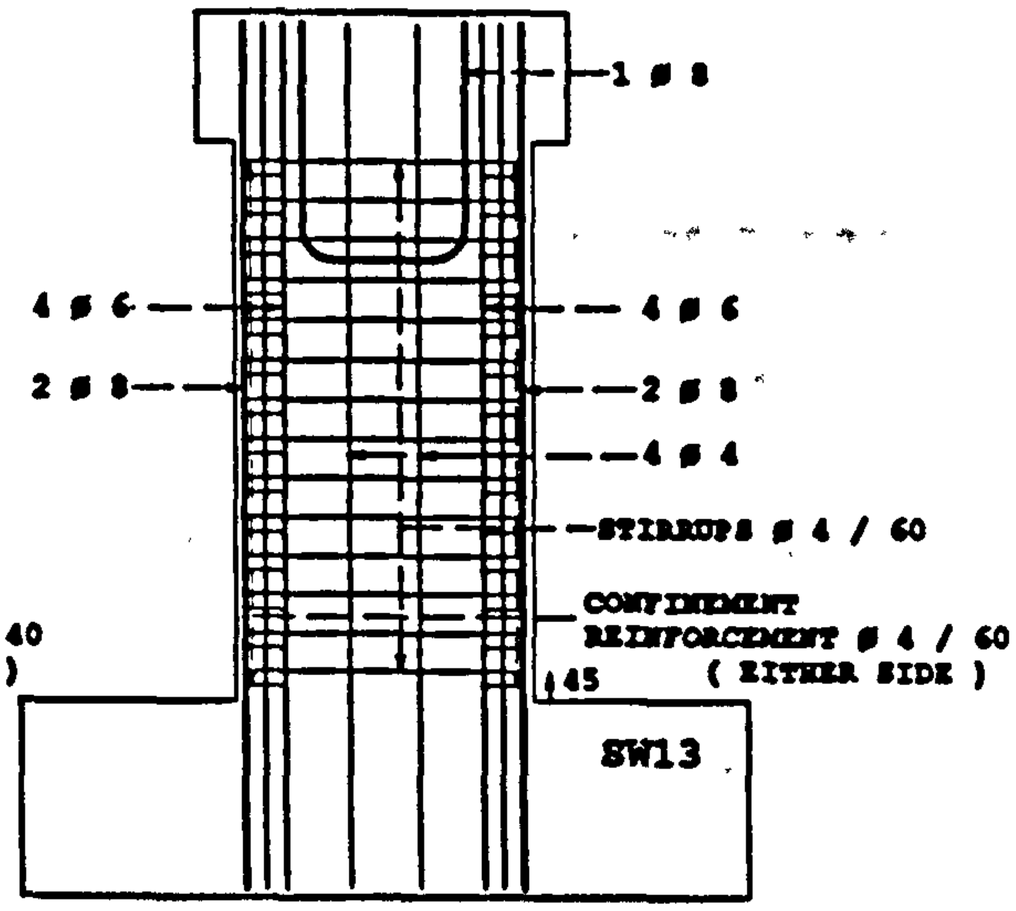


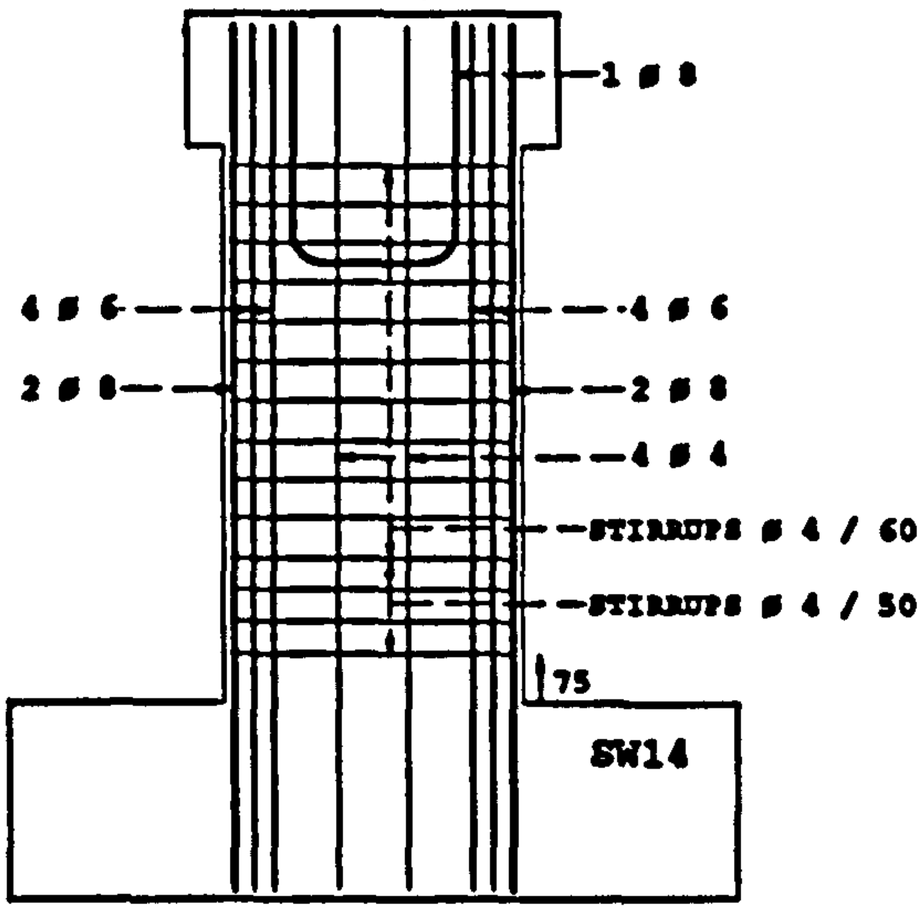
Figure 4.8 Trilinear representation of stress-strain diagram for steel



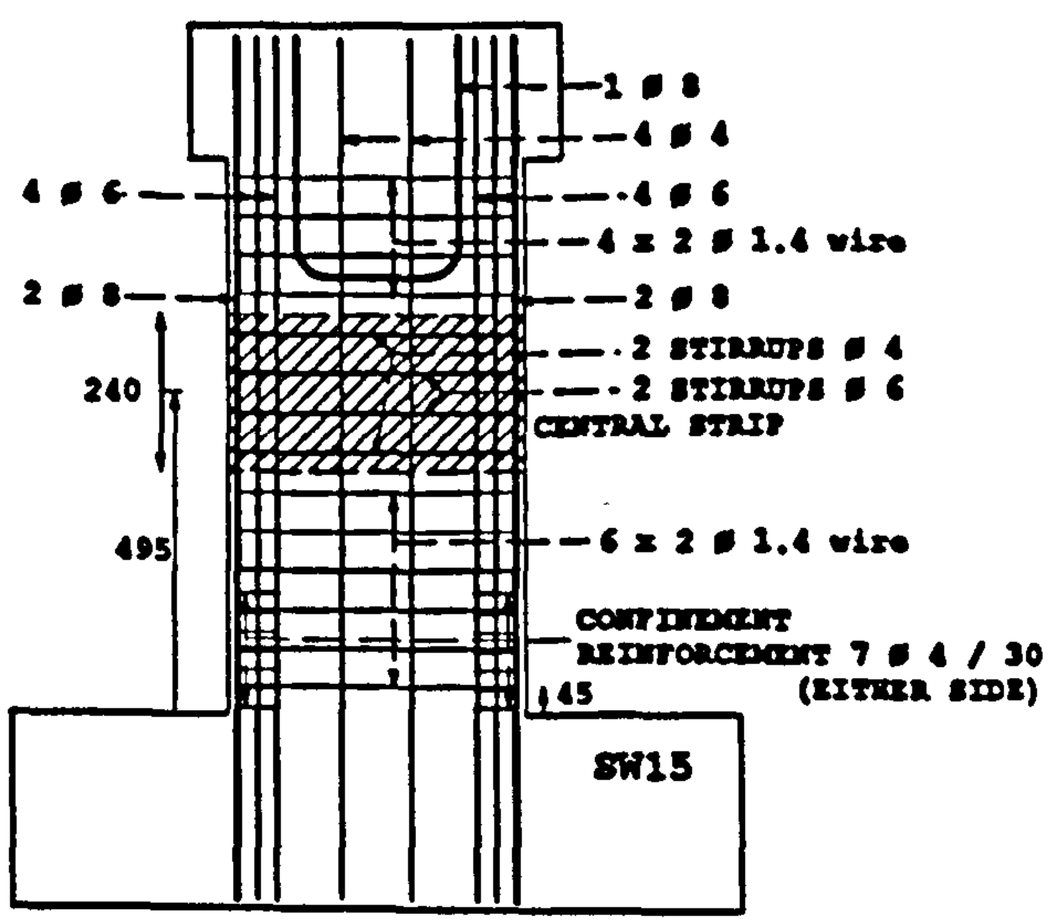
a) SW11 and SW12



b) SW13

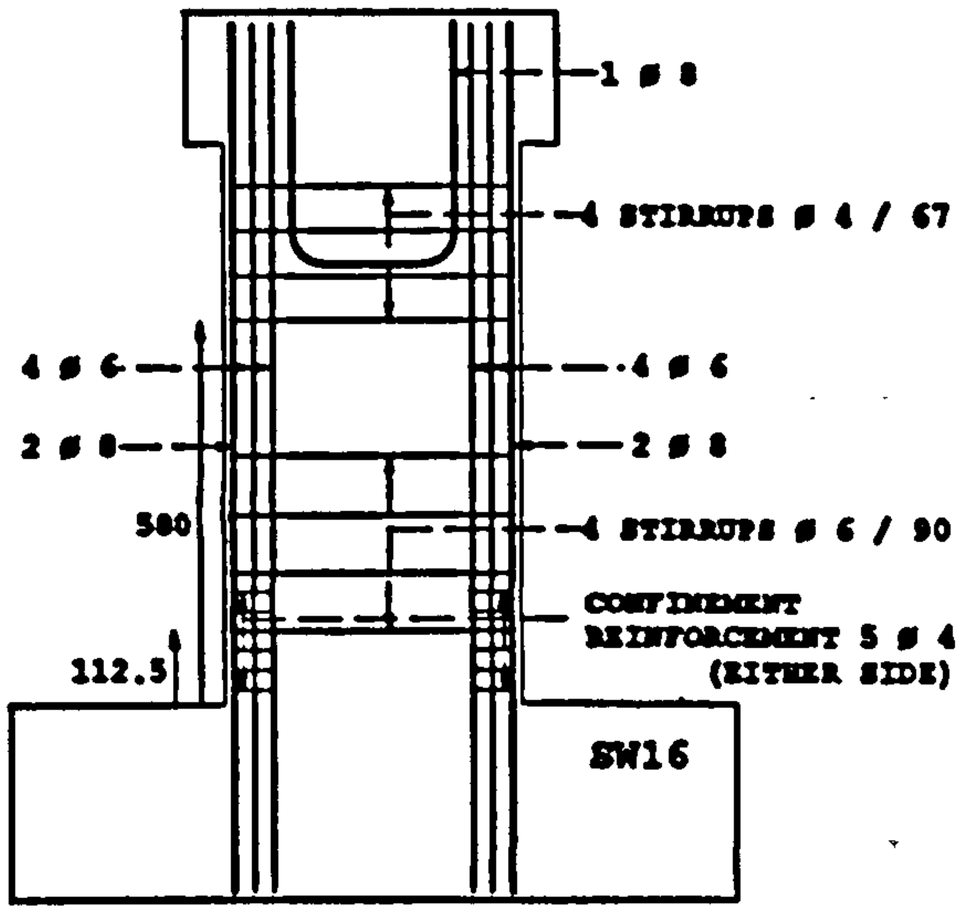


c) SW14

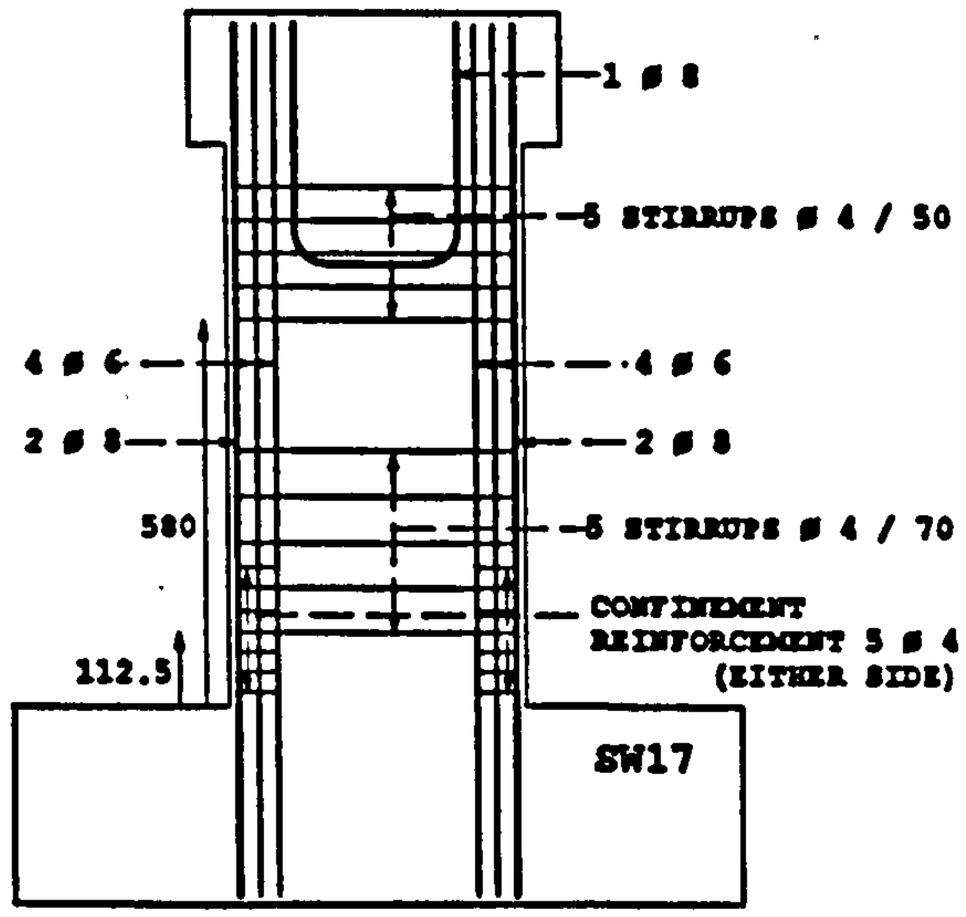


d) SW15

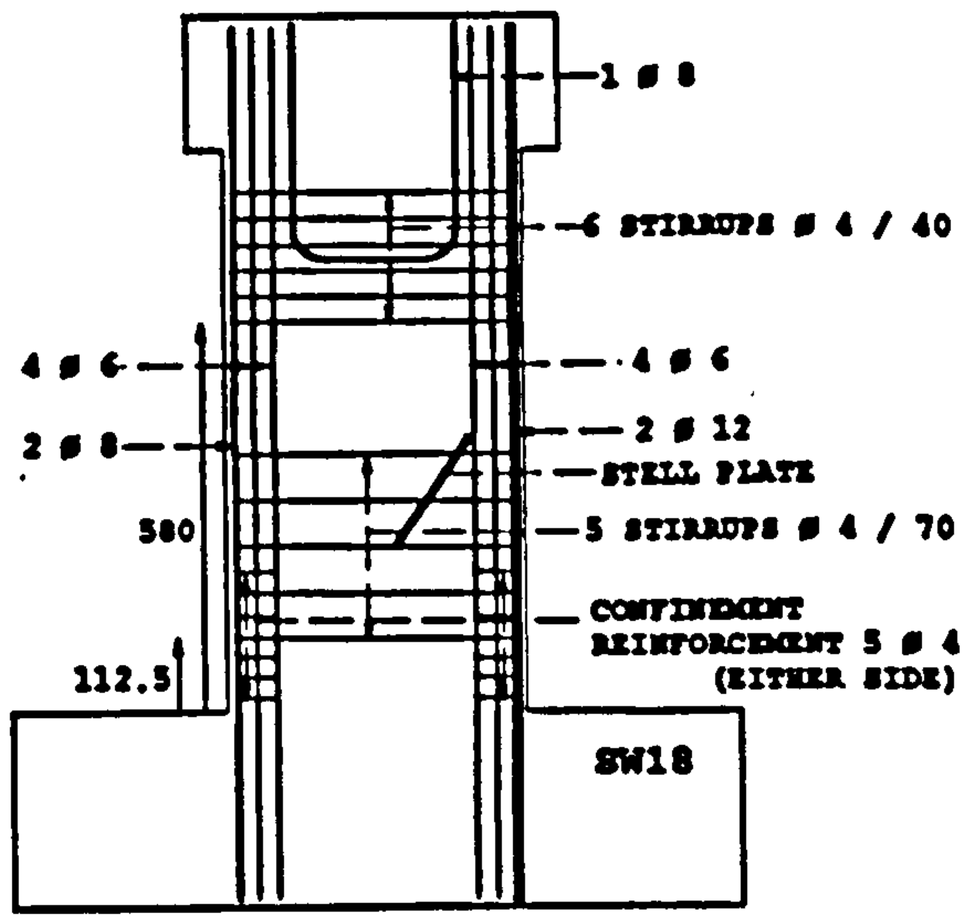
Figure 4.9 Reinforcement details of the specimens



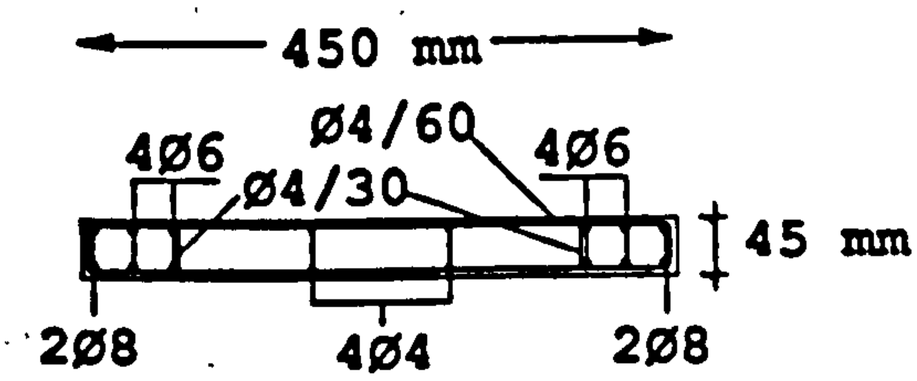
e) SW16



f) SW17



g) SW18



h) Detail of the cross section

Figure 4.9 Reinforcement details of the specimens (cont.)



a) Walls SW11 and SW12 b) All other walls

Figure 4.10 Details of the stirrups

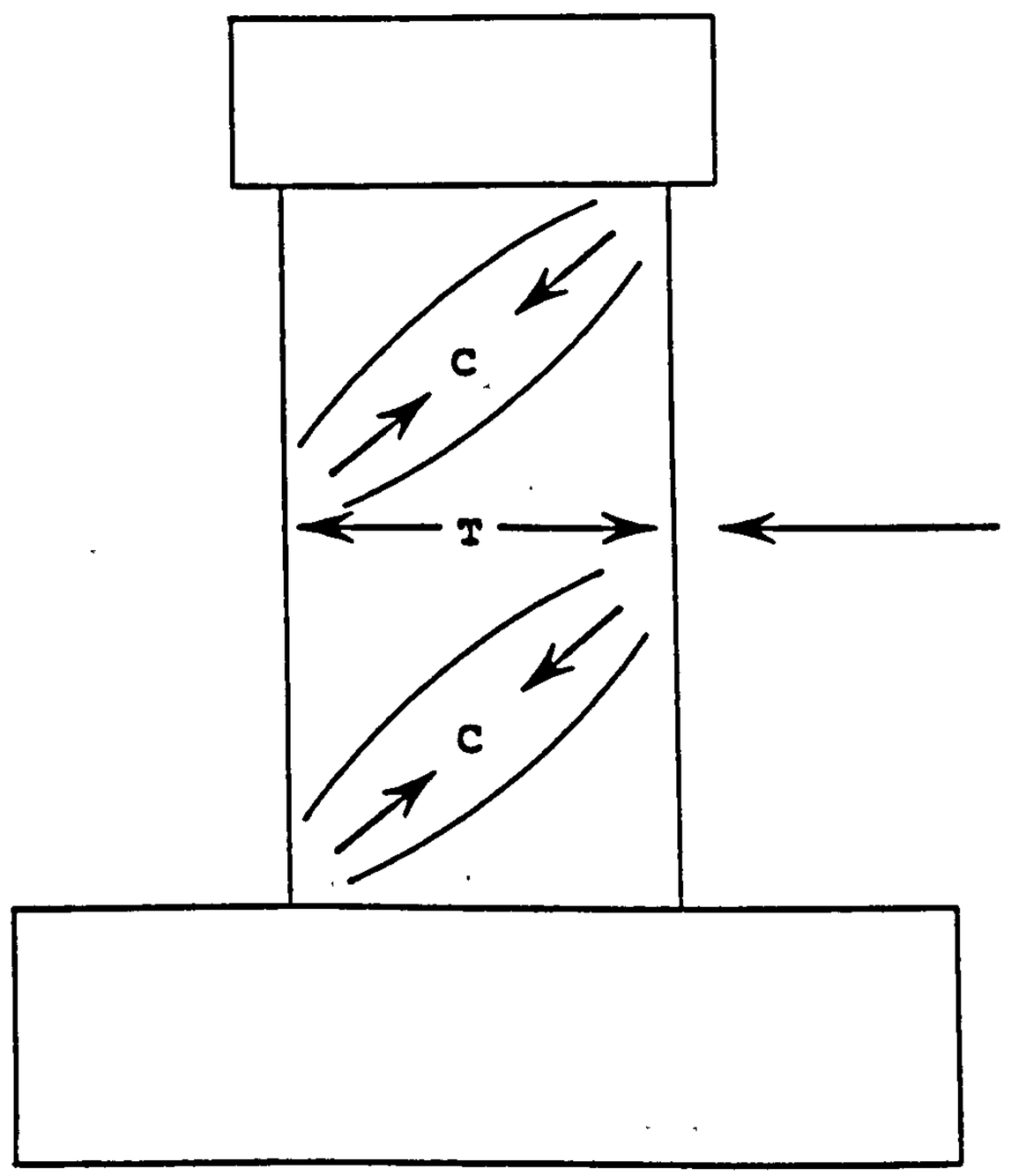


Figure 4.11 Suggested path of the compressive force (Kotsovos, 1989)

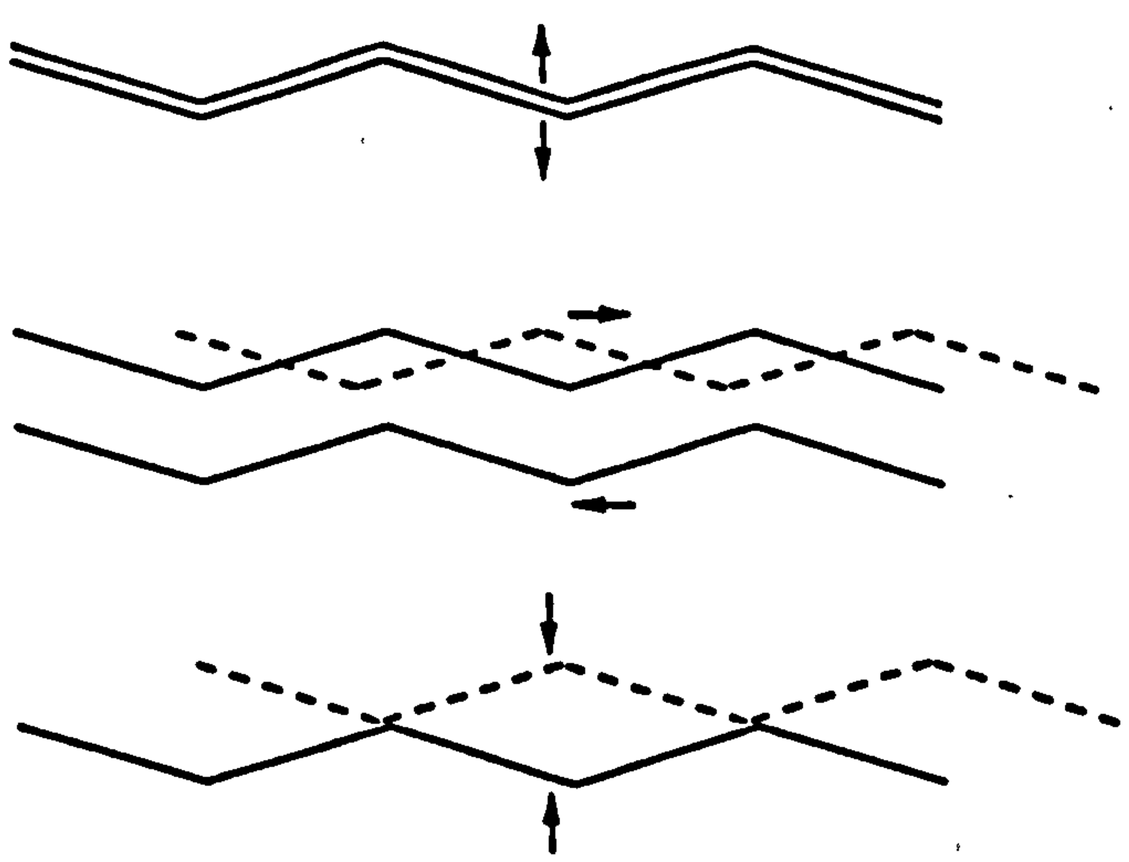


Figure 4.12 Uneven closure of cracks

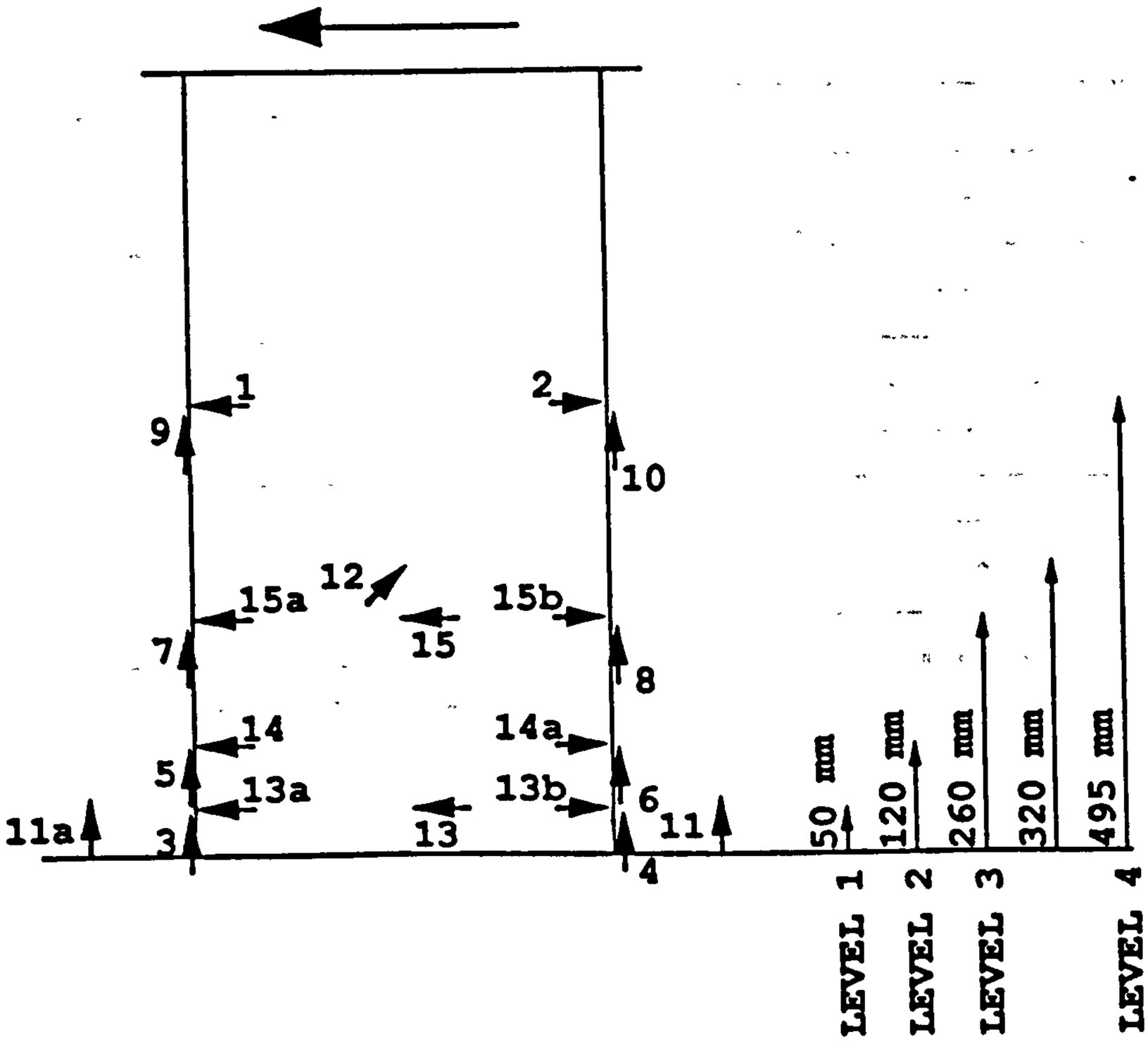


Figure 4.13 Location of the transducers (all walls)

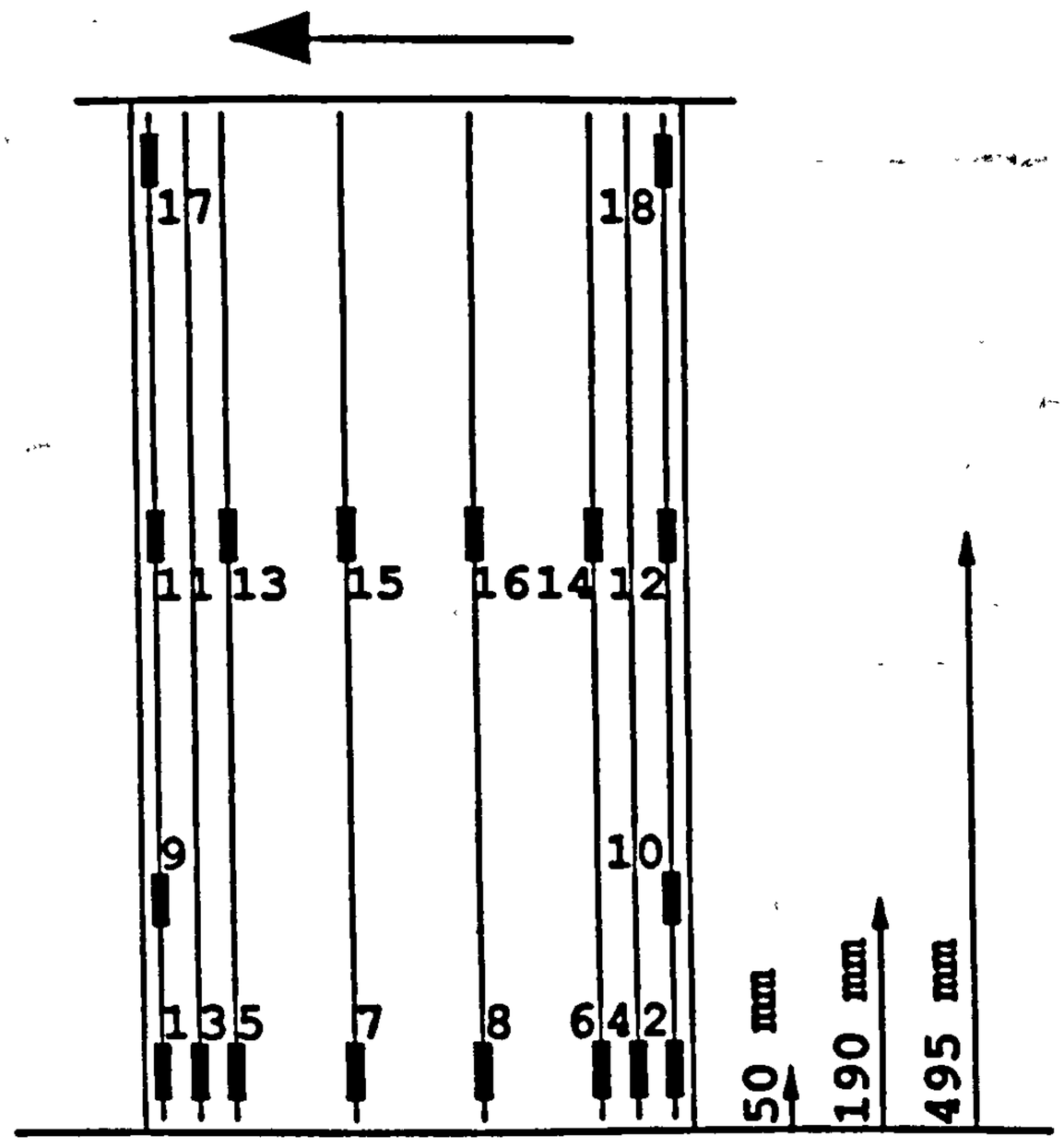
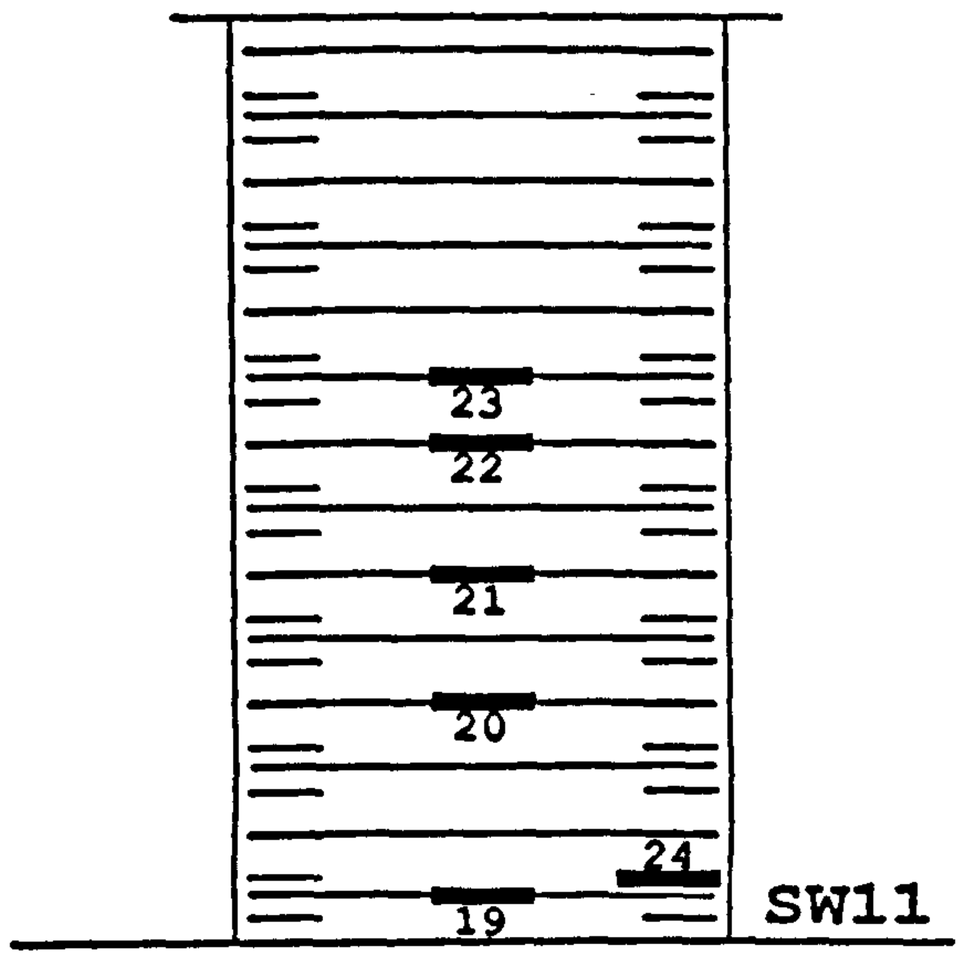
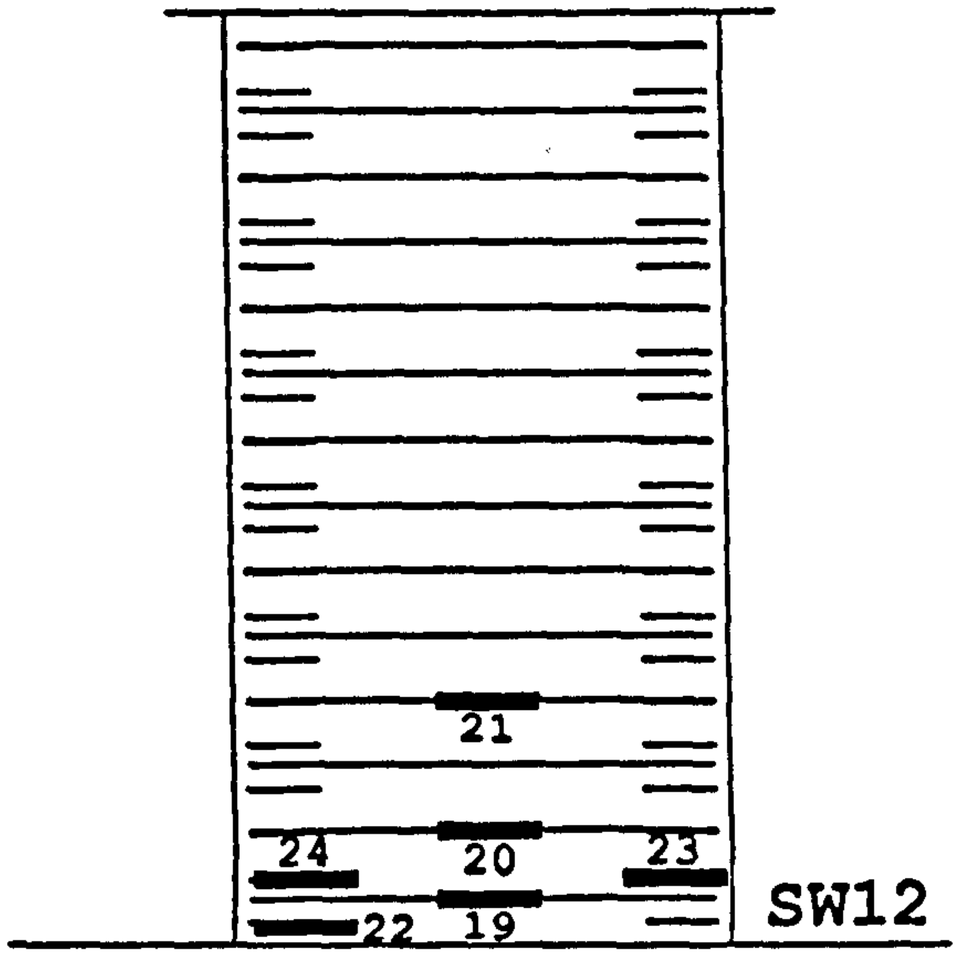


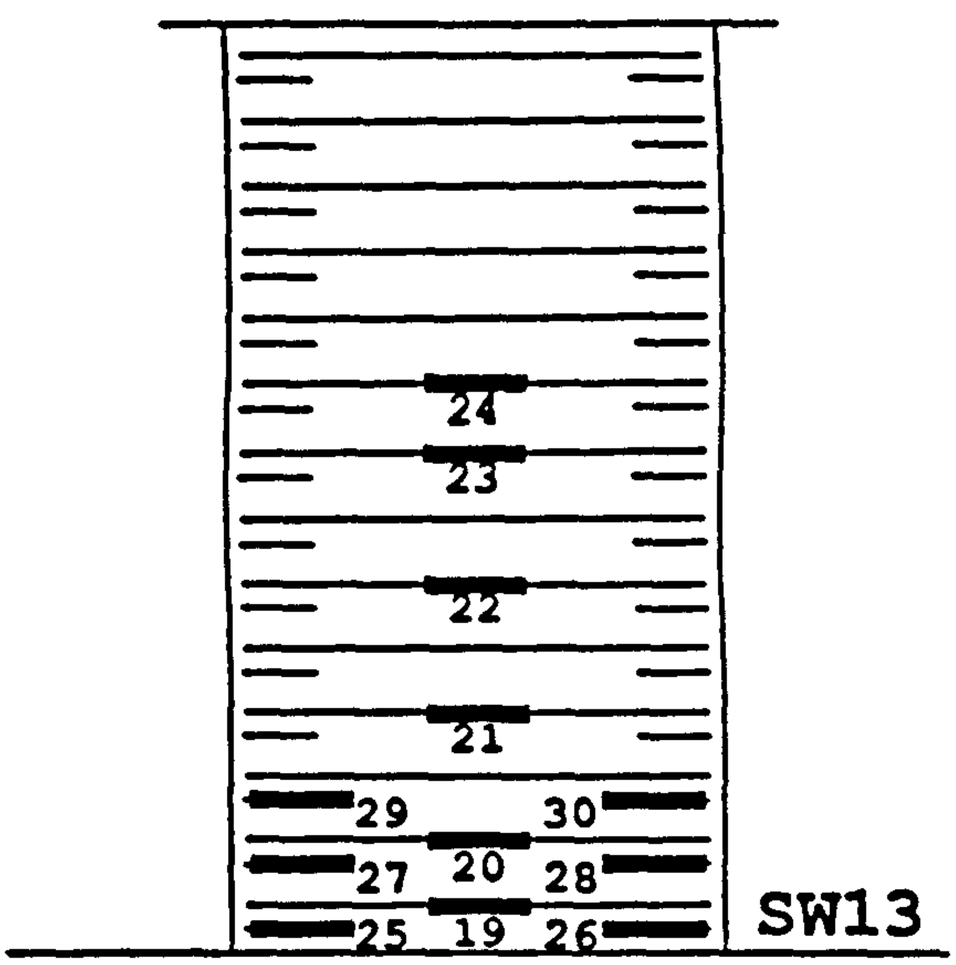
Figure 4.14 Location of strain gauges in vertical bars (all walls)



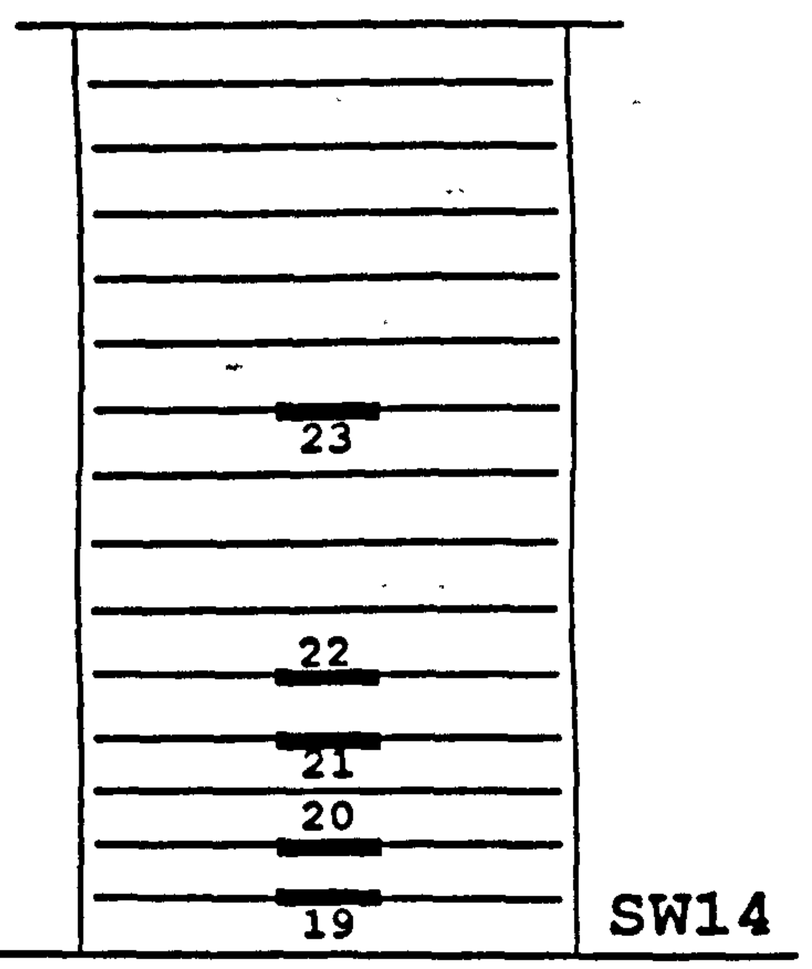
a) Wall SW11



b) Wall SW12

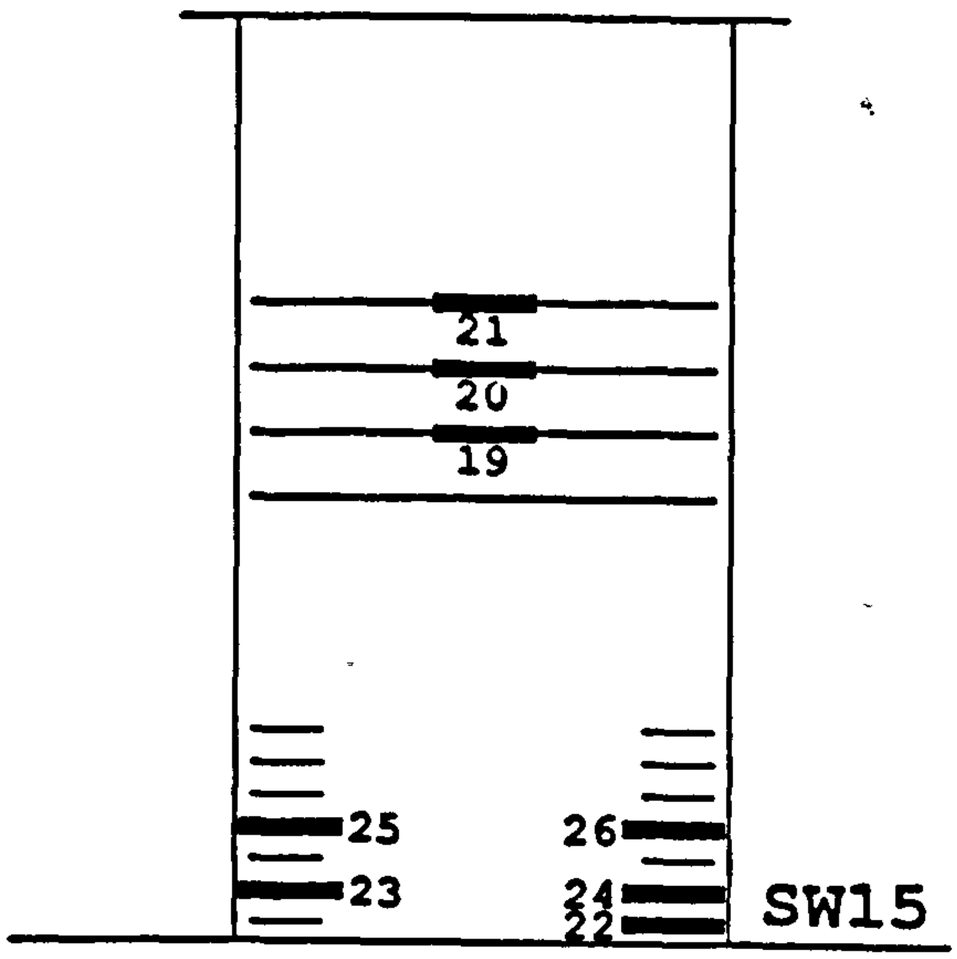


c) Wall SW13

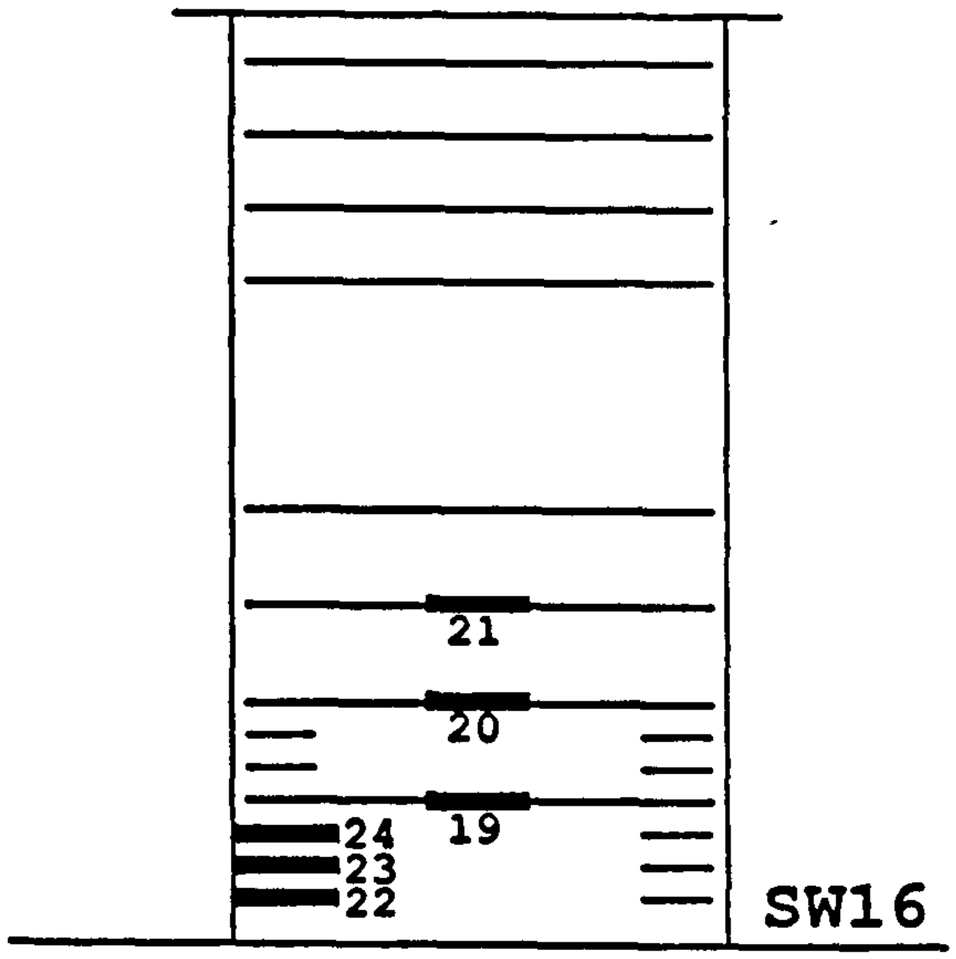


d) Wall SW14

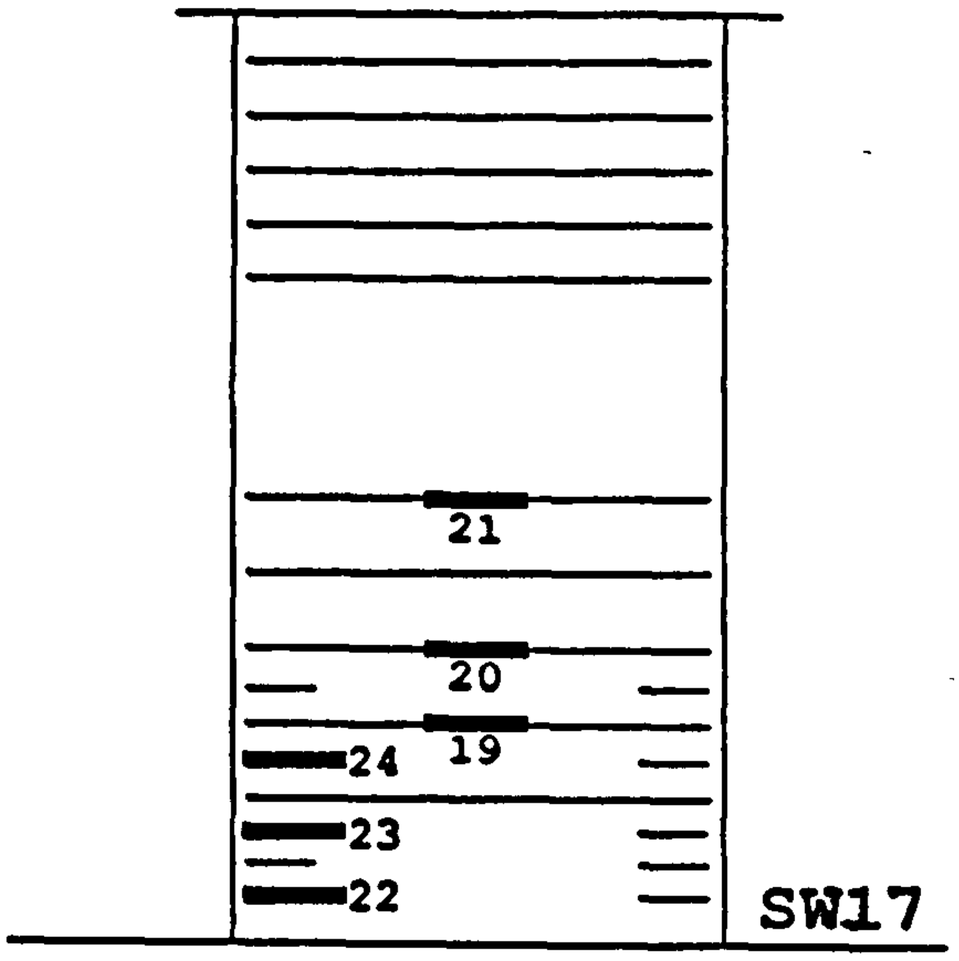
Figure 4.15 Location of strain gauges in horizontal bars



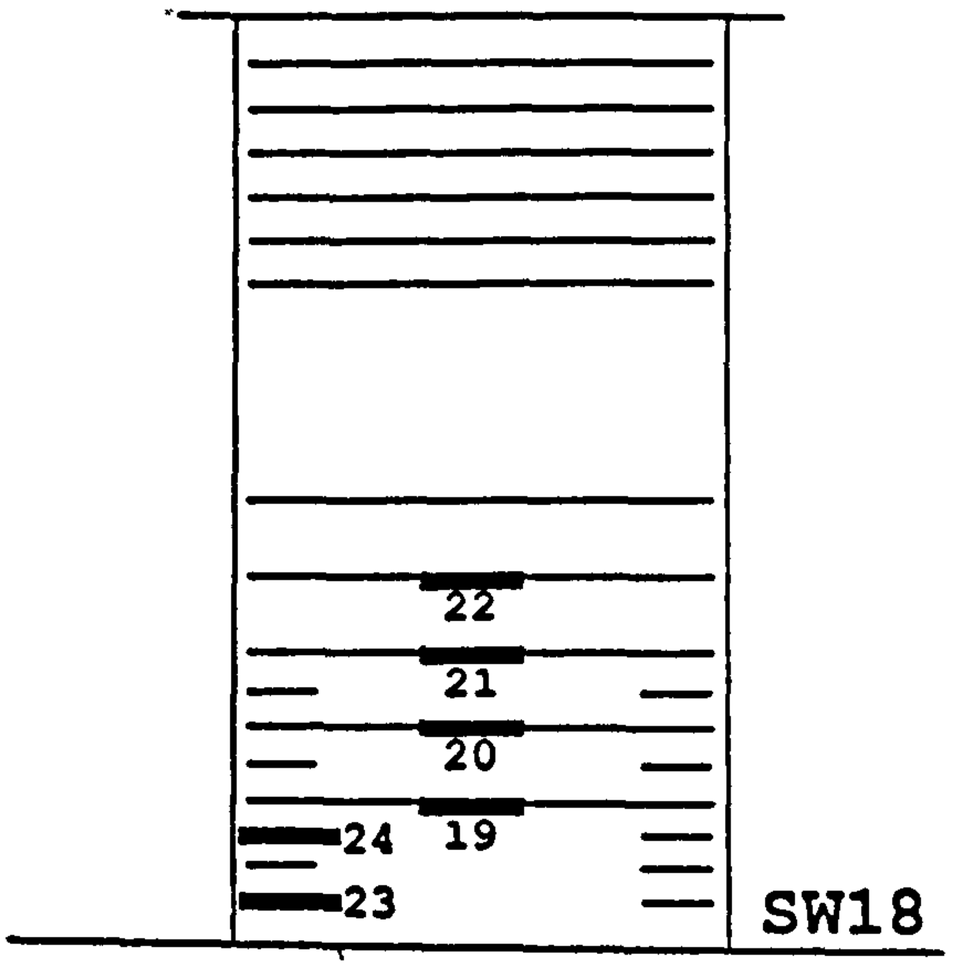
e) Wall SW15



f) Wall SW16

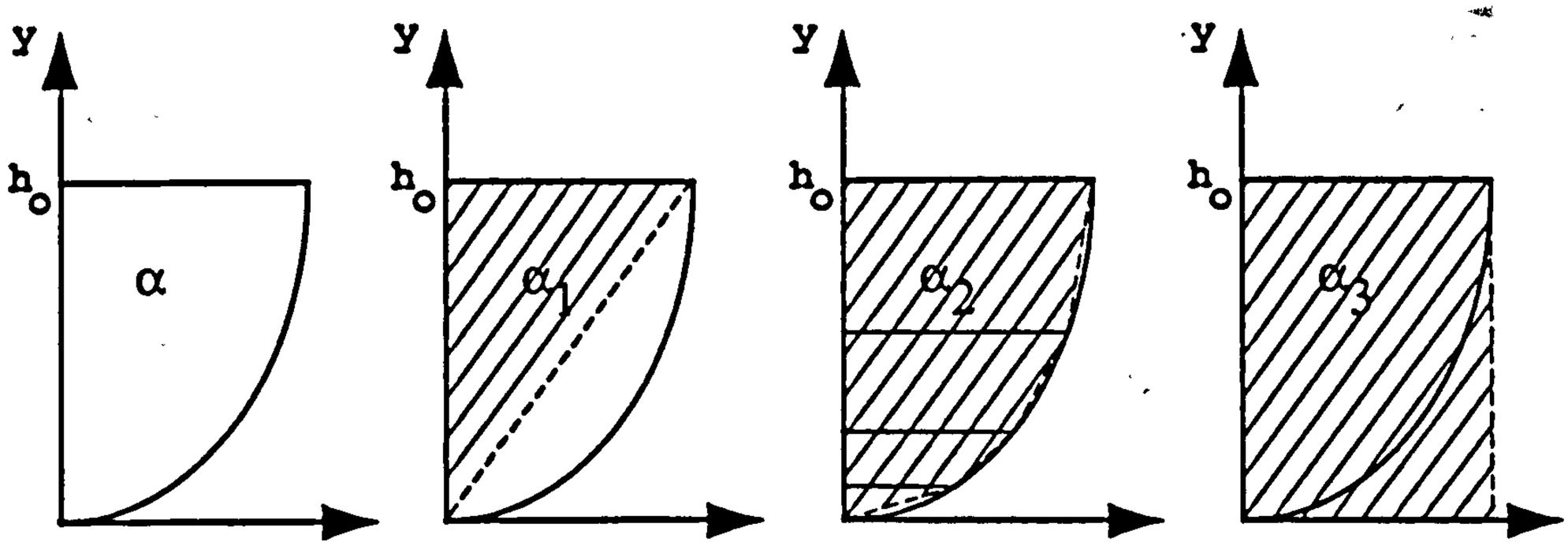


g) Wall SW17



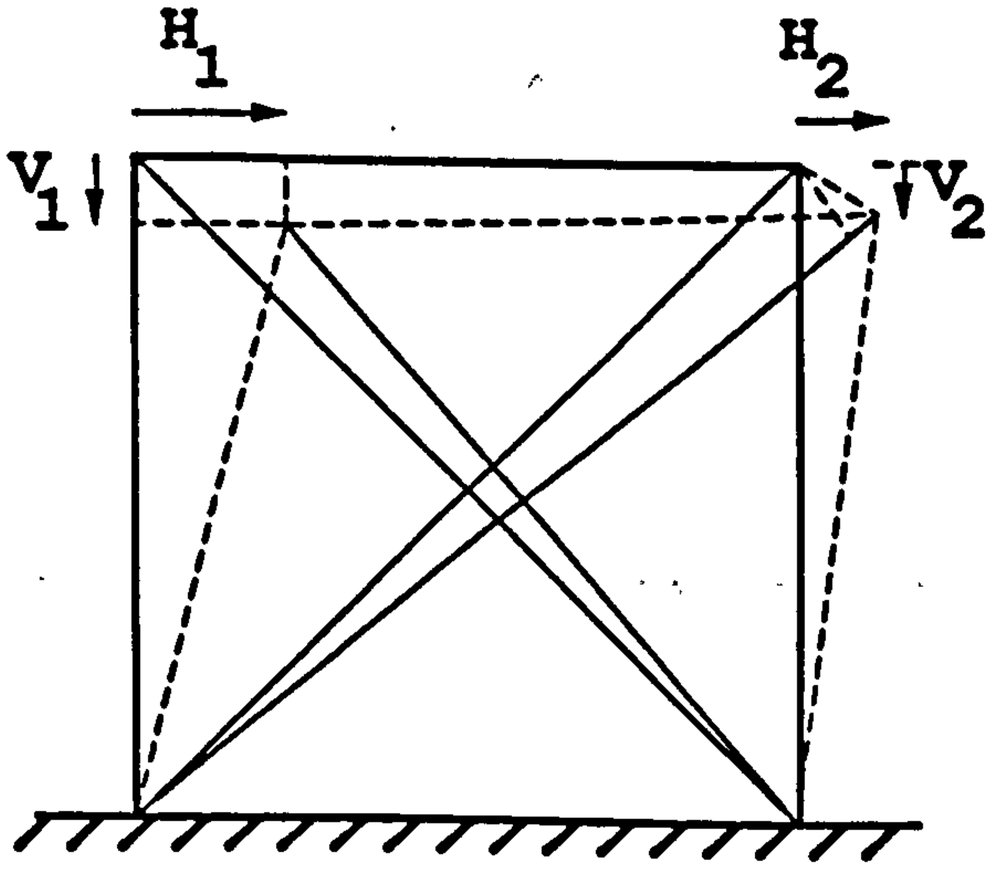
h) Wall SW18

Figure 4.15 Location of strain gauges in horizontal bars (cont.)



a) Real area α b) Method of area α1 c) Method of area α2 d) Method of area α3

Figure 4.16 Evaluation of flexural deformations



$$\Delta_1 = -\Delta_s \frac{L}{L_d} \qquad \Delta_s = -\Delta_1 \frac{L_d}{L}$$

$$\Delta_2 = \Delta_s \frac{L}{L_d} \qquad \Delta_s = \Delta_2 \frac{L_d}{L}$$

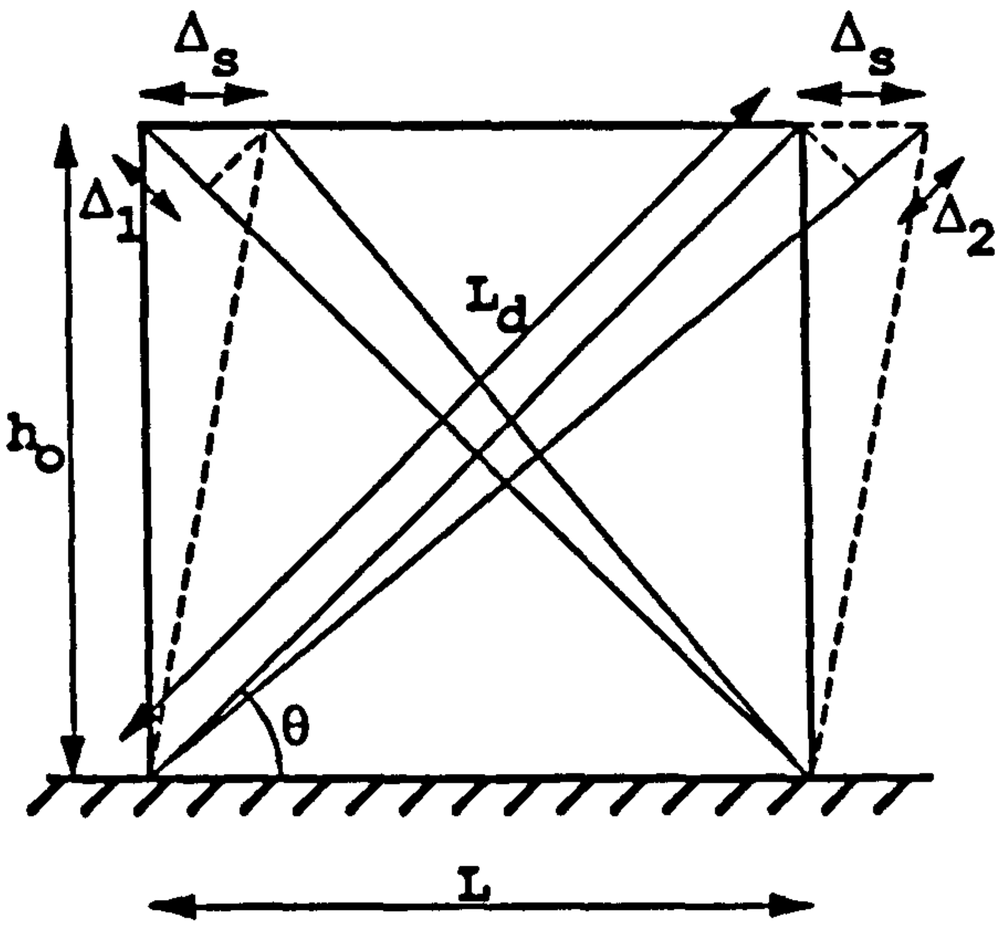
$$\Delta_s = \frac{1}{2} (\Delta_2 - \Delta_1) \frac{L_d}{L}$$

Figure 4.17 Evaluation of shear deformations using diagonal measurements.

$$\Delta_s = \frac{1}{2} \quad (\Delta_2 - \Delta_1) \frac{L_d}{L}$$

$$\Delta_1 = \frac{1}{L_d} \quad (- V_1 \, h_0 - H_1 \, L)$$

$$\Delta_2 = \frac{1}{L_d} \quad (- V_2 \, h_0 - H_2 \, L)$$



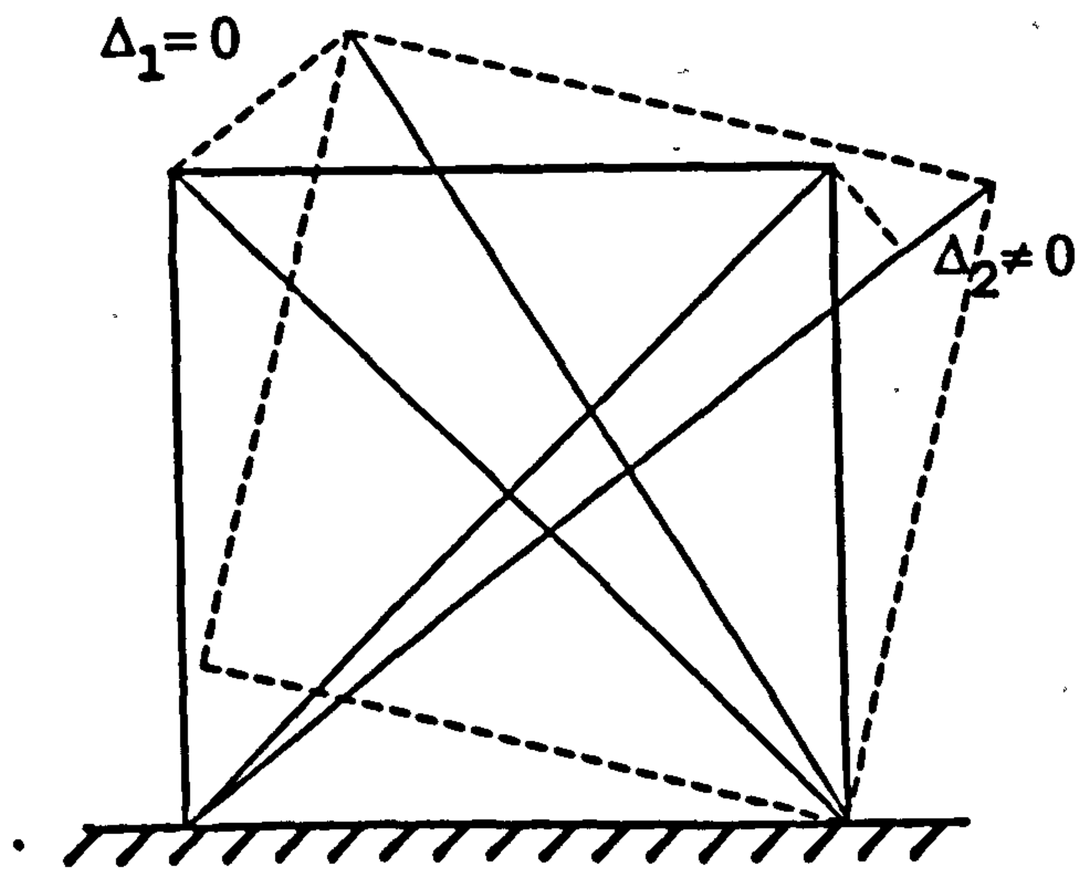
$$\Delta_s = \frac{1}{2} \quad (- V_2 \, h_0 + H_2 \, L + V_1 \, h_0 + H_1 \, L) \quad \frac{1}{L_d} \quad \frac{L_d}{L}$$

$$= \frac{1}{2 \, L} \, [(V_1 - V_2) \, h_0 + (H_2 + H_1) \, L \,]$$

$$= \frac{H_2 + H_1}{2} - \frac{V_2 - V_1}{L} \cdot \frac{h_0}{2}$$

$= TD - h_0$ ROT_{TOP}

Figure 4.18 Components of diagonal measurements



$$\left.\begin{matrix} \Delta_1 = 0 \\ \Delta_2 \neq 0 \end{matrix}\right] \Rightarrow \Delta_s \neq 0$$

Figure 4.19 Measurement of flexural deformations using diagonals

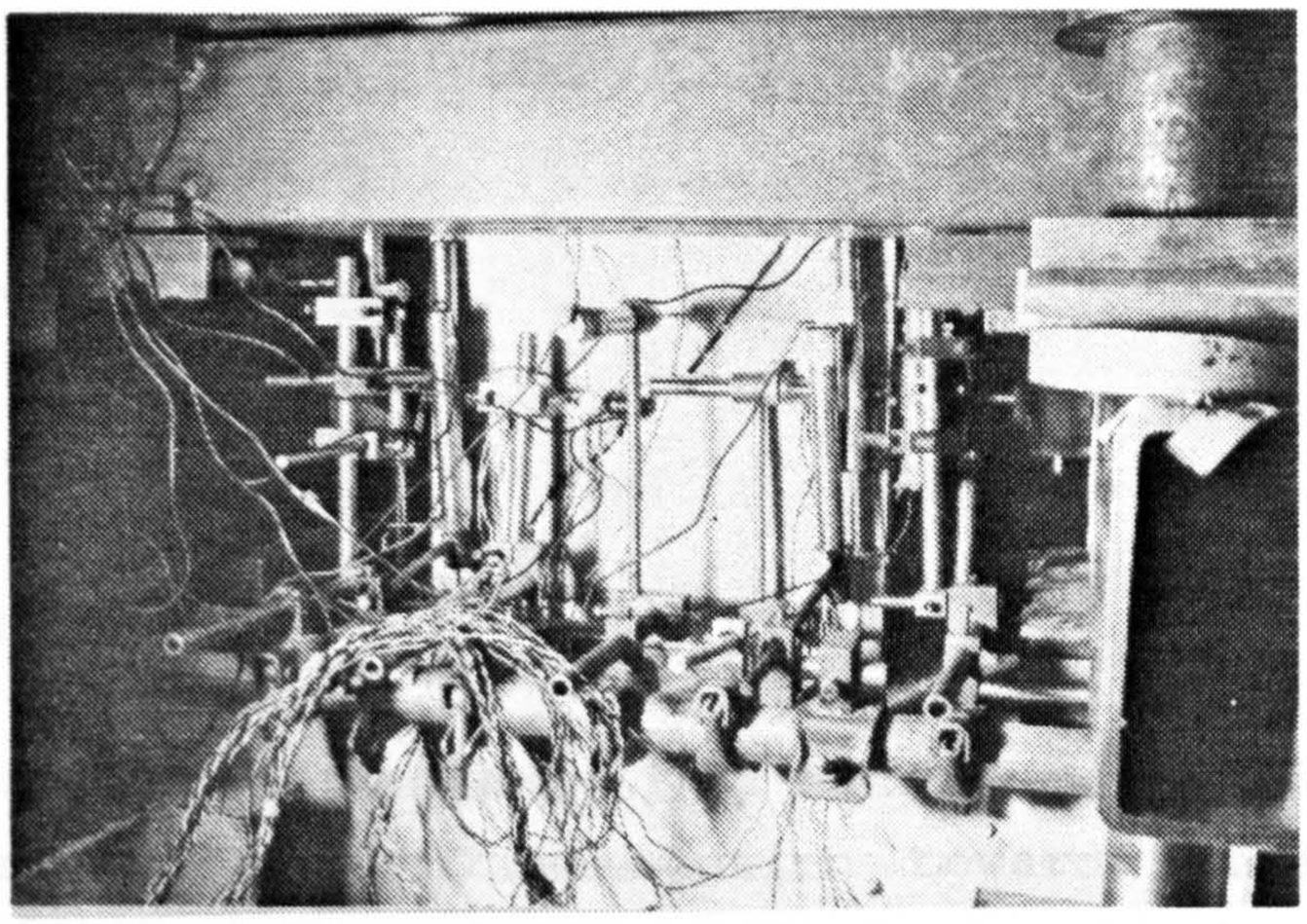


Figure 4.20 External instrumentation

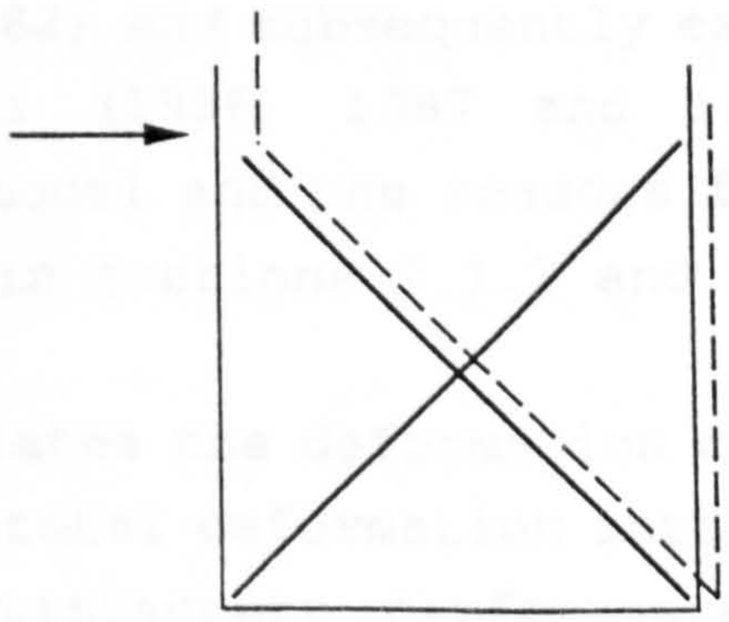


Figure 4.21 Sliping along diagonal cracks in the post-ultimate range

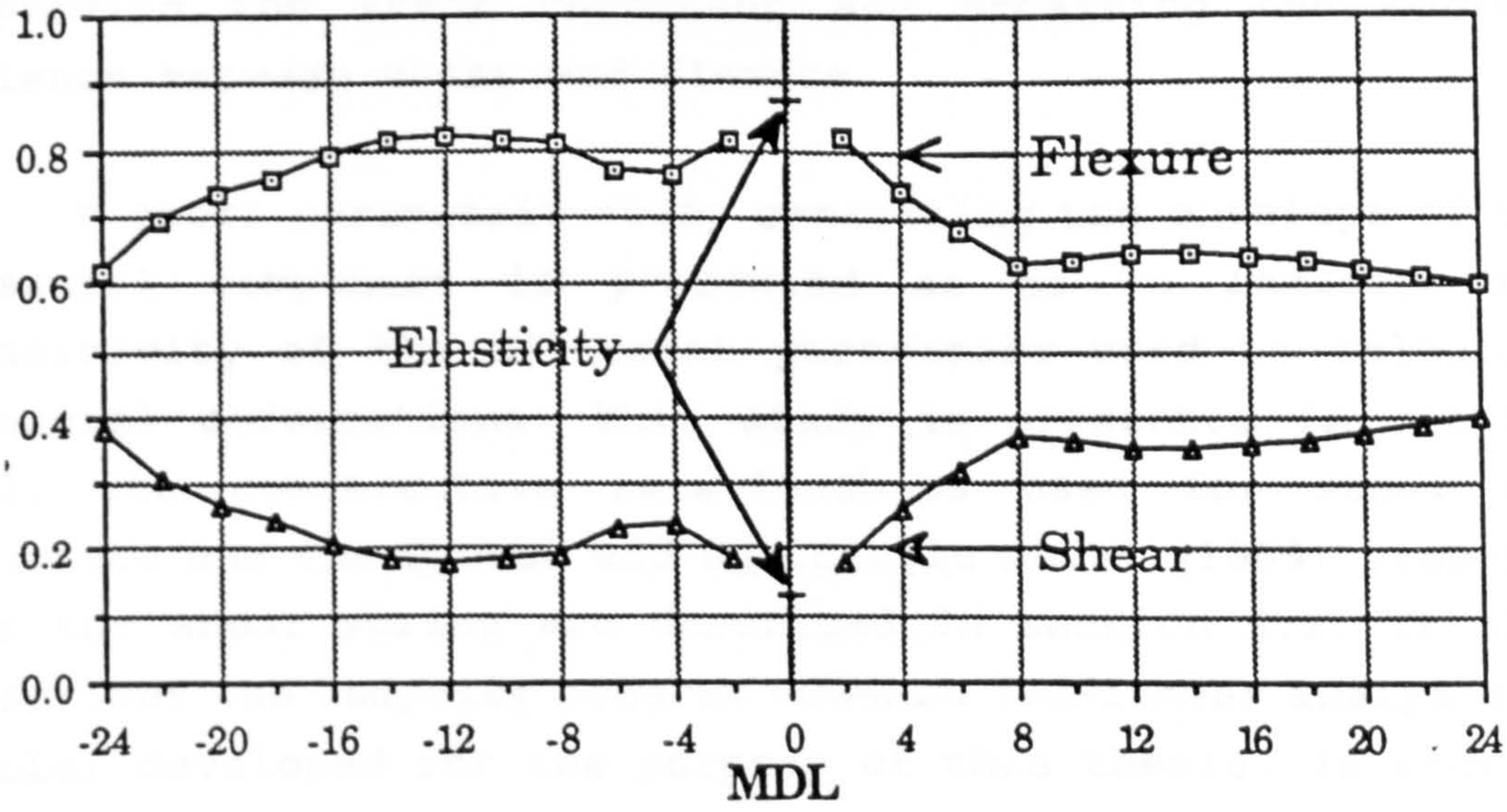


Figure 4.22 Balance between shear and flexural deformations for wall of shear ratio 2 (Pilakoutas, 1990)

CHAPTER 5

5 ANALYTICAL STUDIES

5.1 Introduction

The purpose of the analytical studies presented in this chapter is to make a contribution towards developing a general model for the analysis of the hysteretic behaviour of R/C walls. The model chosen is based on the model proposed by Kabeyasawa et al (1982) and subsequently extended by Vulcano, Bertero and Colotti (1986, 1987 and 1988). The general description of the model and the reasons for its choice have already been given in sections 2.1.2 and 2.3.3.

The model simulates the deformation of a R/C wall member by sub-dividing the total deformation into flexural and shear components. The satisfactory performance of the flexural component of the model has already been highlighted in chapter 2. Therefore, the present study concentrates on improving the shear component and obtaining the correct balance between shear and flexure.

A short parametric study concerning the envelope of the flexural component is presented so as to indicate the sensitivity of the different parameters used to calculate flexural deformations. This study is presented in section 5.3. The constitutive relationships used for steel and concrete and the Ozcebe and Saatcioglu model (1989) proposed for the shear spring are described in section 5.2. It also describes the computer program NONWALL (NONlinear analysis of WALLs) developed for the purpose of this thesis. In section 5.4 the performance of the shear spring is assessed independently of the rest of the model. Comparisons with experimental data are made and improvements are suggested. The performance of the model in the determination of the

correct balance between shear and flexural deformation components is studied in section 5.5. In section 5.6 the performance of the model for different failure modes is discussed and suggestions for improvements are given. In section 5.7 the main observations and conclusions of this chapter are summarised. All the plots showing the results of the study presented in this chapter are given in Appendix C.

5.2 Description of Constitutive Relationships and Computer Programs

The parameter λ which defines the zone where bond is effective and the zone where the deformations of concrete and steel are independent (elements 1 and 2 in figure 2.30, respectively) is considered constant. The constitutive relationships used for steel are the same in both elements of the uniaxial springs and are described in section 5.2.1. The constitutive relationships for the concrete are different for the two elements and are described in section 5.2.2. The model used for the shear spring is described in section 5.2.3. In section 5.3 comparisons are made with results given by the program CRELIC. The main features of this program are highlighted in section 5.2.4. The program NONWALL, which is an implementation of the proposed model, is described in section 5.2.4.

5.2.1 Constitutive Relationships for Steel

The model used was developed by Pilakoutas for the program CRELIC and is a simplified version of the model proposed by Santhanam (1979) for mild steel. The yield plateau before the onset of strain hardening was not considered. The yield growth factor β used by Santhanam to define the yield stress on reloading above the yield plateau was eliminated. A trilinear envelope was used for all kinds of steel, as shown in figure 5.1. The values necessary for

the definition of the envelopes are given in table 4.2 for all types of steel used. The value of the parameter α, which defines the stiffness on reloading, cannot be directly calibrated. In the absence of data from cyclic tests for the steels used in the experiments, α is taken equal to 0.5, as suggested by Pilakoutas (1990).

The proposed steel model is simple since only the current and previous maximum and minimum permanent strains are needed to establish the stiffness and stress at each stage. Notwithstanding, it is able to simulate the most important features of behaviour ignored by the elastoplastic model, often used in design; strain hardening and stiffness degradation on reloading in the post yield range.

5.2.2 Constitutive Relationships for Concrete

The definition of the monotonic curves for confined and unconfined concrete in compression are based on the same equations. The model developed by Mander et al (1988) for concrete subjected to uniaxial compressive loading and confined by transverse reinforcement was used. Figure 5.2 shows the model proposed by Mander et al. The equations that define the model are as follows:

$$f_{cx} = \frac{f_{cc} \; x \; r}{r - 1 + x^r} \qquad (5.1)$$

where:

$$x = \frac{\varepsilon_c}{\varepsilon_{cc}} \qquad (5.2)$$

$$\varepsilon_{cc} = \varepsilon_{co}\left[1 + 5\left(\frac{f_{cc}}{f_c} - 1\right)\right] \qquad (5.3)$$

$$r = \frac{E_c}{E_c - E_{sec}} \qquad (5.4)$$

$$E_c = 5000 \sqrt{f_c} \qquad \text{(units in MPa)} \qquad (5.5)$$

$$E_{sec} = \frac{f_{cc}}{\varepsilon_{cc}} \qquad (5.6)$$

For unconfined concrete f_{cc} is equal to f_{co} in the previous equations. For confined concrete the procedure proposed in Appendix A of EC8 to calculate f_{cc} was used in this work. The ultimate compressive stress for confined concrete is calculated as a function of the average effective confining stresses given by:

$$\text{eff}(\sigma_2 = \sigma_3) \ / \ f_{cc} = 1/2 \ \alpha_n \ \alpha_s \ W_w \qquad (5.7)$$

The values of α_n and α_s can be obtained from figure 5.3 as a function of the type and detail of confinement reinforcement used. A value of $\alpha_n\alpha_s$=0.3 is used. W_w is the volumetric ratio of confinement reinforcement calculated as 0.343. The value of f_{cc} was calculated as shown in figure 5.4 and the value of 47.5 MPa was obtained.

A simplified version of the rules proposed by Mander et al are used to define the unloading and reloading segments. It should be noted that the rules proposed by Mander et al do not account for the progressive closure of cracks in reinforced concrete. Figure 5.5 shows an unloading segment starting on the main compressive loading curve. The determination of a plastic strain ε_{pl} based on the coordinates of the point of the main compressive curve where unloading started needs to be determined. The value of the strain ε_a is calculated using equation (5.8), leads to:

$$\varepsilon_a = a \sqrt{\varepsilon_{un} \ \varepsilon_{cc}} \qquad (5.8)$$

The value of "a" in equation (5.8) is taken as the greater of the values given by equations (5.9) and (5.10):

$$a = \frac{\varepsilon_{cc}}{\varepsilon_{cc} + \varepsilon_{un}} \qquad (5.9)$$

$$a = \frac{0.09\ \varepsilon_{un}}{\varepsilon_{cc}} \qquad (5.10)$$

The plastic strain ε_{pl} is given by:

$$\varepsilon_{pl} = \varepsilon_{un} - \frac{(\varepsilon_{un} + \varepsilon_a)\ f_{un}}{(f_{un} + E_c\ \varepsilon_a)} \qquad (5.11)$$

In the simplified version of Mander model used in this work unloading and reloading in compression follows a straight line from the point of the main curve where unloading starts to the point of strain ε_{pl} in the strain axis. These rules apply to the concrete of both elements of the uniaxial springs. For lower compressive strains or tensile strains the path depends on which element is being considered. In the case of element 2, where it is considered that there is no bond between concrete and steel, the tensile strength of the concrete is disregarded. Therefore, for strains lower than ε_{pl} (considering the notation of figure 5.6 in which compression is positive) both loading and unloading follow the strain axis. For element 1 of the uniaxial springs perfect bond is considered to exist between concrete and steel and the concrete is considered able to resist tension. Unloading and reloading for strains below ε_{pl} follows a straight line with a stiffness equal to the elastic compressive stiffness, as proposed by Colotti and Vulcano (1987). Figure 5.6 shows the constitutive relationships for concrete of elements 1 and 2.

5.2.3 Description of the Shear Model

It is recognized that the OOHM model is not suitable for the shear component of the deformation of R/C walls. The model imposes restrictions which are not observed experimentally, such as the unloading segments aiming at the origin, and does not represent other features, such as the pinching effect. The most likely reason for this has already been pointed out by Hoedejanto (1988); the conditions

existing in the tests whose results were used to establish the model cannot be considered representative of the ones existing in a R/C member subjected to shear and flexure. Therefore, the model is not amenable to improvements and it was decided to replace it by a more suitable characterisation.

The energy dissipation capacity influences the forces for which a structure is to be designed to withstand a given earthquake ground motion. Hence, the energy dissipation capacity must be simulated with some accuracy. The pinching effect, which reduces the energy dissipation capacity, seemed to affect more shear deformations than flexural deformations. Therefore it is considered important that a model for the shear component should simulate the aforementioned effect. The model proposed by Ozcebe and Saatcioglu (1989) was chosen because it represents the most important features that the model should be able to represent, including the pinching effect.

The model is based on a trilinear envelope with well defined cracking and yield points. Any acceptable analytical or experimental procedure can be used to establish the envelope. Ozcebe and Saatcioglu used the Compression Field Theory (Collins and Mitchel, 1980) and Kabeyasawa et al (1982) and Vulcano et al (1986, 1987 and 1988) used empirical relationships. The assessment of these different methods is beyond the scope of this work. Hence, the trilinear envelope will be established from the actual experimental data.

Similar to the OOHM, the derivation of the rules for establishing the response under load reversals of Ozcebe and Saatcioglu model are subject to calibration based on the actual experimental data. All the test specimens from which the data was derived were designed to yield in flexure prior to shear failure. The model only simulates the behaviour up to the onset of strength decay.

Two slopes of the envelope, as shown in figure 5.7 are used as flags to define the unloading segments as follows:

- Unloading follows the primary curve if the shear force at the beginning of unloading is less than the cracking load V_{cr}, and V_{cr} has not been previously exceeded in either direction.

- If V_{cr} has been exceeded at least once in one direction, and the yield load has not been previously exceeded in the quadrant where unloading is taking place, unloading follows a straight line up to the zero load axis. The slope of this line for unloading from a load higher than V_{cr} is given by equation (5.12) below (e.g.: AB, KL). If unloading is from a load lower than V_{cr} is equal to K_1 (e.g., CD).

$$K = K_1 - \frac{K_1 - K_2}{\Delta_y - \Delta_{cr}} (\Delta - \Delta_{cr}) \qquad (5.12)$$

- If V_y has been exceeded at least once in the quadrant where the current unloading is taking place, unloading stiffness above the cracking load is given by equation (5.13) (e.g., GH, MN, RS, VW, YZ), and below the cracking load is given by equation (5.14) (e.g., HI, NO, ST, WX). Figures 5.9 and 5.10 show equations (5.13) and (5.14) given below and the data by which they were calibrated.

$$K = K_2 \left(1 - 0.05 \frac{\Delta}{\Delta_y}\right) \qquad (5.13)$$

$$K = 0.6\ K_2 \left(1 - 0.07 \frac{\Delta}{\Delta_y}\right) \qquad (5.14)$$

Examples of the hysteresis loops are shown in figure 5.8.

The reloading segments are established using the ratios V_p/V_p' and V_m/V_m'. These variables are defined in figure 5.11 and calculated using equations (5.15) to (5.19) given below.

$$V_p' = V_p \, e^{\alpha \left(\frac{\Delta p}{\Delta y}\right)} \qquad (5.15)$$

$$\alpha = 0.82 \left(\frac{N}{N_o}\right) - 0.14 < 0.0 \qquad (5.16)$$

$$V_m' = V_m \, e^{[\beta \, n + \gamma \, (\Delta_m \, / \, \Delta_y)]} \qquad (5.17)$$

$$\beta = - \, 0.014 \, \sqrt{\Delta_m \, / \, \Delta_y} \qquad (5.18)$$

$$\gamma = - \, 0.01 \, \sqrt{n} \qquad (5.19)$$

The rules for loading and reloading proposed by Ozcebe and Saatcioglu (1989) are as follows.

- Initial loading and reloading follow the envelope until the load is reversed at a level higher than the cracking load.

- If the member has not been loaded beyond the cracking load in one direction, the initial loading in that direction aims at the cracking load, even if the member has previously experienced inelastic deformations in the opposite direction (e.g., BJ, IJ).

- If V_{cr} has been exceeded in the direction of loading: (i) reloading up to V_{cr} will follow a straight line passing through point (Δ_p, V_p') (e.g., DE, OP, TU); (ii) reloading beyond V_{cr} will follow a straight line up to the primary curve, passing through point (Δ_m, V_m') (e.g., EF, PQ, UY); and (iii) beyond the intersection of reloading segment with the envelope, loading follows the envelope (e.g.,FG, QR). The parameter "n", which is a

counter of the number of cycles at a given ductility level, is assigned two values, one for each direction of loading. When the maximum displacement is increased to a new value "n" takes the value 1. Every time the load reverses within the range Δ_m-Δ_{cr} to Δ_m+Δ_{cr} after loading in the opposite direction the value of "n" is increased one unit.

- If unloading is complete prior to reaching the zero load axis, reloading in the same quadrant will trace a straight line aiming at the immediate preceding peak point (e.g. XV).

Examples of hysteresis loops are shown in figure 5.8.

5.2.4 Description of Computer Programs

The computer program NONWALL described in this section was developed on the MicroVax computer of the Dynamics Group at Imperial College.

The wall is discretized in a set of elements along the height separated by stiff horizontal beams. The generic element has already been described in section 2.1.2 and is shown in figure 2.29. Each uniaxial spring is simulated by a set of springs, as shown in figure 2.30.

The wall is subjected to a horizontal displacement at the top level. All other degrees of freedom are free with the exception of the bottom section, which is built-in, as shown in figure 5.15. At each step the response is evaluated by an iterative procedure, as shown in figure 5.12. At the beginning of each step the iteration matrix $[K_I]$ is set as the tangent stiffness matrix at that stage. This provides very fast convergence for the majority of steps of the analysis. However, it does not ensure convergence. If the system starts diverging then a new iteration matrix, as

suggested by Vulcano and Bertero (1987), is adopted. This is given by:

$$[K_I] = \{(1-\xi_o)[K_E] + \xi_o[K_T]\} \qquad 0 \leq \xi_o \leq 0.5 \qquad (5.20)$$

$[K_I]$ - iteration matrix
$[K_E]$ - elastic stiffness matrix of wall system
$[K_T]$ - tangent stiffness matrix

The stiffness matrix of each element can be evaluated as shown in figure 5.13 as a function of the stiffness of the individual springs. The stiffness matrix of the whole system is obtained by assembling the stiffness matrices of all wall elements. At each iteration the state of stress and the stiffness in the horizontal springs is evaluated explicitly. For the uniaxial springs this is also the case if $\lambda=0$ or $\lambda=1$. For intermediate values of λ, in which both elements need to be considered, an iterative procedure is needed to satisfy the equilibrium and compatibility conditions expressed in the following equations:

$$\Delta D = \Delta D_1 + \Delta D_2 \qquad (5.21)$$

$$\Delta F_1(\Delta D_1) = \Delta F_2(\Delta D_2) = \Delta F \qquad (5.22)$$

ΔD, ΔF - increments of displacement and force. The subscripts identify the respective elements within the uniaxial spring.

The flow chart of the program NONWALL is shown in figure 5.14

A full description of the program CRELIC, used for comparison of results in section 5.3, can be found elsewhere (Pilakoutas, 1990). Only the main features are referred to in this section. The program was developed on the basis of sectional analysis. Flexural displacements are evaluated by integration of the curvatures and rotations calculated at eight levels along the height of the wall.

The constitutive relationships for steel were described in section 5.2.1. The concrete model of Mander et al (1988), briefly outlined in section 5.2.2, was used for the constitutive relationships of confined and unconfined concrete.

5.3 Flexural Component

As already mentioned, this work is not aimed at improving the flexural component. However, a short parametric study was performed in order to appraise the sensitivity of the results to values of λ and C, which need to be given as input.

The part of the test specimens up to the level where M=0 is simulated. The discretization of the wall is shown in figure 5.15. Four elements along the height are considered. The elements are of shorter length at the lower levels where the inelastic behaviour is concentrated and curvatures are high. The discretization of the cross section comprises 6 elements, which was the minimum in this case, since each uniaxial element can only simulate one type of steel. Two uniaxial elements are used to simulate each boundary element and two for the whole web. The concrete cover was not considered and the concrete of the boundary elements was assigned the properties of confined concrete.

Figures C.1 and C.2 show comparisons of results between the program CRELIC and NONWALL for different values of C and λ. It should be noted that the program CRELIC does not consider the contribution of the concrete in the zone below the neutral axis (in tension) to the stiffness of the wall. This corresponds to λ=1 in program NONWALL. Figure C.1 shows that program NONWALL yields lower forces for the same displacements if a value of λ=1 is adopted, i.e., the system is more flexible.

The parameter C must vary between 0 and 0.5 for monotonic loading. This can be easily understood in the context of figure 4.16. Method of area $\alpha 1$ is equivalent to assuming C=0.5 and method of area $\alpha 3$ to C=0. Under cyclic loading the value of C may vary more. At lower levels of load the distribution of strains along the vertical bars may not follow a regular pattern due to the accumulation of plastic strains at the base. Therefore, the curvature may change sign along the height of the wall, and the corresponding value of C may be outside the range $0<C<0.5$. At higher loads the rotations tend to increase along the whole height and the curvature sign does not change. Under these conditions the value of C should be within the range $0<C<0.5$, as for monotonic loading. In this work a value of C of 0.3 is used in all calculations. Figure C.2 shows the comparison of results obtained with the program CRELIC and the program NONWALL for different values of λ. The variation for different values of λ is considerable. This points towards the need for modelling the tension-stiffening effect described by the parameter λ by a suitable law. However, this is outside the scope of this work and a constant value of $\lambda=0.6$ is used in all subsequent calculations.

Figure C.3 shows the envelopes of the flexural component of the deformation of wall SW13 calculated using method of area $\alpha 2$ and $\alpha 1$ and the predictions of both programs. It is observed that the programs yield good predictions of the ultimate load but overestimate the stiffness. Method of area $\alpha 1$ yields lower displacements than method of area $\alpha 2$, as expected.

To identify the causes of the difference of stiffness between analytical and experimental results, data from walls SW9 and SW3 tested by Pilakoutas (1990) were processed as shown in figures C.4 and C.5, respectively. In the case of wall SW3 no vertical readings were taken along the height of the wall. Therefore, flexural deformations could not be calculated by method of area $\alpha 2$. However, the analysis of figure 4.16 and the results shown in figures C.3 and C.4

indicate that the displacements would be larger than the ones calculated according to method of area $\alpha 1$. The dimensions of walls SW9 and SW3 are shown in figure 5.16. The scale of wall SW9 is larger than the scale of SW13, while SW3 is smaller than SW13.

It is noticeable that while for the larger wall SW9 the comparison of analytical and experimental results is quite reasonable, for the lower scale specimens the analytical models predict higher stiffness. The gap between the stiffness predicted analytically and experimental values increases as the scale decreases. Pilakoutas (1990) considered the effect of micro-cracking due to shrinkage as a possible explanation for this effect. Wagner and Bertero (1982) also pointed out to the effect of micro-cracking initiated during curing in reducing the initial stiffness of the specimens. Aktan et al (1983) observed that the difference in shrinkage of members of different sizes was significant. This phenomena may have been the cause of the reduction in stiffness for the lower scale models.

5.4 Shear Component

The performance of the analytical model for the shear component is assessed in this section. Results obtained using only the shear component of program NONWALL are compared with the shear component of the deformation of walls SW13 and SW16. Wall SW13 was chosen because it exhibited the code-desired behaviour for earthquake resistant design. The comparison with the data from SW16 aims at studying the influence of the failure mode on the intensity of the pinching effect, which is the feature more clearly affected by the failure mode.

In the shear model the cracking load is used to establish the load at which the stiffness increases on reloading. Analysis of the experimental data shows that in

the reloading segments the load starts picking up at a much lower level than the load at which first cracking was observed. This increase in stiffness is due to the closure of cracks opened when loading in the opposite direction and therefore is not related to the load at which first cracking is observed. In section 5.6, this issue is further discussed and a proposal is made for the establishment of an analytical procedure to determine the point at which the transition between the two reloading segments occurs. For this study a value of F=16KN, based on the actual experimental data, was chosen to establish the separation between the two segments in reloading and unloading.

The cracking displacement is used to establish the range within which a reversal of displacement increases the value of the counter n, already mentioned in section 5.2.3. The cracking displacement is very small, below the accuracy of the control system. Under these conditions n would, in general, assume the value 1, even when cycling at similar ductility levels. This would increase artificially the stiffness degradation on reloading at a given displacement amplitude. It was therefore decided to use a value higher than the cracking displacement to establish the range in which n is increased. A value of 0.3mm was chosen since it allows the increase in n for cycles that were supposed to be at the same displacement amplitude. This way, small variations in MD due to lack of precision of the control system do not change the value of n to 1.

Figure C.6.a shows the hysteretic cycles given by the model for the shear displacement history of wall SW13. It is noticeable that several unloading segments cross each other. This can be clearly observed in figure C.6.b which shows the part of figure C.6.a up to MD 2.0 at a larger scale. This feature was not observed in the experimental results. This should be expected as the data shows the plastic nature of shear deformations after yielding of the main flexural reinforcement. Residual shear deformations at zero load are due essentially to the incomplete closure of cracks and

locking of relative displacements along the cracked surfaces. These features tend to become more intense with increased values of MD. Therefore, unloading from a higher displacement should not lead to a smaller displacement at zero load, as predicted by the model.

Features of the analytical predictions discussed above may be due to two reasons. Firstly, in the pre-yield range crossing of the unloading segments is due to the proposed formula to vary the unloading stiffness from the initial stiffness K_1 to the unloading stiffness at yield K_2, expressed in equation (5.12). Since K_1 is much larger than K_2, the relative variation in the unloading stiffness is very small after the cracking displacement but it increases considerably before the yield displacement is achieved. The high variation in unloading stiffness before reaching the yield displacement is responsible for the erroneous crossing of the unloading segments. In order to avoid this, it is proposed that the unloading segments aim at the cracking point in the opposite direction when unloading before reaching the yield displacement . This rule provides a variation between K_1 and K_2 which does not exhibit the lack of realism of the rule proposed by Ozcebe and Saatcioglu. It should be noted that the proposed change is of conceptual importance, but has little practical consequences since very little energy is dissipated before yielding of the main flexural reinforcement.

In the post-yield range the reason for the crossing of the unloading segments is due to equations (5.13) and (5.14), which express stiffness degradation as a function of the absolute value of the displacement. This causes a sudden variation in unloading stiffness as MD is increased beyond the yield displacement. This sudden variation in unloading stiffness can be avoided if stiffness degradation is expressed as a function of the difference between the displacement at unloading and the yield displacement. It is proposed that equations (5.13) and (5.14) are replaced by:

$$K = K_2 \left(1 - \frac{2}{3} \frac{\Delta - \Delta_y}{\Delta_y}\right) \qquad (5.23)$$

$$K = 0.6\ K_2 \left(1 - \frac{2.8}{3} \frac{\Delta - \Delta_y}{\Delta_y}\right) \qquad (5.24)$$

The new expressions were derived from the data provided by Ozcebe and Saatcioglu and lead to the same stiffness degradation as the previous ones for a ductility factor of 4. Figure C.7 shows the hysteretic cycles given by the model after introducing the proposed changes, for the shear displacement history of wall SW13. The new pattern shown in figure C.7 is closer to the experimental results than the one shown in figure C.6 and has a clear conceptual justification.

Figure C.7.a shows that the model does not follow its prescribed envelope, which is plotted as a discontinuous line. This is a load-history-dependent effect since it is due to stiffness degradation on reloading after several cycles at similar displacement amplitudes. However, it is important that the model follows its prescribed envelope, even if this implies a localized decrease in accuracy. This is due to the fact that small variations in the envelope of one of the components of the deformation may produce large variations in the energy dissipation by the overall model. This point is further discussed in section 5.5. It is therefore necessary to investigate the parameters that quantify stiffness degradation on the second segment of reloading. Figure C.8 shows the results obtained by eliminating the influence of the parameter β from equation (5.17). The tendency for the model to generate a new envelope which is at variance to the prescribed envelope is practically eliminated. Consequently, all subsequent calculations are performed considering $\beta=0$.

The comparison of figure C.8 with the figures of appendix B that show the force versus shear displacement of several walls, indicate that the model overestimates stiffness degradation on unloading. The decrease in the unloading stiffness with increased MD in the analytical

results progresses at a lower rate than observed in the experimental results from the walls in which shear deformations were evaluated. As a consequence, the hysteretic cycles enclose a larger area and the model considerably overestimates the energy dissipation capacity of the walls. In general, this would lead to an underestimation of the response to earthquake ground motions, thus producing unsafe designs in most cases. It is therefore necessary to calibrate the unloading stiffness in a way that leads to a better simulation of the energy dissipation capacity of the walls. The following equations are proposed for the unloading segments:

First unloading segment:

$$K = K_2 \left(1 - \frac{\Delta - \Delta_y}{\Delta_y}\right) \qquad (5.25)$$

Second unloading segment:

$$K = 0.6\ K_2 \left(1 - 1.4\ \frac{\Delta - \Delta_y}{\Delta_y}\right) \qquad (5.26)$$

The force versus shear deformation of wall SW13 predicted by the model after introducing the proposed changes is shown in figure C.9. In order to visualise better the comparison with experimental data, some cycles of experimental and analytical results are plotted together in figure C.10. Figure C.11 shows the cumulative energy dissipation in both cases. It can be seen that the shear model still overestimates the energy dissipation capacity. However this is a parameter that is very sensitive to small variations, and the difference between experimental and analytical results is not very high. For instance, the analytical results overstimate the area enclosed by the second and third loops shown in figure C.10 by 14% and 22%, respectively. Therefore, the performance of the model is considered satisfactory. Figure C.11 also shows that very little energy dissipation occurs in the initial stages,

particularly before yielding of the main flexural reinforcement. Note that the approximate displacement at which yielding started was 2.4mm, which was first reached at the 7th cycle. The first increase beyond yield was at the 10th cycle, when a large increase in slope becomes noticeable.

The mode of failure has an effect on the intensity of the pinching effect, as mentioned in section 4.3.2.1. However, the failure mode is a parameter which is not considered by Ozcebe and Saatciouglu model. The stiffness of the first reloading segment seemed to be calibrated from R/C members that failed by crushing of the concrete after yielding of the main flexural reinforcement. In order to simulate the pinching effect more closely in walls which fail in shear by diagonal tension, it is necessary to take into account the failure mode and the ultimate shear force. To achieve this it is suggested to generalize equation (5.15) in the following way:

$$V_p' = V_p \, e^{\alpha \left(\frac{\Delta_p}{\Delta_y}\right)} \cdot A \qquad (5.27)$$

$$A = 1.85 \frac{V_{fc}}{V_u} \qquad A \geq 1 \qquad (5.28)$$

For a wall with strength conditioned by the strength of the concrete in compression after yielding of the main flexural reinforcement, i.e. a wall that fails in flexure or by web crushing, A=1. The reliability of equation (5.28) should be assessed further by comparing the model predictions with data from other walls failing in shear by diagonal tension. The hysteretic cycles calculated by the model for the shear displacement history of wall SW16 are shown in figure C.12. To facilitate the comparison with the salient experimental data, figure C.13 shows part of the data of both cases together. The larger discrepancies observed as compared with the corresponding figure for wall SW13 are essentially due to the envelope. It has already been pointed out in section 4.3.3.3 that the stiffness associated with the

envelopes of both components of the deformation is lower for walls failing in shear by diagonal tension.

5.5 Balance Between Shear and Flexural Components

The total displacement of the wall is the sum of the shear and flexural components. The relative contribution of each component depends on the respective stiffness characteristics. As already discussed in sections 4.3.2.3 and 4.3.3.3, the energy dissipation capacity associated with each component is different. Therefore, if the overall model is to simulate the overall energy dissipation capacity of the wall, it must assign to each component the correct proportion of the total deformation. However, existing versions of the model do not perform this task satisfactorily. The problem has already been observed, as shown in figure 2.27, but not discussed. It is therefore extremely important to identify the causes of the poor performance of the model regarding this problem and to propose solutions.

5.5.1 Coupling of Shear and Flexural Deformations

The force corresponding to the yield point in the shear model is often calculated as the shear capacity of the wall, or the load that corresponds to yielding of the shear reinforcement. In the case of wall SW13 the strength of the shear reinforcement was not reached. Since the mode of failure was not by diagonal tension, the load associated with yielding of the shear reinforcement should be above the ultimate load of 108KN. A trial run of the program NONWALL was performed considering that shear yielding would occur at a load of 120KN. The applied displacement history was the total displacement history applied to wall SW13 during the test. The overall force deformation relationship and both components of the deformation are shown in figure C.14. It is

clear that the balance between shear and flexure is erroneous.

The underlying reasons for the error in the balance between shear and flexure were discussed in section 4.3.3.3. The last segment of the shear envelope is not associated with yielding of the shear reinforcement or exhaustion of shear capacity. Rather, it is associated with triggering large shear deformations due to yielding of the main flexural reinforcement, even when shear reinforcement remains elastic. This observation must be simulated by the model if unrealistic results as shown in figures 2.27 and C.14, are to be avoided. Hence, coupling shear and flexural deformations is necessary.

When yielding of the main flexural reinforcement occurs the "shear yielding" force is assigned the value of the applied shear force at this stage, and the envelope of the shear model enters the post-yield segment. The definition of yielding of the flexural reinforcement is arbitrary as it could be defined as yielding of all the steel bars in one edge member or just as yielding of the extreme vertical bars. In this case yielding of the flexural reinforcement is to be used as an indicator for triggering of large shear deformations. The analysis of the experimental data shows this is noticeable approximately when the extreme tensile bars yield. Therefore, yielding of the flexural reinforcement will be defined as the stage at which the extreme ϕ8mm vertical bars yield.

The program NONWALL, with shear/flexure coupling was run using exactly the same input as in the previous case. The results are shown in figure C.15. The comparison with the experimental data is far better than in the previous case. It shows that if the shear component is not coupled to the flexural component the model is susceptible to large errors with regard to defining the correct balance between shear and flexure deformations.

The coupling of both components of the deformation shifts downwards the post-yield segment of the shear model if the yield load is below the shear capacity. It means that the balance of shear and flexure deformations is sensitive to the definition of the post-yield segment of the shear component. This may be explained as follows. When the flexural reinforcement yields, the stiffness associated with the envelope of the flexural component decreases. If the shear stiffness remains at its pre-yield level, any further increase in the total displacement will be taken essentially by the flexural component. At this stage a slight increase in force is associated with large flexural deformations and small shear deformations. The continuation of this process produces a completely distorted balance between the shear and flexural components, as shown in figures 2.27 and C.14. The analysis of the experimental data has shown that after yielding of the main flexural reinforcement the balance between shear and flexure tends to shift towards the shear component, as referred to in section 4.3.3.3. This observation reinforces the above comment regarding the influence of the post-yield segment of the shear component on the shear/flexure balance. This is due to the observation that the errors of the uncoupled model in finding the balance between shear and flexure are not only quantitative but also qualitative.

5.5.2 Post-Yield Segment of Shear Envelope

Another parameter that influences the post-yield segment of the envelope of the shear model is its inclination, which is an input quantity. In order to study the sensitivity of the global model to variations in the post-yield stiffness of the shear component KH, a short parametric study was performed.

Four analyses using the version of program NONWALL which includes shear/flexure coupling were performed. The displacement history was that applied to wall SW13 in the

test and used in the previous runs referred to in section 5.5.1. The input data was the same in all cases with the exception of KH, for which four different values were considered; 6, 8, 12 and 15KN/mm. The value adopted from the experiments and used in previous runs was KH=9.8KN/mm. Figures C.16 and C.17 show the total deformation and each components for the cases of KH=6KN/mm and KH=15KN/mm, respectively. Figure C.18 shows the total cumulative energy dissipated for all values of the post-yield stiffness of the shear model. Figure C.19 shows the relative contribution of the shear component to the total deformation for the different values of the post-yield stiffness of the shear model. The data shown in figure C.19 was obtained applying to the wall a displacement increasing monotonically up to 15mm. The variations of KH may be considerable in relative terms. However, the absolute values of these variations are very small. Note that the intermediate value of KH=9.8KN/mm is only 2.3% of the elastic shear stiffness.

It was observed that small variations in KH have a strong effect on the balance between shear and flexure. As a consequence they also have a strong influence on the global energy dissipation capacity. Another important feature of the behaviour, observed in figure C.19, is that after a certain stage the value of RSD tends to decrease with increased applied displacement. This feature contradicts the observed behaviour (figures B(11)19, B(12)19, B(13)18), B(14)18 and B(16)18) which showed an increase of RSD with increased level of displacement applied to the wall. This problem is related to the shape of the envelopes of both components of the deformation. The stiffness of the envelope of the flexural component tends to decrease with increased displacements due to the decrease in stiffness of the concrete, which may become negative. The stiffness of the post-yield segment of the shear model is constant. Therefore, the balance between both components tends to shift towards the flexural component. This shows that a linear envelope in the post-yield range, as proposed by Ozcebe and Saatcioglu, is not

suitable for the shear component of this model. A proposal for the solution of this problem is given in section 5.6.

5.6 Discussion and Future Improvements

The increase in shear stiffness on reloading is due to the closure of cracks opened when loading in the opposite direction. An indicator of the stage at which cracks close may be obtained from the strains in the concrete. It is therefore proposed to replace the existing rule for establishing the transition between both segments of reloading in the shear model at a constant force drawn from observation of experimental data. An analytical procedure based on the strains of the concrete, which can be obtained at every stage from the flexural model, may be used to flag the change in shear stiffness between both segments of reloading.

The suggested procedure also has numerical advantages. If the first reloading stiffness is very low, which may happen due to a previous cycle of small amplitude, two undesirable situations may arise. Either the first reloading segment may never reach the load at which the transition to the second segment is made or may achieve it at an excessively large displacement, beyond the previous maximum displacement. Either of the situations has no physical meaning and may lead to numerical problems. If the transition between both segments is defined in terms of strain in the flexural model the problem is eliminated. This is also consistent with the physical interpretation of the observation being modelled.

The same suggestion applies to the unloading segments since the decrease in stiffness during unloading is also due to a decrease in the contribution of concrete to the stiffness of the wall.

The problem of finding the correct balance between both components of the deformation in the post-yield range warrants consideration. The solution of this problem depends on the accurate definition of the envelope of the shear model in the post-yield range. The study presented in the previous section showed that due to the low stiffness of the flexural component after yielding of the flexural reinforcement, any small variation in the stiffness of the shear model may produce substantial differences of results. Therefore, the envelope of shear deformations in the post-yield range should be defined accurately. The fact that most of the energy is dissipated in the post-yield range only emphasizes this point.

In previous studies the value of KH was assigned an arbitrary value without any theoretical or experimental base (usually very low). This was also a consequence of the physical meaning attributed to the yield point in the shear envelope. The yield load in the shear model was considered to represent the ultimate shear capacity. Therefore, KH would represent the post-ultimate shear stiffness of a wall failing in shear. It was shown in the present work that the physical meaning of "shear yielding" is triggering of large shear deformations due to yielding of the main flexural reinforcement. The study discussed in section 5.5.2 also showed the inadequacy of a segment of constant stiffness to represent the shear envelope in the post-yield range. The shear stiffness in the post-yield range must decrease progressively and at a faster rate than the flexural stiffness for the model to establish the correct balance between shear and flexural deformations.

The definition of the shear stiffness in the post-yield range must also be sensitive to small variations in parameters that affect flexural deformations. For instance, any small variation in the hardening stiffness of the flexural steel would change the flexural envelope. For the model to yield accurate results regarding the balance of shear and flexure, the shear envelope would have to be

sensitive to the aforementioned parameters. It is extremely difficult for a theoretical or experimental method to establish the shear envelope directly with the required accuracy. It is therefore suggested that the envelope of the shear component in the post-yield range is established directly from the envelope of the flexural component. This must be done in such a way that the model simulates the trend observed experimentally for an increase in shear deformations faster than the increase in flexural deformations after cracking and yielding of the main flexural reinforcement.

It will be shown in chapter 6 that one of the parameters that controls the shear strength is the depth of the neutral axis. From the yield load to the ultimate load the neutral axis depth decreases continuously and so does the shear capacity. It seems therefore reasonable to associate the variation of the neutral axis depth with shear degradation. Thus, it is suggested to use the neutral axis as an indicator of shear degradation and of the increase in the relative contribution of shear deformations to the total deformation. Since the neutral axis depth may be obtained from the flexural model, the model would be able to generate the envelope of the shear component in the post-yield range.

The analytical predictions of either component of the model for walls failing in shear by diagonal tension are poorer than for walls failing by crushing of the concrete after yielding of the main flexural reinforcement. It was already shown by other researchers that the flexural component yields good predictions of the behaviour of walls that do not fail in shear by diagonal tension. However it does not simulate the effect of diagonal cracks. Thus, it cannot predict the decrease in stiffness associated with the envelope of flexural deformations observed in all walls that failed in shear by diagonal tension. In the case of shear deformations the situation is similar. The procedures for the calculation of the pre-yield shear stiffness in general do not consider, or are not calibrated to account for, the large opening of diagonal cracks.

In its present form the model can only simulate two modes of failure, both in flexure; failure by fracturing of the flexural reinforcement in tension or failure of the concrete in compression. The necessary input data to define these failure modes are the ultimate strains of steel and concrete. However, the model is not yet able to simulate any shear mode of failure. This can be achieved by providing as input the amount of shear reinforcement and the corresponding yield stress. The contribution of concrete can be obtained according to the SRS method, which is described in detail in section 6.2.3. According to this method the resistance to the diagonal tension mode of failure at the ultimate limit state can be evaluated as the sum of two factors; the contribution of the stirrups and the contribution of the concrete, which is equal to the product of the cohesion of the concrete and the compressive area. The compressive area can be obtained from the flexural model at each stage. The resistance to web compression failure can be calculated by the usual methods as the product of the area contributing to shear resistance and a nominal shear stress.

5.7 Summary

The study presented in this chapter is intended as a contribution towards a semi-empirical model for the simulation of the deformation of R/C walls.

The study showed that Ozcebe and Saatcioglu model for the shear component is suitable to represent the shear behaviour of R/C walls with the exception of the post-yield segment of the envelope. It is able to represent the main features of observed behaviour, such as stiffness degradation with increased levels of applied displacement and the pinching effect. Some quantitative and qualitative improvements were suggested. A procedure was suggested to take into account the effect of the failure mode on the intensity of the pinching effect.

The performance of the overall model in establishing the balance between shear and flexural deformations was subject of detailed discussion. It was concluded that coupling shear deformations to flexural deformations is an essential feature to calculate the balance between both components satisfactorily. It was proposed to evaluate the shear yield force as the shear force at which yielding of the main flexural reinforcement occurs. In this way both components enter the post-yield range simultaneously. This simulates triggering of large shear deformations due to yielding of the main flexural reinforcement observed experimentally. It was also proposed to define the envelope of shear deformations in the post-yield range by coupling with the envelope of flexural deformations. It was suggested that the depth of the neutral axis may be a suitable indicator to establish the balance between the envelopes of both components of the deformation in this range.

It was also proposed to use the strains in the tensile concrete to determine the stage at which to terminate the first reloading segment of the shear model. This suggestion was derived from the experimental observation that the increase in stiffness on reloading is associated with the closure of cracks opened when loading in the opposite direction.

The influence of the failure modes on the accuracy of the model was discussed. The model in its present form gives no indication, and takes no account, of the failure mode. Flexural modes of failure can be predicted if the maximum axial strains for steel and concrete are given as input. Shear modes of failure (with the exception of sliding shear) can also be predicted by giving as input the maximum nominal shear stress, the cohesion of the concrete and the area and yield stress of the shear reinforcement crossing the potential failure surface.

FIGURES

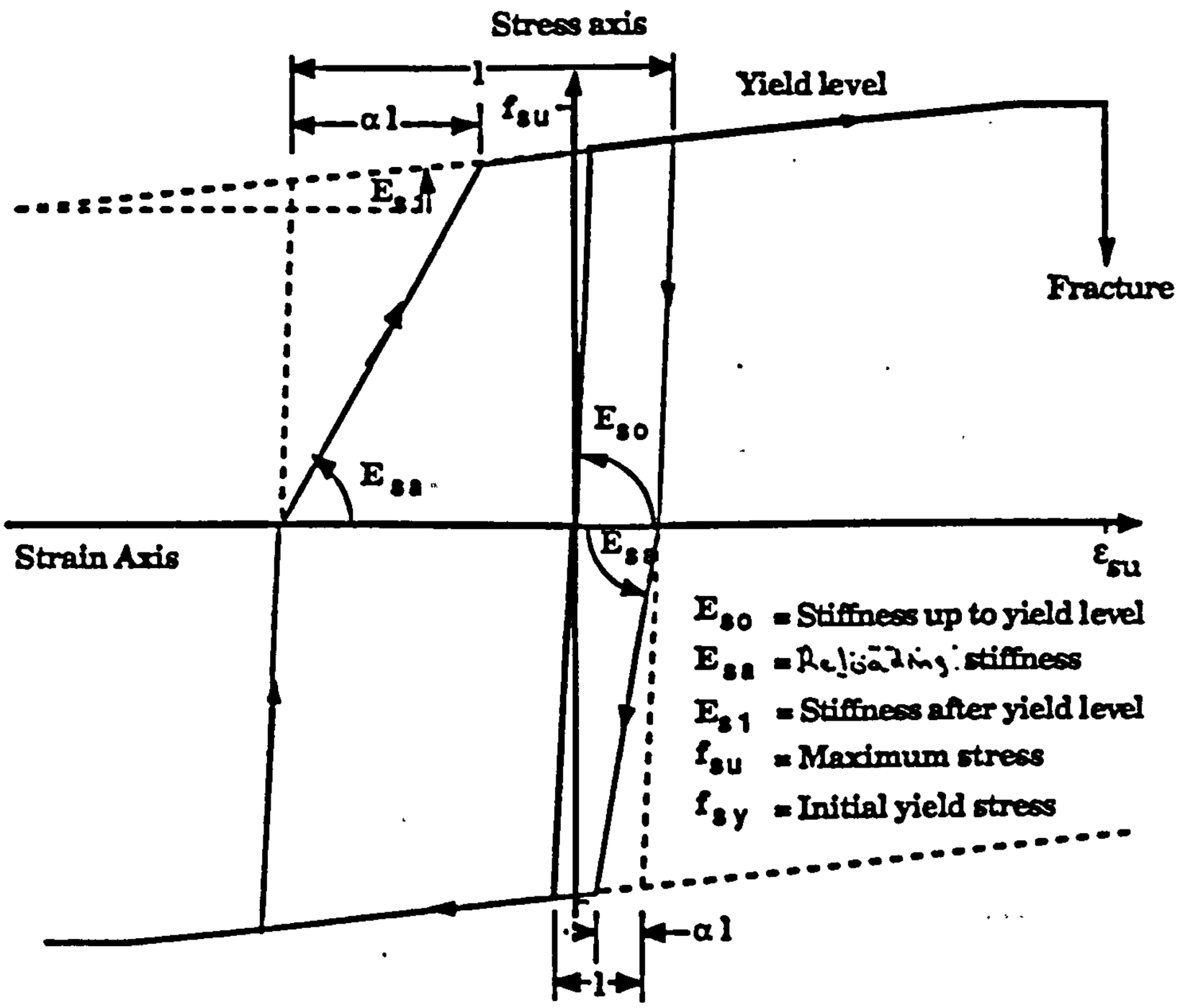


Figure 5.1 Stress-strain diagram for steel used in the analysis (Pilakoutas, 1990)

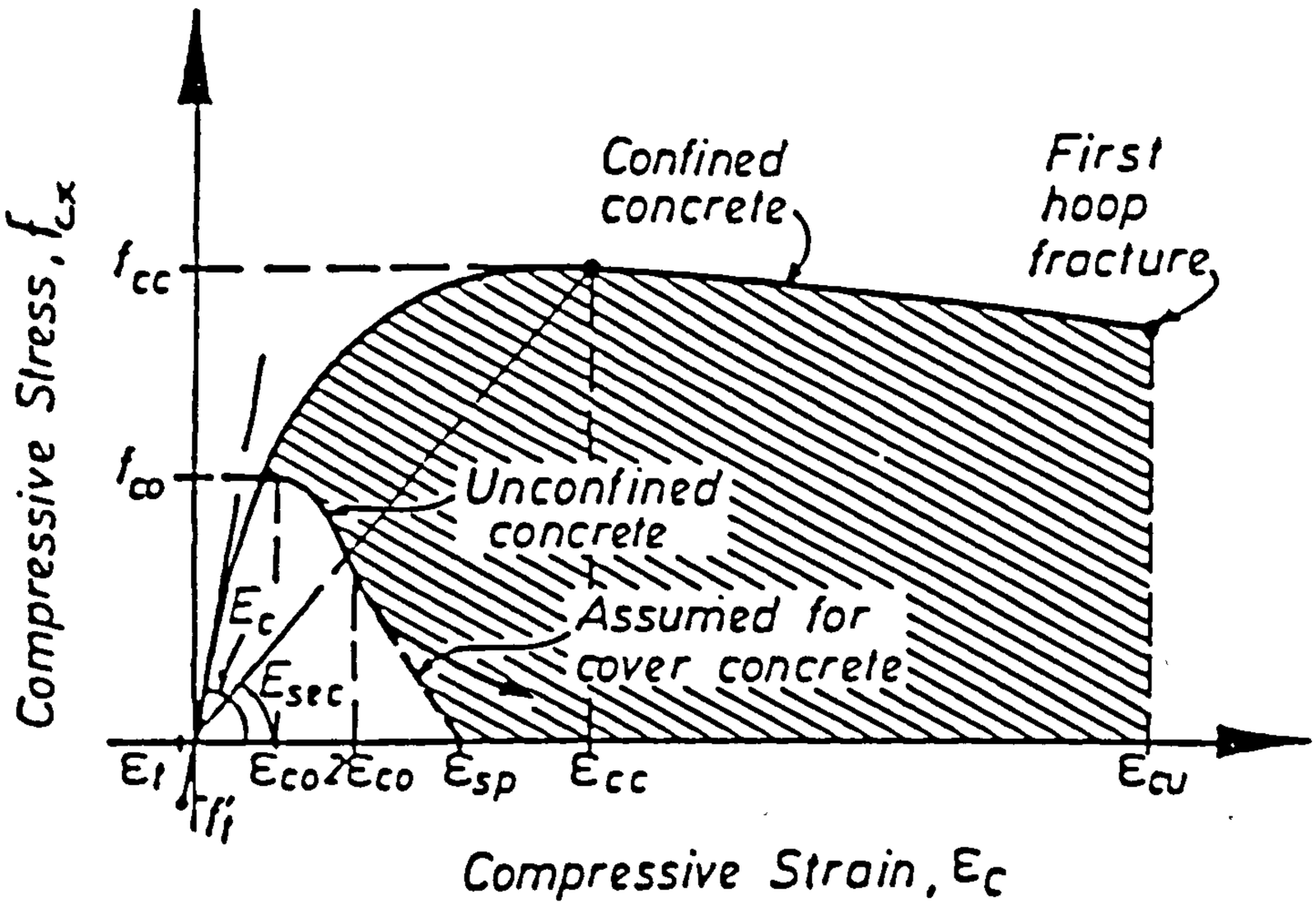


Figure 5.2 Stress-strain model for monotonic loading of confined and unconfined concrete (Mander et al 1988)

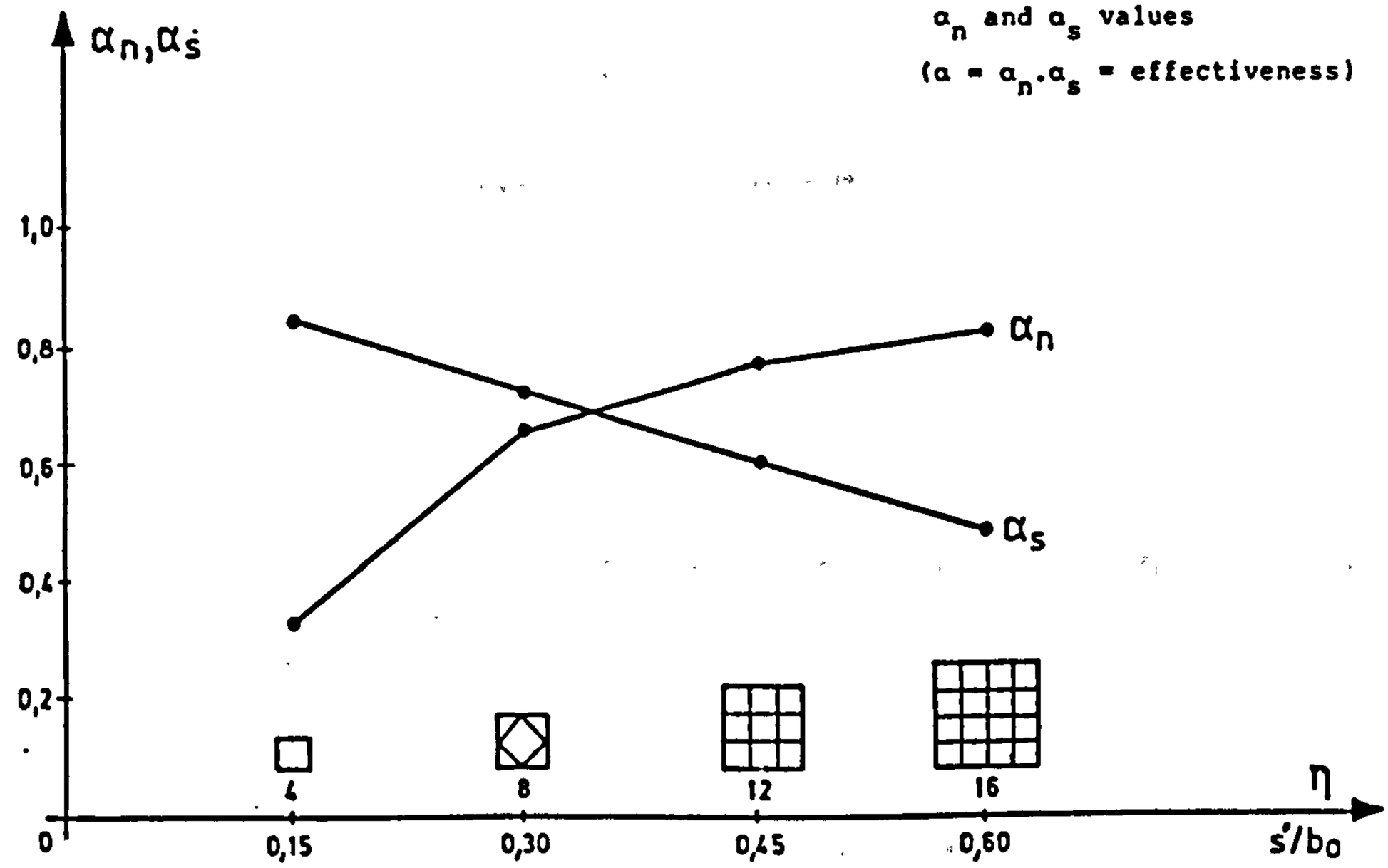


Figure 5.3 Factors α_n and α_s for the evaluation of confining stresses (EC8)

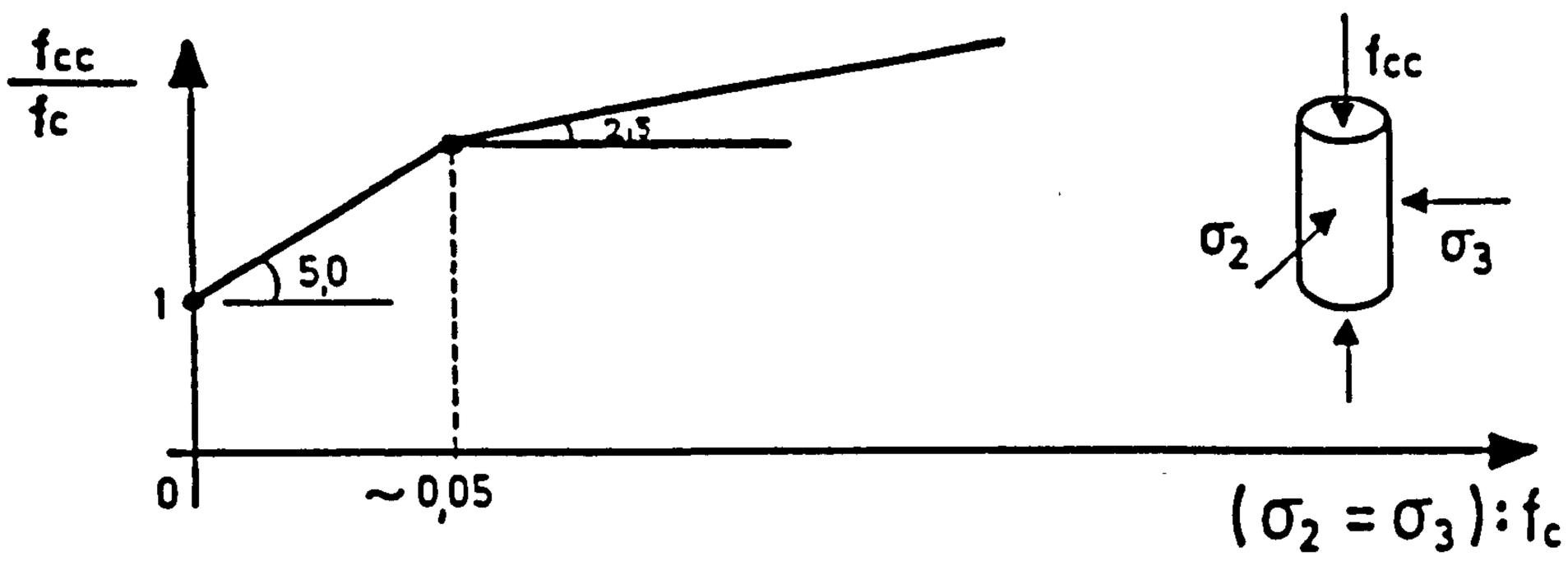


Figure 5.4 Evaluation of the confined compressive strength (EC8)

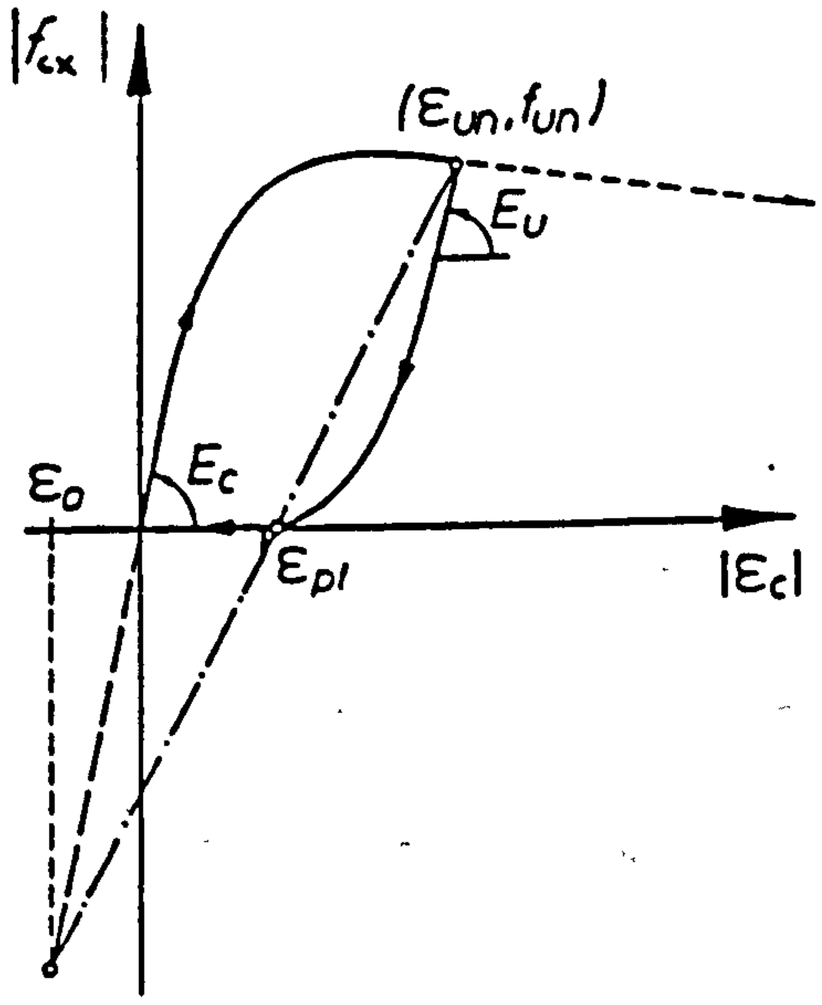
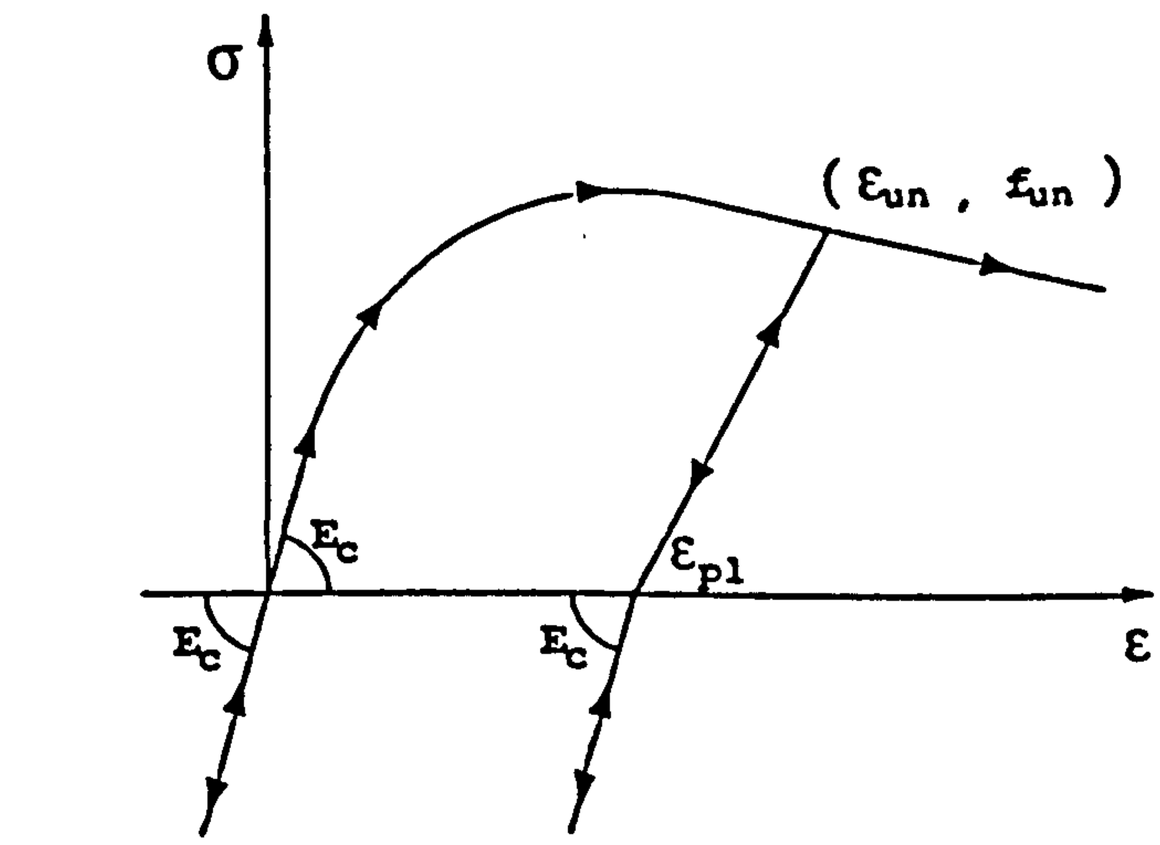
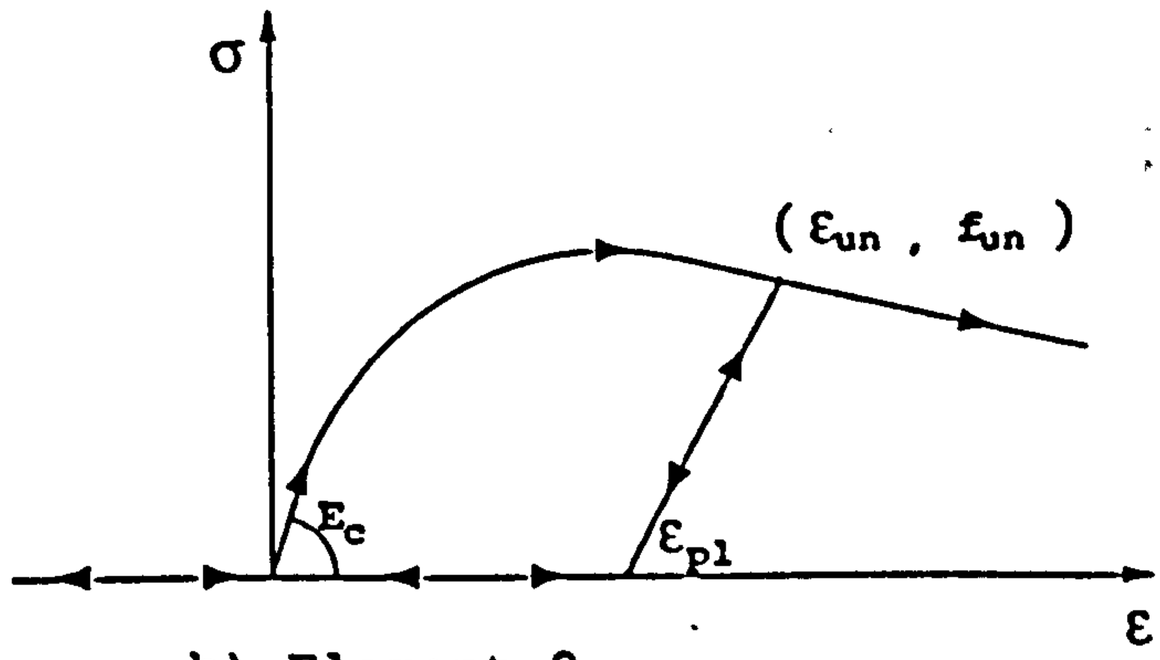


Figure 5.5 Unloading segment of concrete model (Mander et al, 1988)



a) Element 1



b) Element 2

Figure 5.6 Constitutive relationships for concrete

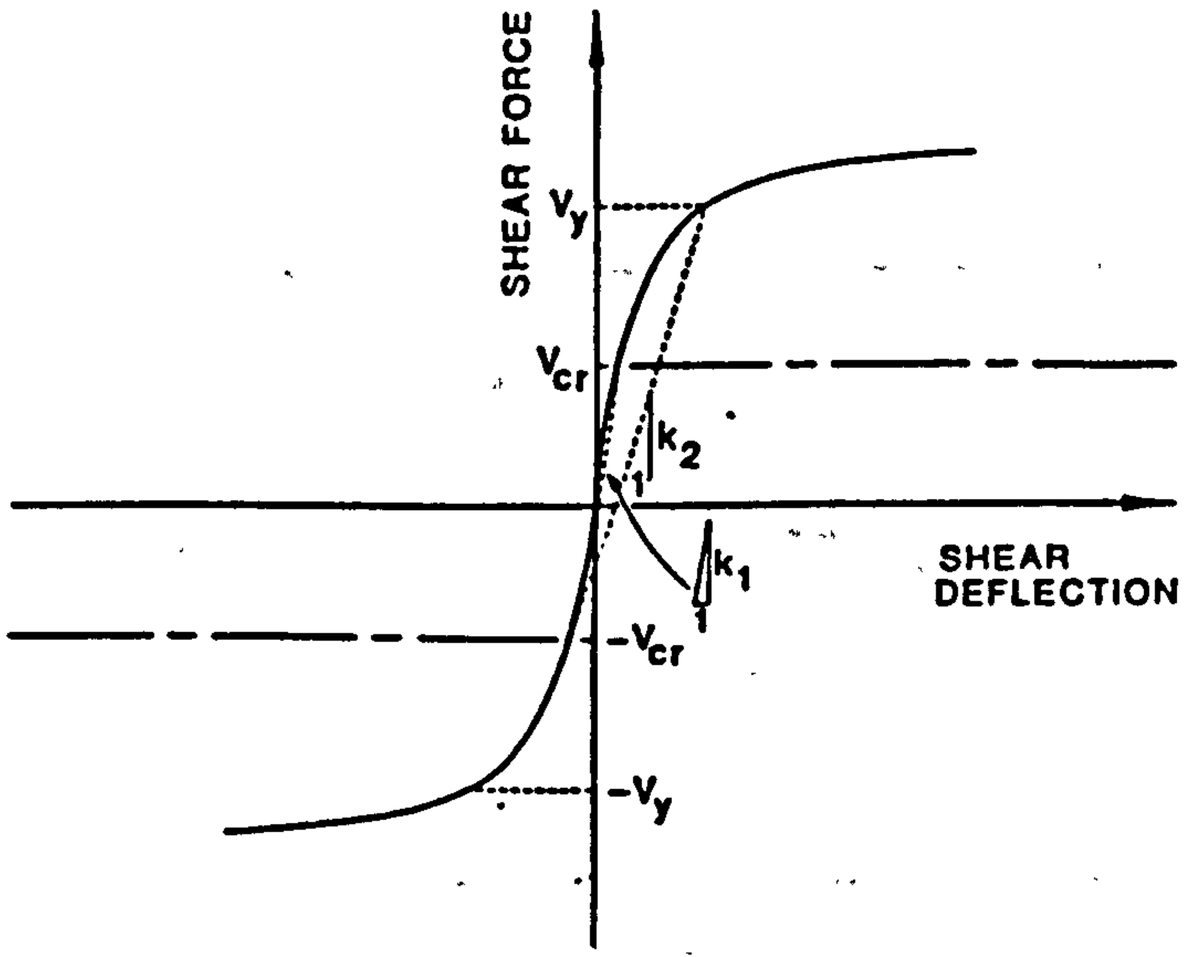


Figure 5.7 Slopes of the envelope used in defining unloading segments (Ozcebe and Saatcioglu, 1989)

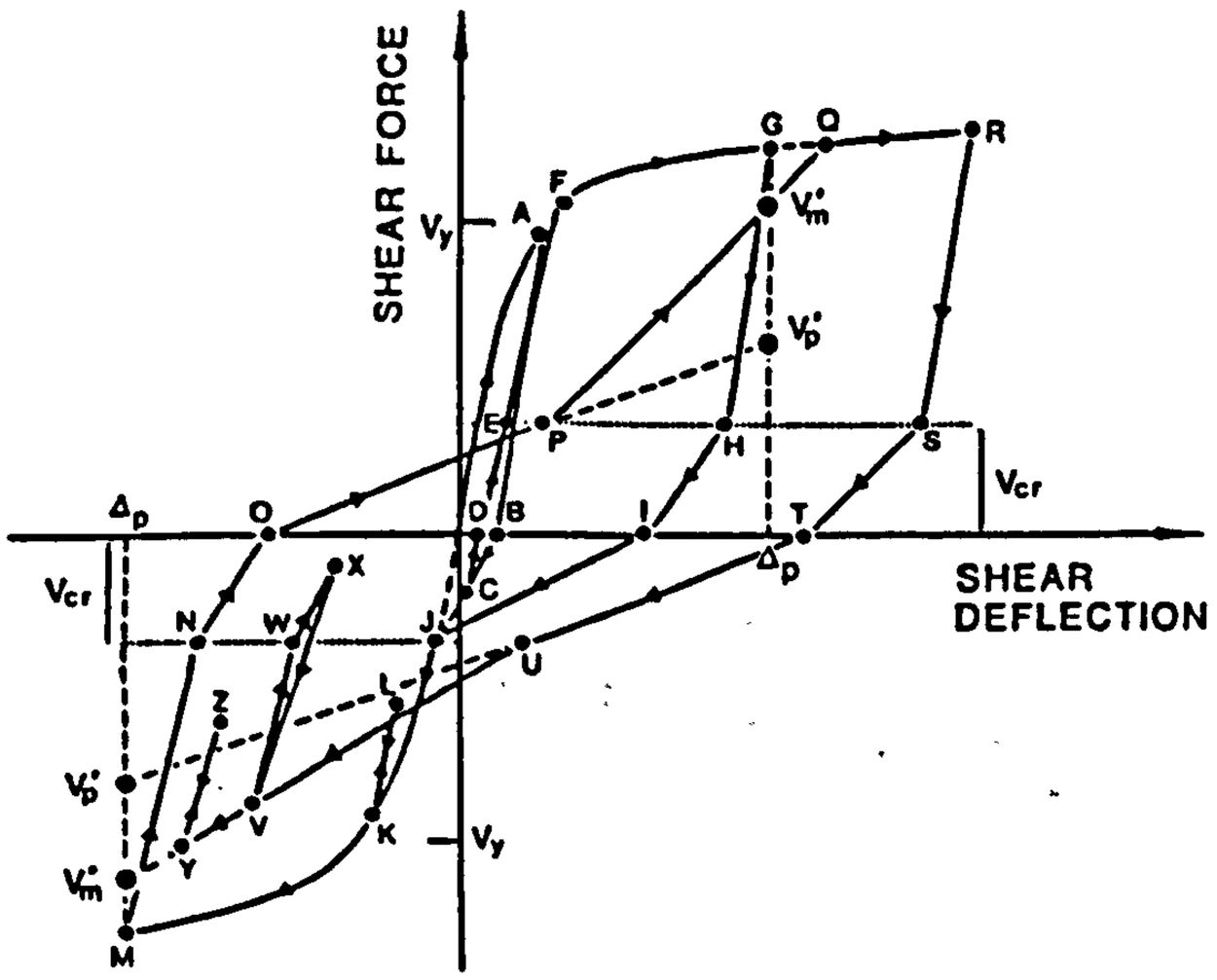


Figure 5.8 Sample segments of shear model (Ozcebe and Saatcioglu, 1989)

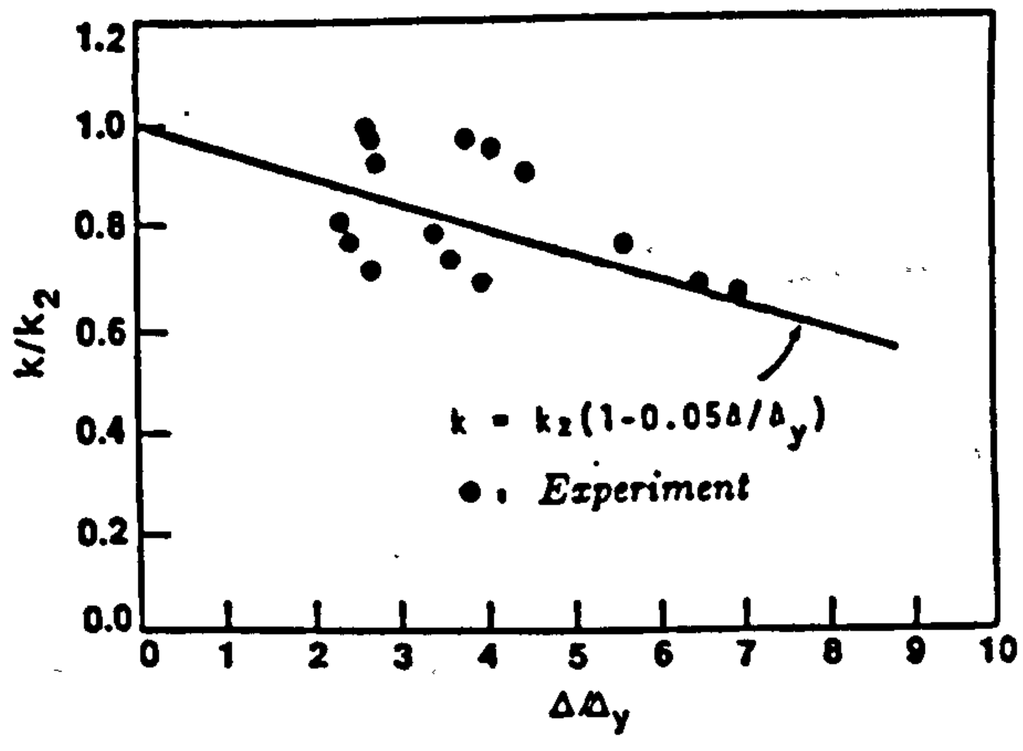


Figure 5.9 Variation of unloading slope above cracking load with ductility in the shear model (Ozcebe and Saatcioglu, 1989)

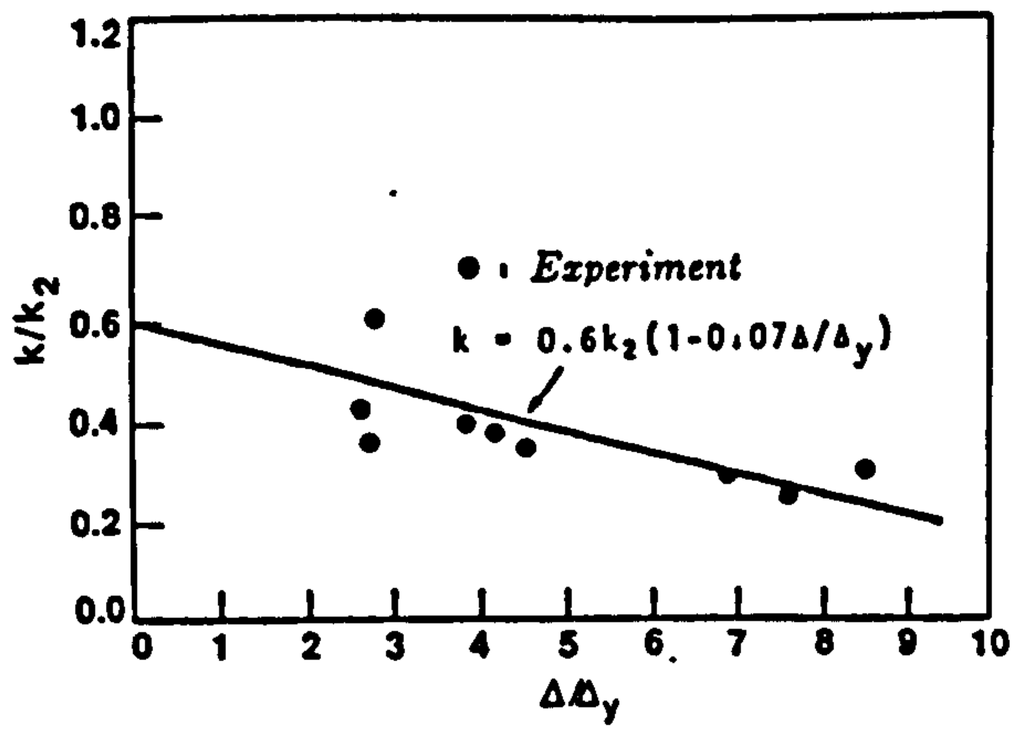


Figure 5.10 Variation of unloading slope below cracking load with ductility in the shear model (Ozcebe and Saatcioglu, 1989)

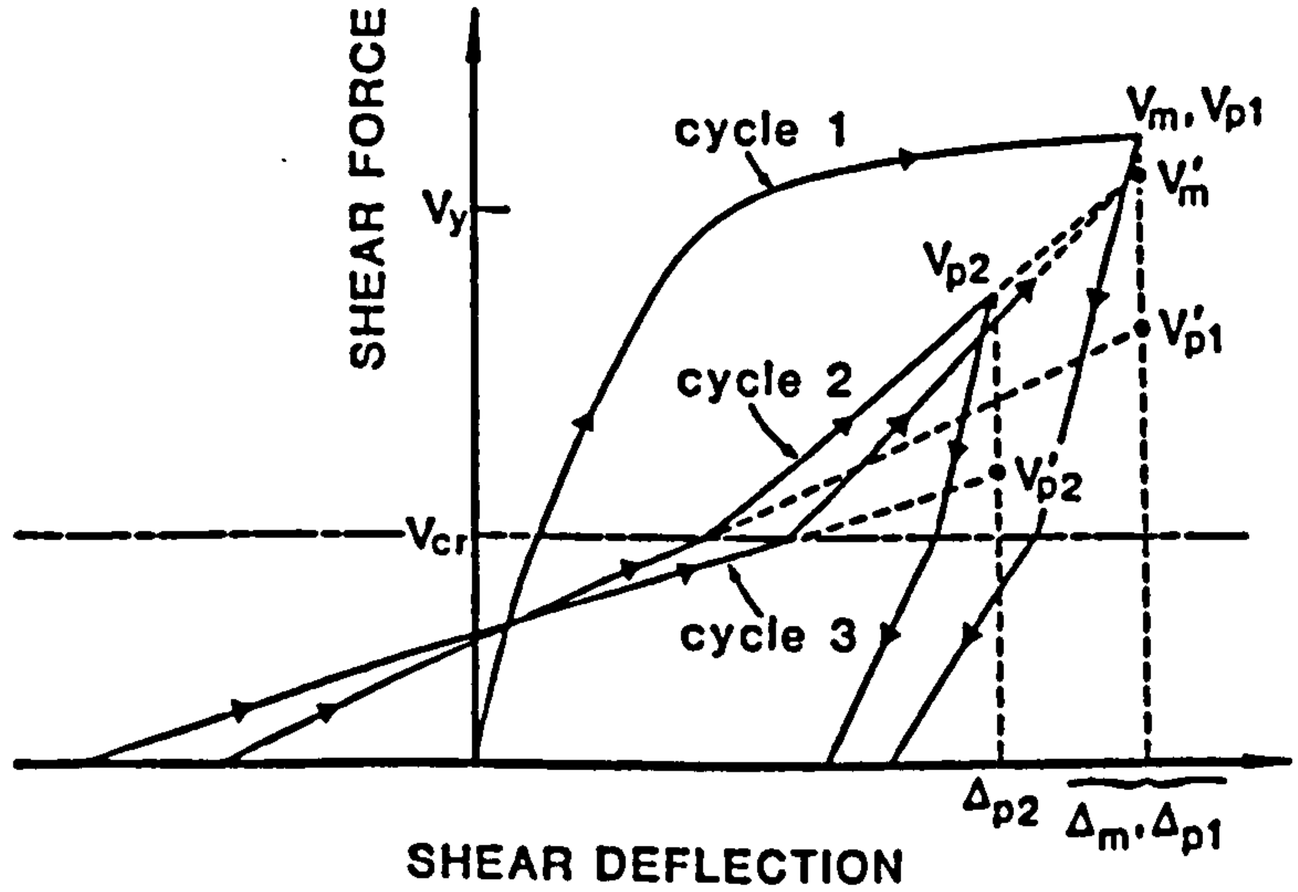


Figure 5.11 Definition of reloading slopes of shear model (Ozcebe and Saatcioglu, 1989)

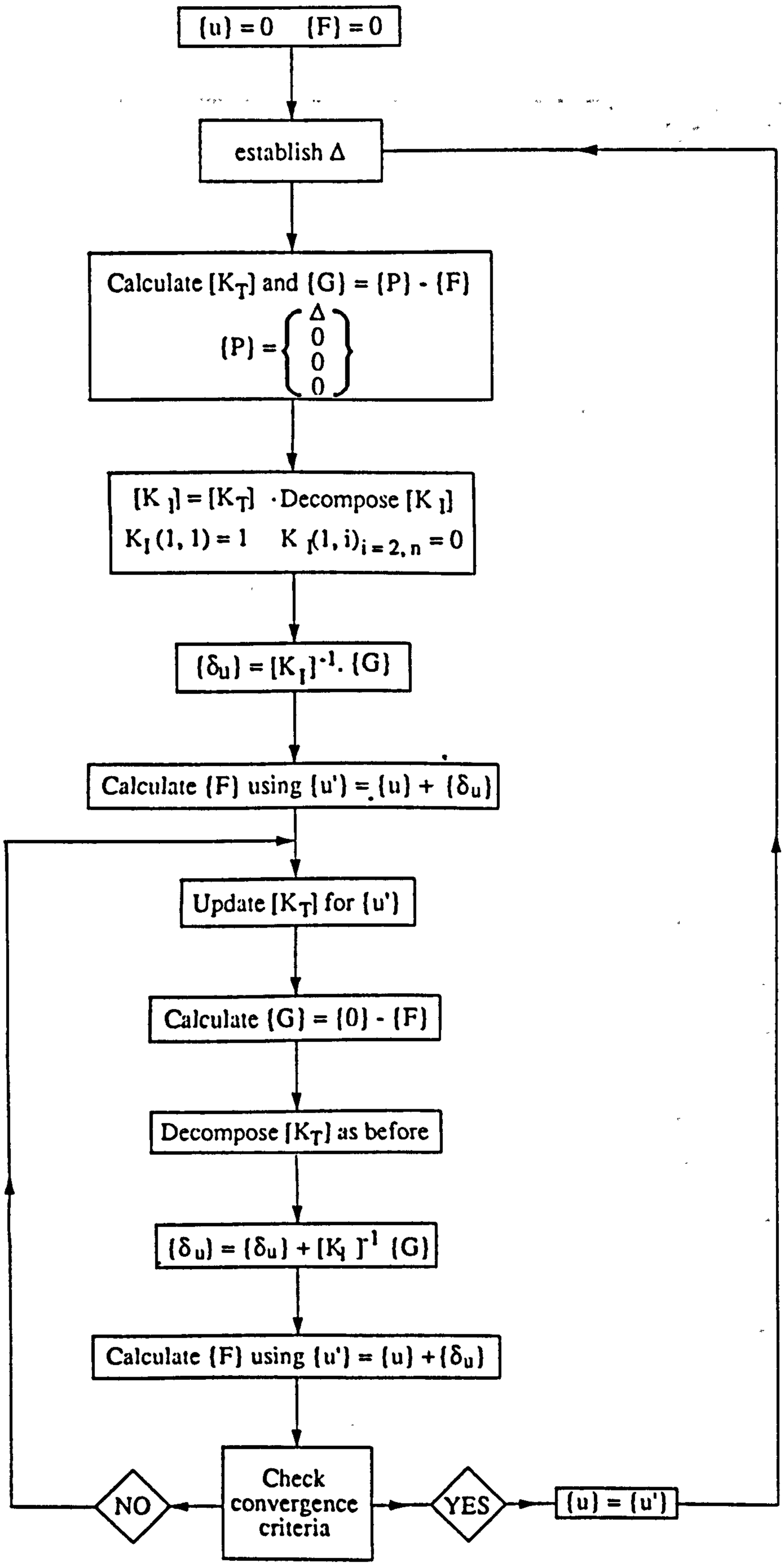


Figure 5.12 - Iterative solution process in the generic step of the analysis

$$K_{ELEM} = \begin{bmatrix} K_H & 0 & K_H\ (1-C)\ h & -K_H & 0 & K_H\ C\ h \\ & \Sigma K_i & \Sigma K_i\ d_i & 0 & -\Sigma K_i & -\Sigma K_i\ d_i \\ & & K_H\ (1-C)^2\ h^2 + \Sigma K_i\ d_i^2 & -K_H\ (1-C)\ h & -\Sigma K_i\ d_i & K_H\ C\ (1-C)\ h^2 - \Sigma K_i\ d_i^2 \\ & & & K_H & 0 & -K_H\ C\ h \\ & & & & \Sigma K_i & \Sigma K_i\ d_i \\ & & & & & K_H\ C^2\ h^2 + \Sigma K_i\ d_i^2 \end{bmatrix}$$

SYMMETRIC

K_H - stiffness of the shear spring

K_i - stiffness of uniaxial element i

d_i - distance of uniaxial element i to mass centre of section

h - height of the element

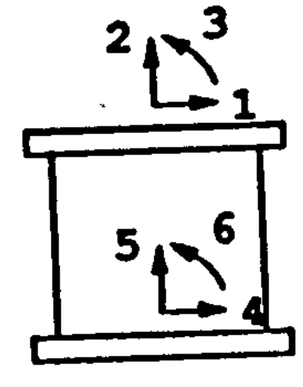


Figure 5.13 - Stiffness matrix of wall element

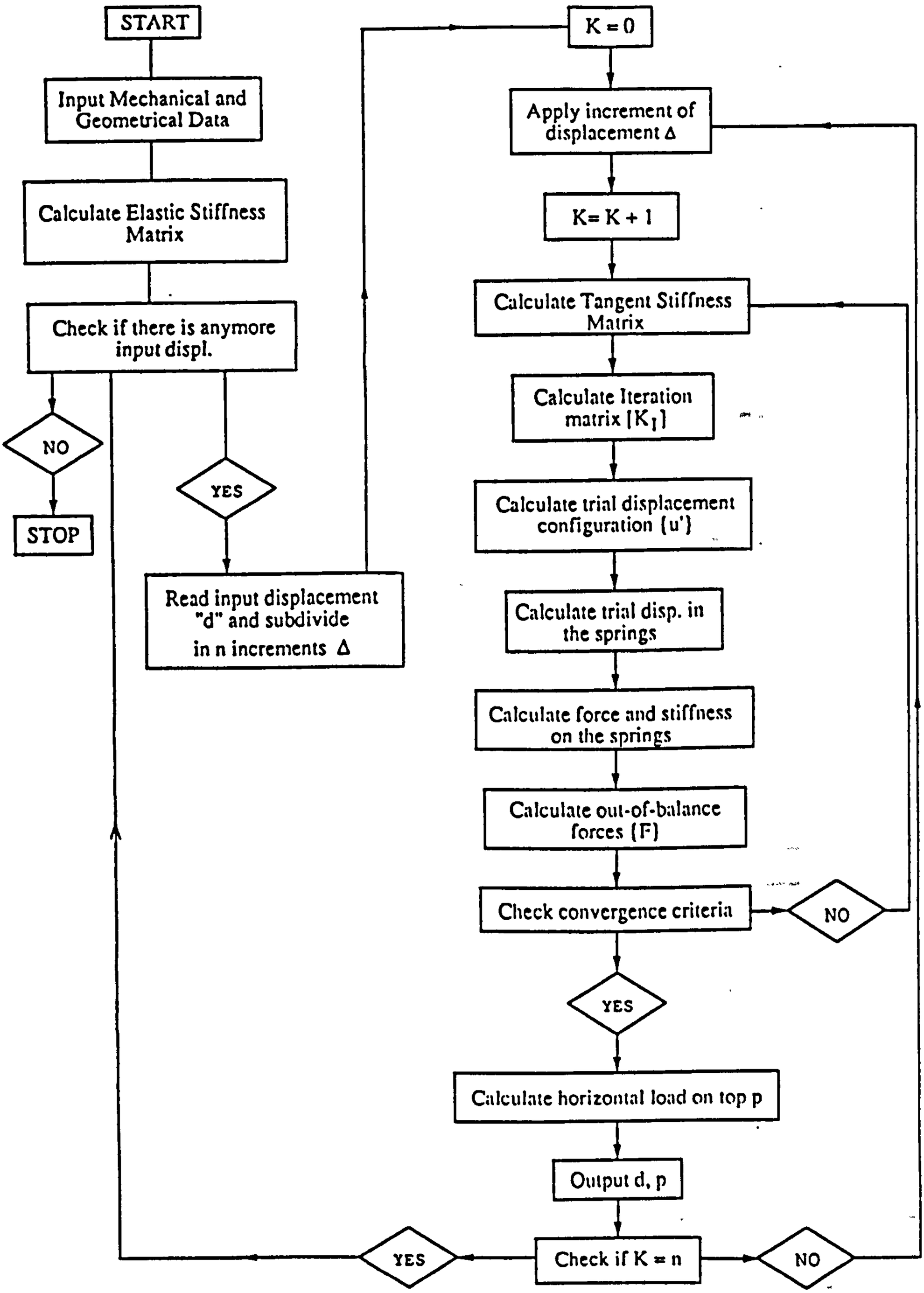


Figure 5.14 - Flow Chart of Program NONWALL

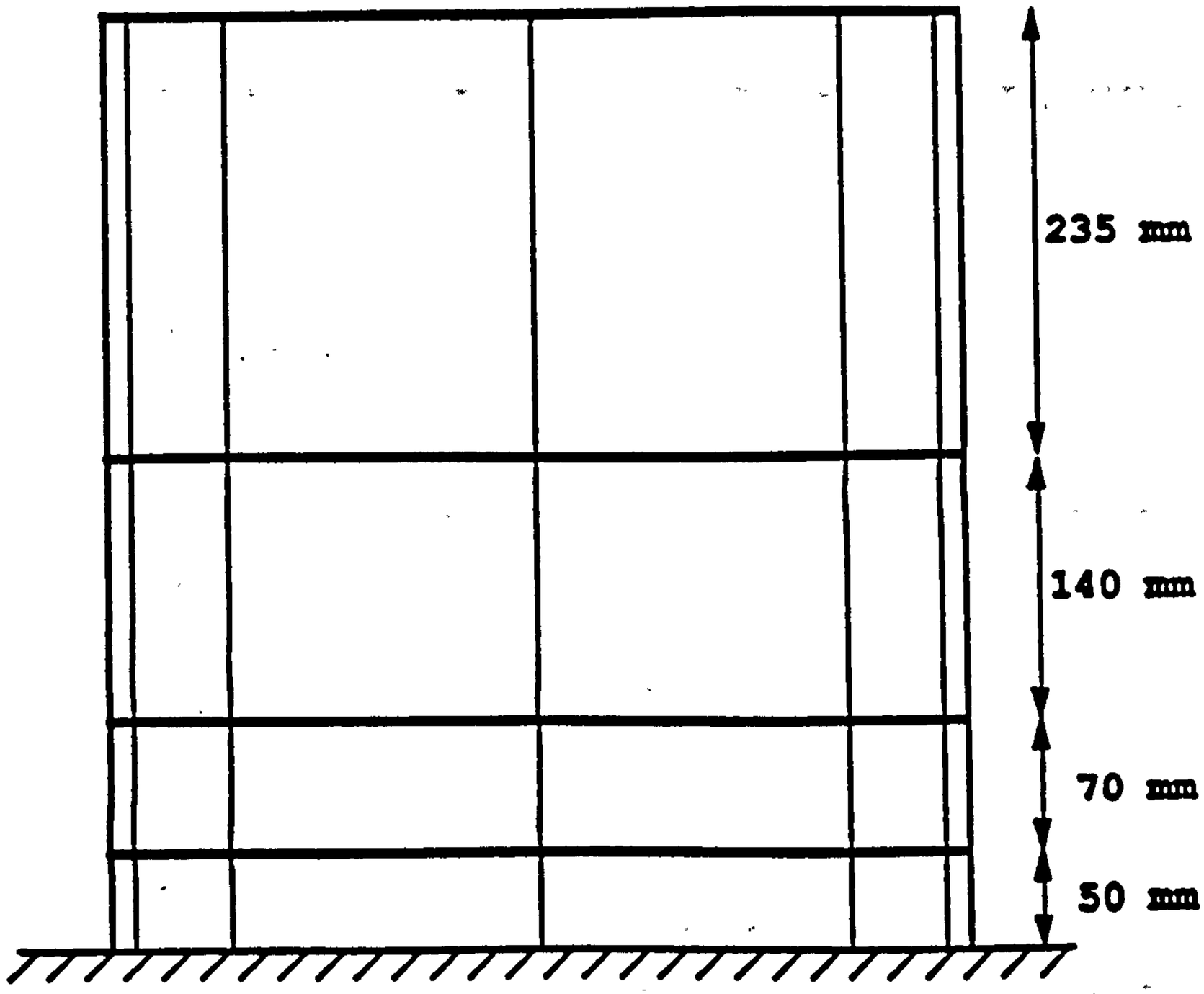


Figure 5.15 Discretization of the wall

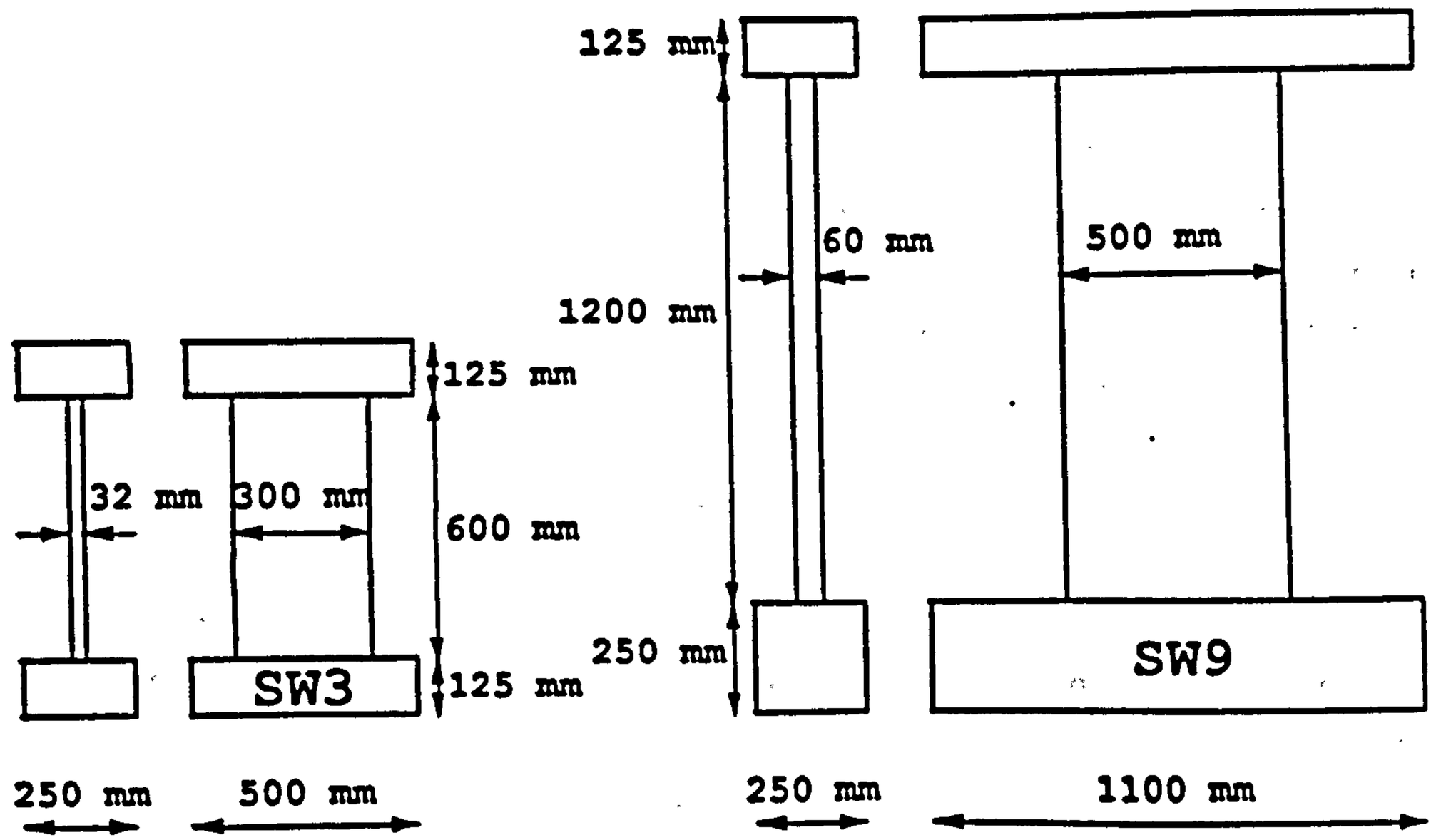


Figure 5.16 Dimensions of walls SW3 and SW9 (Pilakoutas, 1990)

CHAPTER 6

6 DISCUSSION OF RESULTS AND DESIGN IMPLICATIONS

6.1 Introduction

In this chapter the main results of the tests are discussed and recommendations concerning shear design are proposed. Several observations from the tests and analysis of results are discussed and their qualitative implications are highlighted. Suggestions for further work concerning the issues in which the experimental evidence is not considered conclusive are presented.

In section 6.2 analysis of the shear transfer mechanisms across plastic hinges of R/C walls is undertaken. The different theories and methods already referred to in chapter 2 are compared and their potential to explain the observed behaviour is assessed. The most important parameters that control the shear capacity at the ultimate limit state are identified. Analytical predictions are discussed and compared with experimental data. In section 6.3 the influence of confinement reinforcement on the behaviour of walls with low shear ratios is discussed. In section 6.4 current code provisions for the evaluation of the height along which confinement must be provided are appraised. The need to design R/C walls against sliding shear is discussed in section 6.5. Section 6.6 presents a discussion on the influence of the load history, shear ratio and failure mode on the ductility of R/C walls. In section 6.7 the influence of the failure mode and shear design on the energy dissipation capacity is discussed. Changes in the methodology used to evaluate the behaviour factors "q" in EC8 are proposed in section 6.8. The main conclusions of this chapter are summarised in section 6.9.

6.2 Shear Strength of R/C Walls

6.2.1 Shear Transfer Mechanisms

The discussion presented in section 2.3.1.1 has already highlighted shortcomings of the truss analogy and current code provisions for the shear design of plastic hinges. The results presented in chapter 4 also contradict some concepts that form the background of these provisions. For instance, the results of wall SW13 show that the shear strength is well above the predictions of EC8 and NZ 3101 (1982). These predictions are based on the assumption that only the truss mechanism provides shear resistance in the PHZ at the ultimate limit state. This assumption was derived from the observation that the contribution of aggregate interlock can not be relied upon in the PHZ due to the large opening of cracks. The opening of the diagonal cracks in wall SW13 confirms that. The crack width registered at the ultimate load was beyond the limits at which aggregate interlock can be considered effective (Fenwick and Paulay, 1968 and Jimenez, White and Gergely, 1982). Therefore, the ultimate load of wall SW13 cannot be explained using the theory that provides the background to the codes. The explanation requires a better understanding of the shear transfer mechanisms, as discussed at a later stage in this section.

The CFP concept shed some light on the source of shear strength, since it identifies the ability of the compressive zone of the wall to sustain shear forces. In fact, the compressive zone, acting as a large dowel, seems to be the only possible extra source of shear strength at the ultimate limit state. The fact that failure always occurred when the cracks in one direction had closed strengthens this view.

However, serious doubts about the ability of the CFP concept to explain the observed behaviour were raised in the discussion presented in section 2.3.1.1. The behaviour of wall SW15 also points to the fact that the CFP concept on its

own, and as it stands, does not explain the observed behaviour and does not form a suitable basis for design. Wall SW15 was designed in such a way that most of the shear force could not be transferred to the zone below the neutral axis. The result was a brittle shear failure. The observed behaviour could not have occurred if the compressive zone had the ability to sustain all the applied shear. The CFP concept also seems unable to explain the failure mode of wall SW13. According to the CFP concept the concrete below the neutral axis gives almost no contribution to the shear strength. It also does not contribute to flexural strength. Accordingly, failure of the wall cannot be triggered by failure of the concrete below the neutral axis. In other words, according to the CFP concept, web crushing failure cannot take place. However, it should be noted that this failure mode, besides being reported in this work, has been identified and studied by many researchers.

It can be concluded from the above that the compressive zone was responsible for a substantial contribution to shear strength at the ultimate limit state. However, the contribution of the concrete below the neutral axis and the stirrups that transfer shear to that part of the walls are indispensable if diagonal tension failure is to be avoided. Therefore, the resistance to diagonal tension at the state of failure can be evaluated as the sum of two components; the truss mechanism and the shear strength of the compressive zone. The results of all other tests are compatible with this view. All walls exhibited shear strength in excess of that supplied by the truss mechanism and the width of diagonal cracks was such that the aggregate interlock effect could not be relied upon.

The above view about the shear transfer mechanisms applies to walls with low shear ratios, in which a considerable shear force is present. In flexural walls the shear force at failure is comparatively low. The contribution of the compressive zone and a minimum amount of stirrups,

which is always available in real cases, should be sufficient to provide the required shear strength.

6.2.2 Shear Strength of the Compressive Zone

6.2.2.1 Design Concept of the Tests

In order to calculate the resistance of a wall to the diagonal tension mode of failure it is necessary to calculate the shear strength of the compressive zone. The purpose of the last three tests was to identify the most important parameters that control the shear strength of the compressive zone from a design-orientated perspective. All three walls were designed to fail in shear by diagonal tension after diagonal cracks had opened enough for the aggregate interlock effect to vanish. The purpose of this was to measure their resistance to this mode of failure, since if they would fail in flexure or in shear by diagonal compression the ultimate load would only provide a lower bound of their resistance to diagonal tension. This philosophy casts serious doubts on tests conducted by other researchers and used to derive shear resistance expressions, since shear failure was rarely sought, or indeed occurred.

It was sought to eliminate the aggregate interlock effect and no vertical web reinforcement was placed in order to have only two contributors to the shear resistance at the ultimate; the stirrups and the compressive zone. Therefore, the difference between the ultimate load and the strength of the stirrups across the failure surface can be attributed to the shear resistance of the compressive zone. In order to quantify clearly the contribution of the stirrups, the walls were designed in such a way that the number of stirrups crossing the diagonal crack which would lead to failure was known exactly. No stirrups were placed within 100mm of the ends of the potential failure surface. This is the reason for the unusual distribution of stirrups in these walls.

All three walls failed in the desired mode. In the case of wall SW16 the yield strength provided by the stirrups was 41.6KN. Since the ultimate load was 80.3KN, the strength of the compressive zone was about 38.7KN. Wall SW17 was designed with only one difference to wall SW16; the amount of stirrups crossing the potential failure surface. Instead of four, there were five stirrups whose yield strength was 52KN. The flexural reinforcement was the same and both walls were confined up to similar heights. The ultimate load of wall SW17 was 83.6KN, as depicted in table 4.5. Therefore the shear strength provided by the compressive zone was 31.6KN.

6.2.2.2 Comparisons With Different Methods

The above-mentioned results are incompatible with the possibility that the shear strength of the compressive zone is essentially a function of the compressive force in this area, as suggested by Wagner and Bertero (1982) and already mentioned in section 2.1.1.2. In this case, the contribution of the compressive zone to the shear strength would be equal to the product of the total shear force and a factor that is constant for a given shear ratio, as shown in section 2.3.1.1. This means that the ratio between both factors contributing to the shear strength would be the same for both walls. As the contribution of the truss mechanism was increased by 25% from wall SW16 to wall SW17, the total increase in shear strength should also be 25%. In this case the expected shear strength of wall SW17 would be 100.4KN. The contribution of the compressive zone to the shear strength would be 48.4KN.

The fact that the contribution of the compressive zone would be expected to increase derives from the fact that by increasing the strength of the truss mechanism a higher shear force could develop. Therefore, the corresponding bending moment increases and so does the axial force in the zone of the wall under compression. If the shear strength of the compressive zone was proportional to this axial force, its

shear strength should also increase. What happened in fact was exactly the opposite, the shear strength of the compressive zone decreased.

If the strength of the compressive zone was proportional to the depth of the neutral axis a small decrease in the shear strength of the this part of the wall should be expected. This is due to the fact that the neutral axis shifts continuously towards the edge after yielding of the main flexural reinforcement. This should be expected as the neutral axis depth at the state at which yielding of the main flexural reinforcement occurs is much larger than at flexural failure. In between these two stages the neutral axis moves between the corresponding positions. This is also a feature of observed behaviour, as already discussed in section 4.3.4.2. Therefore, the comparison of results from walls SW16 and SW17 points to the fact that the position of the neutral axis is the most important parameter controlling the shear strength of the compressive zone.

6.2.2.3 Verification

In order to provide further evidence of the above conclusion the test of wall SW18 was undertaken. It was sought to design a wall similar to SW17 but with one important difference; a larger neutral axis depth at the ultimate load. In order to increase the neutral axis depth, larger vertical bars were used in the tension side so as to avoid yielding of this reinforcement. This is the reason for the replacement of the extreme ϕ8mm bars by ϕ12mm. Strain gauge readings confirm that the extreme tensile ϕ12mm bars did not yield during the test of wall SW18. The edge member in the opposite side was designed exactly equal to both edge members in wall SW17. The wall was loaded in such a way that failure would occur with the edge member equal to the edge members of wall SW17 being in compression. Therefore, the only difference between the compressive zones of walls SW17 and SW18 at failure would be the neutral axis depth.

However, the fact that the flexural reinforcement was not expected to yield when shear failure would occur was likely to lead to lower crack widths when loading in the direction of failure. In turn it was possible that this could lead to considerable aggregate interlock still resisting shear at the ultimate load. In such a case it would not be possible to evaluate the shear strength of the compressive zone at the ultimate load. In order to eliminate the aggregate interlock effect a pre-formed crack was artificially created with a steel plate, as already referred to in section 4.1.3.3.2. As described in section 4.2.9.1 and as table 4.4 shows, the pre-formed crack increased the crack width in such a way that the effect of aggregate interlock along the failure surface could be considered non-existent when the ultimate load was achieved.

The neutral axis depth of wall SW17 at ultimate load, calculated using the program CRELIC, is shown in table 6.1. This table also shows the depth of the neutral axis for wall SW18 obtained from an elastic analysis of the wall cross-section in which the concrete was considered as a no-tension material. An increase of about 31% in the depth of the neutral axis depth should be expected. This would correspond to an increase in the ultimate load of approximately 10KN. The ultimate load of wall SW18 was 99.9KN, as shown in table 4.5. This corresponds to an increase in shear capacity even higher than expected, which confirms that the neutral axis depth is the key parameter which controls the shear strength of the compressive zone. This shows that the SRS method is the best available method to calculate the contribution of concrete to shear strength.

In section 4.3.4.6 reference was made to the observation that after yielding of the main flexural reinforcement there are large increases in stirrup strain with very little increase in load. This can be attributed not only to the decrease in the aggregate interlock effect but also to the decrease in the neutral axis depth. Both reduce the shear

transfer mechanisms associated with the contribution of the concrete.

6.2.3 The SRS Method

The "shear resistance surface" (SRS) method (Pilakoutas, 1990) already referred to in sections 2.1.1.5 and 2.3.1.1, is described in detail in this section.

According to the SRS method diagonal tension failure occurs along the surface which offers least resistance to this mode of failure. The failure surface must extend across the whole cross section of the wall and comprises two parts; one in the zone under axial tension and another in the zone under axial compression, as depicted in figure 6.1. On the tension side the SRS coincides with the main diagonal crack leading to failure. In the PHZ only the contribution of the stirrups must be considered in the evaluation of the force transferred across the SRS on the tension side. The tests have confirmed the widely held view that the aggregate interlock effect cannot be relied upon in the PHZ. If a value of the angle of the SRS with the horizontal in the tension side ϕ_s=45° is used, which may be slightly conservative in some cases, the shear resistance provided along the SRS in this side of the wall for a uniform distribution of stirrups, is given by:

$$V_t = (1 - \xi)\ L\ (A_s/s)_h\ f_y \qquad (6.1)$$

The above equation yields results similar to the truss analogy. If the distribution of the stirrups is not uniform, as for instances in the case of wall SW15, the SRS of minimum resistance may be different to the surface shown in figure 6.1.

A compressive force, due to the bending moment and axial force, and part of the total shear force are applied on the compressive edge member of the wall, as illustrated in figure

6.2. Failure in this part of the wall also occurs along the surface of least resistance. The resistance of concrete in shear can be expressed by a Mohr-Coulomb envelope, as shown in figure 6.3. Figure 6.2 shows that a surface where the resultant of axial stresses is zero can always be found in the compressive edge member. The inclination of this surface to the horizontal depends on the relative magnitude of the shear and compressive forces. Along this surface the resistance of the concrete to shear (in terms of stress) is the cohesion τ_o, which is a function of the concrete type. The shear force that can be resisted on the surface is:

$$V_\theta = \tau_o \, \xi \, b \, L \, / \, \cos\theta_o \qquad (6.2)$$

The horizontal projection of this force is the contribution of the compressive zone to the shear strength:

$$V_{cc} = V_\theta \cos\theta_o \qquad (6.3)$$

$$V_{cc} = \tau_o \, \xi \, b \, L \qquad (6.4)$$

As equation (6.4) shows, the shear capacity of the compressive zone is independent of the direction along which failure occurs, since the term $\cos\theta_o$ appears both in equations (6.2) and (6.3). This means that the method is valid for any distribution of stresses within the compressive zone, since what matters is the projection of the minimum SRS to the horizontal. Therefore, the neutral axis depth is the only variable required to calculate the shear capacity of the compressive zone. Although the neutral axis depth may increase with the distance from the base of the wall, for design purposes it is acceptable to use the value of the neutral axis depth at the base section.

The method is conservative as it does not consider the contribution of the steel in the compressive zone.

6.2.4 Comparisons With Experimental Data

Table 6.1 shows comparisons of the experimental results with predictions of shear capacity by the SRS method for walls SW13 and SW16 to SW18.

The value of τ_o is a function of the concrete strength. Therefore, it depends on the level of confinement in the compressive zone. However, the enhanced strength of the confined concrete does not need to be evaluated in the design process according to most code provisions. Since the unconfined concrete strength used in design provides a lower bound of the real concrete strength, it is also safe and acceptable for design purposes to use f_c to calculate the cohesion of the concrete. The values of τ_o given in the literature (Wagner and Bertero, 1982, Elnashai, 1984, Divakar, Fafitis and Shah, 1987) vary between $0.15f_c$ and $0.2f_c$.

In the design process the depth of the neutral axis can be obtained from the flexural calculations. In the case of wall SW13 the depth of the neutral axis was calculated using the hypothesis given in EC8 for flexural design. This gives the shear strength at the state of flexural failure. The neutral axis depths of walls SW16 and SW17 were calculated using the program CRELIC. The calculation of the neutral axis depth for a wall failing in shear is more complicated than for a wall failing in flexure. The shear strength of the wall depends on the neutral axis depth, which in turn depends on the bending moment. The values shown in table 6.1 were calculated for the loads at which the walls failed. The neutral axis depth for wall SW18 was calculated as referred to in section 6.2.2. The yield strength of the steel bars was used to evaluate the contribution of the stirrups. Strain gauge readings in the stirrups of walls SW16, SW17 and SW18 did not show strains far above the yield strain at the ultimate load in these walls. Most of the large increase in stirrup strains occurred after the ultimate load, in the descending branch. Therefore it is not advisable to take

advantage of any possible increase in stirrup strength due to strain hardening.

It should be noted that the experimental value of the ultimate load of wall SW13 is a lower limit of its resistance to shear failure by diagonal tension. However, strain gauge readings point to the fact that the resistance of wall SW13 to this failure mode should not be far above its ultimate load, as referred to in section 4.3.4.6

The results shown in table 6.1 indicate that the shear resistance evaluated by the SRS method provides a safe lower bound on the diagonal tension strength if the cohesion of concrete is taken as $\tau_o=0.15f_c$. For design purposes a value of $\tau_o=0.15f_c$ divided by a suitable partial safety coefficient determined by code provisions can be used. If the coefficient $\gamma_c=1.3$ proposed in EC2 for concrete under earthquake actions is chosen, the contribution of concrete to the shear strength of plastic hinges of R/C walls will be given by the following equation:

$$V_{cc} = 0.15\ f_{cd}\ \xi\ L\ b \qquad (6.5)$$

The SRS method may also be used to explain the behaviour and ultimate load of wall SW15. The yield strength of the reinforcement that spanned the failure surface was 22.4KN. This value includes a contribution of 10.4KN of the lower ϕ4mm stirrup of the central strip in addition to the yield strength of the wire below the central strip, which was 12KN. This is far below the ultimate load of wall SW15, which was 85KN. The 62.6KN difference cannot be attributed only to the shear strength of the compressive zone at the base section. The extra source of strength can only be found in the upper part of the failure surface.

In section 4.2.6.1 reference was made to the observation that the diagonal crack along which failure occurred on the tension side of the wall changed direction (becoming more close to the horizontal) on top to avoid the lower ϕ6mm

stirrup of the central strip. This was due to the fact that a surface of less resistance was found. This surface is identified as segment A-B in figure 6.4, which shows a schematic representation of the failure surface of wall SW15. Failure was triggered at a load lower than if the crack would have crossed the lower ϕ6mm stirrup. As the yield strength of one of the ϕ6mm stirrups is 34.4KN, the shear strength offerred by the upper portion of the failure surface was below this value. Therefore, the shear strength of 62.6KN referred to in the previous paragraph is the sum of two contributions; the shear strength of the compressive zone at the base section of the wall and the shear resistance along the less inclined upper part of the failure surface, shown in figures A(15)3 and A(15)4.

Comparisons with the data from walls SW11 and SW12 are not possible since the results of these walls cannot be used in a quantitative basis, as already discussed in section 4.3.4.6. A more detailed discussion of the results of wall SW14 is given in section 6.3

6.2.5 Discussion

In section 6.2.3 it was concluded that the data from the test programme is not compatible with the conclusions of Wagner and Bertero (1982) regarding the shear strength of boundary elements of R/C walls. This is attributed to the fact that the specimens tested by Wagner and Bertero were not suitable for the simulation of the behaviour of the wall edge members. As shown in figure 2.6, the geometry of the specimens is such that the failure surface was imposed on them. Therefore, the results represent the shear strength across a predetermined surface. In the edge member of a wall such restrictions do not exist and the member is free to fail along the surface that offers least resistance. Therefore, the results and conclusions presented by Wagner and Bertero can only be considered representative of the specimens studied or similar R/C members, but should not be

extrapolated to represent the behaviour of edge members of R/C walls.

If a flexural crack in the edge member coincides with the SRS of minimum resistance the cohesion of the concrete would not be available. However this is not possible as flexural cracks are horizontal and tend to be inclined downwards when propagating from the edge to the web. The inclination of the SRS must be parallel to the resultant of the compressive and shear forces acting on the compressive edge member, as shown in figure 6.2. Thus, flexural cracks and the SRS cannot coincide and the cohesion of the concrete is always available along the SRS.

Current code provisions attach importance to the contribution of vertical web reinforcement to the shear strength in walls with low shear ratios. This derives from the formation of an arch mechanism which enhances the contribution of the vertical web reinforcement. In the absence of a strong beam close to the foundation, the latter shear transfer mechanism may not be mobilised and the efficiency of the vertical web reinforcement becomes questionable.

It is considered that vertical web reinforcement is inefficient in transferring shear across diagonal cracks. Relative slip between the faces of a diagonal crack can only be resisted by the vertical web reinforcement as dowel action effect, as shown in figure 6.5. This is a mechanism with very low stiffness which could only provide some strength after a large slip between the crack faces had occurred. Since this only happens after the ultimate shear force is achieved, it is not advisable to consider the contribution of the vertical web reinforcement to transfer shear across diagonal cracks. This is why only the contribution of the stirrups is included in equation (6.1), which gives the contribution along the tension side of the SRS to the diagonal tension strength. However, it should be noted that by contributing to the increase in the neutral axis depth, the vertical web

reinforcement may help indirectly to enhance the contribution of concrete to the total shear strength.

The decrease in the efficiency of the stirrups for walls with low shear ratios, embodied in codes such as EC8, is due to observations from the same tests which lead to the conclusion that vertical web reinforcement is effective in walls with low shear ratios. This is expected, since both observations are a consequence of the same mechanism; the direct transfer of load to the foundation. Therefore, it is advisable not to consider the reduction of effectiveness of the stirrups in walls of multistorey buildings in which the shear ratio is low. This means that for these walls the provisions for the design against diagonal tension should be independent of the shear ratio. It should be noted that this is fully compatible with the SRS method, which intimates that the shear strength is independent of the shear ratio. Current code provisions for walls with low shear ratios should only apply to walls with low aspect ratio, i.e. walls with height close to the length of the cross section.

All previous discussions referred to the PHZ at the base of the walls. It is known that outside the PHZ the shear strength is higher and this is embodied in the most advanced code provisions, such as EC8 and NZ. The higher resistance to the diagonal tension mode of failure outside the PHZ can be attributed to two main causes; the larger depth of the neutral axis and the aggregate interlock effect. Since the flexural reinforcement remains in the elastic range the neutral axis depth is higher than in the PHZ. This effect can be directly evaluated by the SRS method. The aggregate interlock effect may be present due to the fact that shear cracks open less than in the PHZ.

It should be noted that the contribution of the compressive zone to the shear resistance may be more than that implied by the truss mechanism, particularly for flexural walls. Therefore, it seems misleading to consider that shear strength is due essentially to the truss

mechanism, with other sources of resistance playing a secondary role. The relative contribution of the different shear resistance mechanisms, including aggregate interlock and dowel action, may change with factors such as the shear ratio, level of axial force, yielding of the flexural reinforcement, loading regime (cyclic or monotonic) and level of applied shear. Hence, it is considered more appropriate to define the shear strength as the sum of the different mechanisms without establishing their relative importance.

Finally, it is worth mentioning that the SRS method is a safe method for the design against diagonal tension failure and produces more economic results than the provisions of the most advanced codes for earthquake resistant design. Note that according to EC8 and NZ the shear capacity of the walls referred to in table 6.1 would be only the force corresponding to the contribution of the steel. The SRS method also provides a sound theoretical background for the evaluation of the contribution of concrete to the shear resistance.

6.3 Effect of Confinement

It is known that confinement reinforcement increases the capacity of concrete to sustain large compressive strains. Therefore, confinement increases the ductility of walls which fail in flexure. It also contributes to an increase in the flexural capacity for the following two reasons:

- Enhancement of the strength of the compressive concrete, which leads to a slight increase in flexural capacity.

- The consequential development of strain hardening of the steel by delaying the compressive failure of concrete causes further increase in flexural capacity.

The above effects are easily recognisable in walls which behave mainly in flexure, i.e. walls with high shear ratio. However, in walls with low shear ratio, which are more strongly influenced by shear, the effects of the confinement reinforcement are less clear. The comparison of the tests and results of walls SW13 and SW14 may help to provide some insight into the problem, as follows.

As previously discussed in section 4.2.4.1, signs of degradation of the compressive zone of wall SW13 were not visible before a displacement of 6mm was reached. However, in wall SW14 the compressive zone started degrading at a displacement of 3.2mm and the ultimate load was reached on the next displacement step. Therefore, confinement reinforcement seemed to have played an important role in delaying the degradation of the compressive zone of wall SW13. This is the reason to which the higher ductility registered for wall SW13 is attributed.

Confinement reinforcement increases the cohesion of the concrete and therefore the shear strength of the compressive zone. The presence of steel bars that cross the failure surface in the edge member may also contribute to increase the shear strength of the compressive zone. Therefore, wall SW14 should be expected to have less resistance to diagonal tension than wall SW13. The higher values of strain gauge readings registered for wall SW14 as compared with wall SW13 and the respective failure loads confirm this viewpoint.

Confinement reinforcement should also enhance the flexural capacity but less than in the case of flexural walls, since walls with low shear ratios develop lower axial strains. This is relevant only if the failure mode is flexural or strongly influenced by flexure. This could have been the case for wall SW14 in which failure seemed to have been in a mixed mode. It was shown in table 4.4 that after the ultimate load was achieved the width of the main diagonal cracks increased faster than before. This is related to yielding of the stirrups and therefore exhaustion of diagonal

tension strength. However, diagonal cracks of wall SW14 opened less than in the walls that clearly failed in shear by diagonal tension. This suggested that failure may also have been influenced by flexure. The fact that the ultimate load is above the shear force of 97KN, which corresponds to the flexural capacity calculated using code procedures strengthens this viewpoint.

Finally, confinement reinforcement is also important in avoiding a sudden loss of load carrying capacity when the ultimate load is achieved in walls failing in shear by diagonal tension. The reasons for this are discussed in section 6.6.2

6.4 Length of the Plastic Hinge Zone

The most relevant codes establish a minimum length of the PHZ equal to the length of the wall cross section. This is almost up to the level where M=0 in the walls of the current test programme. However, strain gauge readings at this level showed that the bars were far from yield. Therefore, it can be concluded that current code provisions concerning the height of the PHZ are very conservative for walls with low shear ratios. This may be a consequence of observations from tests of walls with low shear ratios where the boundary conditions allowed part of the load to be transferred directly to the foundation. The arch mechanism associated with this load transfer mechanism imposes a constant force on the tensile reinforcement. This observation has been reported in section 2.1.1.1. As a consequence plasticity spreads far more if the arch action is present, rather than for cases in which there is predominantly beam behaviour.

Plasticity in the tensile reinforcement of the walls that failed in shear by diagonal tension did not spread up to the gauges on the intermediate level (190mm above the base

level) in most cases. Nevertheless, plasticity may spread more if this failure mode is prevented, as diagonal tension failure curtailed a more flexural response. Data from strain gauge readings at the intermediate level in wall SW13 indicate that plasticity in the tensile reinforcement spread slightly above the second level of gauges, up to 0.43h. A value of 0.39h is obtained by calculating the PHZ length assuming that when the flexural capacity is achieved the PHZ extends up to a section where the bending moment is equal to the yield moment registered at the base section. Since the flexural capacity was not reached in the experiments, a value of $M=58x10^3$KNmm was calculated assuming that the tensile reinforcement would reach the ultimate stress. This value is 8% higher than the registered ultimate moment of wall SW13. It should be noted that this calculation is based on conservative assumptions since (i) the yield moment is defined as yielding of the extreme ϕ8mm bars only and (ii) the ratio between the ultimate stresses of the ϕ8mm and ϕ6mm bars to the yield stress of the ϕ8mm is 1.43 and 1.53, respectively. EC8 establishes a maximum limit for this ratio of 1.45 for structures of DC "M" and "H".

Analytical studies (Pilakoutas, 1990) indicated that in walls with the flexural reinforcement concentrated essentially at the edge members, plasticity in the tensile reinforcement spreads to aproximately one third of the height of the wall. The analytical predictions overstimated the values registered experimentally in almost all cases.

Based on the above considerations, it is suggested to establish a maximum length of the PHZ of M/(2.5V). This will lead to lower lengths of PHZs, as compared with current code provisions, for walls with shear ratios below 2.5. However, it should be noted that confinement reinforcement may not be needed along all the height of the wall in which the tensile reinforcement yields, since the level of strains on the compressive side is lower than on the tension side. In fact, yielding in compression was not observed on the gauges at the

intermediate level in any wall. Therefore, establishing the height of the wall where confinement reinforcement needs to be provided from the spreading of tensile yielding may be a very conservative criterion. Thus, the above proposal may still be conservative. More research on the subject is needed to establish if it is possible to decrease even further the height of the walls where it is necessary to place confinement reinforcement.

Yielding of the tensile reinforcement in walls with low aspect ratios may spread above the proposed PHZ length due to the formation of the arch mechanism. However, failure of these walls due to lack of confinement in the middle and top of the walls has not been reported in the literature. This observation reinforces the argument that confinement reinforcement may not be necessary all over the height of the wall where the flexural reinforcement yields and allows the extension of the above proposal to walls with low aspect ratios.

6.5 Sliding Shear

According to the provisions of EC8, sliding shear may control the design of walls with shear ratios below 1.4, as shown in figure 3.14. The shear ratio of the walls of the current test programme was below that level but no signs of sliding shear failure were observed. One of the reasons for this observation is the fact that a crack along the entire cross section did not form. Even in the case of wall SW13, which exhibited the highest load carrying capacity and ductility, there were no signs that a horizontal crack along the entire cross section had formed. Therefore, the contribution of the compressive zone to resist sliding shear was available, which is not considered in equation (3.16), given in chapter 3.

The calculations performed in chapter 3 showed that according to EC8 dowel action is sufficient to prevent sliding shear for walls with shear ratios above 1.4. The experimental evidence point to the fact that for walls with a shear ratio below 1.4 a full crack along the entire section, necessary to trigger sliding shear failure, does not form before the wall fails by some other mechanism. Therefore, it seems that the only possible cause of sliding shear failure in R/C walls is poor construction and/or detailing of the construction joint at the base section. This points to the need to revise EC8 provisions concerning sliding shear. However, before EC8 provisions are revised, further research on the subject should be undertaken. Although results from testing wall SW13 point to the fact that it is not necessary to design against sliding shear for walls with shear ratios greater than or equal to 1.1, this conclusion should be extended to low rise walls, in which the shear ratio may be even lower due to a very low level of load application.

6.6 Ductility

6.6.1 Effect of the Load History

Comparison of the results from testing walls SW11 and SW12 can be used to draw qualitative conclusions about the effect of the load history on the ductility of walls. It was already discussed in section 4.3.4.6 that the strength of the stirrups was higher in wall SW12 than in wall SW11. The ultimate load of both walls, given in table 4.5, also points to this conclusion. Therefore, if the load history of both walls was the same, wall SW12 should be expected to be more ductile. However, table 4.5 shows that wall SW12 was less ductile than SW11 and this can only be attributed to the load history.

The reduction in the available ductility due to cyclic loading should be expected, since the materials and the resisting mechanisms of the walls degrade faster under load reversals. Similar conclusions have also been reported by other authors, as referred to in section 2.1.1. However, it should be noted that reversal of load affects some shear resisting mechanisms more intensely than others, as discussed in sections 4.1.4., 4.3.3.2 and 4.3.3.3. Differences of ductility due to differences in the load history should be larger for walls with low shear ratios. The ductility of walls failing in shear by diagonal tension should also be more strongly affected by variations in the load history than the ductility of walls failing in other modes, with the exception of sliding shear. This later failure mode cannot occur under monotonic loading, as discussed in section 4.1.4. The influence of the mode of failure on the ductility is discussed in detail in section 6.6.2.

The above conclusions are in contradiction with Lefas (1988) who came to the conclusion that ductility of cyclically loaded walls could be higher than the ductility of monotonically loaded walls. These conclusions can be attributed essentially to the fact that Lefas tests were performed under load control. It has already been explained in section 4.1.4 that under load control it may not be possible to obtain any reliable measure of the ductility.

6.6.2 Effect of the Failure Mode

Table 4.5 shows that the walls which failed in shear by diagonal tension achieved their ultimate loads at much lower displacements than wall SW13, which failed by web crushing. In the former walls the stirrups offered less resistance to the opening and propagation of diagonal cracks, i.e. the potential surface of diagonal tension failure formed faster. The above argument and the fact that the diagonal tension strength of these walls was lower are the underlying reasons for the earlier attainment of the ultimate load. However, it

is interesting to note that the ultimate displacements of walls SW16, SW17 and SW18 were not far below the ultimate displacement registered for wall SW13. This is due to the relatively ductile behaviour of those walls in the post-ultimate range. This was not expected, since diagonal tension failure is generally thought to be a brittle failure mode, as in the case of wall SW15. The explanation of such differences of behaviour lies in the difference between the failure surfaces and the mechanisms of shear transfer, as discussed below.

In the case of walls SW16, SW17 and SW18, when the ultimate load was achieved the transfer of shear across the failure surface in the zone under axial tension was due only to the steel. The aggregate interlock effect had been eroded progressively and the portion of the shear taken by this mechanism was transferred gradually to the stirrups. Therefore, at the ultimate load the shear transfer mechanism on the tensile side of the wall was a ductile mechanism. After the ultimate load the stirrups entered the post-yield branch and a slight increase in their shear transfer capacity took place due to strain hardening. Hence, the loss of shear capacity after the ultimate load was due to the failure of the compressive zone. However, the results indicate that the compressive zone did not fail in an abrupt manner, since no sudden loss of load carrying capacity was registered after the ultimate load. This was due to the presence of the reinforcement in the compressive zone, which prevented a large slip along the failure surface when its maximum strength was reached. It is thought that confinement reinforcement was more effective than flexural reinforcement in controlling that slip, because the former resisted the slip along the failure surface in tension.

The failure surface of wall SW15, represented by A-B-C-D in figure 6.4, can be subdivided into three zones based on the prevailing failure mechanism. At the ultimate load, a significant part of the shear was transferred to the zone below the failure surface of wall SW15 by the concrete along

the upper segment (A-B in figure 6.4). When the maximum shear transfer capacity along segment A-B was reached, a brittle failure of the concrete took place, which in turn led to a sudden drop in the load carrying capacity of the wall. Failure in the upper segment was brittle due to slippage along this part of the failure surface which was not resisted by stretching of the reinforcement. The latter mechanism was noticeable in segment C-D which is in the compressive zone.

Web crushing failure curtails a more flexural response and therefore reduces the ductility. This reduction may be small if the failure load is close to the load corresponding to the ultimate flexural capacity, which was the case of wall SW13. However, if the load at which web crushing occurs is close to the yield load, a severe reduction in ductility occurs.

6.6.3 Effect of the Shear Ratio

Flexural walls are expected to be more ductile than walls with lower shear ratios. For instances, the displacement ductility ratio of wall SW13 was 3.9 but higher ratios were reported by Pilakoutas (1990) for walls of shear ratio 2. Walls SW8 and SW9, already described in section 2.1.1.5, were reported to have achieved displacement ductility ratios of more than 5. The higher displacement ductilities available in flexural walls are due to the fact that they can achieve higher curvature ductilities by developing their full flexural capacity and by larger spreading of the plastic deformations along the height.

In walls with low shear ratios the flexural response may be curtailed by failure due to shear. This kind of failure may be difficult to avoid, as demonstrated by wall SW13. The full flexural capacity could not develop because web crushing failure occurred prior to flexural failure. This mode of failure was due to the high shear force which led to the compressive failure of the concrete struts in the zone below

the neutral axis. To avoid this mode of failure without reducing the load carrying capacity it would be necessary to re-design the wall. This could be achieved by increasing the width of the web and maintaining or reducing slightly the amount of flexural reinforcement in order to avoid increasing the flexural capacity.

The height of the PHZ extends from the base section up to a section where the applied moment is equal to the yield moment. Therefore the height of the PHZ is given by:

$$h_{PHZ} = (M_{base} / M_{yield} - 1) / V \qquad (6.6)$$

M_{base} - moment at the base section
M_{yield} - yield moment

Equation (6.6) clearly shows that for the lower shear ratios the PHZ is shorter. In the absence of axial force the height of the PHZ is proportional to the shear ratio.

The participation of shear deformation in the overall deformation of the walls with low shear ratios is higher than in flexural walls, as already discussed in section 4.3.3.3. The large shear deformations may have a positive effect, since they reduce the curvature ductility demand for a given displacement ductility demand. Therefore, EC8 provisions are conservative in this respect, since the effect of shear deformations is not considered in the evaluation of curvature ductility from displacement ductility. The conservatism of the code provisions increases as the shear ratio decreases.

6.7 Effect of Shear Design and Failure Mode on Energy Dissipation

The concepts of ductility and energy dissipation are different but are related, as already explained in section 2.3.2. In order to be able to refer to energy dissipation without considering the influence of the ductility level, it is advantageous to express it for a given ductility level. This can be achieved by defining energy dissipation in relative terms, as follows:

$$E_r = E/(F_m\ D_m) \qquad (6.7)$$

in which E is the area enclosed by one hysteresis loop, and F_m and D_m are the corresponding maximum values of force and displacement.

The variables are defined in figure 6.6. The relative energy dissipation E_r measures the area enclosed by the hysteresis loops at a given ductility ratio. Therefore, it can be directly compared for different systems, as it does not depend on the ductility level or the available ductility of the system.

One of the most noticeable features of the force-deformation relationship of all walls tested is the presence of the pinching effect for all failure modes. This effect reduces the area enclosed by the hysteresis loops. The values of E for wall SW13, which exhibited the best inelastic response, were 113.5KNmm and 326.1KNmm at displacement ductilities of 1.3 and 2.3, respectively. However, if the loops were not pinched the corresponding values would be 184.8KNmm and 486.2KNmm. This means that the pinching effect was responsible for a reduction of the energy dissipation capacity of wall SW13 of 39% and 33% at the ductility levels referred to above. This is likely to lead to higher values of the response to earthquake ground motion.

The only way the pinching effect can be avoided in walls with low shear ratios is by providing diagonal reinforcement. With diagonal reinforcement the steel cage forms a truss that can transfer shear without contribution from the concrete or dowel action of the steel. This eliminates the cause of the pinching effect. The effectiveness of diagonal reinforcement in improving the seismic performance of R/C members, including walls, and in eliminating the pinching effect has been reported by several researchers (Paulay, Priestley and Synge, 1982, Bertero, Popov and Wang, 1974 and Bertero and Popov, 1975). Therefore, the use of diagonal reinforcement in shear design of walls with low shear ratios will improve the energy dissipation capacity, which in general will lead to lower values of the response to earthquake ground motion.

The pinching effect cannot be eliminated by adding stirrups beyond the level necessary to avoid diagonal tension failure, as this does not change qualitatively the shear transfer mechanisms. Qualitative changes in behaviour due to variations in the amount of stirrups are related to the stirrups reaching the yield strength. As already discussed in section 4.3.4.6, diagonal tension failure is associated with the exhaustion of the yield strength of the stirrups. This is also the reason why the pinching effect was more intense in the walls which failed in this mode.

The values of E registered for wall SW16 at the displacement ductilities referred to above were 109.6KNmm and 259.2KNmm. Comparison of these values with the corresponding values for wall SW13 illustrates the influence of the failure mode on the energy dissipation capacity of R/C walls. This can be interpreted as follows. After yielding of the stirrups, their stiffness becomes so small that they offer little resistance to the opening and slip along diagonal cracks. This leads to a reduction of stiffness on reloading, which is responsible for the increase in the intensity of the pinching effect and the consequent reduction in energy dissipation capacity. The results indicate that this effect

is noticeable only at large displacements in the post-yield range, especially after yielding of the stirrups.

The lack of stiffness of the stirrups after the attainment of the ultimate load is why the width of diagonal cracks opened much faster in the post-ultimate range in the walls that failed by diagonal tension, as reported in section 4.2. On the other hand, adding stirrups beyond the level necessary for them not to yield produces only a small increase in the global stiffness of the stirrups. The effect of this increase in stiffness in controlling the opening and slipping along diagonal cracks and therefore, in reducing the intensity of the pinching effect and the corresponding loss of energy dissipation capacity, may not even be noticeable. Experimental evidence that increasing the amount of stirrups above the level necessary to prevent yielding has little or no influence on the overall behaviour of R/C walls has been given by other researchers (Goodsir, 1985 and Pilakoutas, 1990).

The effect of the amount of stirrups on the behaviour of R/C walls can be summarised in the following:

- Variations between two levels below the amount necessary to prevent yielding of the stirrups only change the intensity of the pinching effect in the shear component of the deformations.

- Two similar walls, one with an amount of stirrups below the level necessary to prevent yielding and another with an amount above that level will exhibit behaviour patterns qualitatively different; the first will fail in shear by diagonal tension and the pinching effect of the shear deformations will reduce its relative energy dissipation capacity, whilst the other will possibly fail in flexure or web crushing and the pinching effect will be less and the available ductility will be larger than for the first wall.

- Two walls with the only difference being the amount of stirrups, both of which are above the level necessary to prevent yielding in both cases, will exhibit similar behaviour.

An interesting feature of the force deformation relationship of wall SW13 is that the envelope of its response is what should be expected if it had failed in flexure. If the failure mode of wall SW13 was not known, the comparison of its envelope with the diagrams shown in table 2.3 would indicate a ductile flexural failure. The pinching effect visible in the force-total deformation diagram of wall SW13 and not in diagram 1a of table 2.3 is due to the low shear ratio. Even if wall SW13 had failed in flexure, the pinching effect would remain, as the causes of this effect would not be eliminated. This means that web crushing failure curtails a more flexural response, thus reducing the available ductility, but it does not seem to affect the relative energy dissipation capacity. This follows from the fact that the only difference between web crushing failure and flexural failure by crushing of the concrete is the zone where the concrete fails in compression. It has no effect on the widening and propagation of cracks. Therefore it is logical that web crushing has little or no effect on the behaviour up to failure.

It is also worth discussing the importance of reinforcement details. The insufficient anchorage of the stirrups had an effect equivalent to reducing the amount of stirrups to a level that was not enough to avoid yielding. This caused a change in the mode of failure which reduced the load carrying capacity, the available ductility and the total and relative energy dissipation capacities. This is demonstrated by the results from wall SW12.

It can be concluded from the above that the failure mode influences the relative and total energy dissipation capacities. Walls that fail by diagonal tension exhibit less relative energy dissipation than walls that fail by concrete

compression after yielding of the main flexural reinforcement or by fracture of the steel. Walls that fail in flexure or in shear by web crushing have similar relative energy dissipation capacities.

Walls with low shear ratios designed only with conventional reinforcement and failing by crushing of the concrete after yielding of the main flexural reinforcement possess less relative energy dissipation capacity than their high shear ratio conterparts. This due to the increased pinching effect and the lower length of the PHZ in walls with low shear ratios. It should be noted that the lower length of the PHZ may reduce considerably the energy dissipation capacity not only because of the reduction in the contributary part of the wall but also because the strains are lower.

Web crushing failure may strongly limit the ductility of a wall if the ultimate load is clearly below the flexural capacity. However, if the ultimate load is close to the flexural capacity, web crushing only causes a small decrease in ductility.

6.8 Behaviour Factors

EC8 provisions for the evaluation of the behaviour factors "q" consider the influence of the likely mode of failure of R/C walls. This is performed by means of the coefficient ν, which is calculated as shown in equation (2.3) given in chapter 2. In the case of walls of multistorey buildings it is possible for the designer to influence the value of V_{Rd} by either changing the wall cross section or the reinforcement. Hence, in general, there is no need for shear failure to be allowed.

According to capacity design principles shear failure must be avoided in order to provide the zones where plastic

hinges are going to be formed with the most desirable inelastic response. In fact it is considered in EC8 that the application of capacity design principles to frames means that flexural failure must precede shear failure. The same principle must also extend to walls. Therefore, in general, a value of v larger than 1 should be mandatory. However, as web crushing failure does not affect the relative energy dissipation capacity of a wall as compared to walls failing in flexure, it could be allowed as long as the available ductility exceeds the maximum ductility demand. This may be established in terms of interstorey drift, for instance, since it provides an upper limit for the ductility demand. Other exceptions should only be allowed in situations in which it is extremely difficult or impossible that shear capacity exceeds flexural capacity or web crushing capacity at maximum ductility demand. Such situations may arise in low rise walls in which the aspect ratio is very low. For instances EC8 considers that for aspect ratios below 0.75 shear failure is almost certain. However, it should be noted that this situation is unlikely to be found in multistorey buildings.

It was concluded in sections 6.6.3 and 6.7 that even if shear failure is prevented, walls with low shear ratios designed only with conventional reinforcement possess less ductility and relative energy dissipation capacity than if the shear ratio was higher. Therefore, buildings in which the shear ratio of the walls is low should be designed for higher levels of forces than would be necessary if the shear ratio was higher, unless diagonal reinforcement is provided.

Based on the above it is proposed to assign lower "q" factors to walls with low shear ratios unless diagonal reinforcement is provided. For walls with shear ratios higher than 0.75 failure by crushing of the concrete after yielding of the flexural reinforcement should be mandatory.

6.9 Conclusions

Herewith a summary of the discussion of results presented above.

(i) The diagonal tension strength of plastic hinges of R/C walls at the ultimate load is attributed to two mechanisms; the stirrups, which transfer load across the potential failure surface in the zone under axial tension, and the shear strength provided by the compressive zone. It was shown that the most important parameter controlling the shear strength of the compressive zone was the depth of the neutral axis. This led to the conclusion that the SRS method is the most appropriate for the evaluation of the shear strength of R/C walls.

(ii) Code provisions concerning the contribution of vertical web reinforcement to shear strength should only apply to walls with very low aspect ratios. They should not be extrapolated to walls of multistorey buildings with low shear ratios in which it is not possible to transfer load directly from the point of load application to the foundations. The above implies that provisions for the shear design of R/C walls of multistorey buildings with medium and high aspect ratios should be independent of the shear ratio.

(iii) Confinement reinforcement increases the ductility of walls with low shear ratios by delaying the degradation of the compressive zone. It also prevents a sudden loss of shear strength of the compressive zone after the resistance to diagonal tension is exhausted. The effect of confinement reinforcement in the shear and flexural capacity of walls with low shear ratios is moderate.

(iv) Code provisions for the calculation of the plastic hinge length are conservative for walls with low shear ratios. It was proposed to establish a maximum for the plastic hinge length of M/(2.5V). The need to provide confinement up to the level where plasticity spreads in the tensile reinforcement was questioned.

(v) It is not necessary to design against sliding shear for walls whose shear ratio is equal or above 1.1.

(vi) Cyclic loading reduces the ductility of R/C walls. The magnitude of this effect depends on the shear ratio and failure mode, since cyclic loading affects some load resisting mechanisms more than others. The lower the shear ratio and the higher the influence of shear in the failure mode, the larger the difference in behaviour due to the load history.

(vii) The failure mode may have a strong influence on the ductility. The ultimate load of walls that fail by diagonal tension is likely to be achieved at a much lower displacement than for walls in which this failure mode is prevented. However, it was observed that some of the walls which failed by diagonal tension exhibited a considerable ability to deform in the post ultimate range with moderate loss of load carrying capacity. Web crushing failure also curtails a more flexural response. The intensity of the reduction in ductility depends on the difference between the failure load and the flexural capacity.

(viii) Walls with low shear ratios are expected to be less ductile than flexural walls. This is due to the fact that the length of the PHZ is lower and they may achieve lower curvatures since the

flexural response may be curtailed by shear failure. However, the higher participation of shear deformations in the total deformation of the wall increases the ductility, thus the reduction in ductility is attenuated.

(ix) It is not possible to avoid considerable reduction in energy dissipation due to the pinching effect in walls with low shear ratios if they are designed with conventional reinforcement. Web crushing only reduces the overall energy dissipation due to its effect on ductility and not on the shape of the hysteresis loops. Diagonal tension failure reduces energy dissipation by decreasing both the ductility and the area per hysteresis loop.

(x) To increase the amount of stirrups in a wall failing in shear by diagonal tension only has a qualitative effect on the behaviour if yielding of the stirrups is avoided. For walls failing by crushing of the concrete no change of behaviour is achieved by increasing the amount of stirrups.

(xi) It was proposed that for walls with aspect ratio higher than 0.75, flexural failure or web crushing failure after the maximum ductility demand should be mandatory. The behaviour factor q proposed in EC8 should be calculated considering the effect of the shear ratio. The decrease in the q factor due to low shear ratio walls should be reduced if diagonal reinforcement is provided.

Wall	Ultimate load (experiments) (KN)	Neutral axis depth (mm)	Predictions of SRS Method				Failure mode
			Number of bars across potential failure surface	Contribution of the steel (KN)	Contribution of the concrete (KN)	Calculated shear strength (KN)	
SW 13	108.3	74.3	14	72.8	23.4 (31.3)	96.2 (104.1)	Web crushing
SW 16	80.3	110.8	8	41.6	28.3 (37.7)	69.9 (79.3)	Diagonal tension
SW 17	83.6	104.6	10	52	28.4 (37.8)	80.3 (89.8)	Diagonal tension
SW 18	99.9	143.2	10	52	36.6 (48.8)	88.6 (100.8)	Diagonal tension

Where two values are shown, the value above was calculated considering $\tau_0 = 0.15f_c$ and the value in brackets considering $\tau_0 = 0.2f_c$

Table 6.1 - Shear capacity according to SRS Method

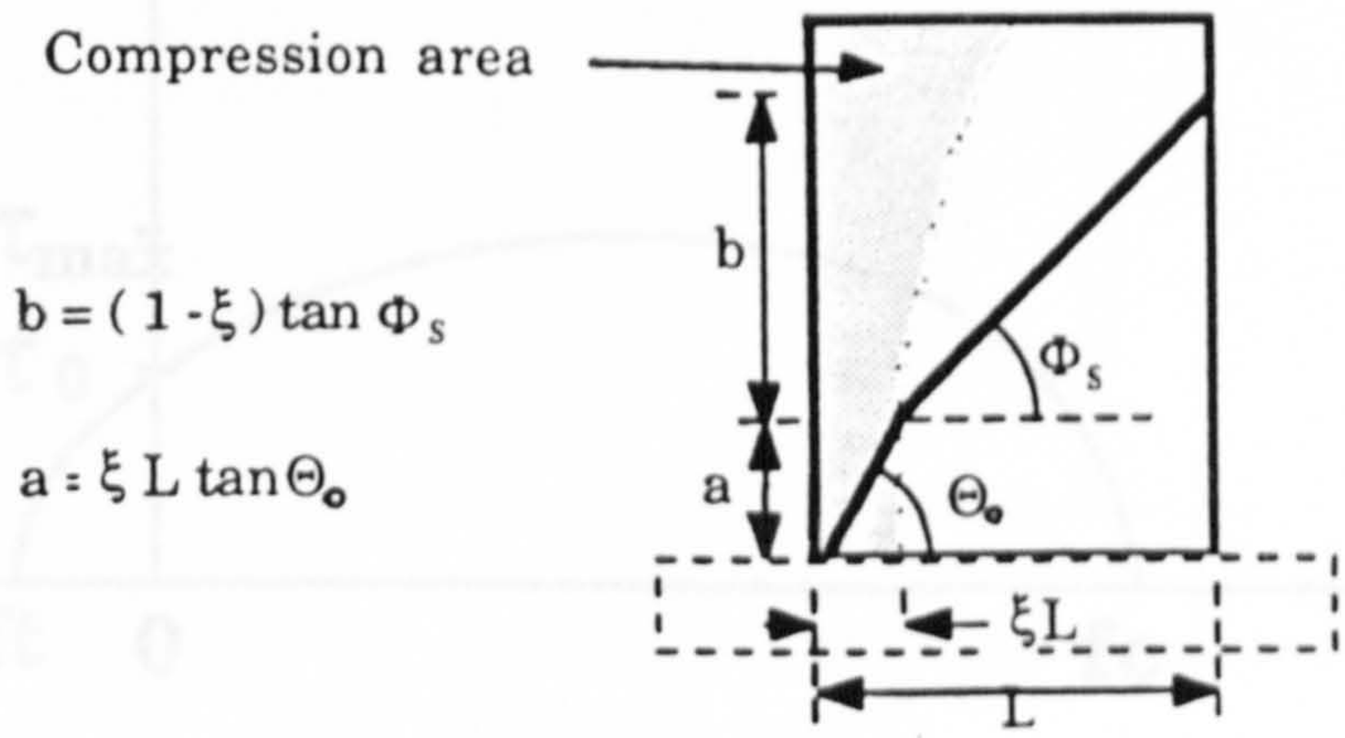
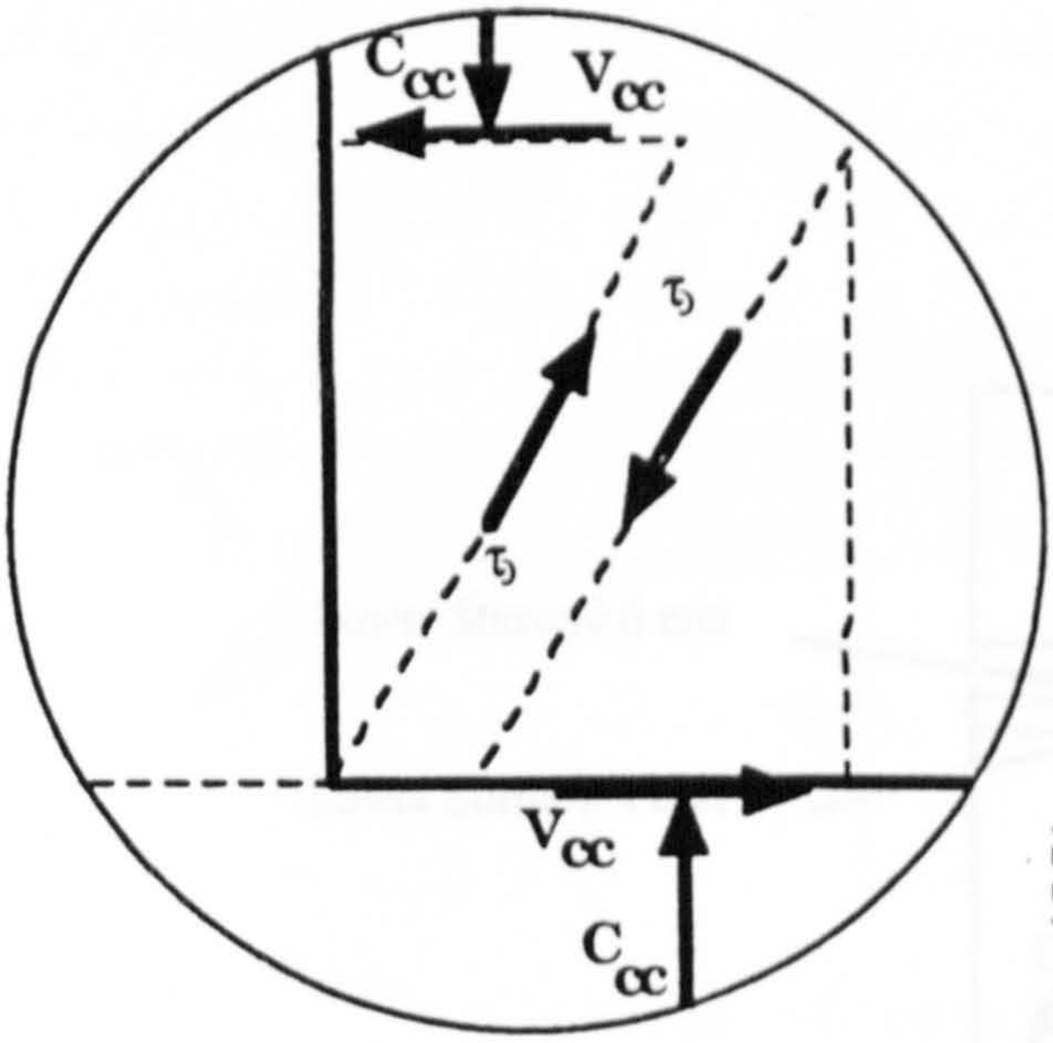


Figure 6.1 Possible minimum SRS (Pilakoutas, 1990)



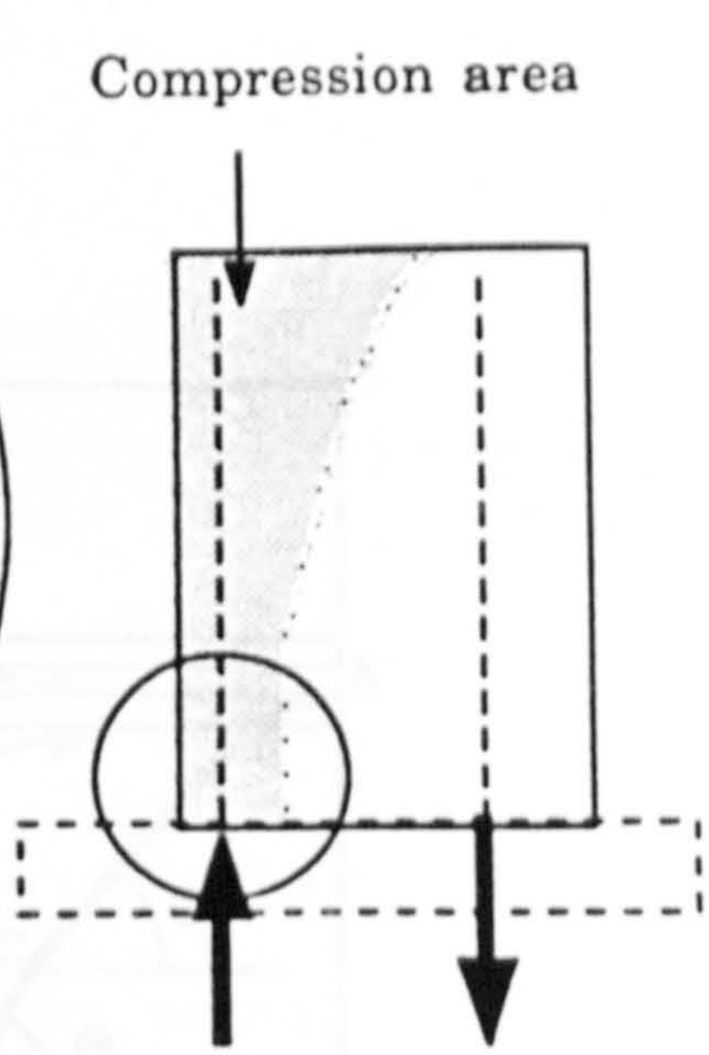


Figure 6.2 Forces and stresses in the compressive edge member (Pilakoutas, 1990)

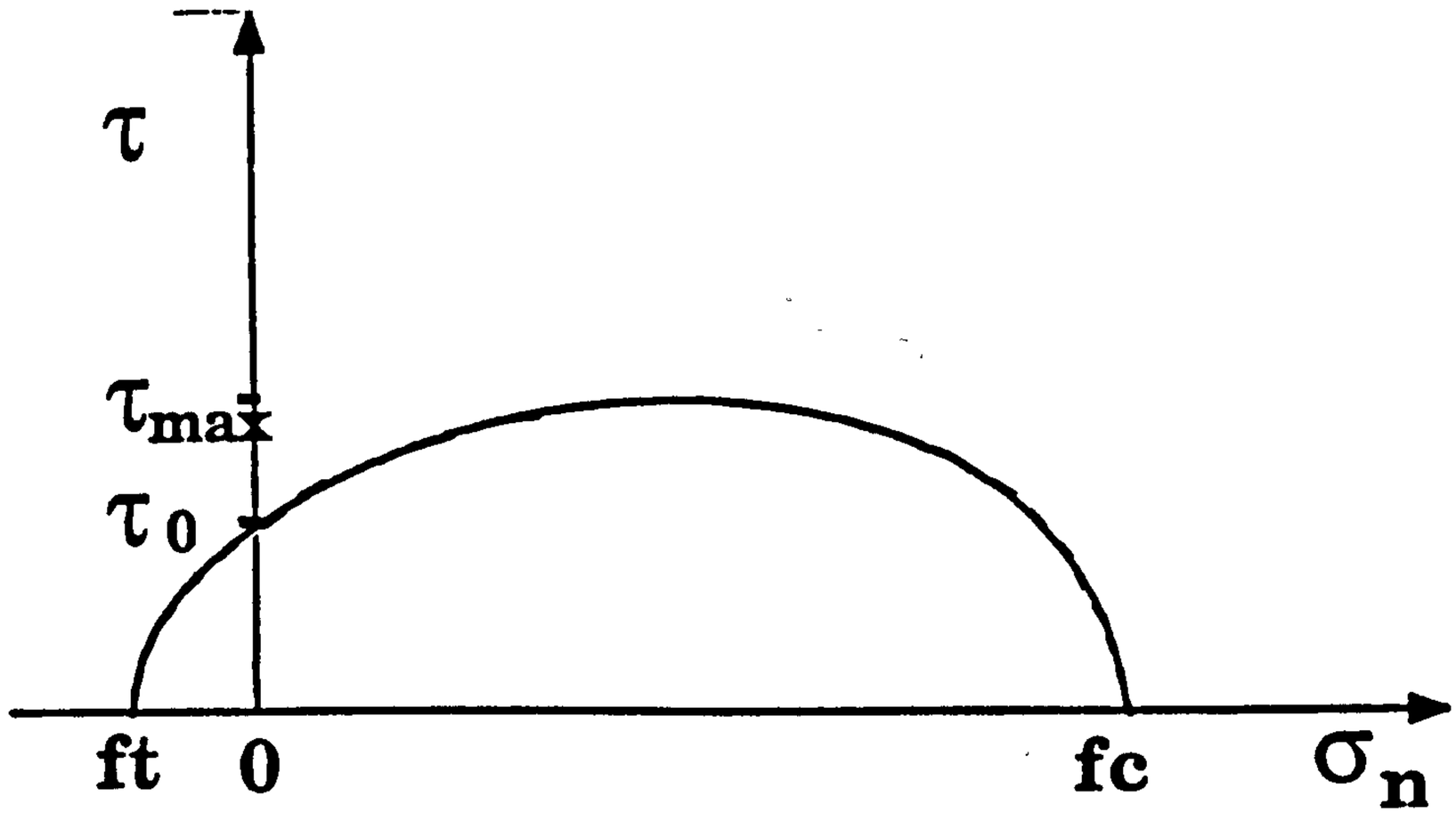


Figure 6.3 Mohr-Coulomb failure envelope for concrete (Pilakoutas, 1990)

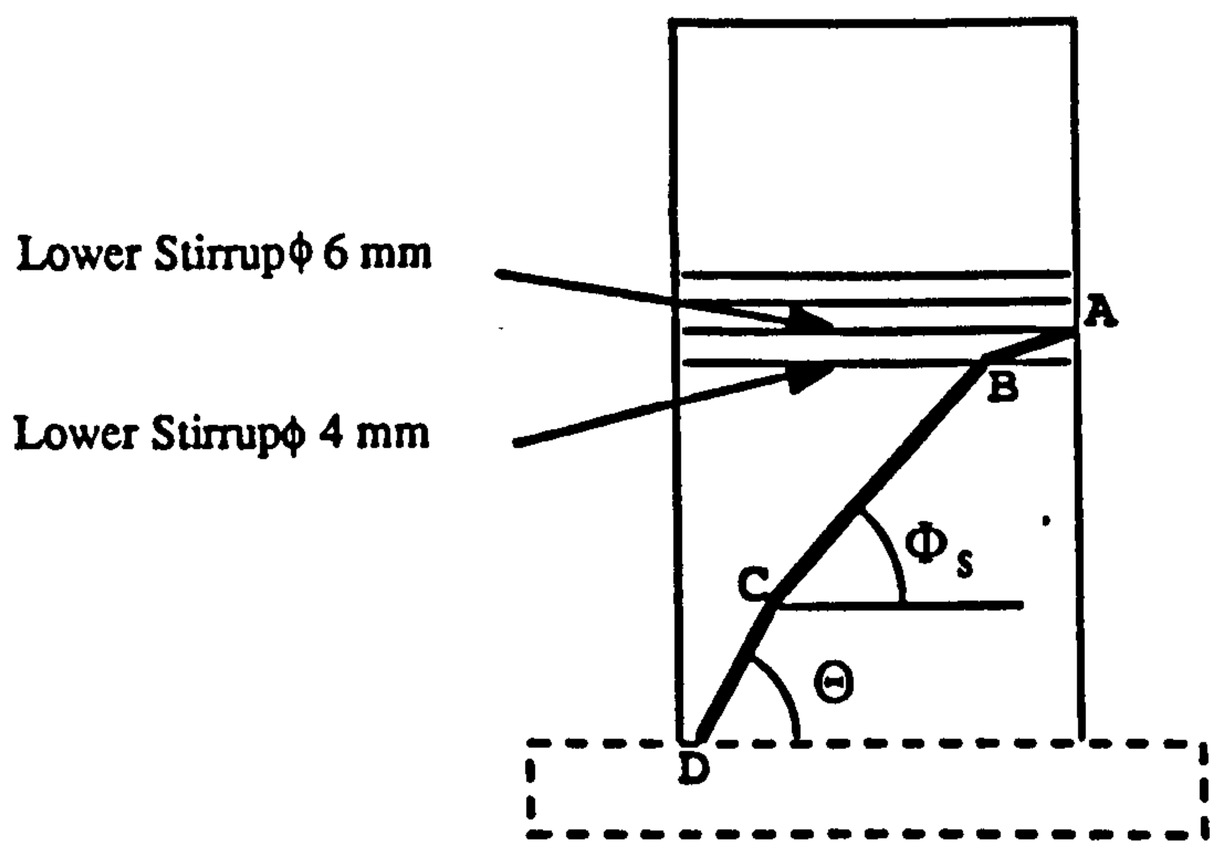


Figure 6.4 Schematic representation of the failure surface of wall SW15

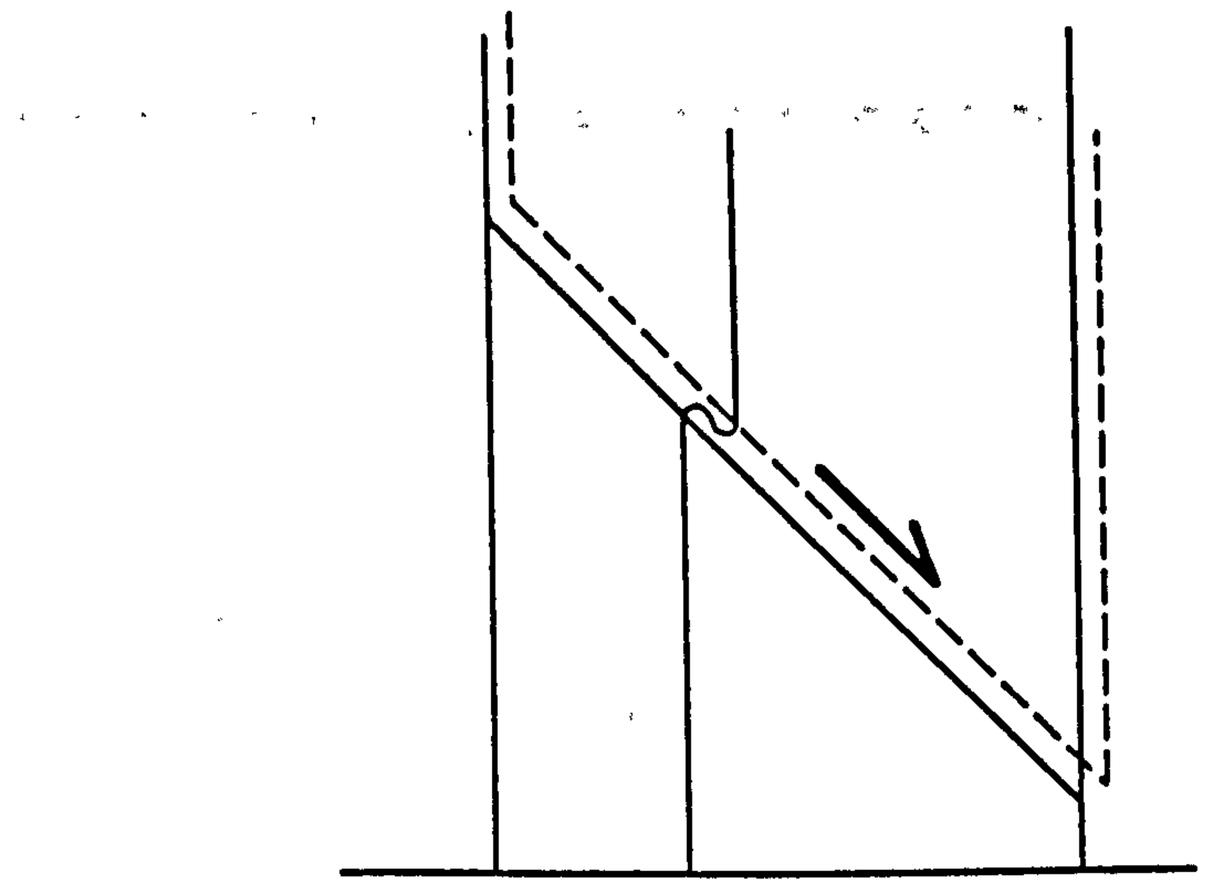


Figure 6.5 Dowel action of vertical web reinforcement along diagonal crack

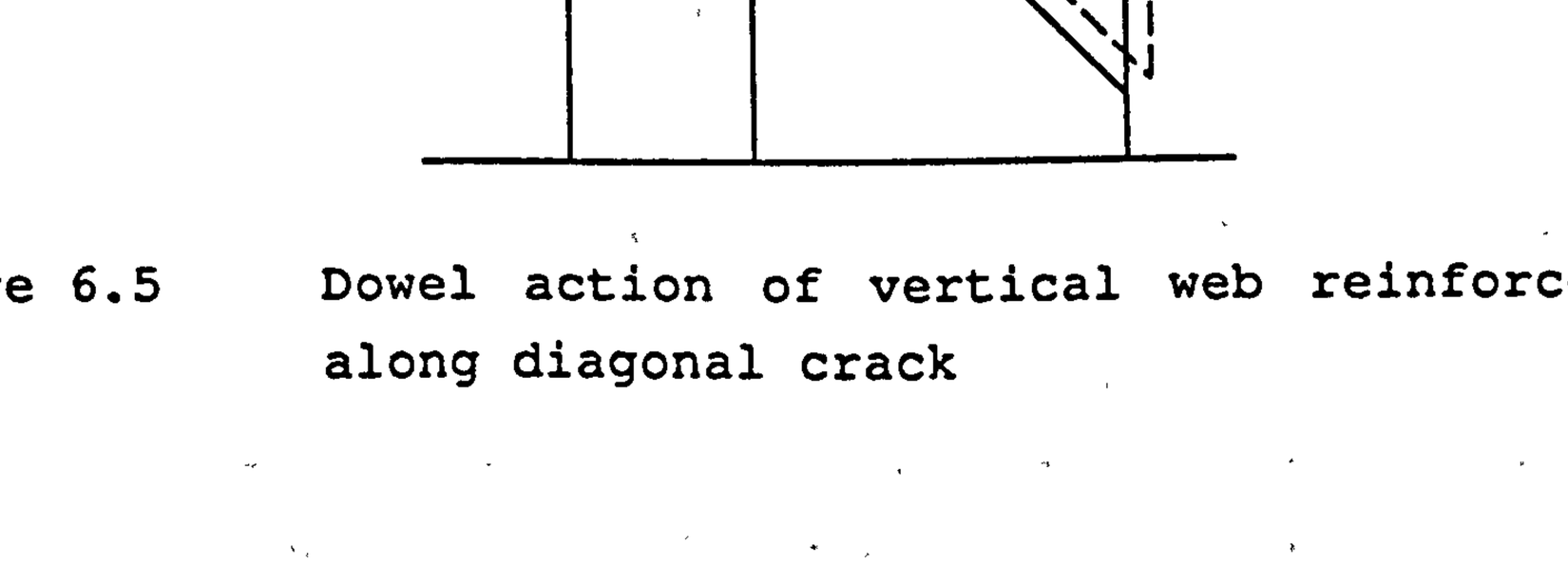


Figure 6.6 Definition of relative energy dissipation

CHAPTER 7

7 CONCLUSIONS AND FUTURE DEVELOPMENTS

7.1 Conclusions

The salient developments and conclusions presented in this work are summarised in this section.

The most important conclusion of this thesis is that at the ultimate limit state the resistance to the diagonal tension mode of failure (shear) in PHZ of R/C walls can be calculated as the sum of two components: the horizontal web reinforcement (stirrups) and the shear strength of the compressive zone. The first component represents the amount of shear that can be transferred across the potential failure surface in the zone of the wall that is under axial tension. The second component represents the part of the shear force that is transferred across the failure surface in the zone of the wall under axial compression. For design purposes the second component can be calculated as the product of the cohesion of concrete, the depth of the neutral axis and the width of the wall. This conclusion shows that the SRS method proposed by Pilakoutas (1990) is the most adequate to evaluate the shear capacity. Therefore, according to the above mentioned findings and the SRS method, the ultimate shear capacity in the PHZ (with regard to the diagonal tension mode of failure) can be expressed by the following equation:

$$V_r = (1 - \xi)\ L\ (A_s/s)_h\ f_y + \xi\ \tau_o\ L\ b \qquad (7.1)$$

The first term of equation (7.1) yields results similar to the truss analogy embodied in the codes of practice. However, the most advanced codes for earthquake resistant design assume that in the PHZ of R/C walls only the

contribution of the stirrups should be relied upon. The conclusions of this work showed that this assumption is excessively conservative. It was also found that an alternative design concept, termed compressive force path (CFP), was not compatible with observed behaviour. According to this concept the shear strength of a R/C member is associated with the strength along which the compressive force is transferred to the supports. The results of the test programme described in this thesis clearly showed that in the presence of high shear forces the contribution of the concrete in the zone under axial tension is indispensable to avoid failure in shear by diagonal tension.

Some features of the behaviour of low rise walls, i.e. walls whose height is close to the length of the cross section, should not be extrapolated for higher walls of multistorey buildings with similar shear ratios M/VL. Those features are essentially the increased effectiveness of the vertical web reinforcement, the lower effectiveness of the stirrups and the spread of plasticity along the vertical reinforcement up to or close to the top of the wall. The difference of behaviour was attributed to the formation of an arch mechanism in walls of low aspect ratios due to the proximity of the top beam to the foundations. This allows part of the load to be transferred directly to the foundations. If the load is not transferred to the wall by a top beam at the level where M=0 but from the part of the wall above this level, the wall is more prone to beam behaviour and the direct transfer of load to the foundations is not possible.

The above led to the conclusion that the shear design of walls of multistorey buildings should be independent of the shear ratio unless their aspect ratio is low. It was also concluded that code provisions to establish the height of the walls along which confinement reinforcement needs to be provided may be excessively conservative for walls with low shear ratios. It was proposed to establish an upper limit to the length of the PHZ of M/(2.5V). The above conclusions also

showed the importance of the boundary conditions in the tests of walls with low shear ratios if they are to be considered representative of the behaviour of the lower regions of walls of multistorey buildings. This pointed to the need of boundary conditions similar to the ones used in the current test programme in tests of walls with low shear ratios.

Confinement reinforcement increases the ductility of walls with low shear ratios by delaying the degradation of the compressive zone. It also prevents a sudden loss of shear strength of the compressive zone after the resistance to diagonal tension is exhausted. The effect of confinement reinforcement in the shear and flexural capacity of walls with low shear ratios is moderate.

Cyclic loading has a negative effect upon the ductility of R/C walls. The intensity of this effect depends on the shear ratio and failure mode, since cyclic loading affects some resisting mechanisms more than others. The lower the shear ratio and the higher the influence of shear in the failure mode, the larger the differences of behaviour that can be expected due to the load history.

The failure mode may have a strong influence on the ductility of R/C walls. The ultimate load of the walls that failed by diagonal tension was achieved at a much lower displacement than in the walls in which this failure mode was prevented. However, it was found that some of the walls that failed by diagonal tension exhibited a considerable ability to deform in the post ultimate range with moderate loss of load carrying capacity. Web crushing failure also curtails a more flexural response. The intensity of the reduction in ductility depends on the difference between the ultimate load and the flexural capacity.

For walls failing in shear by diagonal tension an increase in the amount of stirrups only has a qualitative influence on the behaviour if it prevents yielding of the stirrups. Further increase in the amount of stirrups above

the level necessary to prevent yielding has no noticeable effect on the behaviour.

Due to the pinching effect the energy dissipation capacity associated with shear deformations is lower than the energy dissipation capacity associated with flexural deformations for similar displacements. However, large shear deformations may give a considerable contribution to the ductility of walls with high shear forces. This helps to attenuate the reduction in ductility for walls with low shear ratios as compared with flexural walls.

It is not possible to avoid a considerable reduction in energy dissipation due to the pinching effect in walls with low shear ratios if they are designed only with conventional reinforcement. It was found that web crushing after yielding of the main flexural reinforcement does not reduce energy dissipation up to failure. Web crushing only reduces the overall energy dissipation due to its effect on ductility and not on the shape of the hysteresis loops. Diagonal tension failure reduces energy dissipation by decreasing ductility and also because walls that fail in this mode have less area within the hysteresis loops.

It was proposed to change the methodology used in EC8 to evaluate the behaviour coefficients. It was proposed that for walls whose aspect ratio is higher than 0.75, flexural failure or web crushing failure after the maximum ductility demand should be mandatory. Lower "q" factors should be assigned to walls with low shear ratios.

The hysteretic model proposed by Ozcebe and Saatciouglu (1989) is suitable to represent the shear component of the deformation of R/C walls, as it is able to represent all the important features of observed behaviour. However, the model led, in general, to an overestimation of the energy dissipation capacity associated with shear deformations. Therefore, some quantitative improvements were proposed.

The model could generate an envelope of its own and does not follow the prescribed envelope. As this would change the relative balance between shear and flexure deformations, alterations were suggested in order to avoid this problem.

It was suggested to introduce a new pinching parameter to allow for the lower energy dissipation capacity due to more intense pinching effect in walls that failed in shear by diagonal tension.

The overall force-deformation of the walls was simulated by the model proposed by Kabeyasawa et al (1982) and developed by Vulcano, Bertero and Collotti (1986, 1987 and 1988). The model analyses the deformation of the wall by separating it into shear and flexural components.

The flexural component of the model was found to overestimate the flexural stiffness of the walls. This was not observed in higher scale models, whilst smaller scale models tested by other researchers exhibited higher variation between measured stiffness and analytical predictions. The differences in stiffness were attributed to higher shrinkage effects in the smaller scale models.

If both components of the deformation are defined independently, the separation of the total displacement into shear and flexural components may involve large errors. It was shown that this problem may be solved by coupling both components of the deformation. By imposing "yielding" of the shear component when yielding of the flexural reinforcement occurs, the most important source of error in finding the correct balance between both components of the deformation is eliminated.

The balance between shear and flexural components strongly influences the energy dissipation capacity. This is due to the fact that for a given displacement amplitude the energy dissipation capacity associated with flexural deformations is higher than the energy associated with shear

deformations. The balance between shear and flexural deformations was found to be extremely sensitive to small variations in the post-yield stiffness of the shear model.

Even if the models are coupled as described above, the model proposed by Ozcebe and Saatciouglu tends to increase the participation of the flexural component in the total deformation when the imposed displacement increases in the post yield range. This is a qualitative error since the observed behaviour shows exactly the opposite trend. It was concluded that the linear envelope of the shear component in the post yield range was not suitable and it was necessary to replace it by a nonlinear curve or multilinear segments.

7.2 Future Developments

Suggestions regarding the study of the seismic behaviour of R/C walls with low shear ratios are offered below.

The validation of the SRS method for walls subjected to axial compression should be a priority. The capacity of the horizontal jack within the test-rig designed for the current project is sufficient to apply a force necessary to develop the flexural capacity of the walls with an axial compression of 20% of their compressive strength.

It is not necessary to design R/C walls against sliding shear if the shear ratio is equal or above 1.1. Further studies should be undertaken to assess if specific code provisions concerning sliding shear are necessary.

The suggestions given for the evaluation of the behaviour factors emphasise the need for reliable but simple models that describe the overall behaviour of walls with low shear ratios. Such models are necessary to perform nonlinear dynamic analyses that lead to the evaluation of behaviour factors. Although in this work significant progress has been

achieved in developing a general model to represent the overall force deformation of R/C walls with low shear ratios, further improvements on the model are still necessary.

Reliable and fully validated constitutive relationships for shear transfer across cracks under any load history should be incorporated in finite element programs in order to simulate the hysteretic behaviour of R/C members with high shear forces.

REFERENCES

ACI 318-83, "Building Code Requirements for Reinforced Concrete", American Concrete Institute, Detroit, 1983.

Aktan,A.E. and Bertero,V.V., "Seismic Response of R/C Frame-Wall Structures", Journal of Structural Division, ASCE, Vol. 110, No. 8, August 1984, pp 1803-1821.

Aktan,A.E., Bertero,V.V. Chowdhury,A.A. and Nagashima,T., "Experimental and Analytical predictionsof the Mechanical Characteristicsof a 1/5 Scale Model of a 7-Story R/C Frame-Wall Building Structure" Report N0. EERC-83/13, Earthquake Engineering Research Center, University of California, Berkeley, 1983.

Aktan,A.E., Bertero,V.V. and Piazza,M., "Prediction of the Seismic Responses of R/C Frame-Coupled Wall Structures", Report N0. EERC-82/12, Earthquake Engineering Research Center, University of California, Berkeley, 1982.

Alexander,C.M., Heidebrecht,A.C. and Tso,W.K., "Cyclic Load Tests on Shear Wall Panels", 5th World Conference on Earthquake Engineering, Rome, 1974, Vol. 1, pp 1116-1119.

Aoyama,H. and Yoshimura,M., "Tests on R/C Walls Subjected to Biaxial Loading", 7th World Conference in Earthquake Engineering, Istanbul, Turkey, 1982, Vol. 7, pp 511-518.

Barda,F., Hanson,J.M. and Corley,W.G., "Shear Strength of Low Rise Walls With Boundary Elements", SP-53, American Concrete Institute, Detroit, 1977, pp 149-202.

Benjamin,J.R. and Williams,H.A., "The Behaviour of One-Storey Reinforced Concrete Shear Walls", Journal of Structural Division, ASCE, Vol.83, March 1957, pp. 1-49.

Benjamin,J.R. and Williams,H.A., "Behaviour of One-Storey reinforced Concrete Shear Walls Containing Openings", ACI Journal, Vol. 55, No 5, 1958, pp. 605-618.

Benjamin,J.R. and Williams,H.A., "Reinforced Concrete Shear walls Assemblies", Journal of Structural Division, ASCE, Vol. 86, No. 8, August 1960, pp. 1-32.

Bertero,V.V., Popov,E.P. and Wang,T.Y., "Hysteretic Behaviour of Reinforced Concrete Flexural Members with Special Web Reinforcement", Report No EERC-74/09, Earthquake Engineering Research Center, University of California, Berkeley, 1974.

Bertero,V.V. and Popov,E.P., "Hysteretic Behaviour of Ductile Moment Resisting Reinforced Concrete Frame Components" Report No EERC-75/16, Earthquake Engineering Research Center, University of California, Berkeley, 1975.

Bertero,V.V., "State of the Art and Practice in Seismic Resistant Design of R/C Frame-Wall Structural Systems", 8th World Conference on Earthquake Engineering, San Francisco 1984, Vol V, pp 613-620.

Cardenas,A.E. and Magura,D., "Strength of High-Rise Shear Walls - Rectangular Cross Section", SP-36, American Concrete Institute, Detroit 1973, pp. 119-131.

Cardenas,A.E., Hanson,J.M., Corley,W.G and Hognestad, E., "Design Provisions for Shear Walls", ACI Journal, Vol. 70, 1973, No 3, pp.221-230.

Cardenas,A.E., Russel,H.J. and Corley,W.G., "Strength of Low-Rise Structural Walls", SP-63, American Concrete Institute, Detroit, 1980, pp. 221-241.

Clough,R.W. and Johnston,S.B., "Effect of Stiffness Degradation on Earthquake Ductility Requirements", 2nd Japan National Conference on Earthquake Engineering, 1966, pp 227-232.

Collins,M.P. and Mitchell,D., "Shear and Torsion Design of Prestressed and Non-Prestressed Concrete Beams", PCI Journal, September-October 1980, Vol 25, pp 32-100.

Colotti,V. and Vulcano,A., "Behaviour of R/C Structural Walls Subjected to Severe Cyclic Loadings", (in Italian), Procs. AICAP (Italian Association of Reinforced and Presstressed Concrete) Conference, Stresa, Italy, 1987.

Commentary on ACI 318-83, "Building Code Requirements for Reinforced Concrete", American Concrete Institute, Detroit, 1983.

Divakar,M.P., Fafitis,A. and Shah,S.P., "Constitutive Model for Shear Transfer in Cracked Concrete", Journal of Structural Division, ASCE, Vol 113, May 1987, pp. 1046-1062.

EC2, "Eurocode No.2: Common Unified Rules for Concrete Structures", Report EUR 8848 DE, EN, FR, Industrial Processes, Building and Civil Engineering, Commission of the European Communities, 1984.

EC8, "Eurocode No.8: Structures in Seismic Regions - Design", Part 1, General and Building, Report EUR 12266 EN, Industrial Processes, Building and Civil Engineering, Commission of the European Communities, May 1988.

Elnashai,A.S., "Nonlinear Analysis of Composite Tubular Joints", PhD Thesis, University of London, 1984.

Elnashai,A.S., Pilakoutas,K. and Ambraseys,N.N., "Experimental Behaviour of Reinforced Concrete Walls Under Earthquake Loading", International Journal of Earthquake Engineering and Structural Dynamics, Vol 19, No 3, April 1990, pp 389-407.

Elnashai,A.S., and Pilakoutas,K. , "Interpretation of Testing Results for R/C Panels", ACI Journal, Under Review.

Elwi,A.A. and Murray,D.W., "A 3D hypoelastic concrete constitutive relationship", Journal of Engineering Mechanics, ASCE, VOL. 105, No. 4, April 1979, pp. 623-641.

Fenwick,R.C. and Paulay,T., "Mechanism of Shear Resistance of Concrete Beams", Journal of Structural Division, ASCE, Vol. 94, October 1968, pp 2325-2350.

Fiorato,A.E., Oesterle,R.G. and Corley,W.G., "Importance of Reinforcement Details in Earthquake Resistant Structural Walls", Workshop on "Earthquake Resistant Reinforced Concrete Building Construction", University of California, Berkeley, 1977, Vol. III, pp. 1430-1451.

Fiorato,A.E., Oesterle,R.G. and Corley,W.G., "Ductility of Structural Walls for Design of Earthquake Resistant Buildings" 6th World Conference on Earthquake Engineering, New-Delhi, 1977, Vol. 3, pp. 2797-2802.

Fukada,Y., "Study on the Restoring Force Characteristics of Reinforced Concrete Buildings" (in Japanese), Kanto District Symposium, AIJ, No 40, 1969, pp 121-24.

Goodsir,W.J., "The Design of Coupled Frame-Wall Structures for Seismic Actions", PhD Thesis, University of Canterbury, Christchurch, New Zealand, 1985.

Hirashi,H., "Evaluation of Shear and Flexural Deformations of Flexural Type Shear Walls", Bulletin of the New Zealand National Society for Earthquake Engineering, Vol 17, No 2, June 1984, pp 135-144.

Hiraishi,H., "Evaluation of Shear and Flexural Deformations of Flexural Type Shear Walls", 8th World Conference on Earthquake Engineering, San Francisco, 1984, Vol. 5, pp. 677-685.

Hoedajanto,D., "Simple Model for Shear Response of R/C Panels", 9th World Conference on Earthquake Engineering, Tokyo-Kyoto 1988, Vol VI, pp 29-34.

Hsu,T.T.C. and Mo,L.Y., "Softening of Concrete in Low-Rise Shearwalls", ACI Journal, Vol. 82, November-December 1985, pp. 883-889.

Hsu,T.T.C., Mau,S.T. and Chen,B., "Theory of Shear Transfer Strength of Reinforced Concrete", ACI Journal, Vol 84, March-April 1987, pp 149-160.

Huang,C. and Sheu,M.S., "Experimental and Theoretical Study on Aseismic Behaviour of Low-Rise R.C. Shear Walls", 9th World Conference on Earthquake Engineering, Tokyo-Kyoto 1988, Vol VI, pp 35-40.

Iliya,R. and Bertero,V.V., "Effects of Amount and Arrangement of Wall-Panel Reinforcement on Hysteretic Behaviour of Reinforced Concrete Walls", Report No EERC-80/04, Earthquake Engineering Research Center, University of California, Berkeley, 1980.

Jimenez,R., White,R.N. and Gergely,P., "Cyclic Shear and Dowel Action Models in R/C", Journal of Structural Division, ASCE, Vol. 108, May 1982, pp 1106-1123.

Kabeyasawa,H., Shiohara,H., Otani,S. and Aoyama,H., "Analysis of the Full-Scale Seven-Storey Reinforced Concrete Test Structure: Test PSD3", 3rd Joint Coordinating Committee Mtg of the US-Japan Cooperative Research Program, BRI, Tsukuba, Japan, 1982.

Kanaan,A.E. and Powell,G.H., "DRAIN-2D, A General Purpose Computer Program for Dynamic Analysis of Planar Structures", Report No EERC-73/06, Earthquake Engineering Research Center, University of California, Berkeley, 1973.

Kotsovos,M.D., "Mechanisms of Shear Failure", Magazine of Concrete Research, Vol. 35, No. 123, 1983, pp. 99-106.

Kotsovos,M.D., "Consideration of Triaxial Stress Conditions in Design: a Necessity", ACI Journal, Vol. 84, May-June 1987, pp 266-273.

Kotsovos,M,D., "Compressive Force Path Concept: Basis for Reinforced Concrete Ultimate Limit State Design", ACI Journal, Vol. 85, January-February 1988, pp 68-75.

Kotsovos,M.D., Private communication, 1989.

Lefas,I.D. and Kotsovos,M.D., "Behaviour of Reinforced Concrete Structural Walls: a New Interpretation", IABSE Colloquium on "Computational Mechanics of Concrete Structures, Advances and Applications", Delft 1987.

Lefas,I.D., "Behaviour of Reinforced Concrete Structural Walls", PhD Thesis, University of London, 1988.

Lefas,I.D., Kotsovos,M.D. and Ambraseys,N.N., "Behaviour of Reinforced Concrete Structural Walls: Strength, Deformation Characteristics, and Failure Mechanism", ACI Journal, Vol. 1, January-February 1990, pp 23-30.

Ma,S.M., Bertero,V.V. and Popov,E.P., "Experimental and Analytical Studies of hysteretic Behaviour of Reinforced Concrete Rectangular and T-Beams", Report No EERC-76/02, Earthquake Engineering Research Center, University of California, Berkeley, 1976.

Mander,J.B., Priestley,M.J.N. and Park,R., "Theoretical Stress-Strain Model for Confined Concrete", Journal of Structural Division, ASCE, Vol. 114, No. 8, August 1988, pp. 1804-1826.

Mander,J.B., Priestley,M.J.N., and Park,R., "Observed Stress-Strain Behaviour of Confined Concrete", Journal of Structural Division, ASCE, Vol. 114, No. 8, August 1988, pp. 1804-1826.

Mo,Y.L., "Analysis and Design of Low-Rise Structural Walls Under Dynamically Applied Shear Forces", ACI Journal, Vol 85, March-April 1988, pp 180-189.

Moss,P.J., Carr,A.J. and Buchanan,A.H., "Seismic Response of Low Rise Buildings", Bulletin of the New Zealand Society for Earthquake Engineering, Vol 19, No 3, September 1986, pp 180-199.

Nielsen,N.N. and Imbeault,F.A., "Validity of Various Hysteresis Systems", 3rd Japan National Conference on Earthquake Engineering, 1971, pp 707-714.

NZS 3101:1982, Parts 1&2, "Code of Practice for the Design of Concrete Structures", Standards Association of New Zealand, Wellington, 1982.

NZS 4203:1984, "Code of Practice for General Structural Design and Design Loadings for Buildings", Standards Association of New Zealand, Wellington, 1984.

Oesterle,R.G., Fiorato,A.E., Aristizabal-Ochoa,J.D. and Corley,W.G., "Hysteretic Response of Reinforced Concrete Structural Walls", SP-63, American Concrete Institute, Detroit, 1980, pp. 243-273.

Oesterle,R.G., Aristizabal-Ochoa,J.D., Shiu,K.N. and Corley,W.G., "Web Crushing of Reinforced Concrete Walls", ACI Journal, Vol. 81, May-June 1984, pp. 231-241.

Otani,S., "SAKE - A Computer Program for Inelastic Response of R/C Frames to Earthquakes", Civil Engineering Studies, Structural Research Series, Report No 413, University of Illinois, Urbana, 1974.

Otani,S., "Hysteresis Models of Reinforced Concrete for Earthquake Response Analysis", 8th World Conference on Earthquake Engineering", San Francisco 1984, Vol IV, pp 551-558.

Ozcebe,G. and Saatcioglu,M., "Hysteretic Shear Model for Reinforced Concrete Members", Journal of Structural Division, ASCE, Vol 115, No 1, January 1989, pp 132-148.

Park,R. and Paulay,T., "Reinforced Concrete Structures", John Wiley and Sons, New York, 1975.

Park,Y.J., Reinhorn,A.M. and Kunnath,S.K., "IDARC: Inelastic Damage Analysis of Reinforced Concrete Frame-Shear Wall Structures", Report No NCEER-87/0008, National Center for Earthquake Engineering Research, State University of New York, Buffalo, 1987.

Paulay,T., "Earthquake Resistant Structural Walls", Workshop on "Earthquake Resistant Reinforced Concrete Building Construction", University of California, Berkeley, 1977.

Paulay,T., "Earthquake Resisting Shear Walls - New Zealand Design Trends", ACI Journal, Vol 77, May-June 1980, pp 144-152.

Paulay,T., Priestley,M.J.N. and Synge,A.J., "Ductility in Earthquake Resistant Squat Shear Walls", ACI Journal, Vol. 79, July-August 1982, pp 257-269.

Pilakoutas,K. "Earthquake Resistant Design of Reinforced Concrete Walls", PhD Thesis, University of London, 1990.

Popov,E.P., "Seismic Behaviour of Structural Subassemblages", Journal of Structural Division, ASCE, Vol 106, No ST7, July 1980, pp 1451-1474.

Ramberg,W. and Osgood,W.R., "Description of Stress-Strain Curves by Three Parameters", National Advisory Committee on Aeronautics, Technical Note 902, 1943.

Santhanam,T.K., "Model for Mild Steel in Inelastic Frame Analysis", Journal of Structural Division, ASCE, Vol. 105, No. 1, January 1979, pp. 199-220.

Schlaich,J., Schafer,K. and Jennewein,M., "Toward a Consistent Design of Structural Concrete", PCI Journal, Vol. 32, May-June 1987, pp 74-150.

Smith,B.S. and Girgis,A., "Simple Analogous Frames for Shear Wall Analysis", Journal of Structural Division, ASCE, Vol 110, No ST11, November 1984, pp 2655-2666.

Takeda,T., Sozen,M.A. and Nielsen,N.N., "Reinforced Concrete Response to Simulated Earthquakes", Journal of Structural Division, ASCE, Vol 96, No ST12, 1970, pp 2557-2573.

Uniform Building Code, International Conference of Building Officials, Whittier, California, 1988.

Vallenas,J.M., Bertero,V.V. and Popov,E.P., "Concrete Confined by Rectangular Hoops and Subjected to Axial Load", Report No EERC-77/13, Earthquake Engineering Research Center, University of California, Berkeley, 1977.

Vallenas,J.M., Bertero,V.V. and Popov,E.P., "Hysteretic Behaviour of Reinforced Concrete Walls", Report No EERC-79/20, Earthquake Engineering Research Center, University of California, Berkeley, 1979.

Vecchio,F.J., "The Response of Reinforced Concrete to In-Plane Shear and Normal Stresses", Phd Thesis, Department of Civil Engineering, University of Toronto, 1981.

Vecchio,F.J. and Collins,M.P., "The Modified Compression-Field Theory for Reinforced Concrete Elements Subjected to Shear", ACI Journal, Vol 83, 1986, pp 219-231.

Vecchio,F.J. and Collins,M.P., "Predicting the Response of Reinforced Concrete Beams Subjected to Shear Using Modified Compression Field Theory", ACI Journal, Vol 85, 1988, pp 258-268.

Vulcano,A. and Bertero,V.V., "Nonlinear Analysis of R/C Structural Walls", 8th European Conference on Earthquake Engineering, Vol 6.5, Lisbon 1986, pp 1-8.

Vulcano,A. and Bertero,V.V., "Analytical Models for Predicting the Lateral Response of R/C Shear Walls: Evaluation of Their Reliability", Report No EERC-87/19, Earthquake Engineering Research Center, University of California, Berkeley, 1987.

Vulcano,A., Bertero,V.V. and Colotti,V., "Analytical Modelling of R/C Structural Walls", 9th World Conference on Earthquake Engineering, Vol VI, Tokyo-Kyoto 1988, pp 41-46.

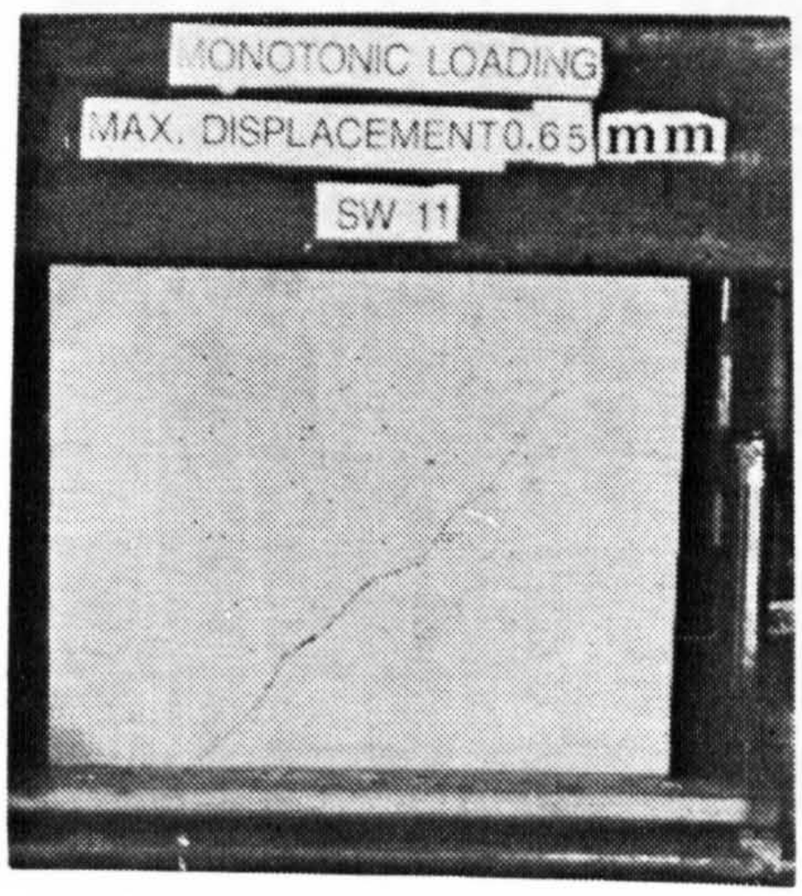
Yamaguchi,K.J., Sugano,S., Higashibata,Y. and Nagashima,T., "Inelastic Cyclic Behaviour of Reinforced Concrete Frame-Wall Structures Subjected to Lateral Forces", 7th World Conference on Earthquake Engineering, Istanbul, Turkey, 1980,Vol. 7, pp 330-340.

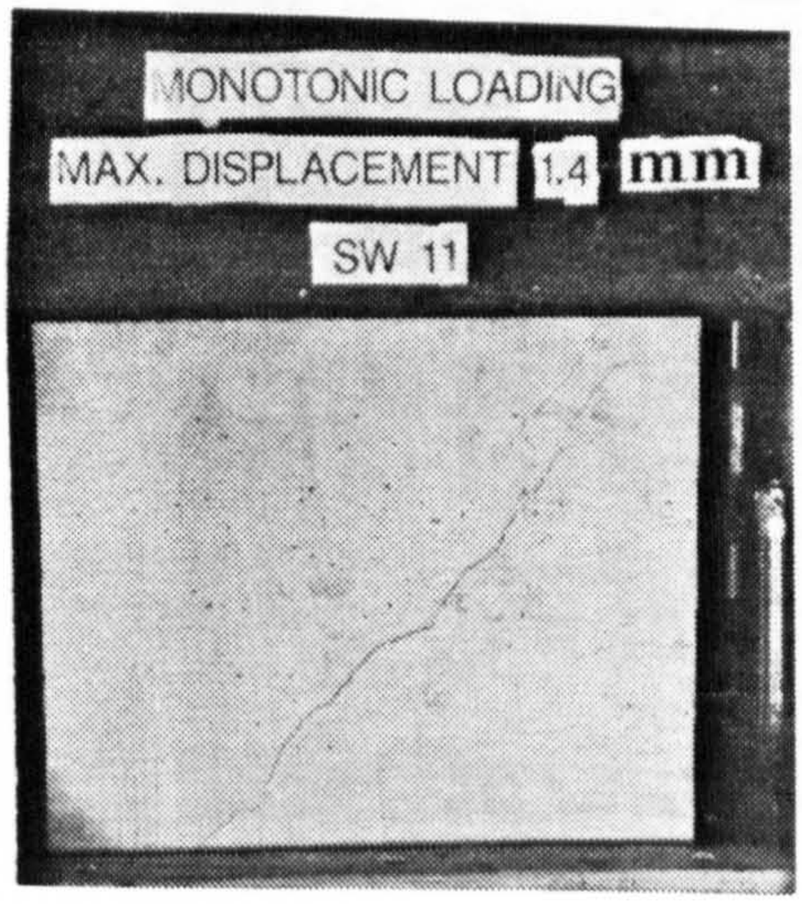
Wagner,T.M. and Bertero,V.V., "Mechanical Behaviour of Shear Wall Vertical Boundary Members: an Experimental Investigation", Report No EERC-82/18, Earthquake Engineering Research Center, University of California, Berkeley, 1982.

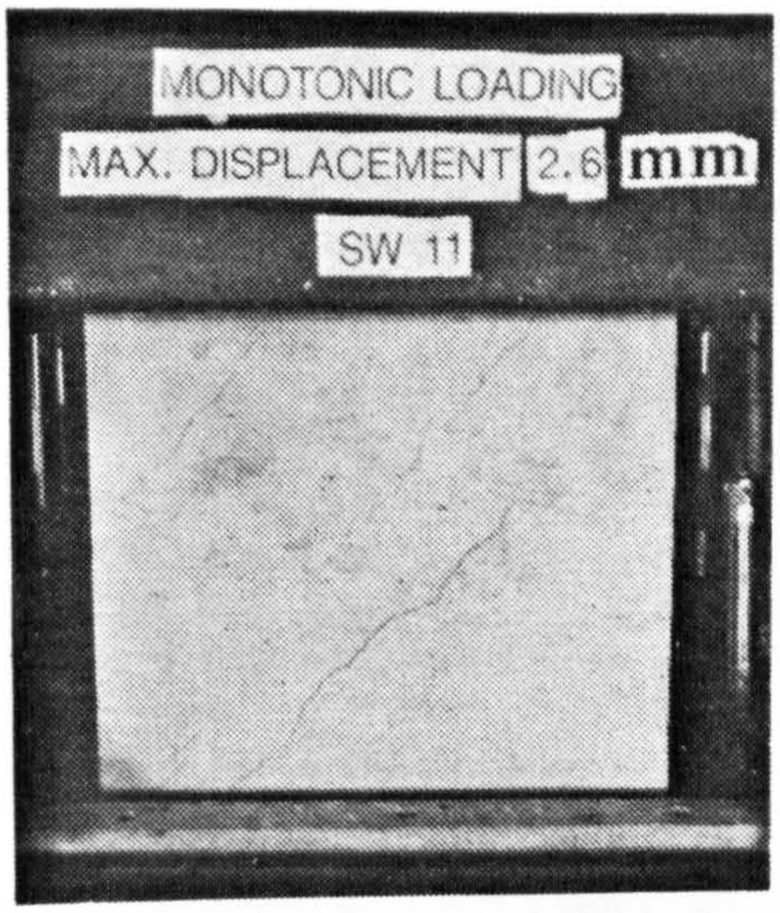
Wang,T.T., Bertero,V.V., and Popov,E.P., "Hysteretic Behaviour of Reinforced Concrete Framed Walls", Report No EERC-75/23, Earthquake Engineering Research Center, University of California, Berkeley, 1975.

APPENDIX A

PHOTOGRAPHS OF THE EXPERIMENTAL PRORAMME







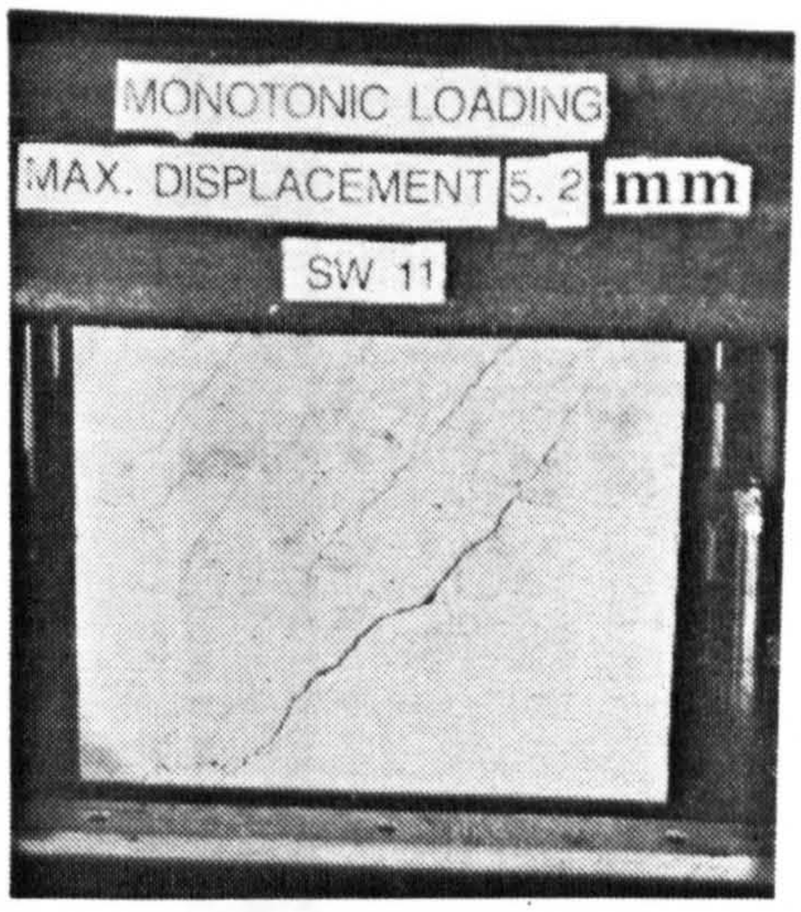


Figure A(11)1 Description of test of wall SW11

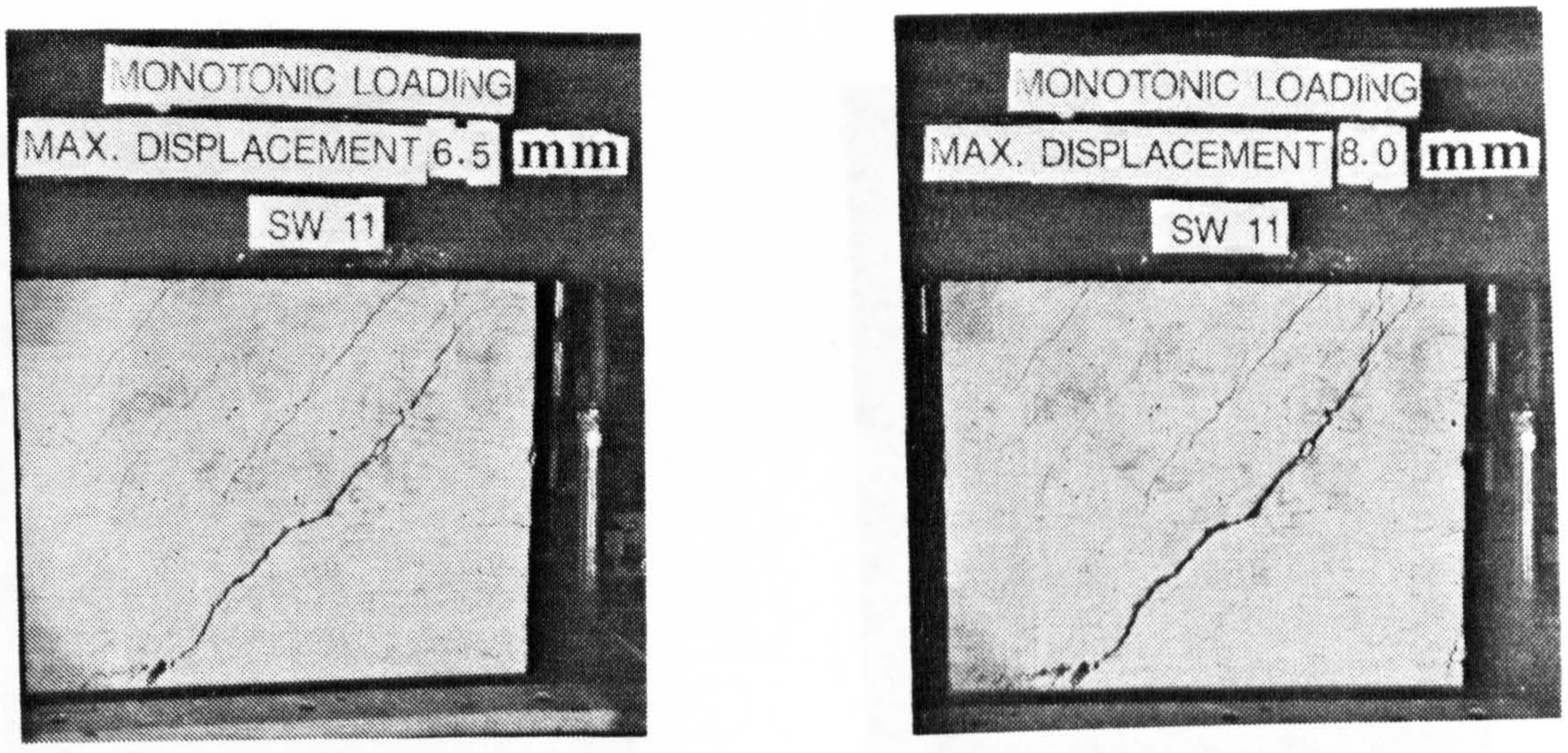


Figure A(11)1 Description of test of wall SW11 (cont.)

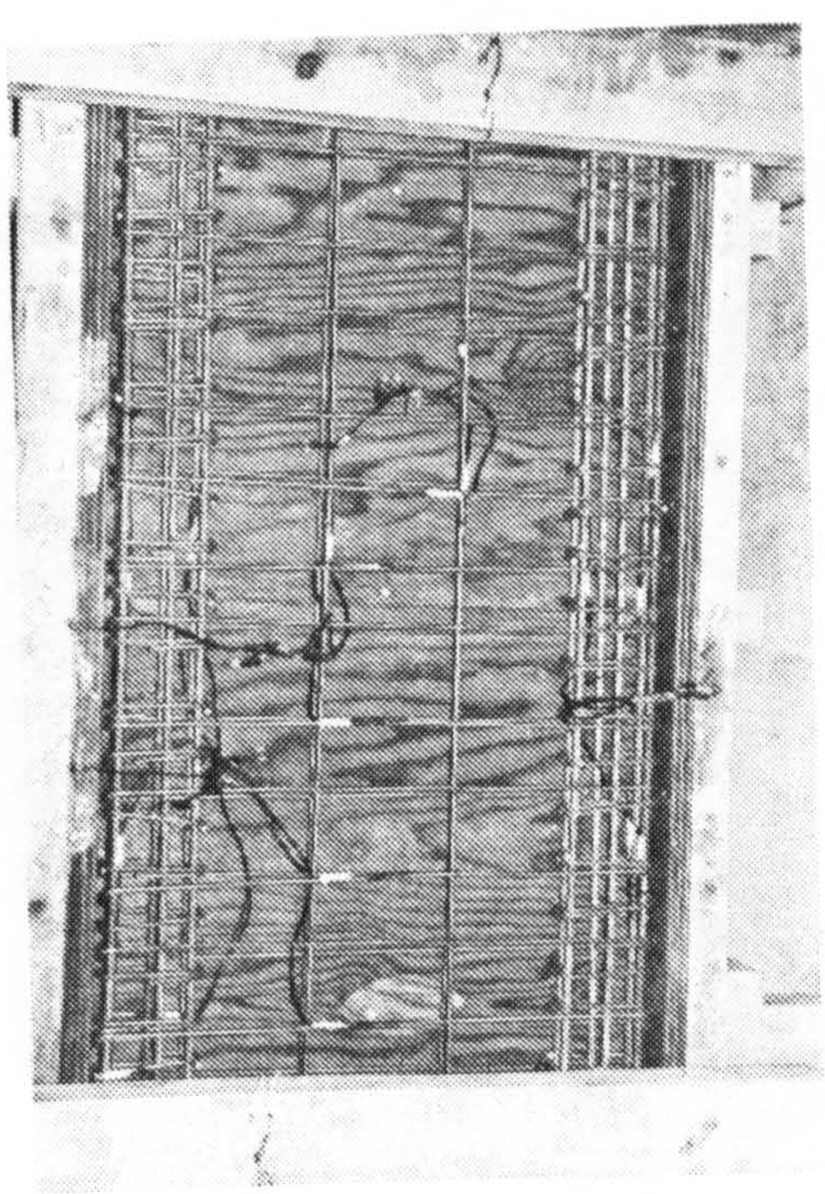


Figure A(11)2 Steel cage of wall SW11

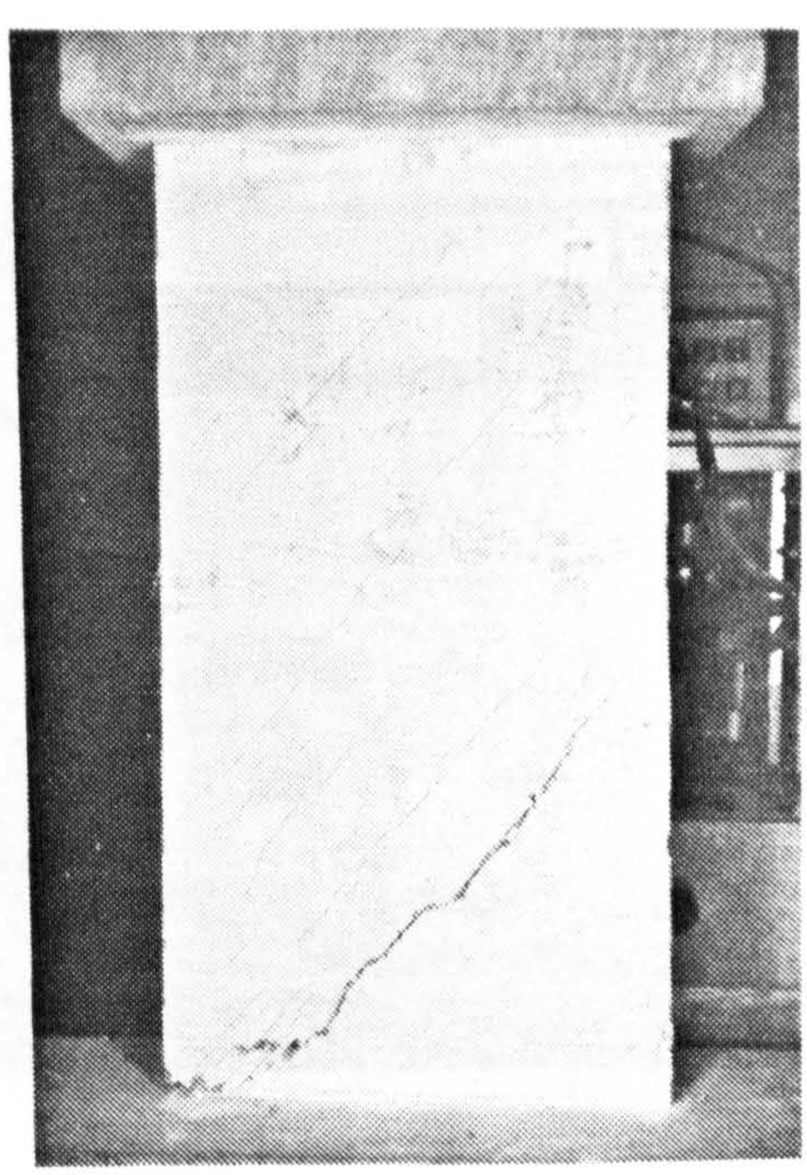
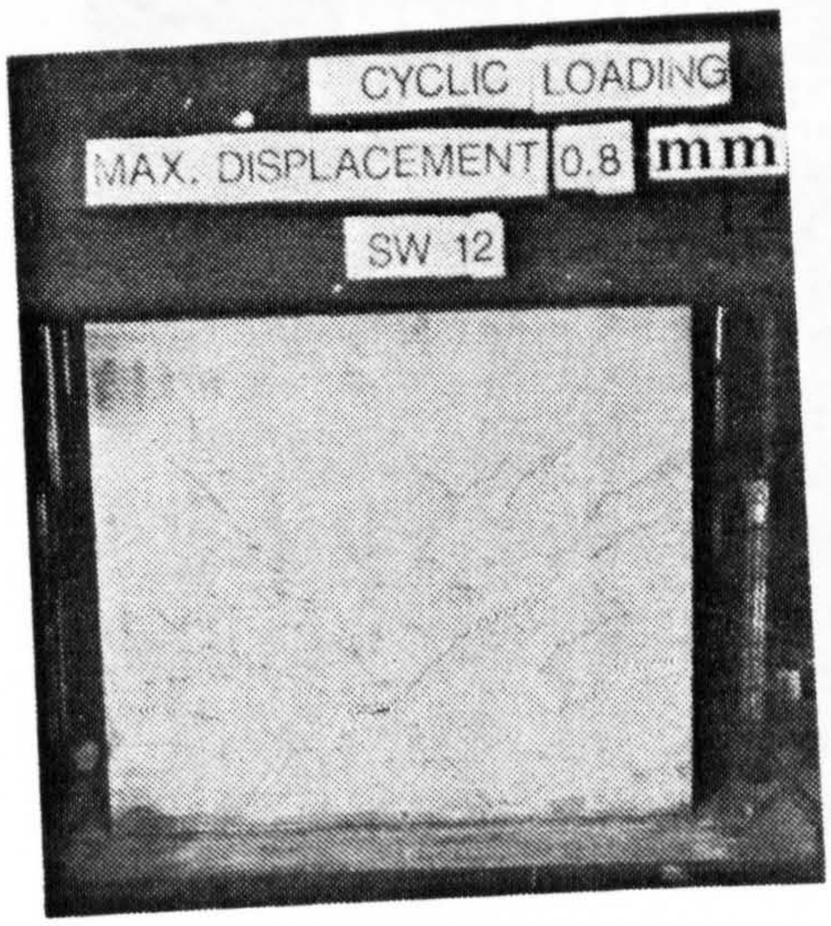
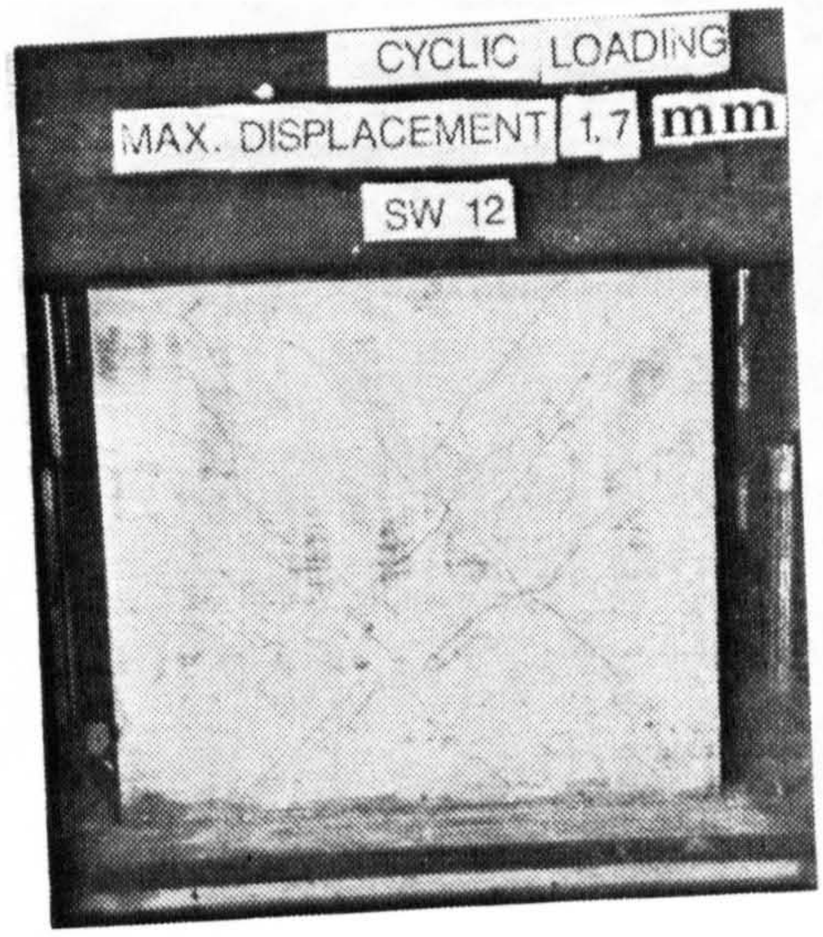
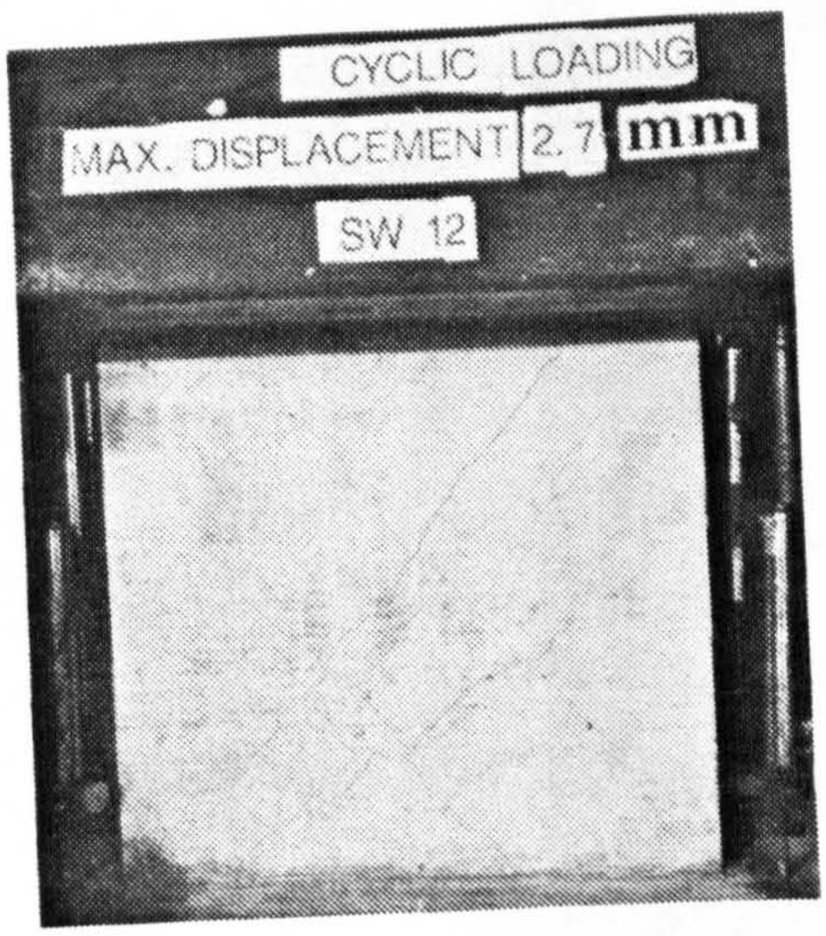


Figure A(11)3 Wall SW11 after the test







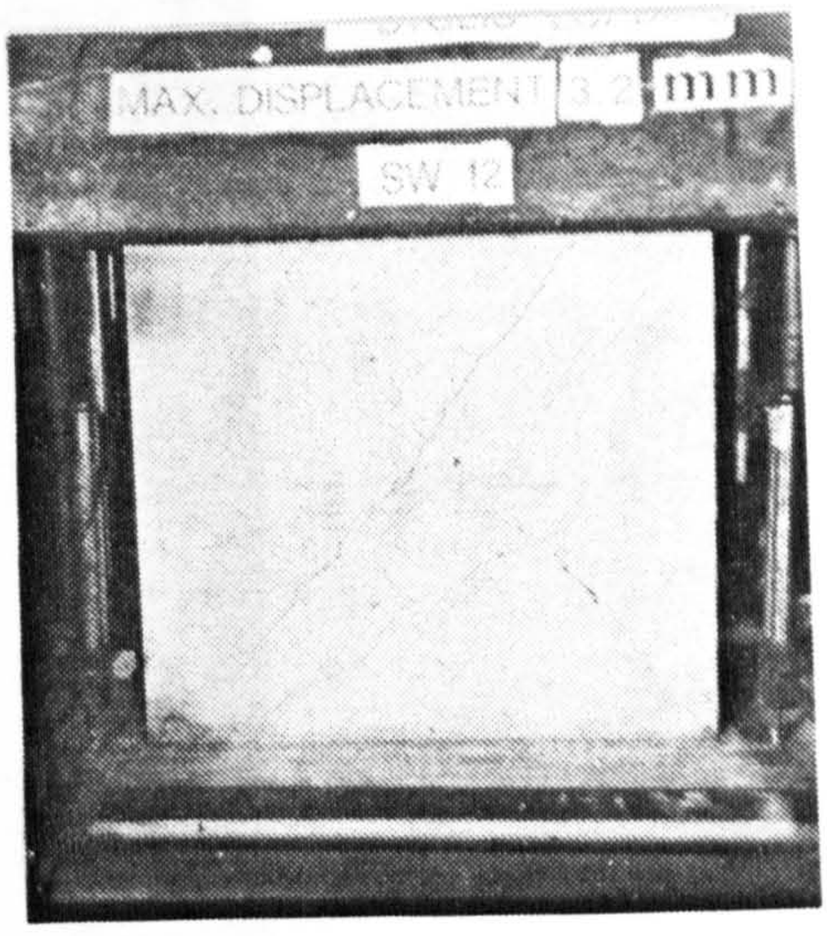
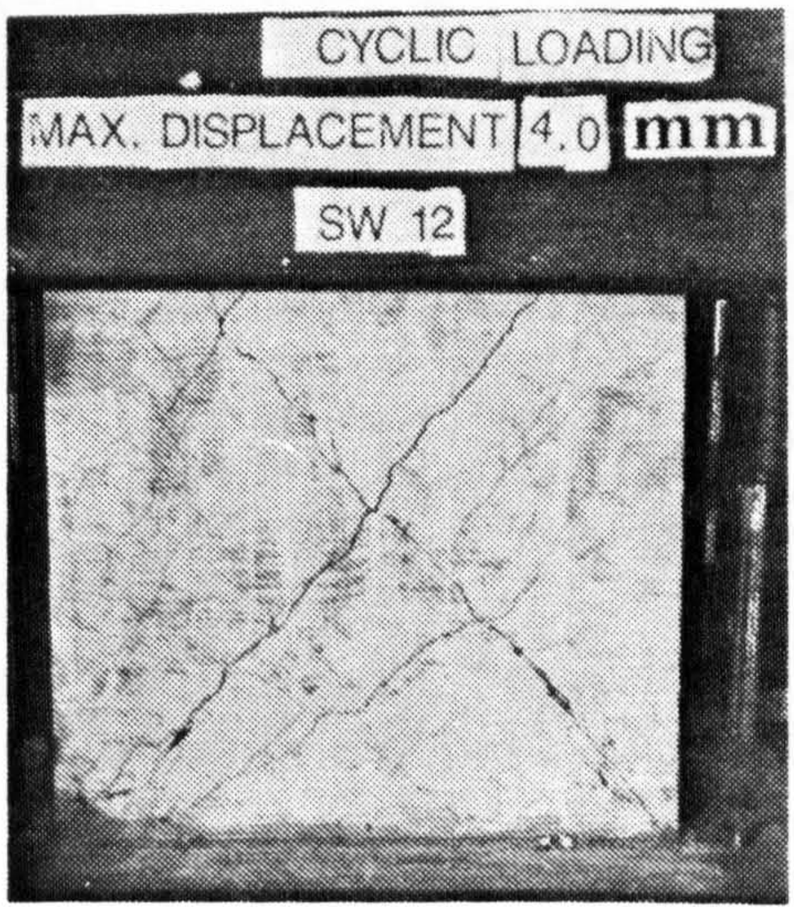


Figure A(12)1 Description of test of wall SW12



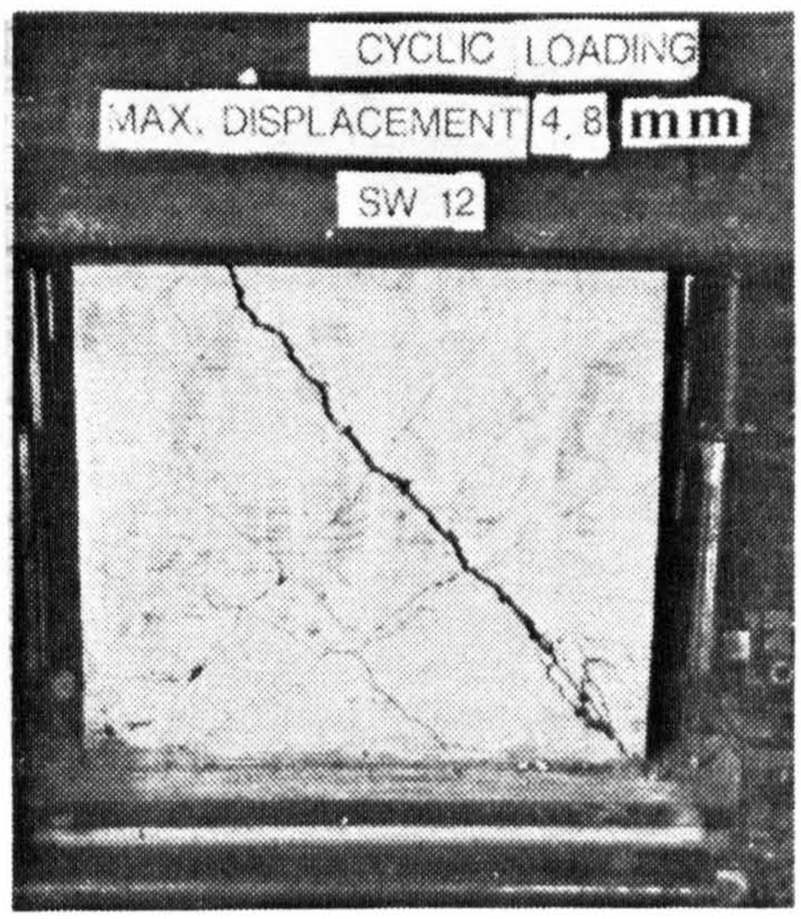


Figure A(12)1 Description of test of wall SW12 (cont.)

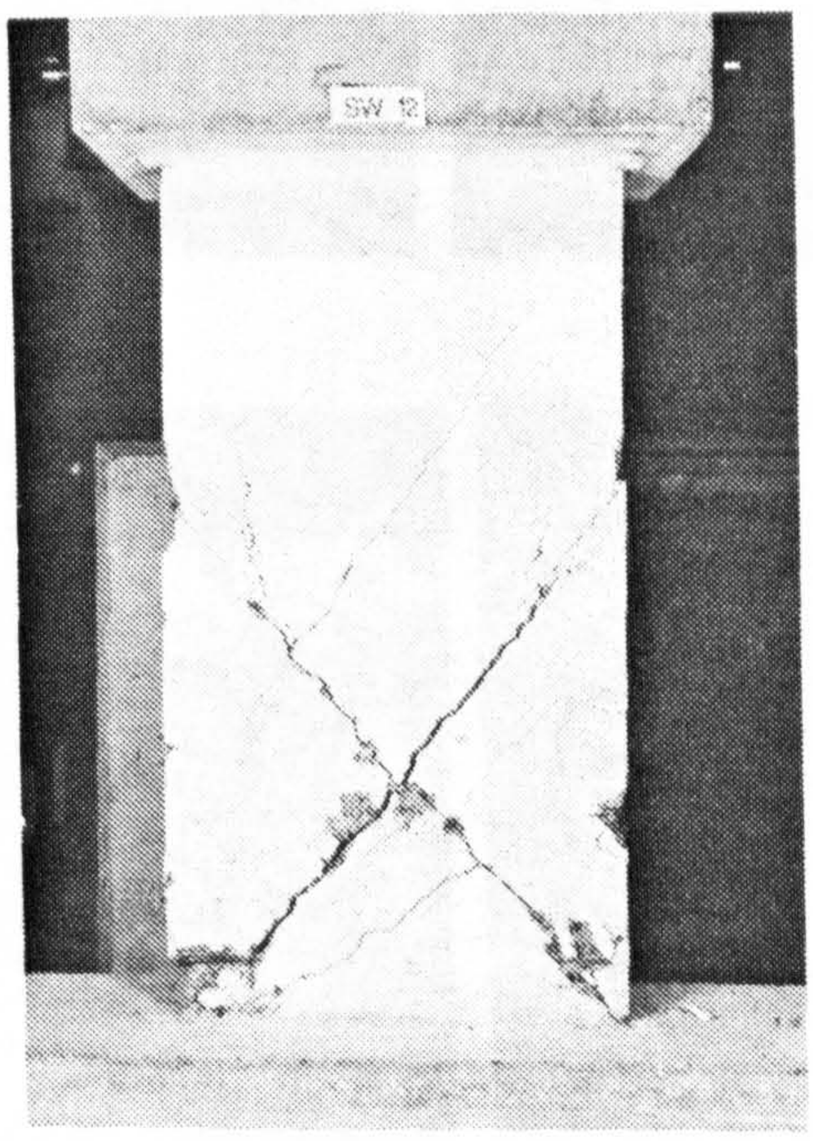


Figure A(12)2 Wall SW12 after the test

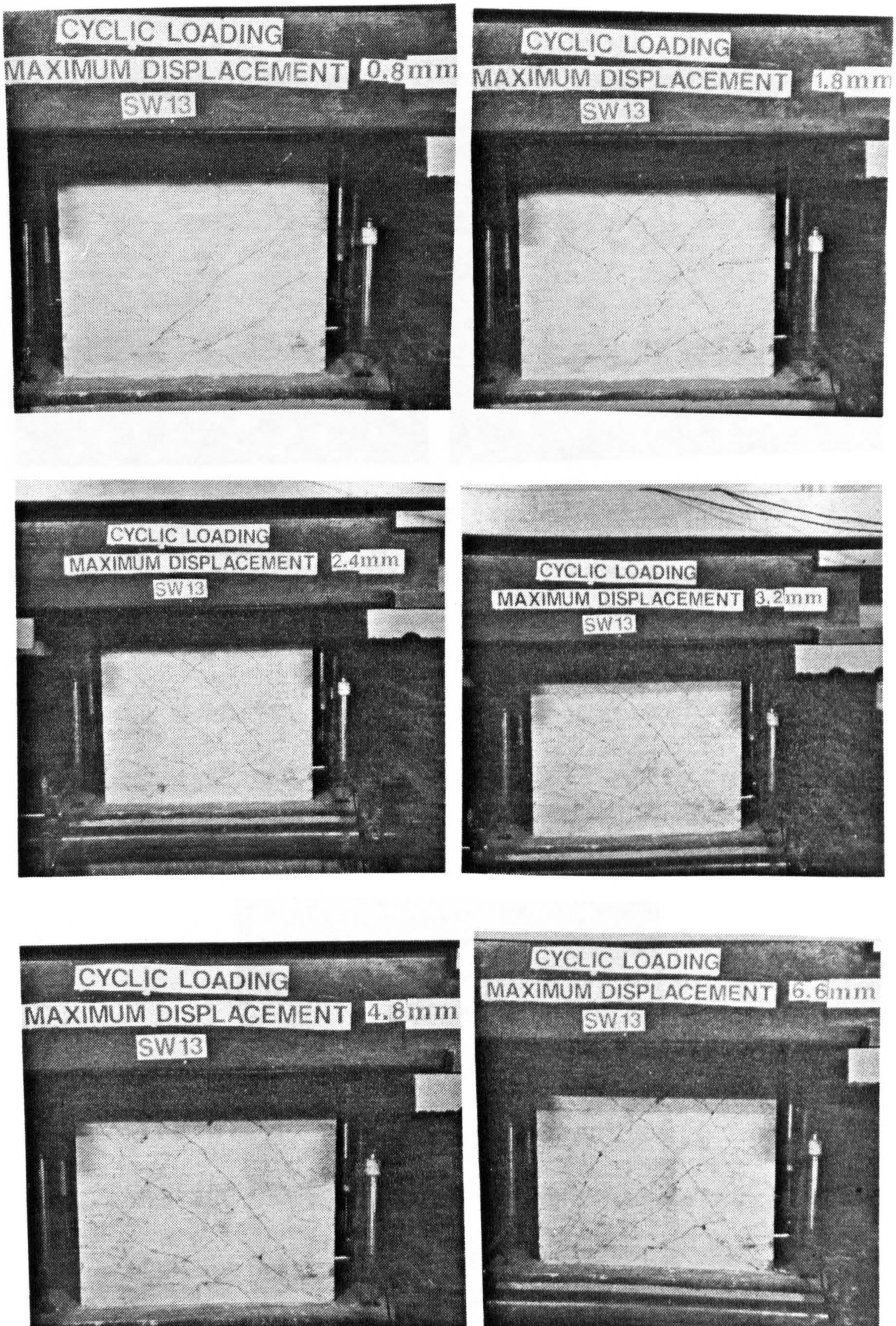


Figure A(13)1 Description of test of wall SW13

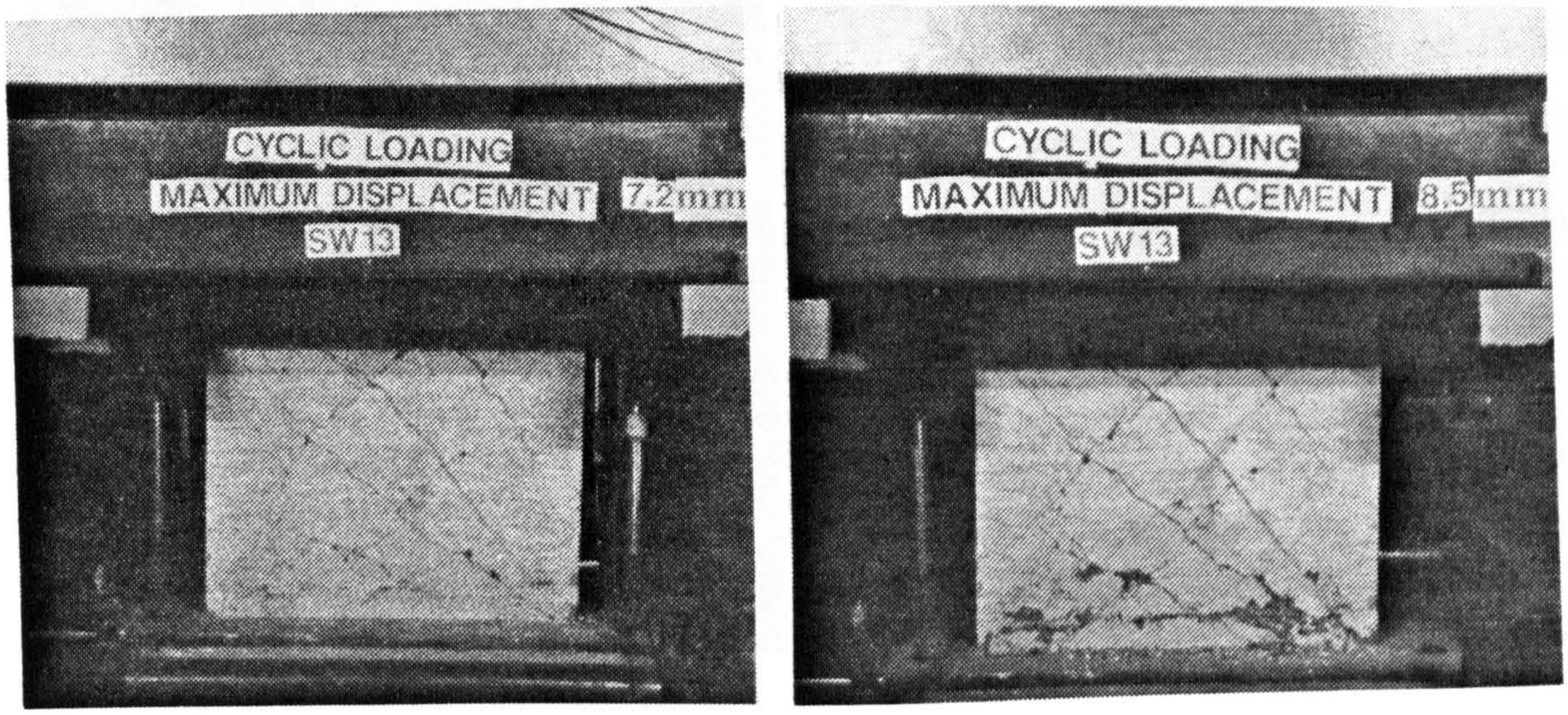


Figure A(13)1 Description of test of wall SW13 (cont.)

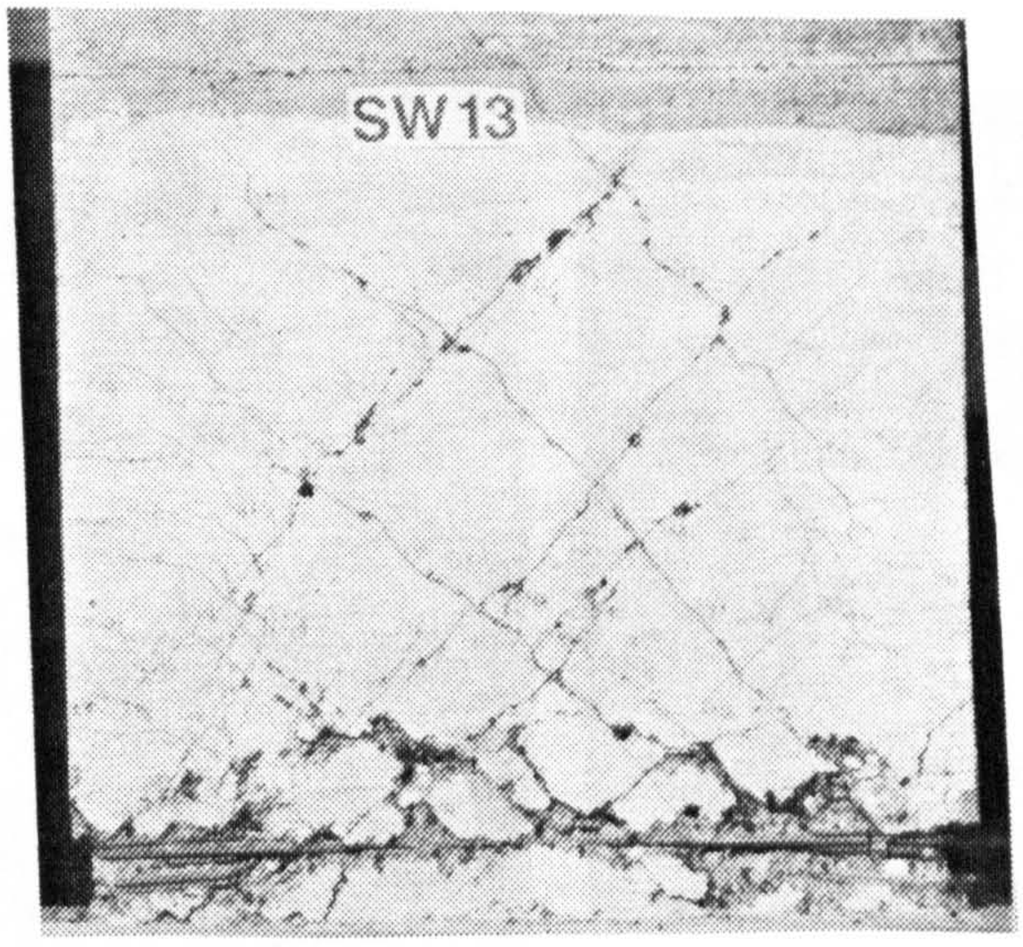
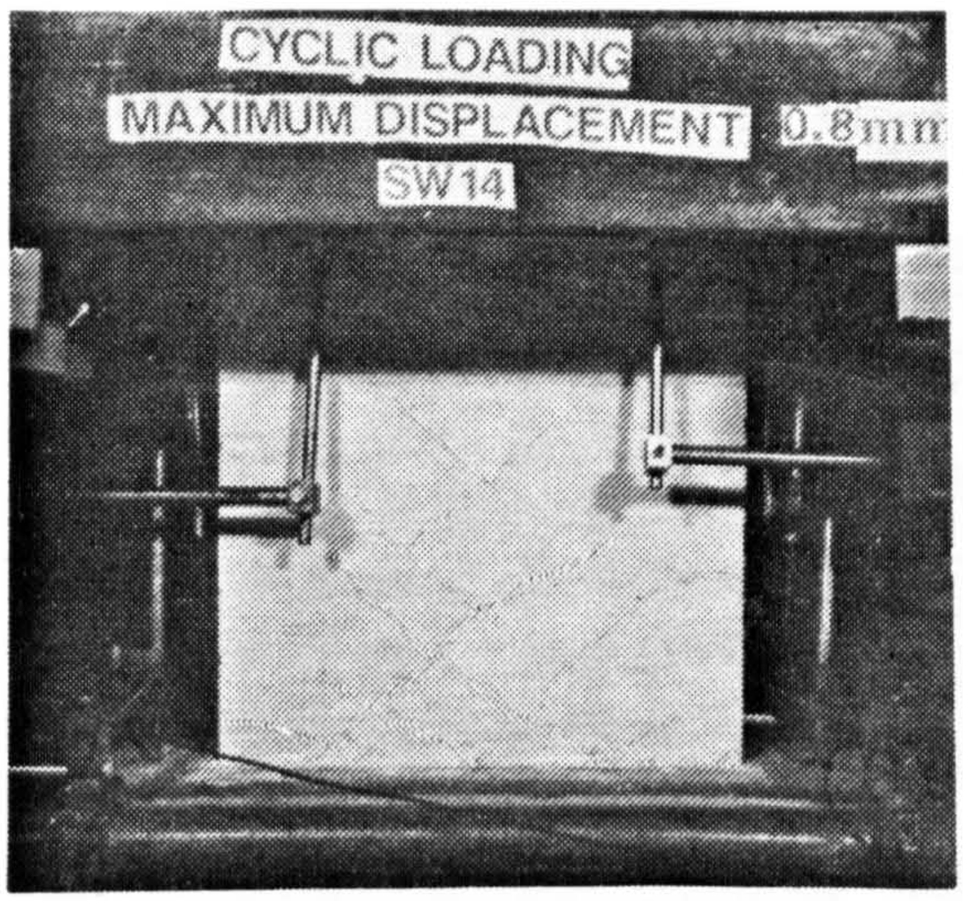
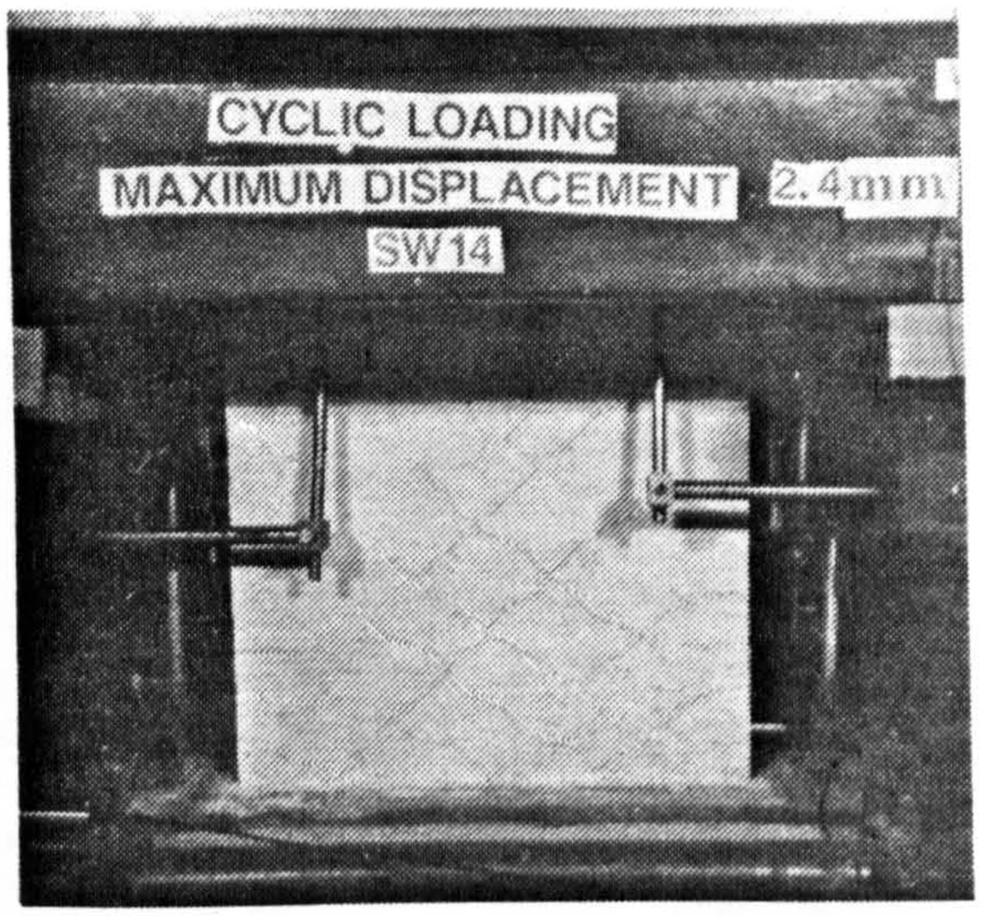
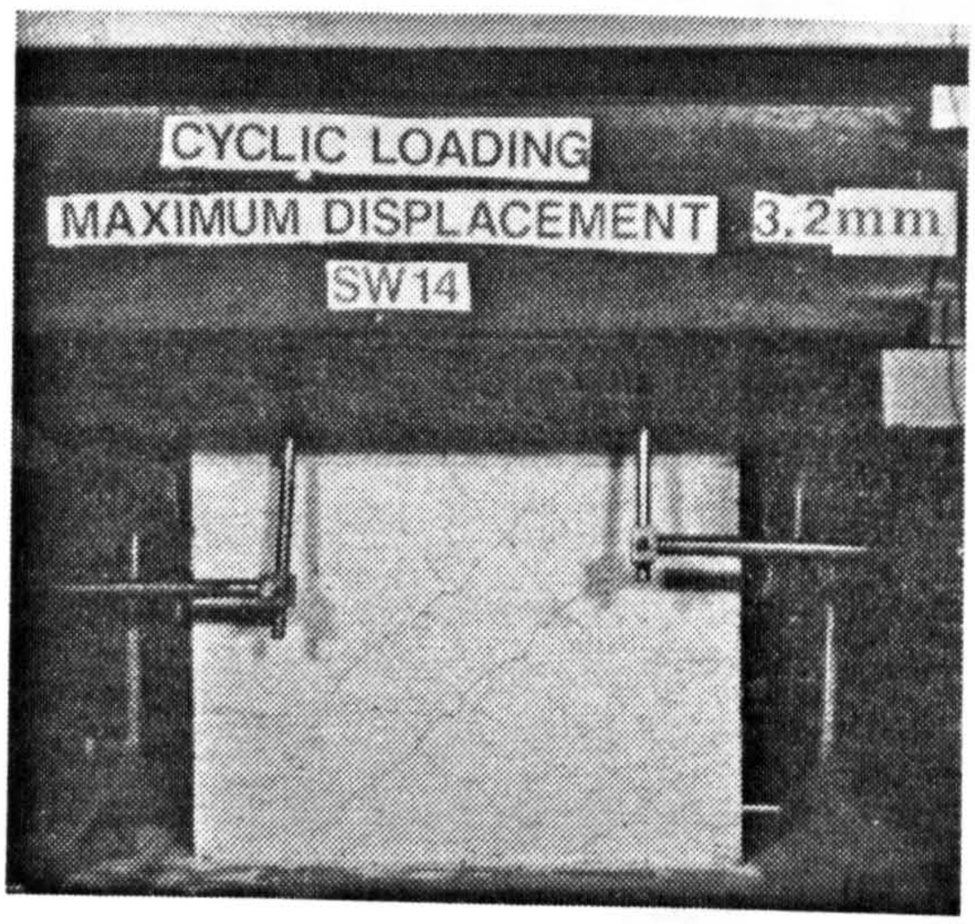
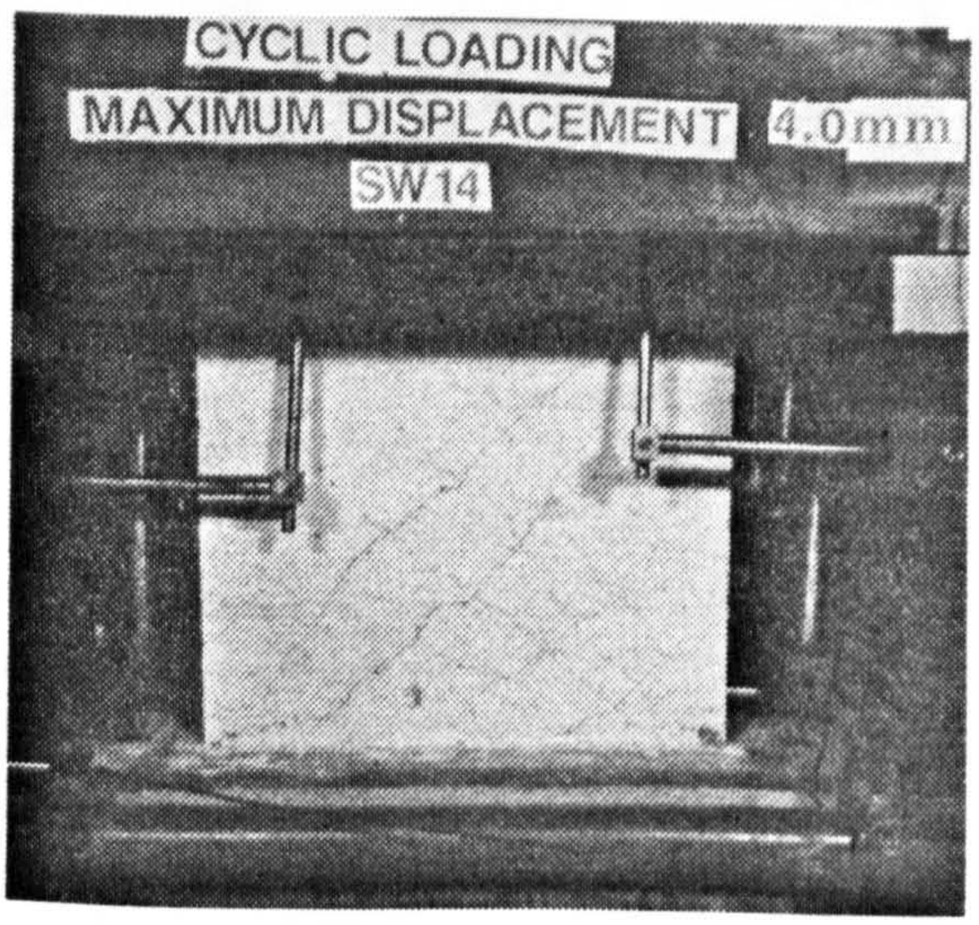


Figure A(13)2 Wall SW13 after the test









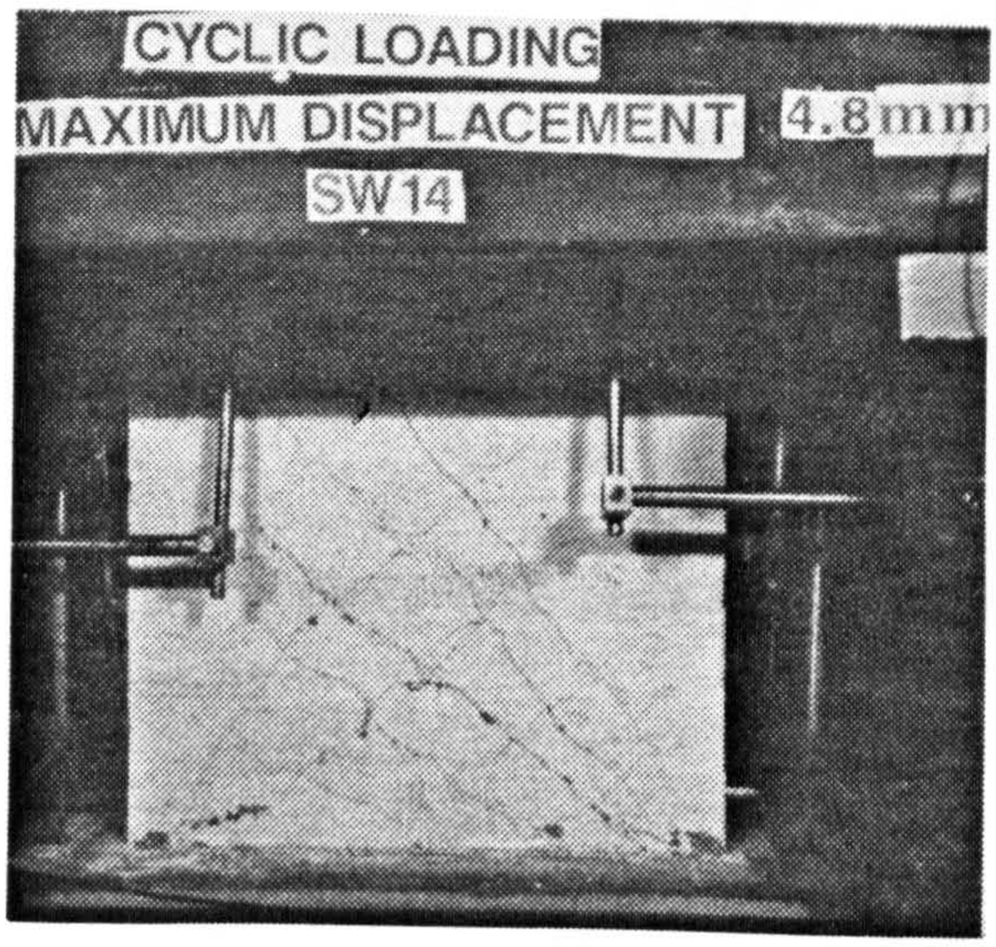




Figure A(14)1 Description of test of wall SW14



Figure A(14)1 Description of test of wall SW14 (cont.)

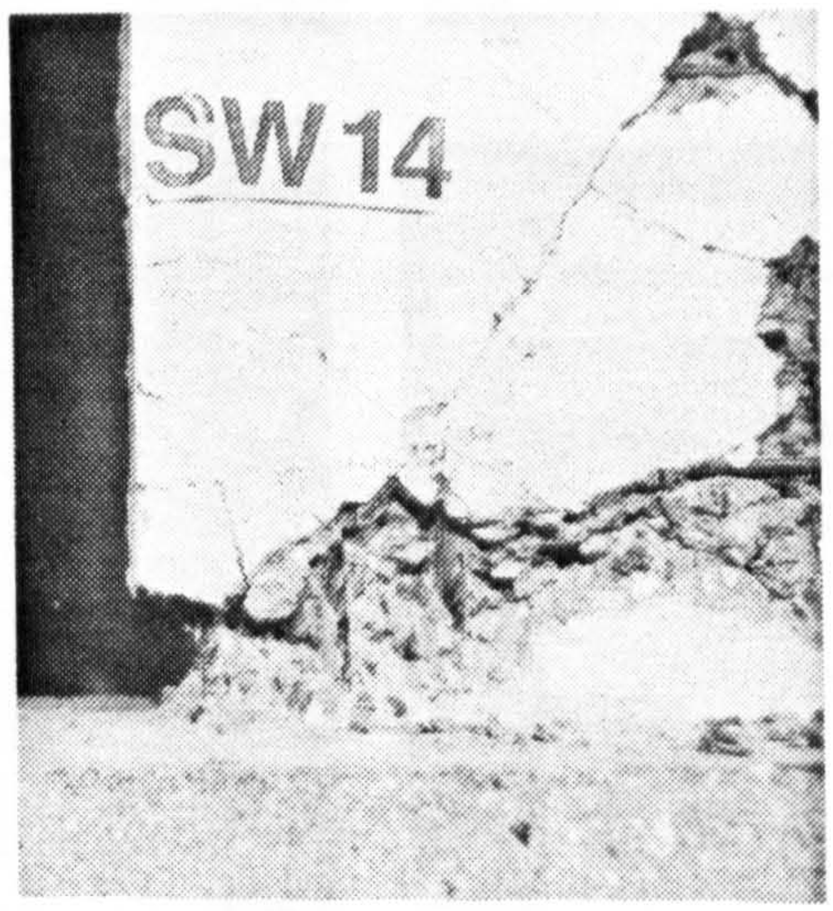
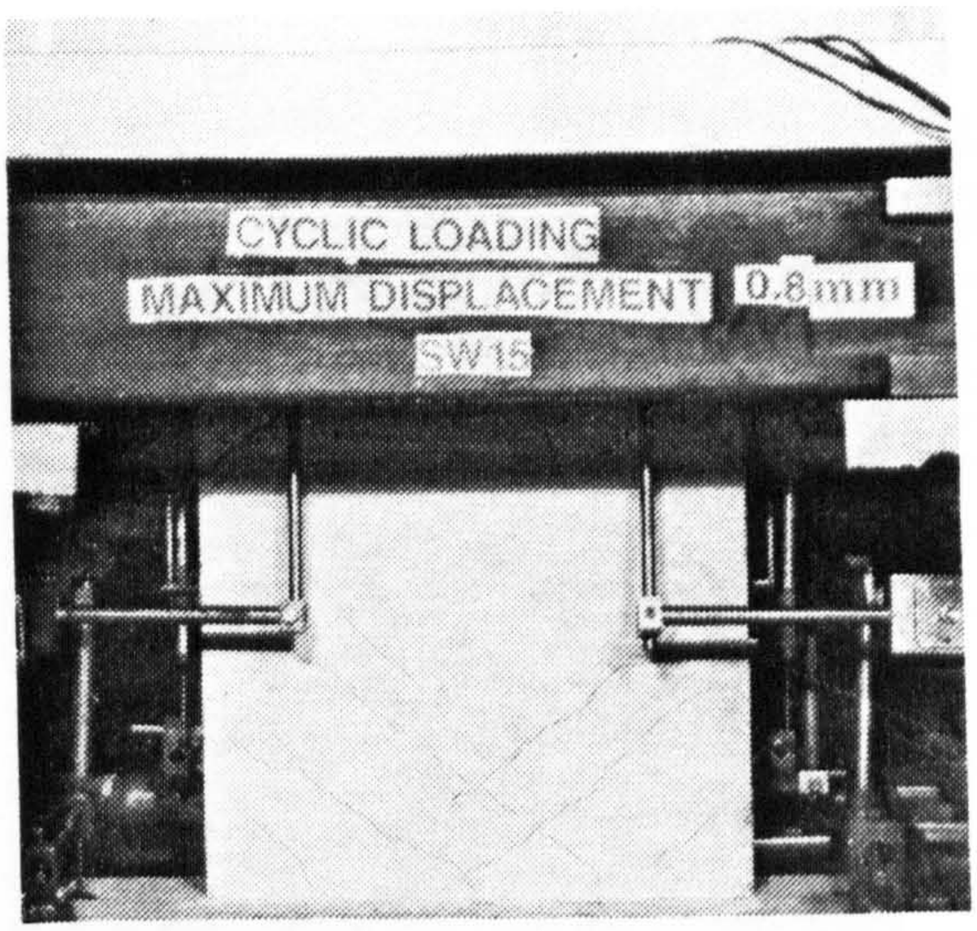
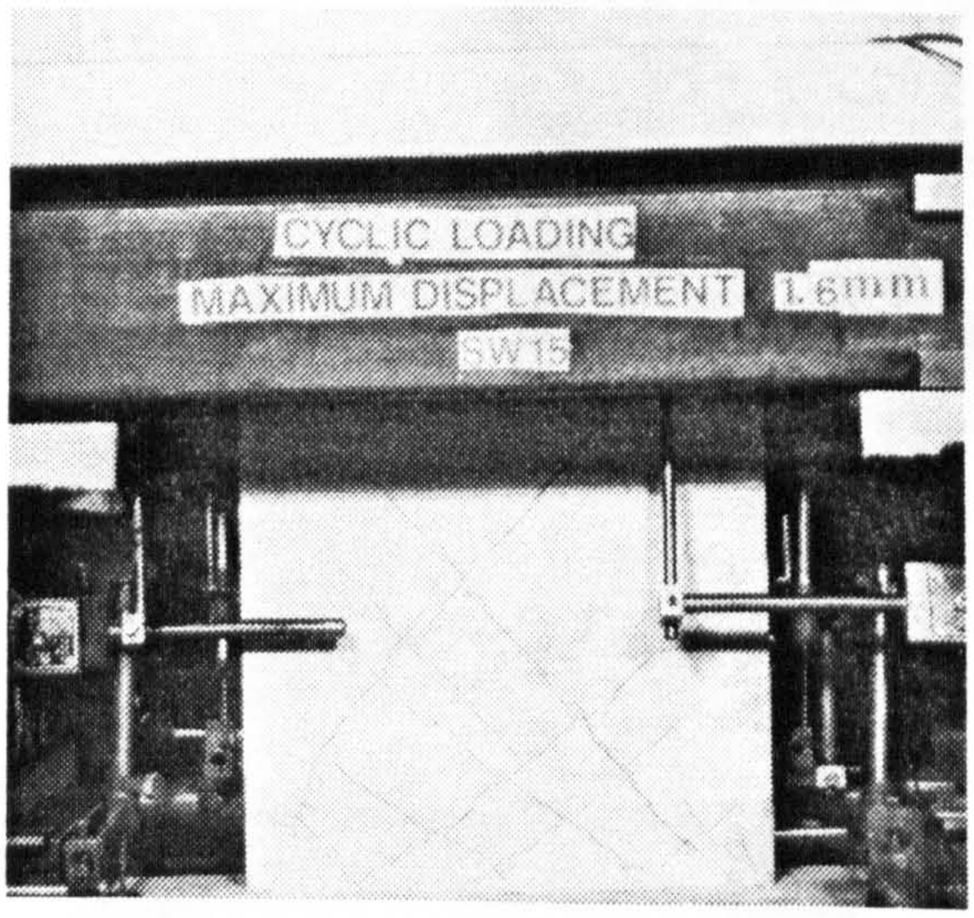
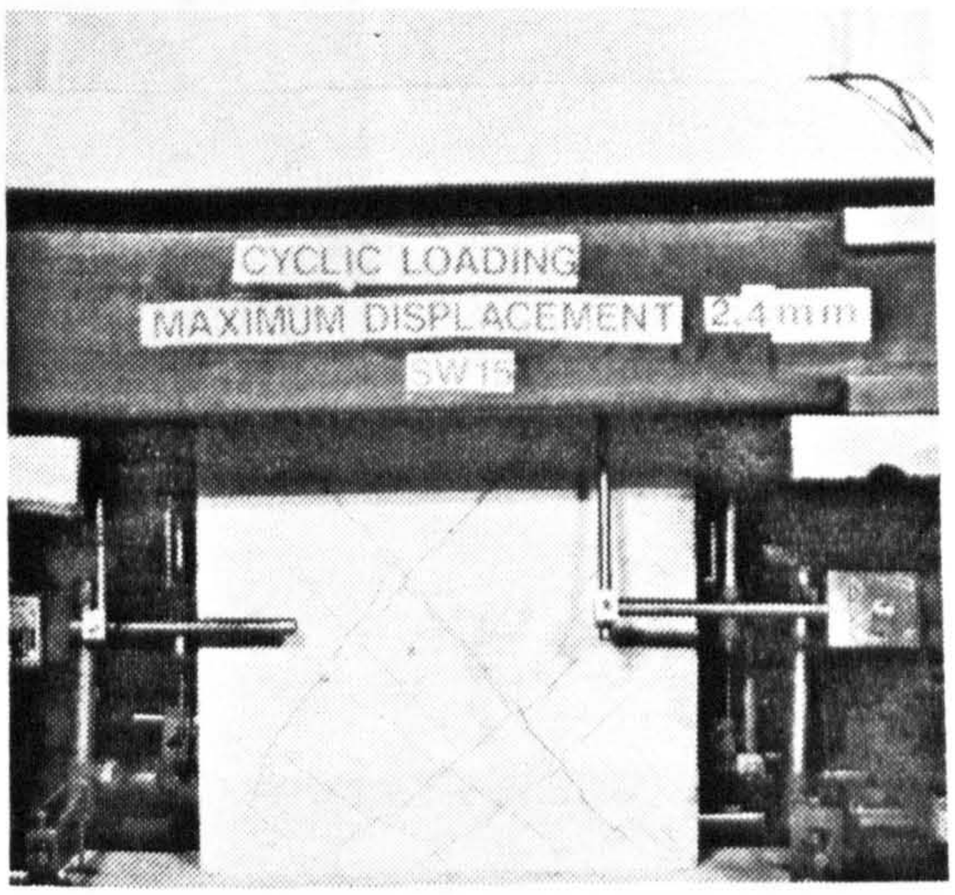
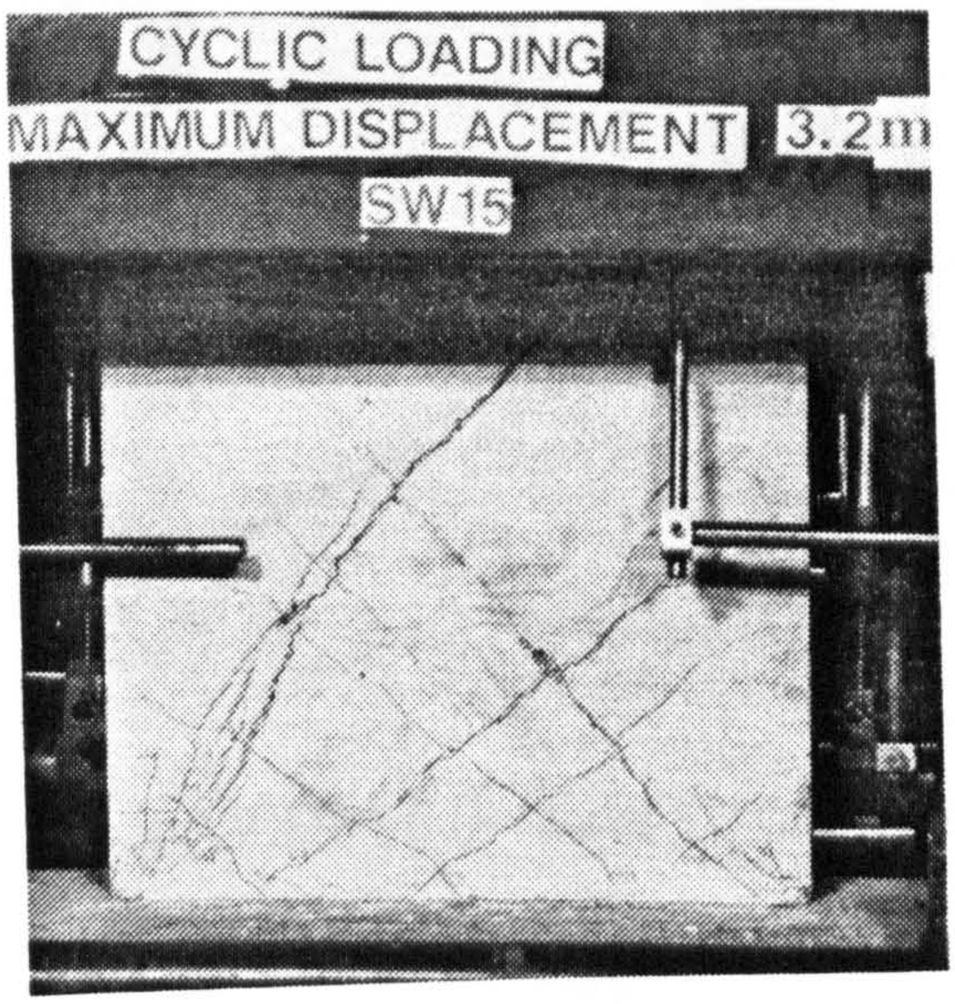


Figure A(14)2 Failure region of wall SW14









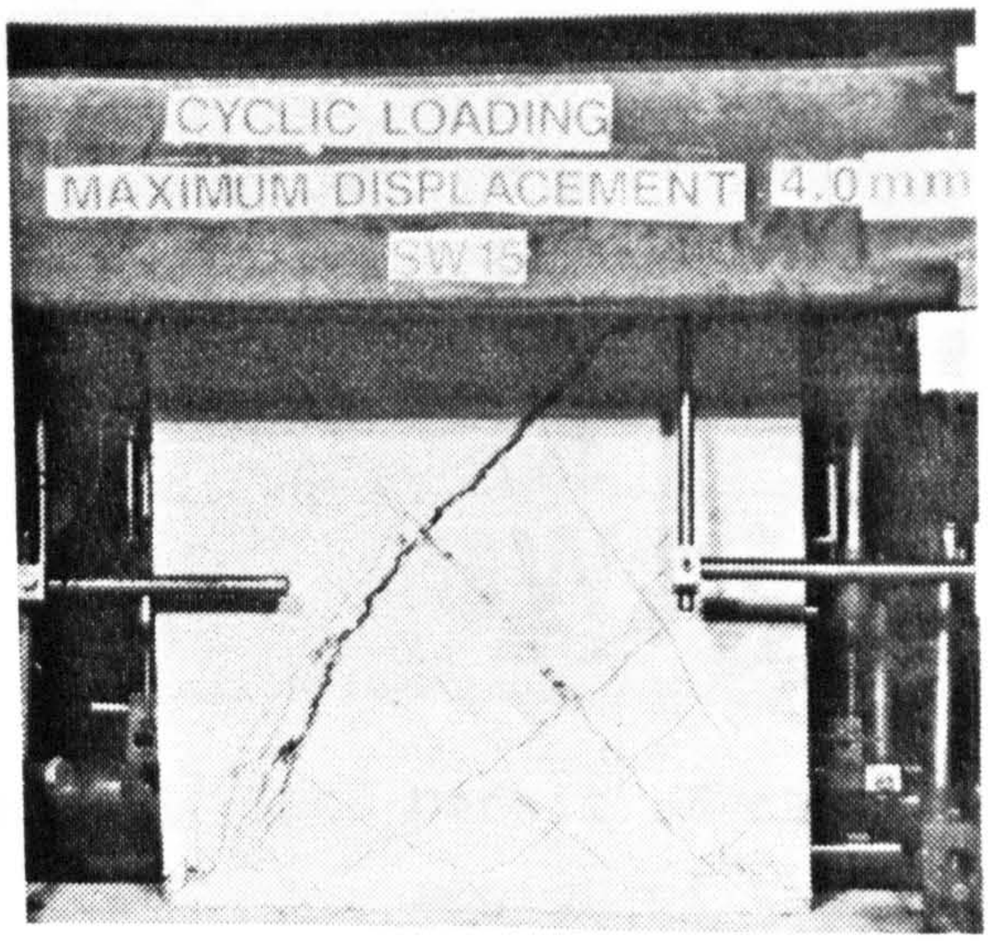


Figure A(15)1 Description of test of wall SW15

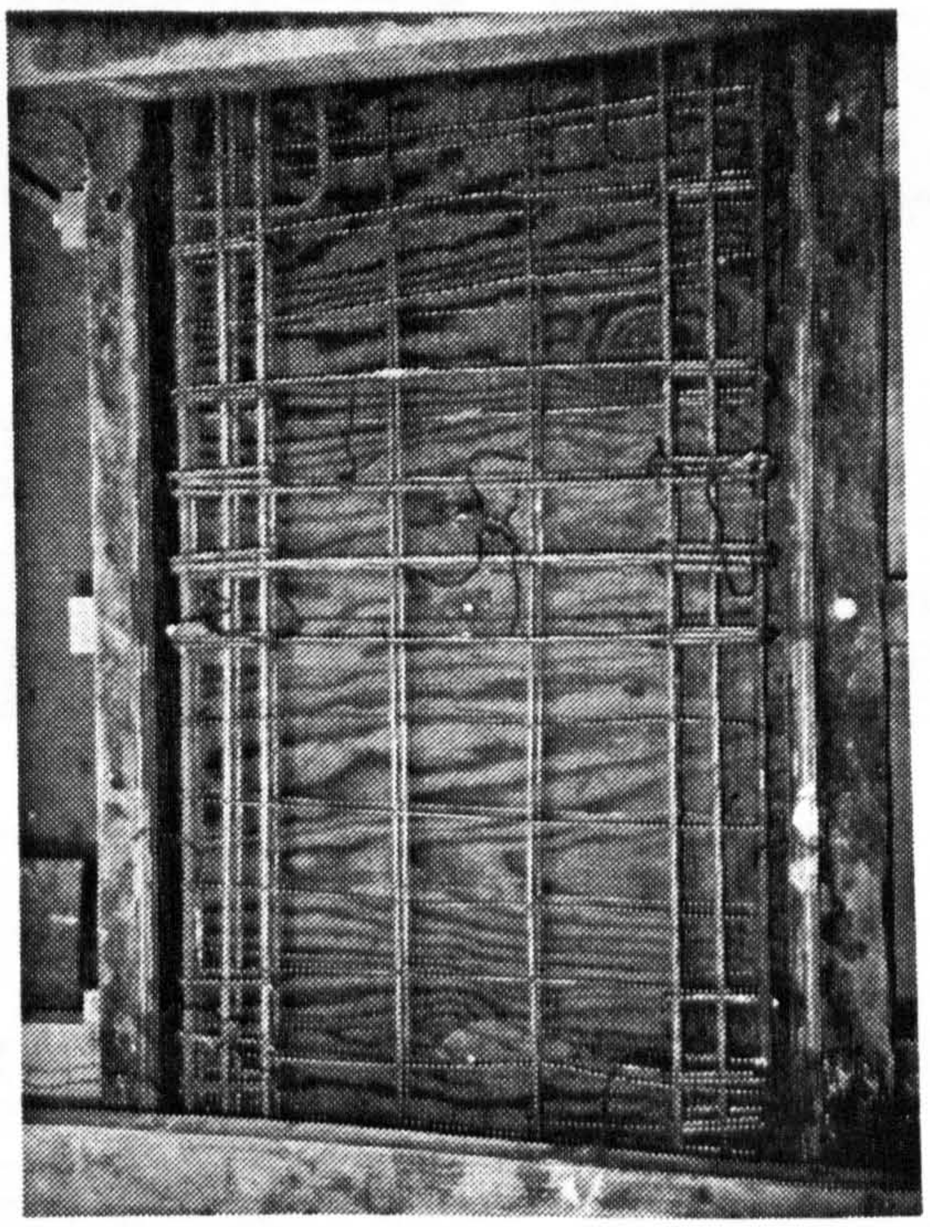


Figure A(15)2 Steel cage of wall SW15

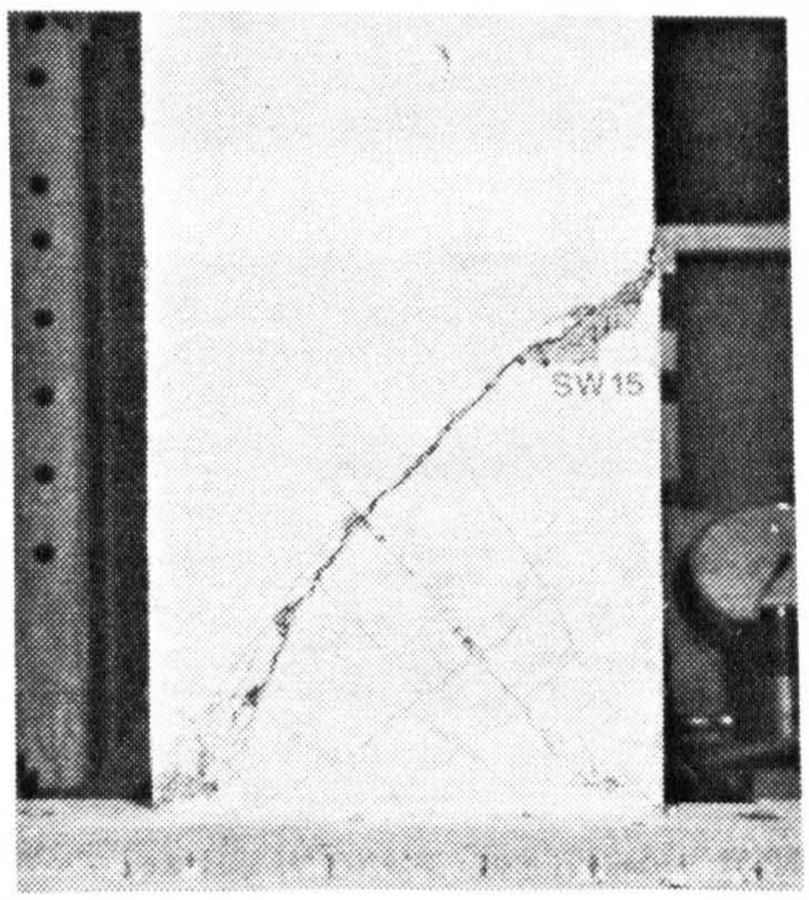


Figure A(15)3 Wall SW15 after the test

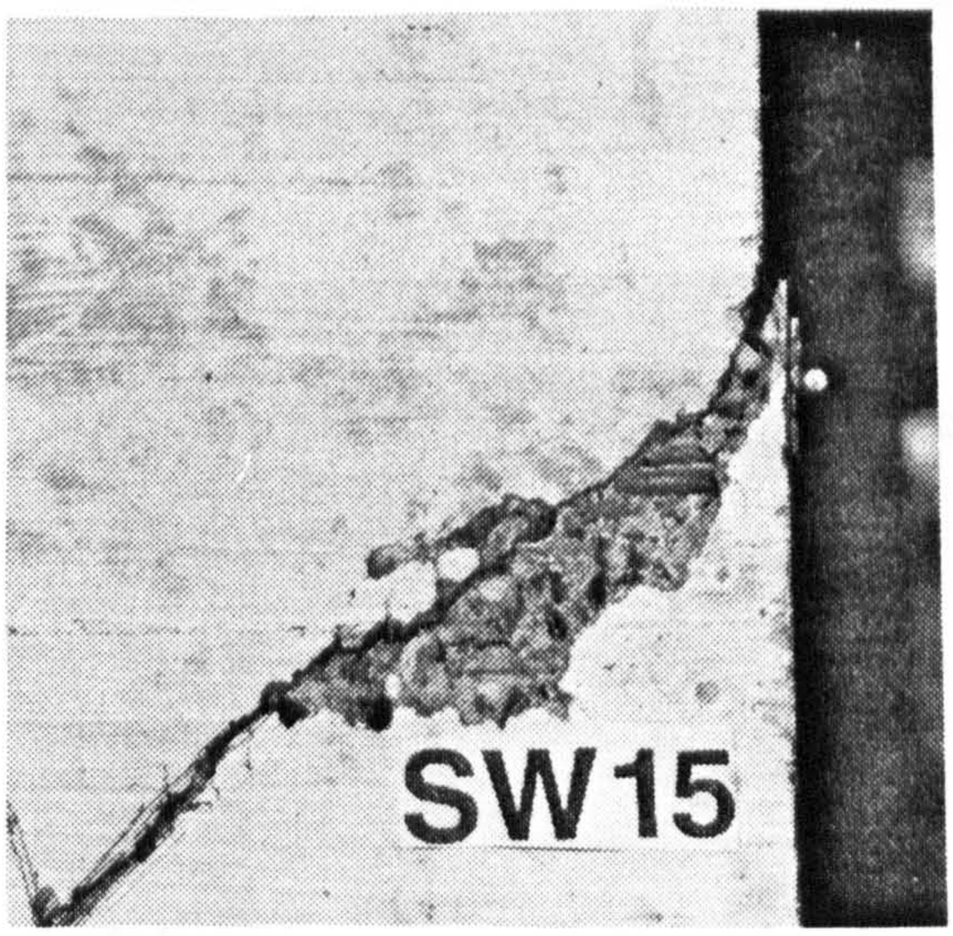
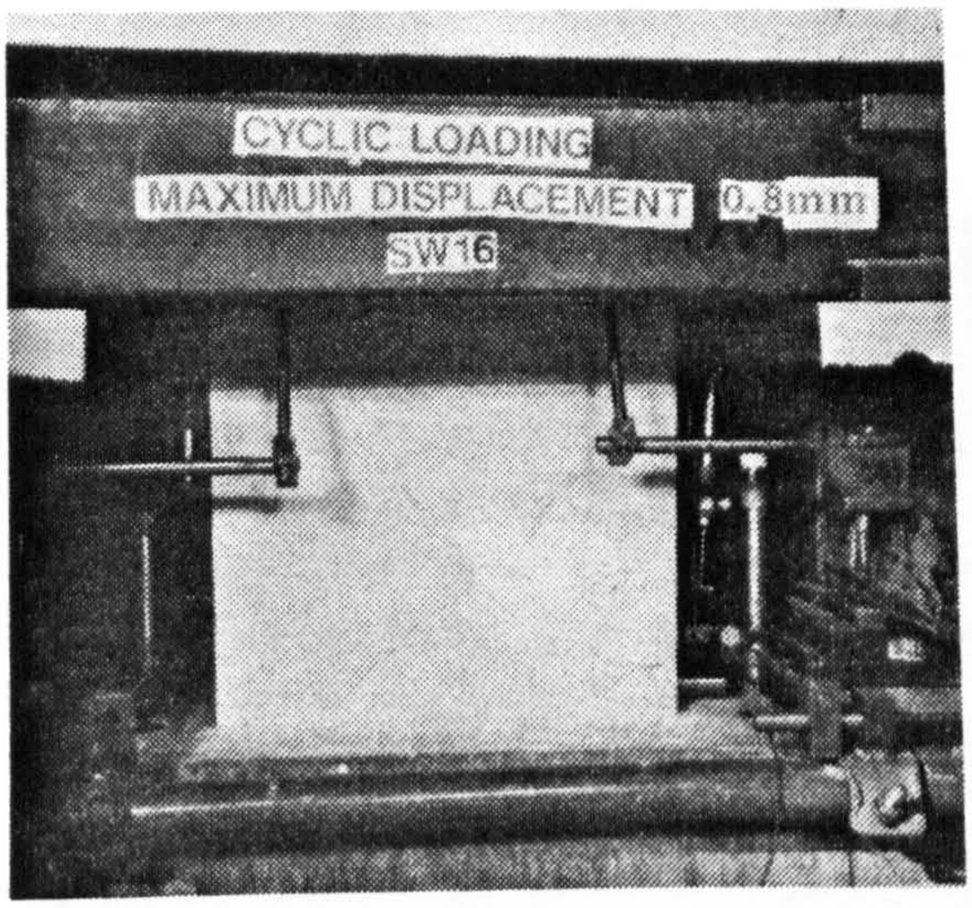
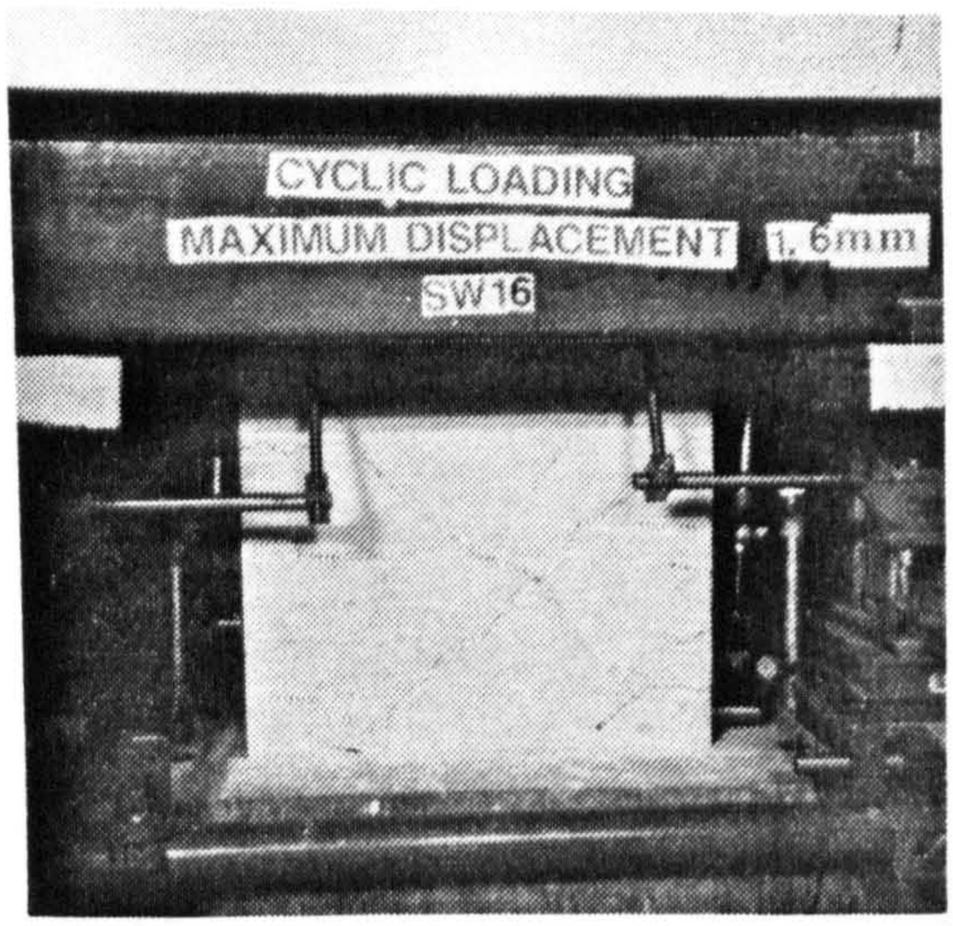
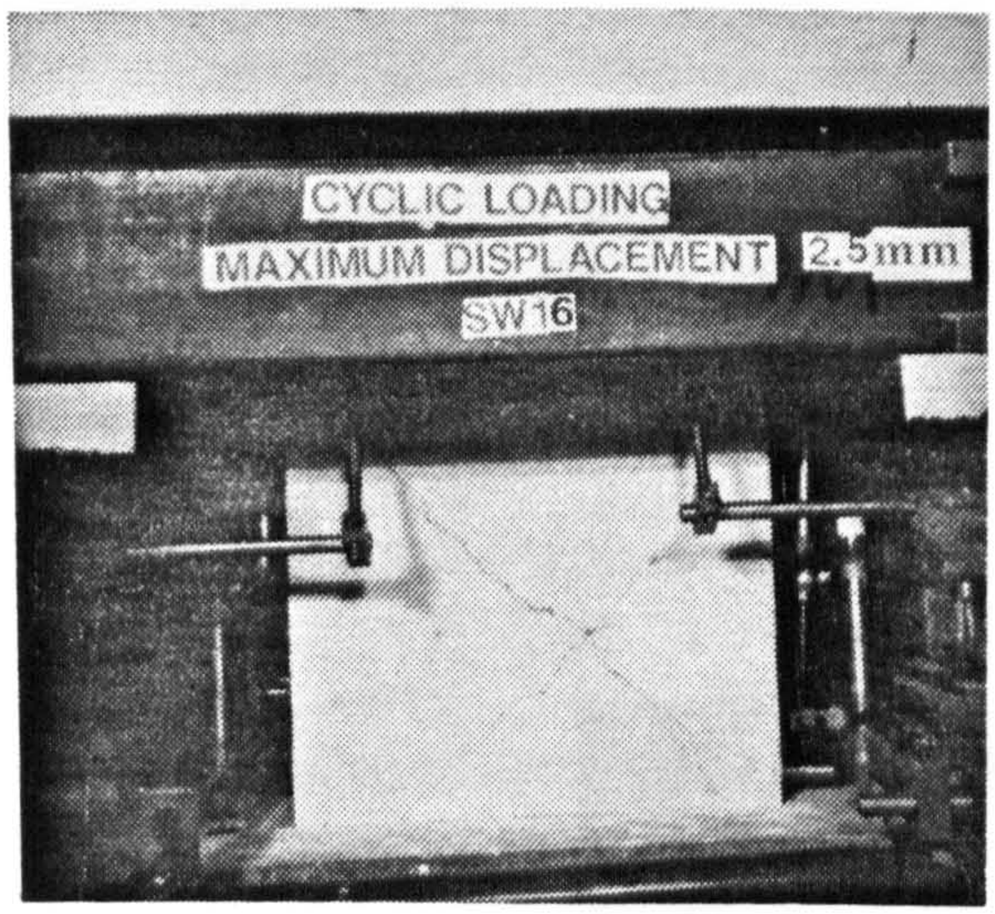
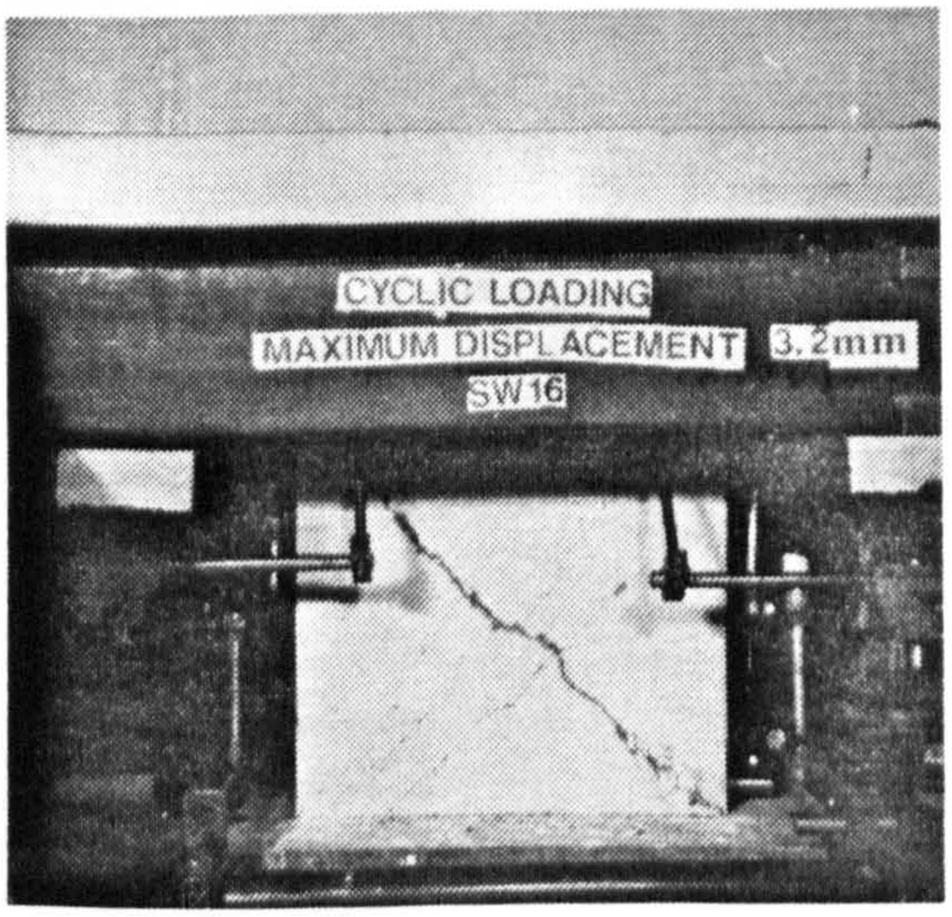


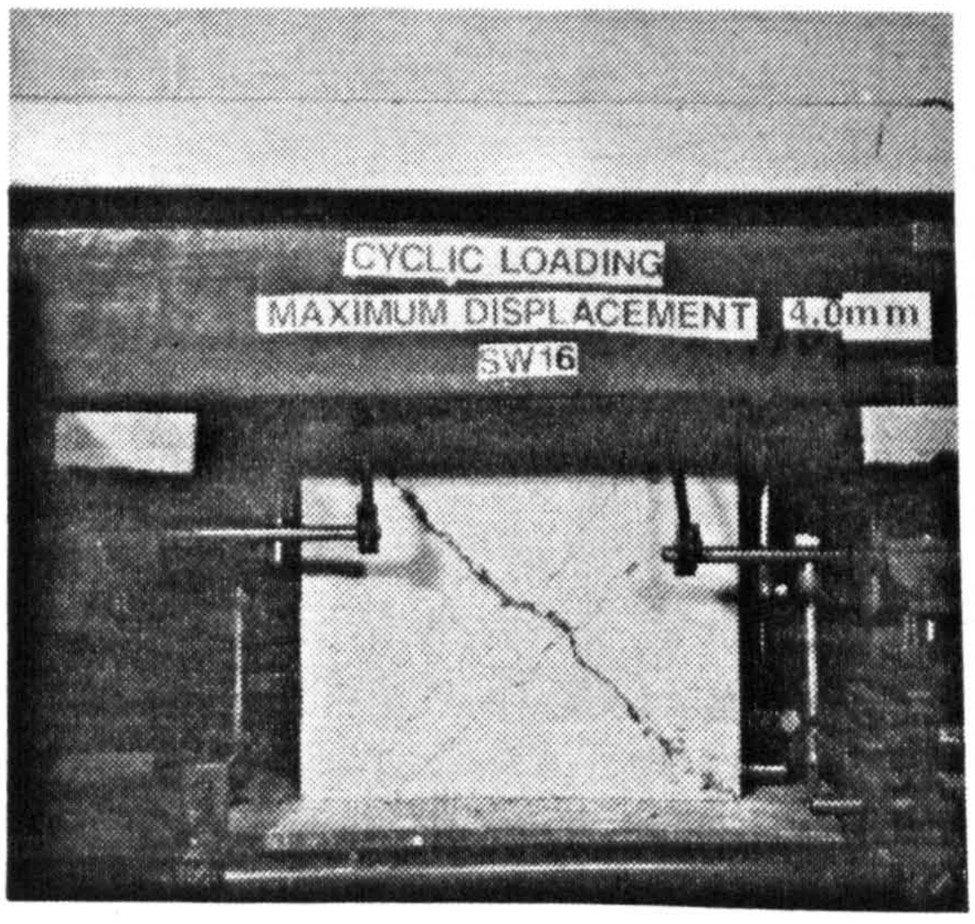
Figure A(15)4 Detail of the top region of the failure surface of wall SW15











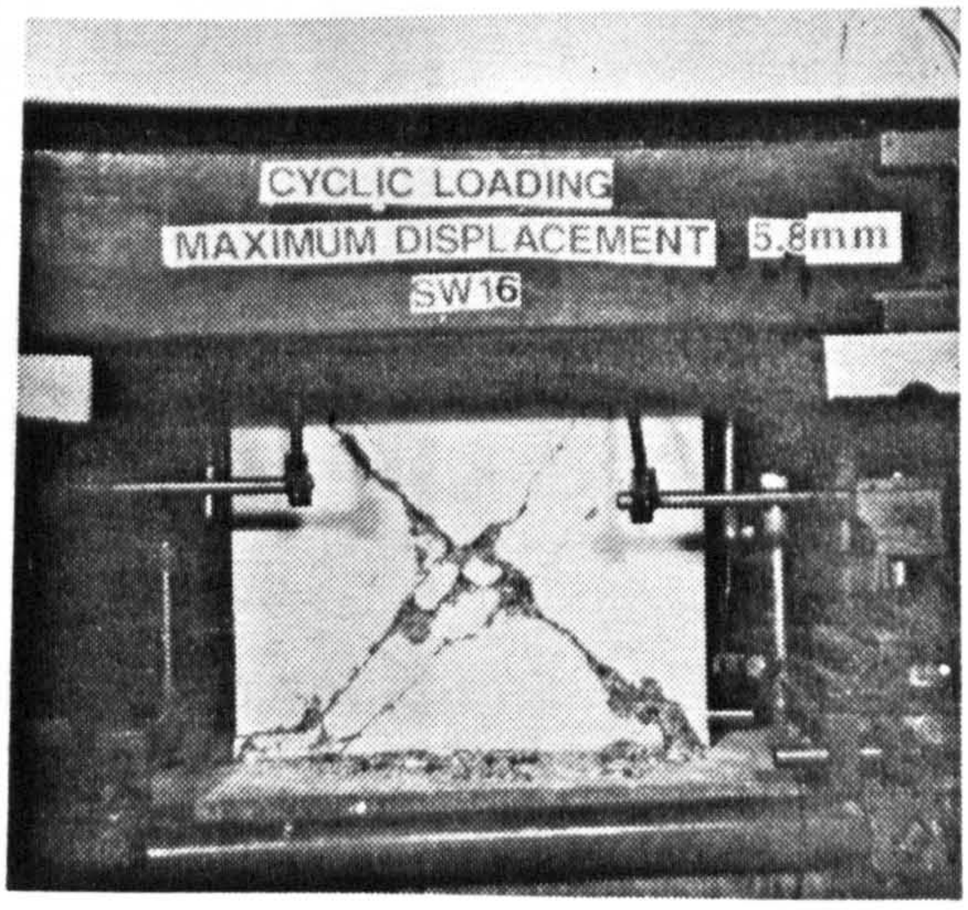


Figure A(16)1 Description of test of wall SW16

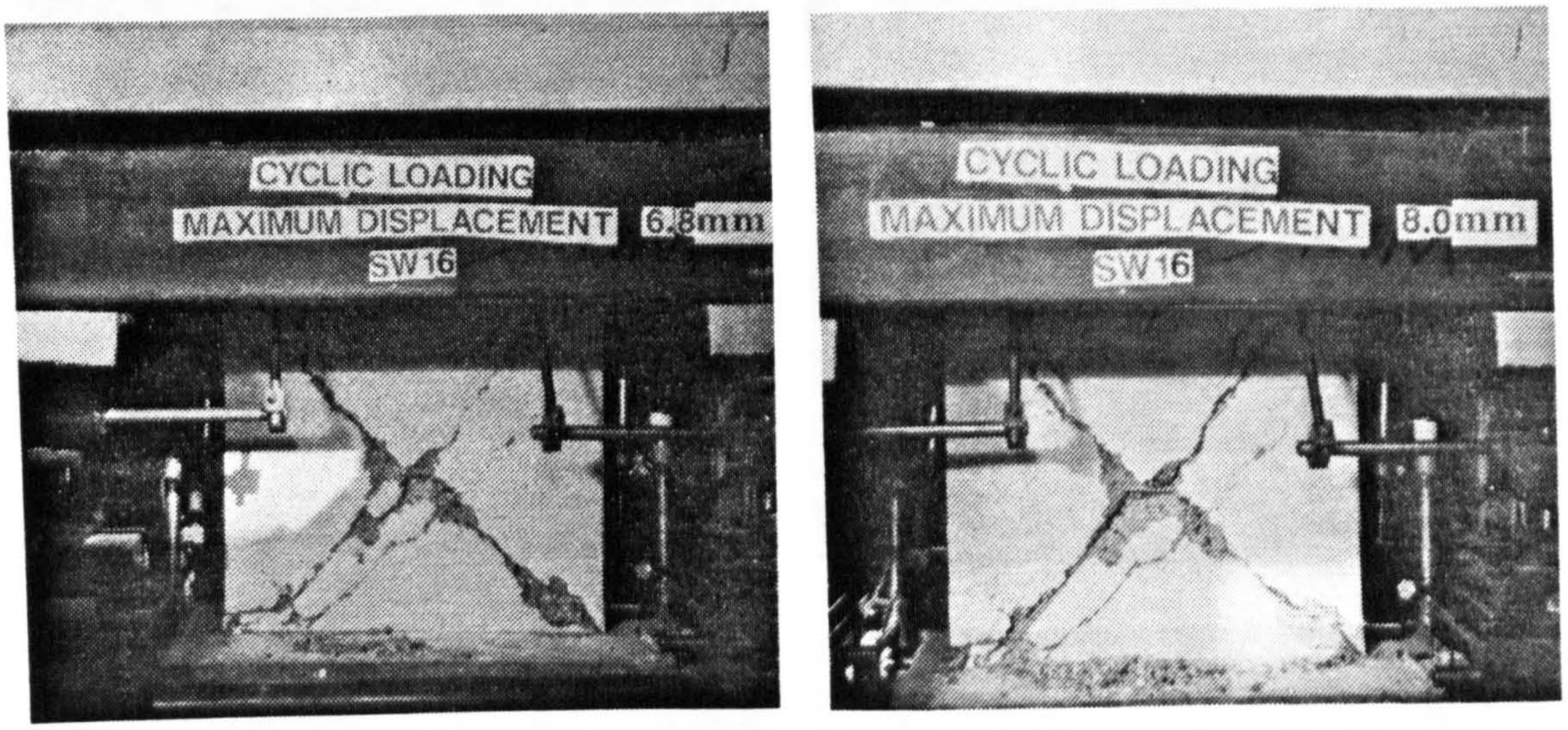


Figure A(16)1 Description of test of wall SW16 (cont.)

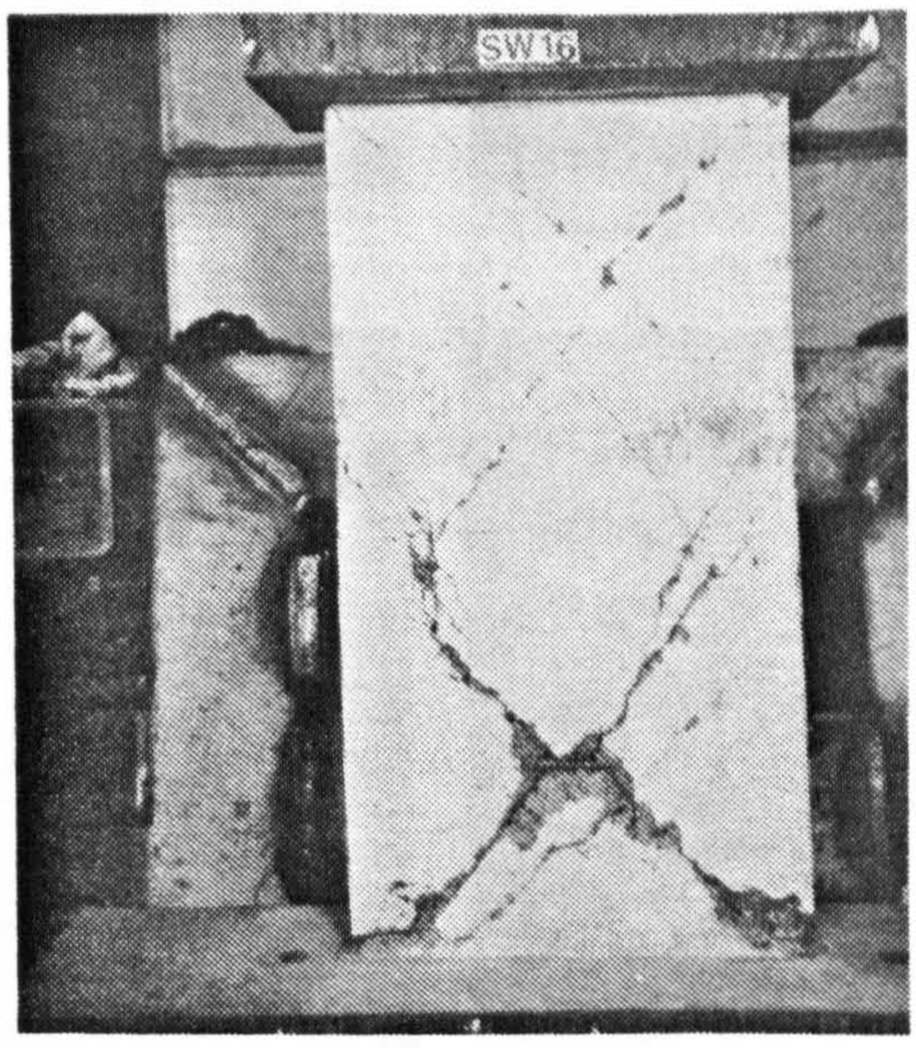
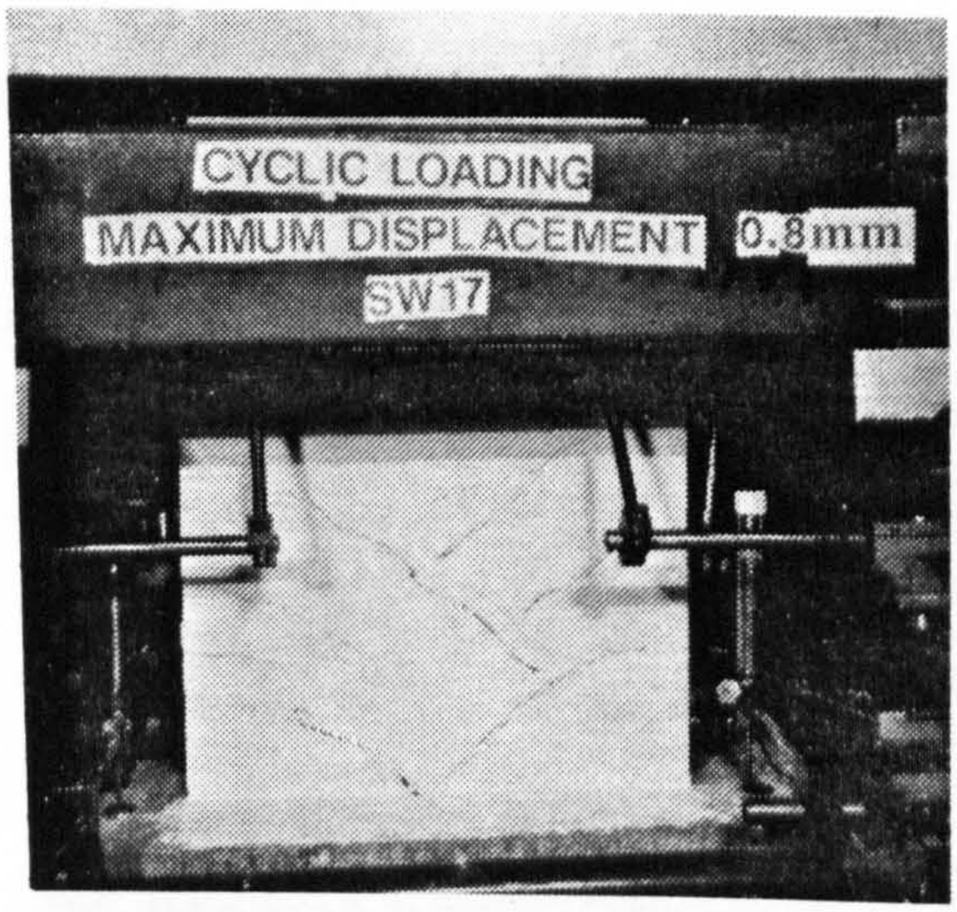
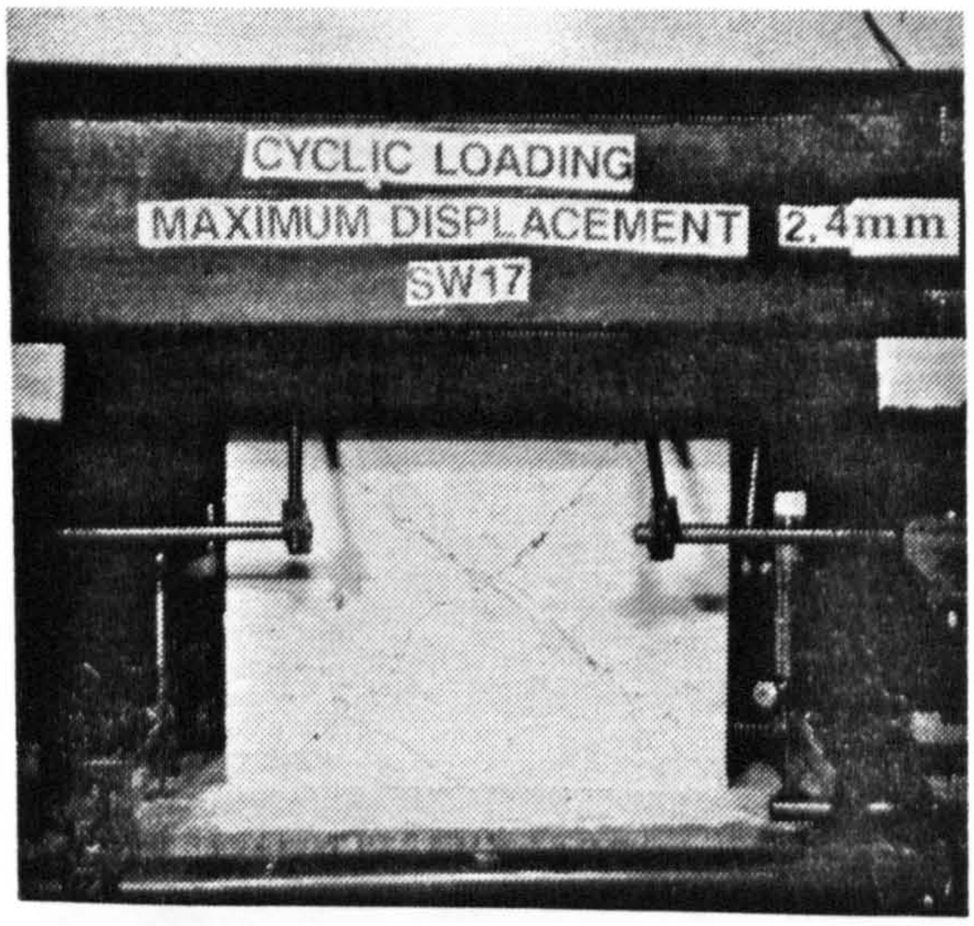
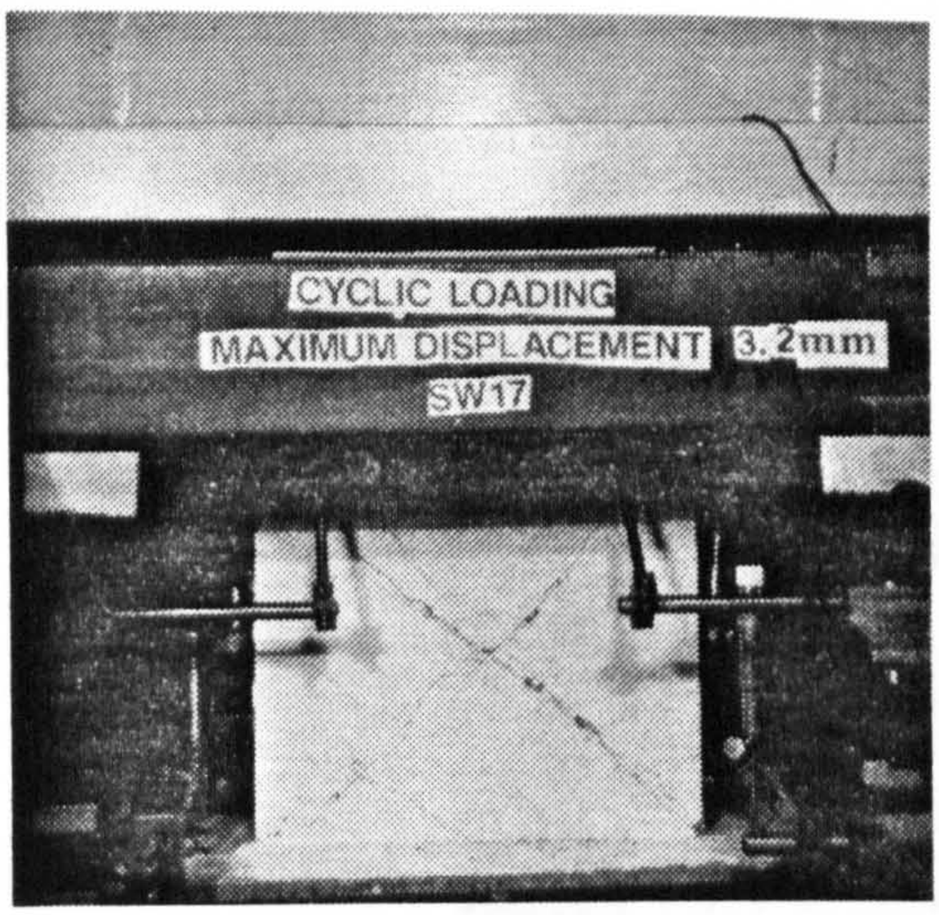
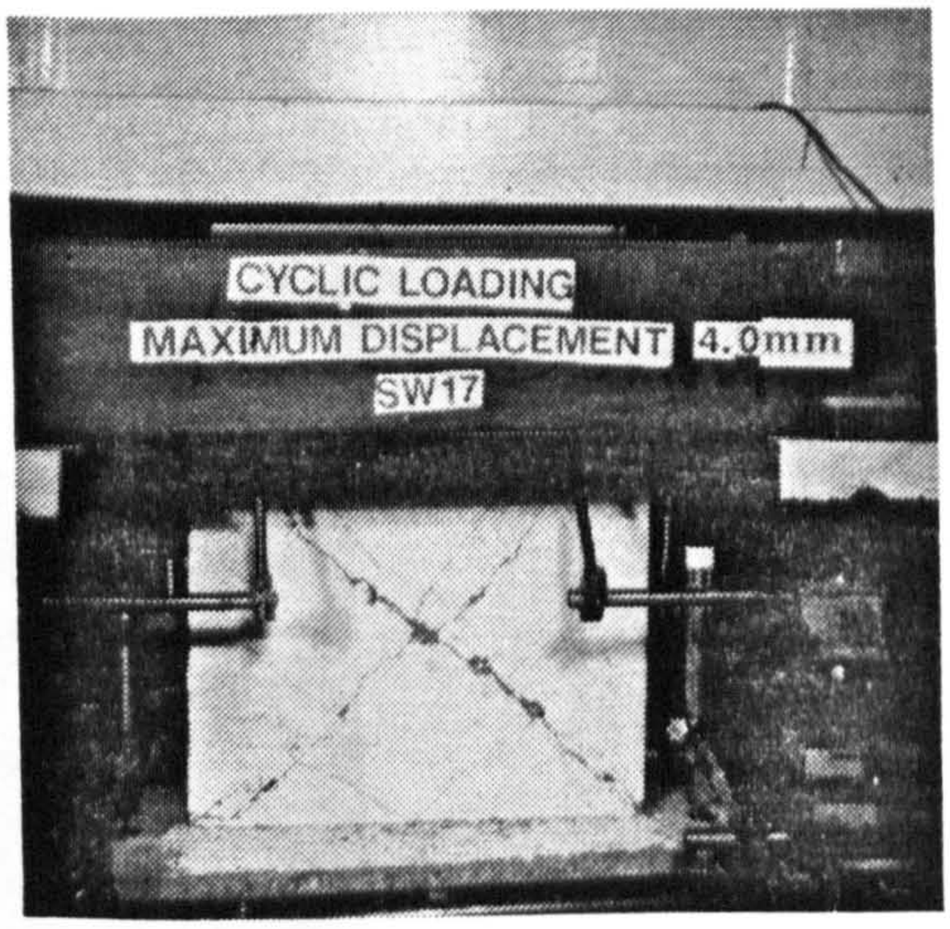


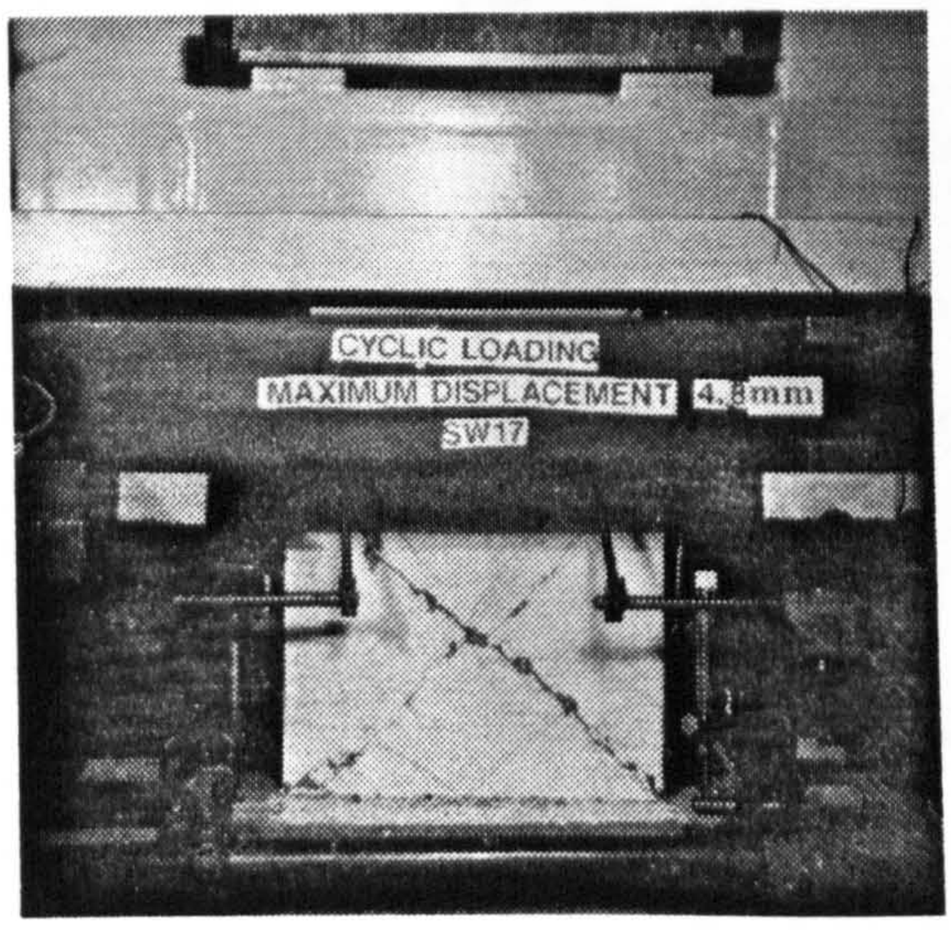
Figure A(16)2 Wall SW16 after the test











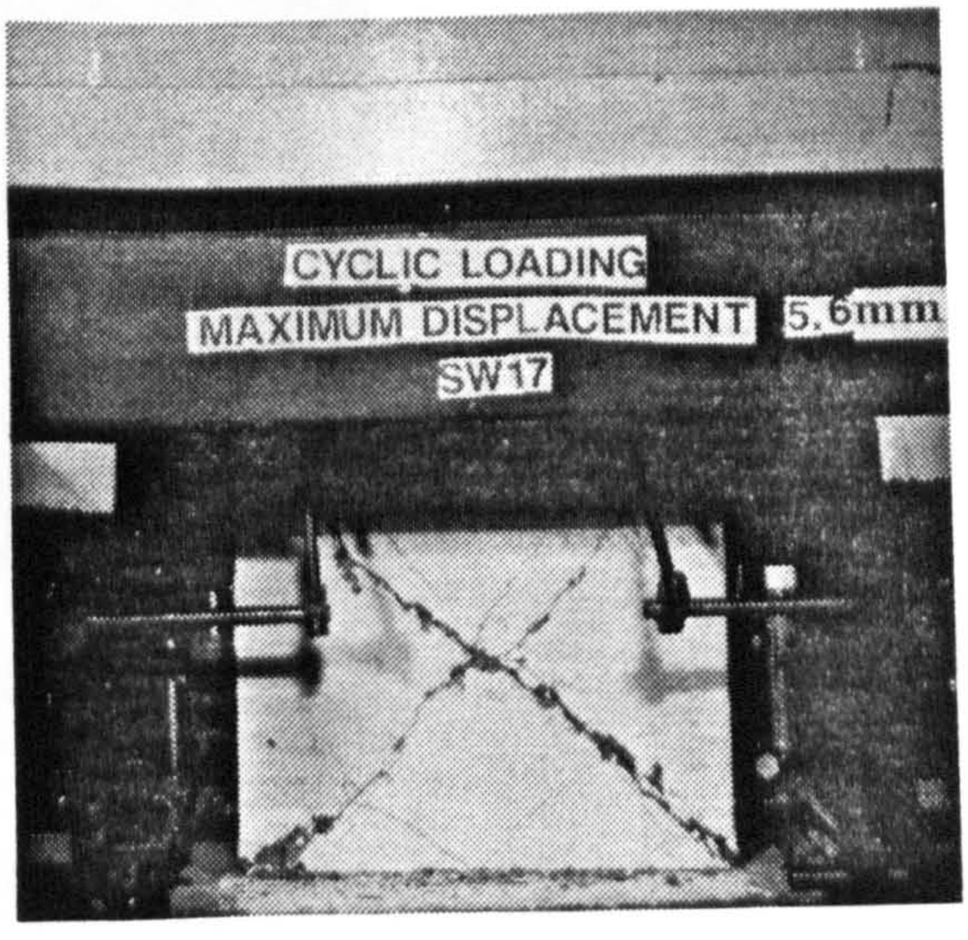


Figure A(17)1 Description of test of wall SW17

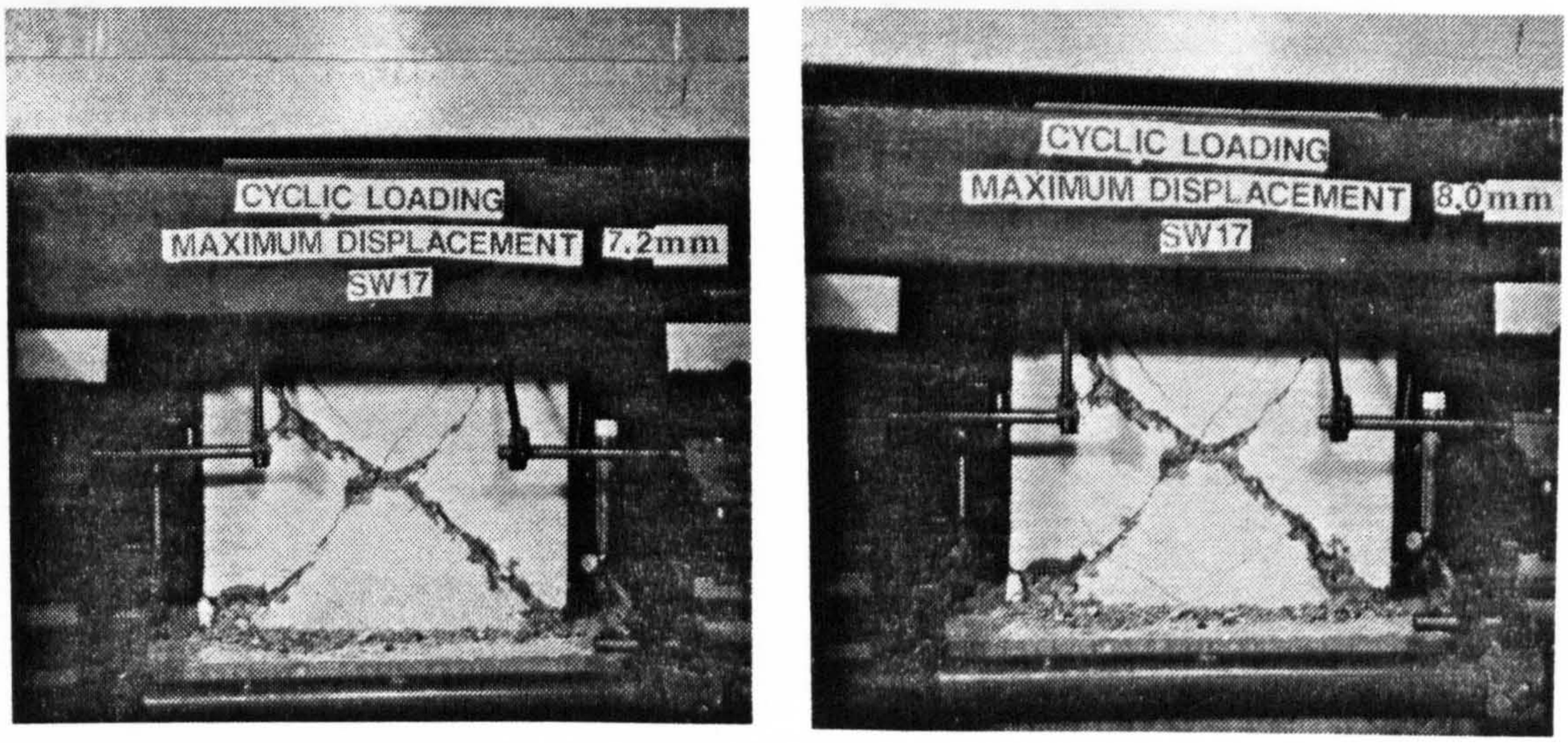


Figure A(17)1 Description of test of wall SW17 (cont.)

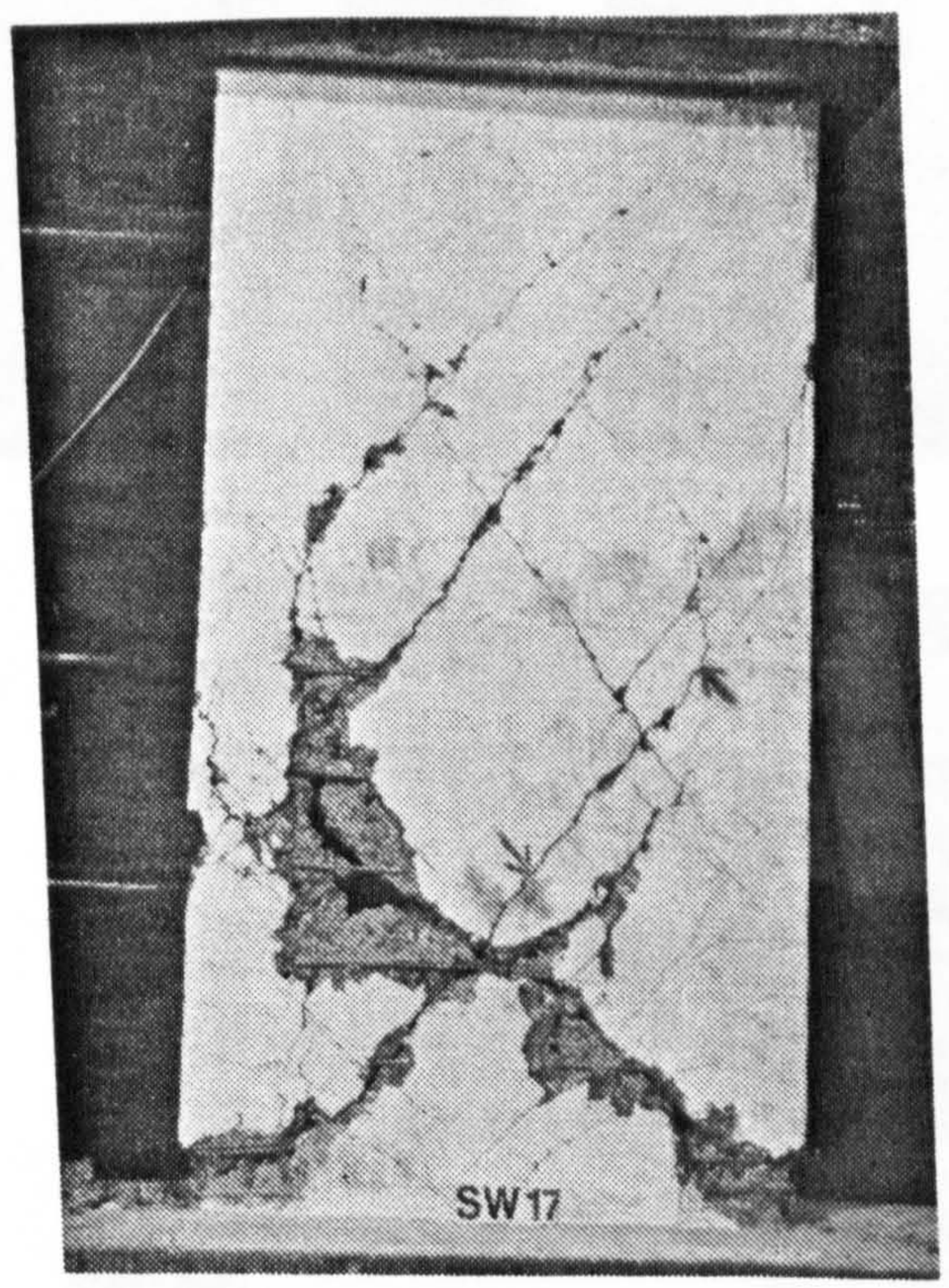
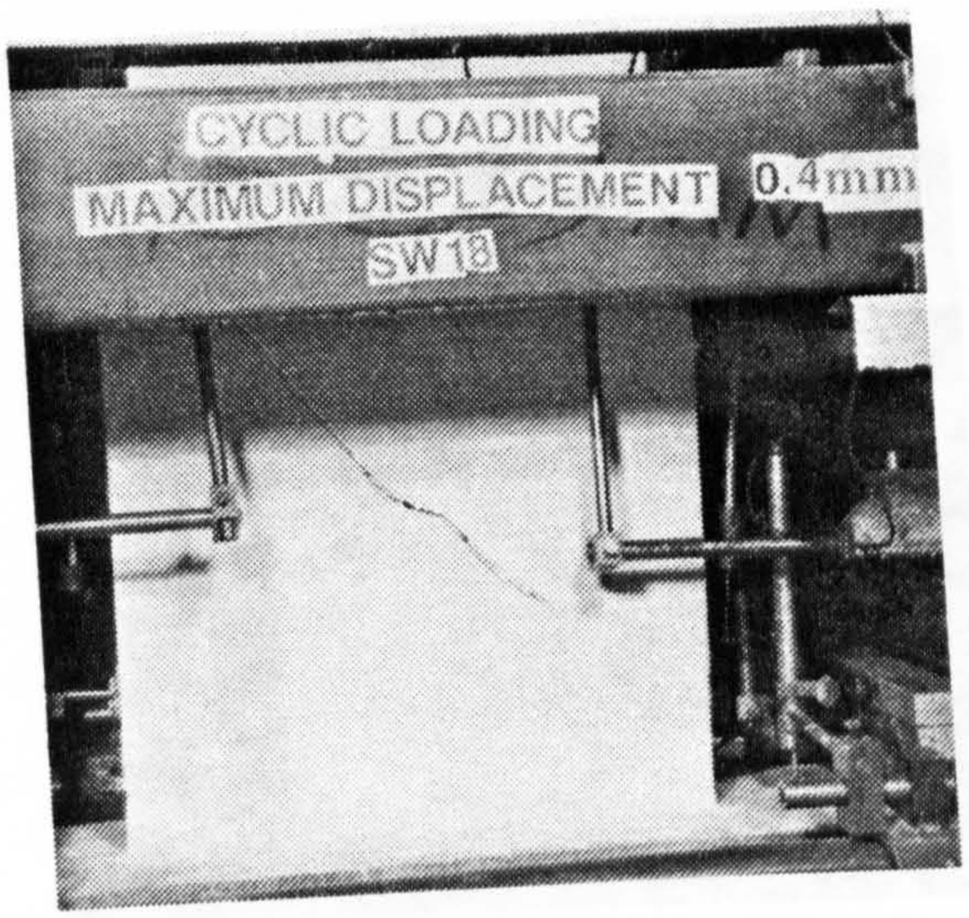
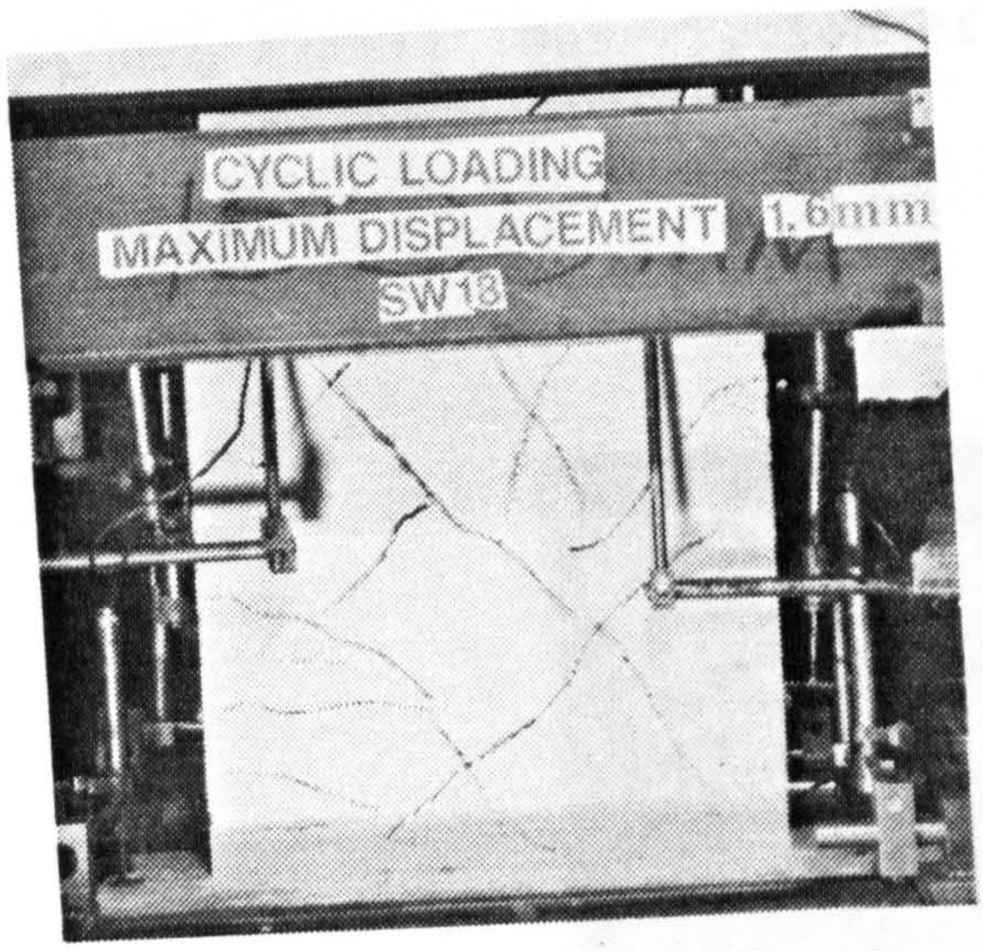
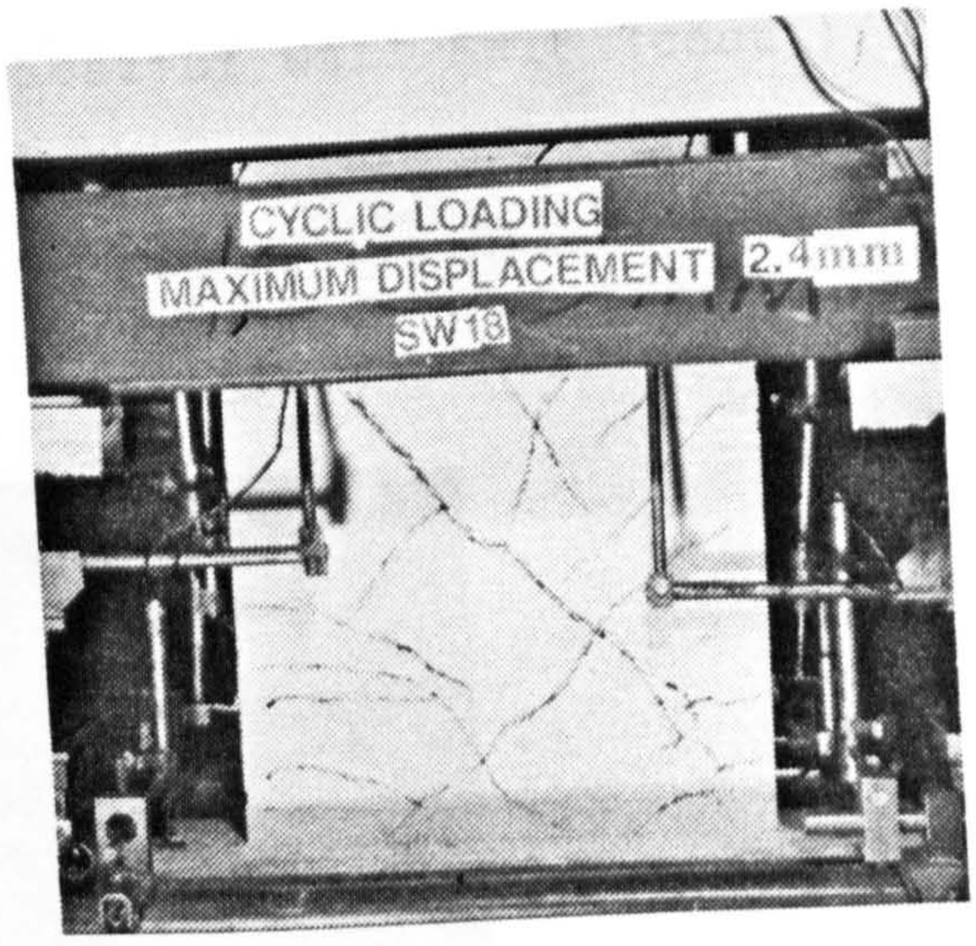


Figure A(17)2 Wall SW17 after the test









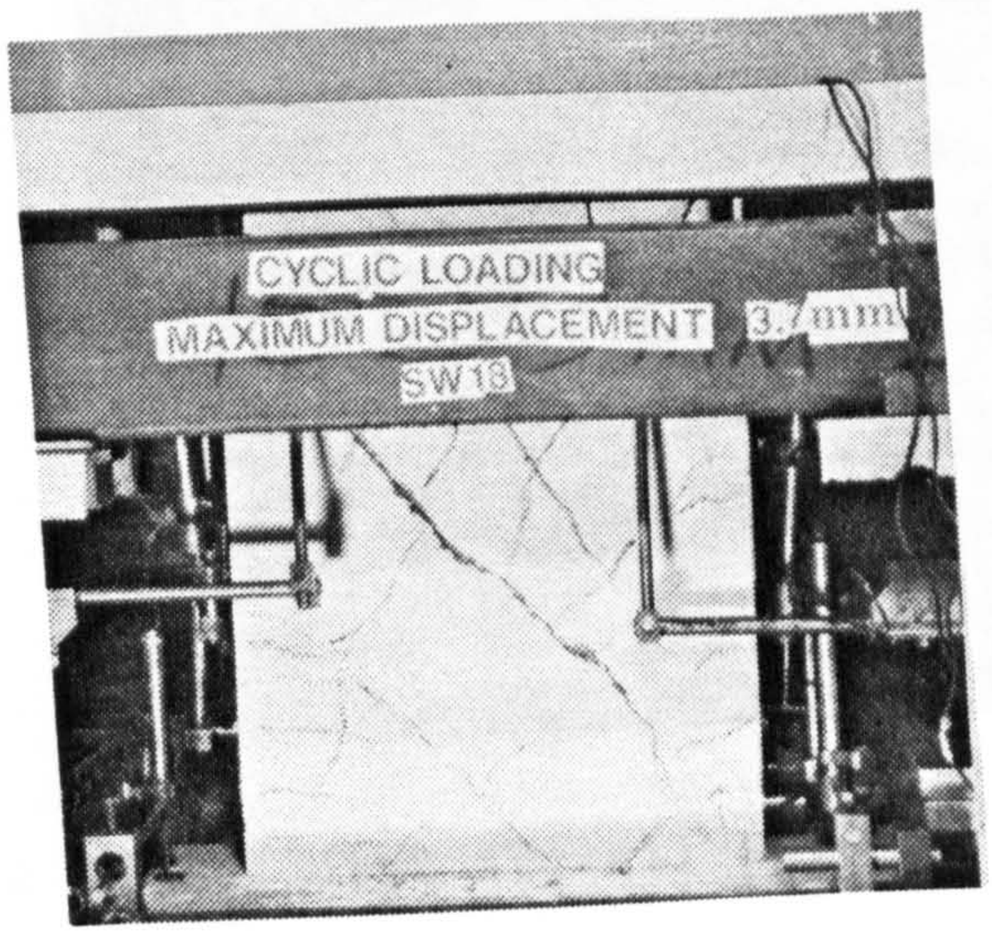


Figure A(18)1 Description of test of wall SW18

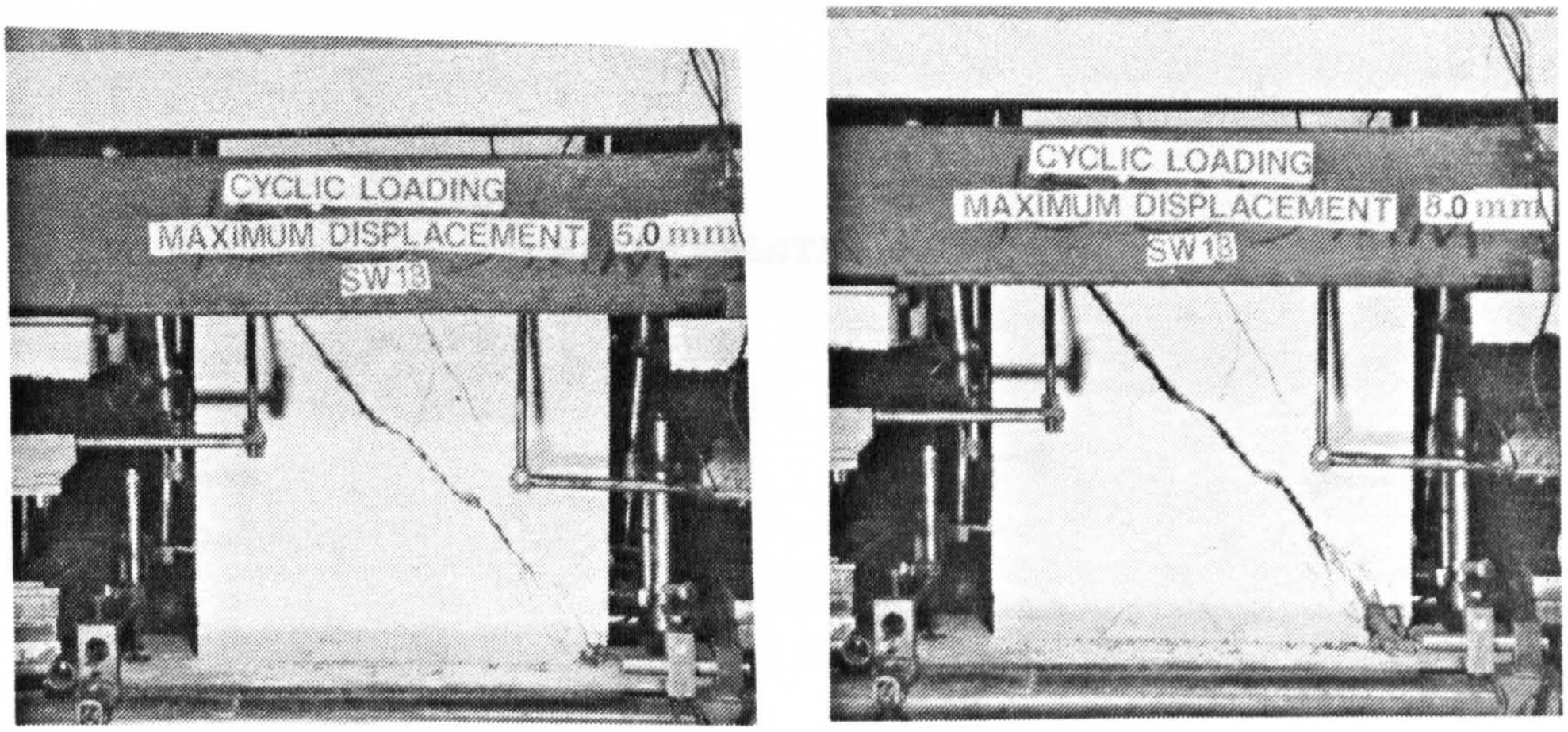


Figure A(18)1 Description of test of wall SW18 (cont.)

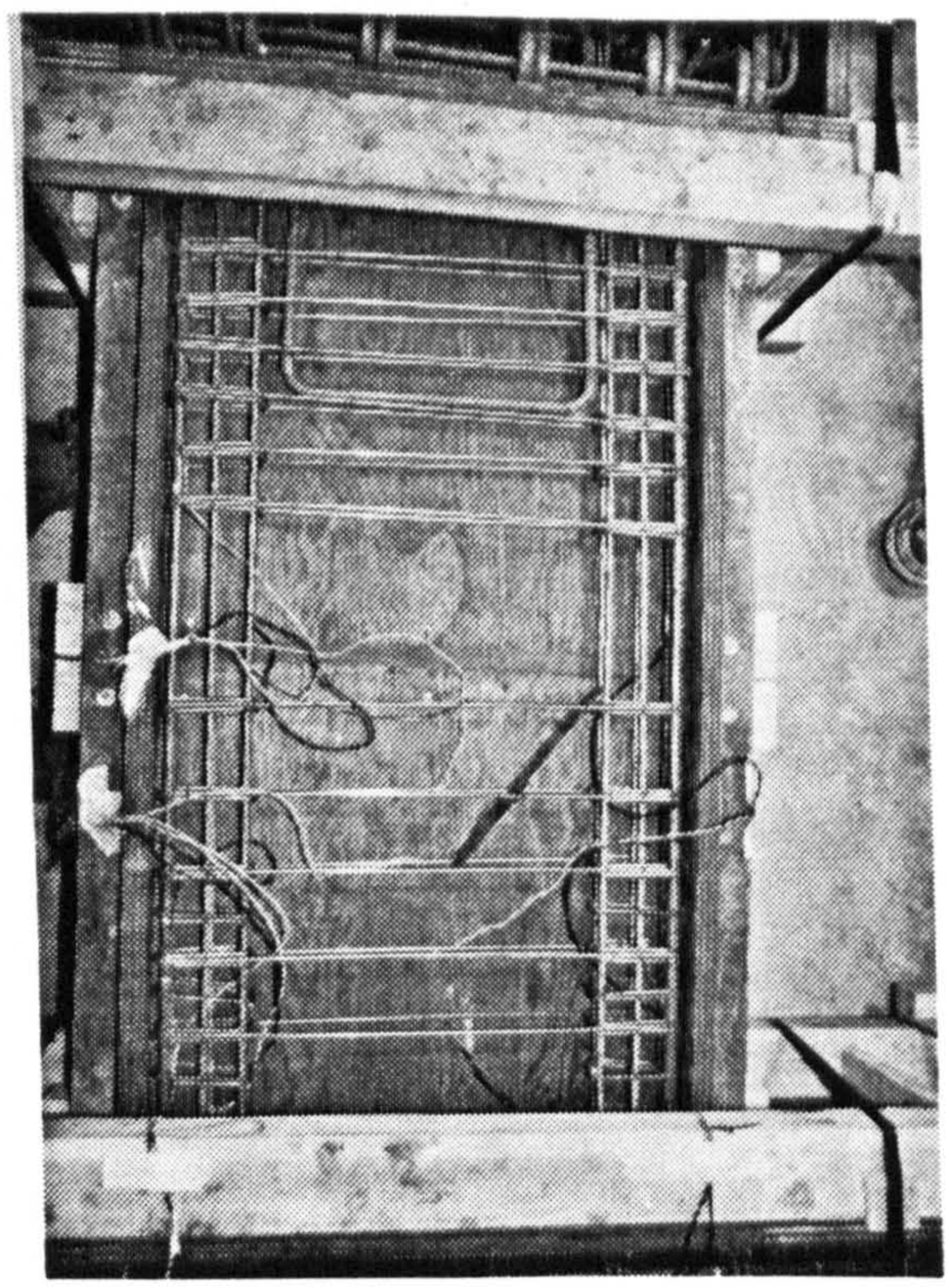


Figure A(18)2 Steel cage of wall SW18

APPENDIX B

EXPERIMENTAL RESULTS

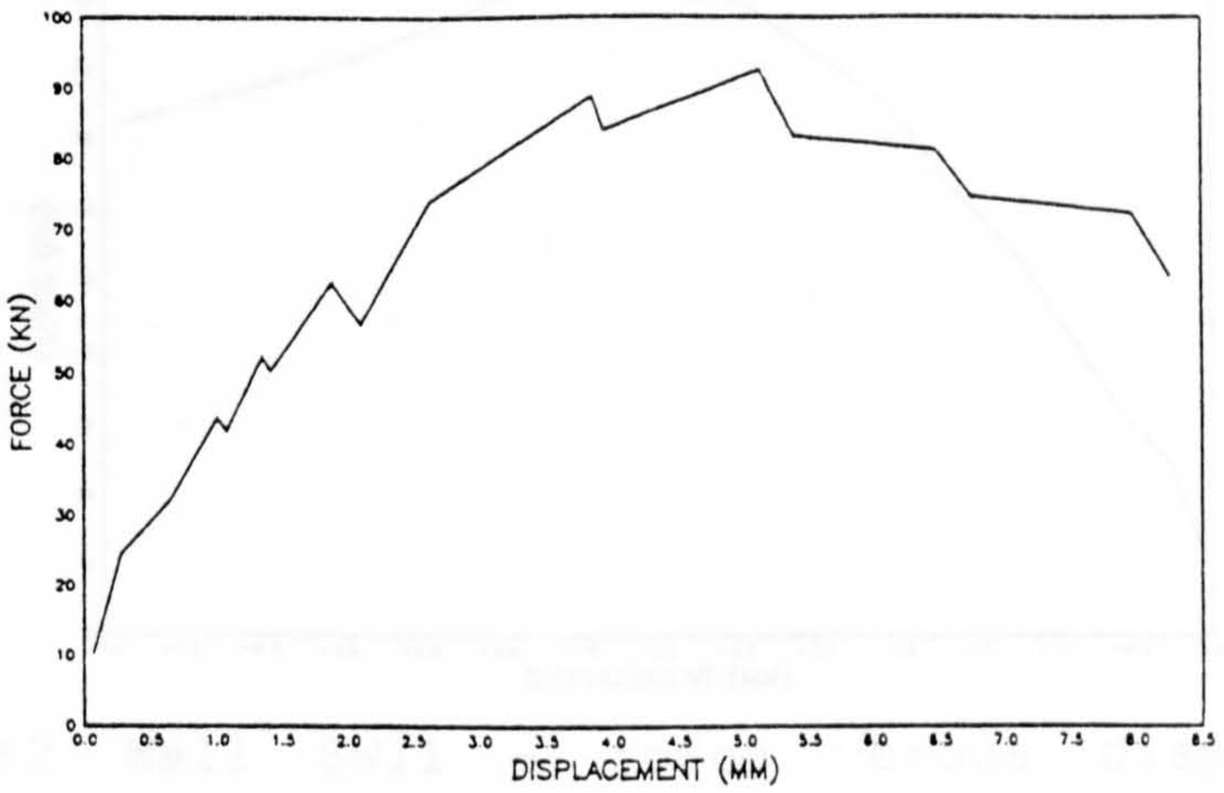


Figure B(11)1.a Wall SW11 - force versus displacement 1 (horizontal, LHS, level 4, all readings)

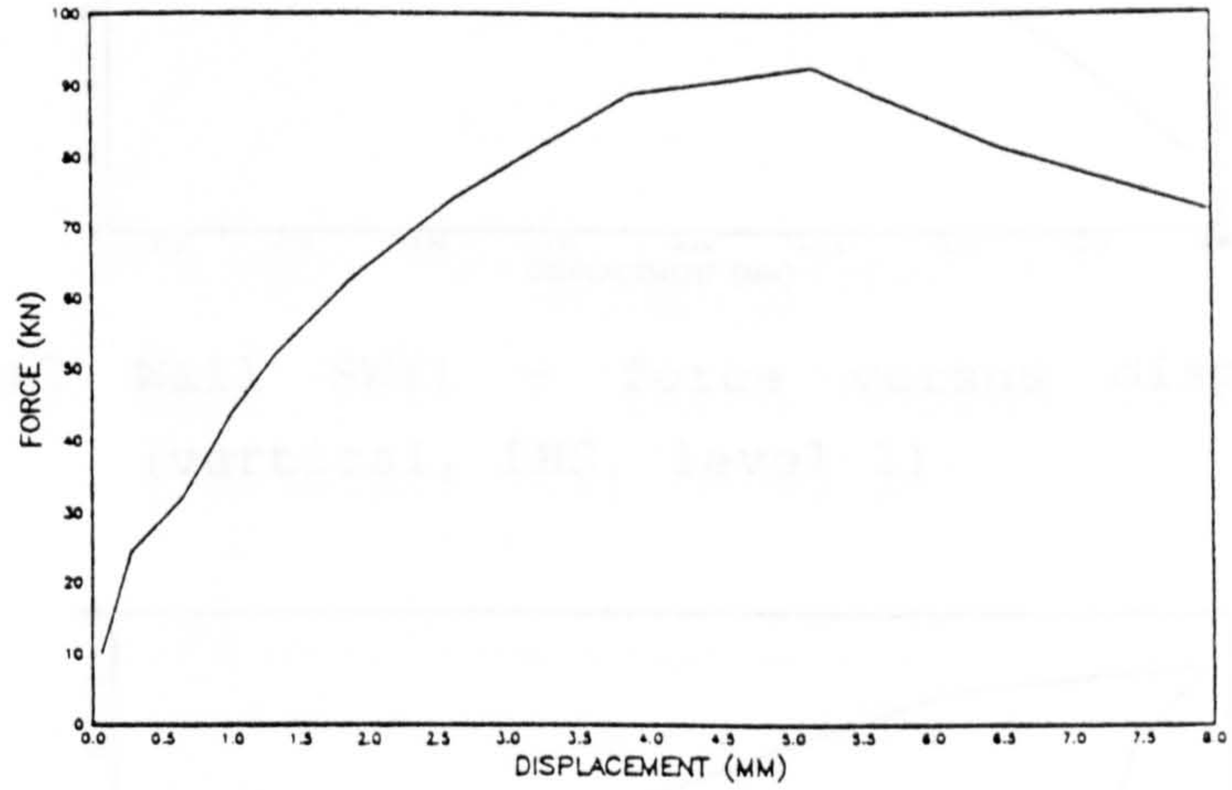


Figure B(11)1.b Wall SW11 - force versus displacement 1 (horizontal, LHS, level 4)

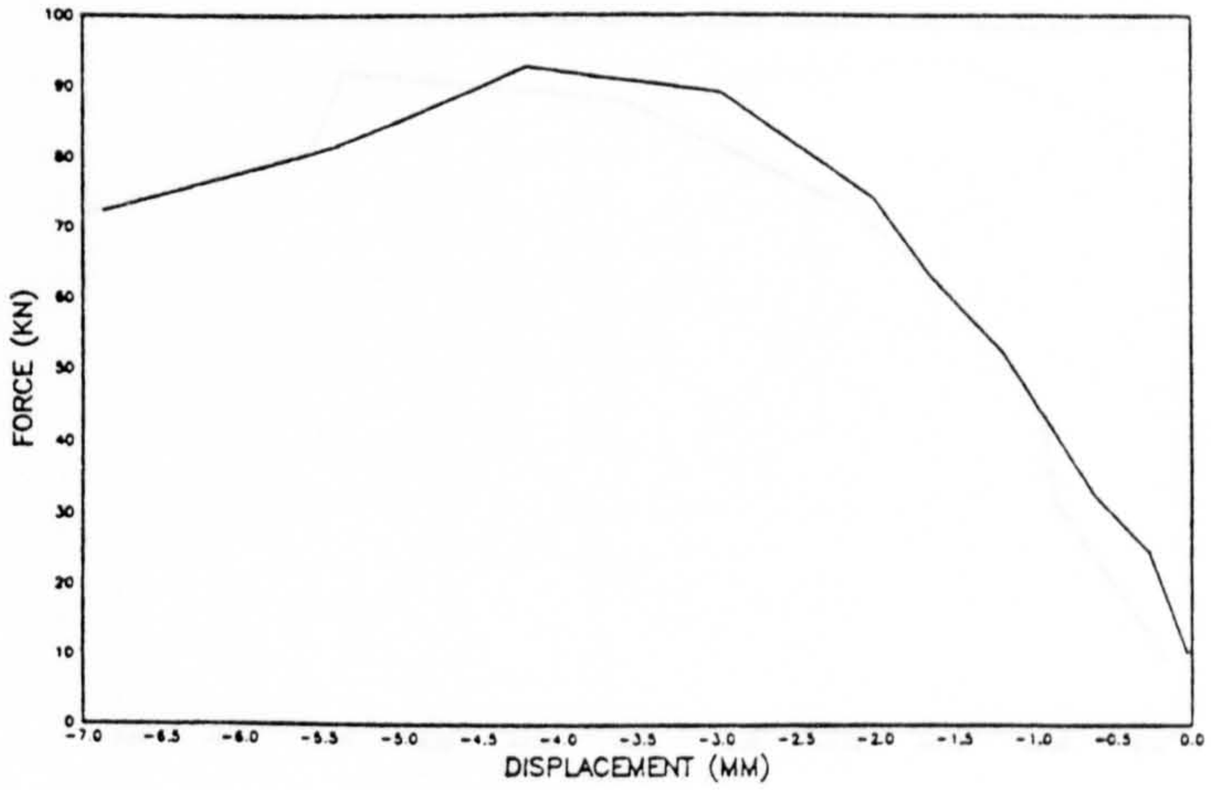


Figure B(11)2 Wall SW11 - force versus displacement 2 (horizontal, RHS, level 4)

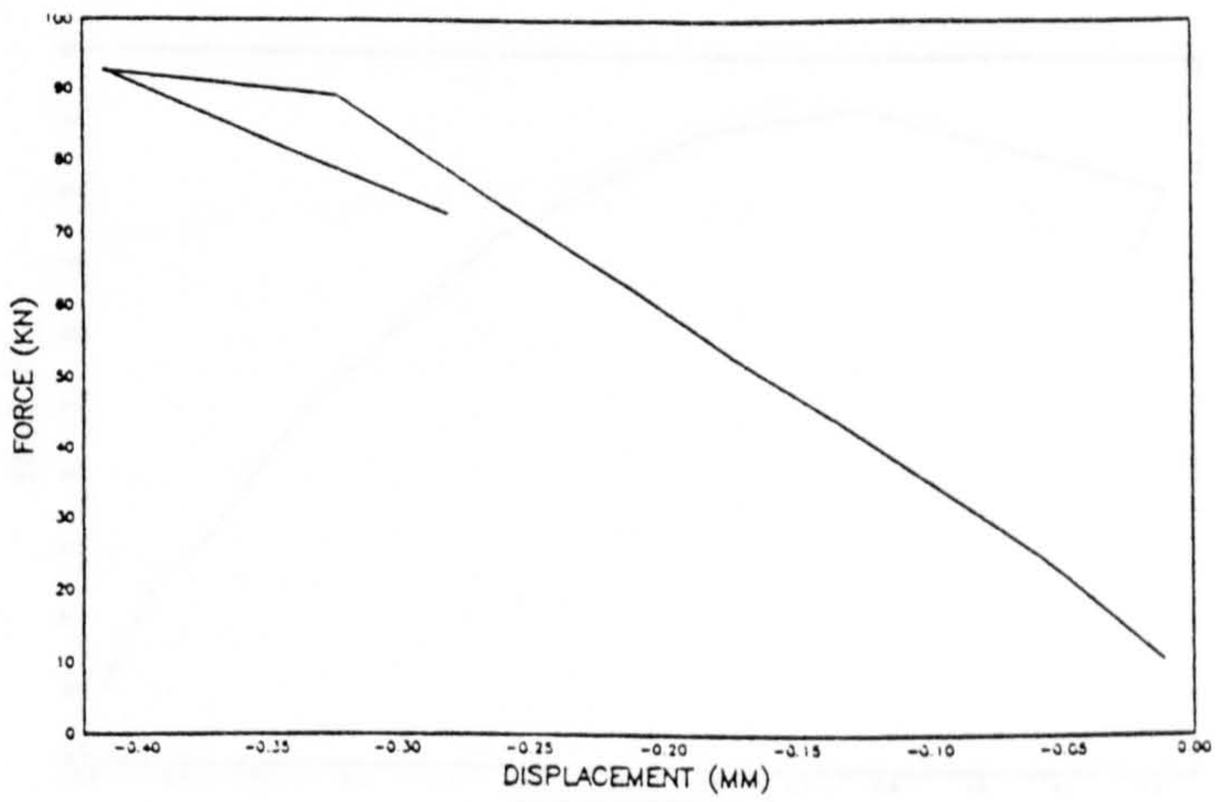


Figure B(11)3 Wall SW11 - force versus displacement 3 (vertical, LHS, level 1)

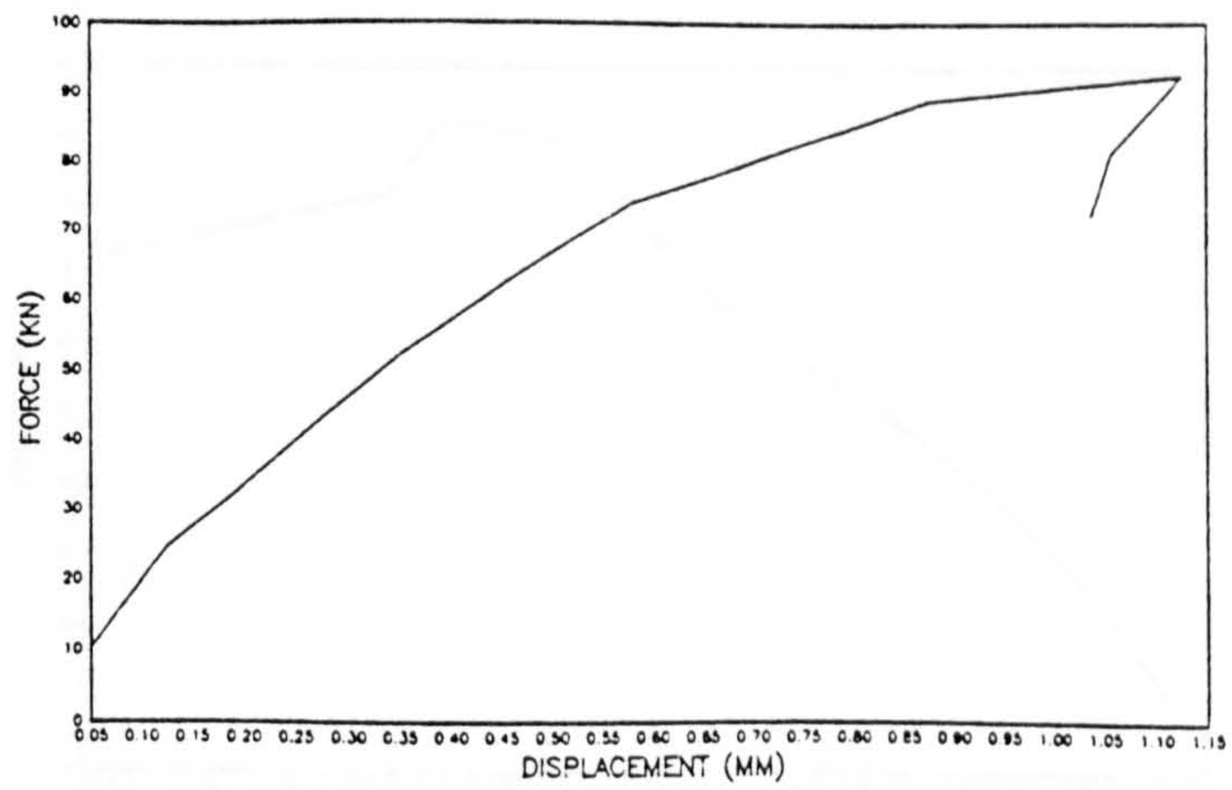


Figure B(11)4 Wall SW11 - force versus displacement 4 (vertical, RHS, level 1)

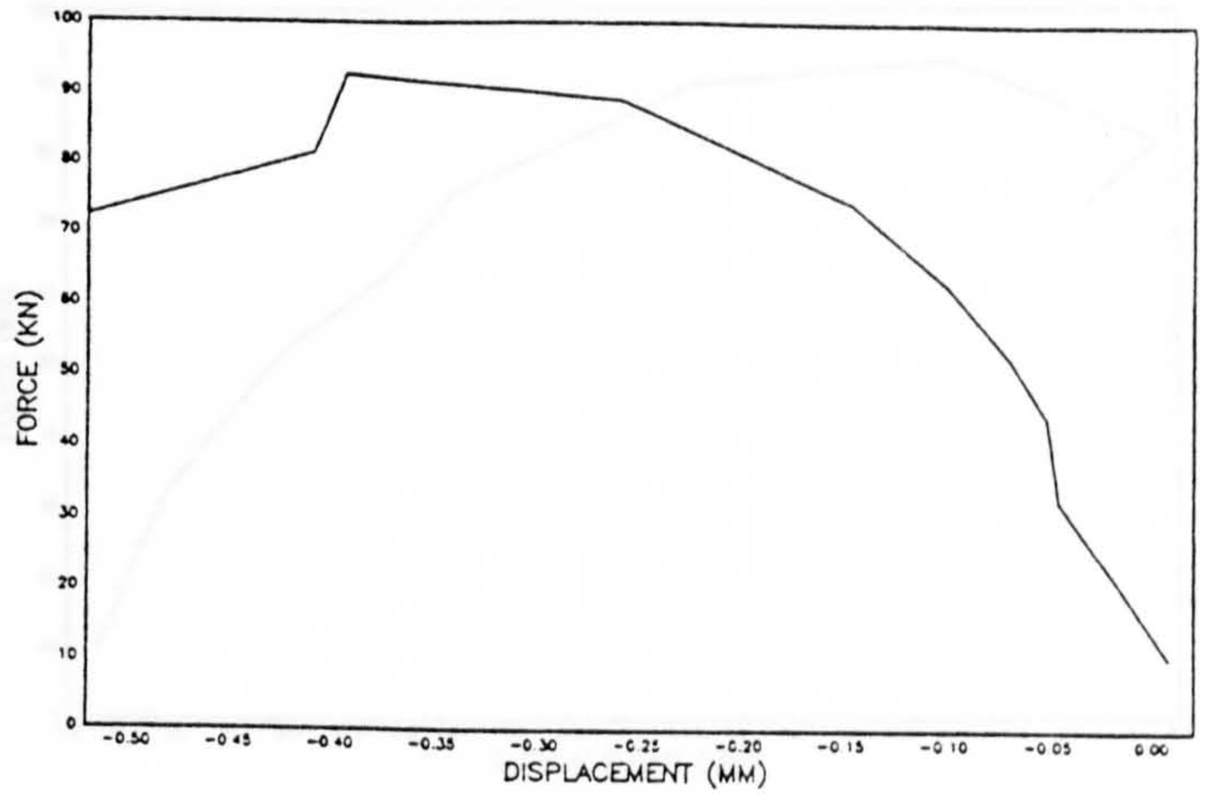


Figure B(11)5 Wall SW11 - force versus displacement 5 (vertical, LHS, level 2)

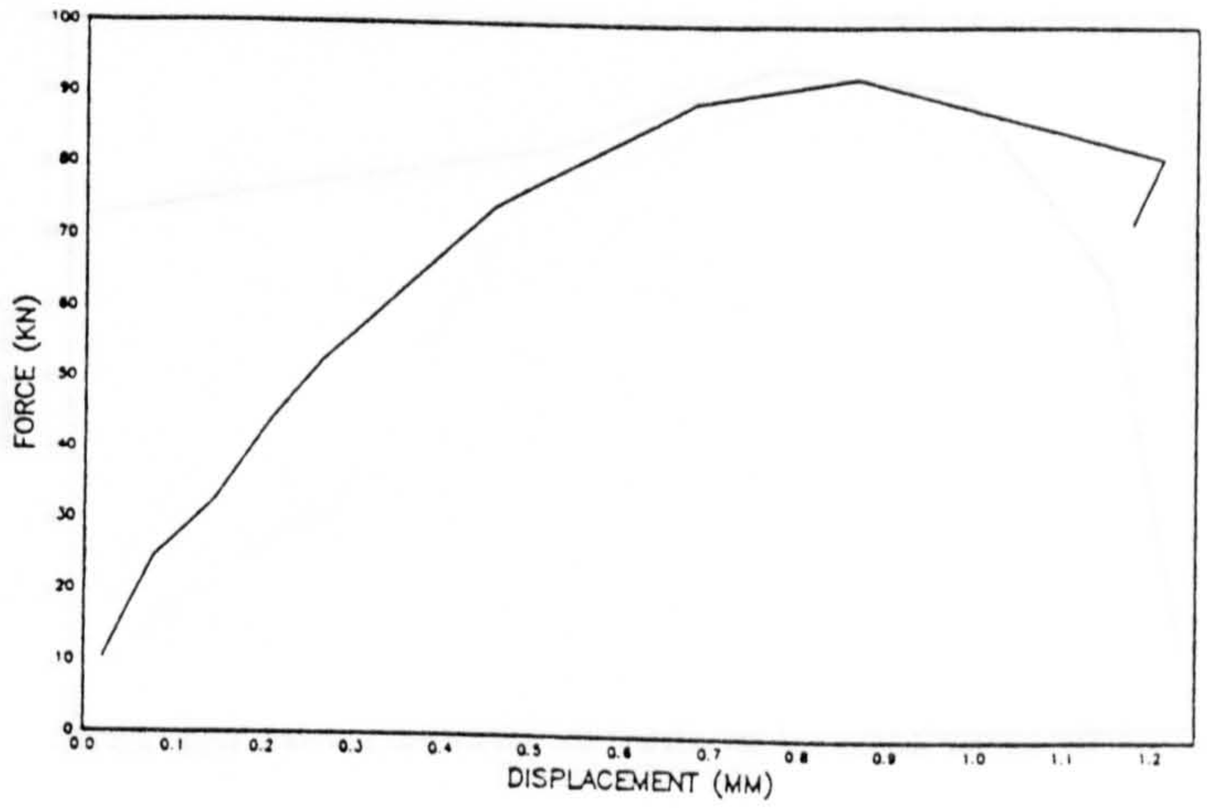


Figure B(11)6 Wall SW11 - force versus displacement 6 (vertical, RHS, level 2)

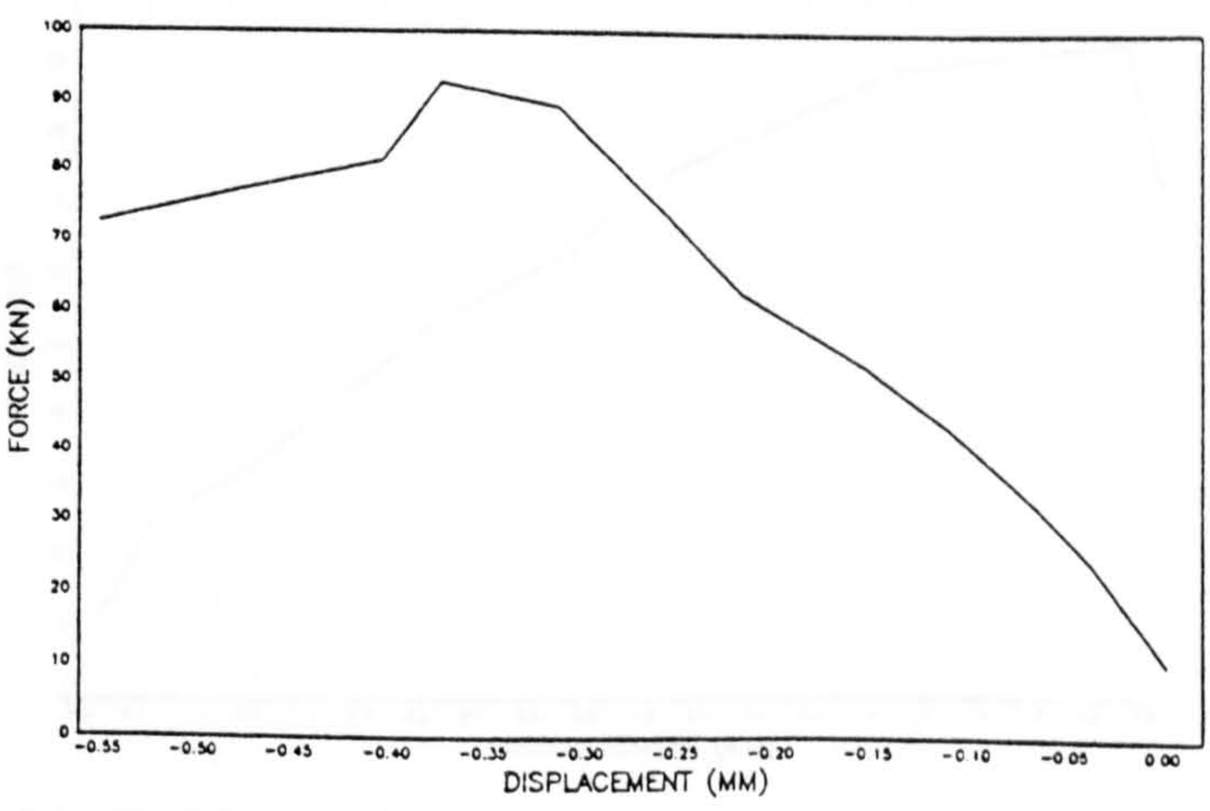


Figure B(11)7 Wall SW11 - force versus displacement 7 (vertical, LHS, level 3)

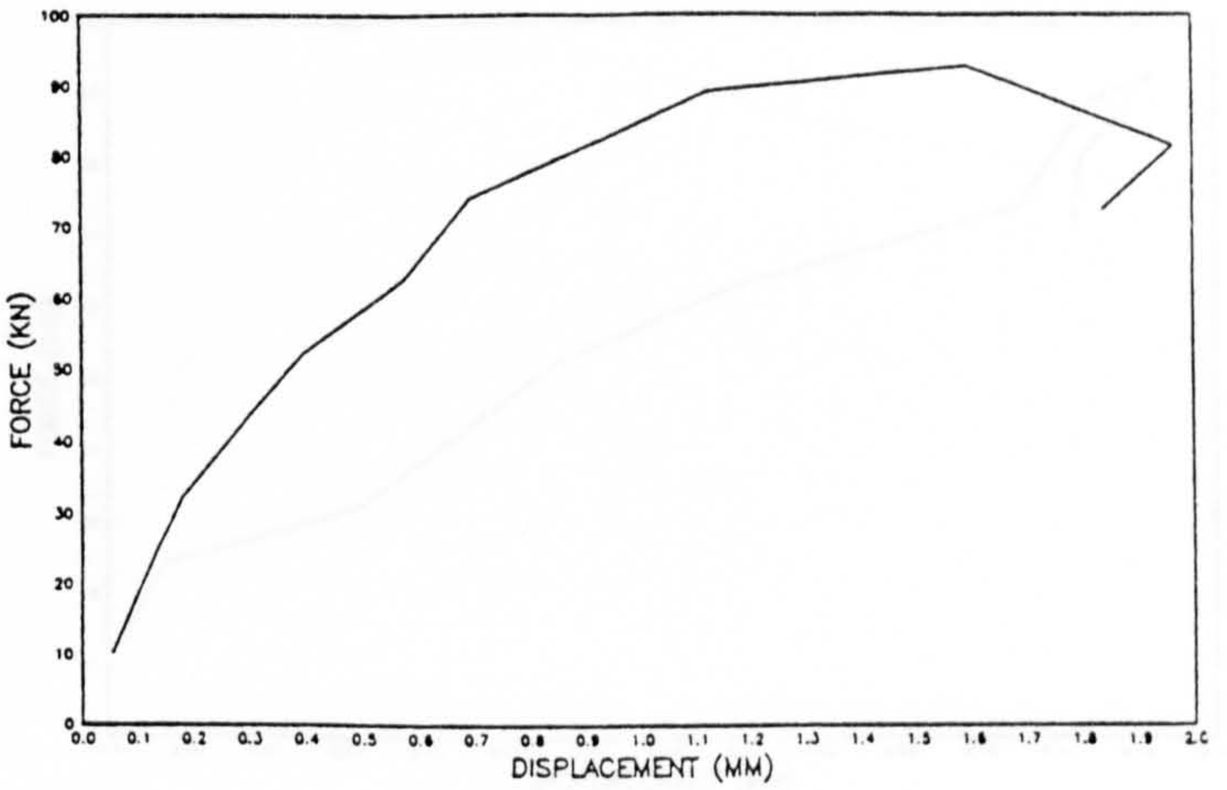


Figure B(11)8 Wall SW11 - force versus displacement 8 (vertical, RHS, level 3)

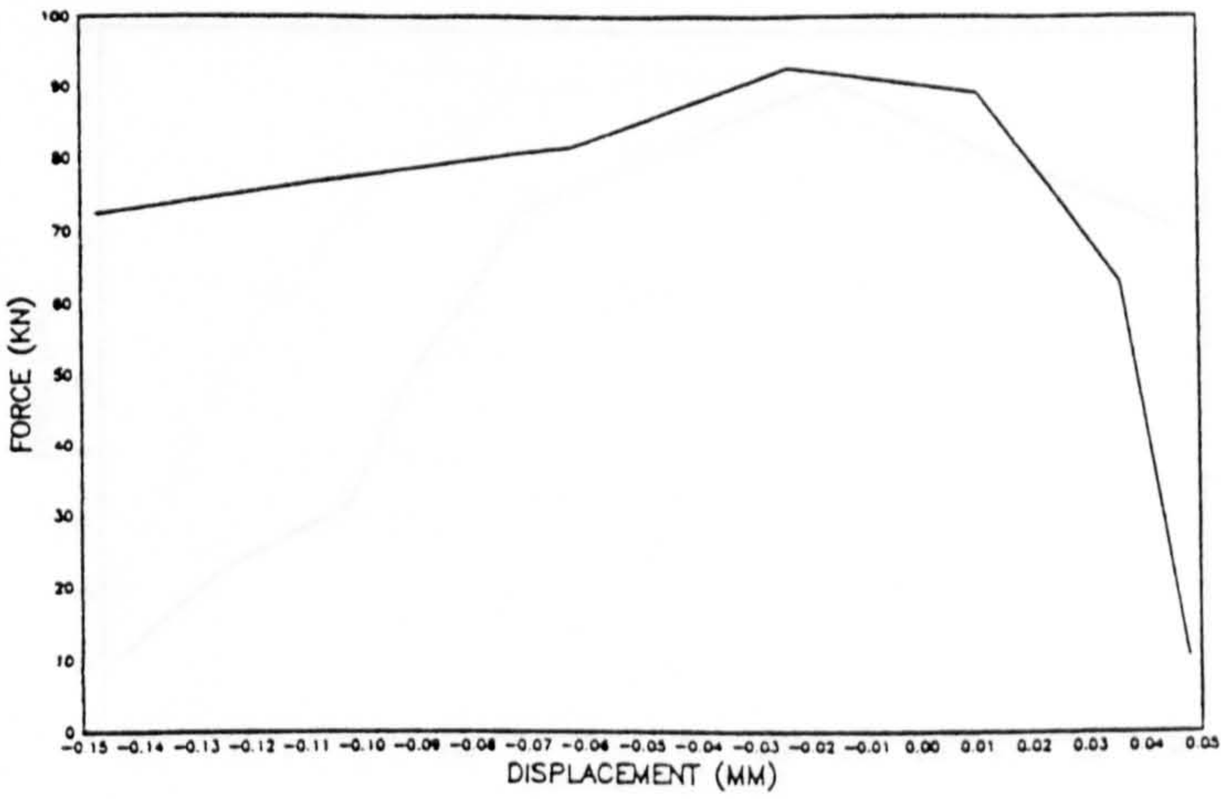


Figure B(11)9 Wall SW11 - force versus displacement 9 (vertical, LHS, level 4)

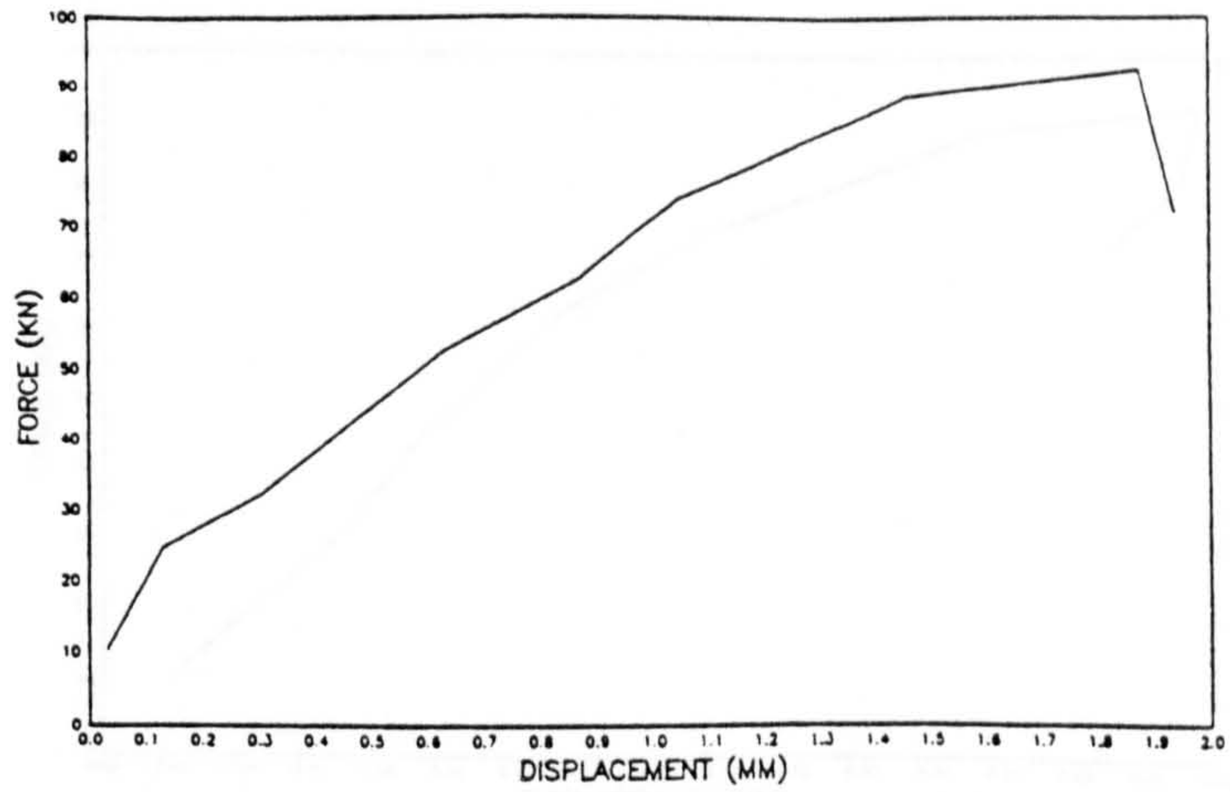


Figure B(11)10 Wall SW11 - force versus displacement 10 (vertical, RHS, level 4)

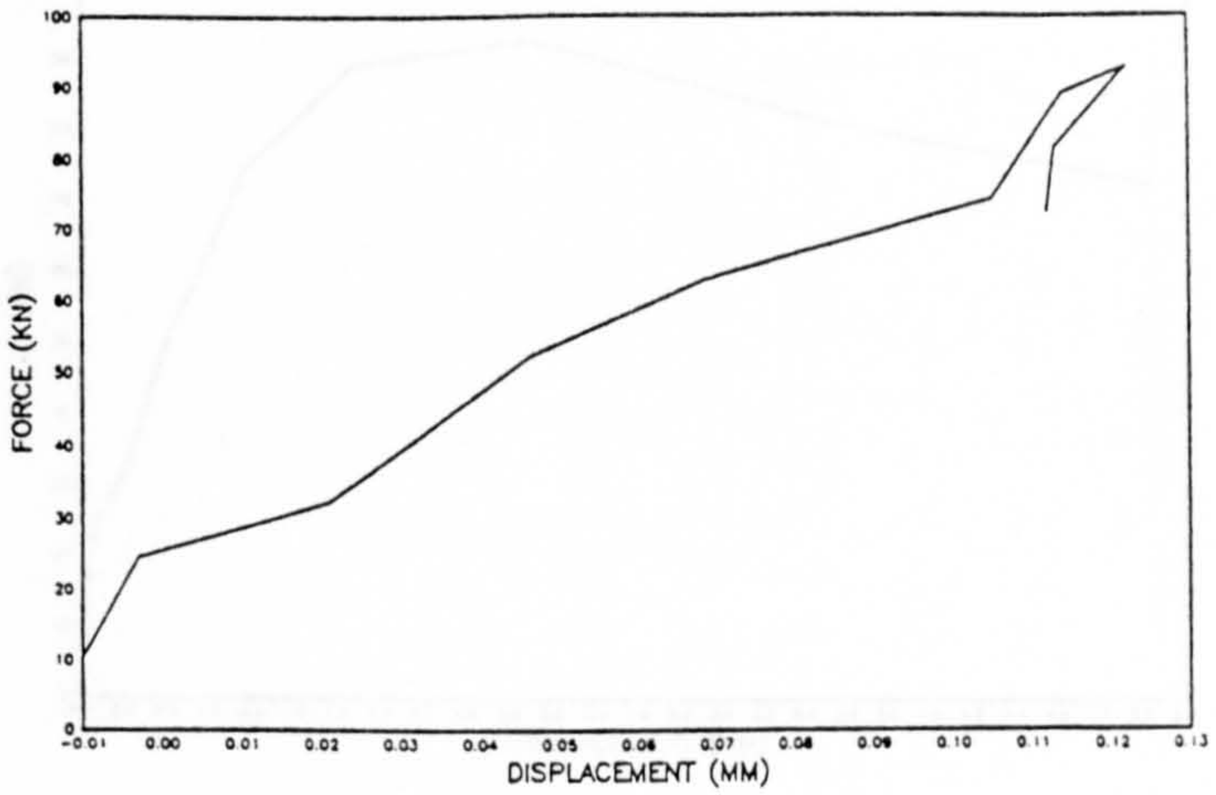


Figure B(11)11 Wall SW11 - force versus displacement 11 (foundation, RHS)

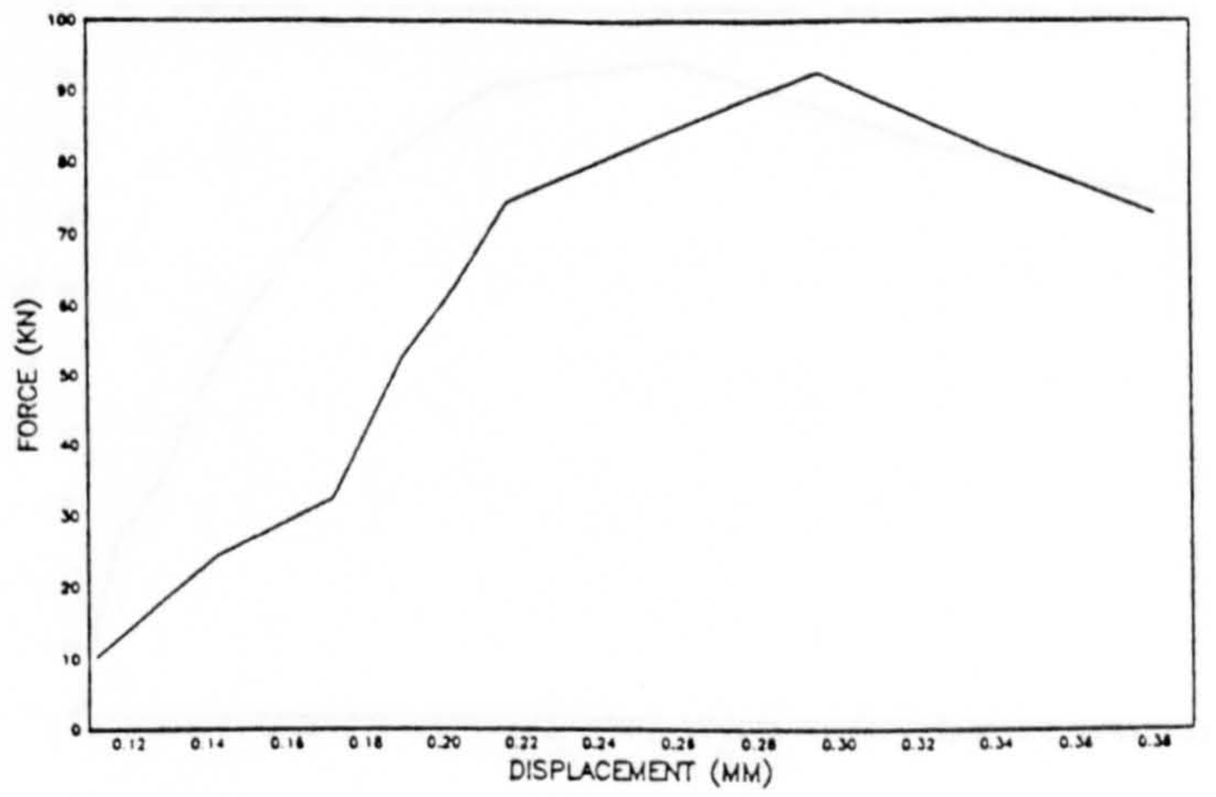


Figure B(11)12 Wall SW11 - force versus displacement 12 (out-of-plane)

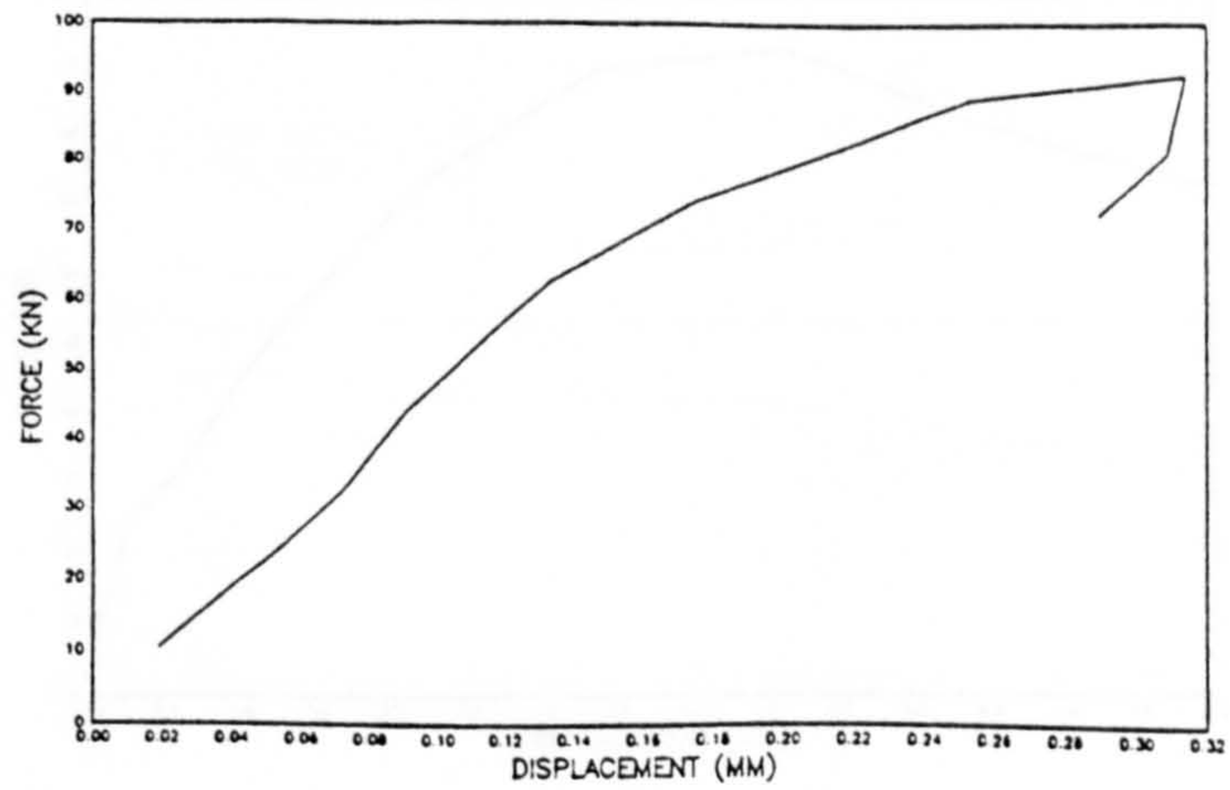


Figure B(11)13 Wall SW11 - force versus displacement 13a (horizontal, LHS, level 1)

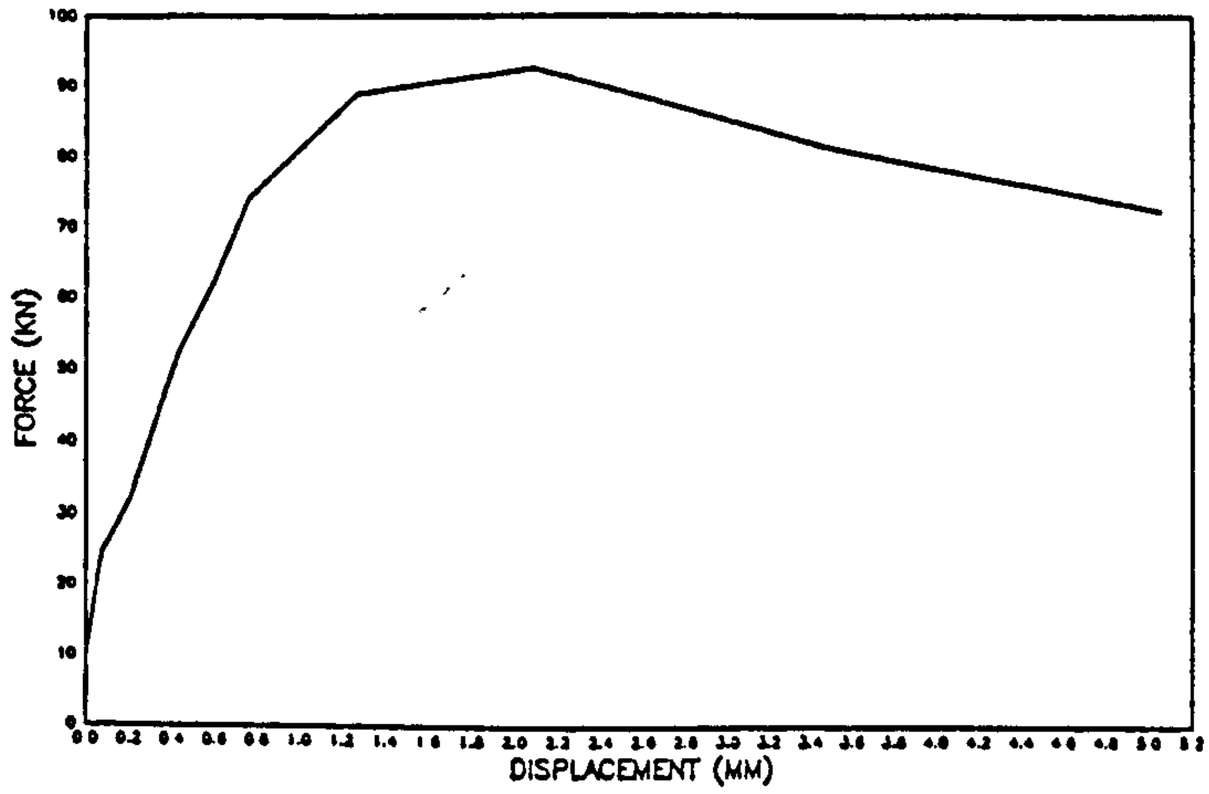


Figure B(11)14 Wall SW11 - force versus displacement 14 (horizontal, LHS, level 2)

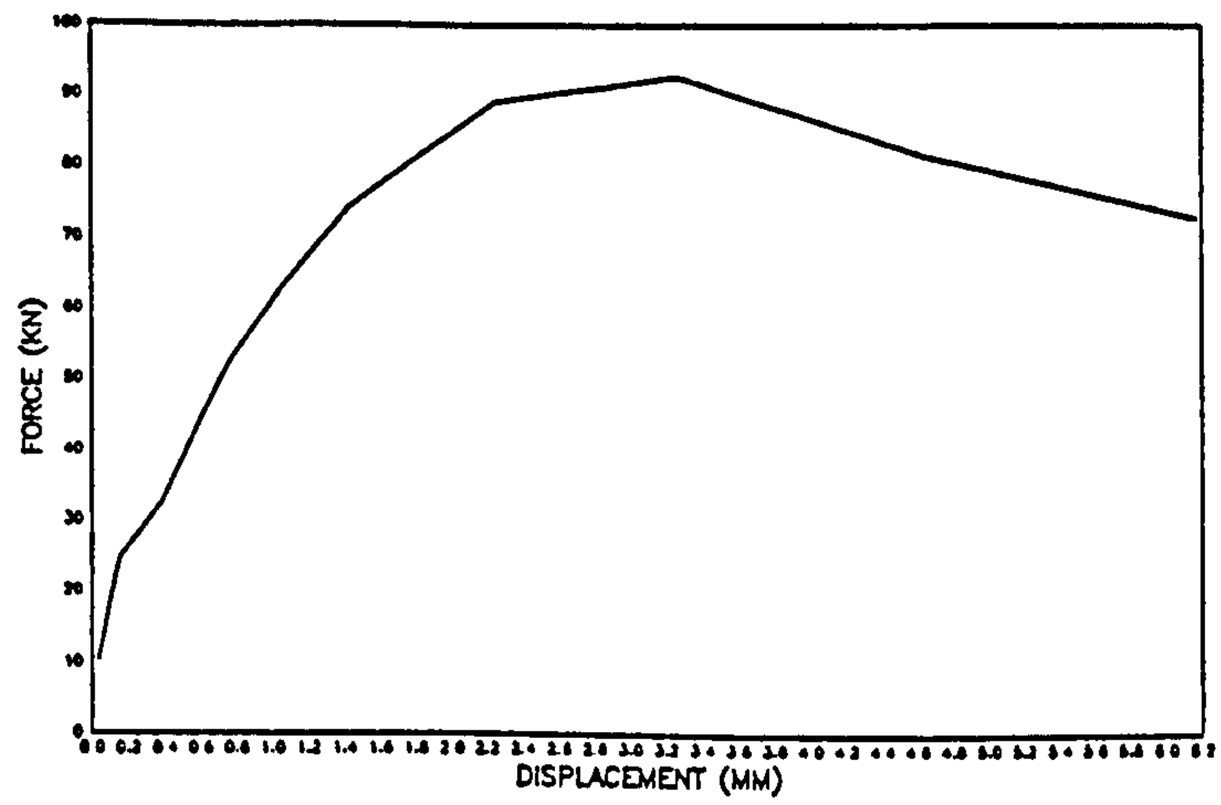


Figure B(11)15 Wall SW11 - force versus displacement 15a (horizontal, LHS, level 3)

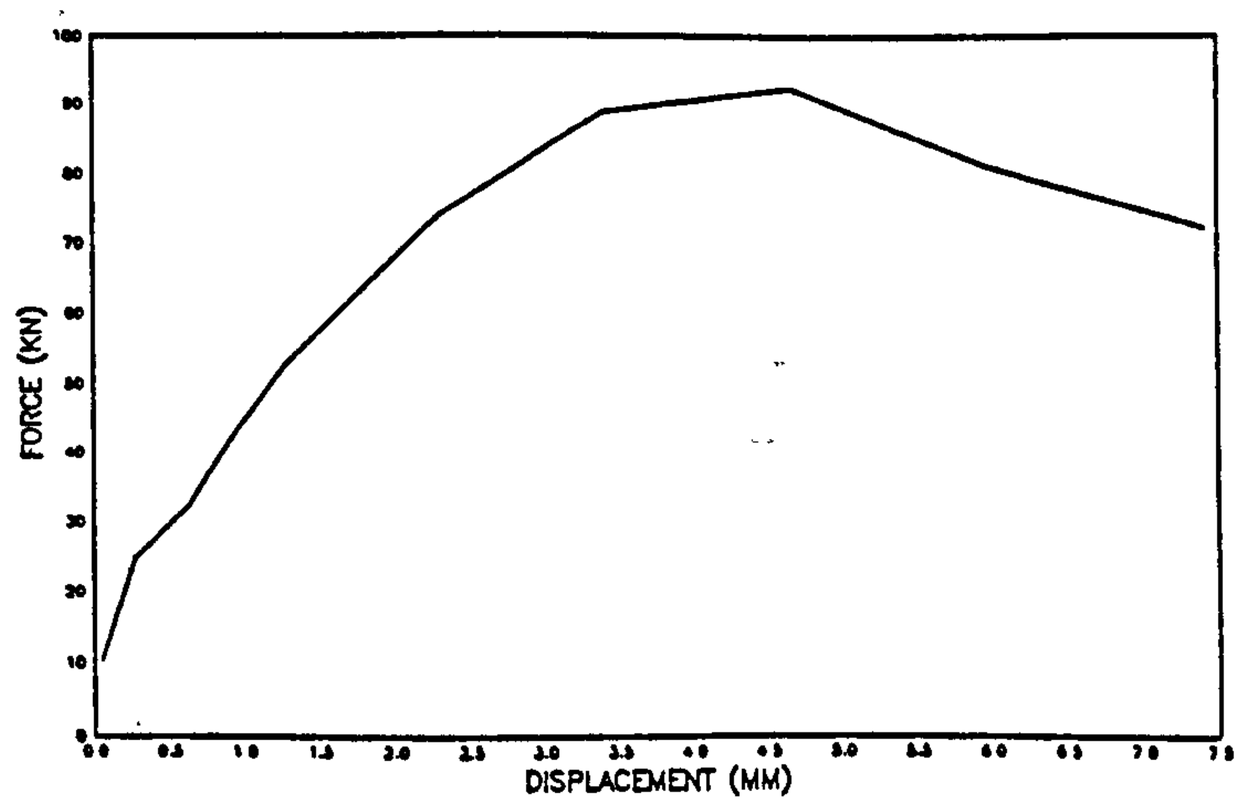


Figure B(11)16 Wall SW11 - force versus top horizontal displacement

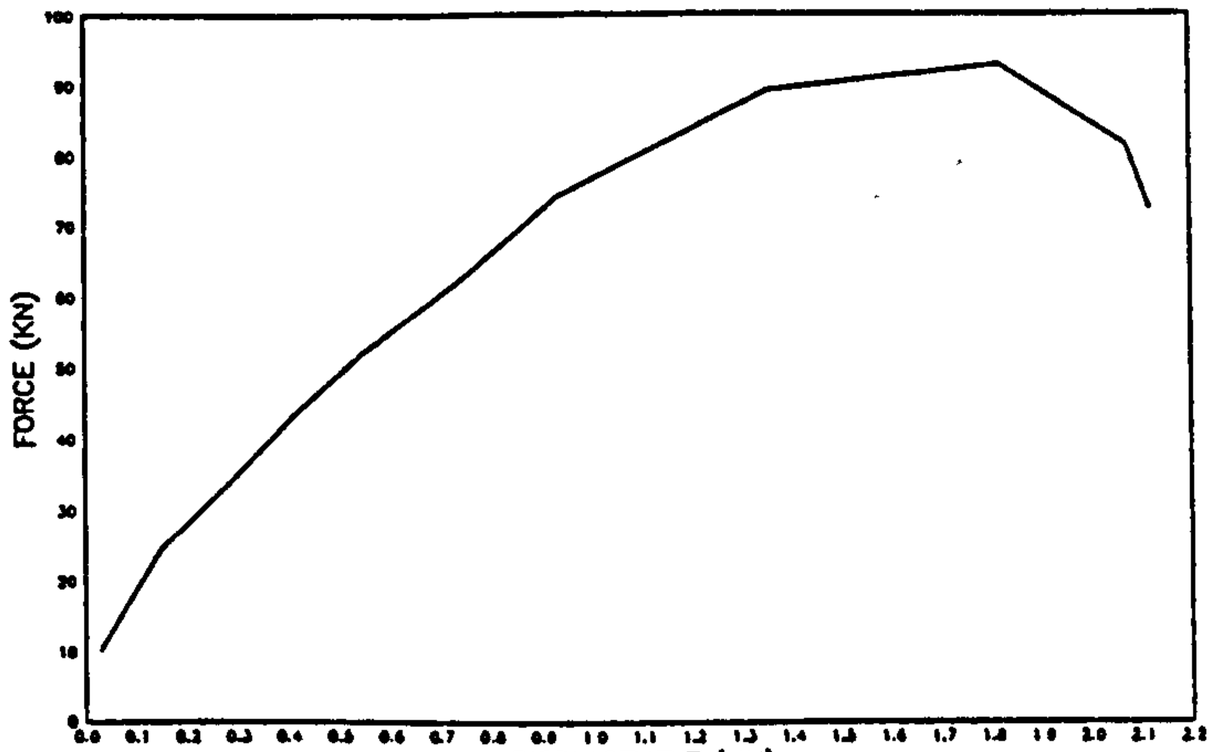


Figure B(11)17 Wall SW11 - force versus flexural component of top horizontal displacement

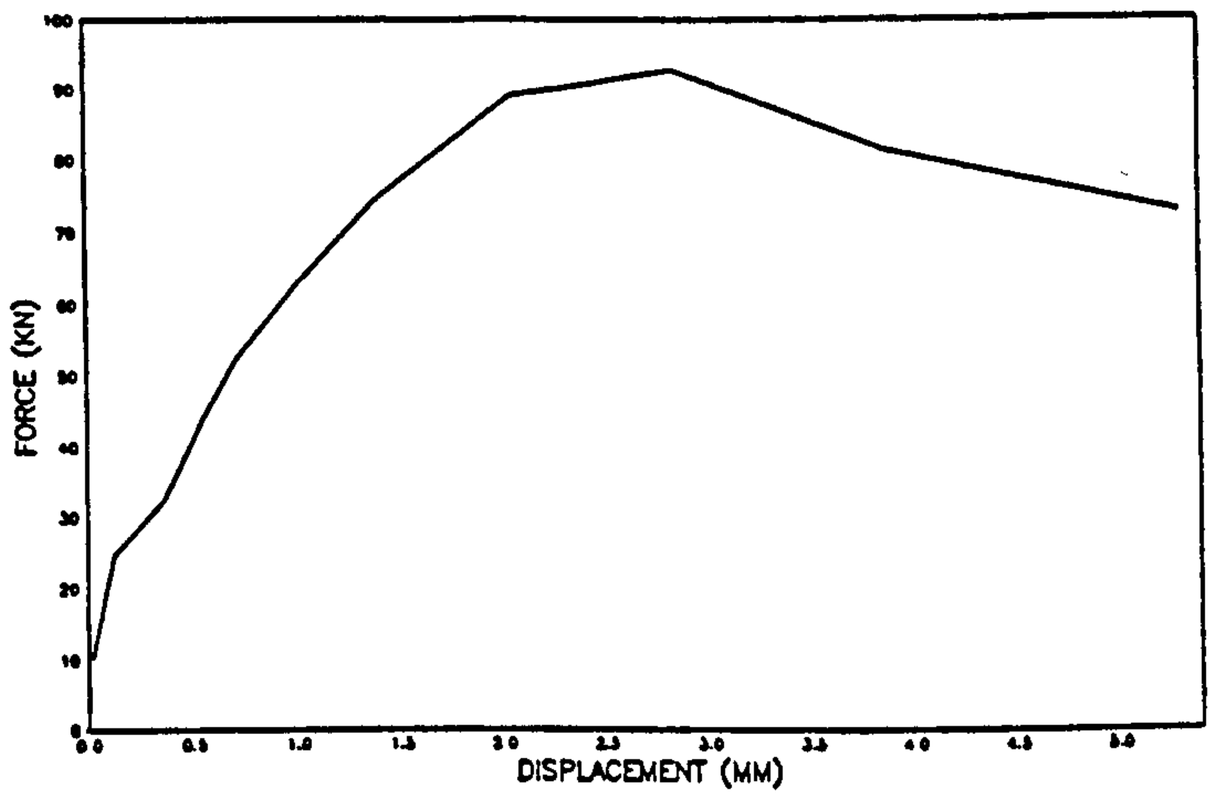


Figure B(11)18 Wall SW11 - force versus shear component of top horizontal displacement

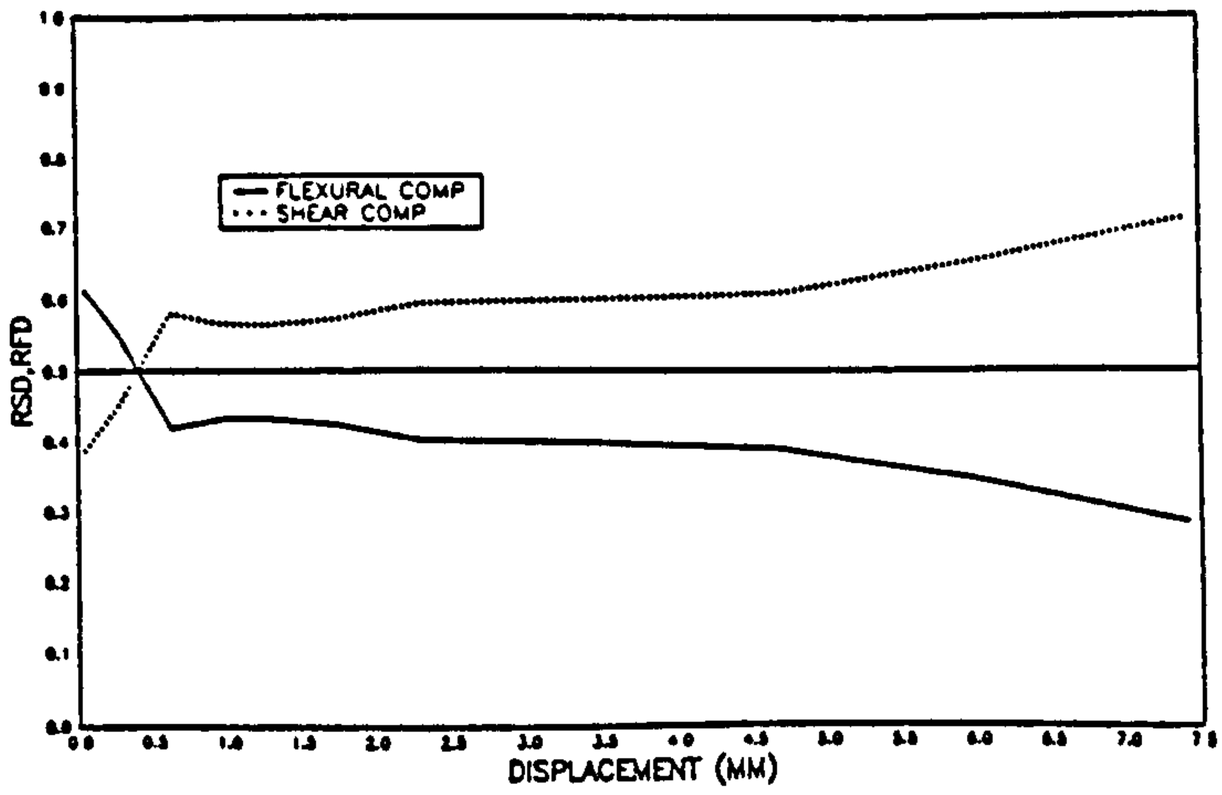


Figure B(11)19 Wall SW11 - RSD,RFD versus top horizontal displacement

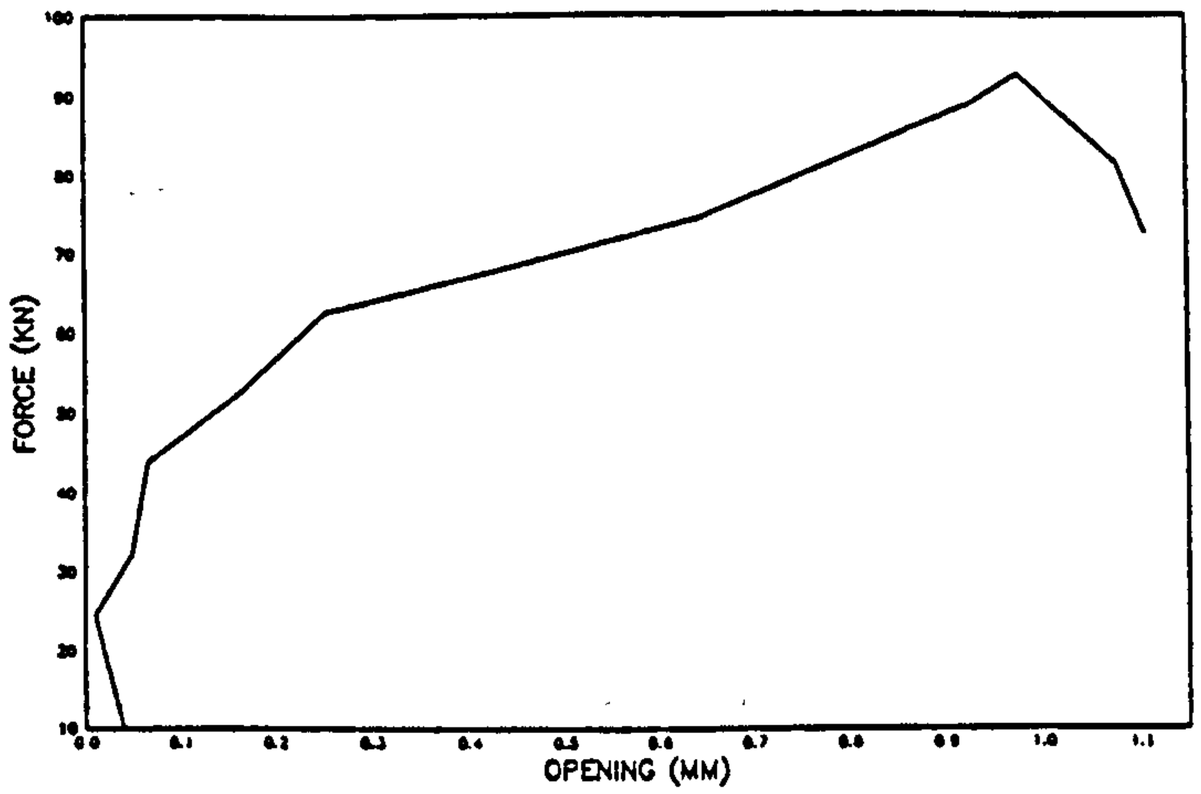


Figure B(11)20 Wall SW11 - force versus opening on top

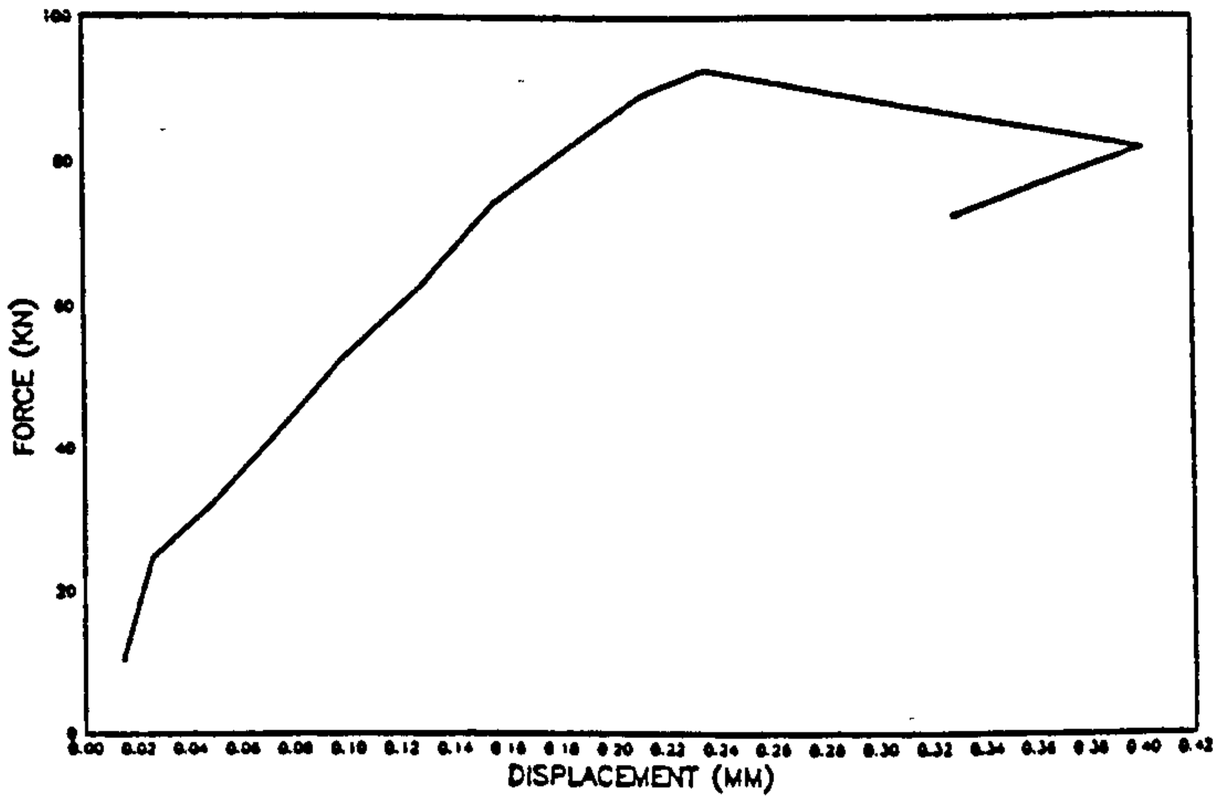


Figure B(11)21 Wall SW11 - force versus extension at a quarter height

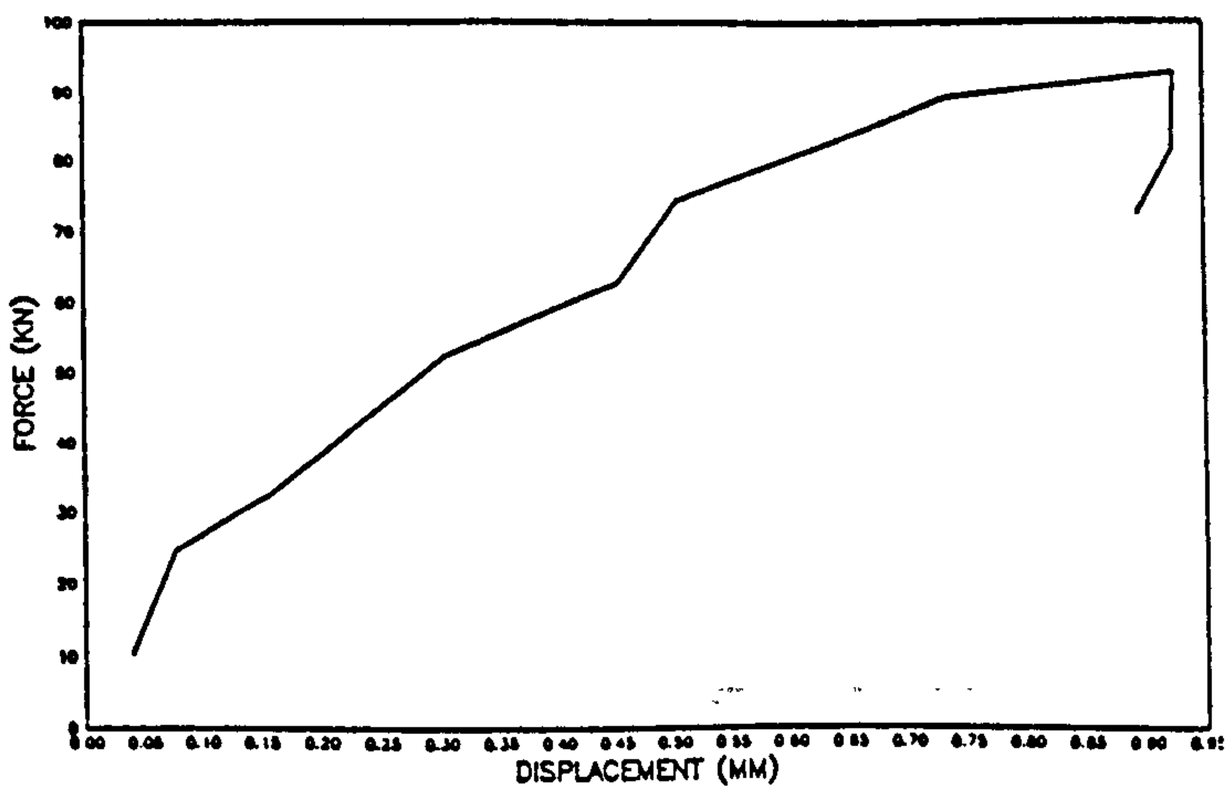


Figure B(11)22 Wall SW11 - force versus extension on top

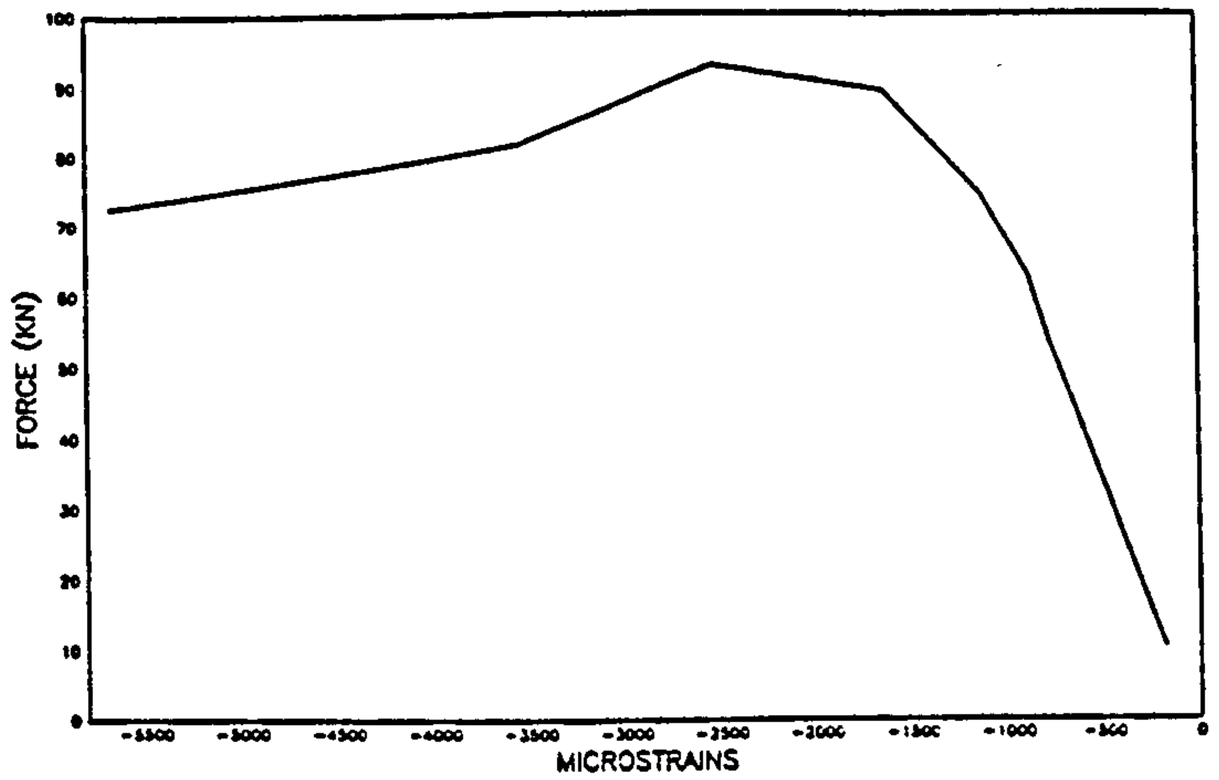


Figure B(11)23.a Wall SW11 - force versus strain 1_I (bottom, ϕ8mm, LHS)

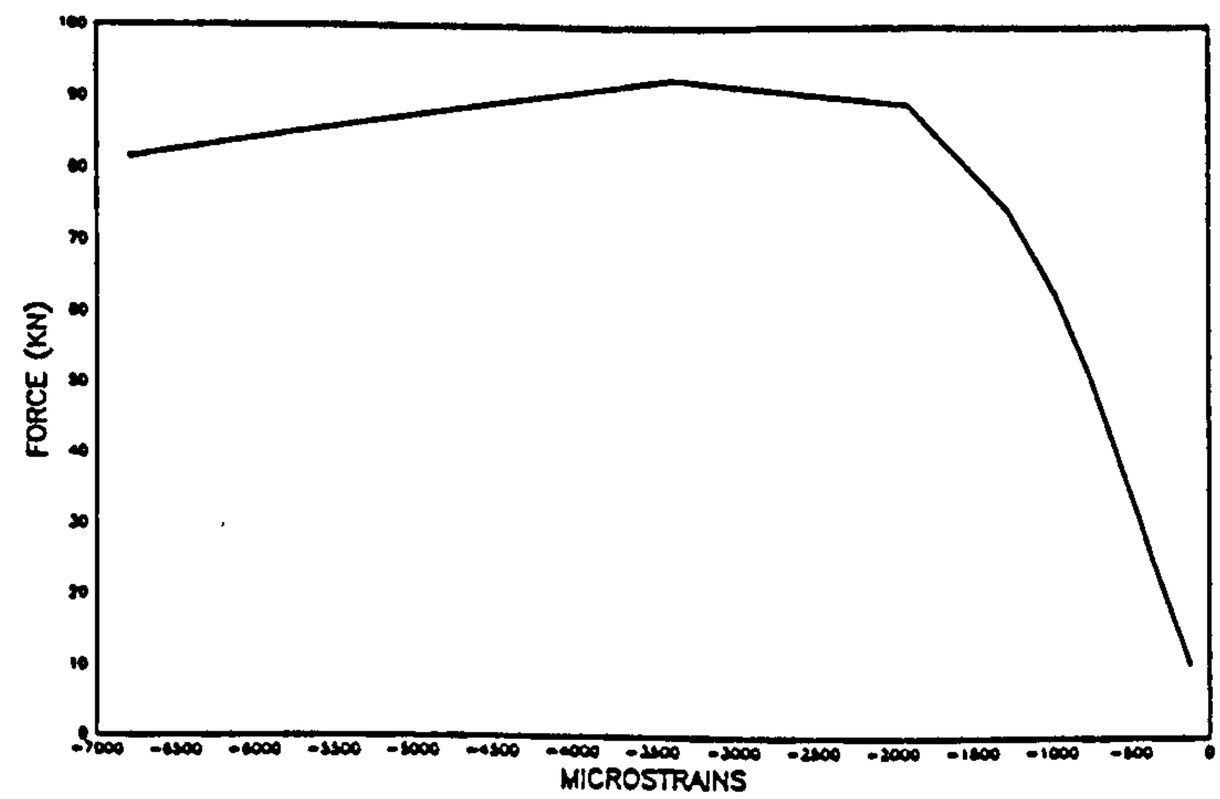


Figure B(11)23.b Wall SW11 - force versus strain 1_{II} (bottom, ϕ8mm, LHS)

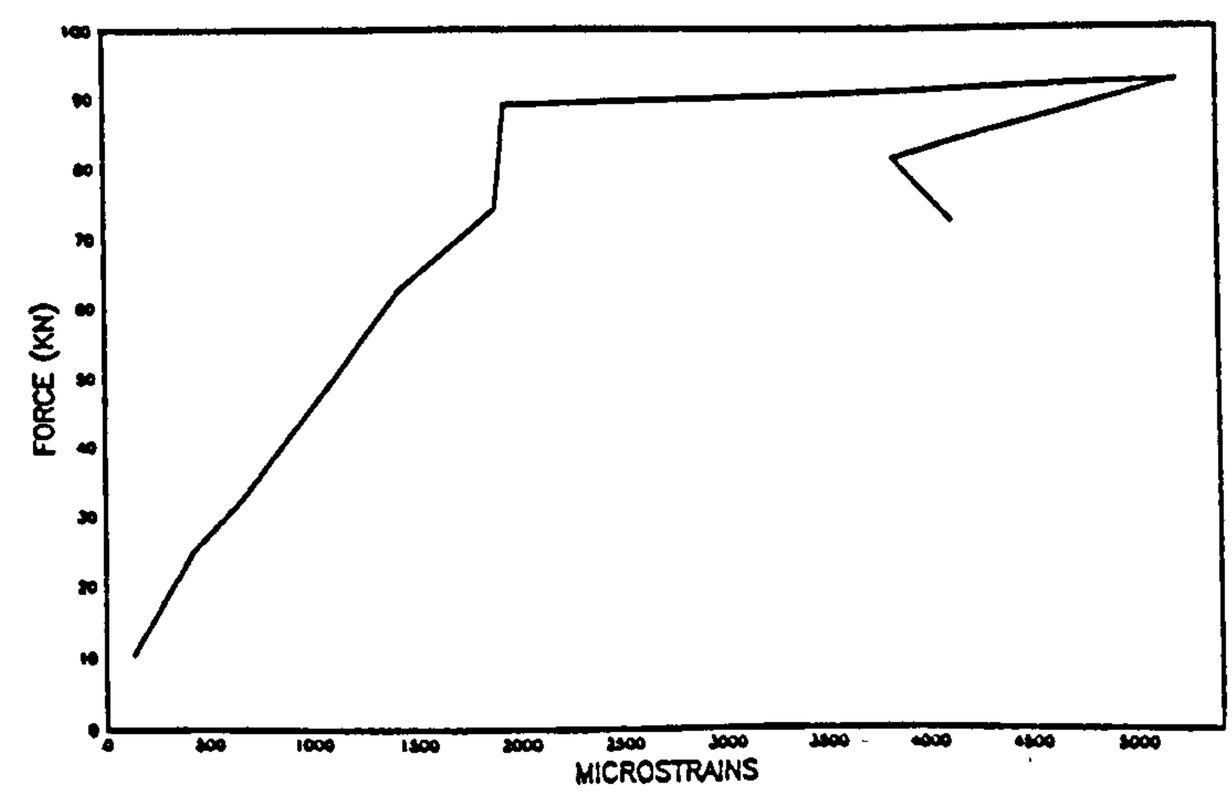


Figure B(11)24.a Wall SW11 - force versus strain 2: (bottom, ϕ8mm, RHS)

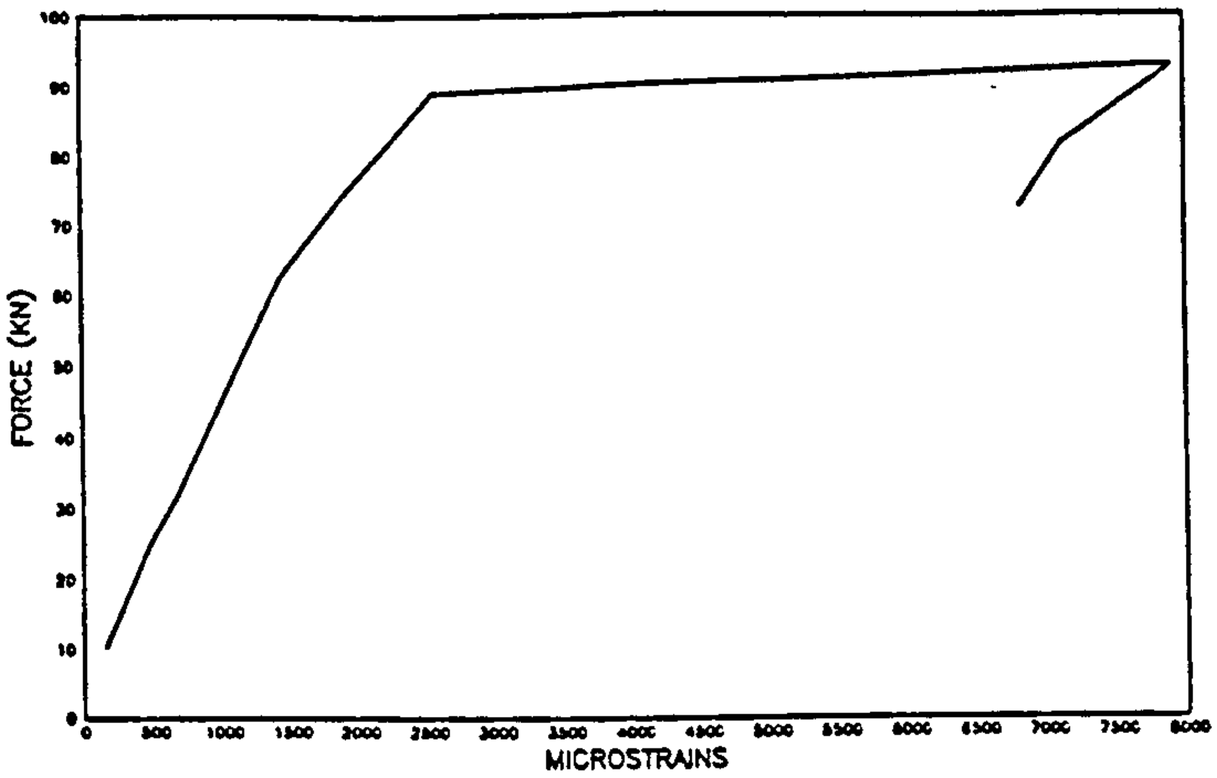


Figure B(11)24.b Wall SW11 - force versus strain 2_{II} (bottom, ϕ8mm, RHS)

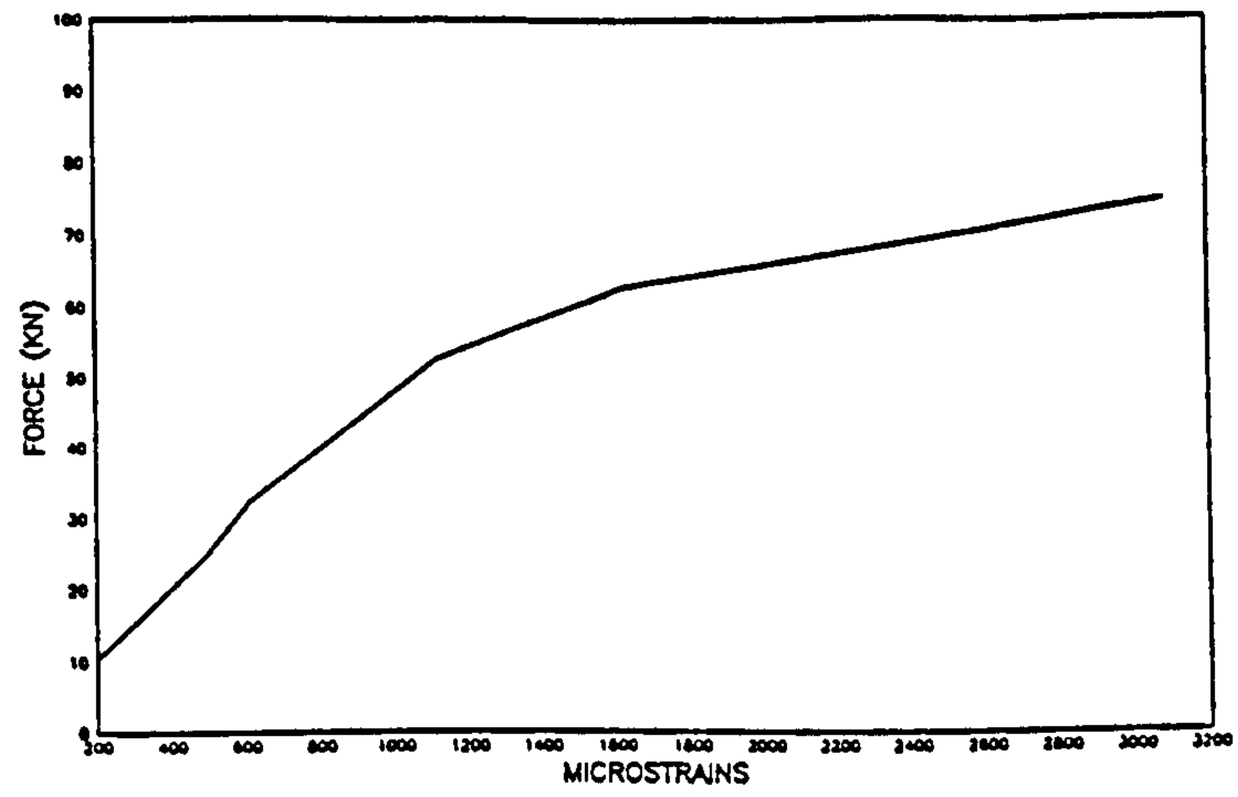


Figure B(11)24.c Wall SW11 - force versus strain 2_{III} (bottom, ϕ8mm, RHS)

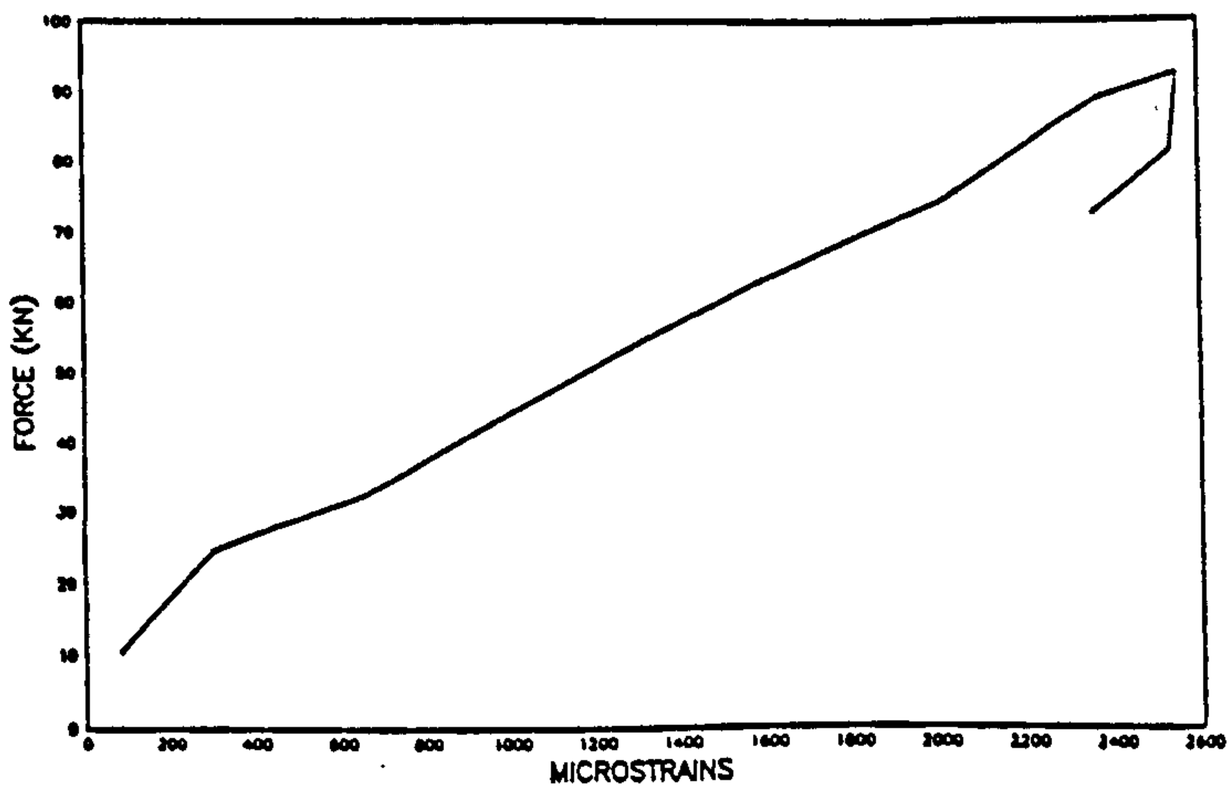


Figure B(11)25.a Wall SW11 - force versus strain 10. (second level, ϕ8mm, RHS)

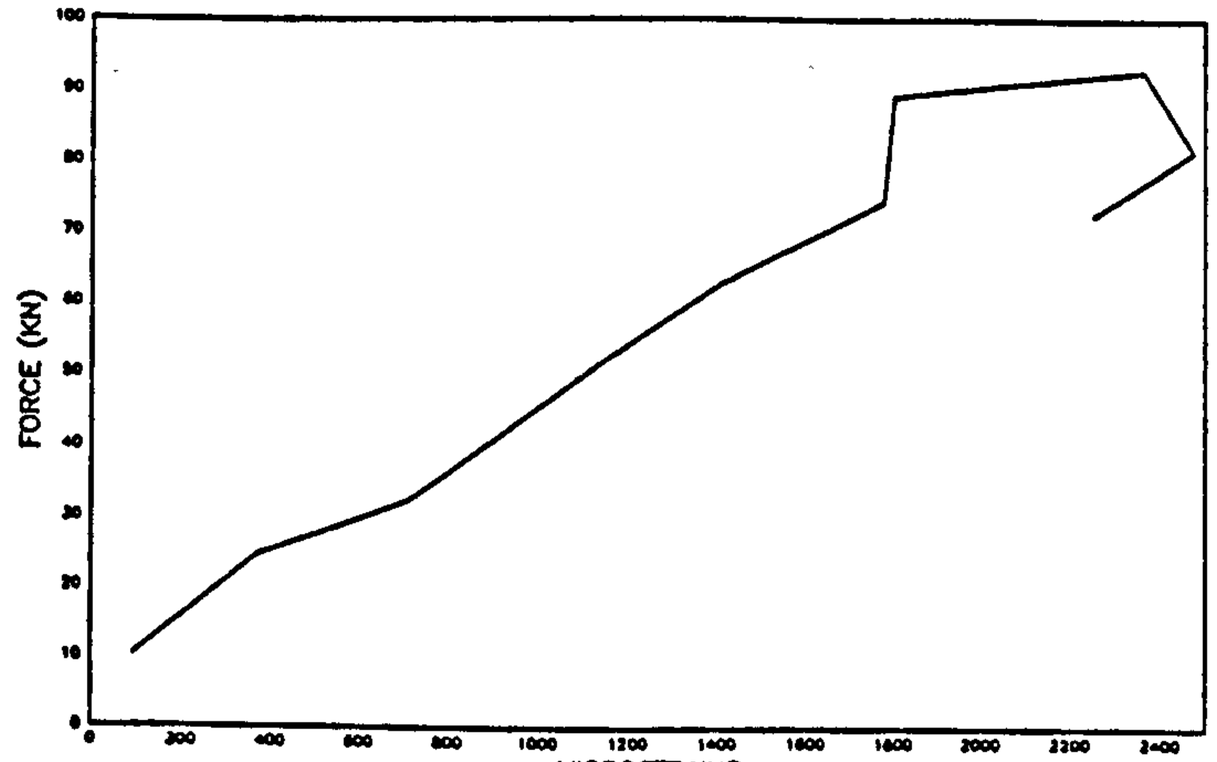


Figure B(11)25.b Wall SW11 - force versus strain $10_{,11}$ (second level, ϕ8mm, RHS)

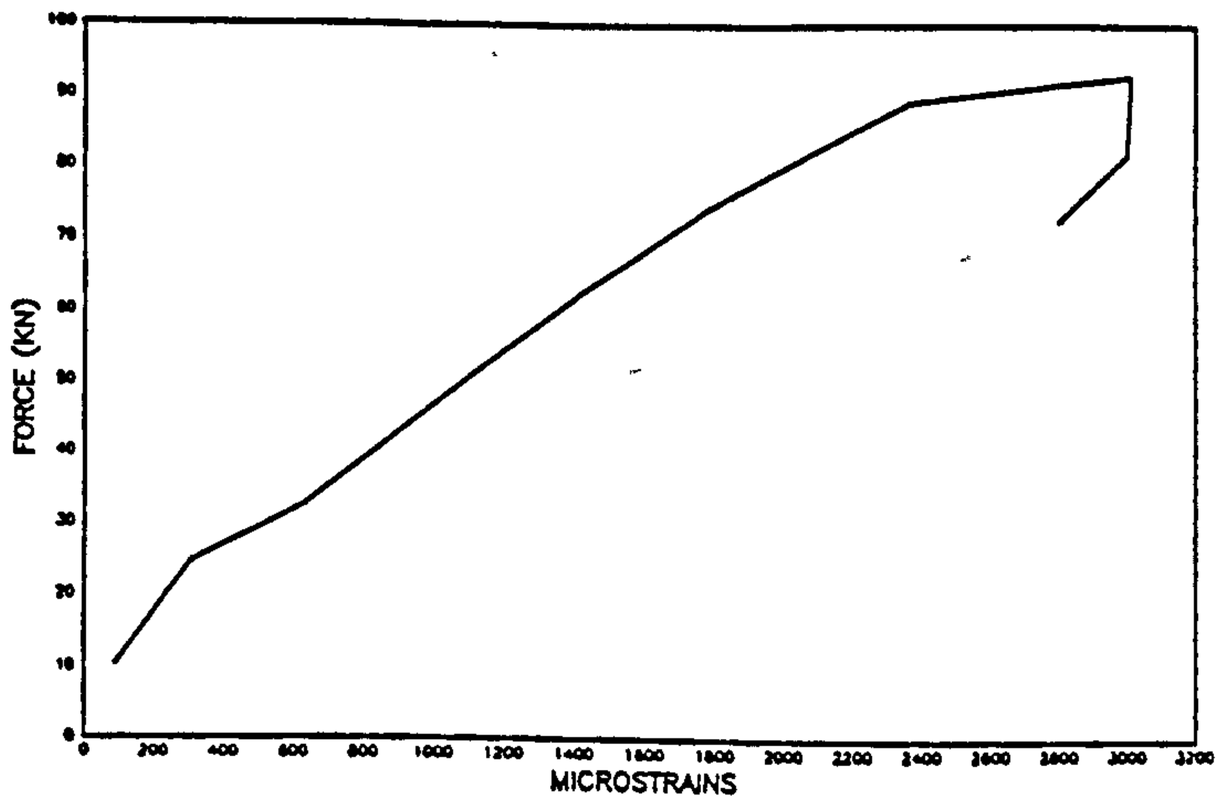


Figure B(11)25.c Wall SW11 - force versus strain $10_{,111}$ (second level, ϕ8mm, RHS)

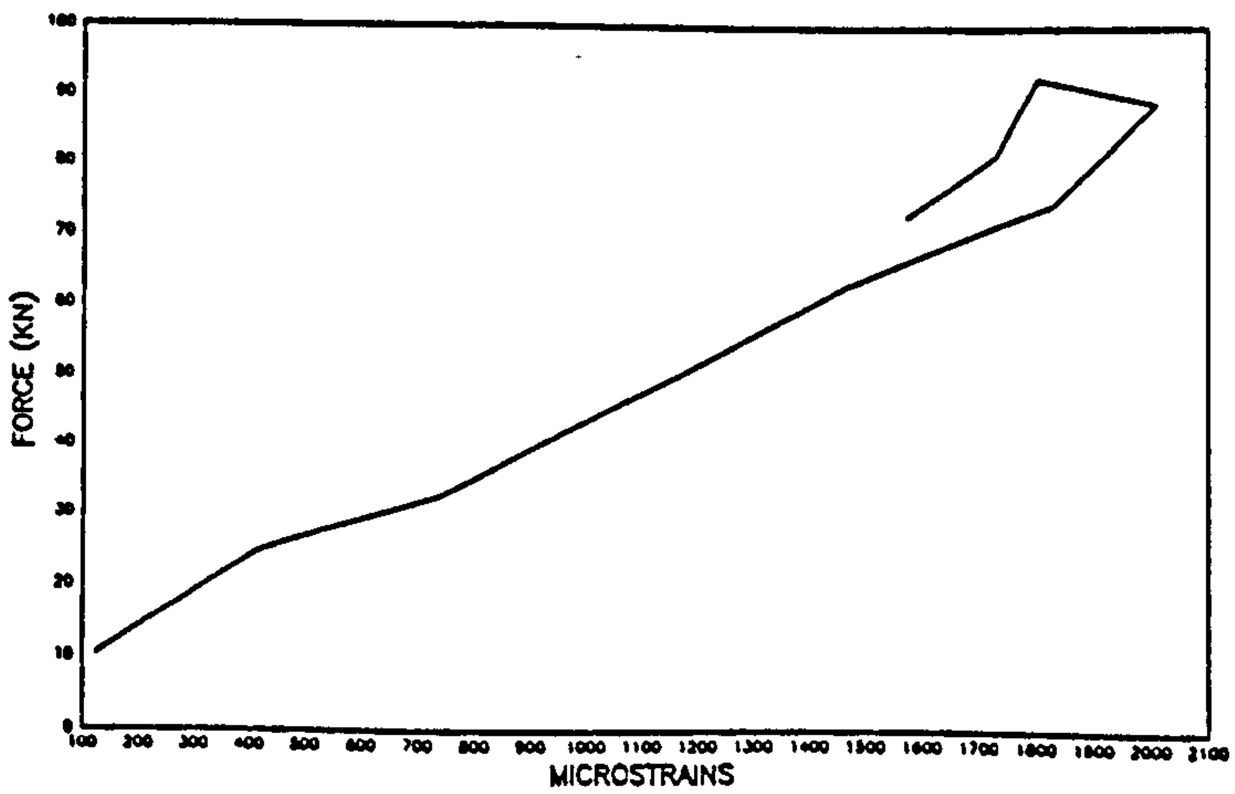


Figure B(11)25.d Wall SW11 - force versus strain $10_{,V}$ (second level, ϕ8mm, RHS)

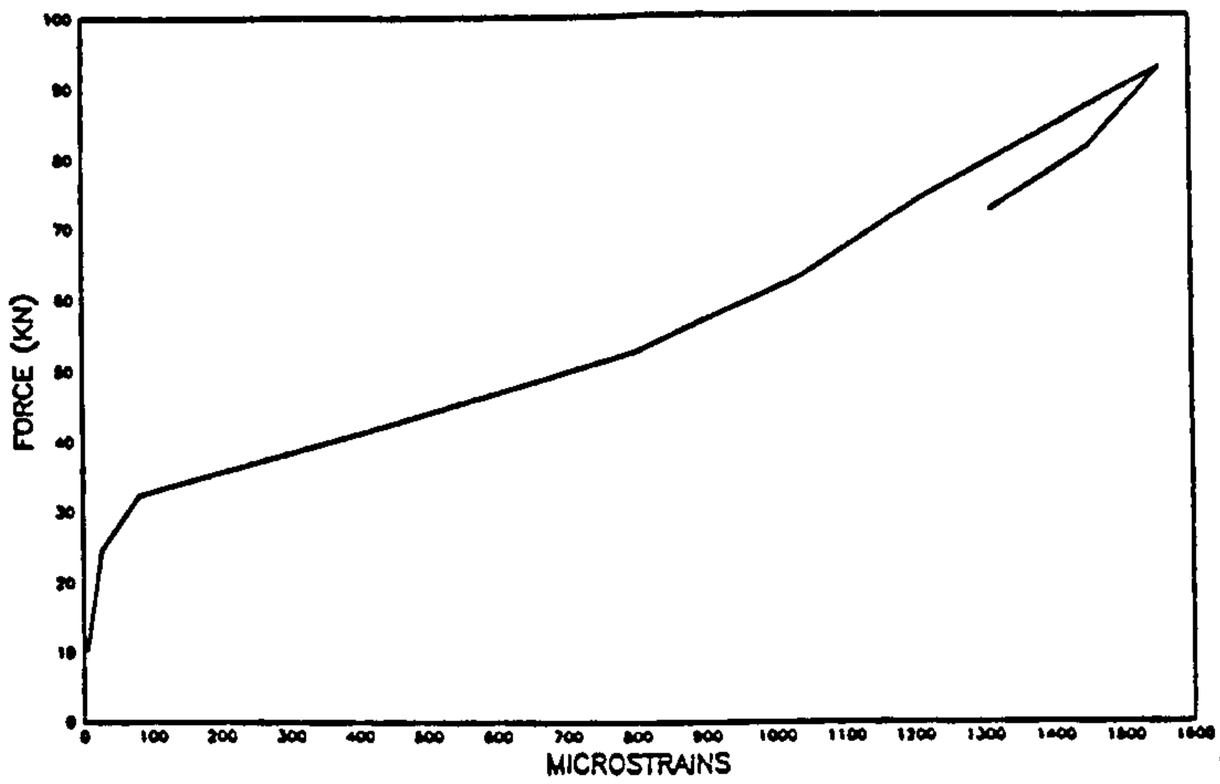


Figure B(11)26 Wall SW11 - force versus strain 11 (level of zero moment, ϕ8mm, LHS)

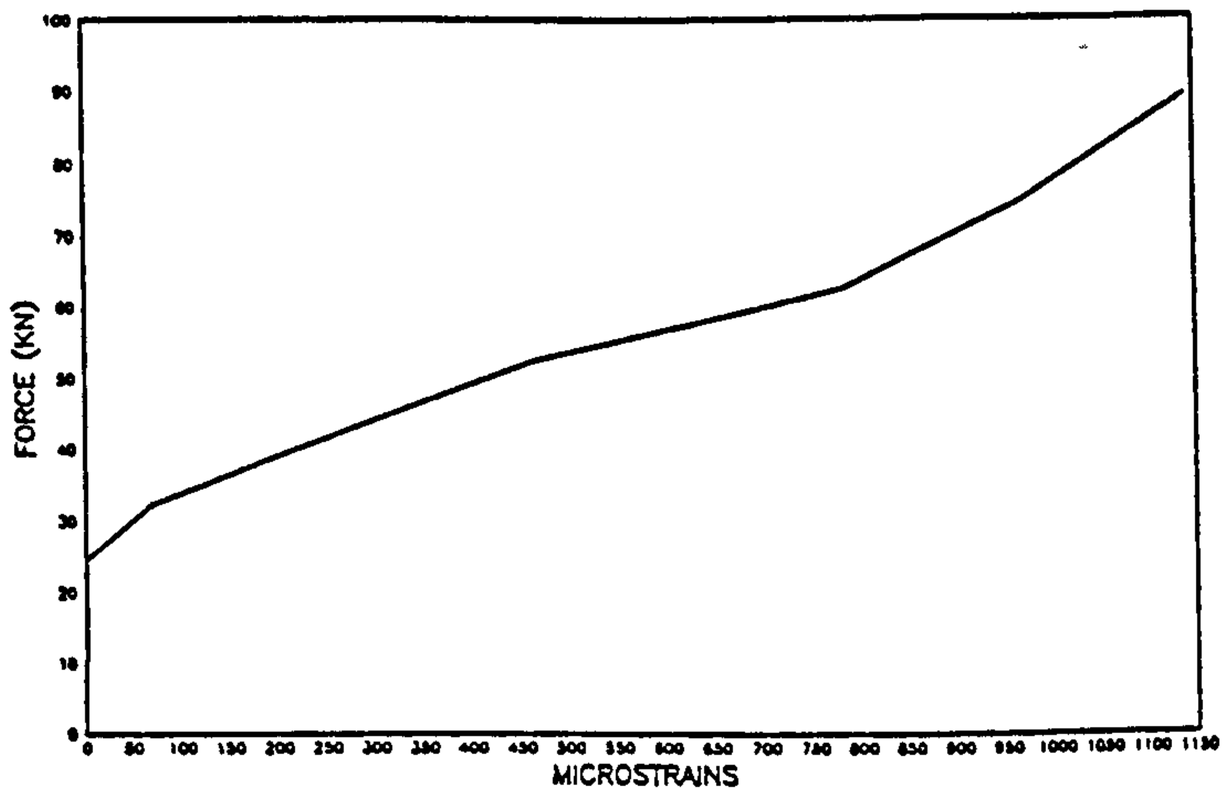


Figure B(11)27 Wall SW11 - force versus strain 12 (level of zero moment, ϕ8mm, RHS)

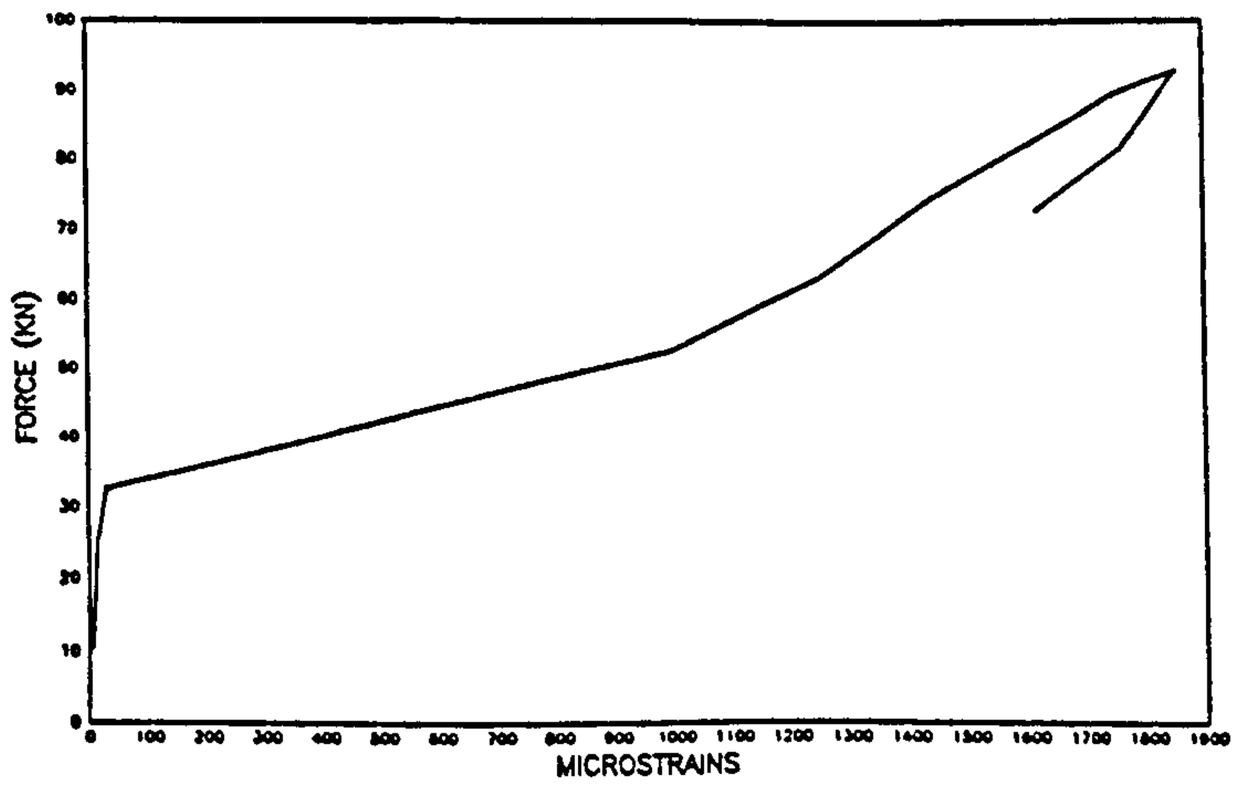


Figure B(11)28 Wall SW11 - force versus strain 13 (level of zero moment, ϕ6mm, LHS)

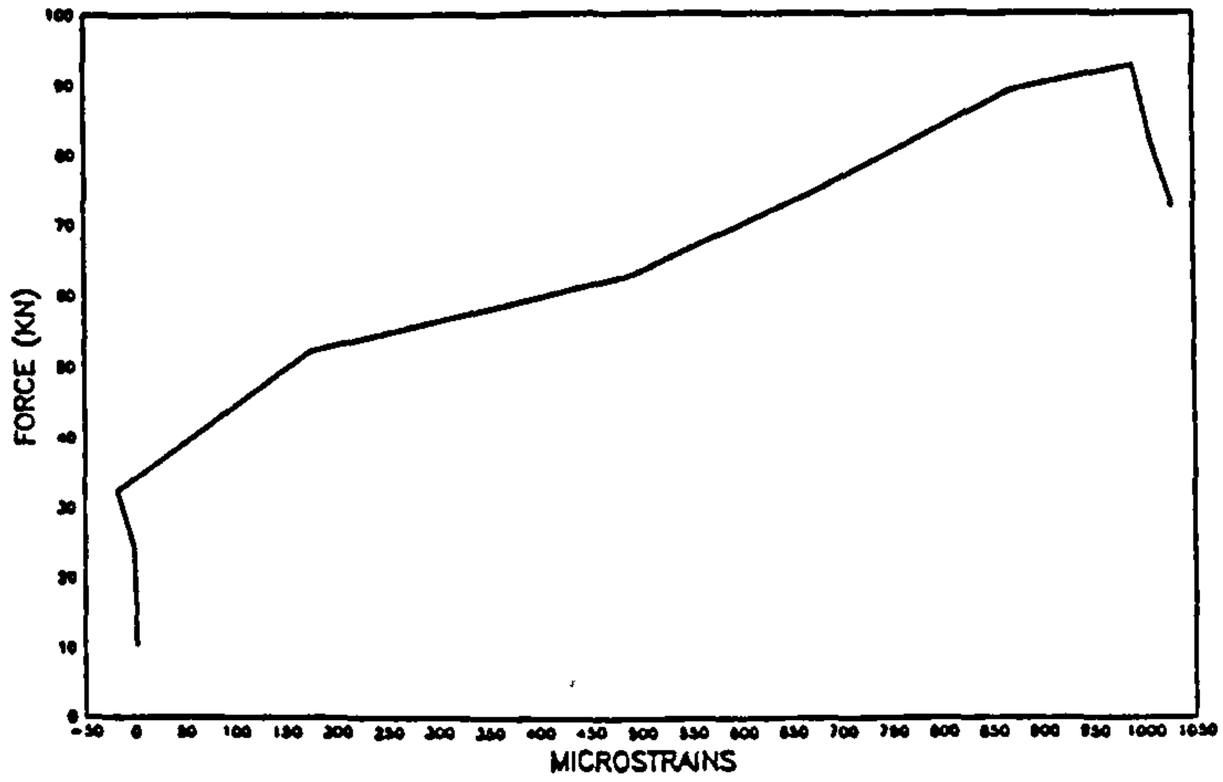


Figure B(11)29 Wall SW11 - force versus strain 15 (level of zero moment, ϕ4mm, LHS)

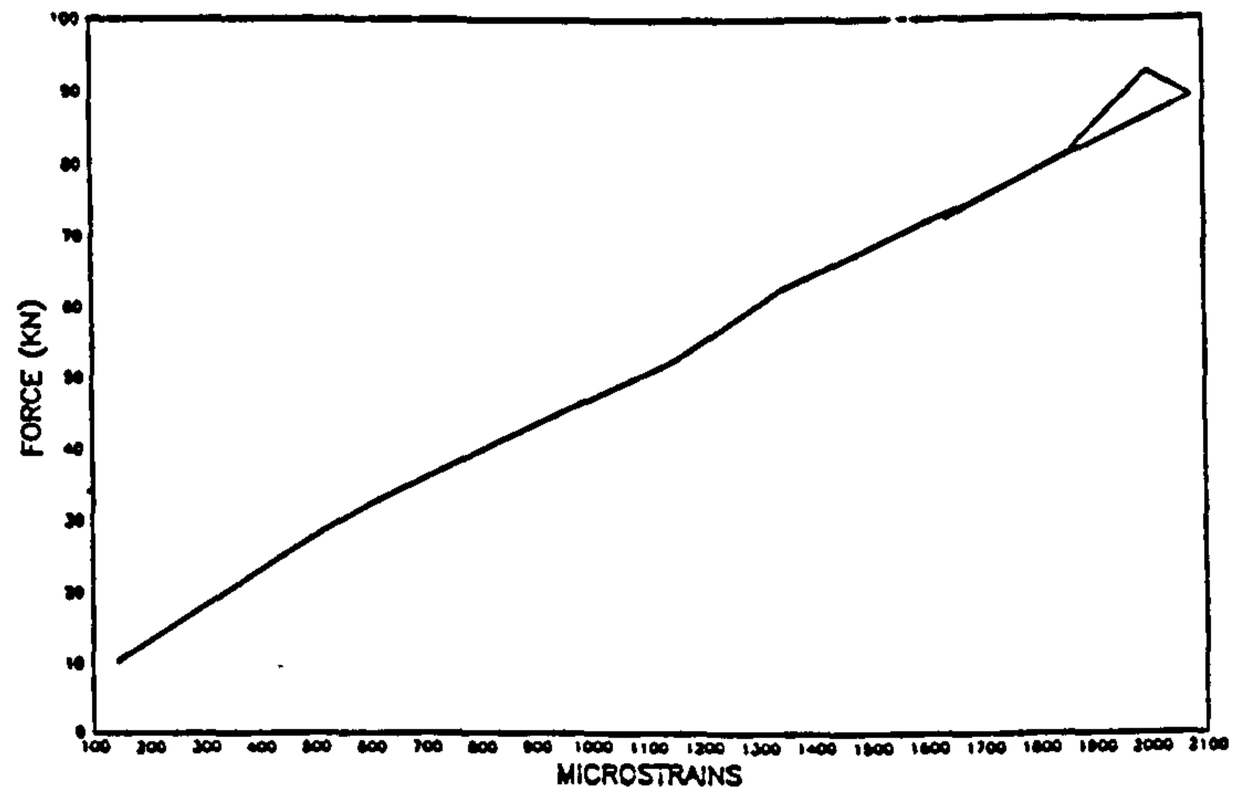


Figure B(11)30.a Wall SW11 - force versus strain 17, (top, ϕ8mm, LHS)

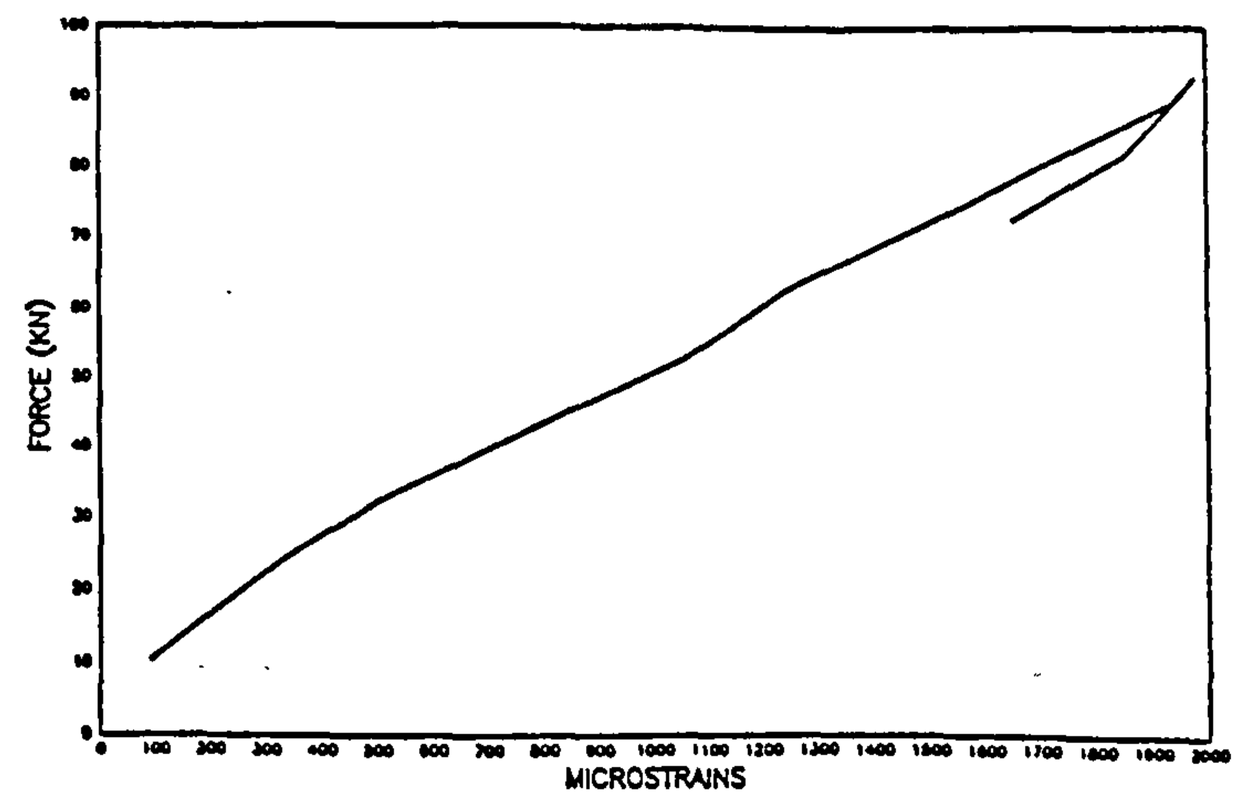


Figure B(11)30.b Wall SW11 - force versus strain 17, (top, ϕ8mm, LHS)

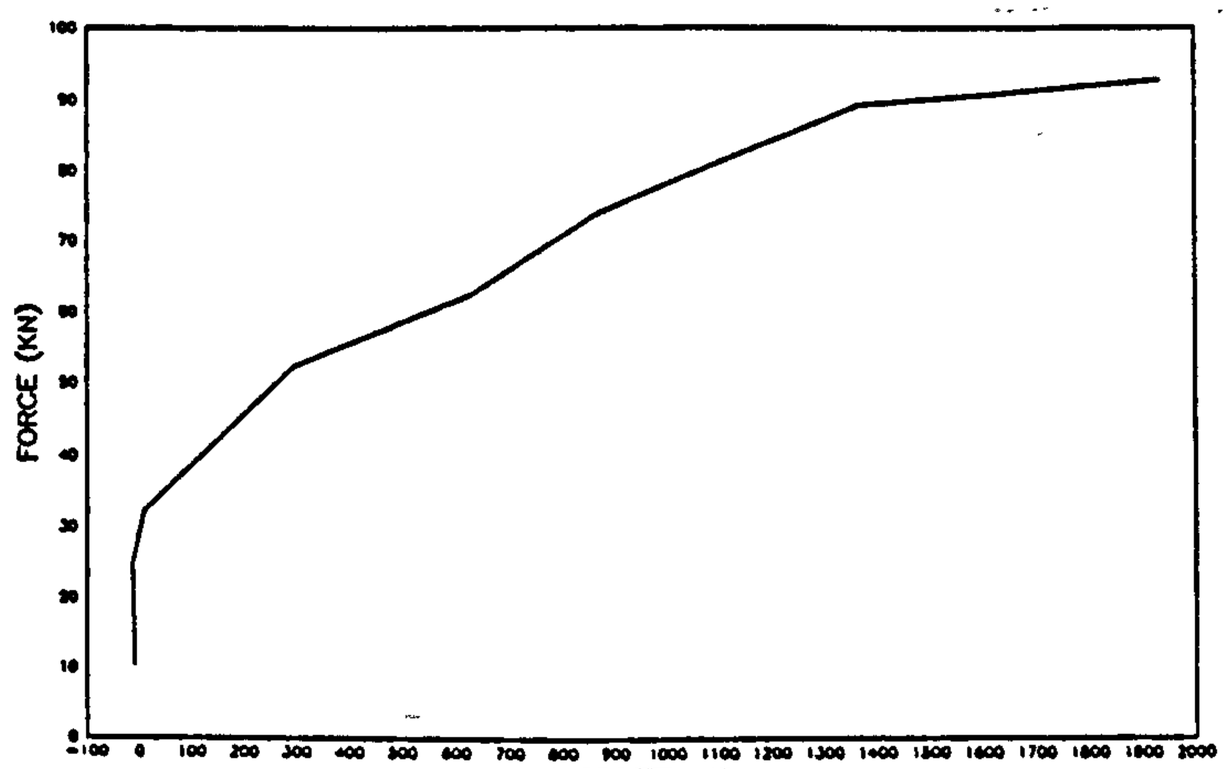


Figure B(11)31 Wall SW11 - force versus strain 19 (stirrup)

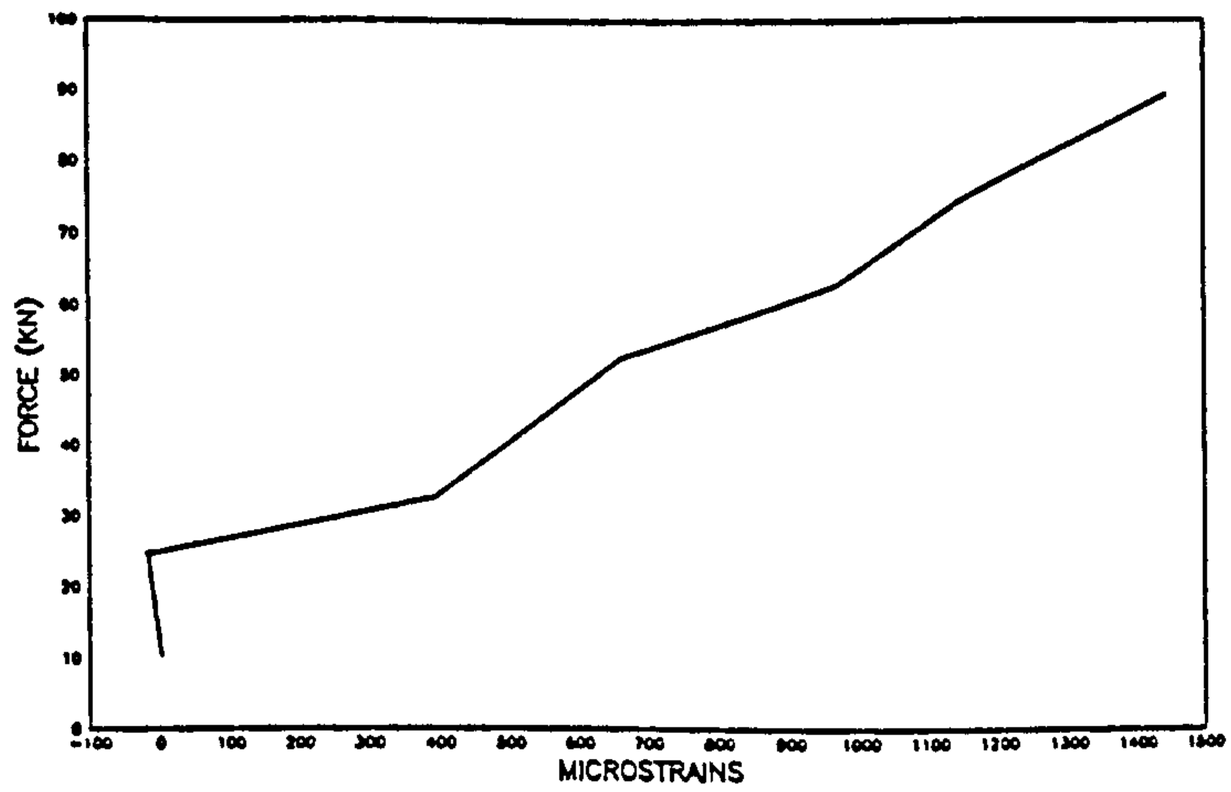


Figure B(11)32 Wall SW11 - force versus strain 20 (stirrup)

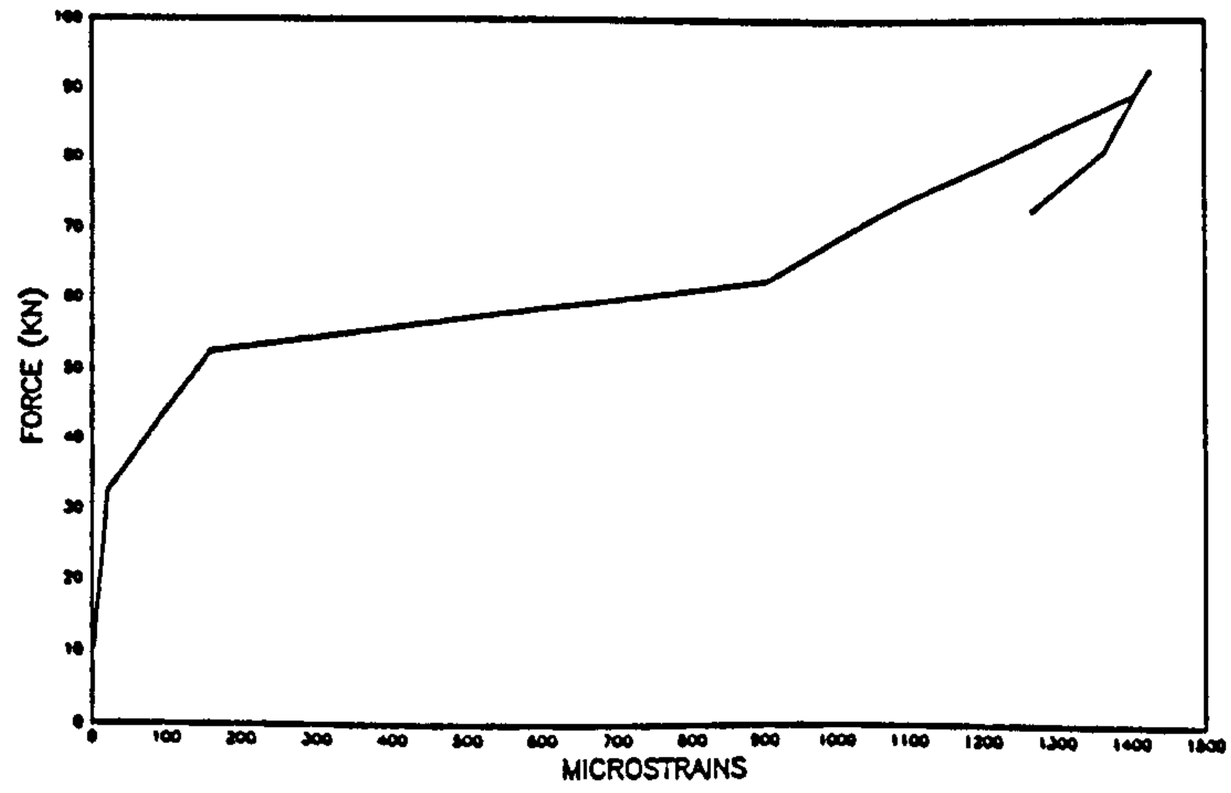


Figure B(11)33 Wall SW11 - force versus strain 21 (stirrup)

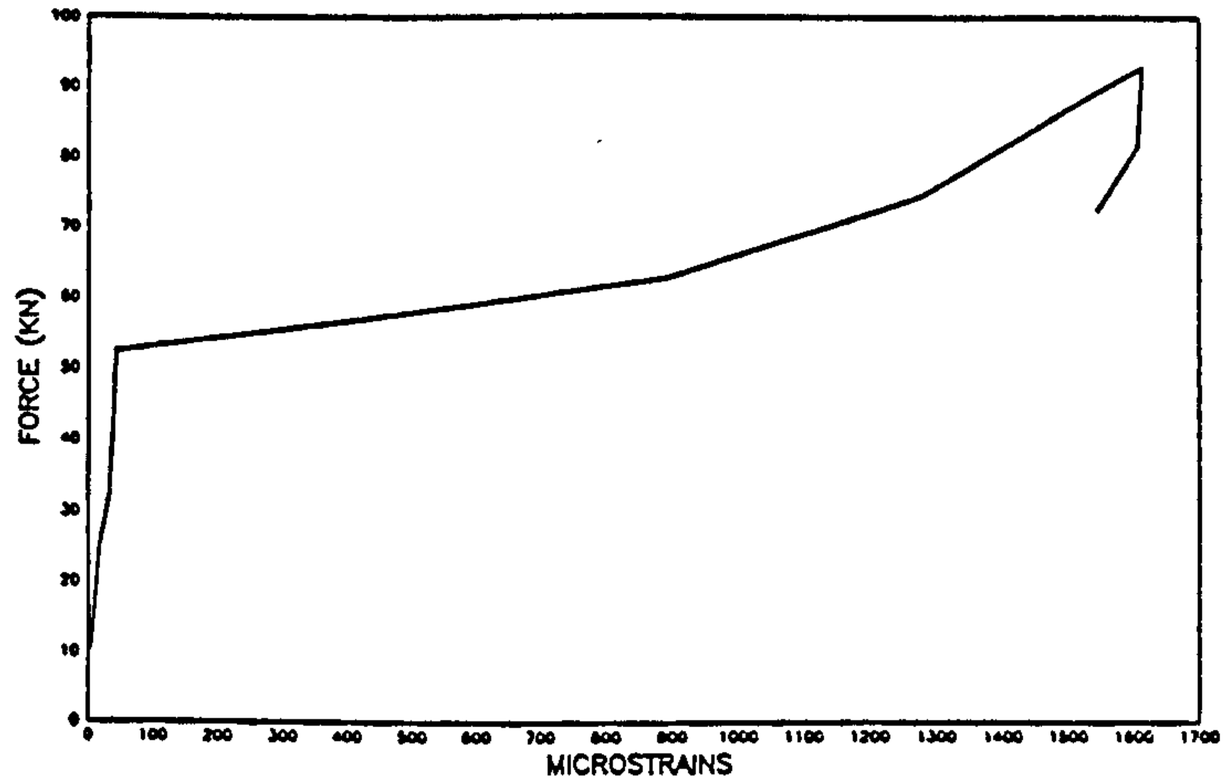


Figure B(11)34 Wall SW11 - force versus strain 22 (stirrup)

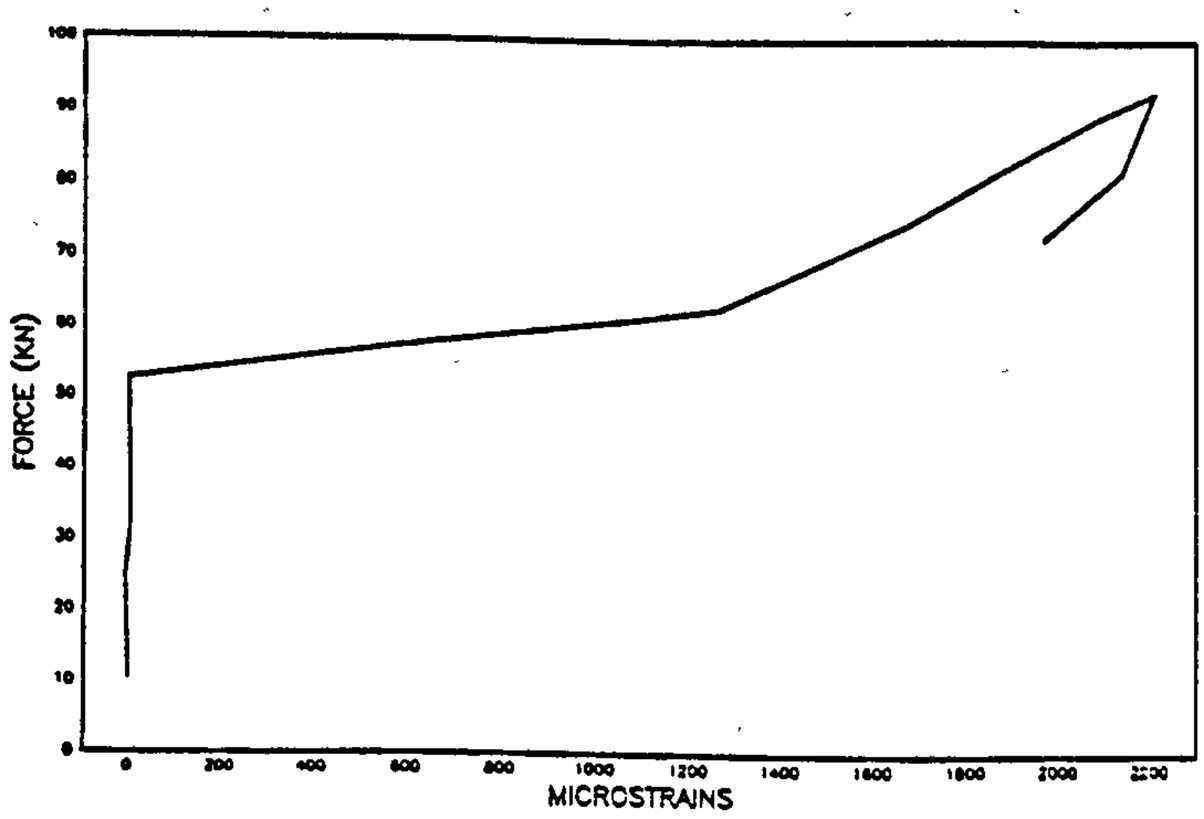


Figure B(11)35 Wall SW11 - force versus strain 23 (stirrup)

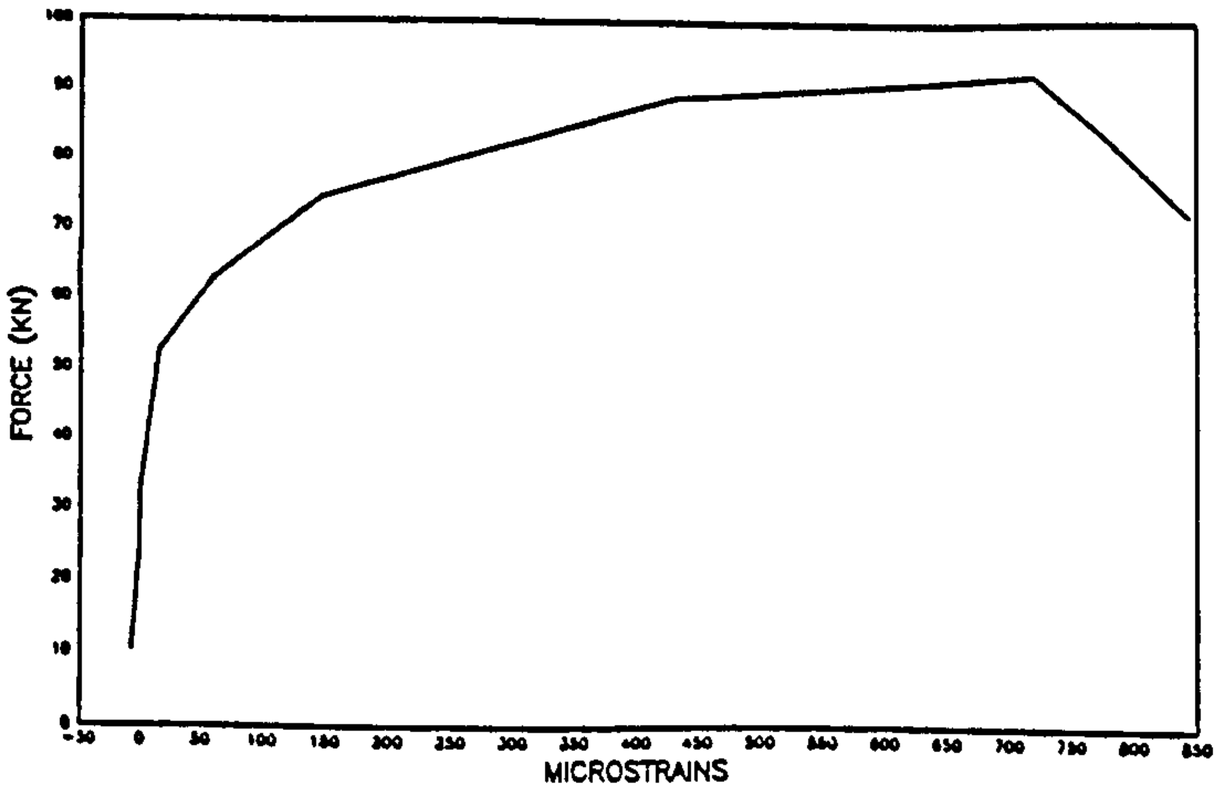


Figure B(11)36.a Wall SW11 - force versus strain 24, (confinement reinforcement)

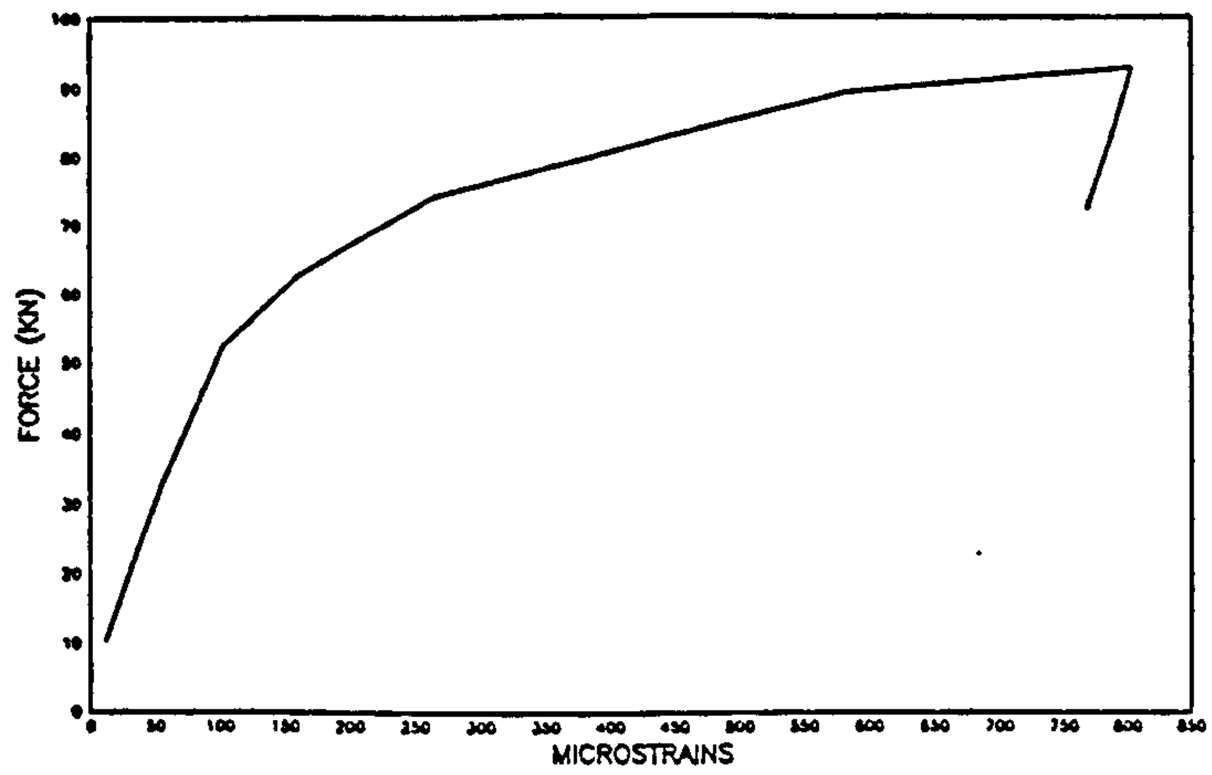


Figure B(11)36.b Wall SW11 - force versus strain 24_{II} (confinement reinforcement)

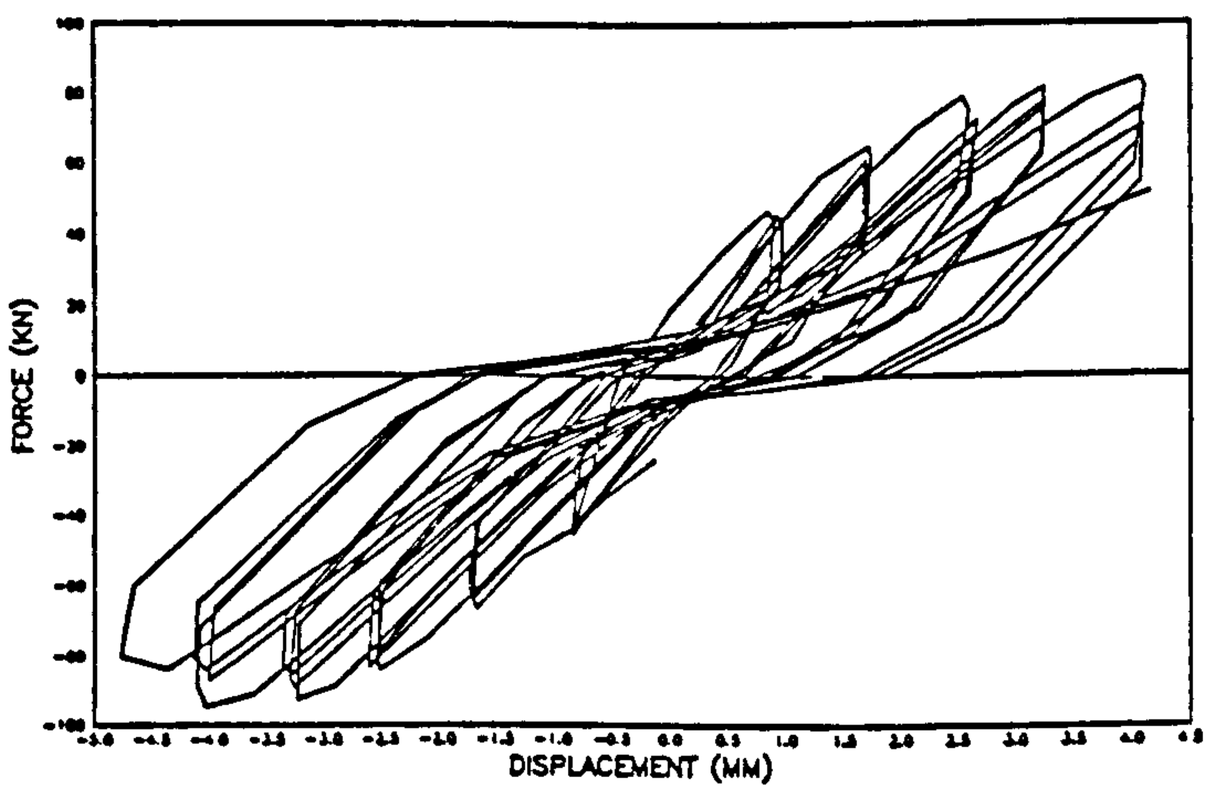


Figure B(12)1 Wall SW12 - force versus displacement 1 (horizontal, LHS, level 4)

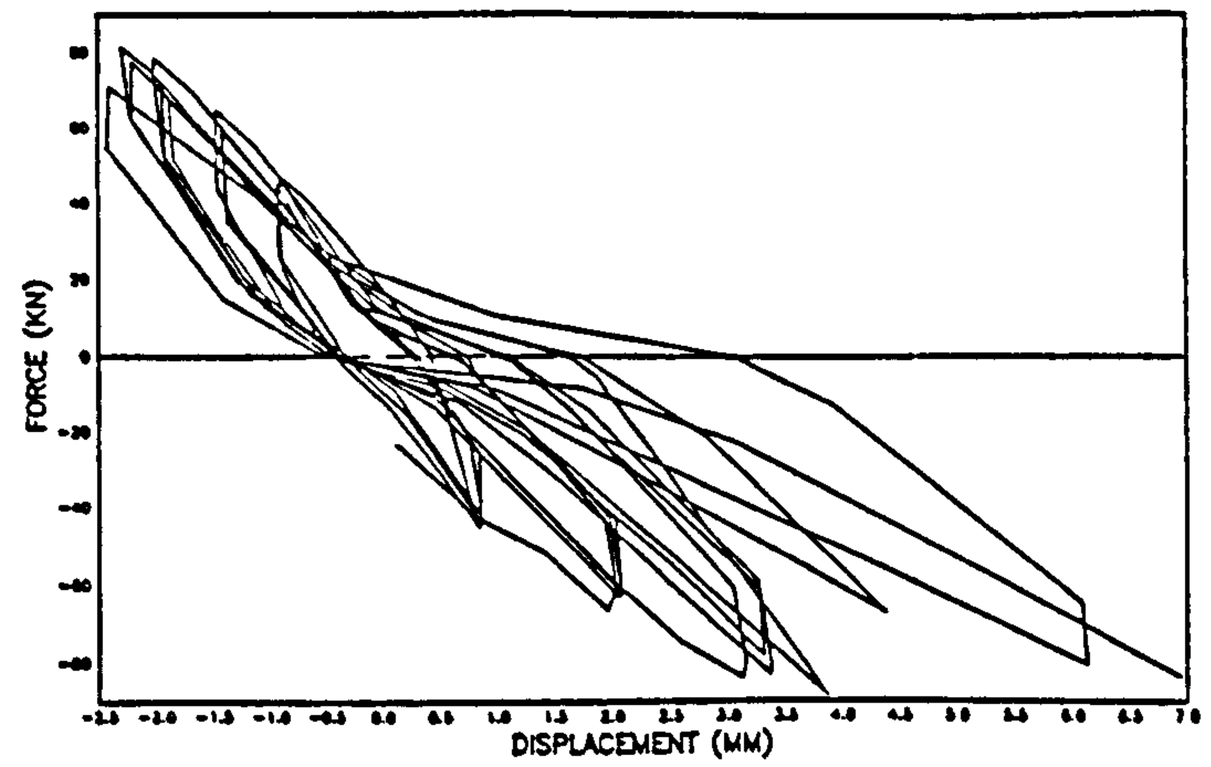


Figure B(12)2 Wall SW12 - force versus displacement 2 (horizontal, RHS, level 4)

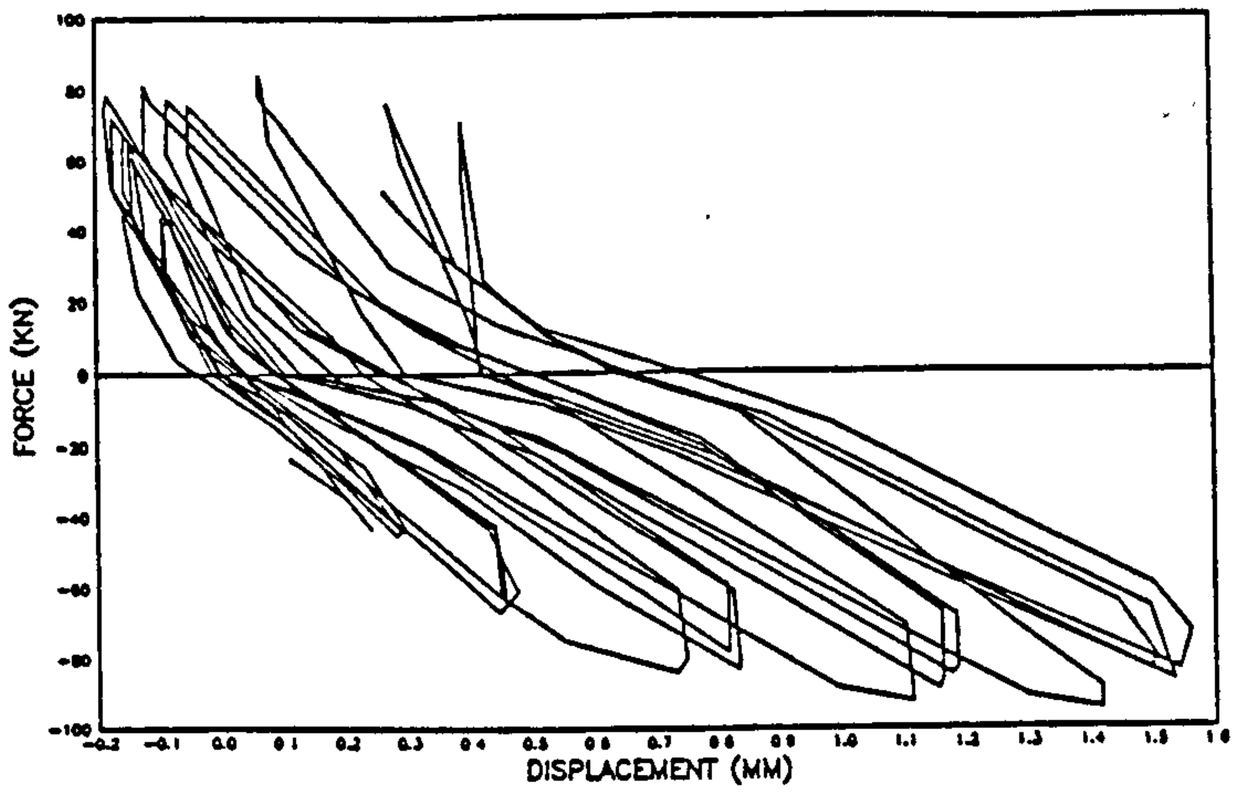


Figure B(12)3 Wall SW12 - force versus displacement 3 (vertical, LHS, level 1)

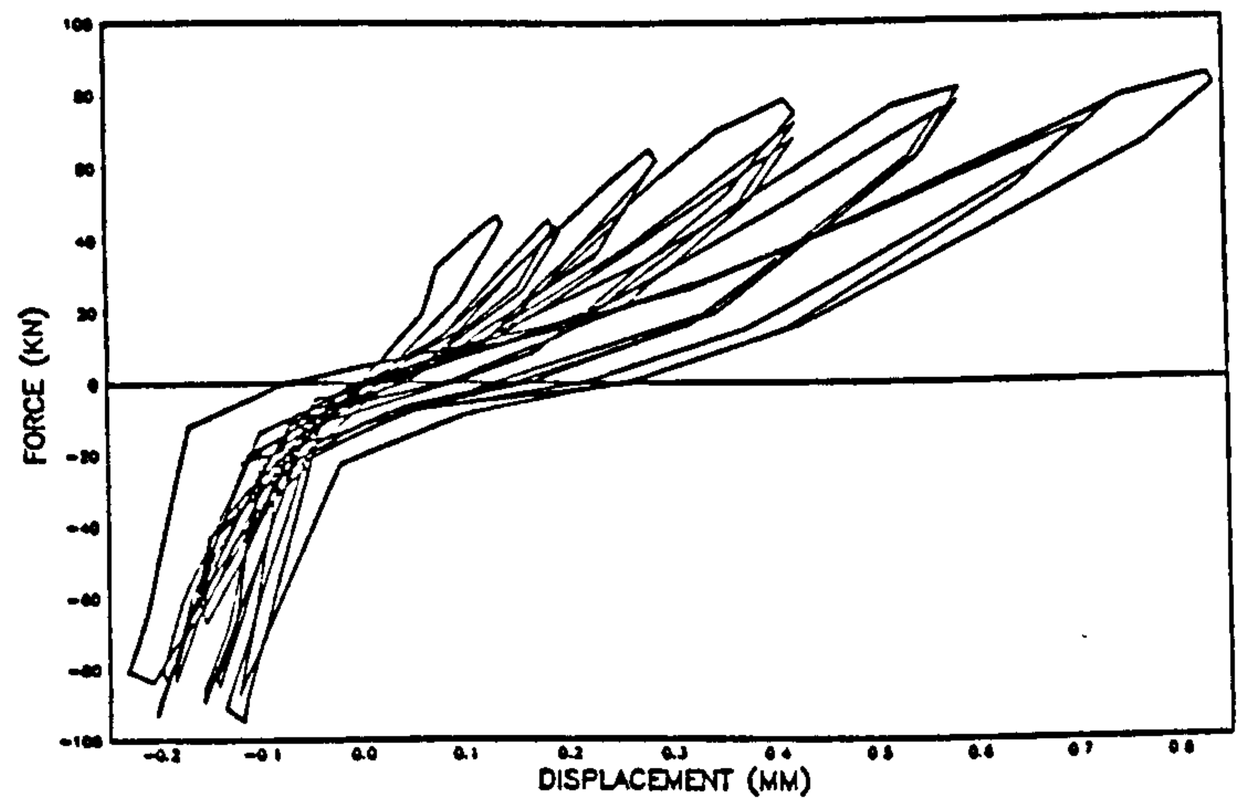


Figure B(12)4 Wall SW12 - force versus displacement 4 (vertical, RHS, level 1)

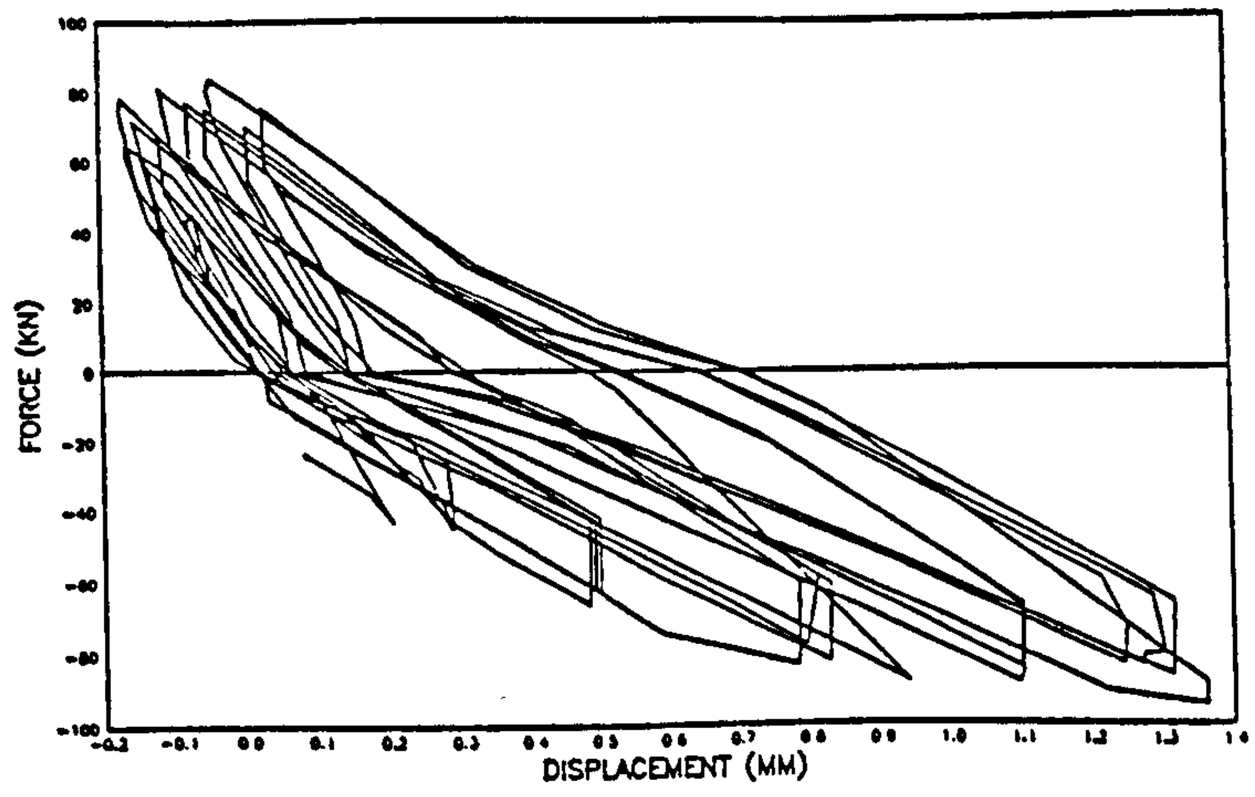


Figure B(12)5 Wall SW12 - force versus displacement 5 (vertical, LHS, level 2)

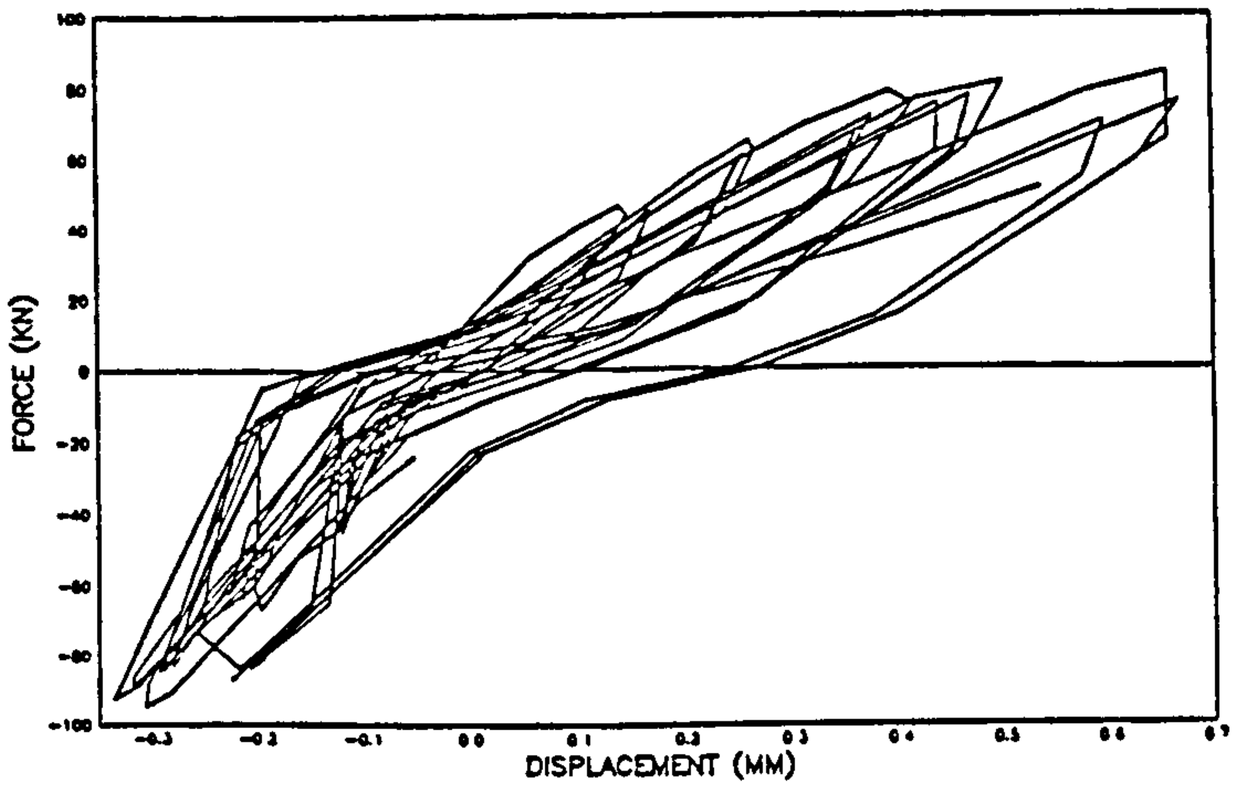


Figure B(12)6 Wall SW12 - force versus displacement 6 (vertical, RHS, level 2)

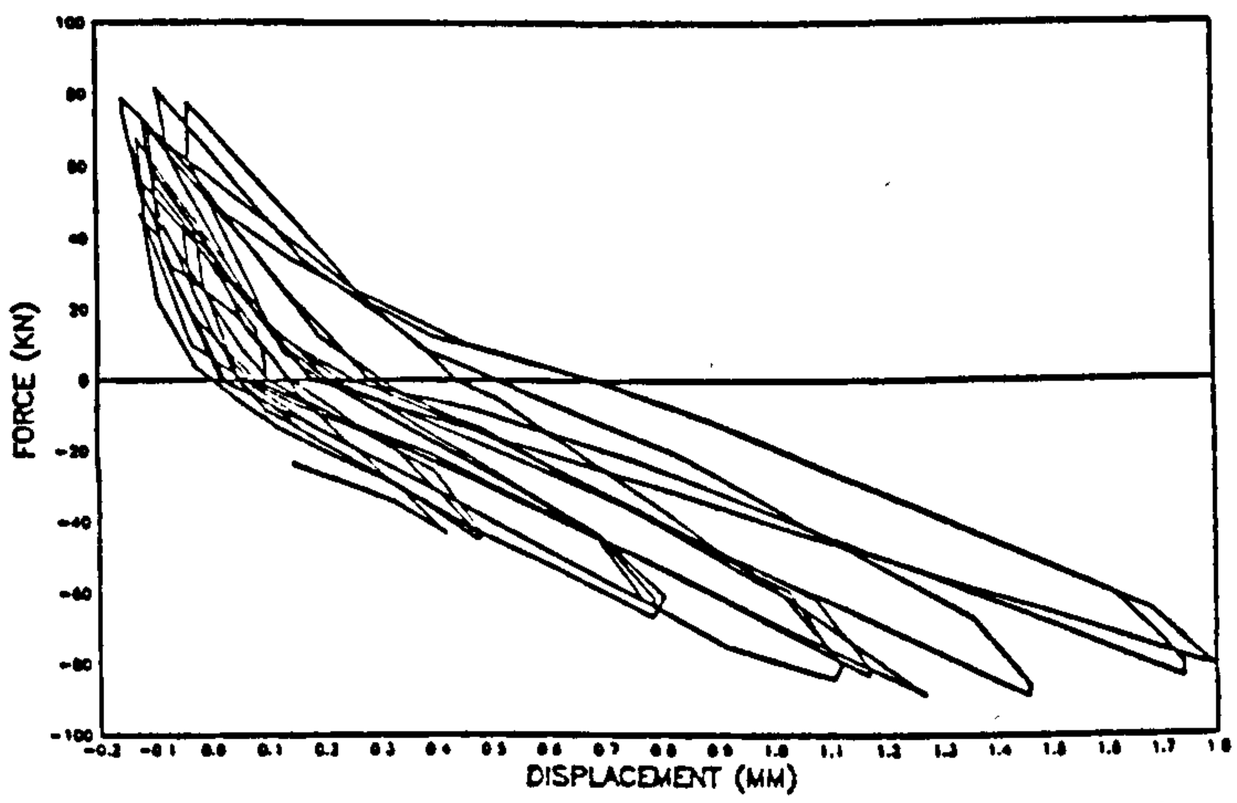


Figure B(12)7 Wall SW12 - force versus displacement 7 (vertical, LHS, level 3)

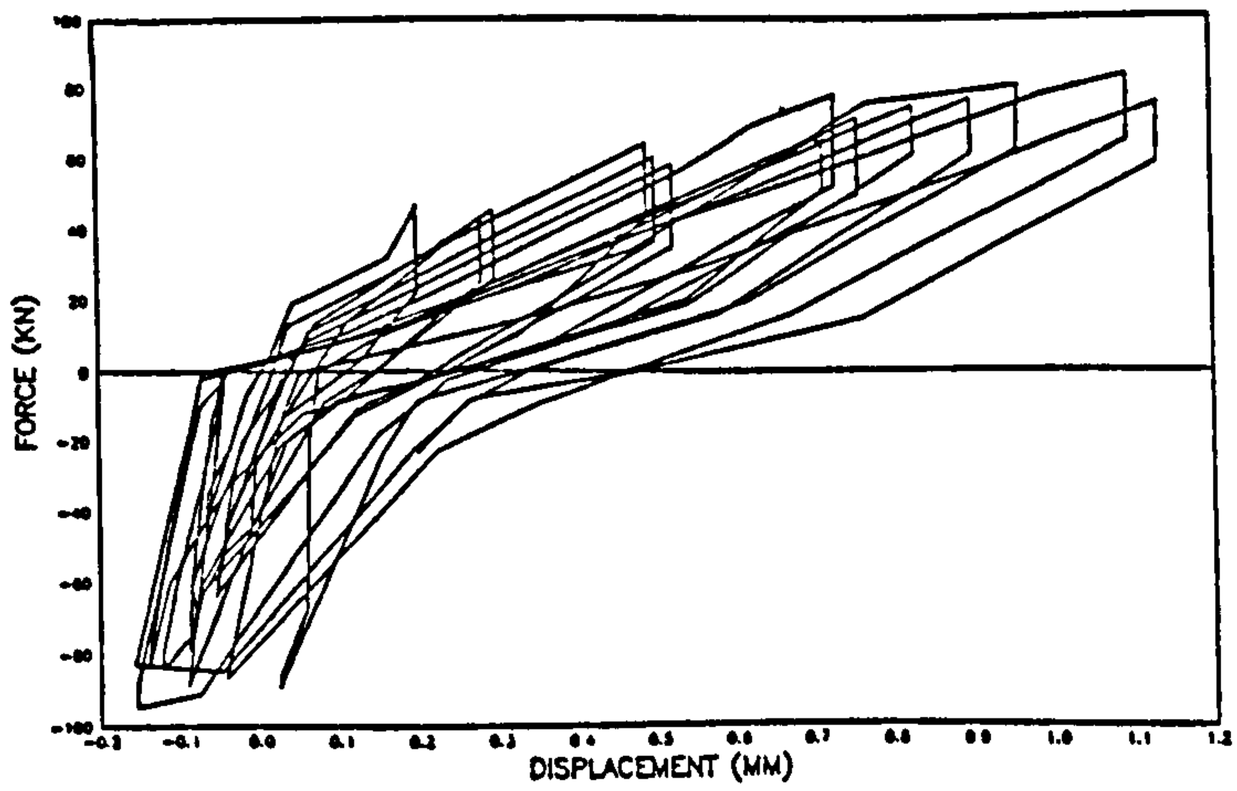


Figure B(12)8 Wall SW12 - force versus displacement 8 (vertical, RHS, level 3)

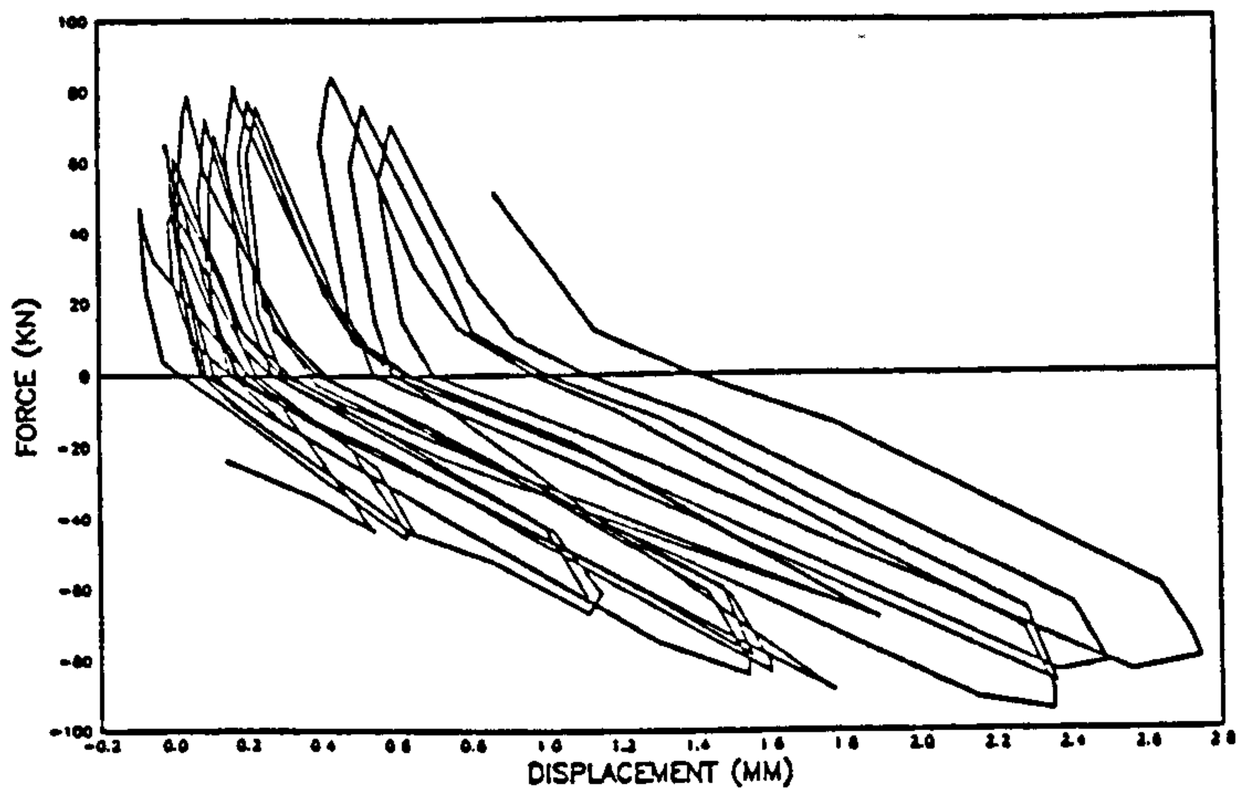


Figure B(12)9 Wall SW12 - force versus displacement 9 (vertical, LHS, level 4)

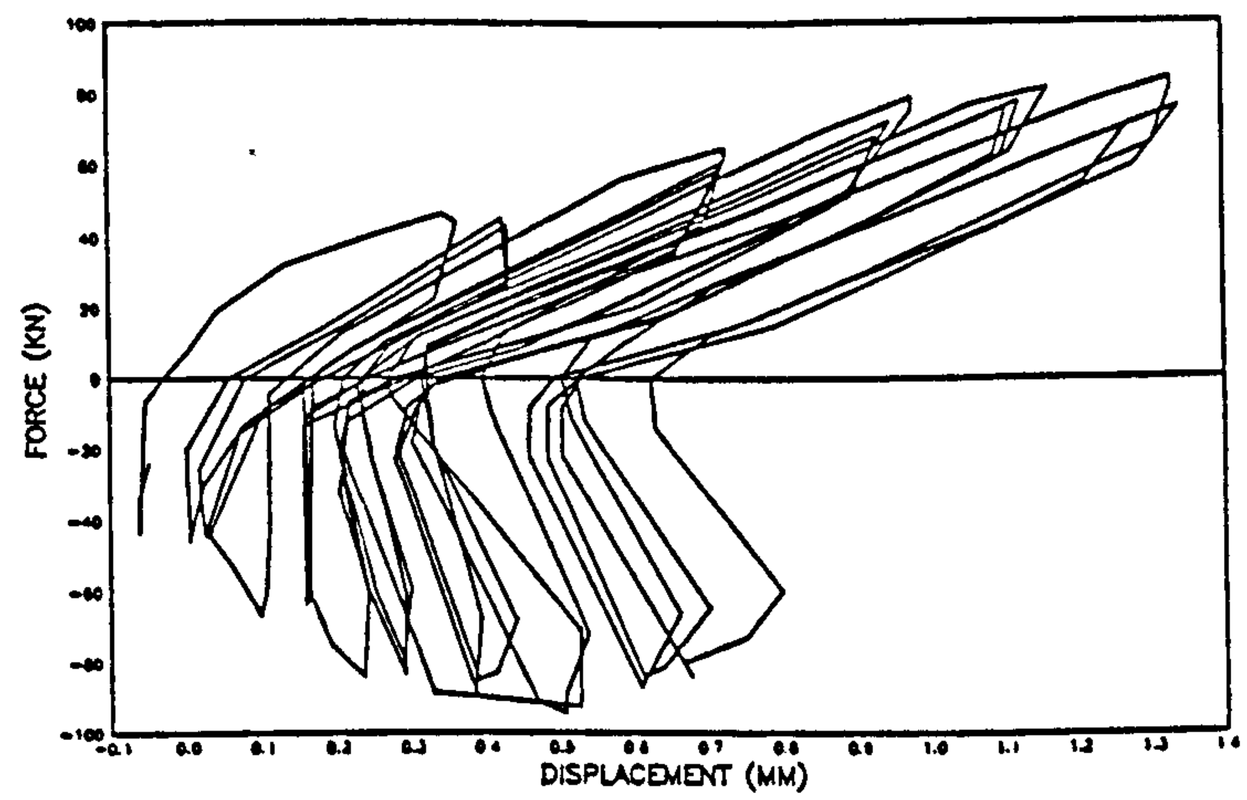


Figure B(12)10 Wall SW12 - force versus displacement 10 (vertical, RHS, level 4)

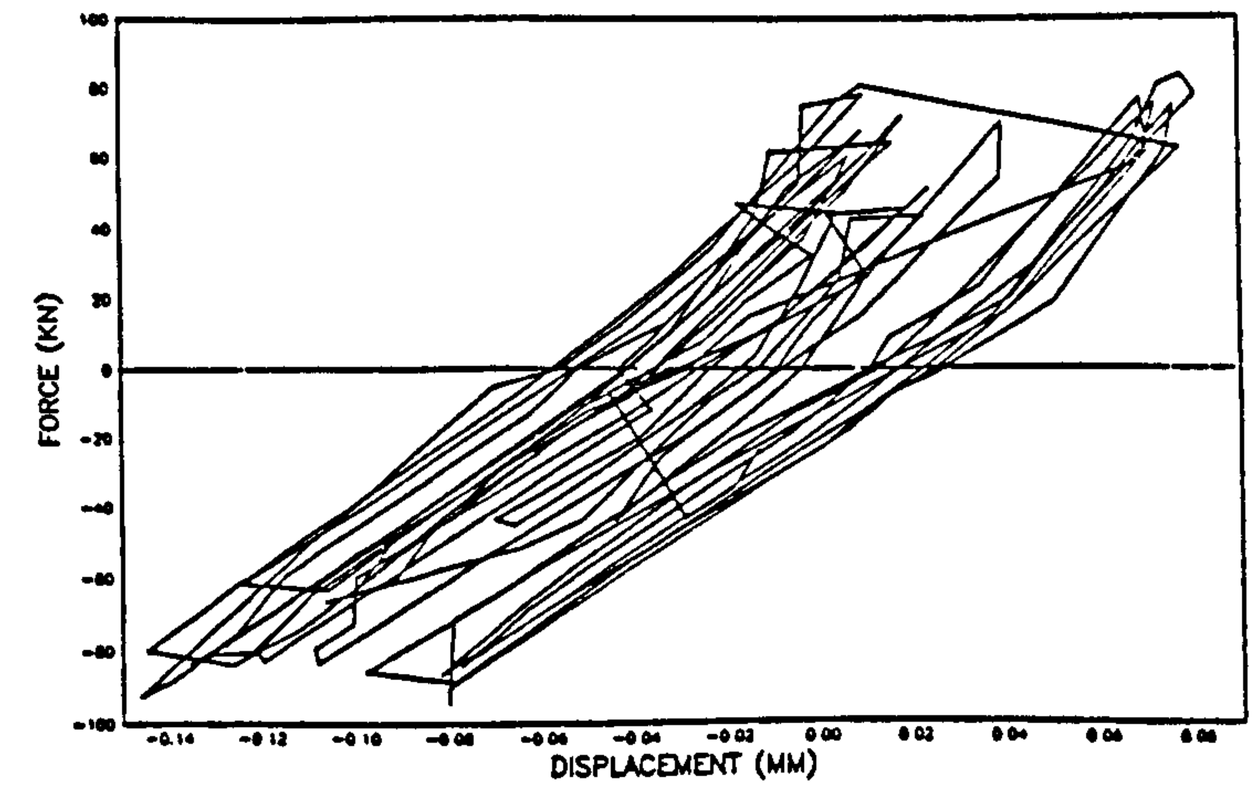


Figure B(12)11 Wall SW12 - force versus displacement 11 (foundation, RHS)

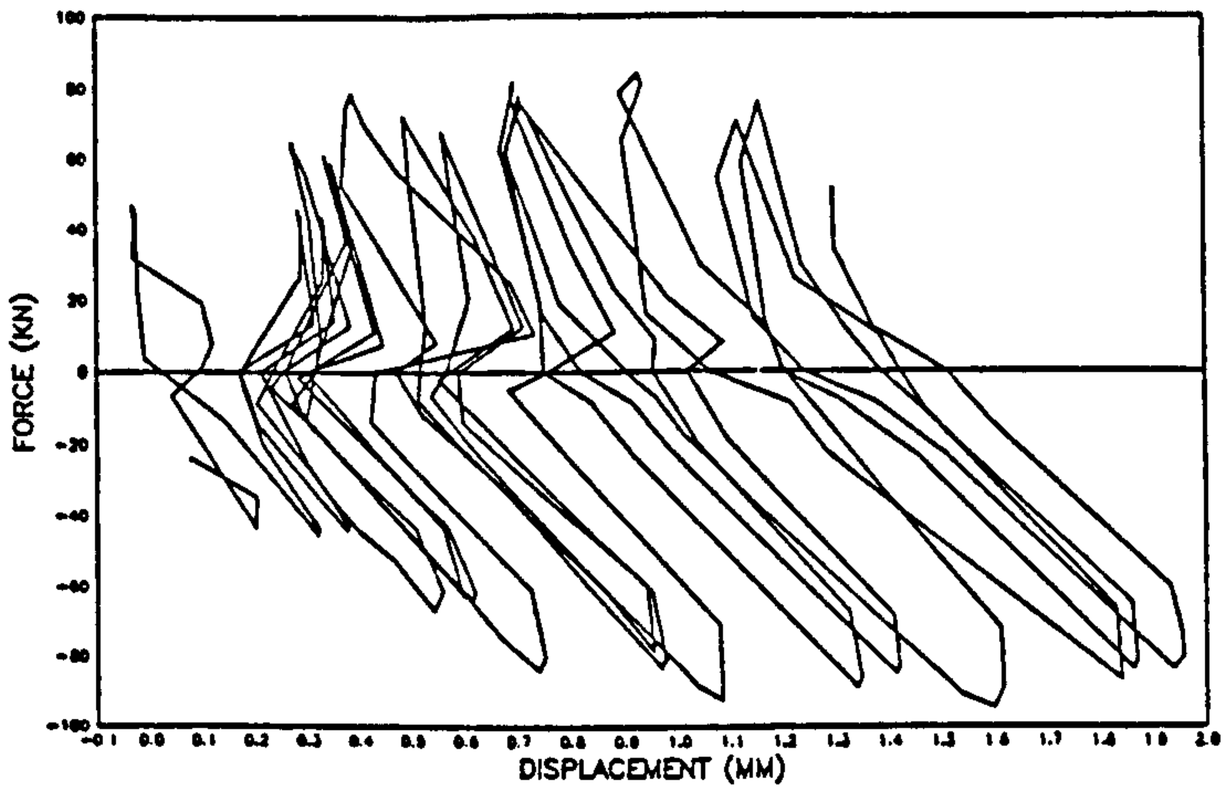


Figure B(12)12 Wall SW12 - force versus displacement 12 (out-of-plane)

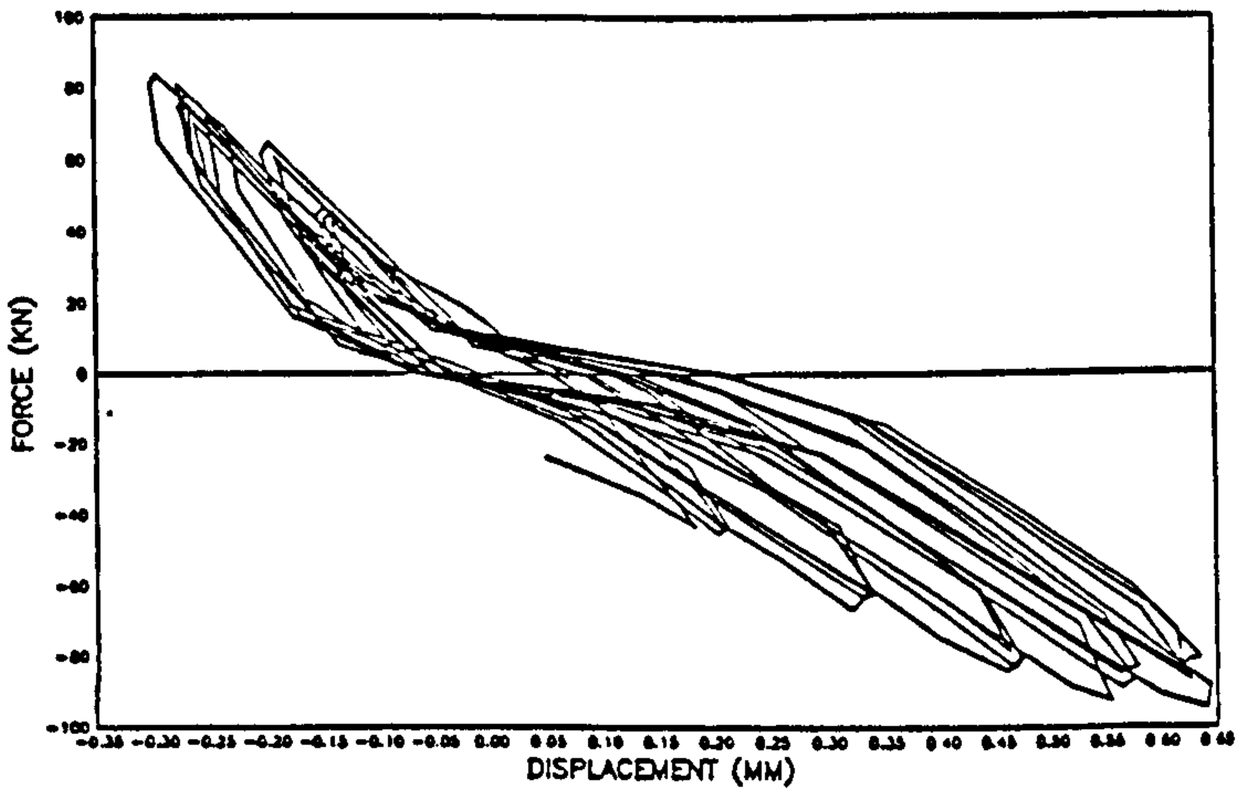


Figure B(12)13 Wall SW12 - force versus displacement 13b (horizontal, RHS, level 1)

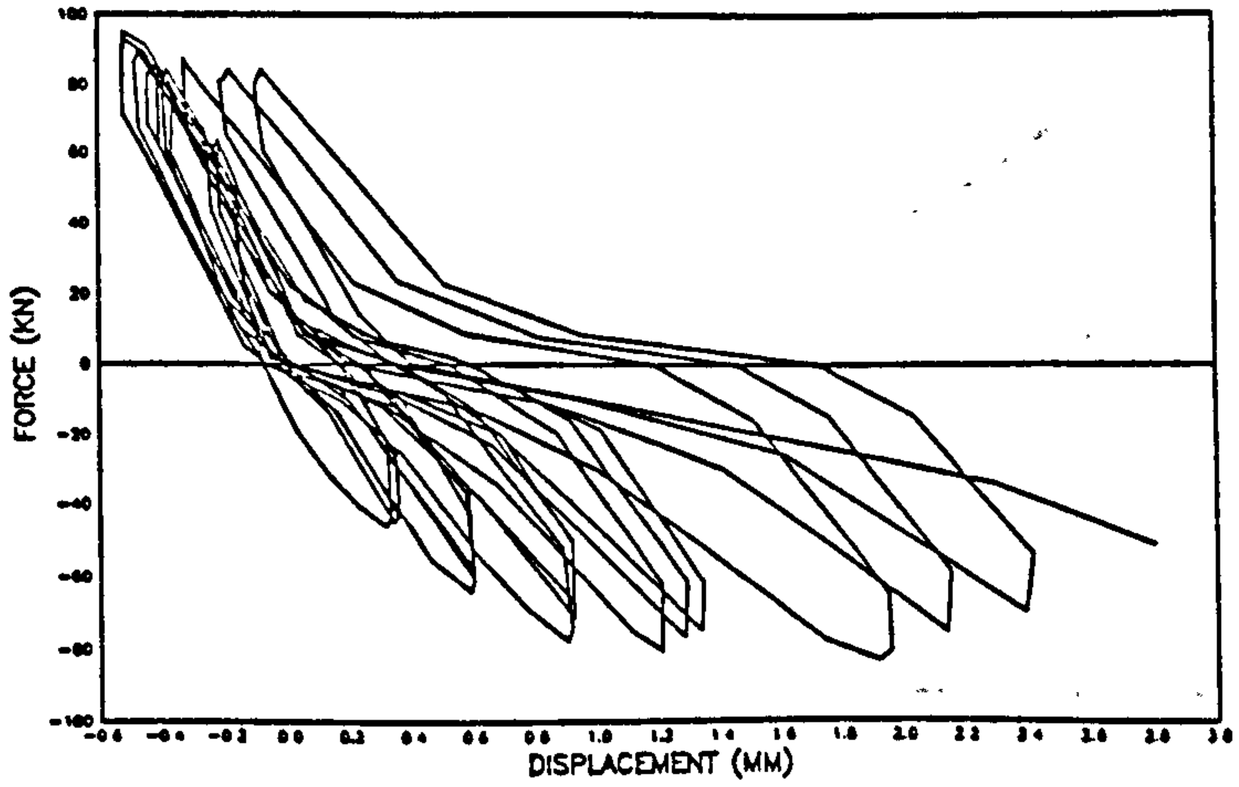


Figure B(12)14 Wall SW12 - force versus displacement 14a (horizontal, RHS, level 2)

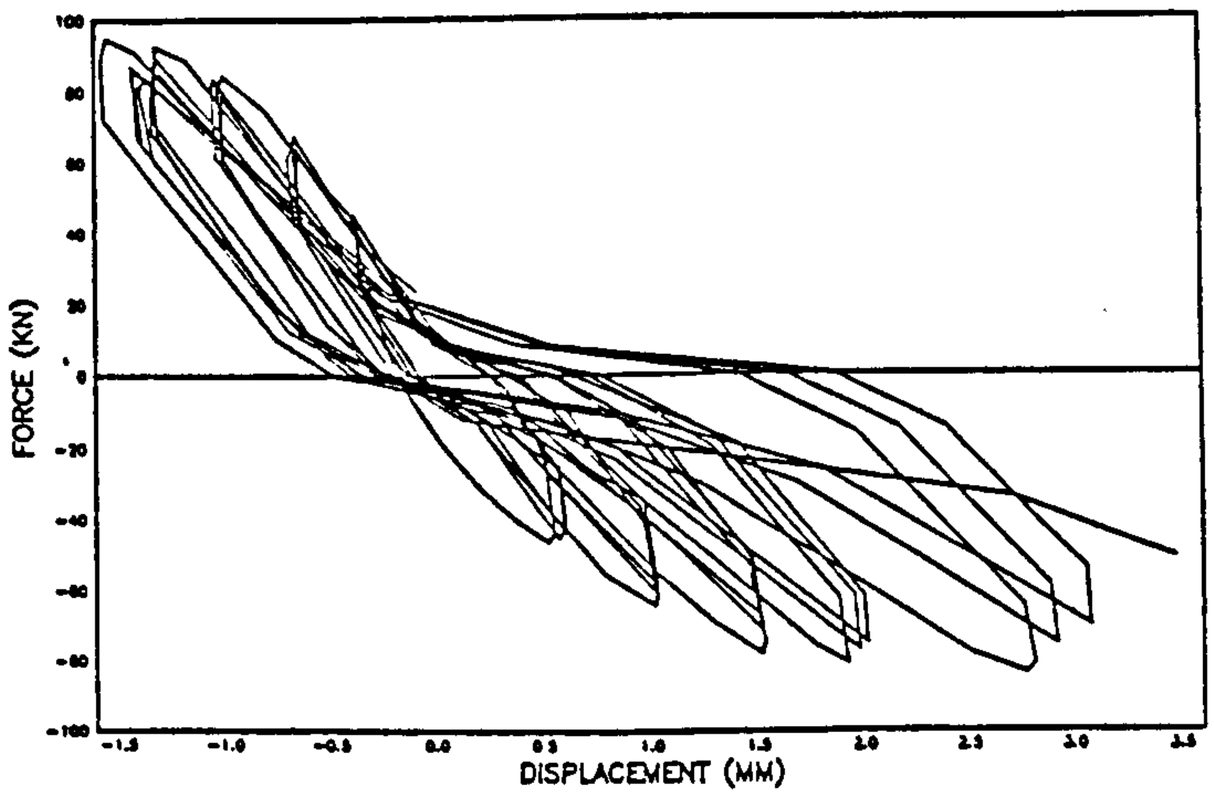


Figure B(12)15 Wall SW12 - force versus displacement 15b (horizontal, RHS, level 3)

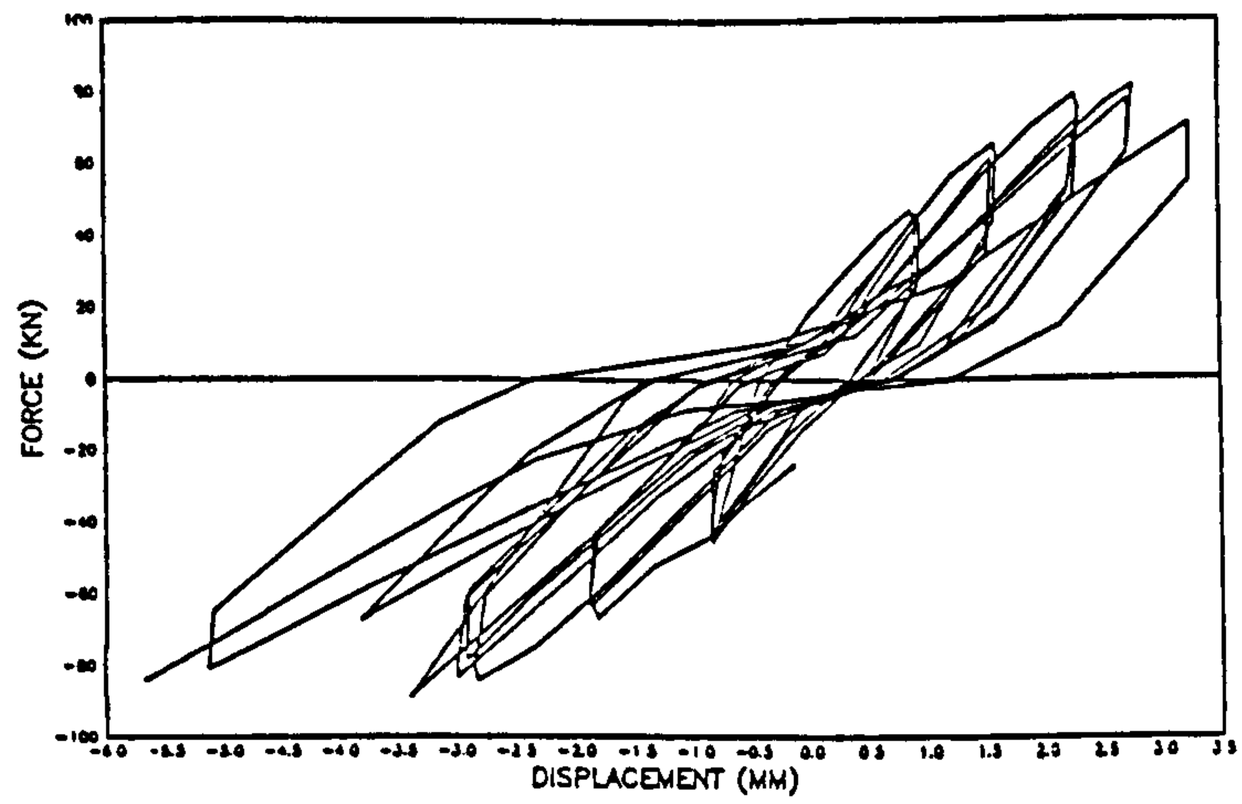


Figure B(12)16 Wall SW12 - force versus top horizontal displacement

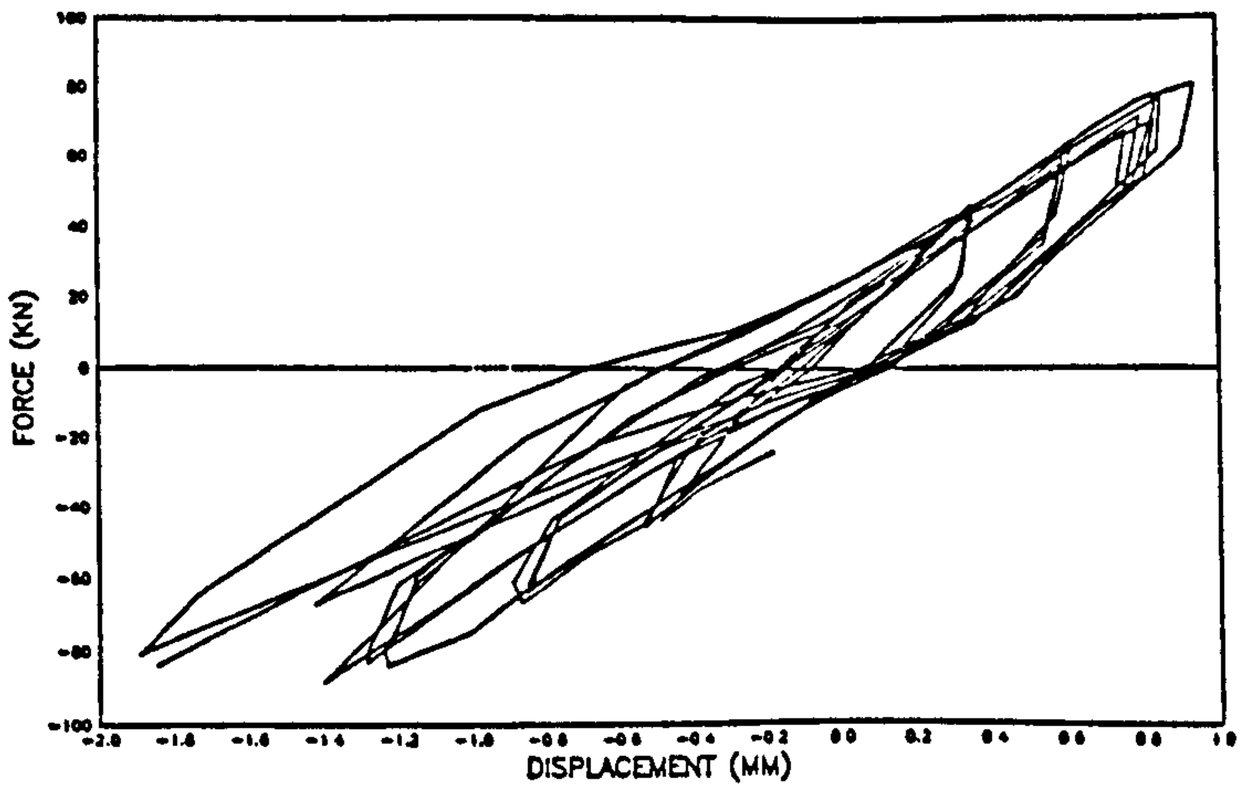


Figure B(12)17 Wall SW12 - force versus flexural component of top horizontal displacement

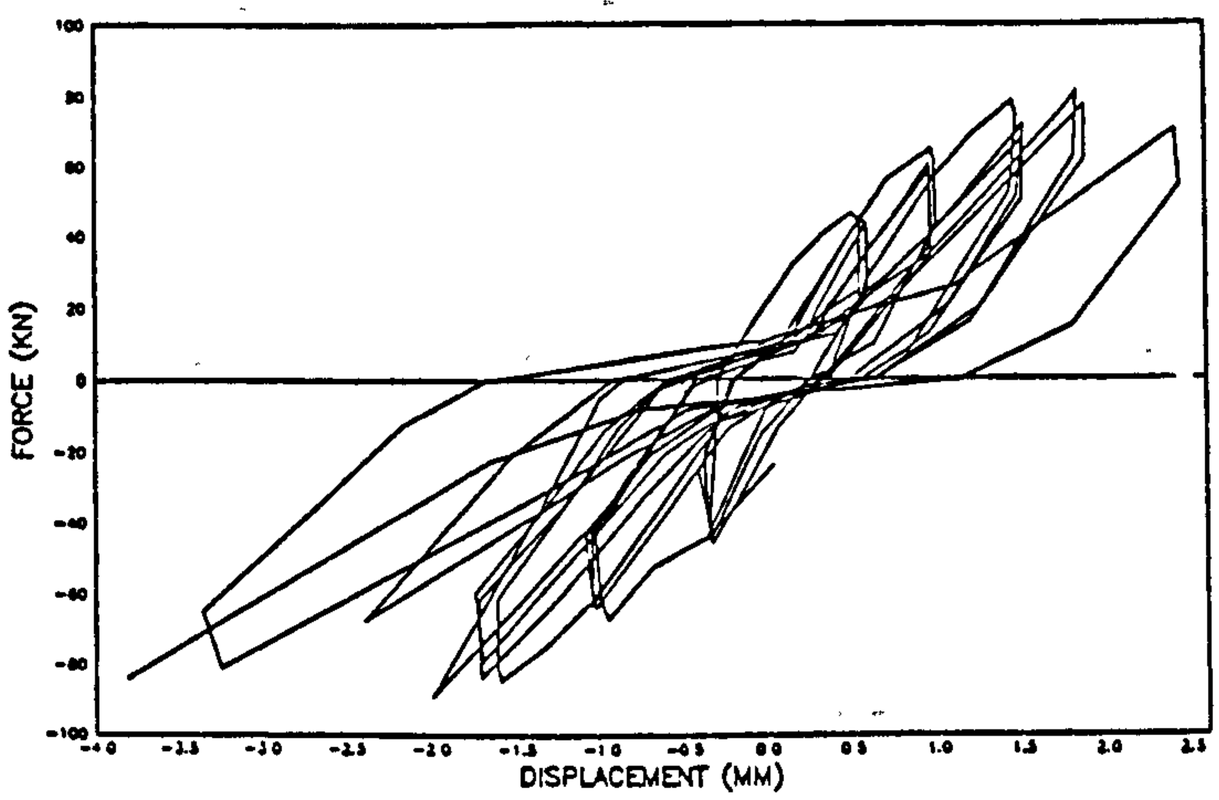


Figure B(12)18 Wall SW12 - force versus shear component of top horizontal displacement

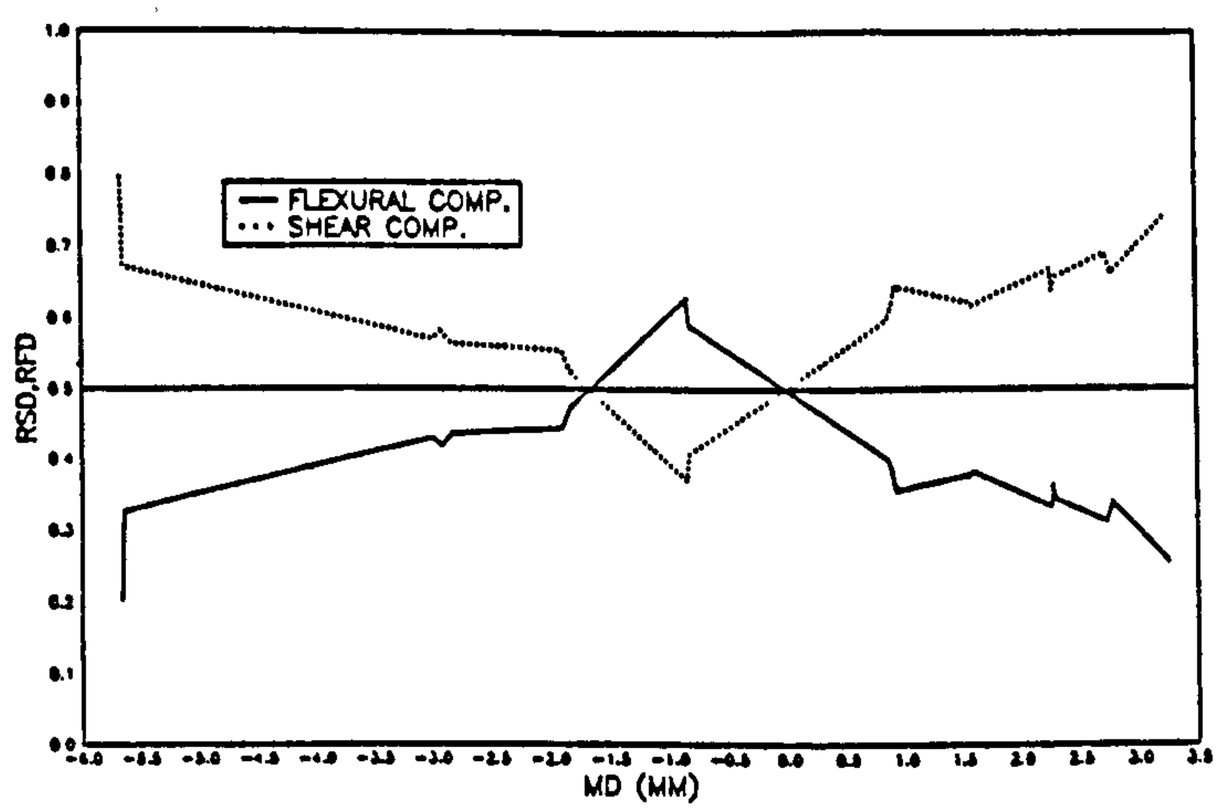


Figure B(12)19 Wall SW12 - RSD,RFD versus MD

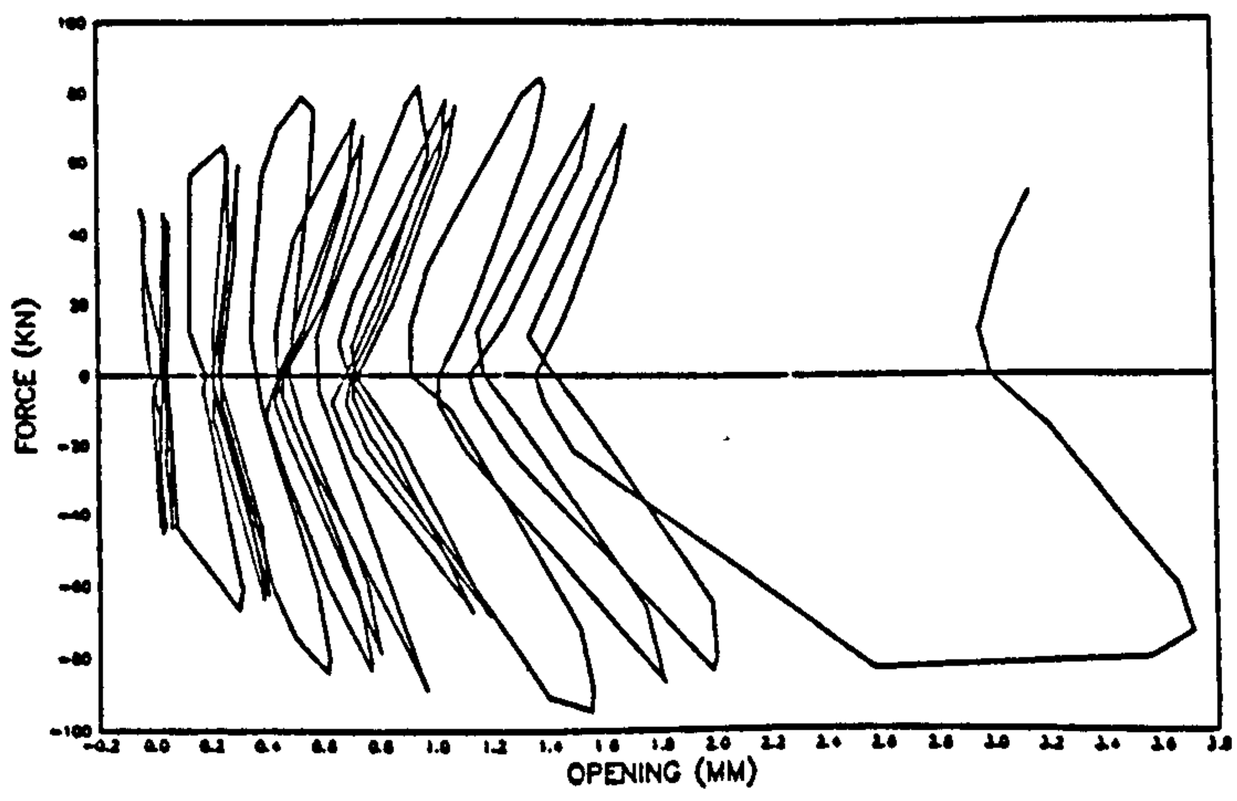


Figure B(12)20 Wall SW12 - force versus opening on top

Figure B(12)21 Wall SW12 - force versus extension at a quarter height

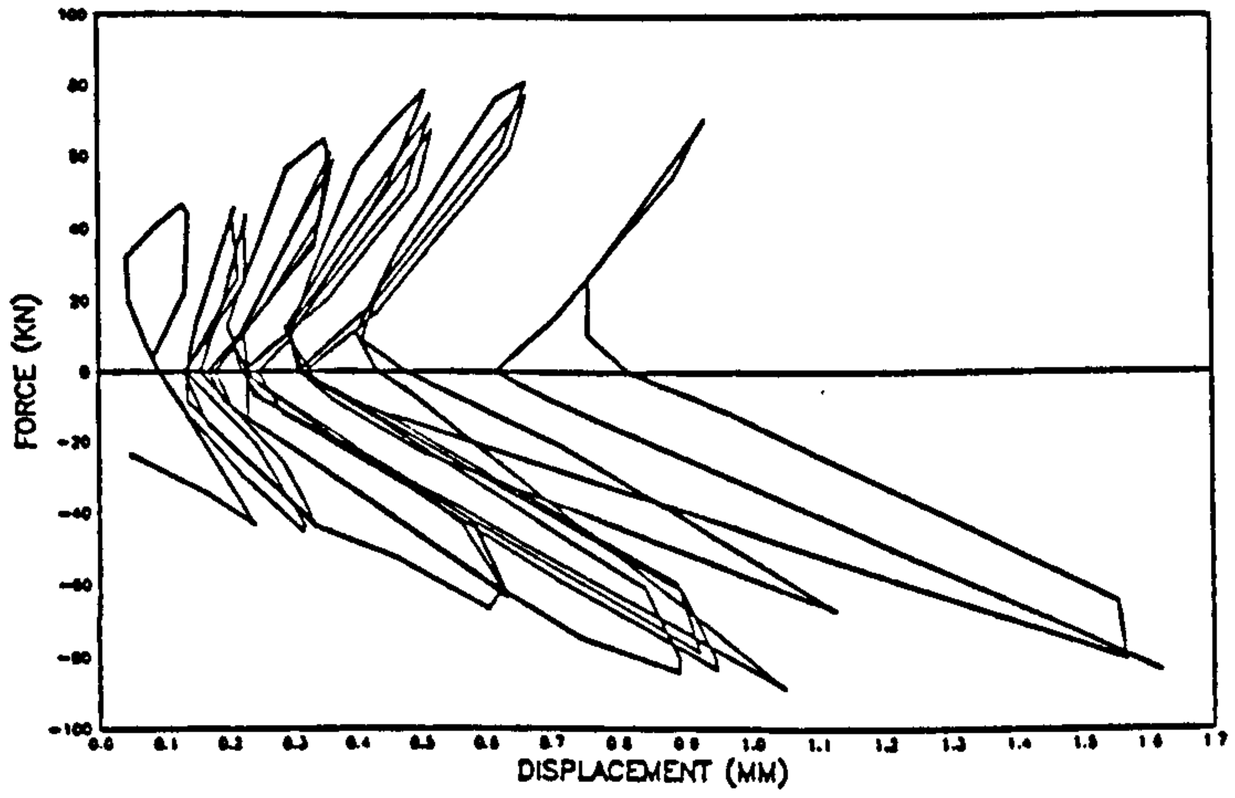


Figure B(12)22 Wall SW12 - force versus extension on top

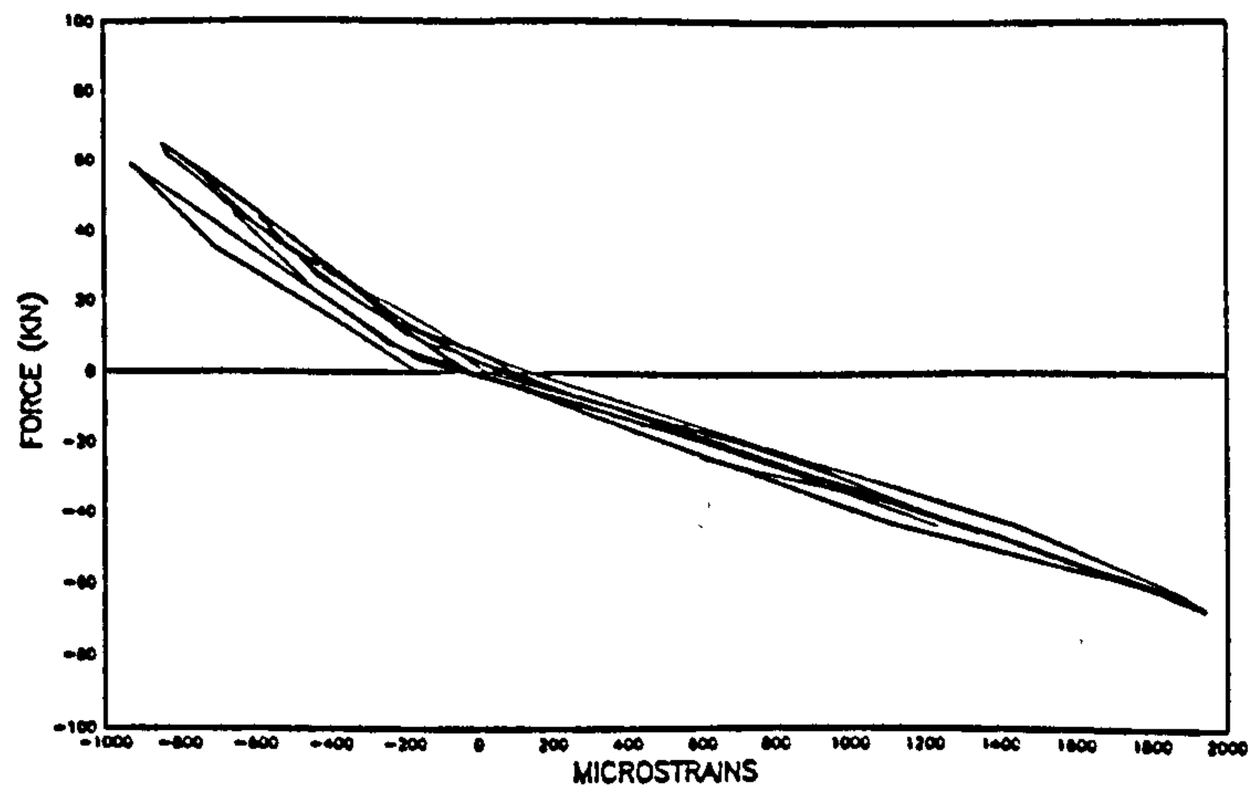


Figure B(12)23 Wall SW12 - force versus strain 1 (bottom, ϕ8mm, LHS)

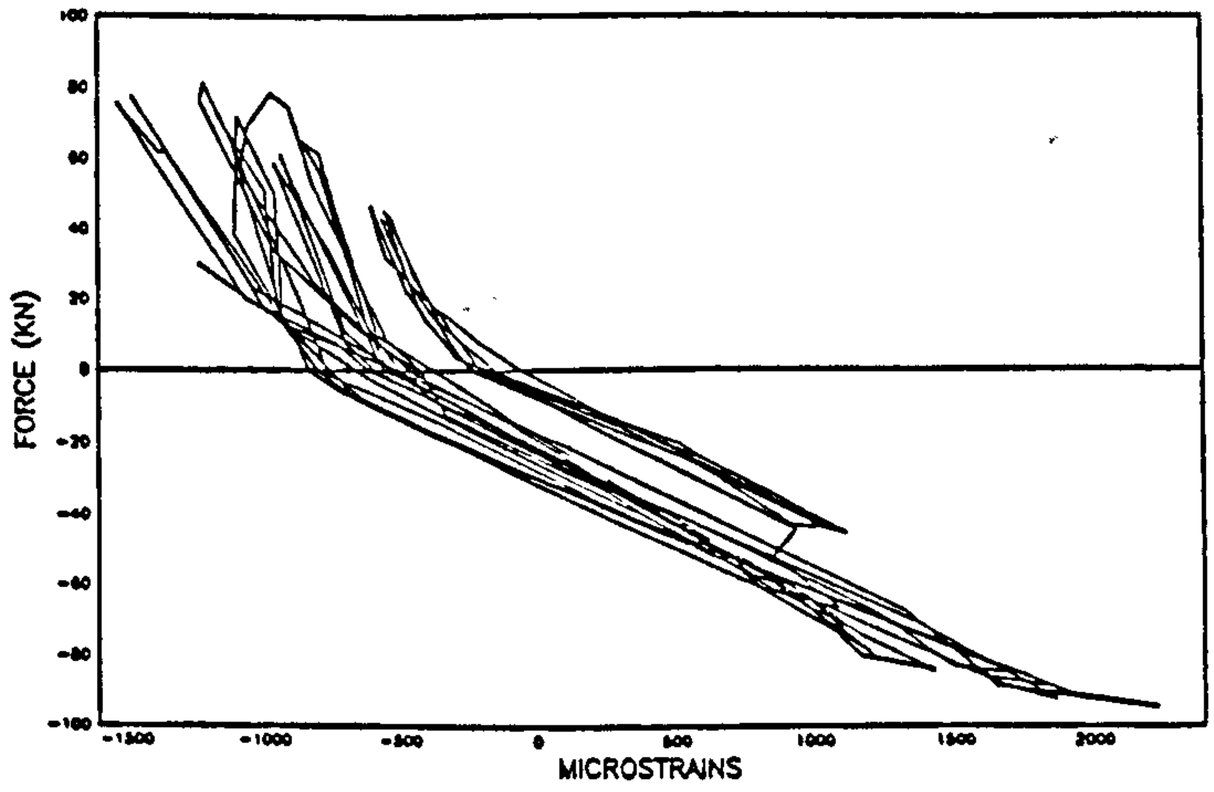


Figure B(12)24 Wall SW12 - force versus strain 3 (bottom, ϕ6mm, LHS)

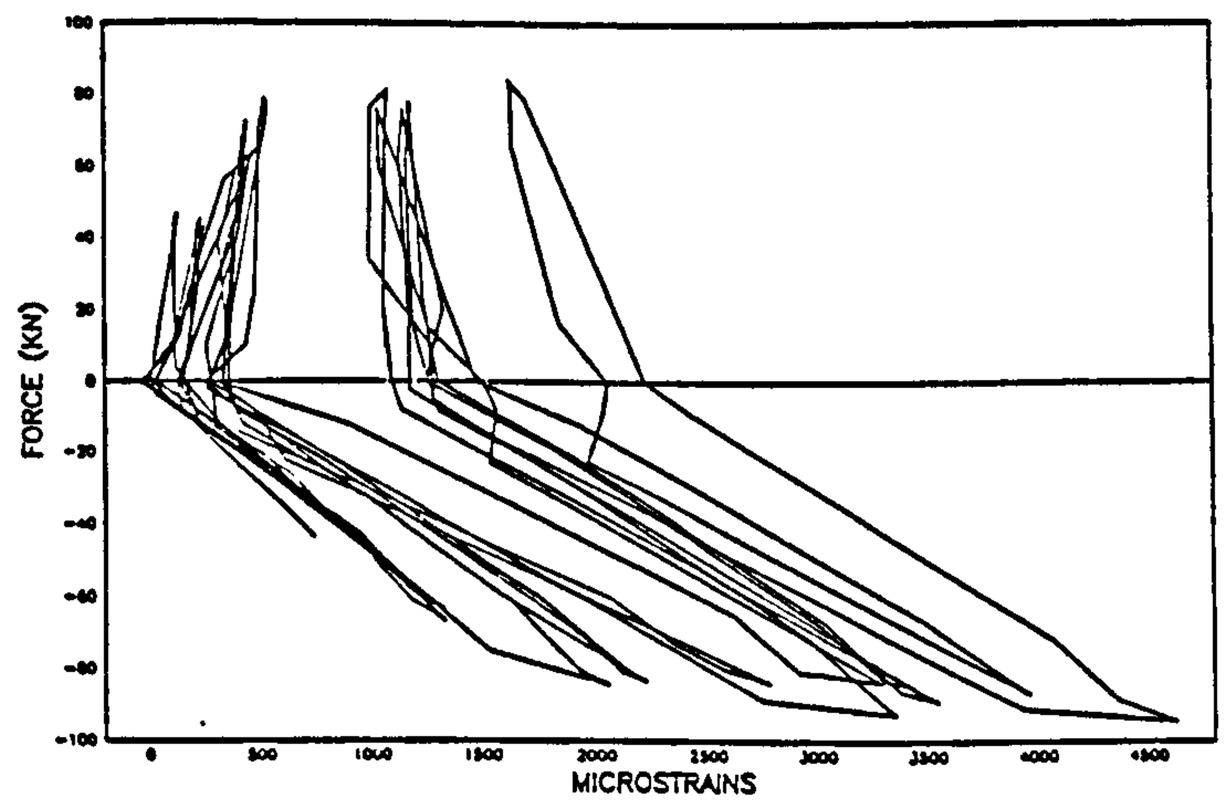


Figure B(12)25 Wall SW12 - force versus strain 5 (bottom, ϕ6mm, LHS)

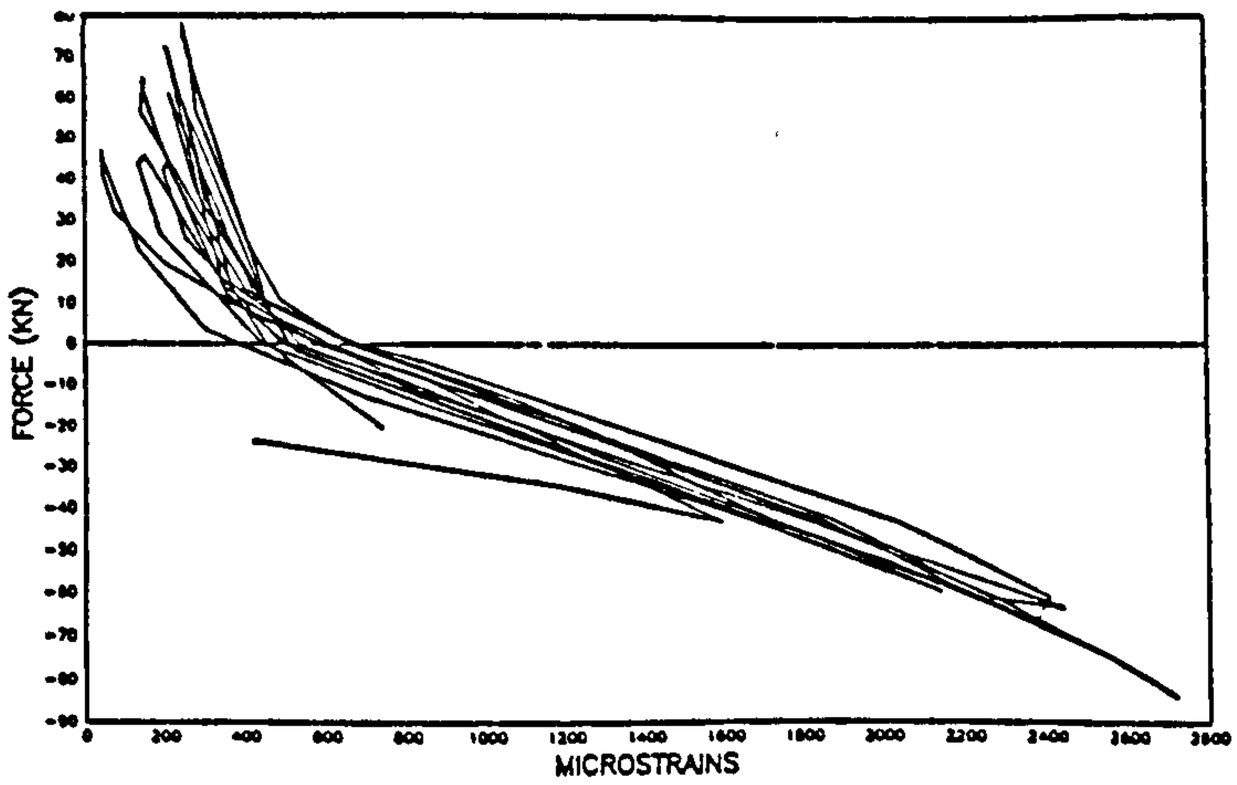


Figure B(12)26 Wall SW12 - force versus strain 9 (second level, ϕ8mm, LHS)

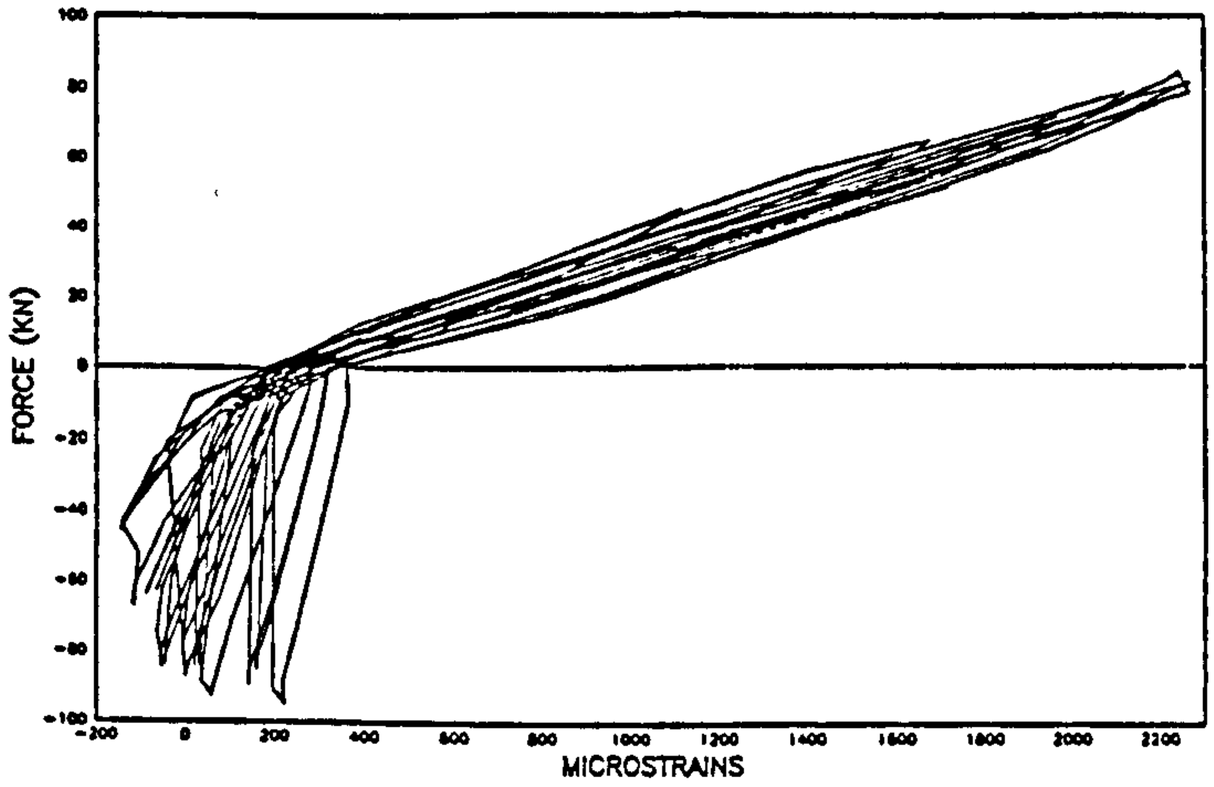


Figure B(12)27 Wall SW12 - force versus strain 10 (second level, ϕ8mm, RHS)

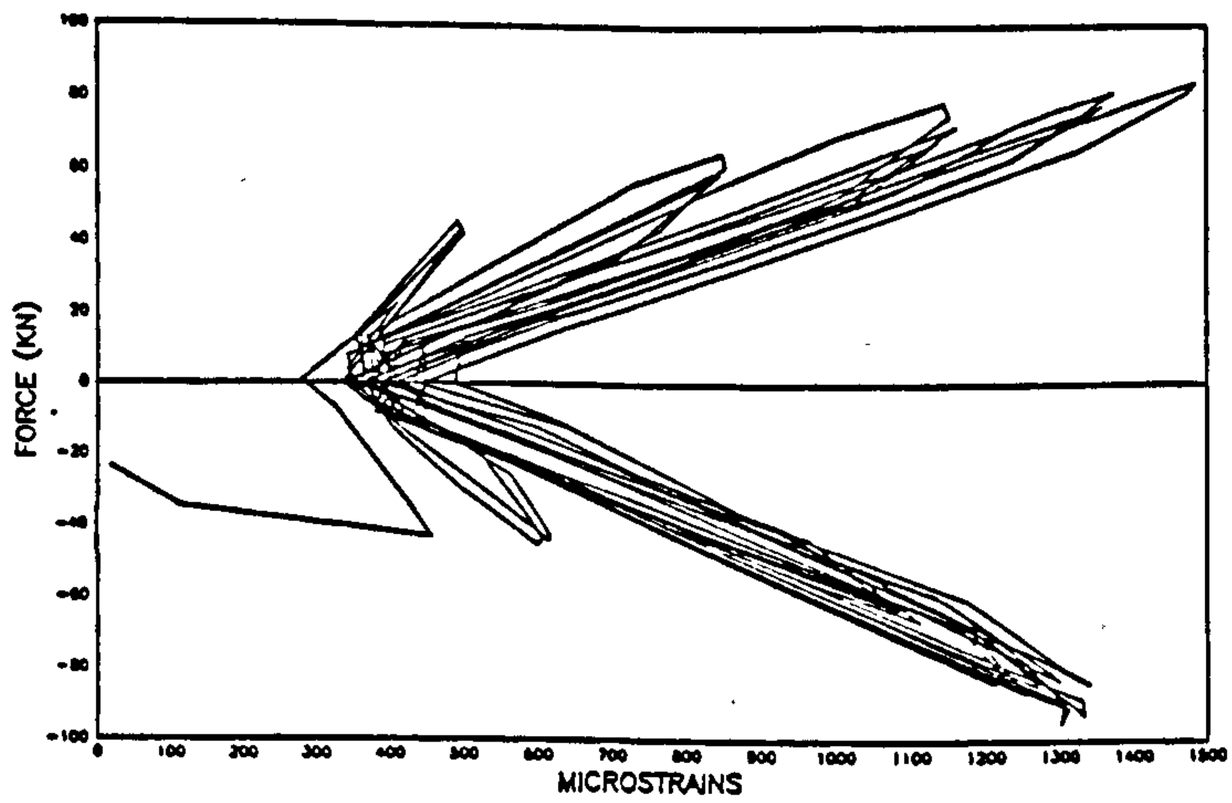


Figure B(12)28 Wall SW12 - force versus strain 11 (level of zero moment, ϕ8mm, LHS)

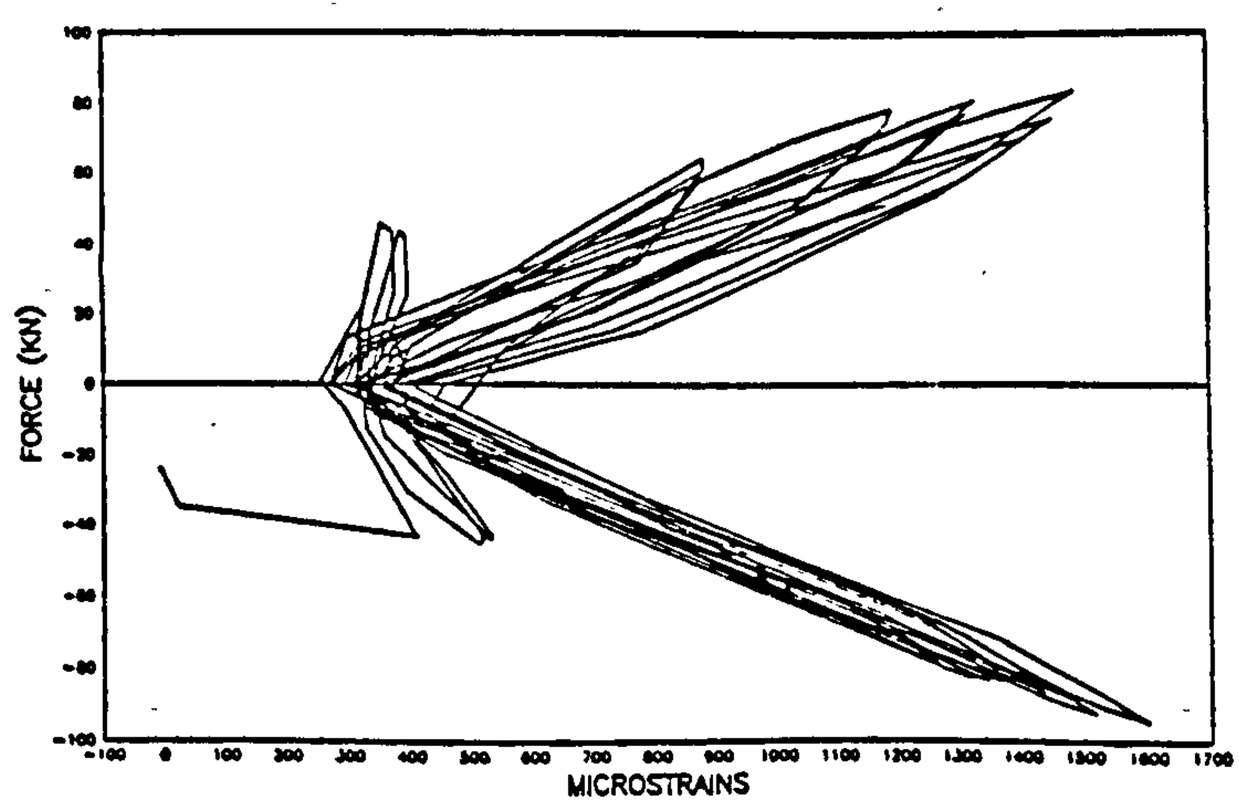


Figure B(12)29 Wall SW12 - force versus strain 12 (level of zero moment, ϕ8mm, RHS)

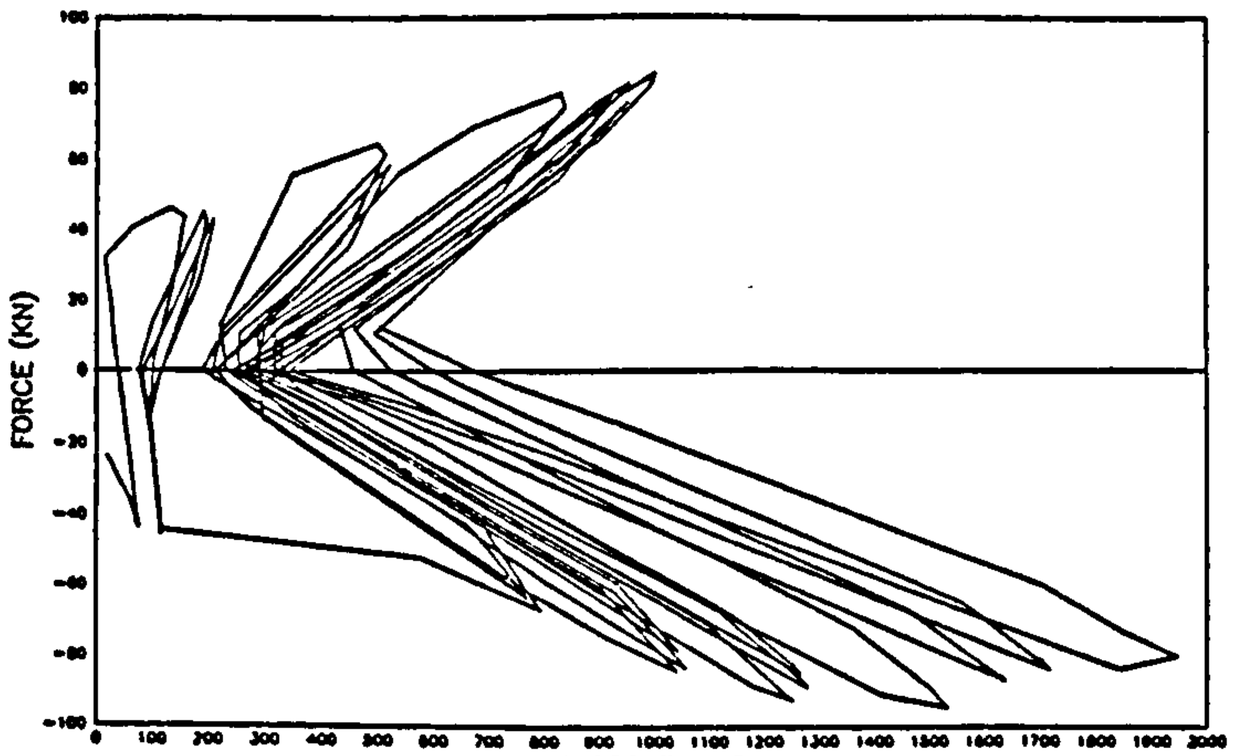


Figure B(12)30 Wall SW12 - force versus strain 13 (level of zero moment, ϕ6mm, LHS)

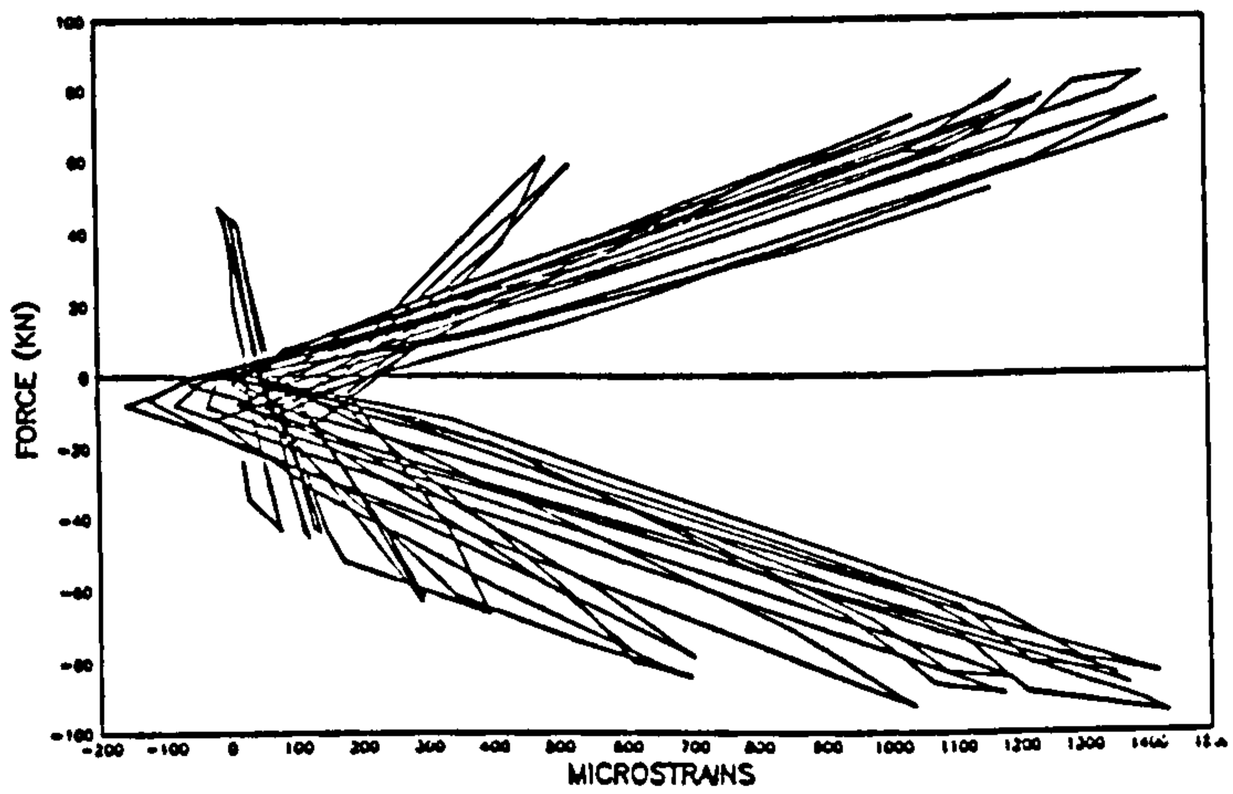


Figure B(12)31 Wall SW12 - force versus strain 14 (level of zero moment, ϕ6mm, RHS)

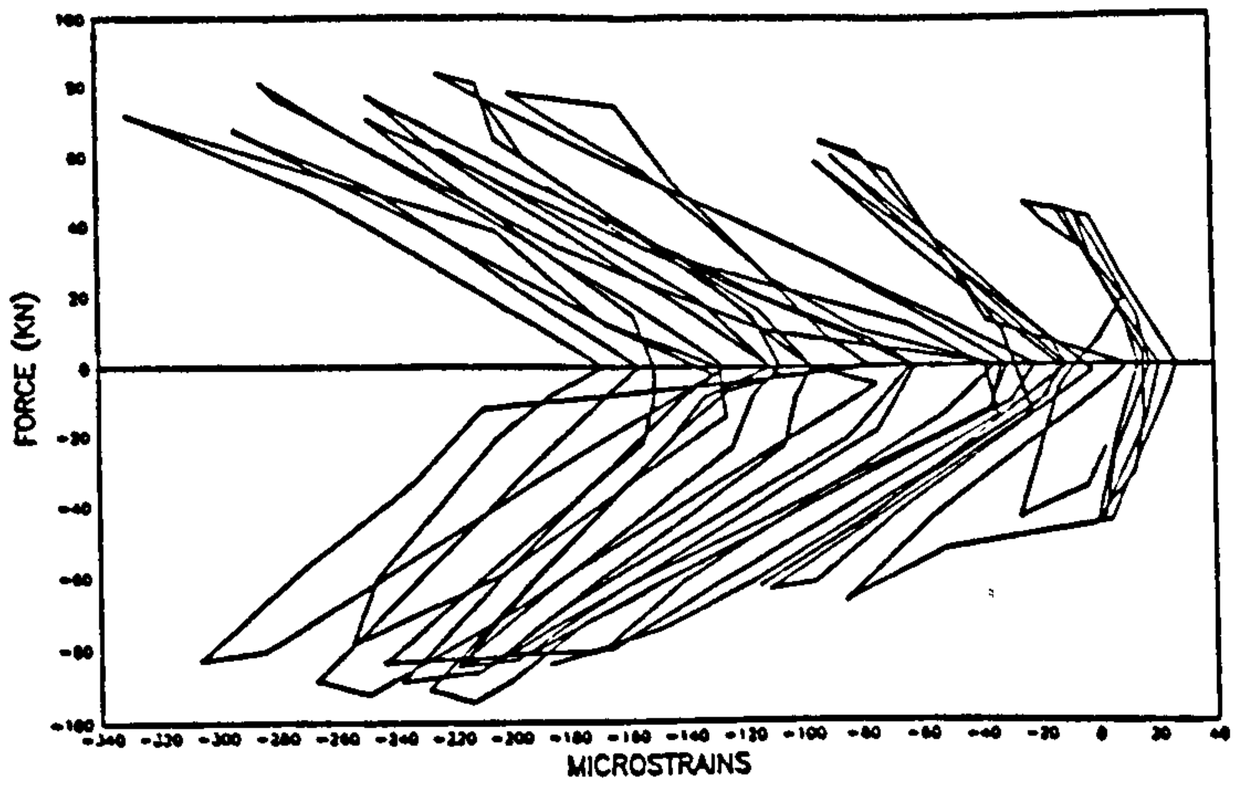


Figure B(12)32 Wall SW12 - force versus strain 15 (level of zero moment, ϕ4mm, LHS)

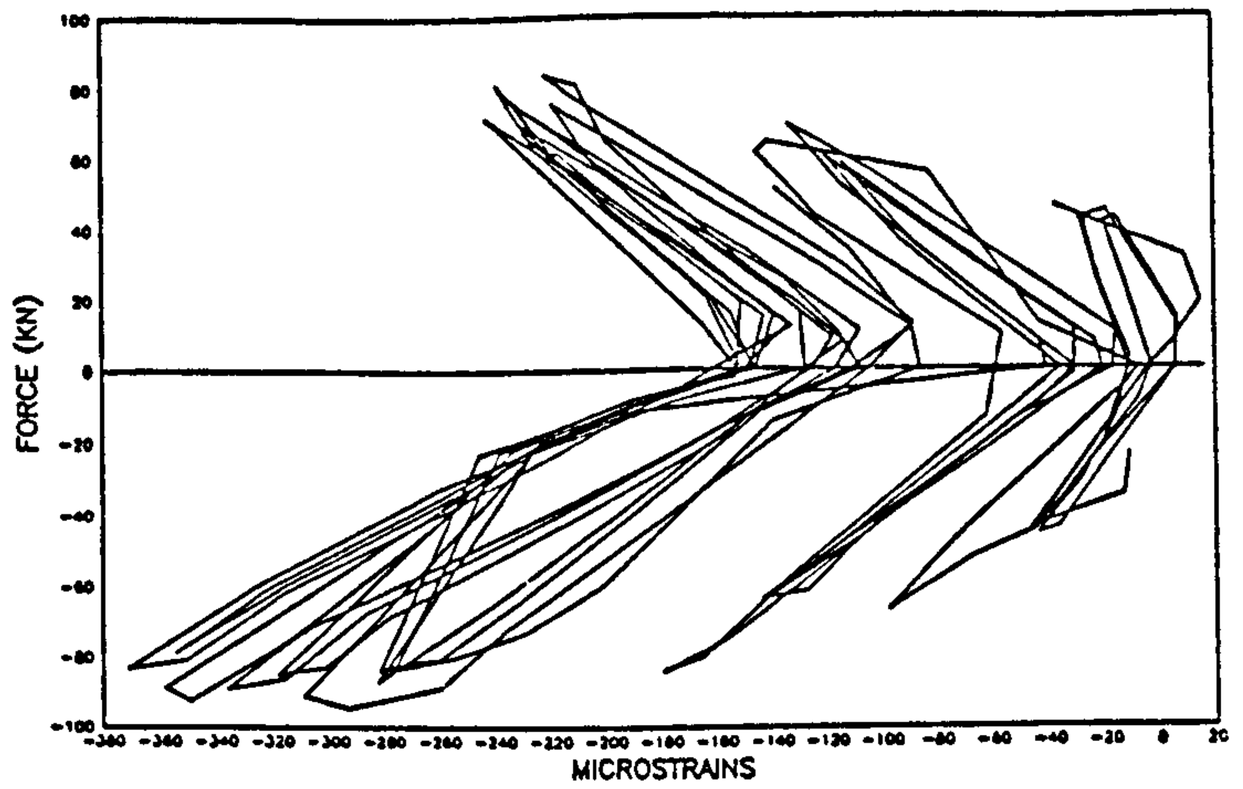


Figure B(12)33 Wall SW12 - force versus strain 16 (level of zero moment, ϕ4mm, RHS)

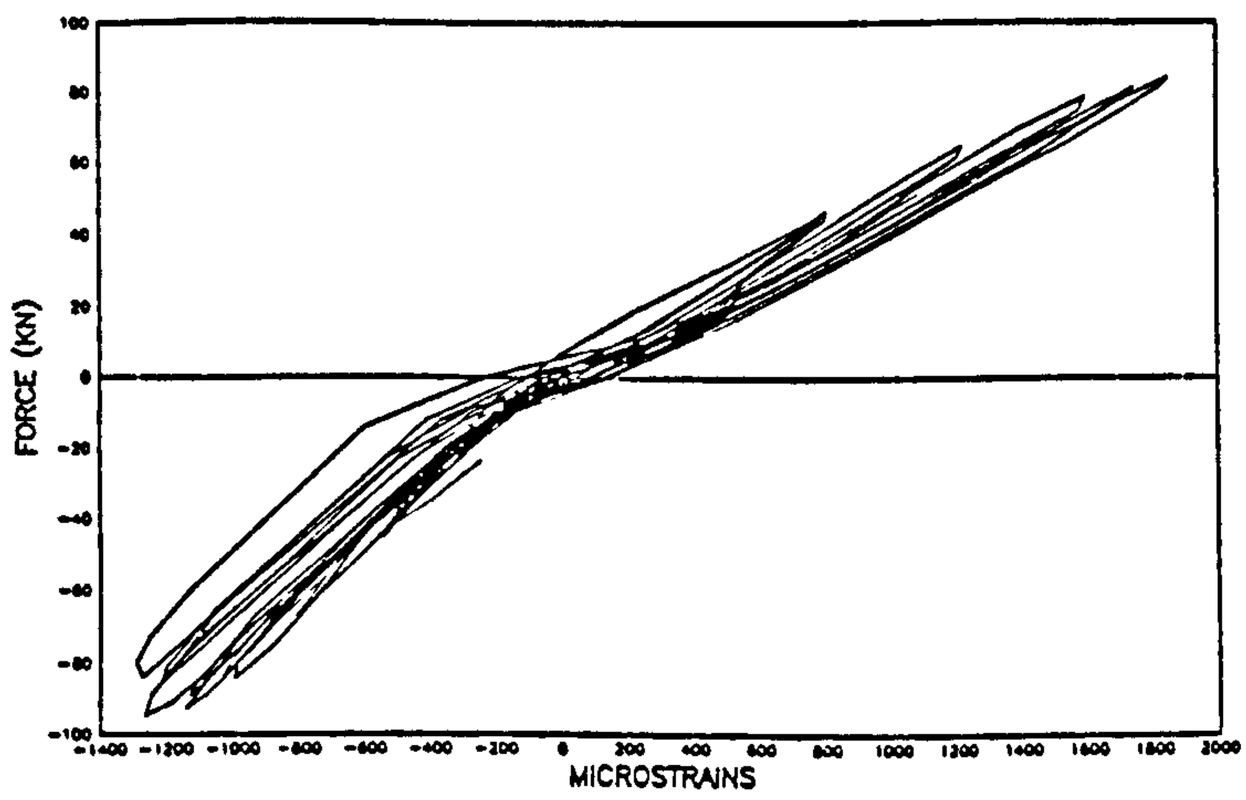


Figure B(12)34 Wall SW12 - force versus strain 17 (top, ϕ8mm, LHS)

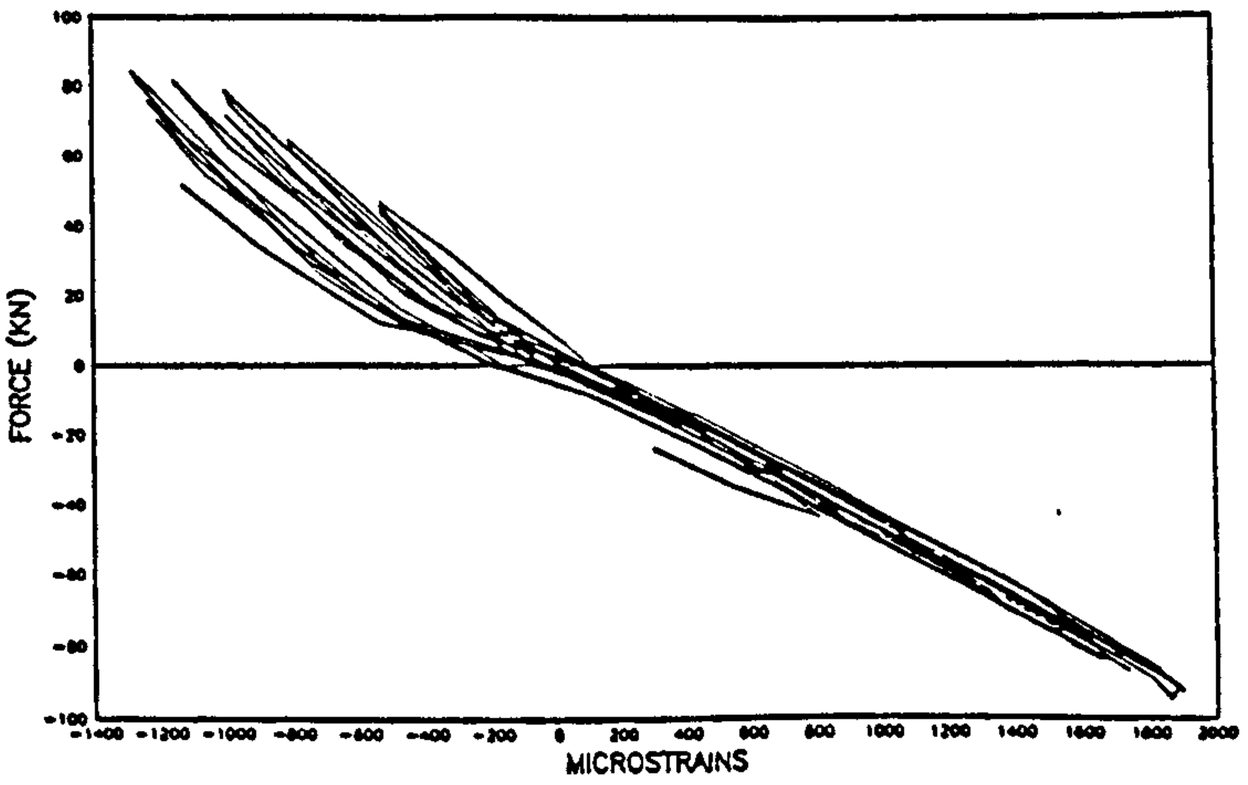


Figure B(12)35 Wall SW12 - force versus strain 18 (top, ϕ8mm, RHS)

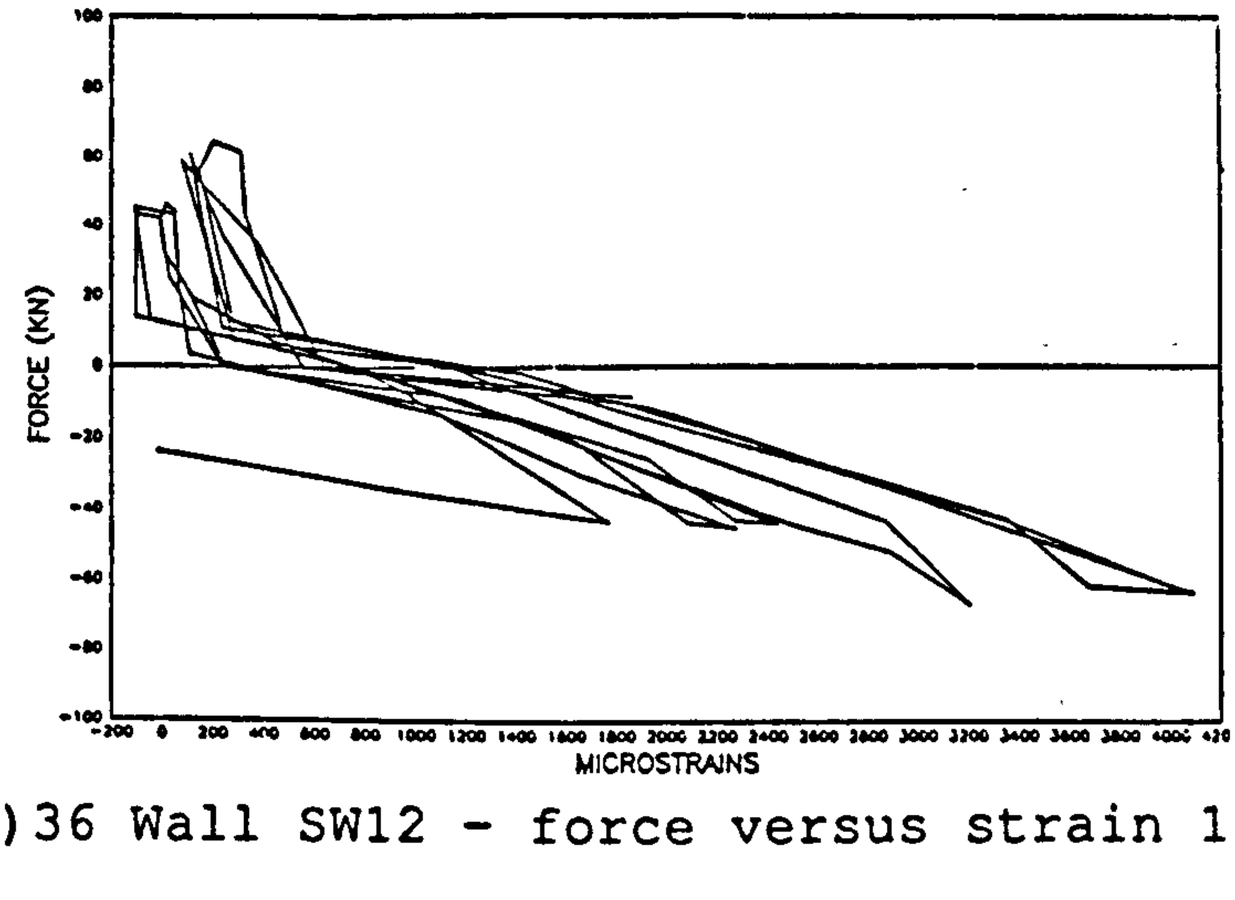


Figure B(12)36 Wall SW12 - force versus strain 19 (stirrup)

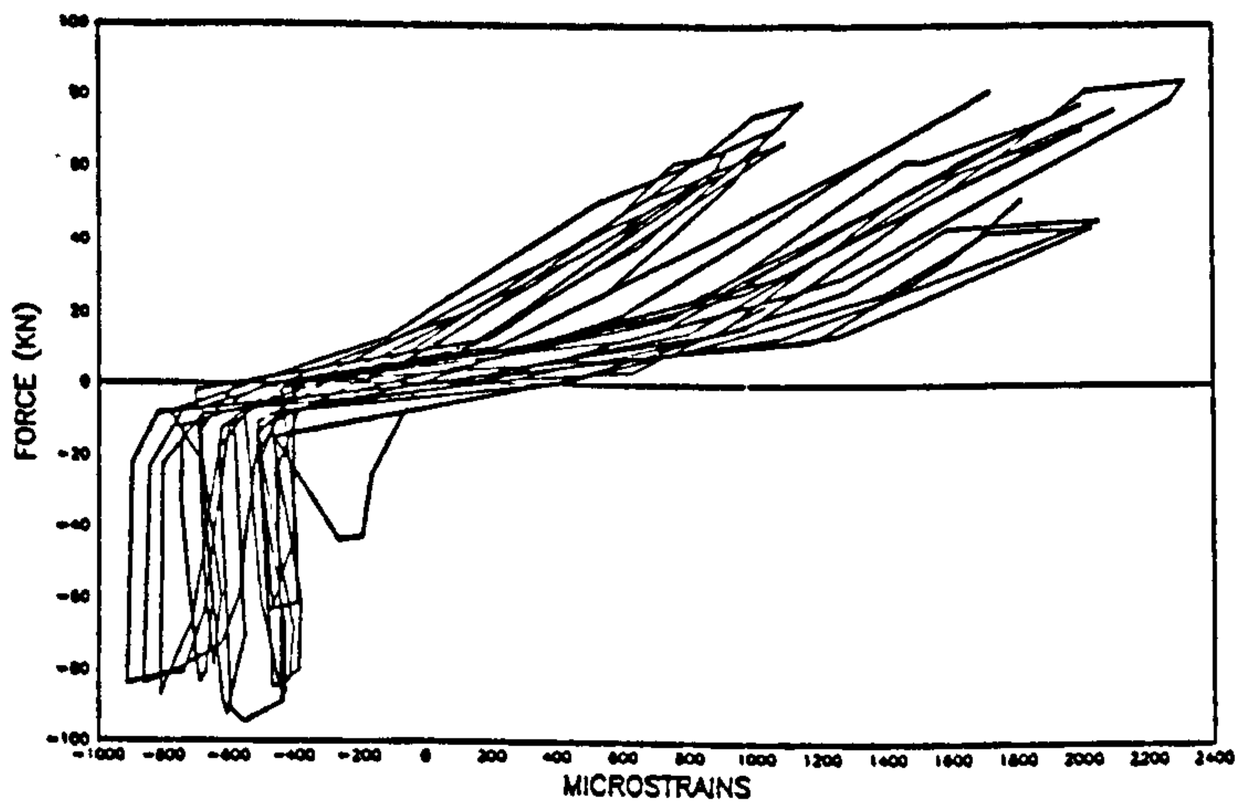


Figure B(12)37 Wall SW12 - force versus strain 20 (stirrup)

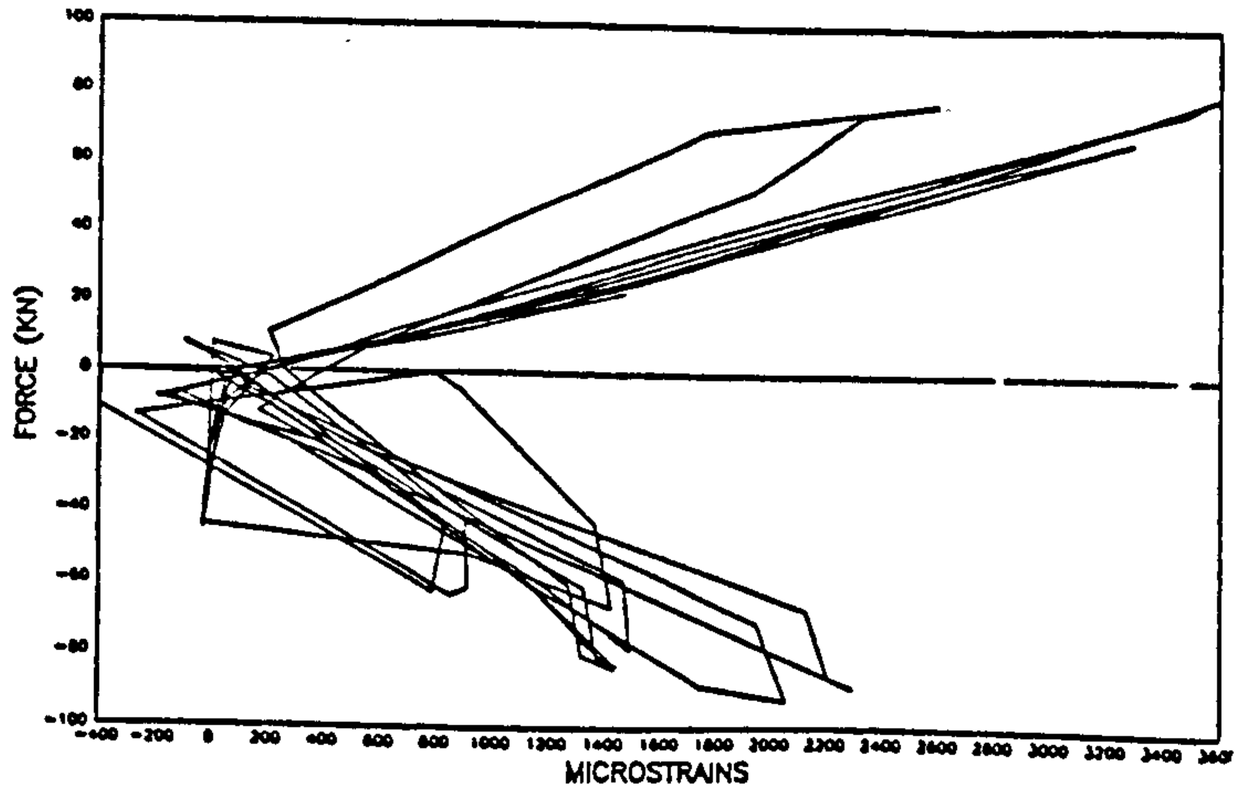


Figure B(12)38 Wall SW12 - force versus strain 21 (stirrup)

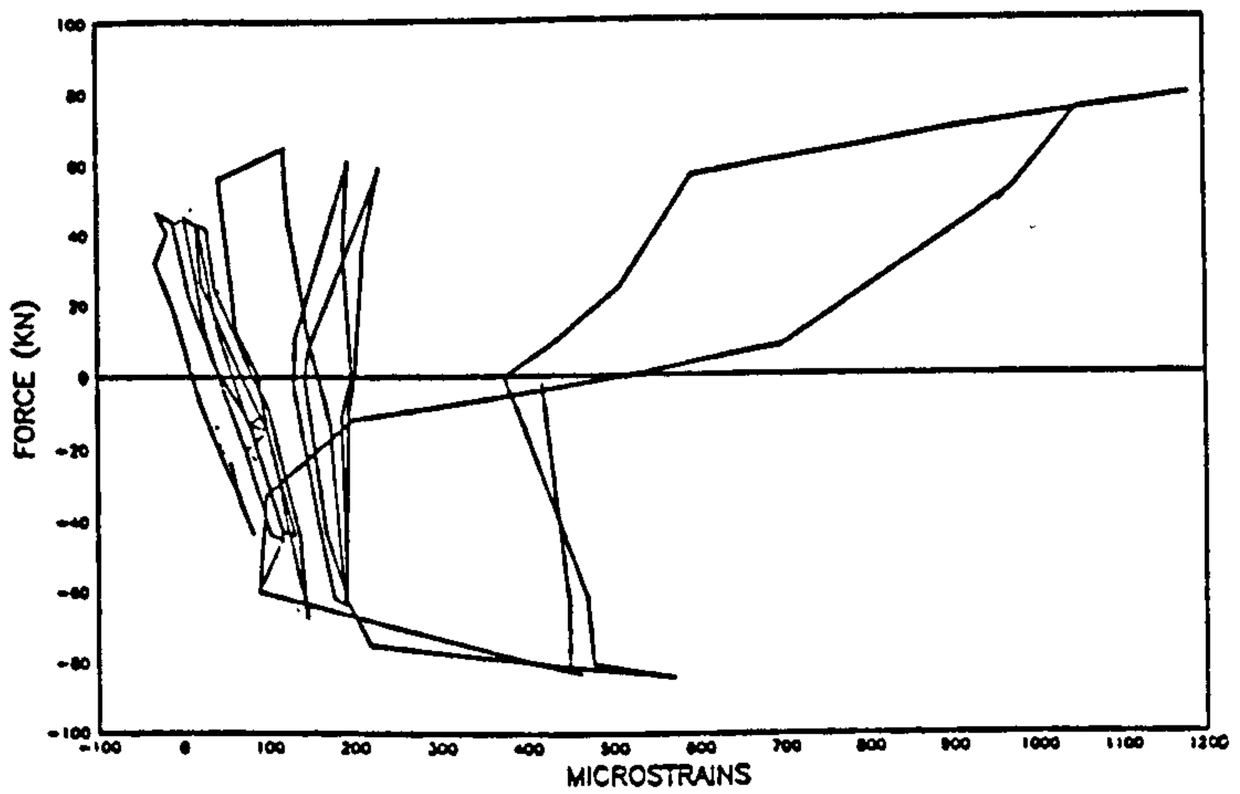


Figure B(12)39 Wall SW12 - force versus strain 22
(confinement reinforcement)

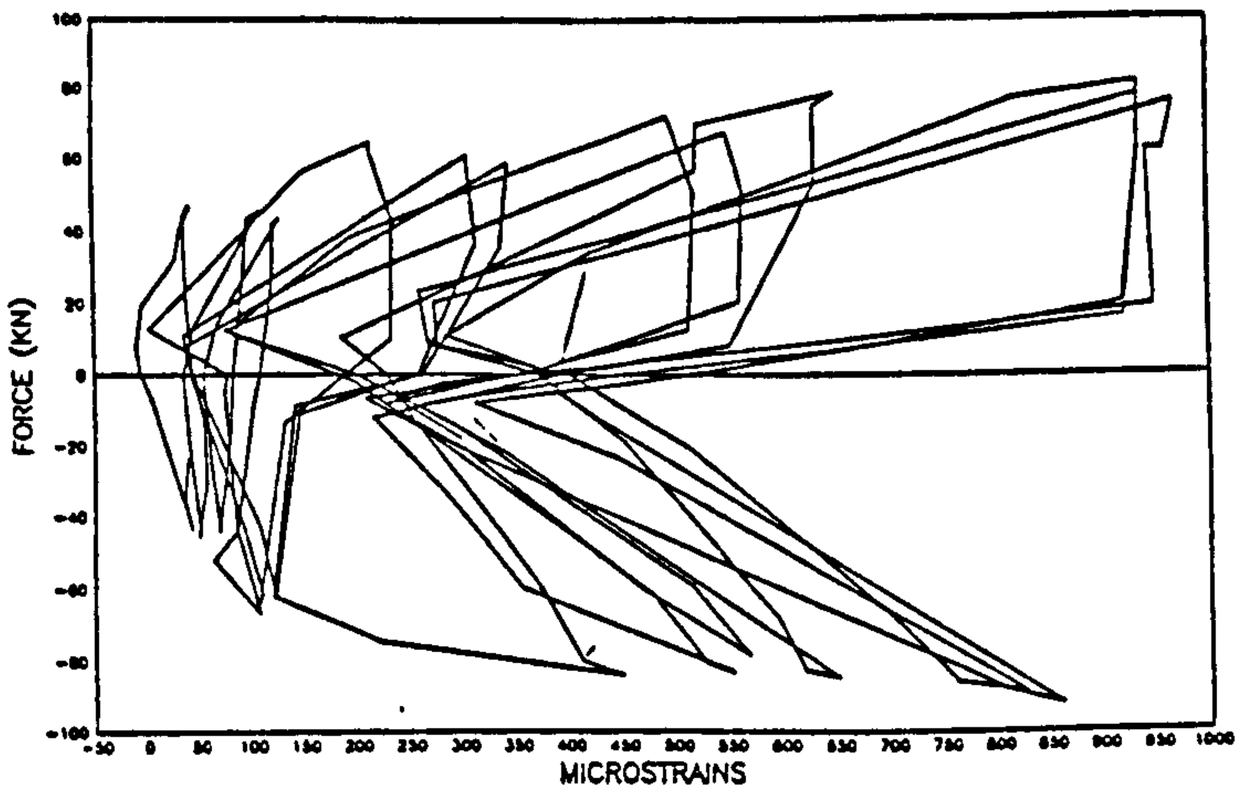


Figure B(12)40 Wall SW12 - force versus strain 23
(confinement reinforcement)

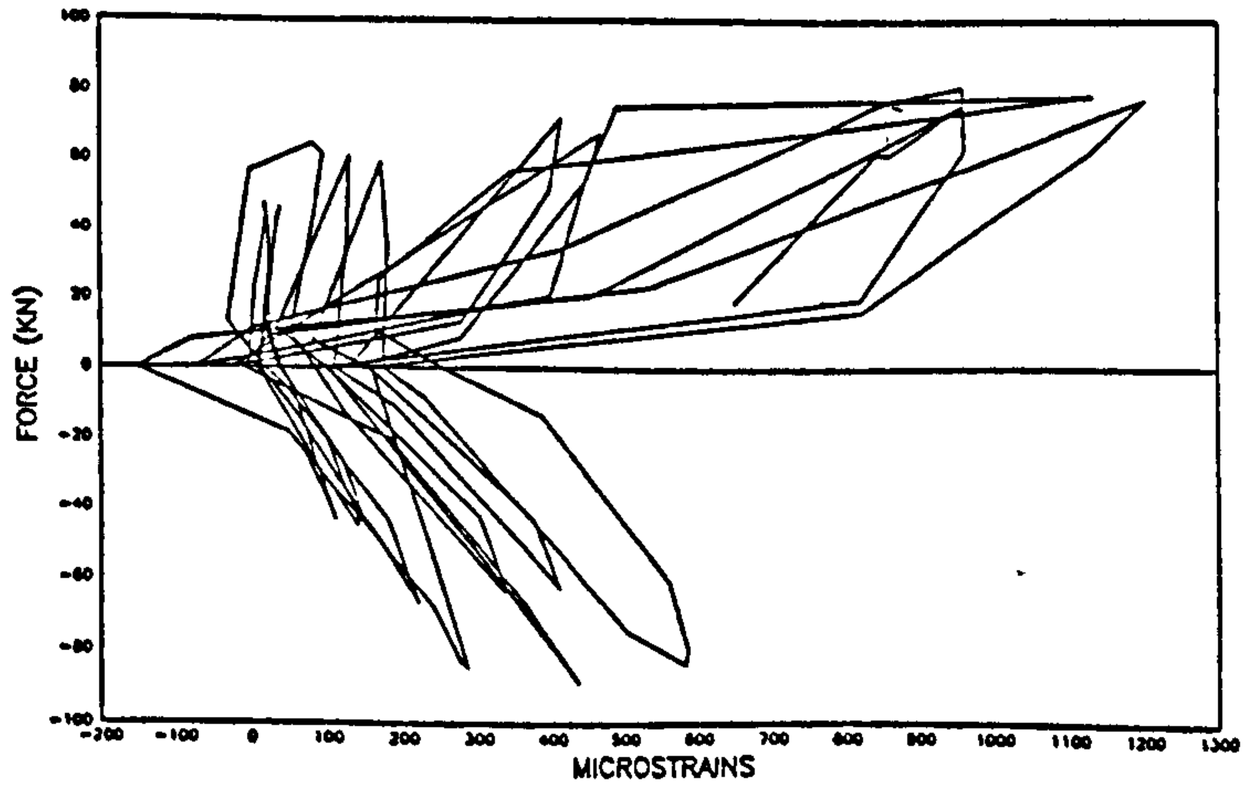


Figure B(12)41 Wall SW12 - force versus strain 24
(confinement reinforcement)

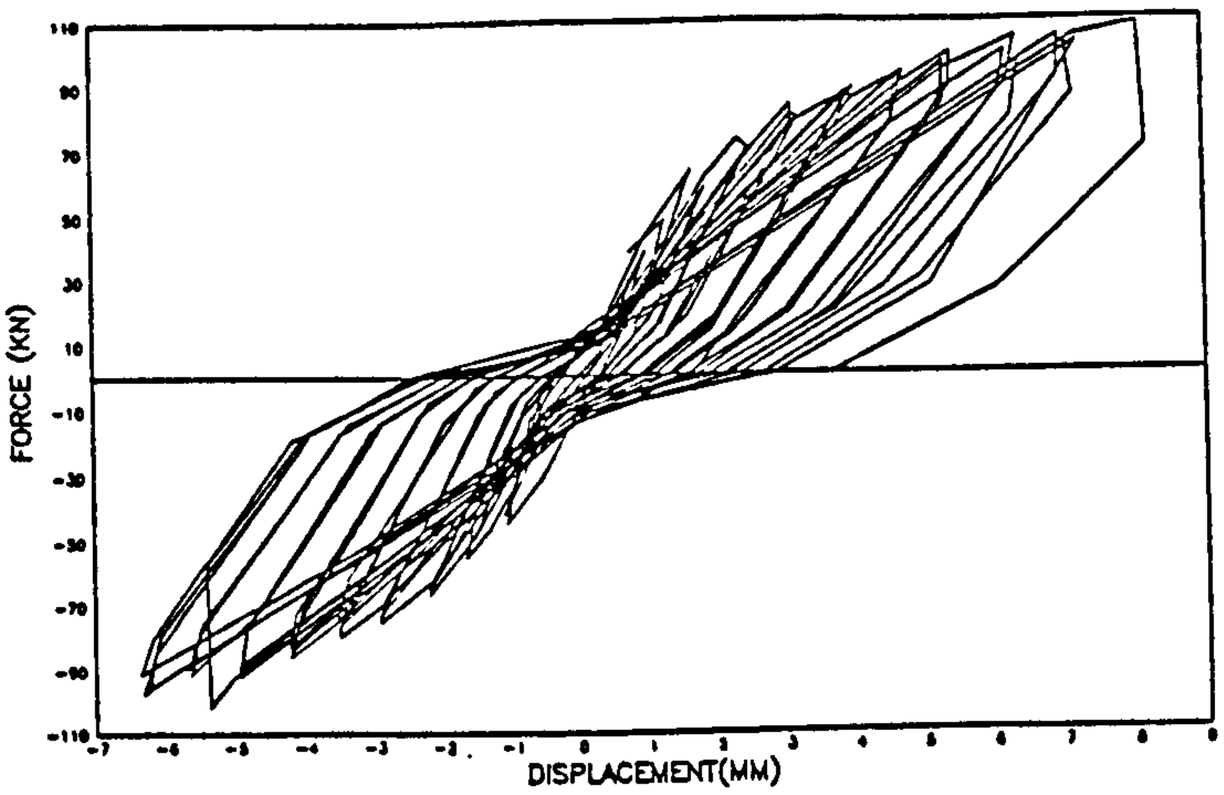


Figure B(13)1 Wall SW13 - force versus displacement 1
(horizontal, LHS, level 4)

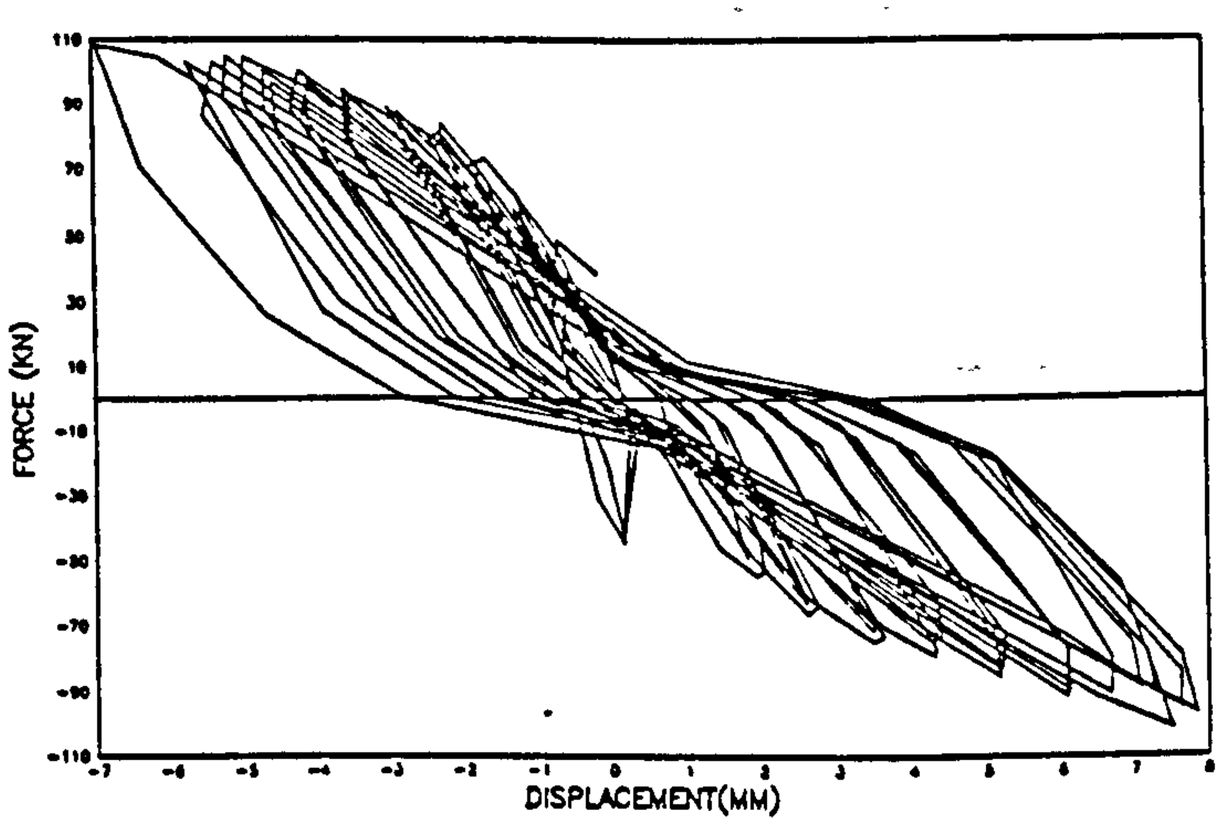


Figure B(13)2 Wall SW13 - force versus displacement 2
(horizontal, RHS, level 4)

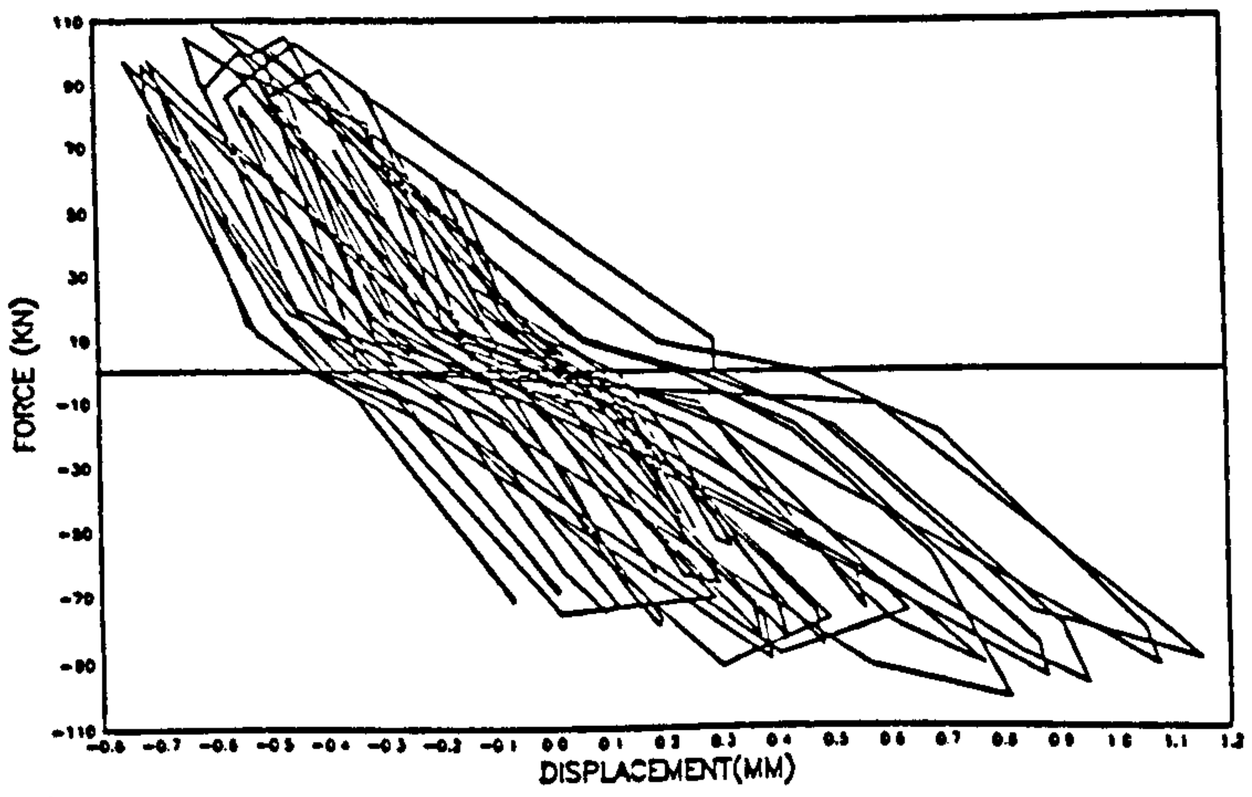


Figure B(13)3 Wall SW13 - force versus displacement 3
(vertical, LHS, level 1)

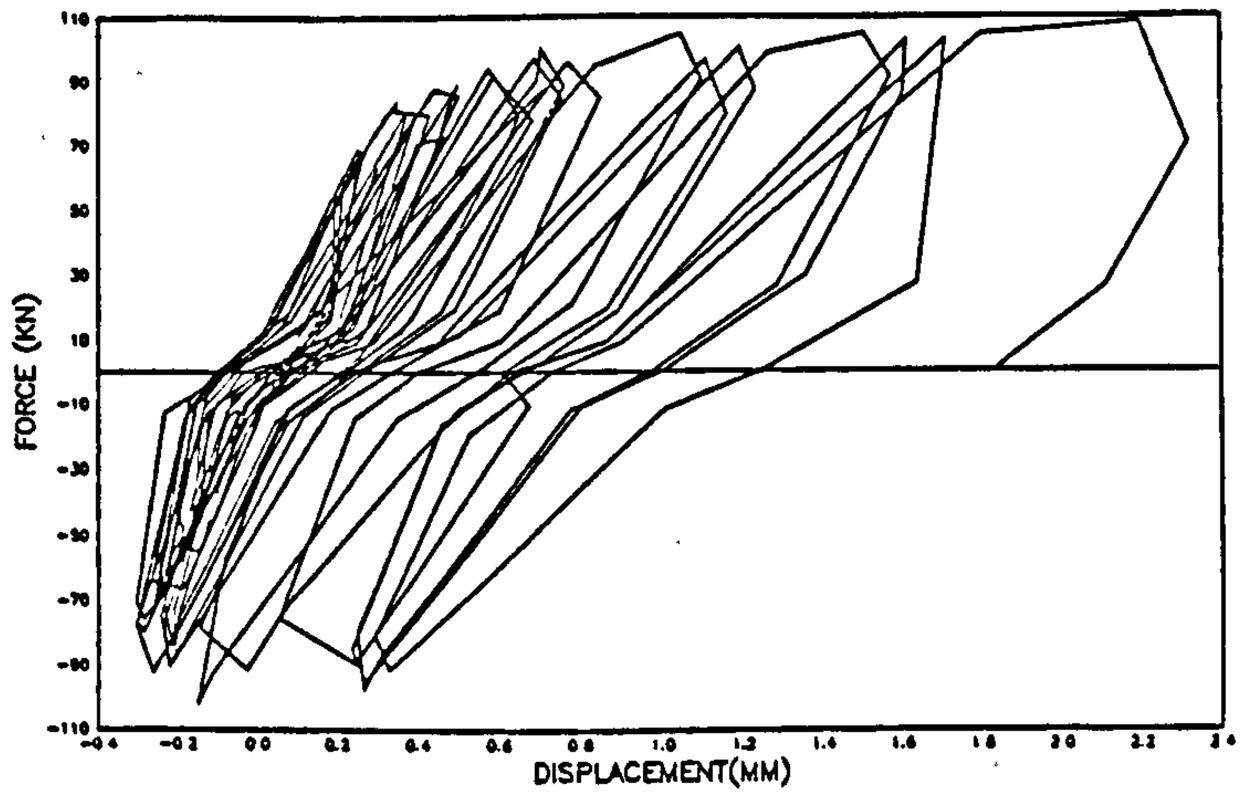


Figure B(13)4 Wall SW13 - force versus displacement 4 (vertical, RHS, level 1)

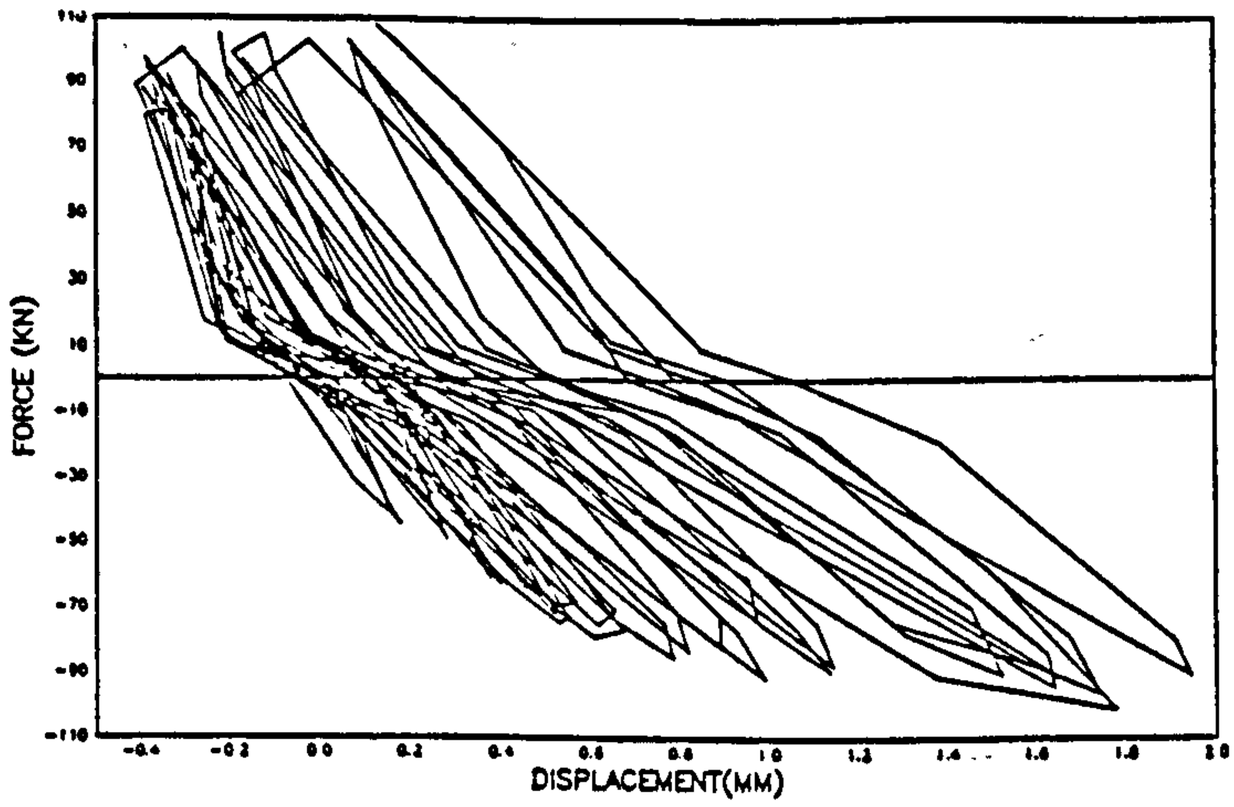


Figure B(13)5 Wall SW13 - force versus displacement 5 (vertical, LHS, level 2)

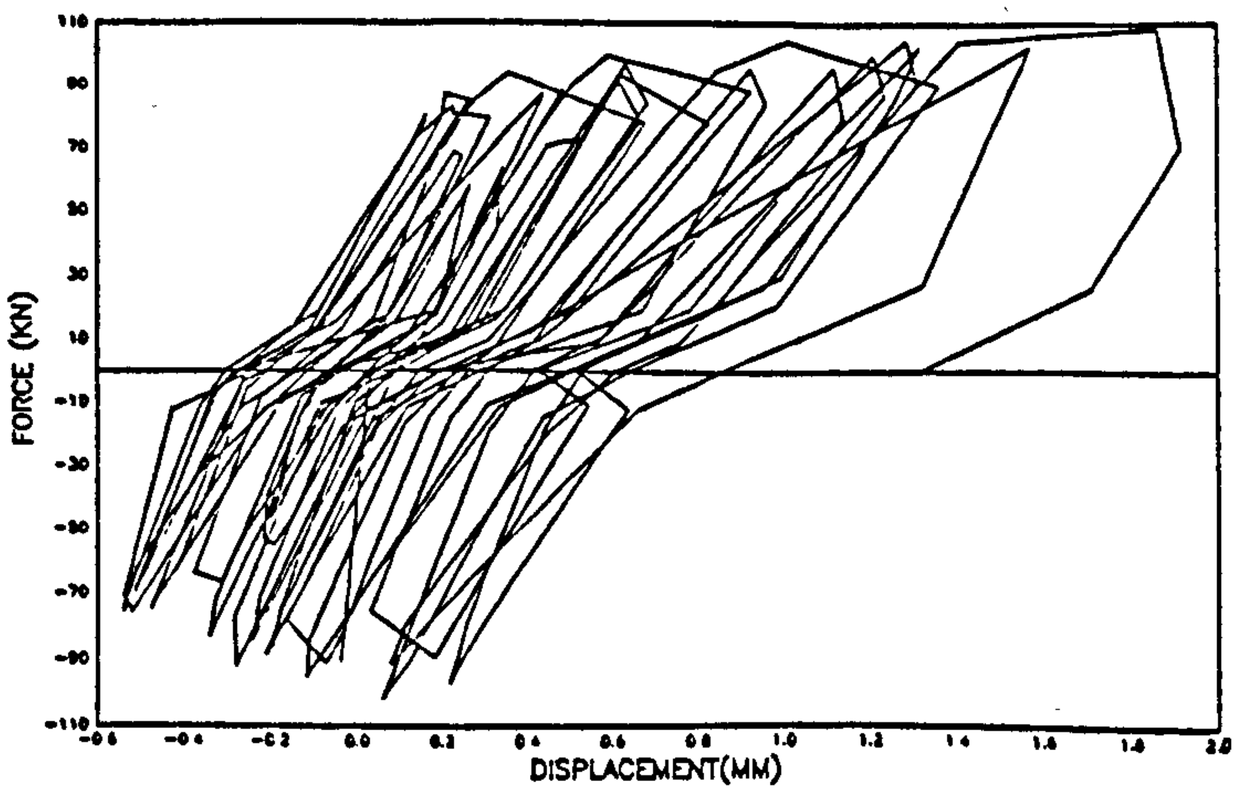


Figure B(13)6 Wall SW13 - force versus displacement 6 (vertical, RHS, level 2)

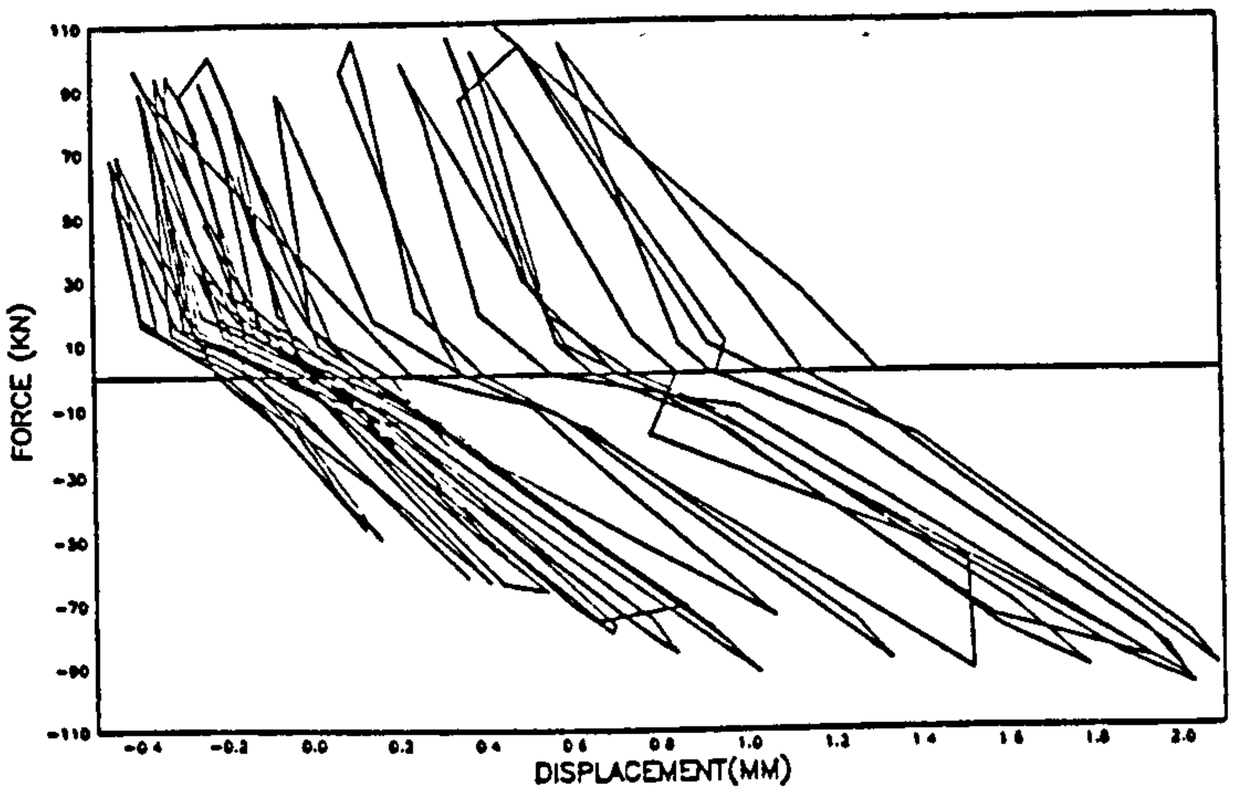


Figure B(13)7 Wall SW13 - force versus displacement 7
(vertical, LHS, level 3)

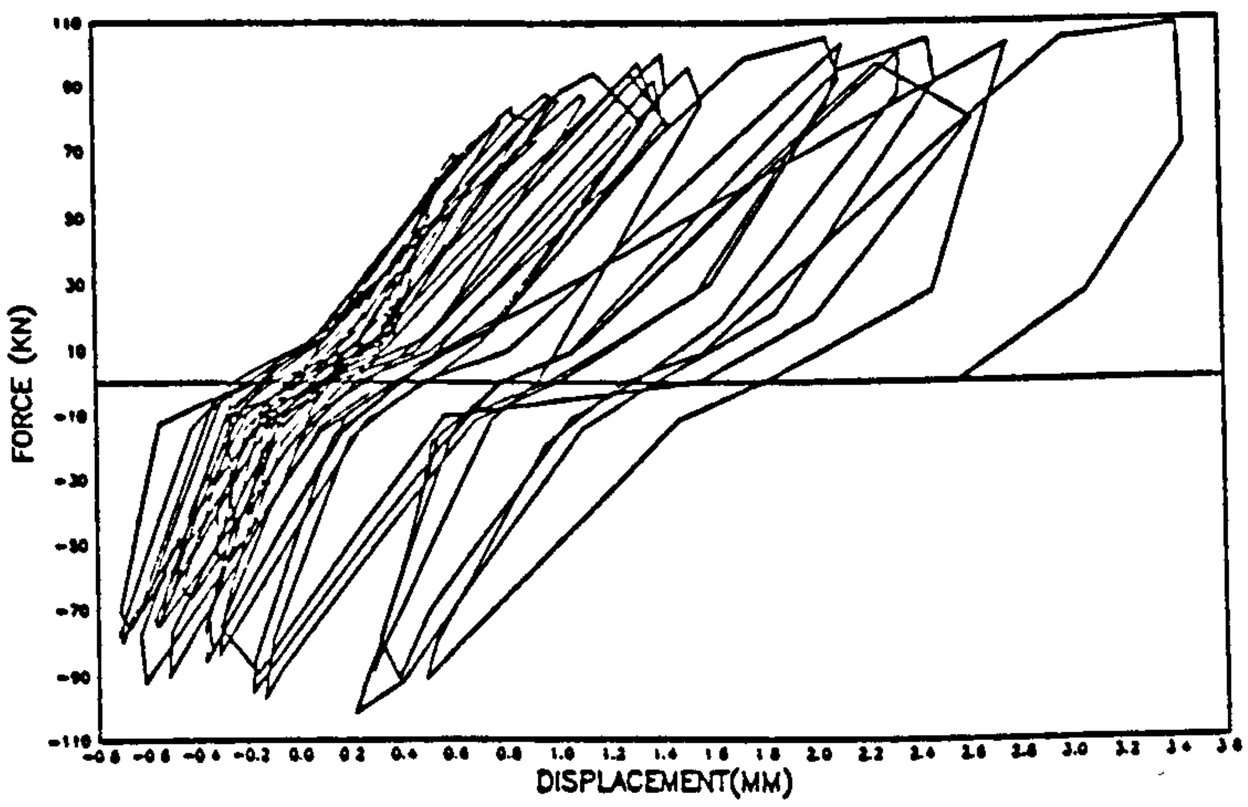


Figure B(13)8 Wall SW13 - force versus displacement 8
(vertical, RHS, level 3)

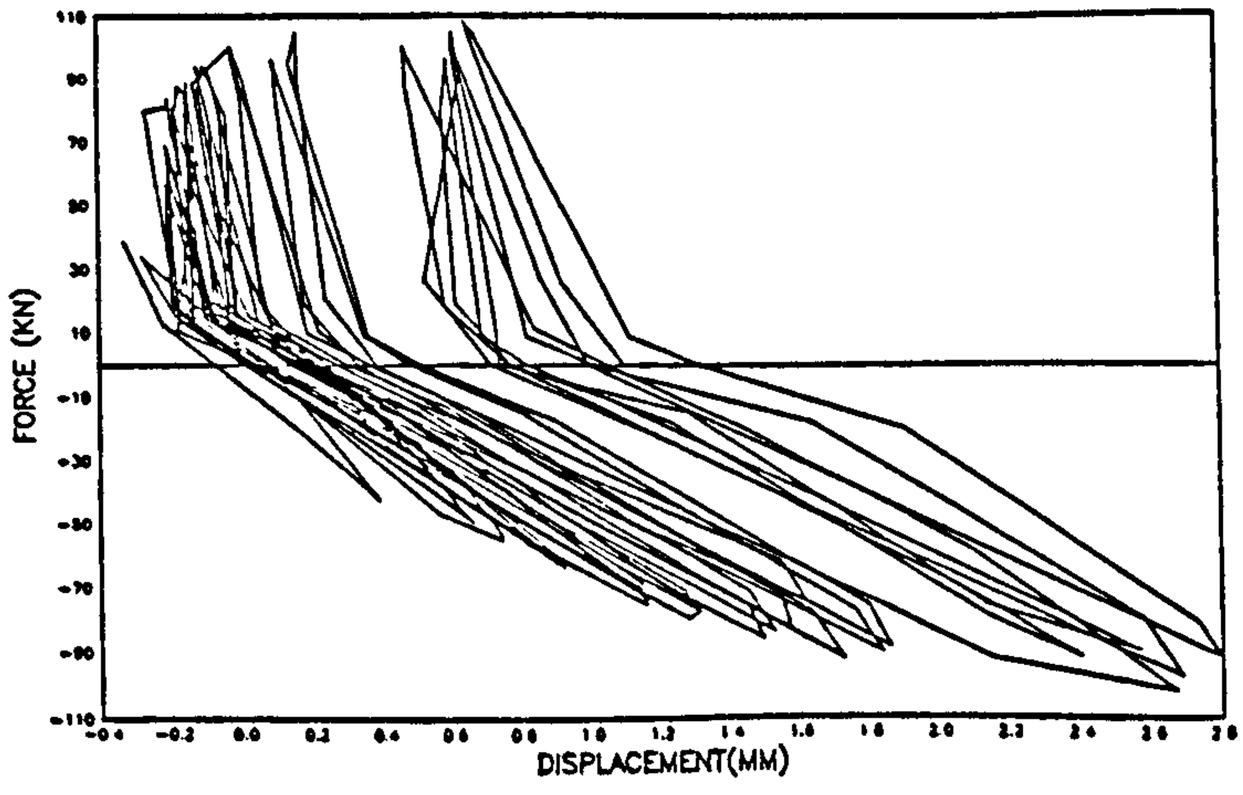


Figure B(13)9 Wall SW13 - force versus displacement 9
(vertical, LHS, level 4)

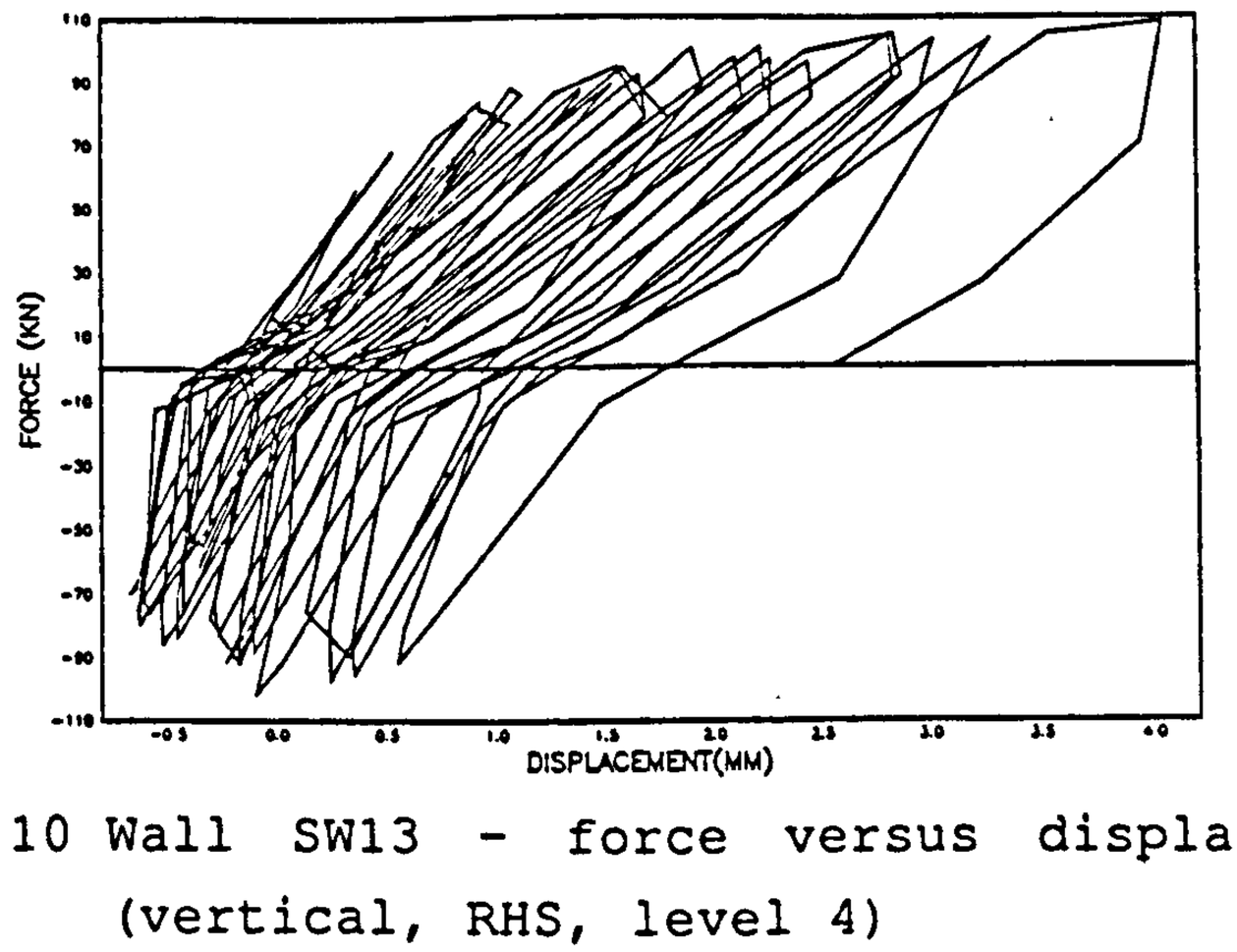


Figure B(13)10 Wall SW13 - force versus displacement 10 (vertical, RHS, level 4)

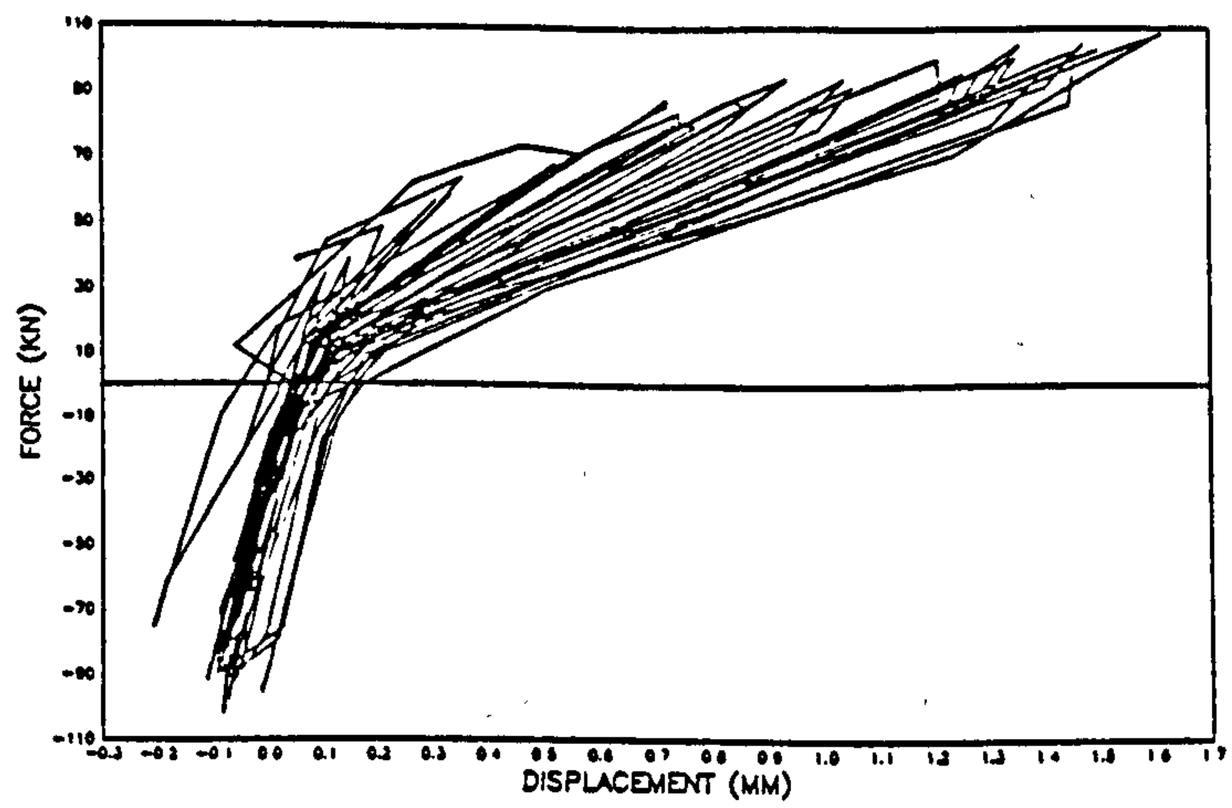


Figure B(13)11.a Wall SW13 - force versus displacement 11 (foundation, RHS)

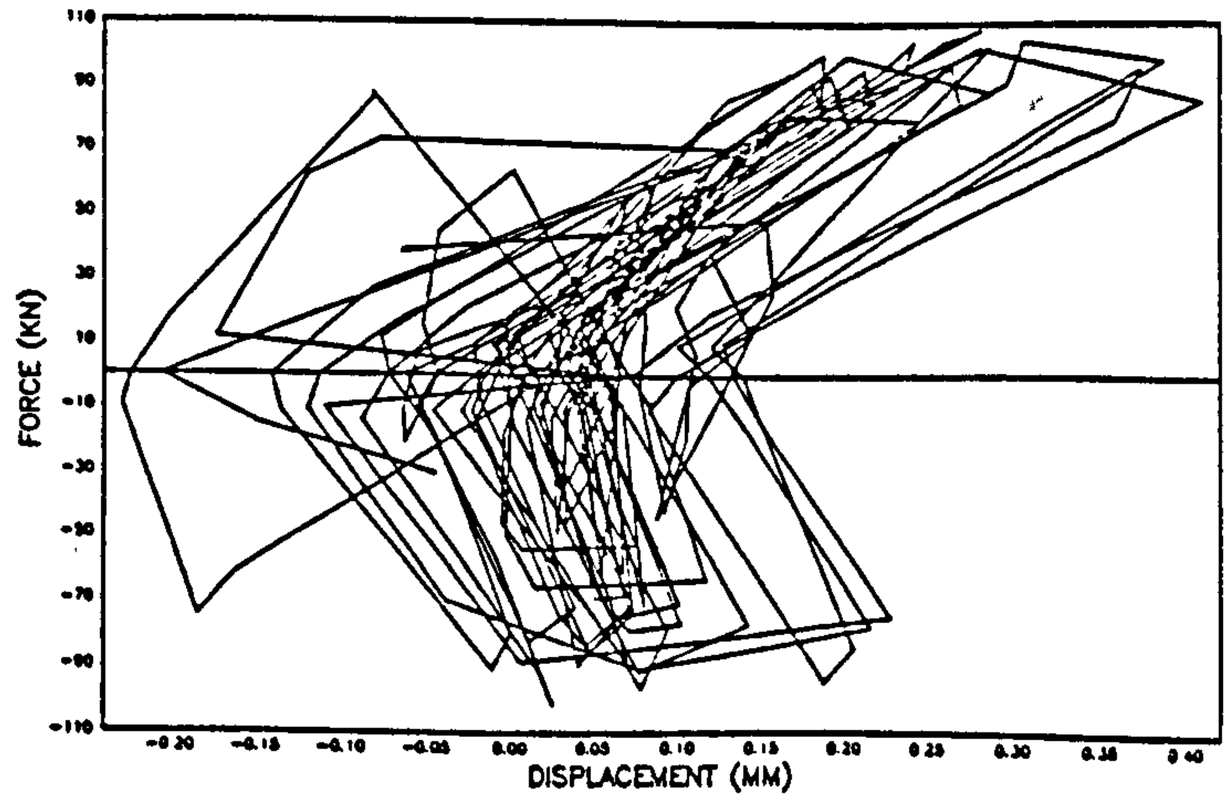


Figure B(13)11.b Wall SW13 - force versus displacement 11a (foundation, LHS)

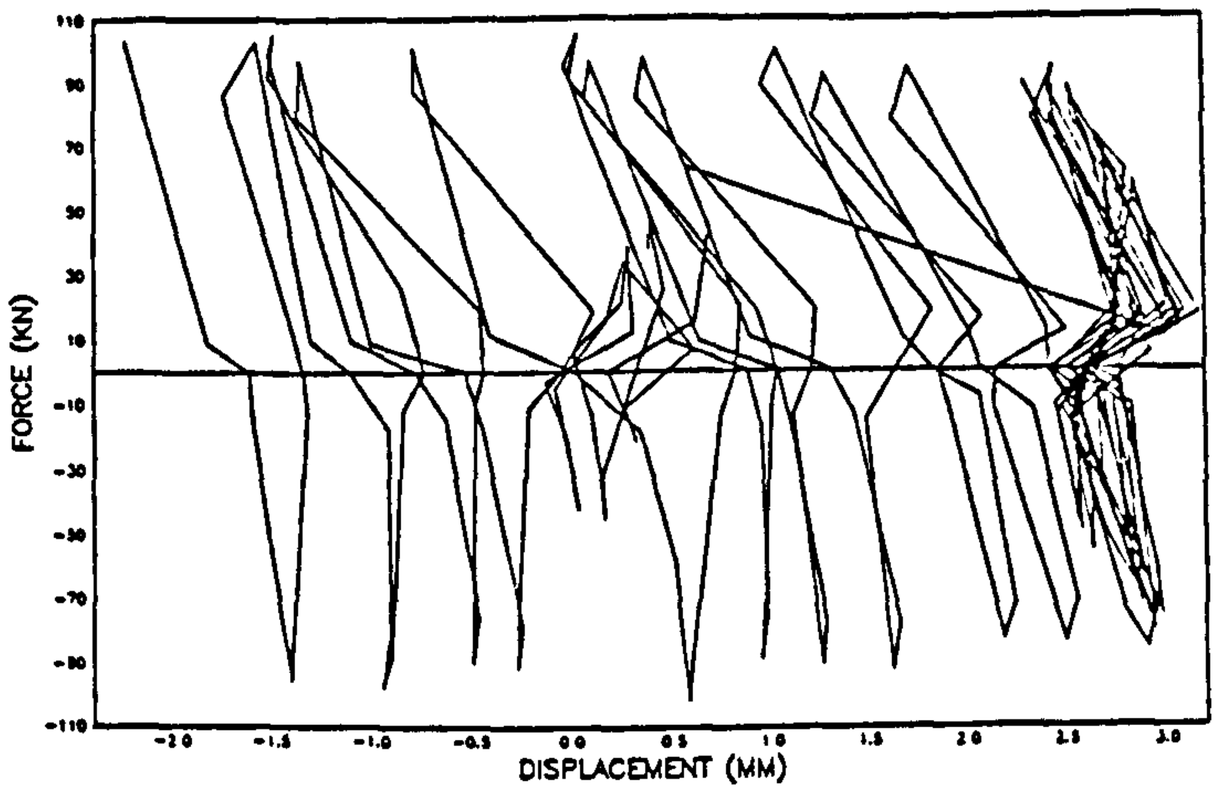


Figure B(13)12 Wall SW13 - force versus displacement 12 (out-of-plane)

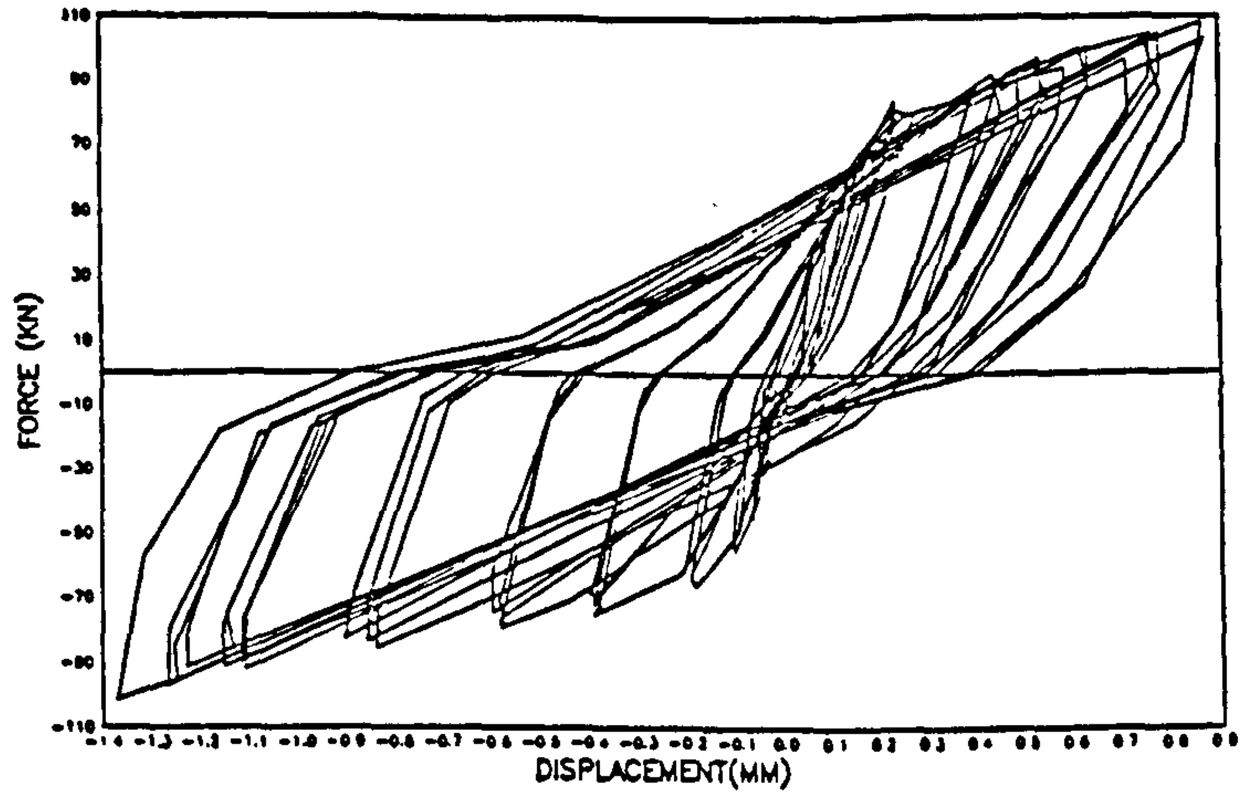


Figure B(13)13 Wall SW13 - force versus displacement 13 (horizontal, centre, level 1)

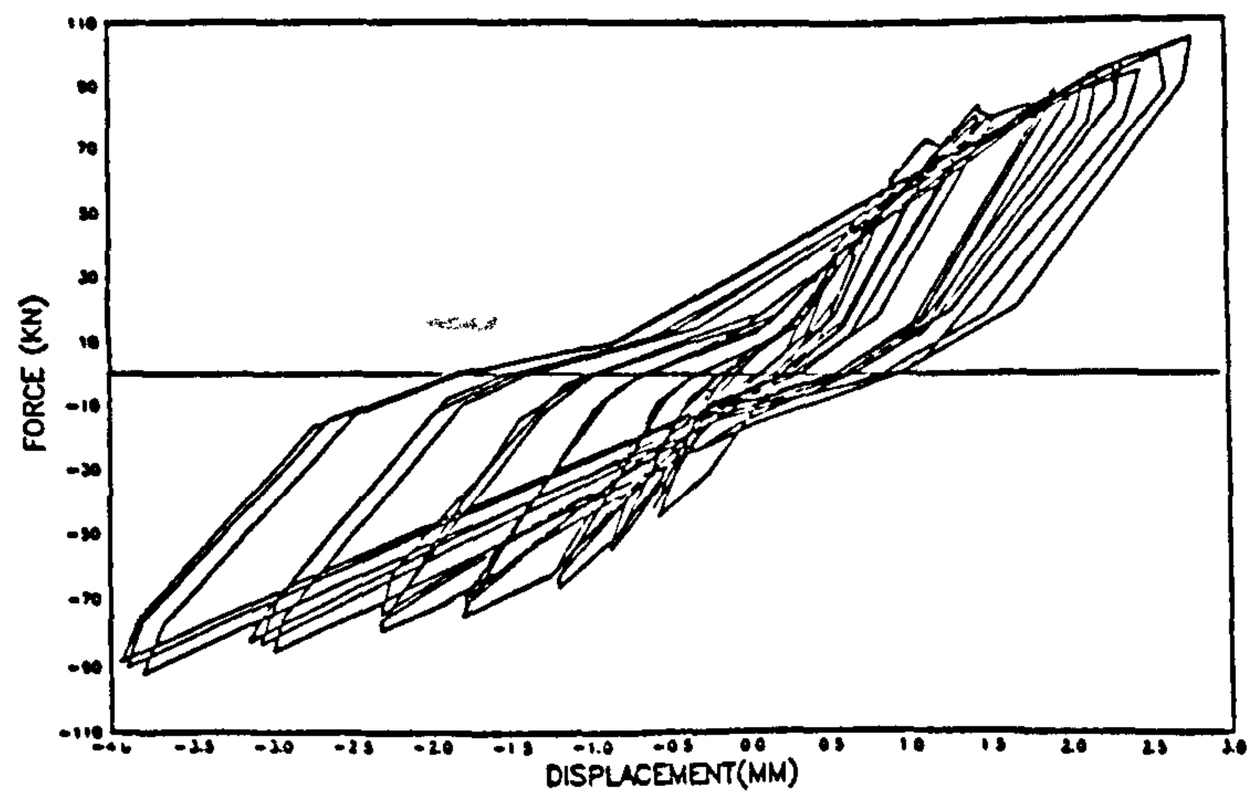


Figure B(13)14 Wall SW13 - force versus displacement 15 (horizontal, centre, level 3)

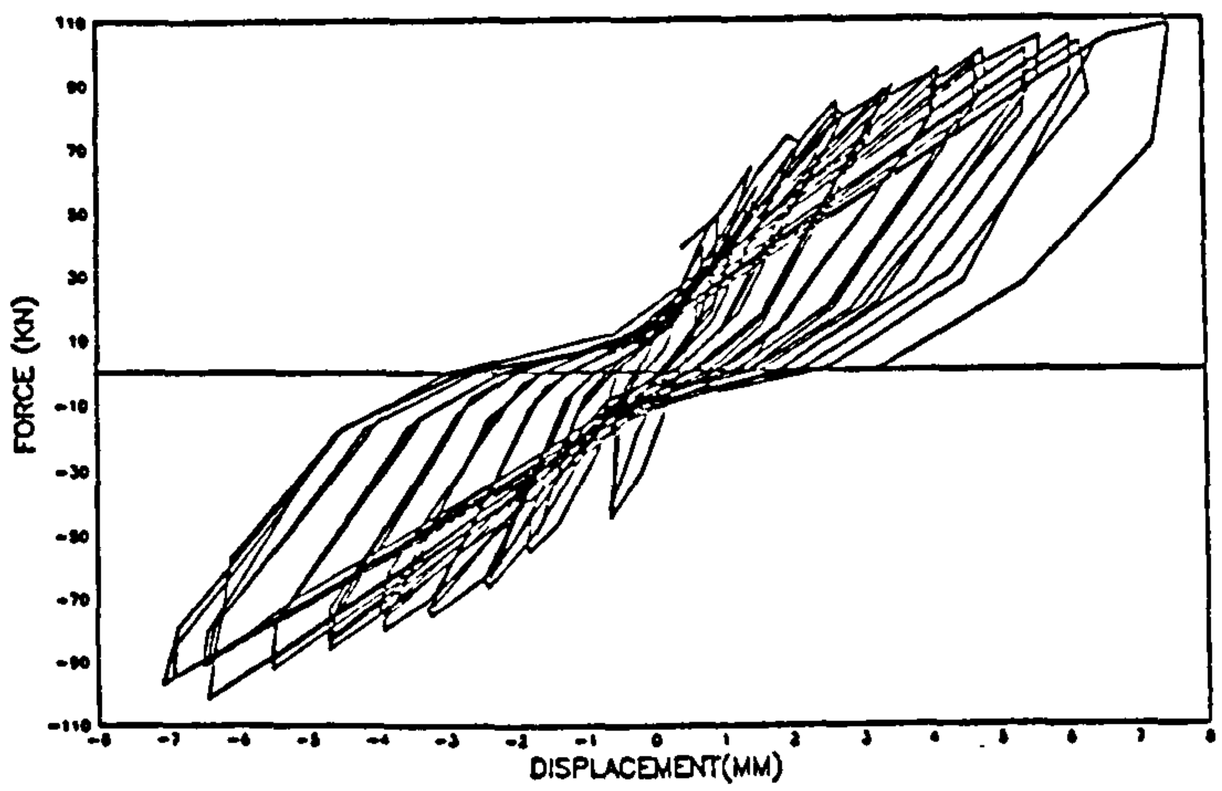


Figure B(13)15 Wall SW13 - force versus top horizontal displacement

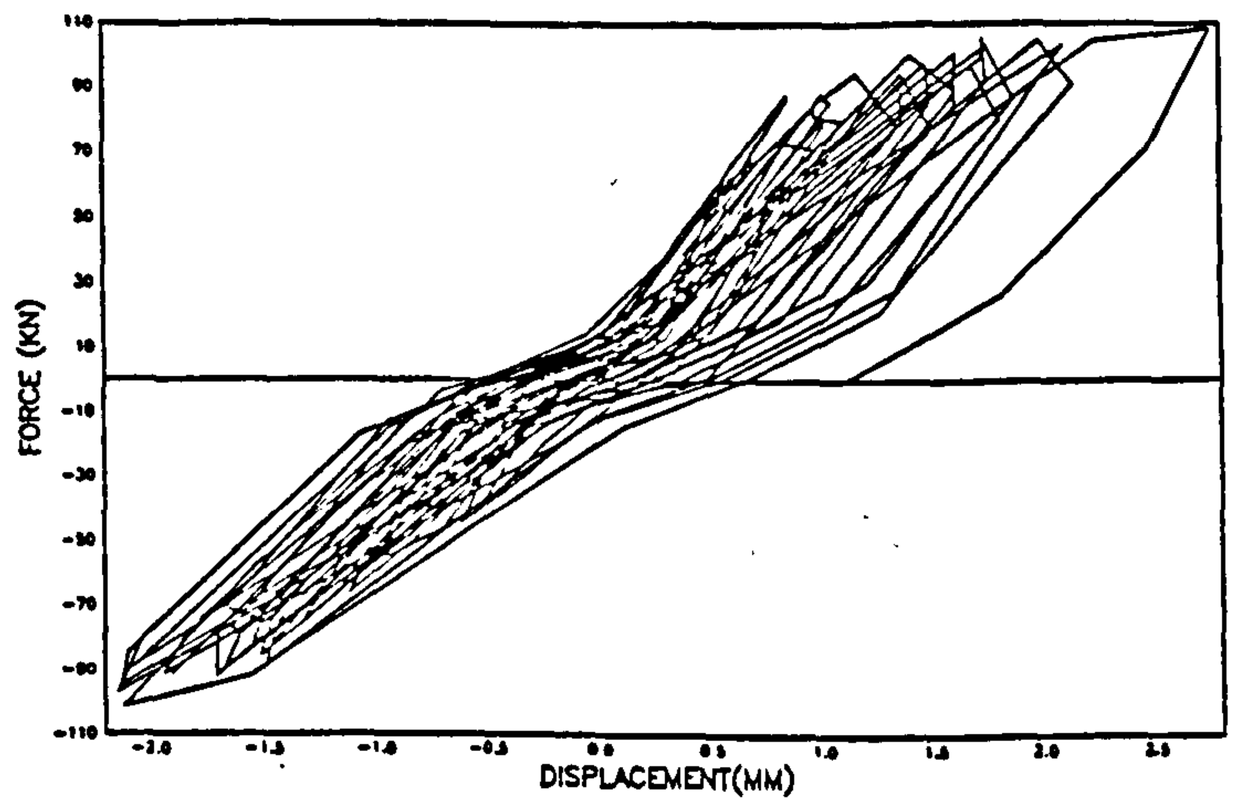


Figure B(13)16 Wall SW13 - force versus flexural component of top horizontal displacement

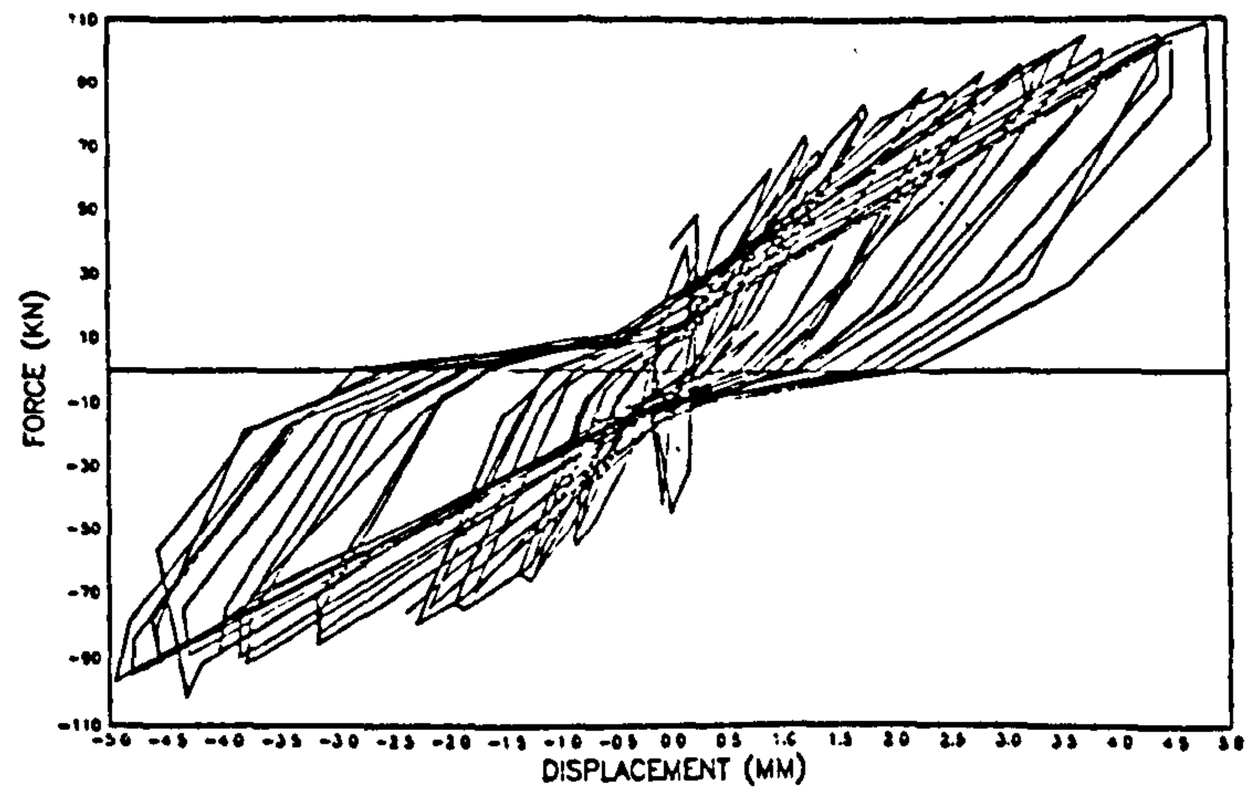


Figure B(13)17 Wall SW13 - force versus shear component of top horizontal displacement

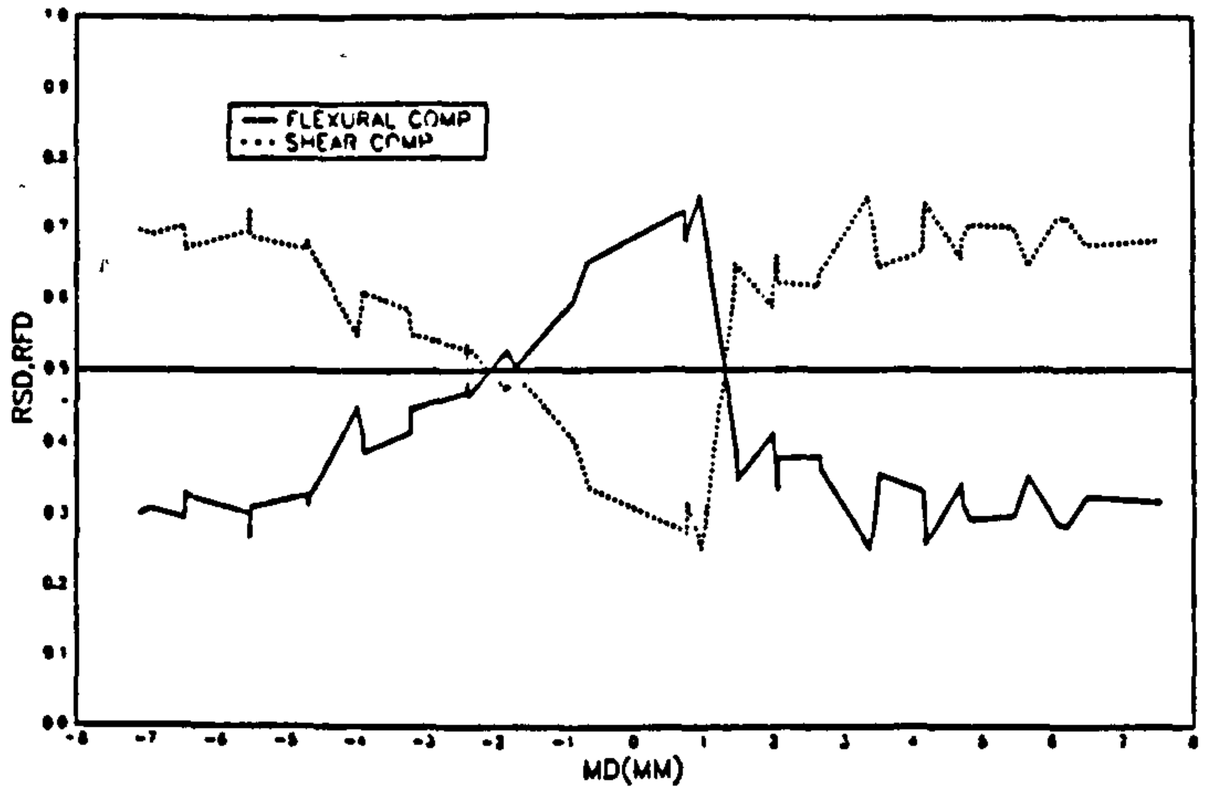


Figure B(13)18 Wall SW13 - RSD,RFD versus MD

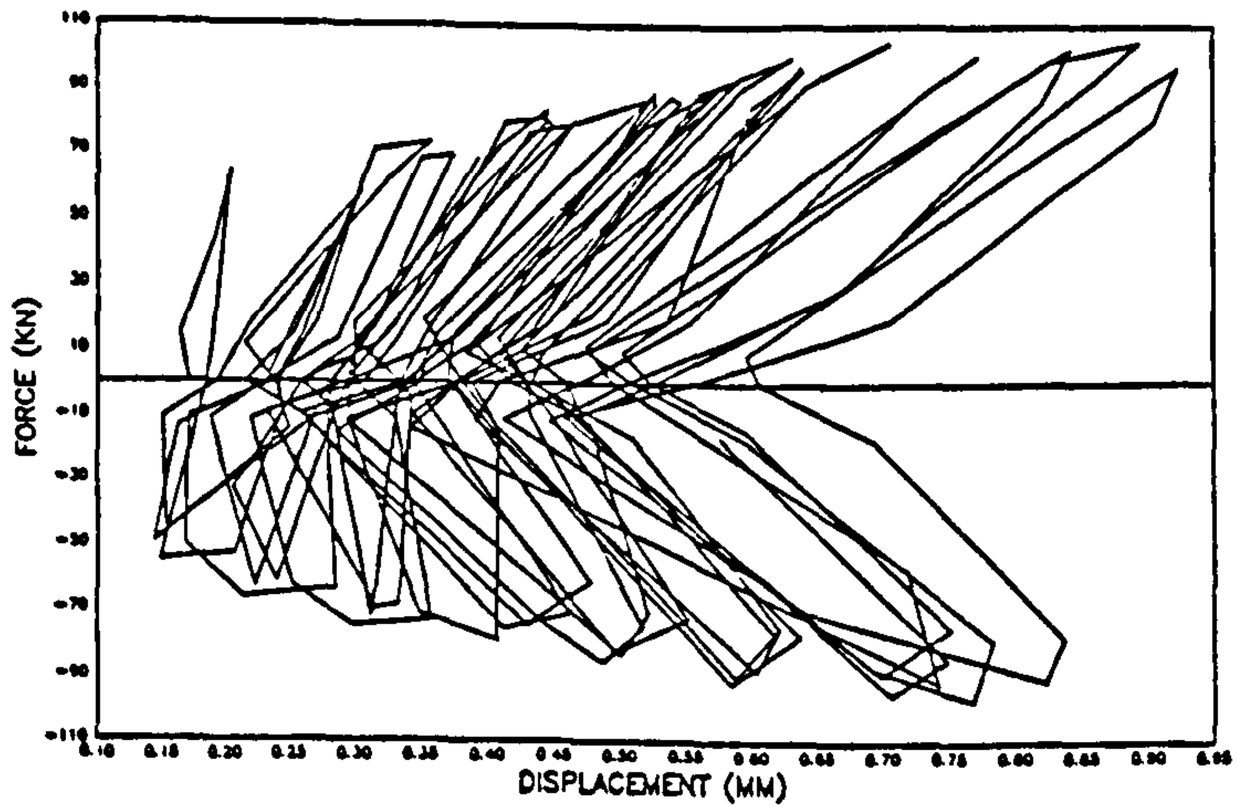


Figure B(13)19 Wall SW13 - force versus opening on top

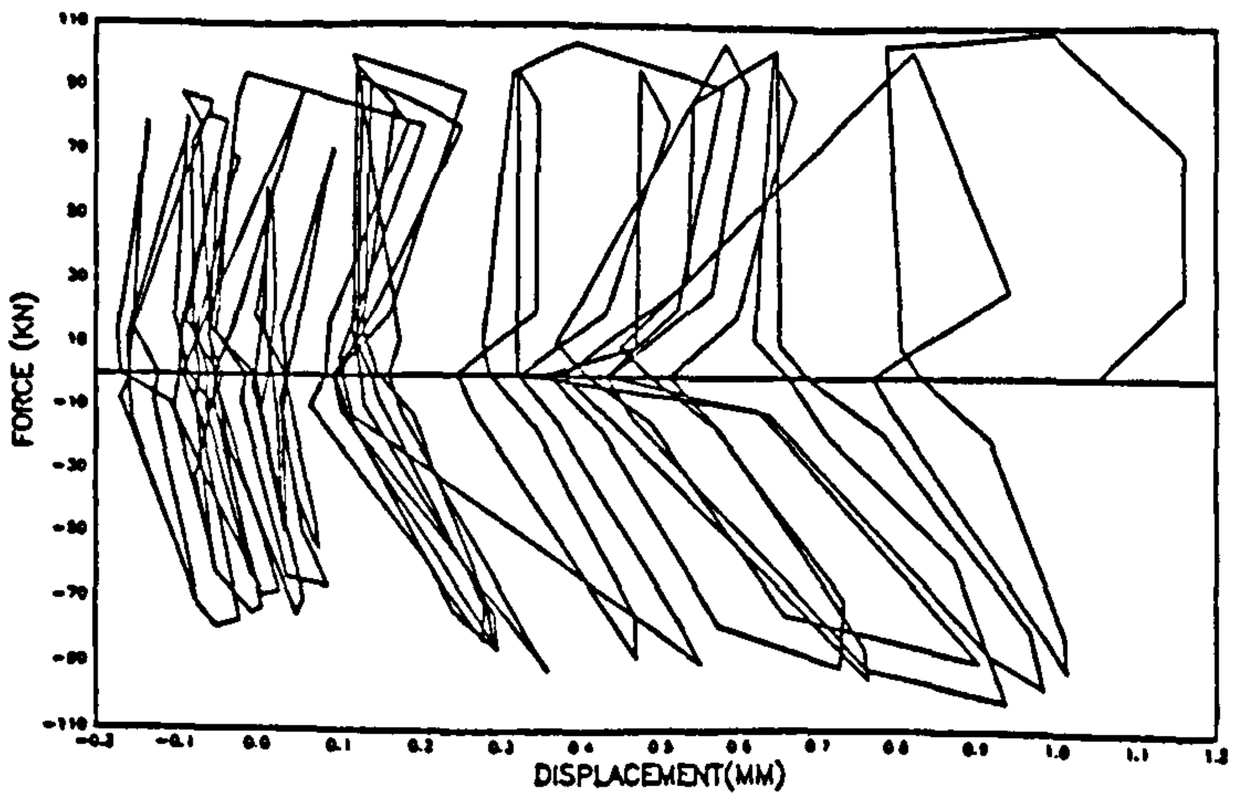


Figure B(13)20 Wall SW13 - force versus extension at a quarter height

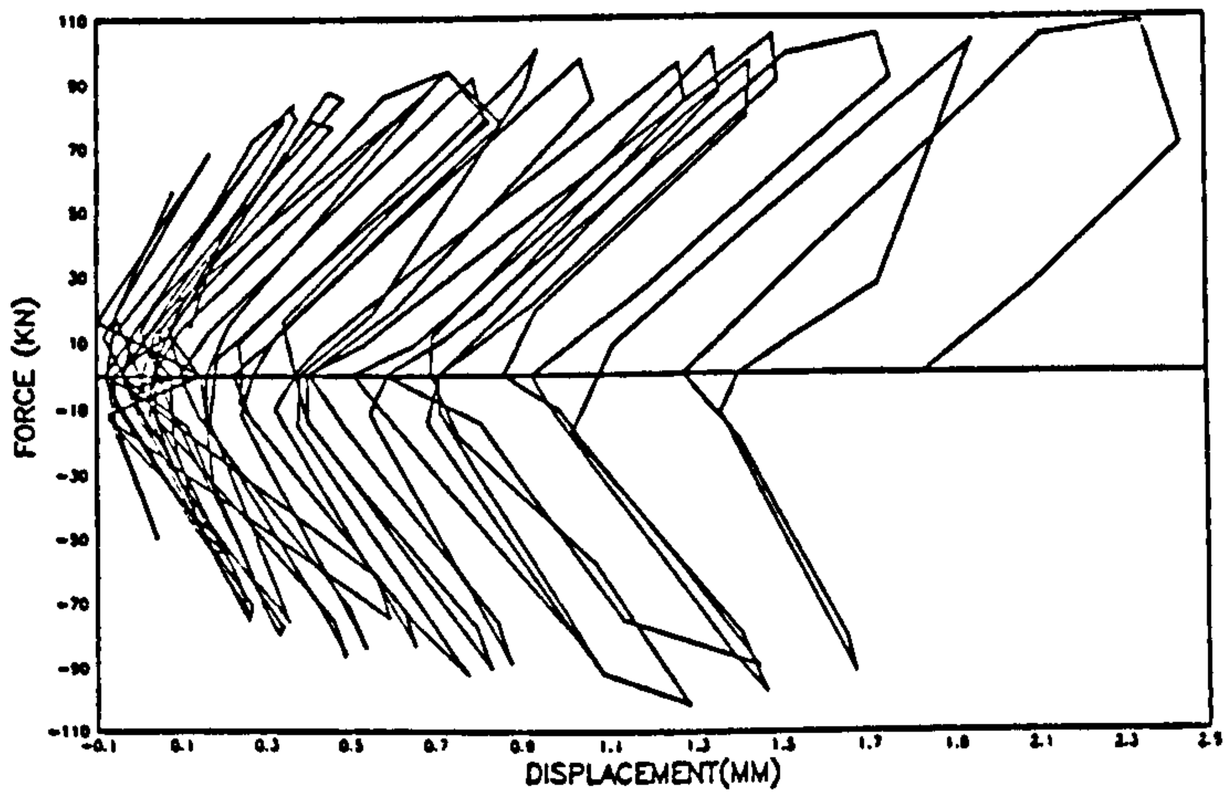


Figure B(13)21 Wall SW13 - force versus extension on top

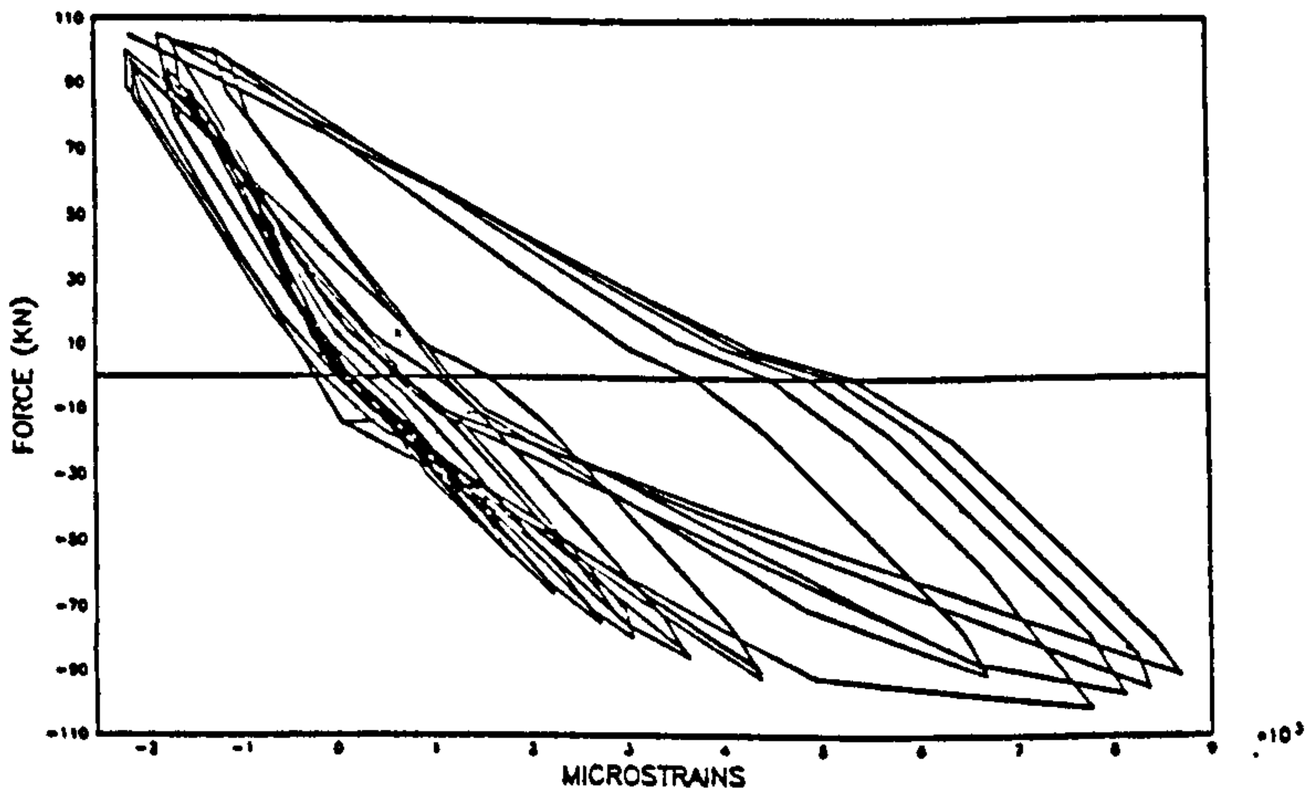


Figure B(13)22.a Wall SW13 - force versus strain 1: (bottom, ϕ8mm, LHS)

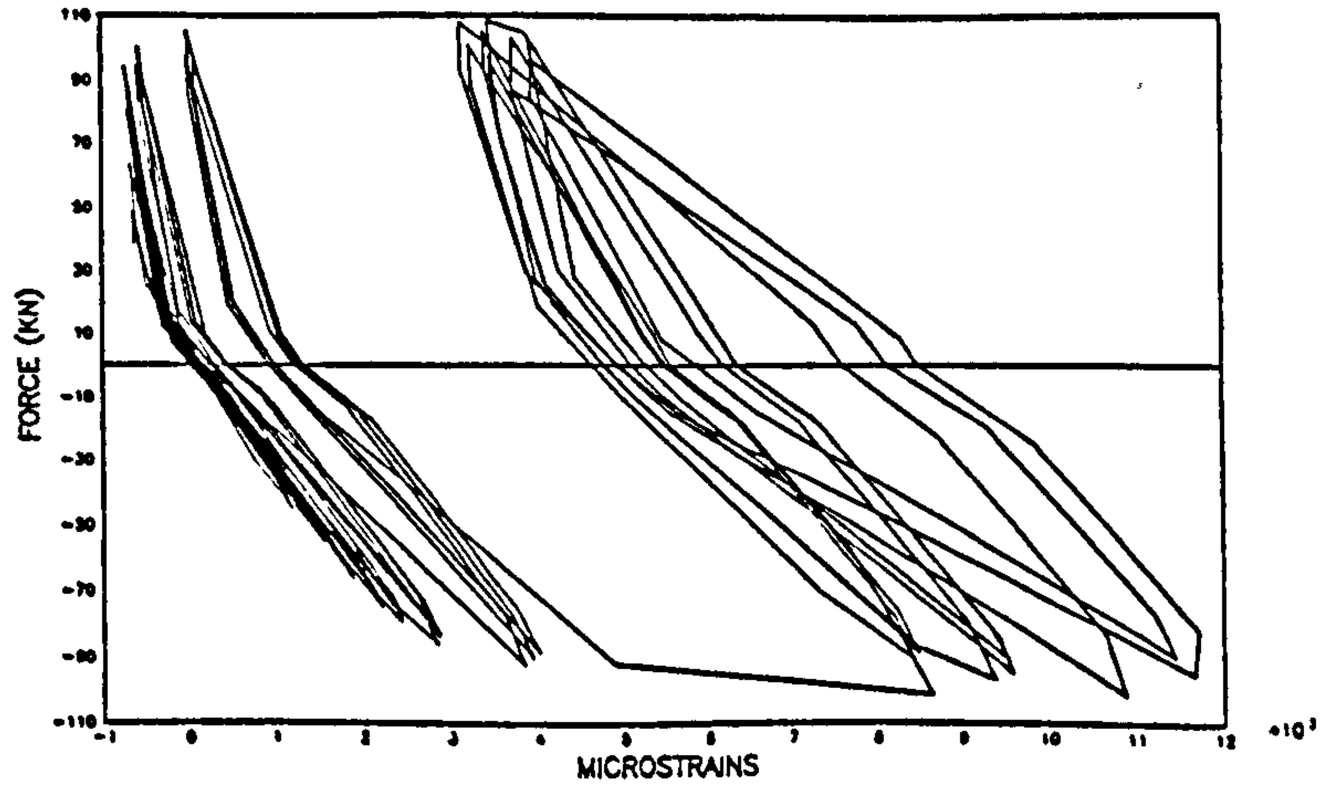


Figure B(13)22.b Wall SW13 - force versus strain 1:: (bottom, ϕ8mm, LHS)

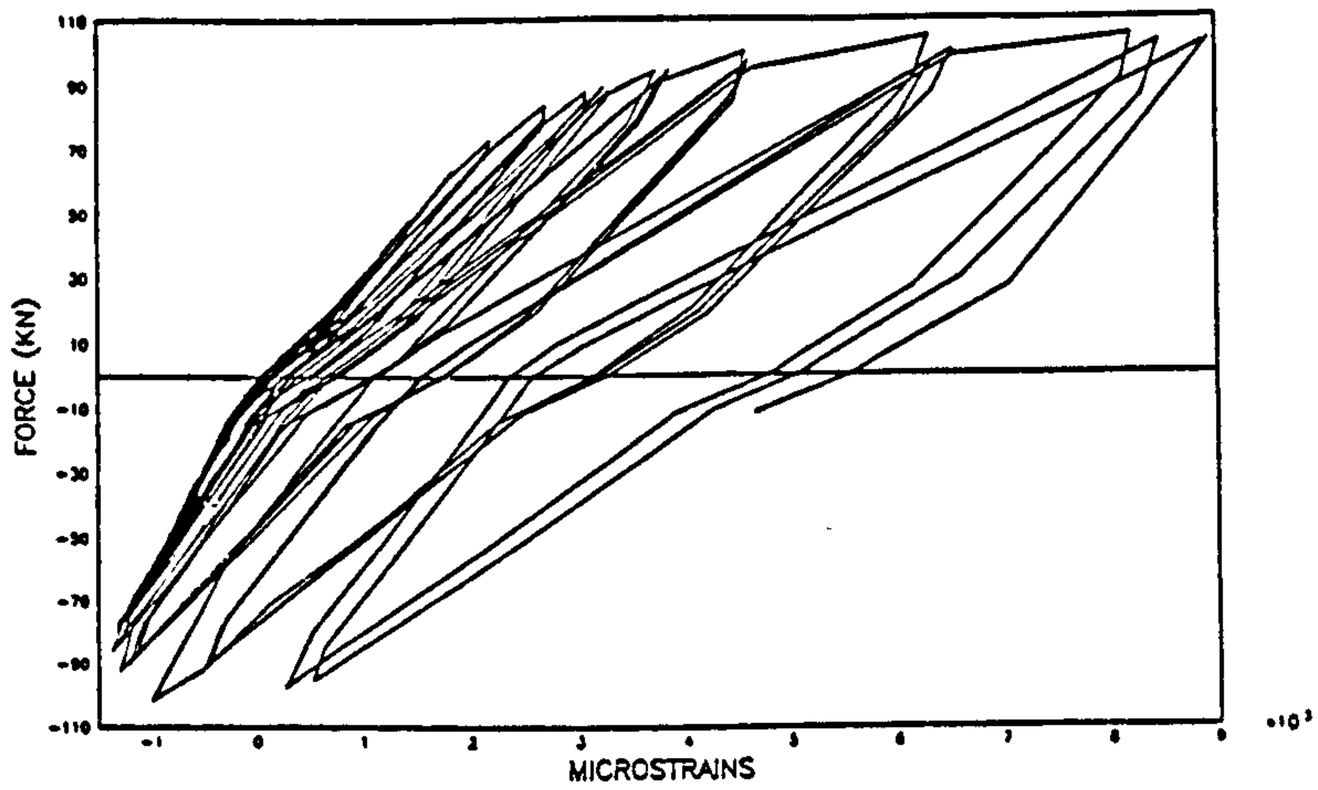


Figure B(13)23.a Wall SW13 - force versus strain 2: (bottom, ϕ8mm, RHS)

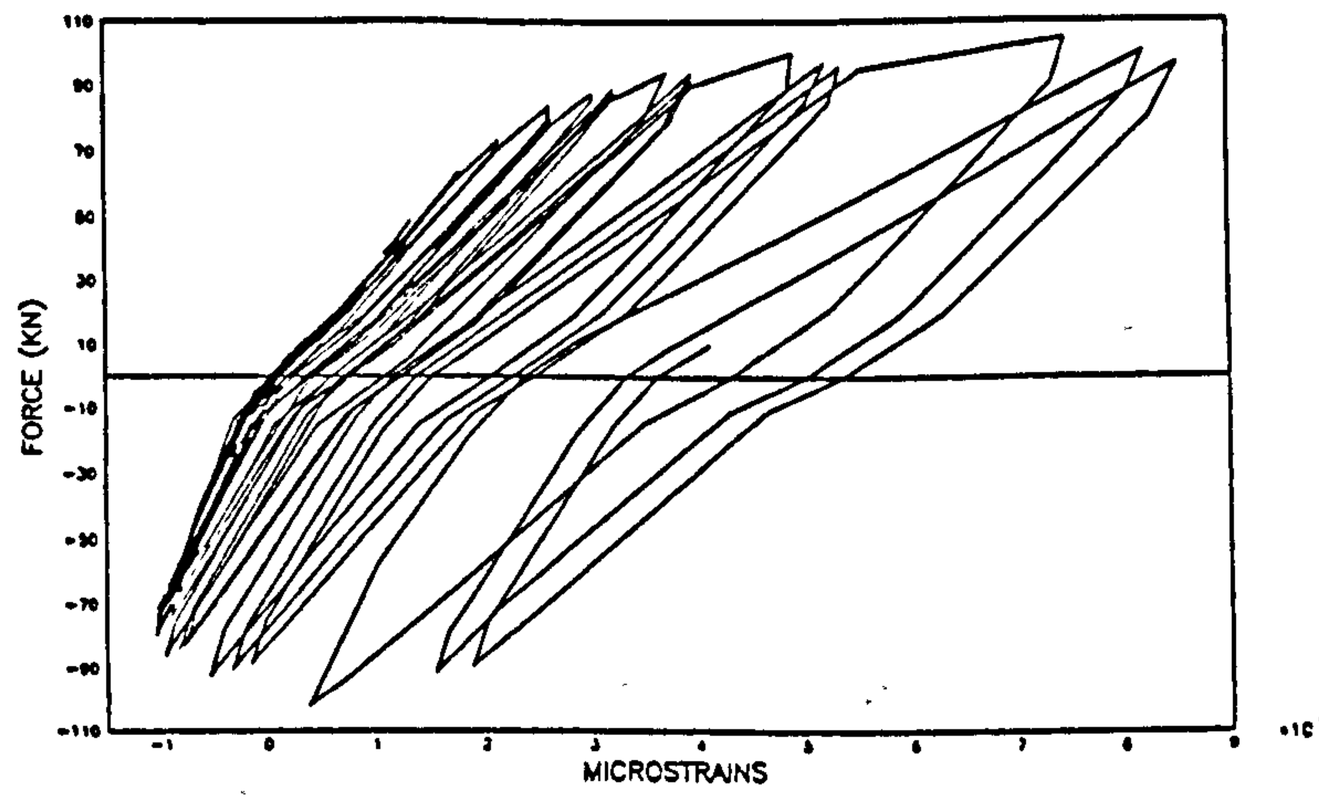


Figure B(13)23.b Wall SW13 - force versus strain 2:: (bottom, ϕ8mm, RHS)

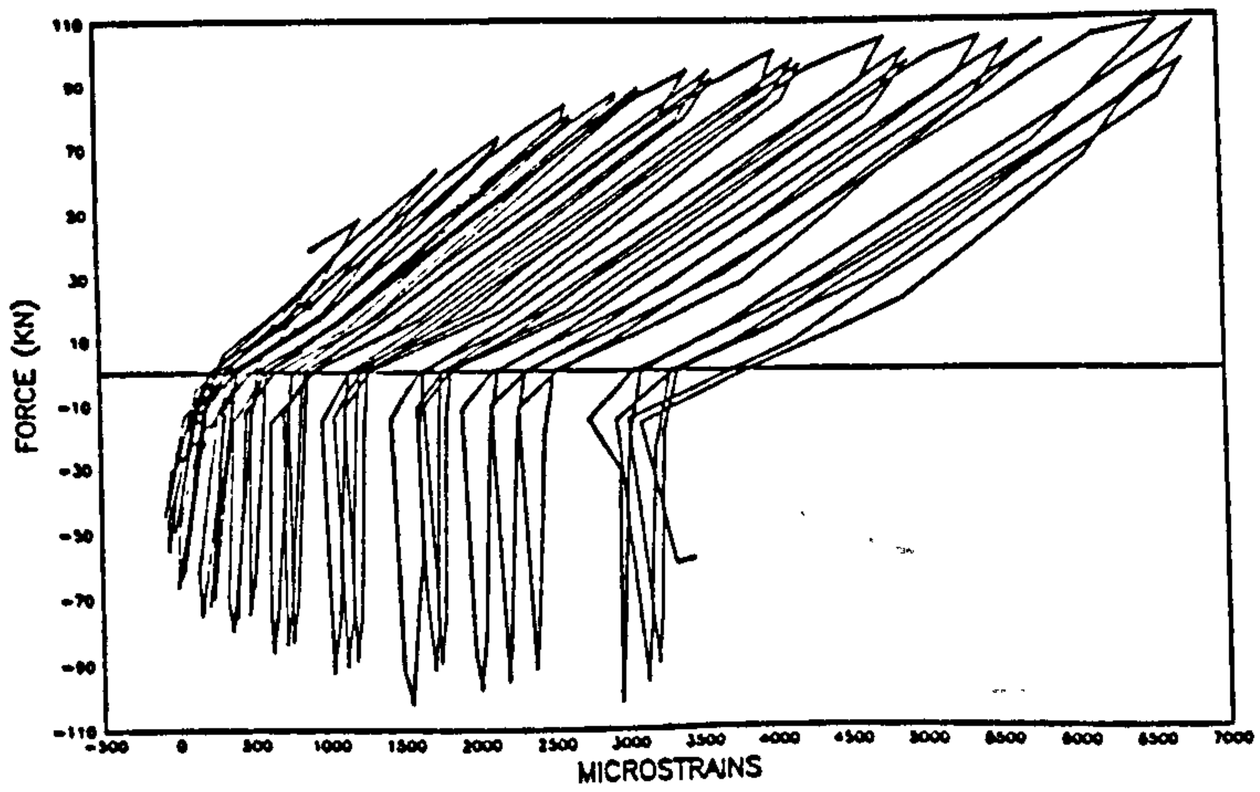


Figure B(13)24 Wall SW13 - force versus strain 4 (bottom, ϕ6mm, RHS)

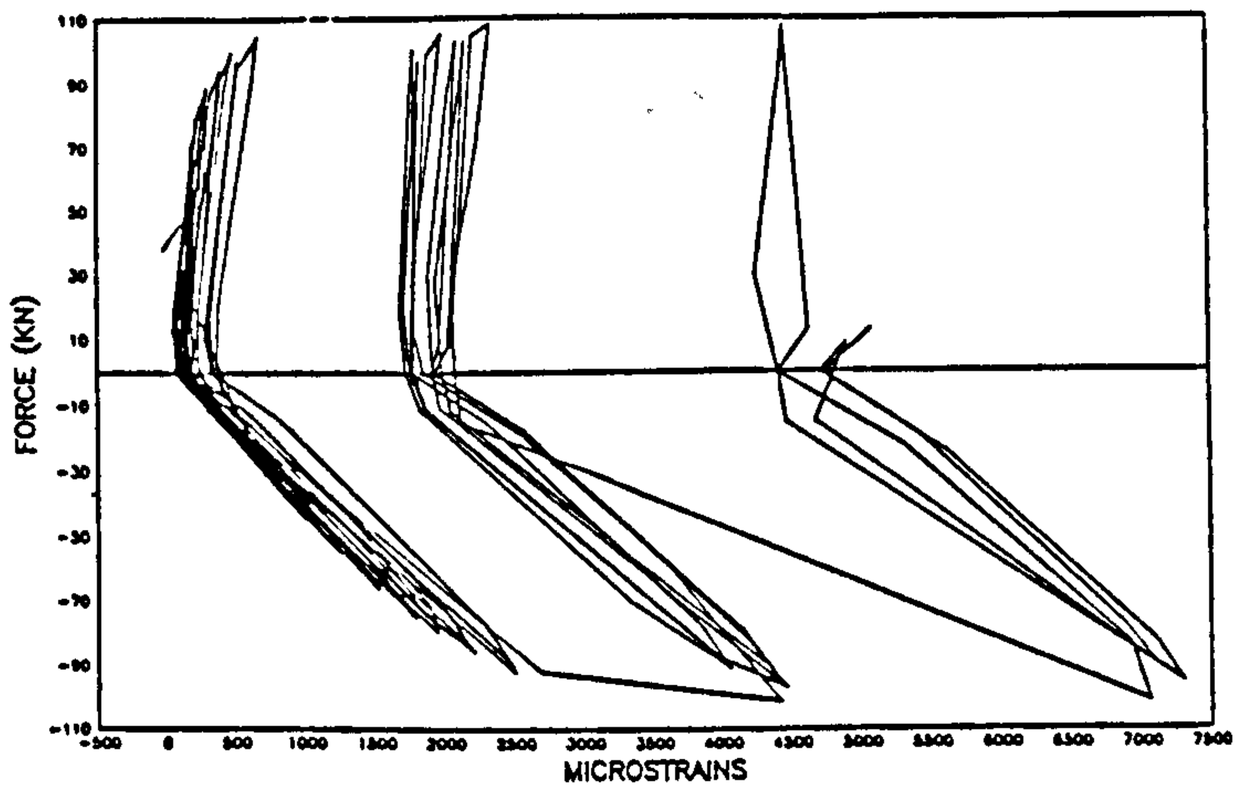


Figure B(13)25 Wall SW13 - force versus strain 5 (bottom, ϕ6mm, LHS)

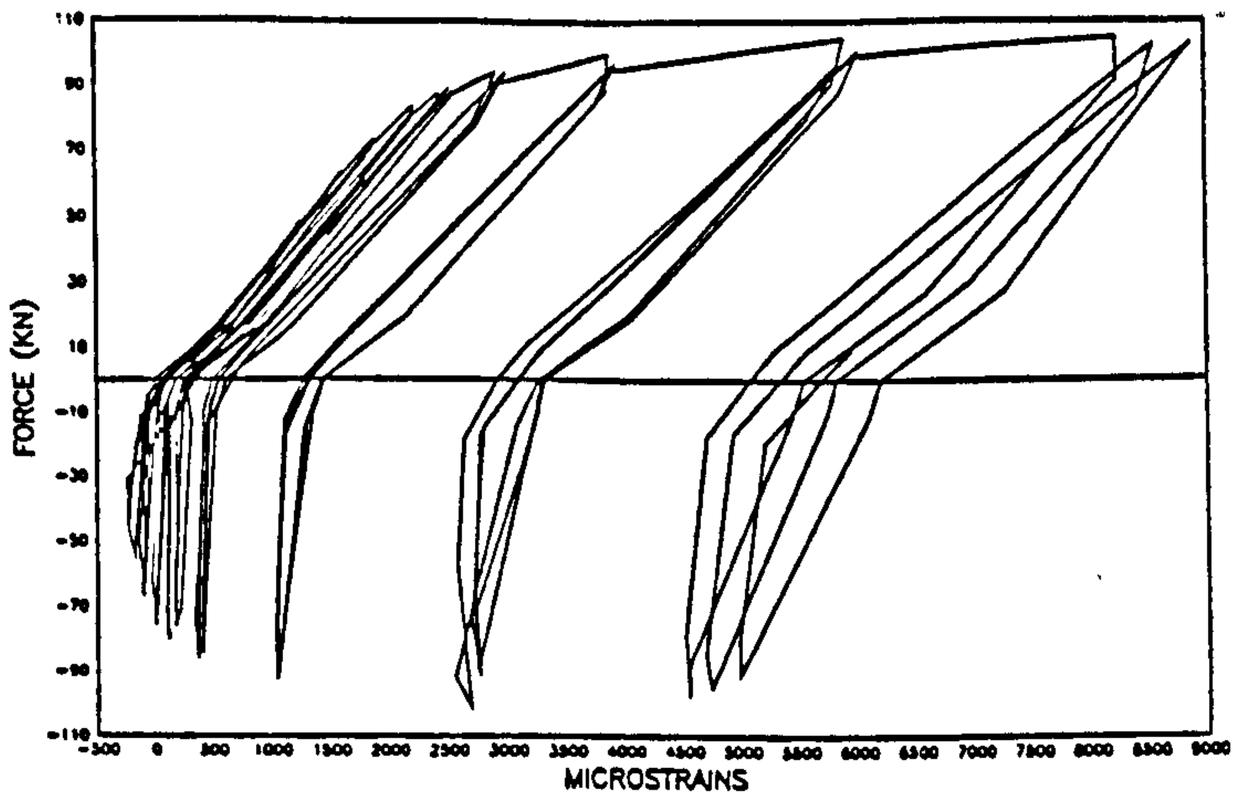


Figure B(13)26 Wall SW13 - force versus strain 6 (bottom, ϕ6mm, RHS)

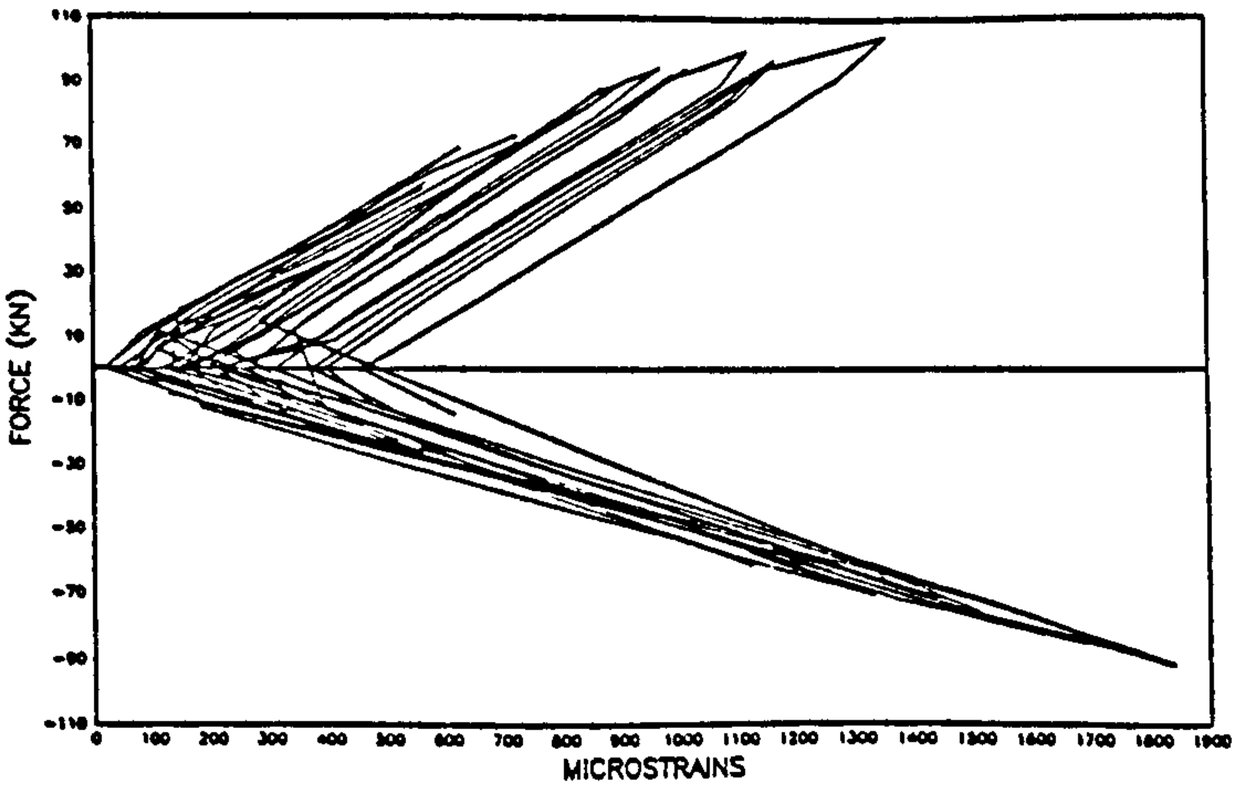


Figure B(13)27 Wall SW13 - force versus strain 7 (bottom, ϕ4mm, LHS)

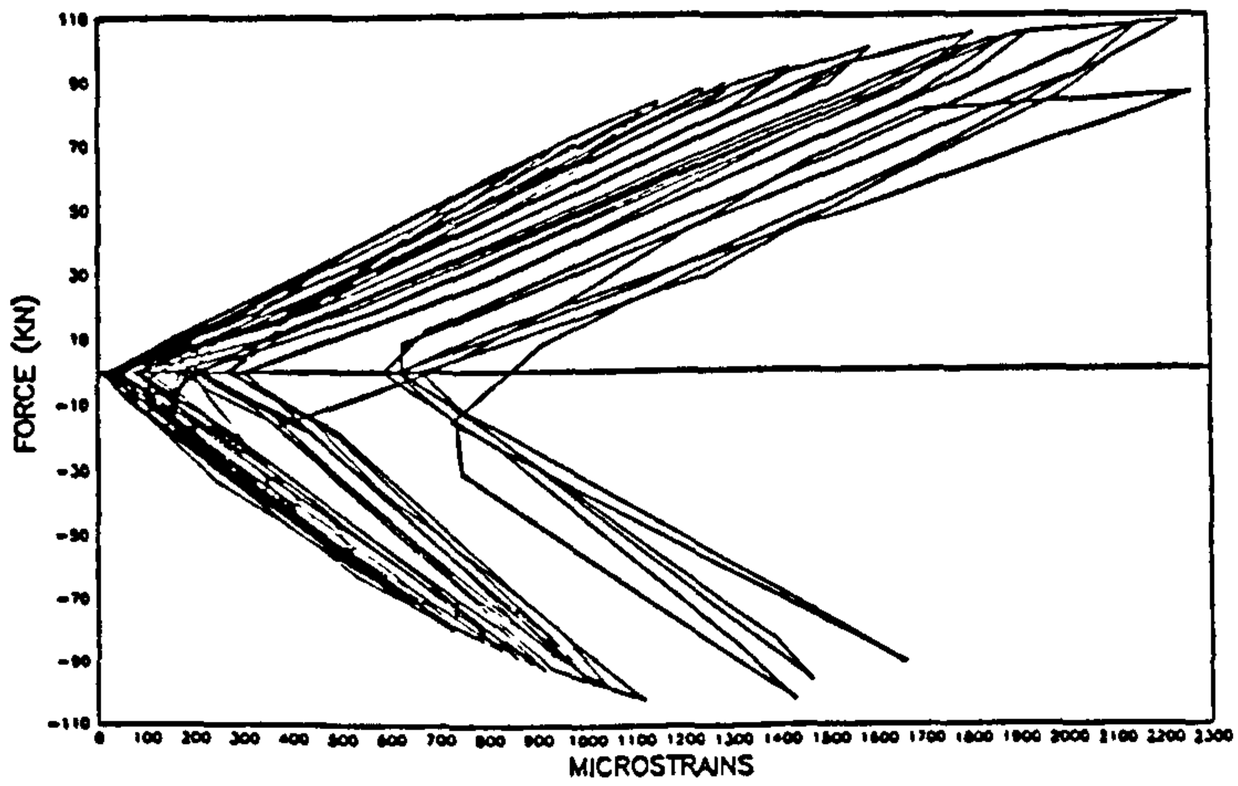


Figure B(13)28 Wall SW13 - force versus strain 8 (bottom, ϕ4mm, RHS)

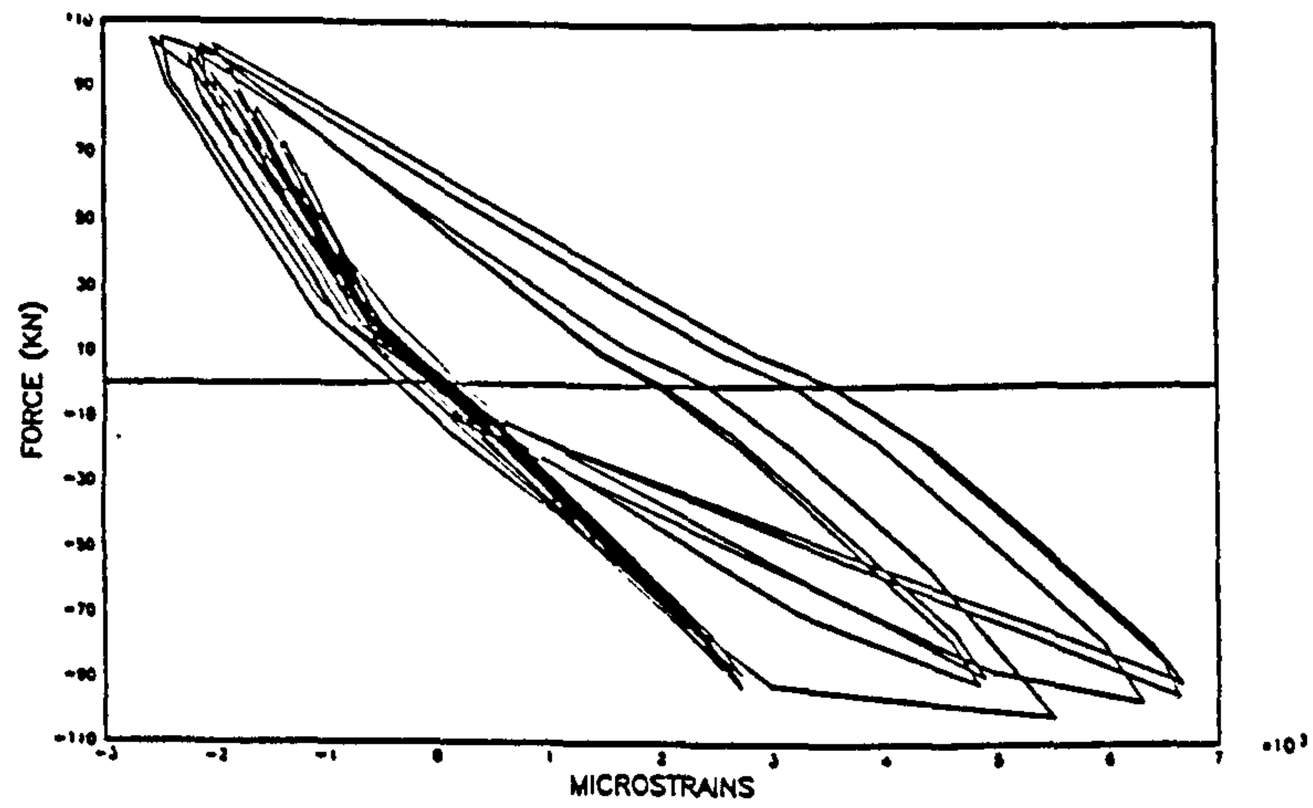


Figure B(13)29 Wall SW13 - force versus strain 9 (second level, ϕ8mm, LHS)

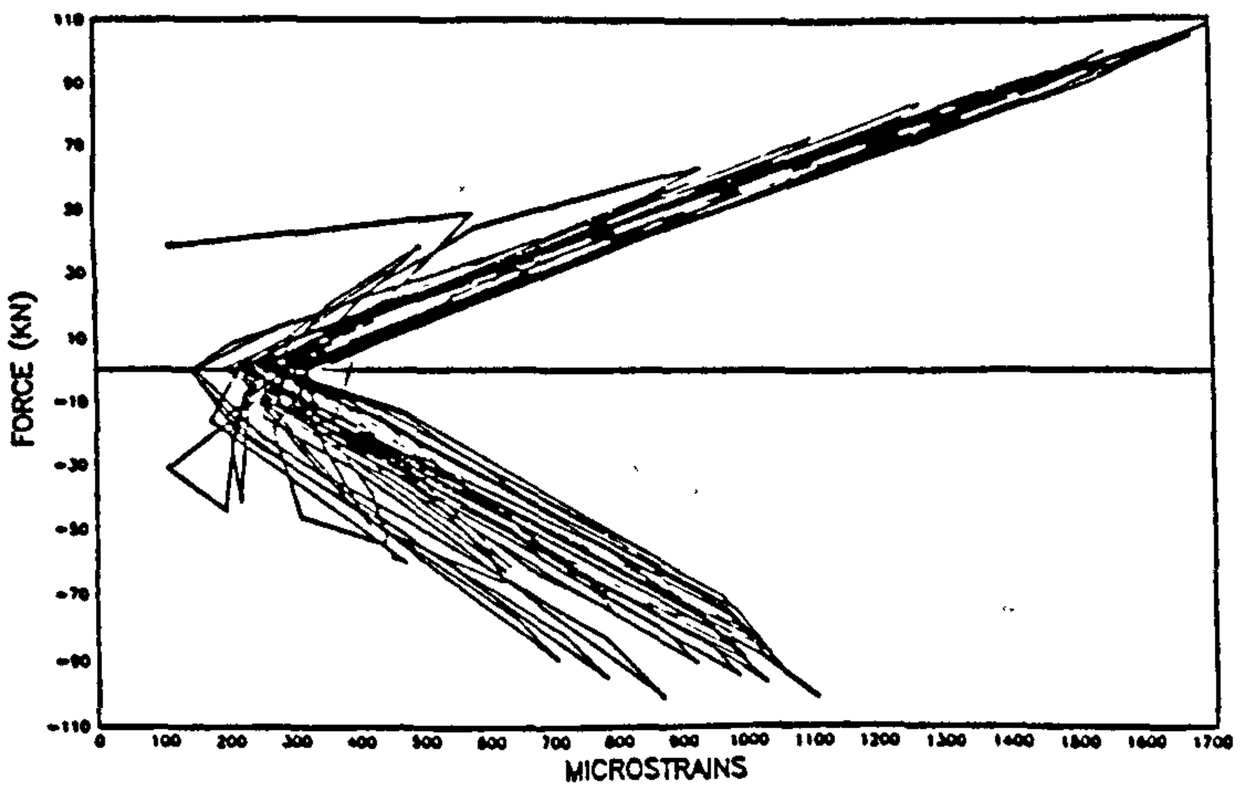


Figure B(13)30 Wall SW13 - force versus strain 11 (level of zero moment, ϕ8mm, LHS)

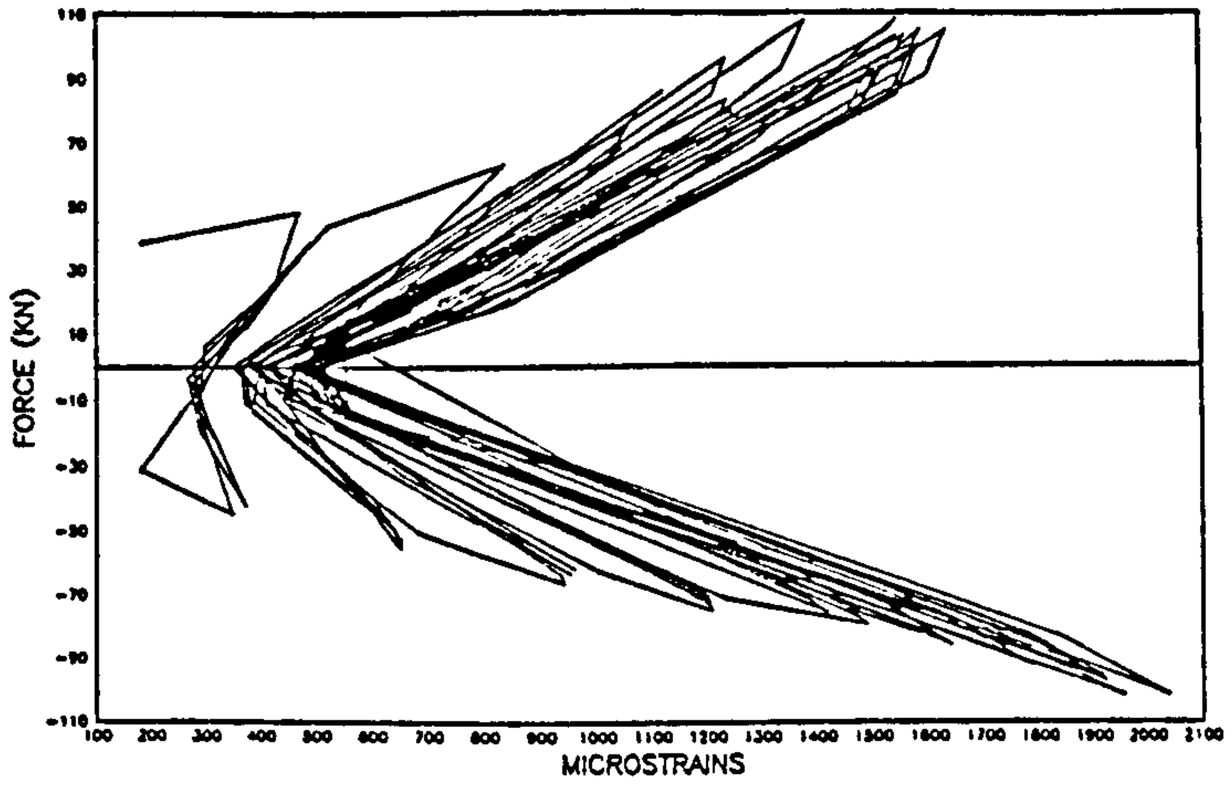


Figure B(13)31 Wall SW13 - force versus strain 12 (level of zero moment, ϕ8mm, RHS)

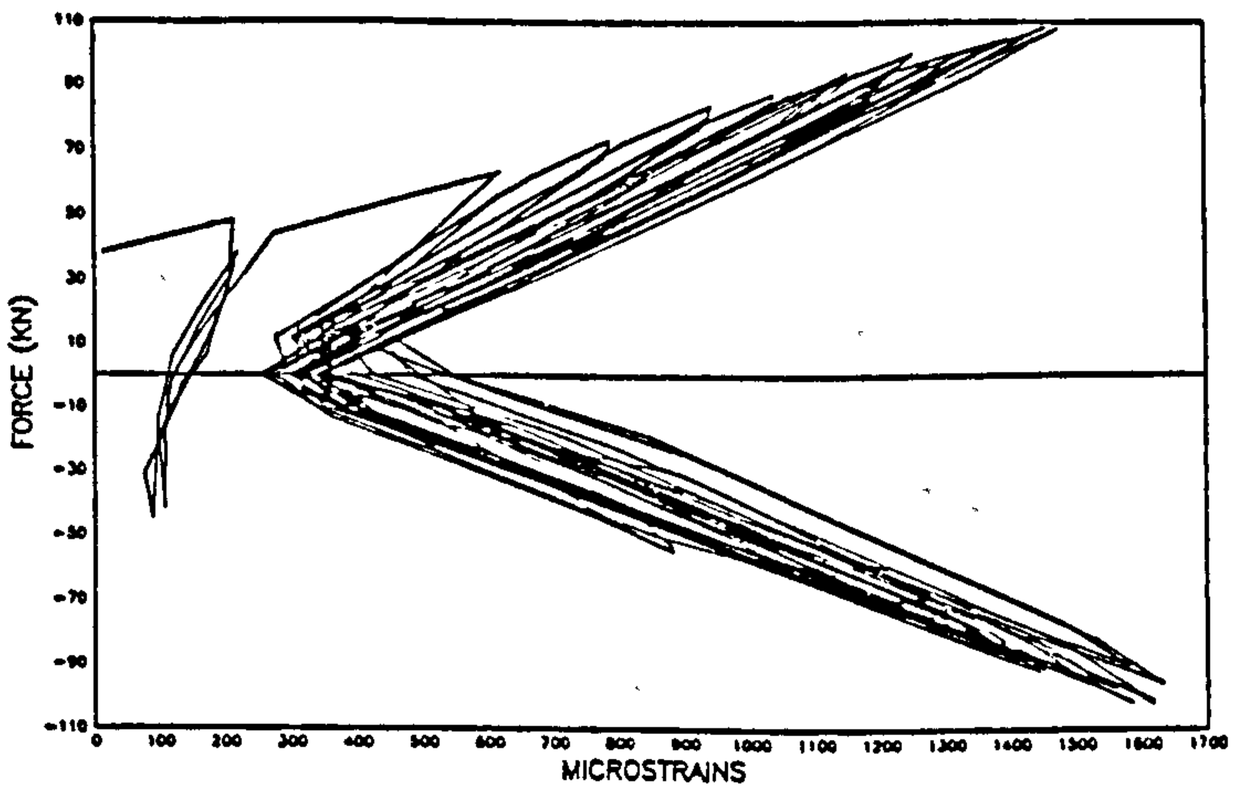


Figure B(13)32 Wall SW13 - force versus strain 13 (level of zero moment, ϕ6mm, LHS)

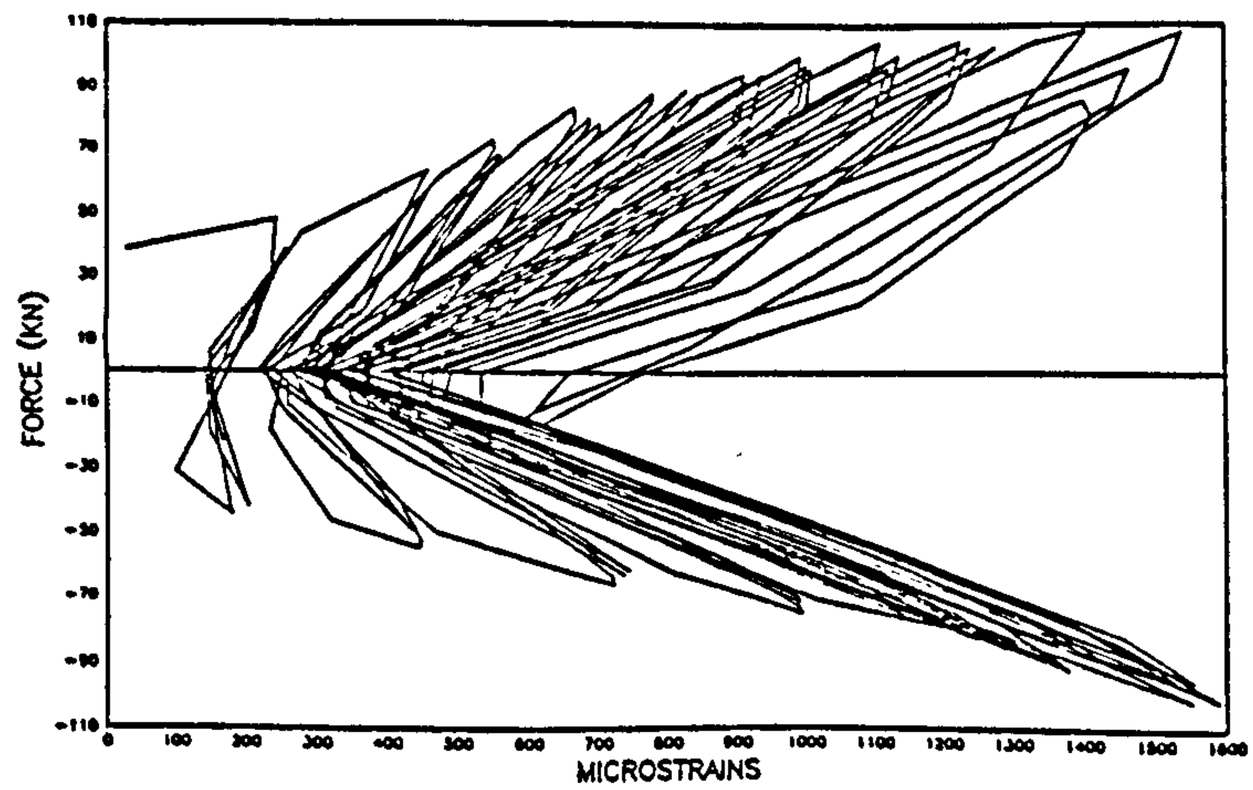


Figure B(13)33 Wall SW13 - force versus strain 14 (level of zero moment, ϕ6mm, RHS)

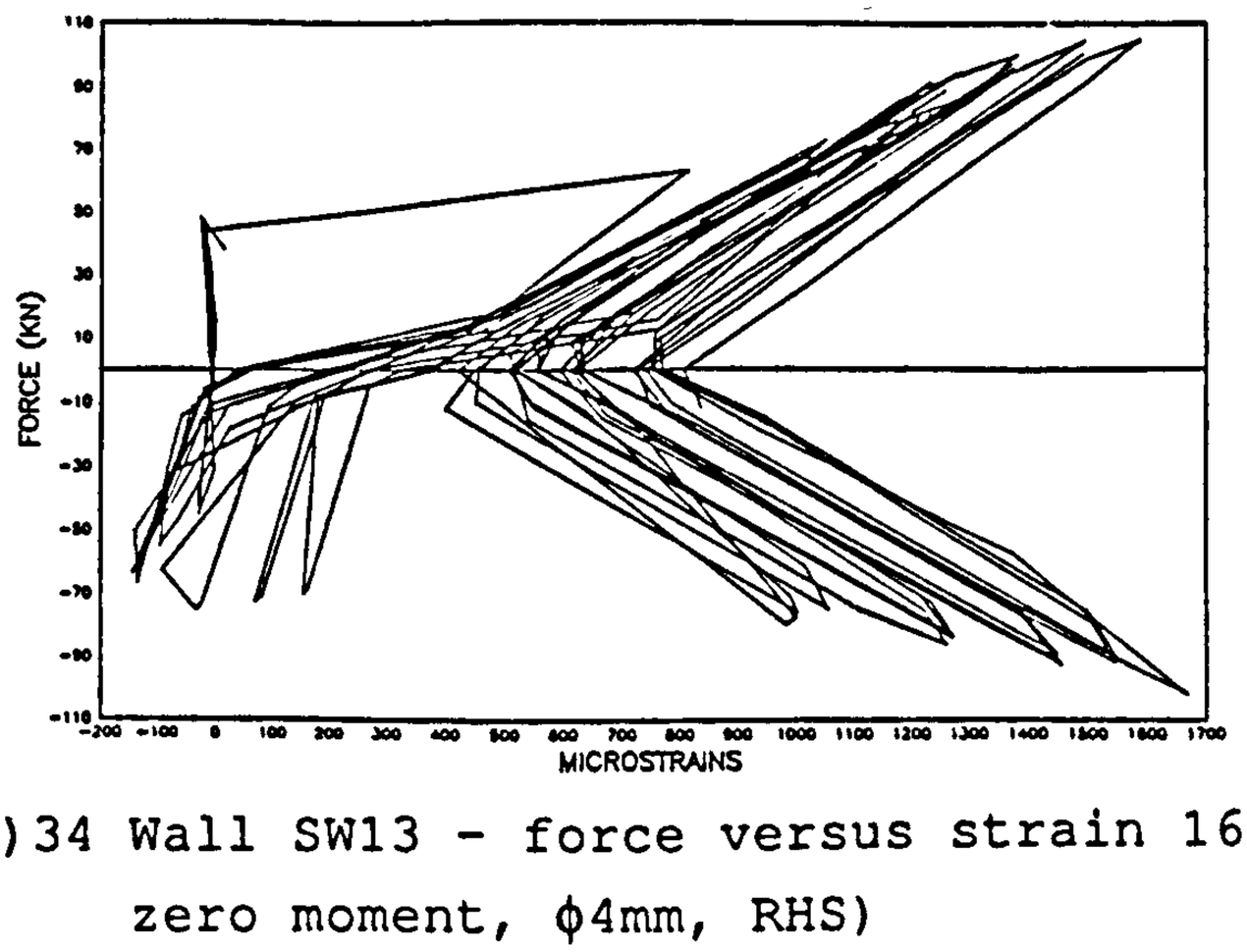


Figure B(13)34 Wall SW13 - force versus strain 16 (level of zero moment, ϕ4mm, RHS)

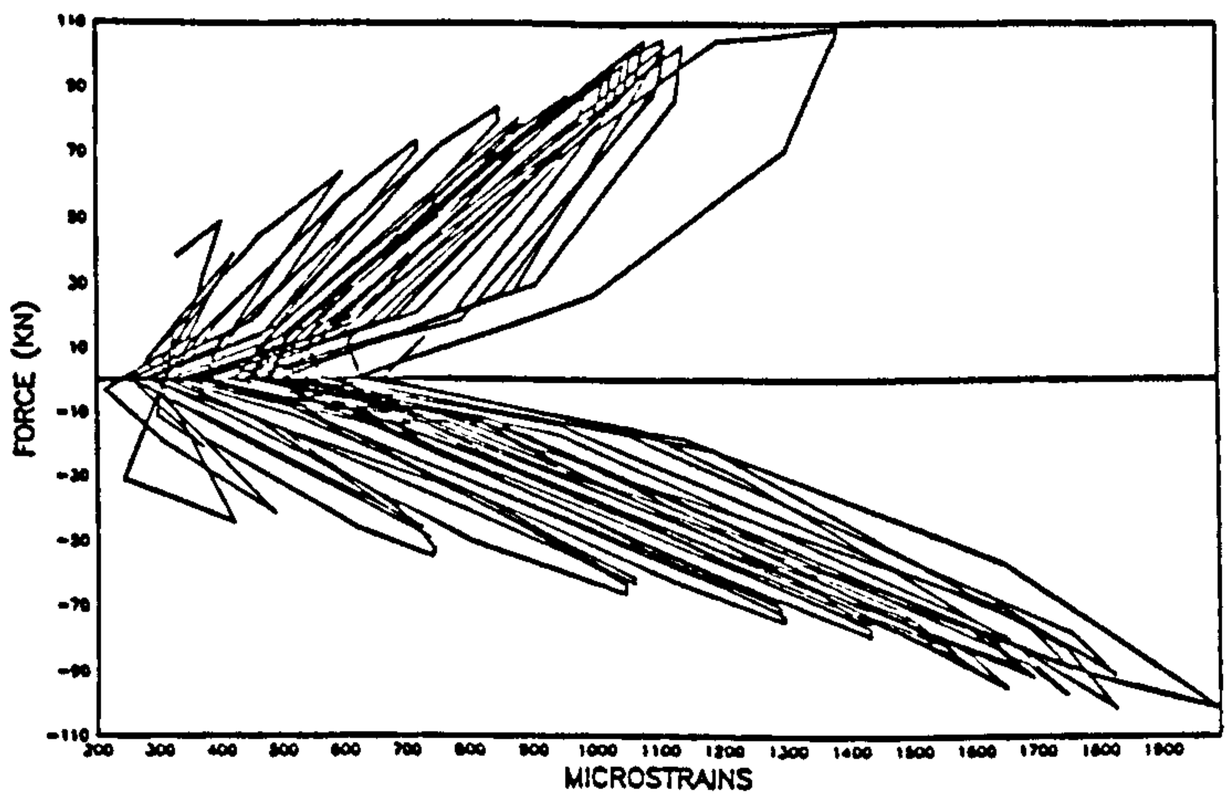


Figure B(13)35 Wall SW13 - force versus strain 19 (stirrup)

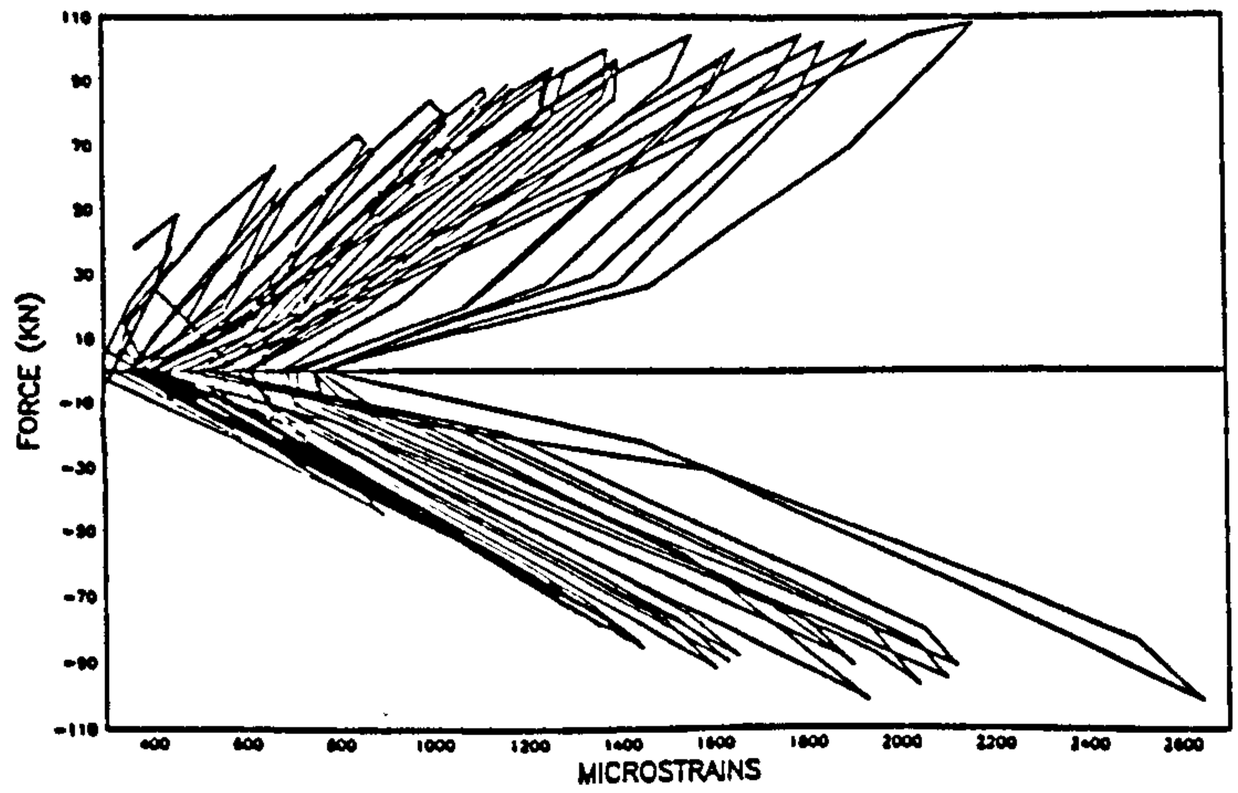


Figure B(13)36 Wall SW13 - force versus strain 20 (stirrup)

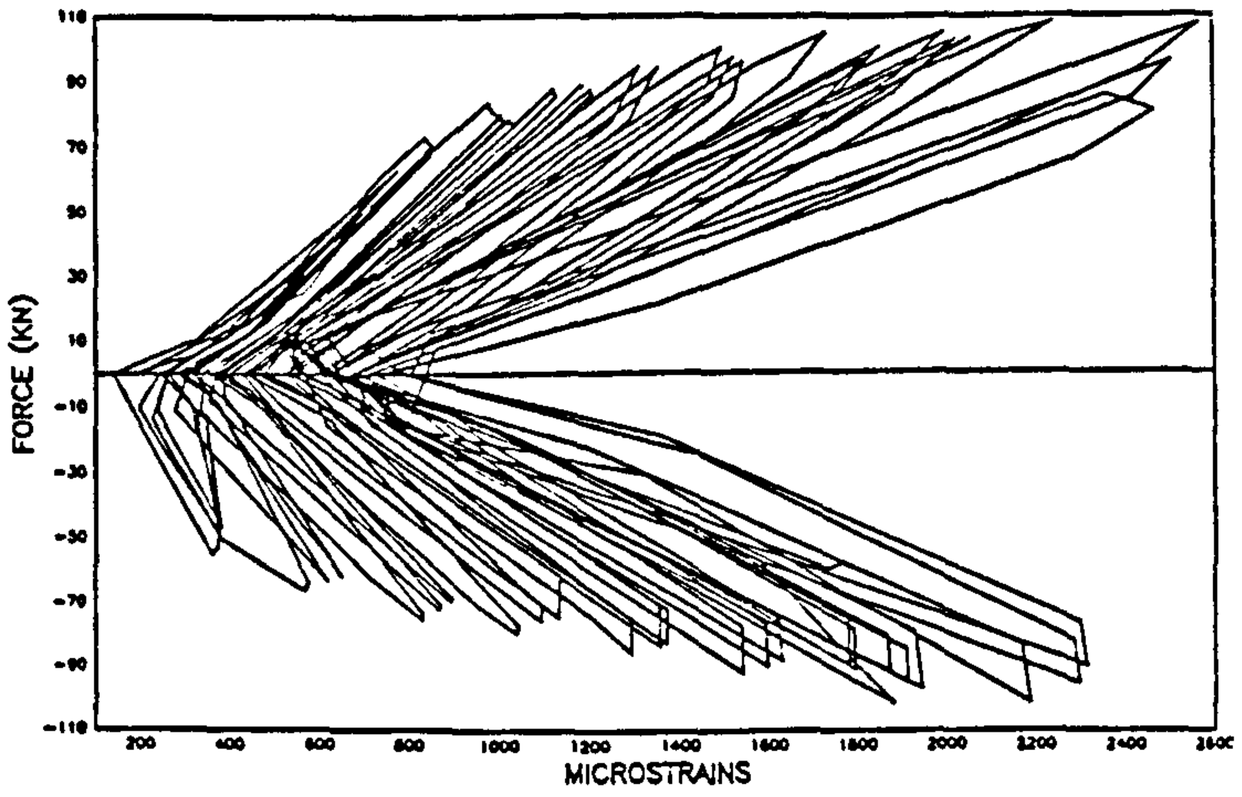


Figure B(13)37 Wall SW13 - force versus strain 21 (stirrup)

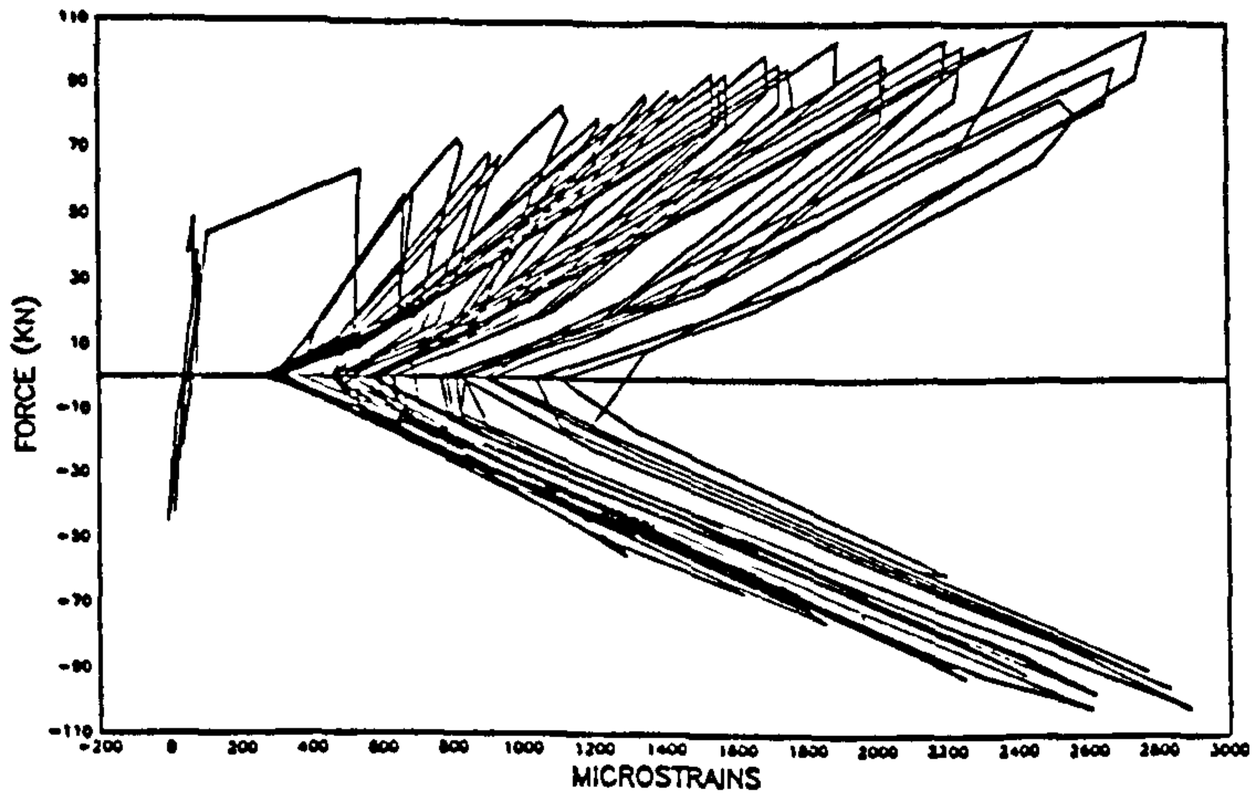


Figure B(13)38 Wall SW13 - force versus strain 22 (stirrup)

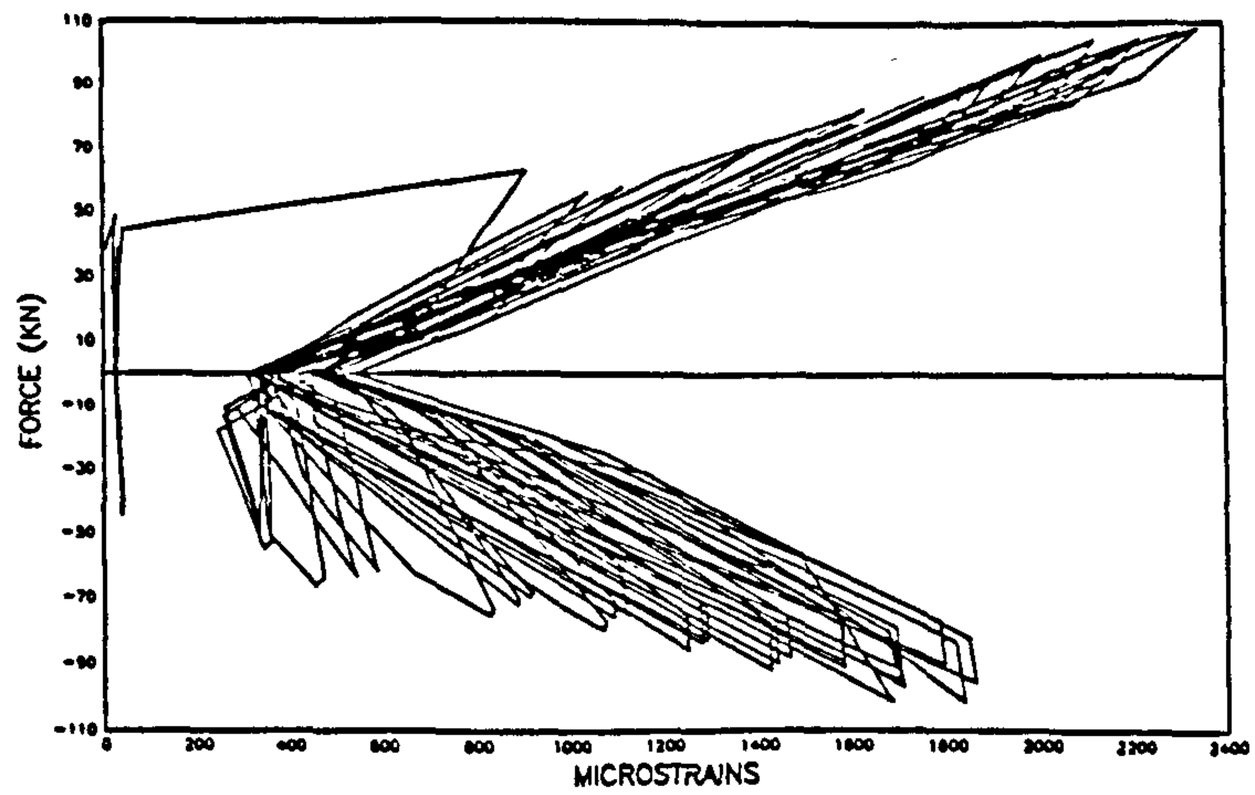


Figure B(13)39 Wall SW13 - force versus strain 23 (stirrup)

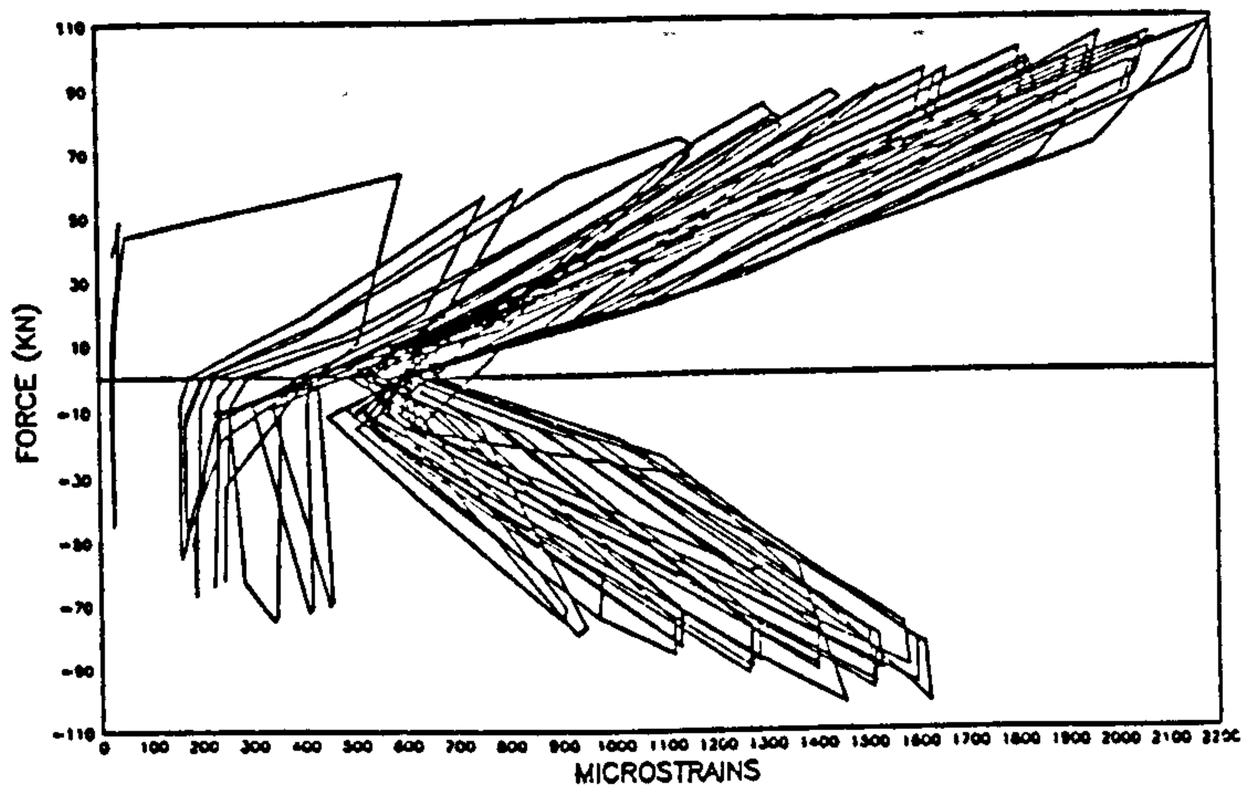


Figure B(13)40 Wall SW13 - force versus strain 24 (stirrup)

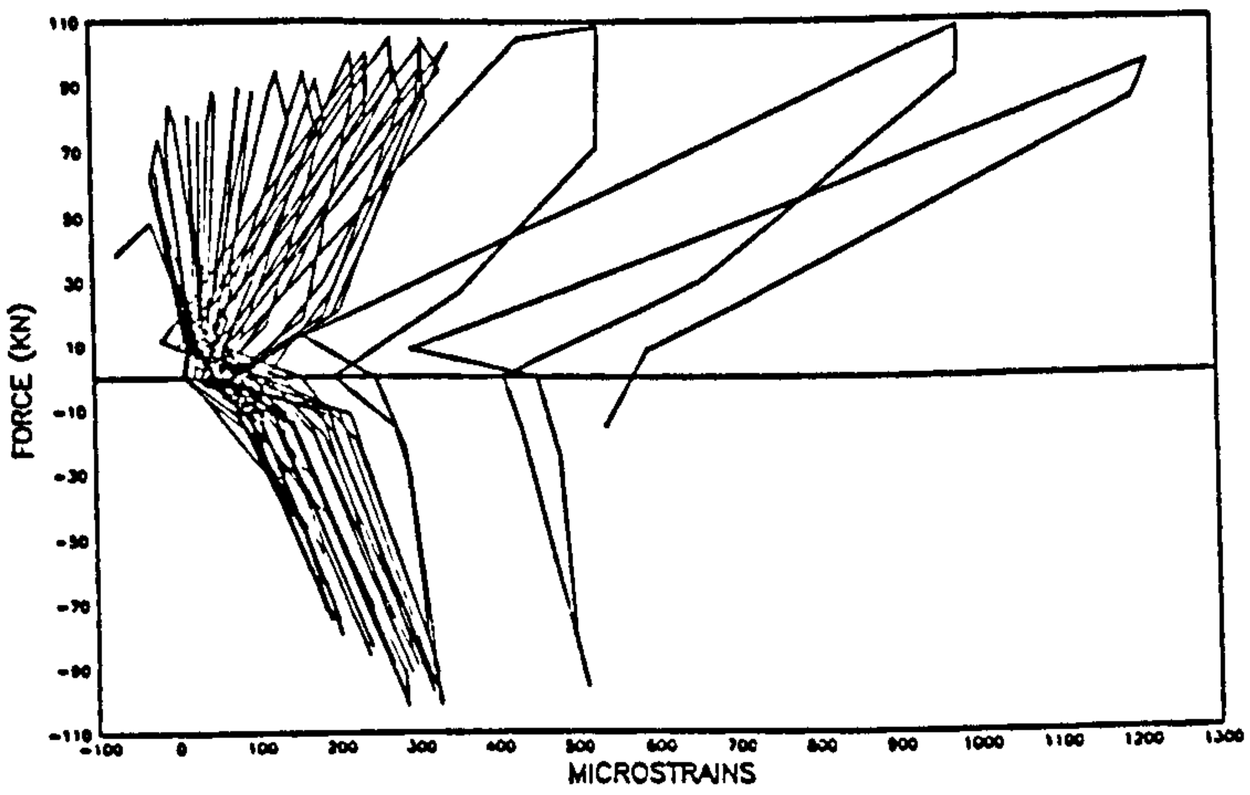


Figure B(13)41 Wall SW13 - force versus strain 25 (confinement reinforcement)

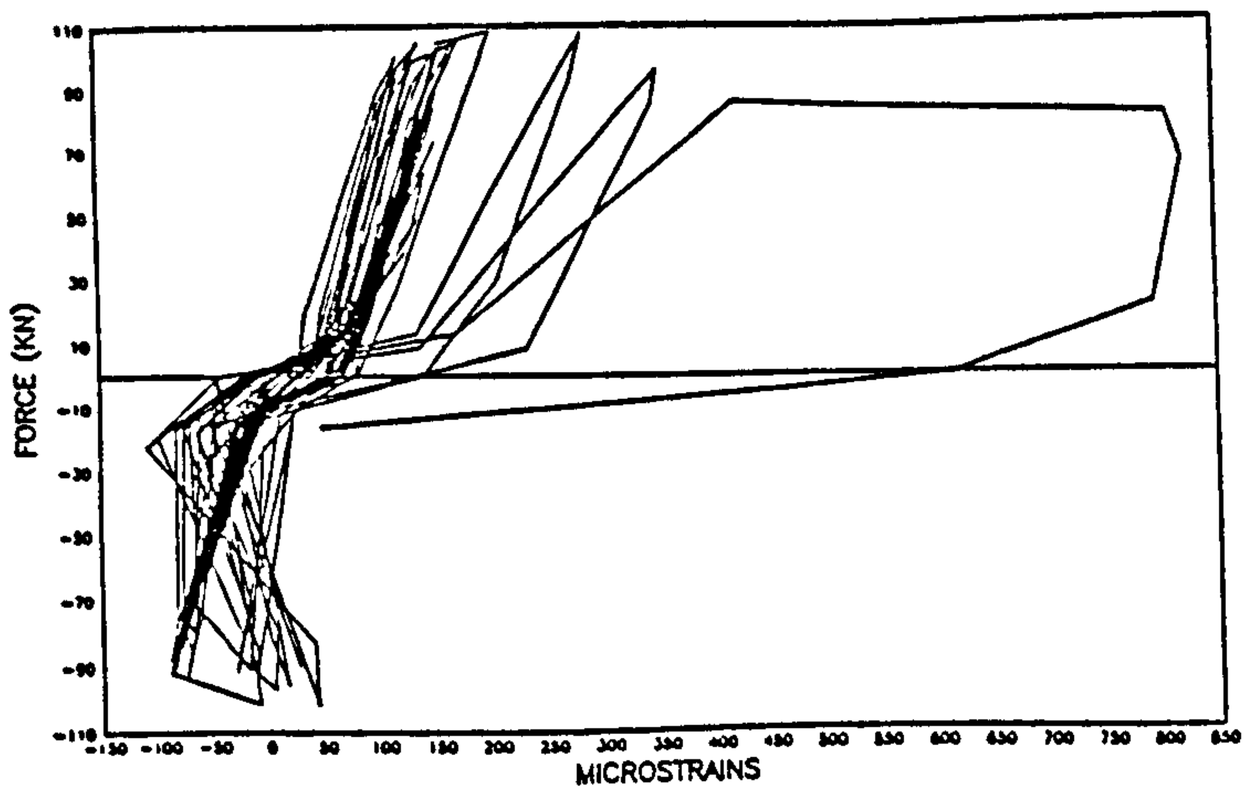


Figure B(13)42 Wall SW13 - force versus strain 26 (confinement reinforcement)

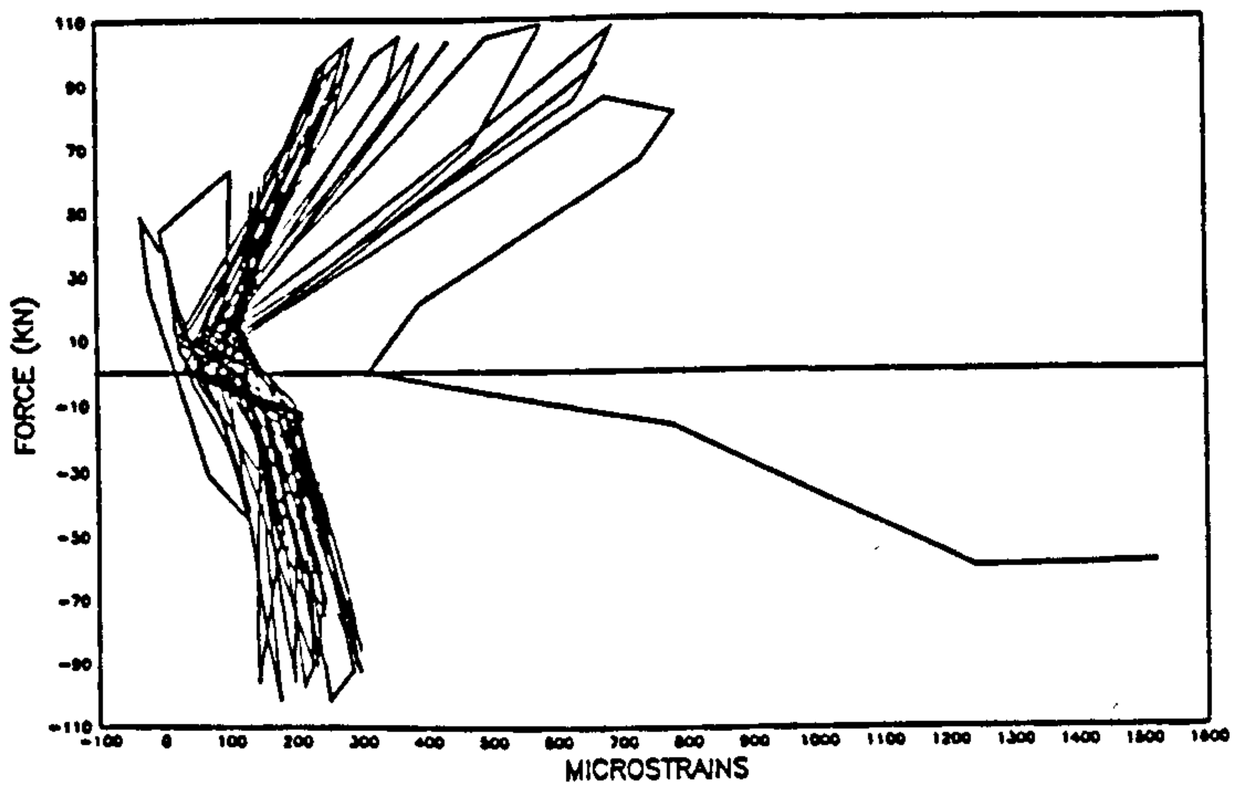


Figure B(13)43 Wall SW13 - force versus strain 27
(confinement reinforcement)

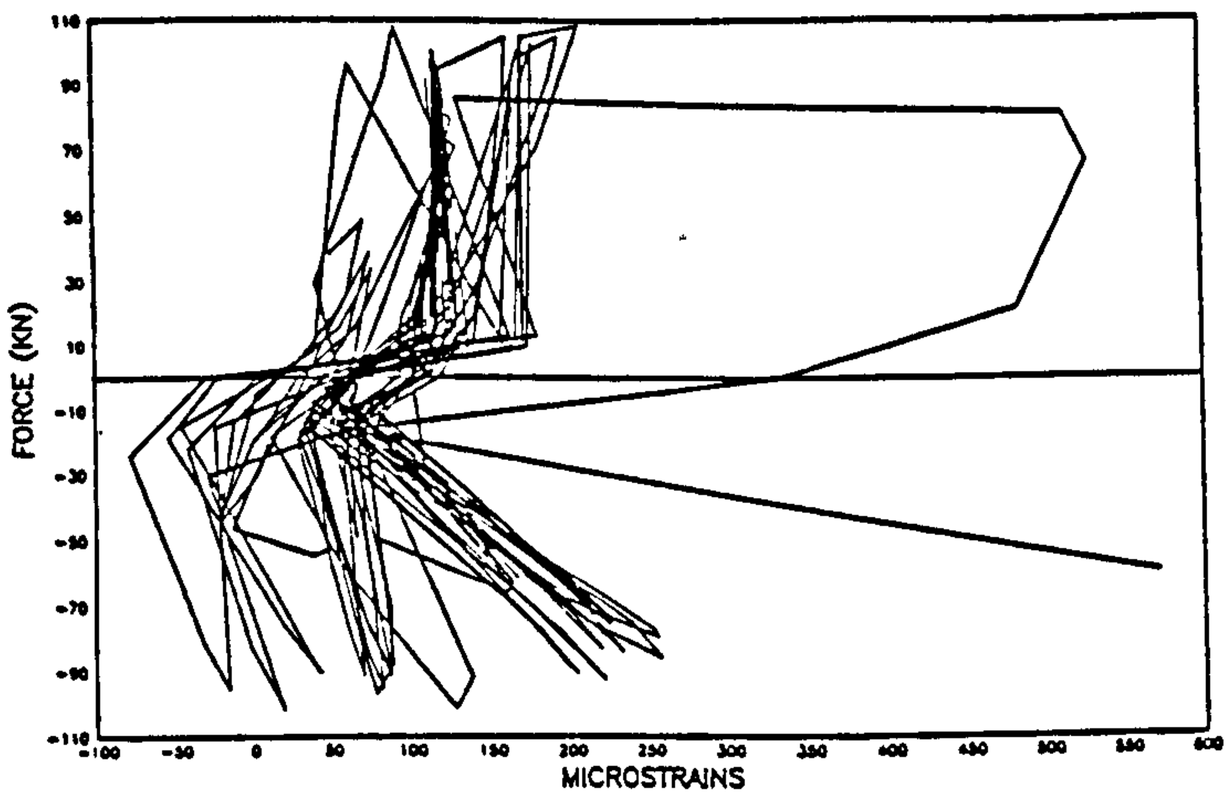


Figure B(13)44 Wall SW13 - force versus strain 28
(confinement reinforcement)

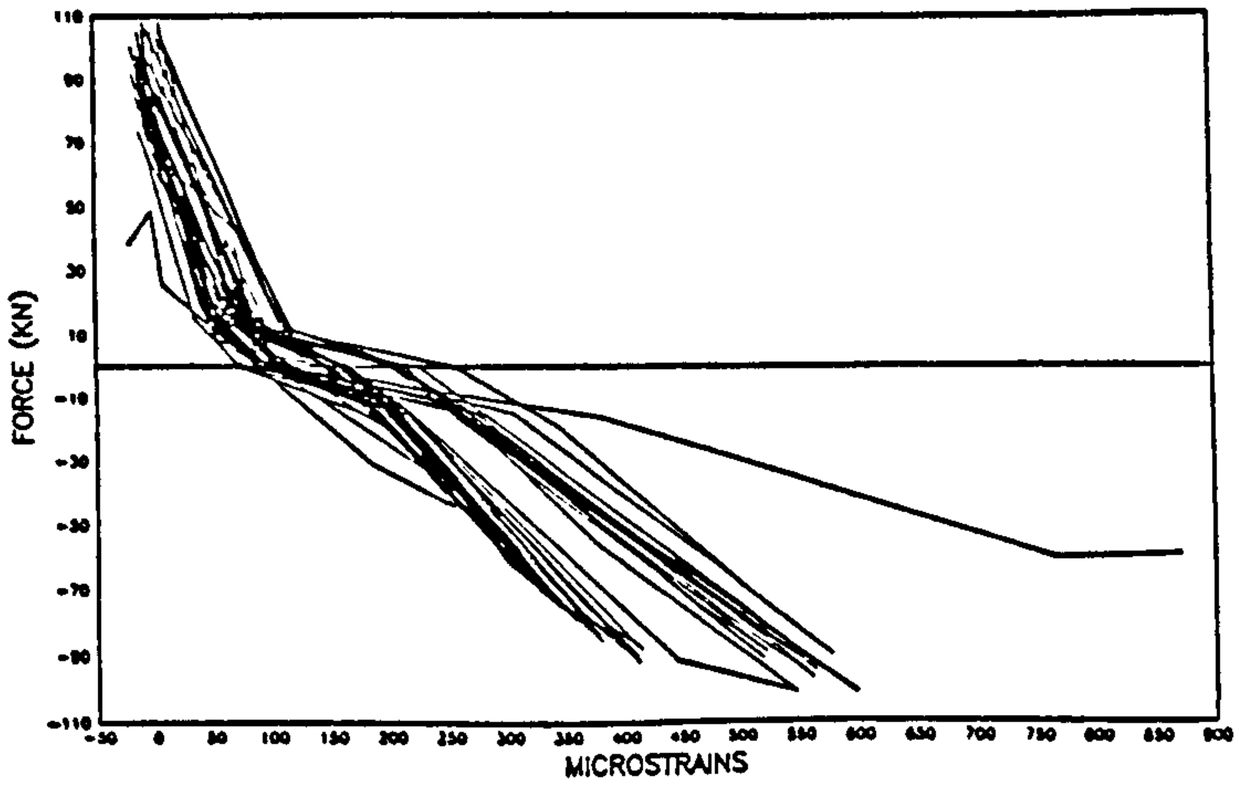


Figure B(13)45 Wall SW13 - force versus strain 29
(confinement reinforcement)

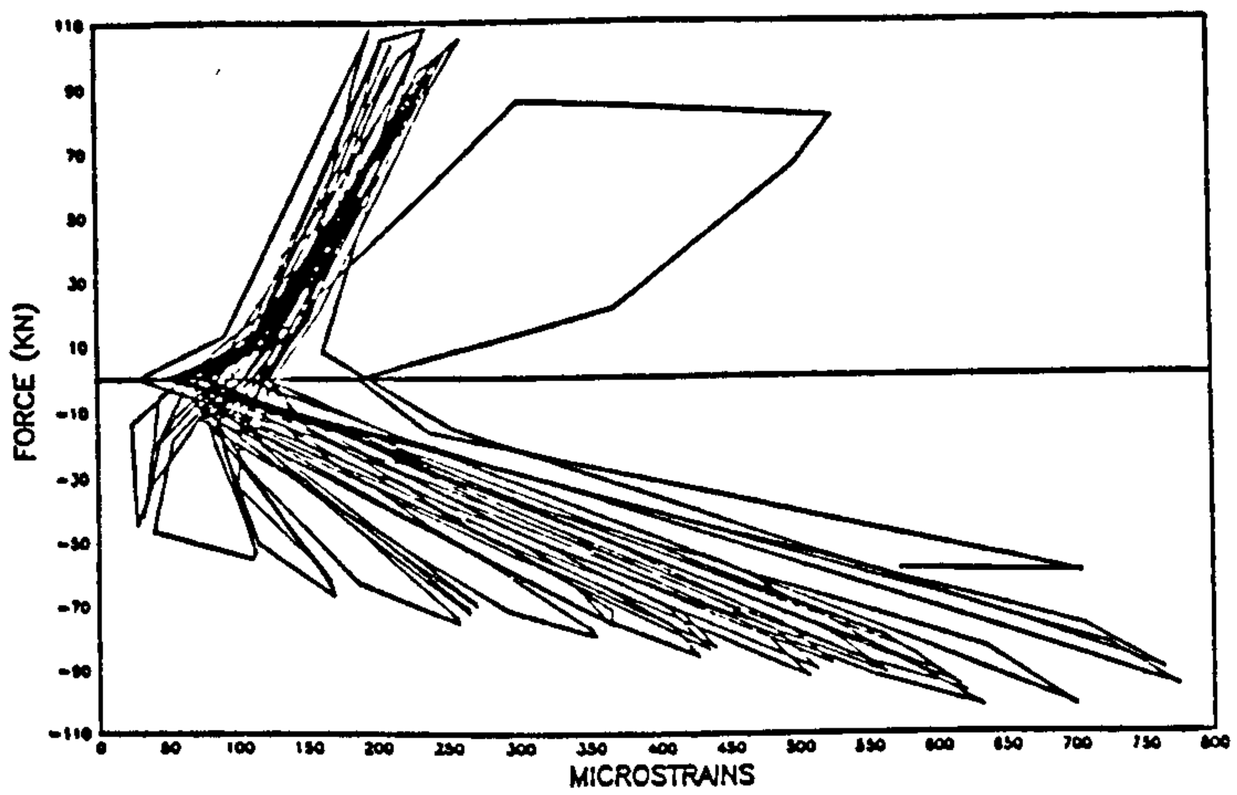


Figure B(13)46 Wall SW13 - force versus strain 30 (confinement reinforcement)

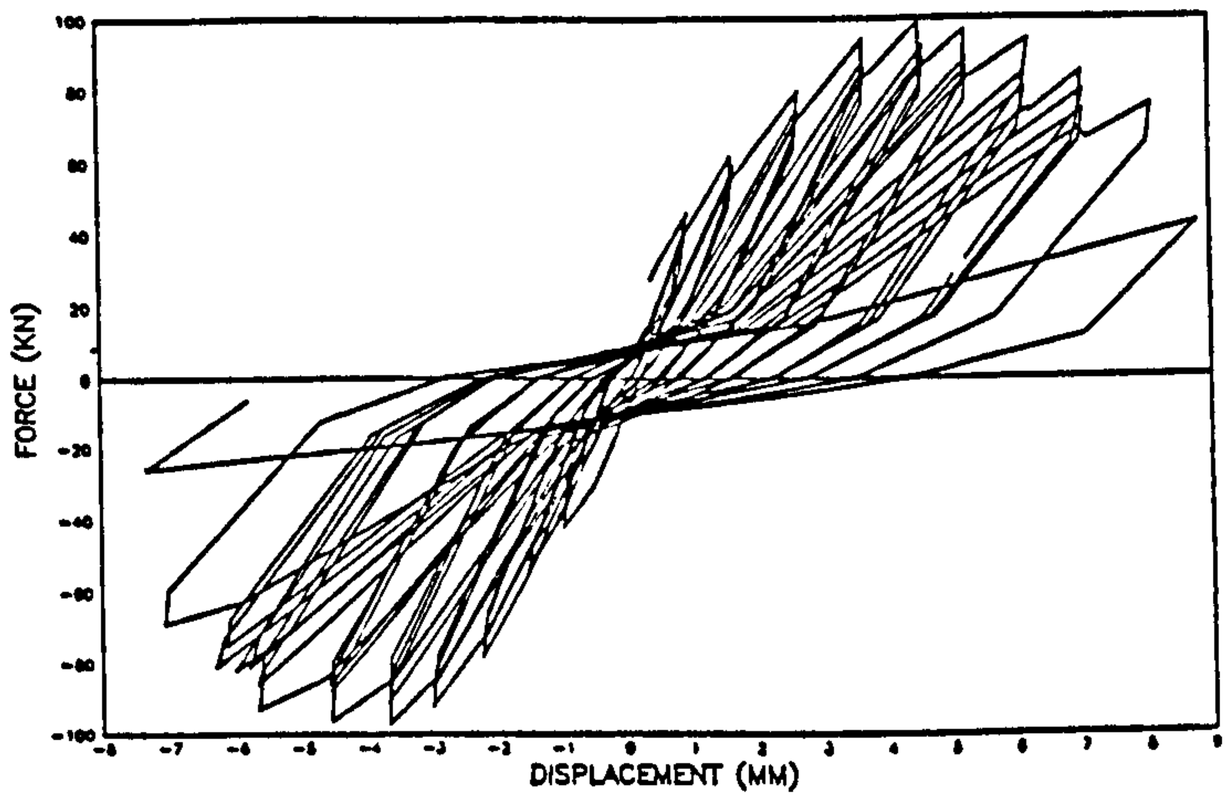


Figure B(14)1 Wall SW14 - force versus displacement 1 (horizontal, LHS, level 4)

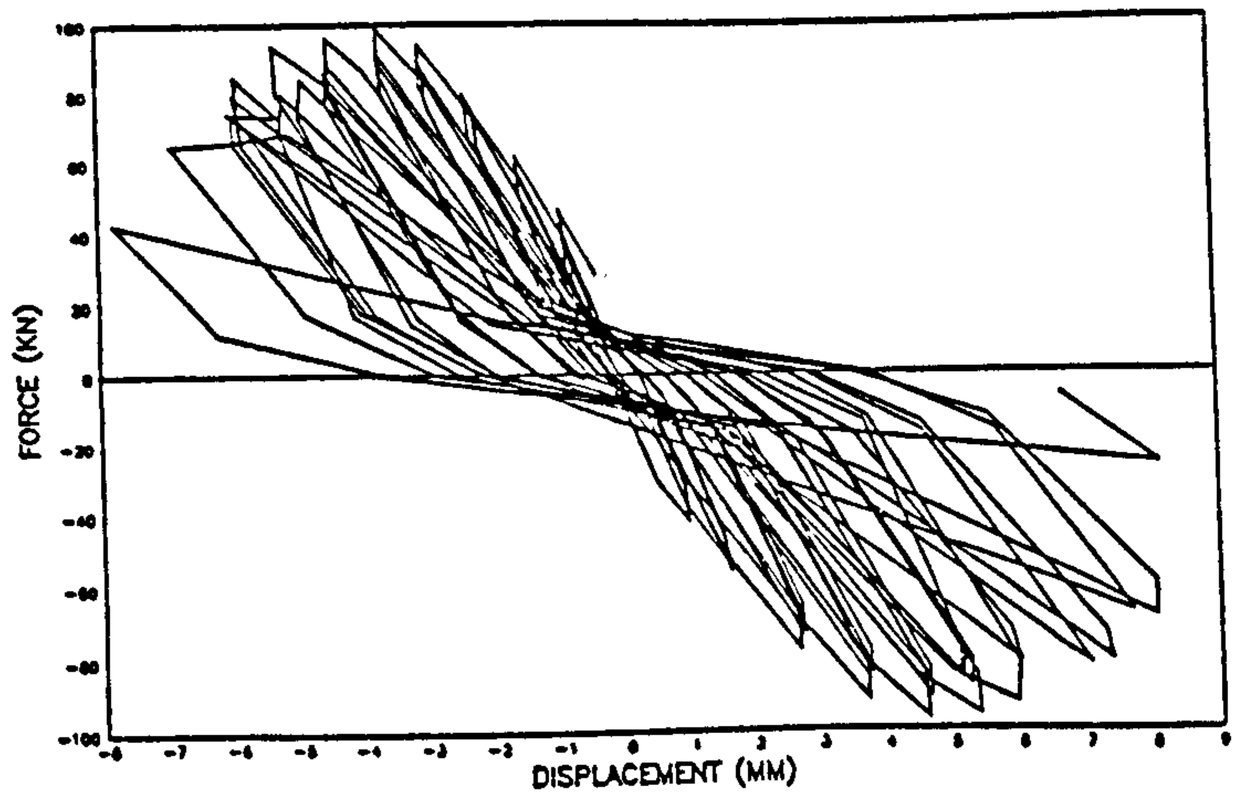


Figure B(14)2 Wall SW14 - force versus displacement 2 (horizontal, RHS, level 4)

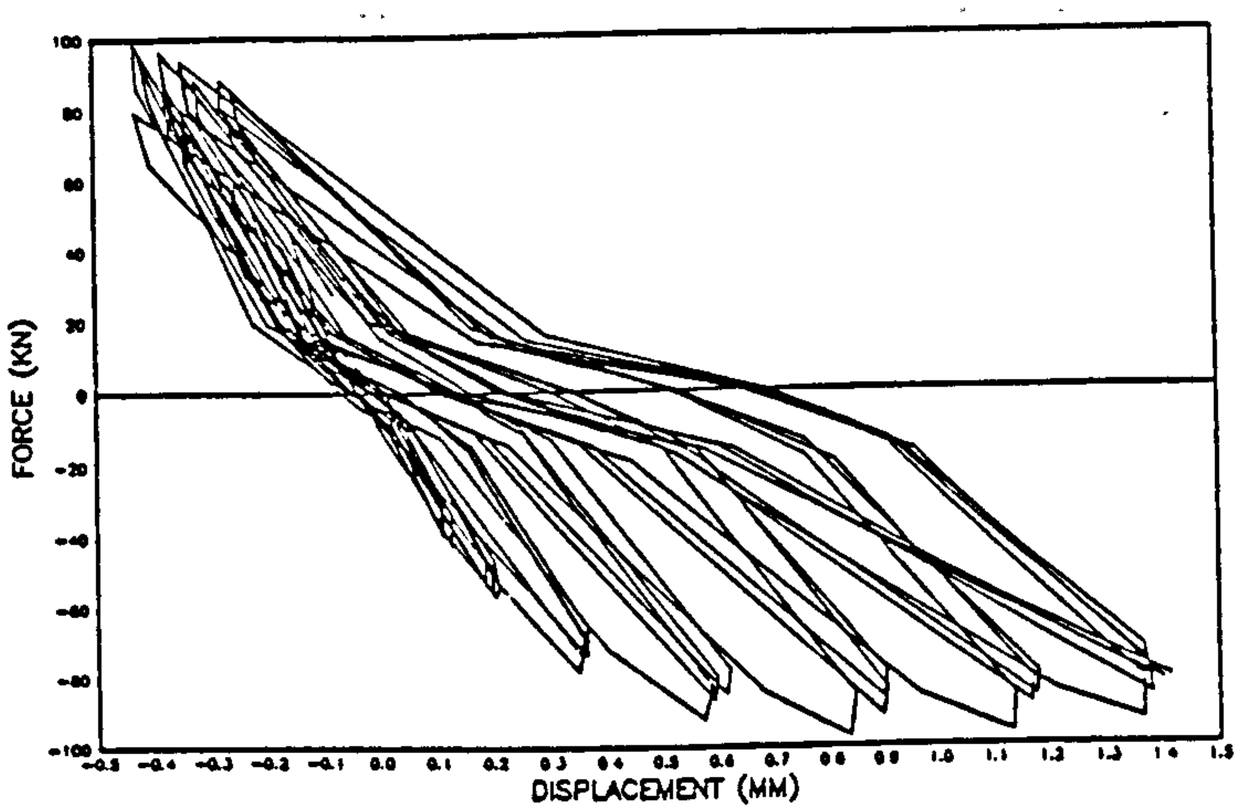


Figure B(14)3 Wall SW14 - force versus displacement 3
(vertical, LHS, level 1)

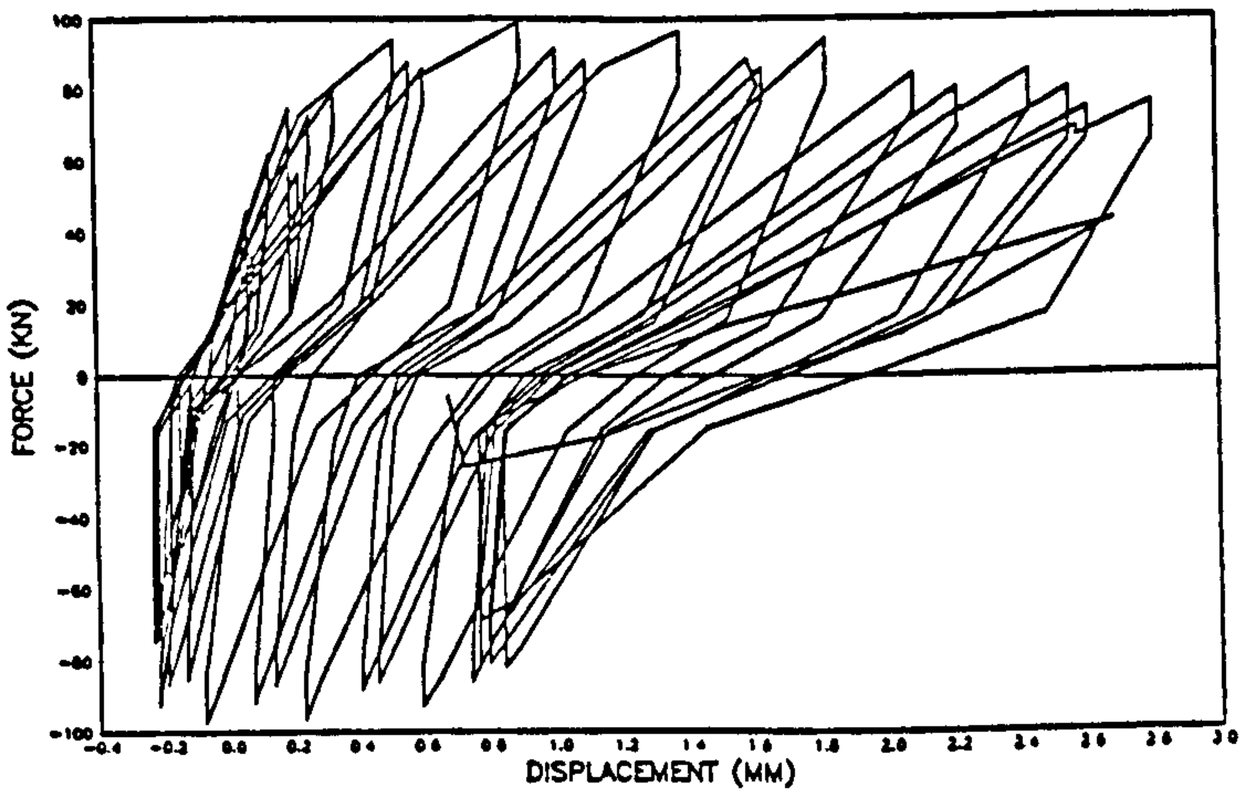


Figure B(14)4 Wall SW14 - force versus displacement 4
(vertical, RHS, level 1)

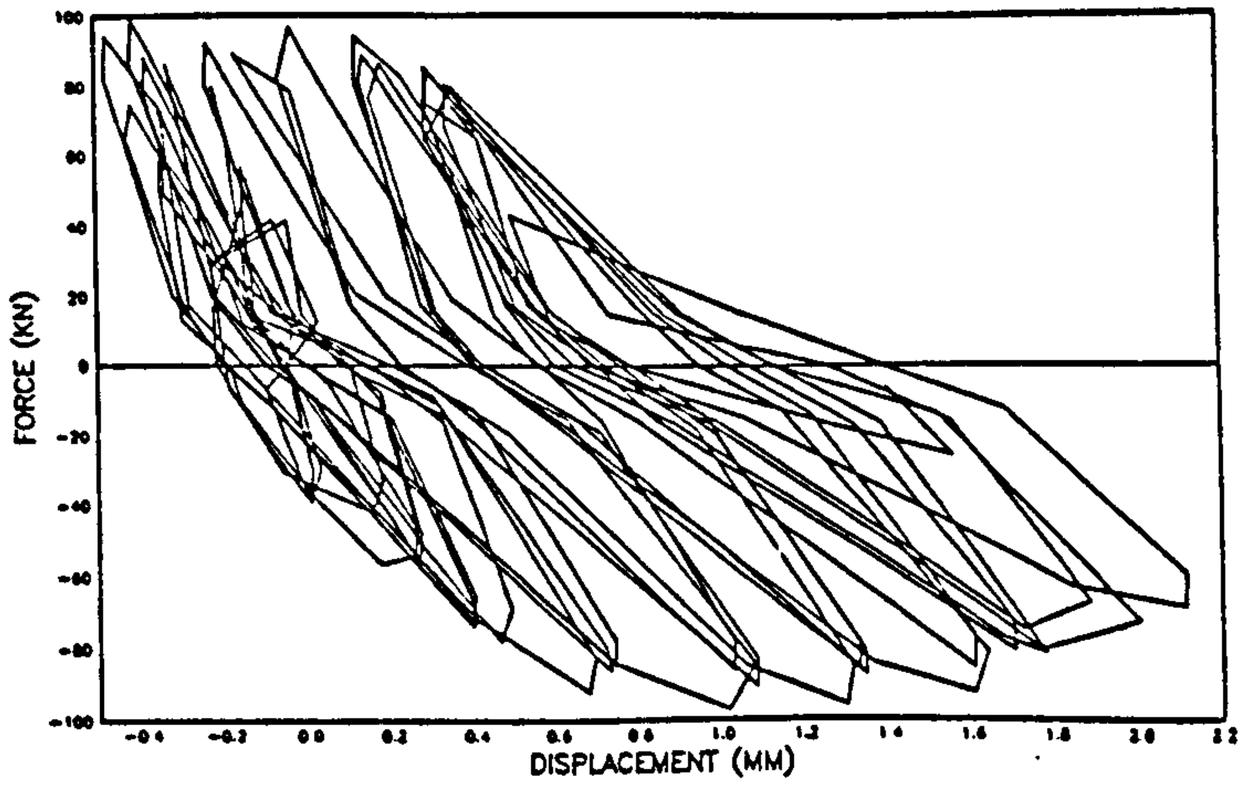


Figure B(14)5 Wall SW14 - force versus displacement 5
(vertical, LHS, level 2)

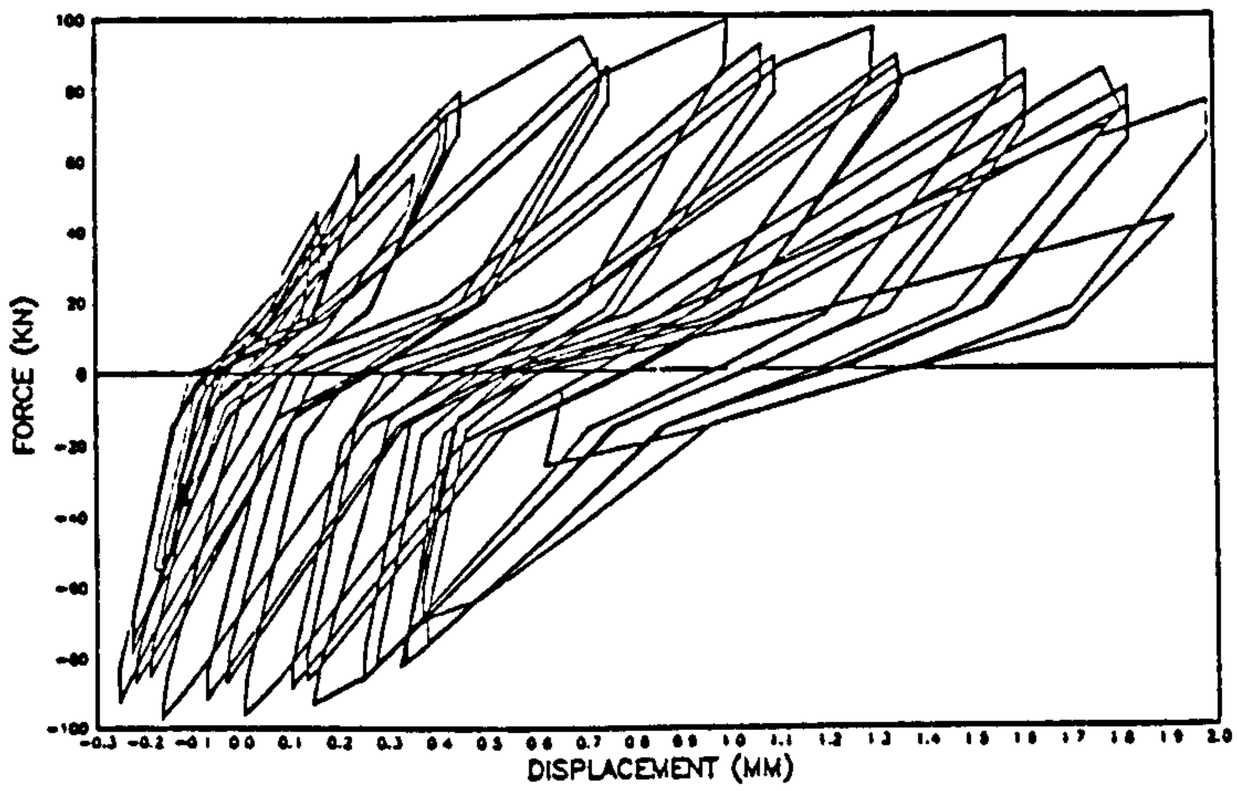


Figure B(14)6 Wall SW14 - force versus displacement 6 (vertical, RHS, level 2)

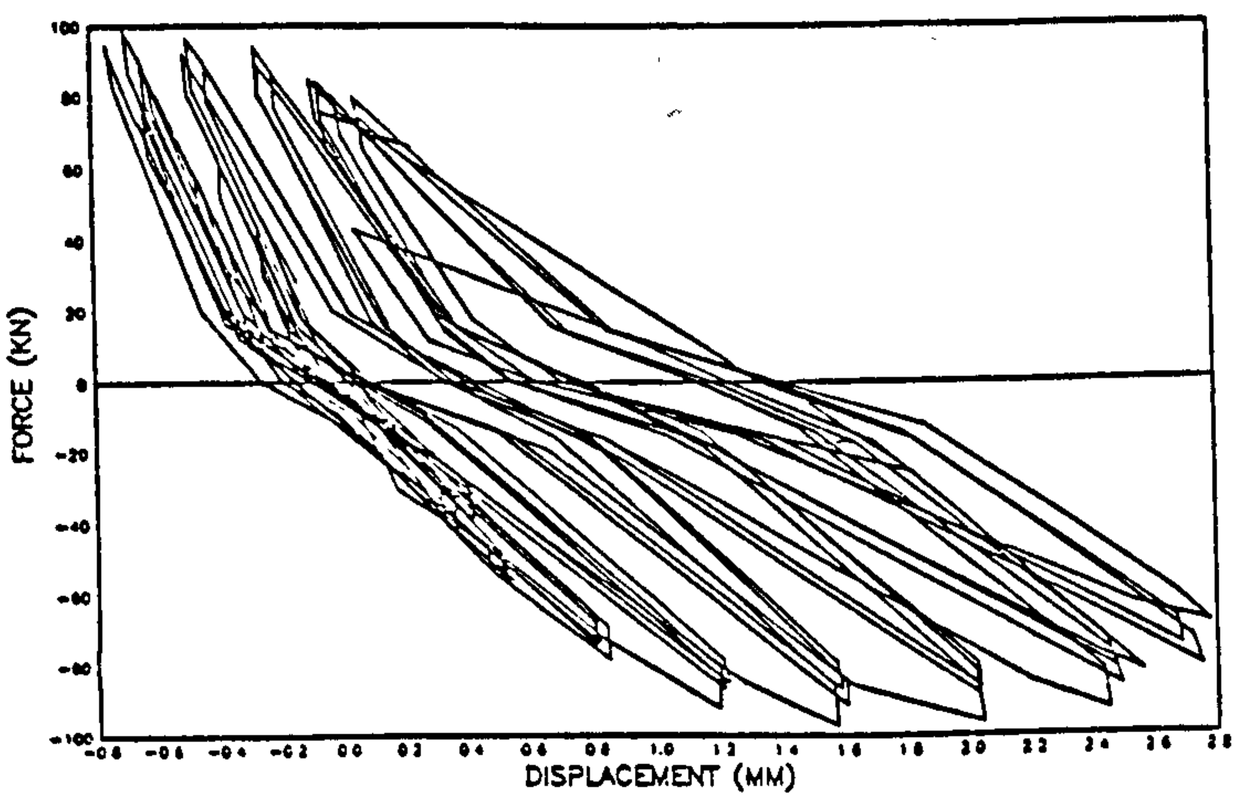


Figure B(14)7 Wall SW14 - force versus displacement 7 (vertical, LHS, level 3)

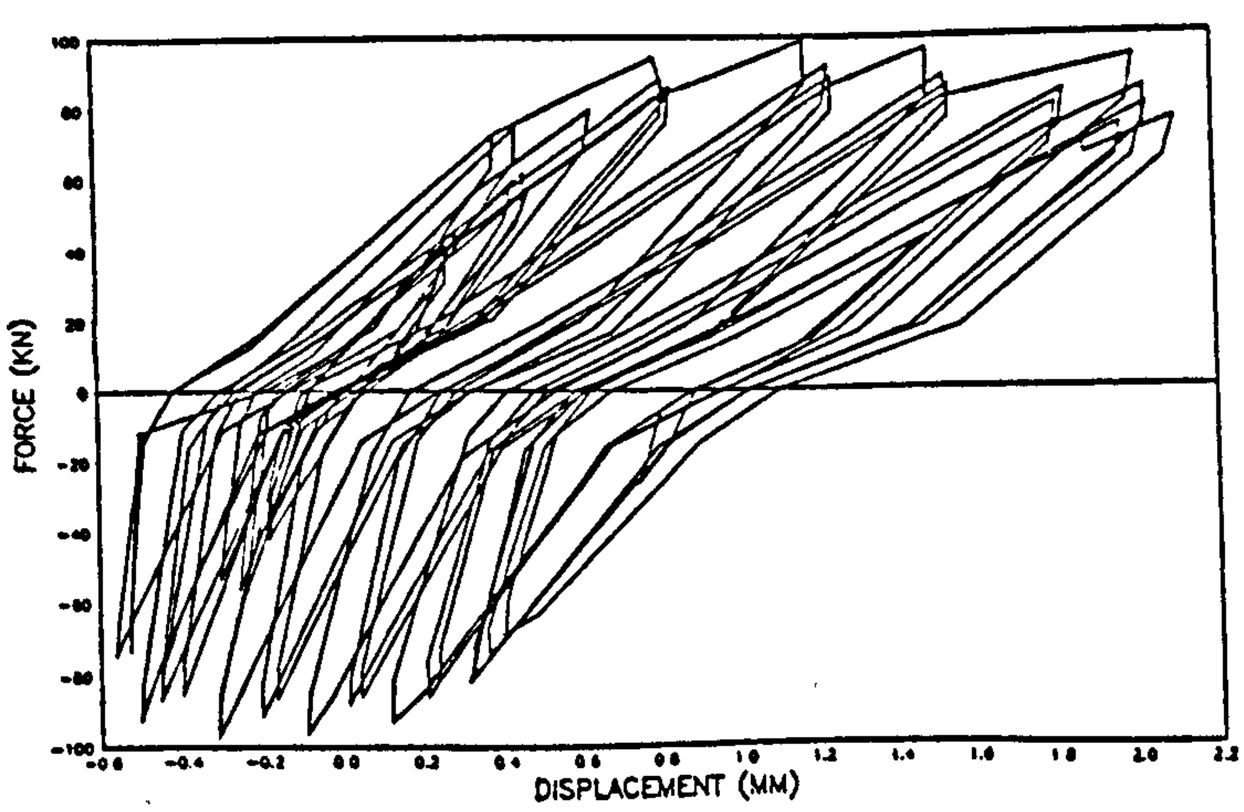


Figure B(14)8 Wall SW14 - force versus displacement 8 (vertical, RHS, level 3)

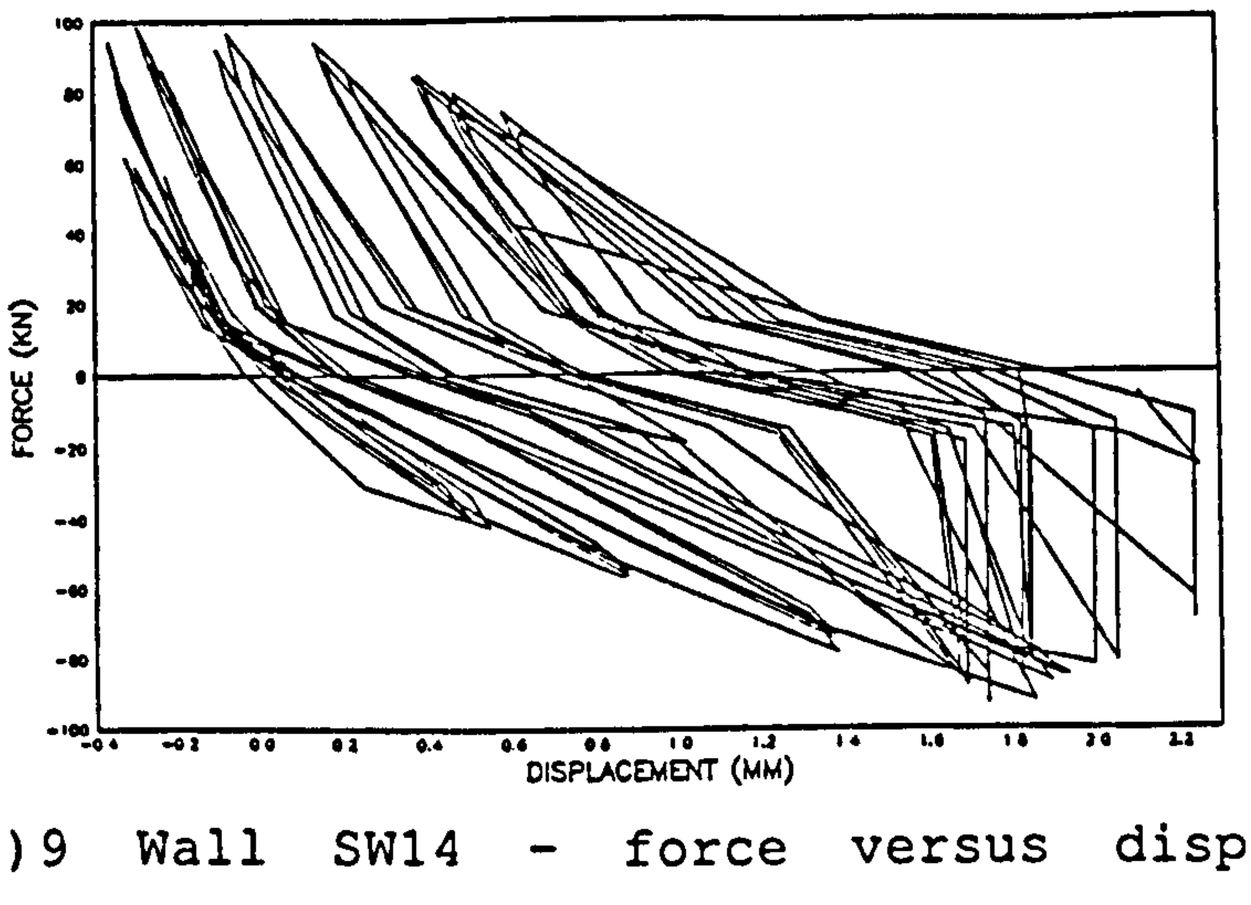


Figure B(14)9 Wall SW14 - force versus displacement 9 (vertical, LHS, level 4)

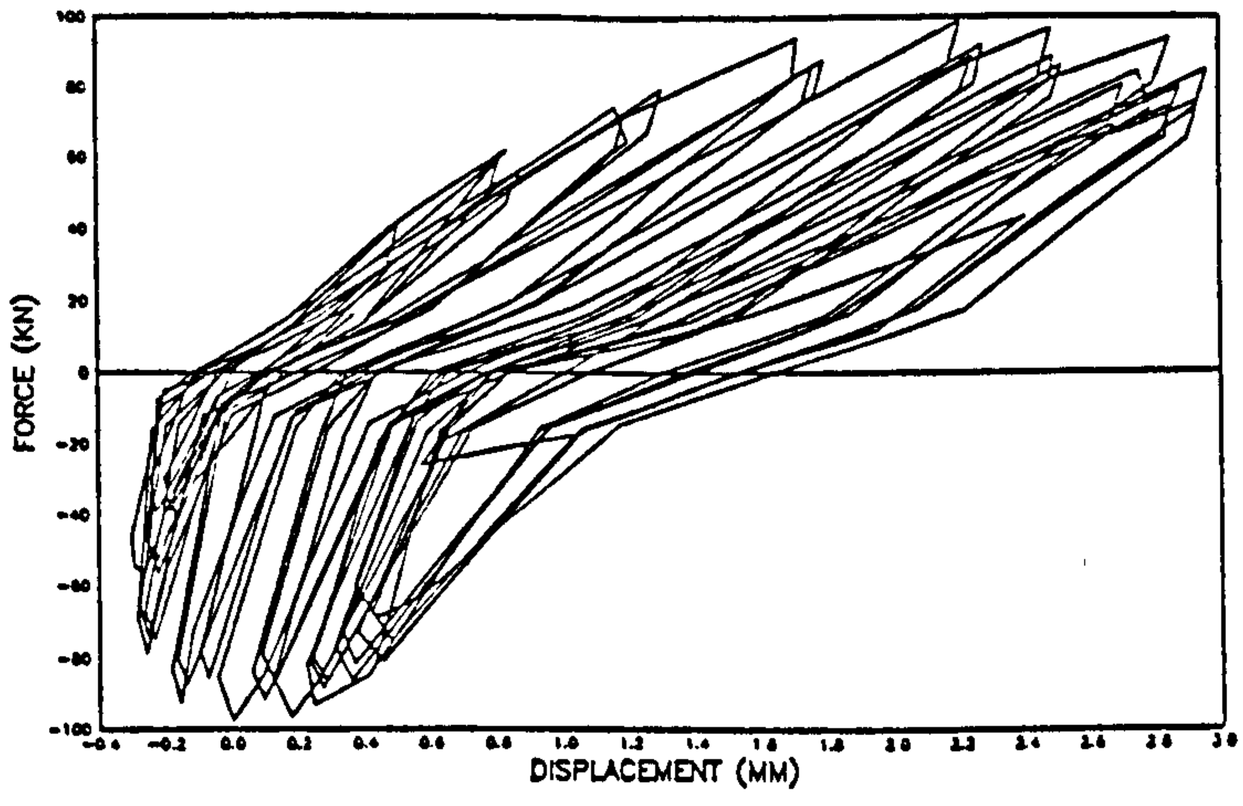


Figure B(14)10 Wall SW14 - force versus displacement 10 (vertical, RHS, level 4)

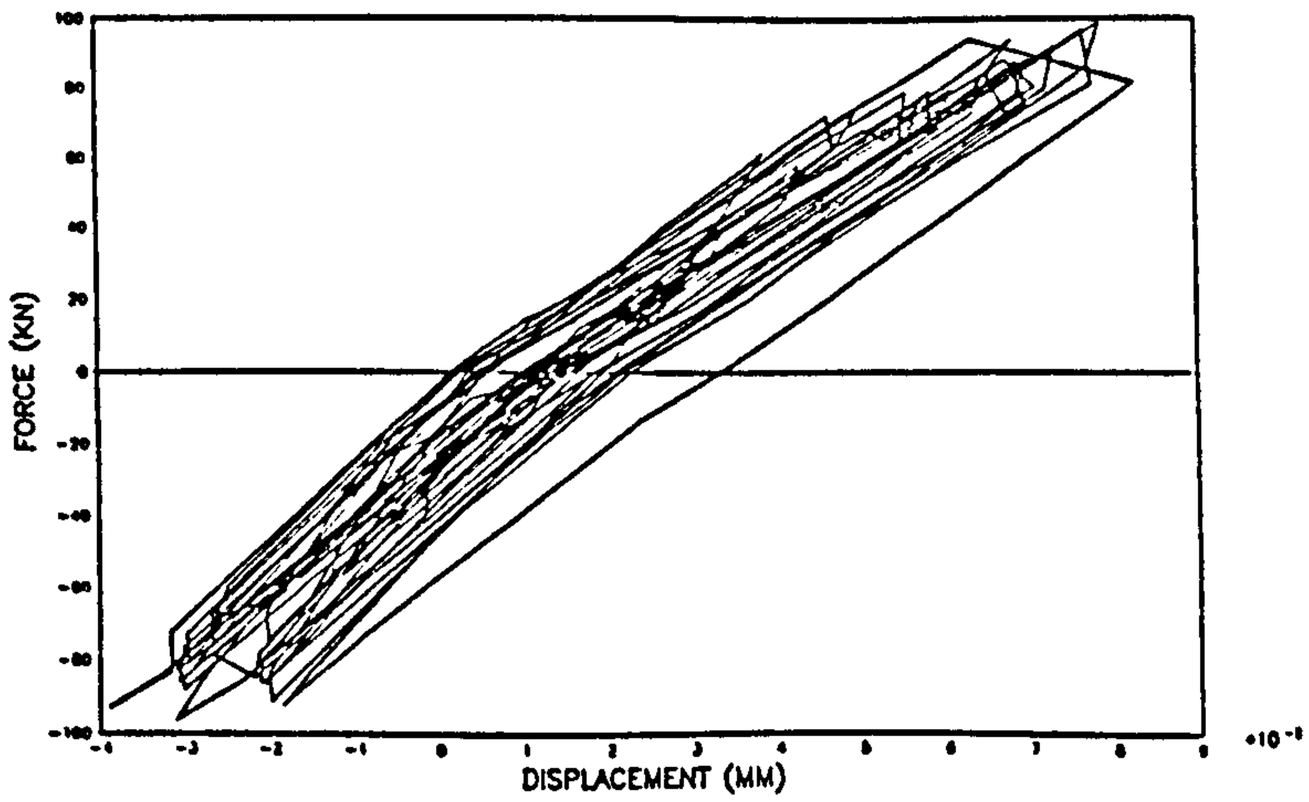


Figure B(14)11 Wall SW14 - force versus displacement 11 (foundation, RHS)

Figure B(14)12 Wall SW14 - force versus displacement 12 (out-of-plane)

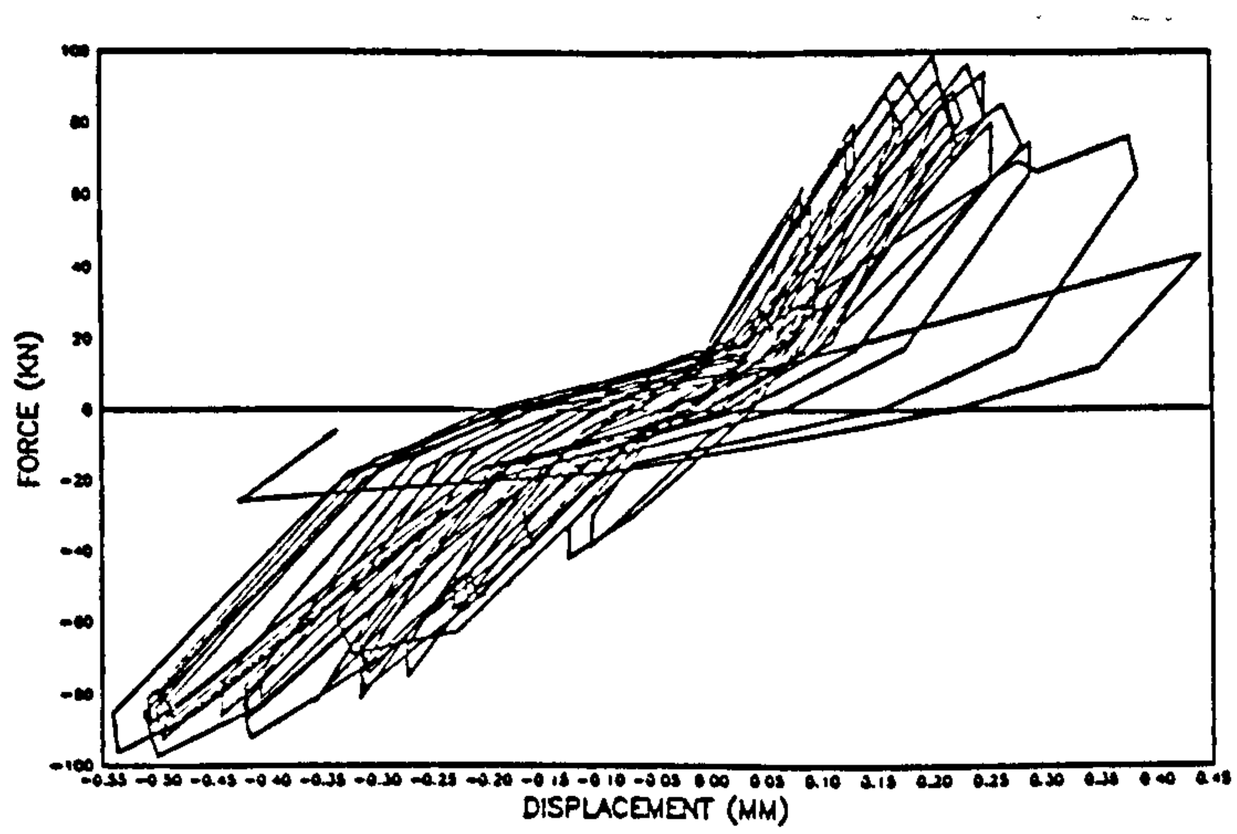


Figure B(14)13 Wall SW14 - force versus displacement 13 (horizontal, centre, level 1)

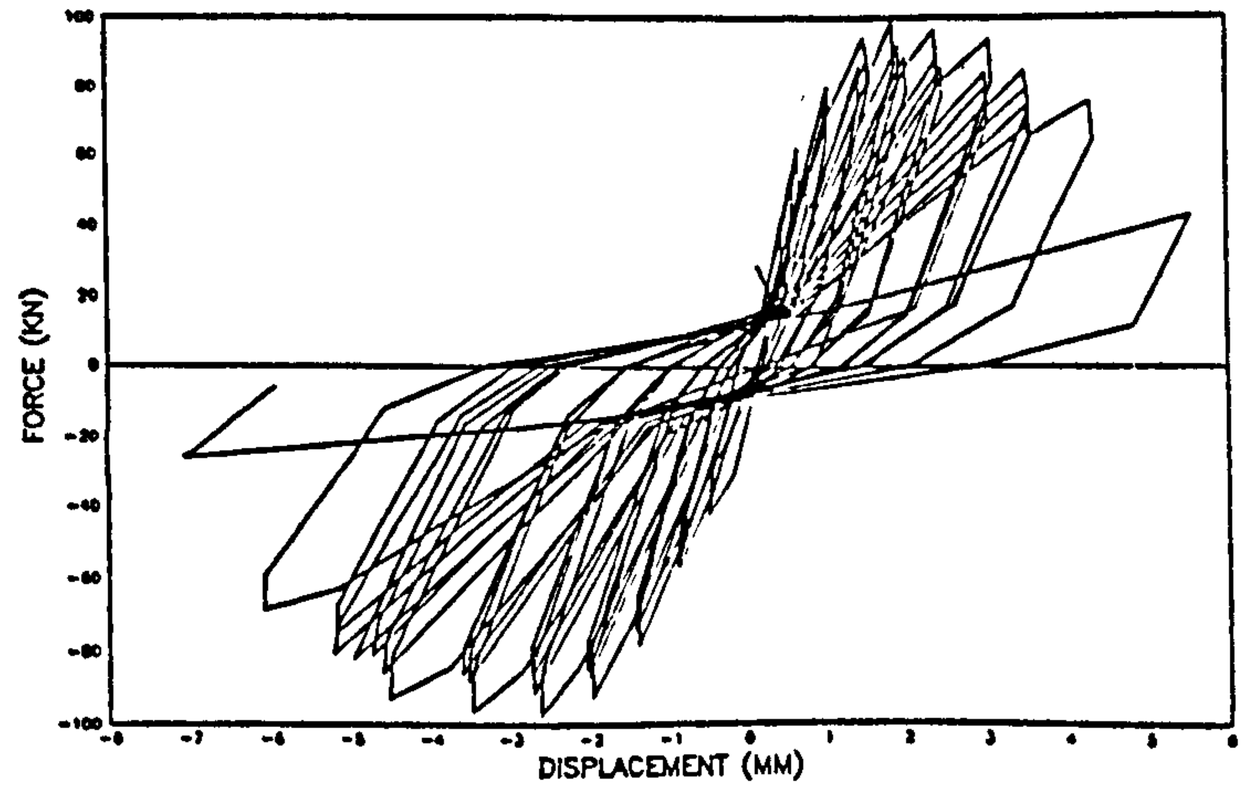


Figure B(14)14 Wall SW14 - force versus displacement 15 (horizontal, centre, level 3)

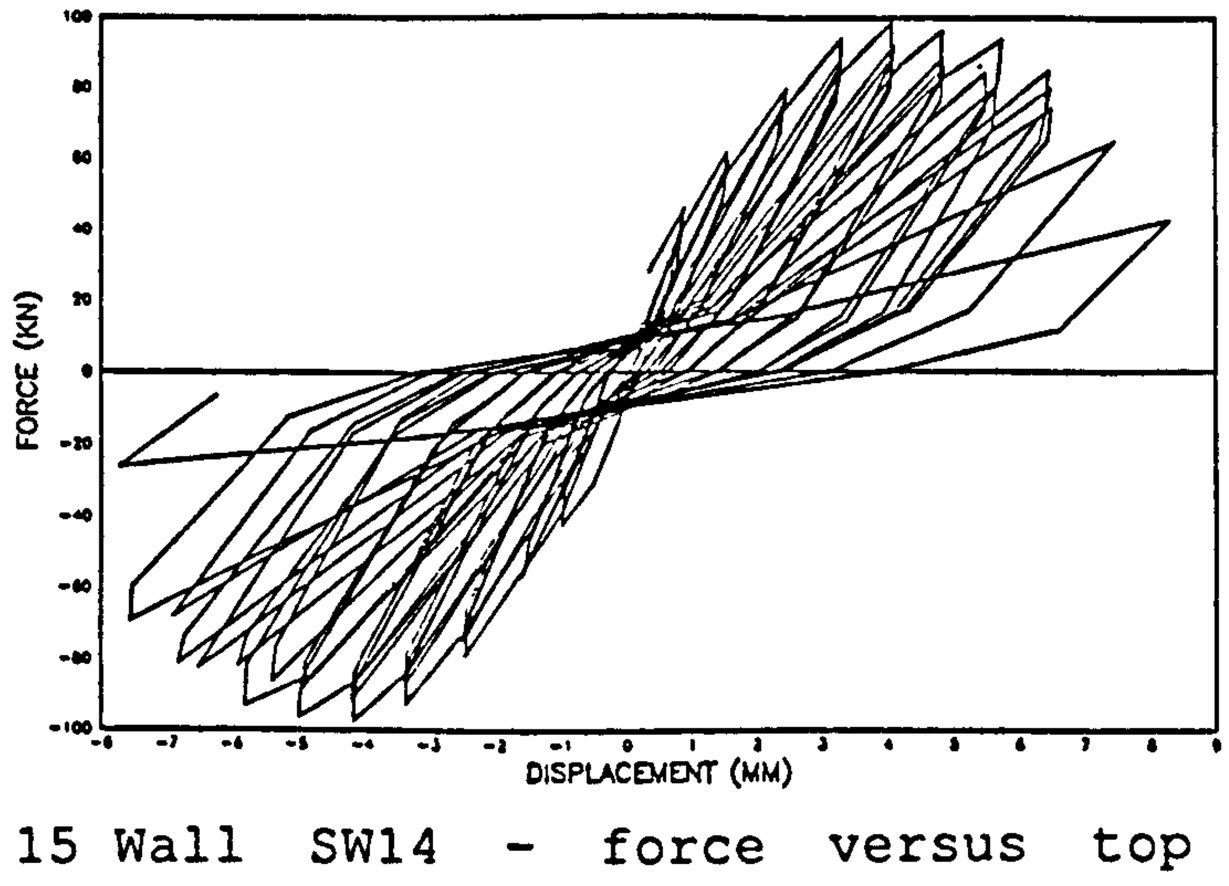


Figure B(14)15 Wall SW14 - force versus top horizontal displacement

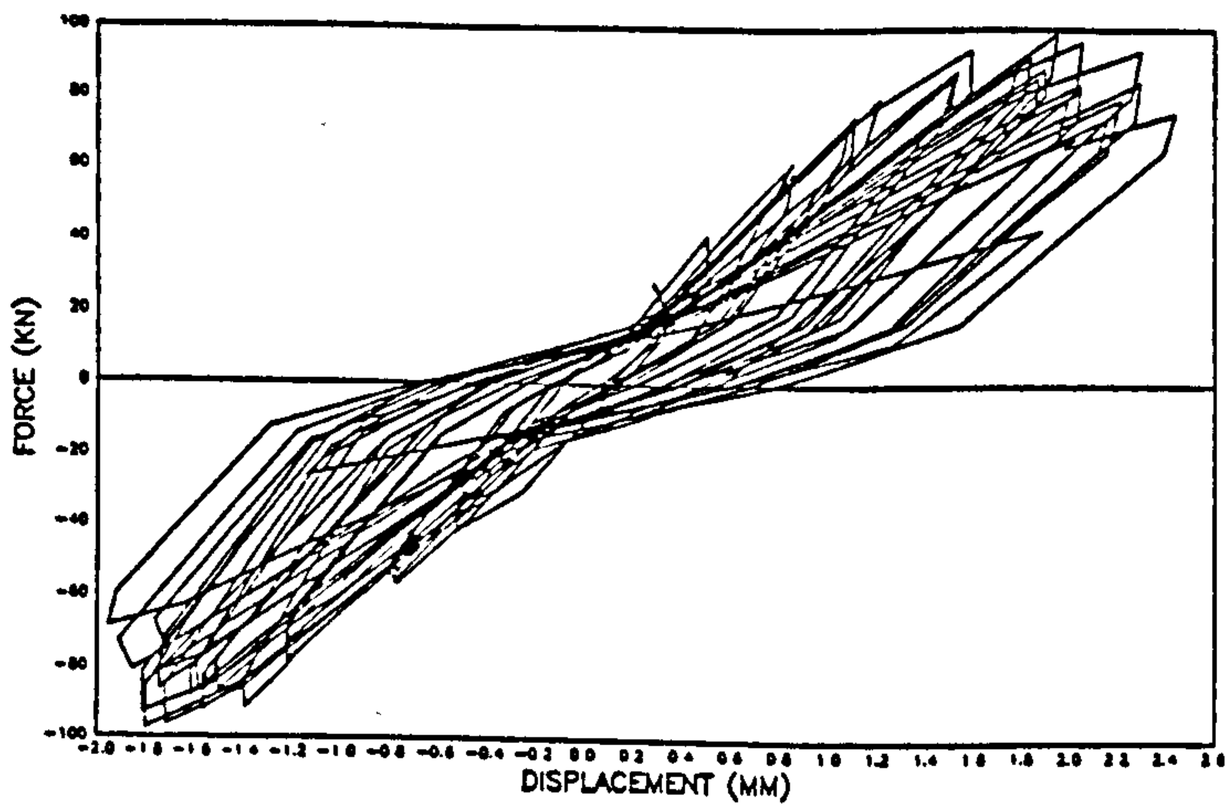


Figure B(14)16 Wall SW14 - force versus flexural component of top horizontal displacement

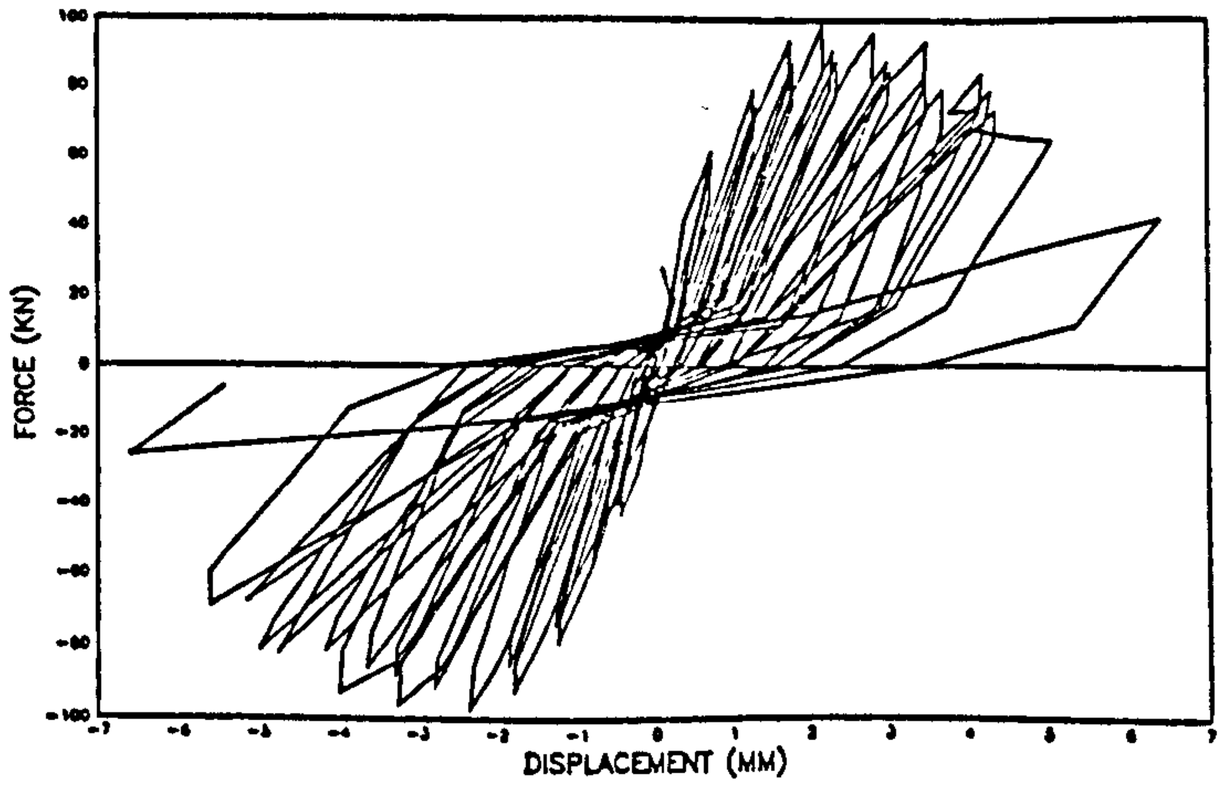


Figure B(14)17 Wall SW14 - force versus shear component of top horizontal displacement

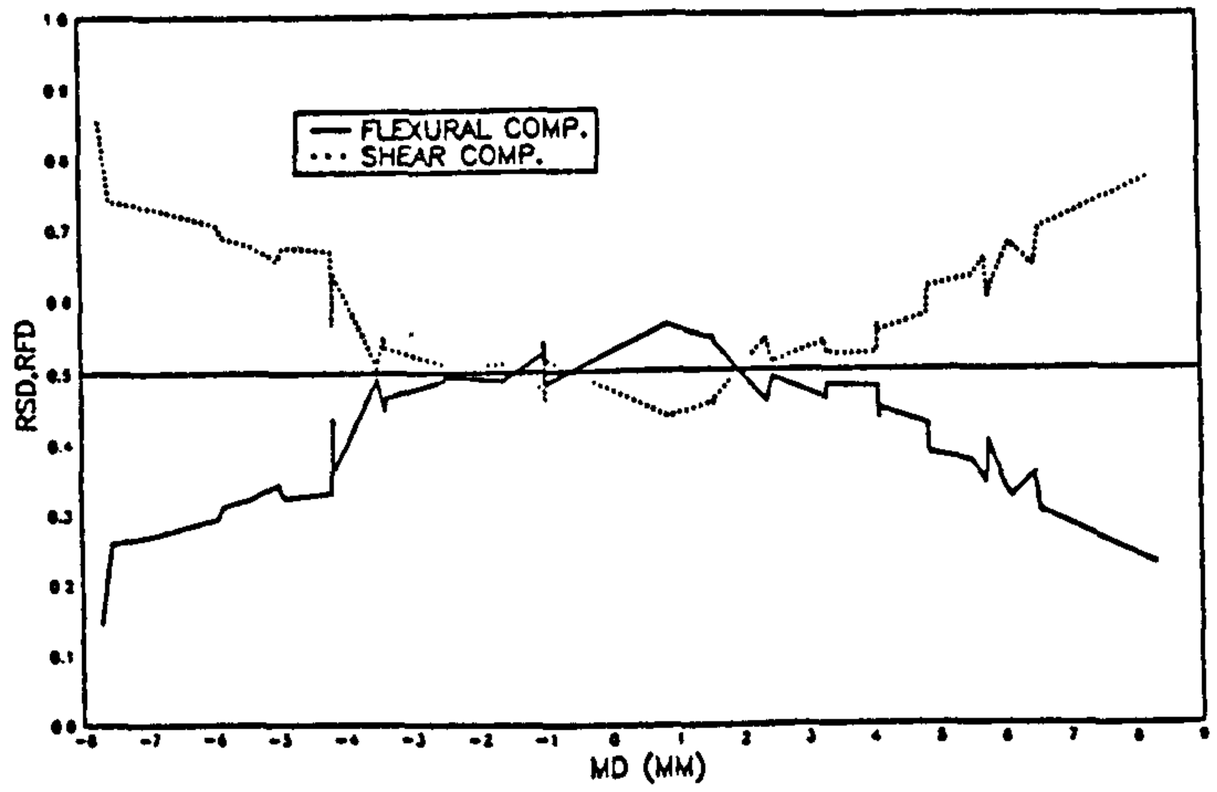


Figure B(14)18 Wall SW14 - RSD,RFD versus MD

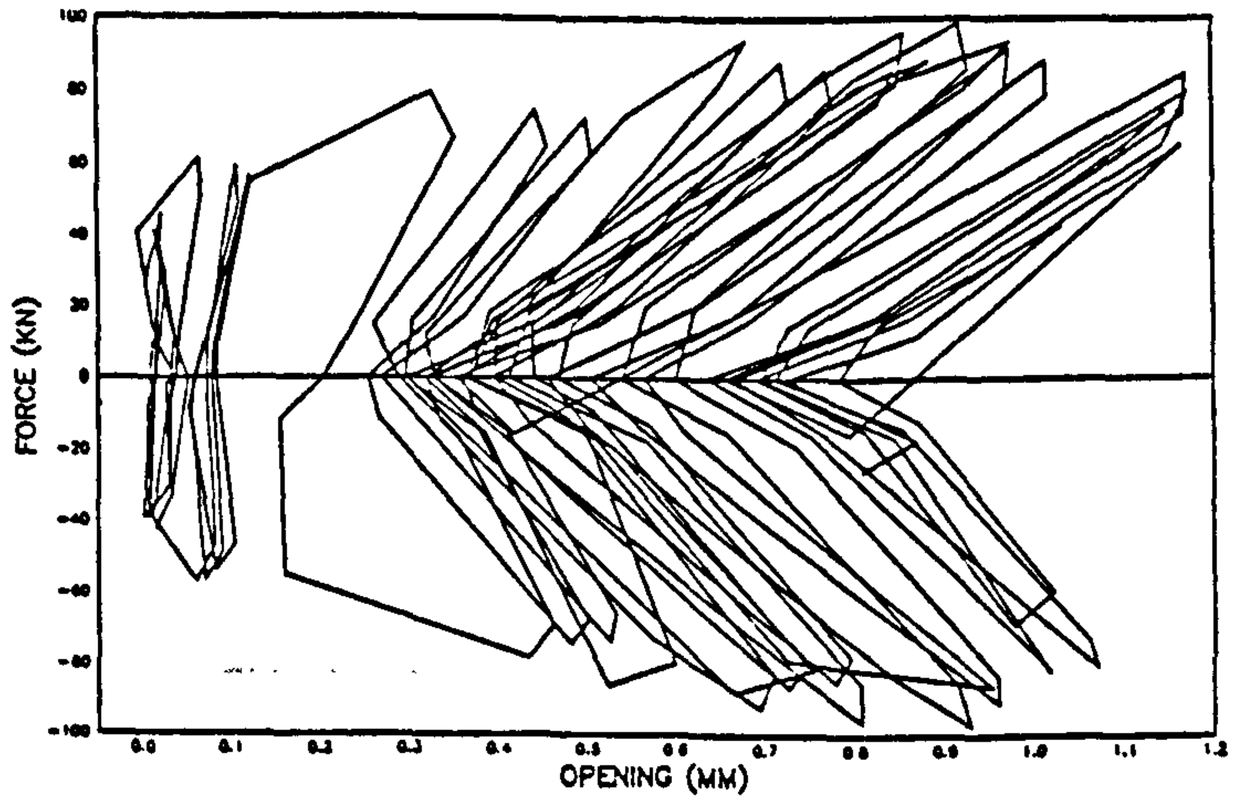


Figure B(14)19 Wall SW14 - force versus opening on top

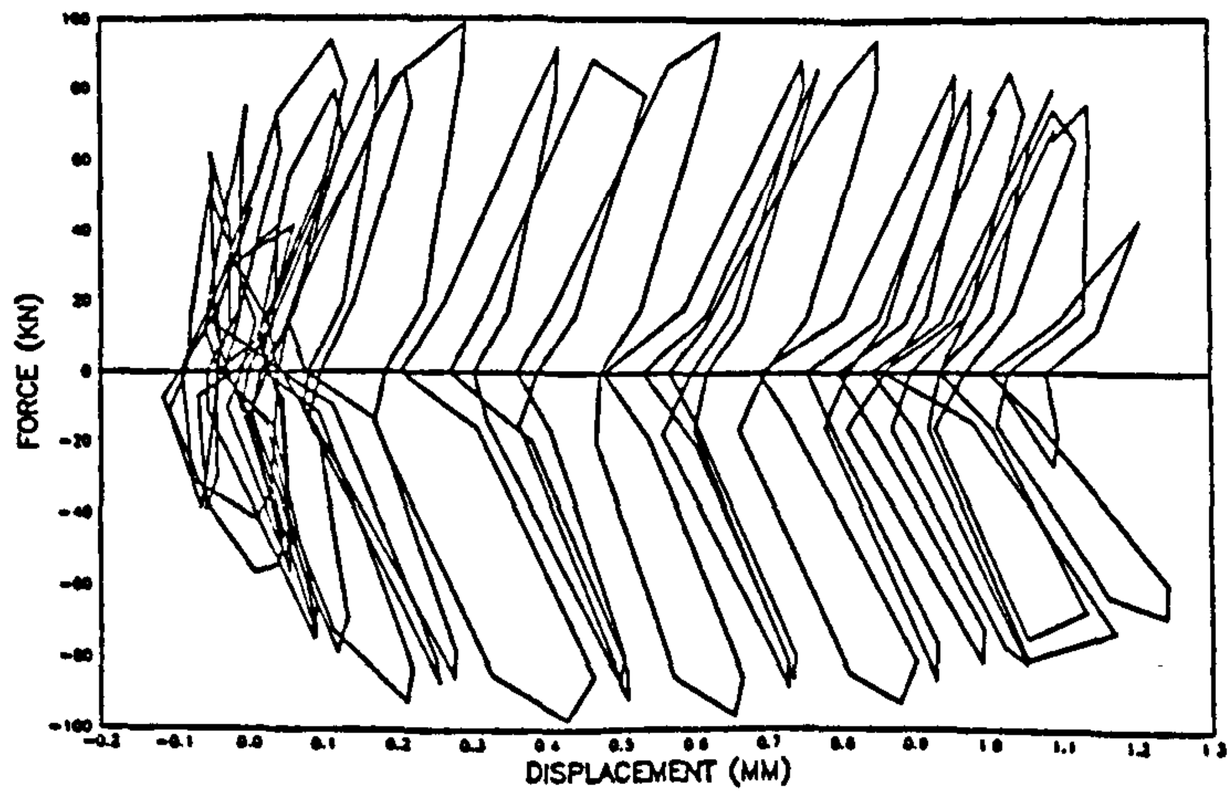


Figure B(14)20 Wall SW14 - force versus extension at a quarter height

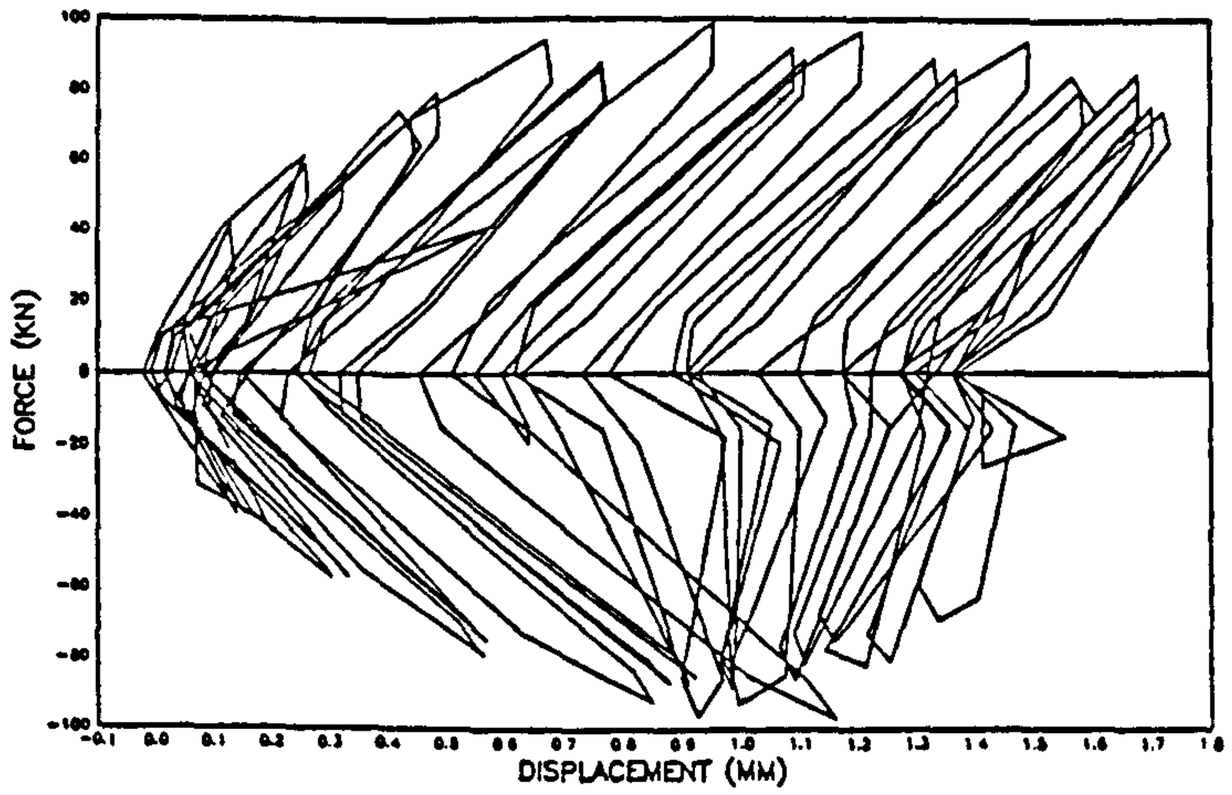


Figure B(14)21 Wall SW14 - force versus extension on top

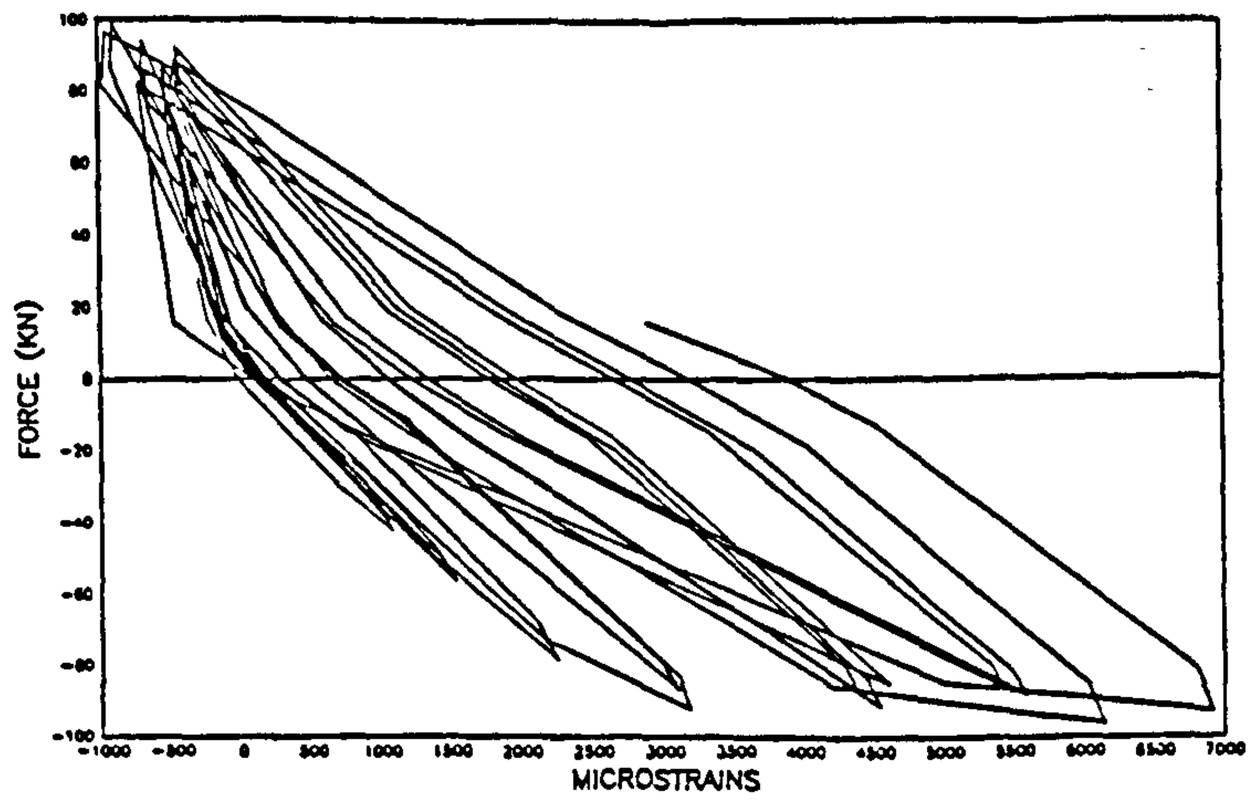


Figure B(14)22 Wall SW14 - force versus strain 3 (bottom, ϕ6mm, LHS)

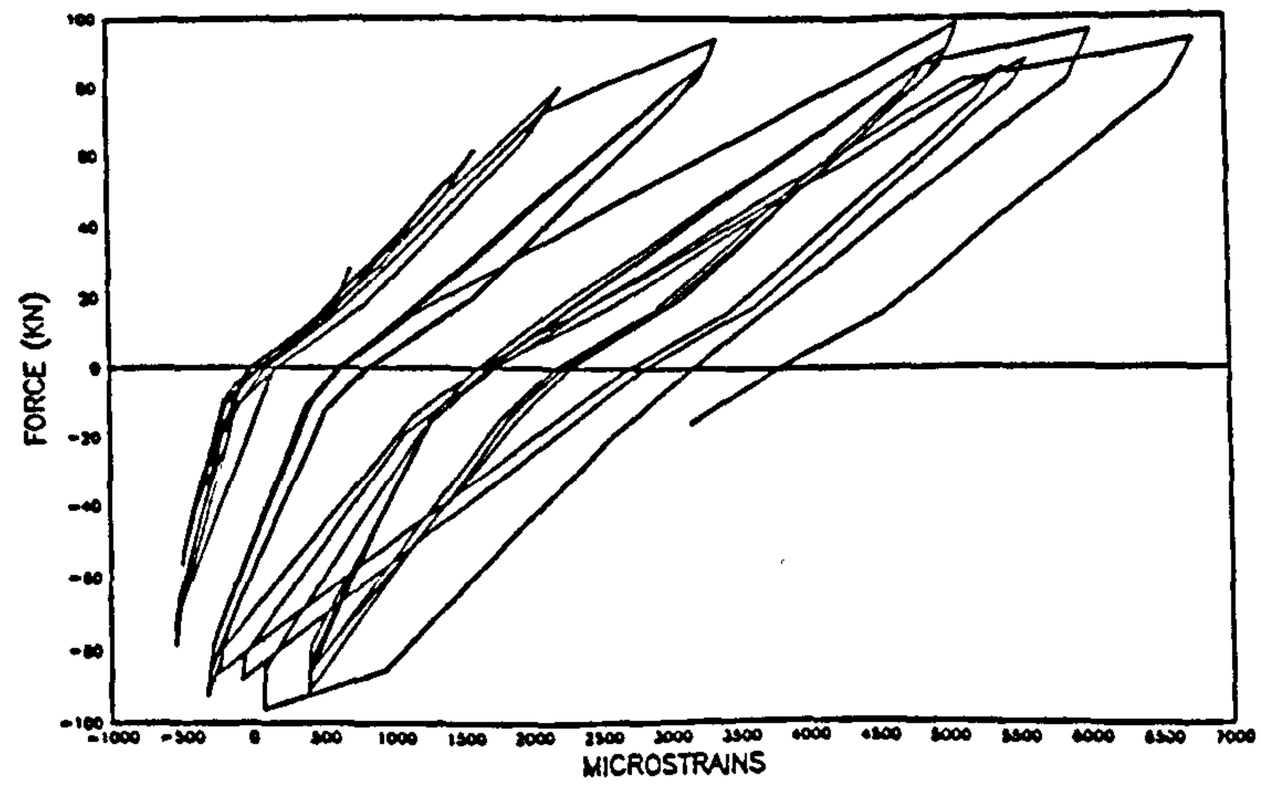


Figure B(14)23 Wall SW14 - force versus strain 4 (bottom, ϕ6mm, RHS)

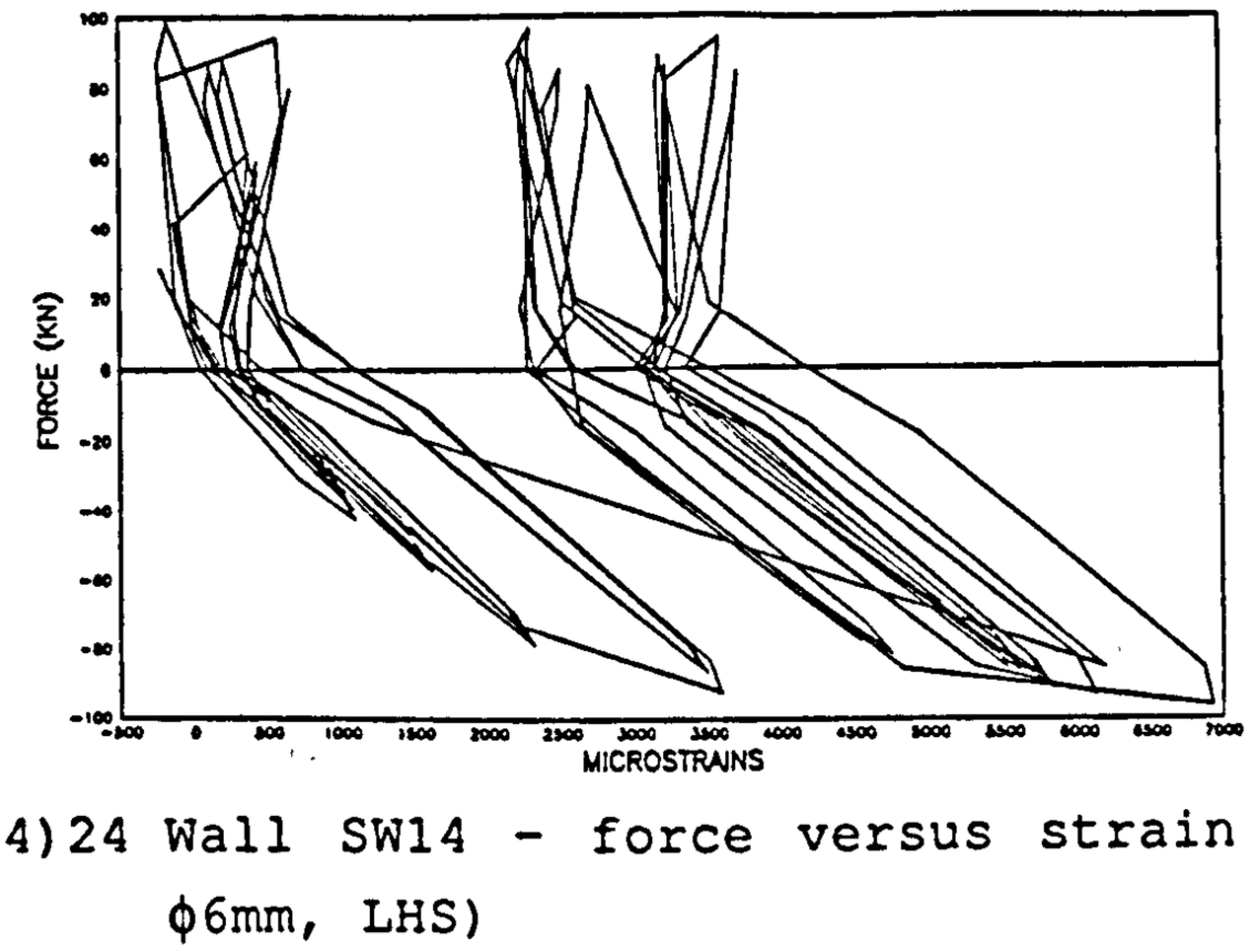


Figure B(14)24 Wall SW14 - force versus strain 5 (bottom, ϕ6mm, LHS)

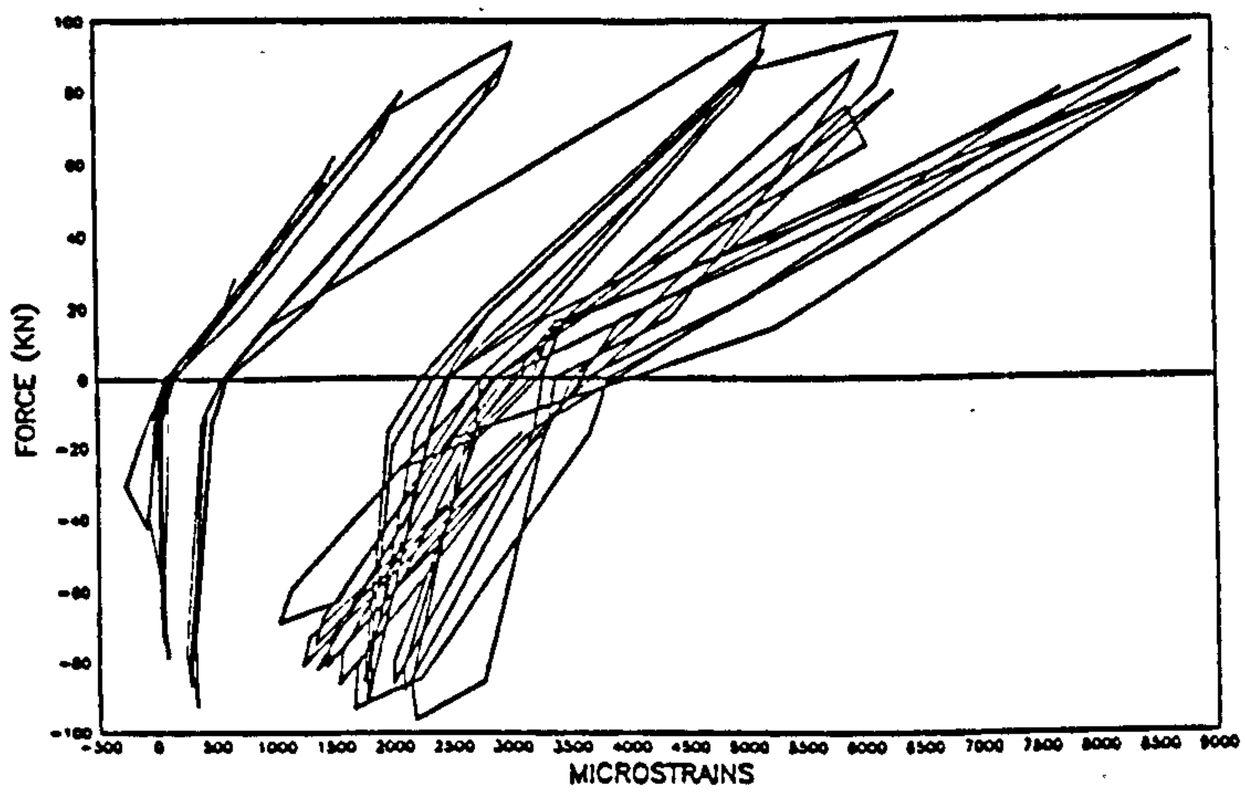


Figure B(14)25 Wall SW14 - force versus strain 6 (bottom, ϕ6mm, RHS)

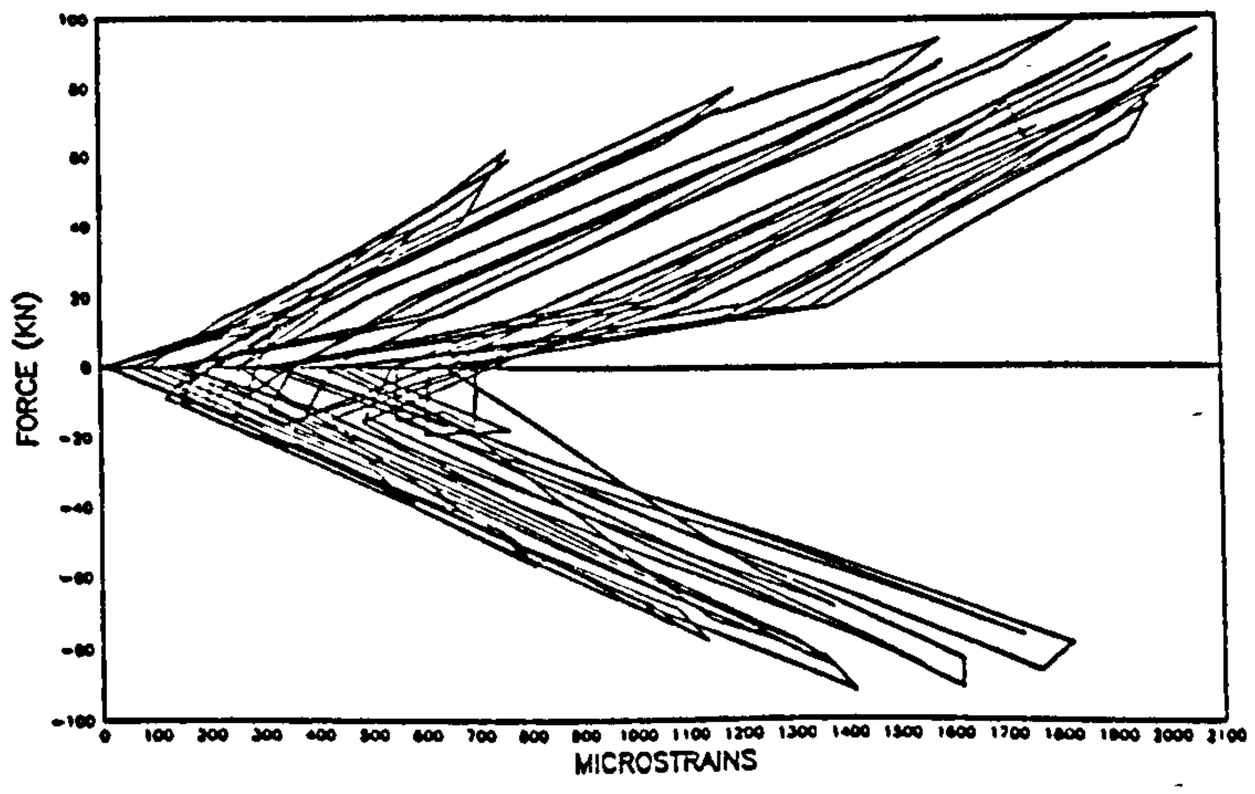


Figure B(14)26 Wall SW14 - force versus strain 7 (bottom, ϕ4mm, LHS)

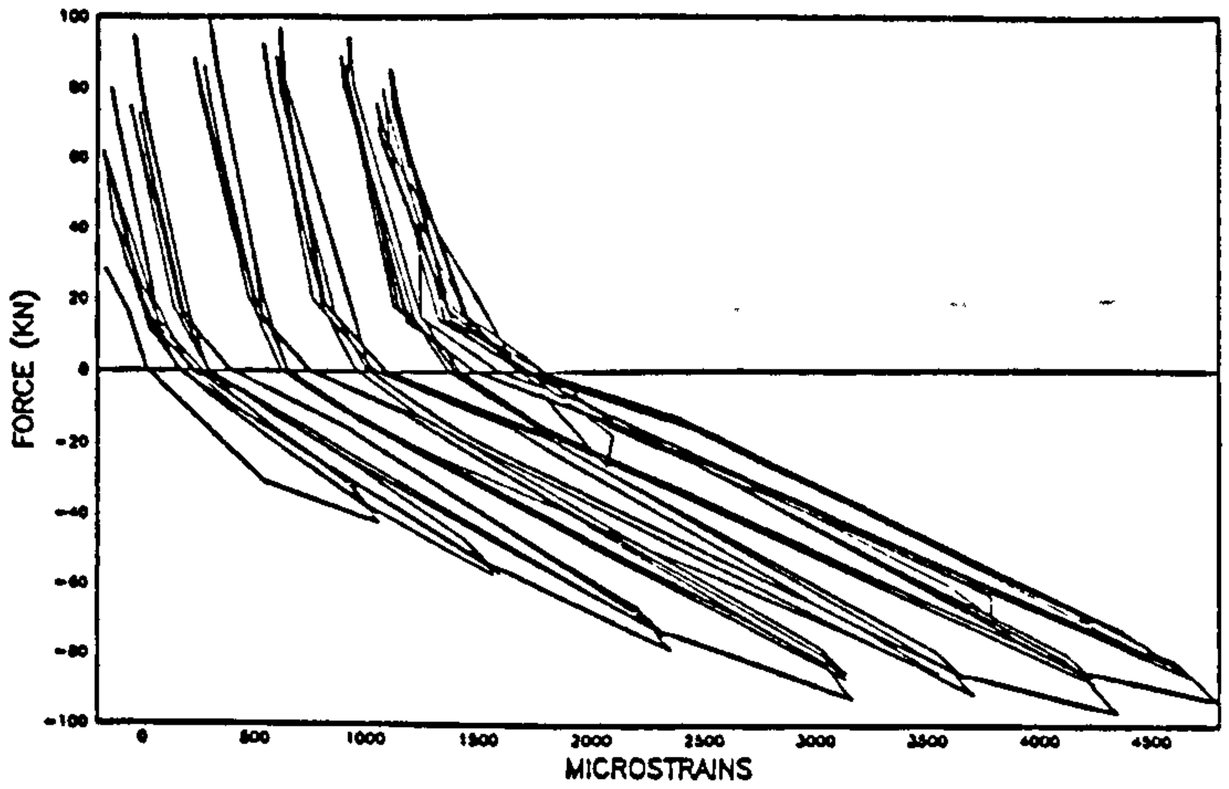


Figure B(14)27 Wall SW14 - force versus strain 9 (second level, ϕ8mm, LHS)

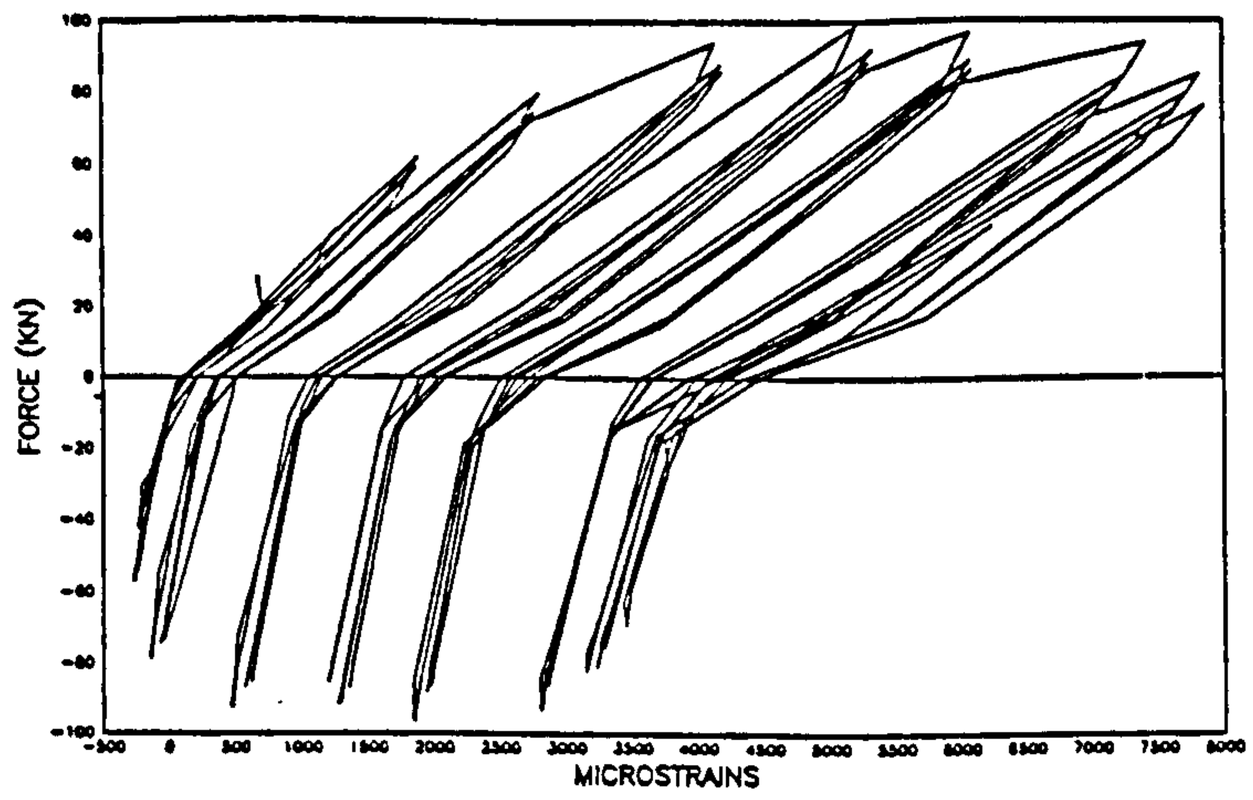


Figure B(14)28 Wall SW14 - force versus strain 10 (second level, ϕ8mm, RHS)

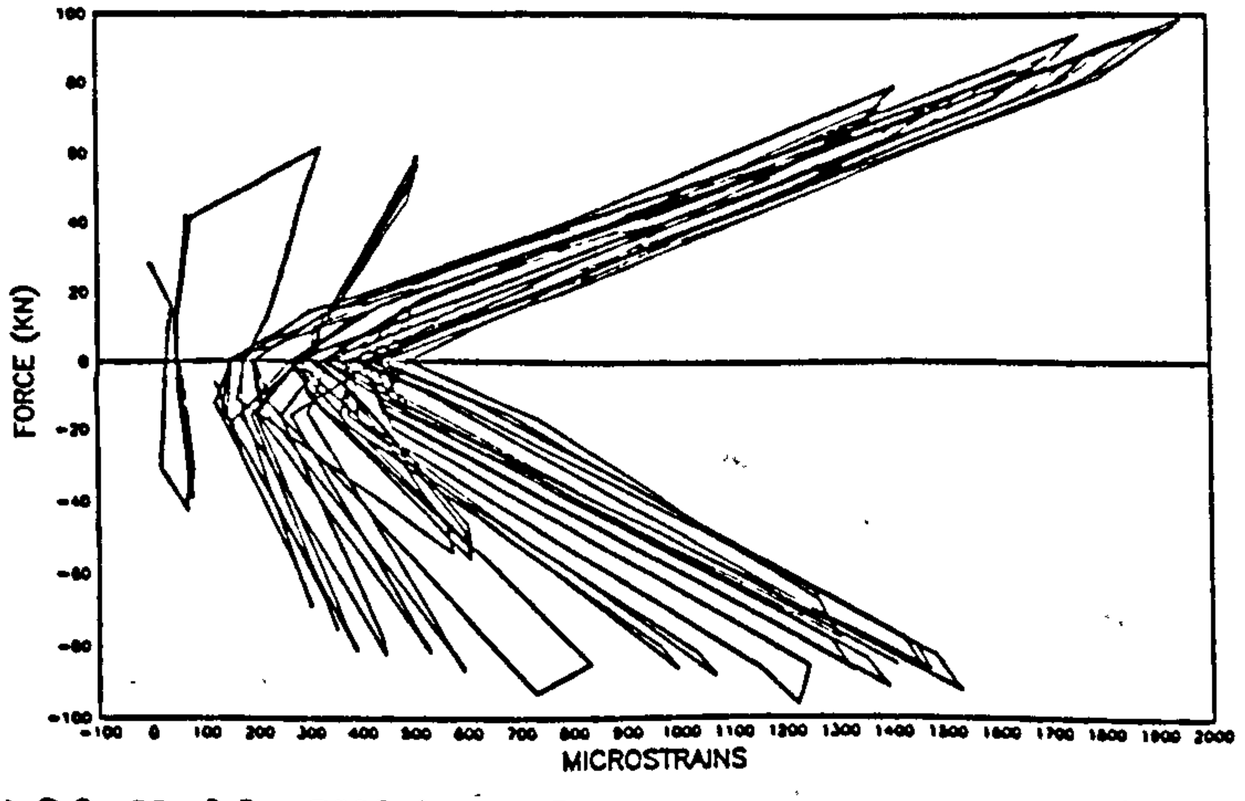


Figure B(14)29 Wall SW14 - force versus strain 11 (level of zero moment, ϕ8mm, LHS)

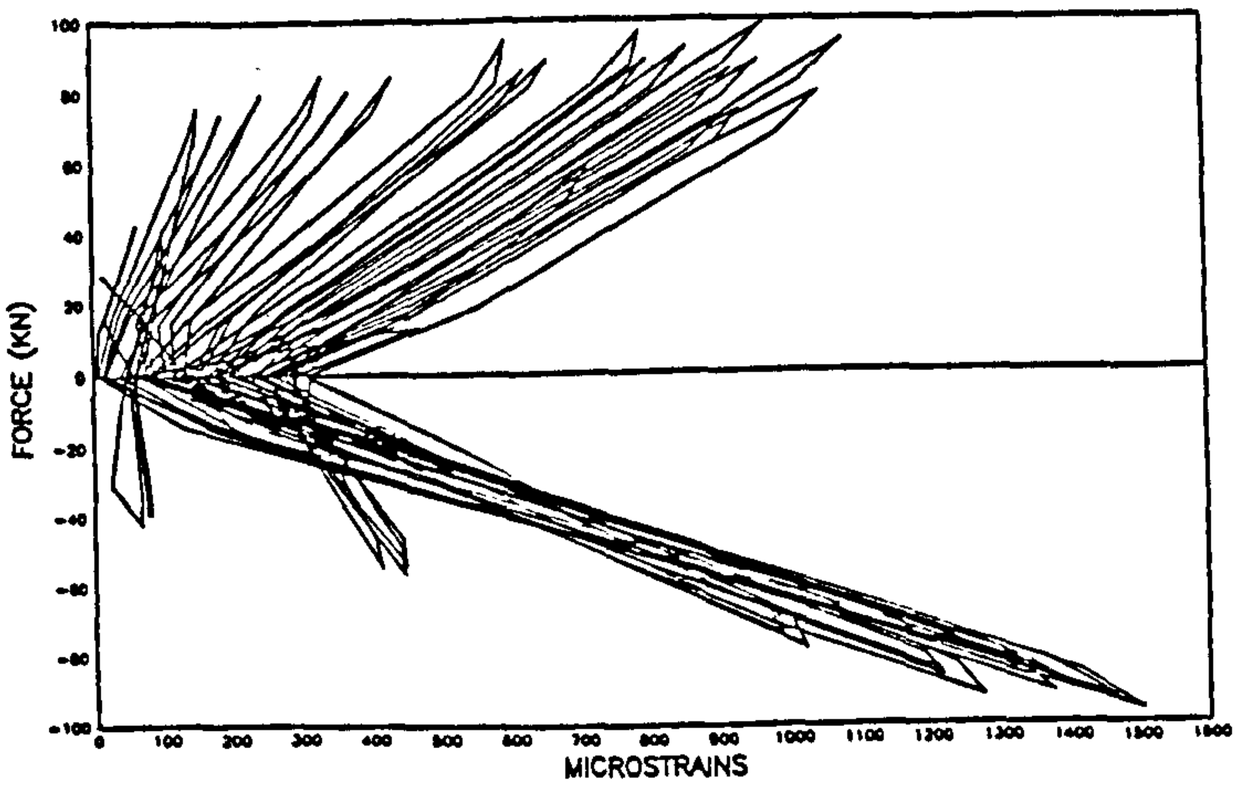


Figure B(14)30 Wall SW14 - force versus strain 12 (level of zero moment, ϕ8mm, RHS)

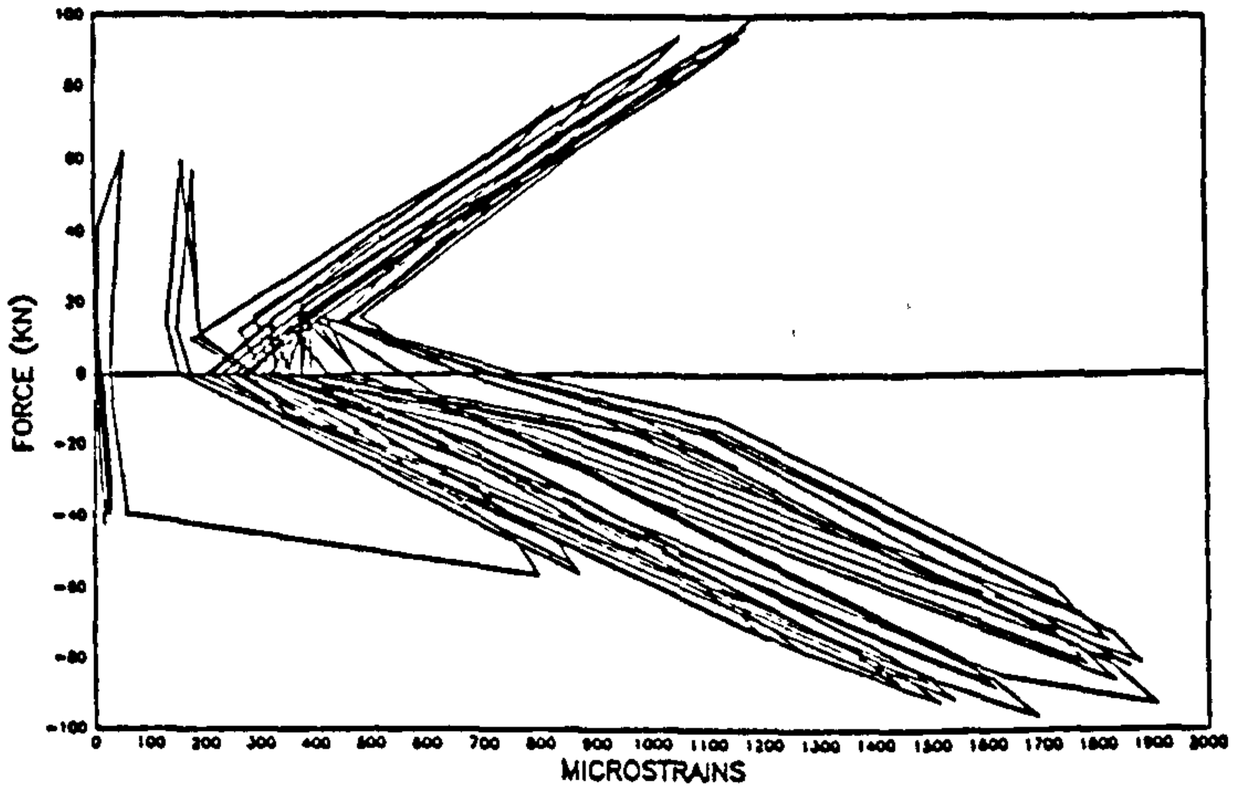


Figure B(14)31 Wall SW14 - force versus strain 13 (level of zero moment, ϕ6mm, LHS)

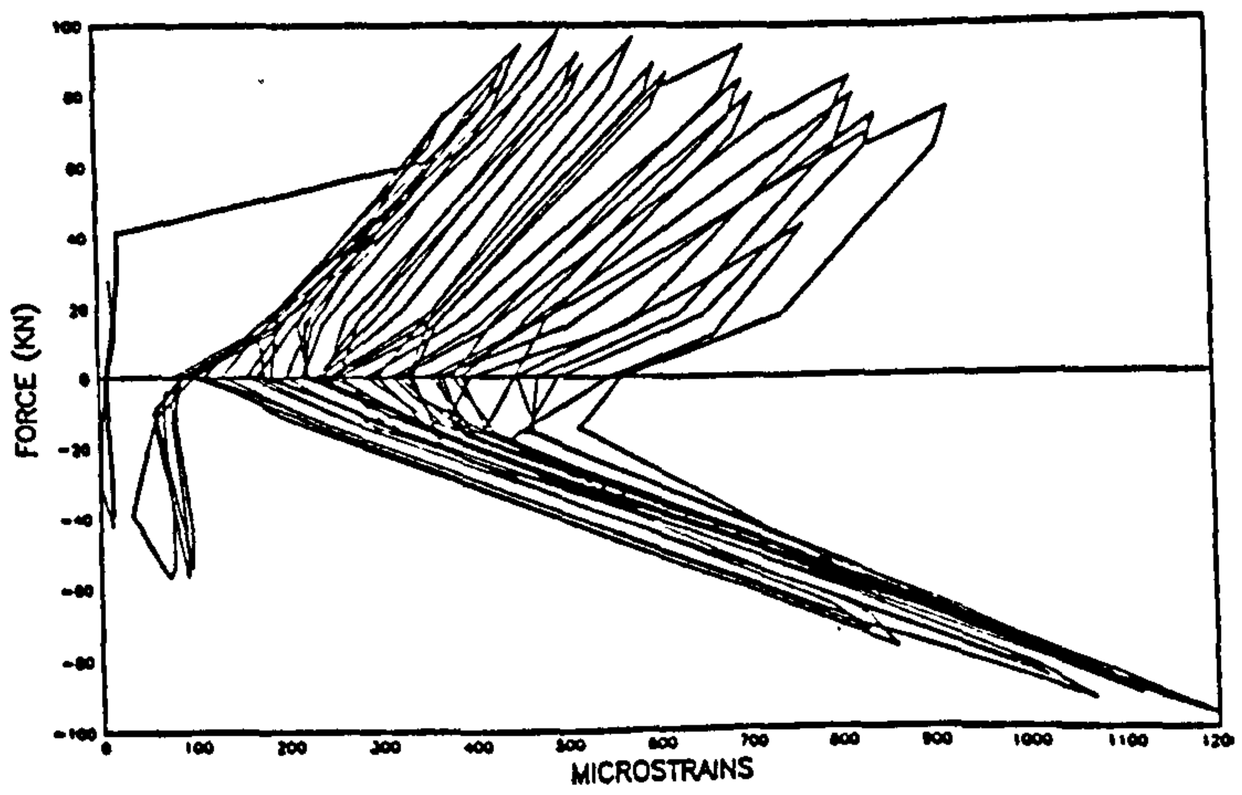


Figure B(14)32 Wall SW14 - force versus strain 14 (level of zero moment, ϕ6mm, RHS)

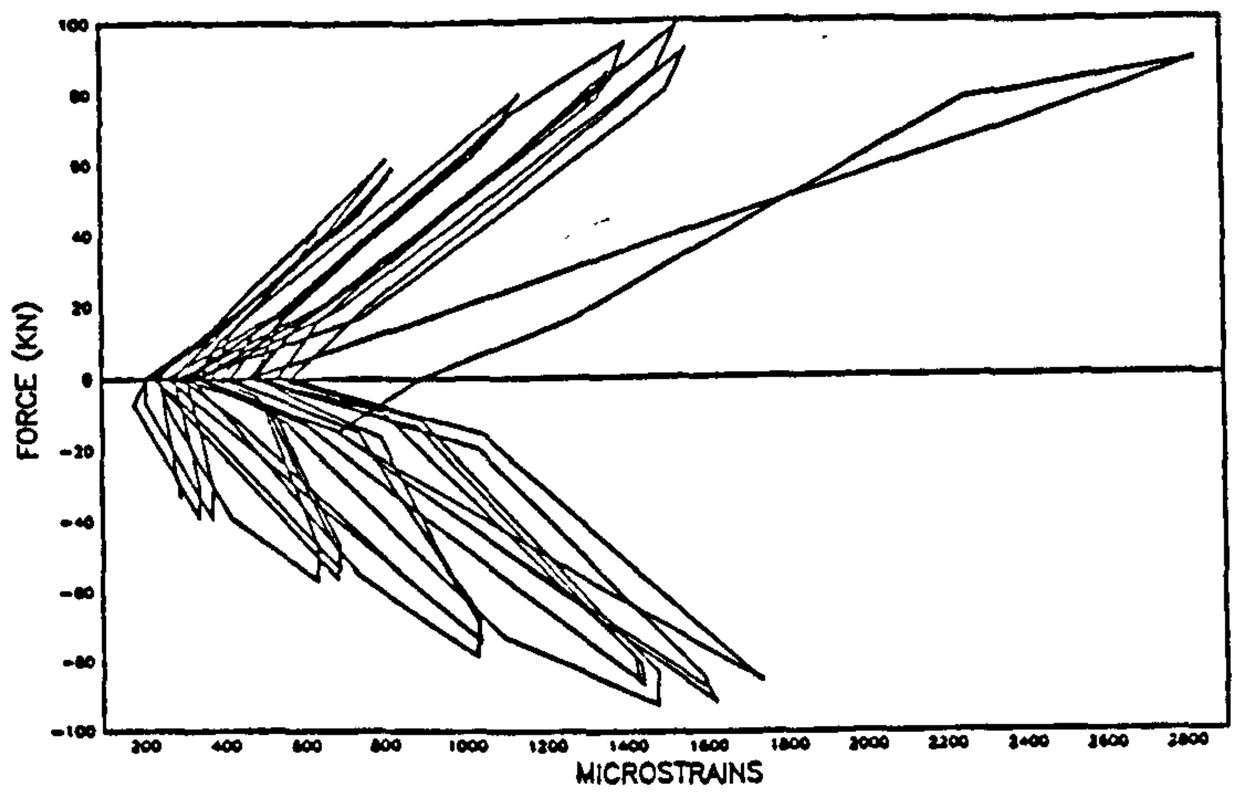


Figure B(14)33 Wall SW14 - force versus strain 19 (stirrup)

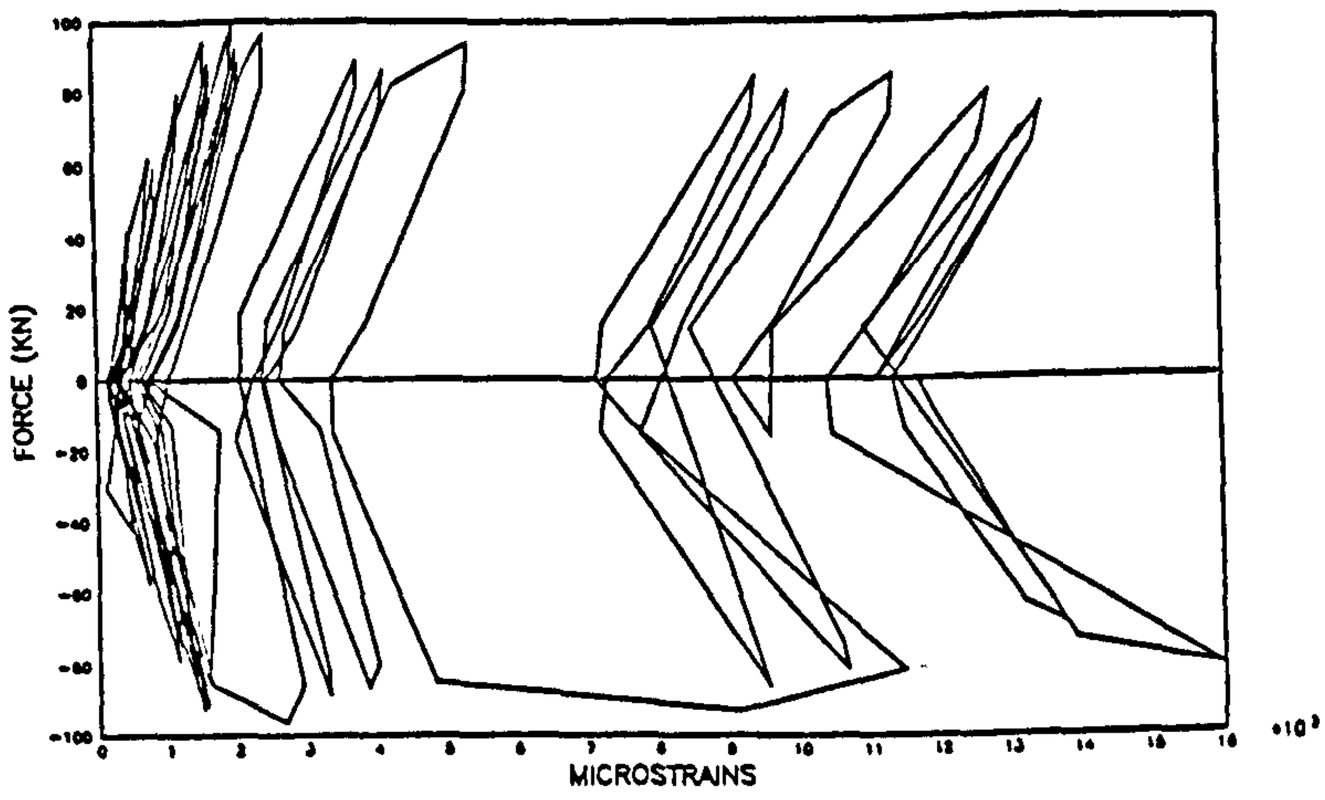


Figure B(14)34 Wall SW14 - force versus strain 20 (stirrup)

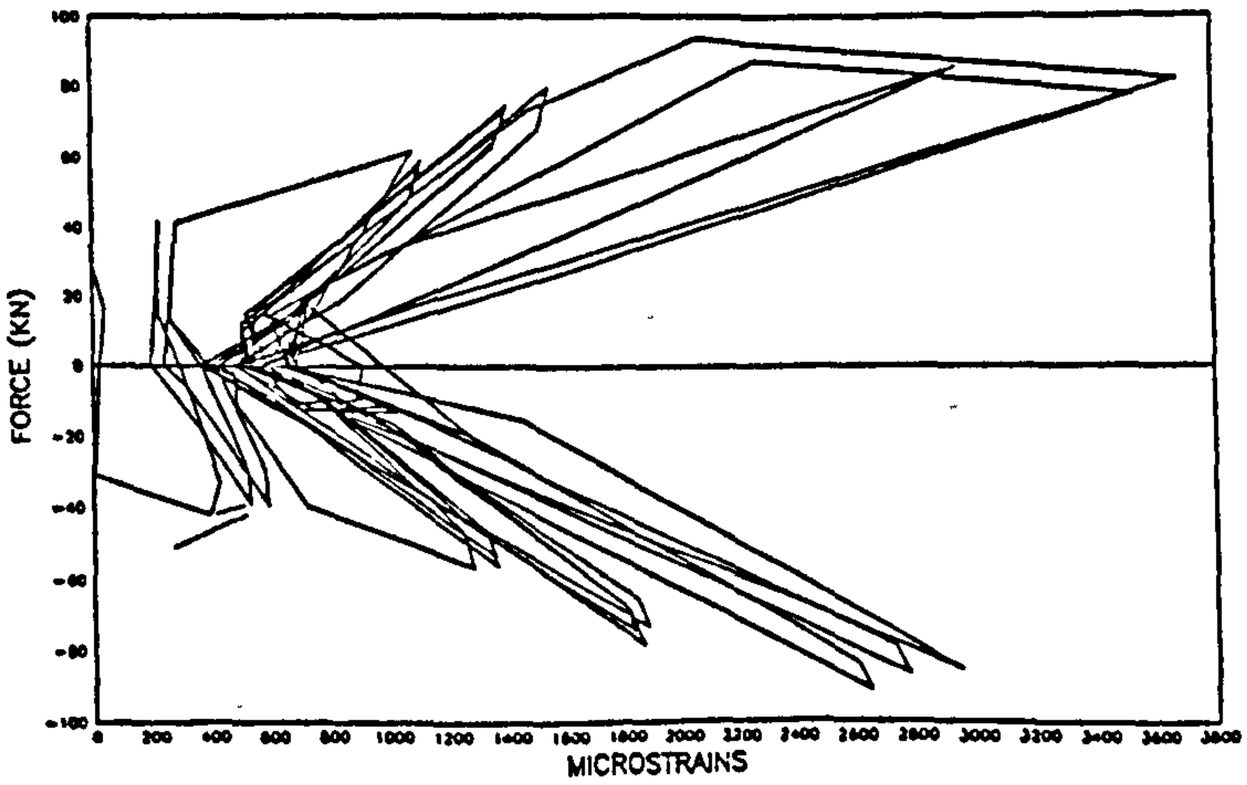


Figure B(14)35 Wall SW14 - force versus strain 21 (stirrup)

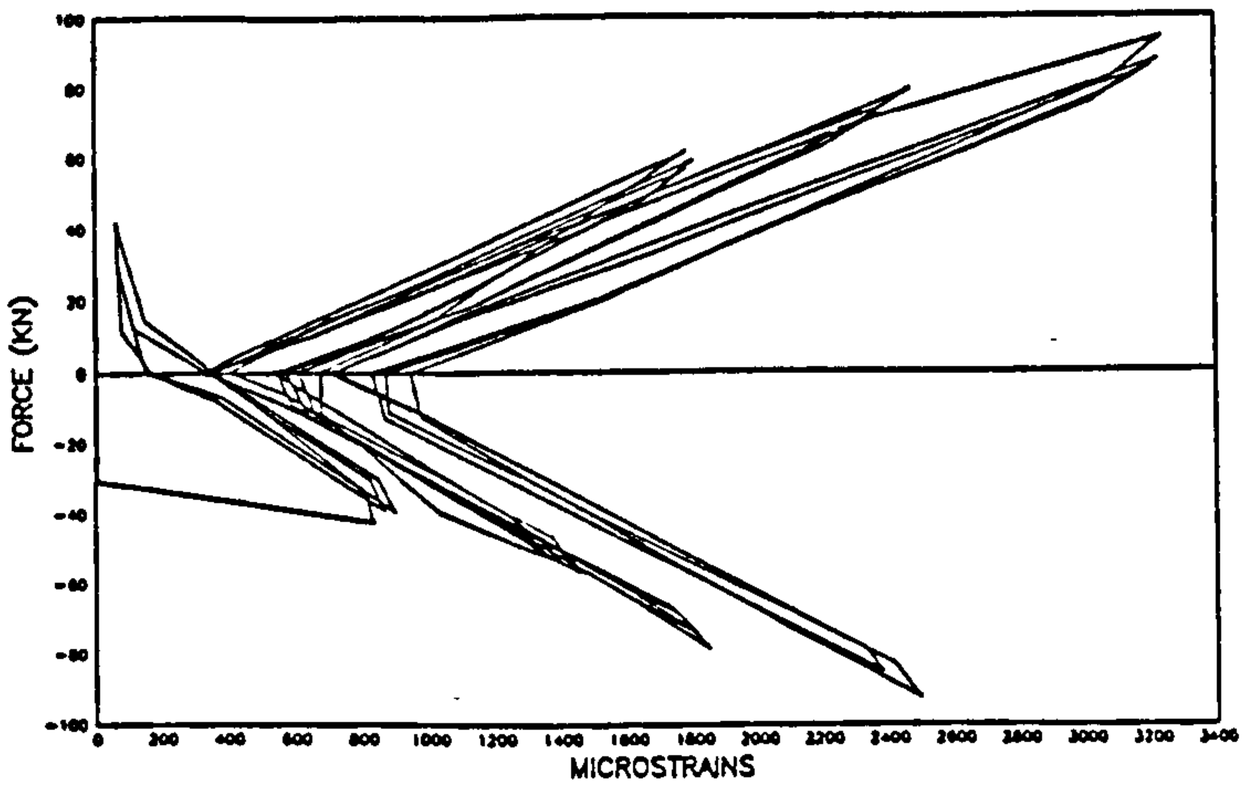


Figure B(14)36 Wall SW14 - force versus strain 22 (stirrup)

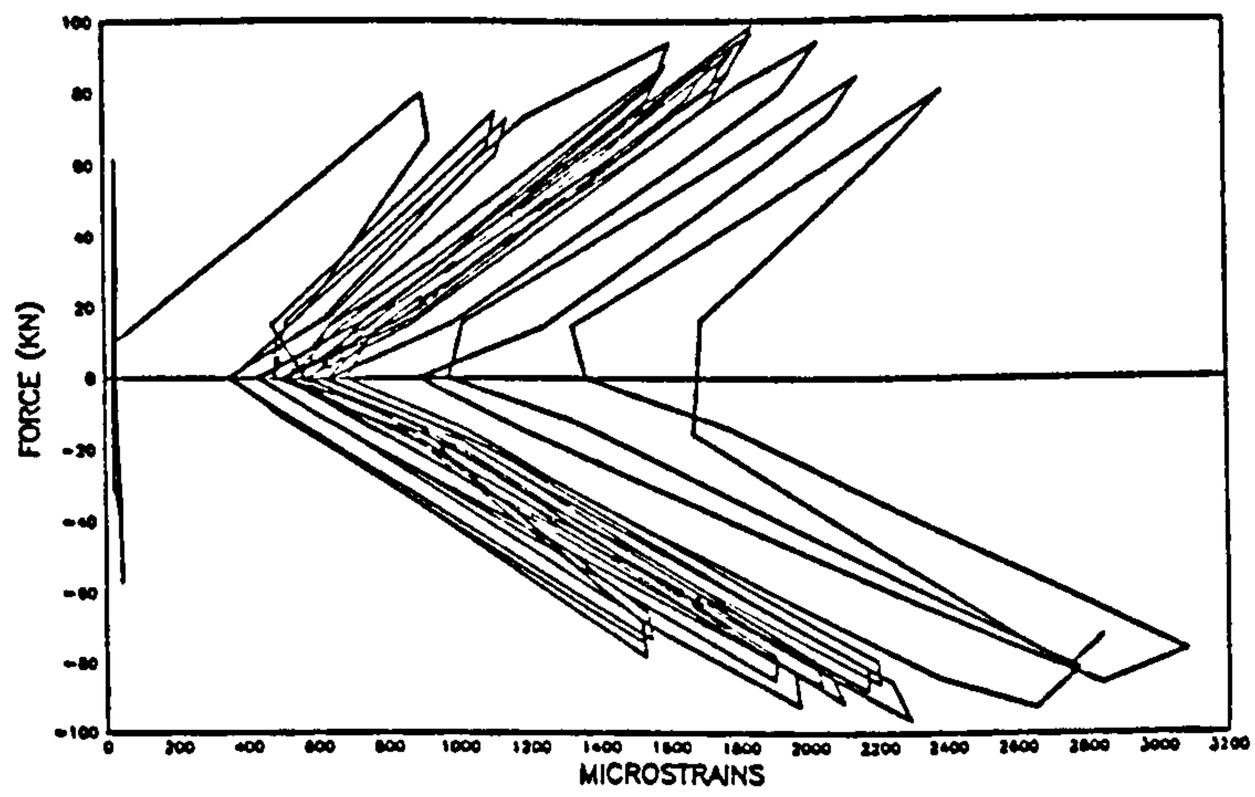


Figure B(14)37 Wall SW14 - force versus strain 23 (stirrup)

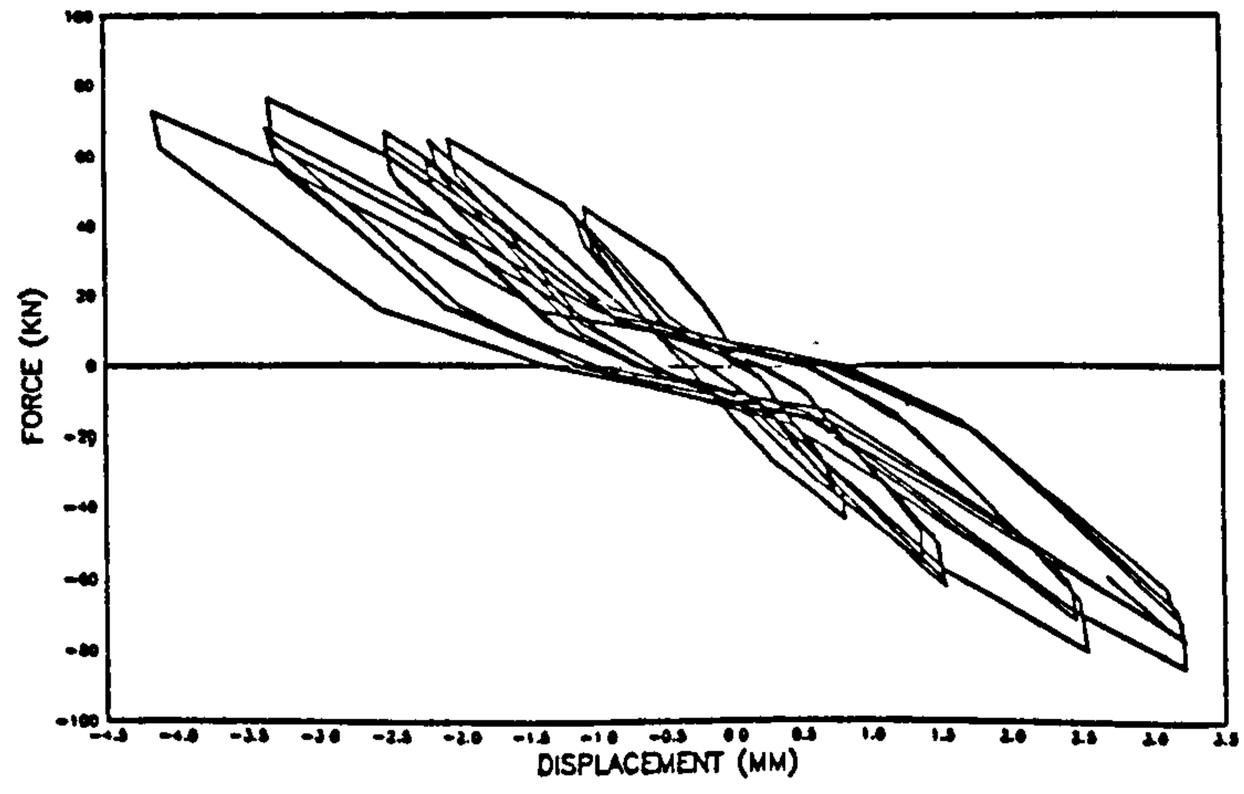


Figure B(15)1 Wall SW15 - force versus displacement 2 (horizontal, RHS, level 4)

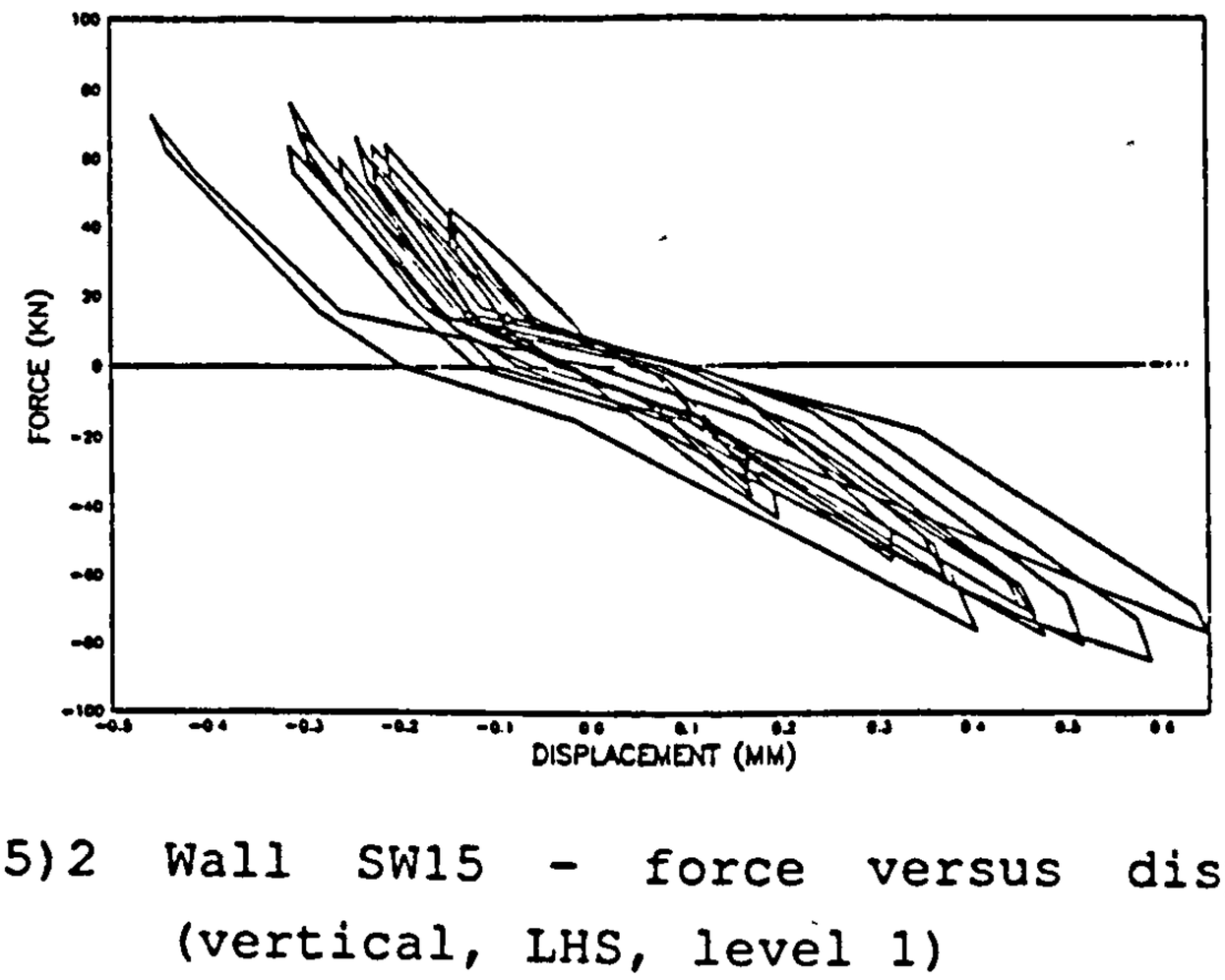


Figure B(15)2 Wall SW15 - force versus displacement 3 (vertical, LHS, level 1)

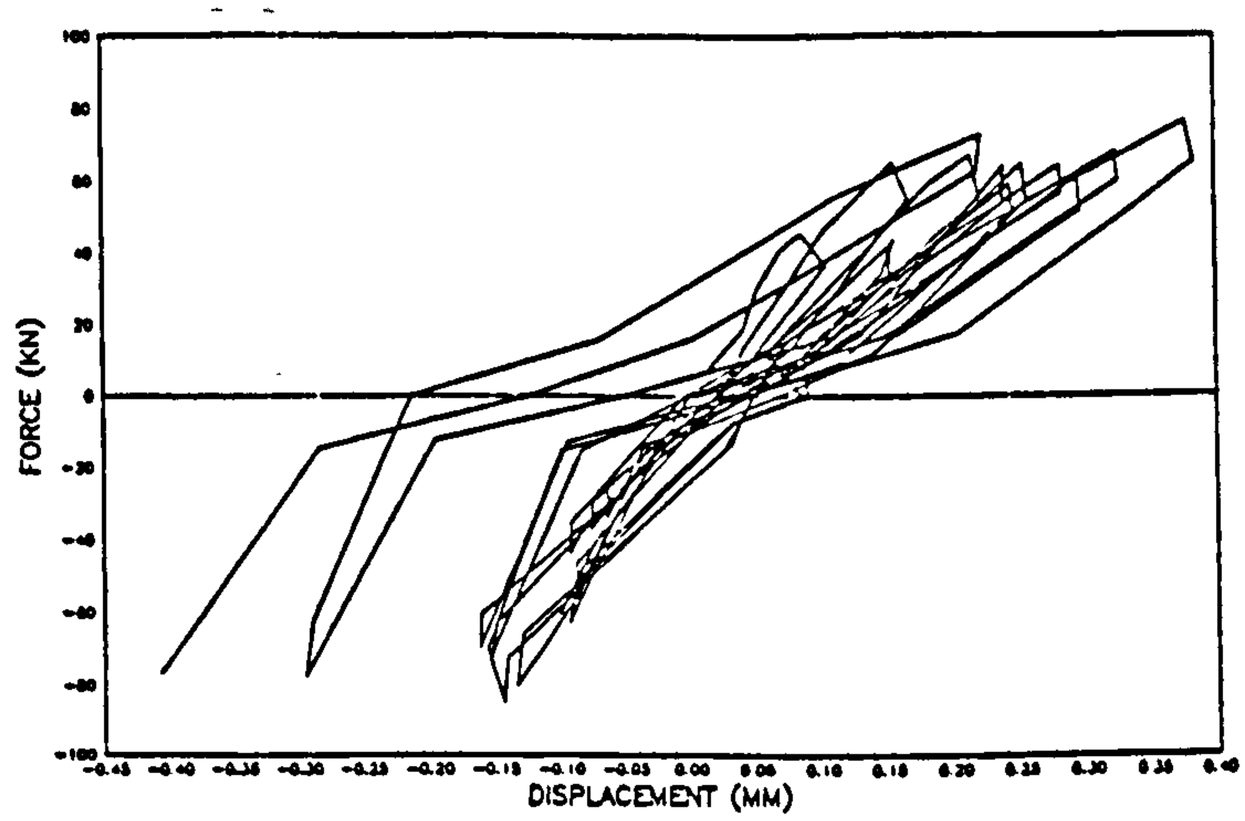


Figure B(15)3 Wall SW15 - force versus displacement 4 (vertical, RHS, level 1)

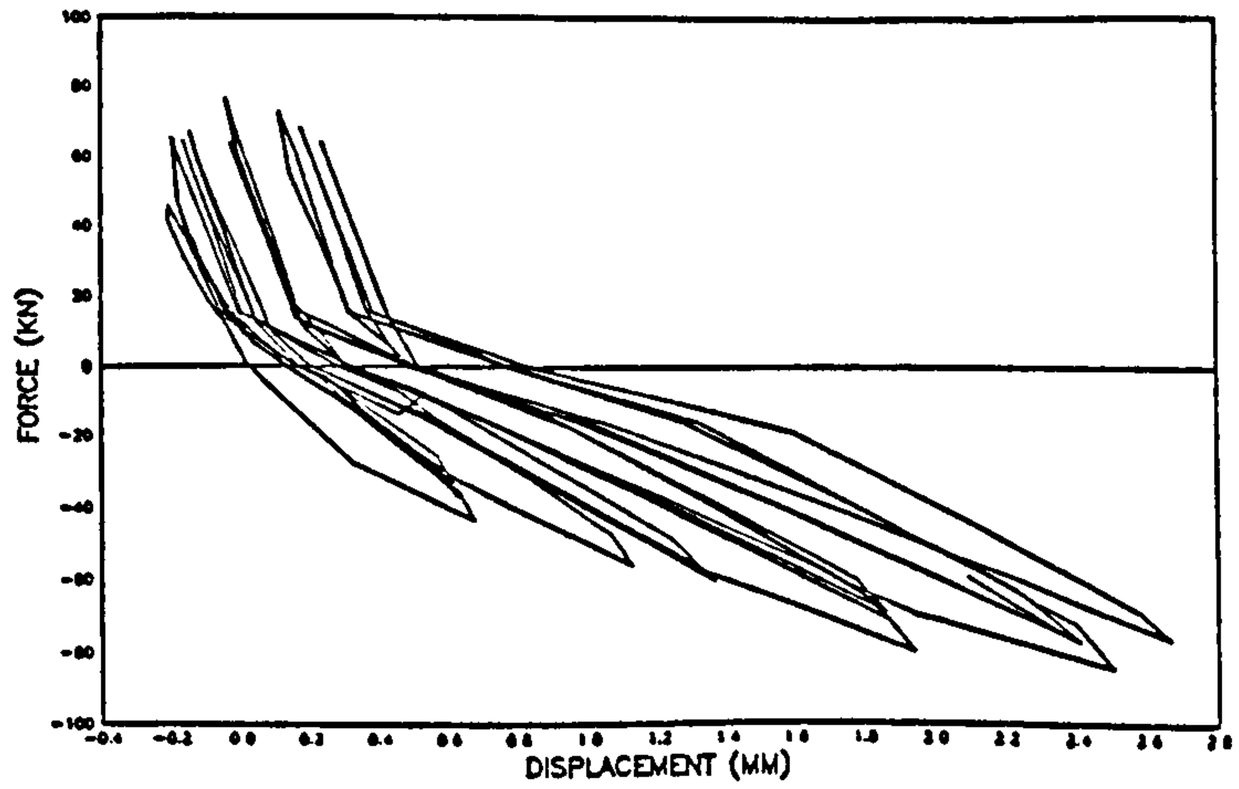


Figure B(15)4 Wall SW15 - force versus displacement 9 (vertical, LHS, level 4)

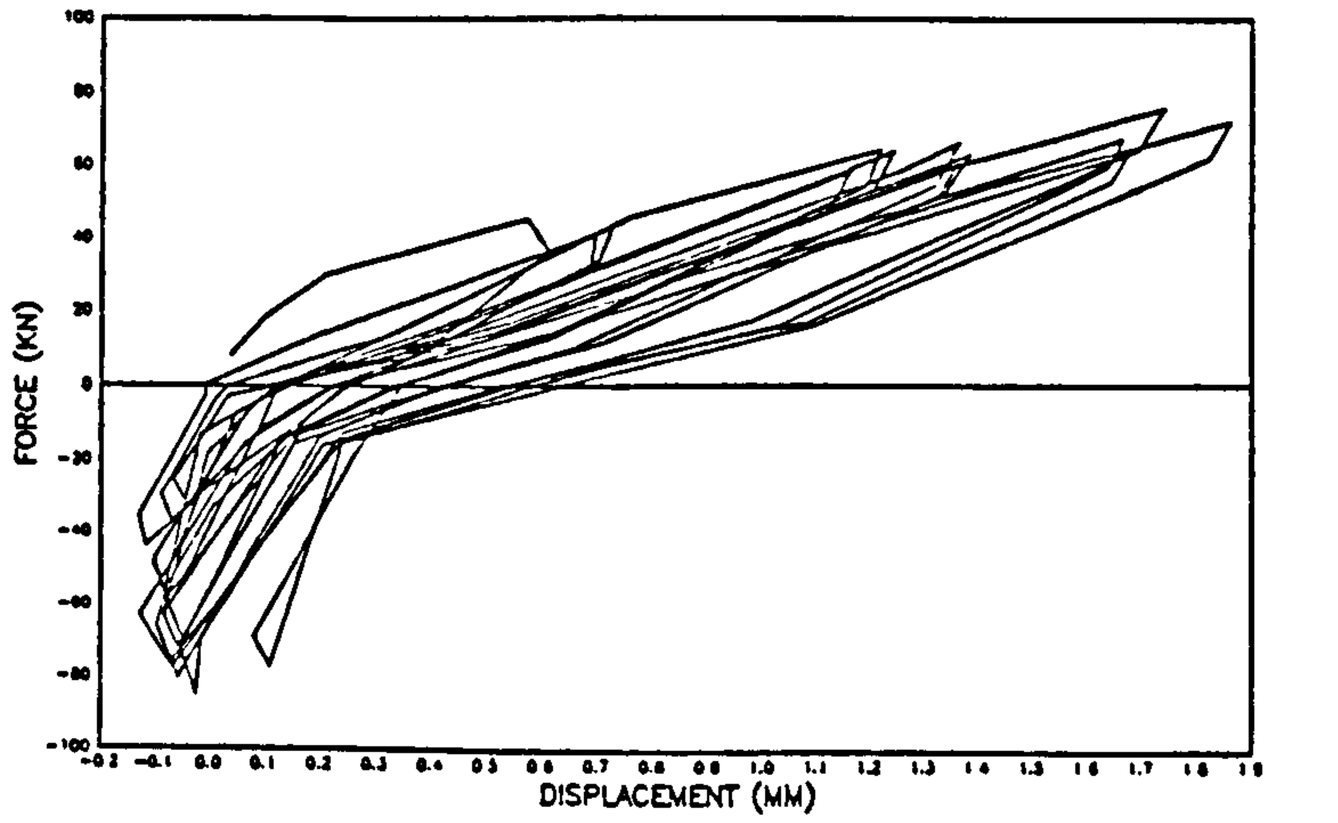


Figure B(15)5 Wall SW15 - force versus displacement 10 (vertical, RHS, level 4)

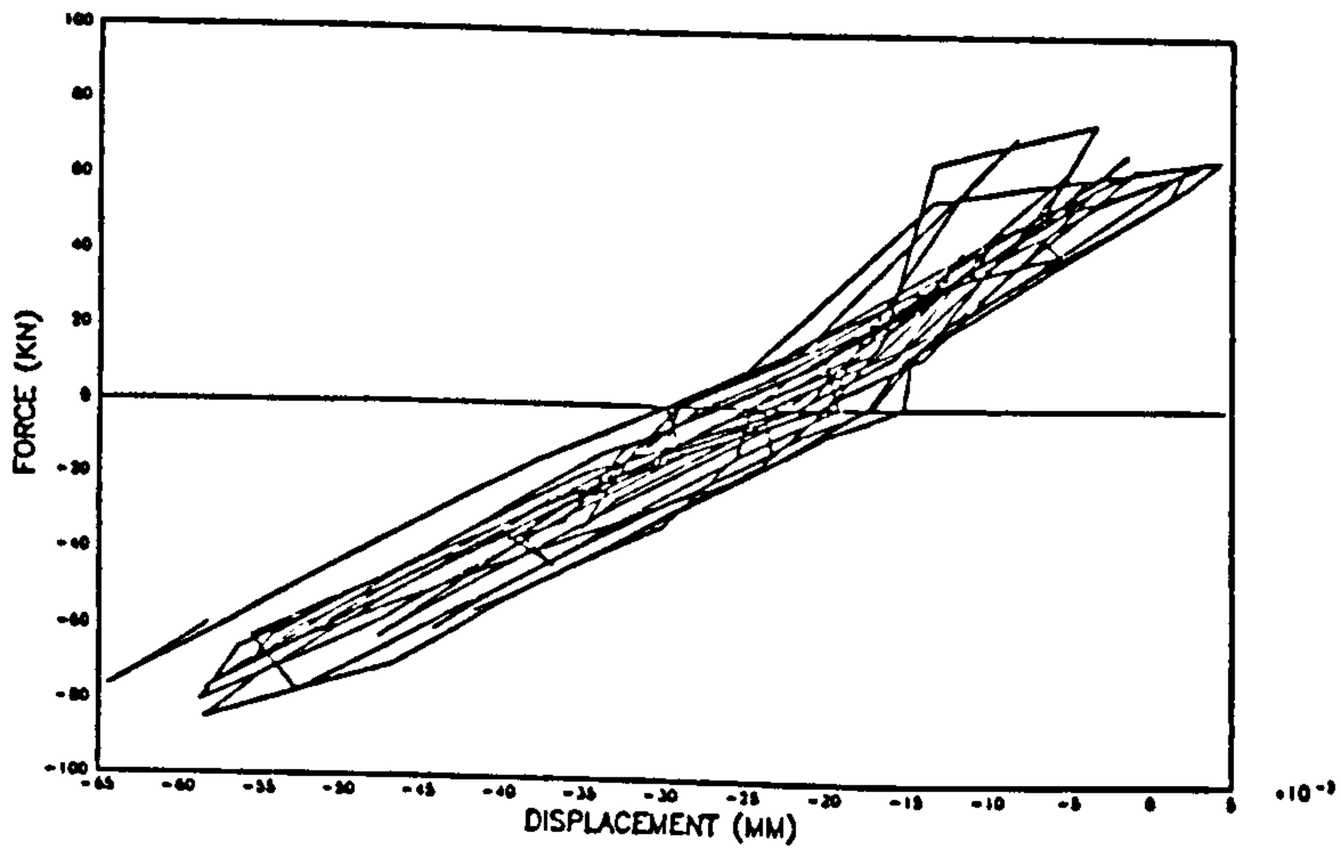


Figure B(15)6 Wall SW15 - force versus displacement 11 (foundation, RHS)

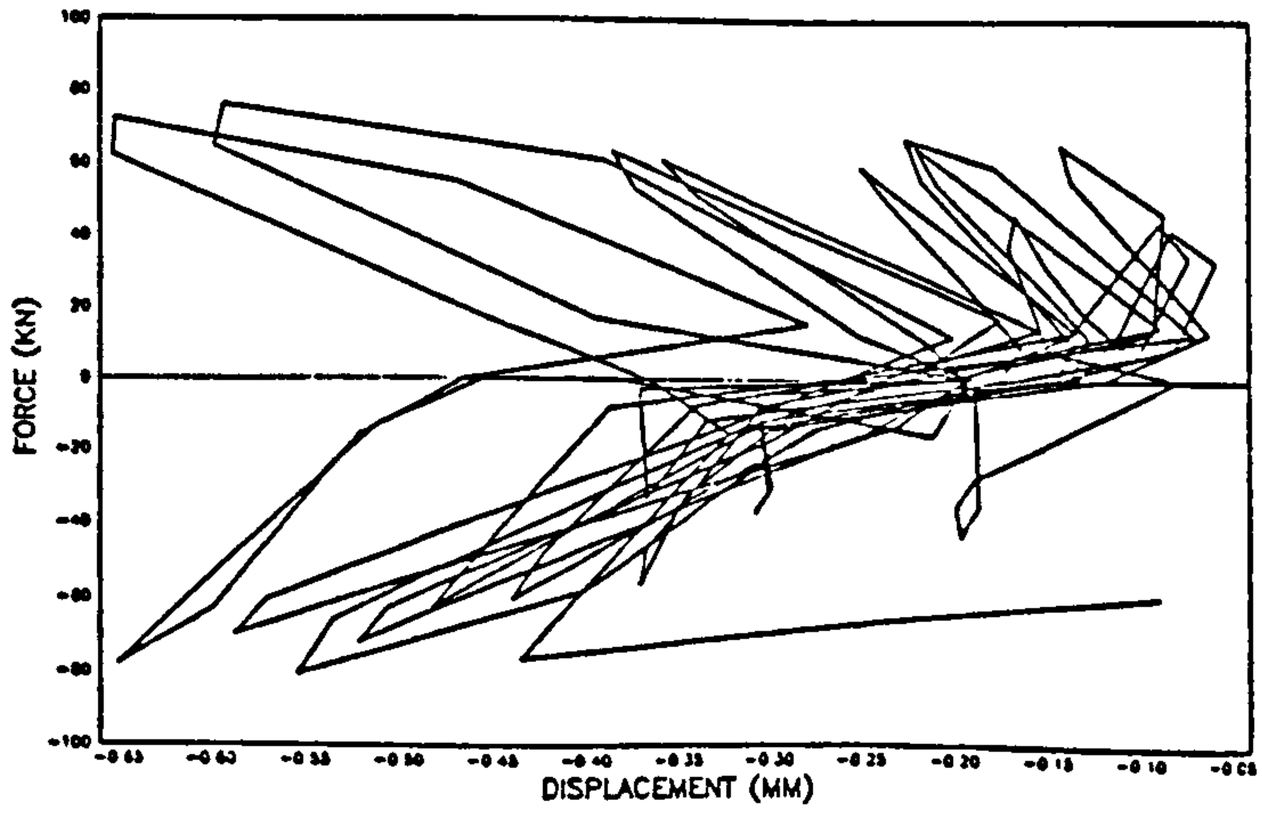


Figure B(15)7 Wall SW15 - force versus displacement 12 (out-of-plane)

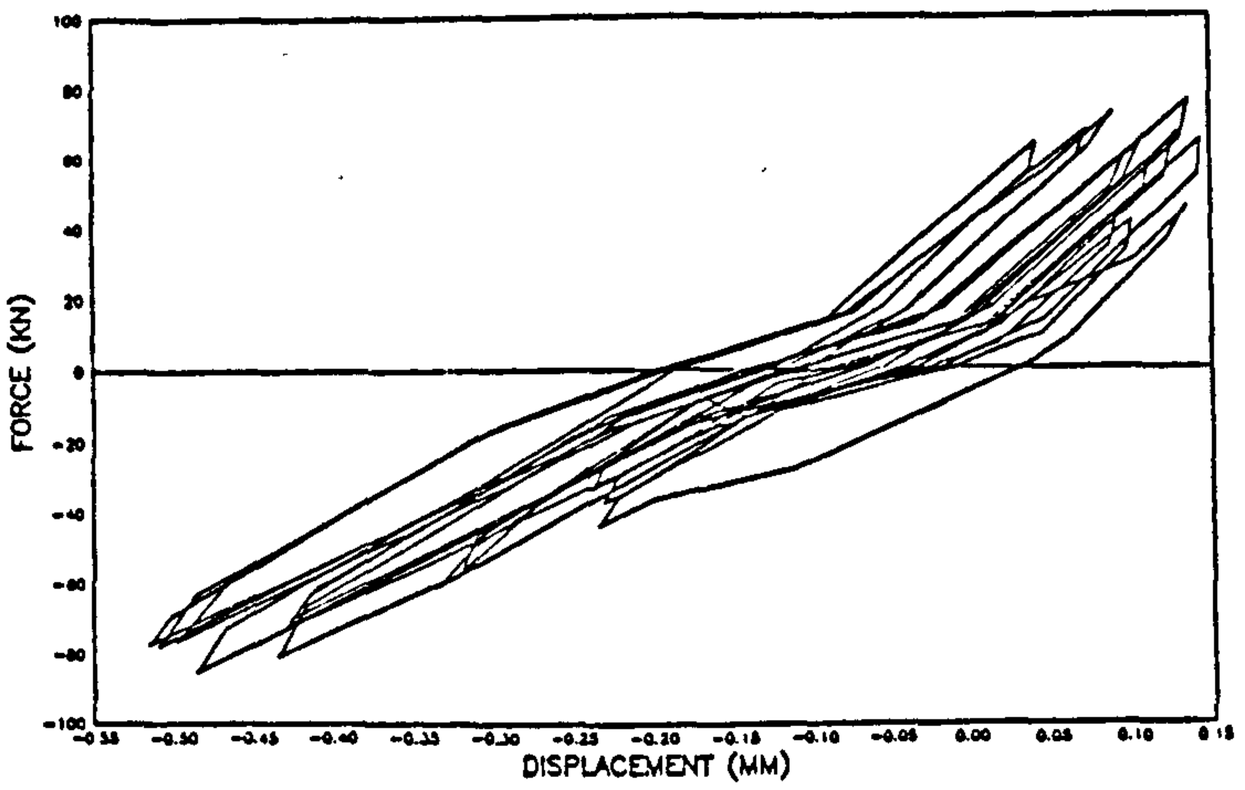


Figure B(15)8 Wall SW15 - force versus displacement 13 (horizontal, centre, level 1)

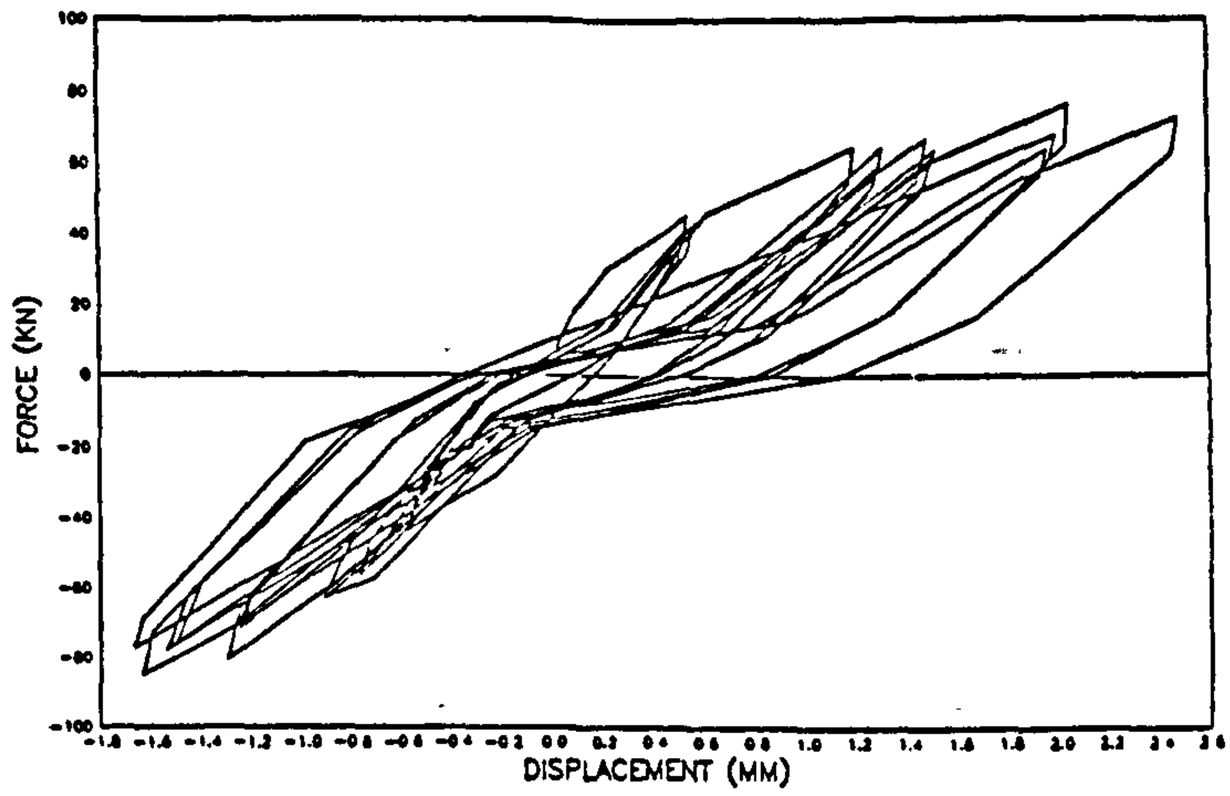


Figure B(15)9 Wall SW15 - force versus displacement 15 (horizontal, centre, level 3)

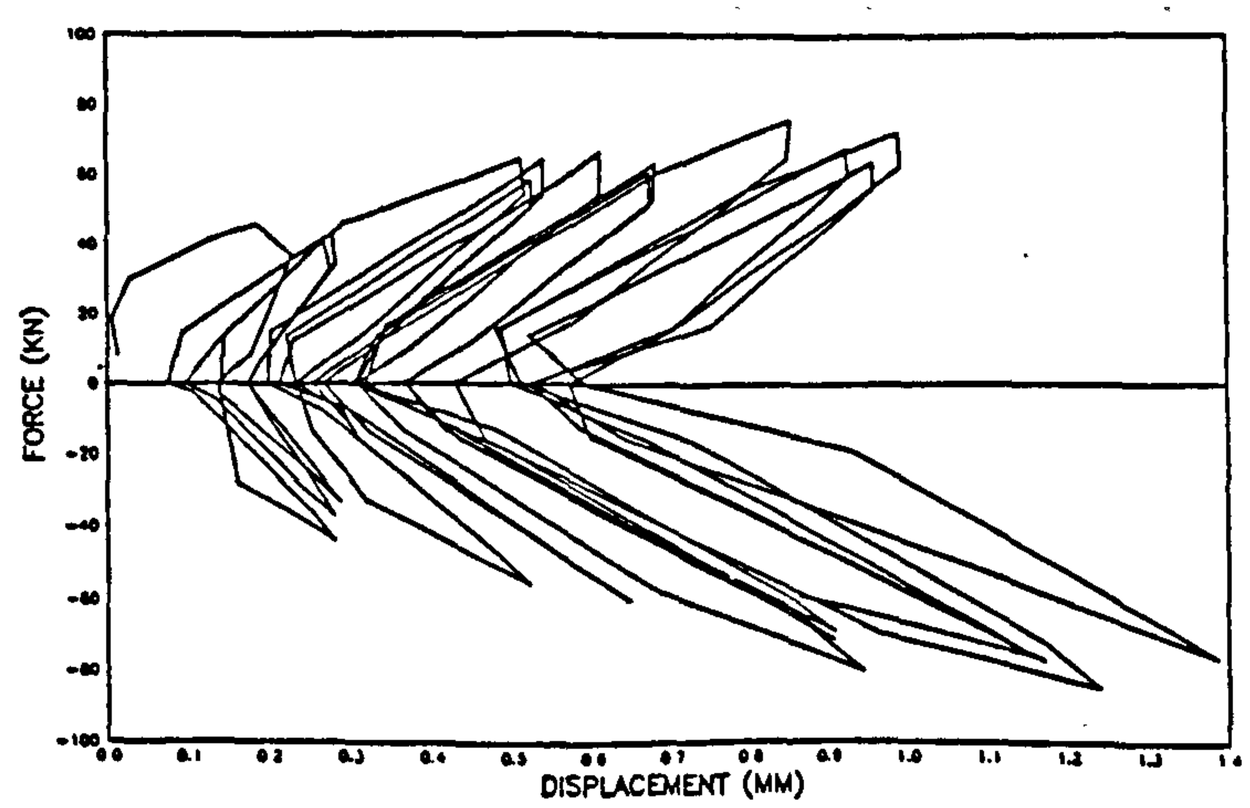


Figure B(15)10 Wall SW15 - force versus extension on top

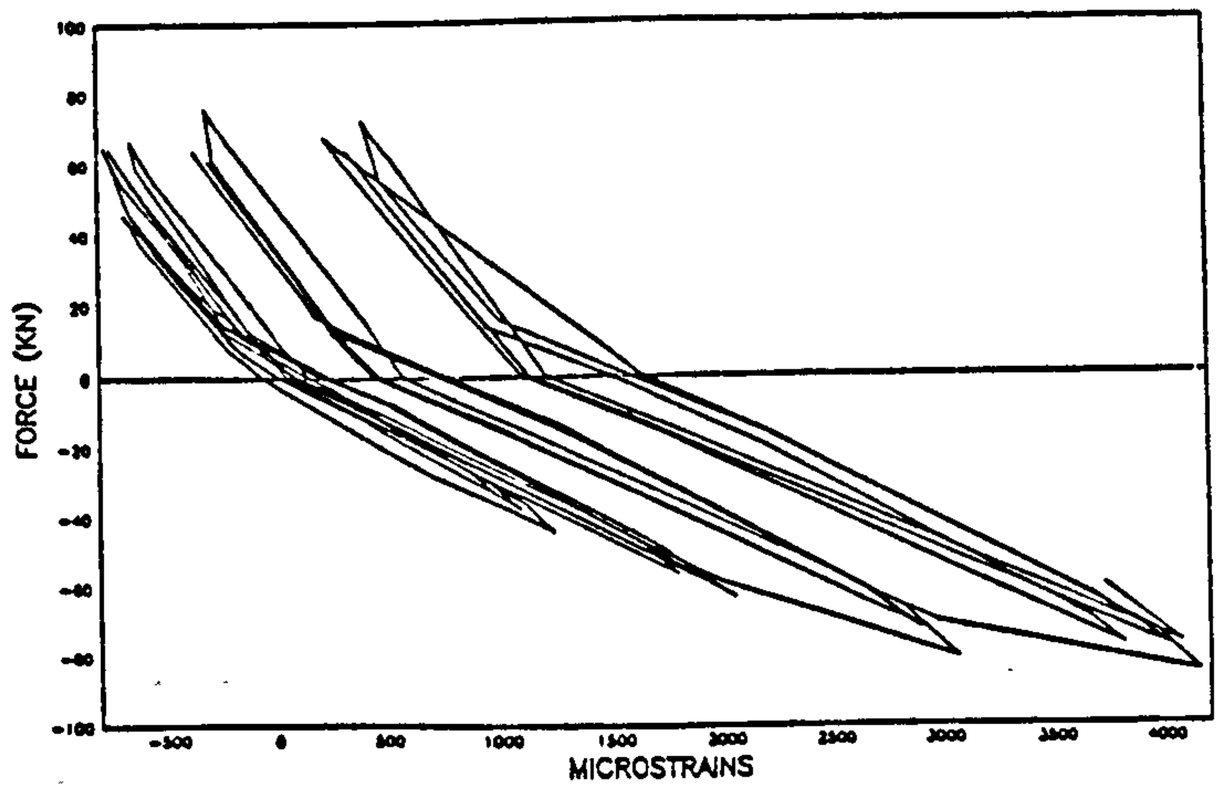


Figure B(15)11 Wall SW15 - force versus strain 1 (bottom, ϕ8mm, LHS)

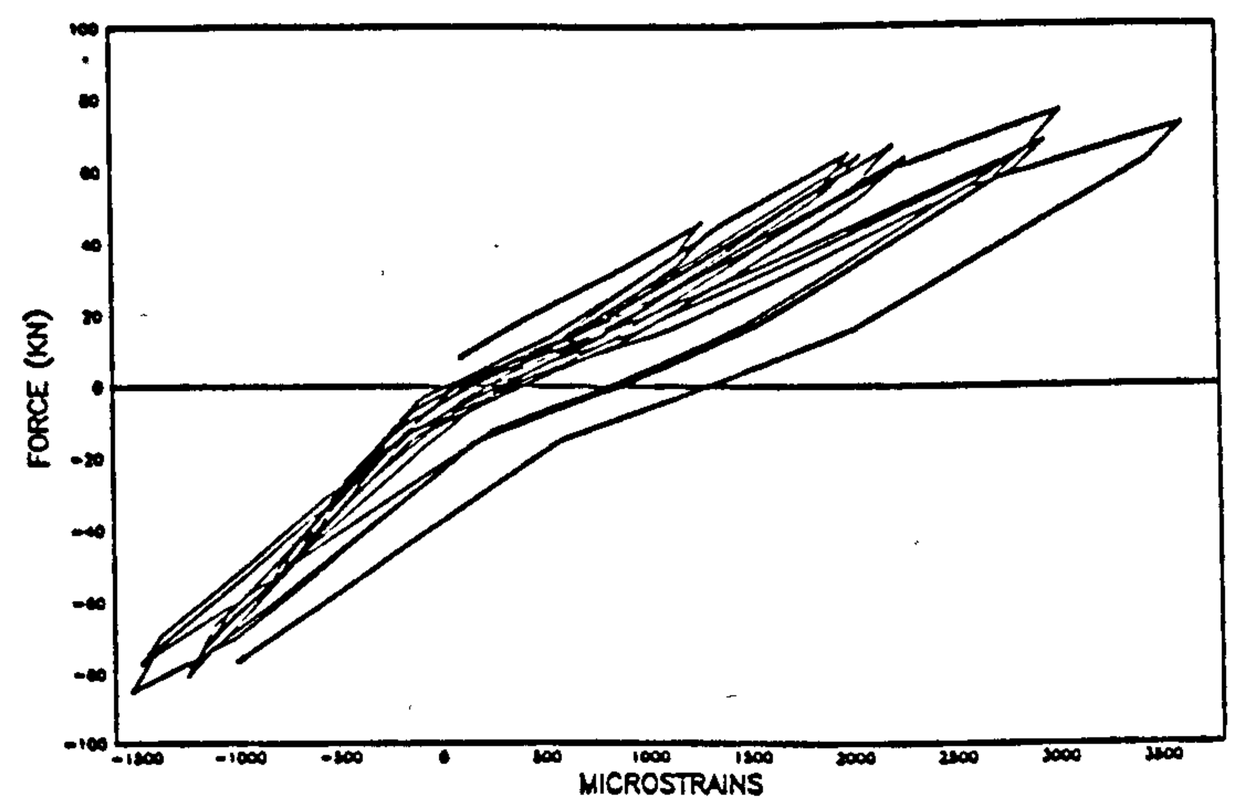


Figure B(15)12 Wall SW15 - force versus strain 2 (bottom, ϕ8mm, RHS)

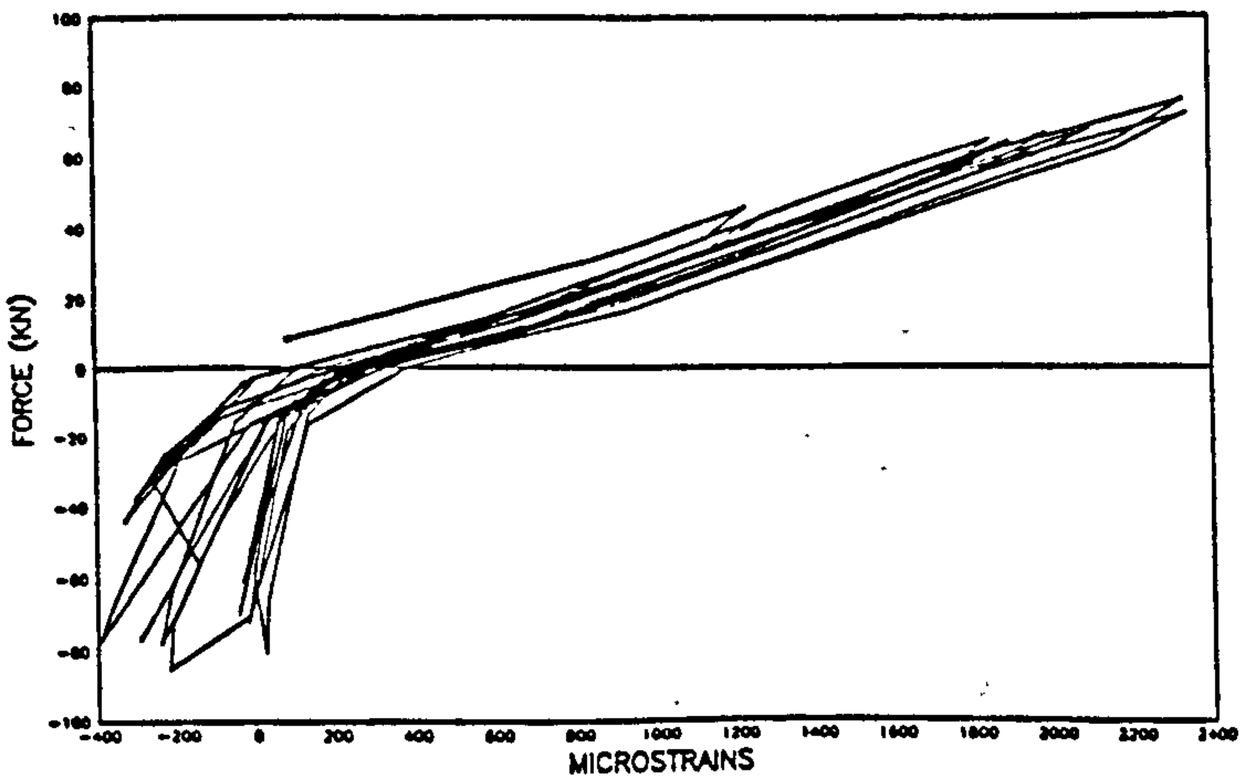


Figure B(15)13 Wall SW15 - force versus strain 4 (bottom, ϕ6mm, RHS)

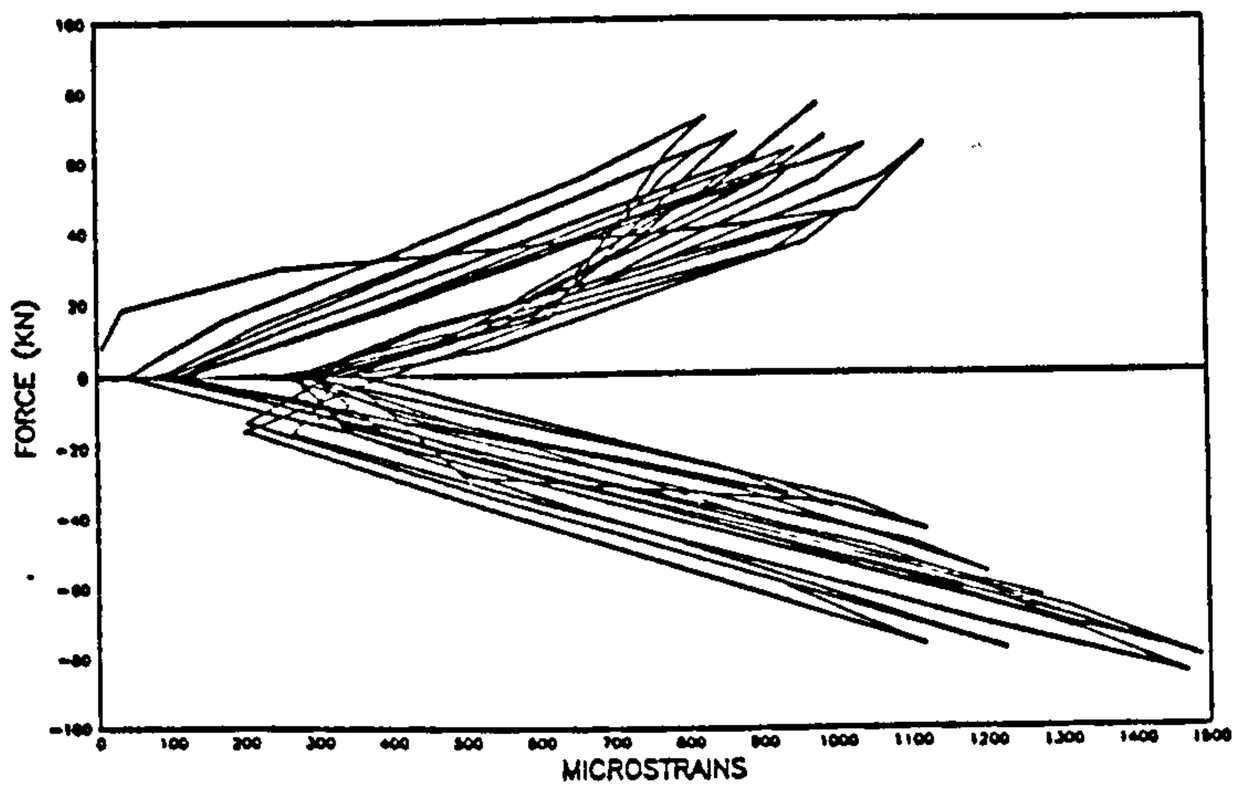


Figure B(15)14 Wall SW15 - force versus strain 7 (bottom, ϕ4mm, LHS)

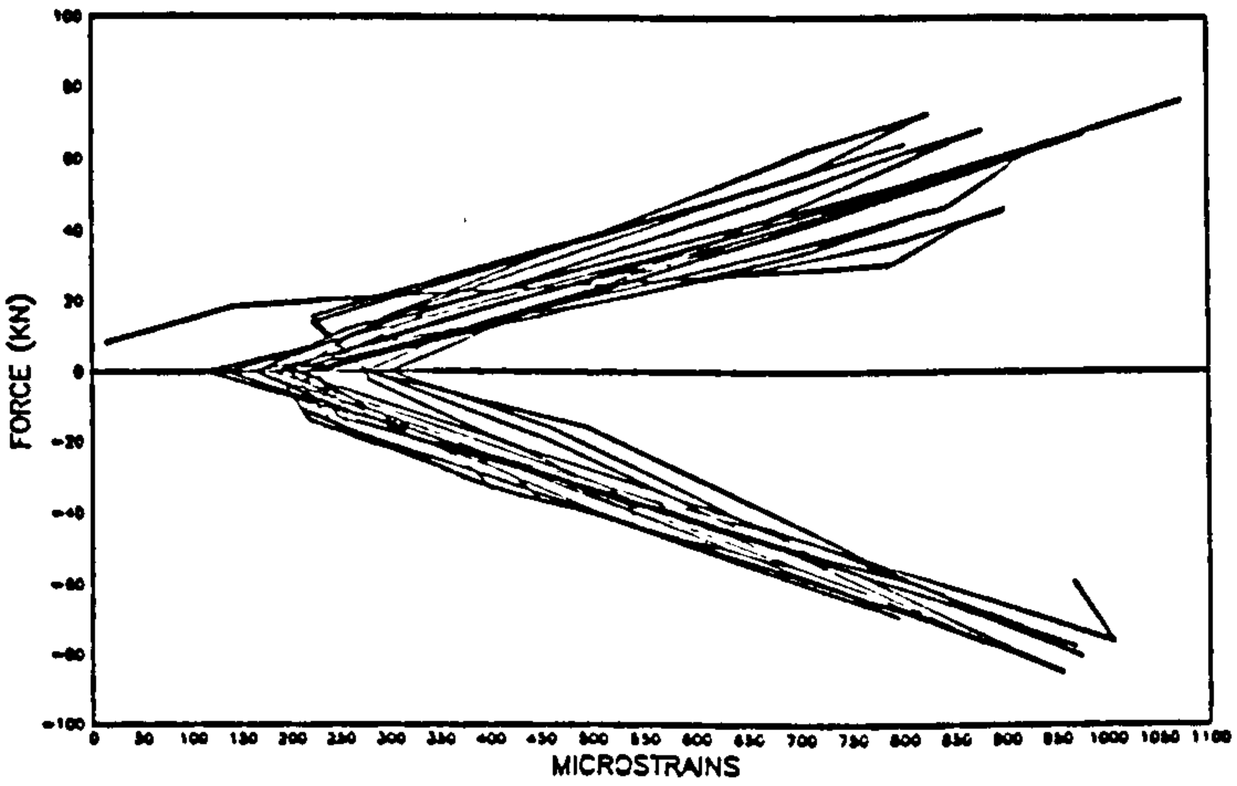


Figure B(15)15 Wall SW15 - force versus strain 8 (bottom, ϕ4mm, RHS)

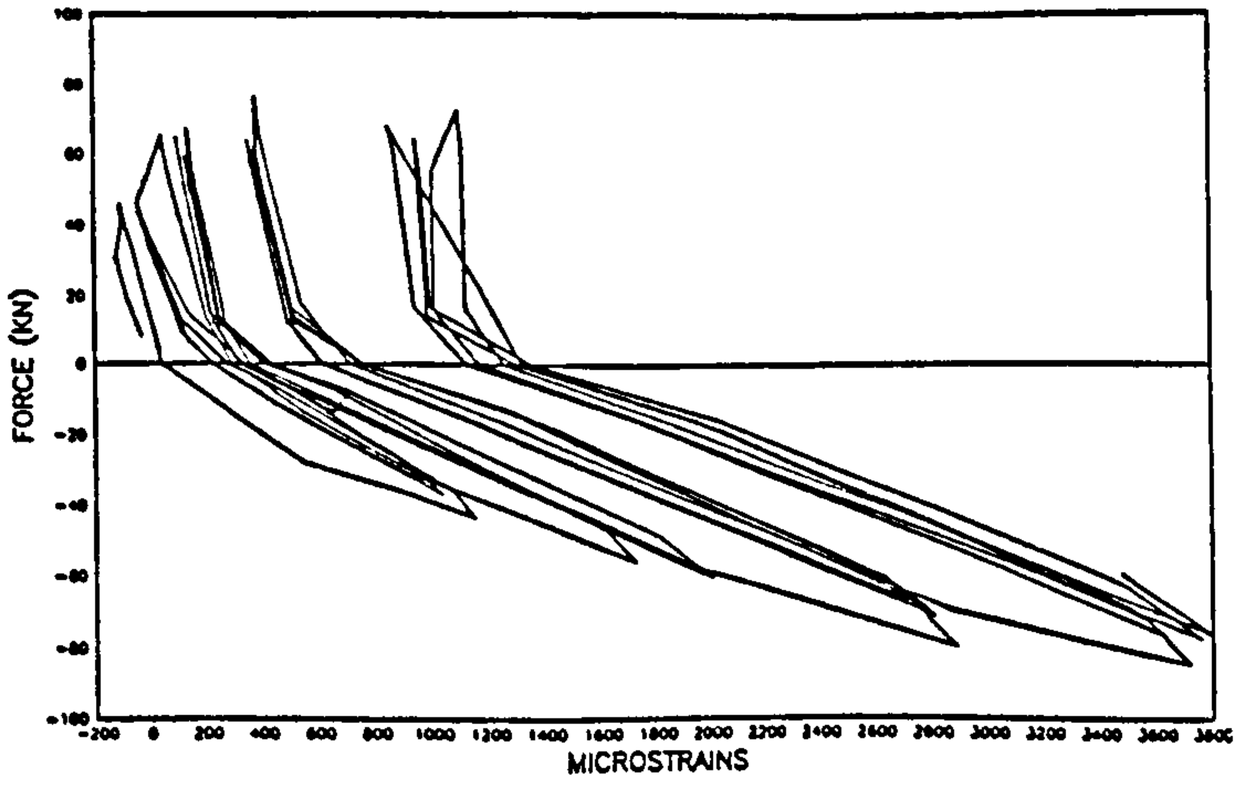


Figure B(15)16 Wall SW15 - force versus strain 9 (second level, ϕ8mm, LHS)

Figure B(15)17 Wall SW15 - force versus strain 10 (second level, ϕ8mm, RHS)

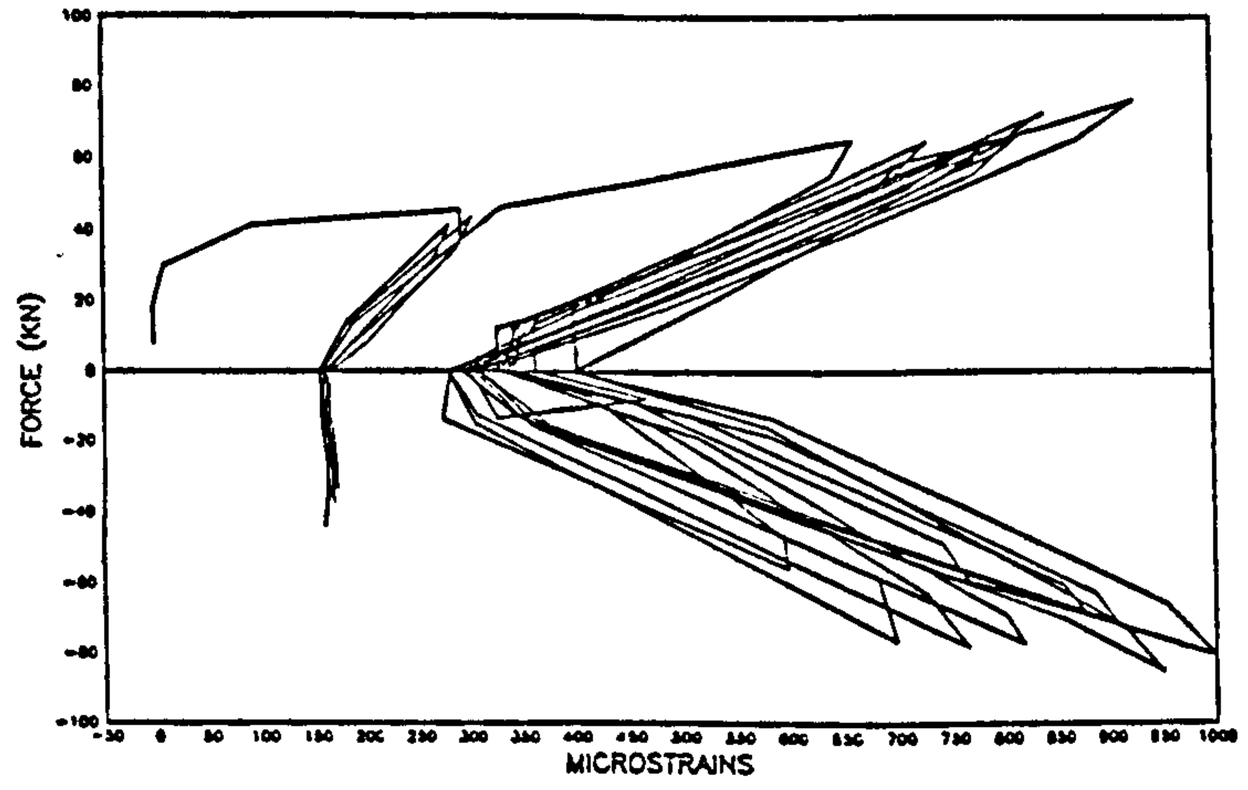


Figure B(15)18 Wall SW15 - force versus strain 11 (level of zero moment, ϕ8mm, LHS)

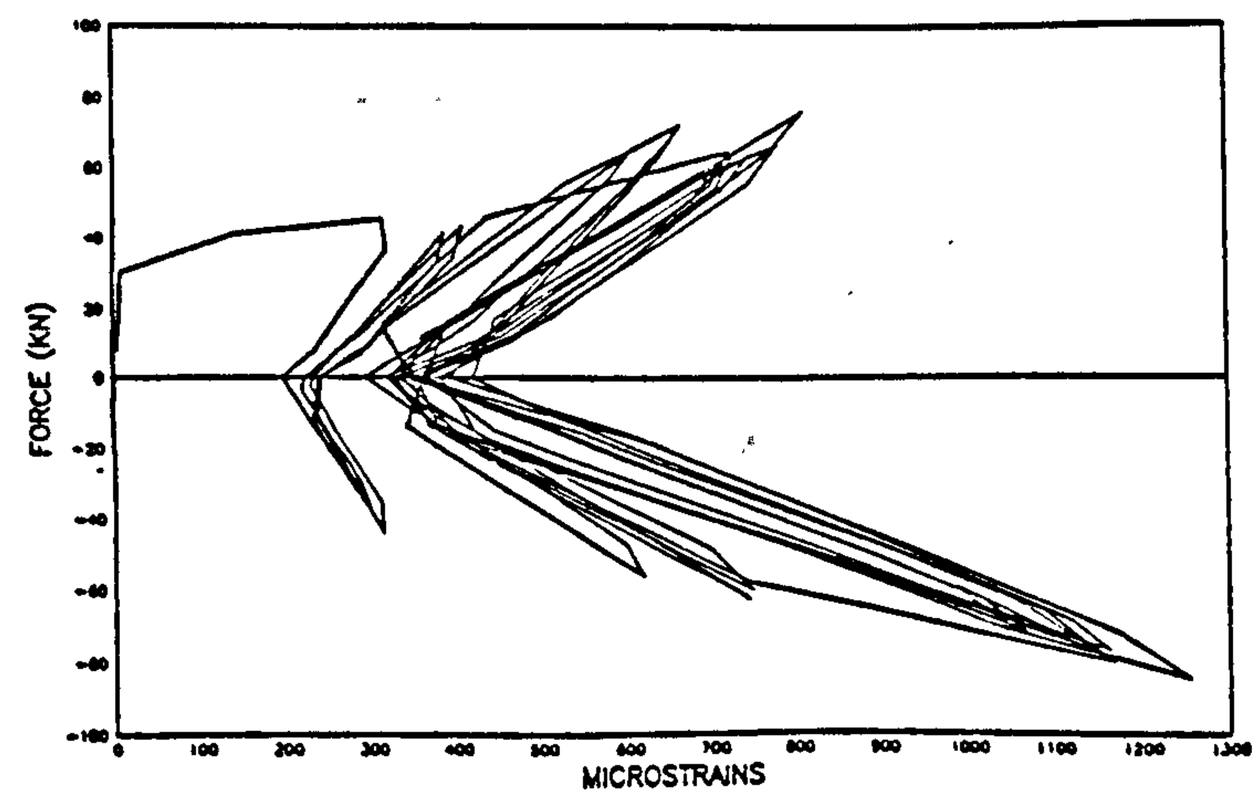


Figure B(15)19 Wall SW15 - force versus strain 12 (level of zero moment, ϕ8mm, RHS)

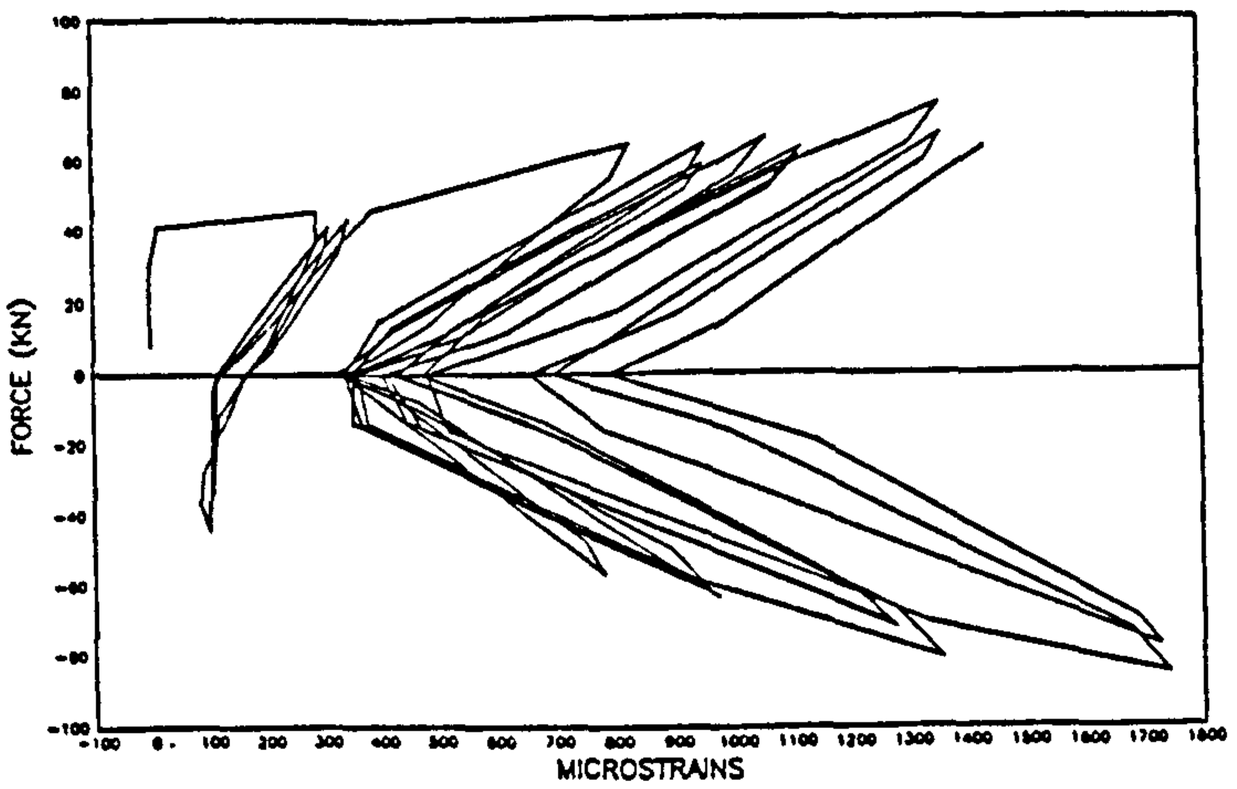


Figure B(15)20 Wall SW15 - force versus strain 13 (level of zero moment, ϕ6mm, LHS)

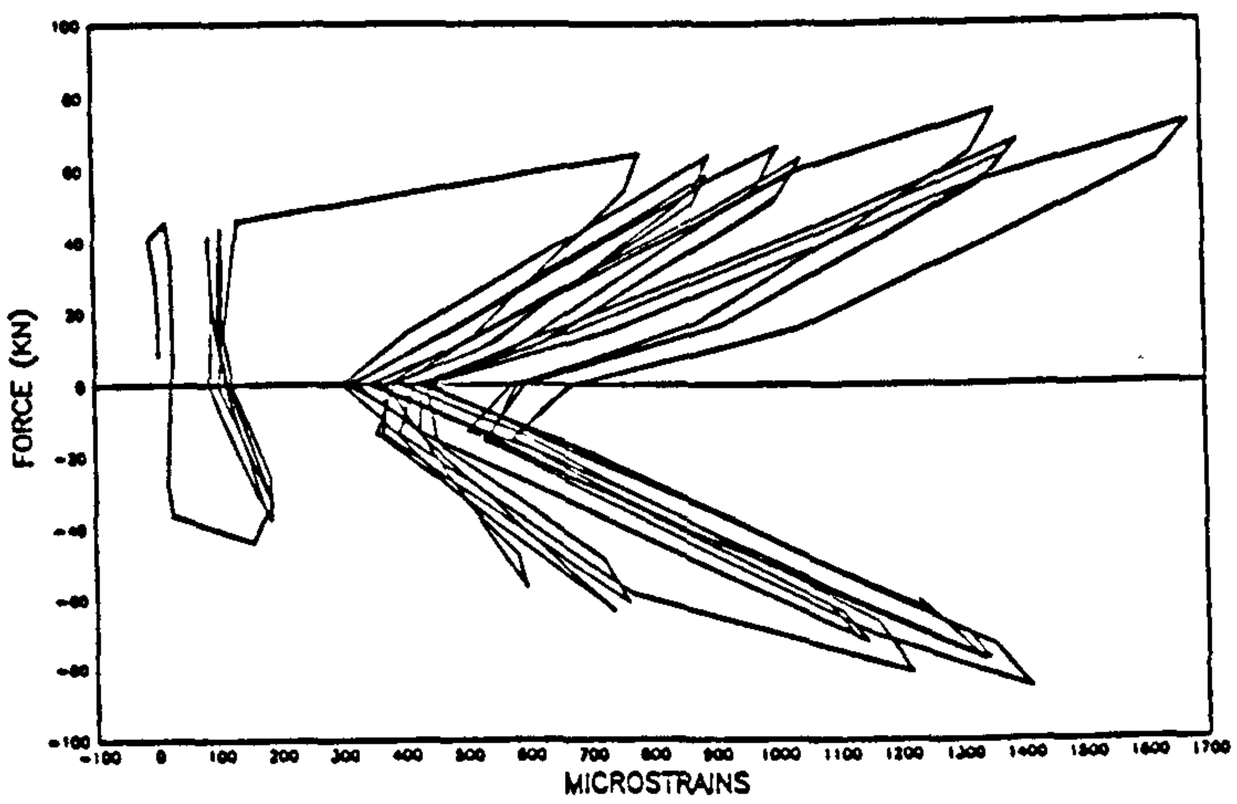


Figure B(15)21 Wall SW15 - force versus strain 14 (level of zero moment, ϕ6mm, RHS)

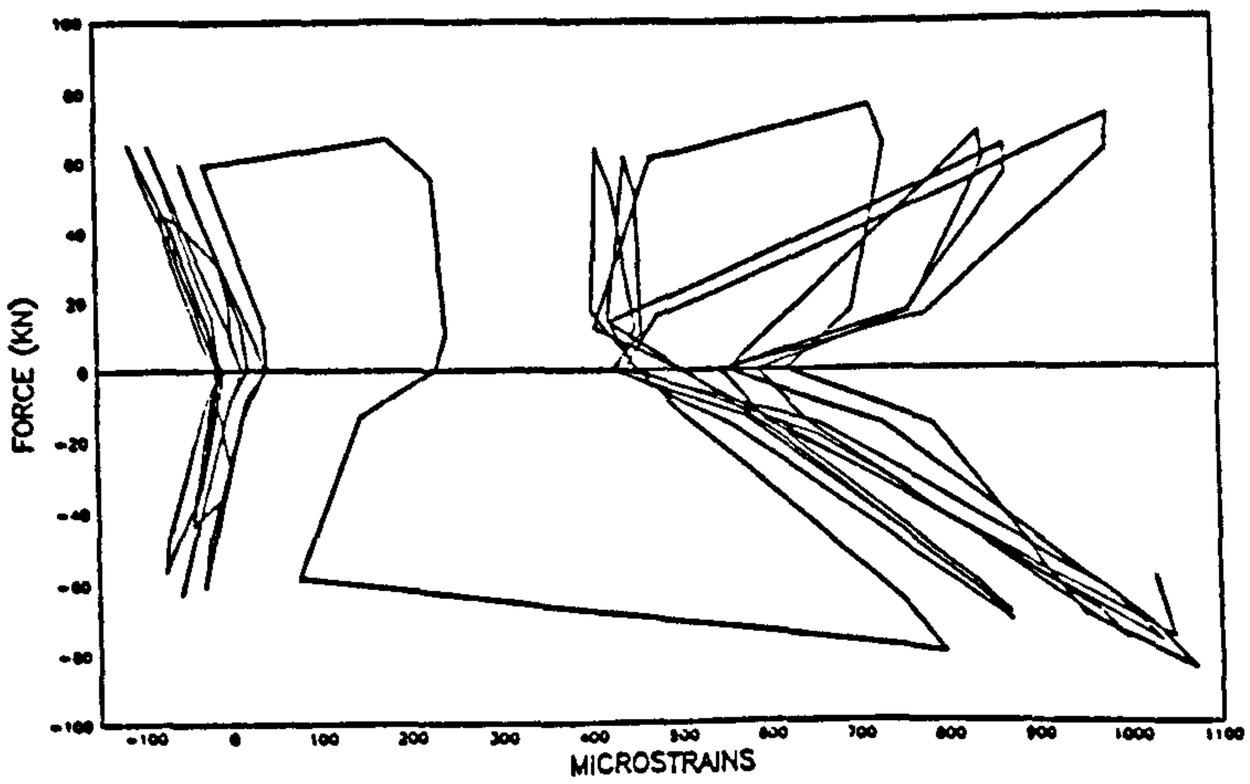


Figure B(15)22 Wall SW15 - force versus strain 16 (level of zero moment, ϕ4mm, RHS)

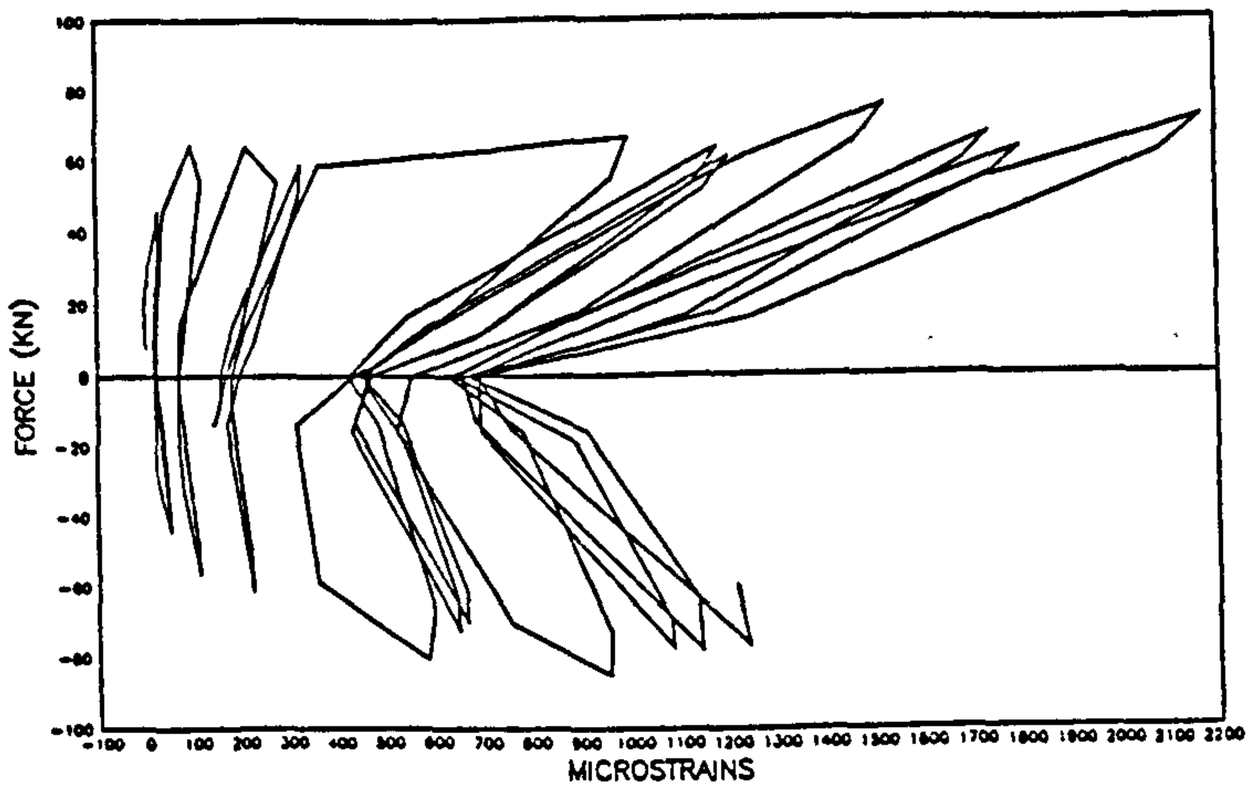


Figure B(15)23 Wall SW15 - force versus strain 19 (stirrup)

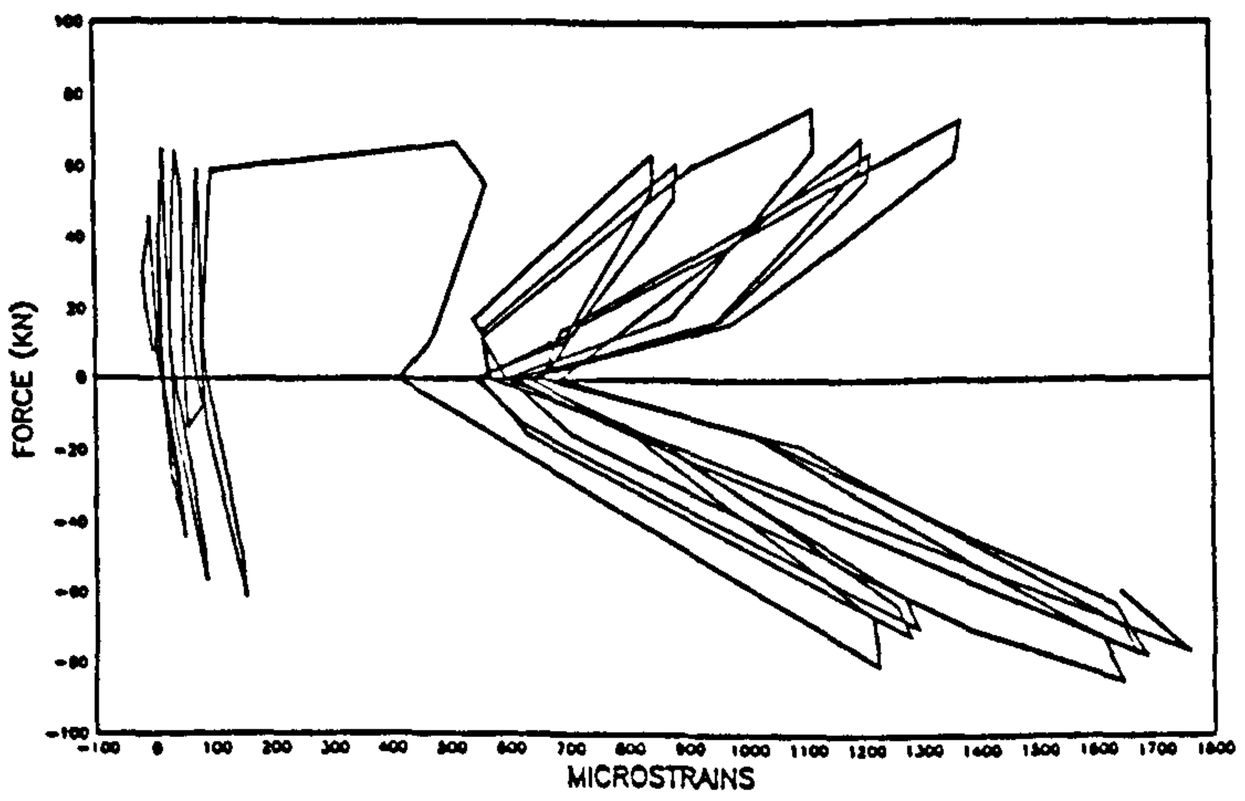


Figure B(15)24 Wall SW15 - force versus strain 20 (stirrup)

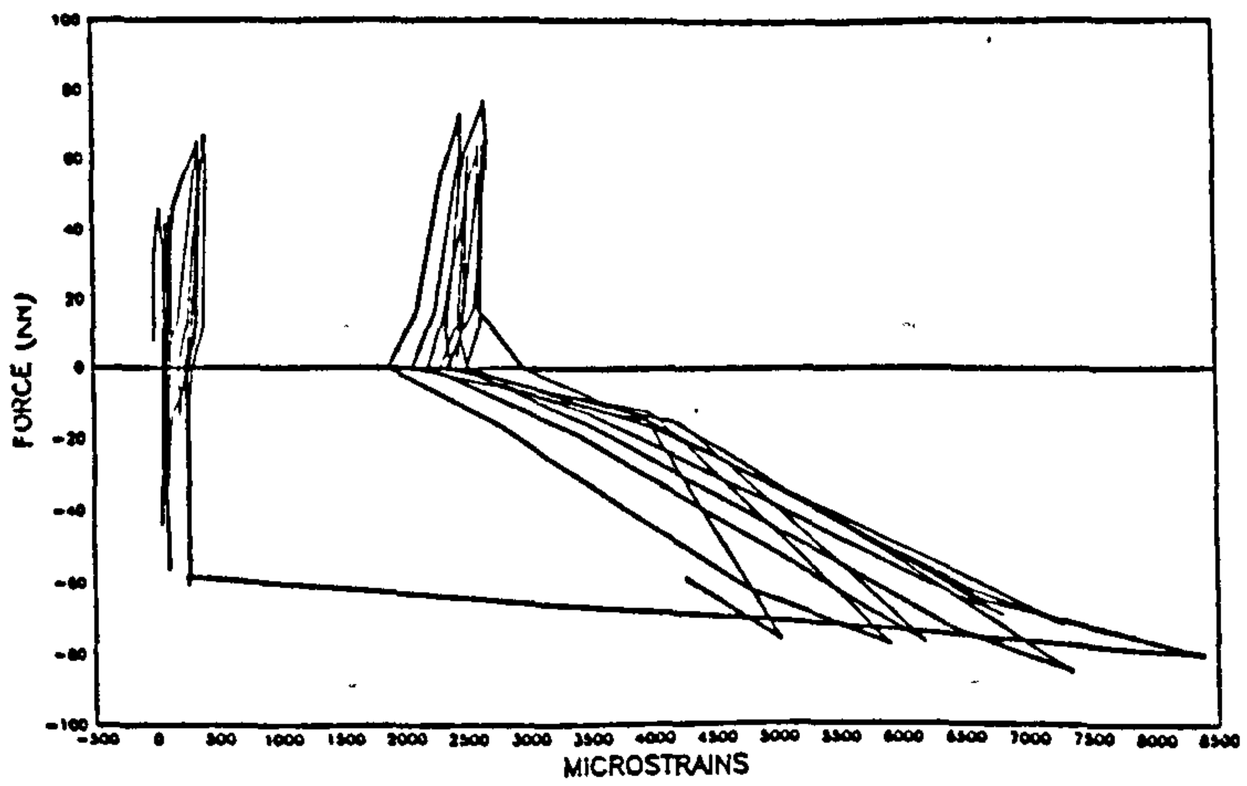


Figure B(15)25 Wall SW15 - force versus strain 21 (stirrup)

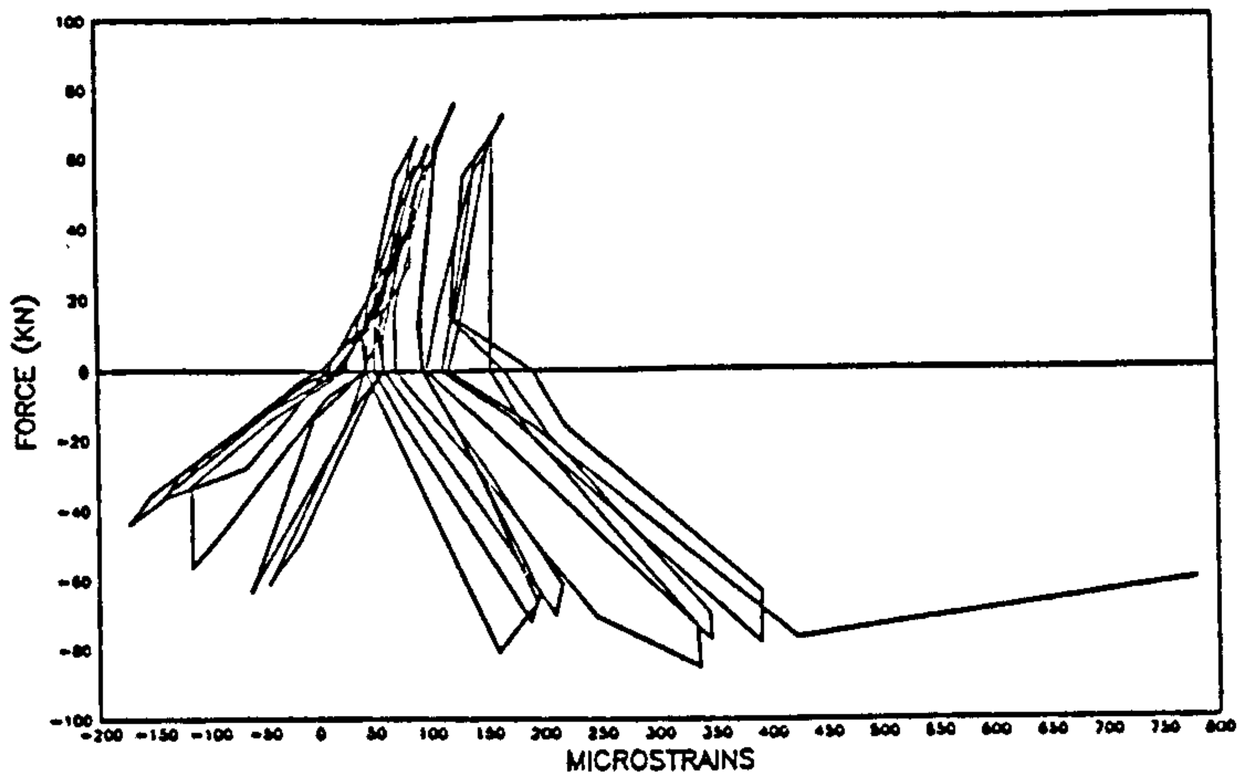


Figure B(15)26 Wall SW15 - force versus strain 22
(confinement reinforcement)

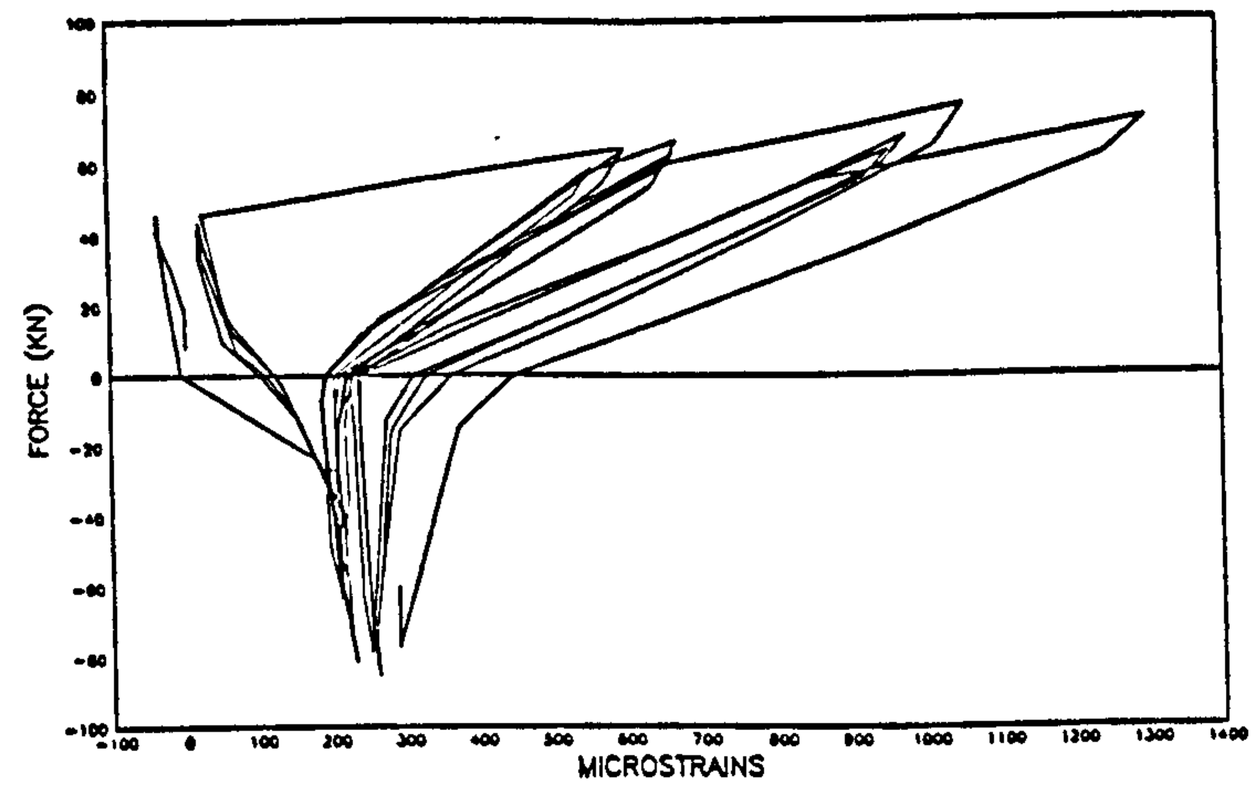


Figure B(15)27 Wall SW15 - force versus strain 23
(confinement reinforcement)

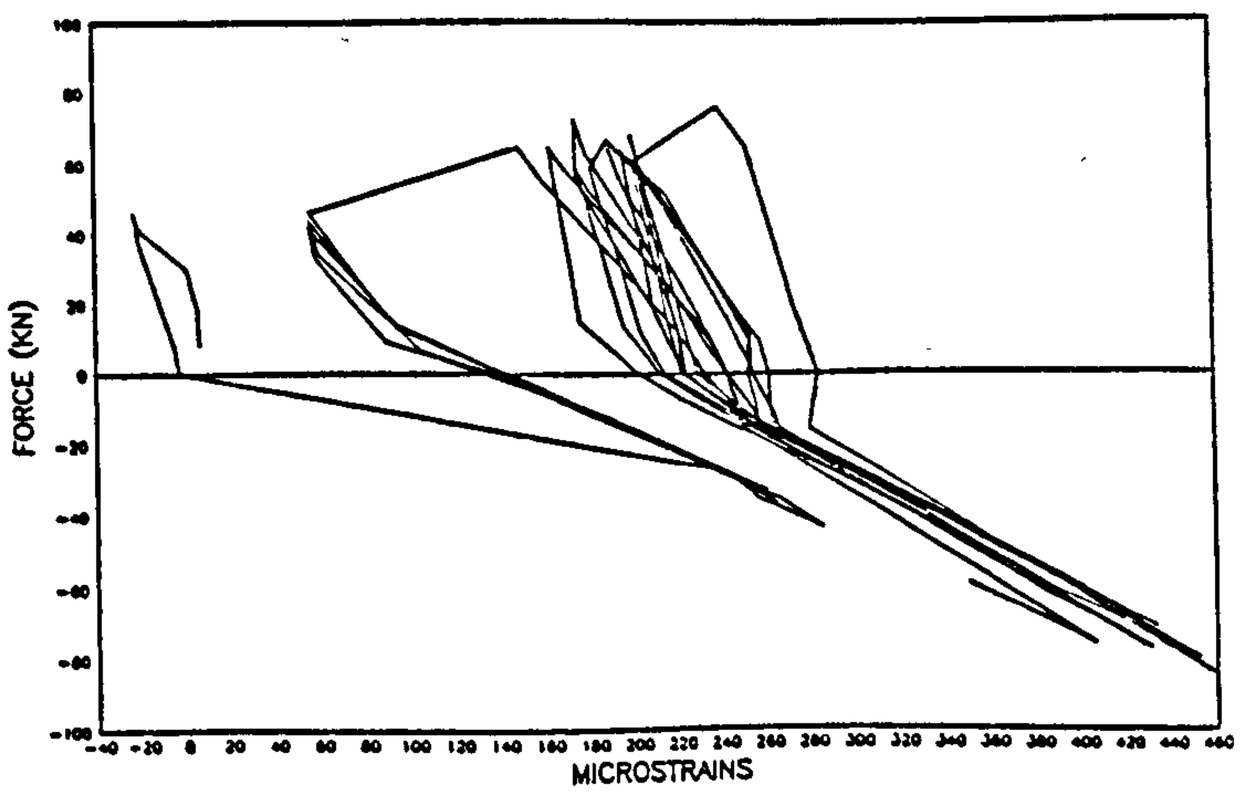


Figure B(15)28 Wall SW15 - force versus strain 24
(confinement reinforcement)

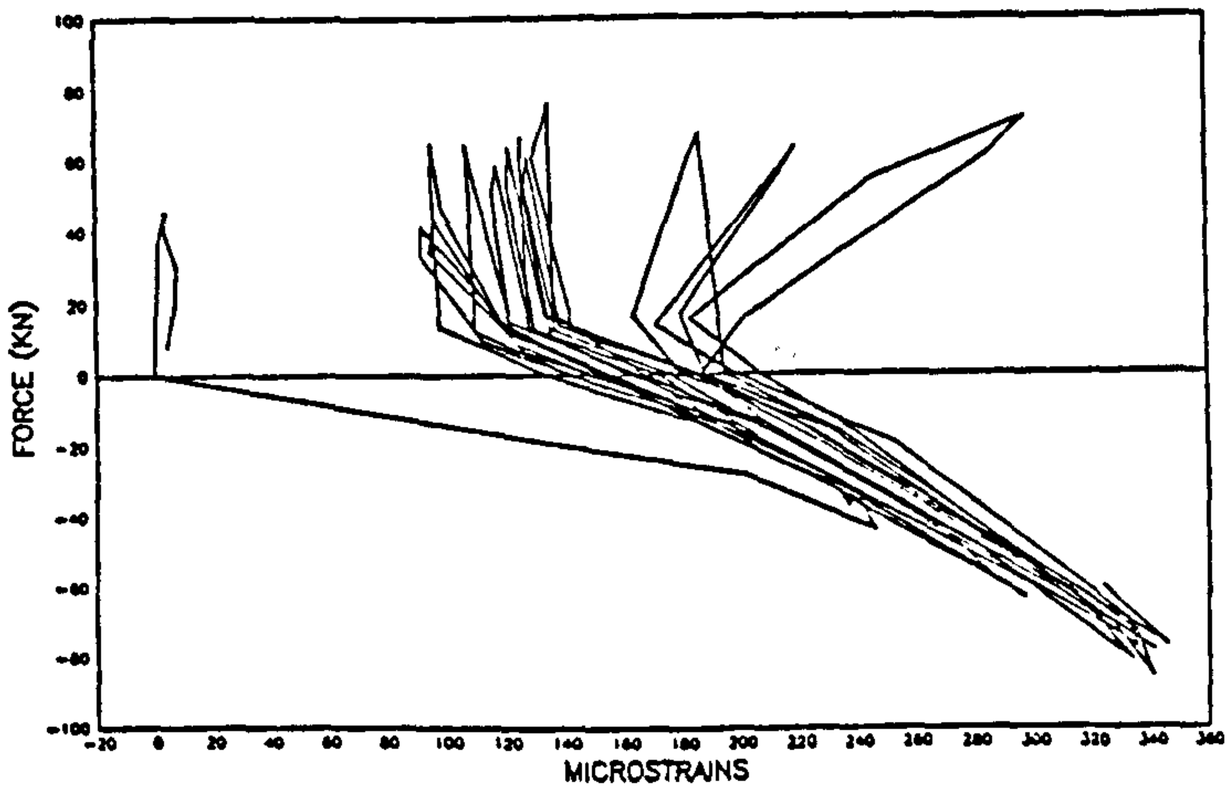


Figure B(15)29 Wall SW15 - force versus strain 25 (confinement reinforcement)

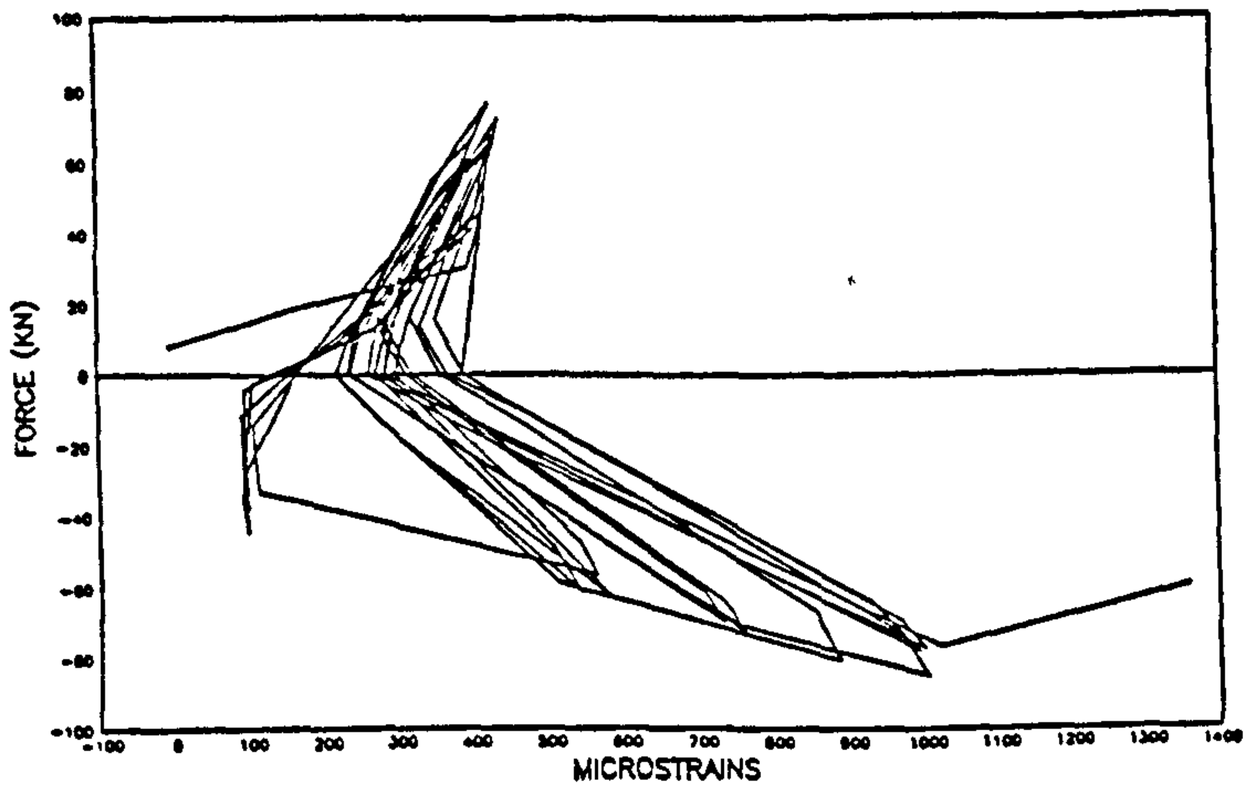


Figure B(15)30 Wall SW15 - force versus strain 26 (confinement reinforcement)

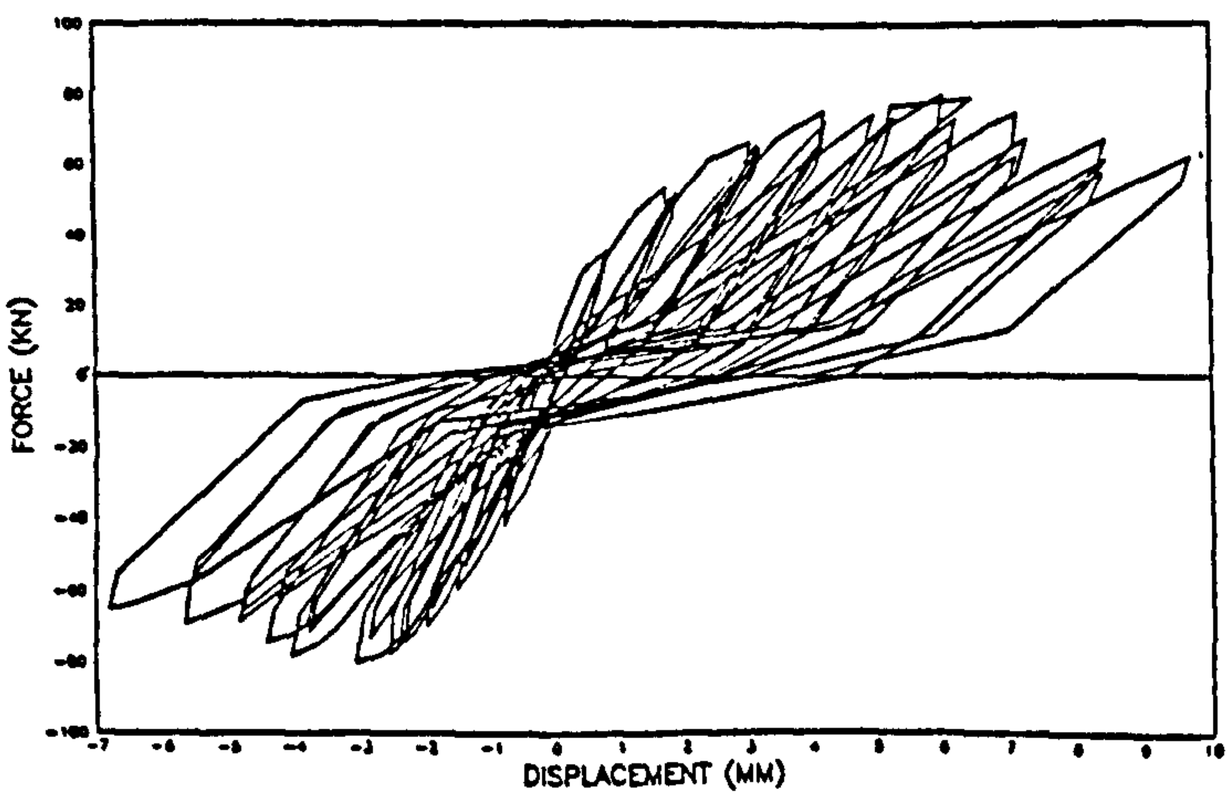


Figure B(16)1 Wall SW16 - force versus displacement 1 (horizontal, LHS, level 4)

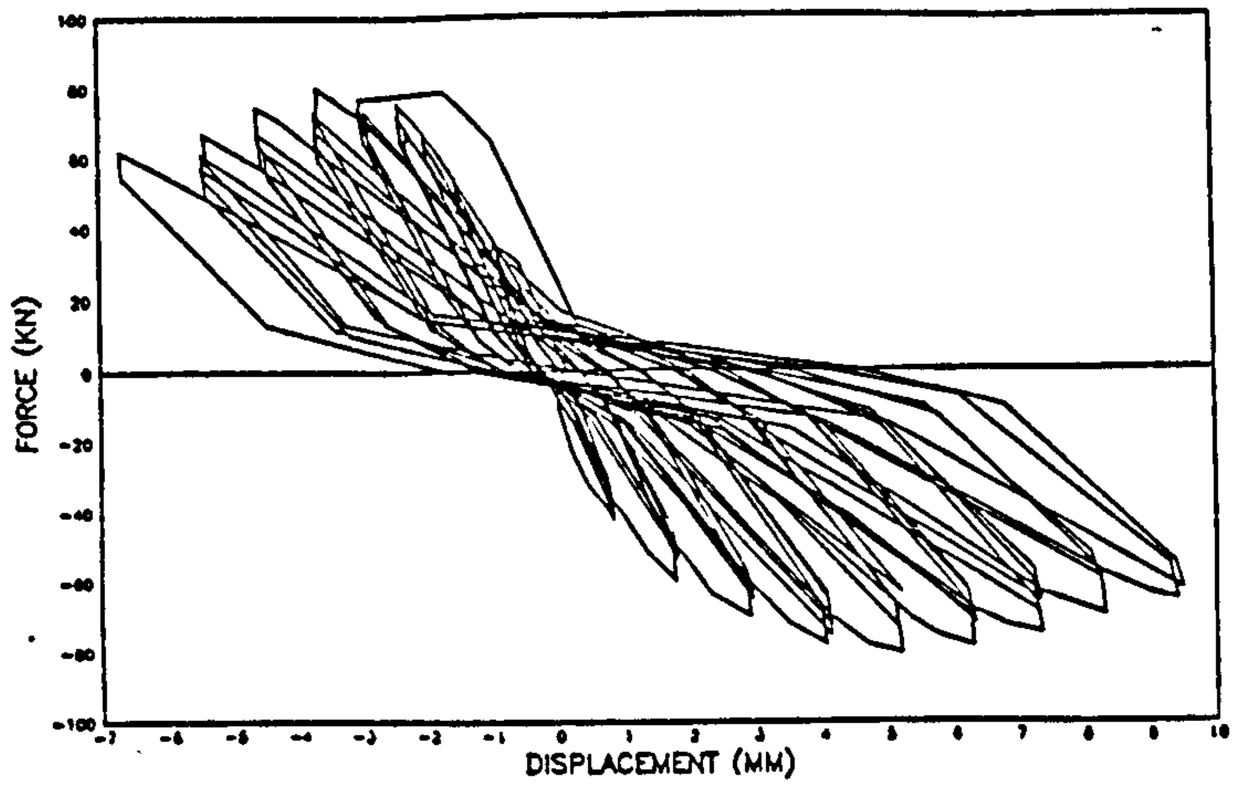


Figure B(16)2 Wall SW16 - force versus displacement 2
(horizontal, RHS, level 4)

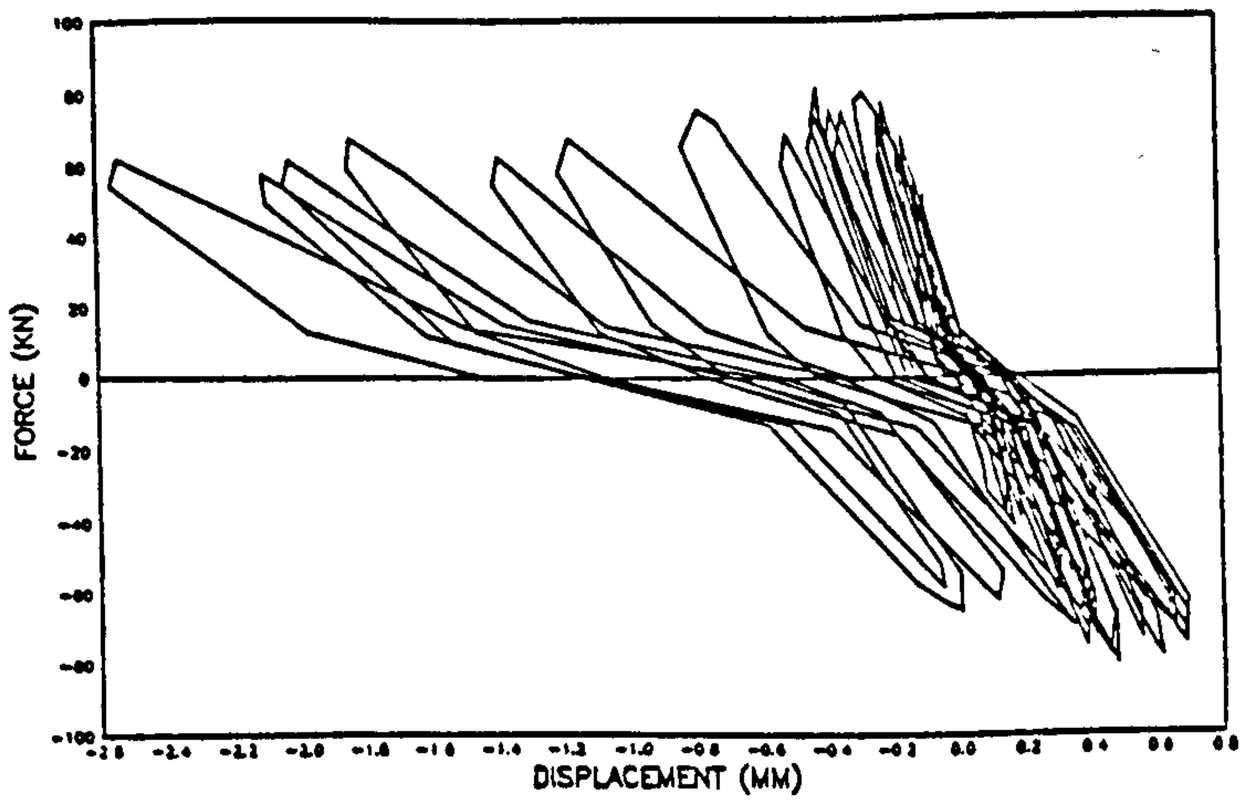


Figure B(16)3 Wall SW16 - force versus displacement 3
(vertical, LHS, level 1)

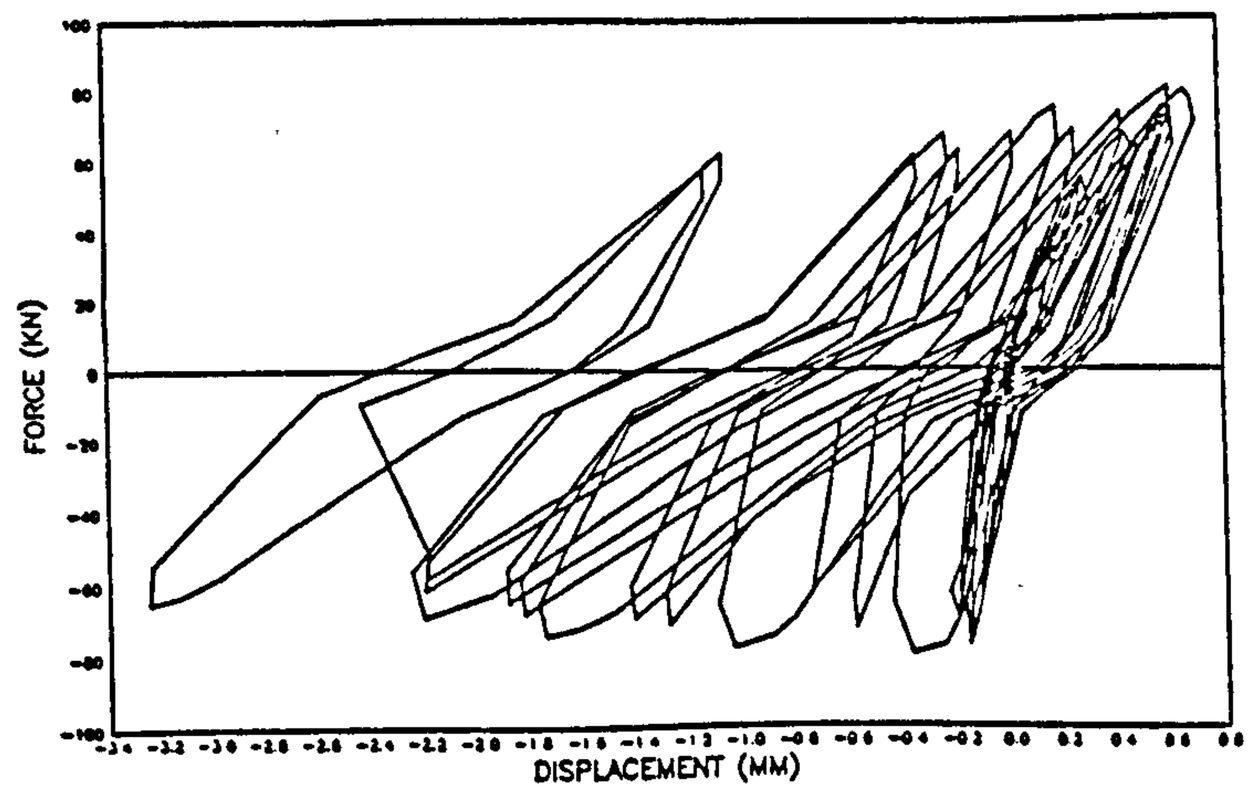


Figure B(16)4 Wall SW16 - force versus displacement 4
(vertical, RHS, level 1)

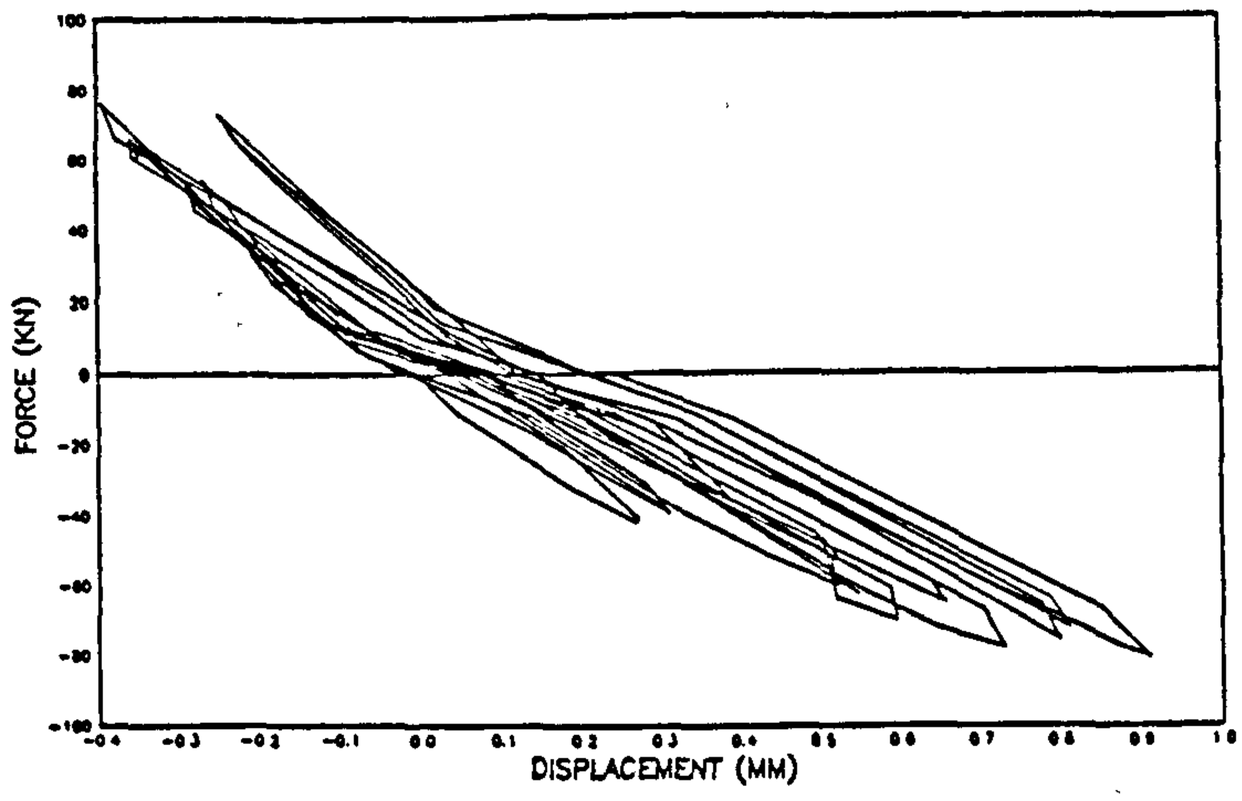


Figure B(16)5 Wall SW16 - force versus displacement 5 (vertical, LHS, level 2)

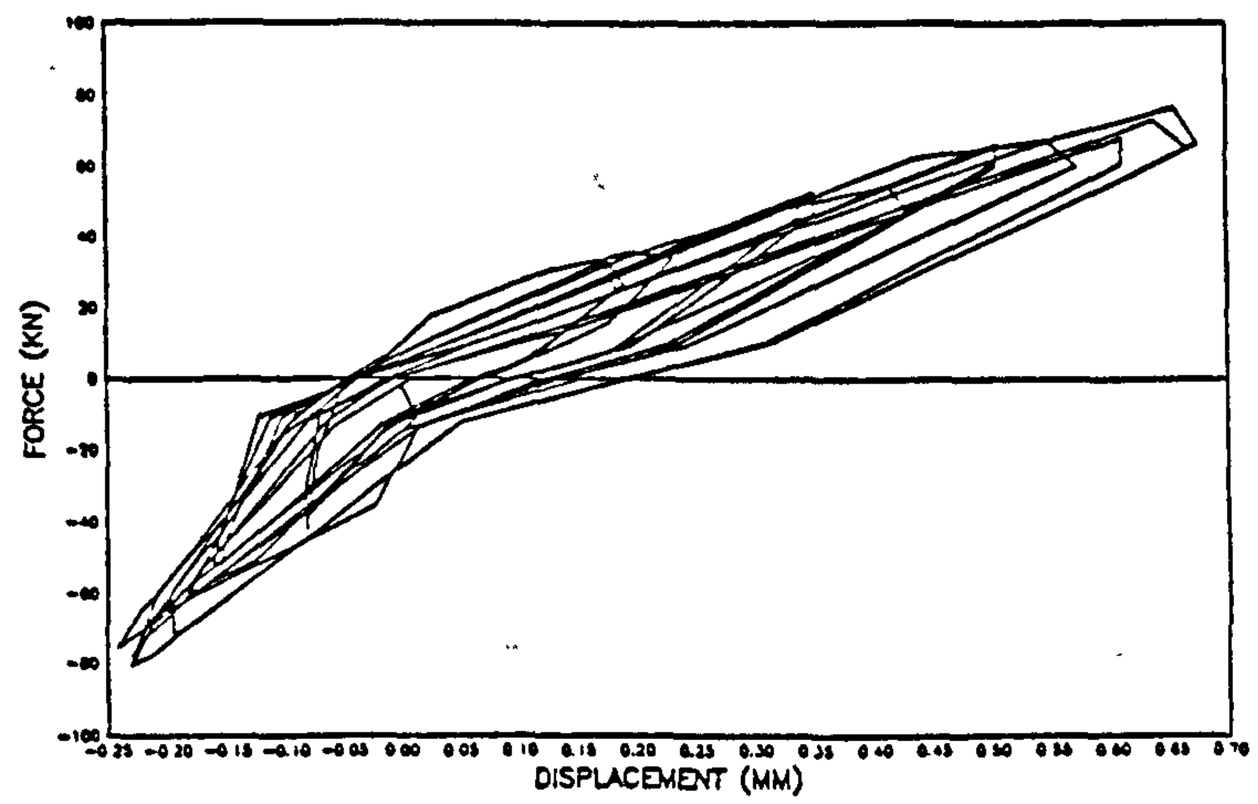


Figure B(16)6 Wall SW16 - force versus displacement 6 (vertical, RHS, level 2)

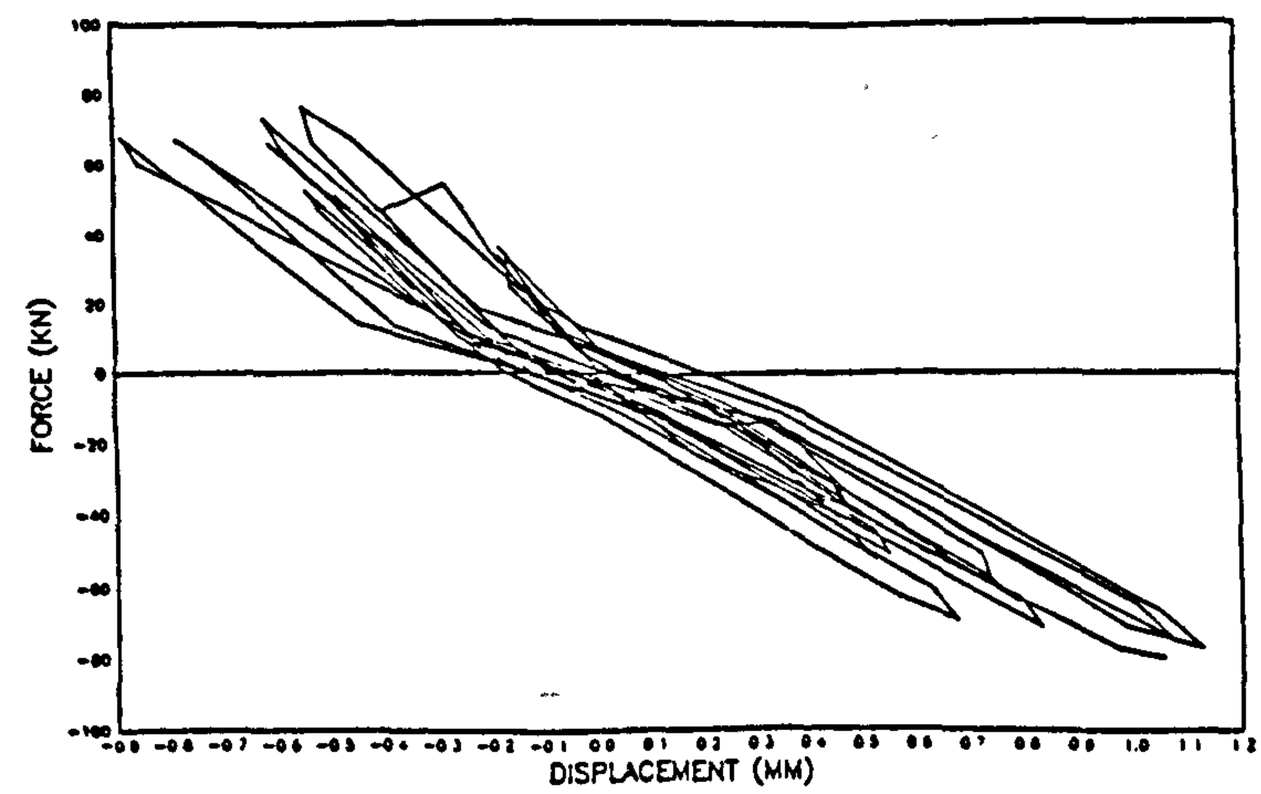


Figure B(16)7 Wall SW16 - force versus displacement 7 (vertical, LHS, level 3)

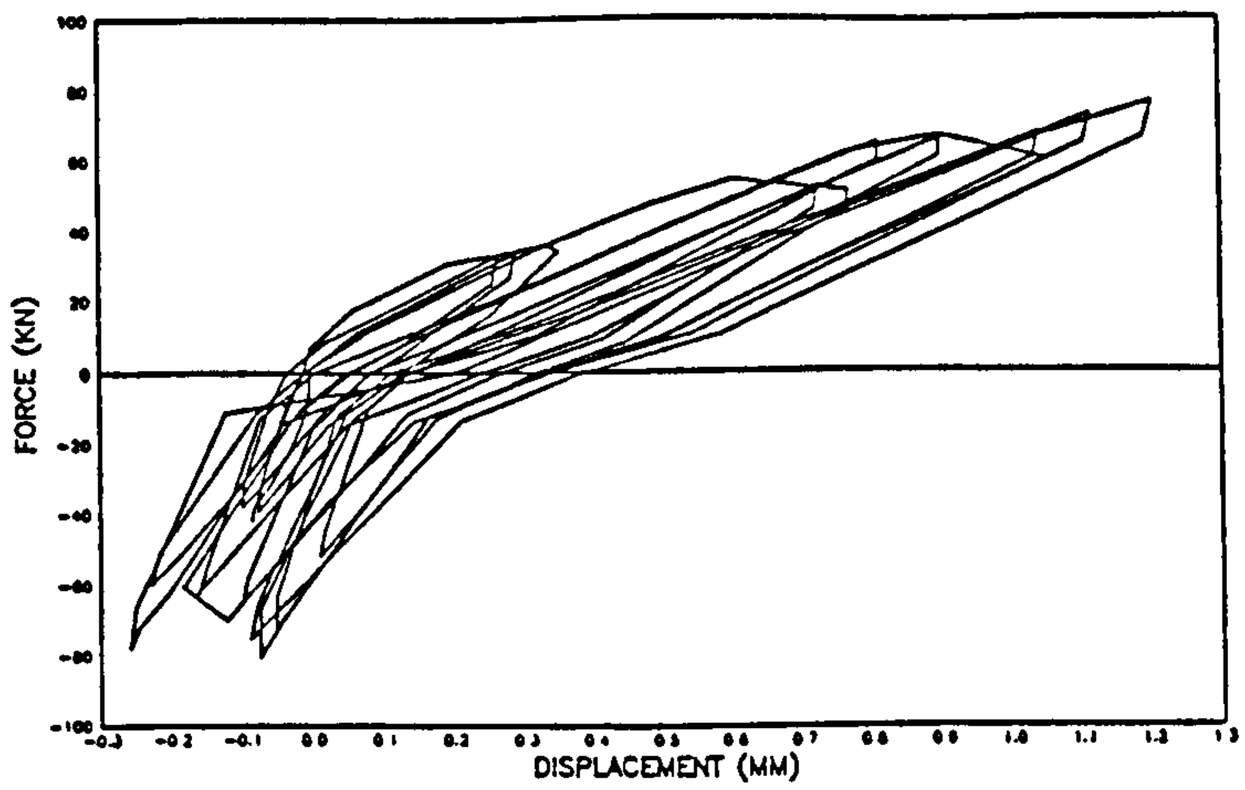


Figure B(16)8 Wall SW16 - force versus displacement 8
(vertical, RHS, level 3)

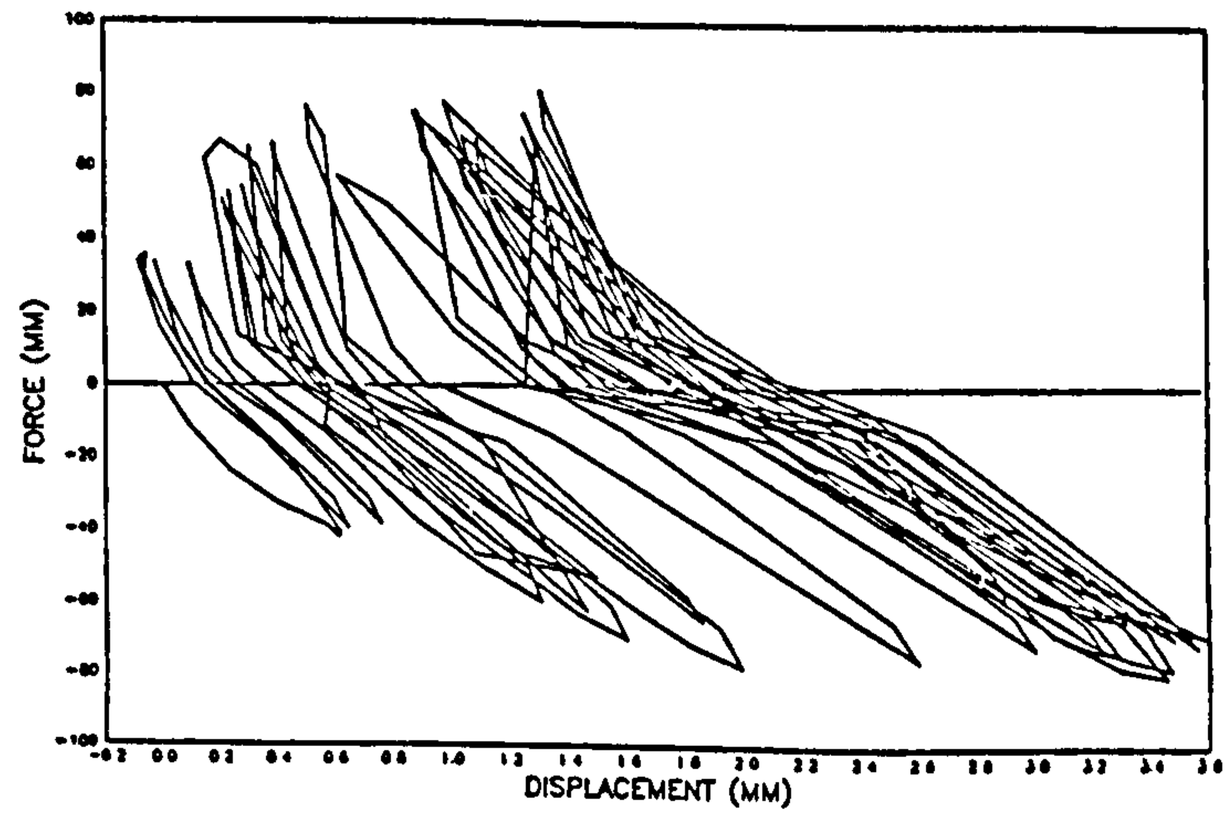


Figure B(16)9 Wall SW16 - force versus displacement 9
(vertical, LHS, level 4)

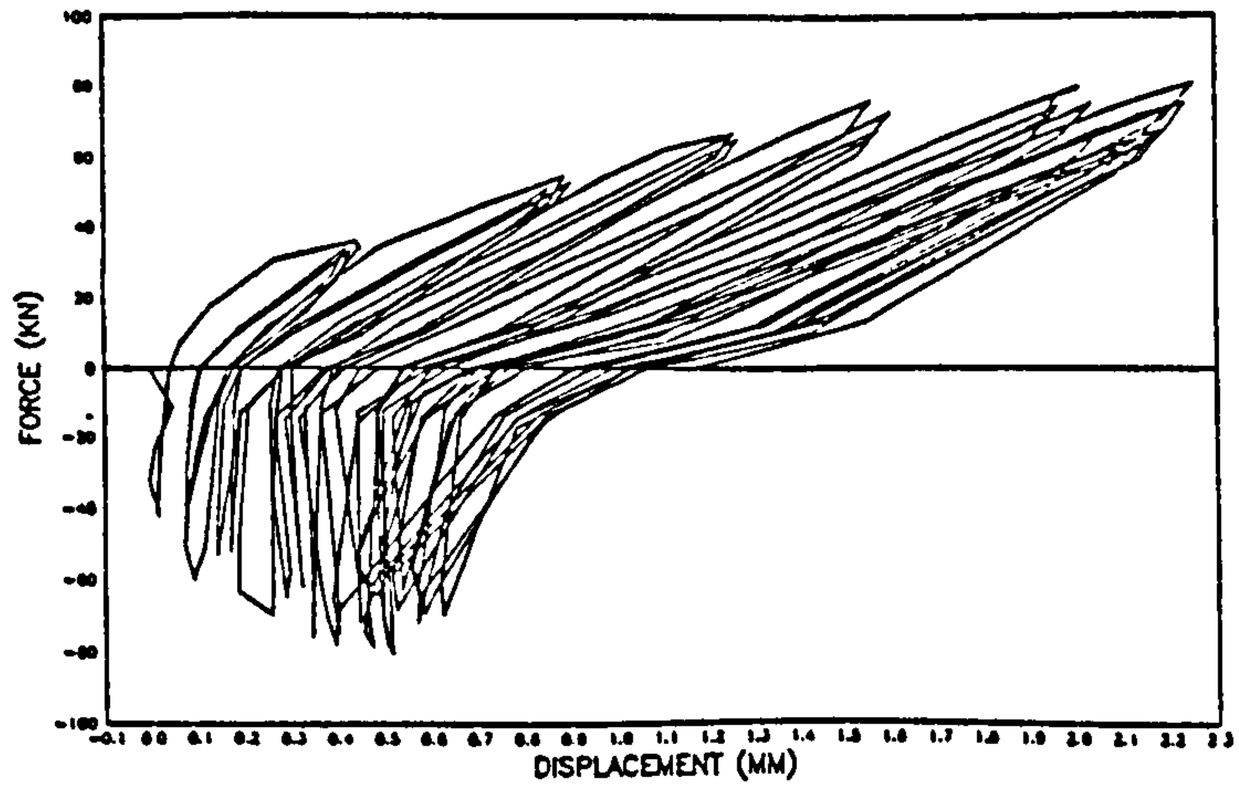


Figure B(16)10 Wall SW16 - force versus displacement 10
(vertical, RHS, level 4)

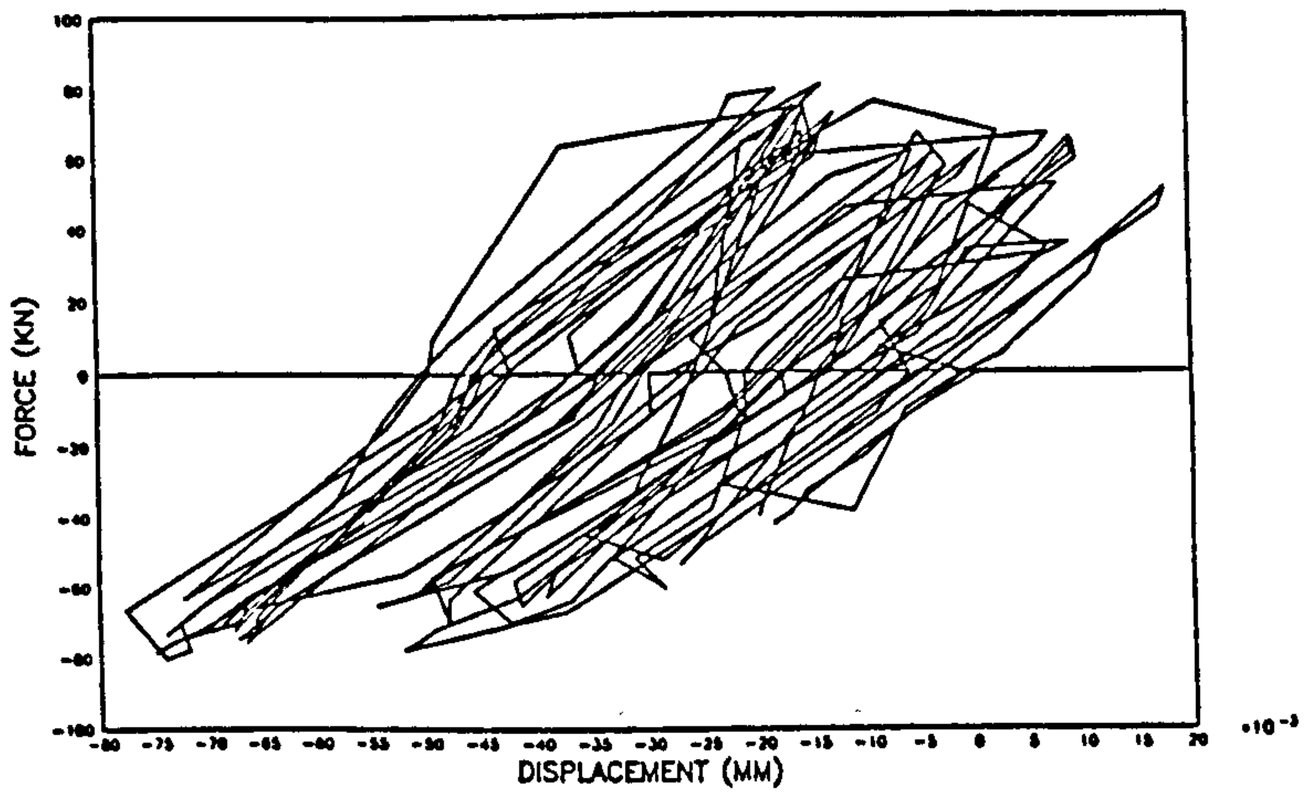


Figure B(16)11 Wall SW16 - force versus displacement 11 (foundation, RHS)

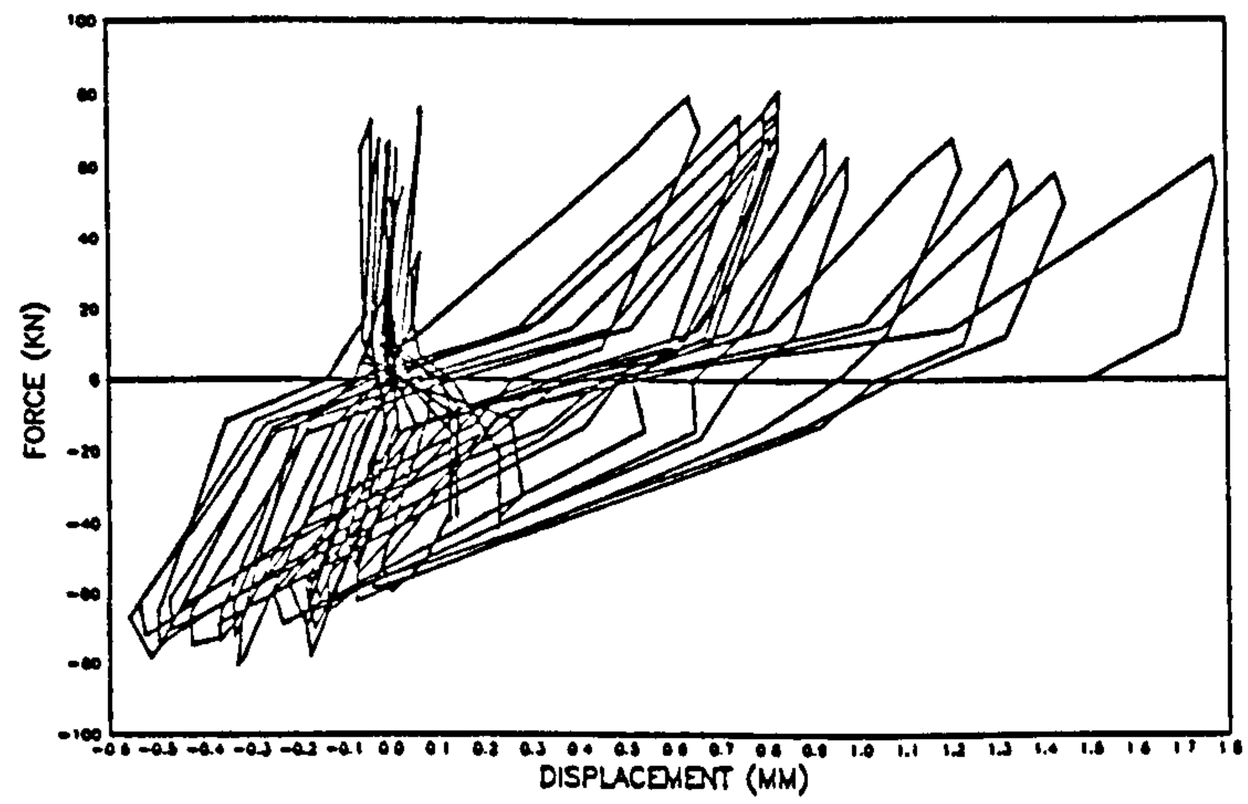


Figure B(16)12 Wall SW16 - force versus displacement 12 (out-of-plane)

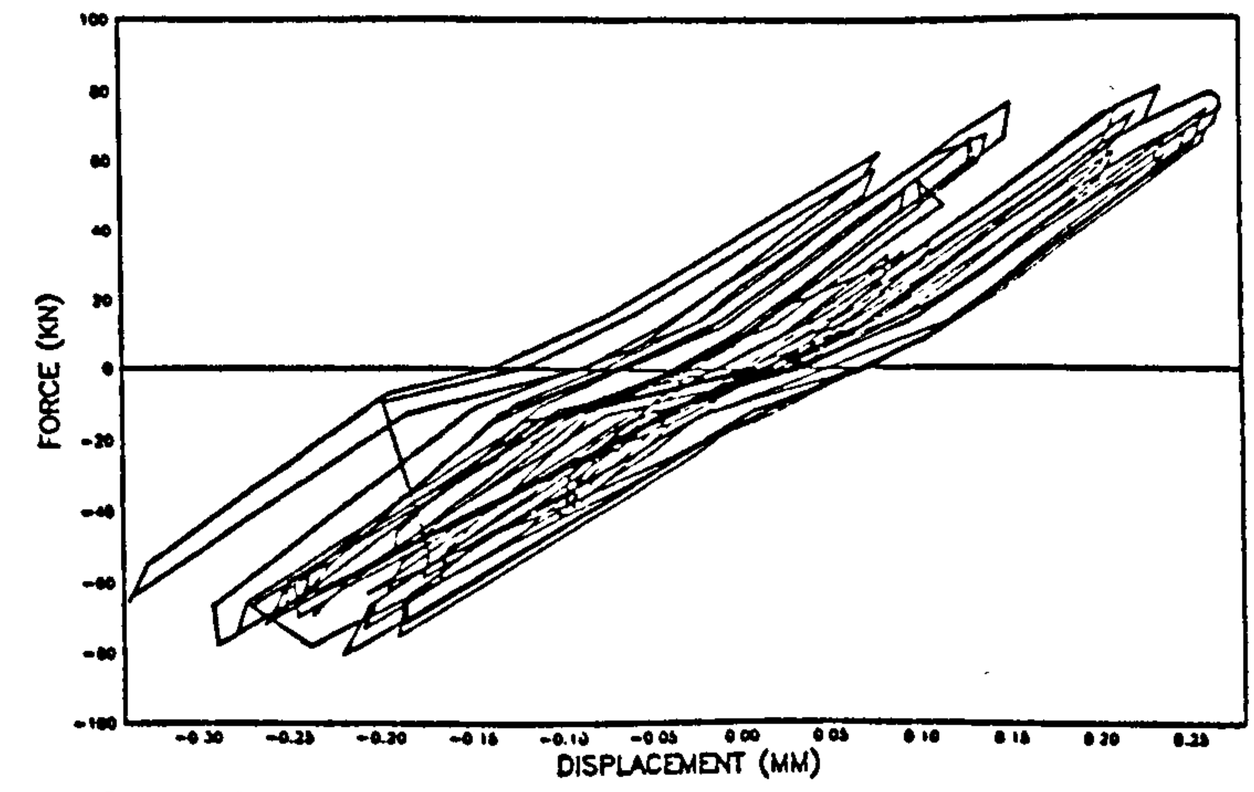


Figure B(16)13 Wall SW16 - force versus displacement 13 (horizontal, centre, level 1)

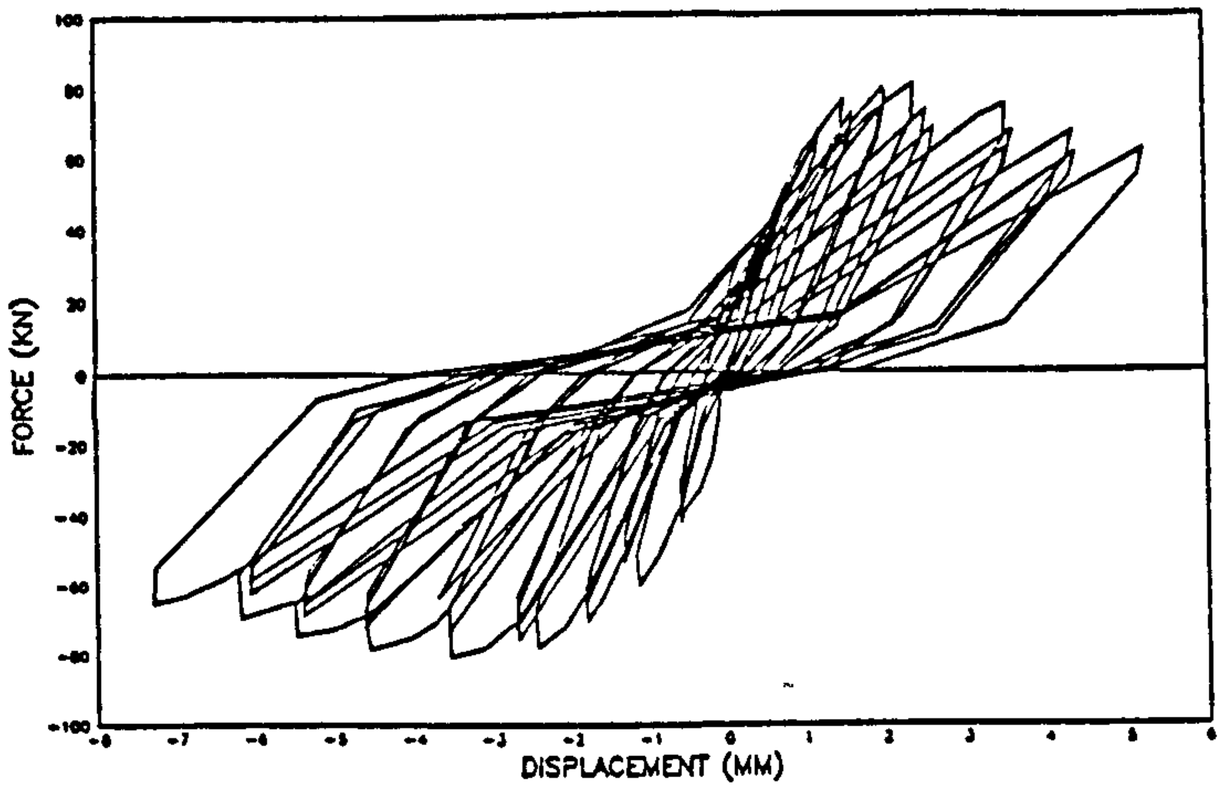


Figure B(16)14 Wall SW16 - force versus displacement 15 (horizontal, centre, level 3)

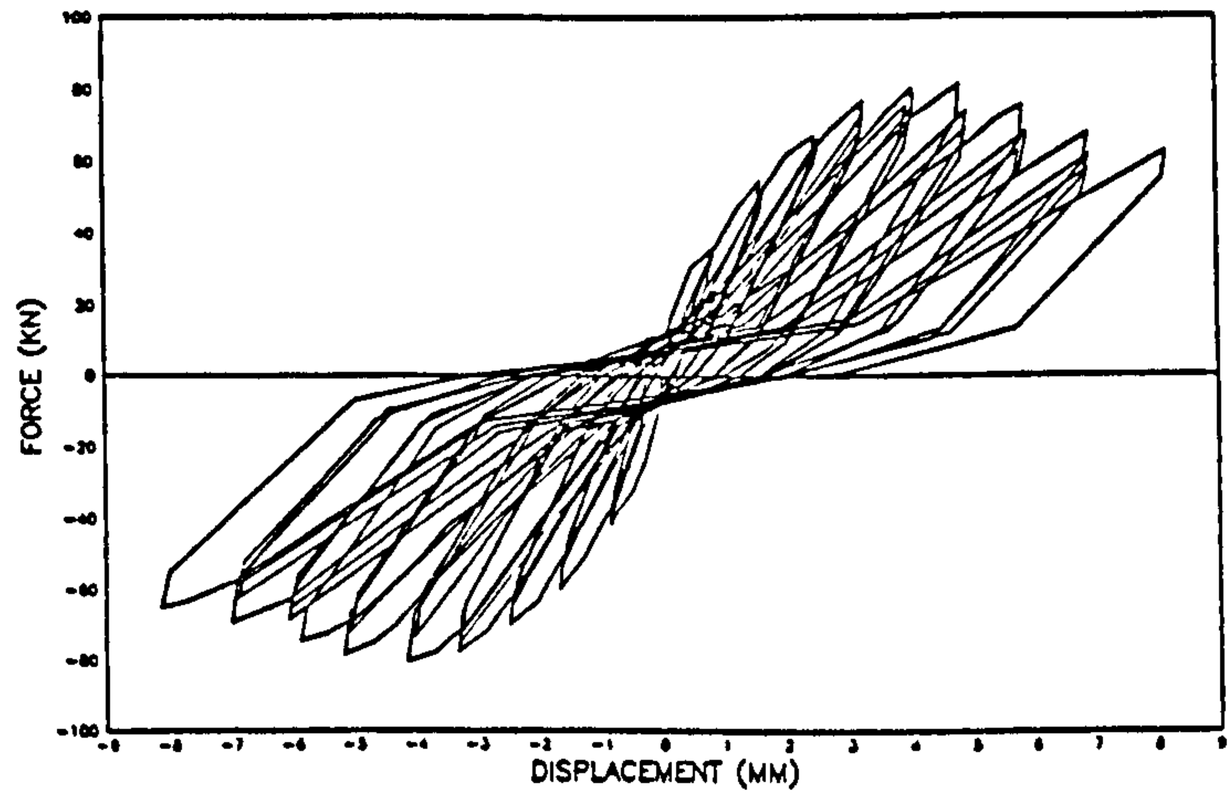


Figure B(16)15 Wall SW16 - force versus top horizontal displacement

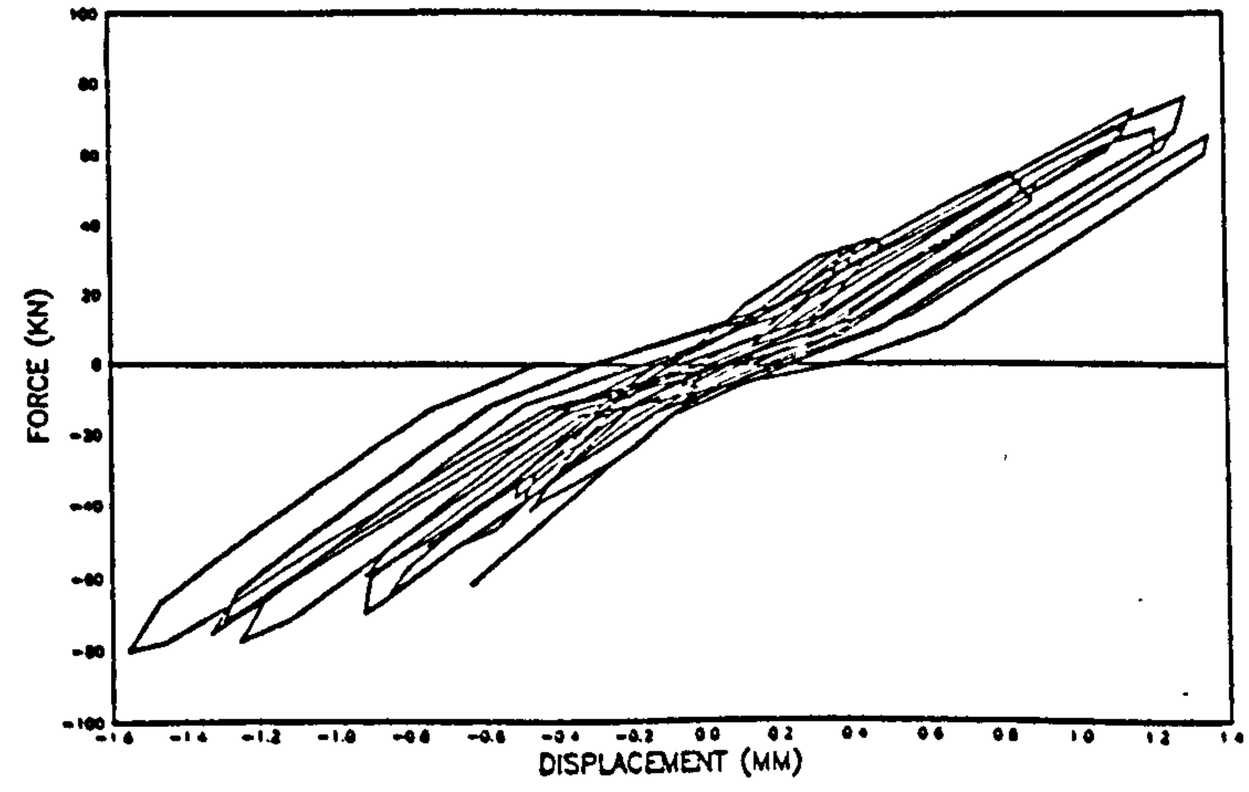


Figure B(16)16 Wall SW16 - force versus flexural component of top horizontal displacement

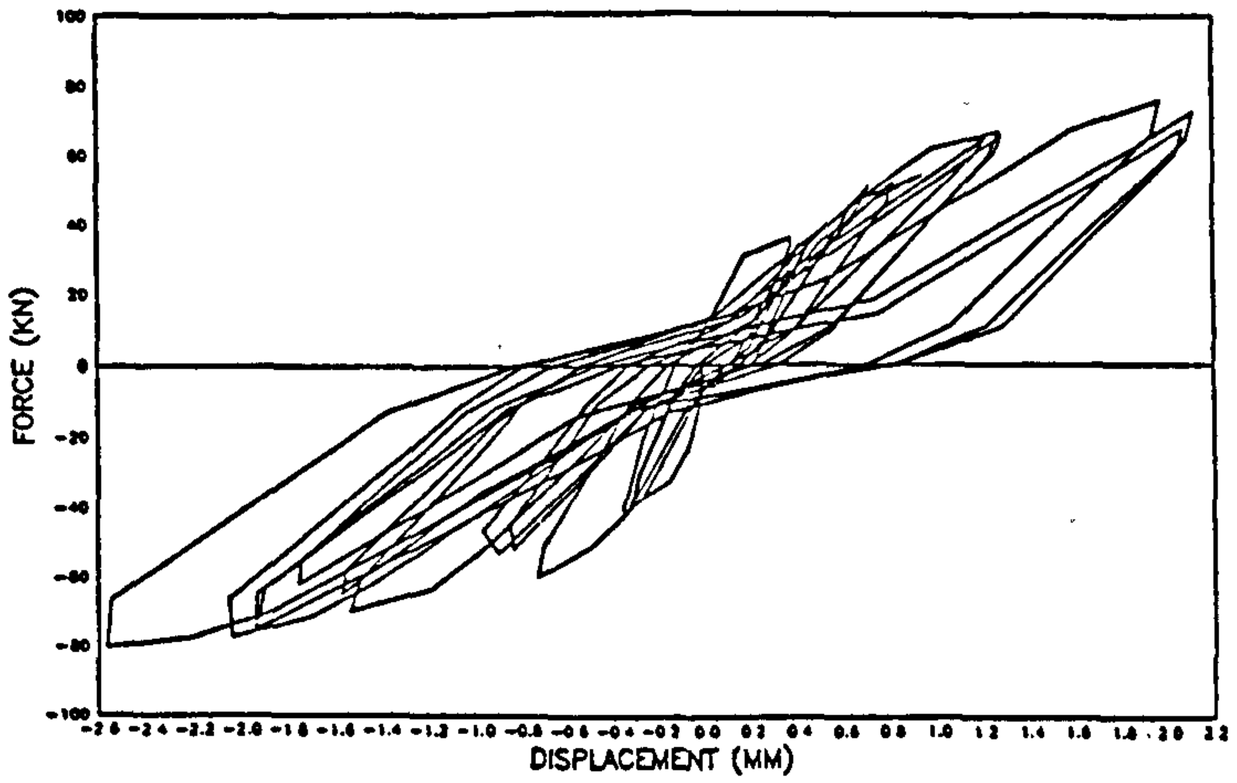


Figure B(16)17 Wall SW16 - force versus shear component of top horizontal displacement

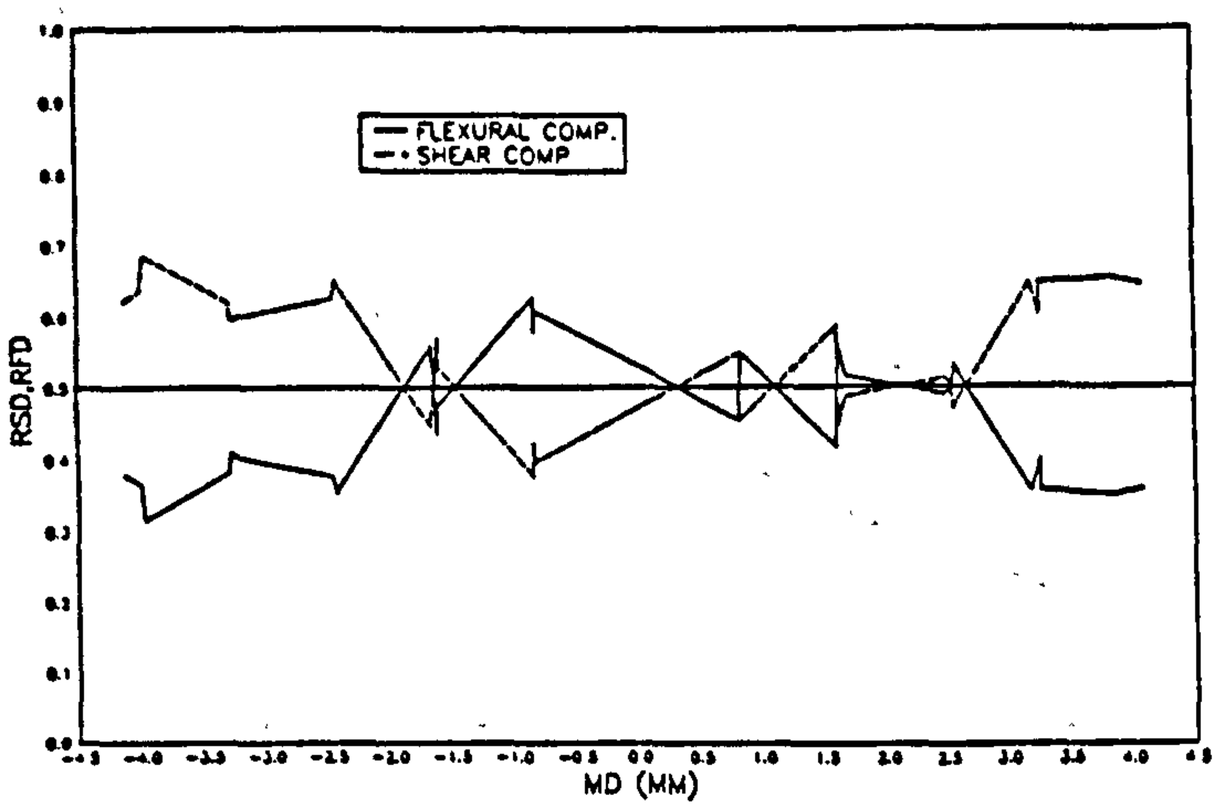


Figure B(16)18 Wall SW16 - RSD,RFD versus MD

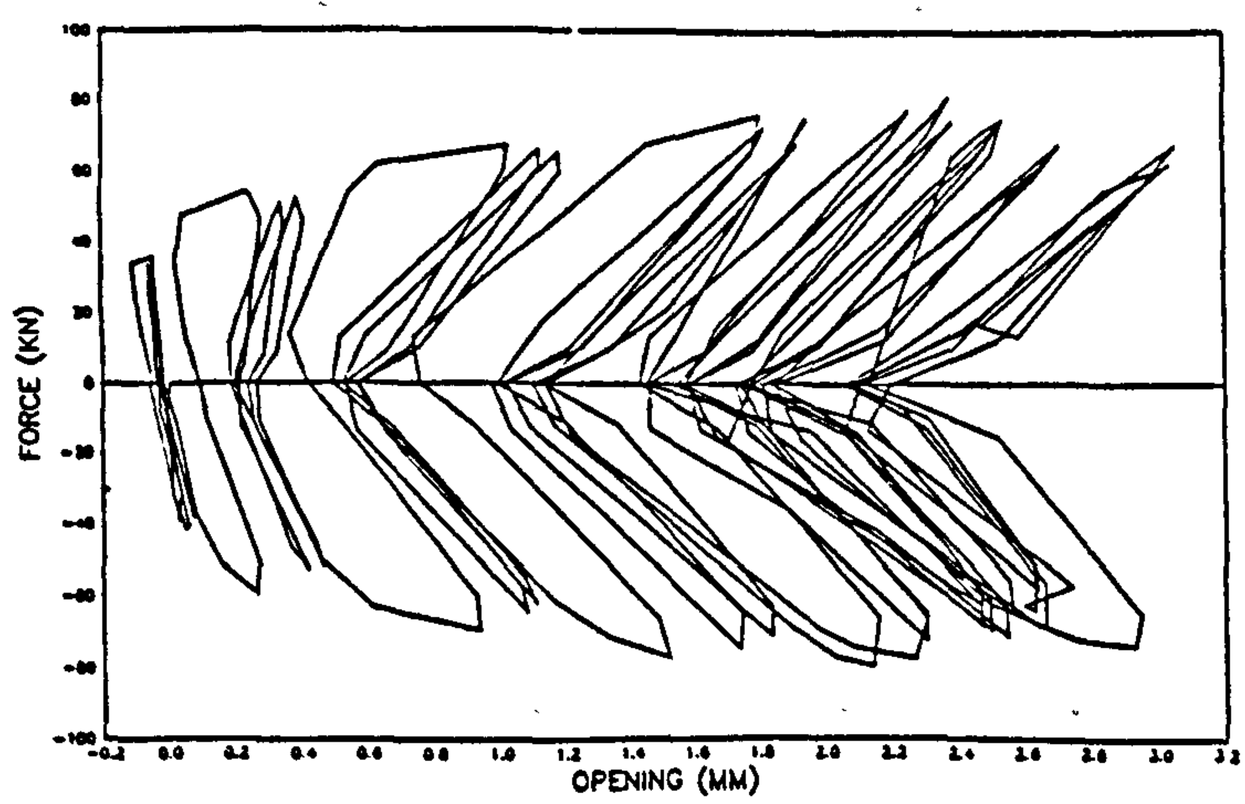


Figure B(16)19 Wall SW16 - force versus opening on top

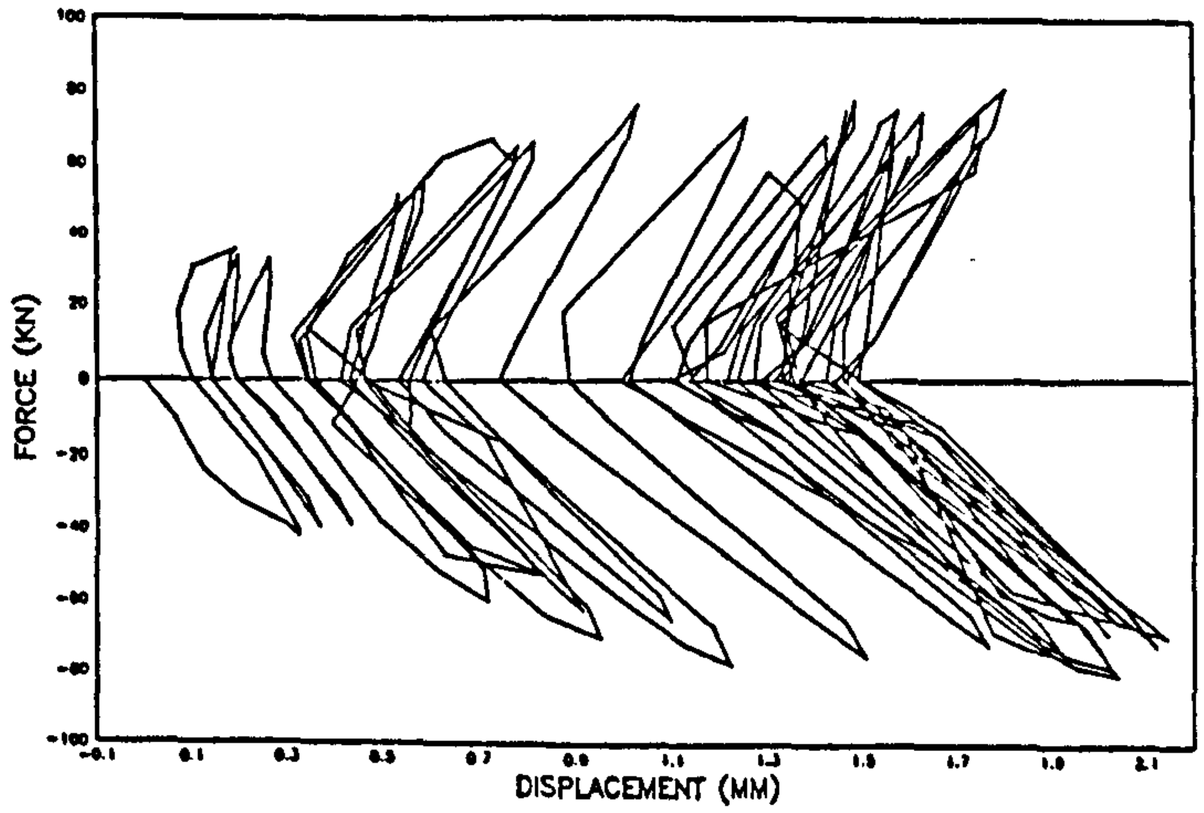


Figure B(16)20 Wall SW16 - force versus extension on top

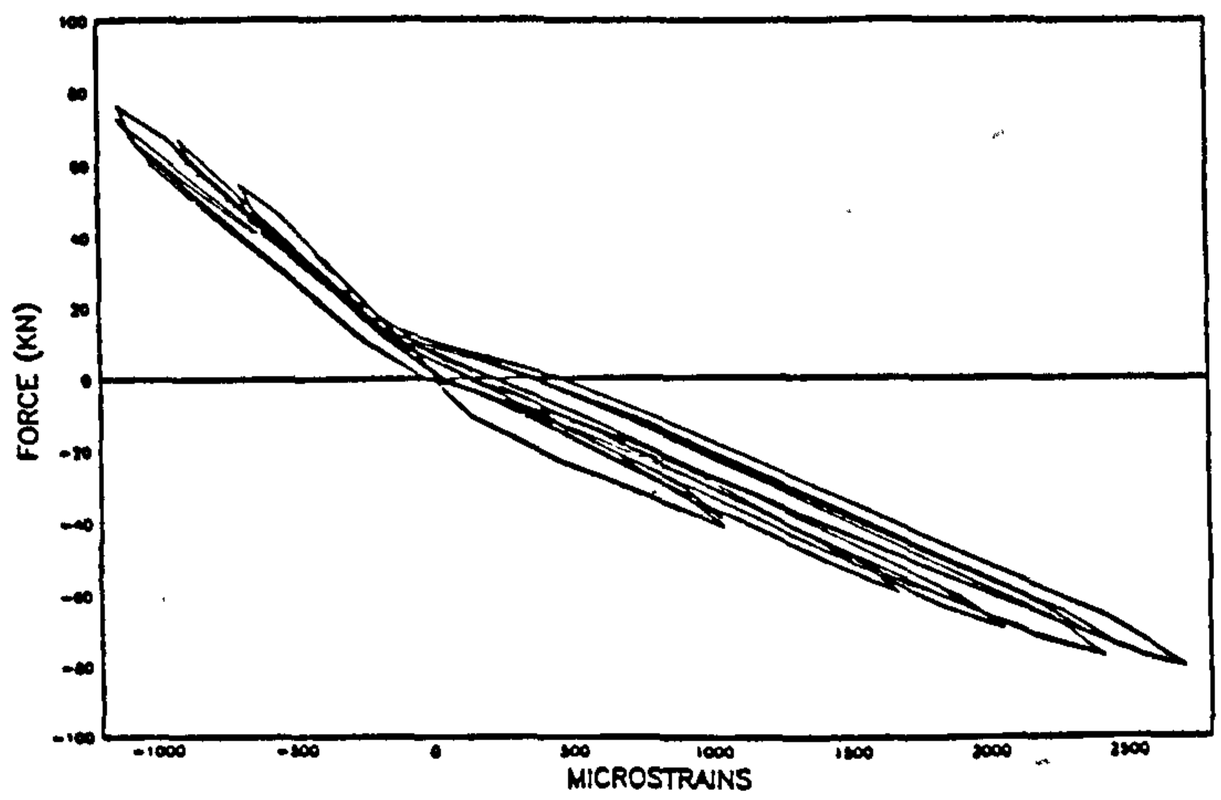


Figure B(16)21.a Wall SW16 - force versus strain 1; (bottom, ϕ8mm, LHS)

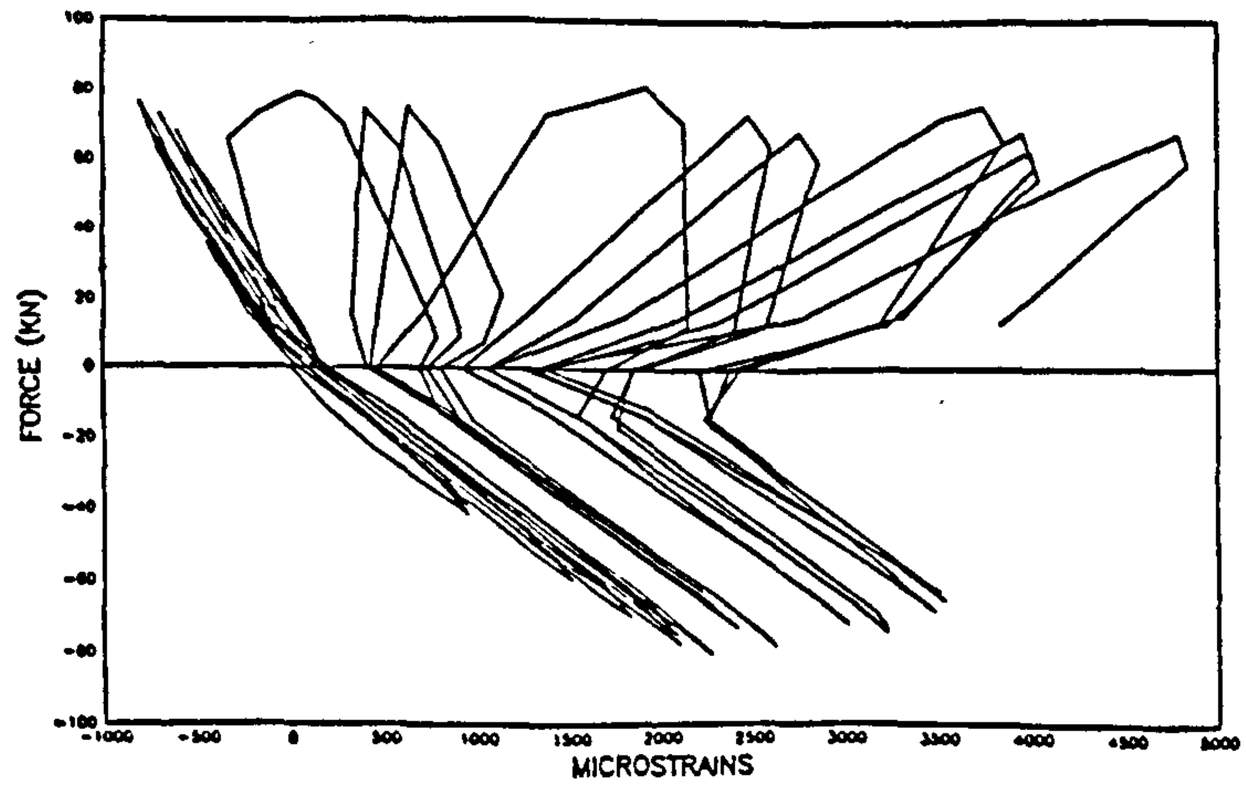


Figure B(16)21.b Wall SW16 - force versus strain 1; (bottom, ϕ8mm, LHS)

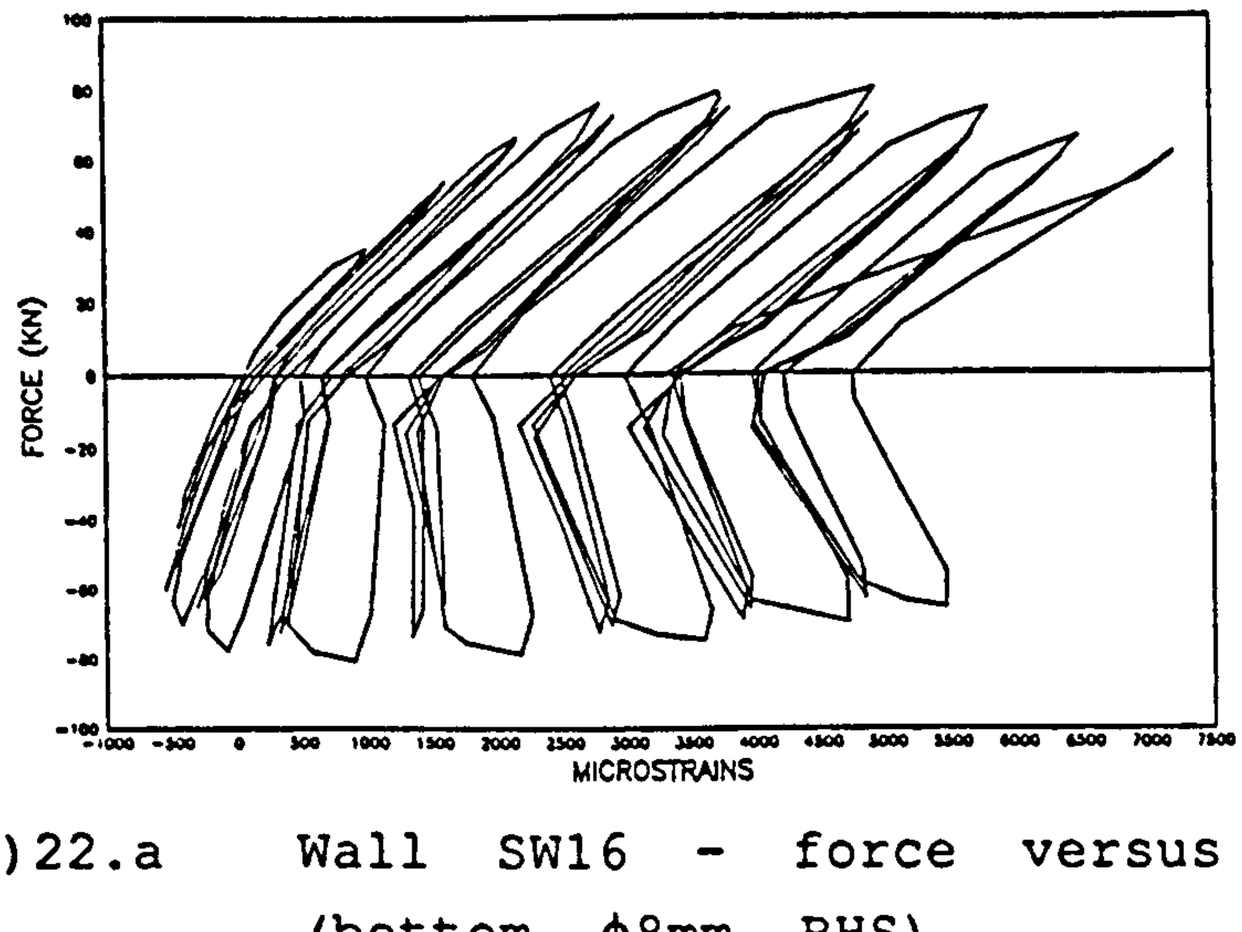


Figure B(16)22.a Wall SW16 - force versus strain 2_1 (bottom, ϕ8mm, RHS)

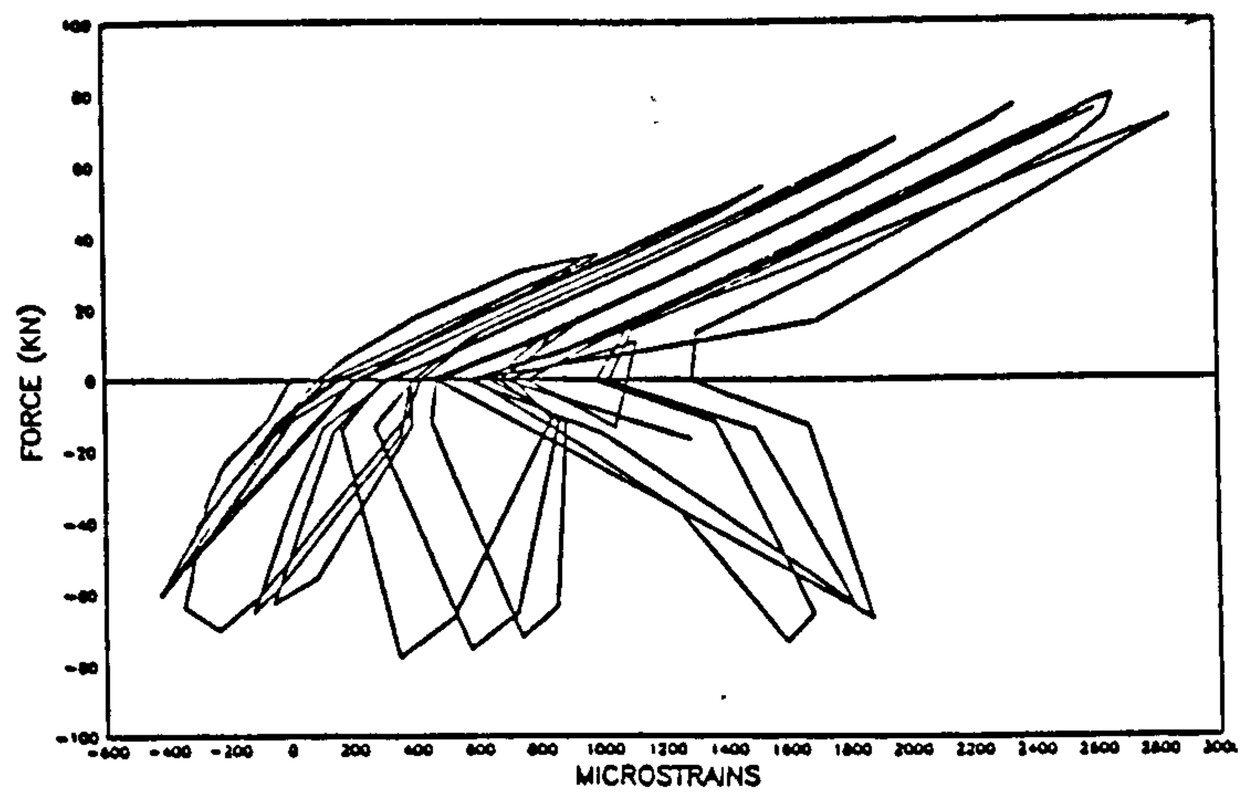


Figure B(16)22.b Wall SW16 - force versus strain 2_2 (bottom, ϕ8mm, RHS)

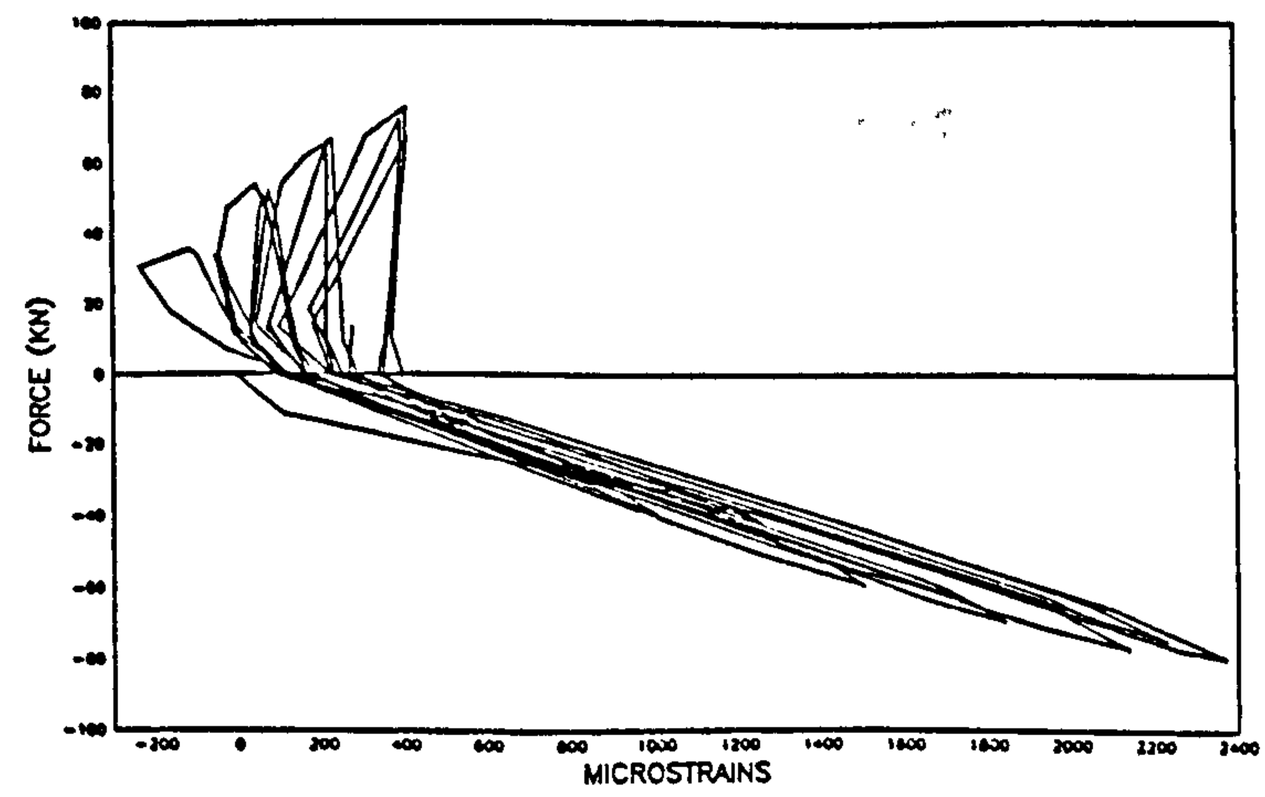


Figure B(16)23 Wall SW16 - force versus strain 5 (bottom, ϕ6mm, LHS)

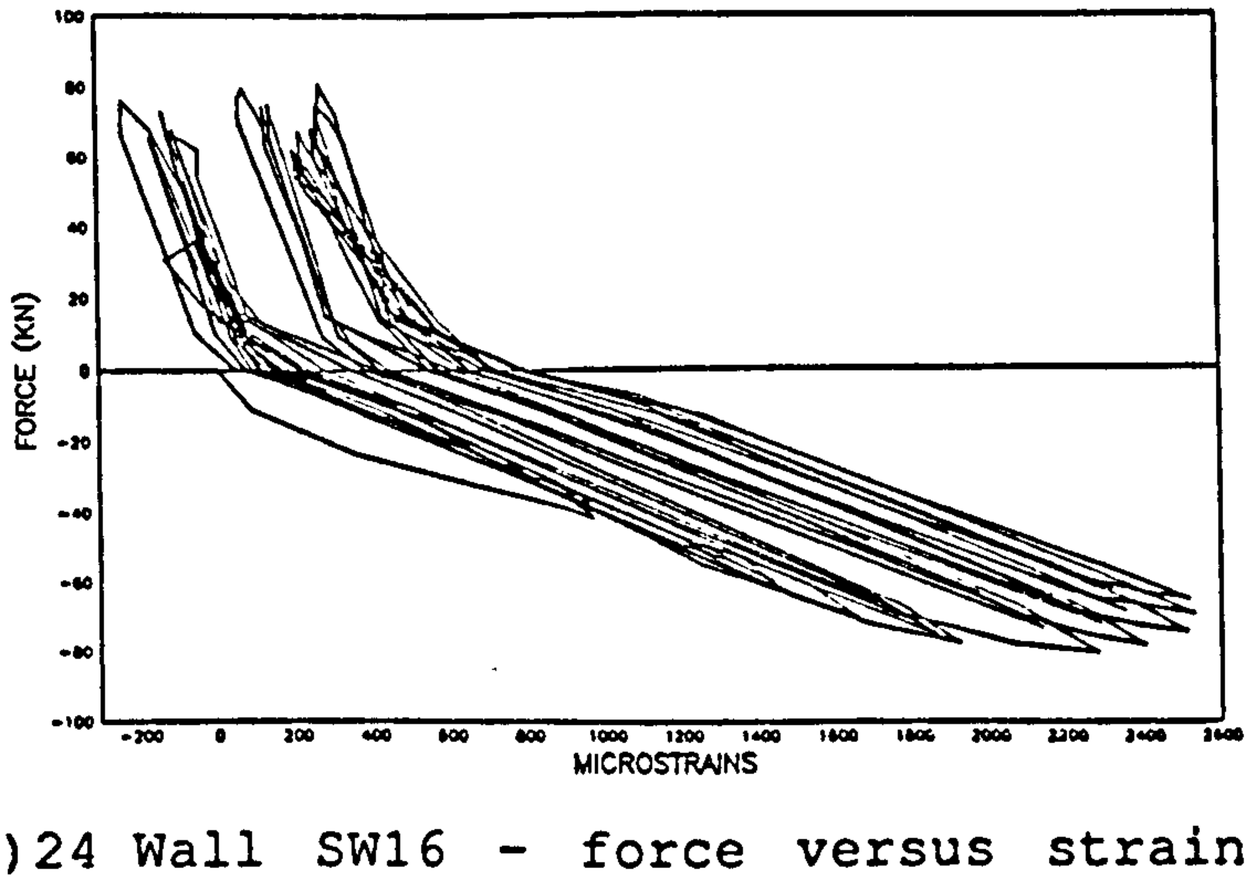


Figure B(16)24 Wall SW16 - force versus strain 9 (second level, ϕ8mm, LHS)

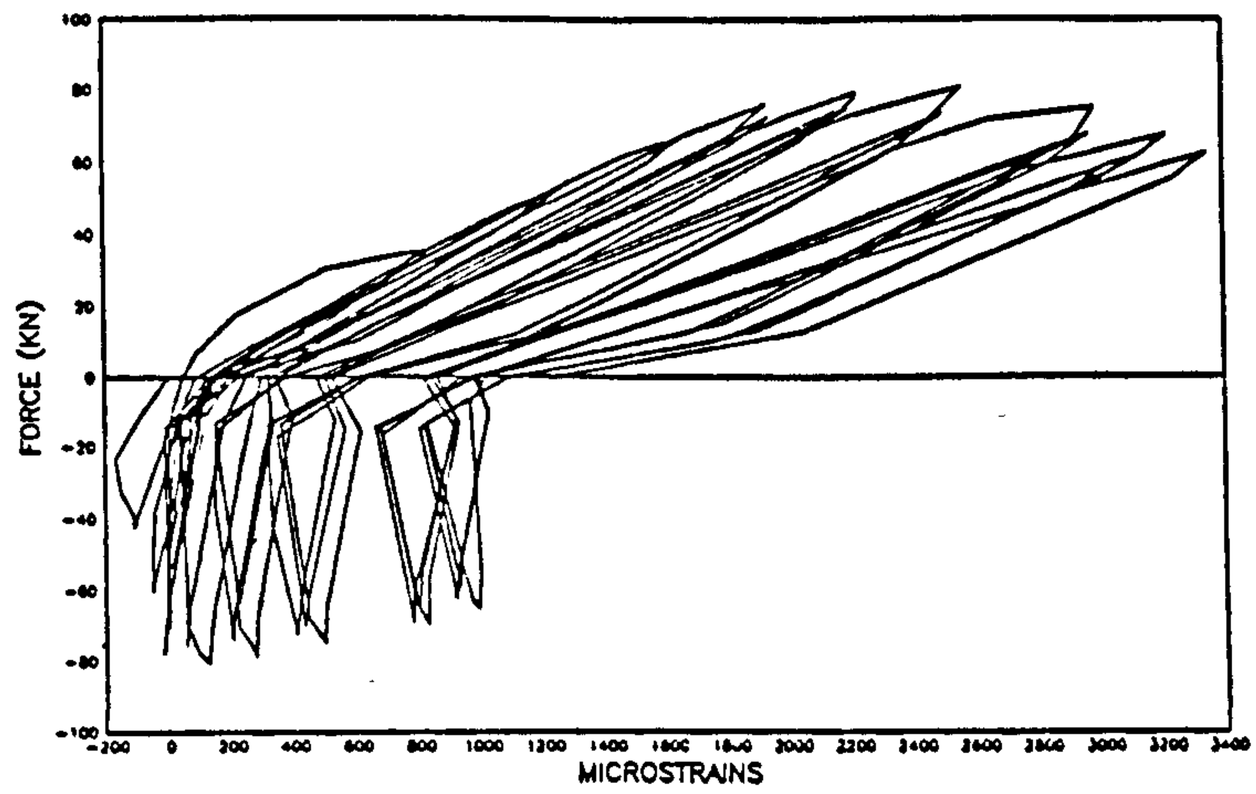


Figure B(16)25 Wall SW16 - force versus strain 10 (second level, ϕ8mm, RHS)

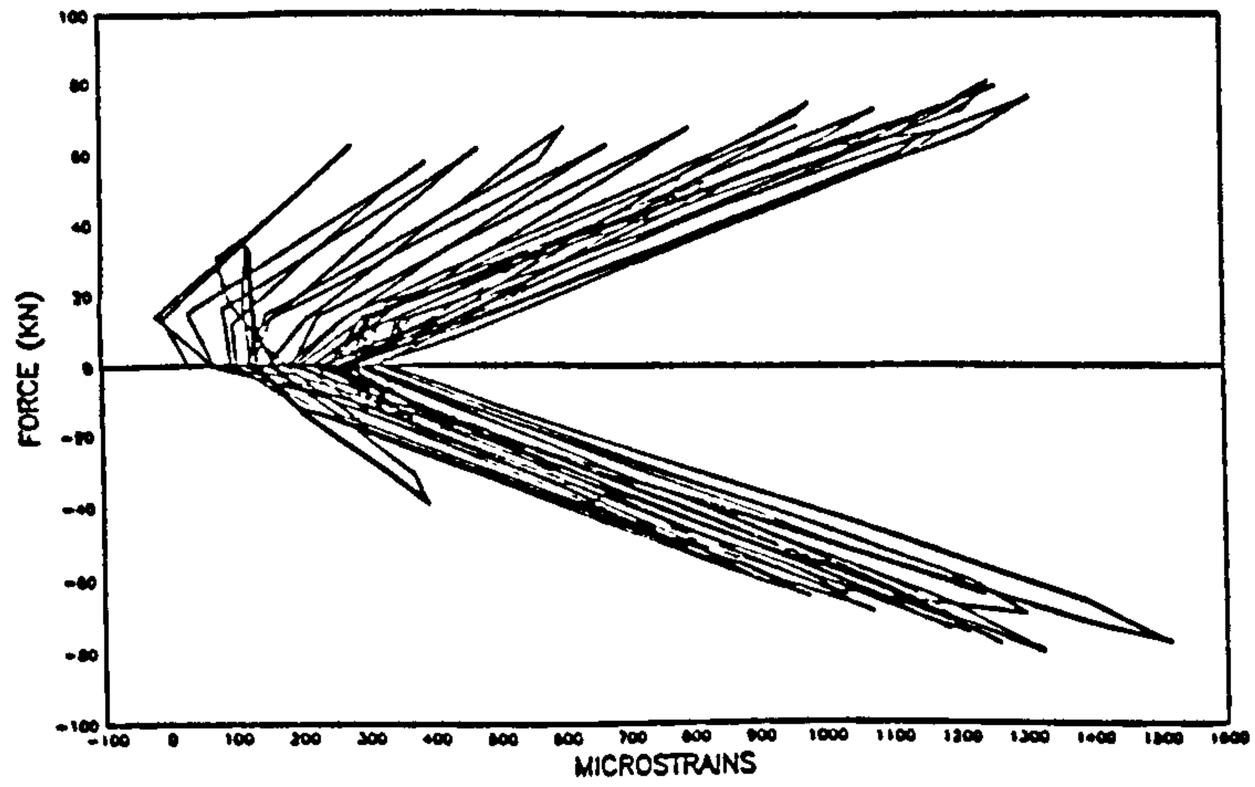


Figure B(16)26 Wall SW16 - force versus strain 12 (level of zero moment, ϕ8mm, RHS)

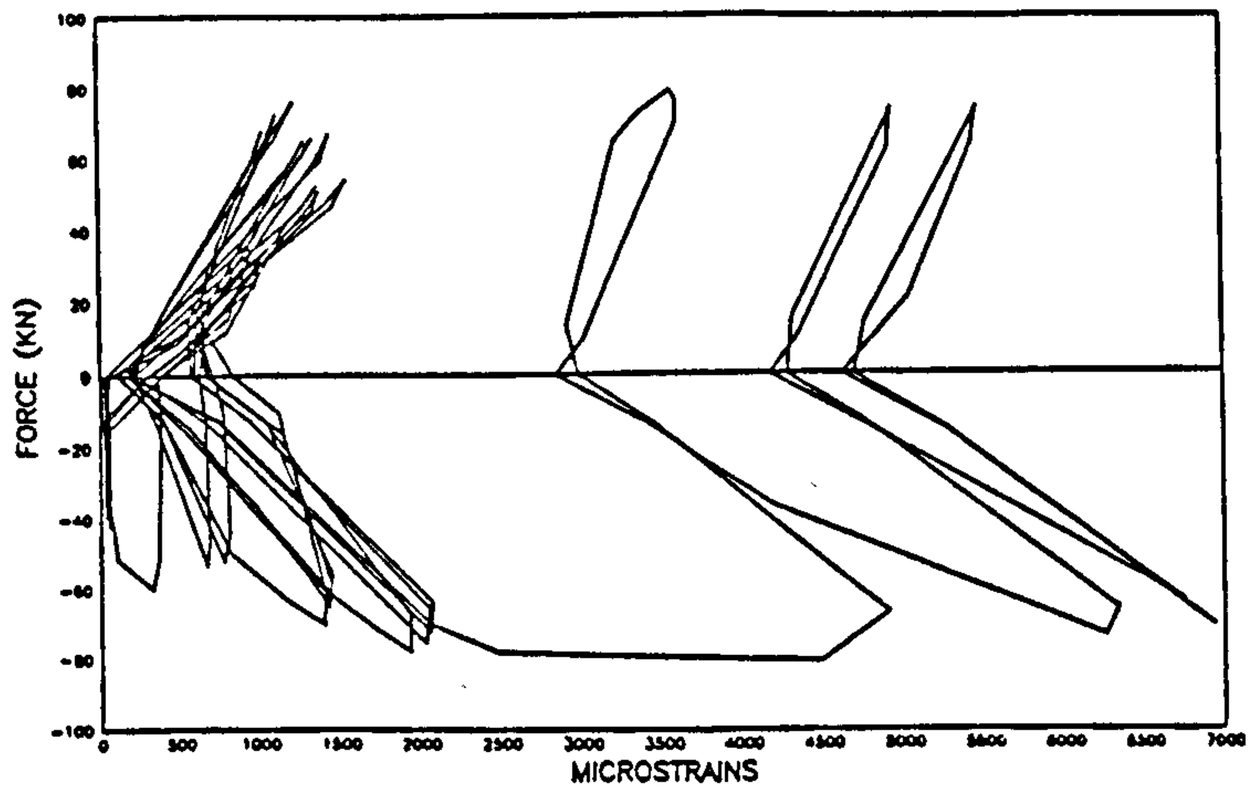


Figure B(16)27 Wall SW16 - force versus strain 19 (stirrup)

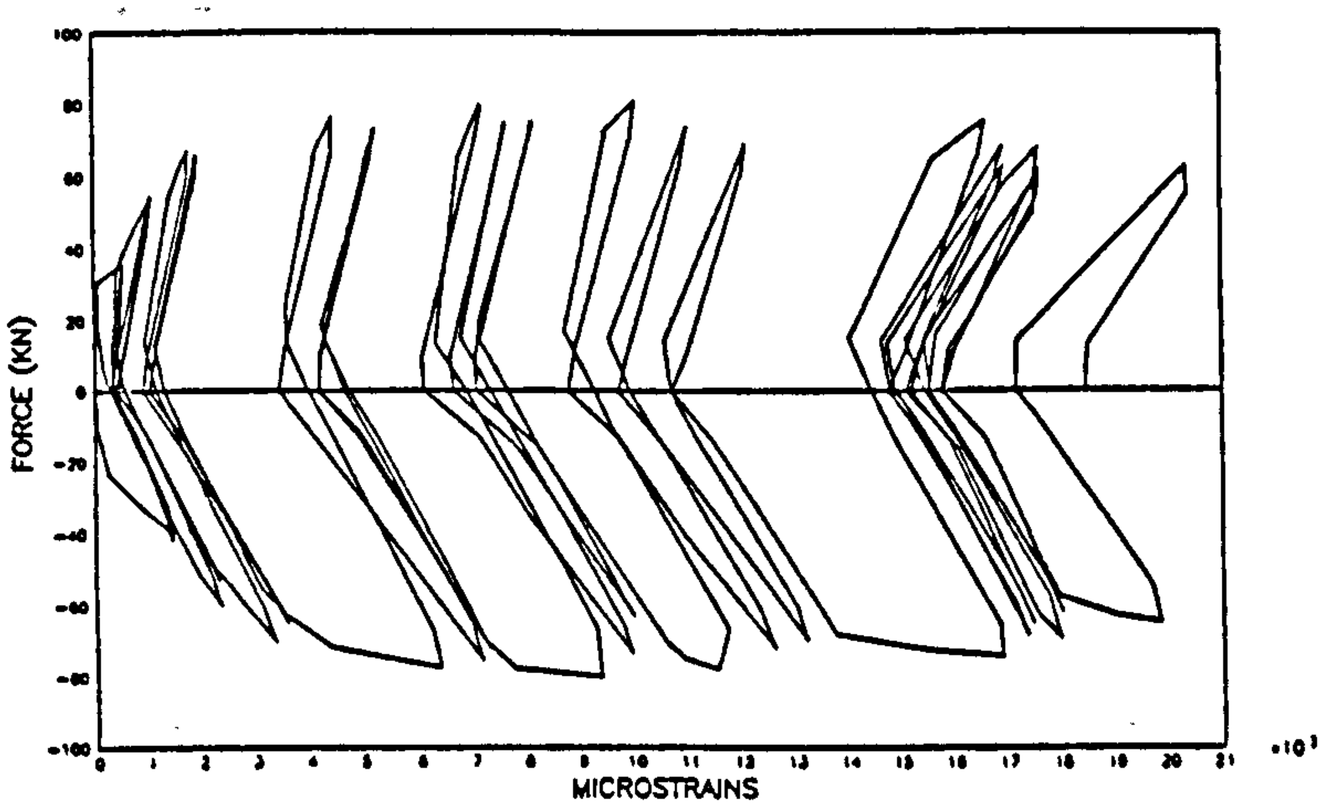


Figure B(16)28 Wall SW16 - force versus strain 20 (stirrup)

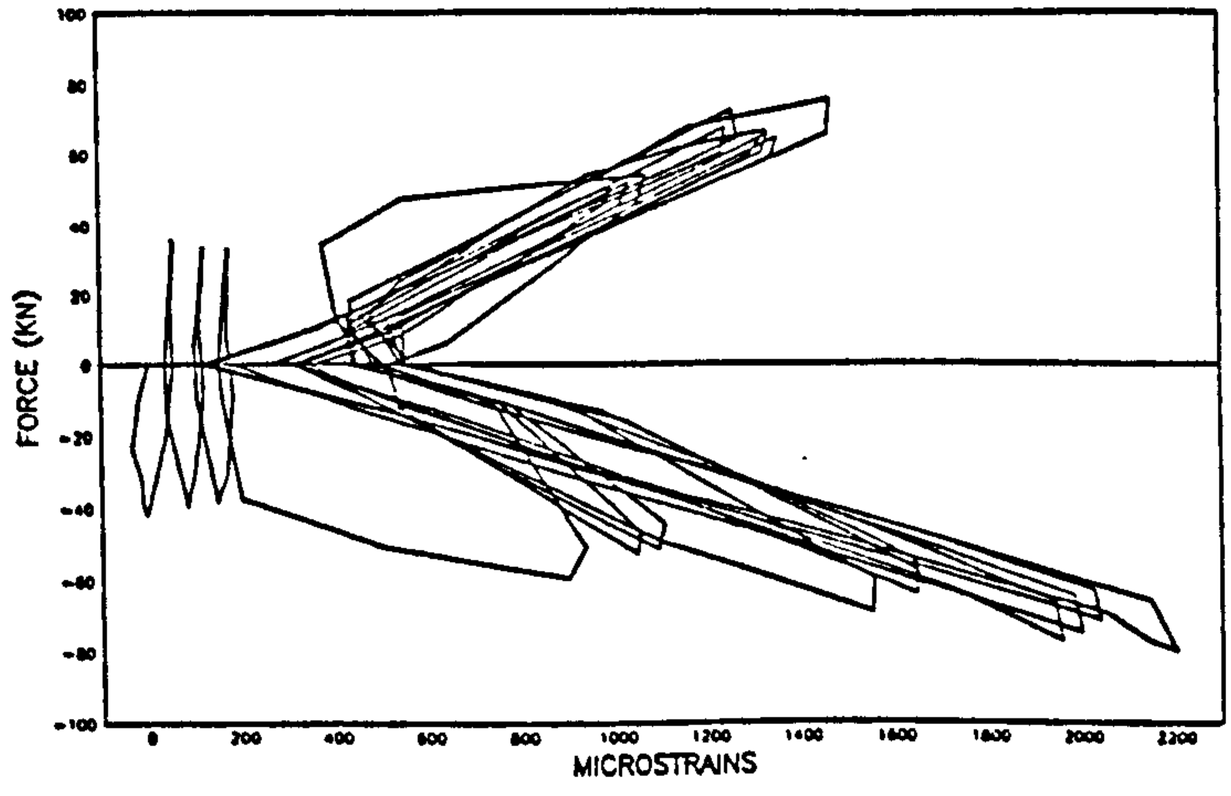


Figure B(16)29 Wall SW16 - force versus strain 21 (stirrup)

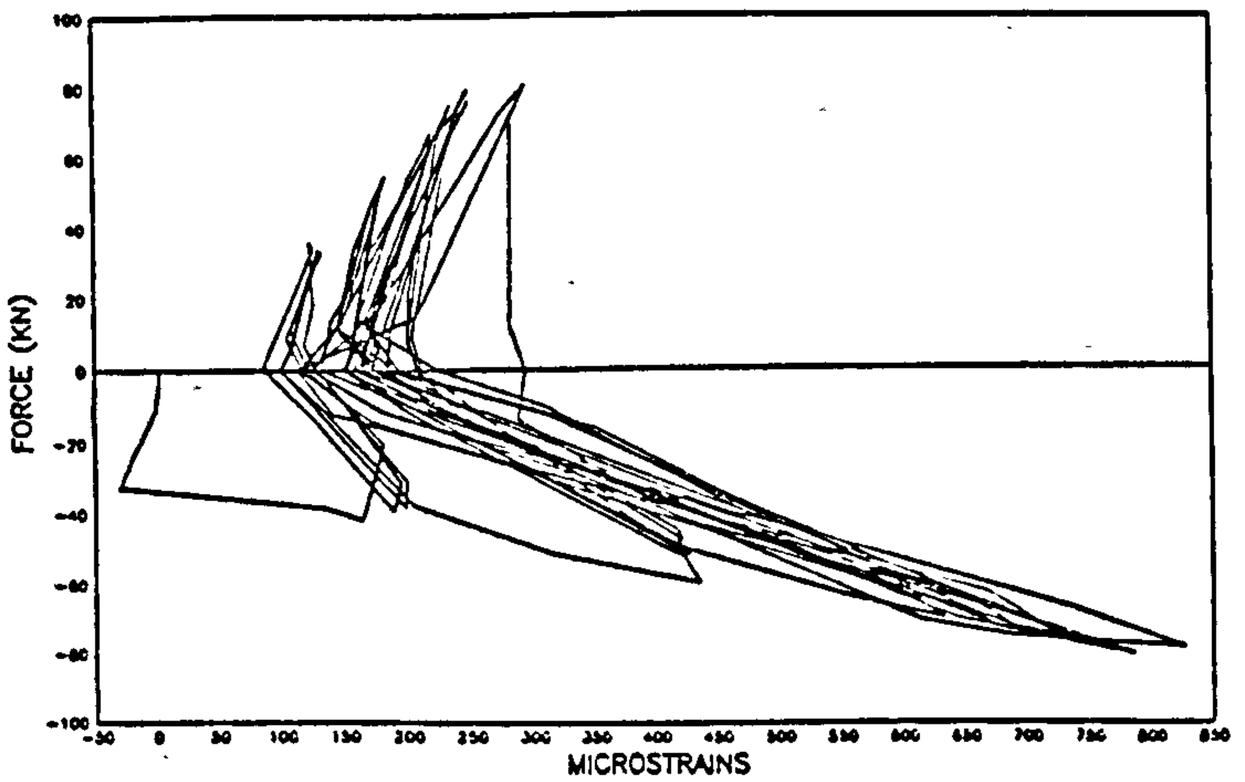


Figure B(16)30 Wall SW16 - force versus strain 22
(confinement reinforcement)

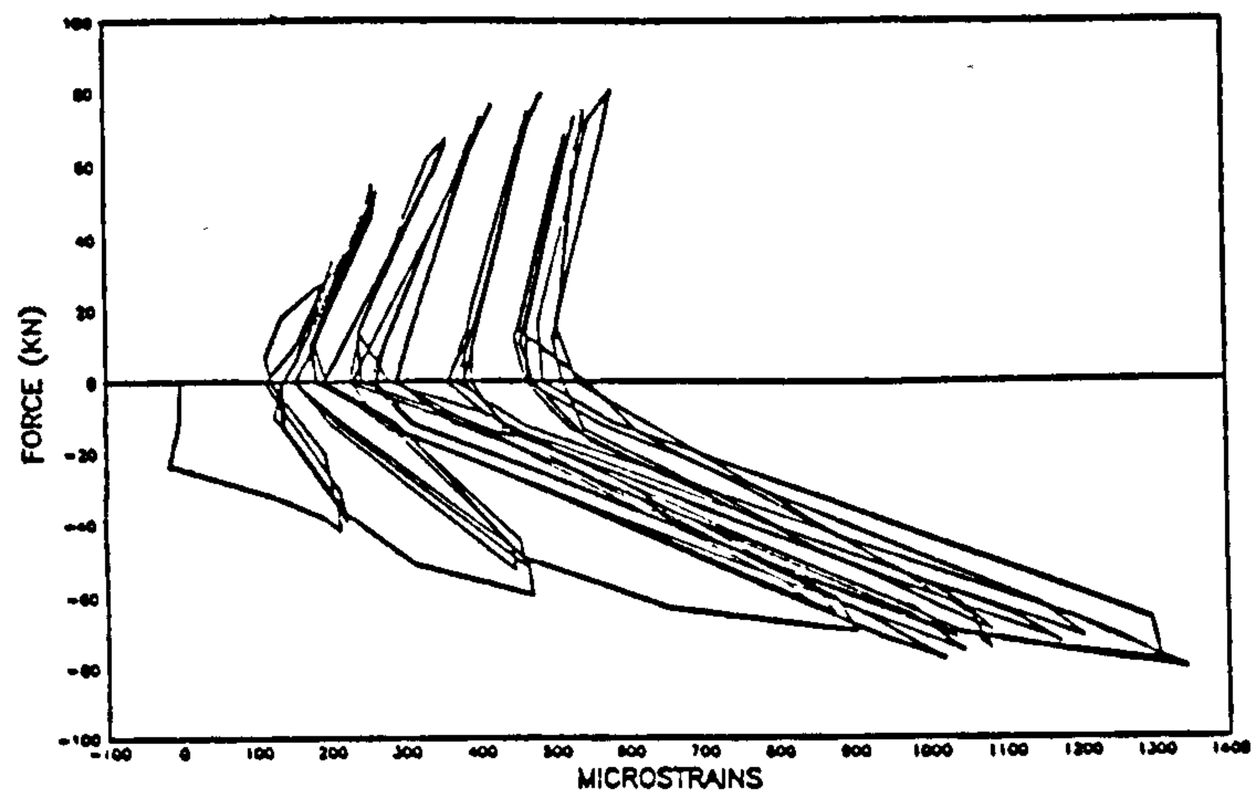


Figure B(16)31 Wall SW16 - force versus strain 23
(confinement reinforcement)

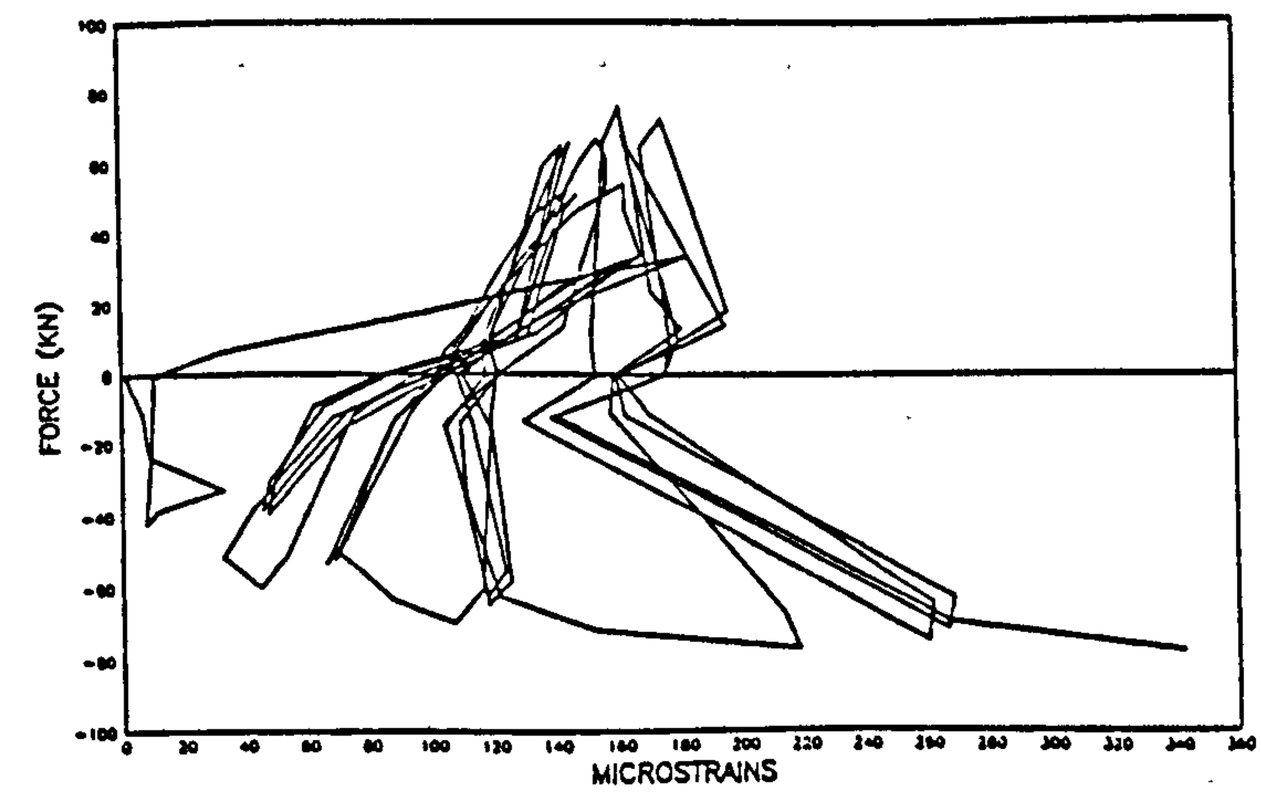


Figure B(16)32 Wall SW16 - force versus strain 24
(confinement reinforcement)

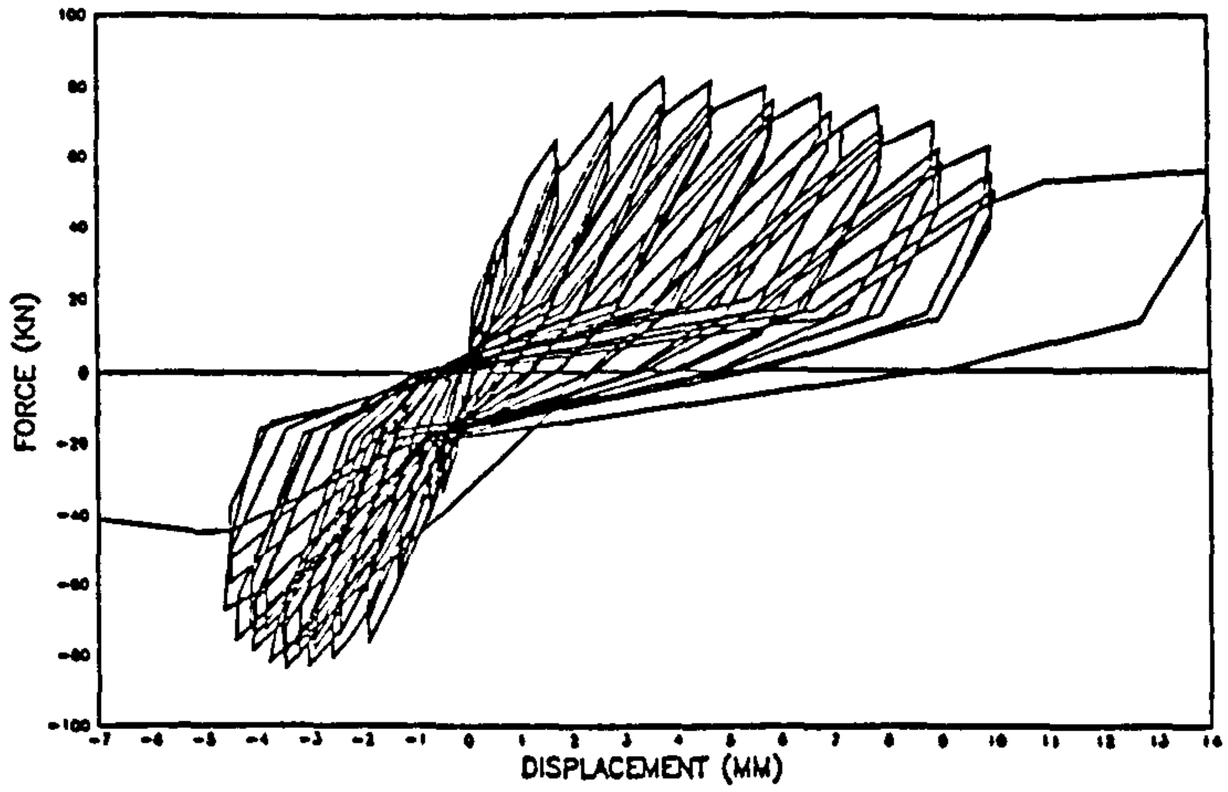


Figure B(17)1 Wall SW17 - force versus displacement 1 (horizontal, LHS, level 4)

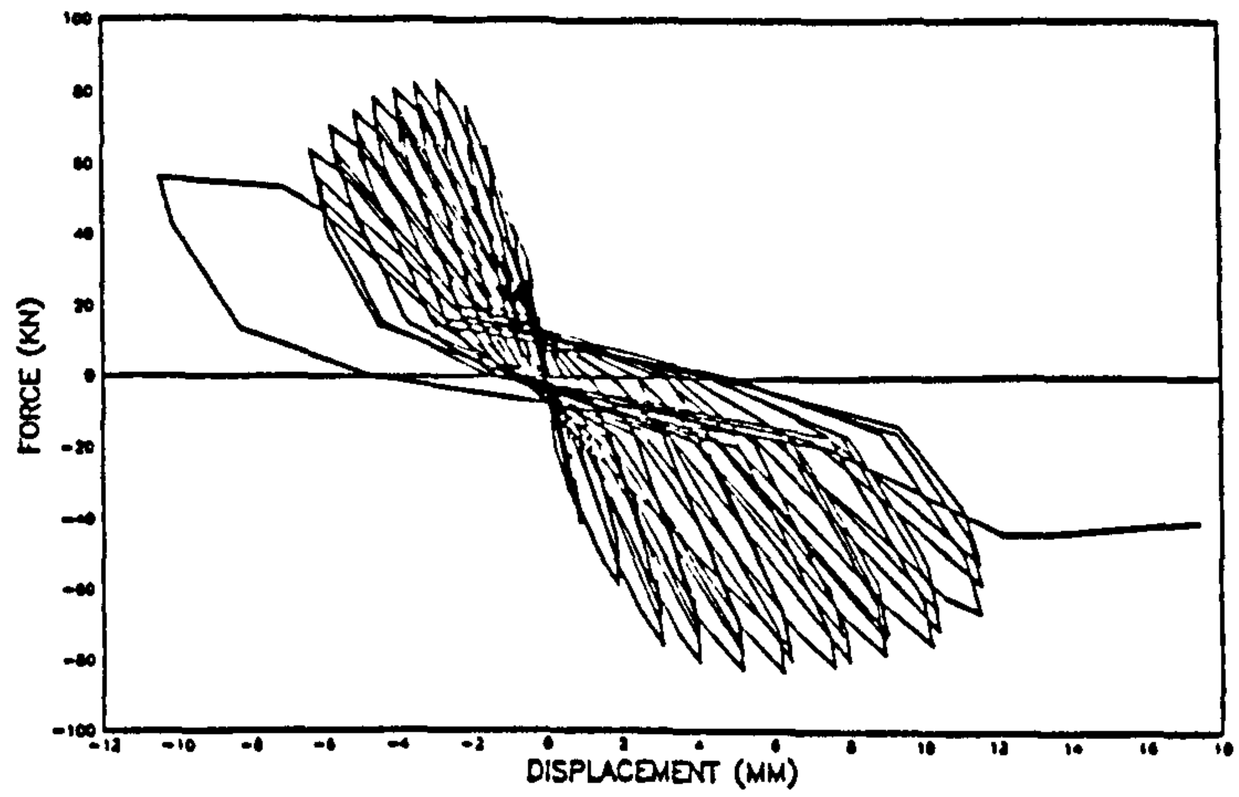


Figure B(17)2 Wall SW17 - force versus displacement 2 (horizontal, RHS, level 4)

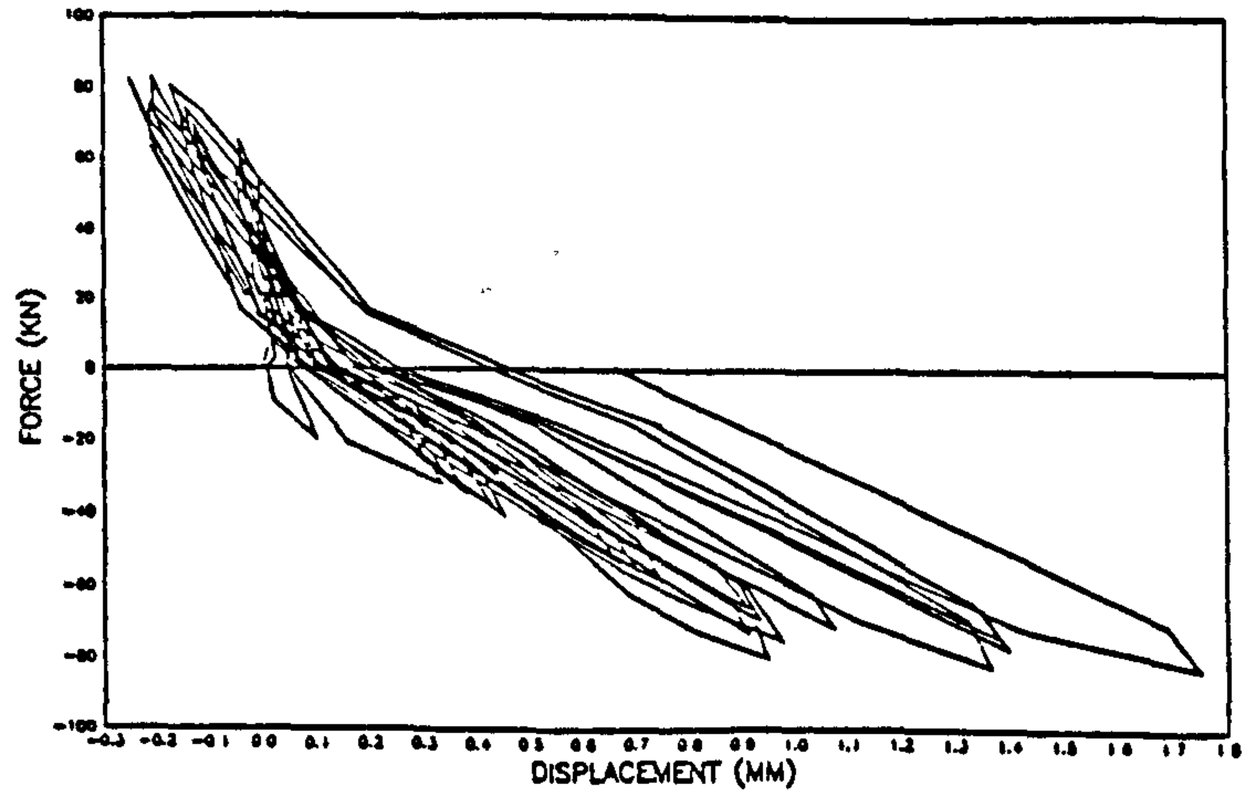


Figure B(17)3 Wall SW17 - force versus displacement 7 (vertical, LHS, level 3)

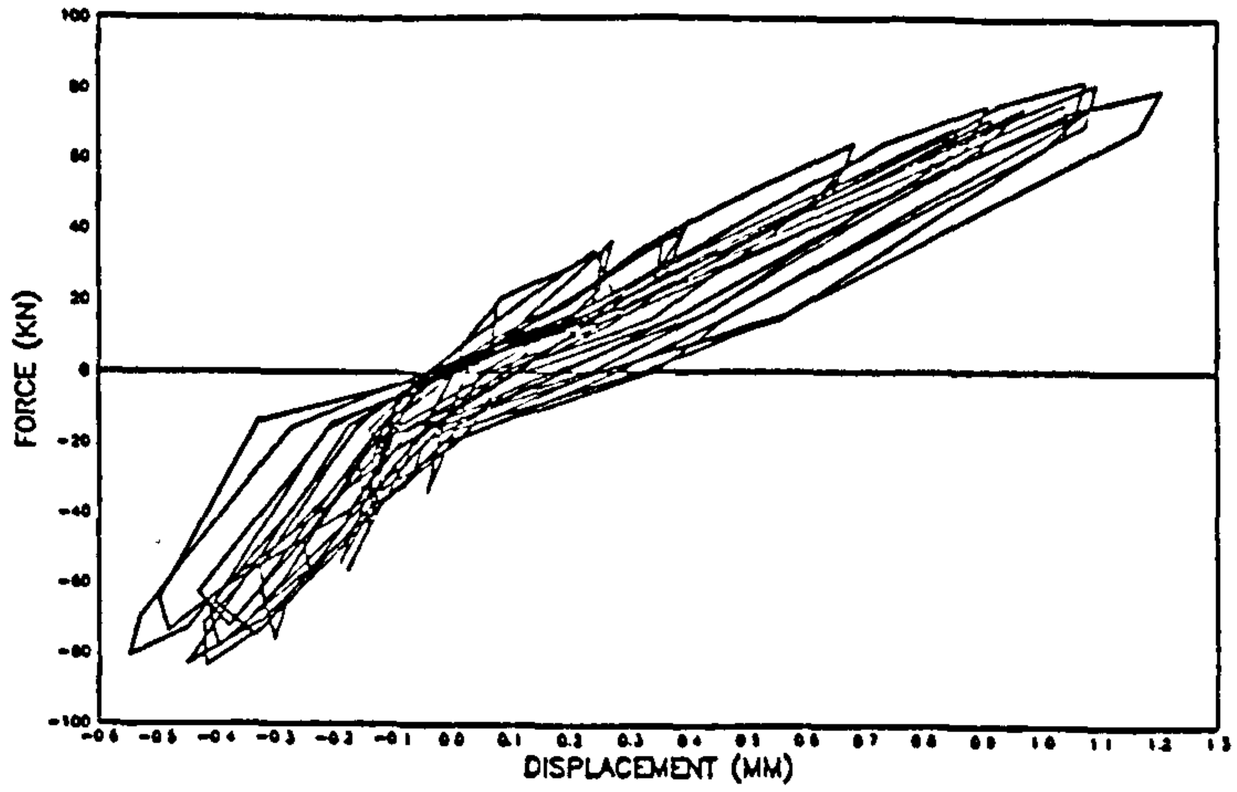


Figure B(17)4 Wall SW17 - force versus displacement 8 (vertical, RHS, level 3)

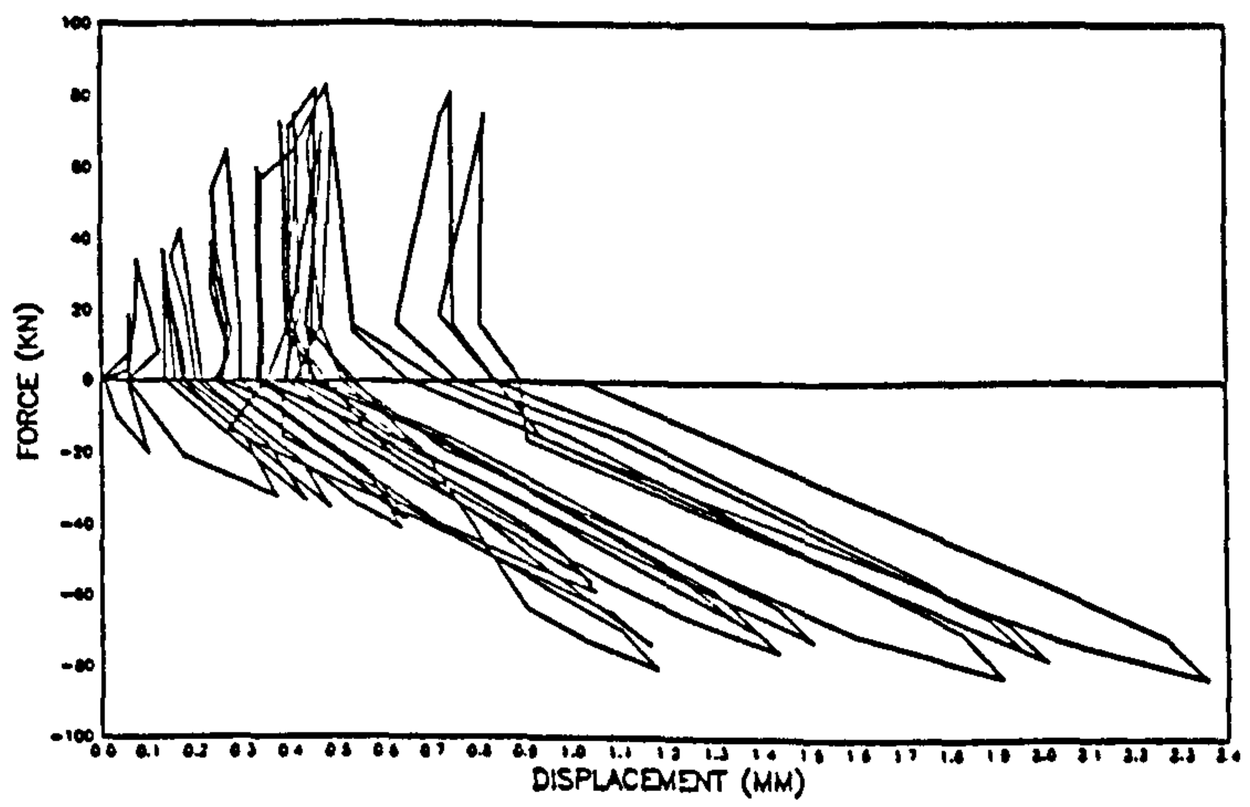


Figure B(17)5 Wall SW17 - force versus displacement 9 (vertical, LHS, level 4)

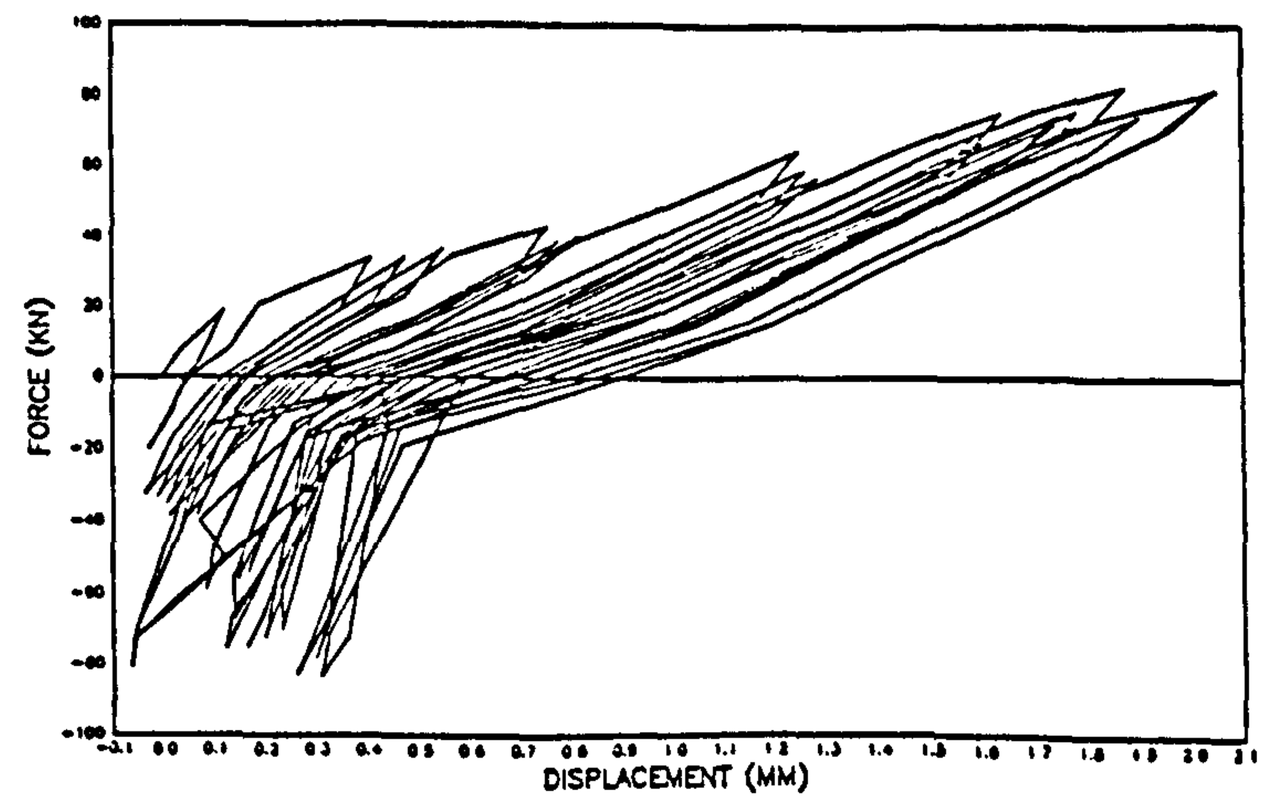


Figure B(17)6 Wall SW17 - force versus displacement 10 (vertical, RHS, level 4)

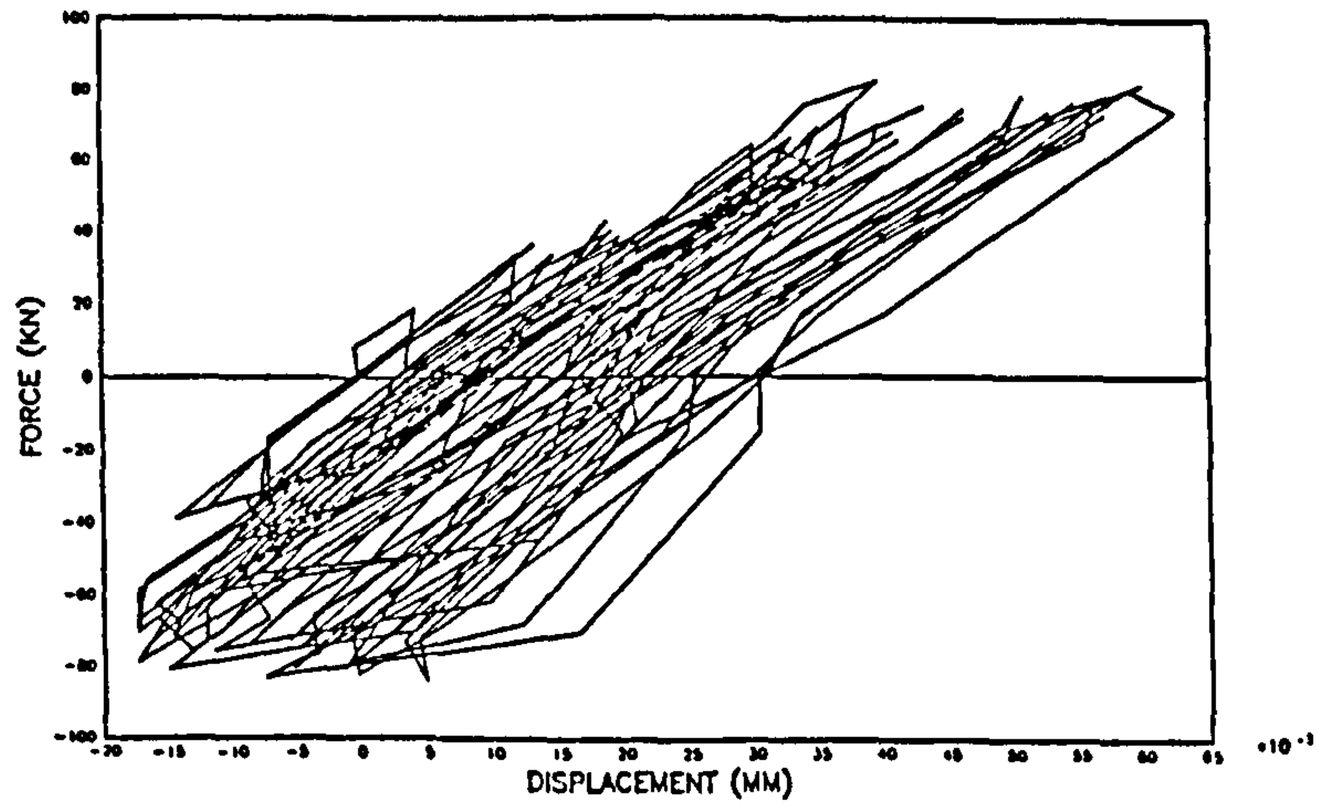


Figure B(17)7 Wall SW17 - force versus displacement 11 (foundation, RHS)

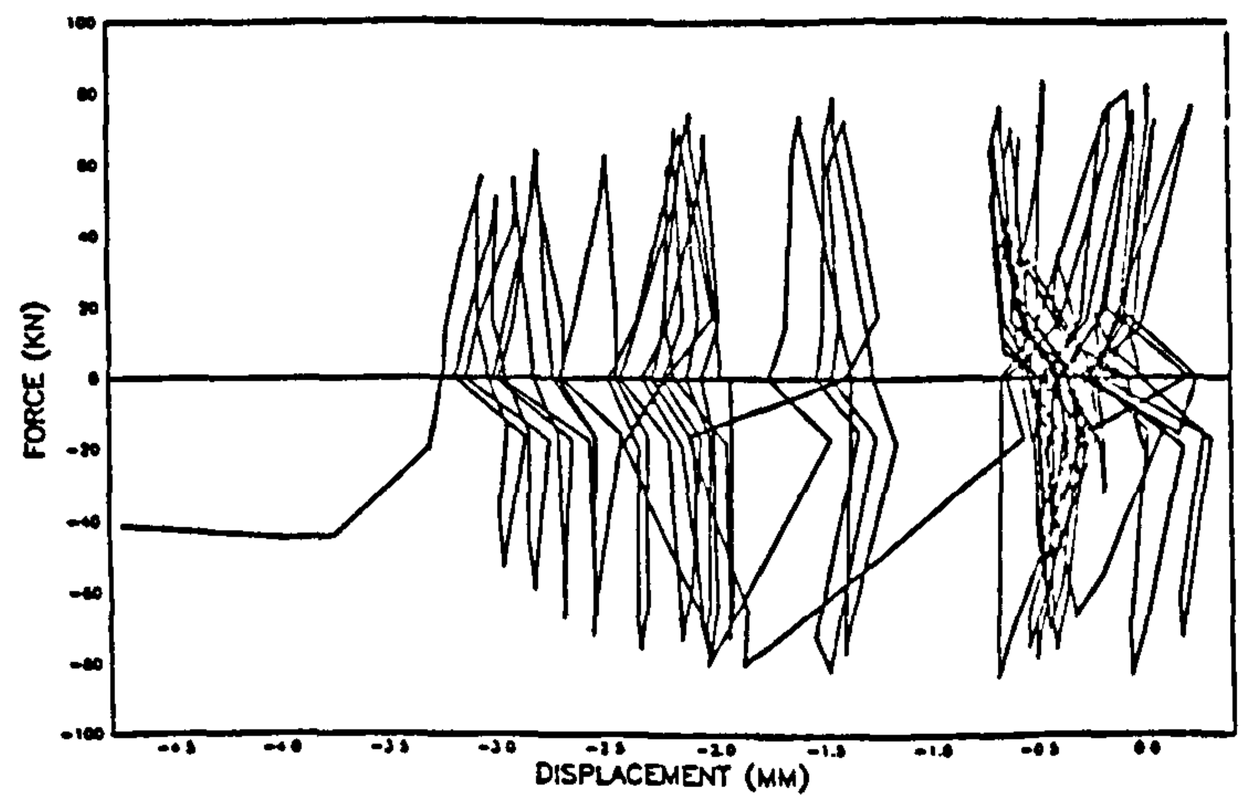


Figure B(17)8 Wall SW17 - force versus displacement 12 (out-of-plane)

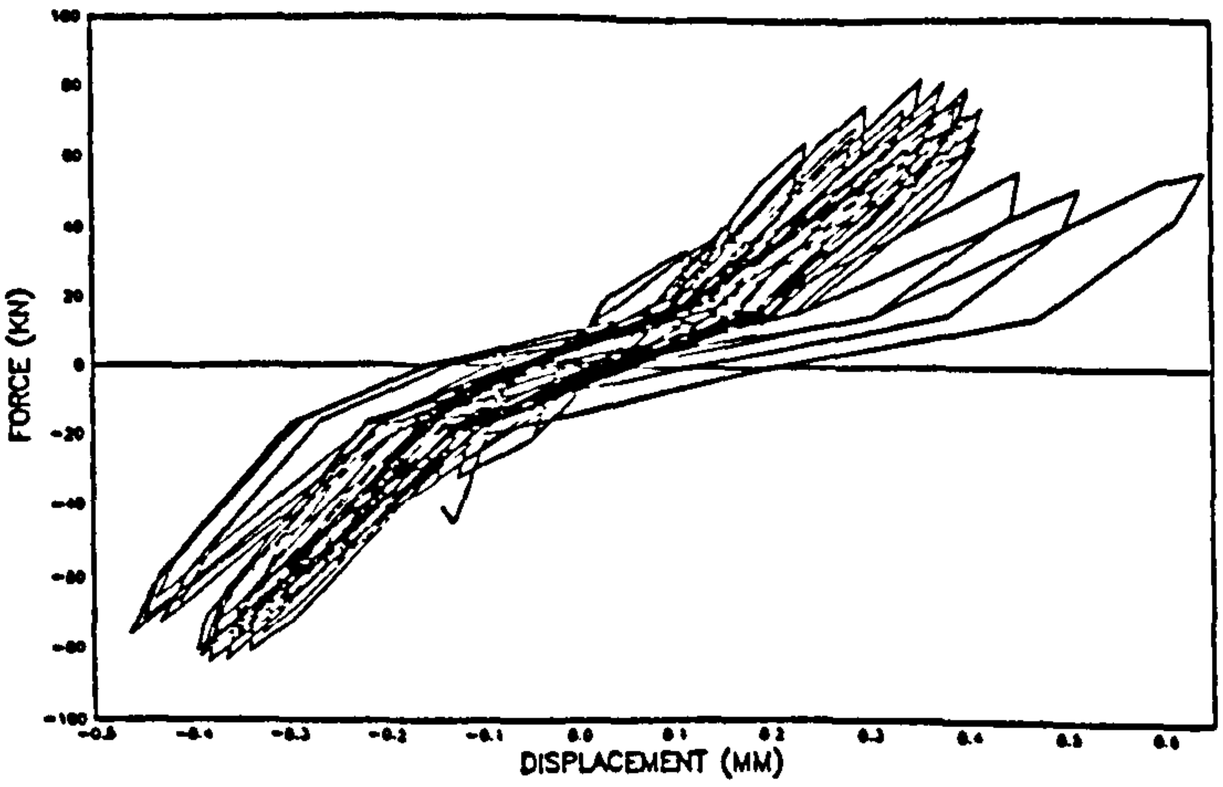


Figure B(17)9 Wall SW17 - force versus displacement 13 (horizontal, centre, level 1)

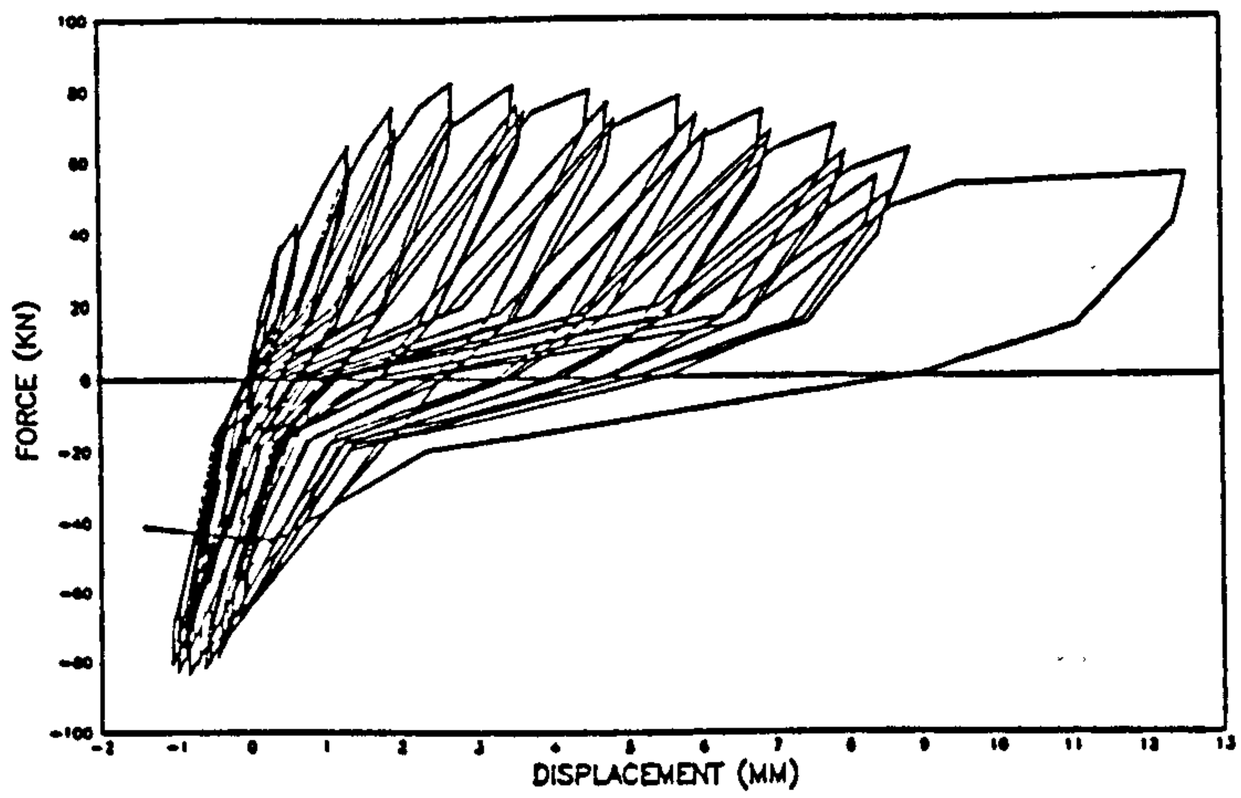


Figure B(17)10.a Wall SW17 - force versus displacement 15a (horizontal, LHS, level 3)

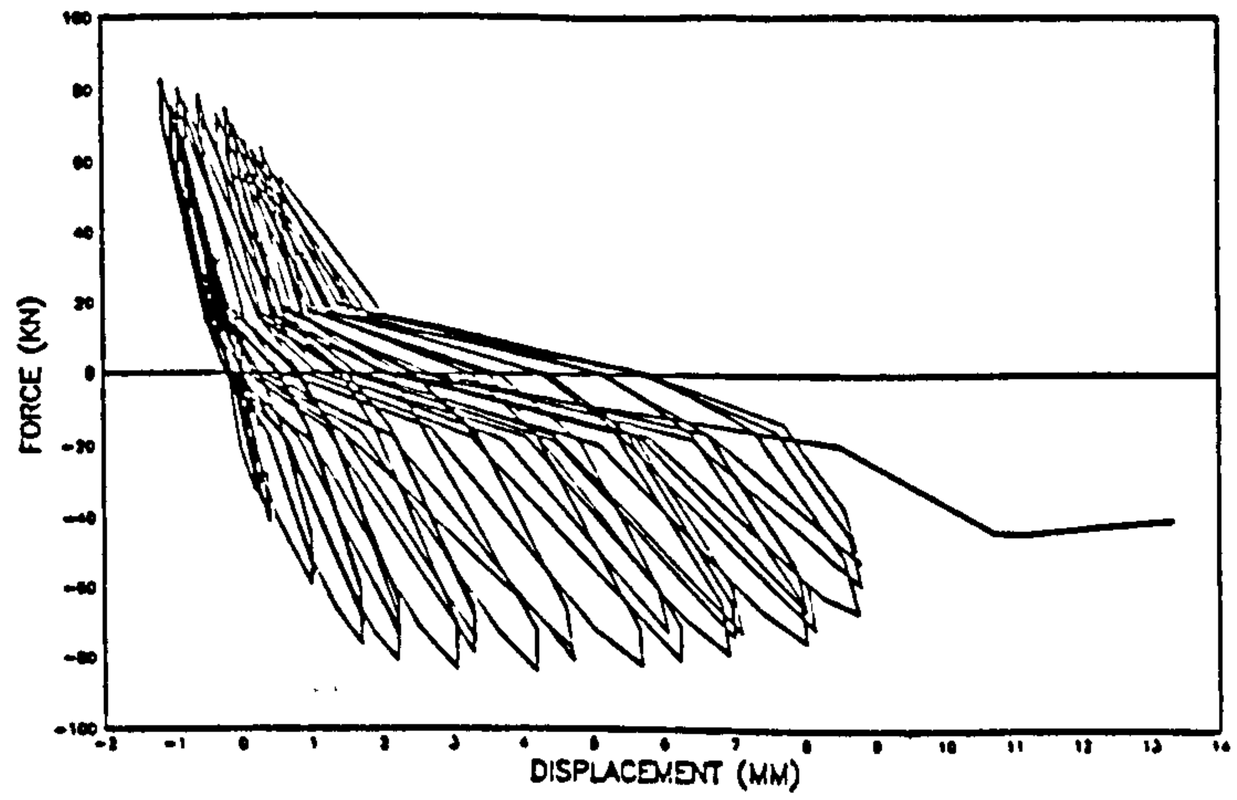


Figure B(17)10.b Wall SW17 - force versus displacement 15b (horizontal, RHS, level 3)

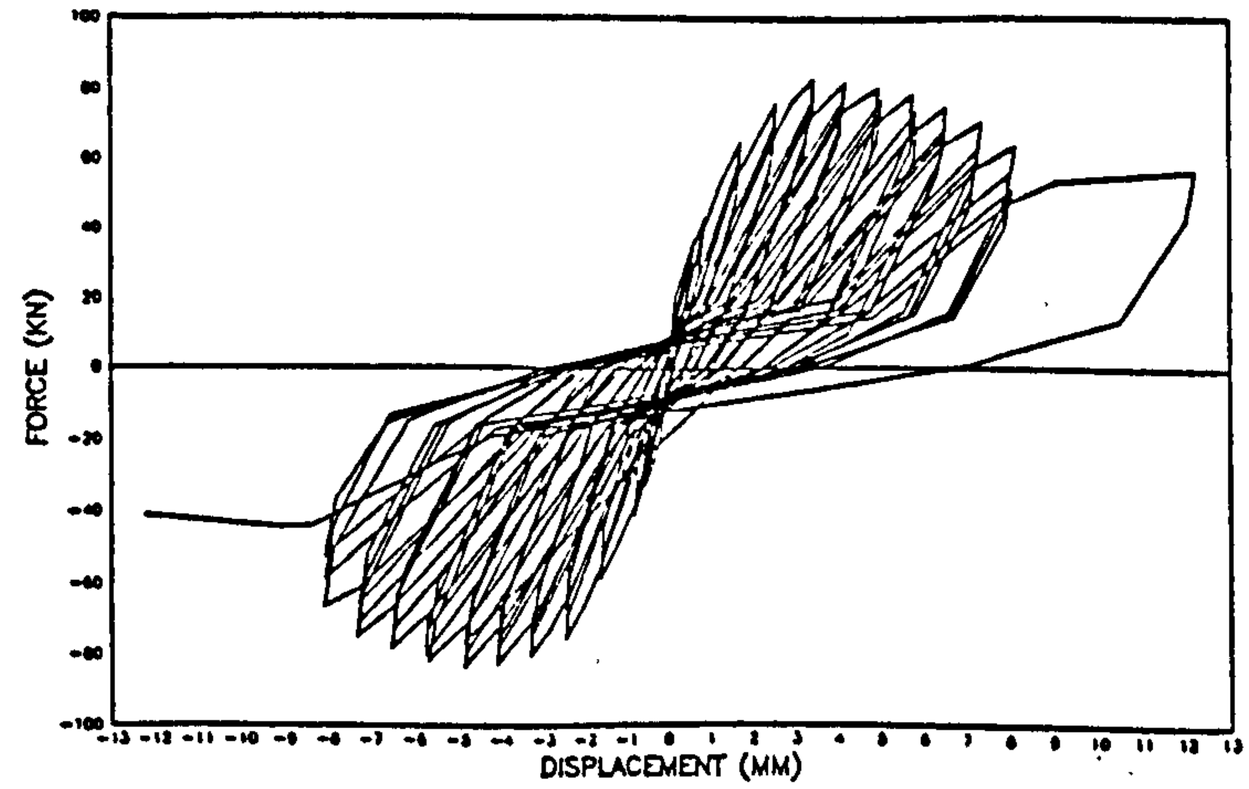


Figure B(17)11 Wall SW17 - force versus top horizontal displacement

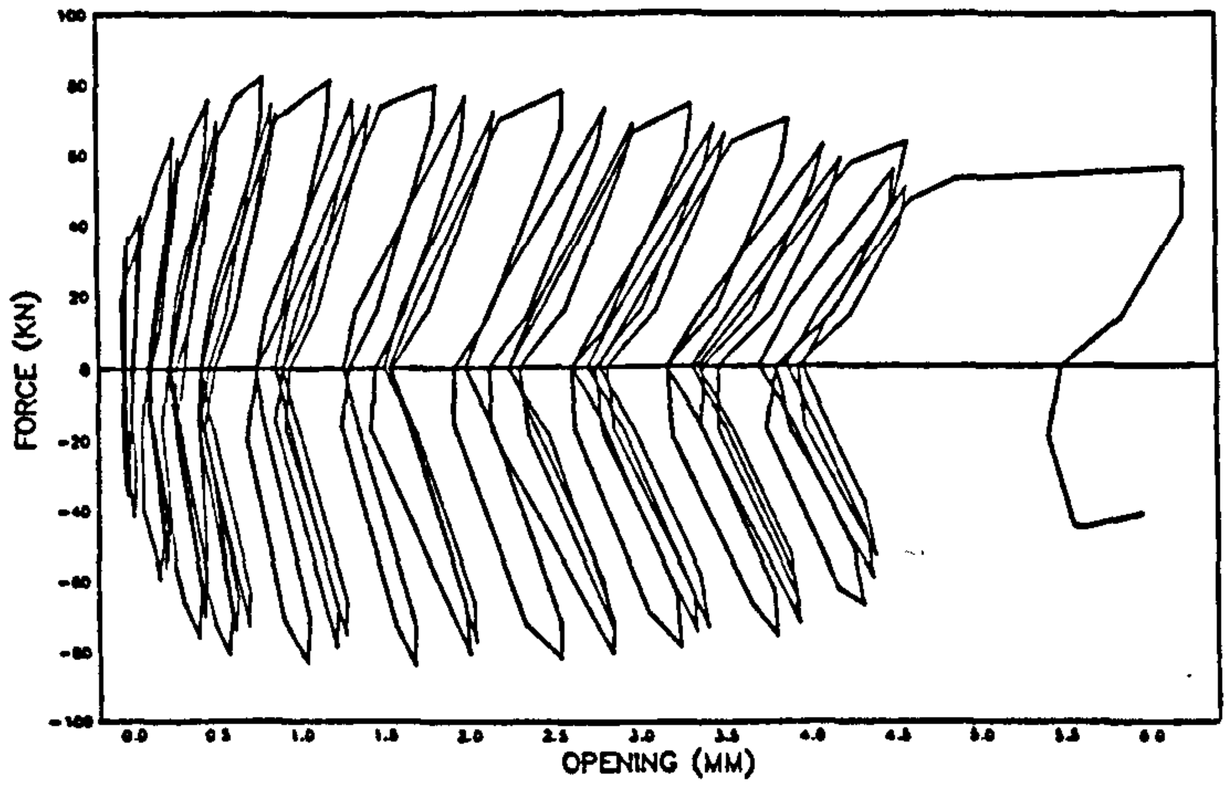


Figure B(17)12 Wall SW17 - force versus opening at third level

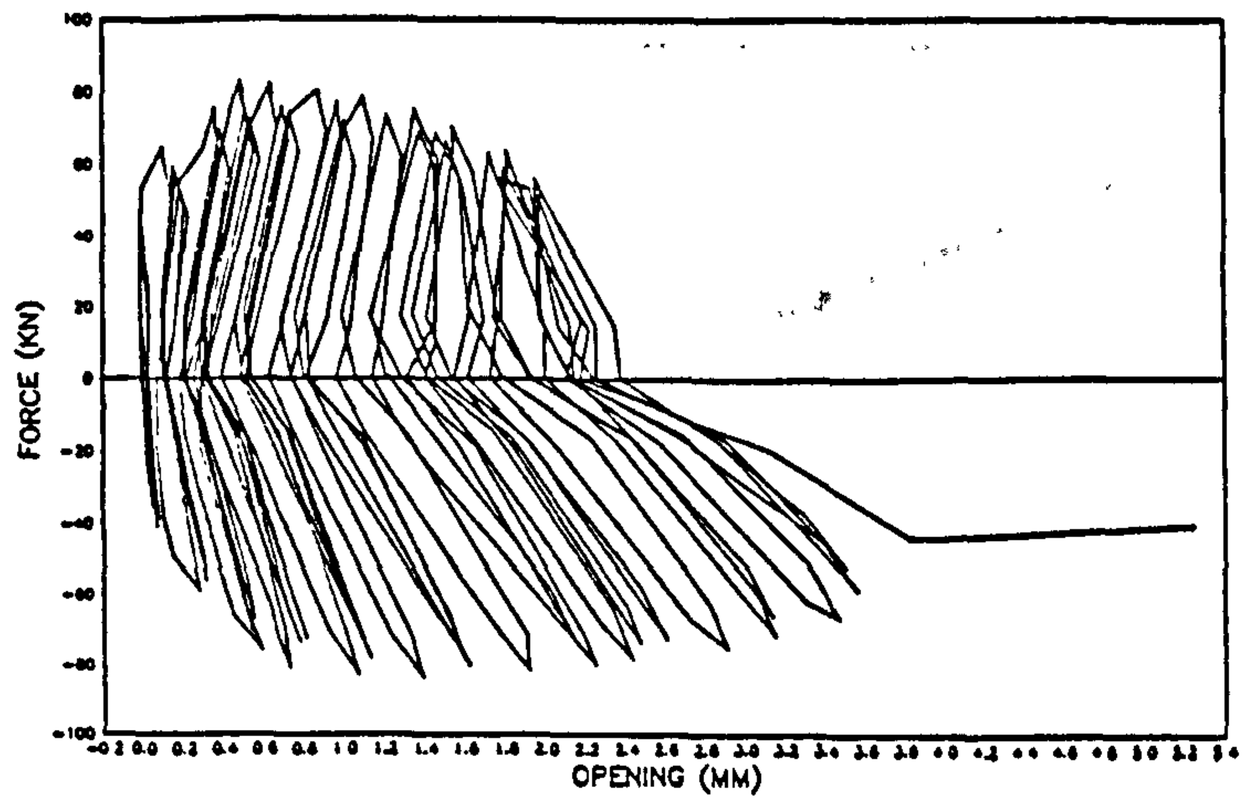


Figure B(17)13 Wall SW17 - force versus opening on top

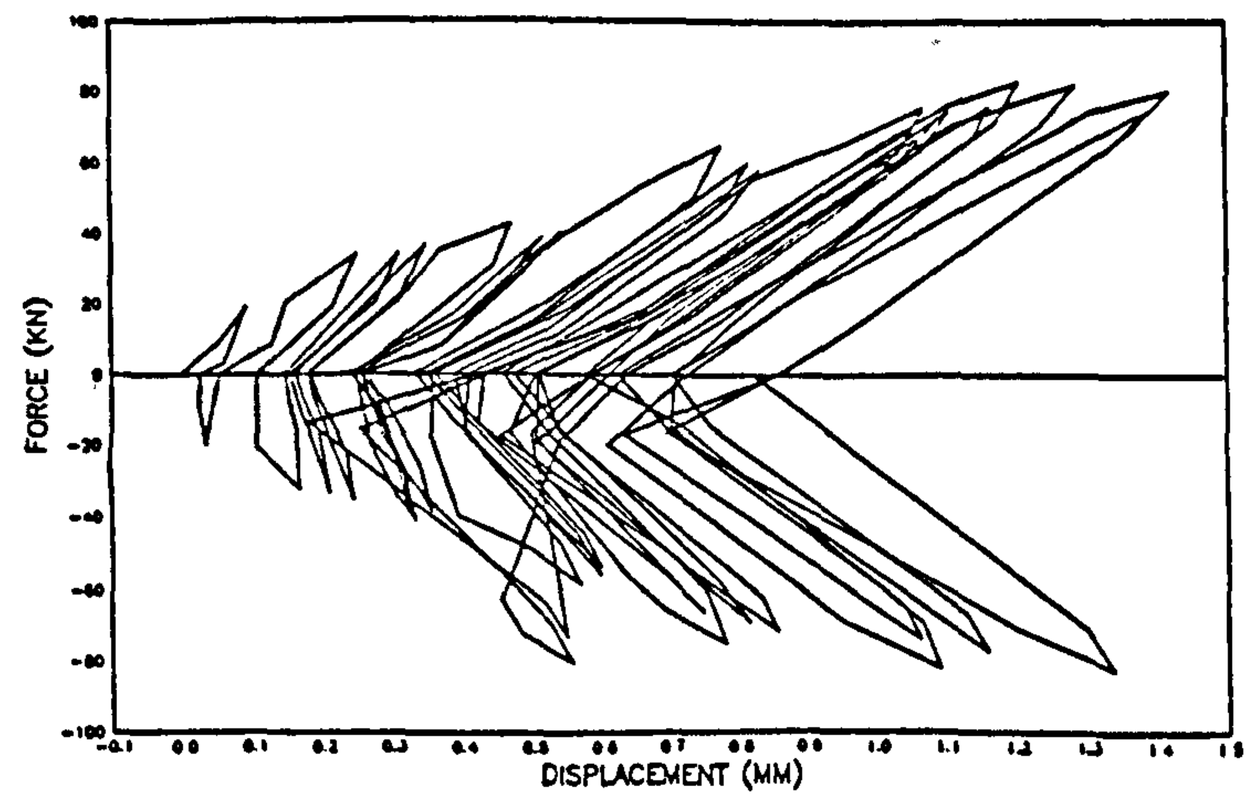


Figure B(17)14 Wall SW17 - force versus extension on top

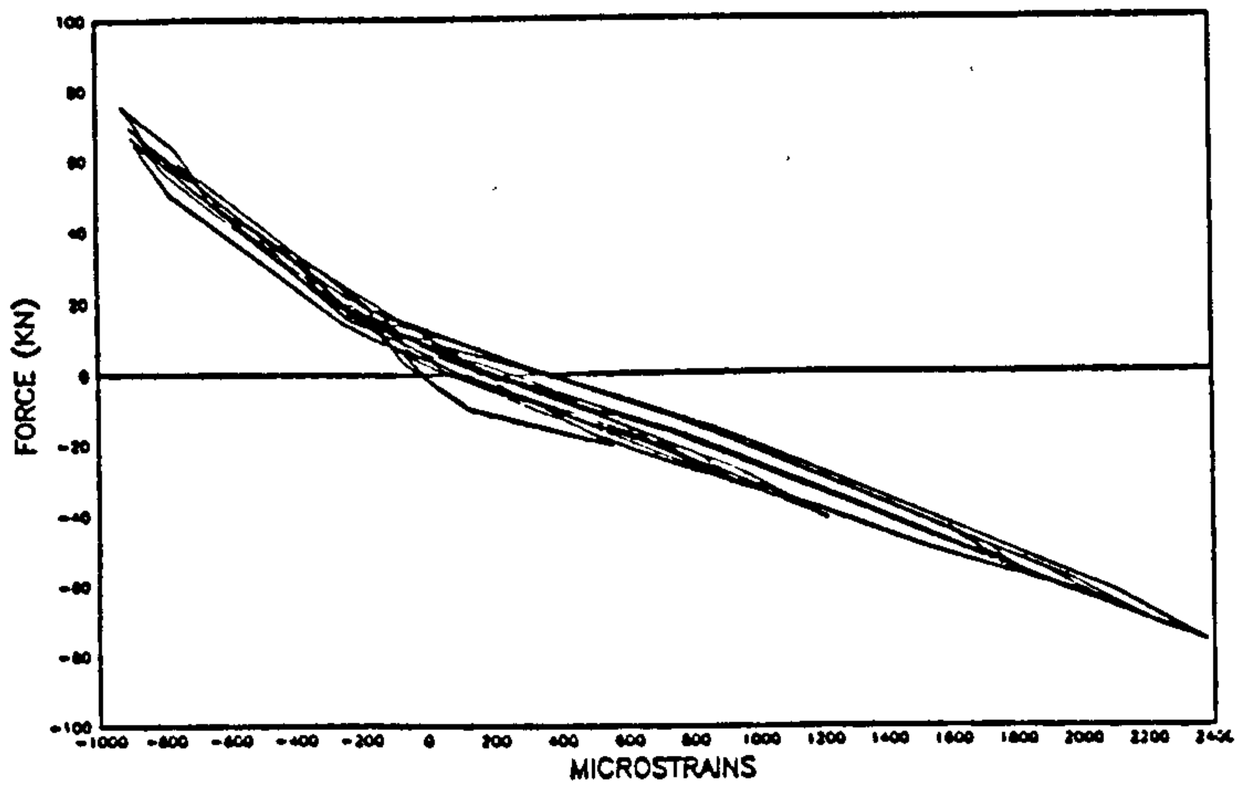


Figure B(17)15 Wall SW17 - force versus strain 1 (bottom, ϕ8mm, LHS)

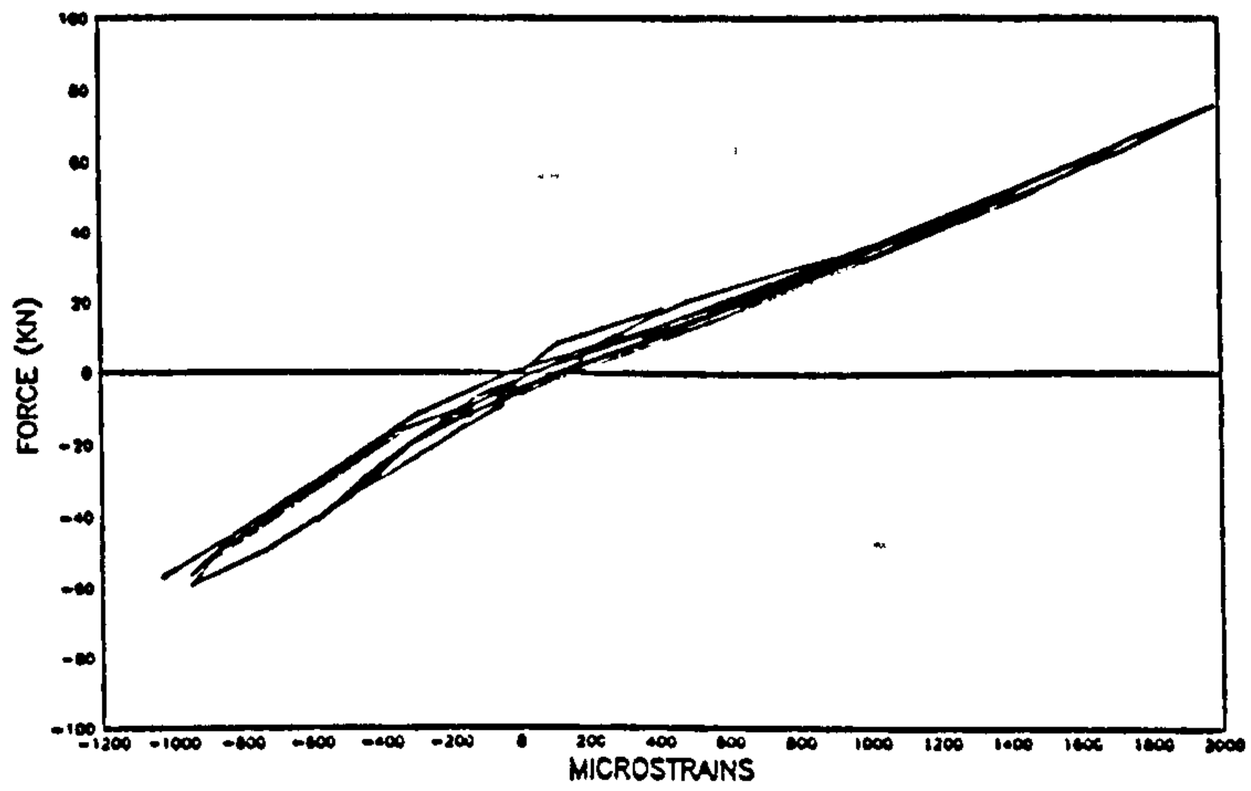


Figure B(17)16 Wall SW17 - force versus strain 2 (bottom, ϕ8mm, RHS)

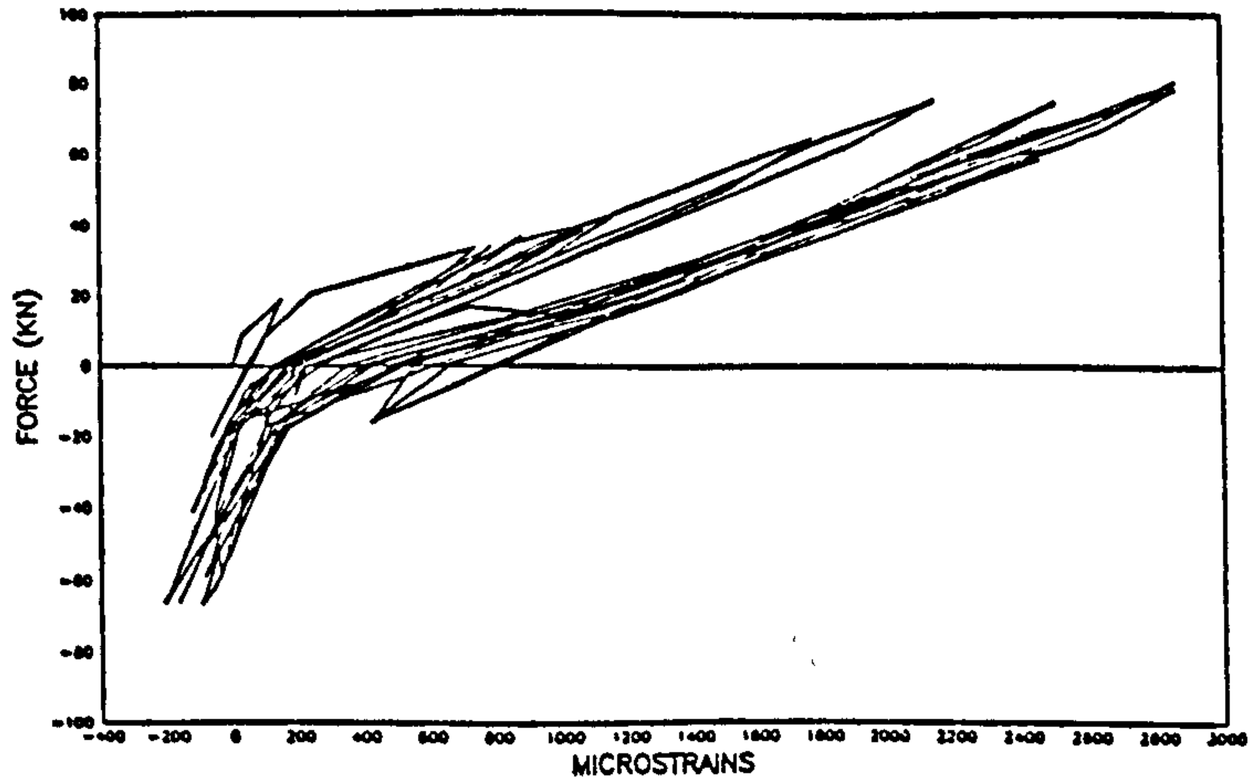


Figure B(17)17 Wall SW17 - force versus strain 10 (second level, ϕ8mm, RHS)

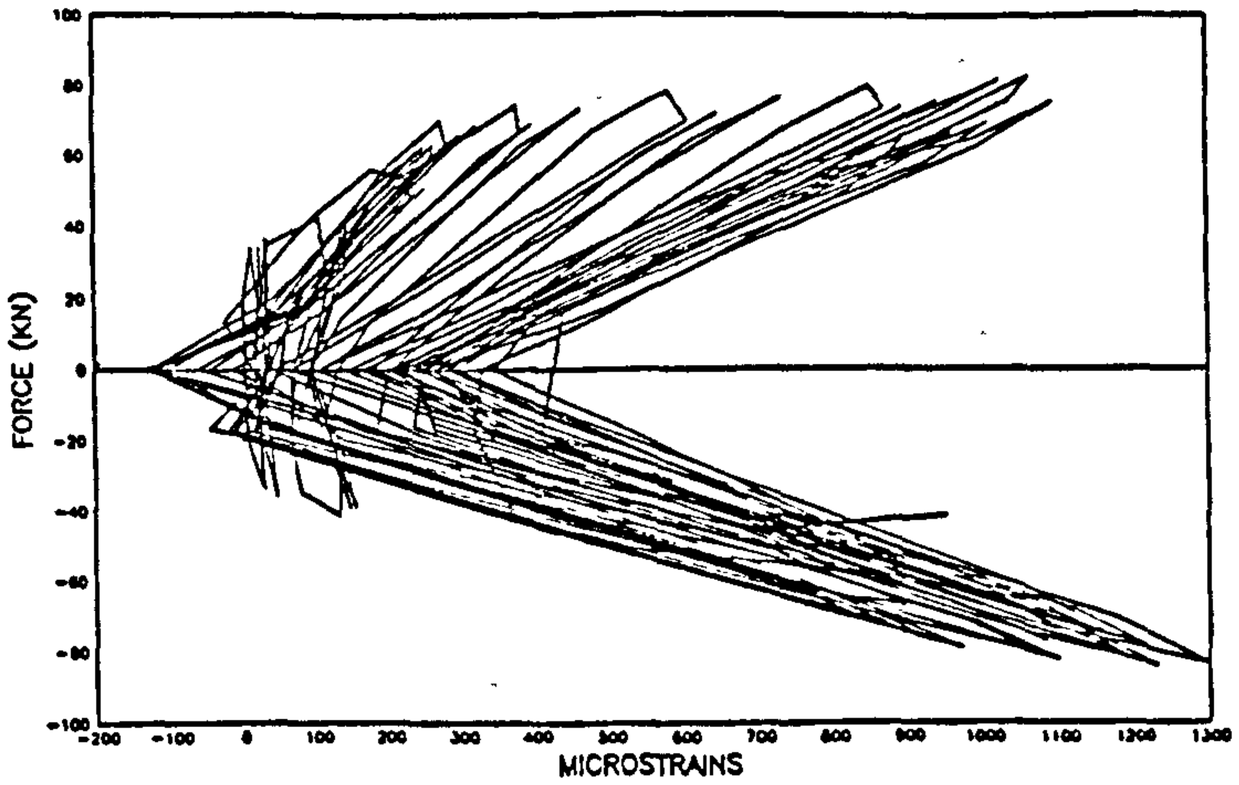


Figure B(17)18 Wall SW17 - force versus strain 12 (level of zero moment, ϕ8mm, RHS)

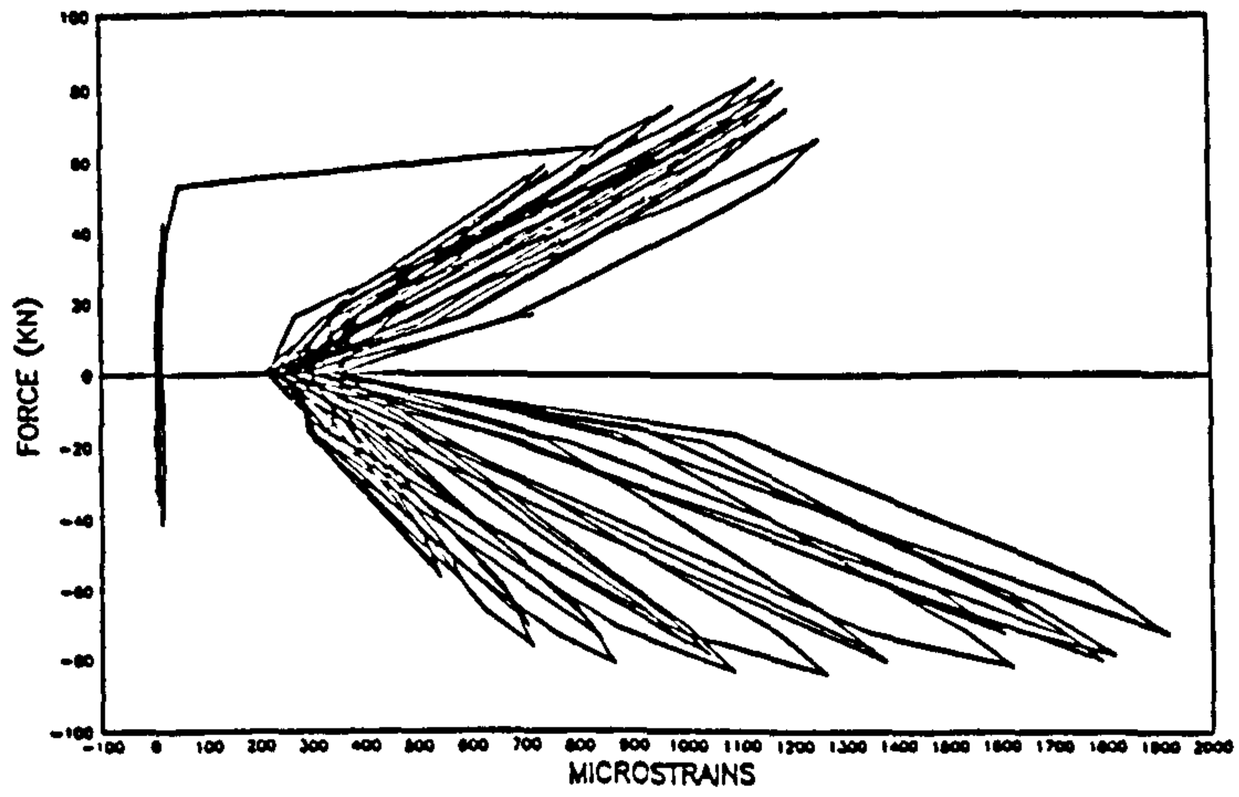


Figure B(17)19 Wall SW17 - force versus strain 13 (level of zero moment, ϕ6mm, LHS)

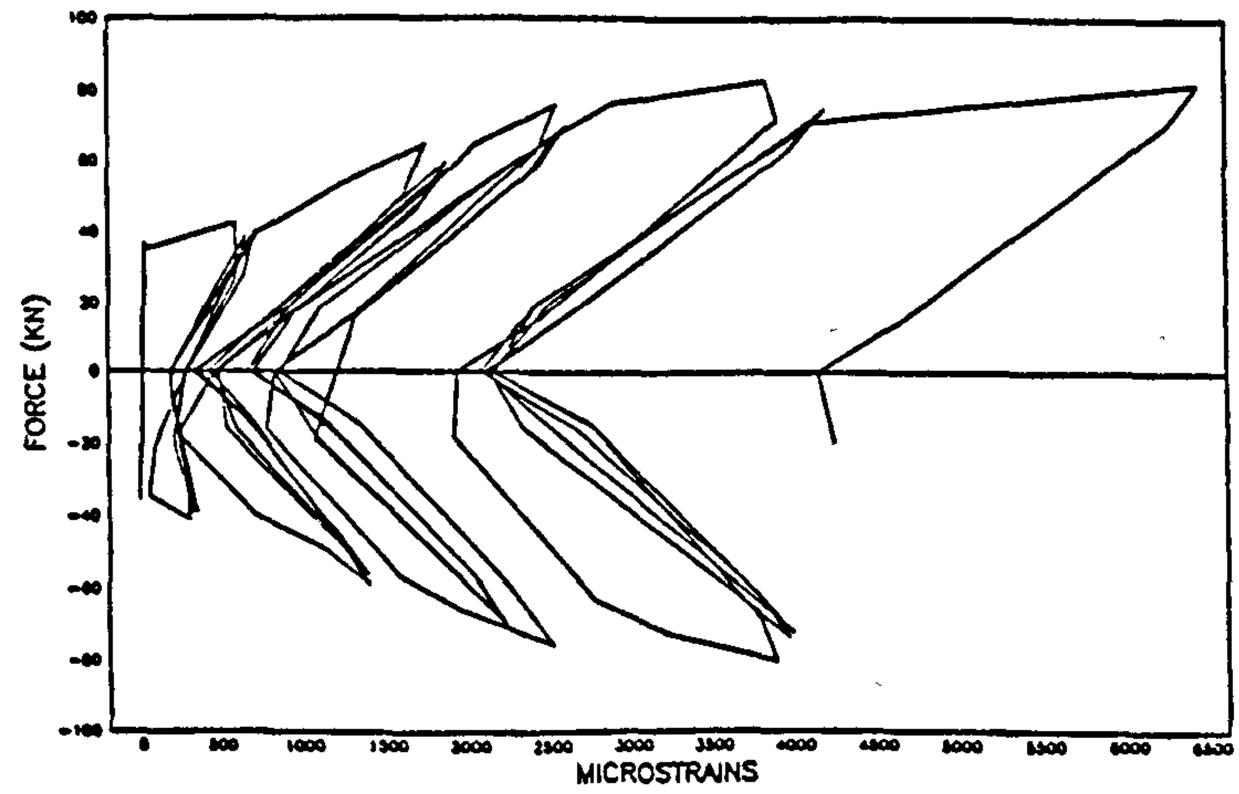


Figure B(17)20 Wall SW17 - force versus strain 19 (stirrup)

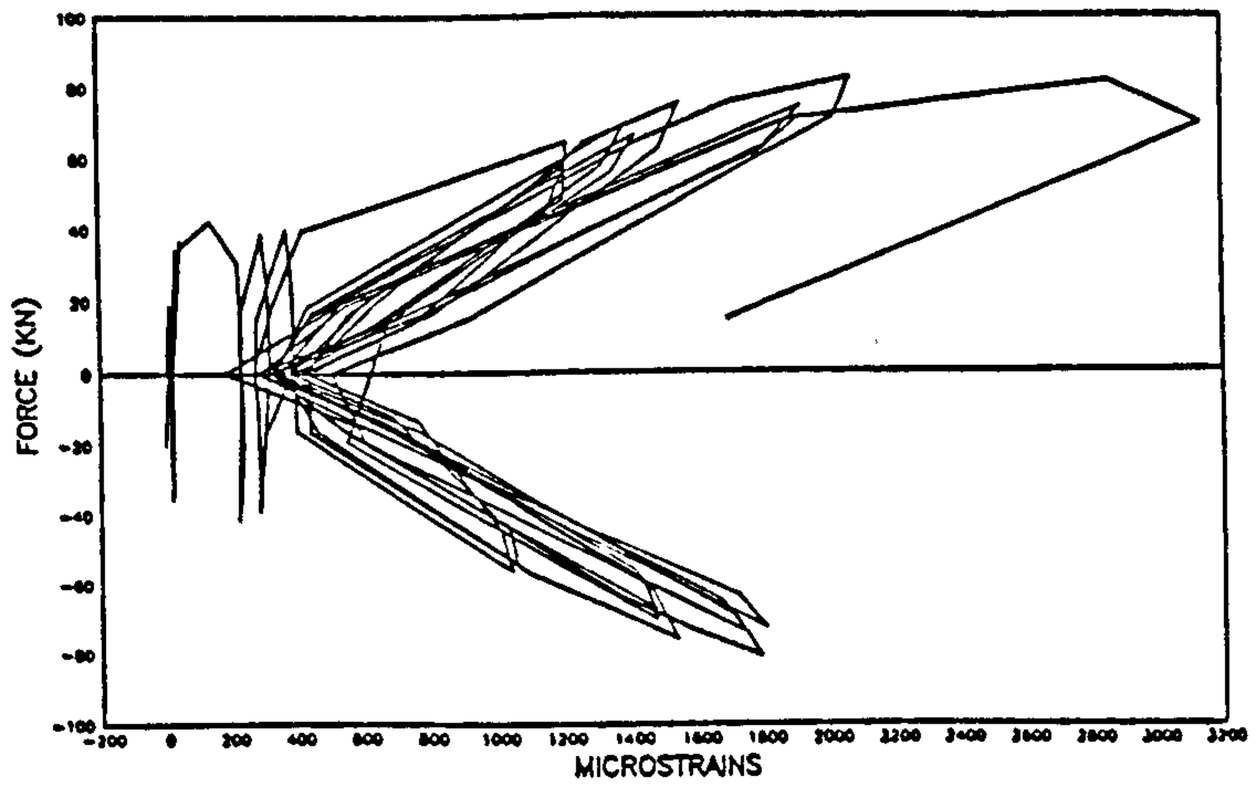


Figure B(17)21 Wall SW17 - force versus strain 20 (stirrup)

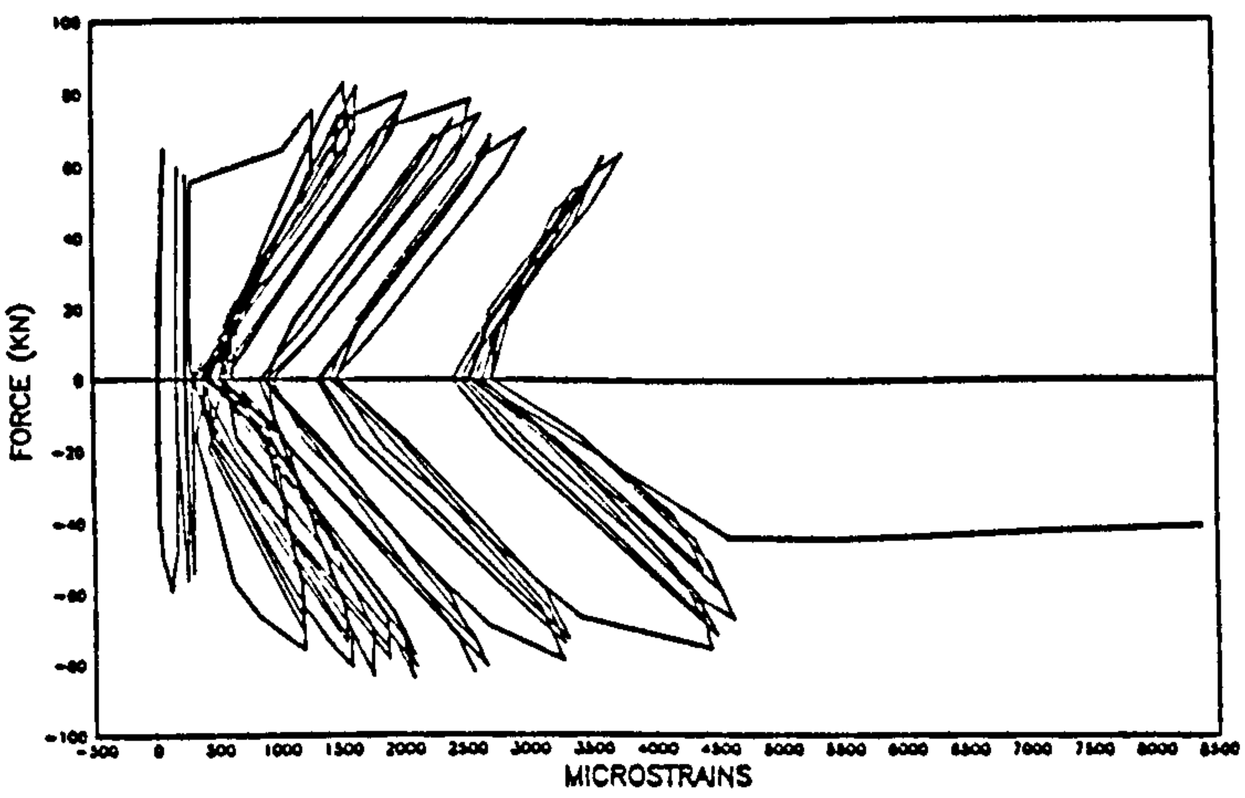


Figure B(17)22 Wall SW17 - force versus strain 21 (stirrup)

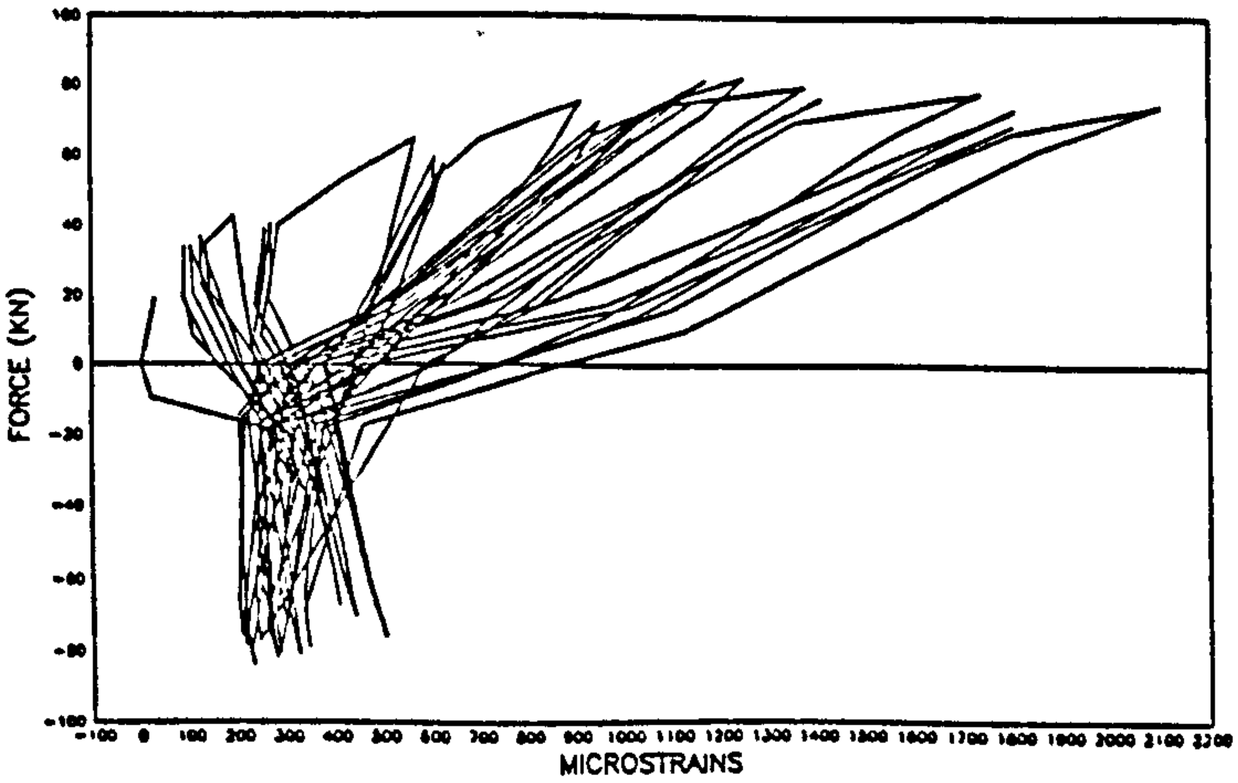


Figure B(17)23 Wall SW17 - force versus strain 22 (confinement reinforcement)

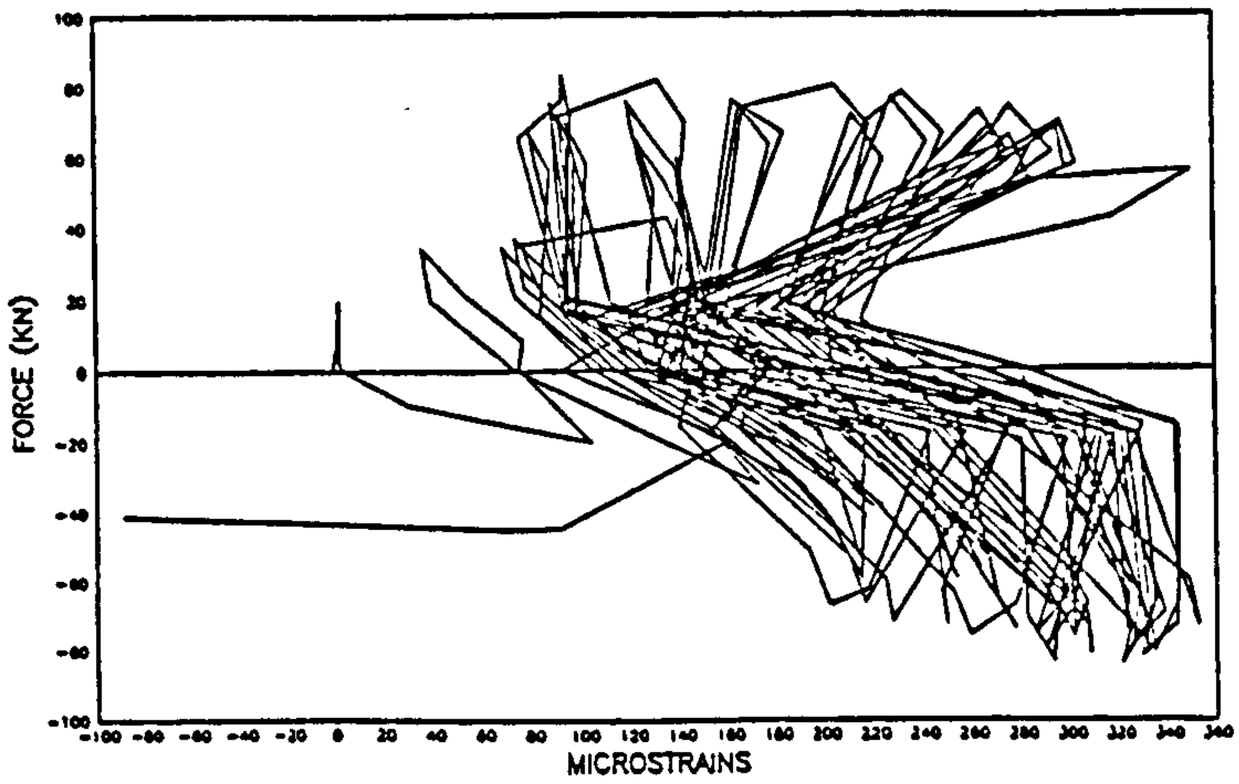


Figure B(17)24 Wall SW17 - force versus strain 23
(confinement reinforcement)

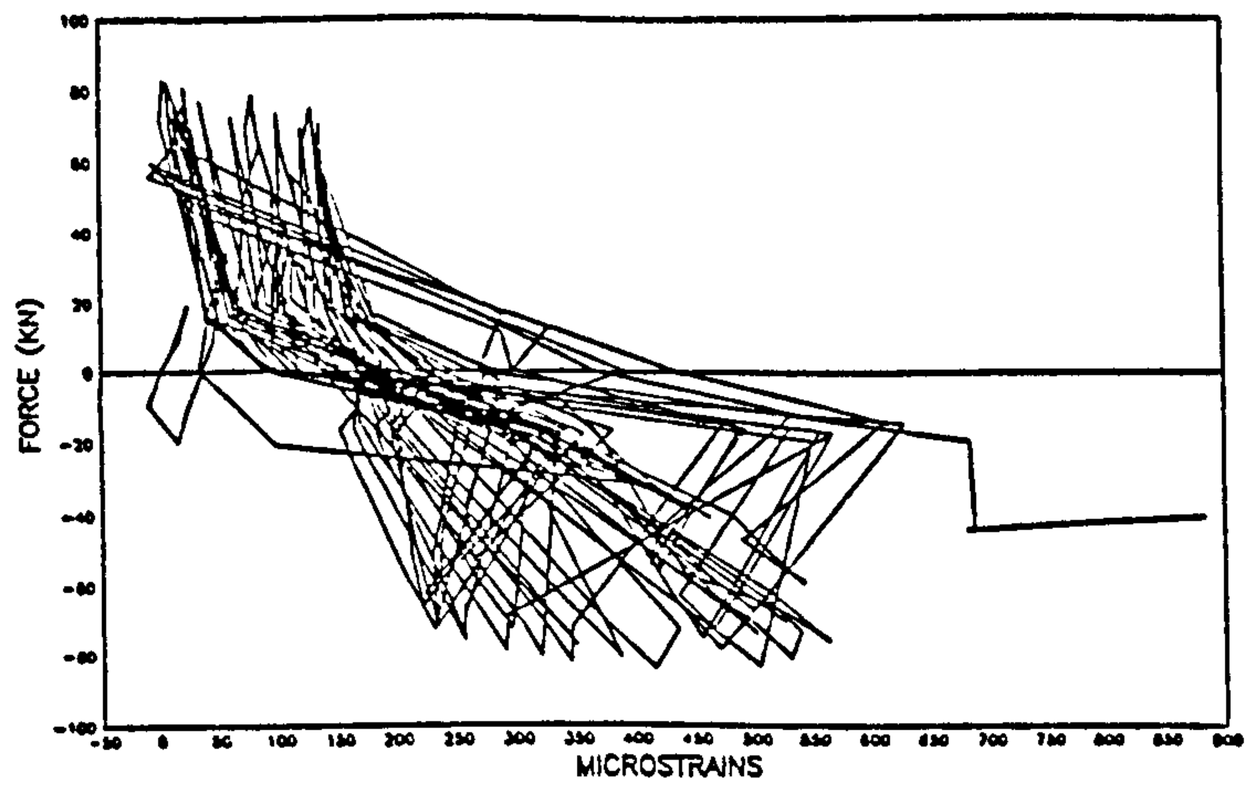


Figure B(17)25 Wall SW17 - force versus strain 24
(confinement reinforcement)

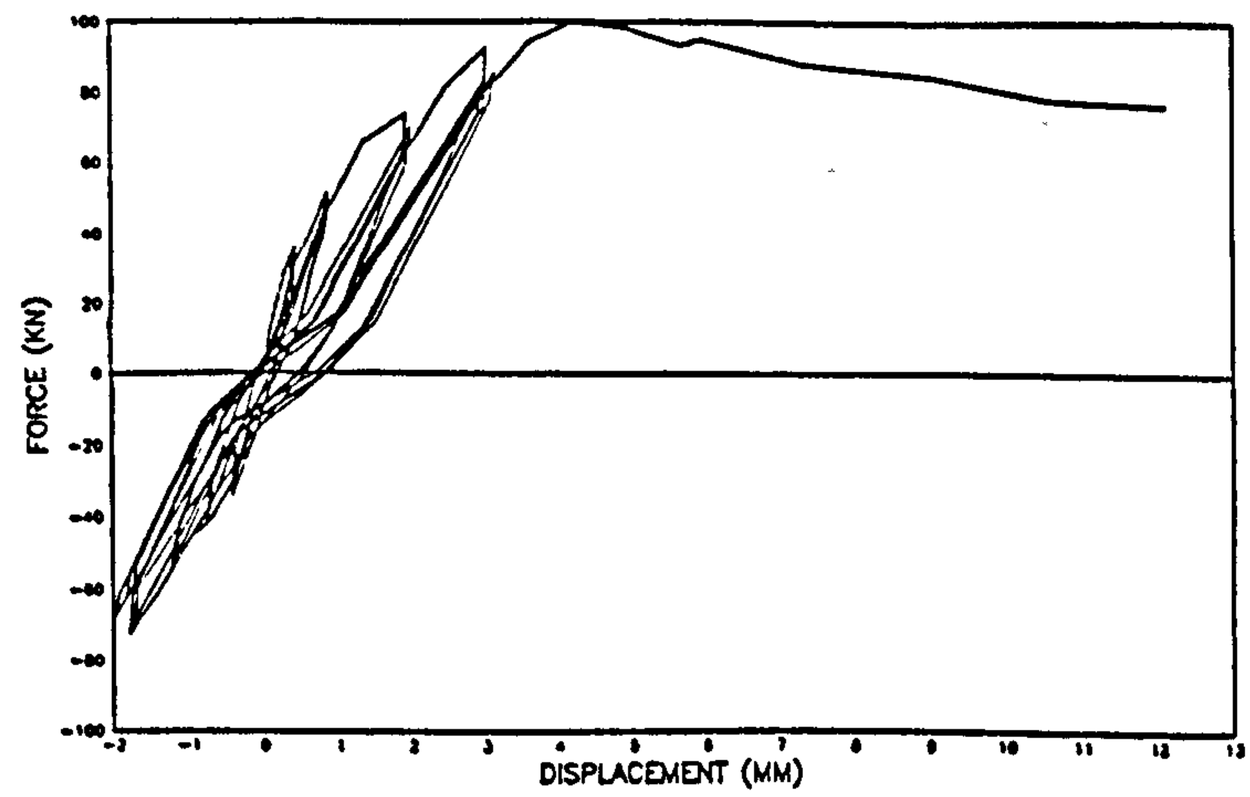


Figure B(18)1 Wall SW18 - force versus displacement 1
(horizontal, LHS, level 4)

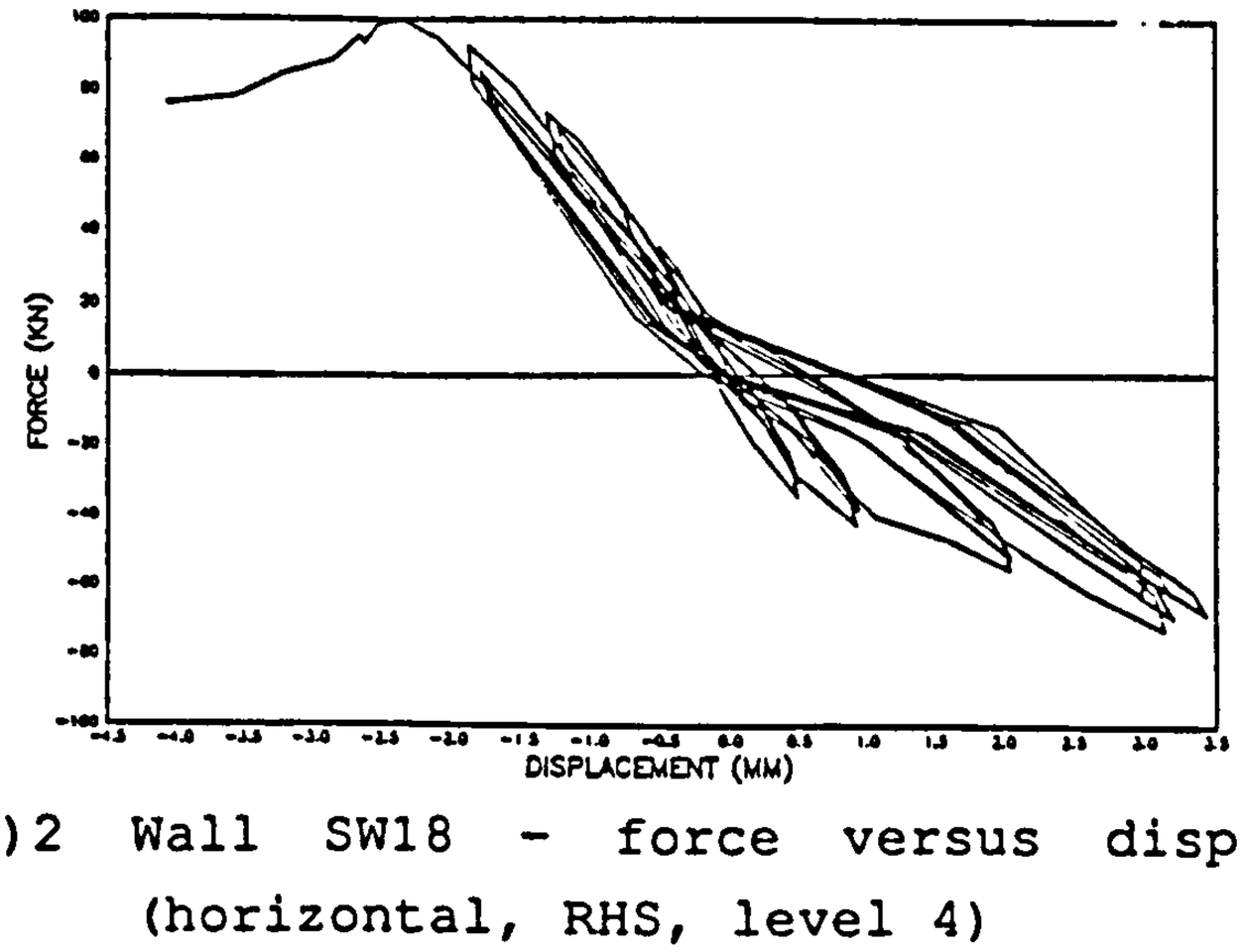


Figure B(18)2 Wall SW18 - force versus displacement 2 (horizontal, RHS, level 4)

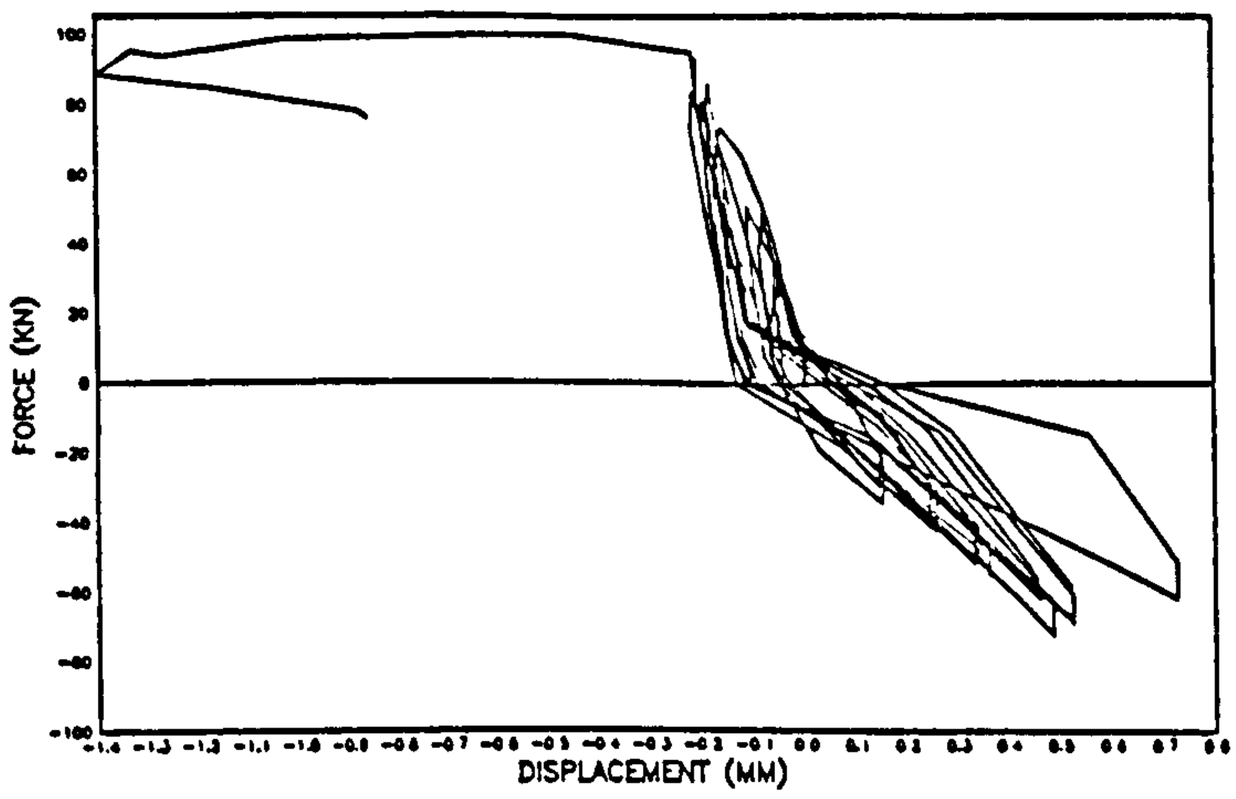


Figure B(18)3 Wall SW18 - force versus displacement 3 (vertical, LHS, level 1)

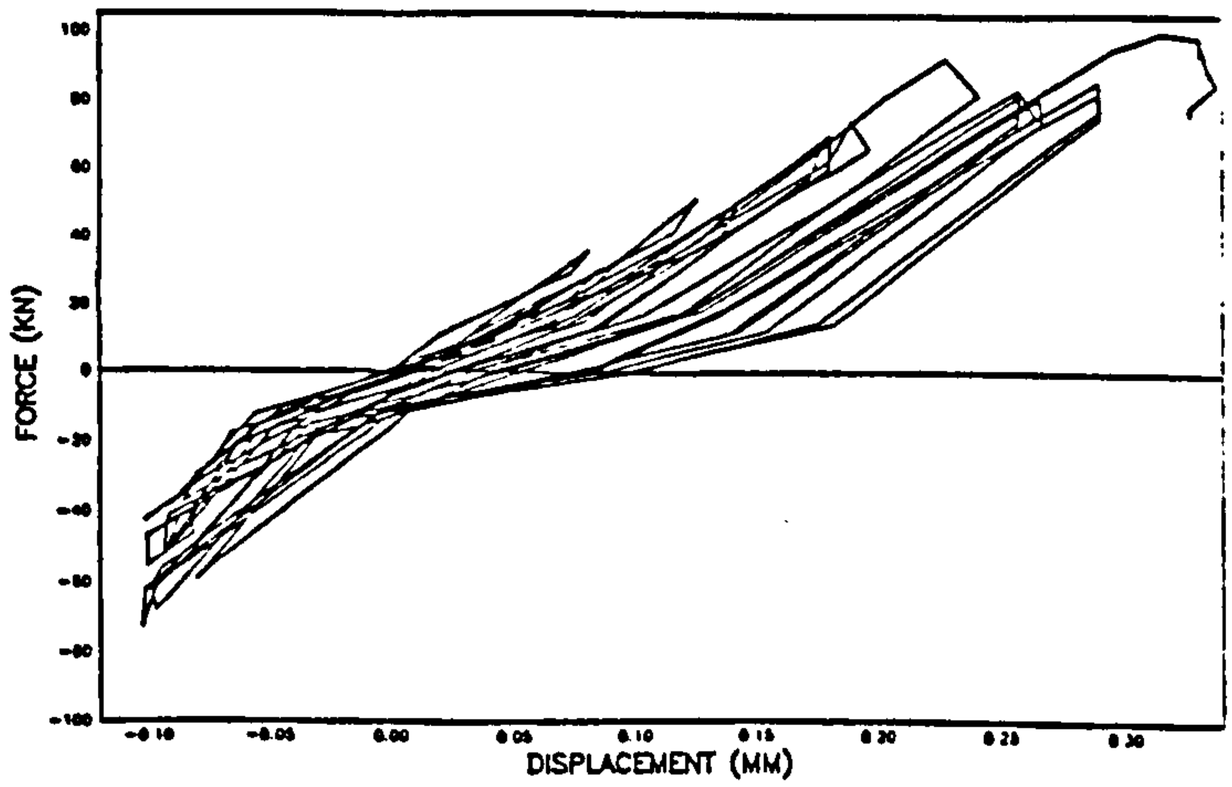


Figure B(18)4 Wall SW18 - force versus displacement 4 (vertical, RHS, level 1)

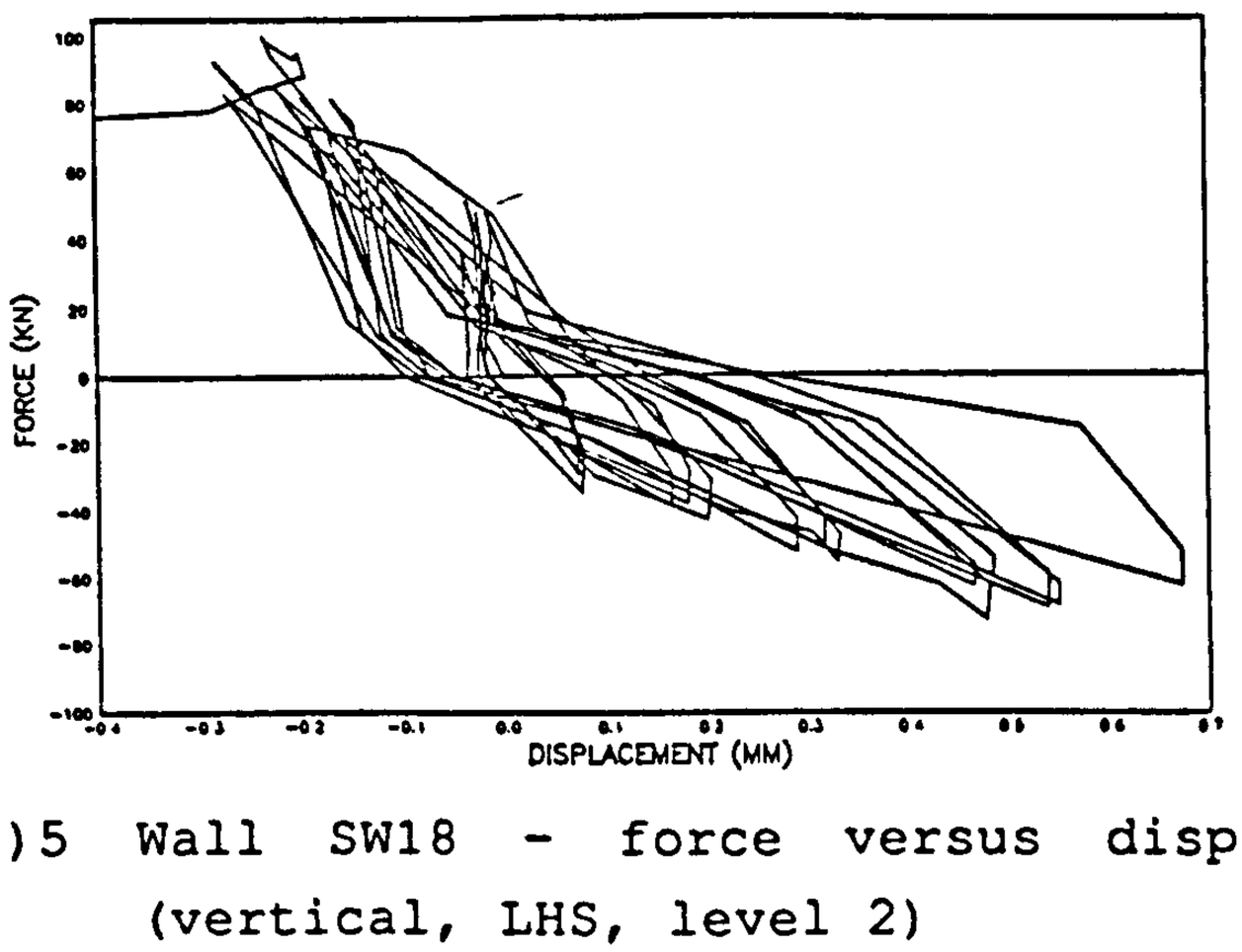


Figure B(18)5 Wall SW18 - force versus displacement 5 (vertical, LHS, level 2)

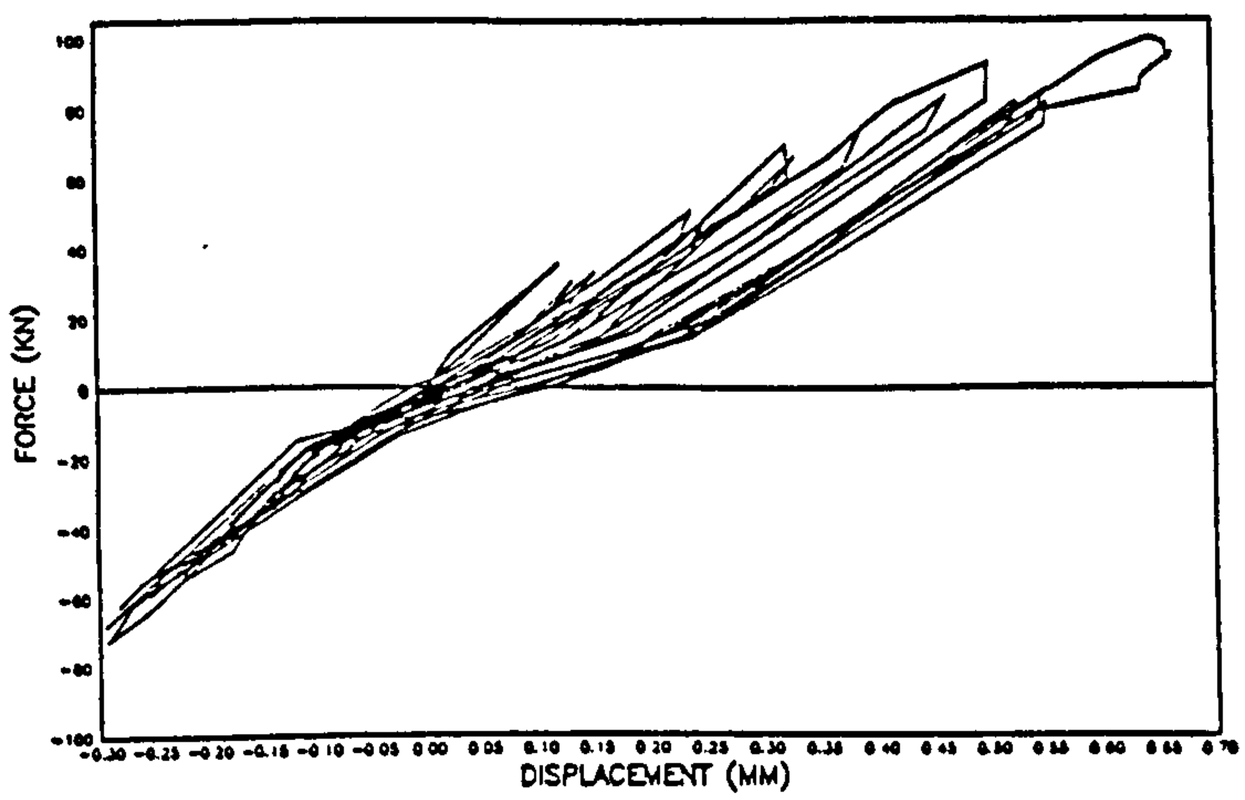


Figure B(18)6 Wall SW18 - force versus displacement 6 (vertical, RHS, level 2)

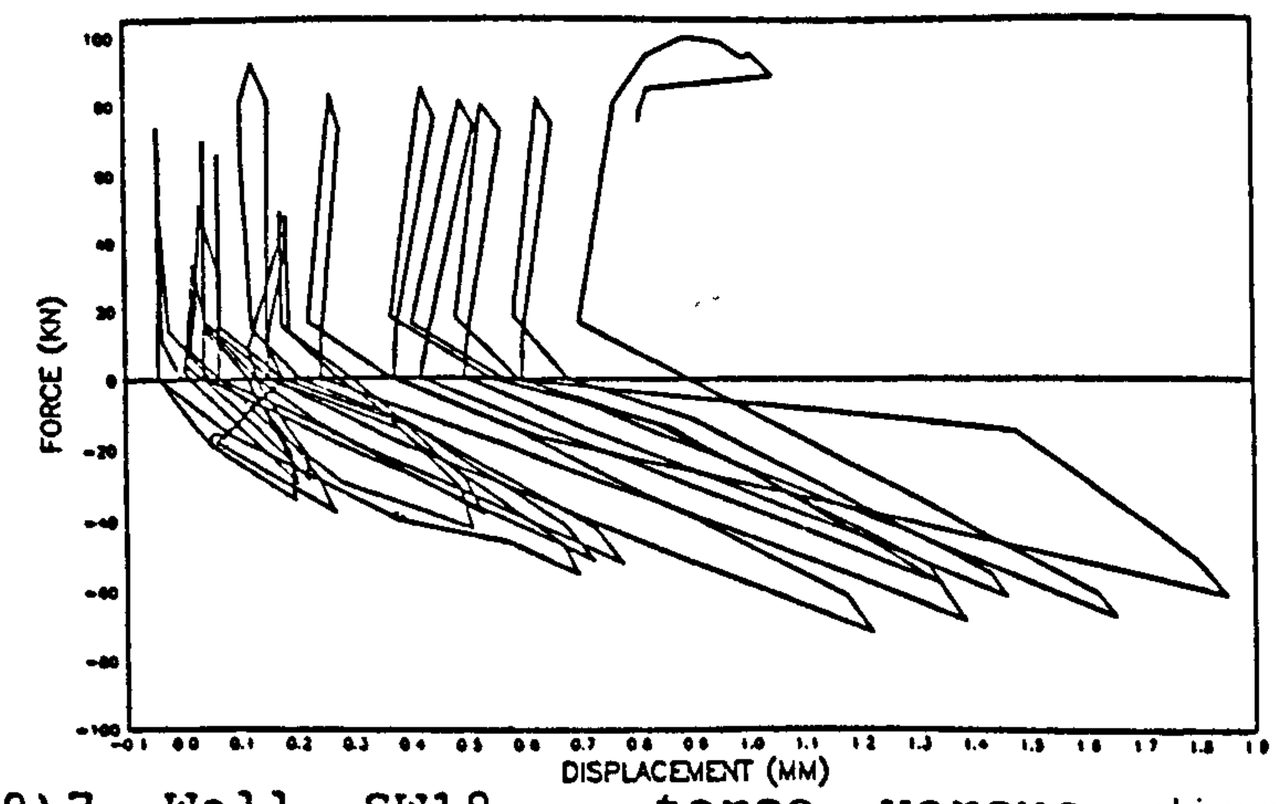


Figure B(18)7 Wall SW18 - force versus displacement 9 (vertical, LHS, level 4)

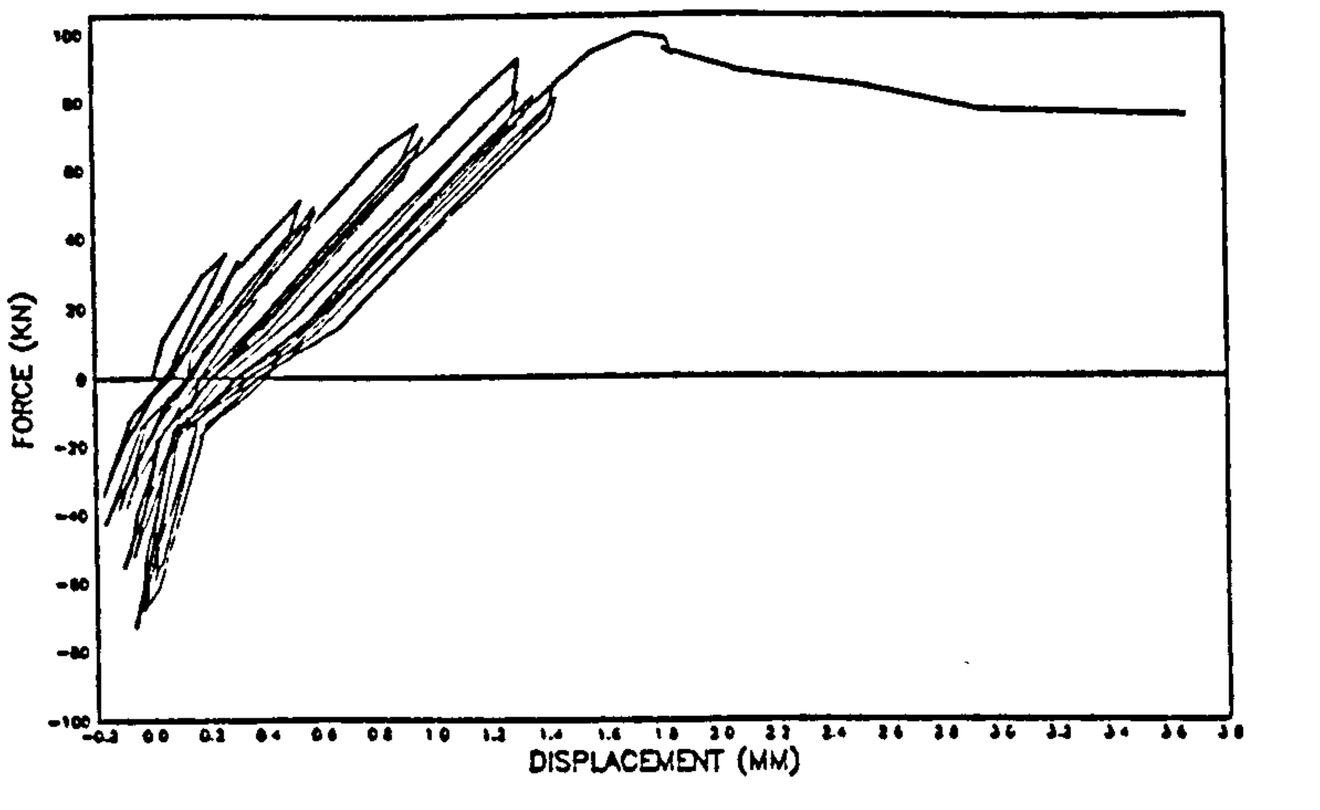


Figure B(18)8 Wall SW18 - force versus displacement 10 (vertical, RHS, level 4)

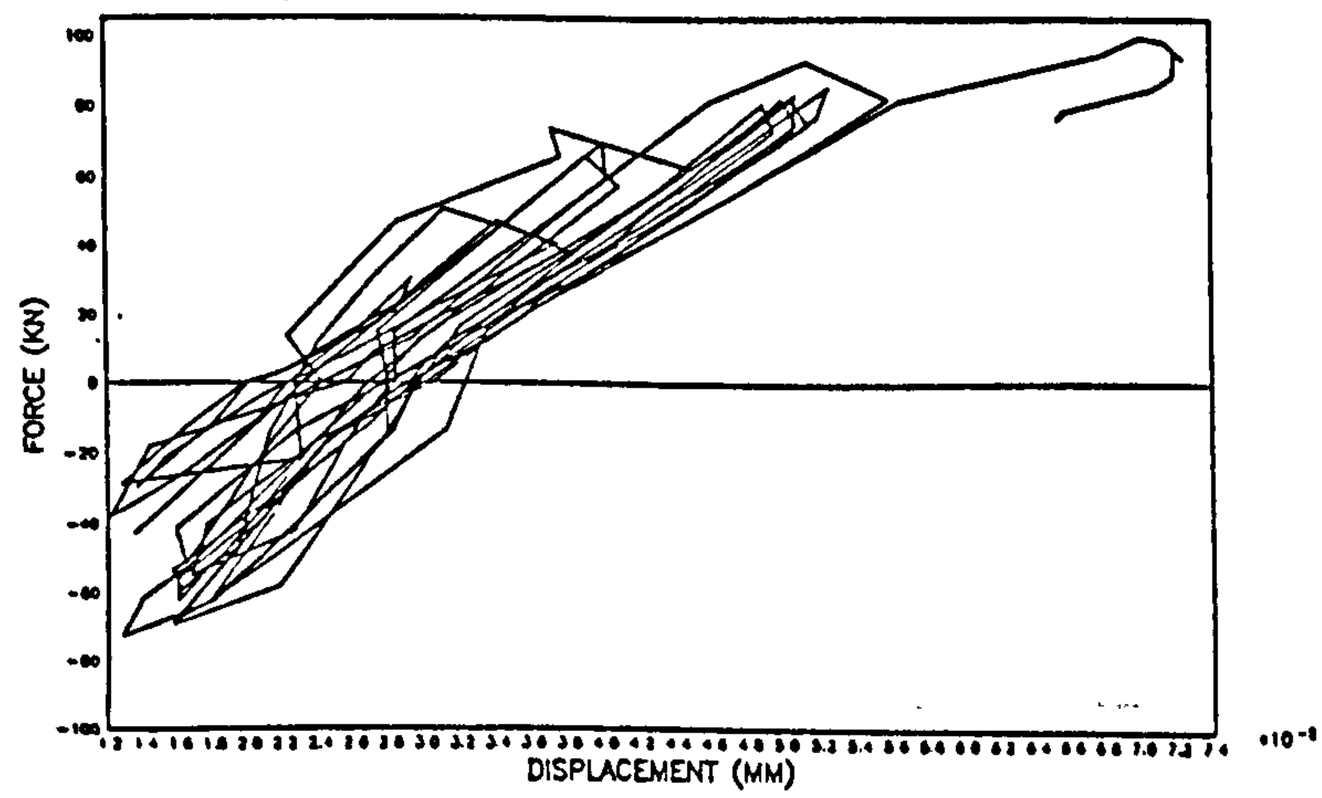


Figure B(18)9 Wall SW18 - force versus displacement 11 (foundation, RHS)

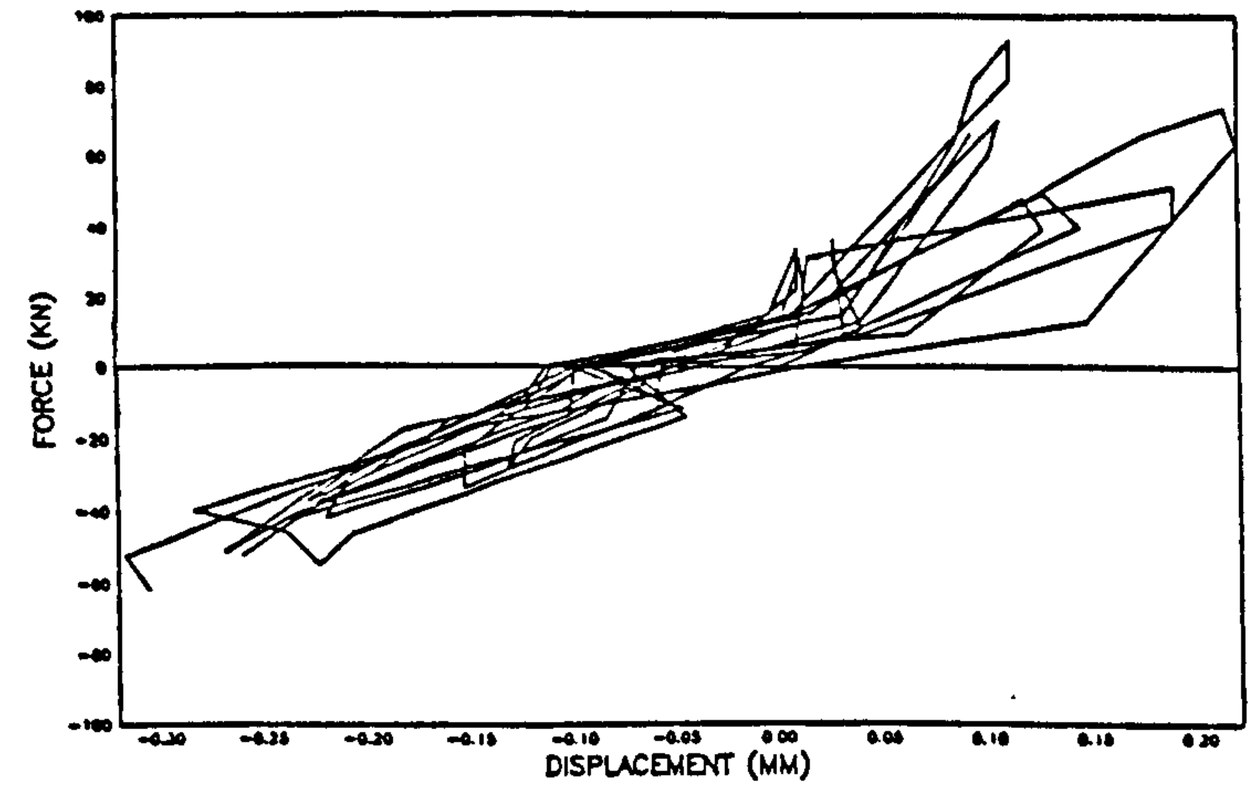


Figure B(18)10 Wall SW18 - force versus displacement 12 (out-of-plane)

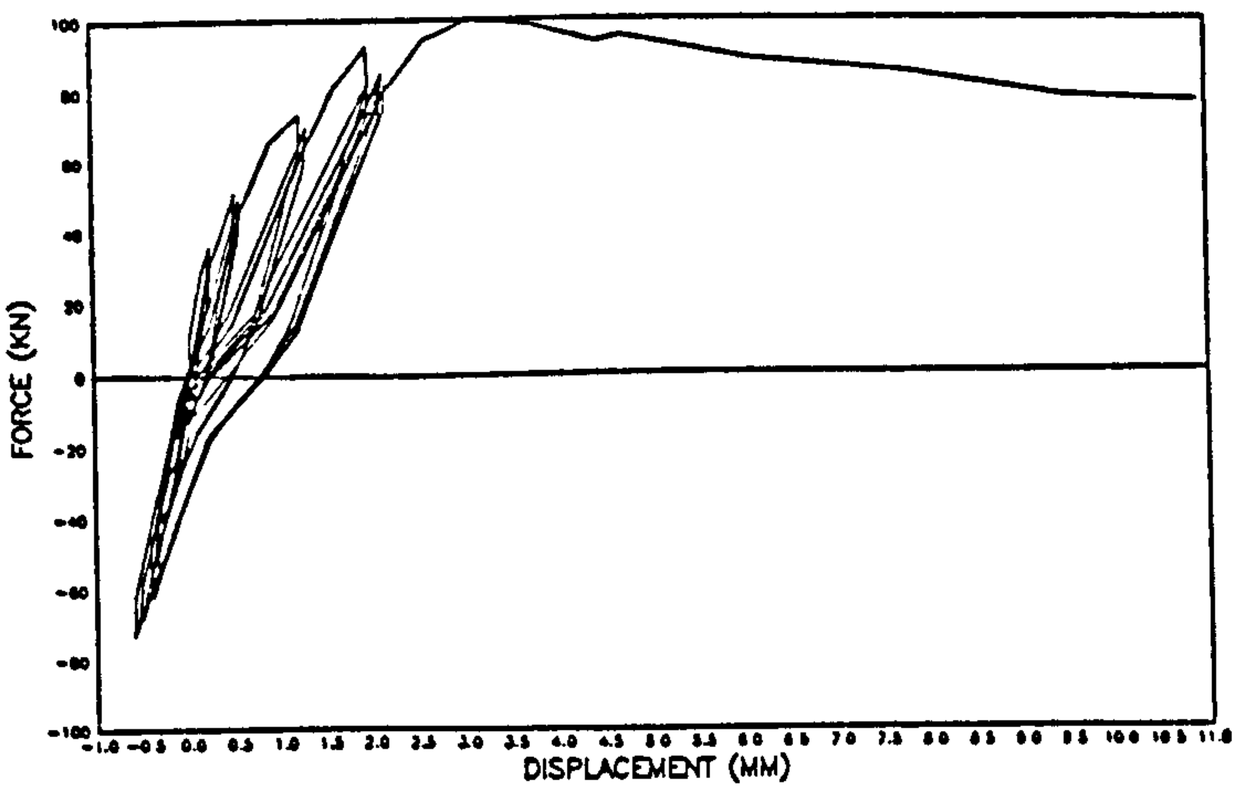


Figure B(18)11.a Wall SW18 - force versus displacement 15a (horizontal, LHS, level 3)

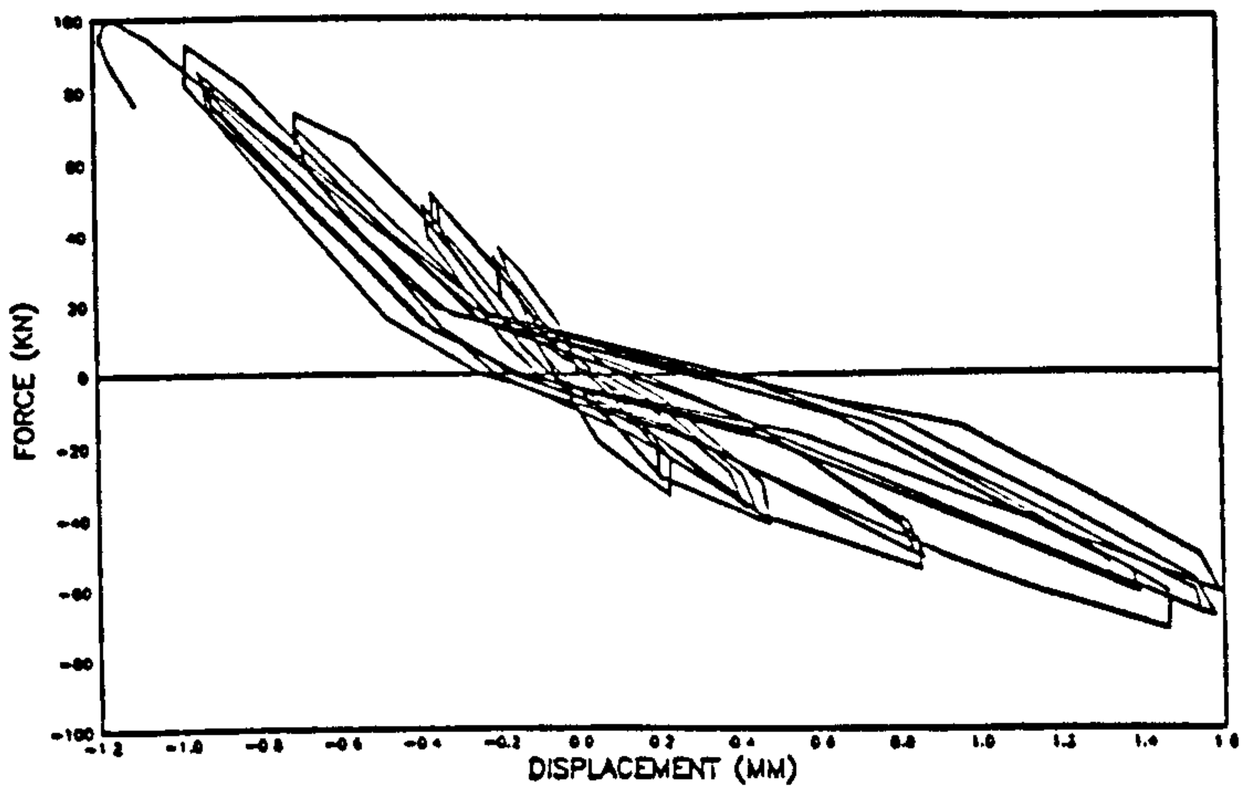


Figure B(18)11.b Wall SW18 - force versus displacement 15b (horizontal, RHS, level 3)

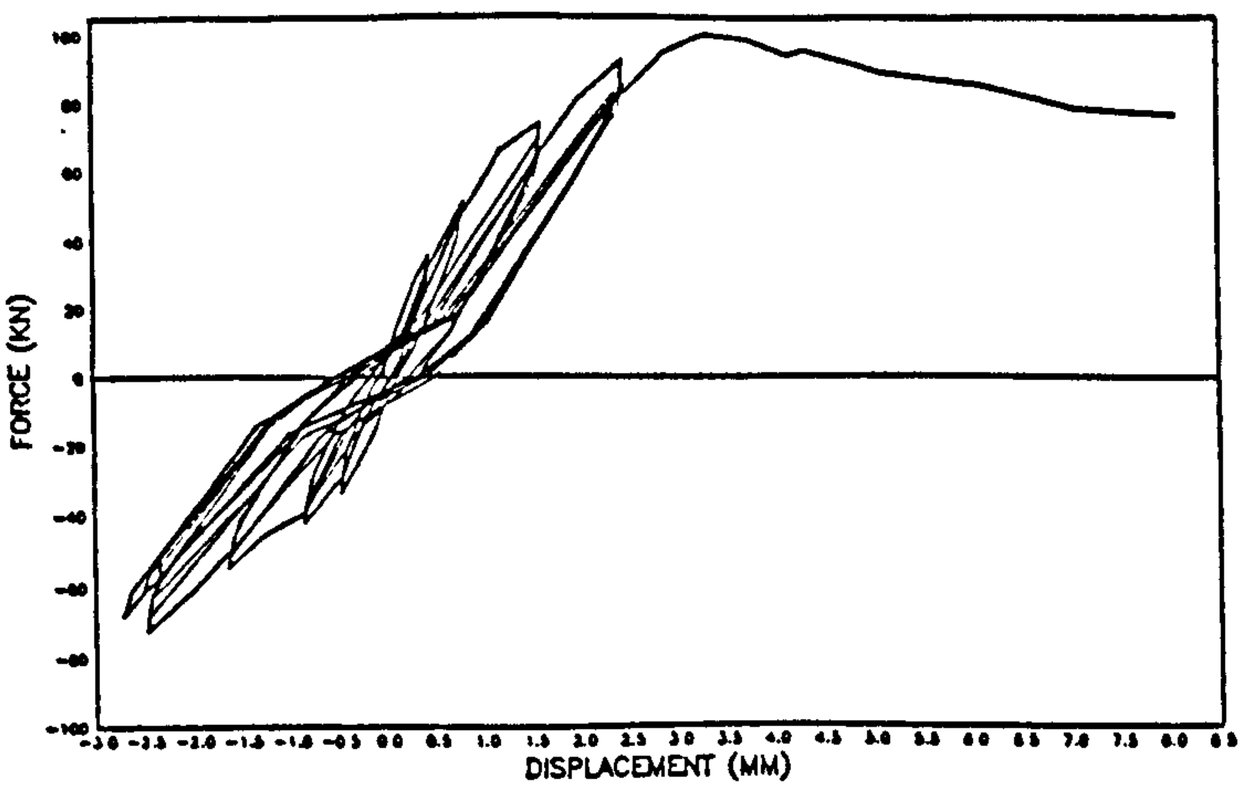


Figure B(18)12 Wall SW18 - force versus top horizontal displacement

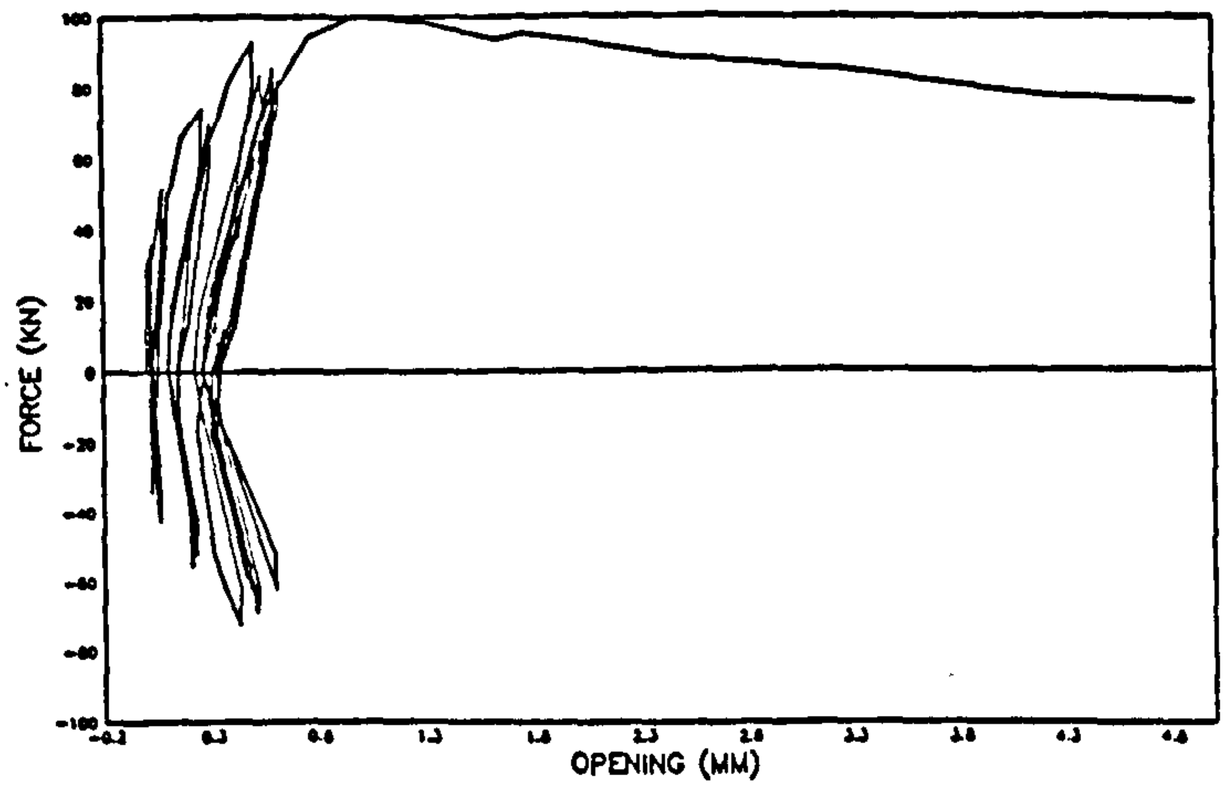


Figure B(18)13 Wall SW18 - force versus opening at third level

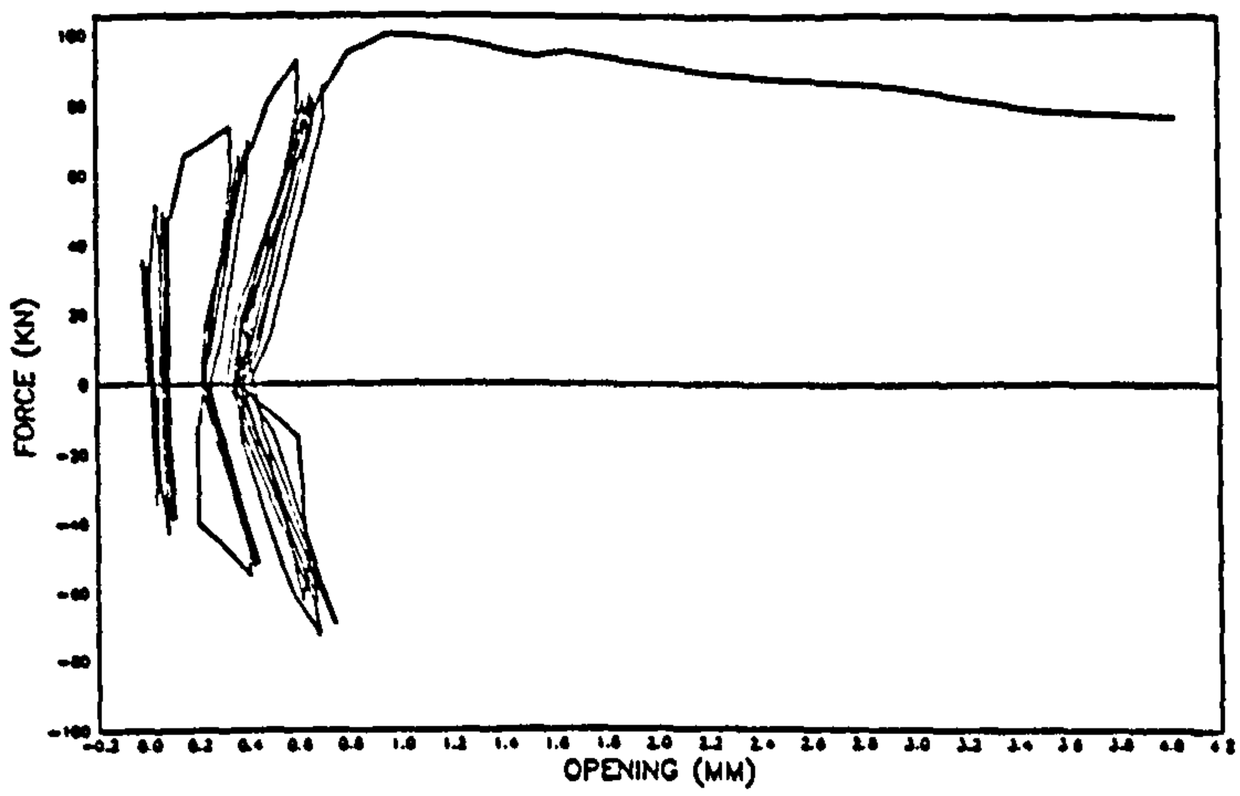


Figure B(18)14 Wall SW18 - force versus opening on top

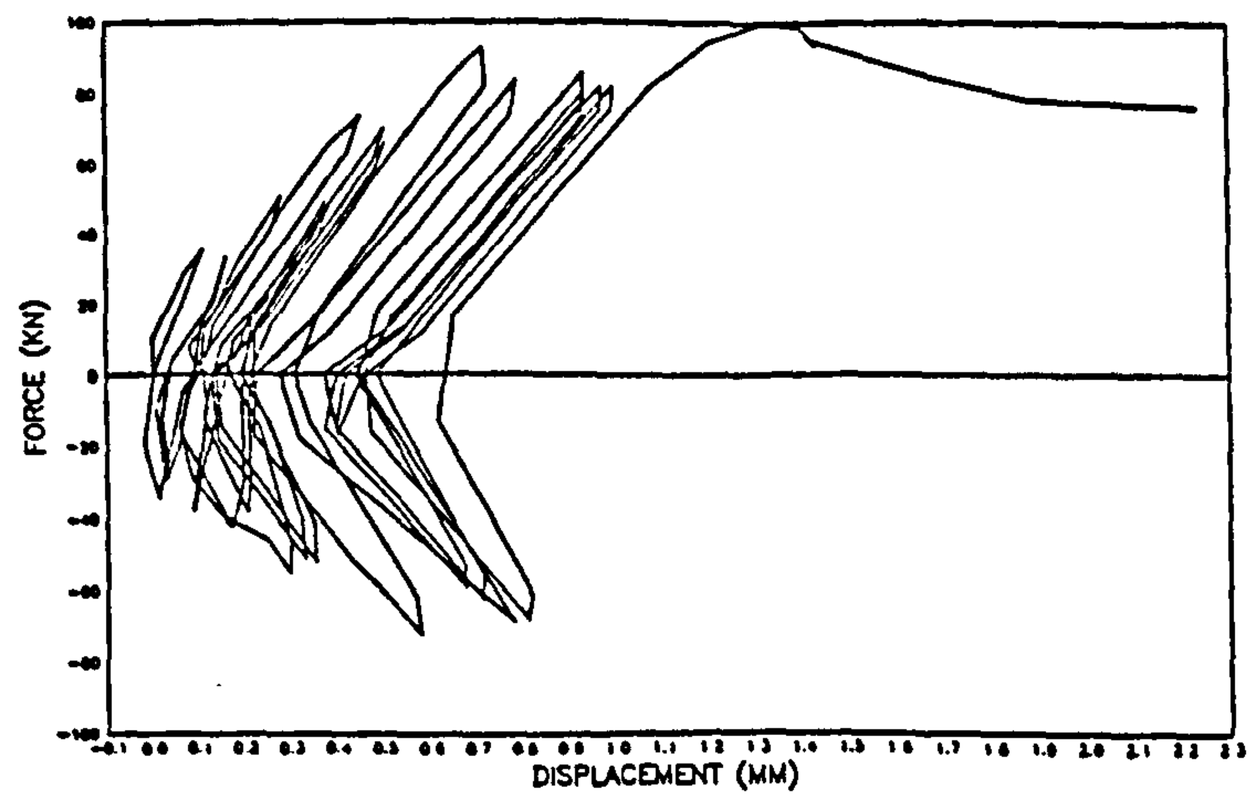


Figure B(18)15 Wall SW18 - force versus extension on top

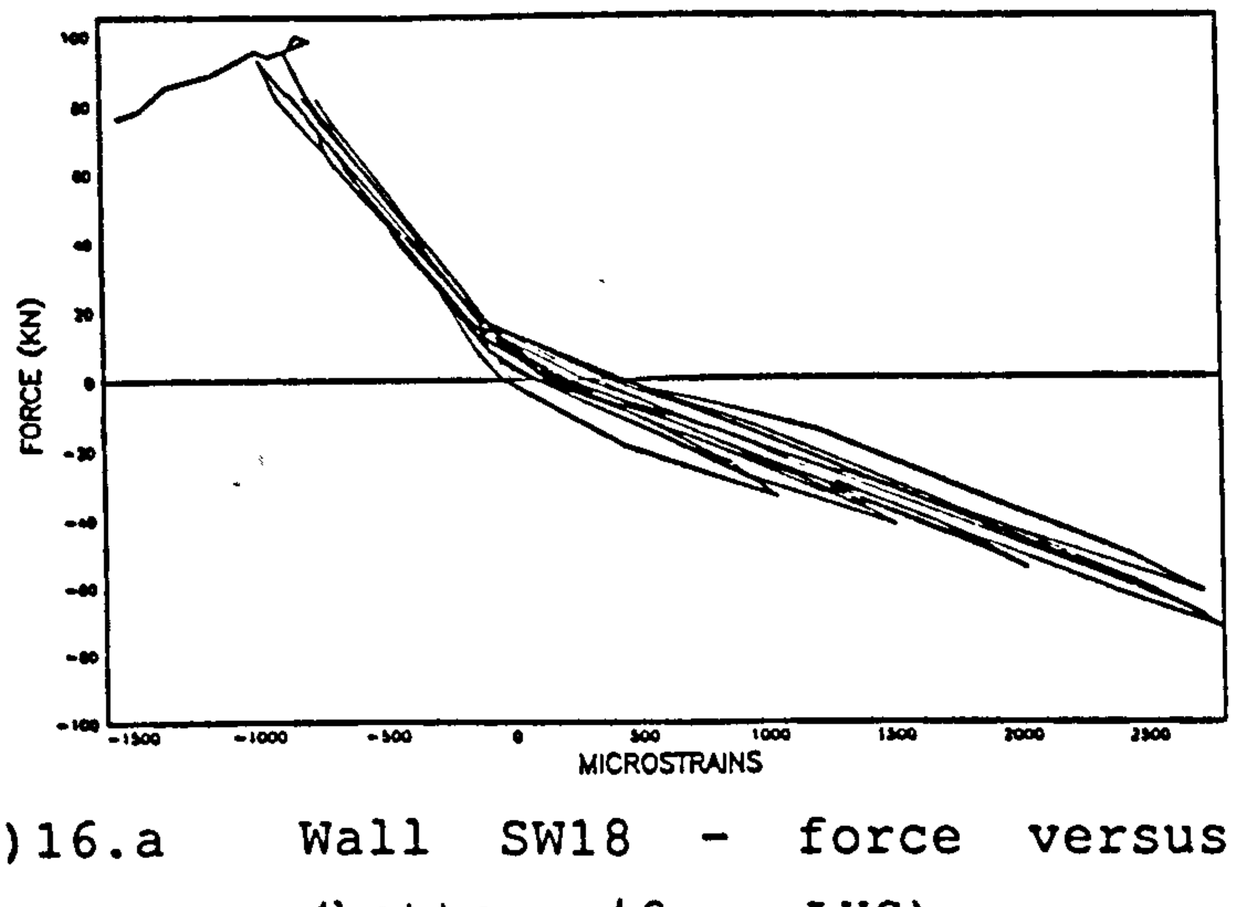


Figure B(18)16.a Wall SW18 - force versus strain 1, (bottom, ϕ8mm, LHS)

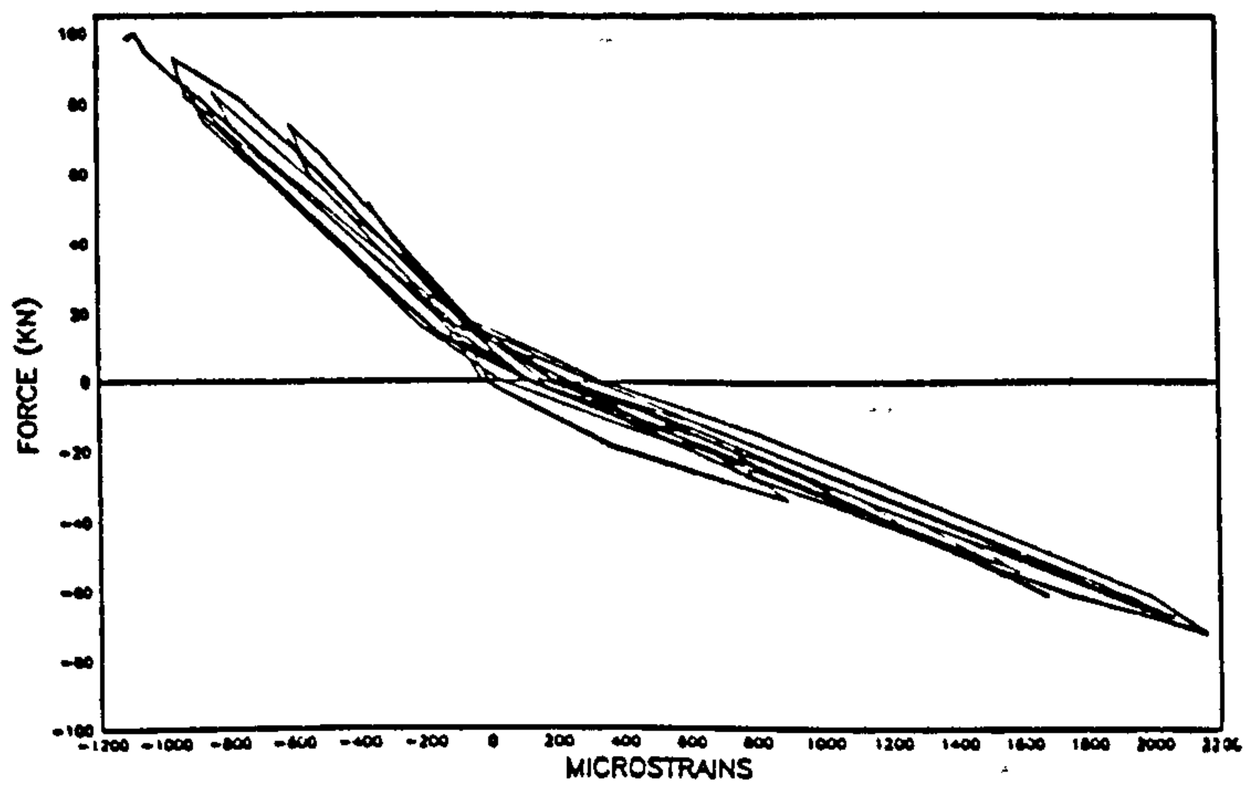


Figure B(18)16.b Wall SW18 - force versus strain 1, (bottom, ϕ8mm, LHS)

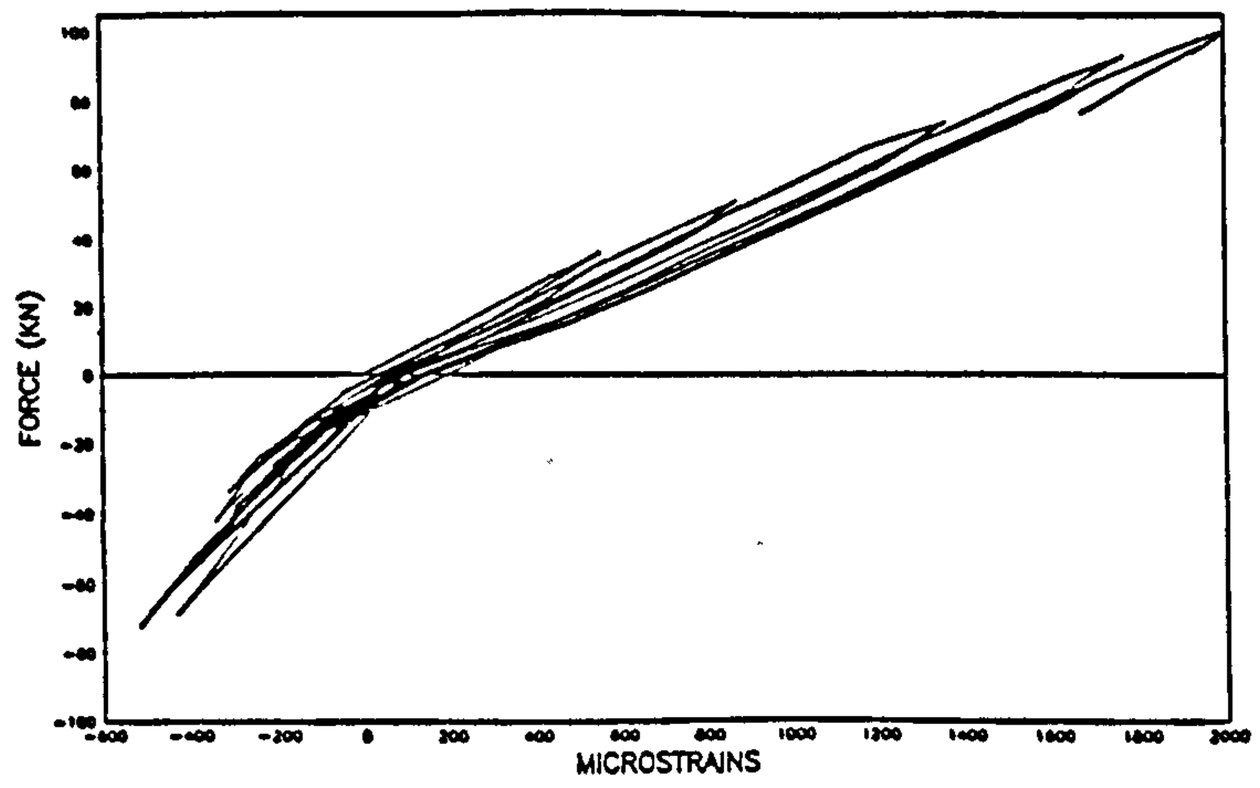


Figure B(18)17.a Wall SW18 - force versus strain 2, (bottom, ϕ12mm, RHS)

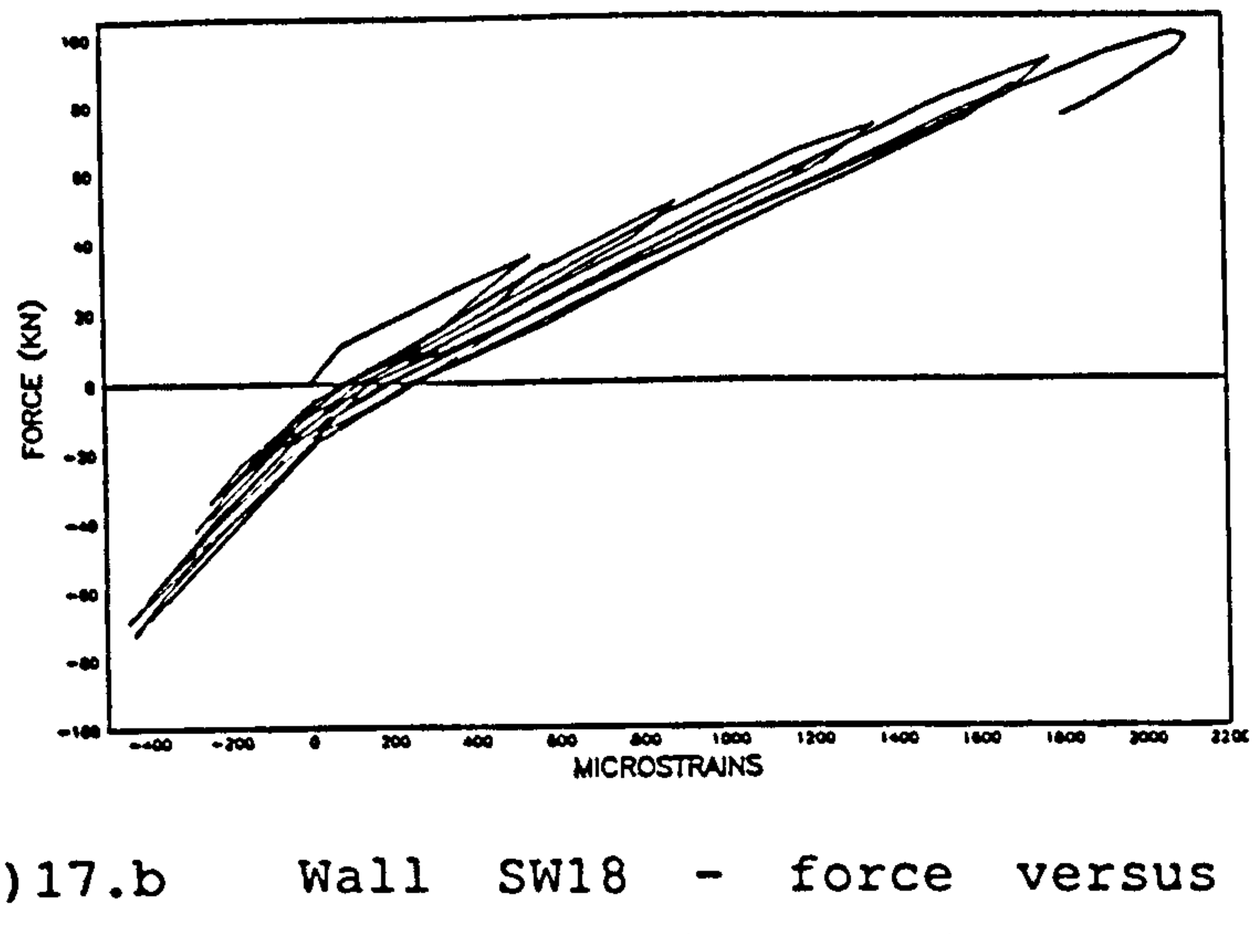


Figure B(18)17.b Wall SW18 - force versus strain 2:: (bottom, ϕ12mm, RHS)

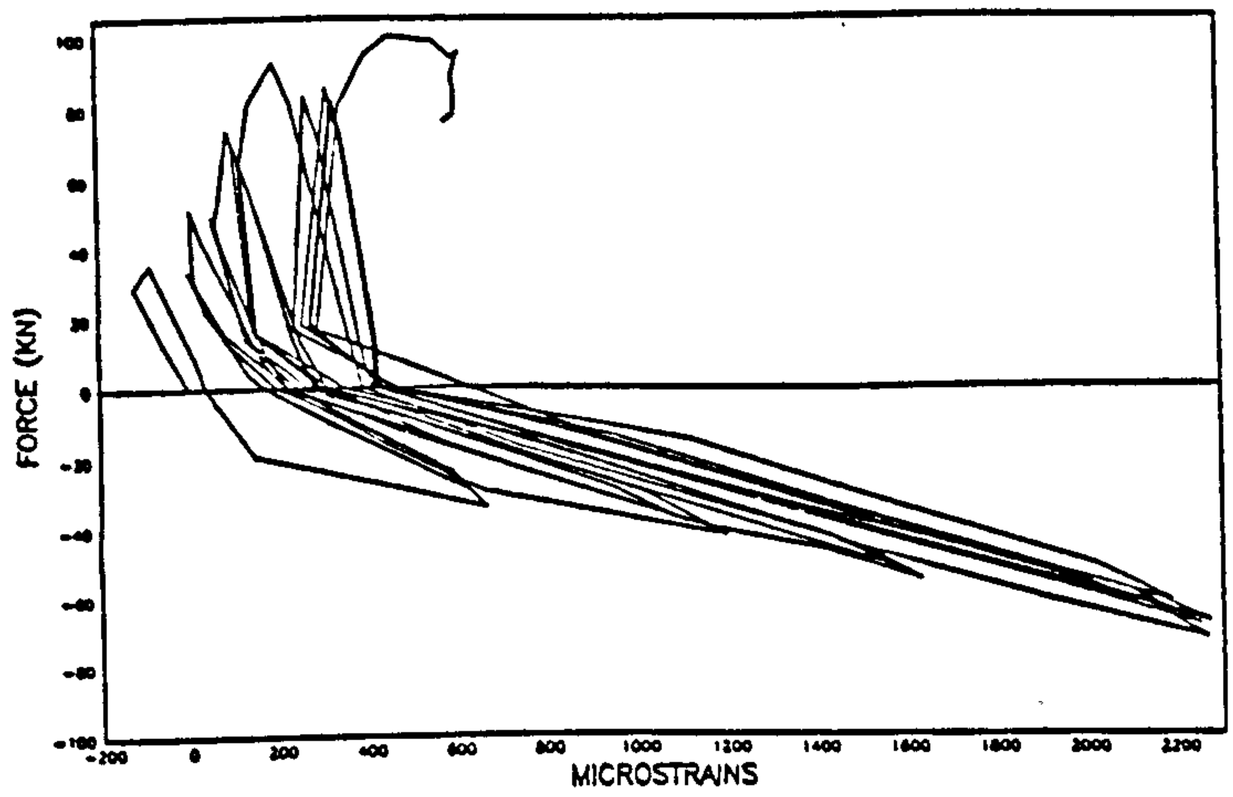


Figure B(18)18 Wall SW18 - force versus strain 9 (second level, ϕ8mm, LHS)

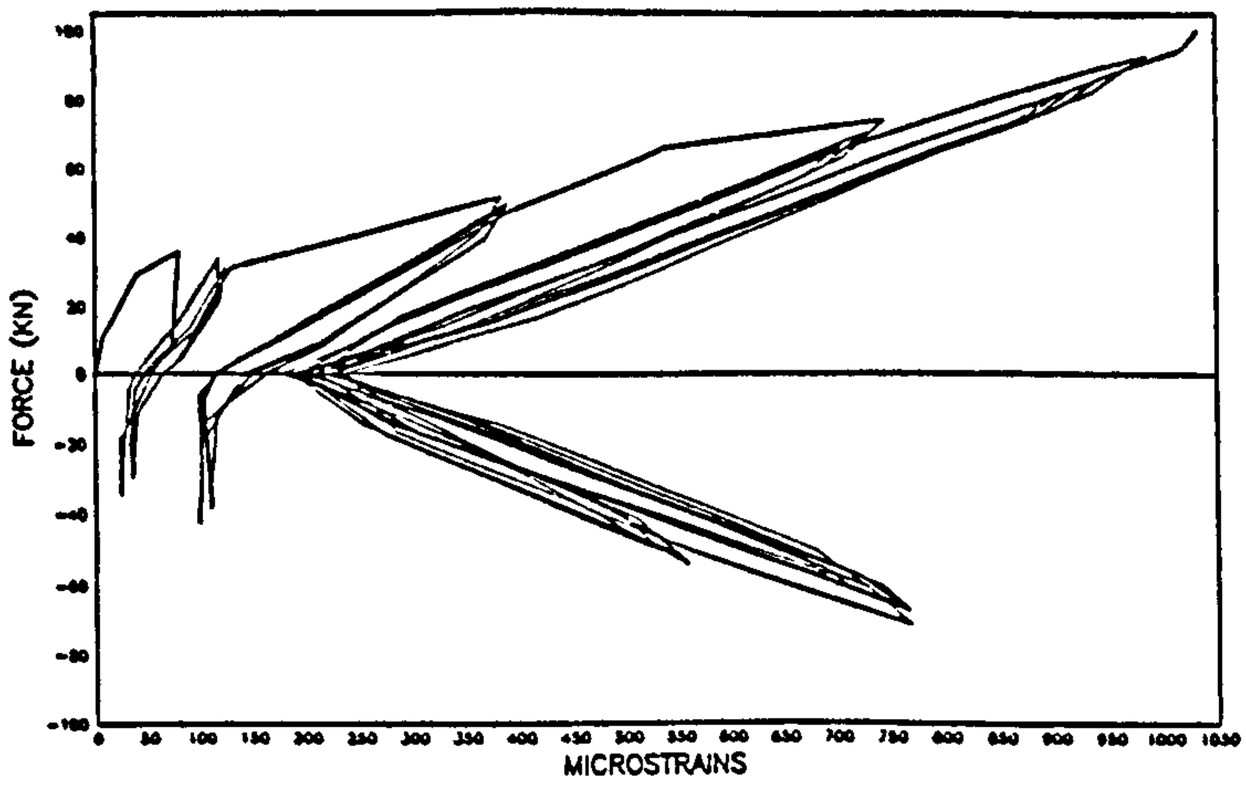


Figure B(18)19 Wall SW18 - force versus strain 12 (level of zero moment, ϕ12mm, RHS)

Figure B(18)20 Wall SW18 - force versus strain 13 (level of zero moment, ϕ6mm, LHS)

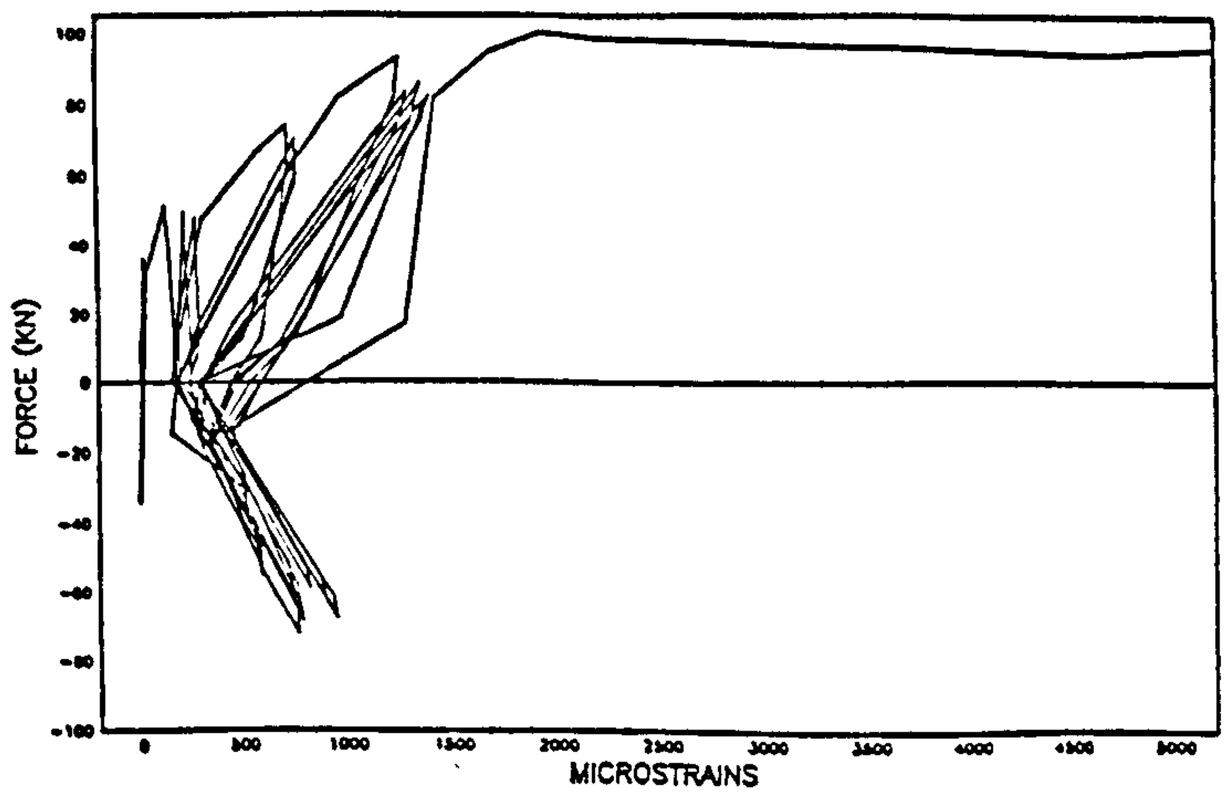


Figure B(18)21 Wall SW18 - force versus strain 19 (stirrup)

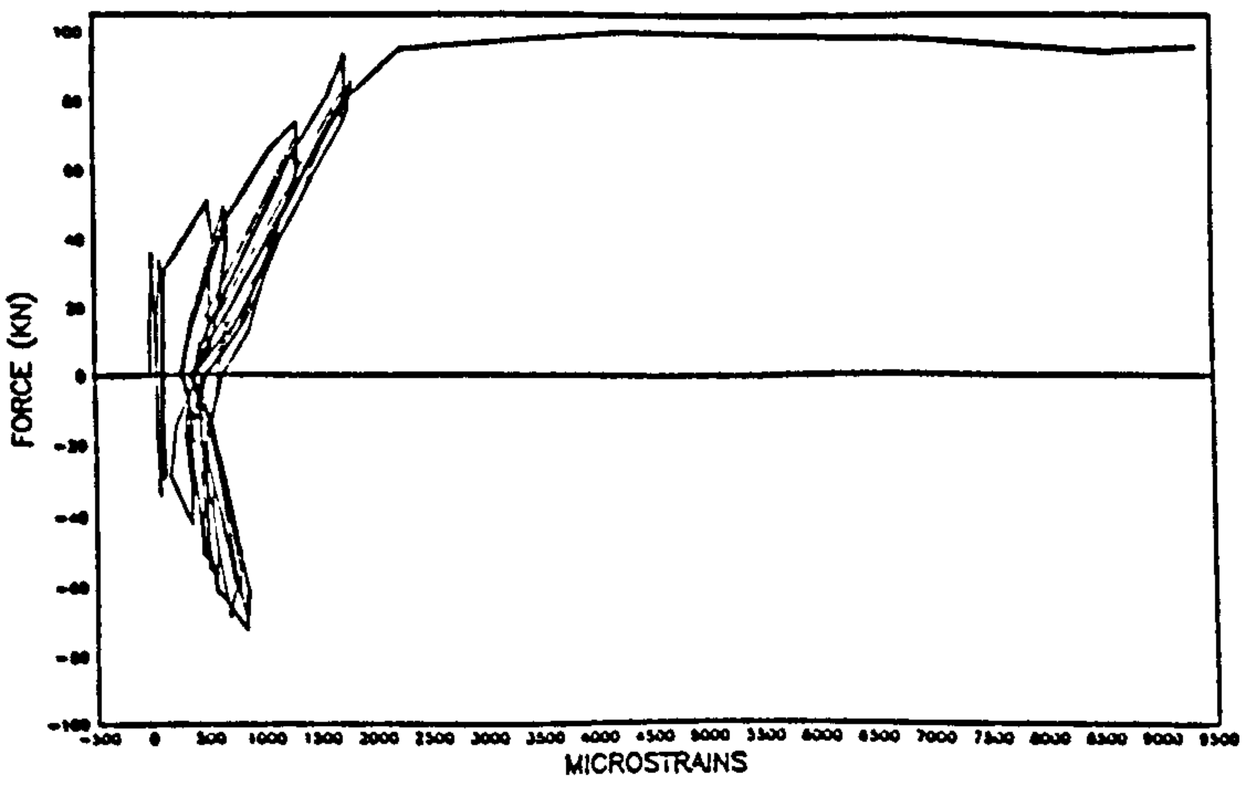


Figure B(18)22 Wall SW18 - force versus strain 20 (stirrup)

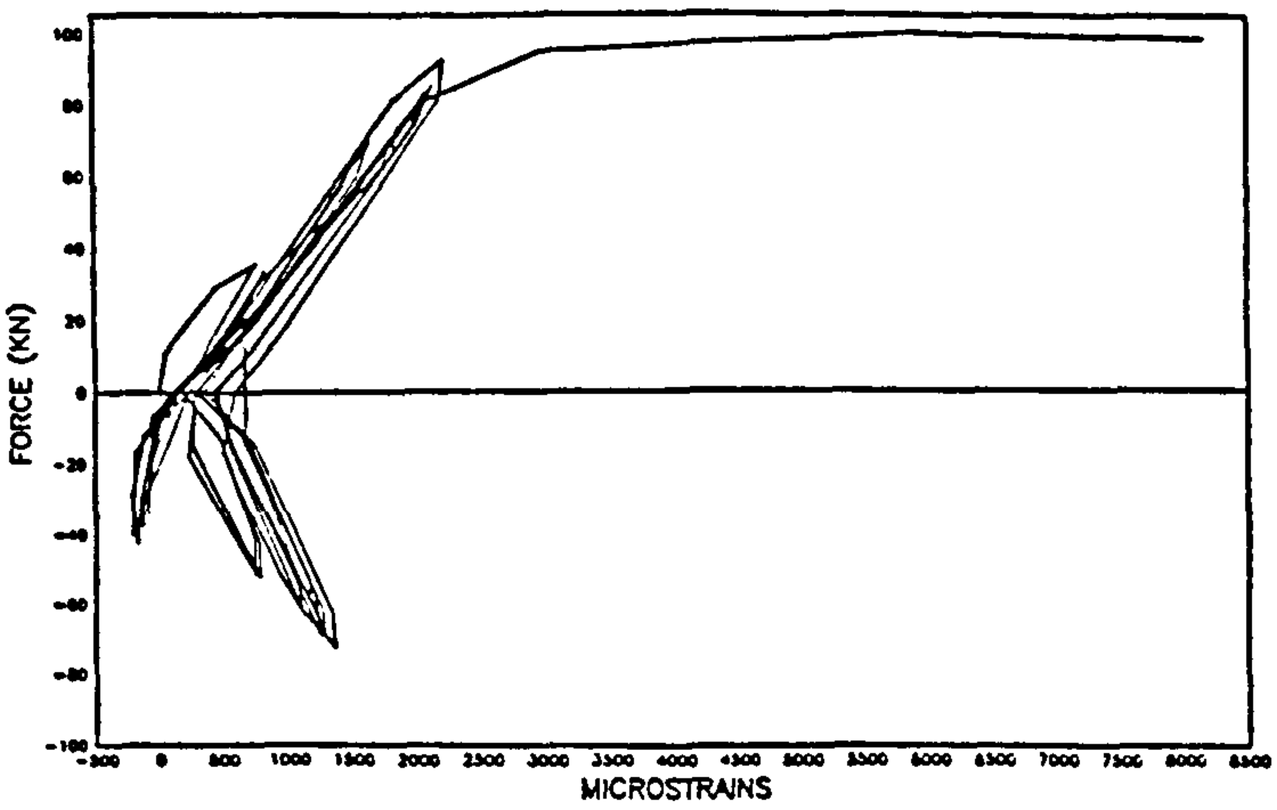


Figure B(18)23 Wall SW18 - force versus strain 21 (stirrup)

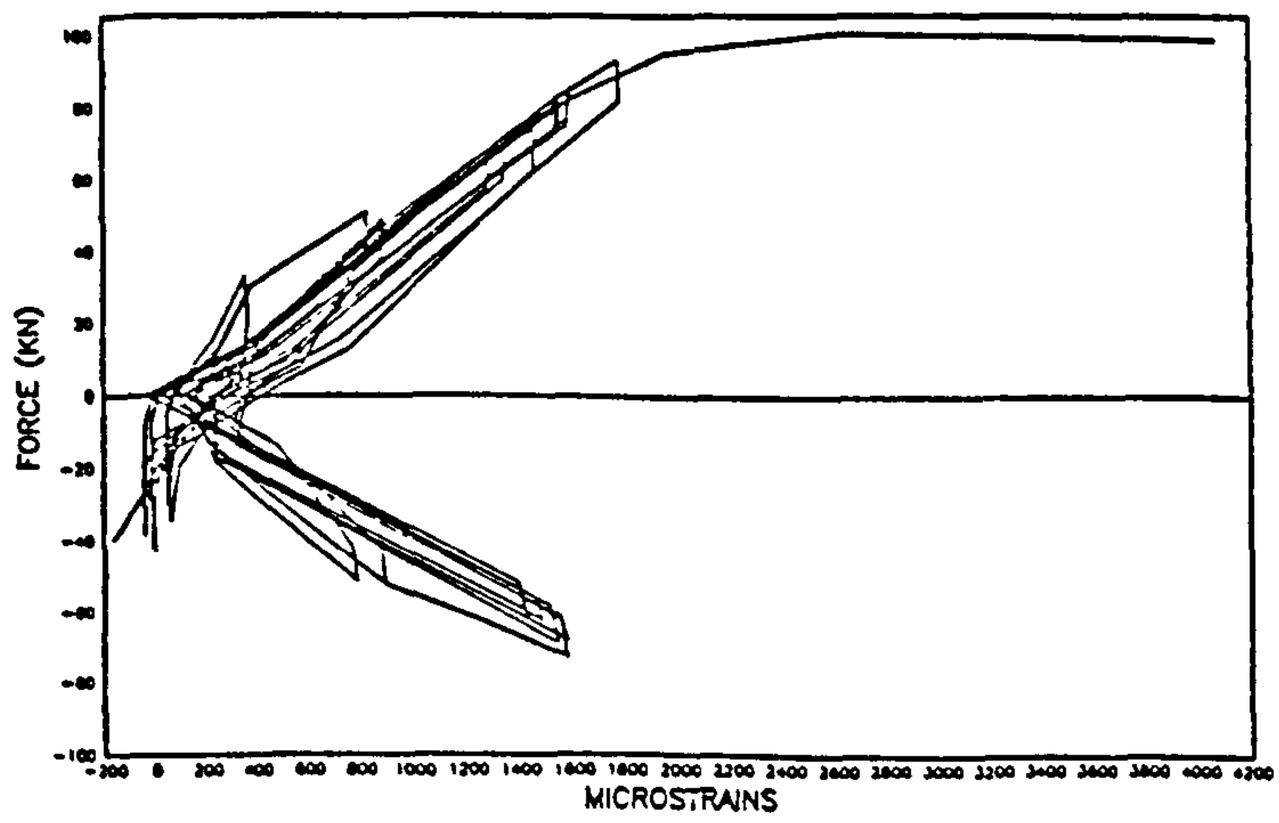


Figure B(18)24 Wall SW18 - force versus strain 22 (stirrup)

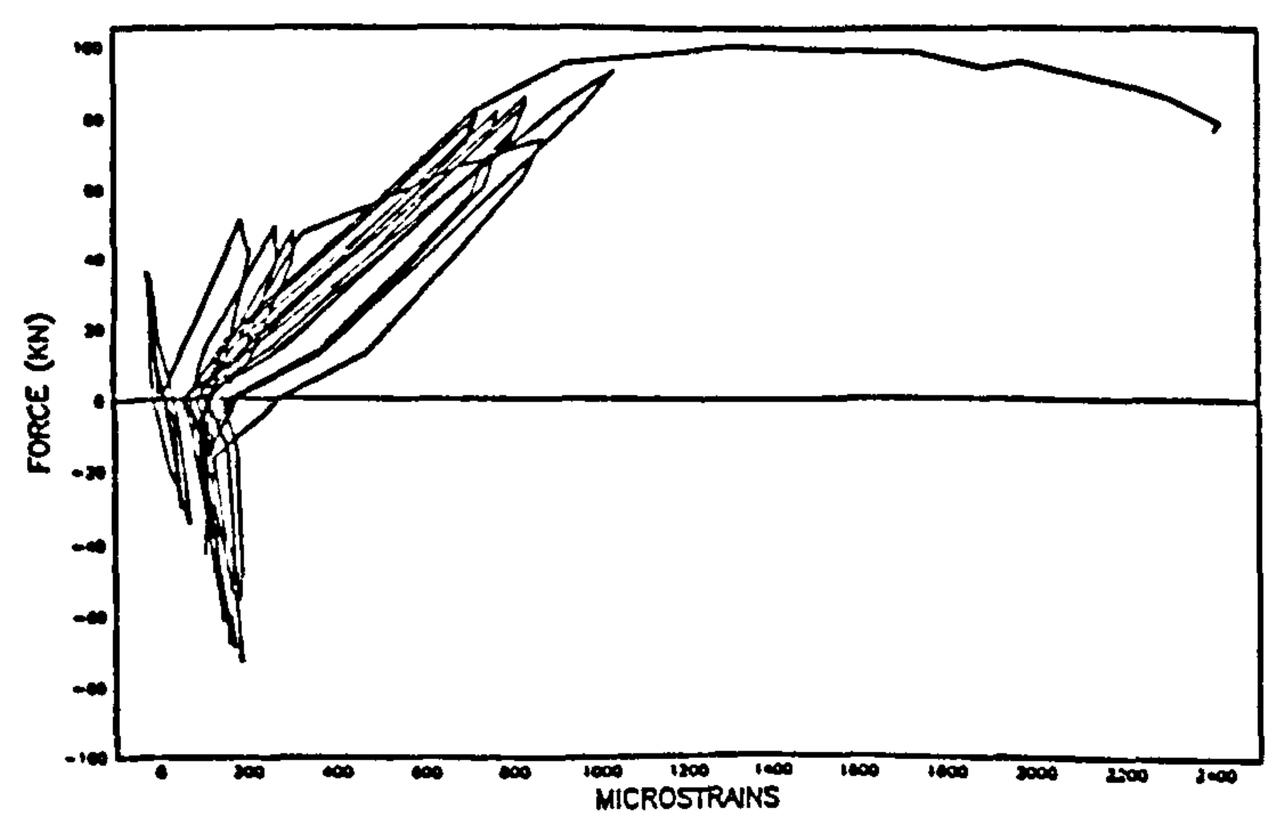


Figure B(18)25 Wall SW18 - force versus strain 23 (confinement reinforcement)

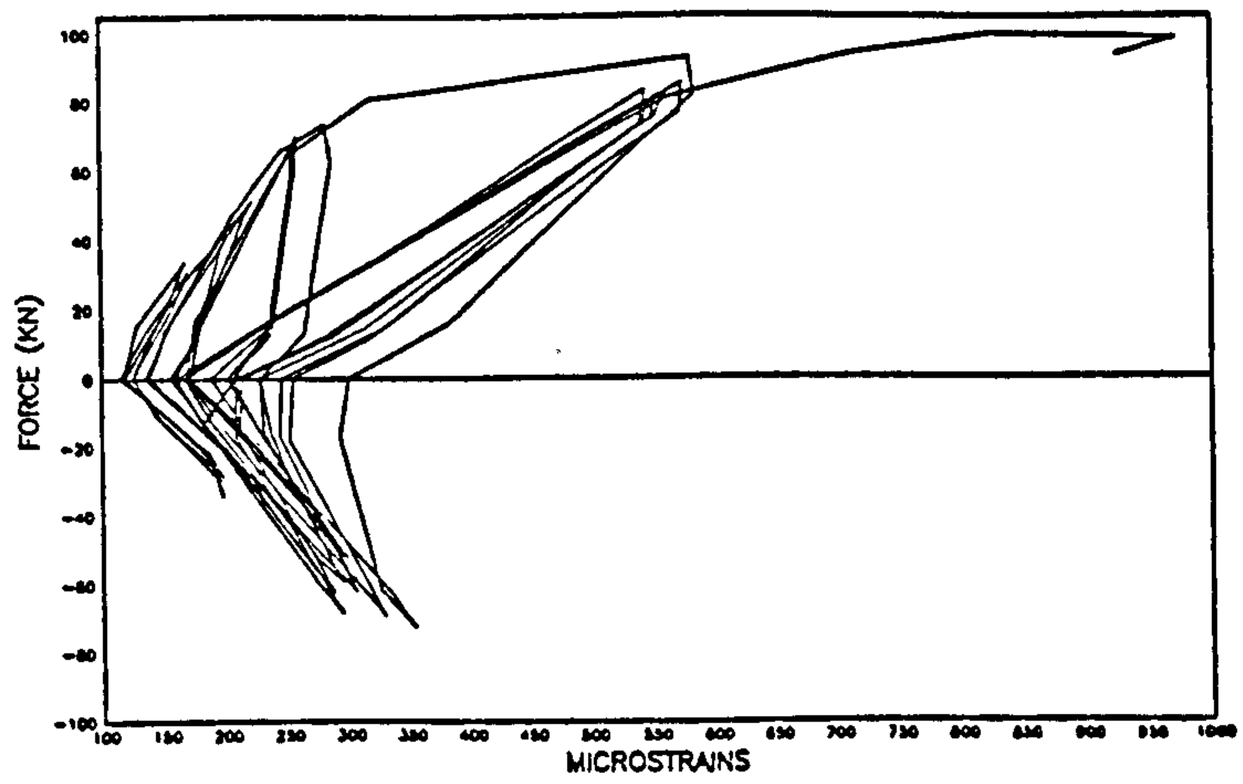


Figure B(18)26 Wall SW18 - force versus strain 24 (confinement reinforcement)

APPENDIX C

RESULTS OF ANALYTICAL STUDIES

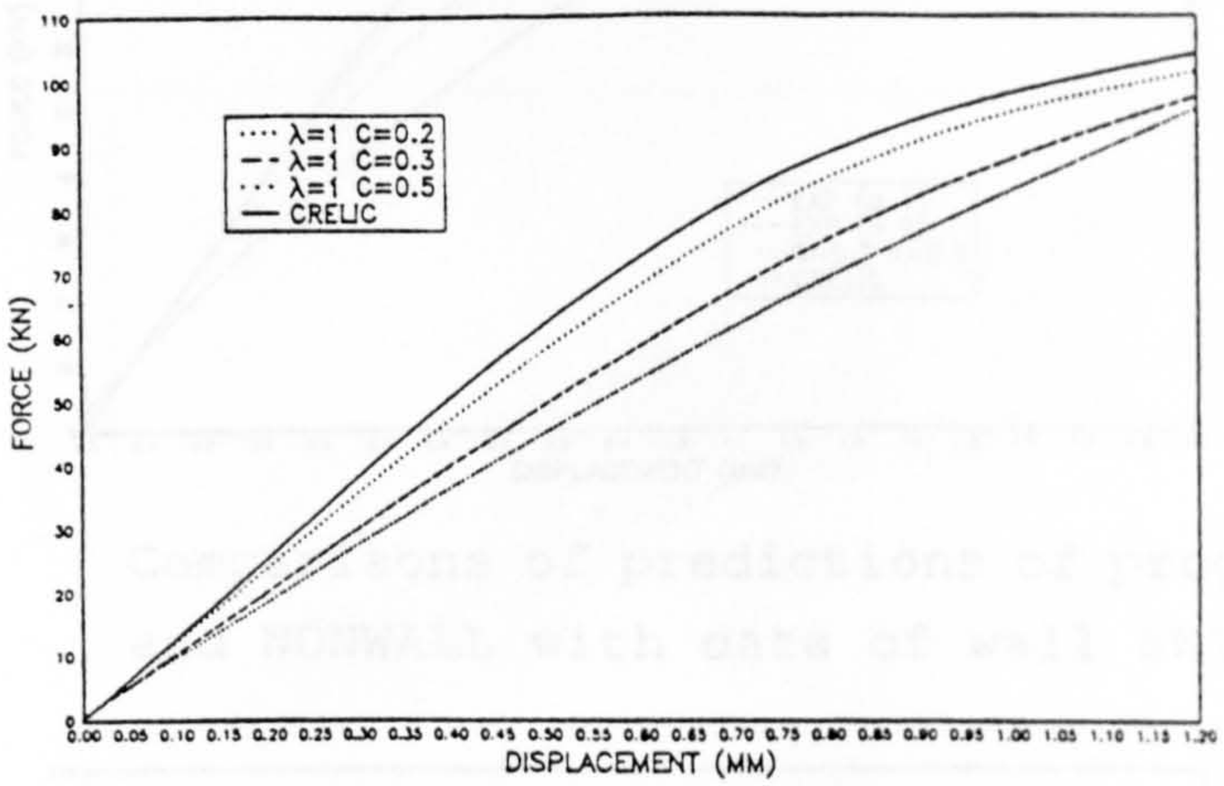


Figure C.1 Comparison of results of programs CRELIC and NONWALL for different values of C

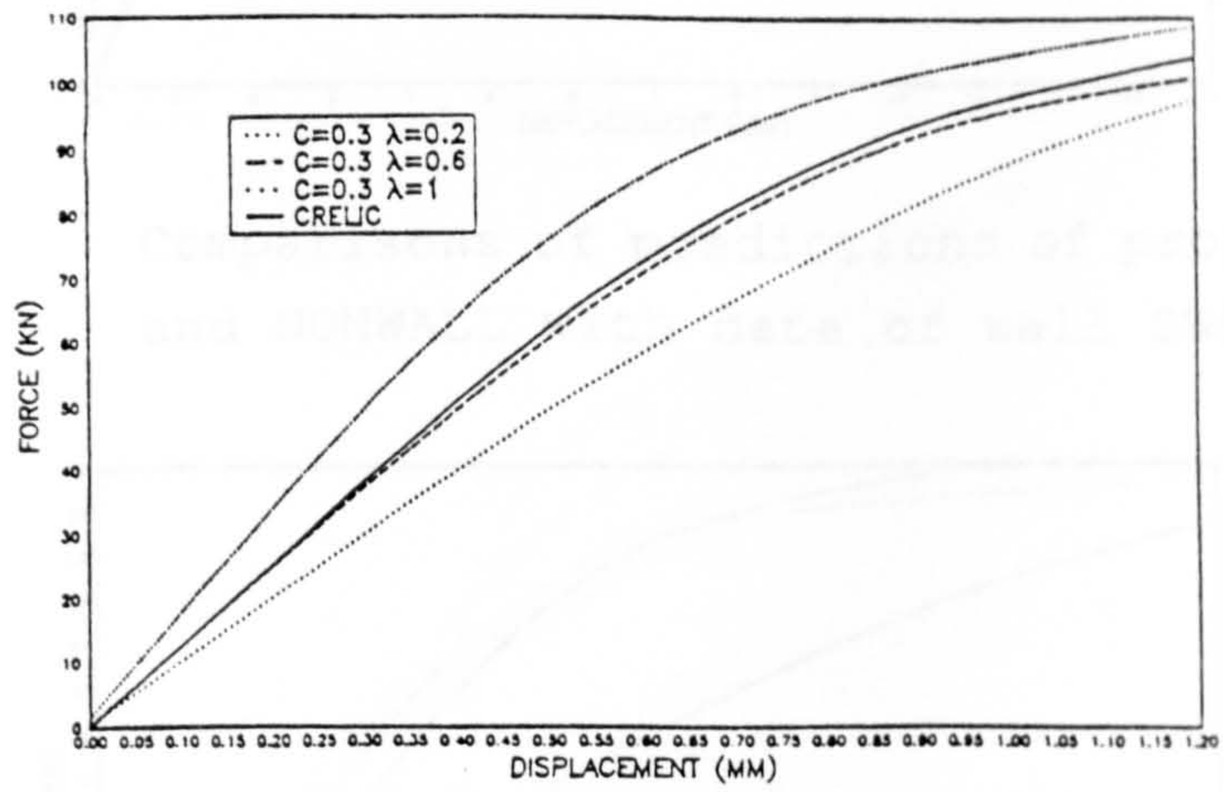


Figure C.2 Comparison of results of programs CRELIC and NONWALL for different values of λ

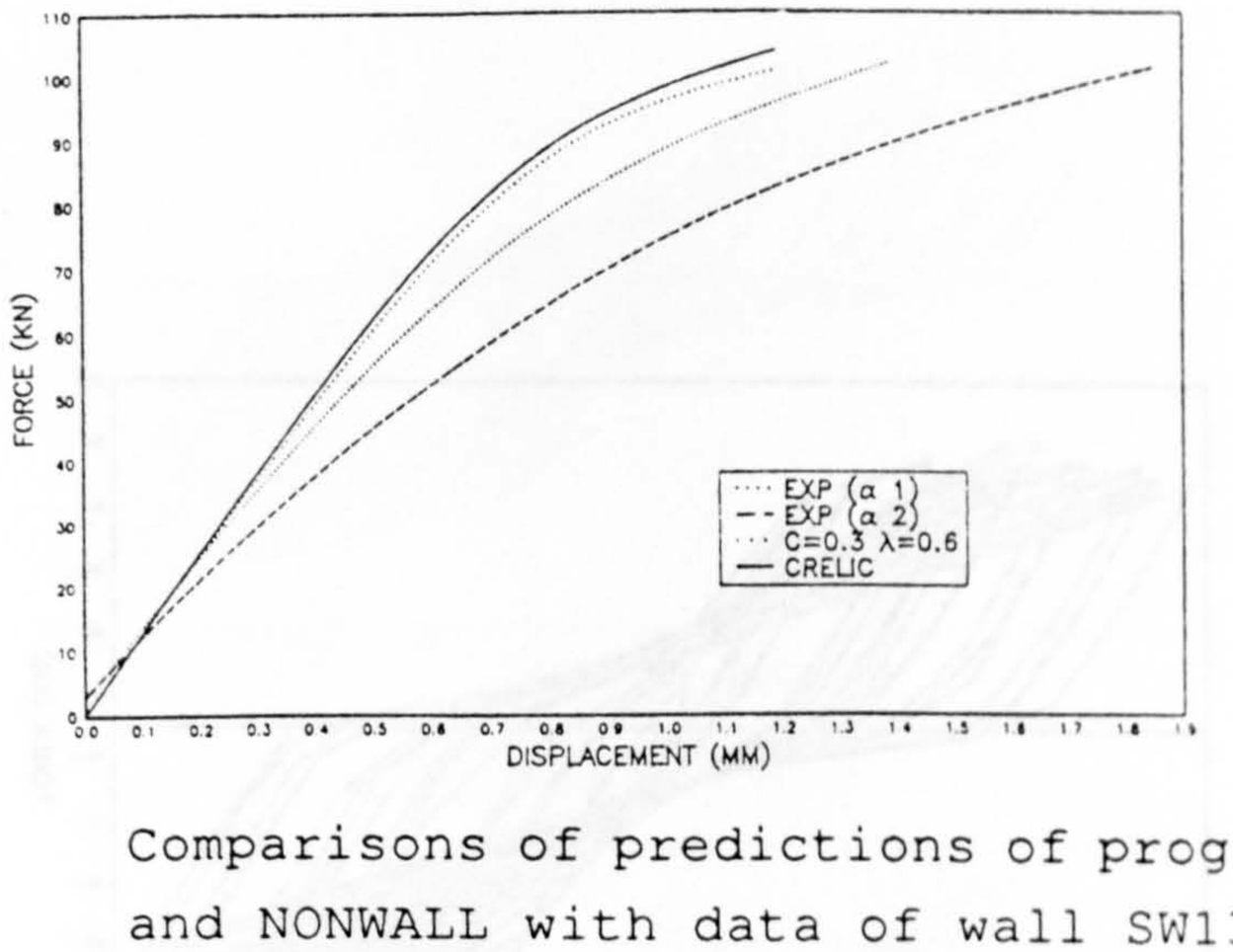


Figure C.3 Comparisons of predictions of programs CRELIC and NONWALL with data of wall SW13

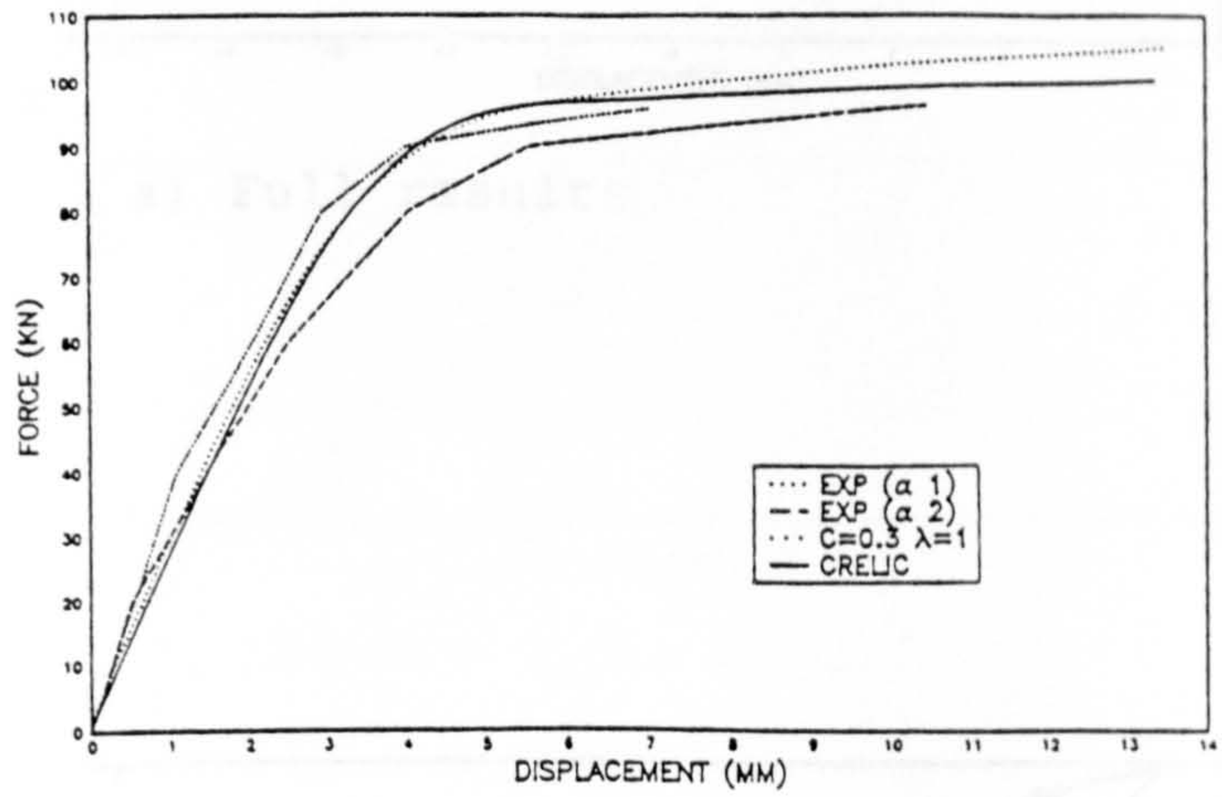


Figure C.4 Comparisons of predictions of programs CRELIC and NONWALL with data of wall SW9

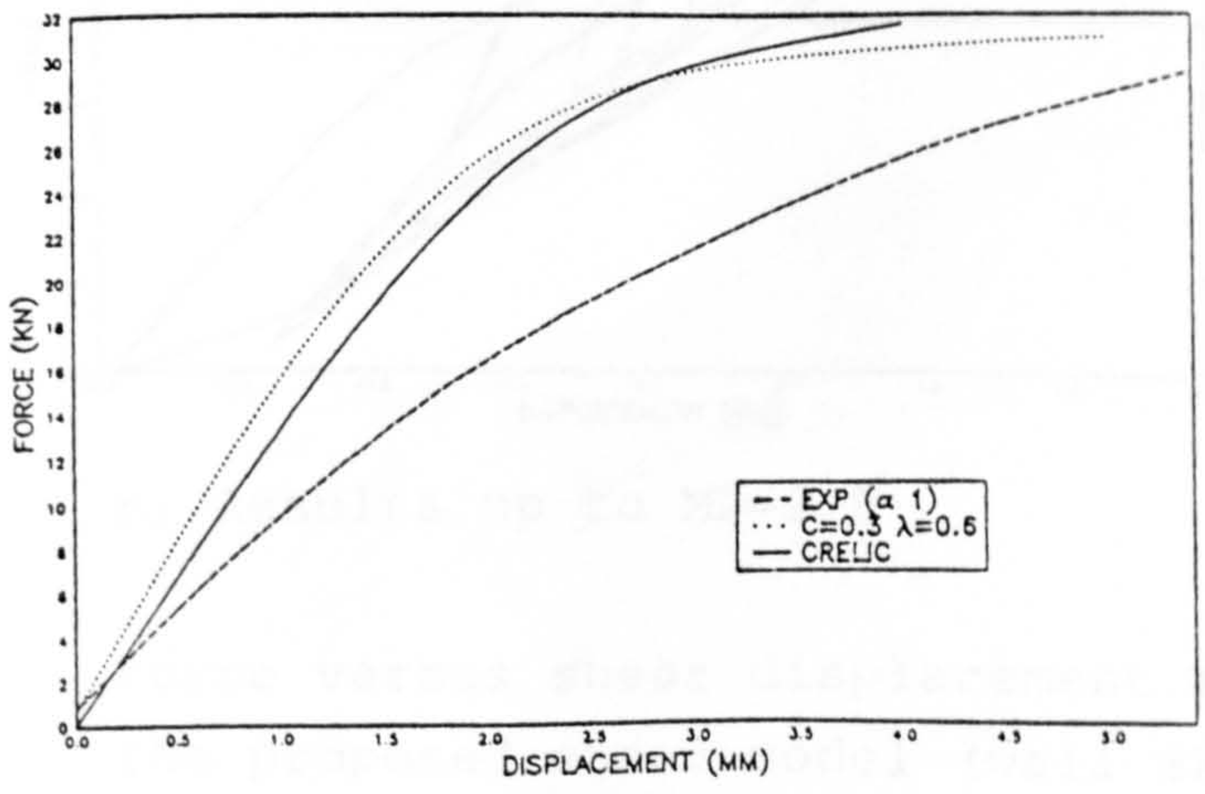
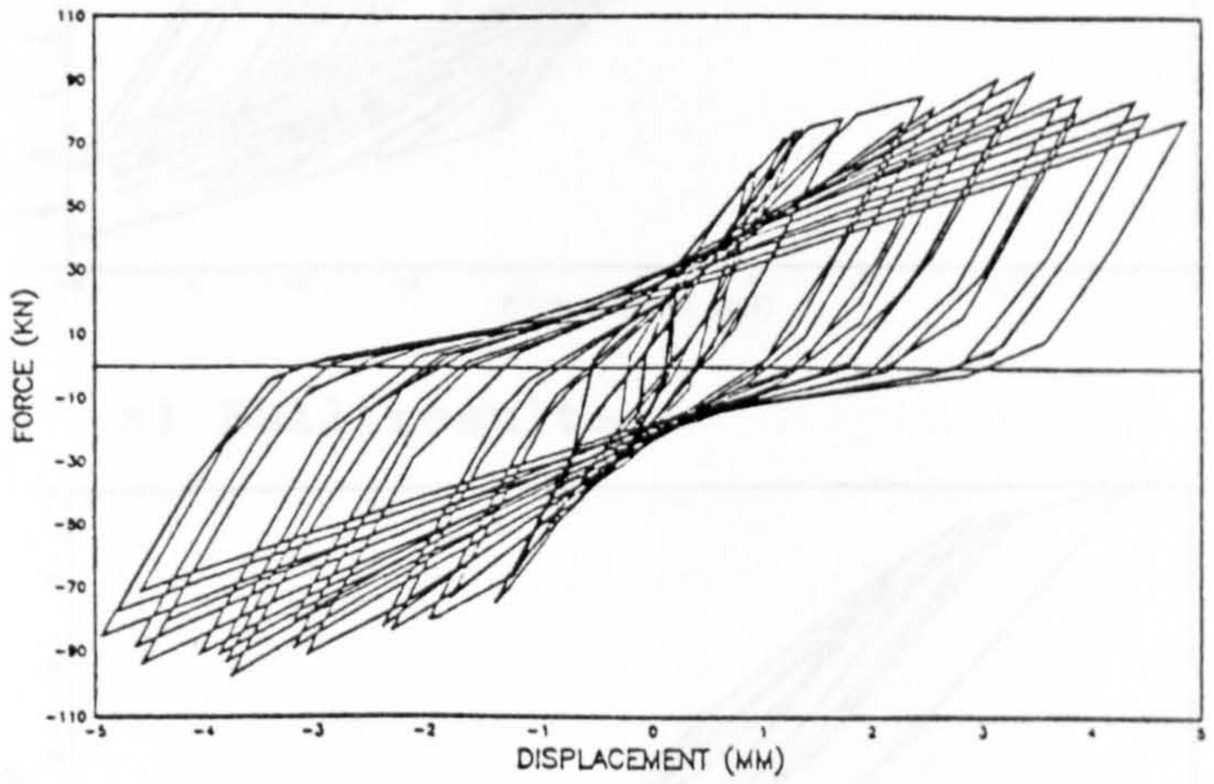
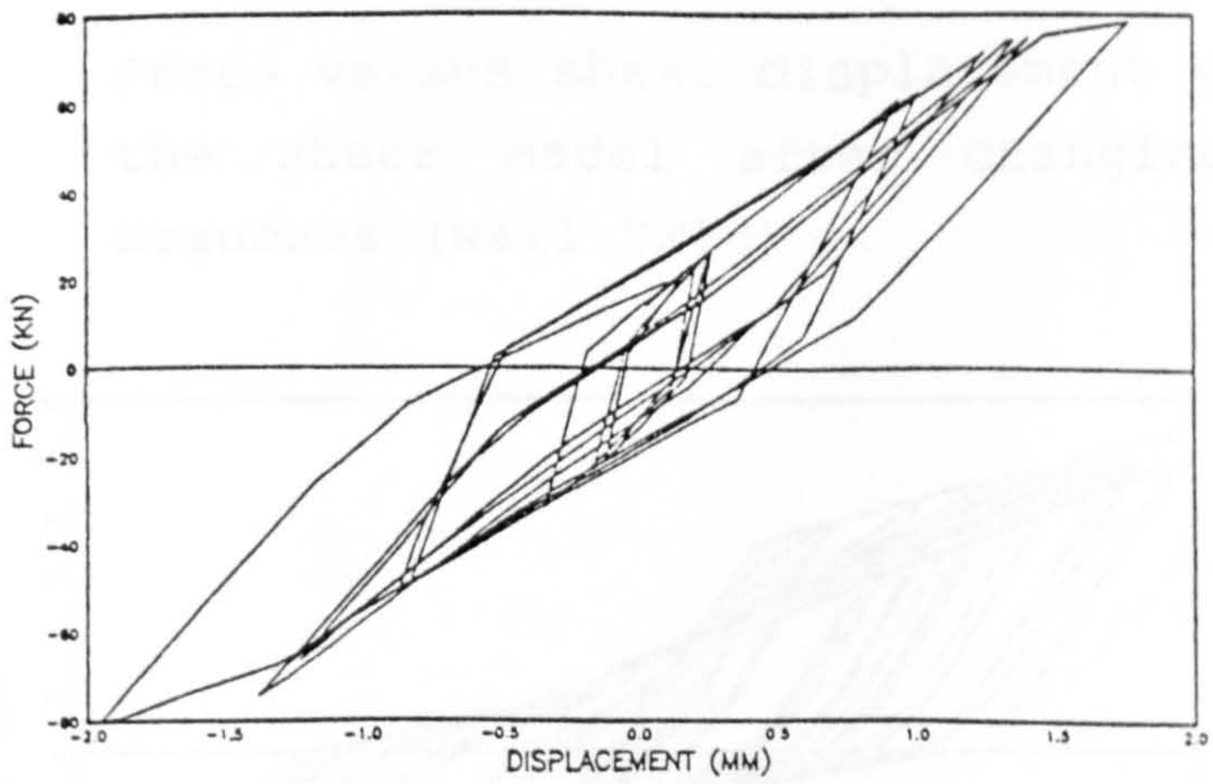


Figure C.5 Comparisons of predictions of programs CRELIC and NLAW with data of wall SW3

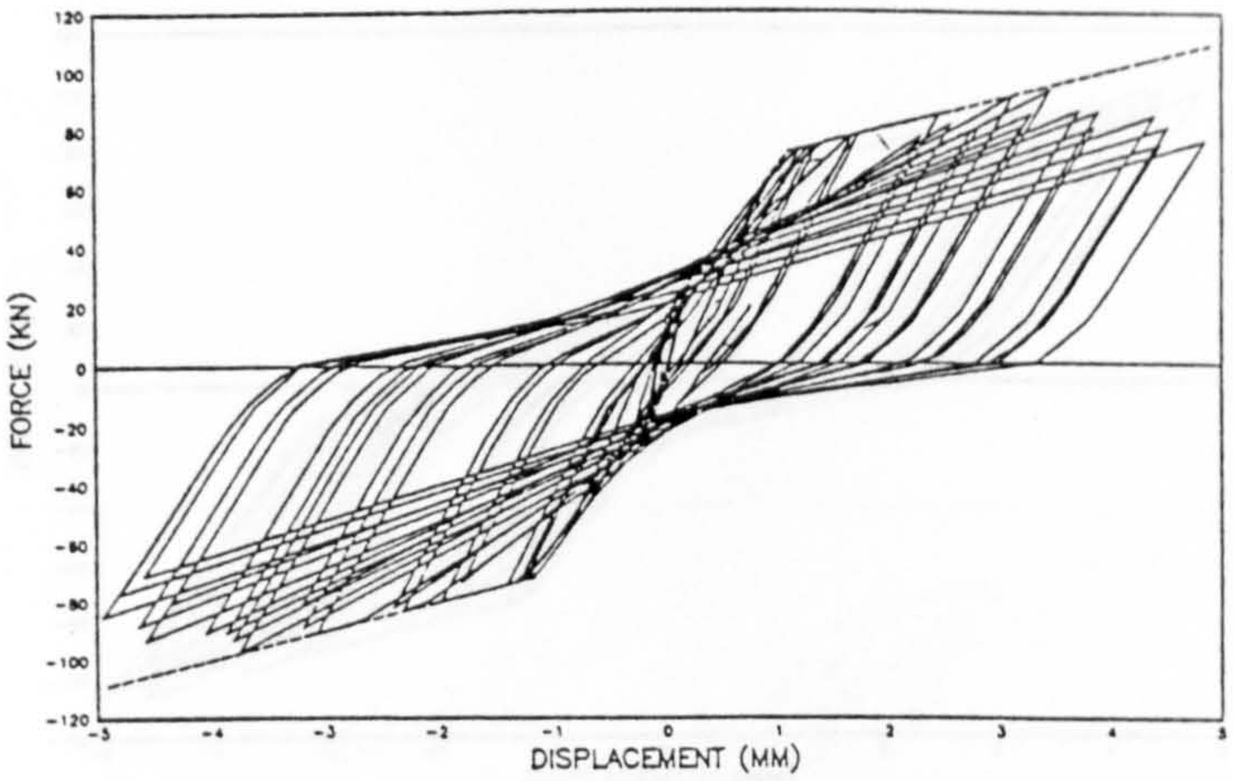


a) Full results

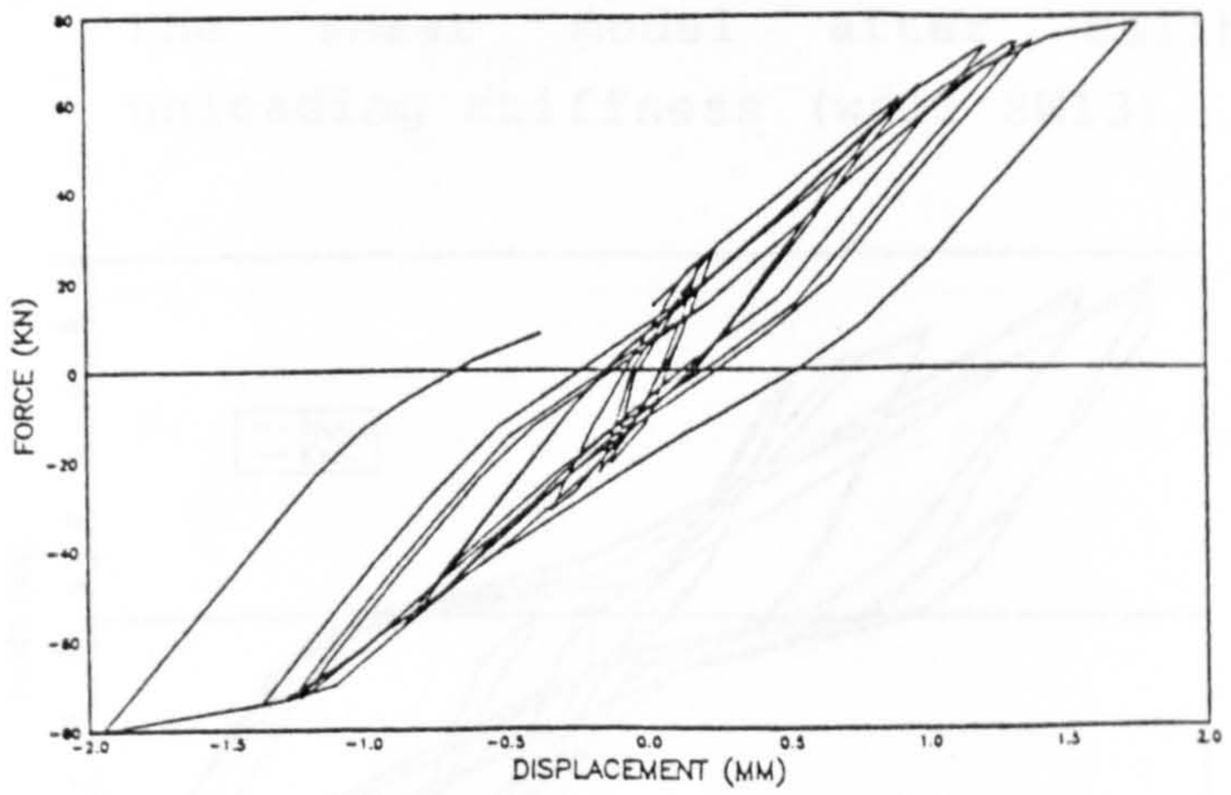


b) Results up to MD=2.0

Figure C.6 Force versus shear displacement evaluated by the proposed shear model (wall SW13)



a) Full results



b) Results up to MD=2.0

Figure C.7 Force versus shear displacement evaluated by the shear model after changing unloading branches (wall SW13)

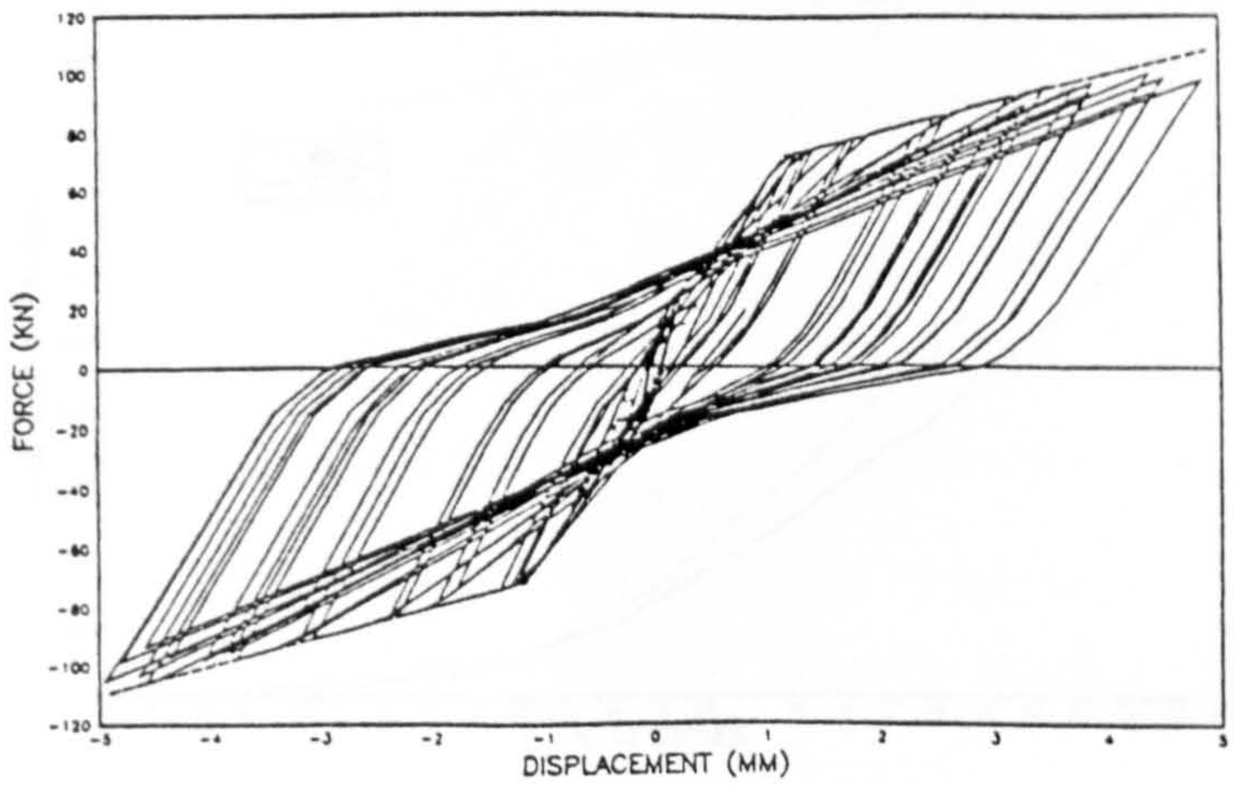


Figure C.8 Force versus shear displacement evaluated by the shear model for β=0 (wall SW13)

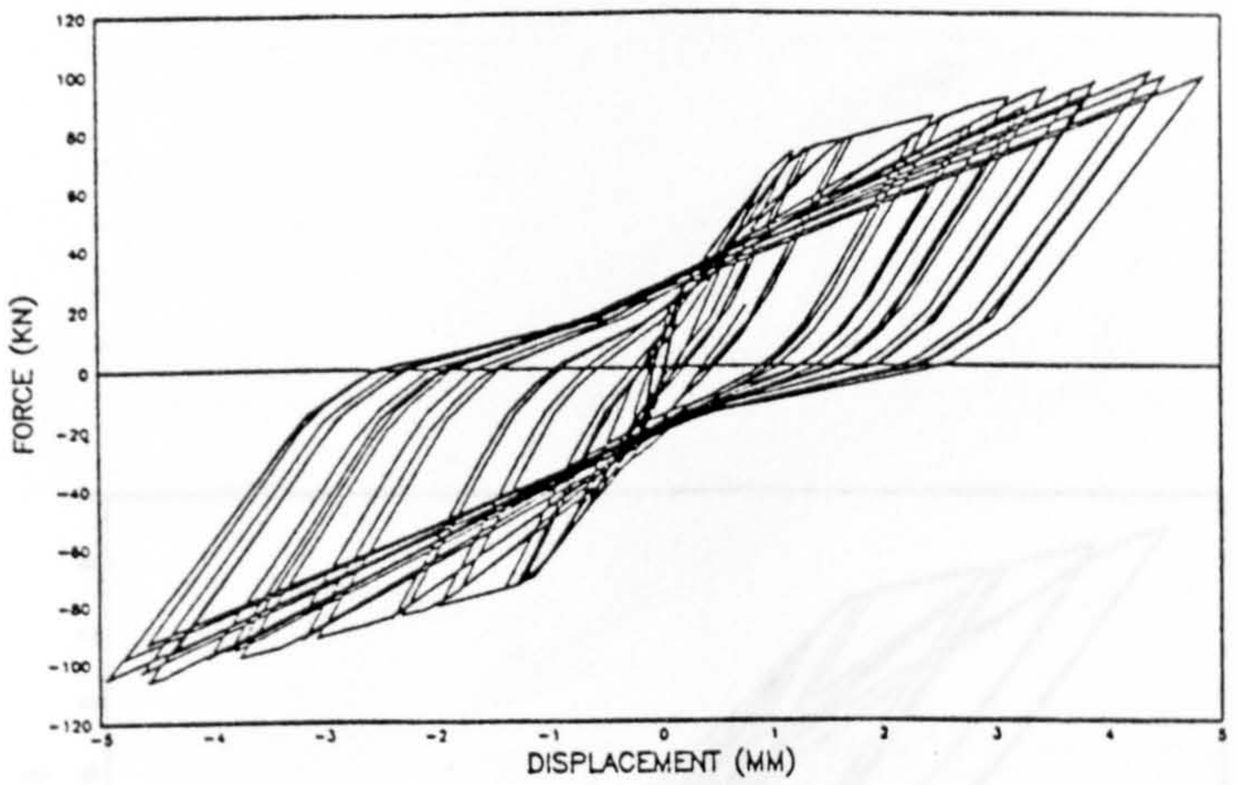


Figure C.9 Force versus shear displacement evaluated by the shear model after calibration of unloading stiffness (wall SW13)

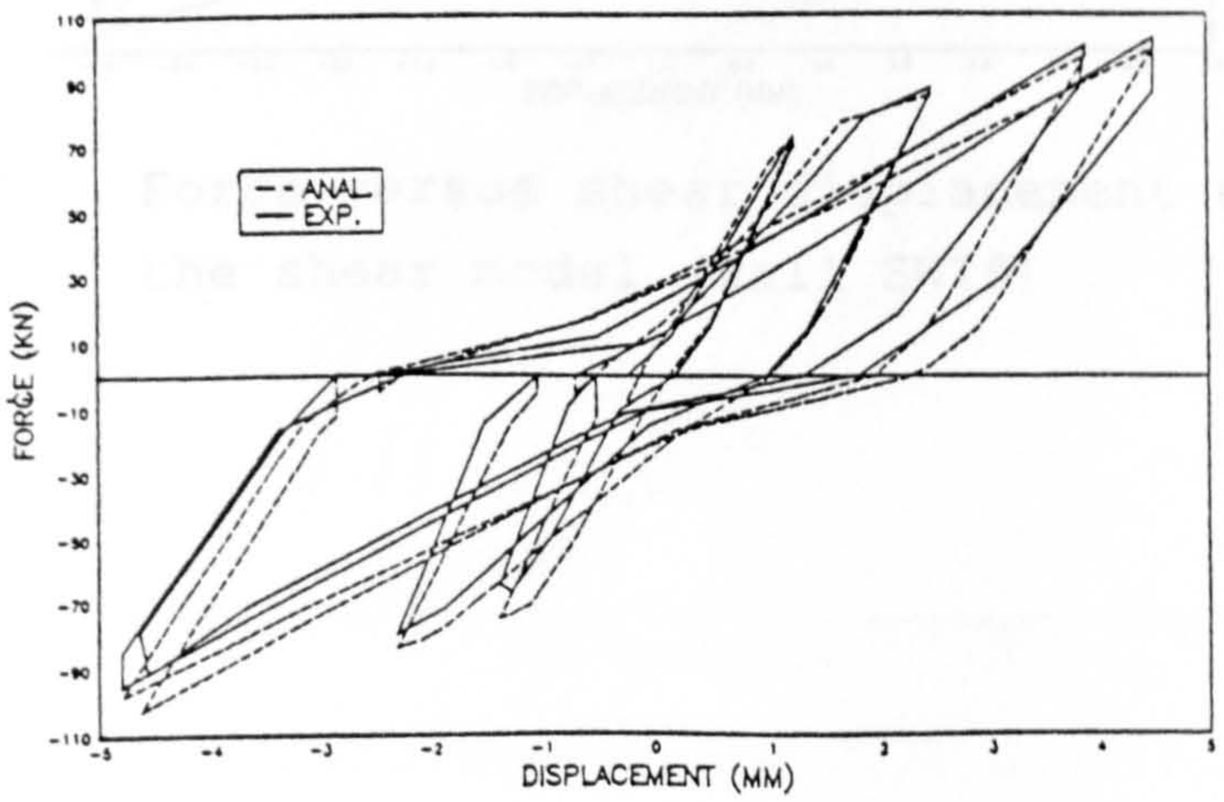


Figure C.10 Comparison of experimental data with predictions of the shear model (wall SW13)

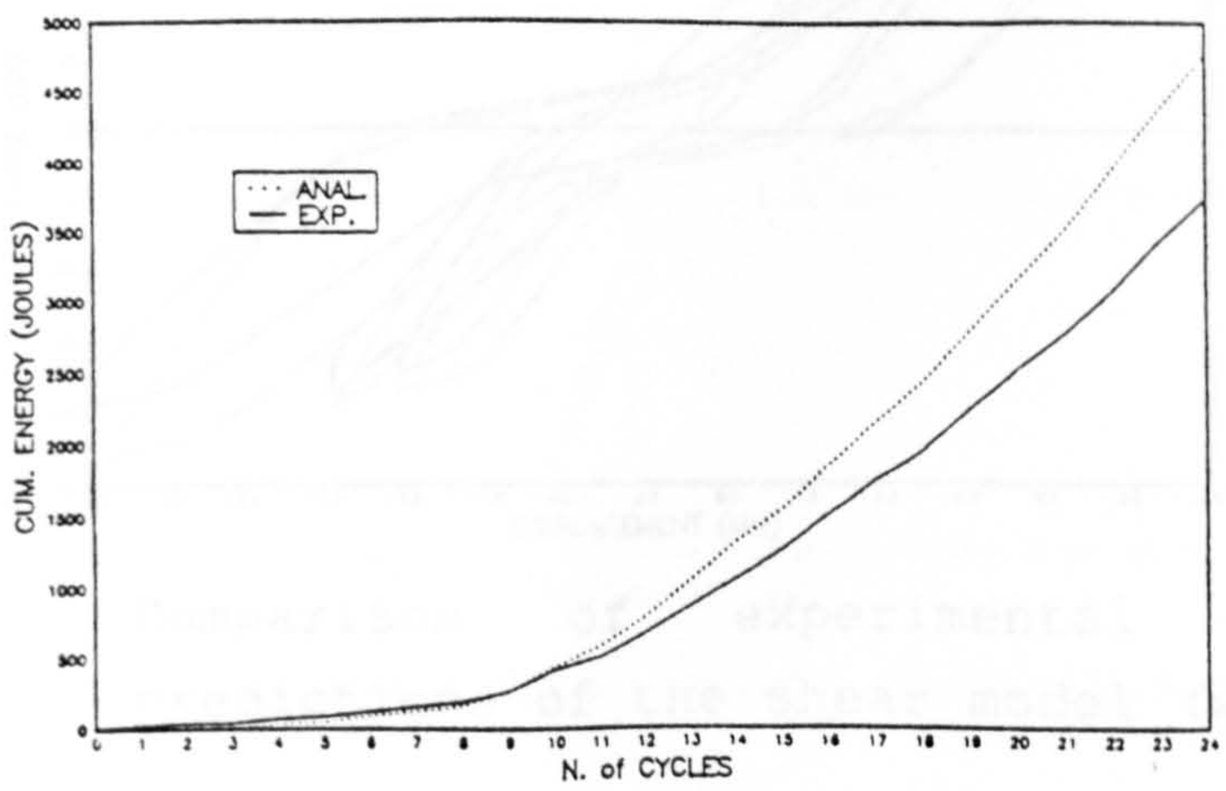


Figure C.11 Comparison of cumulative energy dissipation by the shear component (wall SW13)

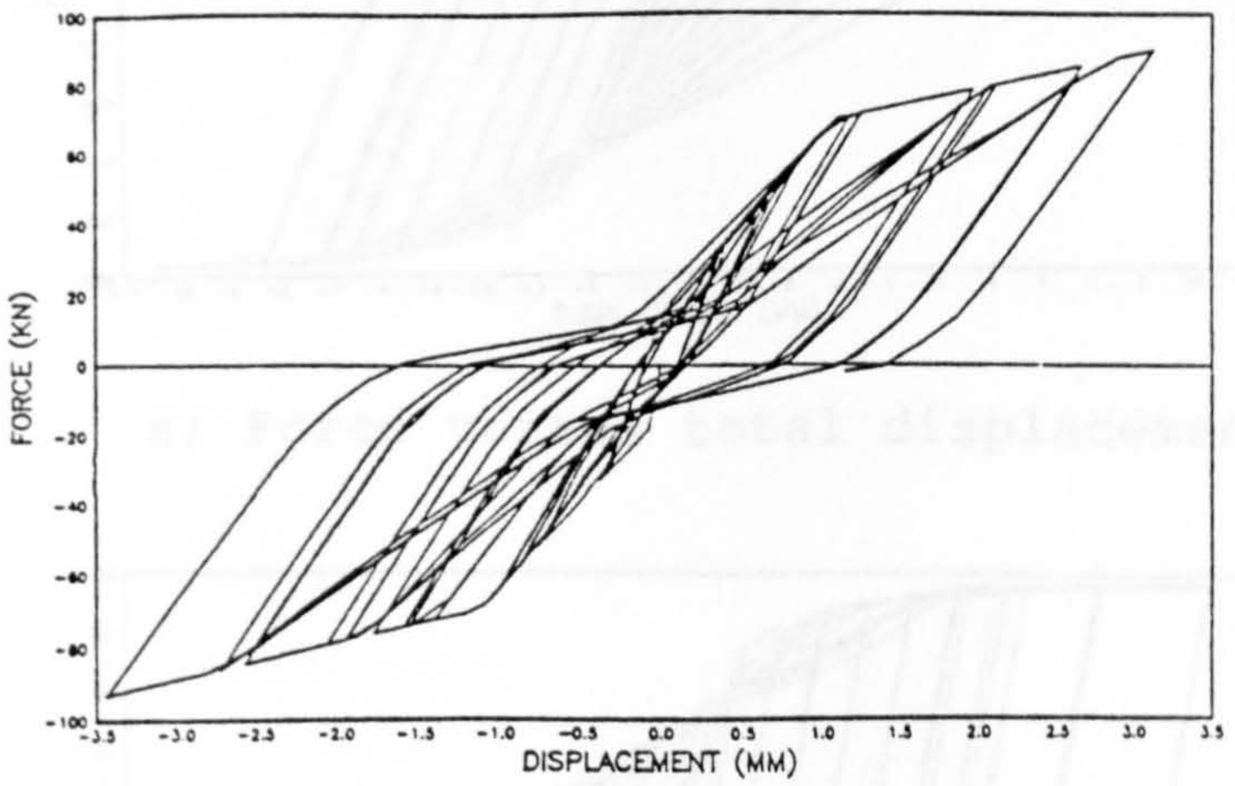


Figure C.12 Force versus shear displacement evaluated by the shear model (wall SW16)

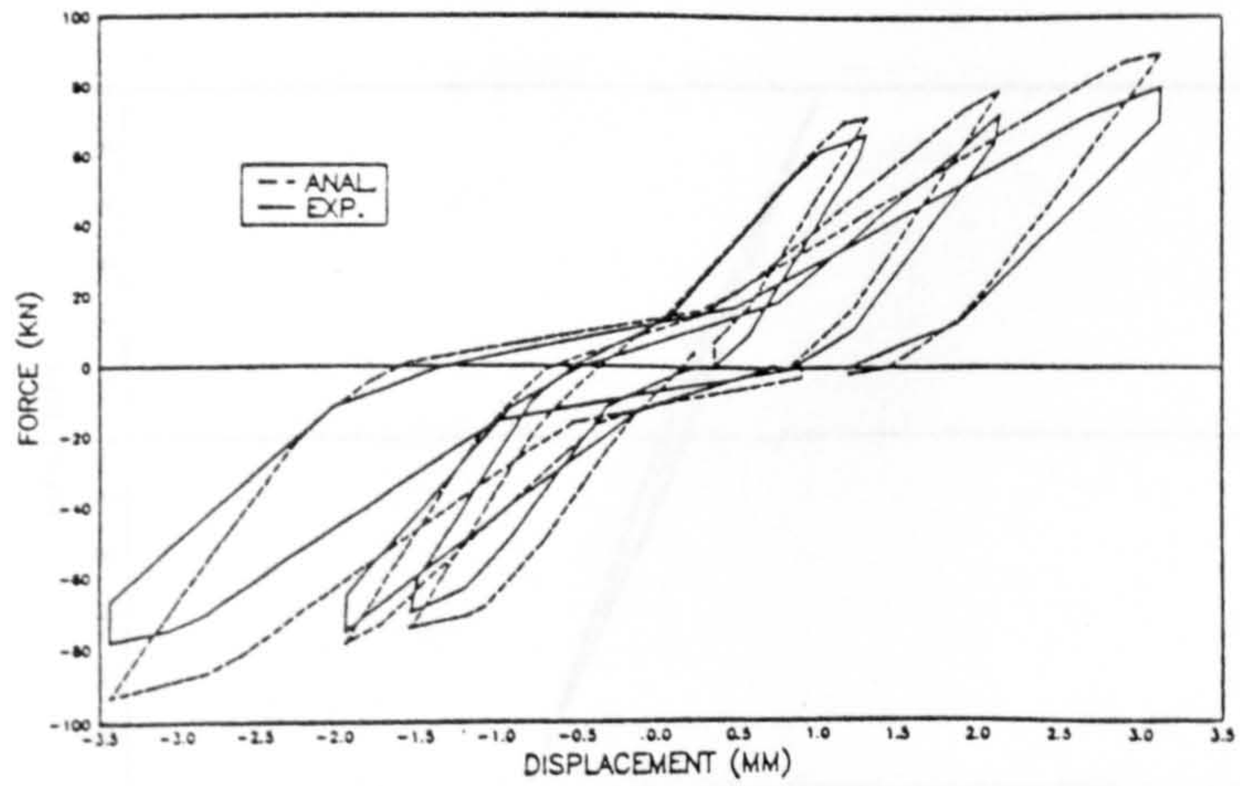
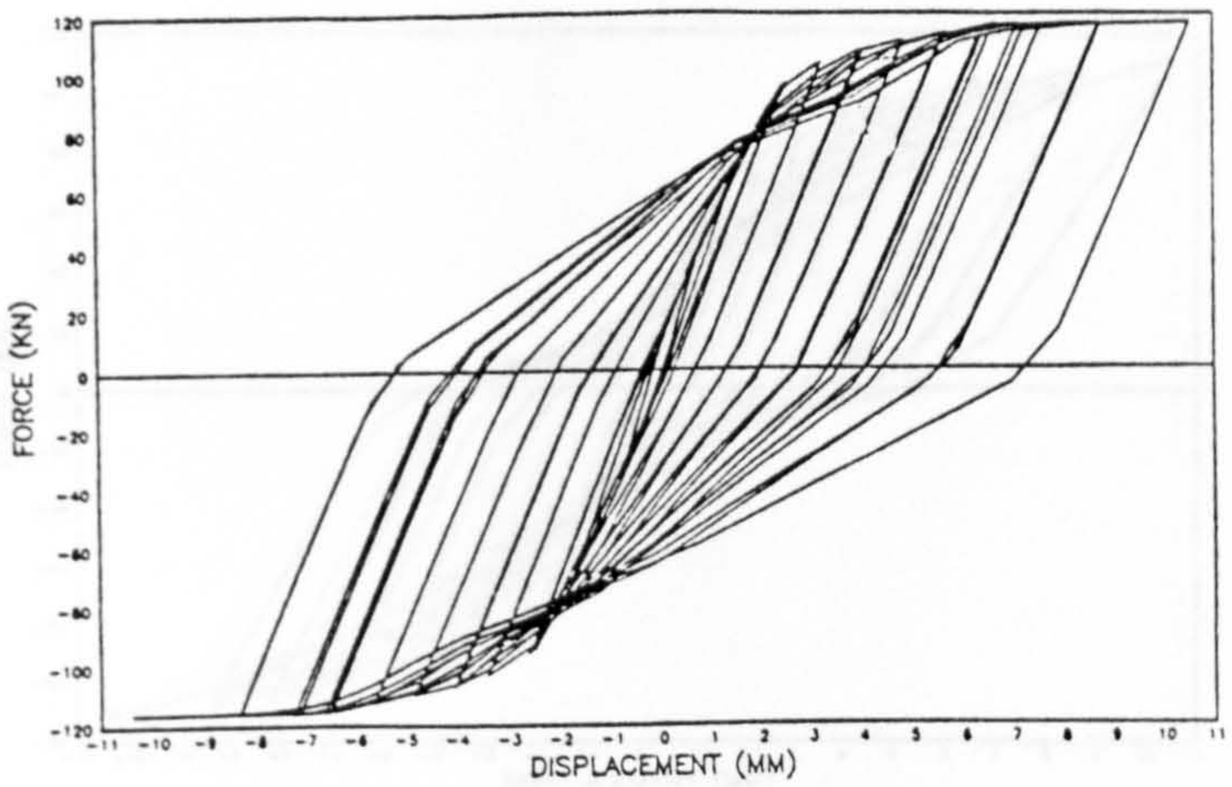
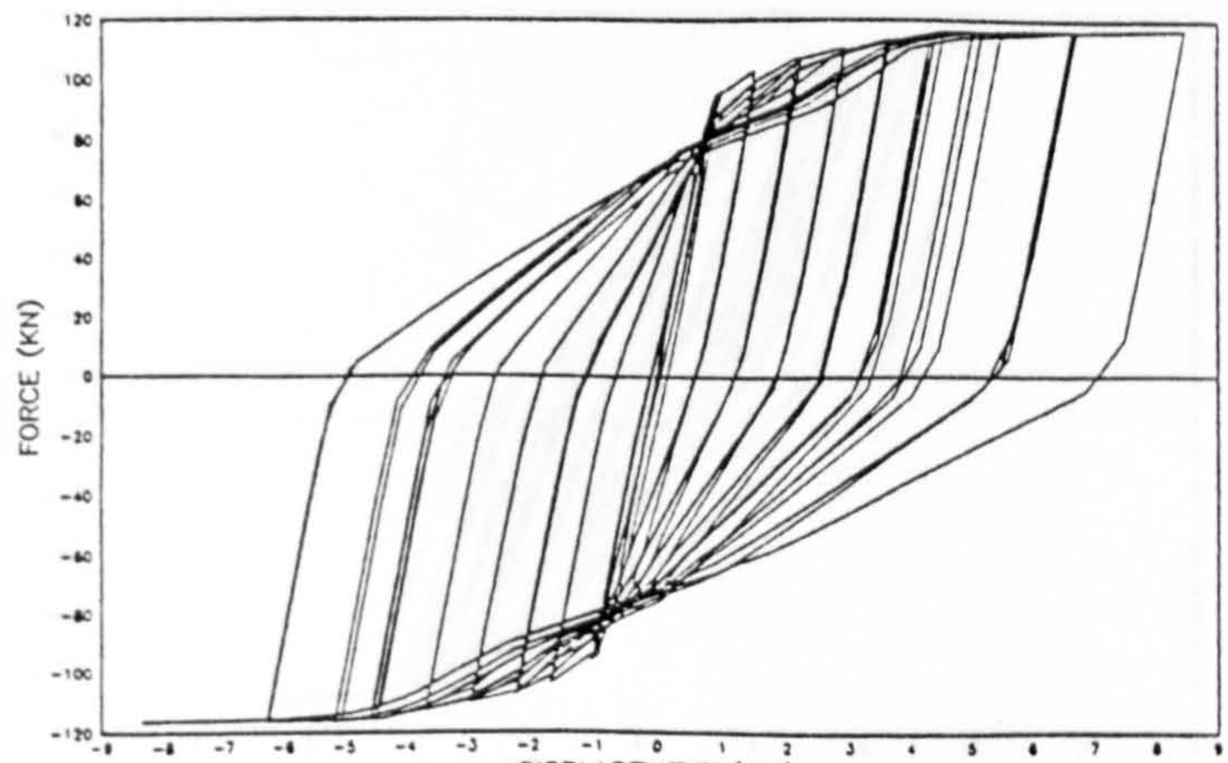


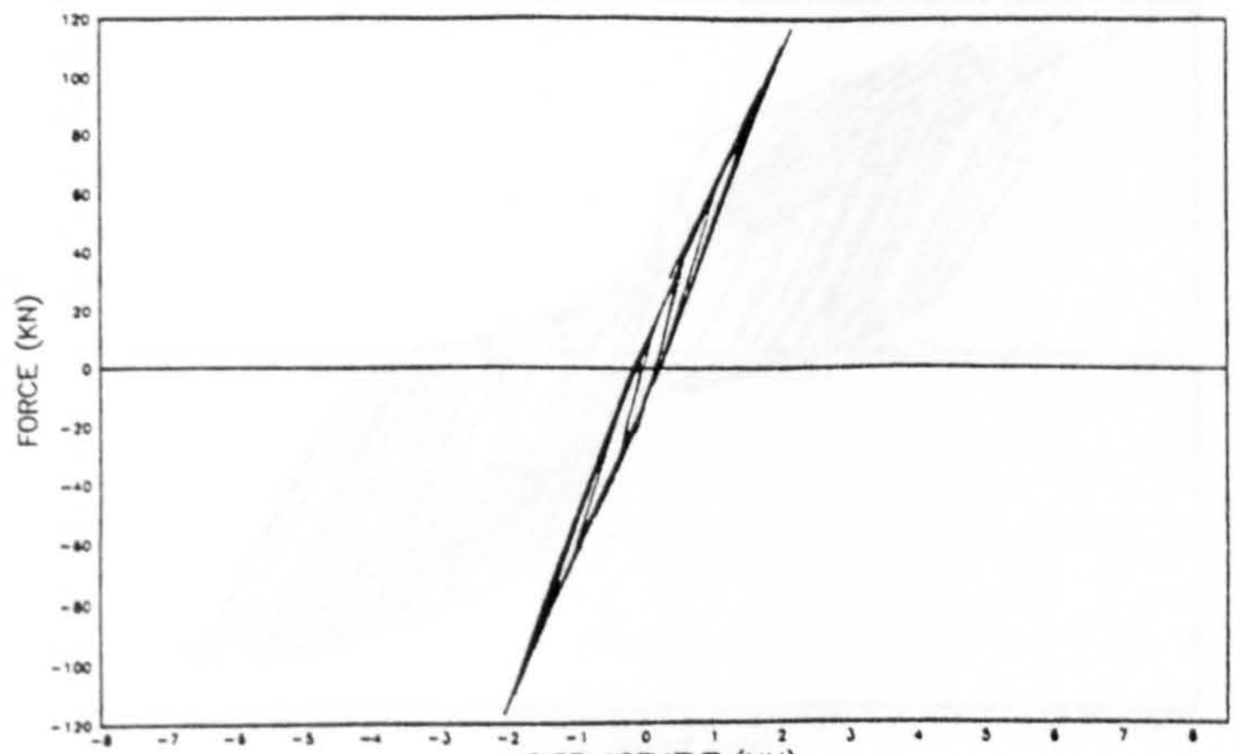
Figure C.13 Comparison of experimental data with predictions of the shear model (wall SW16)



a) Force versus total displacement

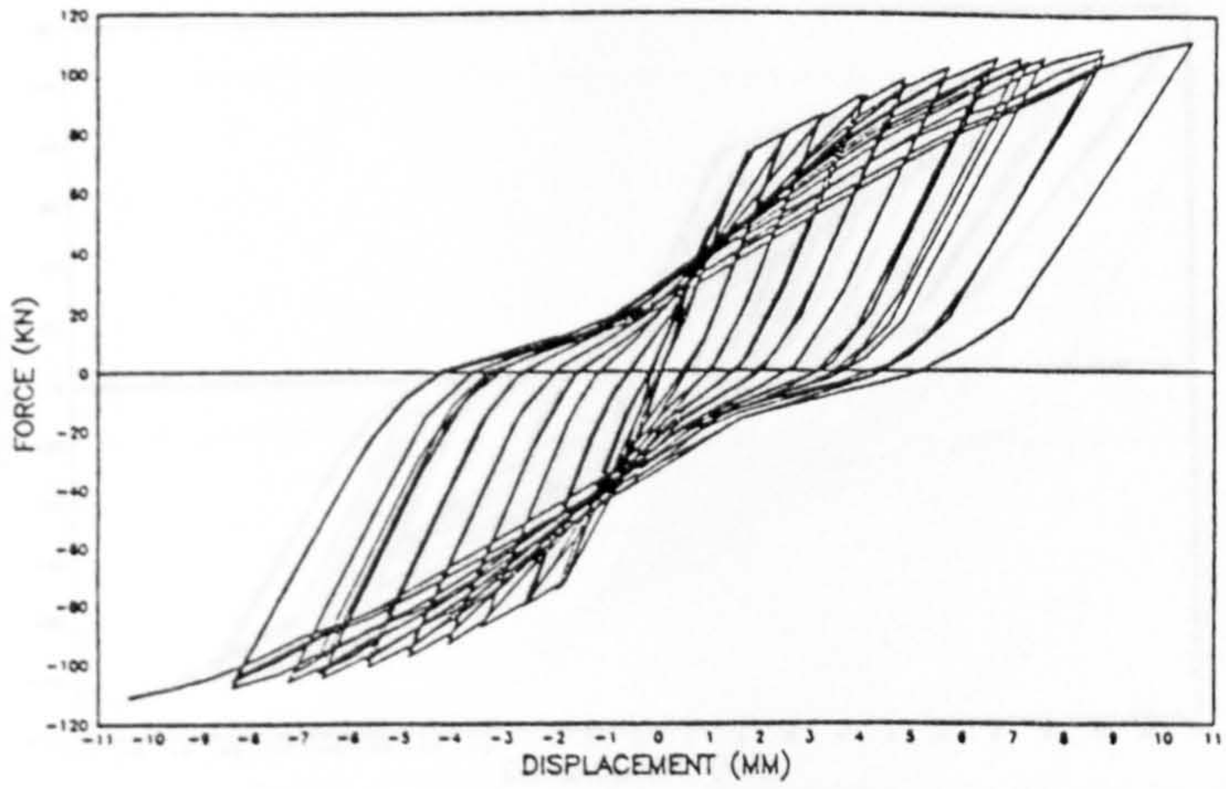


b) Force versus flexural displacement

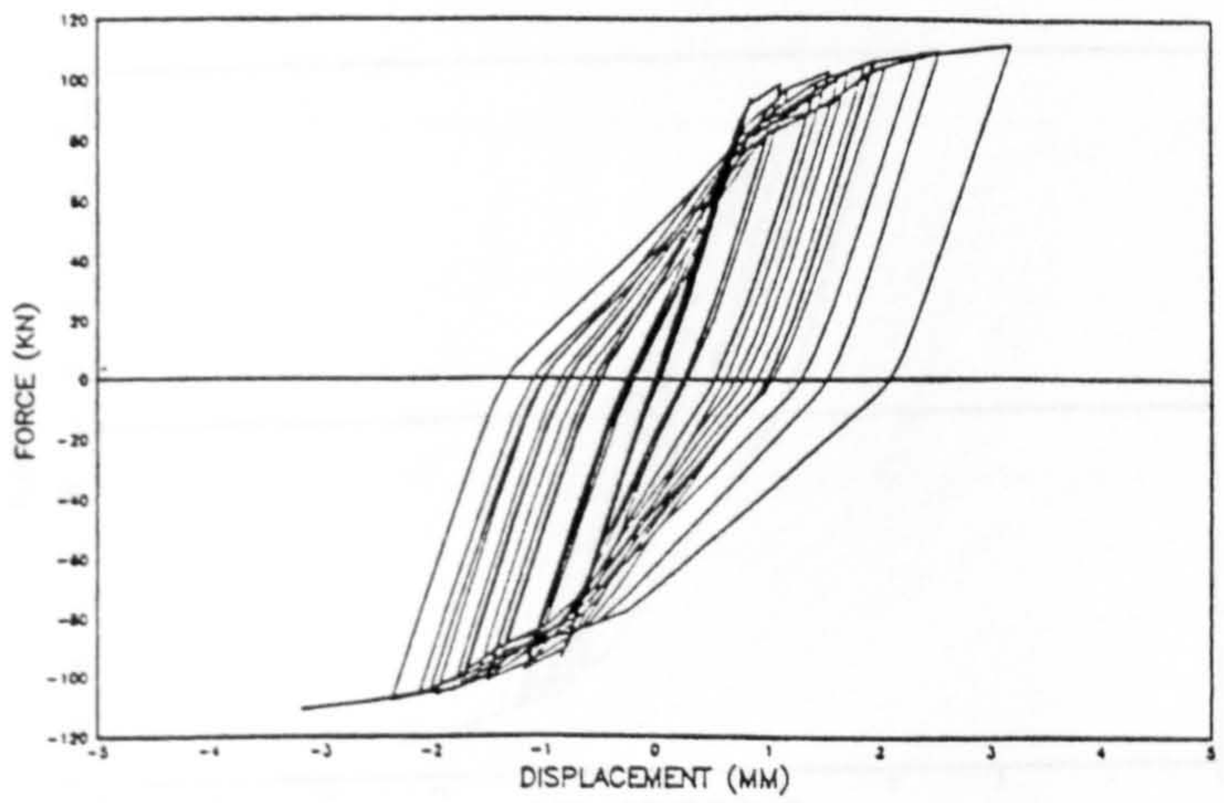


c) Force versus shear displacement

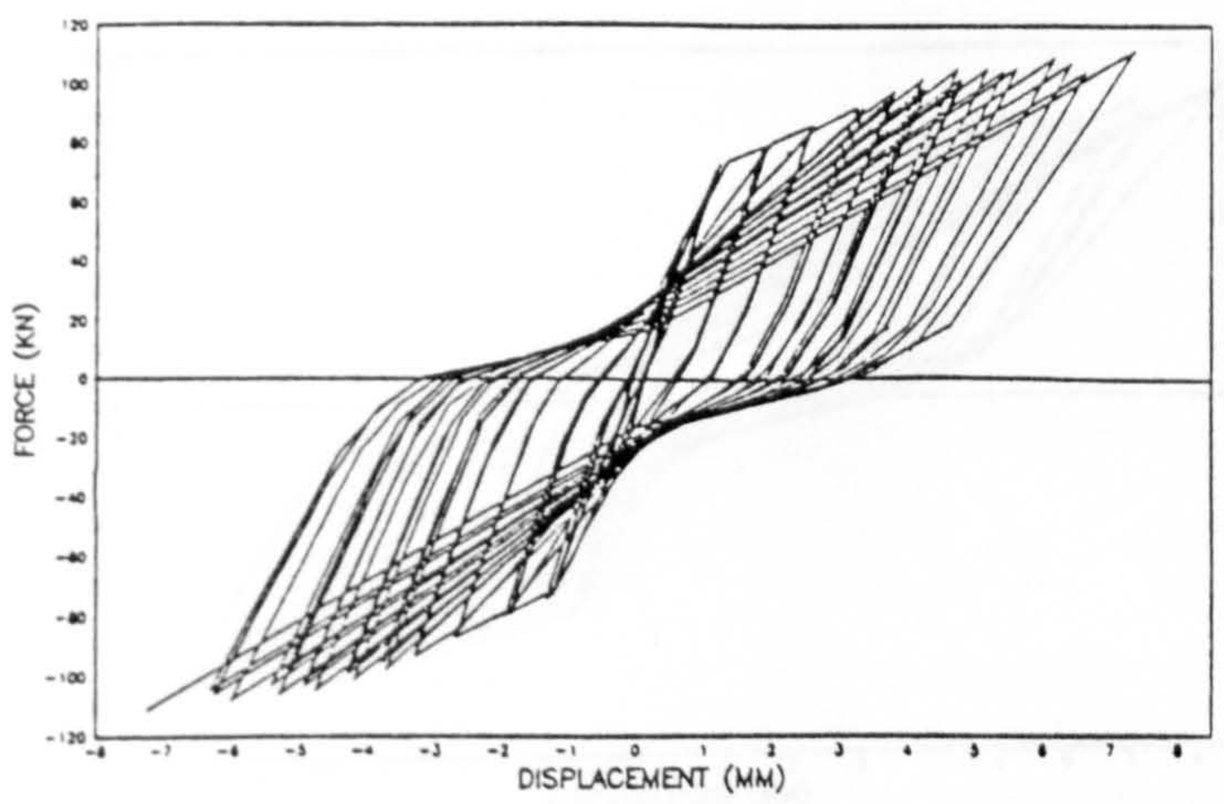
Figure C.14 Analytical results for V_y=120KN (wall SW13)



a) Force versus total displacement

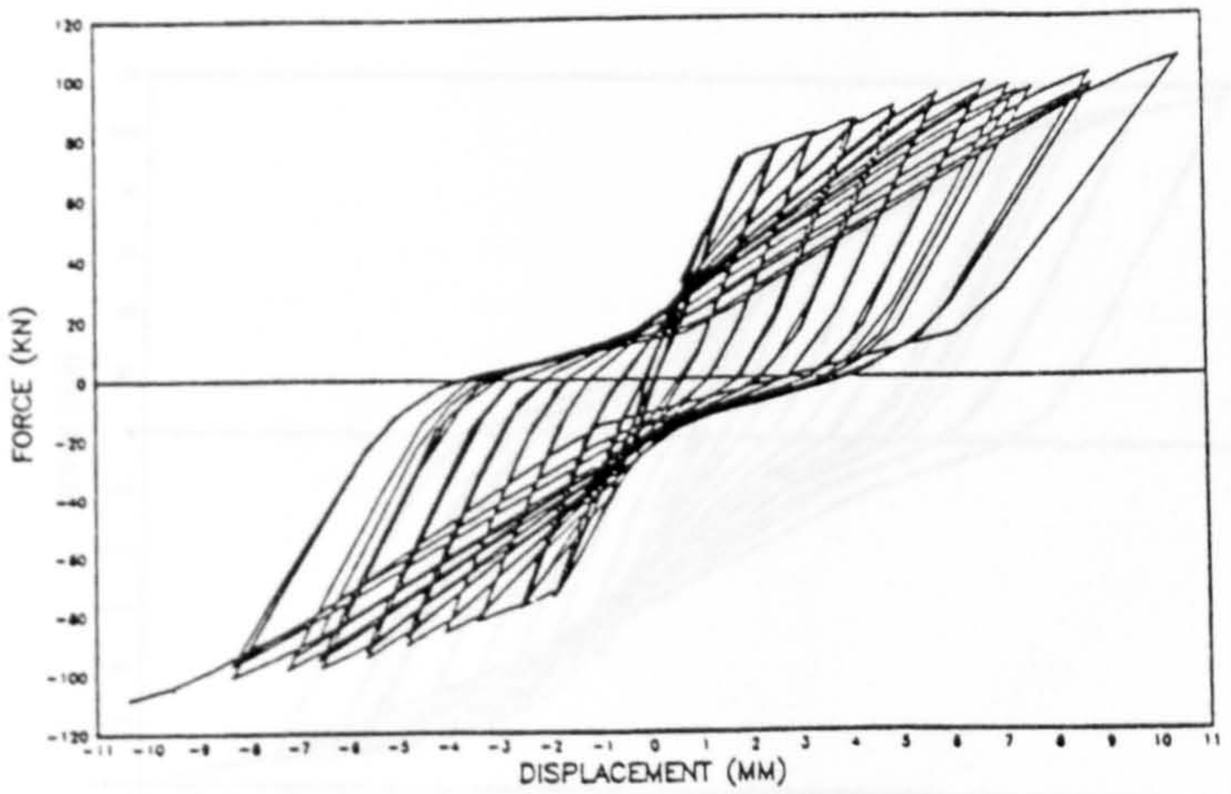


b) Force versus flexural displacement

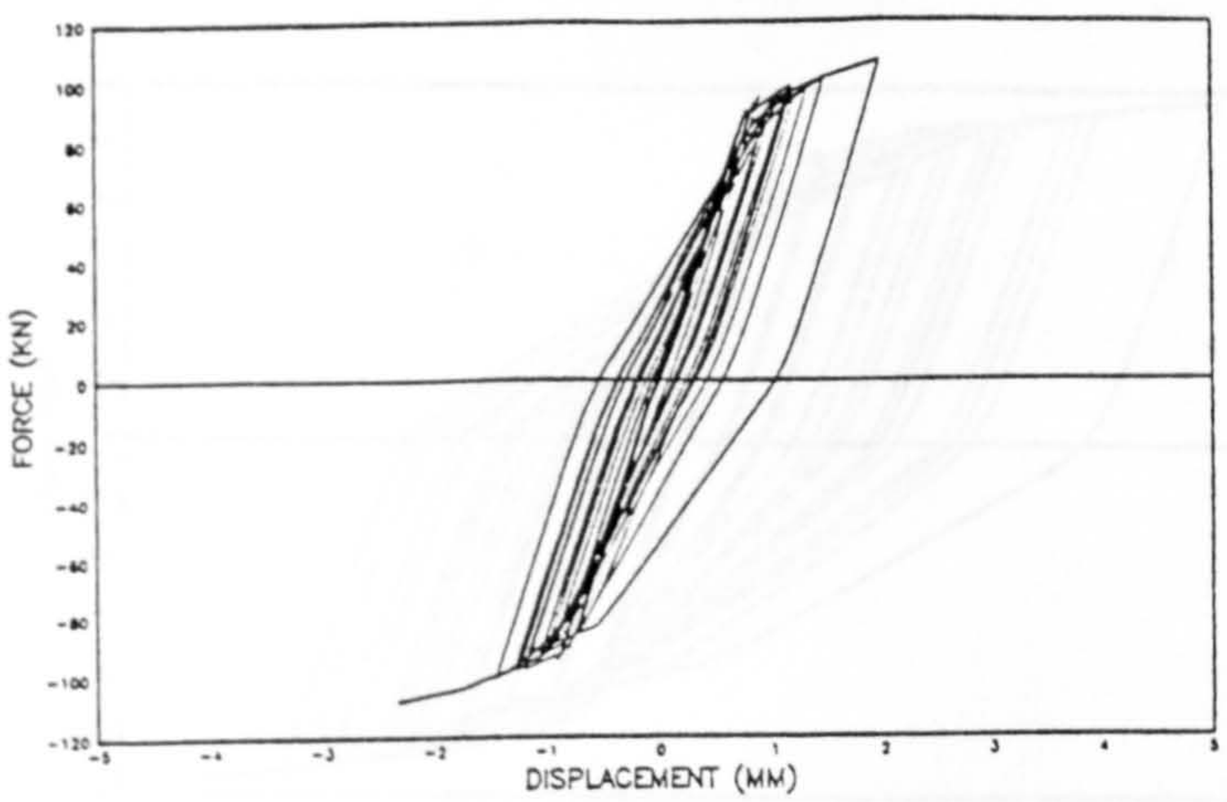


c) Force versus shear displacement

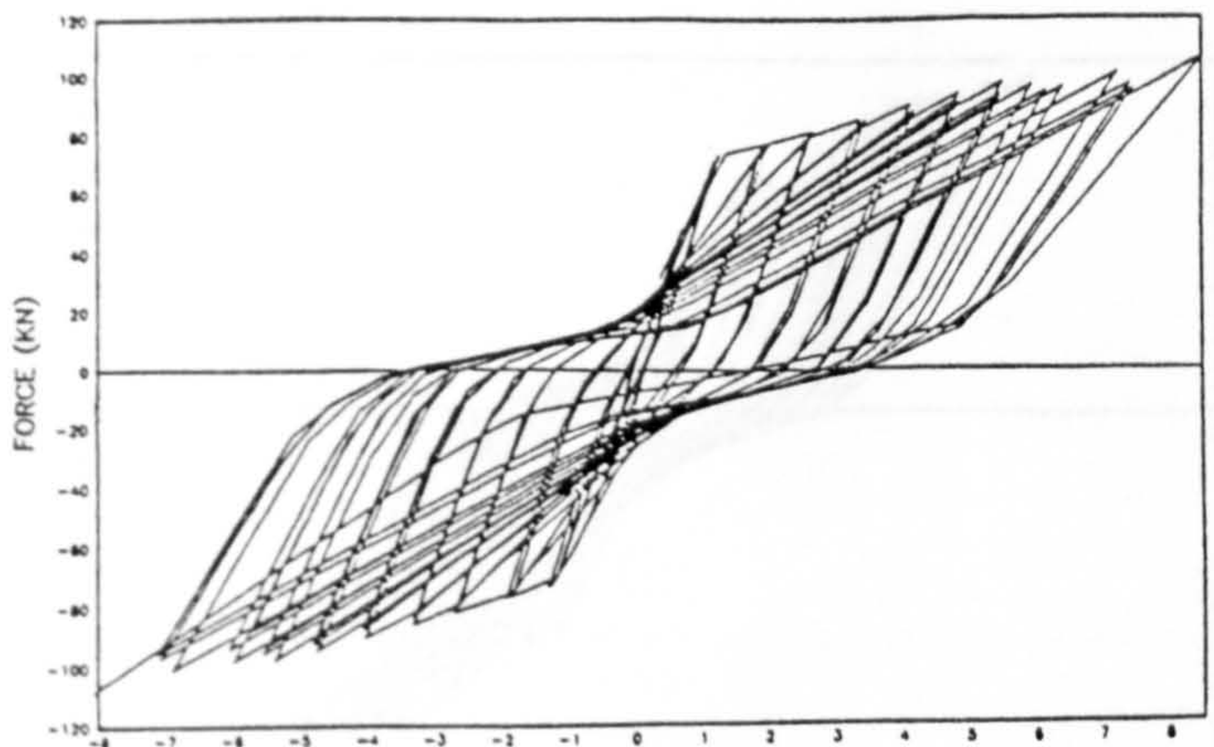
Figure C.15 Analytical results with coupling (wall SW13)



a) Force versus total displacement

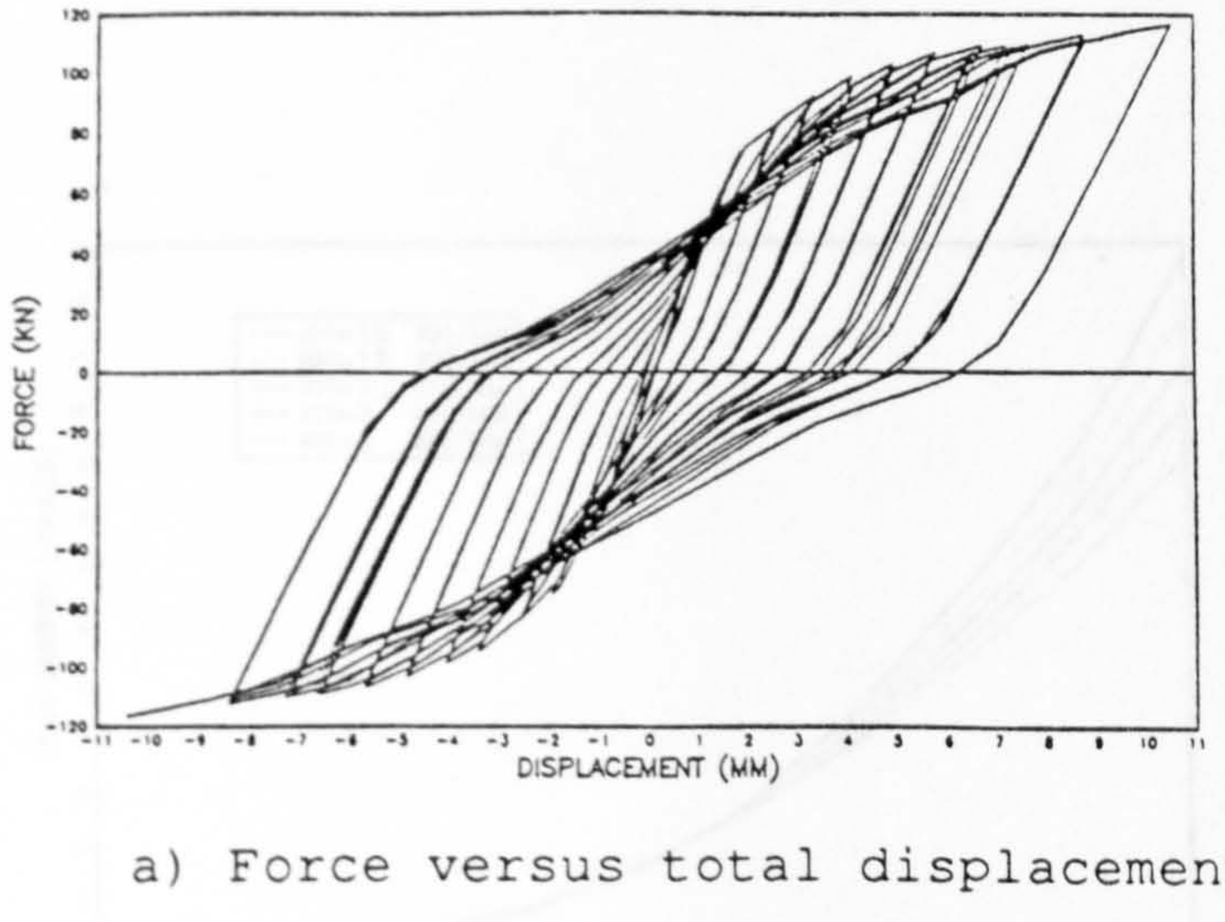


b) Force versus flexural displacement

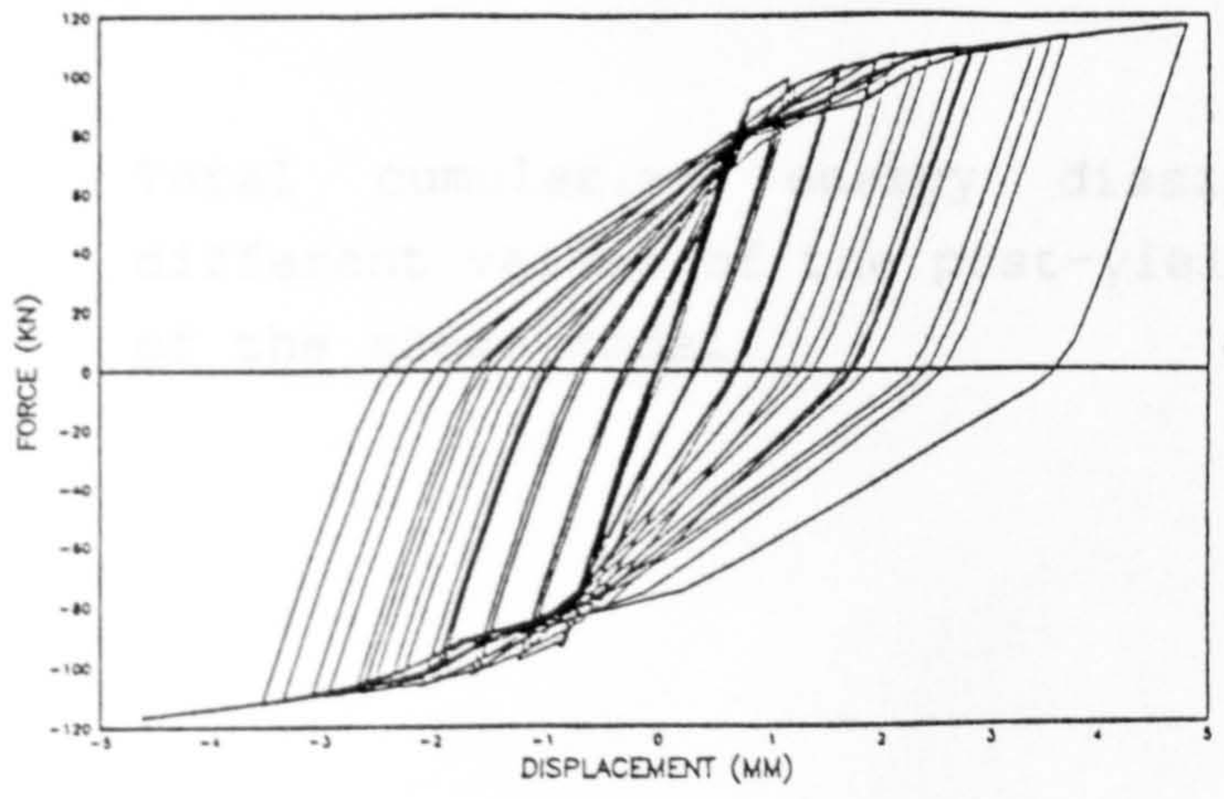


c) Force versus shear displacement

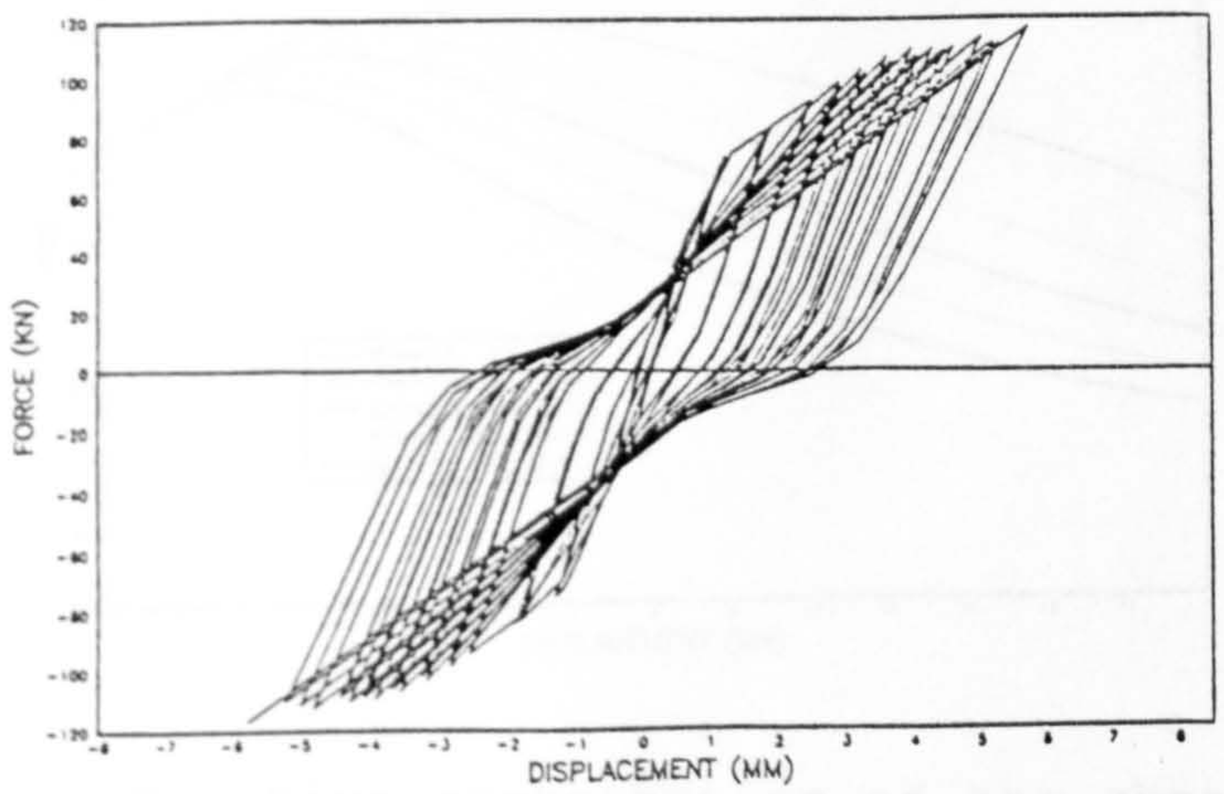
Figure C.16 Analytical results of coupled version for KH=6KN/mm (wall SW13)



a) Force versus total displacement



b) Force versus flexural displacement



c) Force versus shear displacement

Figure C.17 Analytical results of coupled version for KH=15KN/mm (wall SW13)

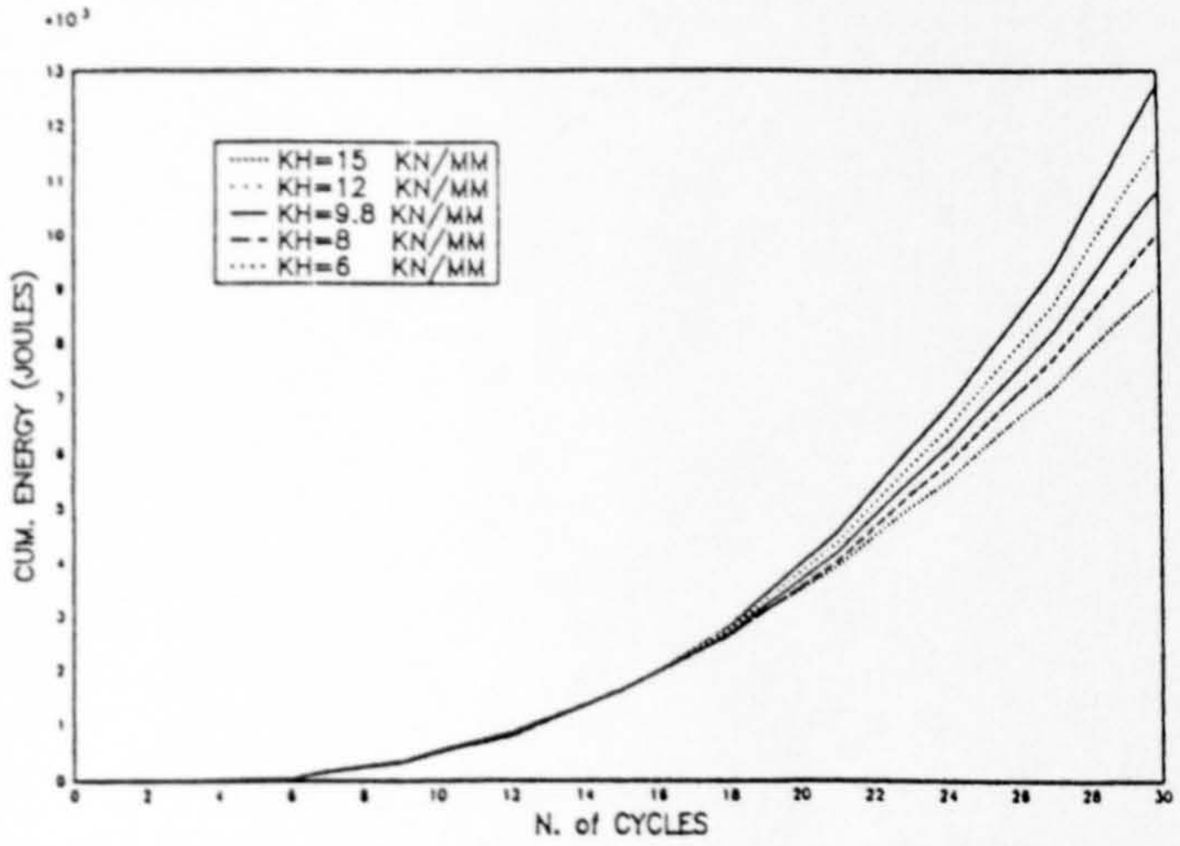


Figure C.18 Total cumulative energy dissipation for different values of the post-yield stiffness of the shear model

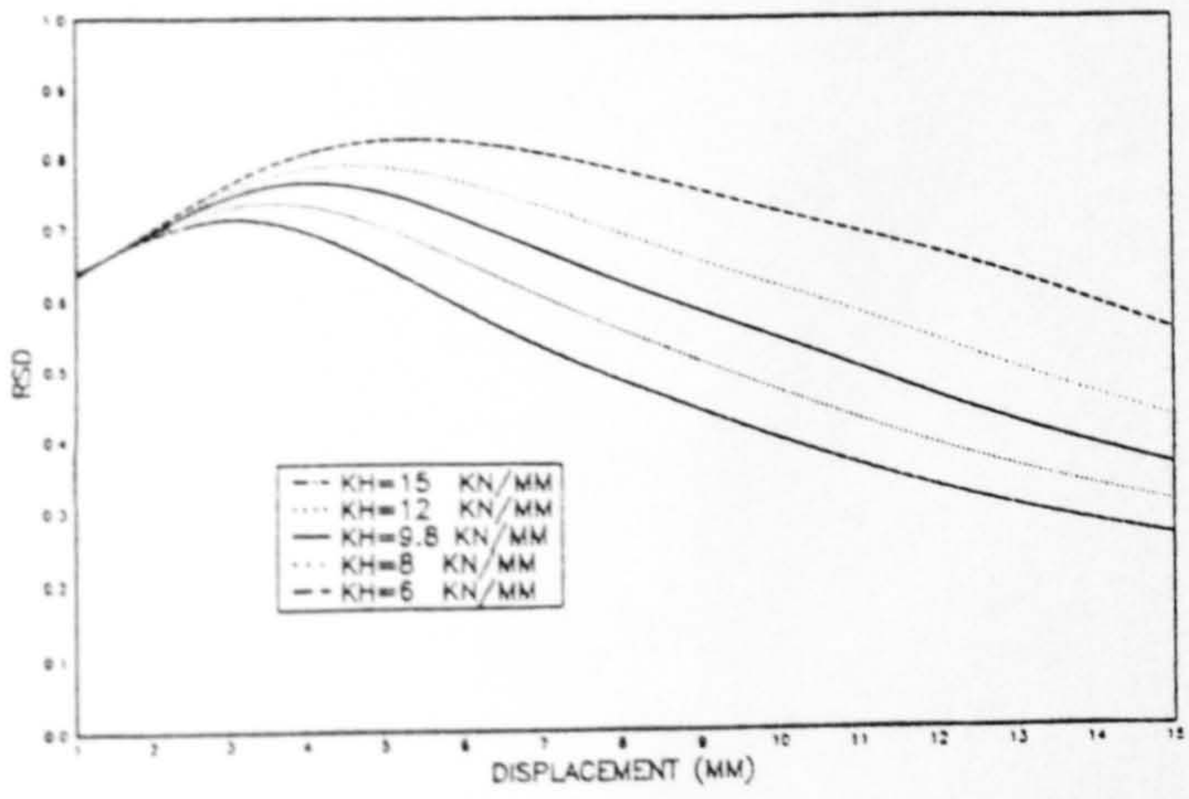


Figure C.19 Relative contribution of the shear component to the total deformation for different values of the post-yield stiffness of the shear model

BIBL. LONDIN. UNIV.